

# **ELECTRONICS FOR ENGINEERS**

---

# **ELECTRONICS FOR ENGINEERS**

***Reference articles, charts, and graphs  
from Electronics magazine***

---

Edited by  
**JOHN MARKUS**  
and  
**VIN ZELUFF**

Associate Editors, Electronics

FIRST EDITION  
FIFTH IMPRESSION

---

McGRAW-HILL BOOK COMPANY, INC.  
NEW YORK AND LONDON  
1945

---



ELECTRONICS FOR ENGINEERS

COPYRIGHT, 1945, BY THE  
MCGRAW-HILL BOOK COMPANY, INC.

---

PRINTED IN THE UNITED STATES OF AMERICA

*All rights reserved. This book, or  
parts thereof, may not be reproduced  
in any form without permission of  
the publishers.*

# Preface

**E**NGINEERS are busy people. They invent all manner of short cuts for themselves; they condense much information into the small space of graphs and charts. In many cases they share this information with other engineers by publishing it in the technical press.

Monthly magazines are not exactly convenient for reference—even in bound volumes—when they have accumulated for a few years. In an earnest attempt to solve this problem for one McGraw-Hill publication—*Electronics*—the editors of this book have gone through the complete files of the magazine from the first issue (April, 1930), and from this wealth of technical data have selected 142 articles, reference sheets, charts, and graphs that have been in greatest demand for their reference value. All this material has been carefully checked, edited, and condensed where desirable to put it into the best possible form for presentation in a book. The individual papers were then grouped into chapters for convenient reference to make the book practically self-indexing.

Designers, builders, and users of electronic equipment and component parts will find here, under the headings of their respective fields of interest, the equations and other data so badly needed yet often so hard to find. One article alone, available when needed, can justify a place for this book on an engineer's desk.

The editorial staff of *Electronics* takes pride in the repeated requests that have come in for tear sheets or photostats and is glad that these articles are now available in handy and economical form between the covers of one book.

The engineer authors whose works appear in this volume deserve congratulations for their permanent contributions to the art and industry of electronics.

KEITH HENNEY,  
Editor, *Electronics*.

NEW YORK, N. Y.,  
October, 1945.

# Contents

		PAGE
PREFACE . . . . .		V

## I. A-F IMPEDANCE-MATCHING NETWORKS

	DATE PUBLISHED	AUTHOR	
Design Charts for Dissymmetrical T Pads . . . . .	July, 1943.	EDWIN Y. WEBB, JR.	1
Design Procedure for Dissymmetrical T and $\pi$ Attenuators . . . . .	Aug., 1942.	P. M. HONNELL	3
Multiple-circuit Pads . . . . .	Mar., 1937.	FREDERICK WHEELER.	6
Forty Commonly Used Pads . . . . .	Apr., 1940.	AARON SHELTON	9
Universal Network Design Chart . . . . .	Mar., 1935.	A. JAMES EBEL.	10
Attenuator-design Formulas . . . . .	Nov., 1941.	DAWKINS ESPY.	11

## II. ANTENNAS

Aircraft Antenna Characteristics . . . . .	Dec., 1942 . . .	PAUL J. HOLMES . . . . .	17
Design of Two-tower Directional Arrays. . . . .	Apr., 1936. . .	E. A. LAPORT. . . . .	19
Directional Radiation Patterns of Two-element Vertical Antenna Arrays. . . . .	Apr., 1936. . .	A. JAMES EBEL. . . . .	23
Antenna Power Divider . . . . .	July, 1944. . .	EARLE TRAVIS . . . . .	25
Computing Performance of Two-tower Directional Arrays . . . . .	Aug., 1937. . .	A. R. RUMBLE . . . . .	26
Voltage Gain Charts for Two-antenna Arrays. . . . .	Feb., 1940 . . .	W. S. DUTTERA. . . . .	29
Field Strength Prediction Charts Based on Sommerfeld's Formula. . . . .	Sept., 1936. . .	WILLIAM A. FITCH . . . . .	30
Radiation Chart for Vertical Antennas. . . . .	July, 1939. . .	L. J. GIACOLETTO. . . . .	32
Design Procedure for Ground Plane Antennas . . . . .	Aug., 1943. . .	H. W. HASENBECK . . . . .	34
Design Chart for Antenna Phase-shifting Networks . . . . .	Oct., 1942 . . .	W. S. DUTTERA. . . . .	37
Phasing Networks for Broadcast Arrays . . . . .	June, 1944. . .	C. RUSSELL COX . . . . .	40
Calculating Broadcast-station Coverage . . . . .	May, 1936. . .	RAYMOND F. GUY. . . . .	45
Radial Ground System Chart. . . . .	Jan., 1938. . .	GEORGE H. BROWN. . . . .	47

## III. AUDIO AMPLIFIERS

Resistance-coupled Amplifier Design Charts . . . . .	Aug., 1936. . .	GLENN KOEHLER. . . . .	48
Design of Class A Push-pull Amplifiers. . . . .	June, 1937. . .	E. W. HOUGHTON. . . . .	50
Design of Class B and AB Output Transformers . . . . .	Feb., 1936 . . .	GLENN KOEHLER. . . . .	52
Cathode-follower Calculations . . . . .	Oct., 1944 . . .	HUMBERT P. PACINI. . . . .	55
Harmonic Analysis of Overbiased Amplifiers . . . . .	Mar., 1944. . .	ULRICH R. FURST. . . . .	56

## IV. AUDIO-CIRCUIT DESIGN

Bass-compensation Design Chart . . . . .	Oct., 1937 . . .	P. A. D'ORIO and R. DE COLA. . . . .	58
Simple RC Equalizer Networks. . . . .	Feb., 1944 . . .	C. J. MERCHANT . . . . .	60
Universal 15-channel Tone Control for Audio Amplifiers. . . . .	Aug., 1943. . .	PAUL H. THOMSEN . . . . .	63
Computing Reactive Attenuation. . . . .	May, 1936. . .	P. F. BECHBERGER . . . . .	65
Time Delay in Resistance-capacitance Circuits . . . . .	Feb., 1937 . . .	E. W. KELLOGG and W. D. PHELPS. . . . .	67

## V. CAPACITORS

Rounded-edge Capacitor Plate Design. . . . .	Oct., 1944 . . .	SAMUEL SABAROFF . . . . .	3
V-h-f Behavior of Capacitors. . . . .	Mar., 1944. . .	E. L. HALL. . . . .	76
Capacitor-discharge Chart . . . . .	June, 1940. . .	LOUIS HANOPOL . . . . .	80
Capacitor Charge-discharge Nomograph . . . . .	Sept., 1937. . .	J. B. HOAG. . . . .	82
Capacitor-lead Resonance Chart . . . . .	Aug., 1939. . .	R. L. HASKINS . . . . .	83
Resonance Chart for Mica Capacitors . . . . .	Mar., 1944. . .	A. P. GREEN and C. T. McCOMB. . . . .	85
Power Factor Correction Charts . . . . .	May, 1944. . .	HARRY HOLUBOW. . . . .	86
Temperature Compensation of Tuned Circuits . . . . .	Apr., 1944. . .	HERBERT SHERMAN. . . . .	88
Determining Frequency Stability of Tuned Circuits. . . . .	Feb., 1944 . . .	G. V. ELTGROTH . . . . .	89

## VI. CATHODE-RAY TUBES

Characteristics of Phosphors for Cathode-ray Tubes. . . . .	Dec., 1938 . . .	L. B. HEADRICK . . . . .	92
Photographing Patterns on Cathode-ray Tubes. . . . .	Feb., 1944 . . .	RUDOLPH FELDT . . . . .	93

## VII. COAXIAL LINES

	DATE PUBLISHED	AUTHOR	PAGE
Design of Terminations for Concentric Lines . . . . .	Dec., 1936 . . .	CARL G. DIETSCH . . . . .	99
Q-factor Charts for Unloaded Concentric Transmission Lines . . . . .	Sept., 1943 . . .	R. C. MIEDKE . . . . .	103
Impedance Determinations of Eccentric Lines . . . . .	Feb., 1942 . . .	GEORGE H. BROWN . . . . .	105
Graph of Impedance of Eccentric-conductor Cable . . . . .	Feb., 1942 . . .	W. J. BARCLAY and K. SPANGENBERG . . . . .	106
Measurement of H-f Lines . . . . .	Apr., 1938 . . .		107

## VIII. ELECTRONIC HEATING

Electronic Heating Design Chart . . . . .	Apr., 1944 . . .	C. V. FIELDS . . . . .	110
Surface Hardening of Metals . . . . .	July, 1944 . . .	H. C. GILLESPIE . . . . .	112
Power Equations for Dielectric Heating . . . . .	Aug., 1943 . . .	CYRIL N. HOYLER . . . . .	114
Design Chart for R-f Heat-treatment Generators . . . . .	Sept., 1941 . . .	EUGENE MITTELMAN . . . . .	116
Design Data for Induction Heating Coils . . . . .	Aug., 1944 . . .	GEORGE H. BROWN . . . . .	117
Magnetic Field Equations for Induction Heating Coils . . . . .	June, 1944 . . .	GEORGE H. BROWN . . . . .	123

## IX. FILTERS

Constant-K Filter-design Chart . . . . .	Aug., 1940 . . .	JOHN BORST . . . . .	127
M-derived Filter-design Chart . . . . .	Oct., 1940 . . .	JOHN BORST . . . . .	129
Filter-conversion Chart . . . . .	Nov., 1940 . . .	JOHN BORST . . . . .	130

## X. INDUSTRIAL CONTROL

Design of Electronic Control Circuits . . . . .	Aug., 1943 . . .	W. A. SCHWARZMANN . . . . .	133
Capacitor Discharge Welding Systems . . . . .	May, 1944 . . .	H. KLEMPERER . . . . .	136
Grid Control of Industrial Gas-filled Tubes . . . . .	June, 1944 . . .	W. D. COCKRELL . . . . .	140

## XI. IRON-CORE TRANSFORMERS AND CHOKES

Notes on Iron-core Transformer Design . . . . .	Feb., 1944 . . .	E. B. HARRISON . . . . .	145
Design of Audio Reactors for D-c Service . . . . .	Sept., 1936 . . .	REUBEN LEE . . . . .	147

## XII. MATHEMATICS

Amplification Factor Chart . . . . .	June, 1939 . . .	E. R. JERVIS . . . . .	151
Polar-rectangular and Rectangular-reciprocal Vector Charts . . . . .	Dec., 1941 . . .	PAUL W. KLIPSCH . . . . .	153
Impedance-conversion Chart . . . . .	Oct., 1944 . . .	PERRY H. WARE . . . . .	155
Impedance-magnitude and Phase-angle Charts . . . . .	Jan., 1943 . . .	T. C. BLOW . . . . .	156
Impedance-combining Chart . . . . .	Mar., 1944 . . .	GARY MUFFLY . . . . .	158
Chart for Equivalent Series and Parallel Circuits . . . . .	Apr., 1943 . . .	R. TOOMBS . . . . .	161
Equivalent Resistance Chart . . . . .	Aug., 1938 . . .	A. E. TEACHMAN . . . . .	163
Chart for Determining Square Root of a Complex Number . . . . .	Aug., 1943 . . .	ROBERT G. NISLE . . . . .	165

## XIII. NETWORKS

Pi Networks as Coupled Tank Circuits . . . . .	Aug., 1944 . . .	F. D. SCHOTTLAND . . . . .	167
Impedance-magnitude and Phase-shift Curves for Linear Networks . . . . .	Nov., 1942 . . .	VITOLD L. EDUTIS . . . . .	171
Equalizer Design . . . . .	Apr., 1944 . . .	MICHAEL J. DiTORO . . . . .	174
Evaluating Performance of Symmetrical Four-terminal Networks . . . . .	Nov., 1942 . . .	E. S. PURINGTON . . . . .	177
Reactance Networks with Resistance Terminations . . . . .	Jan., 1943 . . .	E. S. PURINGTON . . . . .	181
Low- and High-pass Wave Filter Units . . . . .	June, 1943 . . .	E. S. PURINGTON . . . . .	185
Band-pass Wave Filters . . . . .	Sept., 1943 . . .	E. S. PURINGTON . . . . .	189

## XIV. OSCILLATORS

Phase-shift Oscillator Design Charts . . . . .	Nov., 1943 . . .	WALTER W. KUNDE . . . . .	193
Determining Temperature Coefficient of Quartz Crystals . . . . .	Nov., 1943 . . .	NORMAN L. CHALFIN . . . . .	195

## XV. PERMANENT MAGNETS

Permanent-magnet Design . . . . .	Dec., 1943 . . .	EARL M. UNDERHILL . . . . .	197
Designing Stabilized Permanent Magnets . . . . .	Jan., 1944 . . .	EARL M. UNDERHILL . . . . .	203
Mechanical Problems of Permanent-magnet Design . . . . .	Feb., 1944 . . .	EARL M. UNDERHILL . . . . .	207

# CONTENTS

ix

## XVI. PULSES

	DATE PUBLISHED	AUTHOR	PAGE
Determining Shape and Magnitude of Amplified Pulses . . . . .	Nov., 1939.	ERIC A. WALKER.	211
Computing Circuit Response to Pulses. . . . .	July, 1944.	JOHN B. TREVOR . . . . .	213
Circuit Response to Nonsinusoidal Wave Forms. . . . .	Oct., 1944.	P. T. CHIN. . . . .	216
Square-wave Harmonic Amplitude Table. . . . .	May, 1940.	DONALD L. HERR. . . . .	219
Square Waves for Impedance Measurements . . . . .	Sept., 1944.	FRANK ROCKETT . . . . .	220

## XVII. RECTIFIERS

Behavior of Half-wave Rectifiers . . . . .	Sept., 1939.	M. B. STOUT. . . . .	224
Half-wave Gas Rectifier Circuits . . . . .	Oct., 1938.	C. M. WALLIS . . . . .	226
Full-wave Rectifier Analysis . . . . .	Mar., 1940.	C. M. WALLIS . . . . .	229
Filter Performance Charts for Half-wave Rectifiers . . . . .	Apr., 1941.	W. K. H. PANOFSKY and C. F. ROBINSON. . . . .	233
Rectifier Filter Design. . . . .	June, 1938.	HERBERT J. SCOTT . . . . .	236
Filter Design for Grid-controlled Rectifiers. . . . .	Sept., 1944.	HAROLD A. THOMAS. . . . .	239

## XVIII. RELAYS

Choosing Relays for Tube Output Circuits. . . . .	Aug., 1937.	E. E. GEORGE . . . . .	243
Design Chart for Sensitive Relays. . . . .	Oct., 1943.	R. T. FISHER. . . . .	246

## XIX. R-F COILS AND TRANSFORMERS

Distributed Capacitance Chart . . . . .	Mar., 1938.	P. H. MASSAUT. . . . .	249
Nomogram for Single-layer Coils . . . . .	Jan., 1937.	CARL P. NACHOD. . . . .	251
General-purpose Chart for Multilayer Coils. . . . .	Jan., 1939.	J. E. MAYNARD. . . . .	253
Simplified Inductance Chart for Multi-layer Coils. . . . .	Sept., 1942.	E. S. PURINGTON. . . . .	256
Winding the Universal Coil. . . . .	Oct., 1936.	A. W. SIMON. . . . .	258
Mutual-inductance Calculations. . . . .	July, 1937.	DALE POLLACK. . . . .	261
H-f Inductance Charts. . . . .	Mar., 1940.	F. C. EVERETT. . . . .	263
Universal Performance Curves for Tuned Transformers . . . . .	Feb., 1937.	J. E. MAYNARD. . . . .	264
Double-tuned Transformer Design. . . . .	Oct., 1944.	DAWKINS ESPY. . . . .	267

## XX. R-F IMPEDANCE-MATCHING NETWORKS

R-f Impedance-matching Networks . . . . .	Jan., 1936.	RALPH P. GLOVER . . . . .	270
Charts for L-type Impedance-transforming Circuits . . . . .	Mar., 1942.	PHILLIP H. SMITH. . . . .	272
Computing R-f Transition Losses . . . . .	Jan., 1936.	HAROLD A. WHEELER. . . . .	278

## XXI. R-F POWER AMPLIFIERS

R-f Power-amplifier Chart . . . . .	Dec., 1939.	E. H. SCHULZ . . . . .	281
Power-amplifier Plate Tank Circuits. . . . .	Nov., 1941.	ARVID B. NEWHOUSE . . . . .	283
Class B R-f Amplifier Chart . . . . .	Nov., 1937.		286
Power Efficiency of R-f Power-amplifier Stages . . . . .	July, 1944.	HARRY STOCKMAN. . . . .	287
Graphical Determination of Power-amplifier Performance . . . . .	Dec., 1942.	R. I. SARBACHER . . . . .	291
Analysis of Self-biased Modulated Amplifiers. . . . .	Apr., 1943.	R. I. SARBACHER . . . . .	295

## XXII. SOUND

Design for Exponential Horns of Square Cross-section. . . . .	Feb., 1939.	GEORGE H. LOGAN . . . . .	302
Chart of VU-DB Relationships. . . . .	May, 1939.	FRANK B. HALES. . . . .	303
DB Ruler for Christmas-tree Patterns on Records. . . . .	May, 1941.	DON R. KING . . . . .	304

## XXIII. TELEVISION, FREQUENCY MODULATION, AND FACSIMILE

Shunt-peaking Compensation for Video Amplifiers. . . . .	Jan., 1940.	WILLIAM H. FREEMAN. . . . .	305
Television Definitions and Design Equations . . . . .	Mar., 1939.	DONALD G. FINK. . . . .	307
Influence of Feedback in Video Amplifiers . . . . .	Sept., 1944.	RICHARD W. CRANE. . . . .	309
Single-inductor Video Coupling Networks . . . . .	Sept., 1944.	C. T. McCOMB and A. P. GREEN. . . . .	311
Frequency-deviation Measurement of F-m Transmitters . . . . .	Oct., 1941.	L. N. HOLLAND and L. J. GIACOLETTO. . . . .	317
Facsimile Design Chart . . . . .	Apr., 1941.	RAYMOND R. HAUGH . . . . .	320

## CONTENTS

## XXIV. TRANSMISSION LINES

	DATE PUBLISHED	AUTHOR	PAGE
Transmission-line Charts. . . . .	July, 1943. . .	R. F. BAUM . . . . .	321
Characteristics of Resonant Transmission Lines. . . . .	Oct., 1943 . .	J. B. EPPERSON. . . . .	324
Transmission-line Calculator . . . . .	Jan., 1944. . .	PHILLIP H. SMITH. . . . .	326
Impedance Chart for R-f Lines . . . . .	Dec., 1936 . .	A. E. TEACHMAN . . . . .	332
Transmission-loss Charts. . . . .	June, 1944. . .	JACK G. ROOF . . . . .	333
R-f Matching Sections. . . . .	Jan., 1941. . .	A. C. OMBERG . . . . .	335
Universal Wave Guide Chart. . . . .	Dec., 1943 . .	ARTHUR BRONWELL. . . . .	336
Skin-effect Charts and Formulas . . . . .	Feb., 1942 . .	J. R. WHINNERY . . . . .	338
R-f Resistance of Copper Wire . . . . .	Feb., 1936 . .	JOHN H. MILLER. . . . .	343

## XXV. TUBES

Tube Filament and Heater Characteristics. . . . .	July, 1944. . .	CECIL E. HALLER . . . . .	344
Secondary Electron Radiation . . . . .	Sept., 1944. . .	J. H. OWEN HARRIES . . . . .	349
Open-grid Tubes in Low-level Amplifiers. . . . .	Oct., 1944 . .	ROBERT J. MEYER . . . . .	358
28-volt Operation of Receiving Tubes . . . . .	Aug., 1944. . .	C. R. HAMMOND, E. KOHLER and W. J. LATTIN . . . . .	360

## XXVI. TUNED CIRCUITS

Bandwidth Factors for Cascade Tuned Circuits. . . . .	July, 1941. . .	C. E. DEAN . . . . .	365
Frequency Response of Parallel Resonant Wave Traps. . . . .	Aug., 1941. . .	MYRIL B. REED . . . . .	367
Narrow Band-pass Filter Performance. . . . .	May, 1943. . .	H. HOLUBOW. . . . .	369
Attenuation Charts for Band-pass and Band-rejection Filters . . . . .	Aug., 1942. . .	H. HOLUBOW. . . . .	372
Band-pass Characteristics . . . . .	July, 1936. . .	H. W. JADERHOLM . . . . .	375
Superheterodyne Oscillator Tracking Chart. . . . .	Nov., 1942. . .	P. C. GARDINER . . . . .	377

## XXVII. WIDE-BAND AMPLIFIERS

Compensated Amplifier Chart . . . . .	Sept., 1939. . .	Y. J. LIU and J. D. TRIMMER. . . . .	379
Distortion in Compensated Amplifiers. . . . .	July, 1940. . .	J. D. TRIMMER and Y. J. LIU. . . . .	381
D-c Amplifier Design Techniques . . . . .	Mar., 1944. . .	EDWARD L. GINZTON . . . . .	384
Thermal Noise in a Parallel RC Circuit . . . . .	July, 1944. . .	C. J. MERCHANT . . . . .	389

## SECTION I

# A-F IMPEDANCE-MATCHING NETWORKS

	Page
Design Charts for Dissymmetrical T Pads.....	1
Design Procedure for Dissymmetrical T and $\pi$ Attenuators	3
Multiple-circuit Pads.....	6
Forty Commonly Used Pads.....	9
Universal Network Design Chart.....	10
Attenuator-design Formulas.....	11

## Design Charts for Dissymmetrical T Pads

By EDWIN Y. WEBB, Jr.

Graphs for determining the resistance of the three elements of T-pad networks facilitate the design of pads having attenuation of as much as 25 db and impedance mismatch ratios up to 5:1. Graphs are also adaptable to design of symmetrical pads with matched loads

IN radio and communications work the necessity for pads or attenuators of definite electrical loss and definite terminal impedance often arises. The design and construction of such pads of symmetrical or dissymmetrical T configuration are facilitated through simple, rapid, graphical methods, without making necessary recourse to the usual mathematical design equations.

In the following discussion,  $a$  and  $b$  will refer to the series impedances and  $c$  to the shunt impedance of the three-element T network. As pads with elements other than pure resistances are seldom encountered, only the case of a pure resistance network will be discussed, although the symbol  $Z$  will be used. If a balanced pad is desired, it is necessary merely to place half of the value of  $a$  and half of the value of  $b$  in the two lower branches of the pad.

Three individual graphs are given, one for each of the impedance elements in a T network. Each graph contains a family of curves, one for each of several different values of attenuation or loss in decibels. The family of curves is plotted to show the normalized resistance (for the element  $a$ ,  $b$ , or  $c$  of the T for which the curve applies) as ordinates, against the ratio of impedance transformation as

abscissa. Since the curves are plotted for the normalized impedance of 1 ohm, the resistances found from the curves must be multiplied by the actual impedance value of the input circuit to obtain the true values of resistance for the elements of the desired T network. By plotting normalized impedances, only one set of curves is required no matter what the impedance value may be. It should be noted that while the curves are plotted for a dissymmetrical T network, which is useful in matching unequal impedance, the curves are equally useful for the symmetrical T network for matching equal impedances since in the latter case the impedance transformation is 1/1, and  $a$  and  $b$  are equal.

The graphs can be used for any impedance ratio normally encountered in practice. If an impedance ratio less than 1 is encountered, the T network can be reversed, for purposes of analysis, to obtain a transformation ratio greater than 1. The curves can of course be used for uneven ratios, such as 2.5:1 or 3.7:1. The curves can likewise be used for symmetrical T pads, for in this case the terminal impedances  $Z_1$  and  $Z_2$  will be alike. The network impedances  $a$  and  $b$  will also be alike, and hence we need only use the curves for determining

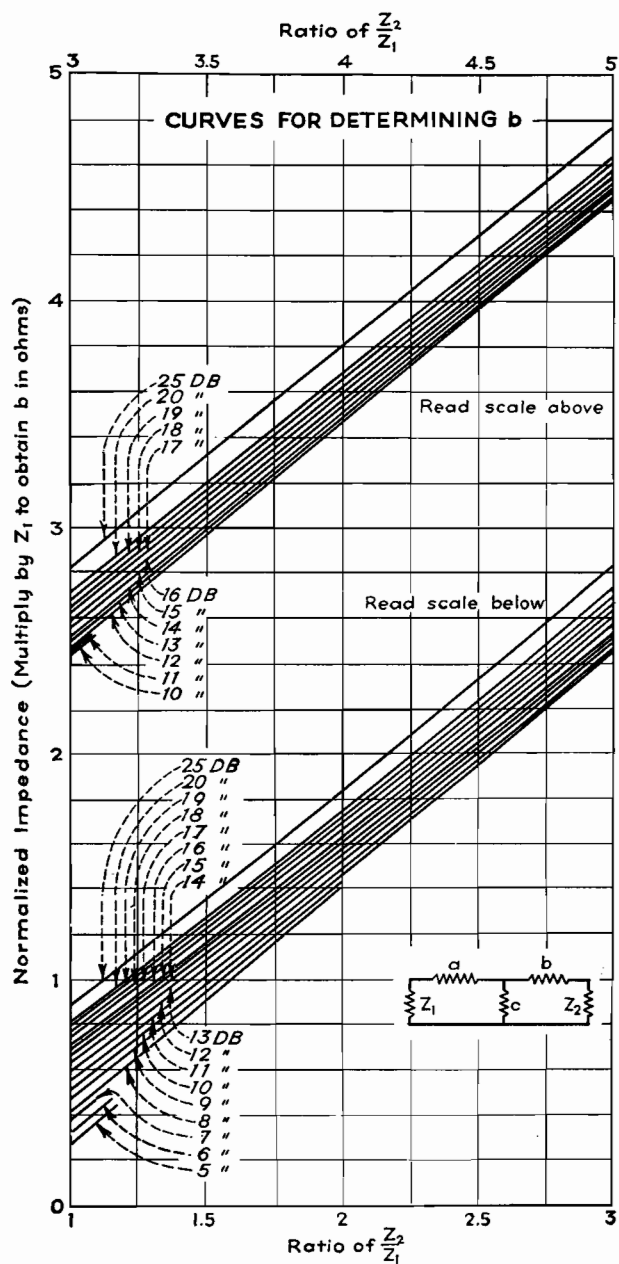
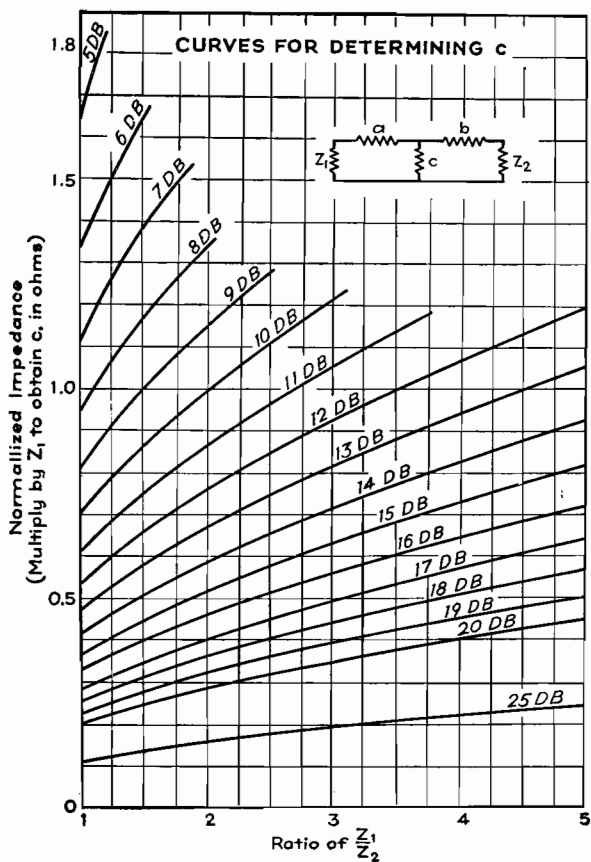
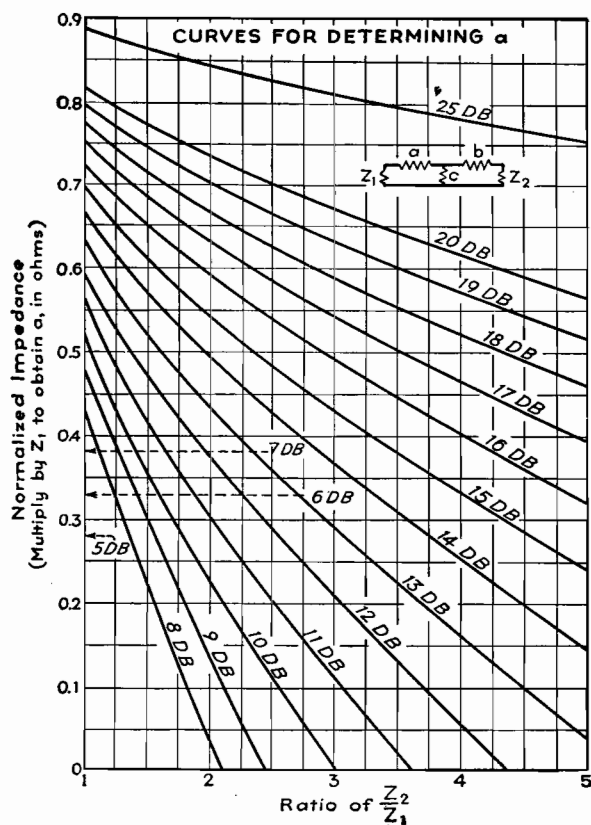
two separate constants  $a$  and  $c$ . The curves are plotted more accurately than the accuracy of commercial resistors, and consequently errors involved from the graphical design method will be negligible for ordinary purposes. Care should be exercised in reading the curves, however, to ascertain that the scales are not misinterpreted.

It is to be particularly noted that the actual values of  $Z_1$  and  $Z_2$  (the terminal impedances) do not affect in any way whatever the values used in plotting the curves as only their ratios were used. Therefore, for a 10-db pad of terminal impedances 5 and 10 ohms, the identical points on the curves will be used as if the terminal impedances were 300 and 600 ohms, as in both cases the ratio of  $Z_2$  to  $Z_1$  is 2:1.

The loss of the pad is obtained by calculating the ratio of the power transferred from  $Z_1$  to  $Z_2$  with the pad in the circuit and again with the pad removed from the circuit. Assuming 1 volt applied, and impedances of 100 and 200 ohms, the power transferred when the pad is out of the circuit is

$$P_0 = I^2 R = \left(\frac{1}{300}\right)^2 \times 200$$

With the pad in the circuit, the power





absorbed by  $Z_2$  is

$$\begin{aligned} P_1 &= I^2 R \\ &= \left[ \left( \frac{1}{200} \right) \left( \frac{99.2}{200 + 145 + 99.2} \right) \right]^2 \times 200 \\ &= \left[ \left( \frac{1}{200} \right) \left( \frac{99.2}{444.2} \right) \right]^2 \times 200 \end{aligned}$$

The loss in decibels is then

$$\begin{aligned} db &= 10 \log_{10} \frac{P_0}{P_1} \\ &= 10 \log_{10} \frac{\left( \frac{1}{300} \right)^2 \times 200}{\left[ \left( \frac{1}{200} \right) \left( \frac{99.2}{444.2} \right) \right]^2 \times 200} \\ &= 10 \log_{10} \left[ \left( \frac{200}{300} \right) \left( \frac{444.2}{99.2} \right) \right]^2 = 9.5 \text{ db} \end{aligned}$$

Hence, the terminal impedances as calculated from the graphs are correct. The loss of the network is actually 9.5 db instead of the 10 db for which it is designed, but the error is sufficiently small to be neglected for nearly all practical purposes.

To use the graphs it is necessary to know (1) the attenuation or loss, in decibels, which the network is to provide; (2) the impedance  $Z_1$  from which power is fed to the T attenuator; and (3) the impedance  $Z_2$  into which the T network feeds. The first condition specifies the

network loss, and hence indicates which curve of the three families is to be selected for any particular problem. The second and third conditions determine the impedance transformation ratio, and hence determine at what point on the abscissa the graph is entered. From this point of entry, project vertically upward until the desired curve is reached; then project to the left and read the normalized resistance for the specified conditions for the element for which the chart applies. Multiply this reading by  $Z_1$  to obtain the true resistance of the element for the specified conditions.

## Design Procedure for Dissymmetrical T and $\Pi$ Attenuators

By P. M. HONNELL

A method of designing symmetrical T or  $\pi$  resistance attenuators is presented here as well as a simplified means of converting to a dissymmetrical network where impedances of different magnitudes must be matched

WHEN the need arises for an attenuator with a given loss that will match terminal apparatus or lines of unequal impedances, it will be found necessary to compute the values of the branch resistances of the required pad since such data cannot ordinarily be found in curves or tables. For a T or  $\pi$  network of constant impedance level, however, such information is usually available. By utilizing a symmetrical pad that matches one of the two impedances and a transformer of proper ratio to match the other impedance, the required network can always be realized. But it is not usually convenient, and certainly not economic, to utilize this combination, especially as it is possible in most instances to replace both the constant impedance pad and the transformer by a dissymmetrical pad.

The purpose here is to summarize the

results of the matrix transformation\* which may be used to obtain the branch resistances of the dissymmetrical pad that will fit the required terminal impedances, from design data for the resistance of the branches of a symmetrical T or  $\pi$  pad of the desired attenuation. If exact branch resistance values for symmetrical T or  $\pi$  pads (of any impedance level) are not available, they may be obtained from the curves with fair accuracy.

### T Pad

It should be understood at the outset that the values of branch resistances of a symmetrical T or  $\pi$  pad of given impedance level (say 600 ohms) may be changed to any other impedance level (say 500 ohms) by multiplying all the branch resistances by the ratio of the required to

given impedance levels (namely, 500:600 or 5:6 in this example). Thus it is always possible to adjust available data for a pad of the desired loss to fit one of the two impedance levels.

In Fig. 1a, for example, the symmetrical pad giving the desired attenuation, and having branch resistances  $r_a$ ,  $r_b = r_a$ , and  $r_c$ , has been chosen to match the input impedance  $Z_1$ . Since the pad is of constant impedance level, the output impedance  $Z_2$  can be matched only by means of the (ideal) transformer of impedance ratio  $1:a^2$ .

The branch resistances  $r_a'$ ,  $r_b'$ , and  $r_c'$  of the dissymmetrical pad (Fig. 1b), which will replace both the symmetrical pad and the transformer (Fig. 1a), are obtainable from the following equations:

$$\left. \begin{aligned} r_a' &= r_a + (1 - a)r_c \\ r_b' &= a^2(r_a + r_c) - ar_c \\ r_c' &= ar_c \end{aligned} \right\} \quad (1)$$

\* GUILLEMIN, E. A., "Communication Networks," Vol. II, Chap. VI, Sec. 5. John Wiley & Sons, Inc., New York, 1935.

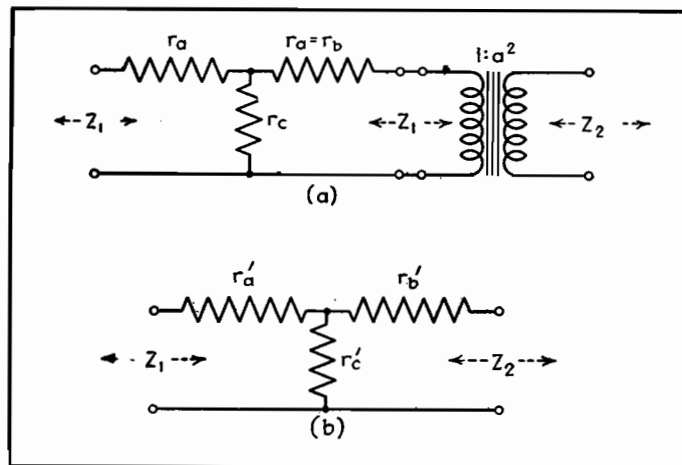


Fig. 1.—Symmetrical T pad and ideal transformer (a) and the electrically equivalent dissymmetrical T pad (b), both having the same loss.

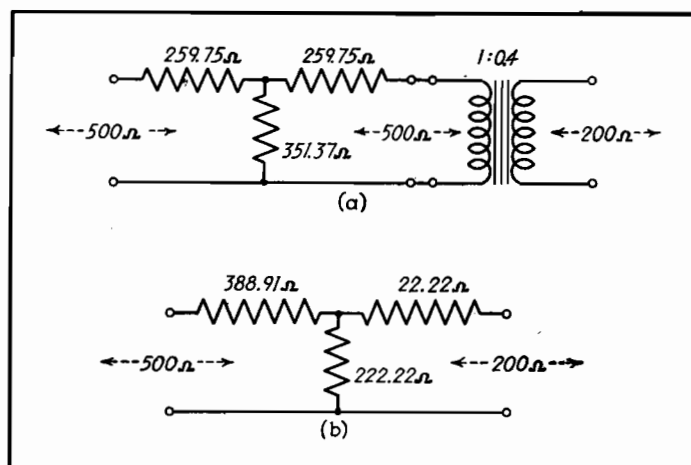


Fig. 2.—Examples of dissymmetrical T network (b) equivalent to symmetrical T network and ideal transformer (a), both with 10-db loss.

where impedance ratio is given by

$$a^2 = \frac{Z_2}{Z_1} \quad (2)$$

the ratio of output to input impedance levels. The equations maintain the loss from input to output terminals of the network invariant.

Without going into an exhaustive analysis, it may be evident that for a given ratio of impedance levels, or  $a^2$ , negative elements for  $r'_a$  or  $r'_b$  may occur. In such an event, the only alternative is to choose a network with more attenuation, which will then result in realizable resistances. Of course, either  $r'_a$  or  $r'_b$  may actually be zero in the limiting case. This result may answer a question that has undoubtedly arisen in the reader's mind: Where does a symmetrical network and (ideal) transformer differ physically

from a dissymmetrical network? The answer lies in the fact that for a given terminal impedance ratio the former can be approximated physically for any attenuation, whereas the latter network has a definite minimum attenuation below which some of its elements become physically unrealizable.

*Example.*—As a concrete example of the application of these equations, consider a 10-db pad, required to match impedances  $Z_1 = 500$  ohms and  $Z_2 = 200$  ohms. From tables, the following resistances for the branches of a symmetrical, 10-db, 500-ohm level pad are obtained:

$$\begin{aligned} r_a &= 259.75 \text{ ohms} \\ r_b &= r_a = 259.75 \text{ ohms} \\ r_c &= 351.37 \text{ ohms} \end{aligned}$$

output to input impedances

$$\begin{aligned} a^2 &= \frac{200}{500} = 0.4 \\ a &= 0.63246 \end{aligned}$$

Substituting these values into Eq. (1), we obtain for the branch resistances of the dissymmetrical pad

$$\begin{aligned} r'_a &= 259.75 + (1 - 0.63246)351.37 \\ &= 388.91 \text{ ohms} \\ r'_b &= 0.4(259.75 + 351.37) \\ &\quad - 0.63246(351.37) = 22.22 \text{ ohms} \\ r'_c &= 0.63246(351.37) = 222.22 \text{ ohms} \end{aligned}$$

The resulting dissymmetrical network equivalent to the symmetrical pad and (ideal) transformer is shown in Fig. 2b.

#### Dissymmetrical $\pi$

In order to simplify the mathematical expressions, it is desirable when dealing with  $\pi$  networks to express all quantities

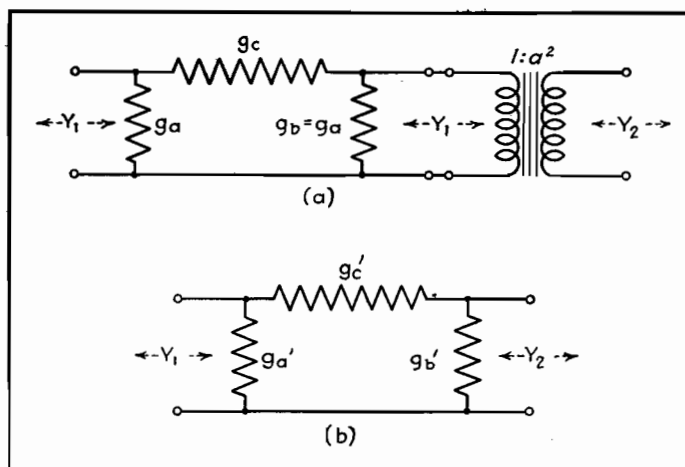


Fig. 3.—Symmetrical attenuator and ideal transformer (a) and equivalent dissymmetrical attenuator (b), with the same loss.

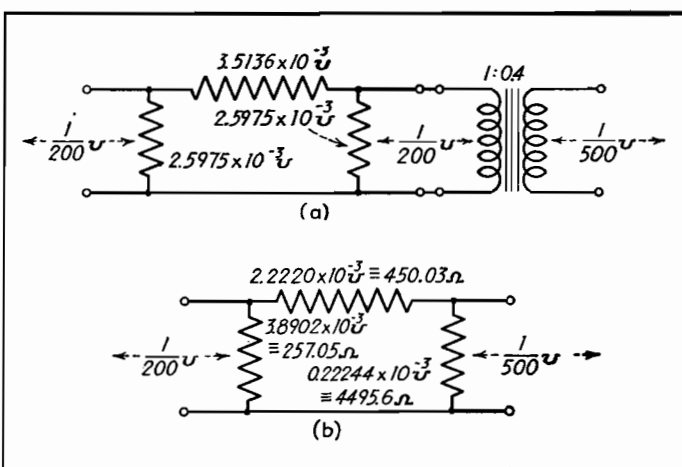


Fig. 4.—Dissymmetrical pad of 10 db loss (b) equivalent to symmetrical and ideal transformer (a), both having the same loss.

as admittances. Since resistors of commercial manufacture and measuring equipment in general are calibrated in terms of impedances, computed circuit admittances must be converted into impedances before the final circuit elements are obtained physically. But this is a mere matter of reciprocation of the branch admittance of the network, and should cause no confusion, if the inverted omega is recognized as the conductance symbol in mhos.

Thus, the equations that relate the symmetrical  $\pi$  pad and (ideal) transformer to the equivalent dissymmetrical  $\pi$ , working between unequal terminal admittances, are as follows:

$$\left. \begin{aligned} g_a' &= g_a + \left(1 - \frac{1}{a}\right) g_c \\ g_b' &= \left(\frac{1}{a^2}\right) (g_b + g_c) - \left(\frac{1}{a}\right) g_c \\ g_c' &= \left(\frac{1}{a}\right) g_c \end{aligned} \right\} \quad (3)$$

where  $1/a^2 = Y_2/Y_1$

is the ratio of output admittance  $Y_2$  to input admittance  $Y_1$  of the terminal equipment.

As shown in Fig. 3a,  $g_a, g_b = g_a$ , and  $g_c$  are the branch conductances of the symmetrical  $\pi$ , with the dissymmetrical  $\pi$  branch conductances  $g_a', g_b'$ , and  $g_c'$  given by Eq. (3) shown in Fig. 3b.

*Example.*—As an example, we consider again a pad with 10-db loss, this time a  $\pi$ , working from 200 into 500 ohms (Fig. 4a). For the ratio of admittances ( $1/a^2$ ) we have, converting the terminal impedances to admittances,

$$\frac{1}{a^2} = \frac{Y_2}{Y_1} = \frac{1/500}{1/200} = 0.400$$

which gives

$$\frac{1}{a} = 0.63246$$

Reference to tables or the curves gives the following values for the branch conductances of a symmetrical  $\pi$  pad of 10-db loss, and 1/200-mho admittance level

$$\begin{aligned} g_a &= 2.5975 \times 10^{-3} \text{ mho} \\ g_b &= g_a = 2.5975 \times 10^{-3} \text{ mho} \\ g_c &= 3.5136 \times 10^{-3} \text{ mho} \end{aligned}$$

The symmetrical 10-db  $\pi$ , therefore, and the required 0.4 admittance ratio (ideal) transformer are shown in Fig. 4a.

To obtain the equivalent dissymmetrical  $\pi$ , substitute these values into Eq. (3), giving:

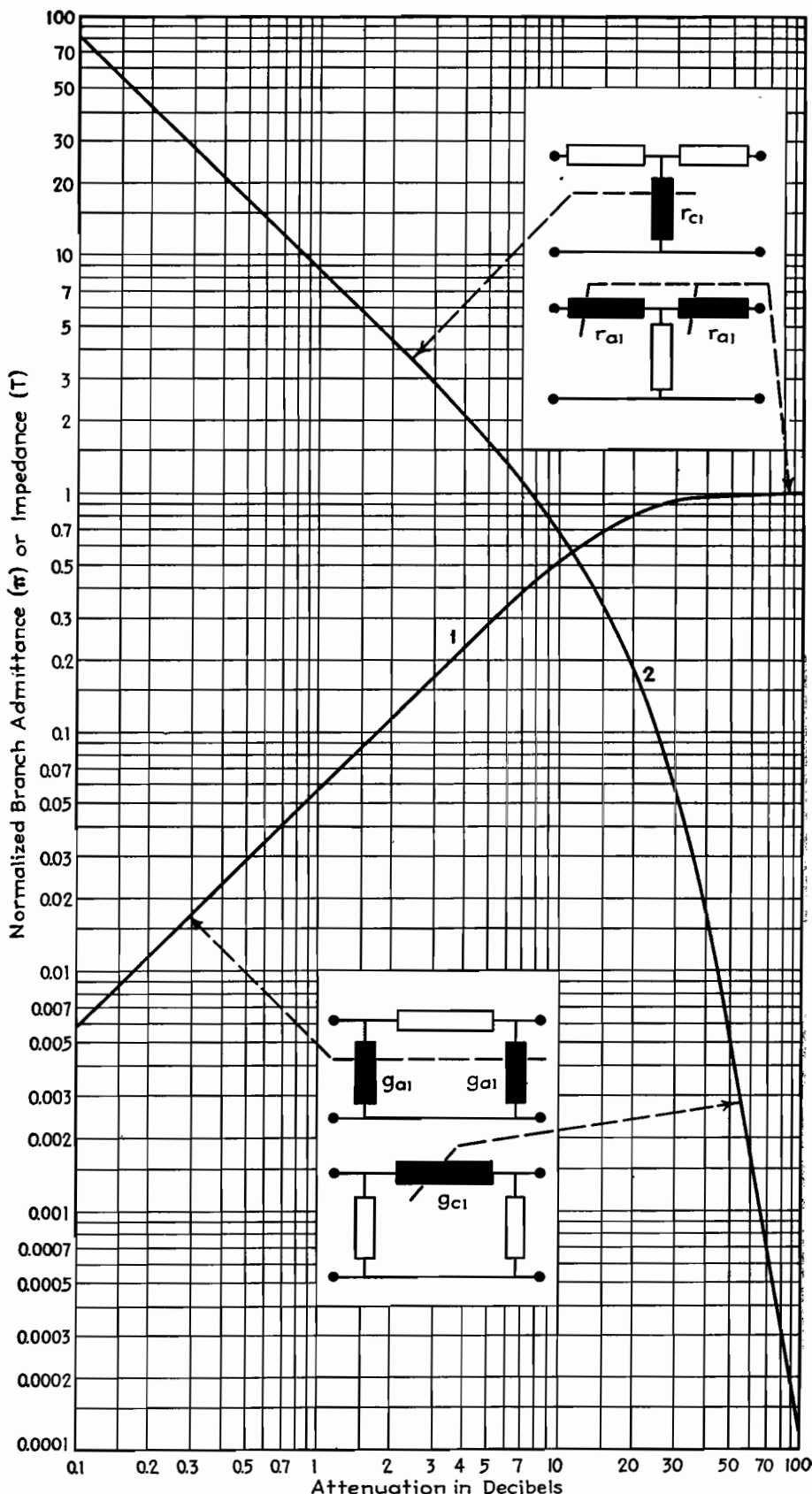


Fig. 5.—The normalized impedance or admittance for the series and shunt arms of T and  $\pi$  networks. Curve 1 applies to shunt elements of  $\pi$  network or series elements of T network, while curve 2 refers to shunt elements of T network or series elements of  $\pi$  network. The values obtained from this graph must be multiplied by the impedance level for which the symmetrical attenuator is designed.

$$\begin{aligned}
 g_a' &= 2.5975 \times 10^{-3} + (1 - 0.63246) \\
 &\quad 3.5136 \times 10^{-3} = 3.8902 \times 10^{-3} \text{ mho} \\
 g_b' &= 0.4(2.5975 + 3.5136) \times 10^{-3} - \\
 &\quad 0.63246(3.5136 \times 10^{-3}) = 0.22243 \times 10^{-3} \\
 &\quad \text{mho} \\
 g_c' &= 0.63246(3.5136 \times 10^{-3}) = 2.2220 \\
 &\quad \times 10^{-3} \text{ mho}
 \end{aligned}$$

The desired dissymmetrical  $\pi$  is shown in Fig. 4b, together with the branch element resistances as well as conductances, obtained, of course, by taking the reciprocals of  $g_a'$ ,  $g_b'$ , and  $g_c'$ .

#### Design of Symmetrical T or $\pi$ Attenuators

There would be no point in repeating here the design equations for symmetrical attenuators, since such information is readily available. However, for those who do not wish to calculate the numerical values of branch resistance or conductance for symmetrical attenuators, the graphs in Fig. 5 are presented for convenience.

The two curves in the figure provide the basic design constants of T or  $\pi$  pads of any constant impedance level, and of 0.1- to 100-db loss. The ordinate of the graph gives the branch impedance of T pads, and the branch admittance of

$\pi$  pads on a normalized basis, i.e., on a 1-ohm or 1-mho level. For any desired impedance or admittance level, multiply all the values from the curves for the particular attenuator by the desired impedance or admittance level. The abscissa of the graph is the desired attenuator loss for which the branch values are to be determined. Although the graph is self-explanatory, it may best be demonstrated by examples.

#### Examples

*Example 1.*—A 10-db T pad, 500-ohm impedance level is required. From curve 1 (Fig. 5) we find, at 10 db on the abscissa, that

$$r_{a1} = r_{b1} = 0.52$$

and from curve 2, still at 10 db on the abscissa, we find that

$$r_{c1} = 0.70$$

These values are on a 1-ohm basis (that is the reason for the subscript 1).

To obtain the branch resistances for the 500-ohm level pad, multiply each factor by 500, giving

$$\begin{aligned}
 r_a &= r_b = 0.52 \times 500 = 260 \text{ ohms} \\
 r_c &= 0.70 \times 500 = 350 \text{ ohms}
 \end{aligned}$$

These values compare with  $r_a = 259.75$  and  $r_c = 351.37$ , obtained from exact equations, as given on page 4.

*Example 2.*—A  $\pi$  pad of 10-db loss, 200-ohm impedance level is required. We first recall that on an admittance basis this would be a 10-db pad of 1/200-mho admittance level. From curve 1 of Fig. 5, we obtain at 10 db on the abscissa

$$g_{a1} = g_{b1} = 0.52$$

and similarly from curve 2

$$g_{c1} = 0.70$$

These values are on a 1-mho basis. To obtain the branch admittances on the required 1/200-mho admittance level, multiply each factor by 1/200, giving the branch conductances as

$$\begin{aligned}
 g_a &= g_b = 0.52 \times \frac{1}{200} = 2.6 \times 10^{-3} \text{ mho} \\
 g_c &= 0.70 \times \frac{1}{200} = 3.5 \times 10^{-3} \text{ mho}
 \end{aligned}$$

These values compare with  $g_a = g_b = 2.5975 \times 10^{-3}$  mho, and  $g_c = 3.5136 \times 10^{-3}$  mho, obtained from exact computations, given on page 5.

## Multiple-circuit Pads

By FREDERICK WHEELER

A chart for determining the resistance values in networks designed to match several like impedances to one other impedance of different value, such as matching several 500-ohm telephone lines to a 2,000-ohm amplifier output

**F**REQUENTLY the communications engineer is confronted with the problem of feeding two or more telephone lines from one amplifier, or the inverse case of feeding two or more amplifiers from one telephone line. In such cases the circuits may be matched by a network, or pad, of resistance elements. While such a pad introduces a loss, the loss is usually not more than 25 db, and in many cases is much less than this amount. The simplicity of the network and its freedom

from frequency error recommend it in preference to transformer coupling.

#### Chart for Six Circuits

The chart (Fig. 1) presents curves for calculating the various constants in such multiple pads for three to six circuits. The curves are calculated for matching one circuit of reflected impedance  $Z_2$  to several circuits of reflected impedance  $Z_1$ . The ratio  $K = Z_2/Z_1$ , the total number

of circuits  $N$  (including both input and output circuits), and the impedance  $Z_1$  are the factors determining the values of the resistances used in the pad. In terms of  $K$  and  $N$ , the factors  $C$  and  $E$  are found from the chart. The resistances  $R_1$  (shown in the diagram) are then  $R_1 = Z_1 C$  and the resistance  $R_2 = Z_1 (K - E)$ . For example, let  $Z_2$  be 2,000 ohms and  $Z_1$  be 500 ohms. Then  $K = 2,000/500 = 4$ . Four impedances  $Z_1$  are to be matched,

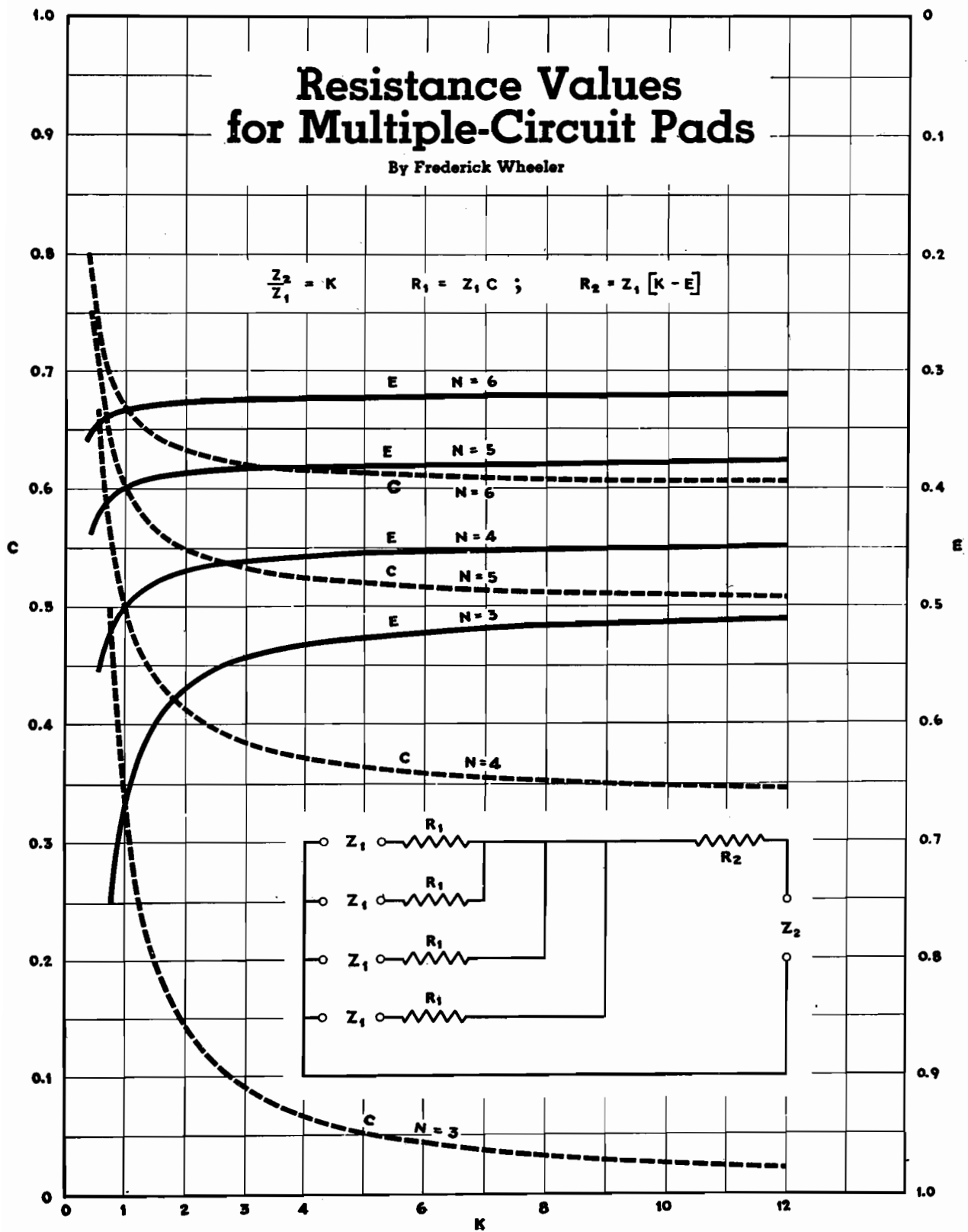


Fig. 1.—Curves for calculating constants in multiple pads for three to six circuits.

with one impedance  $Z_2$ . The number  $N$  is then 5. The chart gives corresponding values of  $C$  and  $E$  to be  $C = 0.525$  and  $E = 0.380$ . The resistances  $R_1$  are then  $R_1 = 500(0.525) = 262.5$  ohms and  $R_2 = 500(4 - 0.380) = 1,810$  ohms.

For cases where  $K$  is greater than 12 and the number of circuits  $N$  is greater than 6, the following formulas may be

used:

$$C = \frac{K(N-3)(N-1) + 1}{K(N-1)^2 - 1}$$

$$E = (C + 1)/(N - 1)$$

The losses between circuits in decibels are given in Fig. 2. For values of  $K$  larger than 12 and  $N$  larger than 6, the formulas are

$$\text{db} = 10 \log_{10} \frac{(2K - E)^2}{K(1 - C)^2}$$

when  $Z_1$  and  $Z_2$  are not equal, and

$$\text{db} = 20 \log_{10} \frac{1 + C}{1 - C}$$

when the loss is between circuits of the same impedance, i.e., between circuits of impedance  $Z_1$  and  $Z_1$ .

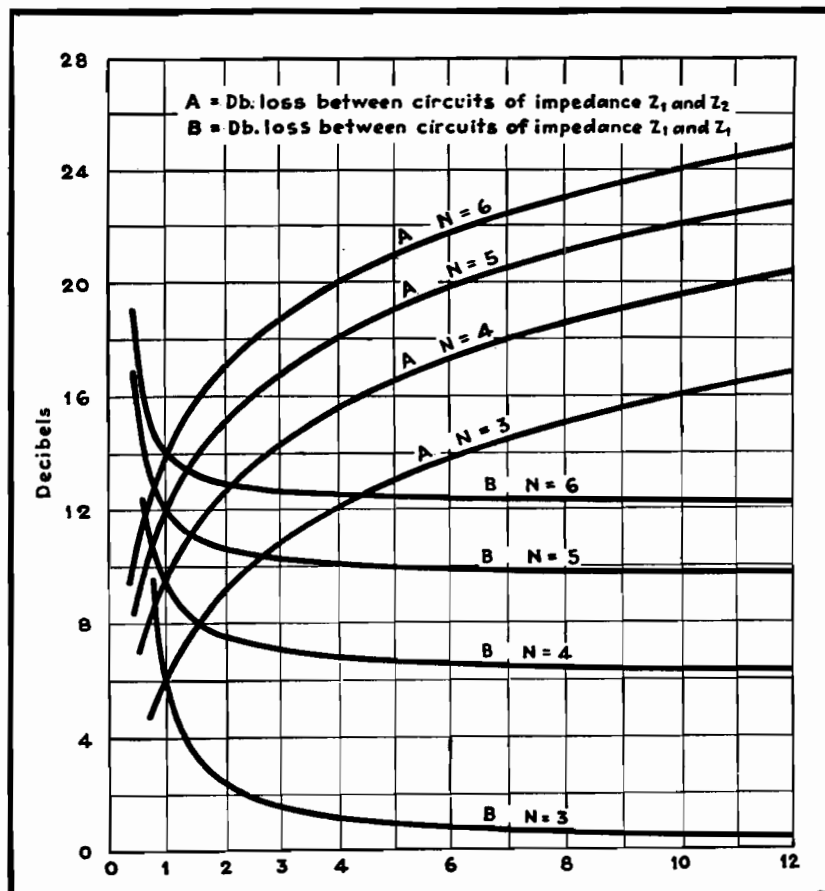
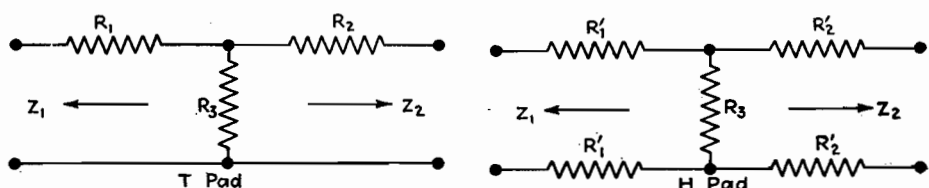


Fig. 2.—Decibels loss between impedances in multiple-circuit pads.

# Forty Commonly Used Pads

By AARON SHELTON

Table of values of the elements of resistive attenuators for various input and output impedances commonly encountered in communications circuits



$Z_1 \leftarrow$ $\rightarrow Z_2$ , ohms	Loss, db	$R_1$ , ohms	$R_2$ , ohms	$R_3$ , ohms	$Z_1 \leftarrow$ $\rightarrow Z_2$ , ohms	Loss, db	$R_1$ , ohms	$R_2$ , ohms	$R_3$ , ohms
50-50	5	14	14	83	500-500	5	138	138	834
	10	26	26	35		10	258	258	352
	15	35	35	18		15	350	350	183
	20	41	41	10		20	410	410	100
50-200	Min loss 11.5	0	175	57	500-2,000	Min loss 11.5	0	1,755	575
	15	16	175	37		15	168	1,775	366
	20	31	185	20		20	307	1,837	203
50-500	Min loss 15.8	0	475	53	500-5,000	Min loss 15.8	0	4,750	528
	20	20	480	31		20	190	4,780	321
50-2,000	Min loss 22	0	1,980	50	2,000-2,000	5	570	570	3,330
200-200	5	35	55	334		10	1,040	1,040	1,410
	10	103	103	140		15	1,400	1,400	735
	15	140	140	75		20	1,634	1,634	406
	20	163	163	40	2,000-5,000	Min loss 9	0	3,910	2,590
200-500	Min loss 9	0	380	270		15	980	4,170	1,160
	10	23	390	222		20	1,400	4,460	640
	15	98	417	116	5,000-5,000	5	1,370	1,370	8,330
	20	140	436	64		10	2,600	2,600	3,520
200-2,000	Min loss 15.8	0	1,886	214		15	3,500	3,500	1,830
	20	76	1,912	128		20	4,085	4,085	1,015

To change T pads to balanced H pads, simply make resistances  $R_1'$  and  $R_2'$  equal to one-half the values as shown for  $R_1$  and  $R_2$  in the T pads.

# Universal Network Design Chart

By A. JAMES EBEL

THE problems of network design that are of practical interest to the radio engineer can be classified in three divisions: (1) the matching network (or taper pad) which matches two impedances and introduces a loss that is of secondary importance; (2) the attenuation network, which is intended to introduce a fixed known loss in the circuit and also to match the ingoing and outgoing impedances of the circuit to which it is connected; and (3) the variable attenuation network which is designed to introduce a variable loss in the circuit while maintaining its terminal impedances constant. The fourth, the constant-loss variable-impedance type, is important only in special applications.

All these network problems can be solved in several ways, by the use of T pads, L pads,  $\pi$  networks (both of the balanced and unbalanced variety), or by more complicated mesh networks. It is usually the wisest plan to design the simplest network that will meet the requirements of the job. And in addition, if the values of the resistors in the network can be found without long-drawn-out calculation, the design problem can be made very simple indeed. Figure 2 will solve the simpler types of network problems of the fixed-value type, and permit the design of variable networks by a point-by-point method.

In Fig. 1 the impedance of the generator  $R_G$  is to be matched to the impedance of the load  $R_L$  by the L pad consisting of  $R_1$ , the series branch, and  $R_2$ , the shunt branch. To accomplish this match,  $R_1$  and  $R_2$  must have the following values, which can be calculated directly from the known values of  $R_G$  and  $R_L$ :

$$R_1 = \sqrt{R_G(R_G - R_L)}$$

$$R_2 = \frac{R_G R_L}{\sqrt{R_G(R_G - R_L)}}$$

where  $R_G$  is assumed to be the larger of the impedances to be matched. For ease in computation, the ratio of the larger to the smaller impedances is

introduced as

$$r = \frac{R_G}{R_L}$$

Using this ratio,  $R_1$  and  $R_2$  can then be found in terms of their ratio to  $R_L$ , a convenient method that makes it possible

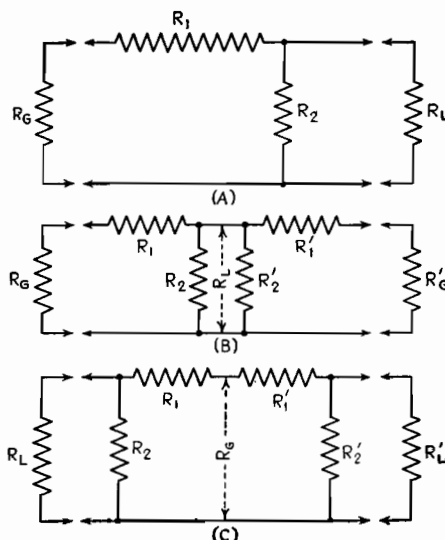


Fig. 1.—The T and  $\pi$  pad developed from an L pad.

to use widely varying magnitudes of  $R_L$  without the use of extended scales.

These ratios are

$$\frac{R_1}{R_L} = \sqrt{r(r-1)}$$

$$\frac{R_2}{R_L} = \frac{r}{\sqrt{r(r-1)}}$$

By plotting the values of these ratios for different values of  $r$ , the required  $R_1$  and  $R_2$  for any value of  $R_L$  can be found from the graph.

If  $n$  is the loss ratio (relative to a perfect matching transformer) introduced by the network, then

$$\frac{n^2 + 1}{2n} = \sqrt{\frac{R_G}{R_L}} = \sqrt{r}$$

from which

$$n = \sqrt{r} + \sqrt{r-1}$$

From this relation, the loss in decibels can be given as

$$\text{db loss} = 20 \log_{10}(\sqrt{r} + \sqrt{r-1})$$

Thus, the decibel loss can also be plotted as a function of  $r$ , as shown in the chart.

## Examples

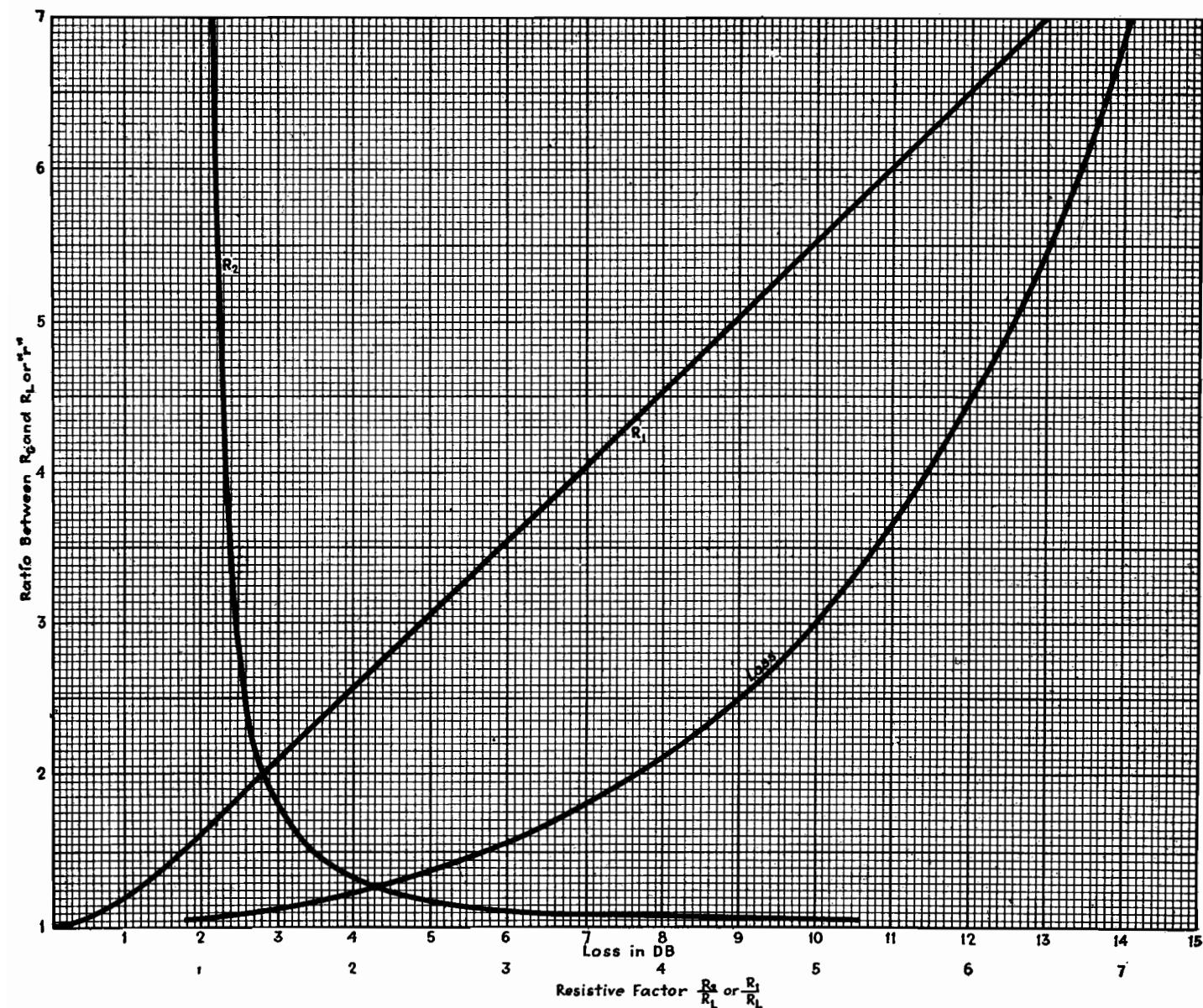
Although the chart has been worked out on the basis of the L type of network, T- and  $\pi$ -type circuits can be built up from the L type as illustrated in the following examples.

**Example 1.**—To calculate the series and shunt branches of a taper pad matching 2,000 to 500 ohms. Since the ratio  $r$  in this case is 4, the abscissa shown by the chart for  $R_1$  is 3.46 and for  $R_2$  is 1.15, which when multiplied by  $R_L$  (500) gives 1,730 ohms for  $R_1$  and 575 ohms for  $R_2$ . The loss of this network, from the graph, is 11.4 db.

**Example 2.**—To design a 500-ohm balanced network with a loss of 20 db. Reading directly from the graph, a 1:1 ratio would give a zero value for  $R_1$ , but it is still possible to introduce a loss by tapering a network to a lower impedance and back to normal again (Fig. 1B). The loss of each half of such a combination would be half the total loss. Therefore, calculations will be made for two 10-db taper pads to be placed "back to back." The ordinate opposite the 10-db abscissa is the ratio 3 and, since  $R_G$  is to be 500 ohms,  $R_L$  will be 500/3, or 133, ohms. From this point the procedure is the same as in Example 1, the value of  $R_1$  being found to be 326 ohms and  $R_2$ , 163 ohms. Therefore the two series branches  $R_1$  and  $R_1'$  of the T pad would equal 326 ohms each, and the shunt branch would equal 163/2, or 81.5 ohms since  $R_2$  and  $R_2'$  are paralleled.

**Example 3.**—To design a 500-ohm balanced  $\pi$  network with a 20-db loss (see Fig. 1C). Here the loss may be obtained by tapering to a higher impedance and back to normal, i.e., just the reverse of the process in Example 2. Since  $R_L$  is 500 ohms in this case, it is found that for a 10-db loss or a ratio of 3 the shunt branches  $R_2$  and  $R_2'$  equal 500  $\times$  1.2, or 600, ohms each, and the series branch, being the sum of  $R_1$  and  $R_1'$ , equals 2  $\times$  500  $\times$  2.45, or 2,450 ohms.





Universal network design chart.

## Attenuator-design Formulas

By DAWKINS ESPY

The design of resistance networks, or pads, for matching the impedances of two connected circuits, or for inserting a definite attenuation in a circuit, is simplified through the use of design charts applicable to a wide variety of networks

NETWORKS whose elements consist of pure resistances and whose attenuation does not vary with frequency are known as attenuator pads. There are two common uses of these resistance pads, namely, to match the impedance between two circuits and to insert a definite loss

in a circuit. The physical interpretation of a pad is a transmission line that has no reactive characteristics, but rather may be considered as a group of series and shunt elements that are pure resistances.

Three factors determine the design of a pad. They are (1) the input impedance,

(2) the output impedance, and (3) the loss in decibels. For every input-to-output impedance ratio, there is a definite minimum loss for which the pad can be designed so that (2) and (3) are not completely independent. To attempt to design a pad with less than this critical

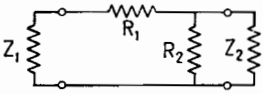
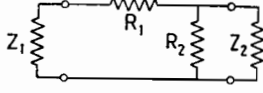
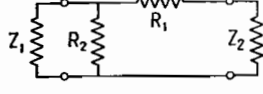
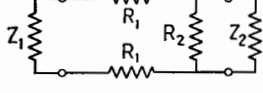
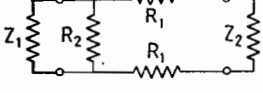
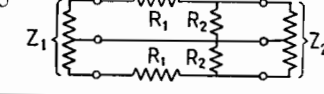
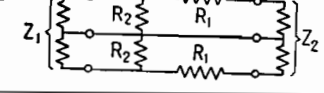
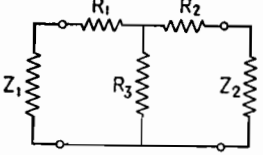
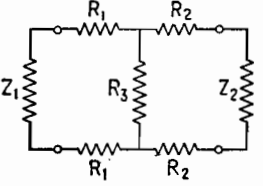
1 Type and configuration	2 Dissymmetrical formulas $S = \frac{Z_1}{Z_2}$ or $\frac{Z_2}{Z_1}$ ( $S \geq 1$ )	3 Symmetrical formulas ( $Z_1 = Z_2$ ) or ( $S = 1$ ) $Z_1$ used for input and output impedance
<b>Potentiometer</b> 	$R_1 = Z_1 \left( \frac{K-1}{K} \right)$ $R_2 = \frac{Z_1}{K}$	
<b>L</b> 	$R_1 = \frac{Z_1}{S} \left( \frac{KS-1}{K} \right)$ $R_2 = \frac{Z_1}{S} \left( \frac{1}{K-S} \right)$	$R_1 = Z_1 \left( \frac{K-1}{K} \right)$ $R_2 = Z_1 \left( \frac{1}{K-1} \right)$
<b>L</b> 	$R_1 = \frac{Z_2}{S} (K-S)$ $R_2 = \frac{Z_2}{S} \left( \frac{K}{KS-1} \right)$	$R_1 = Z_1 (K-1)$ $R_2 = Z_1 \left( \frac{K}{K-1} \right)$
<b>U</b> 	$R_1 = \frac{Z_1}{2S} \left( \frac{KS-1}{K} \right)$ $R_2 = \frac{Z_1}{S} \left( \frac{1}{K-S} \right)$	$R_1 = \frac{Z_1}{2} \left( \frac{K-1}{K} \right)$ $R_2 = Z_1 \left( \frac{1}{K-1} \right)$
<b>U</b> 	$R_1 = \frac{Z_1}{2S} (K-S)$ $R_2 = \frac{Z_1}{S} \left( \frac{K}{KS-1} \right)$	$R_1 = \frac{Z_1}{2} (K-1)$ $R_2 = Z_1 \left( \frac{K}{K-1} \right)$
<b>Balanced U</b> 	$R_1 = \frac{Z_1}{2S} \left( \frac{KS-1}{K} \right)$ $R_2 = \frac{Z_1}{2S} \left( \frac{1}{K-S} \right)$	$R_1 = \frac{Z}{2} \left( \frac{K-1}{K} \right)$ $R_2 = \frac{Z}{2} \left( \frac{1}{K-1} \right)$
<b>Balanced U</b> 	$R_1 = \frac{Z_2}{2S} (K-S)$ $R_2 = \frac{Z_2}{2S} \left( \frac{K}{KS-1} \right)$	$R_1 = \frac{Z}{2} (K-1)$ $R_2 = \frac{Z}{2} \left( \frac{K}{K-1} \right)$
<b>T</b> 	$R_1 = \frac{Z_1}{\tanh \theta} - \frac{\sqrt{Z_1 Z_2}}{\sinh \theta}$ $R_2 = \frac{Z_2}{\tanh \theta} - \frac{\sqrt{Z_1 Z_2}}{\sinh \theta}$ $R_3 = \frac{\sqrt{Z_1 Z_2}}{\sinh \theta}$ <p>or</p> $R_1 = Z_1 \left( \frac{K^2+1}{K^2-1} \right) - 2\sqrt{Z_1 Z_2} \left( \frac{K}{K^2-1} \right)$ $R_2 = Z_2 \left( \frac{K^2+1}{K^2-1} \right) - 2\sqrt{Z_1 Z_2} \left( \frac{K}{K^2-1} \right)$ $R_3 = 2\sqrt{Z_1 Z_2} \left( \frac{K}{K^2-1} \right)$	$R_1 = R_2 = \frac{Z_1}{\tanh \theta} - \frac{Z_1}{\sinh \theta}$ $R_3 = \frac{Z_1}{\sinh \theta}$ <p>or</p> $R_1 = R_2 = \left( \frac{K-1}{K+1} \right) Z_1$ $R_3 = 2Z_1 \left( \frac{K}{K^2-1} \right)$
<b>H</b> 	$R_1 = \frac{1}{2} \left( \frac{Z_1}{\tanh \theta} - \frac{\sqrt{Z_1 Z_2}}{\sinh \theta} \right)$ $R_2 = \frac{1}{2} \left( \frac{Z_2}{\tanh \theta} - \frac{\sqrt{Z_1 Z_2}}{\sinh \theta} \right)$ $R_3 = \frac{\sqrt{Z_1 Z_2}}{\sinh \theta}$ <p>or</p> $R_1 = \frac{Z_1}{2} \left( \frac{K^2+1}{K^2-1} \right) - \sqrt{Z_1 Z_2} \left( \frac{K}{K^2-1} \right)$ $R_2 = \frac{Z_2}{2} \left( \frac{K^2+1}{K^2-1} \right) - \sqrt{Z_1 Z_2} \left( \frac{K}{K^2-1} \right)$ $R_3 = 2\sqrt{Z_1 Z_2} \left( \frac{K}{K^2-1} \right)$	$R_1 = R_2 = \frac{1}{2} \left( \frac{Z_1}{\tanh \theta} - \frac{Z_1}{\sinh \theta} \right)$ $R_3 = \frac{Z_1}{\sinh \theta}$ <p>or</p> $R_1 = R_2 = \frac{Z_1}{2} \left( \frac{K-1}{K+1} \right)$ $R_3 = 2Z_1 \left( \frac{K}{K^2-1} \right)$

Fig. 1.—Common resistance networks for communication uses, together with the design equations for both equal and unequal impedances between which the pad works.

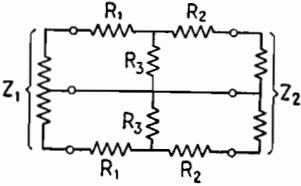
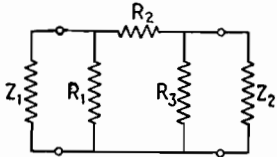
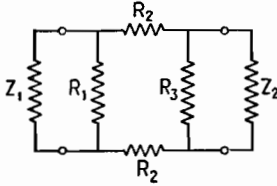
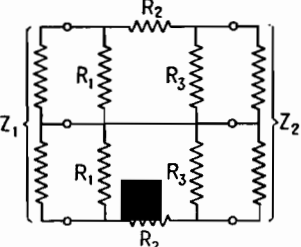
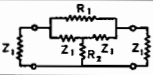
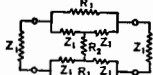
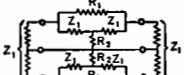
4 Type and configuration	5 Dissymmetrical formulas $S = \frac{Z_1}{Z_2} \text{ or } \frac{Z_2}{Z_1} (S \geq 1)$	6 Symmetrical formulas ( $Z_1 = Z_2$ ) or ( $S = 1$ ) $Z_1$ used for input and output impedance
Balanced H 	$R_1 = \frac{1}{2} \left( \frac{Z_1}{\tanh \theta} - \frac{\sqrt{Z_1 Z_2}}{\sinh \theta} \right)$ $R_2 = \frac{1}{2} \left( \frac{Z_2}{\tanh \theta} - \frac{\sqrt{Z_1 Z_2}}{\sinh \theta} \right)$ $R_3 = \frac{\sqrt{Z_1 Z_2}}{2 \sinh \theta}$ <p>or</p> $R_1 = \frac{Z_1}{2} \left( \frac{K^2 + 1}{K^2 - 1} \right) - \sqrt{Z_1 Z_2} \left( \frac{K}{K^2 - 1} \right)$ $R_2 = \frac{Z_2}{2} \left( \frac{K^2 + 1}{K^2 - 1} \right) - \sqrt{Z_1 Z_2} \left( \frac{K}{K^2 - 1} \right)$ $R_3 = \sqrt{Z_1 Z_2} \left( \frac{K}{K^2 - 1} \right)$	$R_1 = R_2 = \frac{1}{2} \left( \frac{Z_1}{\tanh \theta} - \frac{Z_1}{\sinh \theta} \right)$ $R_3 = \frac{Z_1}{2 \sinh \theta}$ <p>or</p> $R_1 = R_2 = \frac{Z_1}{2} \left( \frac{K - 1}{K + 1} \right)$ $R_3 = Z_1 \left( \frac{K}{K^2 - 1} \right)$
$\pi$ 	$R_1 = \frac{Z_1 Z_2 \sinh \theta}{Z_2 \cosh \theta - \sqrt{Z_1 Z_2}}$ $R_2 = \frac{\sqrt{Z_1 Z_2} \sinh \theta}{Z_1 \cosh \theta - \sqrt{Z_1 Z_2}}$ $R_3 = \frac{Z_1 Z_2 \sinh \theta}{Z_1 \cosh \theta - \sqrt{Z_1 Z_2}}$ <p>or</p> $R_1 = Z_1 \left( \frac{K^2 - 1}{K^2 - 2KS + 1} \right)$ $R_2 = \frac{\sqrt{Z_1 Z_2}}{2} \left( \frac{K^2 - 1}{K} \right)$ $R_3 = Z_2 \left( \frac{K^2 - 1}{K^2 - 2\frac{K}{S} + 1} \right)$	$R_1 = R_3 = \frac{Z_1^2 \sinh \theta}{Z_1 \cosh \theta - Z_1}$ $R_2 = Z_1 \sinh \theta$ <p>or</p> $R_1 = R_3 = Z_1 \left( \frac{K + 1}{K - 1} \right)$ $R_2 = \frac{Z_1}{2} \left( \frac{K^2 - 1}{K} \right)$
$O$ 	$R_1 = \frac{Z_1 Z_2 \sinh \theta}{Z_2 \cosh \theta - \sqrt{Z_1 Z_2}}$ $R_2 = \frac{\sqrt{Z_1 Z_2} \sinh \theta}{2}$ $R_3 = \frac{Z_1 Z_2 \sinh \theta}{Z_1 \cosh \theta - \sqrt{Z_1 Z_2}}$ <p>or</p> $R_1 = Z_1 \left( \frac{K^2 - 1}{K^2 - 2SK + 1} \right)$ $R_2 = \frac{\sqrt{Z_1 Z_2}}{4} \left( \frac{K^2 - 1}{K} \right)$ $R_3 = Z_2 \left( \frac{K^2 - 1}{K^2 - 2\frac{K}{S} + 1} \right)$	$R_1 - R_3 = \frac{Z_1^2 \sinh \theta}{Z_1 \cosh \theta - Z_1}$ $R_2 = \frac{Z_1 \sinh \theta}{2}$ <p>or</p> $R_1 = R_3 = Z_1 \left( \frac{K + 1}{K - 1} \right)$ $R_2 = \frac{Z}{4} \left( \frac{K^2 - 1}{K} \right)$
Balanced O 	$R_1 = \frac{1}{2} \left( \frac{Z_1 Z_2 \sinh \theta}{Z_2 \cosh \theta - \sqrt{Z_1 Z_2}} \right)$ $R_2 = \frac{\sqrt{Z_1 Z_2} \sinh \theta}{2}$ $R_3 = \frac{1}{2} \left( \frac{Z_1 Z_2 \sinh \theta}{Z_1 \cosh \theta - \sqrt{Z_1 Z_2}} \right)$ <p>or</p> $R_1 = \frac{Z_1}{2} \left( \frac{K^2 - 1}{K^2 - 2KS + 1} \right)$ $R_2 = \frac{\sqrt{Z_1 Z_2}}{4} \left( \frac{K^2 - 1}{K} \right)$ $R_3 = \frac{Z_2}{2} \left( \frac{K^2 - 1}{K^2 - 2\frac{K}{S} + 1} \right)$	$R_1 = R_3 = \frac{1}{2} \left( \frac{Z_1^2 \sinh \theta}{Z_1 \cosh \theta - Z_1} \right)$ $R_2 = \frac{Z_1 \sinh \theta}{2}$ <p>or</p> $R_1 = R_3 = \frac{Z_1}{2} \left( \frac{K + 1}{K - 1} \right)$ $R_2 = \frac{Z_1}{4} \left( \frac{K^2 - 1}{K} \right)$
Bridged T 		$R_1 = Z_1 (K - 1)$ $R_2 = Z_1 \left( \frac{1}{K - 1} \right)$
Bridged H 		$R_1 = \frac{Z_1}{2} (K - 1)$ $R_2 = Z_1 \left( \frac{1}{K - 1} \right)$
Bridged-balanced H 		$R_1 = \frac{Z_1}{2} (K - 1)$ $R_2 = \frac{Z_1}{2} \left( \frac{1}{K - 1} \right)$

Fig. 1.—(Continued)

loss would require that at least one of the resistances be negative, which is physically meaningless for attenuators built of customary resistor elements.

In order to know which pad to employ for a particular use, it is necessary to know the electrical characteristics of the various networks. When working into a high-impedance device, it is usually possible to use the simplest form of attenuator, the potentiometer. In this type the sum of the two resistance arms is constant, but their ratio is varied. When it is not necessary that the impedance looking back into the output terminals of the attenuator be equal to the load impedance, an L type of attenuator may be used.

Pads of the T, H,  $\pi$ , and O types are useful where the attenuator impedance must match the load impedance. Such a situation occurs in low-level low-impedance mixing and in amplifiers with critical input impedance. When a pad is in a circuit that must be balanced to ground, such as the input of a push-pull amplifier, the balanced U, O, or H attenuator may be used. Formulas are also included for the bridged T, bridged H, and bridged-balanced H.

The resistance values actually used may deviate from the calculated values by 5 per cent without mismatching the impedance by more than that amount and varying the loss more than 0.5 db. Since the T and  $\pi$  pads occur most frequently, a second set of formulas, easier to work with than the algebraic type, is included.

Very often it is desirable to have a volume control that reflects a constant impedance in both directions. It is for this purpose that the bridged versions of the pads are most frequently used. The bridged T, for example, has the advantage over the ordinary T that one less resistance must be varied, yet it still retains the advantage of the T in having zero insertion loss for matching equal impedances.

### Design Procedure

The steps in the design of any pad may be summarized as follows:

1. Determine from Fig. 1 the type of pad best suited for a particular use. In some cases particular networks will be required; in other cases several network arrangements are possible, as indicated above.

2. Calculate the ratio of input to output impedance (or output to input, which-

ever is the larger), and by using Fig. 2 determine the minimum loss possible for the given impedances. Figure 2 holds for T, H,  $\pi$ , O, balanced H, and balanced O types of pads.

3. From Table I find the value of  $K$  corresponding to the desired loss in decibels, which must be equal to or greater than the minimum loss determined in step 2.

4. Calculate the values of resistance for the various elements from the formulas given in column 2 or 5 of Fig. 1. If the hyperbolic forms of the formulas are used in the case of the T, H,  $\pi$ , O, bal-

anced H, and balanced O pads, it is first necessary to check the desired loss as explained in step 2 and then determine  $\theta$  from the formula  $\theta = 0.115N$ , where  $N$  is the loss in decibels. Then values of  $\sinh \theta$  and  $\tanh \theta$  in the case of the T, H, or balanced H, or the values of  $\sinh \theta$  and  $\cosh \theta$  in the case of the  $\pi$ , O, or balanced O can be found in Fig. 3. It will be noticed that the curves for the  $\sinh \theta$  and the  $\cosh \theta$  are broken up into two sections for increased accuracy.

5. When it is necessary to insert a loss of more than 30 or 40 db, it is usually advisable to use two pads in series, such

Table I.—K Values

Loss, db, $N$	$K$	Loss, db, $N$	$K$	Loss, db, $N$	$K$	Loss, db, $N$	$K$
1.0	1.122	18.0	7.943	35.0	56.234	51.0	354.81
2.0	1.259	19.0	8.912	36.0	63.096	52.0	398.11
3.0	1.412	20.0	10.000	37.0	70.795	54.0	501.19
4.0	1.585	21.0	11.220	38.0	79.433	55.0	562.45
5.0	1.778	22.0	13.335	39.0	89.125	56.0	630.96
6.0	1.995	23.0	14.125	40.0	100.000	57.0	707.95
7.0	2.238	24.0	15.849	41.0	112.202	58.0	794.33
8.0	2.512	25.0	17.783	42.0	125.89	60.0	1,000.0
9.0	2.818	26.0	19.953	43.0	141.25	65.0	1,778.3
10.0	3.162	27.0	22.387	44.0	158.49	70.0	3,162.3
11.0	3.350	28.0	25.119	45.0	177.83	75.0	5,623.4
12.0	3.981	29.0	28.184	46.0	199.53	80.0	10,000.
13.0	4.467	30.0	31.623	47.0	223.87	85.0	17,783.
14.0	5.012	31.0	35.481	48.0	251.19	90.0	31,623.
15.0	5.623	32.0	39.811	49.0	281.84	95.0	56,234.
16.0	6.310	33.0	44.668	50.0	316.23	100.0	10 <sup>5</sup>
17.0	7.079	34.0	50.119				

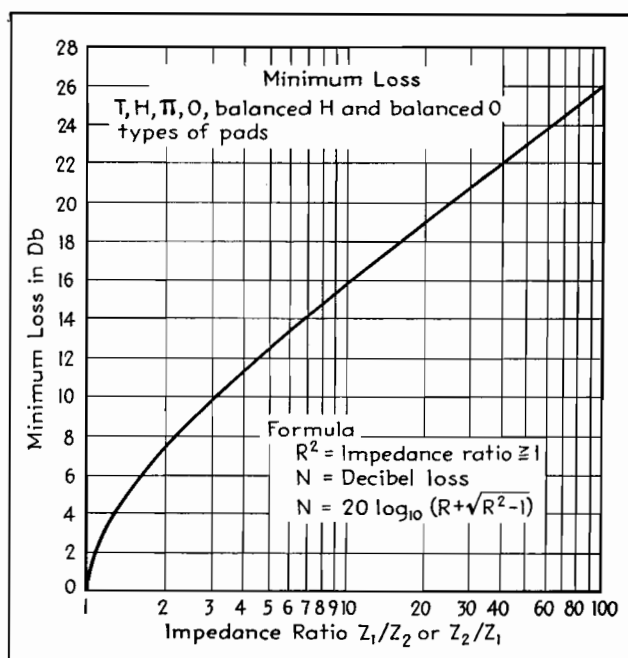


Fig. 2.—The minimum loss of any pad inserted in a circuit is given in decibels for impedance ratios,  $Z_1/Z_2$ , of from 1 to 100. The range may be extended for values of from  $Z_1/Z_2 = 0.01$  to  $Z_1/Z_2 = 1.0$  by forming the ratio  $Z_2/Z_1$  which will be greater than unity.

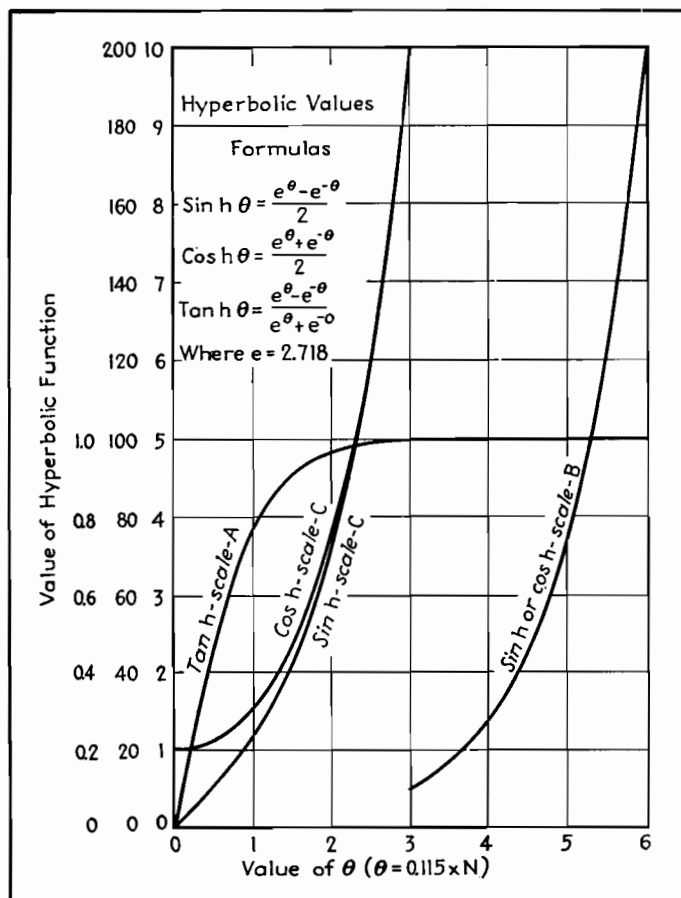


Fig. 3.—Graph of hyperbolic functions, which are used in many design equations of resistance networks. Note that multiple scales for the functions are given, and that the sinh and cosh functions are broken at  $\theta = 3$  so as to obtain greater accuracy.

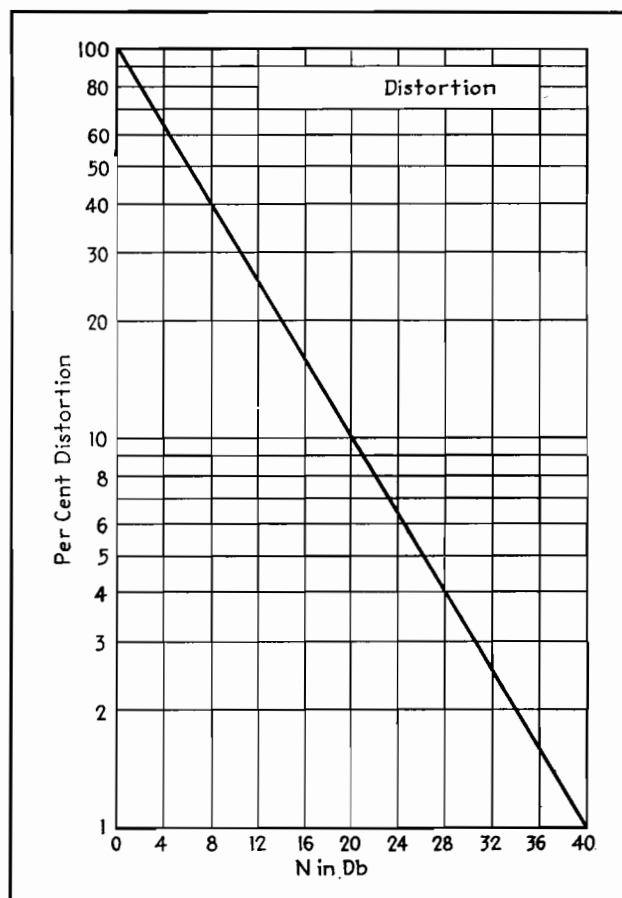


Fig. 4.—Graph for determining per cent distortion by noting the gain required to produce the original output of a network, when the fundamental frequency is removed by use of high-pass filter.

that the sum of their losses is equal to the required amount, rather than a single pad.

### Distortion Measurements

For measuring harmonic distortion, a good method is to adjust the output of the amplifier to the desired level with a constant-frequency input. A frequency of 400 cycles is usually used for this purpose because the distortion at this frequency represents a good average of distortion throughout the audio range. Then a high-pass filter of good characteristics is inserted to eliminate the fundamental, and the amplification in decibels necessary to bring the level back up to the previous value is determined. This may be accomplished by removal of pads of known loss. Then by referring to Fig. 4, the harmonic distortion corresponding to this attenuation may be found. For example, if it were necessary to remove a 30-db pad to regain the original level, there would exist in this particular amplifier 3.16 per cent harmonic distortion.

### Mismatch Loss

If it is desired to calculate the loss incurred by mismatching two circuits, this can be determined from the following equation:

$$N = 20 \log_{10} \frac{R^2 + 1}{2R}$$

where  $N$  is the loss in decibels, and  $R$  is the impedance ratio. This is shown graphically in Fig. 5. If, for example, the mismatch was from a 1,000-ohm circuit to a 500-ohm circuit, or a 500-ohm circuit to a 1,000-ohm circuit, the impedance ratio would be 2:1 and would correspond to a loss of 0.51 db.

### Examples

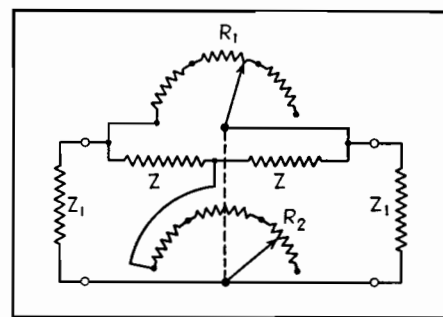
**Example 1.**—Design a potentiometer having an input of 100,000 ohms and a loss of 15 db.

**Solution:**

1. From column 2 of Fig. 1 the formulas are

$$R_1 = Z_1 \frac{(K - 1)}{K}$$

$$R_2 = \frac{Z_1}{K}$$



Simple voltage-dividing network having given input impedance and specified loss, design data for which is worked out in Example 1.

2. From Table I the value of  $K$  for a 15-db loss is found to be 5.62.

3. Using this value of  $K$  in the formulas above, the values of  $R_1$  and  $R_2$  are found to be

$$R_1 = 100,000 \frac{(4.62)}{5.62} = 82,200 \text{ ohms}$$

$$R_2 = \frac{100,000}{5.62} = 17,800 \text{ ohms}$$

**Example 2.**—Design a 20-db T pad having input and output impedances of 500 and 200 ohms, respectively.

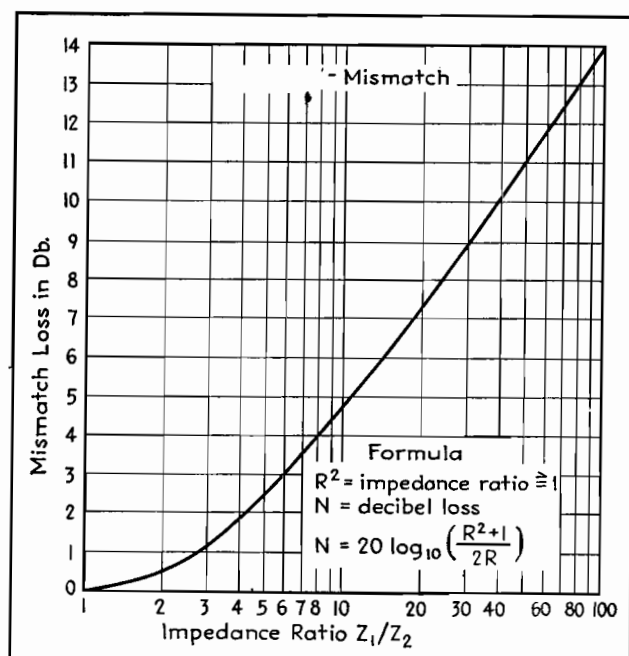


Fig. 5.—The loss incurred by joining together two circuits of different impedance may be determined by finding the impedance ratio and then reading off the mismatch loss,  $K$ , above.

**Solution:**

1. The impedance transformation ratio is  $500/200 = 2.5$ . From Fig. 2 the minimum loss = 9 db.

2. From Fig. 1 the formulas to be used are

$$R_1 = \frac{Z_1}{\tanh \theta} - \frac{\sqrt{Z_1 Z_2}}{\sinh \theta}$$

$$R_2 = \frac{Z_2}{\tanh \theta} - \frac{\sqrt{Z_1 Z_2}}{\sinh \theta}$$

$$R_3 = \frac{\sqrt{Z_1 Z_2}}{\sinh \theta}$$

3. To use the hyperbolic functions, it

is necessary to know the value of  $\theta$ , from which the hyperbolic functions can then be found from Fig. 3.

$$\theta = 0.115N = 0.115 \times 20 = 2.3$$

$$\therefore \tanh \theta = 0.98$$

$$\therefore \sinh \theta = 4.9$$

4. The values of the required resistors are then

$$R_1 = \frac{500}{0.98} - \frac{\sqrt{500 \times 200}}{4.9}$$

$$= 510 - \frac{318}{4.9} = 510 - 65 = 445 \text{ ohms}$$

$$R_2 = \frac{200}{0.98} = 65 = 204 - 65 = 139 \text{ ohms}$$

$$R_3 = \frac{319}{4.9} = 65 \text{ ohms}$$

**Example 3.**—Design a bridged T pad with 25-db loss and 500 ohms input and output impedances.

**Solution:**

1. The formulas in column 6 of Fig. 1 are used.

$$R_1 = Z_1(K - 1)$$

$$R_2 = \frac{Z_1}{K - 1}$$

2. From Table I the value for  $K$  for 25-db loss is found to be 17.78. Thus

$$K - 1 = 16.78$$

$$R_1 = 500 \times 16.78 = 8,390 \text{ ohms}$$

$$R_2 = \frac{500}{16.78} = 29.6 \text{ ohms}$$

**Example 4.**—Design a T network to work between two 500-ohm circuits and having a loss of 10 db.

**Solution:**

1. Formulas for the T network in column 3 of Fig. 1 indicate the desired resistances are

$$R_1 = R_2 = Z_1 \frac{K - 1}{K + 1}$$

$$R_3 = \frac{2Z_1 K}{K^2 - 1}$$

2. From Table I,  $K = 3.162$

3. The resistances of the arms are

$$R_1 = R_2 = 500 \times \frac{2.162}{4.162}$$

$$= 260 \text{ ohms}$$

$$R_3 = 1,000 \times \frac{3.162}{10 - 1}$$

$$= 352 \text{ ohms}$$

## SECTION II

# ANTENNAS

	Page
Aircraft Antenna Characteristics .....	17
Design of Two-tower Directional Arrays.....	19
Directional Radiation Patterns of Two-element Vertical Antenna Arrays.....	23
Antenna Power Divider.....	25
Computing Performance of Two-tower Directional Arrays	26
Voltage Gain Charts for Two-antenna Arrays.....	29
Field-strength Prediction Charts Based on Sommerfeld's Formula.....	30
Radiation Chart for Vertical Antennas.....	32
Design Procedure for Ground-plane Antennas.....	34
Design Chart for Antenna Phase-shifting Networks.....	37
Phasing Networks for Broadcast Arrays.....	40
Calculating Broadcast-station Coverage.....	45
Radial Ground System Chart.....	47

## Aircraft Antenna Characteristics

By PAUL J. HOLMES

By measuring the length of a fixed aircraft antenna, making some empirical allowance for its proximity to the fuselage or the size of the ship, the reactance and radiation resistance may be estimated with sufficient accuracy to permit the design of a dummy antenna

THE charts provide a simple means of determining the approximate electrical characteristics of fixed aircraft antennas by measuring their length, making some slight allowance (dictated by experience) for their proximity to the fuselage or for the size of the ship.

Data obtained through the use of the charts facilitate actual measurement of antenna characteristics and are, ordinarily, sufficiently accurate to permit design of dummy antennas needed when bench-testing aircraft radio equipment.

### Quarter-wave Resonance

Figure 1 is used in determining the approximate length of fixed aircraft antennas for quarter-wave resonance. The intersection points of the vertical lines (measured length of antenna) and the horizontal lines (quarter-wave frequency) with the plotted angular lines indicate the quarter-wave resonance frequency for any length between 10 and 100 ft.

The variation of the angular lines on

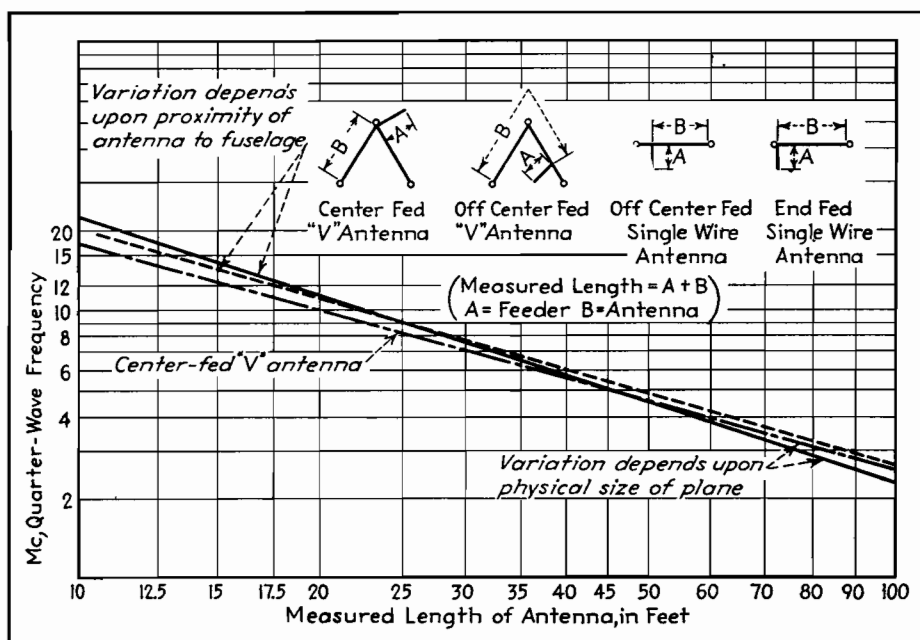


Fig. 1.—Approximate lengths of fixed aircraft antennas for quarter-wave resonance are shown graphically. Empirical variations caused by proximity of the antenna to the fuselage and the physical size of the ship are indicated.



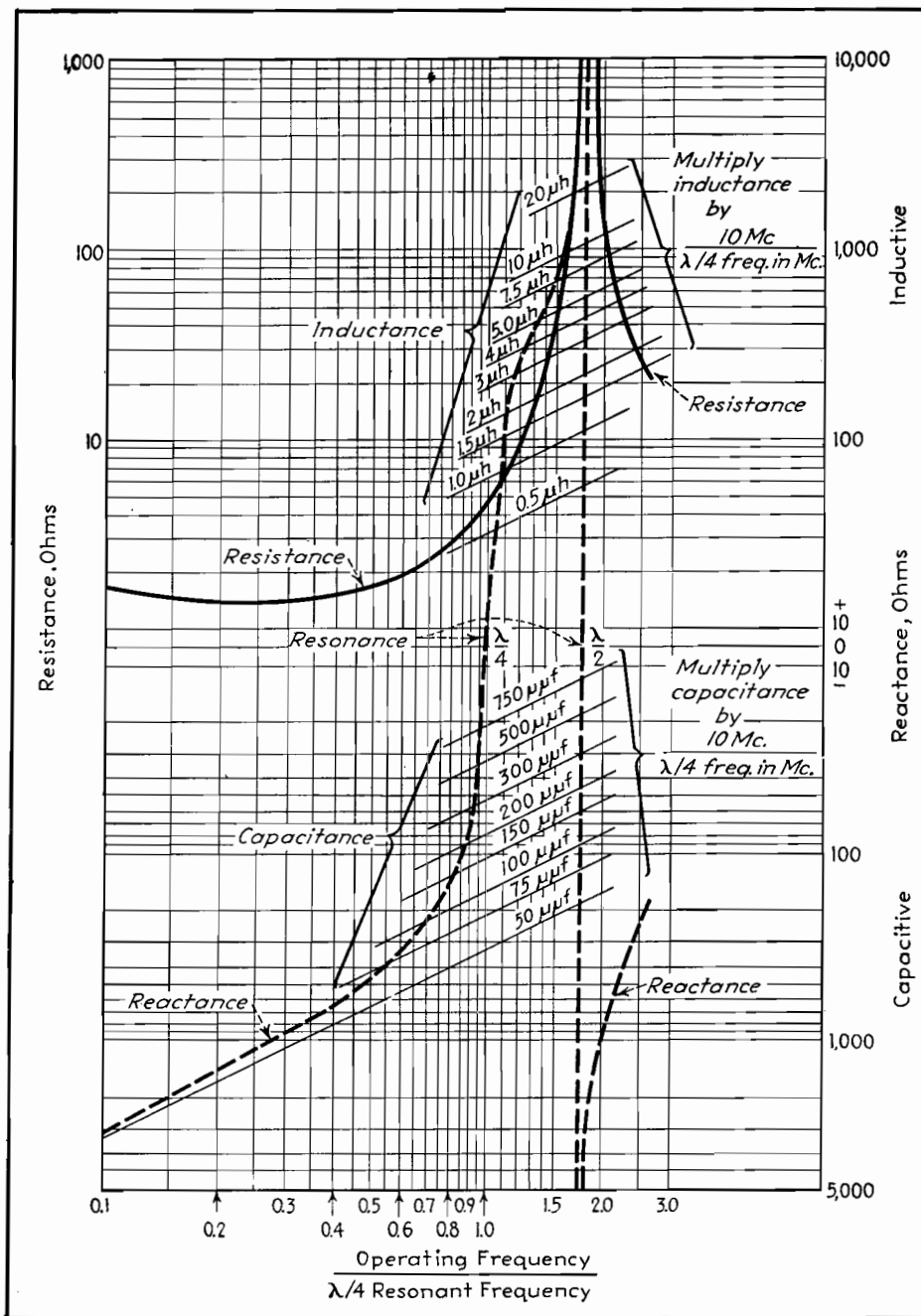


Fig. 2.—Approximate electrical characteristics of a fixed aircraft antenna operated above or below the quarter-wave resonant frequency may be determined by using the chart as outlined in this text.

the right of the vertical dotted line (lengths over 45 ft.) depends largely on the physical size of the airplane as compared with the length of the antenna. The upper dashed line on the right side of the chart is representative of a small airplane, and the solid line represents a large airplane.

The variation shown on the left of the vertical dotted line (lengths under 45 ft.) depends largely on the proximity of short antennas to the metal fuselage of the airplane. The solid line on the left side of the chart is representative of an antenna reasonably distant from the fuselage, such as one running from a wing

tip to the aft portion of the fuselage. The dashed line immediately below the solid line on the left side of the chart represents a short antenna close to the fuselage, such as one run from a short mast near the cockpit directly aft over the fuselage to the fin of the plane.

The following example illustrates the use of Fig. 1. Assume a measured length of antenna as 47 ft. From the chart, the quarter-wave resonant frequency is seen to be approximately 5 Mc. If the plane is small, the resonant frequency will be greater than 5 Mc; if large, it will be less than 5 Mc

### Inductance, Capacitance, Resistance

Figure 2 is used in determining the equivalent electrical components of an antenna at various operating frequencies. In addition to determining such characteristics at the quarter-wave resonant frequency, the equivalent capacitive or inductive reactance and radiation resistance at operating frequencies above or below quarter-wave resonance may be readily determined.

As an example, the equivalent electrical components of the 47-ft. 5-Mc quarter-wave antenna discussed above may be determined for an operating frequency of 3 Mc.

The vertical lines marked across the bottom of the chart from 0.1 to 3.0 represent the ratio of the selected operating frequency to quarter-wave resonant frequency, the latter being determined by the use of Fig. 1.

The horizontal lines marked on the right of the chart represent the antenna's reactance in ohms. Those below the center or zero line indicate negative or capacitive reactance (operating frequency less than quarter wave). Those above the zero line indicate positive or inductive reactance (operating frequency greater than quarter wave). The common intersection point of the horizontal lines with the dashed reactance curve and the vertical lines indicates the reactance of the antenna at the selected operating frequency.

Assume the quarter-wave resonant frequency as 5 Mc (measured length 47 ft). The reactance of this antenna at an operating frequency of 3 Mc is found as follows: Divide the 3-Mc operating frequency by the 5-Mc quarter-wave resonant frequency. The quotient is seen to be 0.6. Following the vertical 0.6 line to the point where it intersects the dashed reactance curve and then proceeding to the right, the reactance is seen to be about -325 ohms.

Referring again to Fig. 1, the upper horizontal lines are marked on the left. These numbers at the left represent the radiation resistance in ohms of the antenna. The common intersection point of these horizontal lines with the solid resistance curve and the vertical lines (ratio of operating frequency to quarter-wave resonant frequency) indicates the radiation resistance of the antenna at the particular operating frequency chosen. Thus, the radiation resistance of the 47-ft 5-Mc quarter-wave antenna at an operating frequency of 3 Mc is seen to be approximately 1.9 ohms (the 0.6 vertical



line intersects with the resistance curve and the 1.9-ohm horizontal line as read on the left).

The lower solid angular lines mark in terms of capacitance values which, when multiplied by a factor shown on the chart, produce a capacitive reactance equal to that of the antenna. For example, the effective value of capacitance of a 47-ft 5-Mc quarter-wave antenna at an operating frequency of 3 Mc is found as follows: The vertical 0.6 line intersects the reactance curve at a point just slightly higher than that of the 75- $\mu\text{mf}$ -capacitance line, indicating a value of capacitance greater than 75  $\mu\text{mf}$  or approximately 80  $\mu\text{mf}$ . This value of 80  $\mu\text{mf}$ , when multiplied by the ratio 10 Mc:5 Mc, is 160  $\mu\text{mf}$ , which is the effective capacitance of the 5-Mc antenna under discussion when operated at 3 Mc.

The upper solid angular lines mark in terms of inductance values which, when multiplied by a factor shown on the chart, produce the equivalent inductance of the antenna at the particular operating frequency chosen. The inductance value is found the same way as capacitance, outlined above, using the angular inductance lines instead of the angular capacitance lines.

(It is important to note when using the chart that the capacitance lines are used only when the antenna has capacitive reactance at the operating frequency, *i.e.*, less than quarter-wave frequency. The inductance lines are used only when the

antenna is inductive, *i.e.*, greater than quarter-wave frequency.)

#### Estimating Procedure

To review the examples illustrated, by the use of the antenna charts a 47-ft aircraft antenna is found to be quarter-wave resonant at a frequency of 5 Mc. At an operating frequency of 3 Mc, it is found to have a capacitive reactance of -325 ohms and a radiation resistance of 1.9 ohms. The value of reactance is equivalent to a capacitance of 160  $\mu\text{mf}$ . Thus, a good grade air dielectric capacitor having a capacitance of 160  $\mu\text{mf}$ , in series with a noninductive resistance of approximately 2.0 ohms, would simulate a 47-ft antenna at a frequency of 3 Mc. This would constitute a suitable dummy antenna for the bench testing of aircraft radio equipment to be installed in an airplane having an antenna 47 ft long and operated on a frequency of 3 Mc.

The characteristics of an aircraft antenna at various operating frequencies may, then, be readily determined by the following procedure:

1. Measure the length of the antenna from the antenna insulator on the skin of the fuselage to its farthest point. If the antenna is an off-center fed V, do not include the short side. Measure the length of lead to the V plus the length of the longest side of the antenna proper to determine the measured length of the antenna.

2. From Fig. 1, determine the quarter-wave resonant frequency, taking into consideration the size of the airplane if the antenna is long or the proximity of the antenna to the fuselage if the antenna is short.

3. Determine the ratio of selected operating frequency to the quarter-wave resonant frequency by dividing the operating frequency by the previously noted quarter-wave frequency. This numerical value coincides with the numerical value of one of the vertical lines on Fig. 2.

4. Determine the reactance by the common intersection of the applicable vertical line, the dashed reactance curve, and the nearest horizontal line, reading the reactance value on the right side of Fig. 2.

5. Determine the effective capacitance or inductance by multiplying the value of capacitance or inductance found on the solid angular line intersecting the point on the reactance curve obtained in connection with 4 above, by the factor shown on the chart.

6. Determine the radiation resistance by the intersection of the vertical line obtained in 3 with the resistance curve and the nearest horizontal line, reading the value on the left.

Both charts were compiled empirically and are the average of the characteristics of a number of antennas of different lengths and types on various types of airplanes.

## Design of Two-tower Directional Arrays

By E. A. LAPORT

---

Practical methods for the design and application of two-element directional arrays in broadcast and communication service. Such arrays are useful for improving coverage and reducing fading

---

**T**HE outstanding problem in antenna design is always to control the distribution of the radiated energy in some desired manner. In the case of single vertical radiators, the control is obtained by adjusting the length of the antenna and the distribution of current in it. Further modification of the radiation distribution is achieved by the use of more than one radiator. As the number of

radiators is increased, a greater degree of control becomes possible. In general, it is electrically possible to mold the radiation pattern in almost any desired manner.

The array of two vertical radiators provides a wide range of radiation patterns, depending on their separation, and the relative magnitudes and phase of the radiator currents. Only two-element arrays in which identical vertical wire

radiators one-quarter wavelength in height are used will be discussed here. These restrictions are only for the purpose of simplification of the discussion, and one can readily remove them when the principles of radiation control are understood.

The radiation pattern, or space characteristic, is a geometrical description of the manner in which the radiant energy is distributed in space around the radiators.

The horizontal pattern represents the distribution in the ground plane, and the various vertical plane patterns represent conditions in directions at various angles above the horizon. These patterns may be drawn in terms of relative or actual field strength or power. Patterns are shown here in terms of relative field intensities.

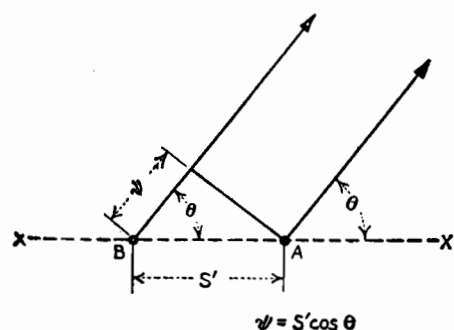


Fig. 1.—Plan view of directive array, showing geometry for computing the horizontal pattern.

The investigation of a directive antenna system usually starts with the choice of a suitable horizontal pattern, since that portion of the entire radiation pattern is of primary importance where ground-wave coverage is intended, as in broadcasting.

Extended tables of diagrams have been published<sup>1</sup> showing the horizontal directivity patterns resulting from two identical parallel linear radiators for various spacings and various phasings of equal radiator currents. These diagrams are always useful in prospecting for an approach to a given problem. The relative directions of nulls, maxima, and their broadness or sharpness, can be roughly determined by inspection of the figures. However, figures of this sort are seldom more than indicators, and the designer must calculate precisely his patterns after he has decided in what range of spacings and phasings he wishes to work.

#### Horizontal Directivity Diagrams

The entire radiation pattern is *symmetrical with respect to the plane drawn through the radiators*, as can be recognized by inspecting a table of directivity diagrams for two radiators. So it is necessary only to calculate the horizontal pattern through an angle of 180 deg. In Fig. 1 is shown the geometrical plan for calculating this pattern. The line of reference is the line X-X' through the radiators A and B, and the angle between this line and the point of observation is  $\theta$ . The point of observation may be considered to be anywhere on a circle drawn from the geometrical center of the array,

and it is assumed that the distance is great enough so that lines drawn from it to each radiator are essentially parallel. At broadcast frequencies and for broadcast applications, points on the 1-mile circle are usually considered.

At any angle  $\theta$ , in the first quadrant, radiations from A arrive in advance of those from B by an angle  $\psi = s' \cos \theta$ . Here  $s'$  is used to indicate the separation of the radiators in electrical degrees, and is the spacing in wavelengths ( $s/\lambda$ , where  $s$  is the actual separation in meters,  $\lambda$  the wavelength, multiplied by 360). In order to establish a basis of reference that can be followed throughout a problem, radiations from B may be arbitrarily considered in their relation to radiations from A. If radiations from B arrive later than those from A (as they do in the first quadrant),  $\psi$  is negative; contrariwise,  $\psi$  is positive when B radiations are in advance of those from A (second quadrant). Representing these radiations by means of rotating vectors exactly as used in a-c analyses, the resultant intensity at the point of observation is obtained by vector addition. If radiations are considered to start from both radiators at the same instant in phase, and travel to the observation point by paths of different lengths, but at the same velocity, the vectors would be added at an angle to obtain the resultant.

In addition to  $\psi$ , the effect of the initial difference of phase of the vectors must be included. Furthermore, since the field intensity is proportional to the antenna current that produces it, account must be made of the relative fields in the vector lengths. The total angle between the vectors is called  $\alpha$ , and it is the algebraic sum of the space angle  $\psi$  and the initial phase difference between radiator currents  $\phi$ . Proper precautions must be taken with signs. Angle  $\phi$  is positive or negative depending upon whether the instantaneous current in radiator B passes through positive maximum value so many electrical degrees in advance or retard of that in radiator A.

The horizontal directivity diagram can be quickly calculated by solving

$$E_{\theta} = 1 + k(\cos \alpha + j \sin \alpha) \quad (1)$$

This equation gives the relative strength of field at any angle  $\theta$ , for any given ratio of the radiator currents  $k$  and initial phase difference  $\phi$ , where  $\alpha = s' \cos \theta + \phi$ . The equation is especially adaptable to graphical solution. The solution for the angle  $\alpha$  is represented in Fig. 2, for two

values of  $\theta$ . A circle with a radius of  $s'$  is intersected by radials drawn at various angles corresponding to values of  $\theta$  from 0 to 180 deg. The projections of these intersections on the axis X-X' give the value of  $\psi = s' \cos \theta$ . According to the conventions adopted,  $\psi$  is negative for first-quadrant angles and positive for second-quadrant angles. In the succeeding operation,  $\phi$  is added algebraically to  $\psi$  to give the angle  $\alpha$ . Lastly, two vectors having a ratio  $k$  are added together at this angle, the resultant being the relative field intensity in the direction of  $\theta$ . Such an addition is shown in Fig. 3.

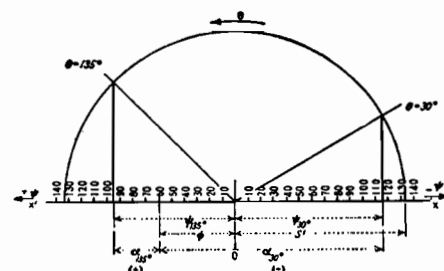


Fig. 2.—Construction used in finding values of  $\alpha$ . Case shown for  $s' = 133^\circ$ ,  $\phi = -60^\circ$ , for  $\theta = 30^\circ$  and  $135^\circ$ . Various values of  $\alpha$  for different values of  $\theta$  are found similarly.

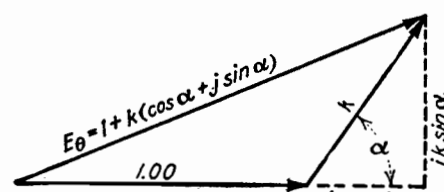


Fig. 3.—When  $\alpha$  is known,  $E_{\theta}$  (the resultant voltage at the observation point) is found by the construction shown here.

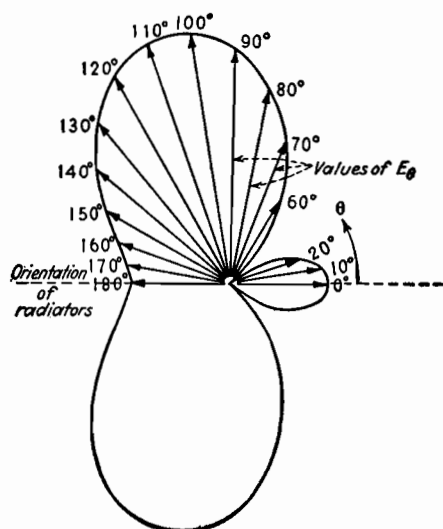


Fig. 4A.—A typical polar plot ( $s' = 180^\circ$ ,  $\phi = -45^\circ$ ,  $k = 1$ ) produced by the method of Figs. 1, 2, and 3.



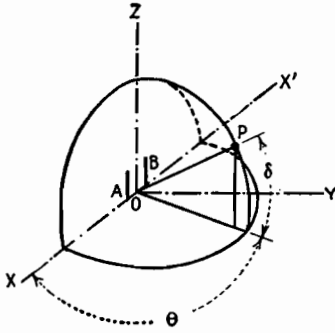


Fig. 8A.—Coordinate system used in computing vertical-plane patterns.

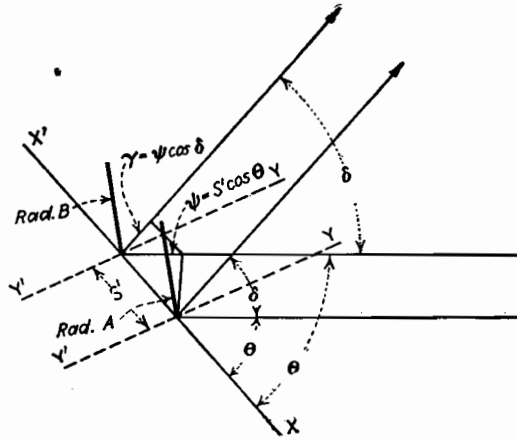


Fig. 8B.—Birdseye view of array showing relation of radiators to observation point.

angles. The pattern for the array, in this plane, is obtained by multiplying the value for  $\theta = 90^\circ$  from Eq. (1) by the values of Eq. (2).

The vertical pattern in this plane can also be determined immediately from inspection of the horizontal pattern.

### The Complete Radiation Pattern

Referring to a suitable spherical coordinate system such as shown in Fig. 8A, the basic geometry for calculating the radiation pattern in any vertical plane is readily developed by the construction of Fig. 8B. From the latter, the following equation is obtained:

$$E_{\theta,\delta} = \{1 + k[\cos(\gamma + \phi) + j(\gamma + \phi)]\} \left\{ \frac{\cos(90^\circ \sin \delta)}{\cos \delta} \right\} \quad (4)$$

In this equation

$E_{\theta,\delta}$  = relative field intensity in directions  $\theta$  and  $\delta$

$k$  = current ratio, as in Eq. (1)

$\gamma$  = total phase difference between radiation vectors A and B due to difference in length of path, and is  $s' \cos \theta \cos \delta$

$\phi$  = initial phase difference of the currents, as in Eq. (1). Equation (2) is used again as a proportionality factor.

The solution of this equation reveals the shape of the space characteristic. One way in which the results of the solution can be plotted for descriptive pur-

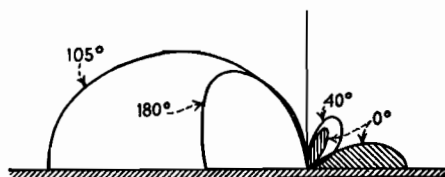


Fig. 9.—Various vertical-plane distributions for the array whose horizontal distribution is shown in Fig. 4A.

poses is shown in Fig. 9, where various vertical patterns in directions of particular interest are drawn.

### Radiation Rules of Thumb

The following notes will be helpful when searching for a suitable radiation characteristic for a particular case:

1. The horizontal pattern is symmetrical with respect to the line through the radiators.

2. When the angle  $\phi$  is either 0 or 180 deg, the horizontal pattern is also symmetrical with respect to a line running normal to the line through the radiators.

3. The three-dimensional pattern is also symmetrical with respect to the line through the radiators.

4. When  $\phi$  is either 0 or 180 deg, the three-dimensional pattern is also symmetrical with respect to the line drawn normal to the line through the radiators.

5. When  $k = 1.00$ , the nulls are directions of zero radiation.

6. When  $k$  is other than unity, the nulls occur at the same angles as in the case of  $k = 1.00$ , but are directions of minimum (not zero) radiation. In the same manner, the maxima are reduced. As the current in one antenna approaches zero, the other current amplitude remaining constant, the horizontal pattern degenerates into a circle.

7. Where there is suppression of radiation along the ground in the line of the radiators, there will be one or more maxima at high angles in that direction.

8. Where a maximum occurs along the ground in the line of the radiators, the vertical pattern in that direction is flatter than that of one radiator alone.

9. Where radiation is suppressed in a direction normal to the line through the radiators, proportional suppression occurs in the vertical plane in that direction.

10. No parts of the radiation pattern extend beyond the limits of the solid of revolution made by rotating the vertical pattern on the line normal to that through the radiators ( $\theta = 90^\circ$ ) about the geometrical center of the array. Maxima approach this surface as a limit wherever they occur.

### Practical Applications of Directional Arrays

In broadcasting, the attempt is made to suppress high-angle radiation to reduce fading. To achieve this with single vertical radiators, it is necessary to build very high structures. Greater suppression of high-angle radiations in two opposite directions can be had by using two radiators with a considerable spacing and proper phasing of the radiator currents. The result is a directive radiating system, but there may arise situations where the undesired horizontal directivity could be tolerated for large-scale high-angle suppression in the favored directions.

Figure 6 is an example, it being the case of two radiators spaced one wavelength with equal cophased currents. The horizontal pattern is shown, together with the vertical pattern in the plane through the radiators and the vertical pattern for one radiator. In the high angles which have the greatest influence on short-range fading, those between 45 and 90 deg, there is a high degree of suppression. A "blind spot" occurs at approximately 60 deg. The extreme inclination of the small high-angle lobe is such as to be of small consequence or negligible, especially in regions of medium or high soil conductivity. Radiation sidewise has the same distribution as one of the radiators, and is also entirely useful. In the directions of the nulls and for a few degrees each side of them, mostly high-angle radiation would be had, and this would be of no value for primary service. In occasional cases where geographical conditions would permit, this attack on the high-angle radiation problem might have some economic advantages over a single high radiator.

An example of a directly opposite case, where the use of two radiators gives generally inferior radiation characteristics, so far as ground-wave coverage and fading are concerned, is that where two radiators spaced  $\frac{1}{2}$  wavelength, with equal cophased currents, are used.

### Protecting One Direction Only

When radiation is to be suppressed in one direction only, one is confined to the

use of some form of cardioid pattern. With two radiators, spaced not more than approximately  $\frac{3}{8}$  wavelength, and properly phased, variously proportioned cardioid patterns can be obtained. A single null direction is desired when the service area of a station lies very nearly round about it and but one direction has to be protected. One unfortunate characteristic of all cardioids is that the null in the ground pattern comes in the line through the radiators, and therefore a lobe of high-angle radiation in the same direction results. This undesired lobe may prove troublesome in the service areas of co-channel stations at moderate distances in that direction, and does not permit complete suppression. Figure 7 shows a  $\lambda/4$  ( $90^\circ$ ),  $\phi = 270^\circ$  couplet cardioid pattern for  $k = 1.00$  and  $k = 0.75$ , and the resulting vertical patterns in the plane through the radiators.

When it is desired to suppress simultaneously radiations in two directions, the problem narrows somewhat at the start to those combinations of spacing and phasing which bring the nulls on the desired bearings. The angle between the two directions to be protected, from the proposed location, must first be determined. Call this angle  $\beta$ . In the patterns that have but two null directions, the orientation of the array must be that of the bisector of the angle  $\beta$ . The spacing and phasing for two radiators, to bring two nulls at the desired angles, can be found from the following equation:

$$\phi = 180^\circ - s' \cos \frac{\beta}{2}$$

where  $\phi$  = phase difference between the antenna currents

$s'$  = spacing between radiators, electrical degrees

$\beta/2$  = angle between a null and the line through the radiators

In many cases it will be found that several space-phase combinations will bring proper bearing of the nulls.

When dependence is placed on a directive array for effective suppression or elimination of radiation in some direction, the space pattern must be stable. Small changes in the phase angle between the radiator currents cause shifts in the null directions. Some patterns are more sensitive than others to the effects of small phase shifts, which may be due to changes in ground conditions, mistuning, etc. It is well to investigate this matter at the time of designing an array by calculating the change in pattern due to small changes in phase. Such a calculation is exhibited in Fig. 10.

Kear and Roder have described methods that are capable of automatically compensating for natural variations in an array, within moderate limits, thus stabilizing the radiation pattern.<sup>2,3</sup> However, such precautions are required only in the most particular broadcast application.

The effect of side-band frequencies in the directive array may be noticeable sometimes in the vicinity of a sharp null, though it will be seldom of importance at broadcast frequencies. Nevertheless the side-band frequencies farthest removed from the carrier work into different impedances from those at the carrier fre-

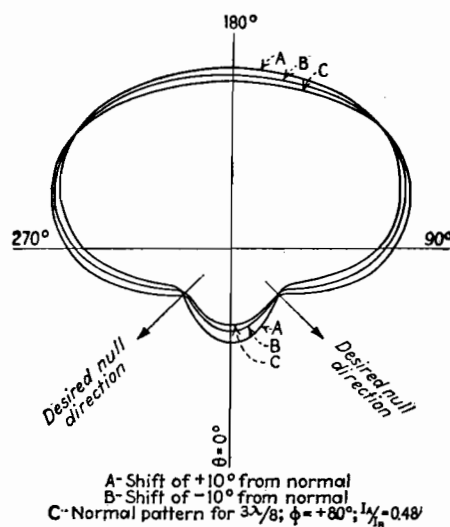


Fig. 10.—Changes in horizontal pattern due to shifts in phase between the antenna currents, which are sometimes difficult to control in practice.

quency, with consequent slight departures from the phase relations, current ratio, and electrical spacing for the latter. With modulation, therefore, we must visualize a faint quivering in the shape of the radiation pattern. The lower the carrier frequency and the higher the modulating frequency, the greater is the deformation of the radiation pattern during modulation.

#### References

- (1) FOSTER, R. M., *Nat. Bur. Standards Tech. Jour.*, April, 1926.
- (2) SOUTHWORTH, G. M. *Proc. I.R.E.* September, 1931. "Radio Engineering Handbook," 2d ed., pp. 744-745, McGraw-Hill Book Company, Inc., New York, 1935.
- (3) KEAR, F. G., *Proc. I.R.E.*, July, 1934.
- (4) RODER, H., *Proc. I.R.E.*, March, 1934.

## Directional Radiation Patterns of Two-element Vertical Antenna Arrays

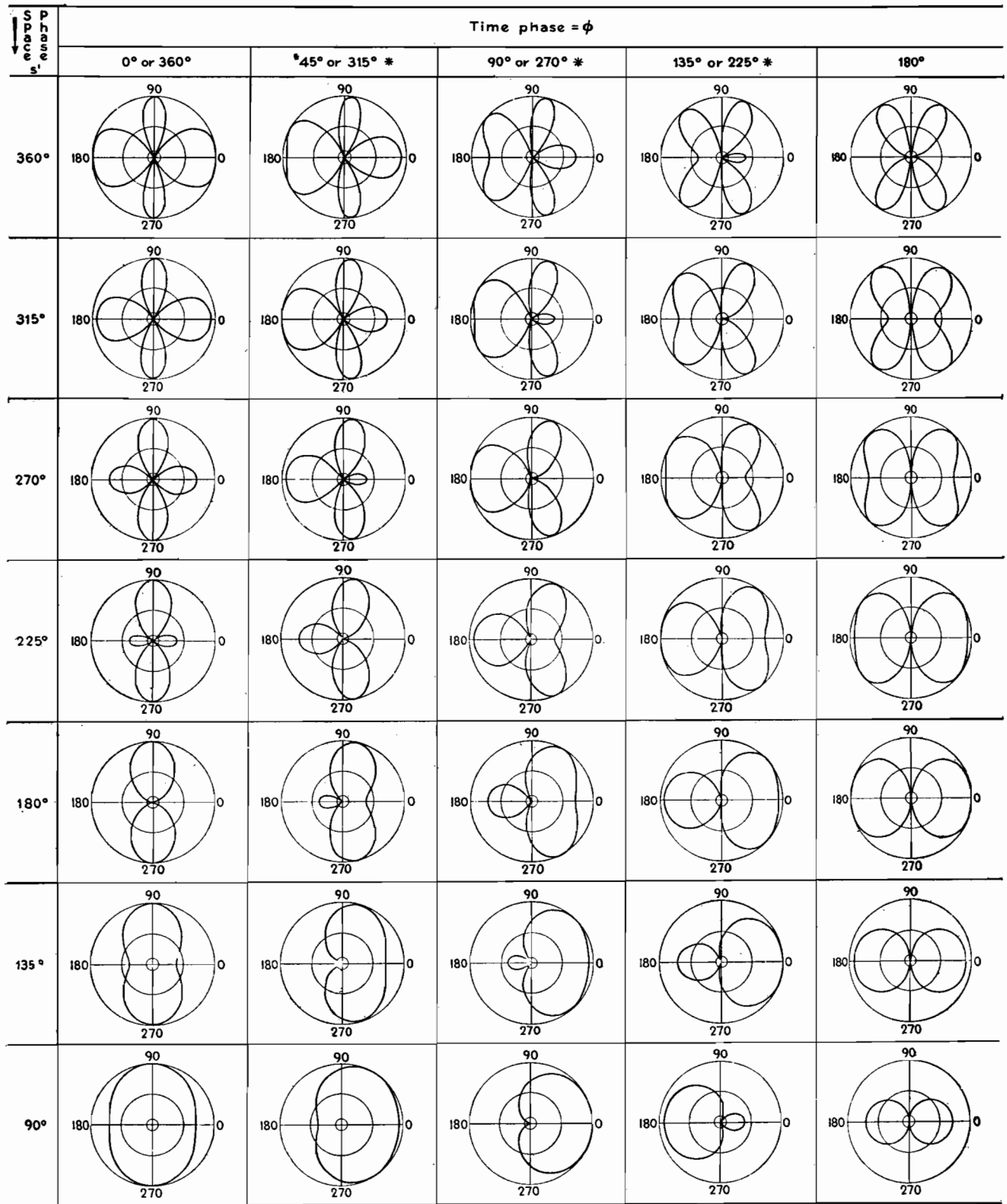
By A. JAMES EBEL

The chart shows the various horizontal signal distributions possible from two-element directional antennas with different current phasing and spacing arrangements, assuming equal maximum current amplitudes in the two radiators

A TWO-ELEMENT directional array consists of a pair of vertical radiators, both of which are radiating energy of the same frequency at the same time. Un-

der these conditions, the energy from one radiator interferes with the energy from the other, the amount of interference depending on the direction relative to the

axis of the array. The result is a directional characteristic that can be made use of in directing the bulk of the signal where it will do the most good. The



\* For  $315^\circ$ ,  $270^\circ$ , and  $225^\circ$  time phase, reverse given pattern from left to right

Fig. 1.—Horizontal signal distributions of two-element directional antenna arrays, arranged according to space phasing  $s'$  and time phasing  $\phi$ .



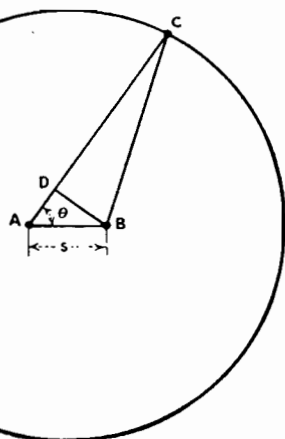


Fig. 2.—Relation of observation point *C* to radiators *A* and *B*.

usual way of representing the horizontal distribution of the signal voltage is to specify the signal strength at various points on a circle surrounding the array and to make a polar plot of these signal strengths. Figure 1 includes 35 such plots, each representing a different combination of space and time phasing.

The space phase  $s'$  is the number of electrical degrees separating the two radiators. If  $s$  is the actual distance separating them, then  $s' = 360^\circ s/\lambda$ , where  $\lambda$  is the wavelength of the radiation in the same units (usually meters) as  $s$ .

The meaning of the space phase can be seen in Fig. 2. *A* and *B* are the two radiators, *C* is a point on the circle surrounding the array, and *D* is a point such that  $DC = BC$ . If  $AB$  is small compared with the radius of the circle, then  $AD = s' \cos \theta$ , which, being expressed in electrical degrees, gives the phase difference between the lengths of the paths from *A* and *B* to *C*.

The total phase difference between the two voltages arriving at point *C* is made up of this space phase and a time phase. The latter is the original difference in phase between the two currents fed to the two radiators. If radiator *B* is fed  $\phi$  deg out of phase with respect to radiator *A* with a lagging voltage, then the total phase difference is  $(s' \cos \theta) = \phi$ .

To determine the vector sum of the voltages at point *C*, which is of course the signal strength at that point, the magnitudes of the voltages must be known in addition to the phase difference between them. It is assumed for the purpose of the chart that the maximum values of the currents in the two radiators are the same, and that, therefore, the magnitudes of the two voltages at point *C* are approximately the same, since  $AC$  is approximately equal to  $BC$ . To show the relative signal strength, therefore, we can

assume that the magnitude of the two vector voltage components is unity and their phase difference is  $(s' \cos \theta) - \phi$ . The magnitude of their sum  $E_c$ , the resultant signal strength at point *C*, then becomes

$$E_c = 2 \cos \frac{(s' \cos \theta) - \phi}{2}$$

$E_c$  can then be plotted as a function of  $\theta$  in polar coordinates, but the form of the resultant signal distribution depends on  $s'$ , a constant depending on physical dimensions and wavelength, and  $\phi$ , also a constant depending on how the radiators are fed. By choosing different discrete values of these two constants, a group of plots of  $E_c$  against  $\theta$  can be made. This procedure has been carried out in preparing the chart.

To aid in plotting, the values of  $\theta$  at which  $E_c$  becomes zero and at which it becomes maximum may be calculated by the use of the following expressions:

$$\theta_0 = \cos^{-1} \frac{k_e 180^\circ + \phi}{s'}, \text{ for } E_c = 0$$

$$\theta_{\max} = \frac{\cos^{-1} k_o 180^\circ + \phi}{s'},$$

for  $E_c = \text{maximum}$

where  $k_e$  is an even integer and  $k_o$  is any odd integer such that  $\theta$  does not exceed  $360^\circ$ .

## Antenna Power Divider

By EARLE TRAVIS

Chart facilitates finding correct values of  $L$  and  $C$  for any desired division of currents in a two-element broadcast array, with constant phase shift and constant resistive input

A SIMPLE power divider for a two-element broadcast antenna array can be built from the basic circuit shown in Fig. 1. Here resistors  $R$  represent actual measured values of characteristic impedance for the two transmission lines and must be equal, while  $L$  and  $C$  are variable and allow for any power division desired. As long as the correct relationships are maintained, the input impedance will be resistive and of a constant value, and, most important, the phase shift between lines will remain constant. This means that the operator can vary tower current without having to change phasing adjustments.

The required relationships are that  $X_L X_C$  always be equal to  $R^2$  and that  $Z_B/Z_A$  always be equal to the current ratio  $K$ , which is equal to the square root of the power ratio.

By means of the chart in Fig. 2, it is possible to observe these relationships automatically and find quickly the values of  $X_L$  and  $X_C$  for any current ratio desired. The chart gives the cosine value for each series circuit. From this, the angle and its tangent can be found in a trigonometry table and the reactance value of each branch computed from  $X_A = R \tan A$  and  $X_B = R \tan B$ . Knowing the operating frequency,  $L$  and

$C$  are computed from  $L = X_A/2\pi f$  and  $C = 1/2\pi f X_B$ .

Usually it is best to let cosine  $B$  be negative so that branch  $B$  is capacitive. This allows for smaller units, but the capacitor must withstand fairly high voltage. In the case of high power it might be better to let cosine  $B$  be positive so its circuit is inductive. This will call for larger units, but the capacitor will not have to withstand such high voltage.

**Example.**—Operating frequency is 1,000 kc, current ratio is 3:1, and  $R$  is 230 ohms. For a current ratio of 3:1, the chart gives a value of 0.950 for  $\cos A$ , and a trigonometry table is then used to find

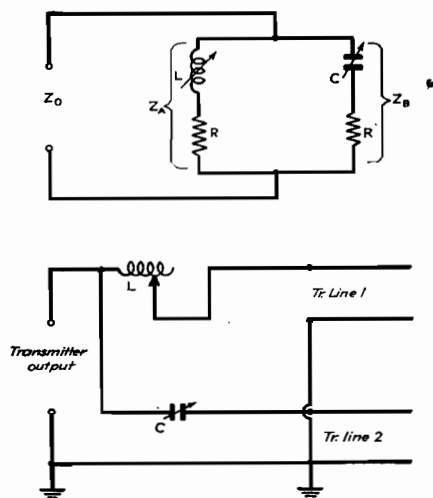


Fig. 1.—Basic power-dividing circuit, with transmission lines represented by  $R$ , and actual circuit.

$\tan A = 0.3284$ . Similarly,  $\cos B = 0.312$  and  $\tan B = 3.044$ . Substituting in  $X_A = R \tan A$ ,  $X_A = 230 \times 0.3284 = 75.51$  ohms. Similarly,  $X_B = 230 \times 3.044 = 700$  ohms. Allowing  $X_B$  to be capacitive,  $C = 1/6.28 \times 1,000,000 \times$

$700 = 227.5 \mu\text{f}$ .  $X_A$  is then inductive, and  $L = 75.51/6.28 \times 1,000,000 = 12 \mu\text{h}$ . The alternate solution with  $X_A$  capacitive and  $X_B$  inductive gives  $C = 0.0021 \mu\text{f}$  and  $L = 111.4 \mu\text{h}$ .

The vector diagrams in Fig. 3 cover three

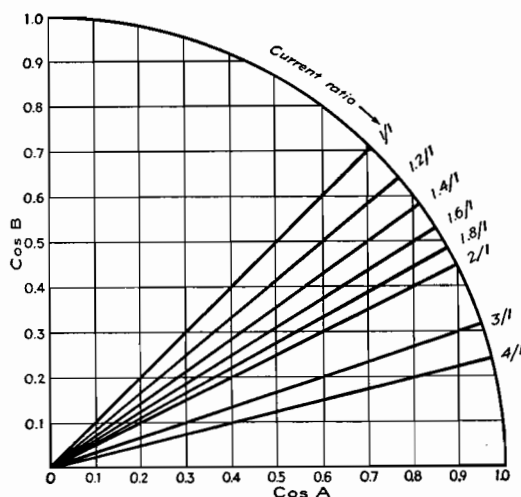


Fig. 2.—Cosine values for finding  $L$  and  $C$  are at intersection of curve with line for desired current ratio.

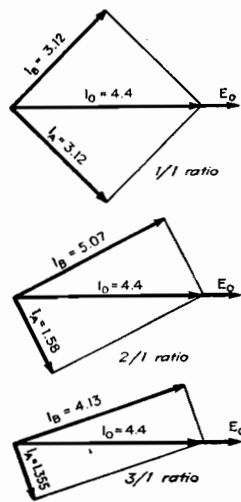


Fig. 3.—Vector diagrams showing that input of circuit is always constant and resistive.

## Computing Performance of Two-tower Directional Arrays

By A. R. RUMBLE

A method for computing the performance of directional arrays and comparing it with the performance of a single vertical radiator of the same height, useful in planning improvements in broadcast radiation systems

THE design of a directional antenna array involves two important factors, the shape of the pattern and the absolute magnitude of the signal strength contours in the pattern. E. A. Laport has previously shown<sup>1</sup> how to calculate the shape of the directional pattern of an array of two vertical grounded radiators. However, his patterns are relative only, and therefore provide no comparison (except shape) between different arrays, or between an array and a single radiator. The purpose here is to show how to extend the usefulness of the method he uses, so as to provide comparisons.

The usual assumptions are made *i.e.*, each radiator is a vertical wire with its

lower end very near a ground of perfect conductivity. Here, as in Laport's article, we shall deal only with arrays composed of radiators of equal height. The field strength of an array will be expressed in terms of the field strength of a single radiator of the same height with the same total power input. Thus we have a direct comparison of the performance of an array and a single tower, or between two arrays.

For purposes of comparison, the horizontal pattern of one radiator alone (*i.e.*, not in the presence of other conductors) will be a circle of unit radius. If the absolute radius of this circle in millivolts per meter at 1 mile is desired, it can be

determined from previously published data.<sup>2</sup> However, for comparison purposes this radius will be unity.

When operating two radiators near each other, the current in each will induce a voltage in the other. The problem then is to determine the total current in each radiator. It is not necessary to determine the actual current, but merely the ratio of current in one element of an array to the current in a single radiator alone with the same total input power as the array.

The following symbols will be used. The element with the greatest current will be designated as element 1.



$I$  = current in single radiator when used alone  
 $I_1$  = current in element 1 of the array  
 $I_2$  = current in element 2 of the array  
 $k$  = ratio of the magnitude of  $I_2$  to  $I_1$   
 $\phi$  = phase angle of  $I_2$  with respect to  $I_1$   
 $Z_{r1} = R_r + jX_{r1}$  = self-impedance of element 1 alone  
 $Z_{r2} = R_r + jX_{r2}$  = self-impedance of No. 2 alone.  $X_{r1}$  and  $X_{r2}$  consist of self reactance plus any loading reactance in each antenna  
 $Z_m = R_m + jX_m$  = mutual impedance between the two elements  
 $Z_1 = R_1 + jX_1$  = total effective impedance of element 1  
 $Z_2 = R_1 + jX_2$  = total effective impedance of element 2

By definition

$$I_2 = kI_1$$

$$I_2 = kI_1(\cos \phi \pm j \sin \phi)$$

And since power in array = power in single radiator alone,

$$I_1^2 R_1 + I_2^2 R_2 = I^2 R_r$$

And by Kirchhoff's laws

$$E_1 = I_1 Z_{r1} + I_2 Z_m$$

$$E_2 = I_2 Z_{r2} + I_1 Z_m$$

Combining the above equations and solving for their current ratio

$$\frac{I_1}{I} = \sqrt{\frac{1}{1 + k^2 + 2k \frac{R_m}{R_r} \cos \phi}}$$

In Laport's equations  $I_1/I$  is always unity. By multiplying his equations by the above correction factor we obtain equations that give a comparison between the performance of a two-element and a single radiator of the same height.

#### Horizontal Pattern

$$E_\theta = \sqrt{\frac{1}{1 + k^2 + 2k \frac{R_m}{R_r} \cos \phi}} \times \sqrt{1 + k^2 + 2k \cos \alpha}$$

#### Vertical Pattern

$$E_{\theta, \delta} = \sqrt{\frac{1}{1 + k^2 + 2k \frac{R_m}{R_r} \cos \phi}} \left[ \frac{\cos(A \sin \delta) - \cos A}{\cos \delta} \right] \sqrt{1 + k^2 + 2k \cos(\gamma + \phi)}$$

where  $\alpha = s' \cos \theta + \phi$

$s'$  = spacing of elements, electrical degrees or radians

$\theta$  = azimuth angle with respect to the line of the two elements. In same units as  $s'$  and  $\phi$

$A$  = height of the two elements, electrical degrees or radians

$\gamma = s'(\cos \theta)(\cos \delta)$  = phase difference due to difference in lengths of paths of two radiations

These are the same units as used in Laport's article except that he dealt only with quarter-wave elements where  $A = 90^\circ$ .

#### Determination of $R_m/R_r$

Values of  $R_m/R_r$  for spacings up to one wavelength of heights of  $\lambda/4$ ,  $3\lambda/8$ , and  $0.528\lambda$  (190 deg) are plotted in Fig. 1. For other heights and spacings approximate values may be estimated from the curves, and exact values may be calculated from the following formulas by G. H. Brown.<sup>3</sup>

#### Example

As an example of the use of this method, suppose it is desired to determine the field strength at right angles to the line of the towers of two quarter-wave towers spaced  $0.7\lambda$  with currents equal and in phase.

$$s' = 0.7 \times 360 = 252^\circ$$

$$\phi = 0$$

$$\alpha = 252 \cos 90 + 0 = 0$$

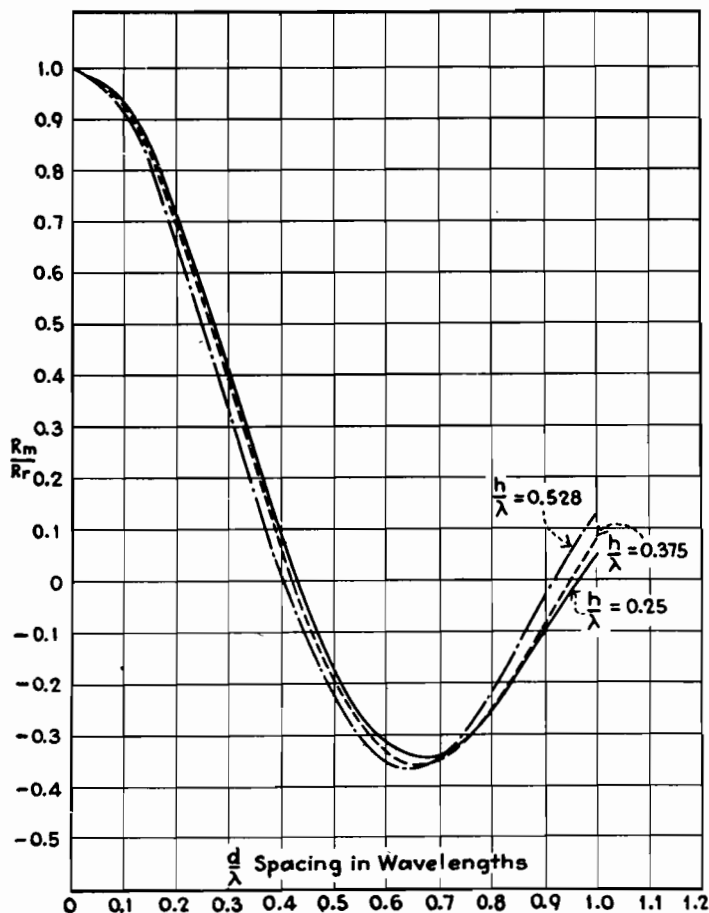


Fig. 1.—Ratio of mutual resistance to self-resistance of two vertical grounded radiators.

$\delta$  = angle of elevation above ground.  
 Same units as other angles

$$\frac{R_m}{R_r} = -0.338$$

$$E_{90} = \sqrt{\frac{1}{1 + 1 + (2 \times 0.338 \times 1)}} \times \sqrt{(1 + 1^2 + 2 \cos 0)}$$

$$= 0.87 \times 2 = 1.74$$

This means that in this direction 74 per cent greater field strength will be obtained than if the same power is used in a single radiator alone. If the absolute theoretical field strength is desired, it is found by determining the field strength of a single radiator alone and multiplying by the above factor. It can be found from the article<sup>2</sup> to which previous reference is made that the theoretical field strength of a quarter-wave vertical grounded radiator is

$$6.2 \text{ mv/meter}/\sqrt{\text{watt}} \text{ at 1 mile}$$

Multiplying this by the above factor gives the theoretical field strength of the array in this direction

$$10.8 \text{ mv/meter}/\sqrt{\text{watt}} \text{ at 1 mile}$$

The power gain of the array is

$$E_{90}^2 = 1.74^2 = 3.02$$

This indicates that using the array gives

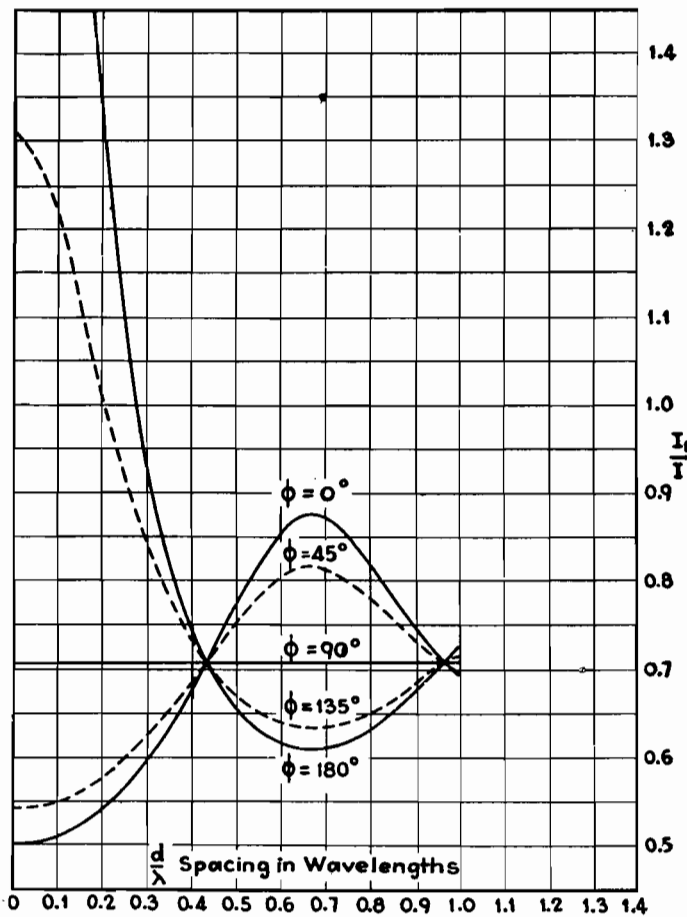


Fig. 2.—Correction factor for two quarter-wave radiators.

an increase of field strength in this direction equivalent to tripling the power in the single radiator. Incidentally this figure checks with the figure given by P. S. Carter<sup>5</sup> for the power gain of two half-wave dipoles in free space, which corresponds to two quarter-wave grounded radiators.

It is only necessary to calculate the

factor once for each complete pattern. Each radius of the pattern is multiplied by the factor. Figure 2 shows how the correction factor varies with spacing and phase angle for two quarter-wave elements with equal currents. There are several points of interest on these curves. At very large spacings there is no appreciable coupling between the two elements

and  $R_m$  approaches zero. If either  $R_m$  or  $\cos \phi = 0$ , then

$$\left(\frac{I_1}{I}\right) = \sqrt{\frac{1}{1+k^2}}$$

and if  $K = 1$

$$\left(\frac{I_1}{I}\right) = 0.707$$

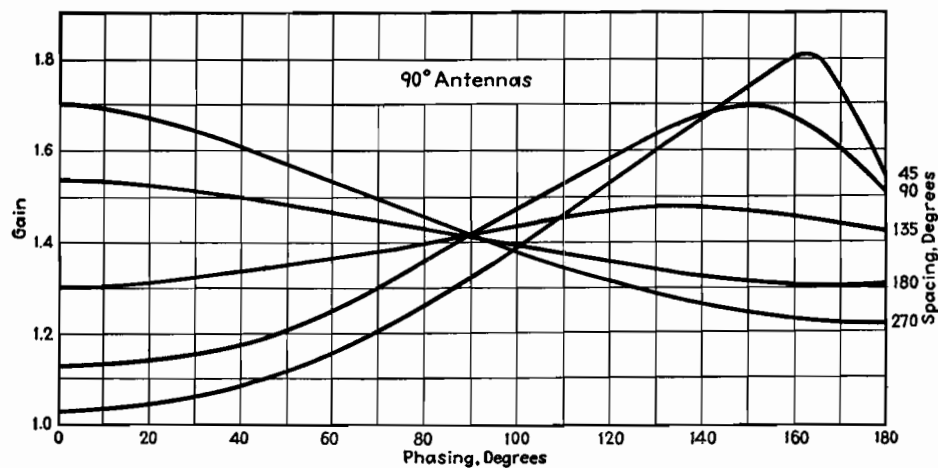
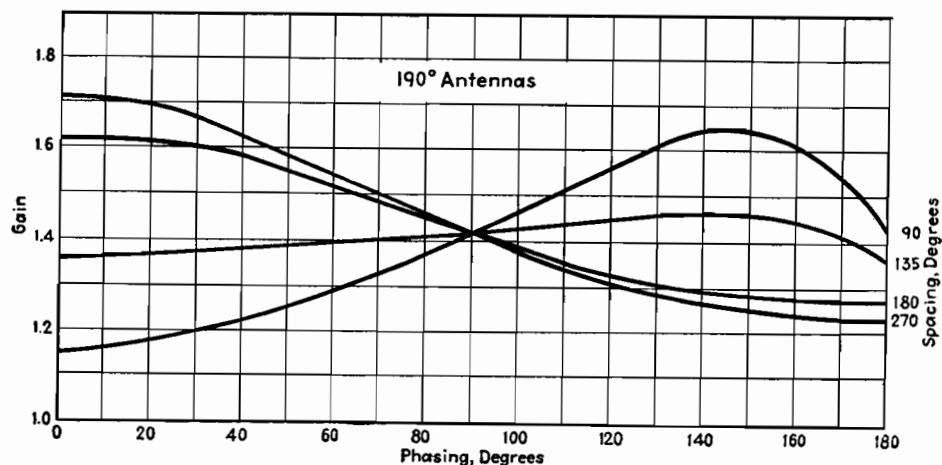
Notice that all the curves are approaching this value at large spacings. At approximately  $0.43\lambda$ , spacing  $R_m$  also equals zero for the quarter-wave elements. At this spacing the only coupling between the elements is purely reactive. Therefore all the curves pass through the point  $0.43\lambda, 0.707$ . The  $\phi = 90^\circ$  curve is constant at 0.707 since the two currents are in quadrature and there is no real component of induced current, and as far as power radiation is concerned each element acts as though the other were not present. Therefore for  $\phi = 90^\circ$  the correction factor depends only on  $k$  and is independent of the height and spacing. The correction factor gives direct comparisons between arrays of the same height. To compare systems of different heights, it will be necessary to determine the actual theoretical field strength as explained previously. The principles applied here could be extended to arrays of more than two elements, but the calculations would probably be rather laborious.

#### References

- (1) *Electronics*, April, 1936, p. 22.
- (2) BROWN, G. H., *Proc. IRE*, January, 1936, p. 53, Fig. 5.
- (3) BROWN, G. H. and KING, ROWOLD, *Proc. IRE* April, 1934, Eq. 7 and reference 2 above (Eq. 7).
- (4) JANKE and EMDE, "Funktionentafeln mit Formeln und Kurven."
- (5) *Proc. IRE*, June, 1932, p. 1019, Fig. 14.

# Voltage Gain Charts for Two-antenna Arrays

By WILLIAM S. DUTTERA



These charts show the voltage gain that may be derived from a two-antenna array when the antennas carry equal currents and are both 90 deg (one-quarter wavelength) high or are both 190 deg high. The voltage gain is the ratio of the maximum directional ground-signal intensity to the nondirectional ground-signal intensity from a similar antenna. The voltage gain is shown as a function of the phasing for various spacings. The approximate gain for other spacings may be found by interpolation or may be computed. The actual gain obtained will of course depend upon the loss in the system and allowance must be made for this loss.

# Field-strength Prediction Charts Based on Sommerfeld's Formula

By WILLIAM A. FITCH

Simplifications to the Sommerfeld formula (field strength at a distance from a broadcast-frequency transmitter) that make it easier to work with and that do not introduce appreciable error

PRIOR to 1930 the Austin-Cohen formula had been in general use for studies of radio transmission. The formula has the advantage of simplicity but was found to be inaccurate for predicting field strengths at a distance, especially for high fre-

quencies, or even medium frequencies over poor soil.

At about this time a number of papers began to appear dealing with the Sommerfeld formula, and results were shown that agreed much more closely with actual

measurements than the Austin-Cohen formula. However, the use of Sommerfeld's theory has not been widespread owing probably to these two reasons: (1) The Sommerfeld formula itself is not so simple as the convenient exponential

Fig. 2.—Attenuation curves for soil having conductivity of  $\sigma = 100 \times 10^{-15}$  emu and inductivity of 14 esu; inverse field strength at 1 mile = 1,000 mv.

Fig. 1.—Conversion chart for soils other than  $\sigma = 100 \times 10^{-15}$  emu.

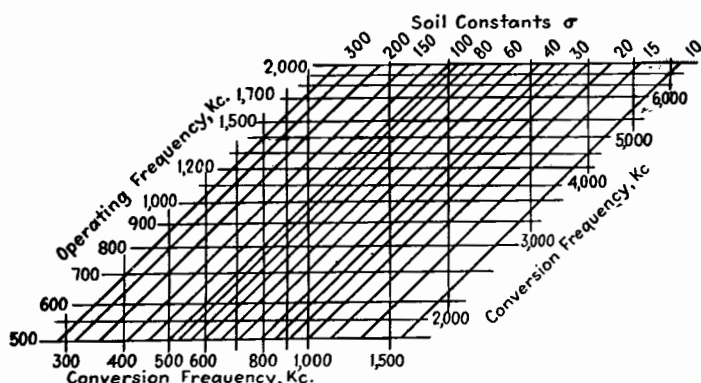


Fig. 3.—Error involved in using simplified method for soils having different conductivity than  $100 \times 10^{-15}$  emu.

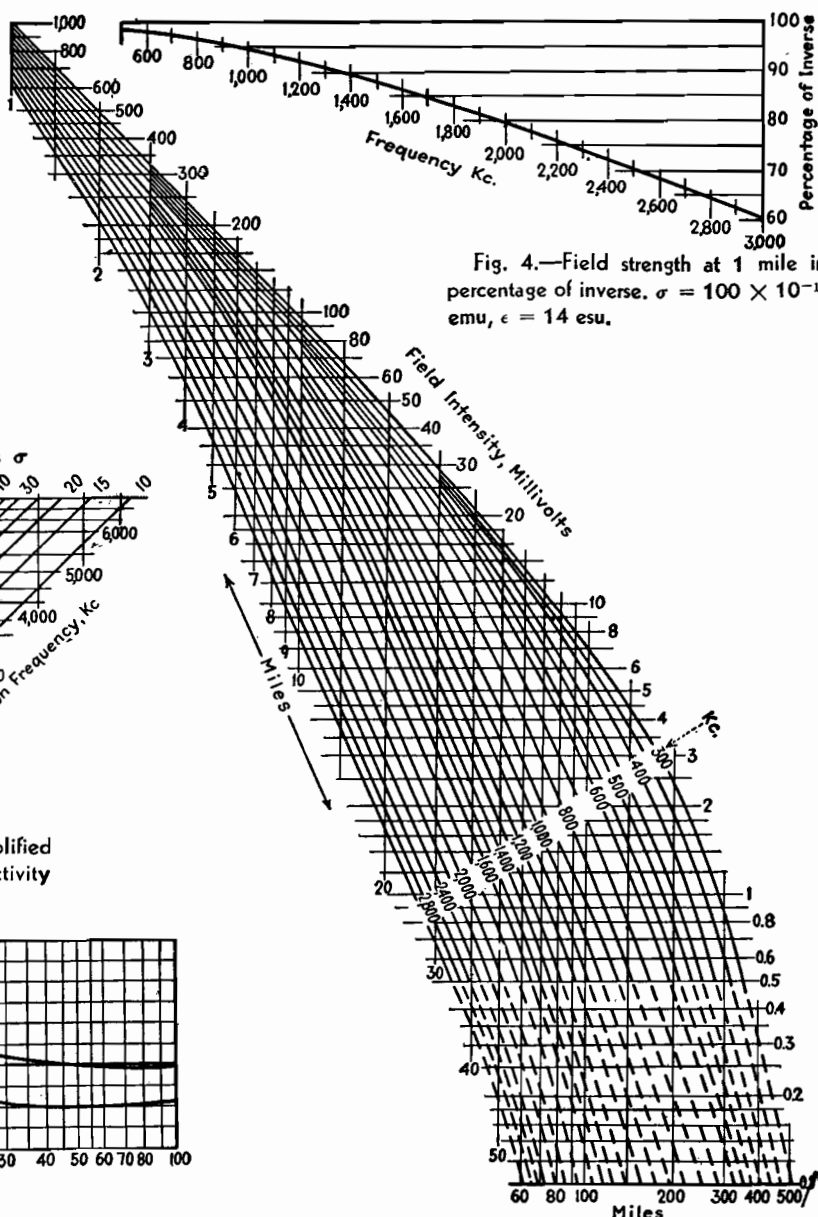
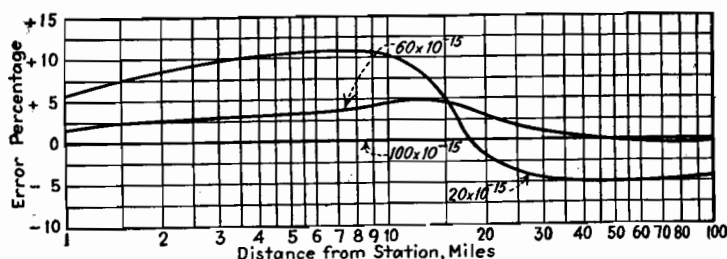


Fig. 5.—Distance to  $\frac{1}{2}$  mv contours:  $\sigma = 100 \times 10^{-15}$  emu,  $\epsilon = 14$  esu.

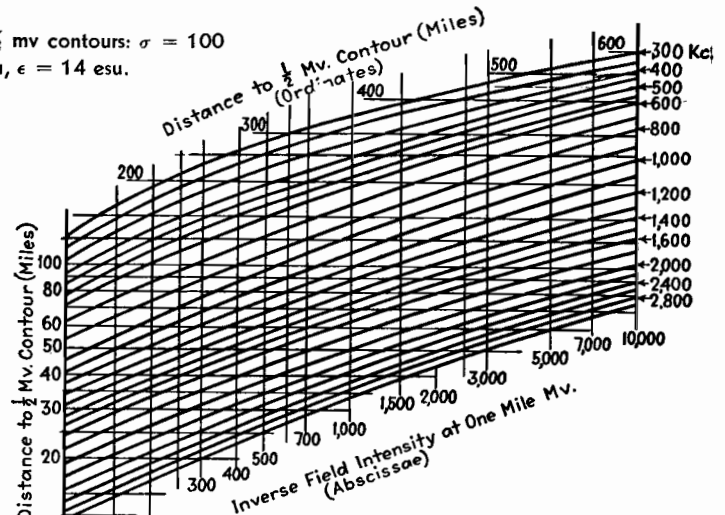
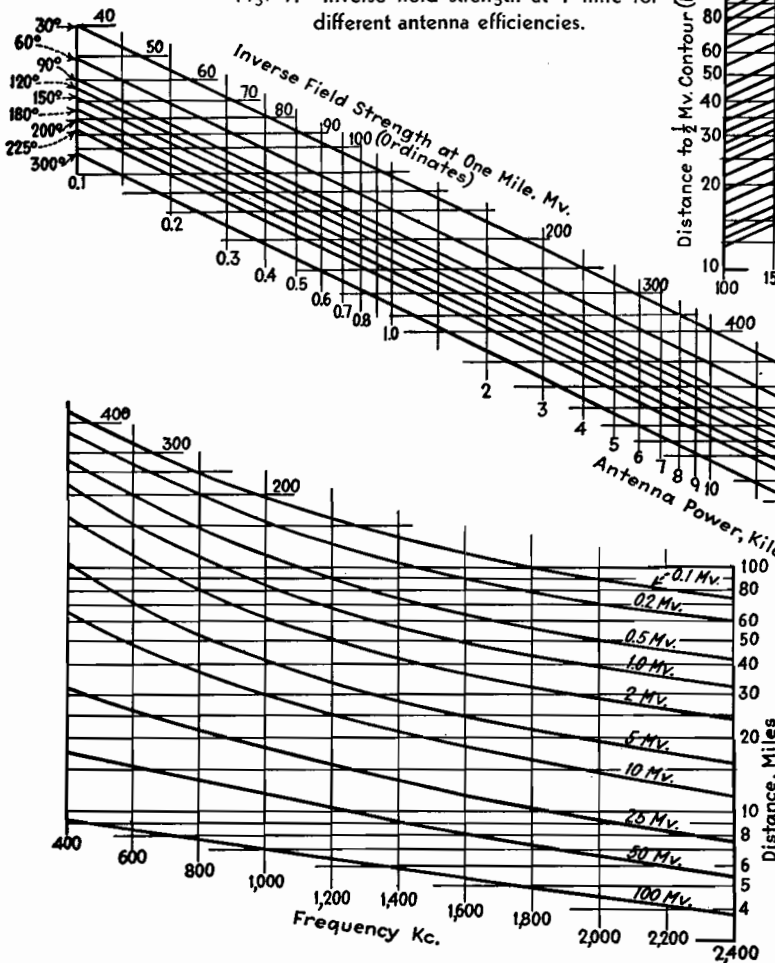
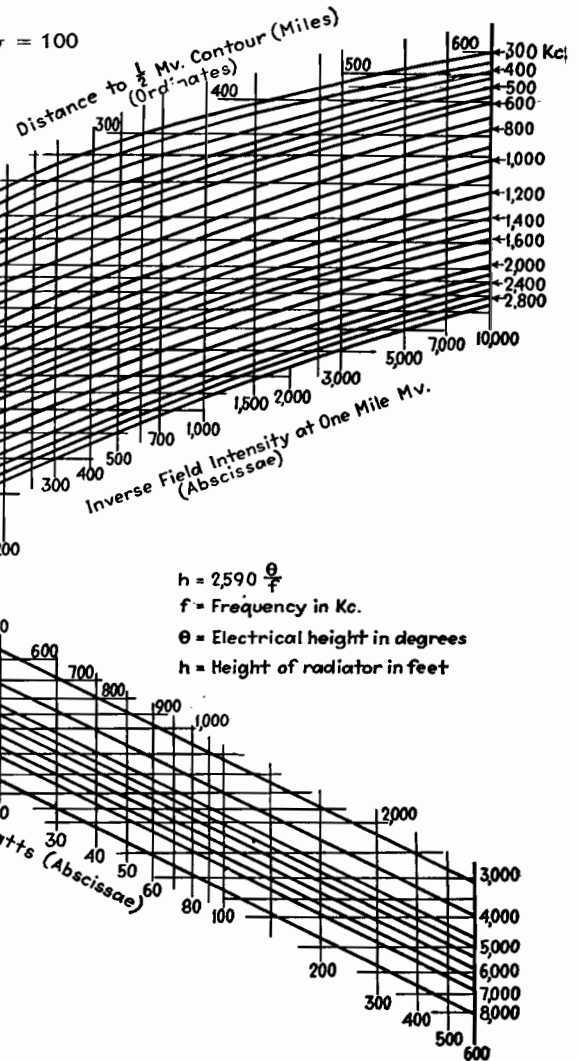


Fig. 7.—Inverse field strength at 1 mile for different antenna efficiencies.



$h = 2590 \frac{\theta}{f}$   
 $f$  = Frequency in Kc.  
 $\theta$  = Electrical height in degrees  
 $h$  = Height of radiator in feet

Fig. 6.—Distance to field intensity contours for 1,000 mv inverse at 1 mile.  $\sigma = 100 \times 10^{-15}$  emu,  $\epsilon = 14$  esu.



Austin-Cohen formula. (2) Sommerfeld uses an extra variable which he calls  $\epsilon$ , representing the inductivity or dielectric constant of the soil.

It is the purpose here to point out certain simplifications that may be used with the Sommerfeld formula without introducing an appreciable error, and to present propagation curves and charts based on these simplifications.

The dielectric constant of soils in this country varies all the way from 5 to about 30. The dielectric constant of water is 80. A good average for most of the soil in the country is 14. This has been used for the charts presented in this article. The error introduced is not of much consequence if only broadcast frequencies are considered.

The other simplification consists of the

elimination of  $\sigma$  (which represents the soil conductivity) as a variable. This may be done if we pick some standard of conductivity and refer all other conductivities to the standard by simply changing the frequency according to the following formula:

$$f_1 = f \sqrt{\sigma / \sigma_1}$$

$f$  = operating frequency  
 $\sigma$  = standard conductivity of chart (assumed to be  $100 \times 10^{-15}$  emu)  
 $\sigma_1$  = actual soil conductivity  
 $f_1$  = conversion frequency

This formula has been plotted in the form of a chart and is shown in Fig. 1. Its use is best explained by an example: If we wanted to find the conversion frequency for a soil constant of  $50 \times 10^{-15}$  emu and an operating frequency of 700 kc,

referring to Fig. 1 we see that a frequency of 1,000 kc and soil constant of  $100 \times 10^{-15}$  emu is equivalent to 700 kc and a soil of  $50 \times 10^{-15}$  emu. A similar chart has previously been prepared by Eckersley,<sup>1</sup> but he used the wavelength instead of frequency as the parameter.

Figure 2 shows a field strength vs. distance chart for a family of frequencies from 300 to 3,000 kc. It is based on a standard conductivity of  $100 \times 10^{-15}$  emu and dielectric constant of 14 esu and inverse field strength at one mile of 1,000 mv. The actual calculation of such a chart has been described in previous papers, and the method followed was that outlined by Rolf.<sup>2</sup> The error pointed out in Rolf's curves by K. H. Norton<sup>3</sup> was corrected. Beyond about 150 miles for the low frequencies and about 60 miles for the

high frequencies, it is necessary to include an earth-curvature correction because Sommerfeld's theory is based on a flat earth. G. N. Watson<sup>4</sup> and others<sup>5</sup> have calculated the effect of earth curvature, assuming a perfectly conducting sphere, but little has been published on the effect of imperfect conductivity over spherical earth. The earth-curvature correction used for the curves in Fig. 2 is based on actual field-intensity surveys of stations. The dotted lines near the bottom of the curves were made to indicate that in this region an indirect ray is received in the daytime which causes a slight fading.

An investigation shows that the maximum error involved in using this one family of curves for all soil constants occurs when the conversion formula is used for very poor soils. About the poorest soil that will be found in the United States is  $20 \times 10^{-15}$  emu. This occurs along the Atlantic seaboard. The error incurred in using  $100 \times 10^{-15}$  emu instead of the exact value is slight. It is expressed on a percentage basis in Fig. 3. It is seen that when using the conversion formula for soils having a conductivity of  $60 \times 10^{-15}$  emu the error is less than 5 per cent. For soils between  $60 \times 10^{-15}$  emu and  $100 \times 10^{-15}$  emu, the error will be even less. A maximum error of about 11 per cent occurs when using the conversion formula for soils having a conductivity of  $20 \times 10^{-15}$  emu. Even here the maximum error is restricted to the first 15 miles. Beyond 15 miles, the error is less than 5 per cent.

Figures 4, 5, and 6 were derived from

Fig. 2. Figure 5 is helpful when the distance to the  $\frac{1}{2}$ -mv contour is desired and the inverse field intensity at 1 mile is known.

Figure 6 shows the distance to field-intensity contours from 100 to 1 mv for a fixed inverse field intensity at 1 mile. It shows distinctly the effect of increased attenuation on the higher frequencies. This disadvantage of the higher frequencies may be partially overcome by the use of more efficient antennas and because of the fact that the noise level is less on the higher frequencies.<sup>6</sup>

All curves are referred to the inverse field strength at 1 mile. This is the intensity that would be produced if no attenuation were encountered. It is well known that with most installations the field strength at 1 mile is seldom equal to the theoretical. It may be as low as 60 per cent of the inverse field in the case of a high frequency on poor soil. The amount of attenuation that may be expected in the first mile with different frequencies is shown by Fig. 4.

Figure 7 is useful for finding the inverse field strength at 1 mile for different powers and antenna efficiencies. The curves are based on antenna installations having good ground systems and uniform cross-section radiators. Lower field strength may be expected if these conditions are not met.

By means of these charts, it is possible to solve rapidly almost any propagation problem. A typical problem might be: The distance to the  $\frac{1}{2}$ -mv contour of a station operating on 1,000 kc with 25 kw

power is 72 miles. The antenna is a quarter wave vertical. Find the soil conductivity of the territory served. By using Fig. 7 it is found that the inverse field strength at 1 mile is 940 mv. From Fig. 5 the conversion frequency is found to be 1,400 kc. By using Fig. 1, the conductivity from the transmitter to the  $\frac{1}{2}$ -mv contour is found to be  $50 \times 10^{-15}$  emu. Other uses for these charts will readily suggest themselves.

In practice, the Austin-Cohen curves and the Sommerfeld curves have the same faults: they are applicable only to a fairly uniform terrain and they fail to take account of natural and artificial irregularities that exert a very marked influence on the propagation of waves. Also, measurements of field intensity made at one point vary from day to day. Some of this variation is caused by changes in conductivity and dielectric constant due to changes in weather. Therefore, it seems that the simplifications, although introducing a slight error, are warranted for practical use.

#### References

- (1) ECKERSLEY, T. L., Direct Ray Broadcast Transmission, *Proc. IRE* 20, No. 10, October, 1932.
- (2) ROLF, B., Numerical Discussion of Prof. Sommerfeld's Attenuation Formula for Radio Waves, *Ing. Vetenskaps Akad., Hand.*, No. 96, (1929); also Graphs to Prof. Sommerfeld's Attenuation Formula for Radio Waves, *Proc. IRE*, 18, March, 1930.
- (3) NORTON, K. H., Propagation of Radio Waves over a Plane Earth, *Nature*, June 8, 1935.
- (4) WATSON, G. N., The Diffraction of Electric Waves by the Earth, *Proc. Roy. Soc. (London)*, A, 95, October, 1918.
- (5) BURROWS, CHARLES R., Radio Propagation over Spherical Earth, *Proc. IRE*, 23, No. 5, May, 1935.
- (6) GILLET, G. D., and EAGER, M., Some Engineering and Economic Aspects of Radio Broadcast Coverage, *Proc. IRE* 24, No. 2, February, 1936.

## Radiation Chart for Vertical Antennas

By L. J. GIACOLETTO

FOR several years, radio engineers have occupied themselves with the problem of predicting the strength of the electromagnetic field at a given distance from an antenna.

If a perfectly conducting plane earth is considered, the Hertzian expression for the electromagnetic field produced at a distance  $R$  is

$$E_0 = \frac{K\sqrt{P}}{R} \quad (1)$$

where  $K$  is a factor depending on the antenna design. For a quarter wave-

length vertical antenna,  $K$  is 6.14 if  $E_0$  is in millivolts per meter,  $P$  in watts, and  $R$  in miles. Equation (1) then becomes

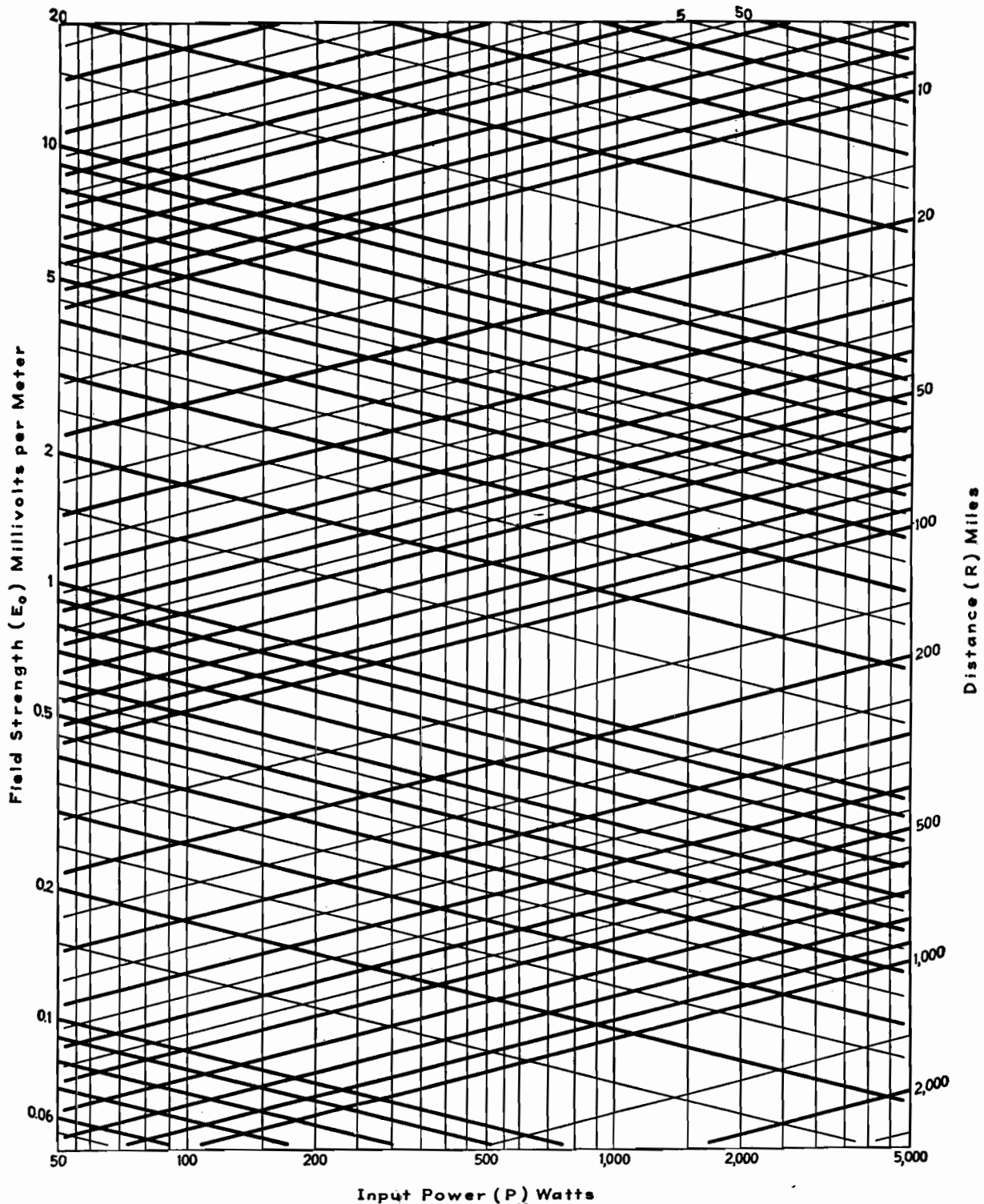
$$E_0 = \frac{6.14\sqrt{P}}{R} \quad (2)$$

The antenna-radiation chart is a plot in triangular logarithmic coordinates of the basic relationship given in Eq. (2).

Effort has been made to cover the range most used in practice. Range extension can be most easily effected by multiplying by powers of 10. Thus if  $P$

is extended by a modulus of 100, and  $R$  by a modulus of 10, the  $E_0$  scale remains unchanged.

The value of  $K$  in Eq. (1) is dependent on the antenna height, and for antenna heights other than one-quarter wave, correction of the radiation chart can be made. For antenna heights of less than one-quarter wave,  $K$  is very closely 5.9, or the value of  $E_0$  found on the radiation chart is to be multiplied by 0.96; for one-half wavelength antenna,  $K$  is 7.45, or  $E_0$  from the chart is to be multiplied by 1.213; for 0.625 wavelength antenna,  $K$  is maximum



equal to 8.6, or  $E_0$  from the chart is to be multiplied by 1.4; for heights above 0.625 wavelength,  $K$  decreases rapidly.

It is true that Eqs. (1) and (2) hold only for a highly idealized case. However, the more exact treatments of the radiation phenomenon introduce only a correction factor to the Hertzian expression of Eq. (1). These more exact solutions can be written in the form

$$E = E_0 A \quad (3)$$

where  $E_0$  is the field strength as obtained from Eq. (1) or (2), and  $A$  is a correction factor.

In the Austin-Cohen formula, the correction factor is

$$A_1 = \epsilon^{-\frac{0.0764R}{\lambda^{0.5}}} \quad (4)$$

where  $\epsilon$  is the natural base (2.72) and  $\lambda$  is the operating wavelength in meters. This correction takes care of the increased attenuation due to currents induced in the

earth of a wave propagated along the ground. A more exact form of the correction was given by L. W. Austin in 1926 as

$$A_2 = \epsilon^{-\frac{0.142R}{\lambda^{0.6}}} \quad (5)$$

A. Sommerfeld has considered the case of propagation of a wave over a plane earth of finite conductivity. The results of this investigation are altogether too complicated for practical application.



Van der Pol has derived an empirical approximation of Sommerfeld's equations for which  $A$  in Eq. (3) is

$$A_3 = \frac{2.0 + 0.3\rho}{2.0 + \rho + 0.6\rho^2} \quad (6)$$

where  $\rho$  is Sommerfeld's numerical distance given approximately by

$$\rho_1 = \frac{8.44 \times 10^{-10} R}{\sigma \lambda^2} = \frac{0.938 \times 10^{-20} f^2 R}{\sigma} \quad (7)$$

where  $\sigma$  = conductivity of the earth, emu  
 $\lambda$  = wavelength, meters  
 $f$  = frequency, kc  
 $R$  = distance, miles

Equation (7) gives the numerical distance quite accurately at low frequencies where the impedance of the earth is primarily resistive. At the high frequencies the impedance of the earth is largely capacitive and the numerical distance is given more exactly by

$$\rho_2 = \frac{0.00505R}{(\xi + 1)\lambda} \quad (8)$$

where  $\xi$  is the dielectric constant of

earth\* assuming air as unity. For  $\rho$  between 5 and 10, a more exact expression for the correction factor is

$$A_4 = \frac{4 + 5\rho}{4 - 16\rho + 10.4\rho^2} \quad (9)$$

For  $\rho$  greater than 10, the correction factor will be given with sufficient accuracy by

$$A_5 = \frac{1}{2\rho} \quad (10)$$

The Sommerfeld analysis neglects entirely the curvature of the earth, and therefore gives calculated field intensities that are slightly too high.

G. N. Watson has studied the propagation of radio waves over a perfectly conducting spherical earth. In his solution, the factor  $A$  in Eq. (3) is

$$A_6 = 0.4558 \frac{R^{1/2}}{\lambda^{1/2}} e^{-\frac{0.0605R}{\lambda^{1/2}}} \quad (11)$$

Watson's formula does not hold for

\* The dielectric constant of soils in this country varies from 5 to about 30, with a good average being 14. The dielectric constant of water is 80.

regions near the transmitter (say within 500 miles). In this region, Sommerfeld's equations will give good results. C. R. Burrows has derived an empirical formula based on Watson's results which will hold up to 8,000 miles. In Burrow's formula the correction factor is

$$A_7 = (1 + 2Z)^{1/2} e^{-Z} \quad (12)$$

where

$$Z = 0.0564 \frac{R}{\lambda^{1/2}} \quad (13)$$

The problem of propagation of radio waves over a spherical earth of finite conductivity has been studied, but as yet only approximate curves are available.

It is seen that the basic radiation formula is the Hertzian expression given in Eqs. (1) and (2) and graphed on the radiation chart. To this basic equation is added a correction factor whose value depends on the degree of approximation desired. The formulas do, however, serve a very useful purpose in engineering work, and, whenever necessary, the computations can be checked with field-intensity surveys.

## Design Procedure for Ground-plane Antennas

By H. W. HASENBECK

The addition of a turnstile element to a v-h-f vertical antenna lowers the angle of radiation. This paper develops the basic formulas for designing such a ground-plane antenna. An example is worked out for a 78-ohm termination at 33.78 Mc

A VERTICAL antenna located several wavelengths aboveground does not display the low angle of radiation expected unless certain features are included as an integral part of the installation.

One type of h-f antenna designed to produce a low vertical angle of radiation is the so-called ground plane. Its design was conceived by Brown and Epstein.<sup>1</sup> It is unique in that its features not only produce the desired low angle of radiation, but also allow for proper termination of the transmission line and place the antenna at ground potential. Figure 1 illustrates the mechanical construction.

Basically, the antenna assembly is so designed that a parallel circuit is formed, whose impedance can be made to match

the characteristic surge impedance of concentric transmission lines commercially available. The equivalent electrical circuit of a ground-plane antenna is shown in Fig. 2. The parallel circuit formed by the ground-plane antenna is accomplished by connecting the base of the antenna to the center conductor of a metallic concentric base support, shown in Fig. 1 as  $L$ . This center conductor, shown as  $L_S$  in Fig. 1, acts as an inductance and is shunted at the top by the antenna base impedance, composed of capacitive reactance and radiation resistance. If the inductance, capacitance, and resistance are of the proper values, the parallel circuit thus formed will act as a pure resistance at the operating frequency.

As illustrated in Fig. 1, the outer conductor of the coaxial transmission line is connected to the outer conductor of the antenna base support. Since the inner conductor is common to the outer conductor, because of a metallic shorting disk at the base of  $L_S$ , the antenna assembly may be placed at ground potential, provided that the antenna supporting structure or the outer sheath of the coaxial line is grounded.

### Design Data

Consider the circuit shown in Fig. 2. If the values of reactance and resistance are properly proportioned, the circuit can be made to act as a pure resistance, practically equal to the surge impedance of



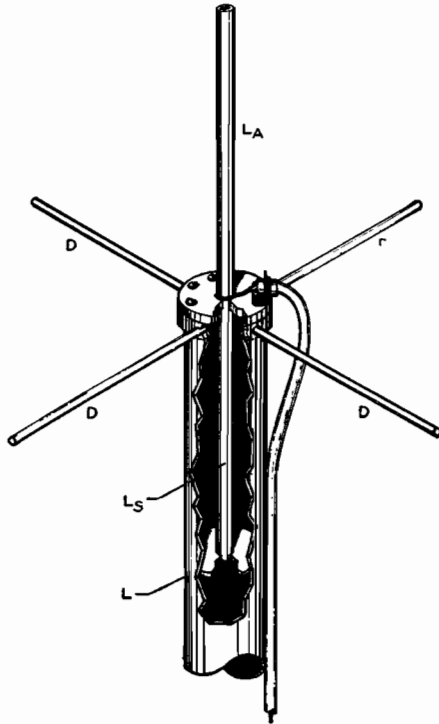


Fig. 1.—Constructional details of ground plane antenna.  $L$  may be any convenient length provided it is at least as long as  $L_s$ .

coaxial transmission lines in common use. Proof of this fact is demonstrated by

$$\frac{j53.3(25 - j36)}{25 + j53.3 - j36} = 77 \text{ ohms} \quad (1)$$

The term  $j53.3$  represents the reactance of  $L_s$  in Fig. 2, and the term  $(25 - j36)$  represents the resistance and reactance of  $L_A$ . The combined branches of the circuit equal 77 ohms and form the termination of the coaxial transmission line.

The four arms extending out from the top end of the outer sleeve of the concentric base support, labeled  $D$ , are ground radials. These radials are necessary to lower the radiation resistance and decrease the effect of high-angle interference radiation originating on the supporting structure or coaxial feed line.

The terms found on the left side of Eq. (1) are entirely possible to obtain in actual practice, and the resulting parallel impedance should be satisfactory for terminating coaxial lines having a characteristic surge impedance between 60 and 90 ohms.

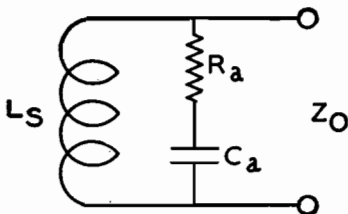


Fig. 2.—Equivalent electrical circuit of ground-plane antenna.

It can be shown mathematically that the base impedance of a quarter-wave antenna, having four radials extending from its base, is approximately 30 ohms. Since Eq. (1) indicates that the antenna must offer a capacitive reactance at its base equal to  $-j36$  ohms, the antenna must be made slightly shorter than a quarter-wave. Obviously, if the antenna is shortened, the radiation resistance will decrease. Measurements indicate that, when the antenna offers  $-j36$  at the base, the radiation resistance decreases to 25 ohms as required by Eq. (1).

The  $j53.3$  term of Eq. (1) is easily obtainable by properly proportioning the length of the concentric base supporting structure. Once the surge impedance of this section has been determined, the reactance of the center conductor can be calculated quite accurately by

$$jX = Z_0 \tan Y \quad (2)$$

Since  $jX$  must equal 53.3,

$$\tan Y = \frac{53.3}{Z_0} \quad (3)$$

$Z_0$  may be calculated once the material has been chosen from which the antenna base support is to be constructed.

$$Z_0 = 138.15 \log \frac{b}{a} \quad (4)$$

where  $b$  is the inside diameter of the outer conductor and  $a$  is the outside diameter of the inner conductor.

The number of electrical degrees that the tangent value represents, as calculated by Eq. (3), may be obtained from a table of trigonometric functions. The length in inches that represents 1 electrical degree at the operating frequency  $f$  in Mc is

$$L = \frac{32.8}{f} \quad (5)$$

The total length of the concentric antenna base supporting section  $L_s$  (as measured from the top of the shorting disk to the top of the outer conductor) is

$$L_s = LY \quad (6)$$

where  $L$  is the length of 1 electrical degree in inches, and  $Y$  is the number of electrical degrees necessary to form 53.3 ohms reactance.

Each of the ground radials should be one quarter-wave in length, and may be calculated by

$$d = 85.5L \quad (7)$$

For those who do not have the necessary equipment to measure the characteristics at the base of the antenna so as to

determine when the antenna length is properly adjusted to fulfill the term  $(25 - j36)$  given by Eq. (1), the following equations may be of interest:

$$\pm jX = Z_{oa} \tan \left\{ \frac{(2\pi h/\lambda) + (1.5\pi)}{+0.01 [\sqrt{2.86(\log \lambda/a) - 4.6 + 3.4}]} \right\} \quad (8)$$

where  $\pm jX$  = reactance of antenna  
 $Z_{oa}$  = characteristic impedance of antenna

$h$  = length of antenna

$\lambda$  = electrical length of one cycle at the operating frequency

$a$  = radius of antenna element

$$Z_{oa} = K_1 + K_2$$

$$K_1 = 138.15 \log h/a$$

$$K_2 = -(60 + 69 \log 2h/\lambda)$$

The reactance of the antenna can be calculated quite accurately by the use of Eq. (8). Since the length of  $h$  must be assumed in solving for  $Z_{oa}$ , several trial values may be necessary before the exact length is ascertained. Previous calculations indicate that the length of  $h$  is usually between 87 and 90 per cent of the 90-deg electrical length. Several values of  $h$  should be chosen between these limits and the reactance calculated. The values should then be plotted as a function of  $h$  to obtain the exact length for a reactance of  $-j36$  ohms at its base.

#### Example of Calculations

A practical example may help in making the included data more easily followed. Assume that it is desired to design a ground-plane antenna to operate on a frequency of 33.780 Mc. The characteristic impedance of the transmission line is 78 ohms. The material available for the antenna base support is a section of copper tubing with an inside diameter of 2 in. and a center conductor having an outside diameter of 0.625 in. The antenna section is to be a continuation of the center conductor of the antenna base support.

If the various sections of the antenna system satisfy the terms given on the left side of Eq. (1), the 78-ohm transmission line should be satisfactorily terminated.

Since the antenna base support  $L_s$  is to offer the required 53.3 ohms reactance to the base of the antenna, the length of this section must be calculated. First, it is necessary to calculate the  $Z_0$  of this section by the use of Eq. (4).  $Z_0 = 138.15 \log 2/0.625 = 70$  ohms.

Substituting known values in Eq. (3), we get  $53.3 = 70 \tan Y$ , or  $\tan Y = 53.3/70 = 0.76143$ . Then  $\tan^{-1} 0.76143 = Y = 37^\circ 17'$ .

From Eq. (5) the length of 1 electrical degree may be calculated:  $L = 32.8/f$

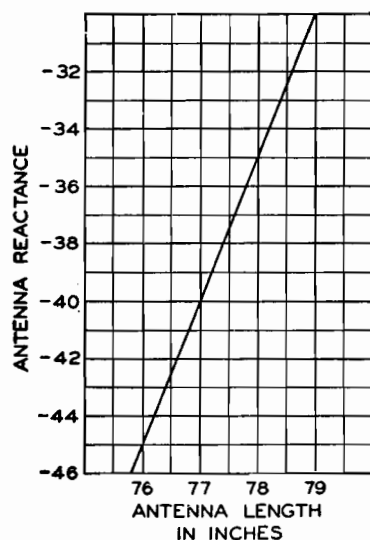


Fig. 3.—Reactance as a function of length  $h$  for the hypothetical antenna design given in the text.

$33.780 = 0.973$  in. From Eq. (6),  $L_s = 37.2833^\circ \times 0.973 = 36.28$  in.

The next operation solves for the length of the ground radials. The length is measured from the outer wall of the outer conductor of the concentric antenna base support to the tip of the radial:  $d = 85.5 \times 0.973 = 93$  in.

The antenna must offer  $-j36$  at its base. The proper length may be calculated by the use of Eqs. (8) and (9). As mentioned, the length usually will be between 87 and 90 per cent of the true 90 deg. electrical length. The 90 deg. length is  $90^\circ L = 90^\circ \times 0.973 = 87.5$  in. The correct length of  $h$  should be between  $0.87 \times 87.5$  in. and  $0.9 \times 87.5$  in., or between 76 in. and 78.8 in.

If the reactance of the antenna is calculated for the lengths 76 and 78.8 in. and these reactive values are plotted as a function of  $h$ , the proper value may be ascertained.

The characteristic impedance of the 76-in. element is  $Z_{oa} = K_1 + K_2$ .

$$K_1 = 138.15 \log 76/0.3125 = 330$$

$$K_2 = -(60 + 69 \log 152/350) = -35.7$$

$$Z_{oa} = 330 - 35.7 = 294.3 \text{ ohms}$$

The characteristic impedance of the 78.8-in. element is

$$K_1 = 138.15 \log 78.8/0.3125 = 331$$

$$K_2 = -(60 + 69 \log 157.6/350) = -36$$

$$Z_{oa} = 331 - 36 = 295 \text{ ohms}$$

From Eq. (8), the reactance of the 76-in. element is

$$\pm jX = 294.3 \tan \{6.28 \times 76/350 + 4.71 + 0.01[\sqrt{2.86(\log 350/0.3125)} - 4.6 + 3.4]\}$$

$$\pm jX = 294.3 \tan (6.073 + 0.0555)$$

$$= 294.3 \tan 6.1285$$

$$= 294.3 \tan 351.3^\circ$$

Since  $351.3^\circ$  is in the fourth quadrant, the tangent value is negative and the reactive component of the antenna will be  $-jX$ .

$$\begin{aligned} -jX &= 294.3 \tan 8.7^\circ \\ &= 294.3 \times 0.153 = 45 \text{ ohms} \end{aligned}$$

The reactance of the 78.8-in. element is

$$\pm jX = 294.3 \tan \{6.28 \times 78.8/350 + 4.71 + 0.01[\sqrt{2.86(\log 350/0.3125)} - 4.6 + 3.4]\}$$

$$\pm jX = 295 \tan 6.1785$$

$$\pm jX = 295 \tan 354^\circ$$

Since  $354^\circ$  is also in the fourth quadrant, the tangent value is negative and the reactive component is  $-jX$ .

$$\begin{aligned} -jX &= 295 \tan 6^\circ = 295 \times 0.1051 \\ &= 31 \text{ ohms} \end{aligned}$$

When these two values are plotted as a function of  $h$  as shown in Fig. 3, the correct value of  $h$  to produce  $-j36$  ohms is 77.8 in.

Thus, to construct a ground-plane antenna to operate on a frequency of 33.78 Mc, which will properly terminate a 78-ohm transmission line, the antenna must be  $\frac{5}{8}$  in. diameter and 77.8 in. long. The antenna base support must have a

surge impedance of 70 ohms and a length of 36.28 in. The lengths of the four ground radials, extending out at right angles from the top of the antenna base support, must be 83 in. each.

The curves in Figs. 4 and 5 illustrate the variation of reactive and resistive component parts of the antenna when the operating frequency is varied from the proper operating frequency of 33.78 Mc. The frequency range represented by both curves is approximately 30 to 37 Mc. Figure 5 combines the reactive and resistive components to illustrate the variation in magnitude of the antenna terminating impedance and its phase angle.

### Appendix

The constant 32.8 in Eq. (5) was derived from

$$\lambda_{\text{meters}} = 3 \times 10^8 / f_{\text{cycles}} = 3 \times 10^2 / f_{\text{Mc}}$$

$$\lambda_{\text{inches}} = 39.37 \times 3 \times 10^2 / f_{\text{Mc}}$$

$$L = 39.37 \times 3 \times 10^2 / 360 f_{\text{Mc}} = 32.8 / f_{\text{Mc}}$$

Measurements indicate that the length of the ground radials is not critical provided that they are equal to 90 deg electrical length or longer. The constant

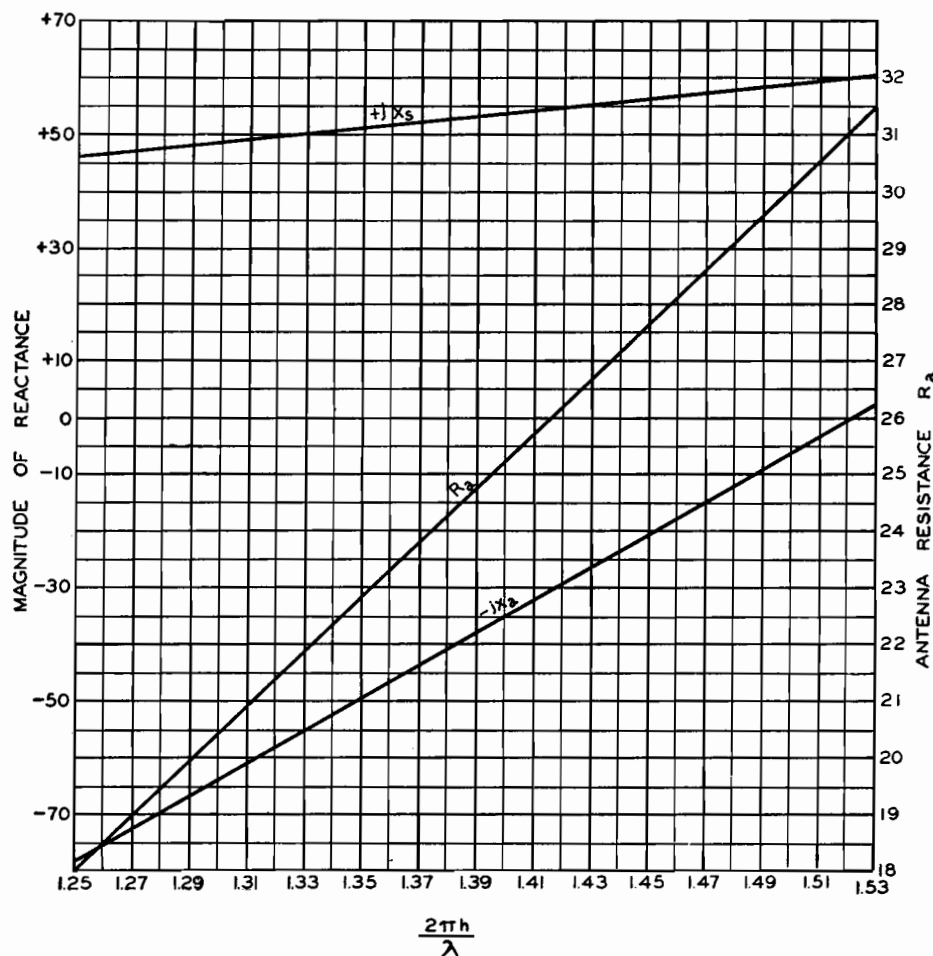


Fig. 4.—Antenna reactance, antenna resistance, and antenna base reactance as a function of  $2\pi h/\lambda$ .

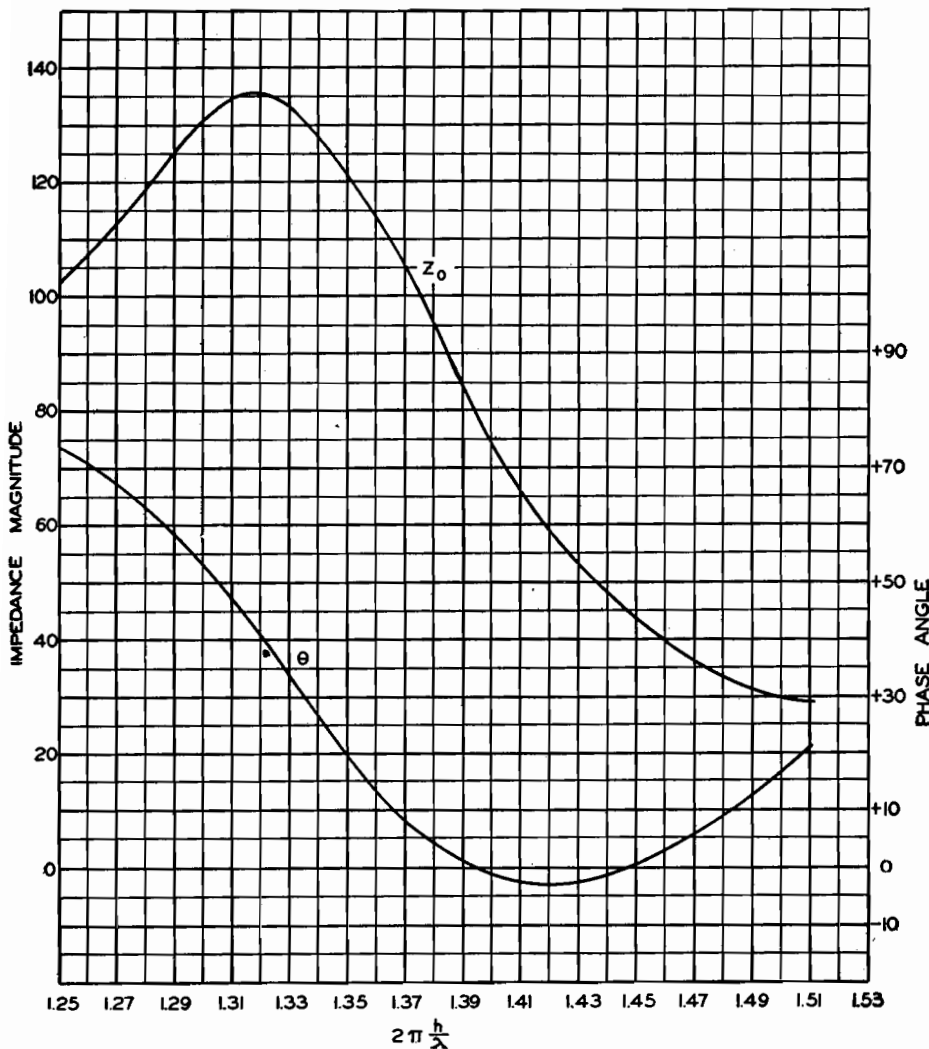


Fig. 5.—Antenna terminating impedance and its phase angle as a function of  $2\pi h/\lambda$ .

85.5 when multiplied by  $L$  gives the approximate 90 deg electrical length, after allowance has been made for end effect. (85.5 is 95 per cent of 90 deg.)

In computing the resistance and reactance at the base of the antenna, the antenna was considered as an open-circuited transmission line. The methods

used in obtaining the characteristic impedance  $Z_{oa}$  of the antenna were developed by Morrison and Smith.<sup>2</sup> (For a complete derivation, refer to page 693 of their paper.<sup>2</sup>) The accuracy of Morrison and Smith's methods of calculation seems to be substantiated by the correlation between the reactance values calculated by the use of Eq. (8) and the results obtained by the more rigorous formula given by King and Blake.<sup>3</sup>

By including the  $1.5\pi$  term in Eq. (8), a rotation of 270 deg is produced, making it possible to multiply the  $Z_{oa}$  term by the tangent value without regard to the antenna length, up to  $\lambda/2$ .

The square-root term in Eq. (8) corrects for end effect which is influenced by the relationship between the antenna radius and operating wavelength.

Over the range of  $2\pi h/\lambda$  under consideration for this investigation (1.25 to 1.53), the reactance values calculated by Eq. (8) are in complete agreement with those calculated by the formula given by King and Blake.<sup>3</sup>

The values of resistance used in formulating curve  $R_a$  in Fig. 4 and calculation to obtain the impedance and phase-angle curves of Fig. 5 were derived from the data given by King and Blake.

#### References

- (1) BROWN, G. H., and EPSTEIN, J., An Ultra-high-frequency Antenna of Simple Construction, *Communications*, **20**, 3-5, 1940.
- (2) MORRISON, J. F., and SMITH, P. H., The Shunt-excited Antenna, *Proc. IRE*, **25**, 691-695, June, 1937.
- (3) KING, R., and BLAKE, JR., F. G., The Self-impedance of a Symmetrical Antenna, *Proc. IRE*, **30**, 335-349, 1942.
- (4) HUND, A., "Phenomena in High-frequency Systems," p. 418, McGraw-Hill Book Company, Inc., New York.

## Design Chart for Antenna Phase-shifting Networks

By W. S. DUTTERA

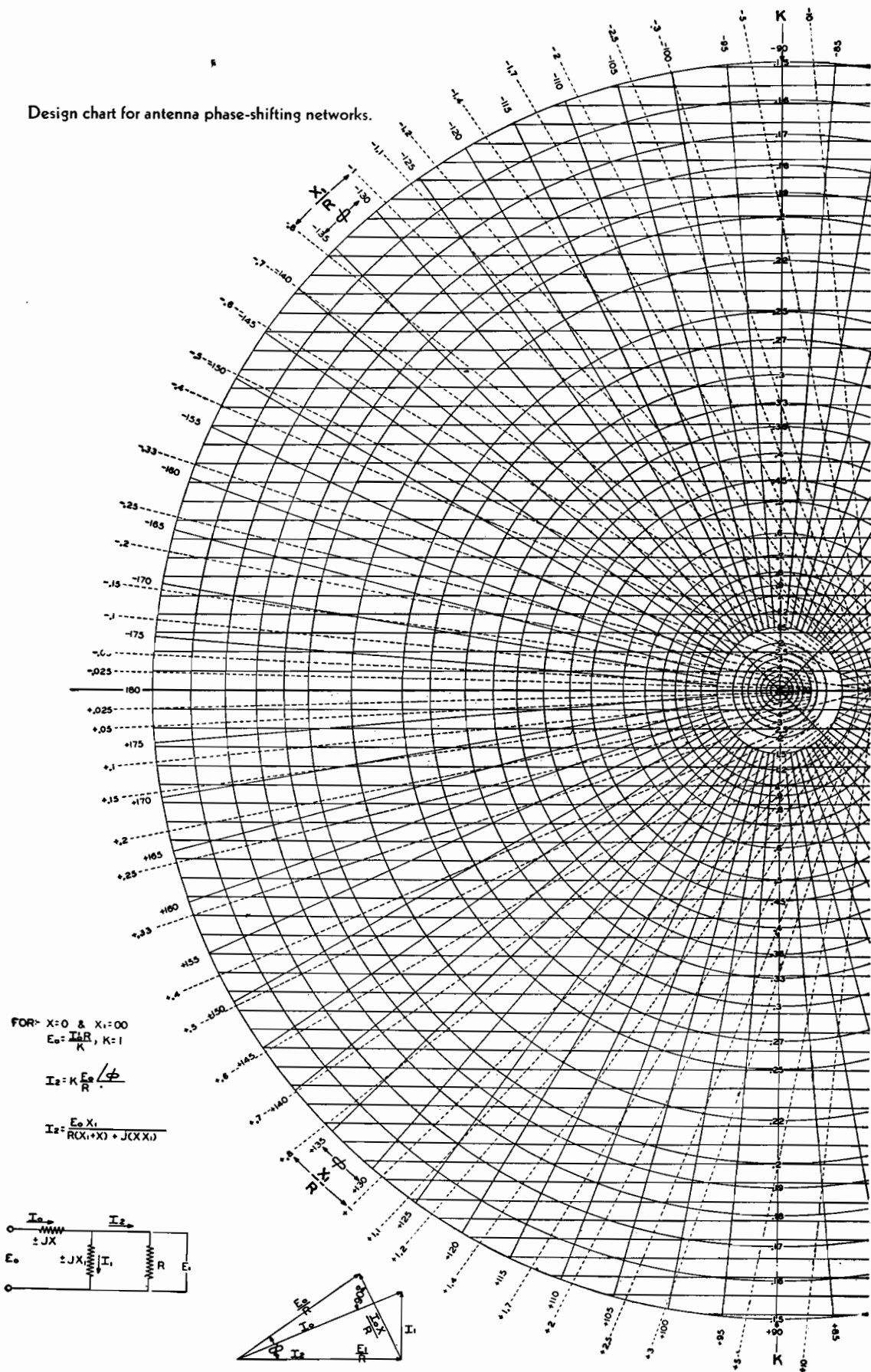
Design charts present a graphical solution to the problem of determining the network required to deliver proper power to each of several directional antenna towers or other loads fed by the same source. Phase and amplitude relations of coupling network are easily determined

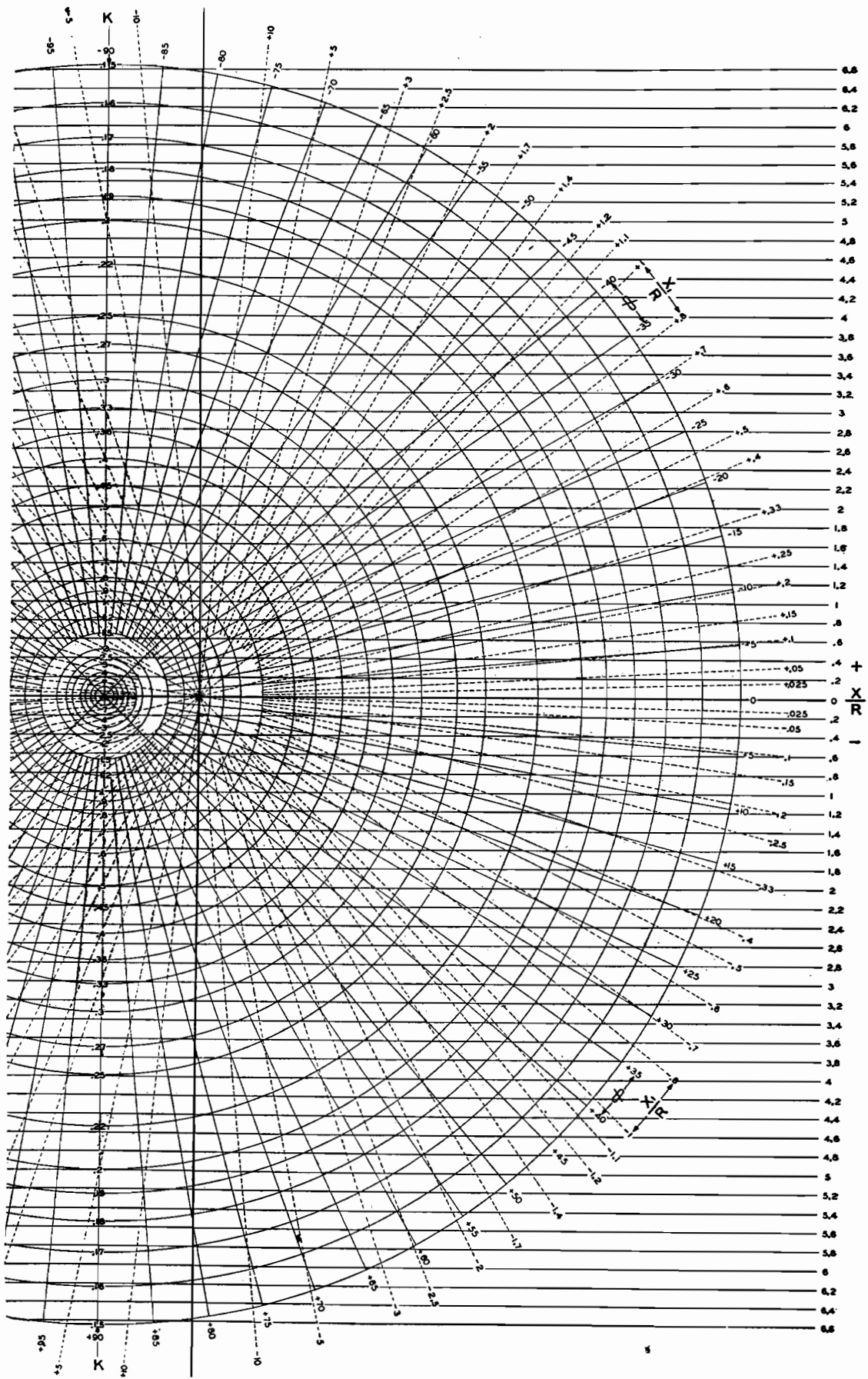
WHEN a transmitter feeds, simultaneously, the various elements in a directional antenna system, suitable networks must be designed for insertion

between the source and the loads, to deliver the desired power to each load. The purpose of the network is to alter the effective impedance of the load so that

the current and voltage fed to it are of the proper amplitude and phase relations. The graphical chart permits the rapid determination of the reactive elements,

Design chart for antenna phase-shifting networks.





in the simplest  $L$  network, which will suffice.

As may be seen from the schematic diagram, the source delivers a voltage  $E_o$  and a current  $I_o$  to a resistive load  $R$ . The voltage across this load is  $E_1$ , and the current through it is  $I_2$ . The required network is composed of  $X$  and  $X_1$  whose function is to change the magnitude and phase of the current  $I_2$  so that the load  $R$  may take the required amount of power.

In the absence of reactances  $X$  and  $X_1$ , the current to the load is  $I_2 = E_o/R$  at an angle 0 deg with respect to  $E_o$  and  $I_2$ . The introduction of the reactive elements will alter the magnitude of  $I_2$  by a factor  $K$ , and the phase by the factor  $\phi$ . The value of  $K$  may be greater or less than 1, and  $\phi$  may be a positive or negative angle up to 180 deg.

When  $K$ ,  $\phi$ , and  $R$  are specified, from the requirements of the problem, the chart enables us to determine the normalized reactances  $X$  and  $X_1$ . These normalized reactances are expressed in terms of  $X/R$  and  $X_1/R$ , so that we must multiply the values as determined from the chart by the value of the load resistance  $R$  to ascertain the true values of the reactances actually required. The advantage of plotting the normalized re-

actance is that, by so doing, the chart is applicable to loads of any resistance.

When the proper values of  $K$  and  $\phi$  are known from a statement of the problem, the chart is entered along the vertical line  $K$  until the concentric circle corresponding to the appropriate  $K$  value is obtained. This circle is then followed until it intersects the correct angle  $\phi$ . From this point, the values of  $X/R$  may be read from the scale at the right edge of the graph, while the values of  $X_1/R$  are read from a set of dotted radial lines having  $K = 1.0$  and  $\phi = 0$  as their origin.

Suppose three transmission lines  $A$ ,  $B$ , and  $C$  are to be fed in parallel from a single generator. Let the relative magnitudes and phases of these three currents be given, in polar form, as  $I_A = 0.60/+160^\circ$ ,  $I_B = 0.40/+50^\circ$ , and  $I_C = 1.0/0^\circ$ . The first transmission line will require a correcting network which reduces the magnitude of the current to 60 per cent of its value without the network and which shifts the phase by  $+160$  deg. Thus, for the network required for transmission line  $A$ , we have  $K_A = 0.6$  and  $\phi_A = +160$  deg. The network for line  $B$  reduces the current magnitude to 40 per cent of its original value without the network, and shifts the phase  $+50$  deg. Thus, for the network to be inserted in line  $B$ , we re-

quire  $K_B = 0.4$  and  $\phi_B = +50$  deg. No network is required for transmission line  $C$ .

The problem is now to find the reactances  $X$  and  $X_1$  for lines  $A$  and  $B$  from the chart. For the corrective network for line  $A$ , we enter the chart on the vertical line  $K$  until we reach the circle whose  $K$  value is 0.60. Follow this circle toward the left until we reach the solid radial line whose value is  $\phi = +160$  deg. From this point of intersection, we project to the scale at the extreme right and find  $X_A/R = -0.55R$ . From the same point of intersection, we read the value of  $X_{1A}/R$  from the dotted radial lines intersecting the heavy vertical line. This gives  $X_{1A}/R = 0.22$ . By multiplying these values through by the load resistance  $R$ , we find  $X_A = -0.55R$  and  $X_{1A} = 0.22R$ . The negative sign indicates a capacitance while a positive sign indicates an inductance. From these values of  $X_A$  and  $X_{1A}$ , the network elements are easily determined.

The corrective network for the line  $B$  is found in a similar manner. From the point  $K_B = 0.4$  and  $\phi = +50$  deg, we find  $X_B = 1.95R$  and  $X_{1B} = -3.3R$ . Thus,  $X_B$  is an inductance of  $1.95R$  ohms reactance, and  $X_{1B}$  is a capacitance of  $3.3R$  ohms reactance.

## Phasing Networks for Broadcast Arrays

By C. RUSSELL COX

Graphical methods are applied to the design of phase-shifting and impedance-matching networks required to distribute power properly in directional antennas. Compared with conventional network analysis the vector method results in economy of circuit components and simplified design procedure

VECTOR synthesis is a convenient mathematical tool which is very helpful to the designer of r-f phase-shifting and impedance-matching networks for the directional arrays used by many broadcast stations. Not only does this combination graphical and mechanical technique afford a clear understanding of the operation of a-c circuits, but it can also be used to synthesize network designs which display great simplicity when compared with circuits determined by ordinary methods. Problems in the design of

phasing networks for directional antenna arrays are particularly susceptible to solution by vector methods.

### Principles of Vector Synthesis

In general, the synthesis of a network by vector manipulation usually reduces to the following problem: Given a pair of vectors  $I_1$  and  $E_1$ , representing the current through and the voltage across an impedance, it is required to establish a circuit that will transform  $I_1$  and  $E_1$  into another pair of vectors  $I_2$  and  $E_2$ . The

latter pair of vectors is usually specified by the conditions of the problem.\*

When the input and output impedances  $R_1$  and  $R_2$  between which the network must operate are known, the two currents are related by a simple law that equates input and output powers

$$I_1^2 R_1 = I_2^2 R_2$$

\* If the circuit is free from dissipation, the second pair of vectors is subject to the restriction.

$$\frac{1}{2}(E_1 I_1^* + E_1 I_1) = \frac{1}{2}(E_2 I_2^* + E_2 I_2)$$

in which the asterisk (\*) denotes the conjugate function. This equation states that the network must neither create nor destroy power



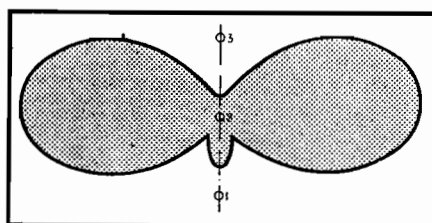


Fig. 1.—Desired radiation pattern, which can be produced by the antenna array of Fig. 2.

The method of designing a network by vector synthesis may be most easily outlined by means of a specific example. To illustrate the general method, let it be required to design phasing networks suitable for providing currents of the desired magnitude and phase to three vertical radiators, in order to produce the radiation pattern shown in Fig. 1.

An analysis of this radiation pattern reveals that the towers must be  $0.25\lambda$  high, separated by a distance  $0.301\lambda$ , and fed with currents whose magnitudes and relative phases are as given in Fig. 2. A block diagram showing the elements of a suitable system of networks to produce the desired radiation pattern is shown in Fig. 3.

The problem at hand is now to design, by methods of vector synthesis, impedance-matching networks between the transmission lines and the antennas, power-dividing and phase-shift networks, and the impedance-matching circuit that connects the transmission line from the transmitter to the three power-dividing and phase-shift networks. (It should be noted from Fig. 2 that antenna 1 is located at the transmitter and consequently does not require a transmission line, as do the other two antennas.)

#### Example of Vector Synthesis

To design a feed system for the array of Fig. 3, it is necessary to start at the antenna and work back through each network and transmission line toward the transmitter. The conditions of the problem yield the following information re-

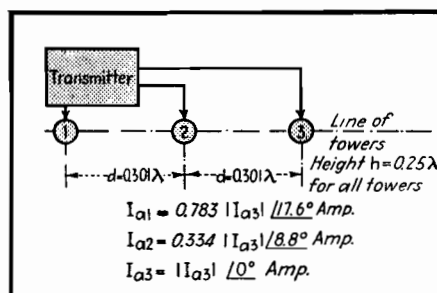


Fig. 2.—Antenna array required to produce the radiation pattern of Fig. 1.

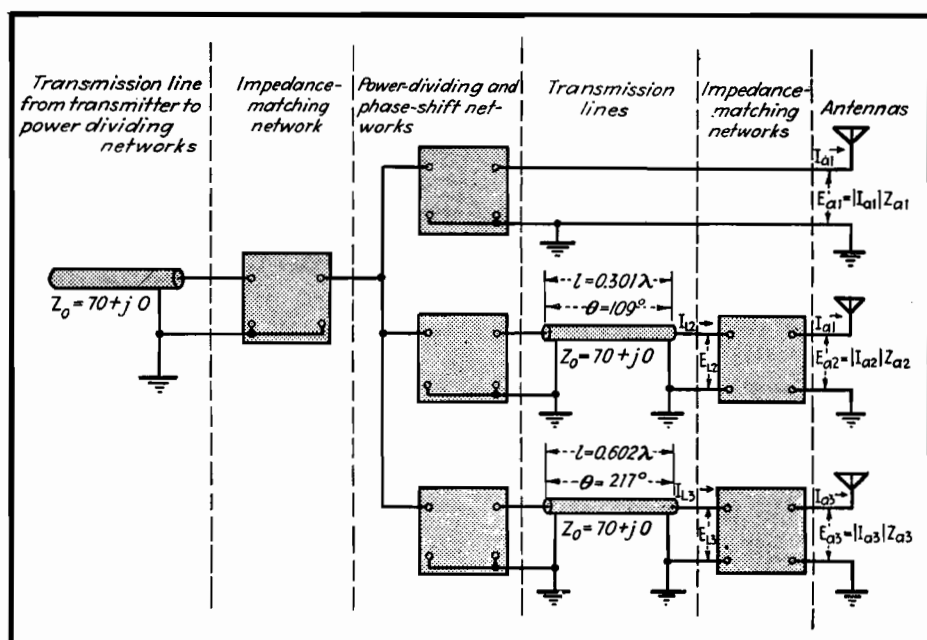


Fig. 3.—Block diagram of system of networks and transmission lines for feeding antennas with the currents and voltages necessary to produce directional radiation pattern.

garding antenna currents, impedances, and powers:

$$\begin{aligned} I_{a1} &= 6.7/17.6^\circ \text{ amp} \\ I_{a2} &= 2.86/8.8^\circ \text{ amp} \\ I_{a3} &= 8.56/0^\circ \text{ amp} \\ Z_{a1} &= 28.7 + j39 = 48.4/53.67^\circ \text{ ohms} \\ Z_{a2} &= 108 - j45 = 117/-22.63^\circ \\ Z_{a3} &= 38.5 + j37 = 53.5/43.83^\circ \\ P_{a1} &= 1,290 \text{ watts} \\ P_{a2} &= 890 \text{ watts} \\ P_{a3} &= 2,820 \text{ watts} \end{aligned}$$

where  $I_{a1}$ ,  $I_{a2}$ , and  $I_{a3}$  are currents in antennas 1, 2, and 3, respectively, and the angles represent phases relative to that of  $I_{a3}$ . The quantities  $Z_{a1}$ ,  $Z_{a2}$ , and  $Z_{a3}$  are the impedances of antennas 1, 2, and 3, respectively, and  $P_{a1}$ ,  $P_{a2}$ , and  $P_{a3}$  are the powers in antennas 1, 2, and 3, respectively.

From these data the voltage applied to the antennas and the currents in the transmission lines (whose impedance is  $Z_0 = 70 + j0$ ) can be determined as follows:

$$\begin{aligned} E_{a1} &= |I_{a1}|Z_{a1} = 6.7 \times 48.4/53.67^\circ \\ &= 324/53.67^\circ \text{ volts} \\ E_{a2} &= |I_{a2}|Z_{a2} = 2.86 \times 117/-22.63^\circ \\ &= 335/-22.63^\circ \text{ volts} \\ E_{a3} &= |I_{a3}|Z_{a3} = 8.56 \times 53.5/43.83^\circ \\ &= 458/43.83^\circ \text{ volts} \end{aligned}$$

$$\begin{aligned} I_{L2} &= \sqrt{P_{a2}/Z_0} = \sqrt{890/70} = 3.56 \text{ amp} \\ I_{L3} &= \sqrt{P_{a3}/Z_0} = \sqrt{2,820/70} = 6.35 \text{ amp} \\ E_{L2} &= Z_0 I_{L2} = 70 \times 3.56 = 250 \text{ volts} \\ E_{L3} &= Z_0 I_{L3} = 70 \times 6.35 = 444 \text{ volts} \end{aligned}$$

where  $E_{a1}$ ,  $E_{a2}$ , and  $E_{a3}$  are the voltages

applied to antennas 1, 2, and 3, respectively, and the phase angle of each voltage is referred to the corresponding antenna current as a reference.  $I_{L2}$  and  $I_{L3}$  are the magnitudes of the currents in the transmission lines feeding antennas 2 and 3, and  $E_{L2}$  and  $E_{L3}$  are the magnitudes of the voltages across these transmission lines. With these data, the impedance-matching networks between the transmission lines and the antennas can now be designed.

#### Design of Network for Matching Impedances

The sketch in Fig. 4 illustrates the synthesis of a network for matching the line impedance of  $Z_0 = 70/0^\circ$  ohms to the center antenna impedance of  $117/-22.63^\circ$  ohms. We begin by drawing a vector of length 2.86 units to represent the antenna current  $I_{a2}$ . This vector can be drawn in any convenient direction, but since it is used as the reference vector, it will be drawn along the x axis. To some suitable voltage scale, the vector for the antenna voltage  $E_{a2}$ , at an angle of  $-22.63^\circ$  deg with respect to  $I_{a2}$ , can also be drawn.

An  $L$  network of the type shown will give the impedance transformation. For such a network, Kirchhoff's law for branching currents must be satisfied, i.e.,  $I_{L2} = I_{a2} + I_c$ , where  $I_c$  is the current through the capacitor. Therefore the tips of  $I_{L2}$  and  $I_c$  must coincide at some point  $P$  which lies on a circle of radius  $I_{L2} = 3.56$ , drawn from zero as a center. Since the current through a reactance forms a 90-deg angle with the voltage across it, we may lay out  $I_c$  at right

angles to  $E_{a2}$ , and the intersection of  $I_c$  with the circle locates the point  $P$ .

The potential  $E_{L2}$  must equal the sum of  $E_x$  and  $E_{a2}$ . Therefore, the tail of  $E_x$  must lie on the tip of  $E_{a2}$ , and the direction of  $E_x$  is normal to the current  $I_{L2}$  through

the inductance. The magnitude of  $E_x$  is determined by the point of intersection with  $I_{L2}$ , and the voltage triangle is completed by drawing  $E_{L2}$  from zero to the point of intersection of  $E_x$  with current  $I_{L2}$ .

Because  $I_c$  leads  $E_{a2}$  by 90 deg, the

parallel reactance must be that due to a capacitance. Similarly, since  $E_x$  leads  $I_{L2}$  by 90 deg, the series reactance must be that due to an inductance. The magnitudes of the required reactances are obtained by dividing the length of a vector representing voltage across a reactance by the length of the corresponding current vector, i.e.,  $X_L = E_x/I_{L2}$ , and  $X_c = E_{a2}/I_c$ .

The network of Fig. 4 is a delay network because  $I_{a2}$  lags behind  $I_{L2}$ . Had we chosen to extend  $I_c$  in the opposite direction, intersecting the circle at  $P_1$ , a phase-advance network would have been obtained.

### Choice of Configuration

The choice between the phase-advance and the phase-delay configuration is purely a matter of convenience. Any impedance transformation problem may be solved by either network. However, in designing the matching circuit for antenna 3 we choose the phase-advance network because this choice happens to simplify the design of the phasing networks. We begin the construction of the vector diagram for antenna 3 (Fig. 5) by drawing vectors  $I_{a3}$  and  $E_{a3}$ . The series capacitor introduces a voltage  $E_c$  which adds to  $E_{a3}$ , but in a direction normal to  $I_{a3}$ . Then, a circle of radius  $E_{L3}$  locates the tip of  $E_c$ , and the vector  $I_{L3}$ , whose length is known, is drawn through the point of intersection. The vector  $I_p$ , drawn normal to and lagging  $I_{L3}$ , completes the construction.

### Phasing Networks

A summary of the phase shifts in the lines and antenna tuning units is given in Fig. 6. Each of the two transmission lines introduces a delay (in degrees) of  $\theta = 360l/\lambda$ , where  $l$  is the length of the line and  $\lambda$  is the wavelength. For  $\lambda = 0.301$  the delay is 109 deg, and for  $\lambda = 0.602$  the delay is 217 deg. The apparatus to the left of the dotted line in Fig. 6 is required to divide the transmitter power into three parts and distribute it among the three antennas with the required phase angles and amplitudes. Figure 7 represents the three voltages and currents leaving the phasing apparatus at the dotted lines of Fig. 6.

The remaining problem is that of selecting a voltage vector  $E$  which can be rotated and transformed by means of three separate reactance networks to produce  $E_{a1}$ ,  $E_{L2}$ , and  $E_{L3}$ . An important point is that the vector  $E$  may be of any magnitude and of any phase, and we may

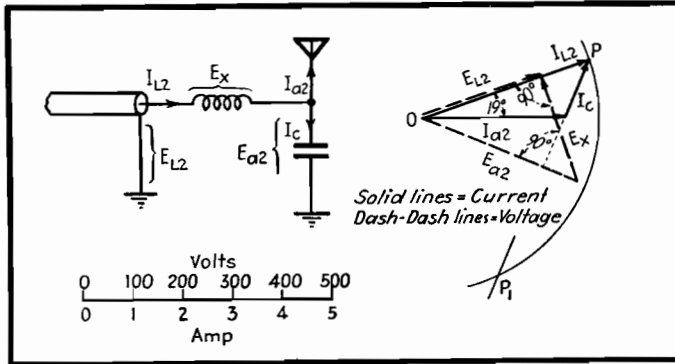


Fig. 4.—L-type network for matching impedance of transmission line to impedance of antenna 2, with vector diagram from which design of the network is derived.

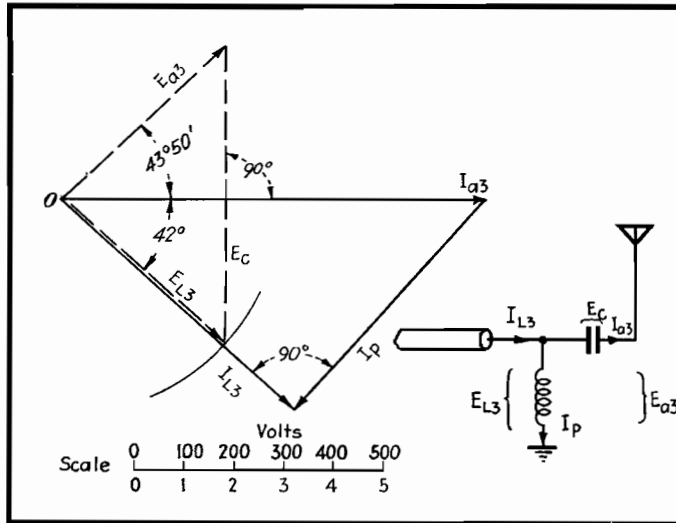


Fig. 5.—Impedance-matching network of the L-type for matching antenna 3 to a 70-ohm transmission line. Vector diagram illustrates method of designing this circuit.

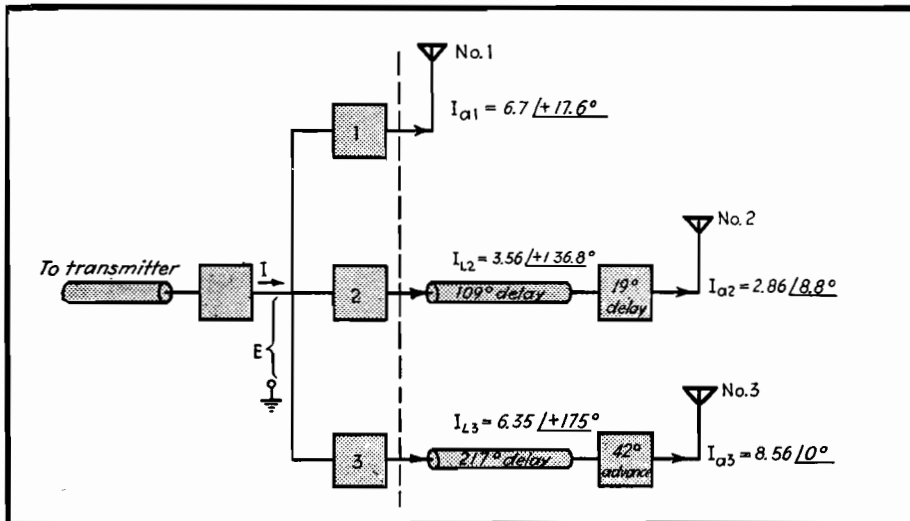


Fig. 6—Block design illustrating the summary of phase shifts occurring between the power-dividing networks and the antenna.



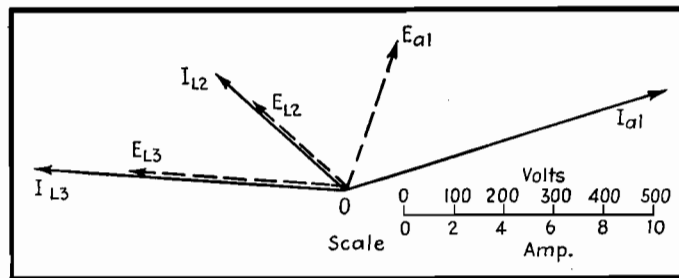


Fig. 7.—Vector diagram of voltages and currents that must be produced by phase-shifting and power-dividing networks.

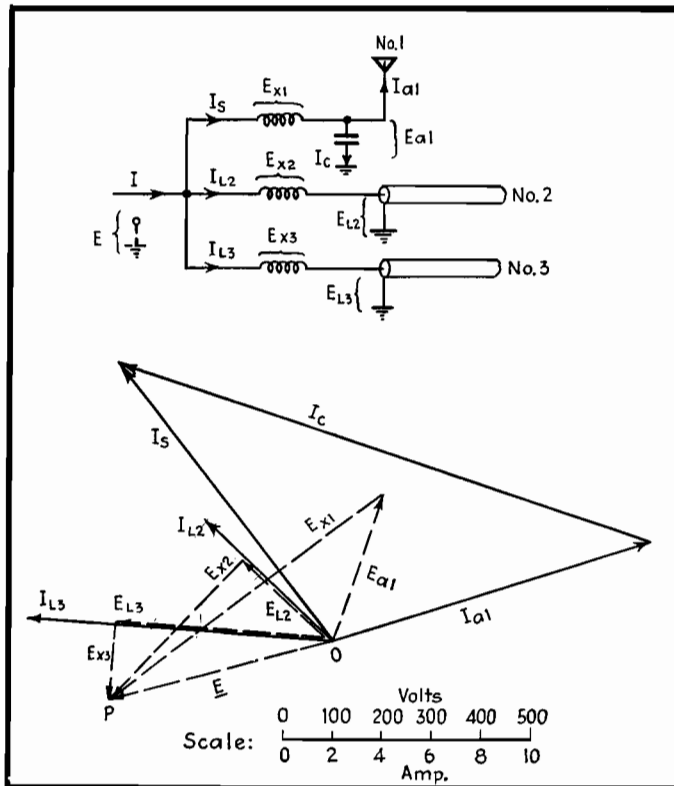


Fig. 8.—Synthesis of phasing and power-dividing networks.

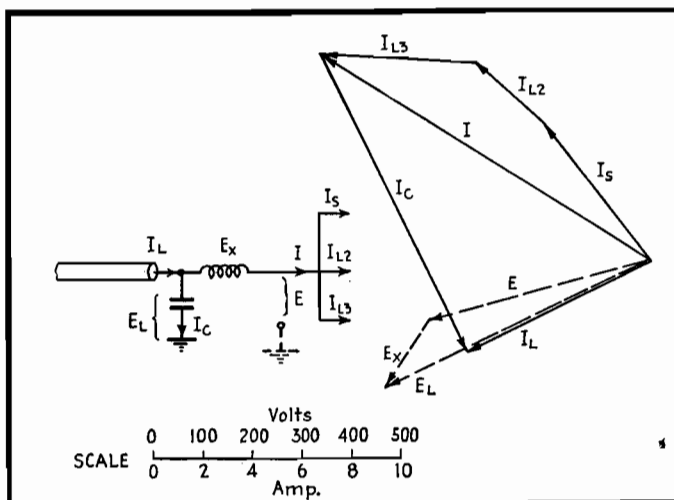


Fig. 9.—Vector diagram for input circuits.

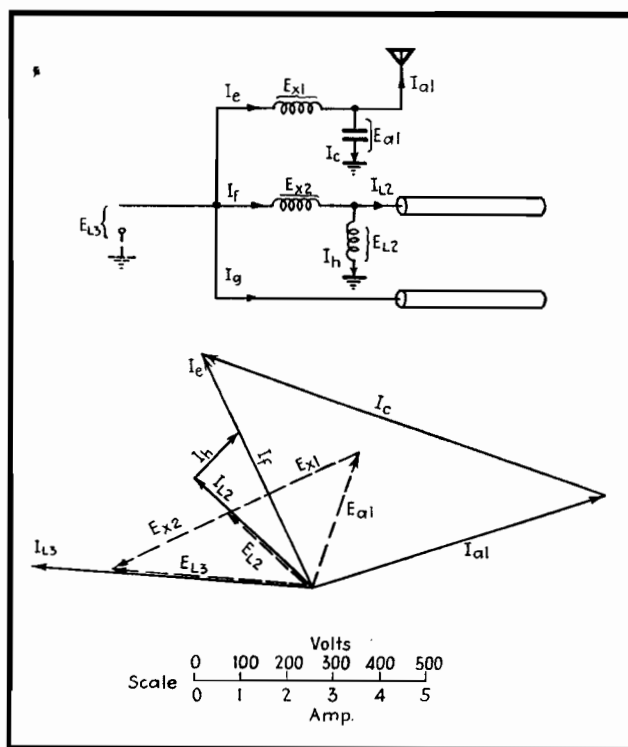


Fig. 10.—Alternative design of phasing networks.

therefore select  $E$  to suit our own convenience. Referring to Fig. 8 we see that reactances in series with transmission lines 2 and 3 produce voltage vectors  $E_{x2}$  and  $E_{x3}$  which intersect at  $P$ . The vector  $E$ , drawn from zero to  $P$ , is then a convenient vector to represent the input voltage.

Since the antenna current  $I_{a1}$  is far removed in direction from  $E$ , it is necessary to obtain somehow a new current  $I_s$  that is at least within 90 deg of  $E$ . This is accomplished by introducing a parallel capacitance across antenna  $I_s$ , producing the current  $I_e$  leading  $E_{a1}$  by 90 deg. An

inductance in series with  $I_s$  introduces a voltage vector  $E_{x1}$ , drawn from the tip of  $E_{a1}$  by 90 deg. An inductance in  $I_s$  perpendicular to  $E_{x1}$  satisfies all the conditions of the problem.

#### Input Circuit

An input circuit, to provide a load impedance of  $70 + j0$  ohms for the transmitter is illustrated in Fig. 9. The total current  $I$  is obtained by adding vectorially the three branch currents  $I_s$ ,  $I_{L2}$ , and  $I_{L3}$ . By adding a series inductance to produce  $E_x$ , and a parallel capacitance to produce

$I_c$ , the voltage and current triangles are all properly completed.

#### Alternative Solution

In an earlier paragraph, it was stated that any voltage vector  $E$  (Fig. 8) could be selected when designing the phasing networks. Suppose, for instance, that antenna 3 is thought to be the dominant element in the array and that we wish to do all the tuning in the networks feeding antennas 1 and 2. Then,  $E_{L3}$  is the input voltage, as shown in Fig. 10. The design in this case follows the same principles established in previous examples.

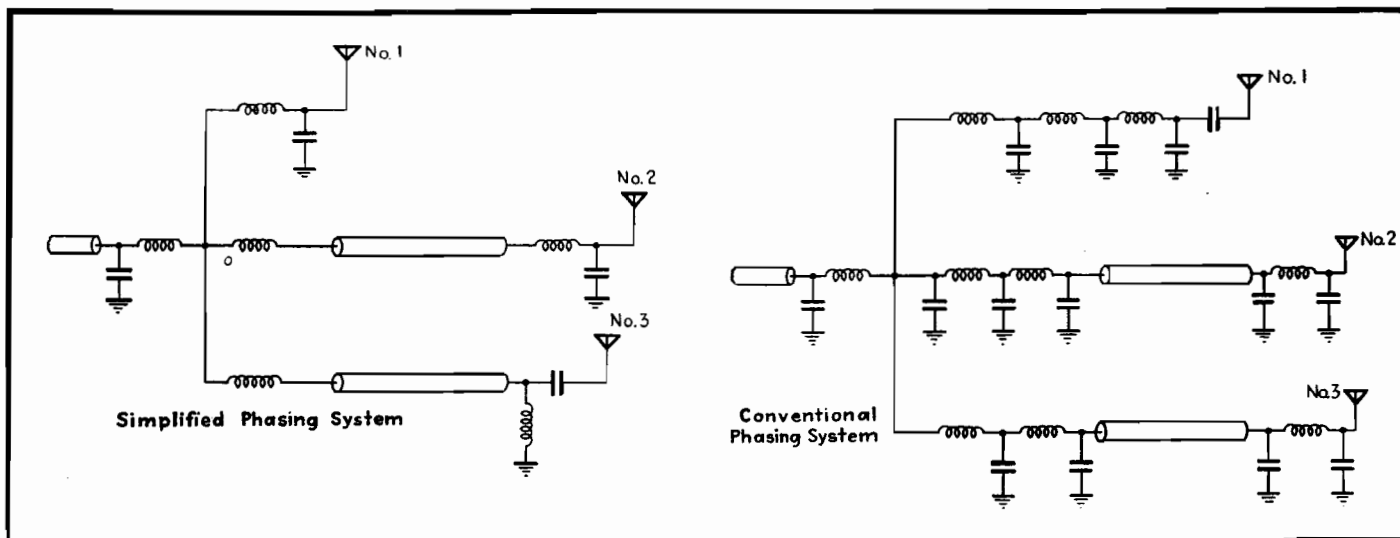


Fig. 11.—Complete, simplified system of networks designed by vector synthesis, and equivalent system of networks designed by conventional methods.

# Calculating Broadcast-station Coverage

By RAYMOND F. GUY

Broadcast stations, like newspapers, must prove the size of their audience, and improve it. Equations for calculating the coverage are given, and they show clearly the influence of frequency, power, and ground conductivity on signal intensity

THE coverage of a station is dependent on the following factors:

1. Power.
2. Antenna design.
3. Soil conditions as they determine the rate of decay of waves over the earth.
4. Interference from other stations.
5. Local noise levels.

The influence of power on coverage is well known. The field intensity produced from a station, exclusive of everything but power, is proportional to the square root of the power increase or decrease.

$$E = \sqrt{P} \quad (1)$$

where  $E$  is the field intensity and  $P$  is the power.

## Effect of Frequency Assignment

It is well known that the frequency assignment has a considerable effect on the coverage obtainable in the primary area. Figure 1 shows a comparison of coverage obtainable from a 50,000-watt station over average soil when operating on approximately the highest broadcast frequency in one case, and approximately

the lowest frequency in the other case. An inspection of the expression for propagation of waves, following, will show the effect of  $\lambda$ , the wavelength.

The most satisfactory expression for computing field intensities along the surface of the earth is the Sommerfeld solution in the empirical form due to Van der Pol.

The field from an antenna decays for two reasons:

1. Dispersion, in which field intensity varies directly with distance.
2. Losses in the earth due to heating, at a variable rate.

These effects are combined in the following Van der Pol expression:

$$E = \frac{E_0}{d} A \quad (2)$$

where  $E$  = field intensity, microvolts per meter, and

$$E_0 = 1.86(10^5) \frac{P}{d} \quad (3)$$

if radiated power is known, or

$E_0$  = field intensity in microvolts per meter at 1 mile in the absence of attenuation

$d$  = distance in miles at which  $E$  is evaluated

$P$  = radiated power in kilowatts, and

$$A = \frac{2 + 0.3p}{2 + p + 0.6p^2} \quad (4)$$

where Sommerfeld's numerical distance  $p$  is

$$p = \frac{0.842 - d}{\sigma \lambda^2 \times 10^{15}} \quad (5)$$

where  $\lambda$  = wavelength in meters, and

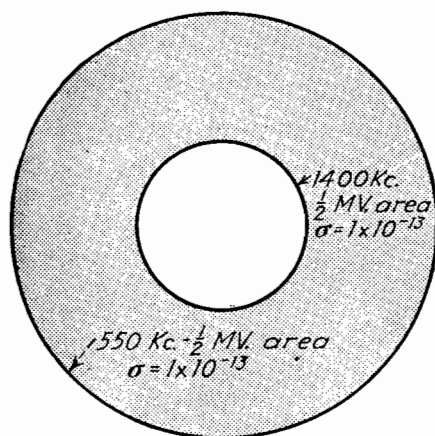
$\sigma$  = ground conductivity in emu which varies approximately from  $4 \times 10^{-11}$  for sea water to  $10 \times 10^{-15}$  for very dry earth.

Equation (4) neglects the dielectric constant of the soil, which in most cases is permissible. Inclusion of the effect of the dielectric constant is treated in the literature.\*

## Soil Conditions

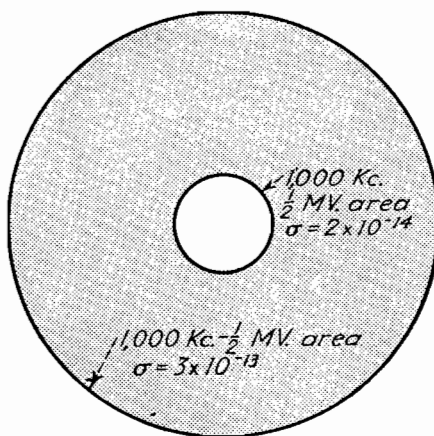
Unfortunately, soil constants have a very great influence on the coverage of a radio station, and, except for locating a station to the best advantage within a small area, nothing can be done about it.

\* NORTON, K. A., Propagation of Radio Waves over a Plane Earth, *Nature*, June 8, 1935.



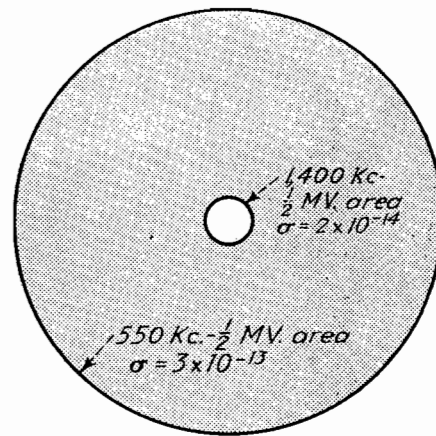
1,700 V/M at one mile

Fig. 1.



1,700 MV/M at one mile

Fig. 2.



1,700 MV/M at one mile

Fig. 3.

Figs. 1, 2, and 3.—Coverage areas, showing the effects of frequency and soil constants, all referred to a field strength of 1,700 mv per meter at 1 mile. The shaded areas show the increased coverage made possible by low frequency assignment, high soil conductivity, and by the combination of the two factors.

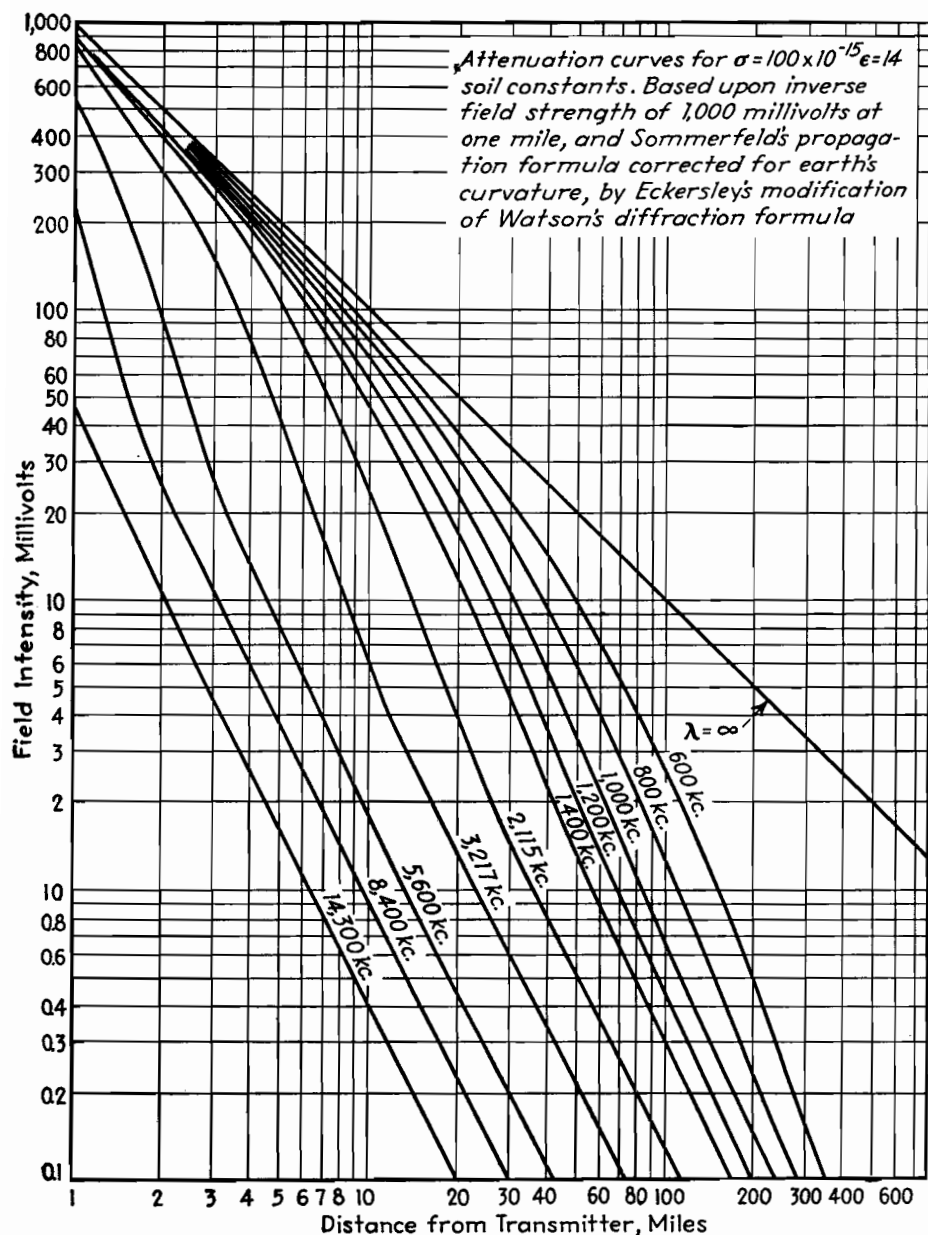


Fig. 4.—Typical chart used to compute field intensities when the soil constant is known (in this case  $100 \times 10^{-15}$ ), taking into account the effect of frequency assignment.

Once the soil constants have been evaluated by measurements, preferably by measurement of the rate of decay of field intensity with distance, the calculation of station performance using the above expression is comparatively simple.

A number of representative soil constants  $\sigma$  for various sections of the United States are given below. They apply only to localized areas and are intended to show only the range of constants encountered.

#### Typical Soil Constants

Texas, around Dallas and Fort

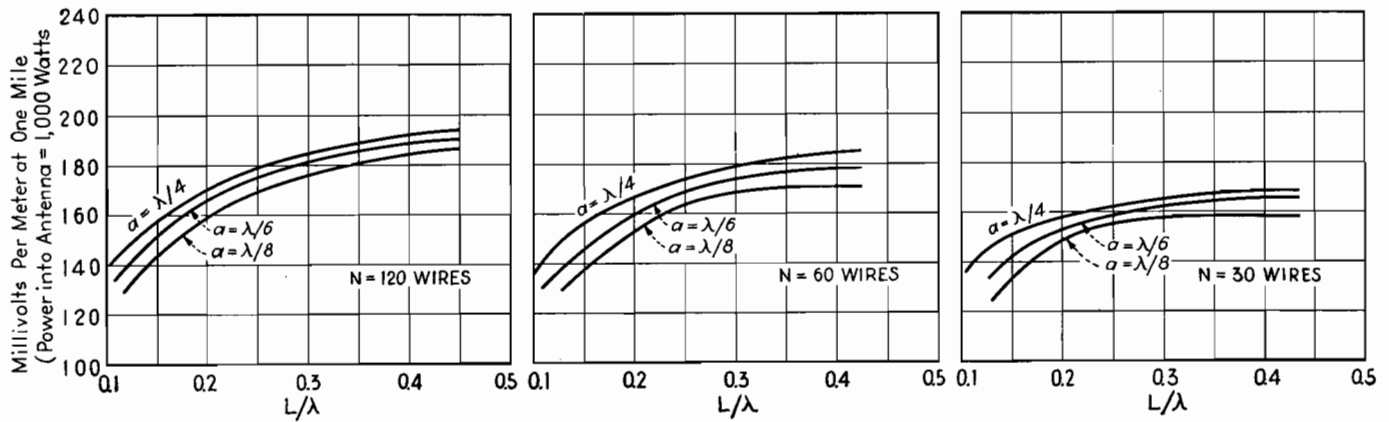
Worth.....	$15 \times 10^{-14}$
Upper Mississippi Valley.....	$1 \times 10^{-13}$
Lower New Jersey.....	5 to $10 \times 10^{-14}$
Vicinity of Pittsburgh.....	3 to $5 \times 10^{-14}$
Salt marshes.....	$1 \times 10^{-12}$
Very dry earth, approximately.....	$1 \times 10^{-15}$
Moist black loam.....	1 to $2 \times 10^{-13}$
Mountainous country.....	5 to $10 \times 10^{-15}$
Upper New York State.....	3 to $8 \times 10^{-15}$
Area about Chicago.....	$1.25 \times 10^{-13}$
Denver, except to West.....	$1 \times 10^{-13}$
Central Massachusetts, approximately.....	$4 \times 10^{-15}$
Ohio.....	$1 \times 10^{-13}$
Pennsylvania.....	3 to $7 \times 10^{-14}$
North Carolina, around Charlotte and Raleigh.....	2 to $5 \times 10^{-14}$
Upper New Jersey exclusive of mountains.....	7 to $10 \times 10^{-14}$
South Atlantic States, approximately.....	3 to $5 \times 10^{-14}$
Sand, approximately.....	$3 \times 10^{-14}$

Figure 4 shows a chart used for computing field intensities when the soil constant is  $100 \times 10^{-15}$ , a typical value. A reference level of 1,000 mv at 1 mile is used.

# Radial Ground System Chart

By GEORGE H. BROWN

Signal strength in millivolts per meter at 1 mile from a vertical antenna using a radial-wire ground system.  $L$  = length of radial ground wires;  $\lambda$  = operating wavelength;  $a$  = antenna height;  $N$  = number of radial wires



## SECTION III

# AUDIO AMPLIFIERS

	Page
Resistance-coupled Amplifier Design Charts.....	48
Design of Class A Push-pull Amplifiers.....	50
Design of Class B and AB Output Transformers.....	52
Cathode-follower Calculations.....	55
Harmonic Analysis of Overbiased Amplifiers.....	56

## Resistance-coupled Amplifier Design Charts

By GLENN KOEHLER

Charts for determining the gain of resistance-capacitance-coupled audio amplifiers in terms of tube and circuit constants at low, medium, and high frequencies

**T**HE formulas used in designing resistance-capacitance-coupled audio units have not been considered suitable for graphical representation, but it is quite possible to bring together all the determining factors in chart form, if separate charts for low, medium, and high frequencies are prepared. At low frequencies the coupling capacitor is of primary importance; at medium frequencies the resistance values alone determine the gain; while at high frequencies the parallel capacitances of tube elements and wiring are the limiting factors.

The complete diagram of connections for a two-stage resistance-capacitance-coupled amplifier is shown in Fig. 1. The dotted-line connections represent the interelectrode capacitances of the tubes and the sockets. At the medium frequencies of the range for which the amplifier is designed, the gain-frequency characteristics of the amplifier are not appreciably affected by the coupling capacitor or the interelectrode capacitances. At these frequencies, the gain per stage, *i.e.*,  $E_{g2}/E_{g1}$ , is a function of the amplification constant  $\mu_1$  and the plate resistance  $R_{p1}$  of the input tube and the two resistors labeled  $R_{o1}$  and  $R_{g2}$ . Chart 1 is constructed to give the voltage amplification  $E_{g2}/E_{g1}$  in per cent of the amplification constant of this tube for any specified values of  $R_{p1}$ ,  $R_{o1}$ , and  $R_{g2}$ .

The range of the chart covers practically all cases that are usually encountered in design.

At the low frequencies, the coupling capacitor causes the gain of the amplifier to decrease with decrease in frequency. It is usually customary to specify the loss in amplification at a particular low frequency in terms of the gain at the medium frequency. This loss is usually designated in decibels. Specifically, the decibel loss at a low frequency  $f_l$  is equal to  $20 \log_{10}$  (voltage amplification at a medium frequency divided by the voltage amplification at the frequency  $f_l$ ). By a medium frequency is meant a frequency for which neither the coupling condenser nor the interelectrode capacitances have any effect. Chart 2 is constructed to show how the decibel loss at 50 cycles depends on the size of the coupling capacitor  $C_{1-2}$ , the resistances  $R_{o1}$ ,  $R_{g2}$ , and the plate resistance  $R_{p1}$ . This chart may be used for any frequency  $f_l$  simply by multiplying the size of the coupling condenser by  $f_l/50$ . If the chart is used for finding the size of the coupling capacitor for preassigned values of  $R_{o1}$ ,  $R_{g2}$ , and  $R_{p1}$  which will give a certain decibel loss at a frequency  $f_l$ , then multiply the value of  $C_{1-2}$  as read on the chart by  $50/f_l$ .

For the high frequencies, the voltage amplification decreases with increase in

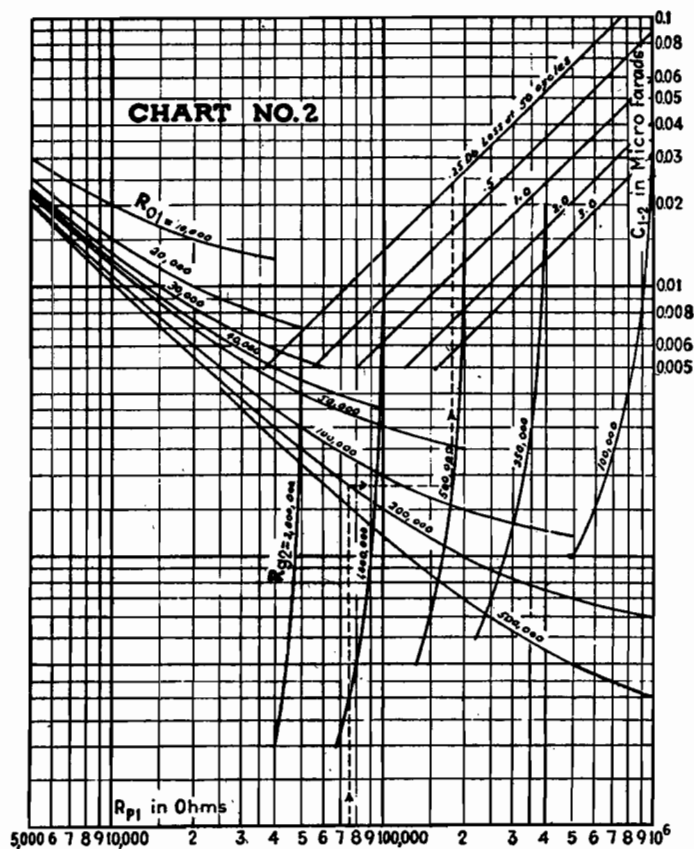
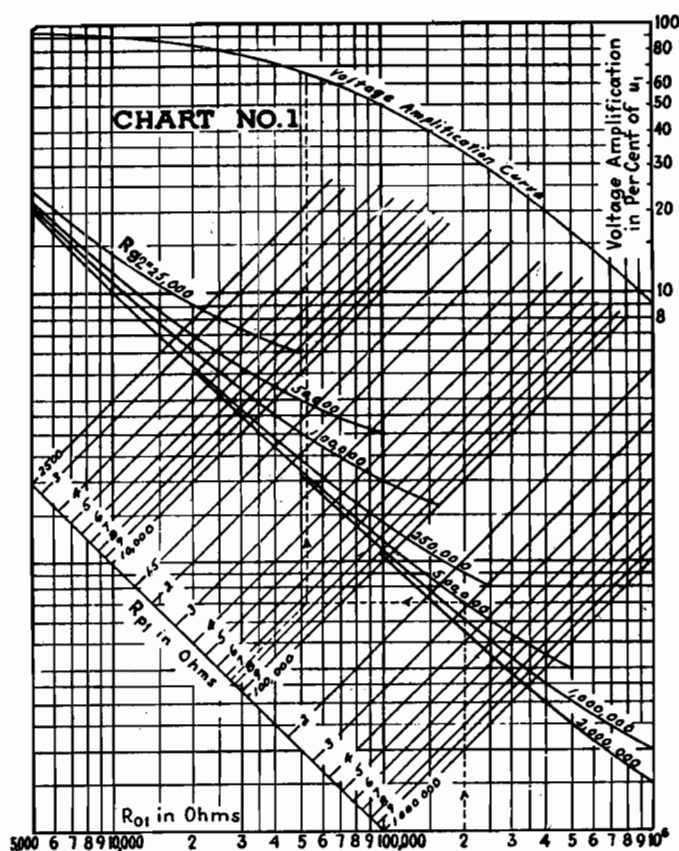
frequency because of the interelectrode capacitances of the tubes and sockets. The principal effect of these capacitances is to shunt the two resistors  $R_{o1}$  and  $R_{g2}$  with a capacitance  $C_e$  which has the value given approximately by the relation

$$C_e = C_{gp1} + C_{pk1} + C_{gk2} + C_{gp2}(1 + |A_{v2}|)$$

where  $A_{v2}$  is the voltage amplification of the second tube and the  $C$ 's are as shown in Fig. 1. Most of these capacitances for the tubes alone can be obtained from the tube handbooks. Allowance must be made for the sockets and leads because in some cases the capacitances of these may be as large as the corresponding values for the tubes alone. The decibel loss at a high frequency  $f_h$  is  $20 \log_{10}$  (voltage amplification at the medium frequency divided by the voltage amplification at the frequency  $f_h$ ). Chart 3 is so constructed that the decibel loss at 10,000 cycles may be evaluated when  $R_{o1}$ ,  $R_{g2}$ ,  $R_{p1}$ , and  $C_e$  are known. This chart may be used for any frequency  $f_h$  simply by multiplying the actual  $C_e$  of the tubes and sockets by  $f_h/10,000$  and using the scale shown.

### Example of the Use of the Charts

Suppose the problem is to design a multistage resistance-capacitance-coupled amplifier. The range of the amplifier is, for example, 50 to 10,000 cycles. The



The values marked in each chart correspond to the component parts given in the circuit diagram below. Chart 1 is used for computing the gain (in percentage of tube amplification constant) of the stage in the medium audio frequencies. Chart 2 gives the decibel loss at low frequencies (50 cycles) in terms of the size of the coupling condenser. Chart 3 gives the decibel loss at high frequencies (10,000 cycles) in terms of parallel (tube and wiring) capacitances.

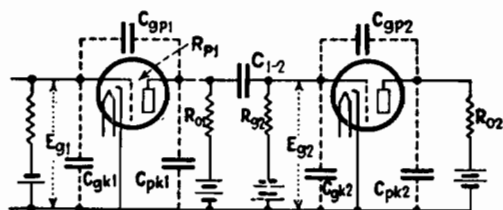
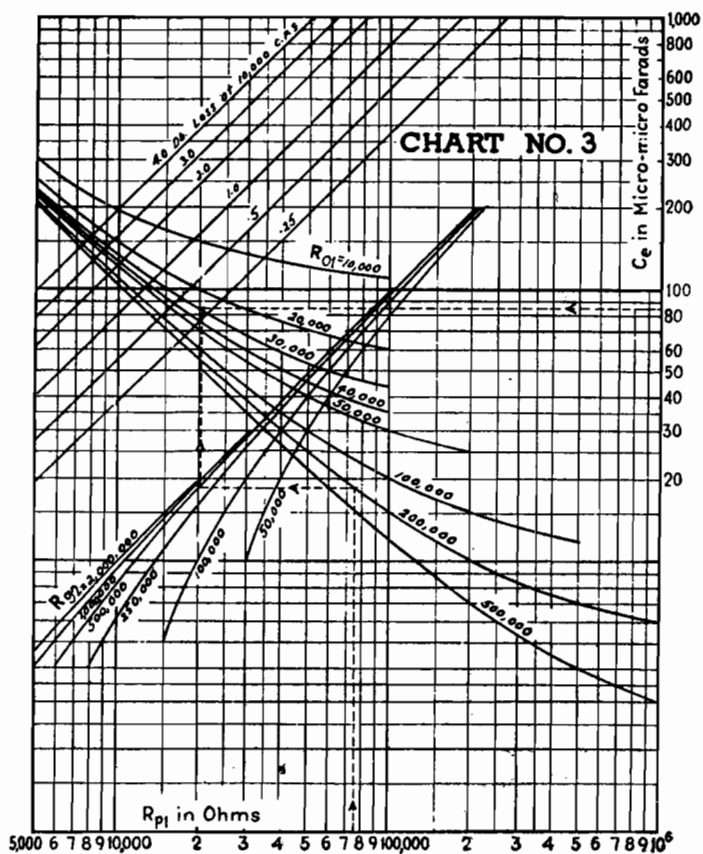


Fig. 1.—Circuit of two-stage resistance-capacitance-coupled amplifier.



over-all voltage amplification and the decibel variation over the frequency range are given certain preassigned values. The design problem becomes one of treating each stage separately and arriving at such characteristics for each stage that the entire amplifier will have the preassigned characteristics. The over-all characteristics of the multistage amplifier are obtained by adding the gains in decibels of each of the stages or taking the product of the voltage amplifications for all the stages. The gain in decibels is  $20 \log_{10}$  of the voltage amplification.

The procedure in design is a trial-and-error process which usually starts with selecting the tubes and the resistors that will give the desired voltage amplification at the medium frequencies. The voltage

amplification per stage for a selected tube and set of resistors is determined from Chart 1. The method of using Chart 1 is to locate first the intersection of the  $R_{o1}$  and the  $R_{o2}$  lines. Through this intersection a horizontal line is drawn to intersect with the  $R_{p1}$  line. From this latter intersection a vertical line is drawn to the voltage-amplification curve at the top of the chart, and the voltage amplification in per cent of the amplification constant of the tube is read at the right of the chart. This gives  $E_{o2}/E_{o1}$  or the voltage amplification of the input stage. The dotted line on the chart illustrates the case of  $R_{o1} = 200,000$  ohms,  $R_{o2} = 500,000$  ohms, and  $R_{p1} = 75,000$  ohms. The voltage amplification is approximately equal to  $0.65 \mu_1$ .

The next step in the design is to see what the decibel loss will be at the highest frequency. If it is not within the pre-assigned limits,  $R_{o1}$  and  $R_{o2}$  will have to be lowered. The dotted line on Chart 3 illustrates the method of determining the decibel loss at 10,000 cycles. For the example illustrated  $R_{o1} = 200,000$  ohms,  $R_{o2} = 500,000$  ohms,  $R_{p1} = 75,000$  ohms, and  $C_o = 85 \mu\text{f}$ . The decibel loss at 10,000 cycles is approximately 0.3.

The final step is to fix the size of the coupling capacitor  $C_{1-2}$  for a given decibel loss at the lowest frequency. For this procedure Chart 2 is used. For the example given above, the dotted line construction which illustrated the procedure yields a value of approximately  $0.025 \mu\text{f}$  for a 0.25-db loss at 50 cycles.

## Design of Class A Push-pull Amplifiers

By E. W. HOUGHTON

Push-pull power output calculations for Class A amplifiers can be made as readily as for single-ended amplifiers. A simplified method of obtaining circuit operation from tube characteristics is given

A push-pull circuit is represented diagrammatically in Fig. 1. Assuming a perfect output transformer by neglecting leakage reactance and resistance and exciting current, then transferring the load resistance  $R_L$  to its equivalent value in the primary, the simplified circuit in Fig. 2 results.

The voltage developed across the transferred plate-to-plate load is

$$E = (I_1 - I_2)R_p \quad (1)$$

The power output is then

$$\begin{aligned} P_o &= E(I_1 - I_2) \\ &= (I_1 - I_2)^2 R_p \end{aligned} \quad (2)$$

The use of static  $E_p I_p$  curves for obtaining the power output and distortion of a single tube operating in class A is quite familiar. As indicated by Eqs. (1) and (2) the calculation of push-pull performance must involve the use of plate current difference characteristics ( $I_1 - I_2$ ). These characteristics can be obtained by a convenient method due to B. J. Thompson. This is illustrated in Fig. 3 for two type 2A3's operating with 250 volts on the plate and 50 volts grid bias. These curves were produced by constructing two individual static characteristic families, one inverted with respect to the other, with a common

zero-signal plate voltage  $E_o$ , then subtracting corresponding static characteristics point by point. The resultant dotted lines trace out the plate current difference characteristics ( $I_1 - I_2$ ) flowing in the output transformer for different grid-excitation values.

The dotted lines representing the equivalent static family of  $E_p I_p$  curves for the two tubes in push-pull can be utilized for predicting their combined effect just as the individual static  $E_p I_p$  characteristics for a single tube in class A can be used for calculating its output and distortion for a given load. Similarly, the

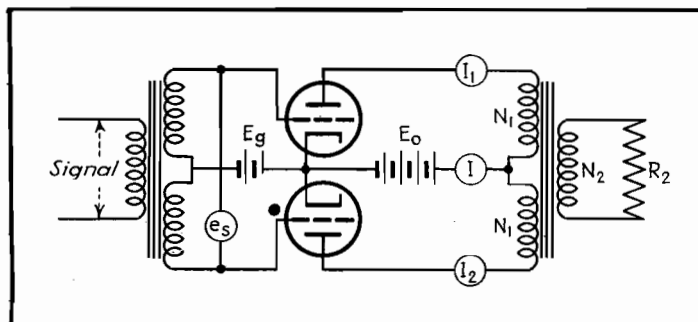


Fig. 1.—Actual diagram of push-pull amplifier.

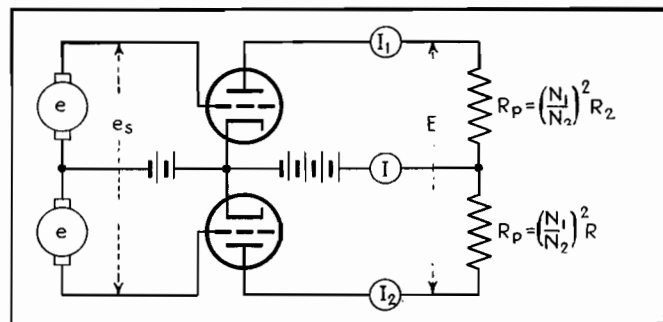


Fig. 2.—Simplified push-pull amplifier circuit.



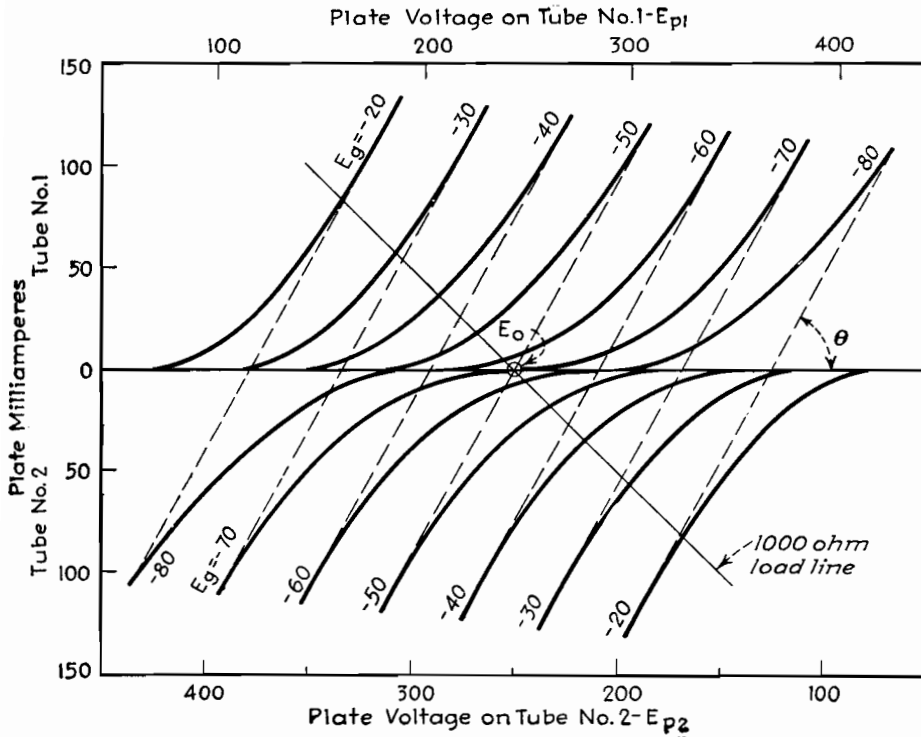


Fig. 3.—Double set of plate characteristics for 2A3 tubes.

equivalent plate resistance  $r_p$  of the push-pull tubes is equal to the reciprocal of the slope of the static difference characteristics or to  $\cot \theta$  in Fig. 3. Thus, the plate-generator circuit for push-pull tubes evolves from the above considerations as shown in Fig. 4.

The alternating current flowing in the output circuit is

$$i_p = \frac{\mu e}{R_p + r_p} \quad (3)$$

The power output is

$$P_o = \frac{\mu^2 e^2 R_p}{(R_p + r_p)^2} \quad (4)$$

These plate-generator equations are identical to those used for a single class A stage; however, notice that  $\mu$  is the amplification factor of the tubes,  $e$  the rms signal applied to one grid,  $R_p$  the load transferred to one-half of the output transformer primary, and  $r_p$  the reciprocal of the slope of the plate current difference characteristics.

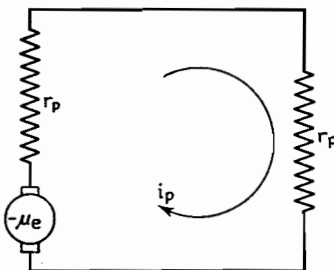


Fig. 4.—Equivalent circuit of push-pull amplifier.

The chief objection to this method of applying the plate-generator attack is that the evaluation of  $r_p$  must be obtained by the cumbersome construction of two sets of curves. Examination of the effect of changing either the grid bias or plate voltage further increases the task, since new plots must be made for each different static voltage condition (Fig. 3). A simplifying method that removes the necessity of plotting curves and utilizes only the plate characteristic curves sent out by the manufacturer will be shown.

Notice from Fig. 3 that the resultant characteristics are all very nearly parallel lines; hence the effective plate resistance  $r_p$  can be closely approximated by constructing only one pair of inverted curves. Further simplicity results by using the zero-signal characteristics ( $E_g = -50$ ,  $E_p = 250$ , in Fig. 3). This difference characteristic passes through the common plate voltage  $E_o$  and becomes tangent to the static curve of tube 1 when the plate current in tube 2 becomes zero ( $E_{p1} = 300$ ). This point of tangency  $E_t$  can be calculated by a fundamental relationship

$$E_t = 2E_o - \mu E_g \quad (5)$$

where  $E_t$  is the plate voltage at which the difference curve touches the static curve,  $E_o$  the zero-signal voltage,  $\mu$  the amplification factor of the tubes, and  $E_g$  the grid biasing voltage.

With the two points  $E_t$  and  $E_o$  known, it is now possible to connect them with a straight line, which represents the upper half of the difference characteristic for zero signal. The value of  $r_p$  can then be readily calculated.

To illustrate the expediency of this plan, calculations will be made using the static plate characteristics of the type 2A3 (Fig. 5).

With a grid bias of 50 volts and 250 volts on the plates, the tangential point is given from Eq. (5) as  $E_t = (2 \times 250) - (4 \times 50) = 300$  volts. The upper half of the difference curve  $E_oA$  is shown in Fig. 5. The equivalent plate resistance is

$$r_p = \cot \theta = \frac{50}{0.095} = 525 \text{ ohms}$$

Comparison of this result with that obtained by taking point-by-point differences (Fig. 3) shows an exact agreement. This method was used to investigate the conditions of push-pull circuit operation for several values of grid and plate operating voltages, the results being given in the following table:

Plate voltage	Grid voltage	Equivalent plate resistance, ohms	Difference line on Fig. 5
200	-30	323	$E_o'E$
200	-40	625	$E_o'D$
250	-40	375	$E_oB$
250	-50	525	$E_oA$
250	-60	1,000-600	$E_oC$

It is evident that a plate voltage of 250 and a grid bias of 60 volts results in an undesirable curved difference characteristic, prohibiting the use of a higher bias than about 50 volts. The chief effects of reducing the bias below -50 volts are to decrease the equivalent plate resistance, and to increase the zero-signal plate current. Therefore, the answer to the problem must be about 50 volts grid bias, the most economical bias value to give low-percentage distortion. The expected output can now be quickly approximated.

If  $E_o = 250$  volts,  $E_g = -50$  volts, and  $r_p = 525$  ohms, then for maximum undistorted output, the external load resistance is  $R_p = 2r_p = 1,000$  ohms and  $R_2 = 4,000$  ohms if a unity ratio exists between the secondary and entire primary of the output transformer. With a grid-to-grid signal  $e_s = 100$  volts (maximum value), or  $e = 50$  volts (maximum value), we

can calculate the power output from Eq. (4) to be

$$P_o = \frac{4^2 \times 50^2 \times 1,000}{2(525 + 1,000)^2} = 8.6 \text{ watts}$$

This plan is an effective means of quickly making a tentative selection of the best grid bias for a given plate voltage. The expected output can be approximated for the push-pull tubes by predicting their combined effect directly from individual static plate characteristics, obviating the necessity of tedious constructions. If greater accuracy is needed, the output and distortion can be predicted by the usual constructional operations performed on a point-by-point curve, such as Fig. 3.

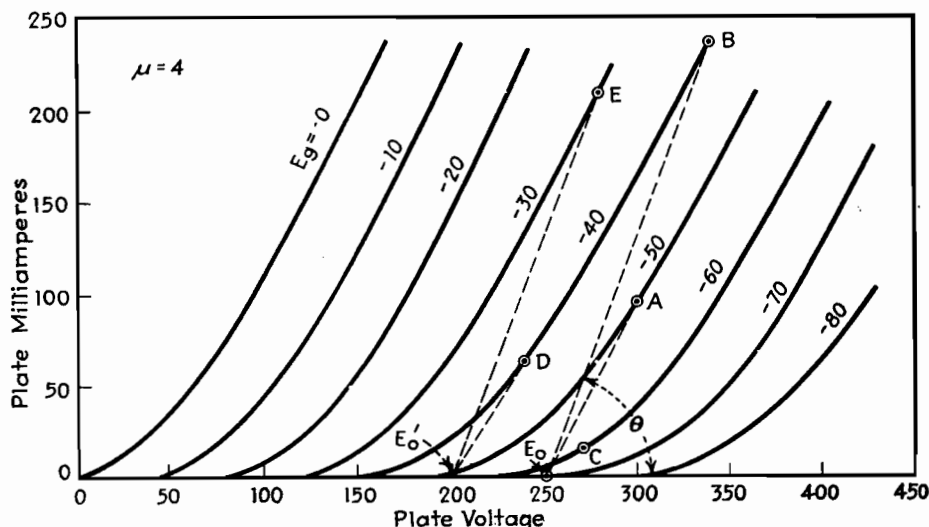


Fig. 5.—Plate characteristics of 2A3 tube.

## Design of Class B and AB Output Transformers

By GLENN KOEHLER

Output transformer design, with approximate methods of determining load resistance and power output

It is the purpose here to aid in designing output transformers for class B and class AB amplifiers, to describe an approximate way of determining the load resistance and power output in the fundamental, and to give a way in which the distortion components may be determined approximately from the characteristic curves of the tube.

The class B amplifier requires two primary windings on the output transformer to transfer the output power to the load. The two windings together serve the same purpose as a single winding of the same number of turns as each of the two for the single equivalent class A

tube. Figure 1 shows how the windings are related to each other.

For a swing of the input voltage that is positive to the upper tube, the winding in the plate circuit of this tube carries alternating current toward the plate while the current in the other winding is practically zero. When the input voltage becomes positive with respect to the lower tube, the winding in the plate circuit of that tube carries alternating current toward the plate while the current in the other winding is practically zero. This gives the same results so far as the voltage induced into the secondary is concerned as would be obtained if the two class B tubes were replaced by an equivalent tube operated as class A and only one primary winding used to carry alternating current in alternate directions for the two halves of the input cycle.

The graphical analysis of Fig. 2 illustrates the currents through each of the two windings as derived from an ideal dynamic characteristic of the class B tubes as a unit. The dotted line current waves on this graph illustrate currents whose effects are practically balanced

out in the magnetic medium of the transformer. Actually it is never possible to obtain such an ideal dynamic characteristic for a class B unit. If the load resistance is too high, the  $E_g I_p$  characteristic will flatten off at the two extremes of the grid swing as shown by the dotted lines and if too low they will follow the dashed lines. Distortion will result in either case.

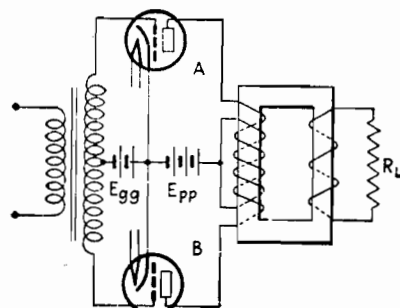


Fig. 1.—Class B or AB amplifier.

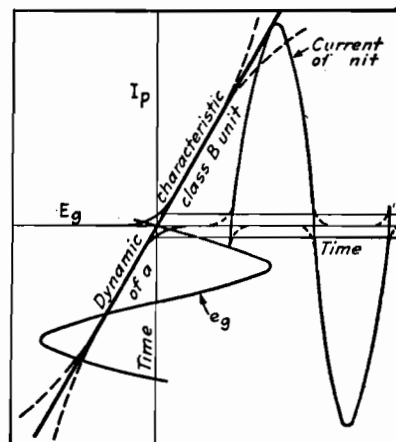


Fig. 2.— $I_q$ - $E_g$  dynamic characteristics of class B unit.

For an ideal transformer, if  $N$  is the ratio of the turns of one primary winding to the secondary winding, the load resistance  $R_L$  is transferred as a resistance  $R_L N^2$  to the two class B tubes as a unit or to the single equivalent class A tube. This is the impedance that determines the dynamic characteristics of the unit and the power output of the unit and not the so-called plate-to-plate impedance. By analogy to the equivalent class A tube, the power in the fundamental is

$$P_o = \frac{\mu^2 E_g^2 R_L N^2}{(R_L N^2 + r_p)^2}$$

in which  $\mu E_g$  is the equivalent generated voltage and  $r_p$  is the internal impedance for the class B unit. The tube factors  $\mu$  and  $r_p$  have the same significance for the class B unit as they do for the single equivalent class A tube. Because the class B tubes are driven over a much greater range, these factors vary some over the range of operation. This is especially true of  $r_p$ . The factors  $\mu$  and  $r_p$  may be measured by direct methods for several values of d-c plate and grid voltages and the average taken. These constants may also be obtained from the characteristic curves of the tube as follows:

The factor  $r_p$  is the reciprocal of the slope of the straighter portion of the  $E_p I_p$  curve at some constant value of grid potential. Since the  $E_p I_p$  curves do not all have the same slope, the average of several curves should be determined. Usually it is sufficiently accurate to evaluate  $r_p$  from an  $E_p I_p$  curve which corresponds to a d-c grid potential equal to the rms value of the a-c grid potential above the grid bias potential  $E_{gg}$ . Since  $\mu = G_{pg} r_p$ , where  $G_{pg}$  is the transconductance of the tube, it is necessary to evaluate  $G_{pg}$  to get  $\mu$ . The tube factor  $G_{pg}$  is the slope of a line that coincides with the greater portion of the  $E_g I_p$  characteristic for a particular value of plate potential. Because the slopes of all such lines for different values of  $E_p$  differ, the average must be taken. When the  $E_g I_p$  curves are not available,  $G_{pg}$  may be evaluated from the  $E_p I_p$  curves by dividing the change in plate current by the change in grid potential which produces the change in plate current when reading such changes along a constant plate-potential line.

#### Distortion

The expression for the power output of the class B unit gives only the power in the fundamental. The expression is

quite accurate for tubes operated with negative bias like the 45, but not for tubes like the 46 operated only in the positive region of the grid swing. There is no simple expression from which the distortion power may be calculated. For low values of input voltage, the distortion is due to the upward curvature of the dynamic characteristic. Distortion of this nature is largest when the load impedance  $R_L N^2$  to the class B unit is smallest.

For a high input voltage, the distortion decreases at first with increase in load resistance, reaches a minimum, and then increases when the downward curvature of the dynamic characteristic becomes excessive. This means that there is some value of load resistance that results in minimum distortion for a given input voltage. This value of load resistance does not generally agree with the value that will result in maximum power in the fundamental for a fixed input voltage, nor with the value that will result in the maximum possible power for a given amount of distortion.

It is possible to predict from the characteristic curves of the tubes the load resistance that gives the maximum possible power output for a limited amount of distortion. The procedure is exactly the same as for the equivalent class A tube. From a given load line (Fig. 3) the dynamic characteristic of  $I_p$  vs.  $E_g$  can be determined as for a class A tube. Then it is possible to determine the distortion fairly accurately.\* The distortion will not be serious if the load resistance  $R_L N^2$  is such that the load line crosses the  $E_p I_p$  characteristic for the peak swing of the grid voltage above the knee of this characteristic.

#### Class B Output Transformer

The above theory gives the conditions, with reference to the equivalent impedance of the source, which must be

\* Proc. IRE, 19, No. 8, p. 1481.

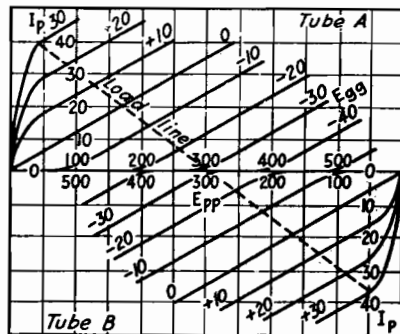


Fig. 3.—Composite  $I_p$ - $E_g$  characteristics of class B unit.

considered in the design of the output transformer. The class B unit is replaced by a single equivalent class A tube. The equivalent source is a generator of  $\mu E_g$  volts with an internal impedance of  $r_p$  ohms. From this equivalent source, power is supplied to the load through only one of the primary windings. Hence the inductive reactance  $\omega L_m$  of each primary winding, with the secondary open, must satisfy

$$\omega L_m = \frac{R_L N^2 r_p}{(R_L N^2 + r_p) \sqrt{\left(\text{antilog}_{10} \frac{\text{db loss}}{20}\right)^2 - 1}}$$

where the decibel loss is the loss in decibels allowed at the lowest frequency over the losses in the transformer at medium frequencies. The d-c resistances of the windings should be added to  $R_L$  for the secondary and to  $r_p$  for the primary.

The ratio of turns  $N$  of one primary winding to the secondary winding must be such as to transfer the load resistance  $R_L$  to whatever resistance is necessary for the class B unit. The load resistance for a given amount of distortion is determined largely by experiment.

Since only one primary winding carries current at a time, it is good practice to interspace the primary windings with each other so they will have the same resistance and will also have the same leakage inductances with respect to the secondary. The two primary windings should also be interspaced with the secondary winding and preferably be placed between the two halves of the secondary. This interspacing improves the h-f response.

#### The Class AB Amplifier

In the case of the class B amplifier, the unit acts as a source of  $\mu E_g$  volts having an internal resistance  $r_p$  ohms. In the case of a push-pull class A amplifier, if put on a unit basis, the voltage of the equivalent generator would be  $\mu E_g$  and the internal impedance  $r_p/2$  ohms, if analyzed on the basis of a single class A tube which would be coupled to the load resistor through a transformer having a ratio of primary turns on each primary to the secondary turns equal to  $N$ .

For a class AB amplifier, since each tube supplies more power to the load on one half cycle of the input than on the alternate half cycle, the internal impedance of the equivalent generator is  $r_p'$  somewhere between  $r_p$  and  $r_p/2$ .

The power output in the fundamental for the class AB unit is

$$P_o = \frac{(\mu E_g)^2 R_L N^2}{(R_L N^2 + r_p')^2}$$

in which  $R_L$  is the load resistance and  $N$  is the ratio of the turns of one primary winding to the secondary turns. It is assumed that the transformer losses are negligible or included as a part of  $R_L N^2$ .

To evaluate  $r_p'$ , draw the composite  $E_p I_p$  characteristics obtained by adding algebraically the  $I_p E_p$  curve of tube A for a grid voltage of  $E_{g0} + X$  volts to the  $I_p E_p$  curve of tube B for a grid voltage of  $E_{g0} - X$  volts. The quantity  $X$  may be either positive or negative. These composite characteristics are the dotted lines of Fig. 4.

It is assumed here that the  $E_p I_p$  curves give straight-line composite characteristics. If this were true, there would be no distortion. Since the distortion is only a few per cent for a good amplifier, these composite characteristics are nearly straight lines for any tube that performs well in a class AB amplifier.  $r_p'$  is the reciprocal of the slope of a composite characteristic. When these characteristics do not all have the same slope,  $r_p'$  should be averaged from several values.

Since  $\mu = G_{pg}/G_p$  it may be evaluated from  $E_p I_p$  characteristics by evaluating the transconductance  $G_{pg}$  and the plate conductance  $G_p$  (the slope of the straighter part of an  $E_p I_p$  curve).  $G_{pg}$  is the ratio of a change in plate current to the change in grid voltage which produces the change

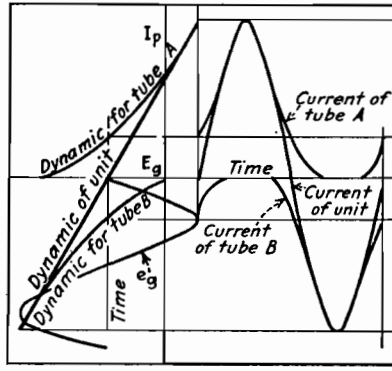


Fig. 5.— $I_p$ - $E_g$  dynamic characteristics of class AB amplifier.

in plate current, when working along a constant plate voltage line.  $\mu$  may also be evaluated from the composite characteristics by determining  $G_{pg}'$  from the composite characteristics and dividing by  $G_p'$ , the slope of a composite characteristic.

In Fig. 4 is shown the load line for each tube as compared with the load line of the unit derived as follows: Constant  $E_p$  lines are drawn through the intersections of the composite characteristics and the load line of the unit. Where each of these vertical lines intersects the  $I_p E_p$  curves from which the composite characteristics were derived, it locates a point on the load line for each tube.

The dynamic  $E_g I_p$  characteristics can be derived from the load lines and composite characteristics. The dynamic  $E_g I_p$  characteristic of the unit is obtained by

plotting the values of  $I_p$  where the unit load line crosses the composite characteristics against the corresponding values of  $E_g$ . The individual dynamic characteristics are obtained by plotting the value of  $I_p$  where the individual load lines cross the  $I_p E_p$  curves against the corresponding values of  $E_g$ . A typical set of dynamic  $E_g I_p$  characteristics is shown in Fig. 5. The current of the unit shown in Fig. 5 is the current that would be delivered to one primary winding by an equivalent single class A tube.

#### Class AB Output Transformer

The general design of the output transformer for a class AB amplifier is the same as for a class B amplifier. The quantity  $r_p'$  is substituted for  $r_p$  in the expression from which the impedance of the transformer is determined to give a particular decibel loss at the lowest frequency.  $r_p'$  is the reciprocal of the slope of a composite characteristic.  $r_p'$  is smaller than  $r_p$ , the plate resistance of the tube. For class AB,  $r_p'$  is somewhere in between  $r_p$  and  $r_p/2$ .

To improve the h-f response, it is preferable to place the two primary windings between the two halves of the secondary. Unless these two windings have nearly the same leakage inductances with respect to the secondary, some distortion will be introduced into the output.

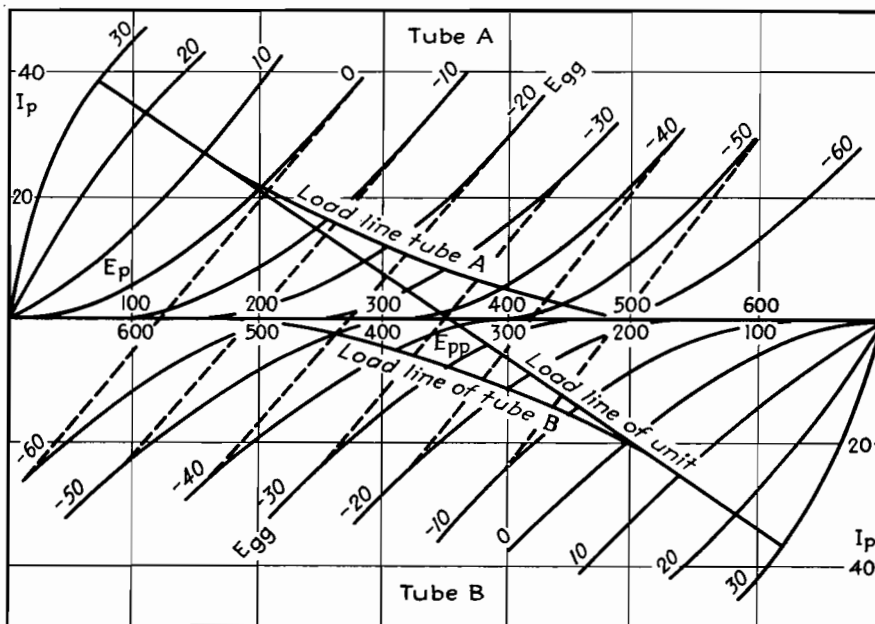


Fig. 4.—Composite characteristics of class AB amplifier.

# Cathode-follower Calculations

By HUMBERT P. PACINI

Equations relating cathode-follower output impedance to the value of the cathode resistor, the plate load resistance of the cathode follower tube, and the transconductance of the tube

IN solving for the output impedance of a cathode follower, such as the one shown in Fig. 1a, it is most convenient to set up the required circuit equations by assuming the cathode of the tube driven by a generator of voltage  $E_1$  and internal resistance  $R_1$ . Figure 1b shows the addition of this generator, and Fig. 1c is the resulting equivalent circuit.

The general equations for a two-loop network are\*

$$Z_{11}I_1 + Z_{12}I_2 = E_1 \quad (1)$$

$$Z_{12}I_1 + Z_{22}I_2 = E_2 \quad (2)$$

where  $Z_{11}$  is the total impedance in loop 1,  $Z_{22}$  the total impedance in loop 2,  $Z_{12}$  the mutual impedance between loops 1 and 2, and  $E_1$  and  $E_2$  are the generator voltages in loops 1 and 2, respectively.

According to Fig. 1c the equivalent voltage acting in the grid circuit, or the rise in voltage from cathode to grid, is  $(I_2 - I_1)R_2$ , and  $-\mu(I_2 - I_1)R_2$  is the voltage acting in the plate circuit in the direction shown if it is taken as voltage

\* EVERITT, W. L., "Communication Engineering," pp. 217-229, McGraw-Hill Book Company, Inc., New York.

driving  $I_2$  clockwise. Upon substitution of these values in Eqs. (1) and (2) there results

$$(R_1 + R_2)I_1 - R_2I_2 = E_1 \quad (3)$$

$$-R_2I_1 + (R_2 + R_p)I_2 = -\mu(I_2 - I_1)R_2 \quad (4)$$

Solving these two simultaneous equations yields for the driving point impedance

$$Z_1 = R_1 + R_2 - \frac{R_2^2(1 + \mu)}{R_p + (1 + \mu)R_2} \quad (5)$$

from which it is obvious that the impedance looking into the cathode, i.e., the output impedance of the cathode follower, is

$$Z_1 - R_1 = R_2 - \frac{R_2^2(1 + \mu)}{R_p + (1 + \mu)R_2} = Z_{out} \quad (6)$$

Since  $\mu$  is much larger than 1, especially in high-gain triodes and pentodes, Eq. (6) may be converted to

$$Z_{out} = R_2 - \frac{R_2^2}{(R_p/\mu) + R_2} = R_2 - \frac{R_2^2}{(1/g_m) + R_2} \quad (7)$$

This impedance is made up of the cathode resistance and the internal impedance of the cathode in parallel; and if

$Z_c$  represents the latter, Eq. (7) can be written

$$Z_{out} = \frac{Z_c R_2}{Z_c + R_2} \quad (8)$$

After transformation and substitution of Eq. (7) for  $Z_{out}$

$$Z_c = \frac{1 + g_m R_2}{g_m} - R_2 = \frac{1}{g_m} \quad (9)$$

If the cathode follower tube had been used with a plate load, either to limit the plate current or to provide a push-pull voltage, the equation for the internal impedance of the cathode follower would be

$$Z_c = \frac{1}{g_m} + \frac{Z_L}{\mu} \quad (10)$$

where  $Z_L$  is the plate load.

The internal impedance of a cathode follower is given by Eq. (9) for the case of no plate load, or by Eq. (10) if there is plate load. It is seen from Eq. (8) that the effect of the internal impedance of the cathode follower tube is to add an impedance  $Z_c$ , in parallel with the cathode load impedance.

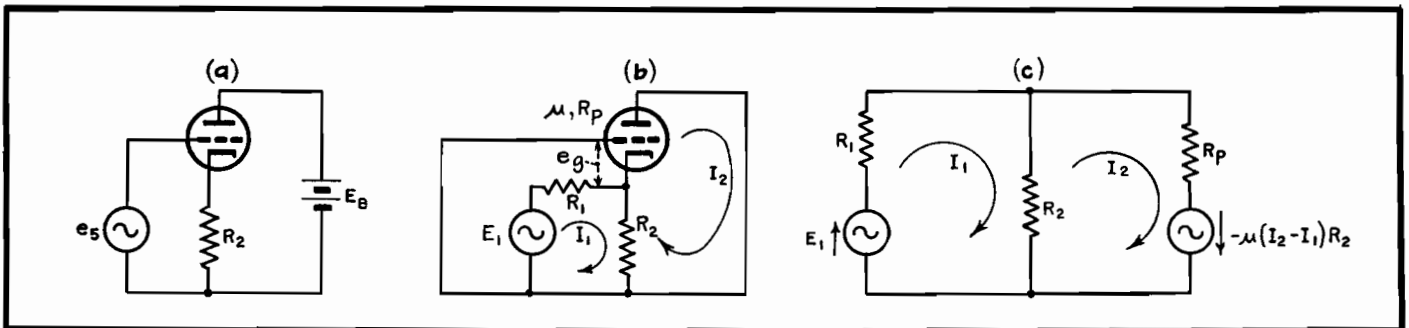


Fig. 1.—a. The actual circuit in which the impedance across  $R_2$  is sought. In b a fictitious generator,  $E_1$ , of internal impedance  $R_1$ , is introduced. The equivalent circuit from which the derivation begins is shown at c.

# Harmonic Analysis of Overbiased Amplifiers

By ULRICH R. FURST

Quick graphical method of determining harmonic components up to the tenth for voltage or current in various classes of amplifiers. Amount of distortion can thus be predicted

WHEN the efficiency of an amplifier is improved by increasing its grid bias so that no plate current flows during a part of the cycle, considerable harmonic distortion is introduced at the same time. The amount of this distortion and its distribution among the various harmonic frequencies depends mainly on the fraction of the cycle during which the tube conducts and to a small extent also on the curvature of the characteristic of the tube. It is important that the designer of such amplifiers can predict what distortion is to be expected.

Harmonic distortion can be computed with the assumption that the tube characteristic can be approximated by a straight line intersecting the abscissa axis at the point of plate-current cutoff as shown in Fig. 1. The curves have been plotted from values obtained by a Fourier analysis of that part of a sine function which has been shown shaded in Fig. 1. This portion of the function represents

the current actually flowing in a tube having an idealized straight-line characteristic. If the coordinate system is selected so that the ordinate axis coincides with the line of symmetry, only cosine terms appear in our Fourier series

$$f(x) = \frac{A_0}{2} + A_1 \cos x + A_2 \cos 2x + A_3 \cos 3x + \dots$$

where the coefficients  $A_0, A_1, A_2, A_3, \dots$  are not constants, but depend on the angle of conduction, *i.e.*, that fraction of the full cycle of the signal voltage during which the tube is conducting, expressed in electrical degrees. They are the peak values of the harmonic currents, expressed as a fraction of the peak value  $I_m$  (Fig. 1) of the current actually flowing through the tube.

Mathematically, these coefficients are expressed by the integral

$$A_n = \frac{1}{\pi} \int_{-\pi}^{+\pi} f(\phi) \cos n\phi d\phi$$

Evaluating this integral we obtain

$$A_0 = \frac{2}{\pi} \frac{1}{1 - \cos \frac{\theta}{2}} \left( \sin \frac{\theta}{2} - \frac{\theta}{2} \cos \frac{\theta}{2} \right)$$

$$A_n = \frac{1}{n\pi} \frac{1}{\left(1 - \cos \frac{\theta}{2}\right)} \left[ \frac{\sin(n-1)\frac{\theta}{2}}{n-1} - \frac{\sin(n+1)\frac{\theta}{2}}{n+1} \right] \text{ for } n \geq 1$$

where  $\theta$  is the angle of conduction (as defined above) in radians and  $n$  is the order of the harmonic. For the first few harmonics, this can be rewritten for greater ease in calculating as

$$A_1 = \frac{1}{2\pi} \frac{1}{1 - \cos \theta/2} \left( \theta - \sin \frac{\theta}{2} \right)$$

$$A_2 = \frac{2}{3\pi} \frac{1}{1 - \cos \theta/2} \sin^3 \frac{\theta}{2}$$

$$A_3 = \frac{2}{3\pi} \frac{1}{1 - \cos \theta/2} \sin^3 \frac{\theta}{2} \cos \frac{\theta}{2} = A_2 \cos \frac{\theta}{2}$$

It can be seen that these coefficients are oscillating functions of  $\theta$ , *i.e.*, they assume positive and negative values in alternate ranges of  $\theta$ .

It is desirable to have curves of this kind plotted in a logarithmic rather than in a linear scale, as the former permits reading all values with the same percentage of accuracy as compared with the absolute accuracy of a linear scale. Unfortunately, a logarithmic scale does not allow the plotting of negative values. In most cases, however, no distinction need be made between the positive and the negative values, so their absolute values only have been plotted.

For the rare case that the phase relation of the components is important, the symbols + and - have been added on the chart after the number designating the order of the harmonic. All values marked + are in phase with a harmonic produced by a very short impulse.

The scale on the abscissa axis has been so selected that the chart can be used for all types of amplifiers: class A ( $\theta = 360^\circ$ ), class AB ( $\theta = 360^\circ - 180^\circ$ ), class B ( $\theta = 180^\circ$ ) for high-power audio

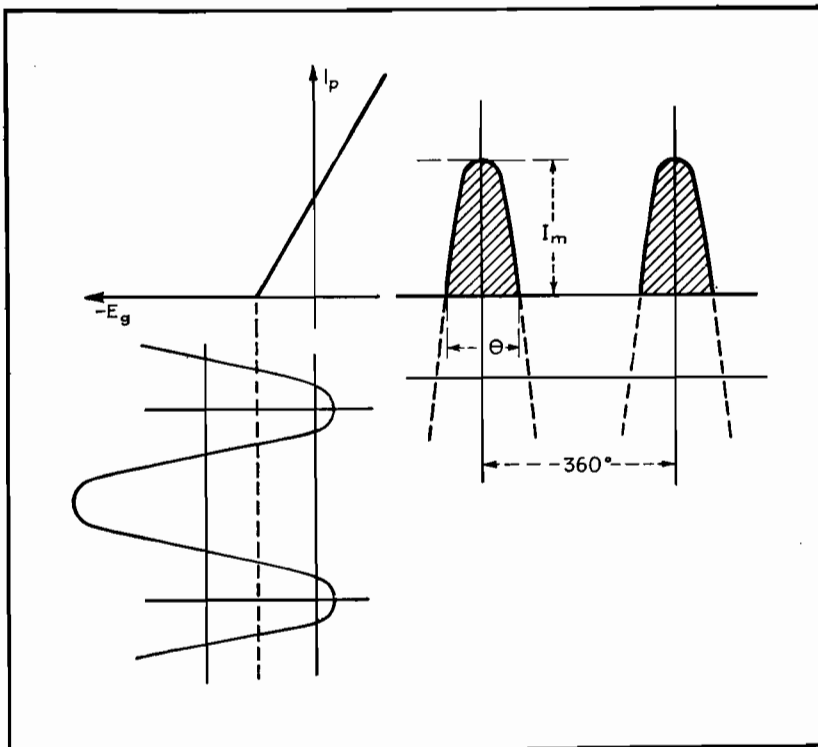


Fig. 1.—The idealized linear amplifier characteristics on which the main graph in Fig. 2 is based.

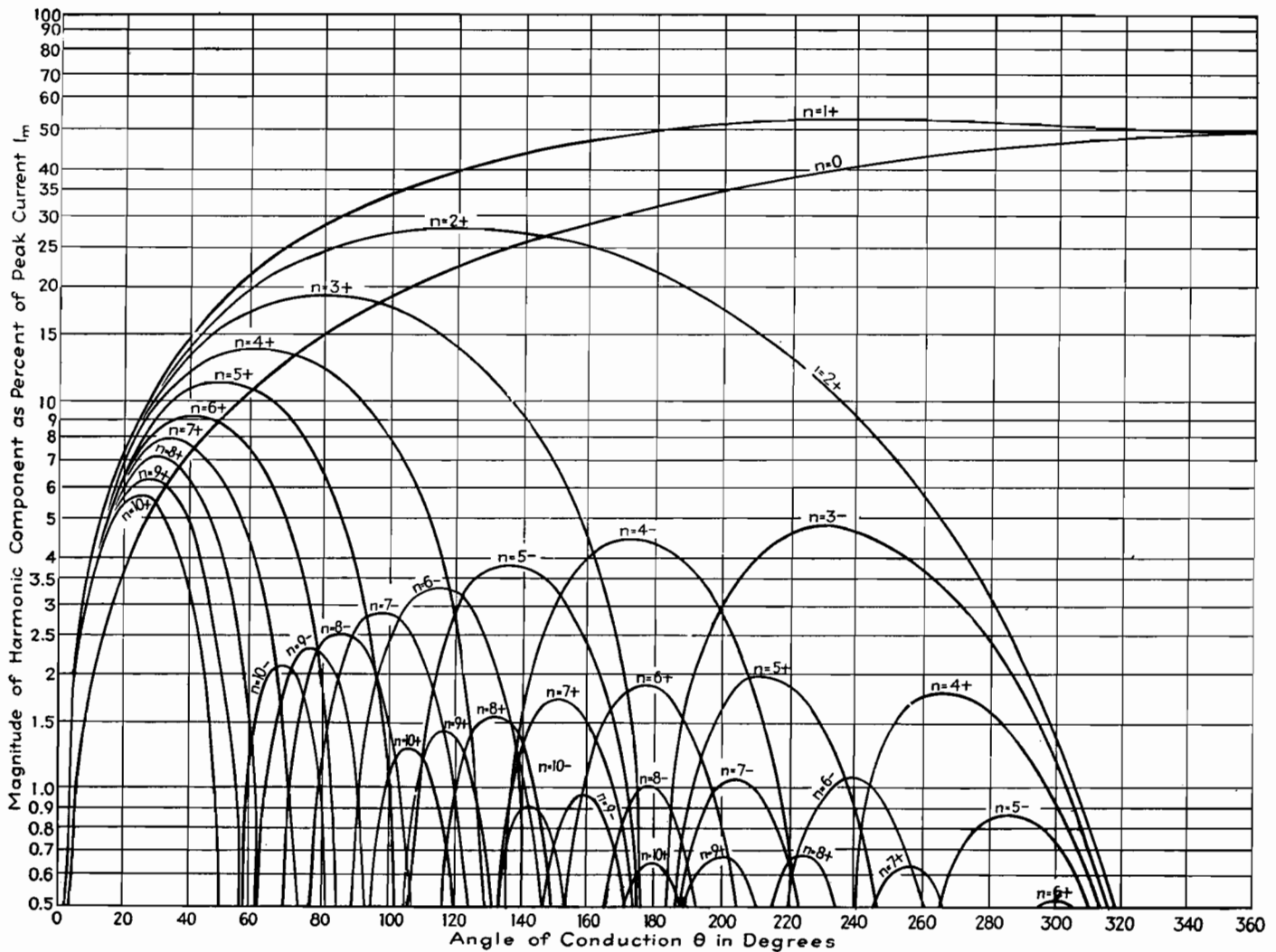


Fig. 2.—The magnitude and phase of the first ten harmonics of an overbiased amplifier. The harmonic amplitudes are expressed in percentages of the peak current for various conducting angles in degrees.

amplifiers and modulators, and class C ( $\theta = 180^\circ - 0^\circ$ ) for r-f oscillators and frequency multipliers.

### Examples

The following examples explain the use of the diagram:

**Example 1.**—A frequency quintupler ( $n = 5$ ) shall be operated under such conditions that the amplitudes of the neighboring harmonics ( $n = 4$  and  $n = 6$ ) of the output frequency are much smaller than the amplitude of the output frequency. Inspection of the chart shows that at  $\theta = 140$  deg the peak current of the fifth harmonic is 3.7 per cent, and those of the fourth and sixth harmonics

are, respectively, only 1.5 and 1.0 per cent of the peak value of the actual current  $I_m$ .

**Example 2.**—The peak value of the third harmonic of a class C amplifier operated at  $\theta = 100$  deg is 17 per cent, that of the fundamental 34 per cent and the d-c component ( $n = 0$ ) 18 per cent of the peak value of the actual current  $I_m$ .

**Example 3.**—To operate a push-pull audio amplifier for good fidelity, no odd harmonic distortion should be present. Inspection of the chart shows that this is the case for  $\theta = 180$  deg, a well-known property of class B amplifiers which makes it possible to use them in push-pull as audio power amplifiers. Of course, the curvature of the tube characteristics will

produce some additional distortion that is not covered by this chart.

**Example 4.**—A class AB amplifier shall be operated with an angle of conduction of  $280$  deg. The direct current will be found to be 46 per cent, the peak signal current is 53 per cent and the second and third harmonics are 3.2 and 2.4 per cent, respectively, of the actual peak current  $I_m$ , which corresponds to 6.1 and 4.5 per cent, respectively, of the signal current.

It should be noted that the plotted curves represent peak currents; these must be multiplied by 0.707 to obtain rms values of current, and multiplied by the impedance of the load at the particular frequency to obtain the desired voltage values.



## SECTION IV

# AUDIO-CIRCUIT DESIGN

	Page
Bass-compensation Design Chart.....	58
Simple RC Equalizer Networks.....	60
Universal 15-channel Tone Control for Audio Amplifiers..	63
Computing Reactive Attenuation.....	65
Time Delay in Resistance-capacitance Circuits.....	67

## Bass-compensation Design Chart

By P. A. D'ORIO and RINALDO De COLA

A direct method of choosing the proper capacitor and series resistance values in tapped-volume-control bass compensators to obtain the maximum degree of compensation between 100 and 400 cycles

To achieve the necessary bass response in radio receivers, resort is frequently made to bass-boost circuits. The most popular by far of these circuits is shown in Fig. 1. Resistors  $R_3$  and  $R_1$  constitute the usual tapped volume control. The resistor  $R_2$  is inserted in the circuit in order that there will not be too great a loss in the higher audio frequencies, and also to fix the output level of the receiver, when the volume control arm is set at the tap, at which point maximum compensation occurs. The problem arises of finding the proper value for  $C$  that will give the greatest attenuation ratio between two arbitrarily chosen frequencies.

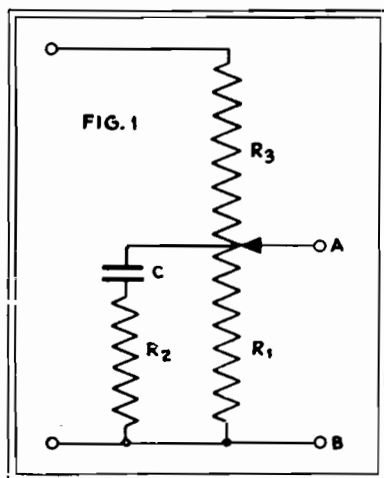


Fig. 1.—Tapped-control bass-boost circuit.

In most development laboratories these frequencies are usually chosen as 400 and 100 cycles.

In Fig. 1, looking into the network between points  $A$  and  $B$  (considering  $R_3$  open), the impedance between these two points will, at two different frequencies, reach a maximum ratio for a certain combination of  $R_1$ ,  $R_2$ , and  $C$ . Now if terminals  $A$  and  $B$  are fed from a high-impedance source, say through  $R_3$ , the ratio of voltages across  $A$  and  $B$ , for two different impressed frequencies, will have the same ratio as the impedances at these same two frequencies.

If the impedance across  $A$  and  $B$  were a pure capacitive reactance, the ratio of reactances at 400 and 100 cycles would be 4 and there would be no point to our analysis. However,  $R_2$  is always required to prevent the higher audio frequencies from being entirely lost; hence there will be a certain value of  $C$  that will yield the maximum impedance or voltage ratio across the terminals.

### Developing the Basic Equation

We can write the equation for the impedance at any arbitrary frequency  $f_a$  across terminals  $A$  and  $B$

$$Z_a = \frac{R_1 \left( R_2 - j \frac{1}{\omega_a C} \right)}{R_1 + R_2 - j \frac{1}{\omega_a C}}$$

and the equation for a certain reference frequency  $f_r$

$$Z_r = \frac{R_1 \left( R_2 - j \frac{1}{\omega_r C} \right)}{R_1 + R_2 - j \frac{1}{\omega_r C}}$$

where  $\omega_a = 2\pi f_a$  and  $\omega_r = 2\pi f_r$ .

If we now write  $Z_a/Z_r$  and maximize with respect to  $C$ , set the resulting equation to zero, and solve for  $C$ , we obtain

$$C = \sqrt{\frac{1}{\omega_a \omega_r R_2 (R_1 + R_2)}} \quad (1)$$

This value of  $C$  gives, therefore, a maximum ratio of the impedances at  $f_a$  and  $f_r$ .

Writing Eq. (1) for  $C$  in equations for  $Z_a$  and  $Z_r$ , we obtain

$$Z_a = \sqrt{\frac{A^2 + R_1 A B N}{B^2 + N B R_2}} \quad (2)$$

and

$$Z_r = \sqrt{\frac{N A^2 + R_1 B A}{B^2 N + R_2 B}} \quad (3)$$

then

$$K = \frac{E_a}{E_r} = \frac{Z_a}{Z_r} = \sqrt{\frac{(A + N B R_1)(N B + R_2)}{(A N + B R_1)(B + N R_2)}} \quad (4)$$

where  $A$  is  $R_1 R_2$ ,  $B$  is  $(R_1 + R_2)$ , and  $N$  is  $f_r/f_a$ . These equations are perfectly general. However, because they are somewhat cumbersome, Fig. 2 has been con-



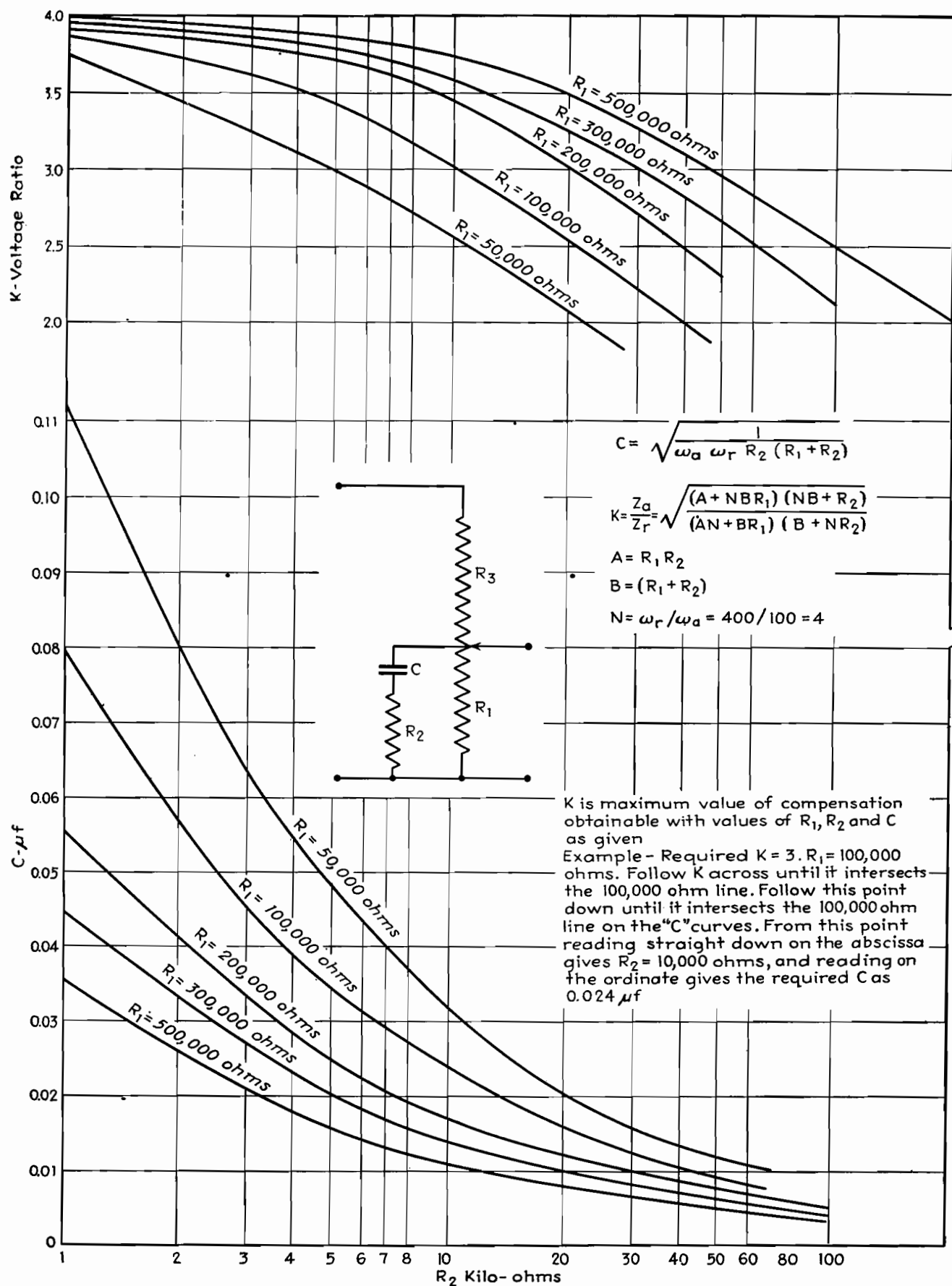


Fig. 2.—Bass compensation design chart.

structed, for a range of values that covers most practical cases. The frequency ratio  $N$  was taken as 400 cycles per 100 cycles.  $K$  is the ratio of the voltages at these two frequencies. Say that  $K$  is chosen at 3 and that  $R_1$  (one of the resistors must be known or assumed) is 100,000 ohms. Then on Fig. 2 follow  $K$  over parallel to the abscissa, until it

intersects  $R_1$  at 100,000 ohms; then follow this point down, until it again intersects the  $R_1$  line at 100,000 ohms, on the  $C$  curves; then, reading straight down from this point,  $R_2$  is given as 10,000 ohms; and reading straight across toward  $C$  gives  $C$  as 0.024  $\mu$ f. The values of  $C$  and  $R_2$  thus derived will give maximum value for compensation with the

chosen value of  $R_1$ . Increasing or decreasing either  $R_1$  or  $R_2$  will require a new value of  $C$  for maximum compensation to be attained. Experimental checks of values derived from the chart show a high order of accuracy. The addition of h-f compensation networks across the volume control will not affect the values of  $R_1$ ,  $R_2$ , and  $C$  for maximum compensation.

## Simple RC Equalizer Networks

By CHARLES J. MERCHANT

Two charts give directly the attenuation in decibels and the phase shift of simple RC equalizer networks employing several resistors and only one capacitor

IN designing amplifiers, it is often desirable to secure some degree of equalization without resorting to the more elaborate LC filters. Simple RC networks are commonly used to perform this function.

Here we are concerned exclusively with networks containing any arbitrary number of resistors and one capacitor. Such networks will be referred to as admissible networks. It will be assumed that we are interested only in the voltage output of such networks, or, in other words, that these networks will be terminated in an infinite load. Since such networks are generally used for coupling between stages, this is almost always the case of greatest interest.

Examples of what are meant by admissible networks are shown at *a* and *b* in Fig. 1, while an example of a network that is not admissible is given at *c*. It should be noted, however, that in case capacitor  $C_2$  and resistor  $R_4$  in Fig. 1c are large enough, the network is approxi-

mately an admissible network, down to a very low frequency.

Two cases will be considered: (1) The case where the network is driven by a constant-voltage generator, i.e., a generator of zero internal impedance. (2) The case where the network is driven by a constant-current generator, i.e., a generator of substantially infinite internal impedance. Cases not included under one of these headings can be placed under one of them by including the generator impedance, if this is purely resistive, in the network itself.

The following definitions apply throughout:

$E$  = voltage output of the driving generator, if voltage is constant

$I$  = current output of the driving generator, if current is constant

$V$  = voltage output of the network

$a$  = attenuation  $E/V$  of the network, taking into account phase as well as magnitude

$\bar{a}$  = absolute value of  $a$

$\theta$  = phase angle of  $a$

$\alpha$  = value of  $a$ , decibels

$a_0$  = attenuation of the network at zero frequency, i.e., the attenuation with the capacitor open-circuited

$a_\infty$  = attenuation of the network at infinite frequency, i.e., the attenuation with the capacitor short-circuited. (It is obvious that both  $a_0$  and  $a_\infty$  have zero phase angle.)

$A$  = ratio of the attenuation of the network at zero frequency to the attenuation of the network at infinite frequency, i.e.,  $a_0/a_\infty$

$A_{db}$  = value of  $A$ , decibels

### Attenuation Formula for Constant-voltage Case

It can be shown that the attenuation  $a$  of any admissible network is given for any frequency  $f$  by the following formula:

$$a = a_\infty \frac{f - jF_1}{f - jF_2} \quad (1)$$

In this formula,  $F_1$  and  $F_2$  are two fixed frequencies that are associated with any such network and are generally referred to as the turnover frequencies. When  $A_{db}$  is large, i.e., greater than 14 db, these two frequencies will lie almost exactly at those points where the curve is within 3 db of its zero and infinite-frequency values of attenuation. Later on a rule will be given for finding these two turnover frequencies by inspection.

Upon setting  $f = 0$  in Eq. (1), we can immediately deduce one important relation. We then have

$$a_0 = a_\infty \frac{F_1}{F_2}$$

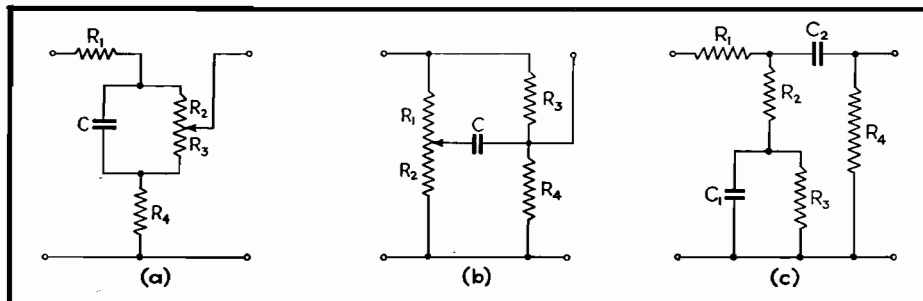


Fig. 1.—Examples of tone-control circuits using several resistors and only one capacitor are shown in *a* and *b*. A type of circuit not considered because it has more than one capacitor is indicated in *c*.

$$\frac{a_0}{a_\infty} = A = \frac{F_1}{F_2} \quad (2)$$

In other words, the ratio of the turnover frequencies is the same as the ratio of the zero and infinite-frequency attenuations of the network. Given one of the turnover frequencies, we can immediately find the other, because the computation of the zero and infinite-frequency attenuations of the network are matters of simple arithmetic.

#### $F_1$ Rule for Constant-voltage Case

It may be shown that we can always find  $F_1$  for any given admissible network driven by a constant-voltage generator, by the following:

**RULE:**  $F_1$  is that frequency at which the reactance of the capacitor equals the resistance it looks into from its own terminals when the driving generator is short-circuited.

$F_1$  is thus seen to be nothing more nor less than the frequency associated with the generalized time constant  $R'C$  of the network, where  $R'$  is the resistance seen by  $C$  from its own terminals and is given by the formula

$$F_1 = \frac{1}{2\pi} R'C \quad (3)$$

#### Driving-point Impedance of an Admissible Network

In the event that the network is driven by a constant-current generator, the output voltage of the network will be the product of the driving generator current, the impedance of the network as seen from the driving generator, and the attenuation of the network if it were driven by a constant-voltage generator. We first, therefore, investigate the impedance function for such networks.

The impedance of any admissible network as seen from any two points in the network whatever is given by the following formula:

$$Z = Z_\infty \frac{f - jF_1}{f - jF_2} \quad (4)$$

where  $F_1$  is given as the frequency at which the reactance of the capacitor equals the resistance it looks into at its own terminals when the driving generator is short-circuited, and  $F_2$  is the frequency at which the reactance of the capacitor equals the resistance it looks into at its own terminals when the driving generator is open-circuited.  $Z_\infty$  is the impedance of the network to current of infinite frequency, i.e., the impedance of the net-

work when the capacitor is short-circuited; it is obvious that  $Z_\infty$  is purely resistive.

#### Attenuation Formula for Constant-current Case

Before considering the case where the network is driven by a constant-current generator, it would be well to indicate what is meant by attenuation in this case. In general, the term attenuation is reserved for a voltage-voltage or current-current ratio. In the present case, however, we are interested only in the voltage output of the network; hence, it would seem, the term attenuation does not apply.

However, we are often interested in the case where such a network is driven by a generator, commonly a pentode, which converts constant voltage to constant current. We may then say that the current output of such a generator is equal to a constant  $g$  times a voltage, where  $g$  has the dimension of current divided by voltage, i.e., conductance. In view of this fact, we may legitimately speak of the attenuation of such networks when they are driven by constant-current generators, if we bear in mind that a constant of the dimensions of  $1/g$  is implied in the formula.

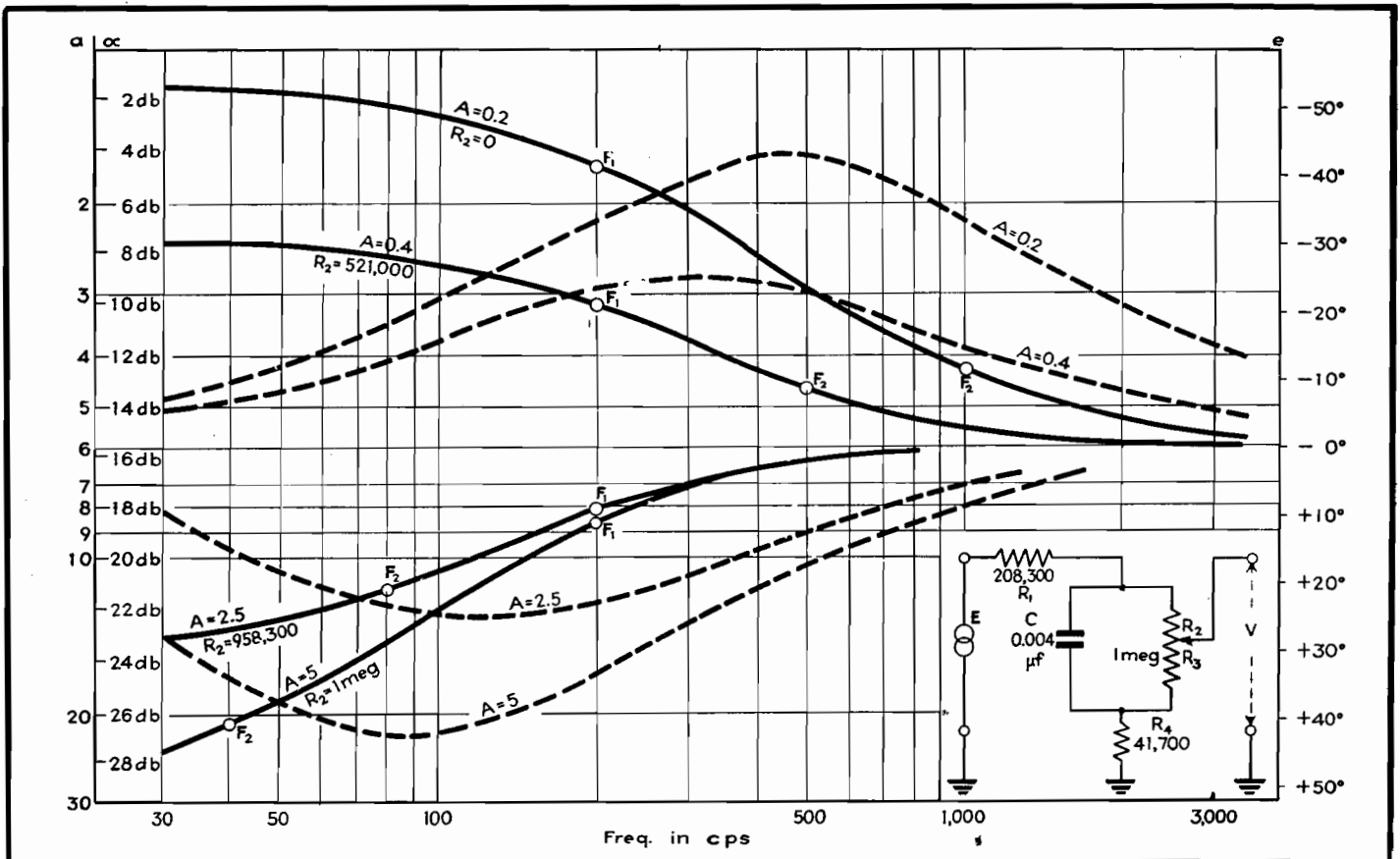


Fig. 2.—Applications of the author's RC equalizer network formulas to practical variable tone-control design. Solid curves show attenuation. Dotted curves indicate the phase shift.

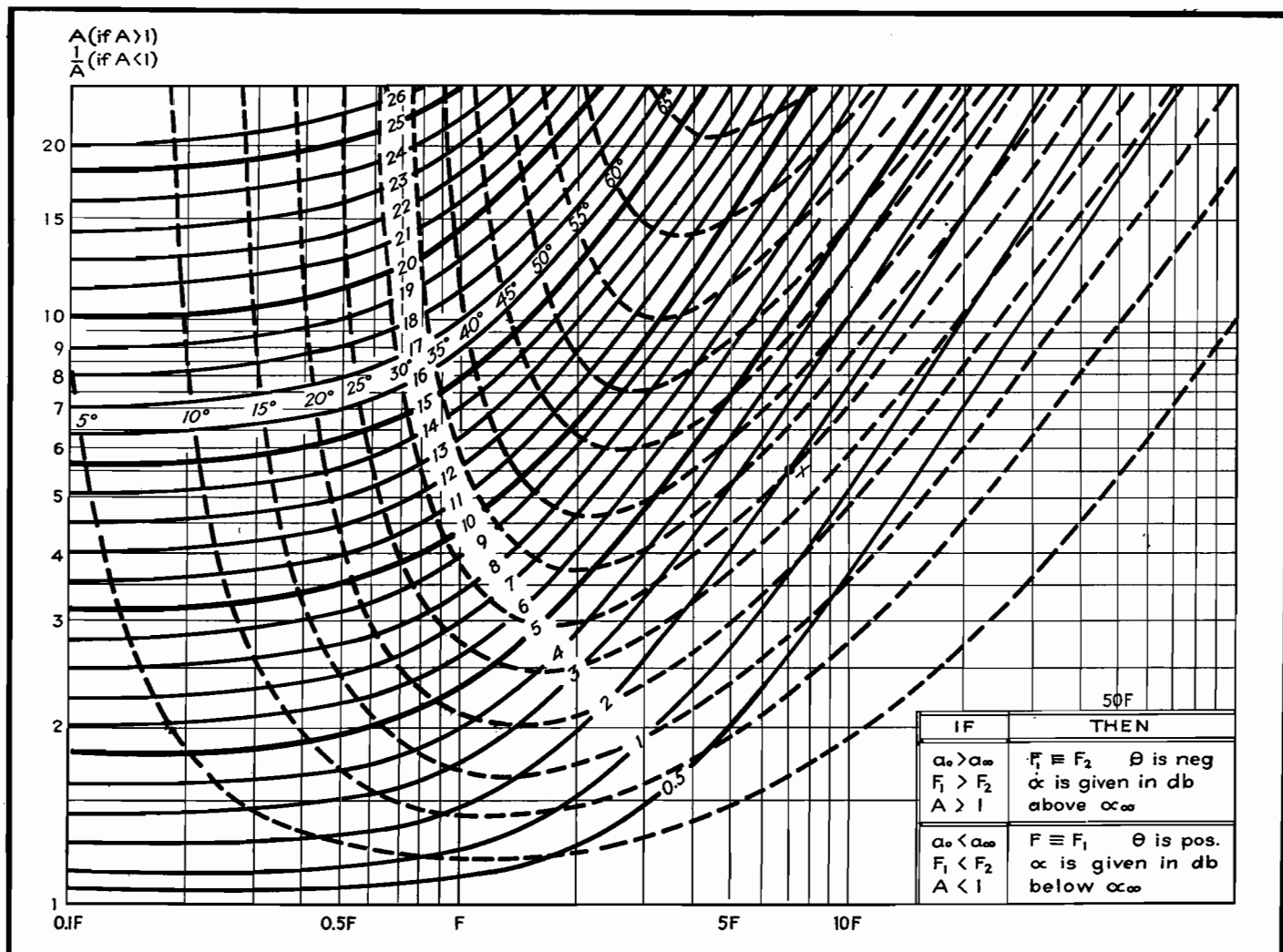


Fig. 3.—Graphical determination in decibels of the attenuation and phase shift of simple RC equalizer circuits. Solid contour lines give the attenuation and dotted contour lines show the phase shift.

Since the attenuation of an admissible network is always given by Eq. (1) when we know the voltage across its input terminals, it follows immediately that the voltage output of an admissible network when driven by a constant-current generator is given by the following:

$$V = IZ_\infty \left( \frac{f - jF_1}{f - jF_2} \right) \frac{1}{a_\infty} \left( \frac{f - jF_2'}{f - jF_1'} \right) \quad (5)$$

where  $F_2$  is given as under Eq. (4) and  $F_2' = F_1/A$ , where  $A$  is computed considering the network as being driven by a constant-voltage generator. This equation simplifies to

$$V = I \frac{Z_\infty}{A} \left( \frac{f - jF_2'}{f - jF_2} \right) \quad (6)$$

If we write  $gE$  for  $I$ , then the attenuation is given by

$$a = \frac{E}{V} = \frac{1}{g} \frac{a_\infty}{Z_\infty} \left( \frac{f - jF_2}{f - jF_2'} \right) \quad (7)$$

We see that the quantity  $a_\infty/gZ_\infty$  must be

the attenuation at infinite frequency. Therefore writing  $a_\infty'$  for this quantity and  $F_1'$  for  $F_2$ , we have

$$a = a_\infty' \left( \frac{f - jF_1'}{f - jF_2'} \right) \quad (8)$$

It will be noted in this case, however, that the turnover frequency that now appears in the numerator is determined by open-circuiting the driving generator.

#### Polar Form of Attenuation Formula

The form of the expression for the attenuation is the same whether the network is driven by a constant-voltage or a constant-current generator. Up to this point, the formula was exclusively in the complex form. For most purposes, however, it is more convenient to make use of the polar form  $a = \bar{a}/\theta$ . By straightforward manipulation of Eq. (1), we derive the following expressions for  $\bar{a}$  and  $\theta$ :

$$\bar{a} = a_\infty \sqrt{\frac{f^2 + F_1^2}{f^2 + F_2^2}} \quad (9)$$

$$\theta = \tan^{-1} \left( \frac{F_2}{f} \right) - \tan^{-1} \left( \frac{F_1}{f} \right) \quad (10)$$

Here  $\theta$  is either a maximum or a minimum when  $f = \sqrt{F_1 F_2}$ , depending on whether  $A$  is less than or greater than unity.

#### Application to Variable Tone Control

As an example of the application of these formulas to a practical case, consider the tone-control circuit of Fig. 1a, with the values shown in Fig. 2. These values were so chosen as to give either a maximum bass boost of 14 db, or a maximum bass cut of 14 db.

The position of the control has no effect on  $F_1$ , since, with the driving generator  $E$  short-circuited,  $C$  always looks into the same resistance no matter where the control is set. This resistance is given by  $R_1 + R_4$  in parallel with  $R_2 + R_3$ , which, for the values given these

resistances, equals 200,000 ohms.  $F_1$  is given by the rule as the frequency at which 0.004  $\mu$ f has a reactance of 200,000 ohms, and from a reactance chart we find this to be 200 cycles.

$a_\infty$  is given as the attenuation of the network when  $C$  is short-circuited. This is also independent of the control setting, and is given by  $(R_1 + R_4)/R_4$ ; for the given values,  $a_\infty$  is thus seen to be equal to 6, which corresponds to a value of 15.6 db.

The control setting affects only  $a_o$ , and this may be varied from a value of 30, with the control all the way down ( $R_3 = 0$ ), to a value of 1.2, with the control all the way up ( $R_2 = 0$ ). These values of  $a_o$  correspond to values of  $\alpha_o$  of 29.6 and 1.6 db, respectively. It is to be noted that for the setting of the control at which  $R_2 = 833,000$  ohms,  $a_o$  and  $a$  are equal, and the attenuation is constant for all frequencies.

$A$  is given as  $a_o/a_\infty$ , which, for the maximum bass-boost setting ( $a_o = 1.2$ ), equals 0.2, and for the maximum bass-cut setting ( $a_o = 30$ ) equals 5. From Eq. (2),  $F_2$  equals  $F_1/A$ , and hence for the maximum bass-boost setting  $F_2 = 1,000$  cycles. Similarly, for the maximum bass-cut setting  $F_2 = 40$  cycles.

Substituting these values of  $F_1$ ,  $F_2$ , and  $a_\infty$  in Eqs. (9) and (10), we obtain the following expressions for  $\alpha$  and  $\theta$ .

$$\begin{aligned} \bar{a} &= 6 \sqrt{\frac{f^2 + (200)^2}{f^2 + (1,000)^2}} \\ \theta &= \tan^{-1} \left( \frac{1,000}{f} \right) - \tan^{-1} \left( \frac{200}{f} \right) \end{aligned} \quad \left\{ \begin{array}{l} \text{(bass-boost)} \\ (A = 0.2) \end{array} \right. \quad (11)$$

$$\begin{aligned} \bar{a} &= 6 \sqrt{\frac{f^2 + (200)^2}{f^2 + (40)^2}} \\ \theta &= \tan^{-1} \left( \frac{40}{f} \right) - \tan^{-1} \left( \frac{200}{f} \right) \end{aligned} \quad \left\{ \begin{array}{l} \text{(bass-cut)} \\ (A = 5) \end{array} \right. \quad (12)$$

The graphs of these functions, together with those for two intermediate settings of the control ( $A = 0.4$  and  $A = 2.5$ ), are given in Fig. 2.

#### Use of Attenuation—Phase-shift Chart

Given any particular admissible network, it is a perfectly straightforward task to plot its attenuation and phase-shift curves using Eqs. (9) and (10). The computations are rather laborious, however, especially if the results are desired in decibels. These quantities are therefore given graphically in Fig. 3 at intervals of 1 db and 5 deg for any multiple of the lower turnover frequency from 0.1 to 100, and for any value of  $A$  between 1 and 20; if  $A$  is less than unity we work with the reciprocal  $1/A$ .

#### Typical Examples

Assuming for the moment that  $A$  is greater than unity, let us suppose we

wish to find the attenuation of a given network where  $A = 5.5$ , at a frequency equal to seven times the lower turnover frequency, which in this case is  $F_2$ . Through the point  $x$  ( $f = 7F_2$ ,  $A = 5.5$ ) passes the solid contour line labeled 2, which means that at this frequency  $\alpha = \alpha_\infty + 2$  db. Keeping the same value of  $A$ , we see that at  $3F_2$ ,  $\alpha = \alpha_\infty + 6$  db, and at  $0.4F_2$ ,  $\alpha = \alpha_\infty + 14.1$  db. The attenuation at multiples of  $F_2$  through which contour lines do not pass can be estimated to an accuracy sufficient for nearly all practical purposes.

Returning to the original point  $x$  we see that the dotted contour line labeled  $30^\circ$  passes through this point also; hence, the phase-shift at this point is  $-30$  deg (since when  $A$  is greater than unity,  $\theta$  is negative). Similarly, for the same value of  $A$ , at  $3F_2$ ,  $\theta = -42.5^\circ$ , and at  $0.4F_2$ ,  $\theta = -18^\circ$ .

When  $A$  is less than unity, we use  $1/A$  instead. Thus, had  $A$  been given as 0.182, we take the reciprocal, or 5.5, and work with that. Now, however, the attenuation is given in decibels below  $\alpha_\infty$ , and the phase shifts are positive. We still take the lower turnover frequency, which is now  $F_1$ . Thus for  $A = 0.182$ ,  $f = 7F_1$ ,  $\alpha = \alpha_\infty - 2$  db, and  $\theta = 30^\circ$ . Similarly, for  $A = 0.182$ ,  $f = 3F_1$ ,  $\alpha = \alpha_\infty - 6$  db, and  $\theta = 42.5^\circ$ .

## Universal 15-channel Tone Control for Audio Amplifiers

By PAUL H. THOMSEN

Design data for an instrument that automatically provides on its panel a response curve from which required equalizer circuit constants to improve response characteristics can be determined

**I**N audio work, there are many uses for an instrument that makes it possible to change the response curve of an amplifier at will. Such an instrument is shown in the circuit of Fig. 1. It consists essentially of 15 separate calibrated tone-control channels connected in parallel but acting independently, each controlling a different portion of the audio spectrum.

To determine the over-all response requirements of an audio amplifier intended for high-fidelity sound reproduction, the unit is inserted in the circuit of the amplifier to be tested, at some point where the signal voltage is about 2 volts. The 15 channel controls are adjusted until the output of the amplifier is the same at all audio frequencies. The response curve then shows on the front

panel, since the positions of control levers connected to each potentiometer  $R_2$  form the visual curve on a panel that is calibrated directly in decibels.

With the unit, the response of a theater sound system or public-address system can be adjusted to suit various acoustic conditions. When the channel controls are set to give the desired tone balance, as determined by listening at various posi-

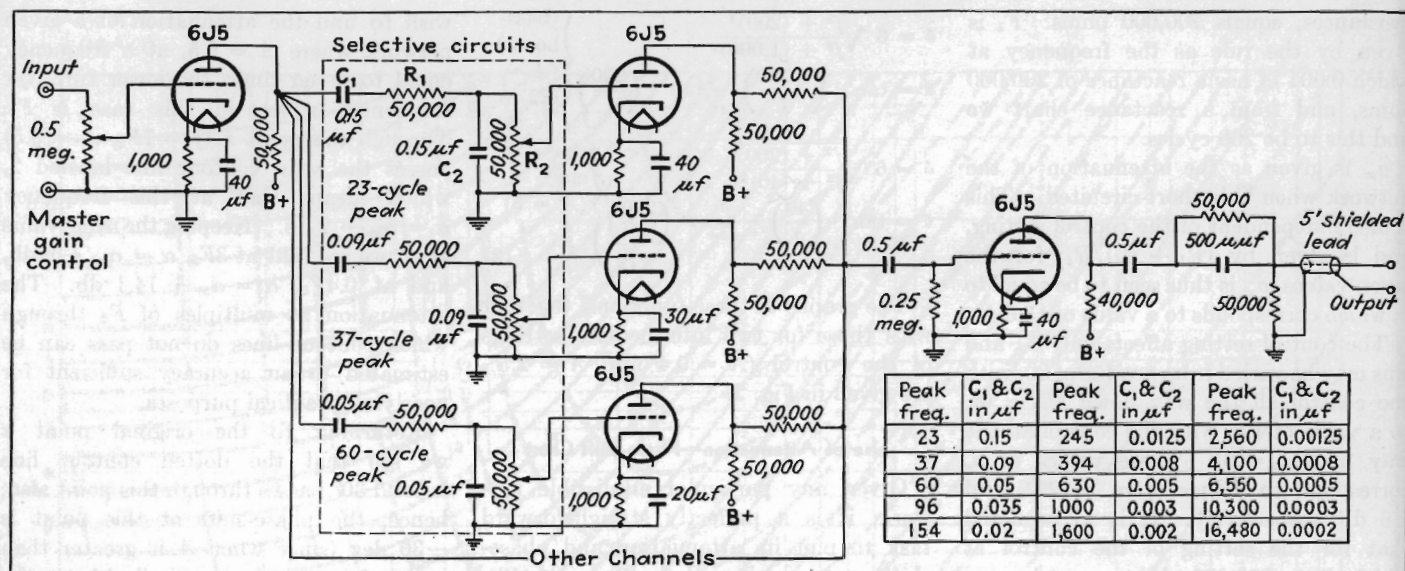


Fig. 1.—Tonalizer circuit with values of parts for a 15-channel arrangement. Fewer or more channels may be used if desired by appropriately spacing the peak frequencies. By-pass capacitors for cathode resistors in remaining channels can be 10  $\mu$ f each.

tions in the audience while the system is in use, the required compensation can be determined from these settings and the necessary permanent equalization inserted later. Numerous other uses will suggest themselves to sound engineers.

The unit, called a tonalizer, is fundamentally a test instrument, due to its multiplicity of tubes and circuits, and is not ordinarily left in a circuit. It may, however, be used permanently as a near-ideal tone control in applications where cost is not a limiting factor.

The basic circuit is shown in Fig. 1. The input voltage amplifier stage with its master gain control permits adjusting the over-all gain of the system and has a sufficiently high input impedance for a plate-circuit connection to any stage when the signal level is about 2 volts in the amplifier to be tested. The plate circuit of the 6J5 input stage feeds each of the 15 selective channels in parallel. (For simplicity, only three channels are shown in the diagram.)

#### Circuit Details

RC circuits are used as a-f filters to eliminate phase distortion and other drawbacks of tuned LC circuits. Each RC circuit is broadly peaked at a particular frequency and has its own individual gain control.

The output matching circuit and shielded cable are optional, and are used only when it is inadvisable for some reason to connect the 0.5- $\mu$ f output capacitor directly to the grid of a tube in the amplifier being tested.

The response curve for an individual

selective RC circuit is given in Fig. 2. The value of the peak frequency of this curve depends on the values of R and C employed and is determined by the formula

$$f = \frac{1}{2\pi \sqrt{R_1 R_2 C_1 C_2}}$$

If  $R_1$  is made equal to  $R_2$  and  $C_1$  is made equal to  $C_2$ , the equation becomes

$$f = \frac{1}{2\pi RC}$$

This equation shows that the peak frequency is inversely proportional to

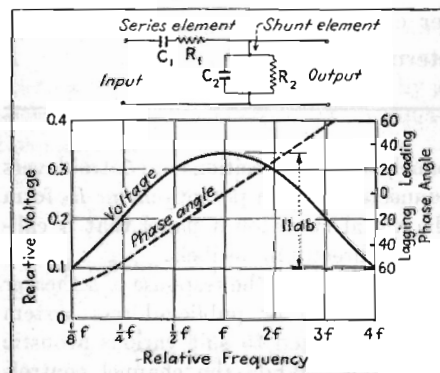


Fig. 2.—RC selective circuit used in tonalizer and voltage response curve it provides.

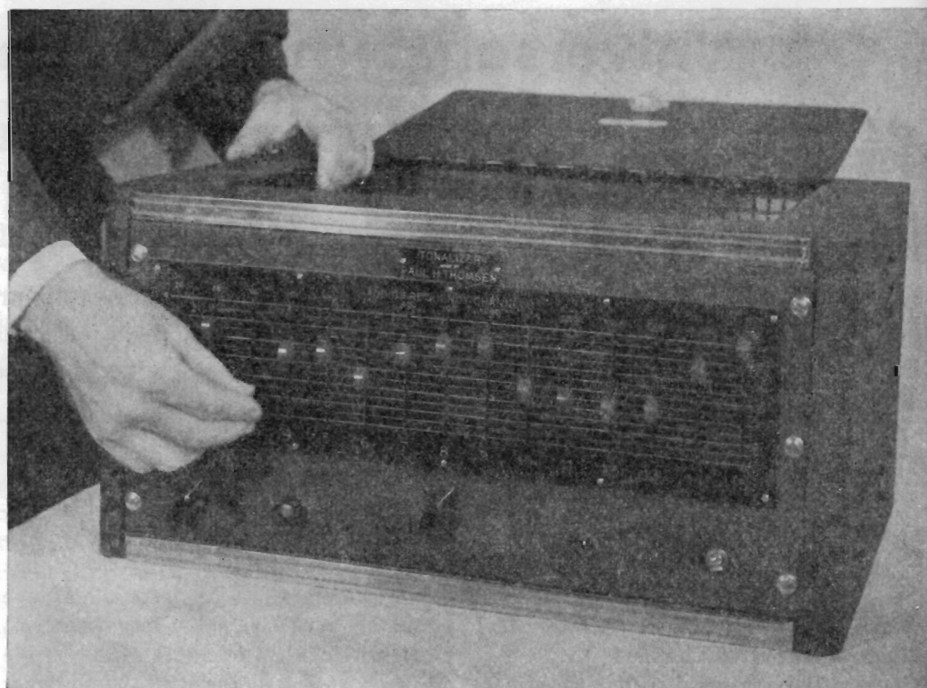


Fig. 3.—Front panel of 15-channel tonalizer. The levers move up and down through the vertical slots in the panel with their ends tracing the response curve to which the instrument is set.



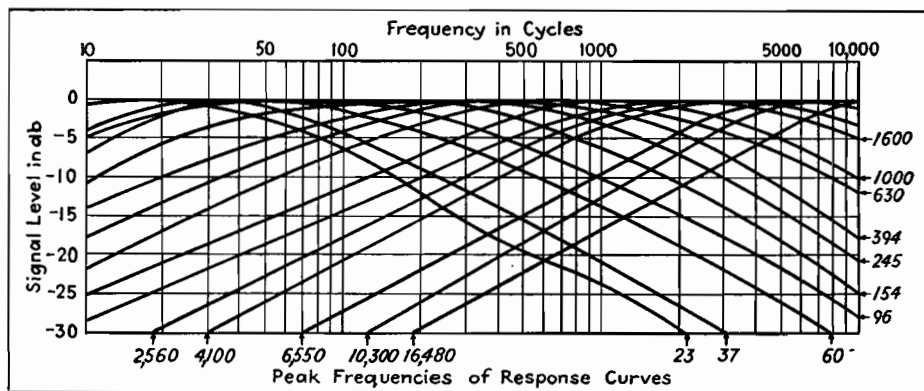


Fig. 4.—The individual responses of all 15 channels combine to give a flat response, as shown here, when all controls are set at maximum.

capacitance, instead of being inversely proportional to the square root of capacitance as in tuned *LC* circuits.

#### Theory of Selective Circuit

Each selective circuit consists of a series element  $C_1R_1$  and a parallel element  $C_2R_2$ , forming a voltage divider as shown in Fig. 2.  $R_1$  and  $R_2$  are 50,000 ohms for all channels, but  $C_1$  and  $C_2$  are equal in individual channels only.

At low audio frequencies, most of the signal voltage is dropped across the series element, and only a relatively small voltage is available across  $R_2$  for transfer to the amplifying portion of the channel.

At high audio frequencies (above 4*f* in Fig. 2), the impedance of the shunt element is much lower than that of the series element, and again the voltage across  $R_2$  for transfer to the amplifier tube is relatively small.

As the frequency is decreased from a high value, the impedances of both the series and shunt elements increase but at different rates. The peak response occurs at the point where the two impedances increase at the same rate, for the two impedances are then increasing at the same proportional rate and giving a high constant output voltage across  $R_2$ , corresponding to the peak of the response curve.

#### Performance Data

The lowest peak frequency employed in a 15-channel tonalizer is 23 cycles. Successive peaks are each approximately 1.6 times the preceding value, namely, 37, 60, 96, 154, 245, 394, 630, 1,000, 1,600, 2,560, 4,100, 6,550, 10,300, and 16,480 cycles. This gives considerable overlap of response curves, with smooth changes in response and with a maximum possible variation of about 5 db between adjacent peaks.

When all 15 channel controls are set for equal or maximum gain, the response curves combine to give essentially flat over-all response, as shown in Fig. 4. Here the signal levels are plotted in decibels and cover a much greater range than the voltage ratios of Fig. 2.

The width of each individual response curve and the amount of overlap together make it impossible to cut out a frequency completely with one channel control. The maximum possible variation from one channel to the next is about 5 db; hence essentially complete suppression (30 db below the original level, from a practical standpoint) can be obtained at the lowest peak of 23 cycles by setting the first six channel controls to zero.

## Computing Reactive Attenuation

By P. F. BECHBERGER

The chart aids attenuation calculations which take into account the presence of series or parallel reactances, useful in predicting audio-transformer frequency response, etc.

**A**TENUATION calculations are usually made on the assumption that the circuit elements involved contain resistance only. In many cases, such as in the design of resistance attenuators and pads, this assumption is correct or at least so nearly correct that no serious error results. But in many cases, the reactance present in the so-called resistance elements is large enough to affect the result by an error of several decibels. When this occurs, especially in rating audio equipment which must be flat to within a small fraction of a decibel, the reactance present must be taken into ac-

count. The chart aids in computing attenuation due to reactive components, for series and parallel cases.

#### Series vs. Parallel Circuits

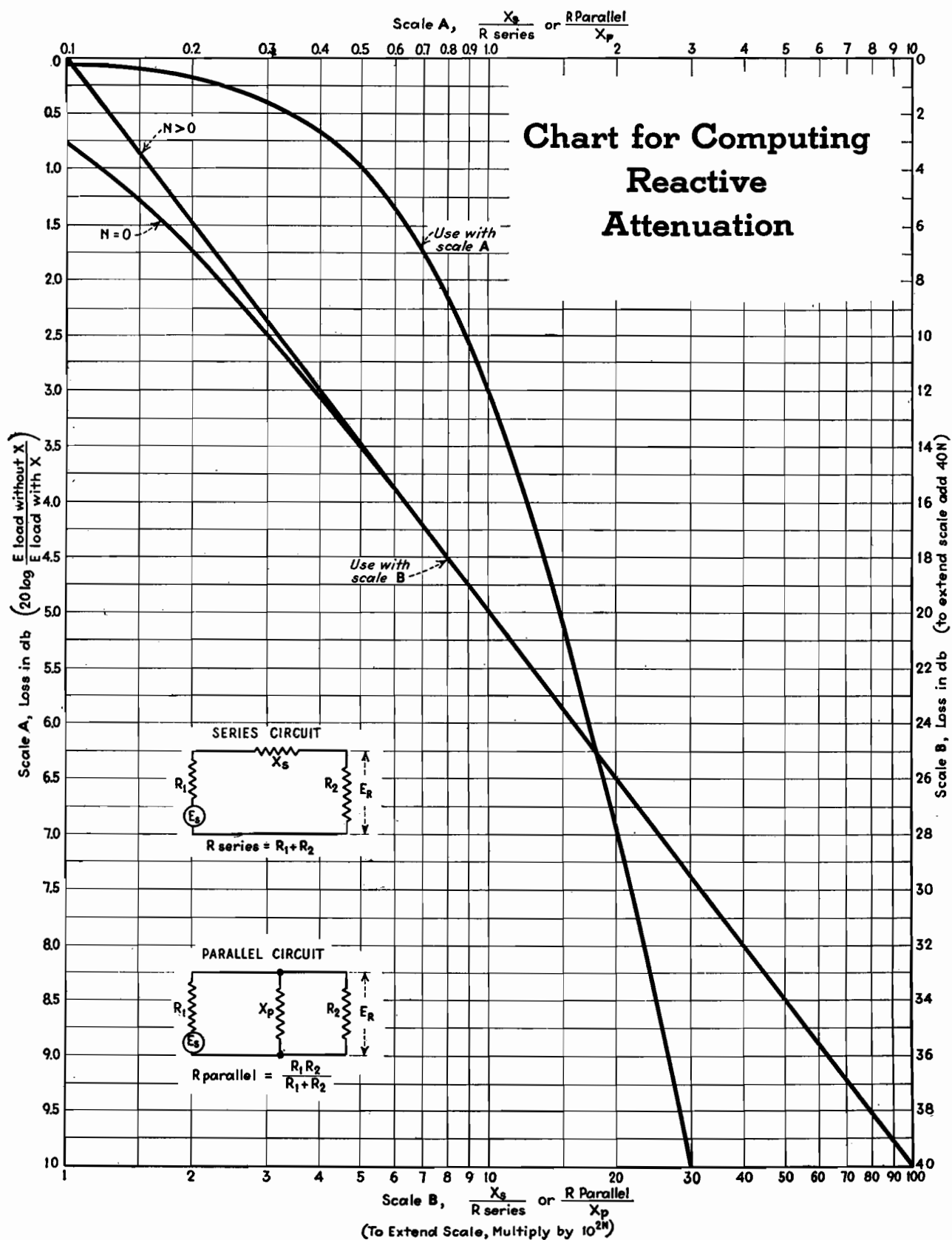
Consider the series circuit, containing a source of emf, the source resistance  $R_1$ , the load resistance  $R_2$ , and a reactance  $X_s$  in series between  $R_1$  and  $R_2$ . Then in computing the attenuation caused by the presence of the reactance, the following expression is set up:

Loss in db

$$= 20 \log_{10} \frac{\text{voltage across load without } X_s}{\text{voltage across load with } X_s}$$

The same expression can be used for the parallel circuit, in which the source of emf and the source resistance are shunted by the load resistance and load reactance in parallel. In this case, the parallel reactance  $X_p$  causes the change in the load voltage, the ratio of voltage change being expressed in decibels by the above expression.

The attenuation so introduced can be expressed in terms of the ratio of the reactance to the series resistance in the series case, or by the ratio of the parallel resistance to the reactance in the parallel case. In the chart, the relation between





the attenuation and these ratios is given. The reactance-resistance ratios are formed by taking the series resistance  $R_1 + R_2$  and dividing into the reactance in the series case, or by dividing the parallel resistance  $(R_1 R_2)/(R_1 + R_2)$  by the reactance in the parallel case. The scales for the resistance-reactance ratio run from 0.1 to 10.0 in scale *A*, and from 0.01 to 1.0 in scale *B*. If it is desired to extend scale *B* upward, the scale value may be multiplied by any even positive power of 10 (by  $10^{2N}$ ), and by adding  $40N$  to the horizontal attenuation values for scale *B*. When the scale is so extended, the curve marked  $N > 0$  should be used. In this manner all the values of  $X$  and  $R_{\text{series}}$  or  $R_{\text{parallel}}$  likely to occur can be accommodated.

The usefulness of the chart is particularly apparent in the case of the a-f interstage coupling or output transformer. At high frequencies, the leakage inductance of such transformers may produce a noticeable reactive component in the load presented by the transformer. The attenuation thus introduced is a function of frequency which must be calculated;

the chart permits rapid determinations of the decibel loss produced by this effect. At low frequencies, the response of transformer and resistance-capacity-coupled stages can likewise be determined directly from resistance, inductance, and capacity values.

### Examples

As an example of the use of the chart, consider an output transformer that is fed from push-pull 2A3's. The source resistance ( $R_1$ ) in this case is the plate resistance of the two 2A3's in series, approximately 1,600 ohms. The load resistance  $R_2$  is the plate-to-plate resistance offered by the transformer, which is in this case 3,000 ohms. The transformer has a leakage resistance of 0.026 henrys, referred to the primary, which at 10,000 cycles gives a series reactance  $X_s(2\pi fL)$  of 1,630 ohms. Then  $X_s/R_{\text{series}}$  is 0.354, which, referring to scale *A* on the chart, gives an attenuation of 0.5 db. Since the ratio  $X_s/R_{\text{series}}$  increases linearly with frequency, the ratio at 15,000 and 20,000 cycles can be calculated by proportion,

giving values of 0.516 and 0.708, respectively, with attenuation, taken from the chart, of 1.05 and 1.75 db. The leakage reactance referred to here may often be measured by shorting the secondary terminals and measuring the primary reactance.

### Low-frequency Response

If the same transformer has a primary inductance of 11 henrys, the attenuation at low frequencies is computed as follows: The primary reactance (which is in parallel with the load) at 30 cycles is 2,080 ohms. The parallel resistance of tube output and load  $R_{\text{parallel}}$  is  $(1,600 \times 3,000)/(1,600 + 3,000)$  or 1,040 ohms. The ratio  $R_{\text{parallel}}/X_p$  is 0.5, and the attenuation taken from the chart (scale *A*) is 1.0 db. Since the ratio is inversely proportional to frequency, its value at 15 and 10 cycles is 1 and 1.5 with attenuations of 3.0 and 5.1 db, respectively.

From the examples it is clear that if the attenuation is known at one frequency the attenuation at other frequencies may be determined without a knowledge of the actual values of resistance and reactance.

## Time Delay in Resistance-capacitance Circuits

By E. W. KELLOGG and W. D. PHELPS

How to calculate and how to use time-delay networks in audio circuits. Several practical applications of such filters are analyzed in detail

THE curves and approximate formulas given here show the manner in which the output voltage or current of a resistance-capacitance filter changes in response to a sudden change in input, and give a simple way of estimating the effective time constant for two stages.

If a capacitor  $c$  (charged to a voltage  $E_o$ ) is discharged through a resistance  $r$ , the voltage  $e_2$  will fall to  $(1/e)E_o$  or  $0.368E_o$  in  $T = rc$  sec. Similarly, the time required for it to charge to within 36.8 per cent or  $1/e$  of the supplied voltage is  $rc$  sec. A corresponding definition of the effective time constant for a two-stage filter may be adopted, and although such a definition may be more or less arbitrary, it is useful in estimating the rapidity of action of filters of the resistance-capacitance type.

Two cases are considered, (1) in which the second stage is either isolated from the first by a tube, or else the connecting resistance is so high as to prevent material reaction on the first stage, and (2) in which the stages are cascaded in the usual manner and the reaction of the second stage on the voltage across the first capacitor is taken into account.

Only filters of the resistance-capacitance type have been considered, although the general conclusions might be applied to numerous other combinations. For example, we might be interested in the current through an inductance in the plate circuit of a tube having a resistance-capacitance filter in the grid circuit; or in the velocity of a mass, actuated by a magnet, the current through which is controlled by resistance and inductance.

In the last case there would be some coupling between the stages, and mechanical resistance would have to be present if the same formulas are to apply.

**Example 1. Uncoupled Filters.**—If the voltage applied to the first stage of the filter is suddenly changed from  $E_o$  to 0, the voltage applied to the second stage will be

$$e_1 = E_o e^{-nt} \quad (1)$$

where  $n = 1/r_1 c_1$ .

If the second stage has a time constant  $1/r_2 c_2 = k$ , the voltage across the second capacitor will be

$$e_2 = E_o \left( \frac{1}{1 - n/k} e^{-nt} + \frac{1}{1 - k/n} e^{-kt} \right) \quad (2)$$

It will be noted that if  $n = k$  this is indeterminate and for this special case

$$e_2 = E_o (nt + 1) e^{-nt} \quad (3)$$

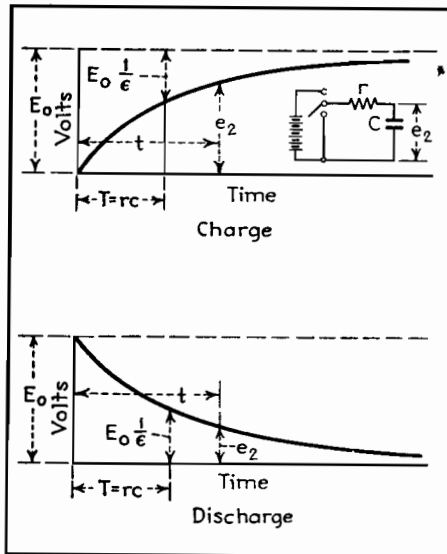


Fig. 1.—Charge and discharge of single stage.

For all other cases, Eq. (2) is applicable. The two terms of Eq. (2) are of opposite sign, the smaller term being negative, and the larger exponent going with the negative term. The value of  $e_2$  is thus represented by a larger term with a decrement corresponding to the slower of the two filter stages, from which is subtracted a smaller term with higher decrement, and therefore fairly rapidly becoming negligible (unless  $n$  and  $k$  are nearly the same).

Using effective time constant to mean the time required for  $e_2$  to fall to  $(1/e)E_0$  or  $0.368E_0$ , it may be said in general for the uncoupled case that the time constant for the two stages is approximately equal to the sum of those for the filter stages taken separately. Table I shows the degree of approximation. The same is true, but with somewhat more error in the

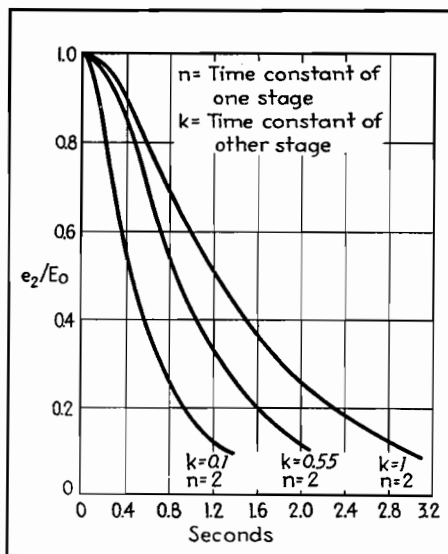


Fig. 2.—Uncoupled case with various time constants.

approximation, if the stages are coupled. If the stages are uncoupled, it makes no difference which stage comes first. If they are coupled, the order makes a difference.

If we are concerned with the time required for the voltage to drop to a lower value than 36.8 per cent of the initial value, or with how quickly it executes a smaller change, it will not be sufficient to depend on the effective time constant. The calculation of the curves from the formulas indicated is comparatively simple, but there are some approximations that may be of use.

If, in the case of uncoupled filters, the time constant for one filter is short compared with the other, the lower part of the curve may be approximated by a single exponential having the exponent

of the slower filter circuit and displaced along the time axis by the time constant of the faster filter. This approximation, which is equivalent to ignoring the smaller term in Eq. (2), becomes poorer as the time constants of the two filters approach equality, and can hardly be recommended unless one time constant is at least twice the other. A good approximation for the case of equal time constants consists in a simple exponential curve of time constant equal to 1.4 times that for one filter, and displaced along the time axis by 0.7 of the time constant.

Table I.— $1/n = 0.5$ 

Uncoupled case. Comparison of actual and approximate time constants

$t$ , sec	$1/k + 1/n$ , sec	$r_2 c_2 = 1/k$ , sec
10.45	10.5	10.0
1.15	1.05	0.55
0.61	0.60	0.1

Since in the uncoupled case the relative impedance of the two filter sections is not a factor in determining the build-up or decay curve, the cases illustrated are representative of about all the conditions likely to be encountered. In the coupled case, there are so many variables that only a few of the many possible combinations can be illustrated, and it will have to suffice to give the formulas, and a few illustrations, together with some approximate expressions for the effective time constant for the two stages.

**Example 2. Coupled Stages.**—If an emf  $E_0$  of the form shown in Fig. 5B is applied to the two-stage filter,  $e_2$  and  $e_1$  are given by the following relations:

$$e_2 = \frac{E_0}{1 - m_1/m_2} e^{m_1 t} + \frac{E_0}{1 - m_2/m_1} e^{m_2 t} \dots (4)$$

$$e_1 = \left( \frac{1 + m_1 r_2 c_2}{1 - m_1/m_2} \right) E_0 e^{m_1 t} + \left( \frac{1 + m_2 r_2 c_2}{1 - m_2/m_1} \right) E_0 e^{m_2 t} \dots (5)$$

Also if the emf is of the form shown in Fig. 5-A

$$e_2 = E_0 - \left( \frac{E_0}{1 - m_1/m_2} e^{m_1 t} + \frac{E_0}{1 - m_2/m_1} e^{m_2 t} \right) \dots (6)$$

$$\text{where } m_1 = \frac{-\lambda + \sqrt{\lambda^2 - 4\mu}}{2}$$

$$m_2 = \frac{-\lambda - \sqrt{\lambda^2 - 4\mu}}{2}$$

$$\lambda = \frac{1}{r_1 c_1} + \frac{1}{r_2 c_2} + \frac{1}{r_2 c_1}$$

$$\mu = \frac{1}{r_1 c_1 r_2 c_2}$$

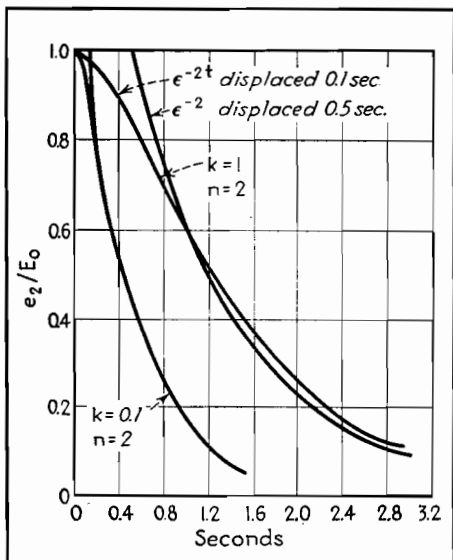


Fig. 3.—Curves for uncoupled case.

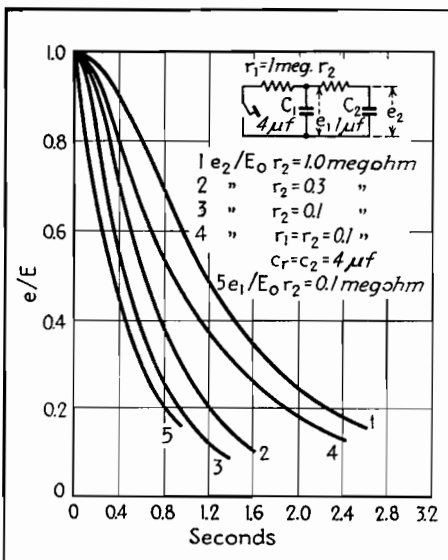


Fig. 4.—Curves for coupled case.

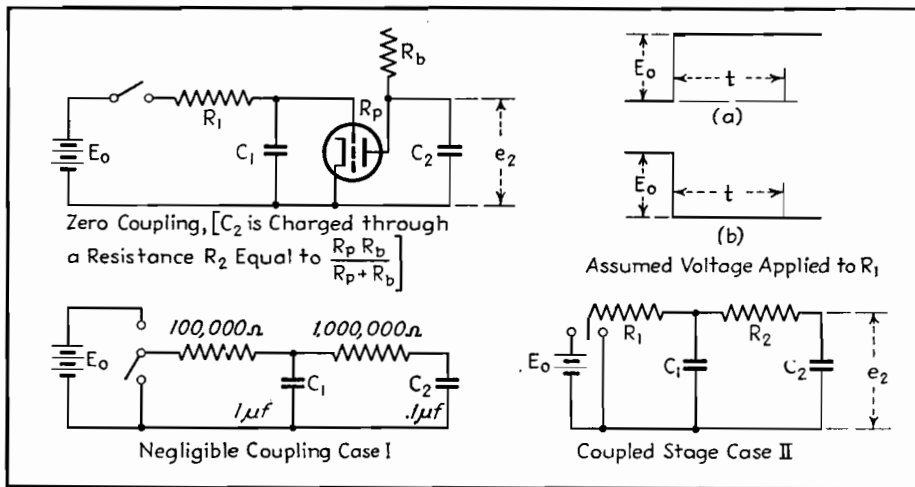


Fig. 5.—Coupled and uncoupled two-stage filters.

Although in the above formulas the change in impressed voltage is either from 0 to  $E_0$  or from  $E_0$  to 0, they show the manner in which the voltages  $e_1$  and  $e_2$  change from any initial to any final value. For calculating such a case, if  $E_a$  is the initial and  $E_b$  the final impressed voltage, Eqs. (1) to (5) may be used, letting  $E_0$  in the formula stand for  $E_a - E_b$ , and the total voltages across the first and second stages will be  $E_b + e_1$  and  $E_b + e_2$ , respectively.

In Fig. 4 curves of  $e_2$  and  $e_1$ , calculated from Eq. 4, are plotted for three different values of  $r_2$ . Only one curve for  $e_1$  is shown because the other two lie nearly on it.

A curve is also shown for the case where both filter stages are identical. The discharge times of  $C_2$  and  $C_1$ , designated as  $t_2$  and  $t_1$ , respectively, determined from the curves are shown in columns 3 and 2 of Table II.

Table II.—Coupled Case

Actual and approximate time constants compared

$r_2$ , meg.	$t_1$ , sec.	$t_2$ , sec.	$r_1 C_1 + (r_1 + r_2) C_2$ , sec.
1.0	0.44	1.58	1.50
0.3	0.47	0.83	0.80
0.1	0.496	0.61	0.60
0.005	0.499	0.504	0.505

Approximate values of  $t_2$  obtained by a combination of the filter constants are shown for purposes of comparison. It is seen that a reasonably good approximation to  $t_2$  is obtained simply by using the equation

$$t_2 = (r_1 + r_2)c_2 + r_1 c_1 \quad (7)$$

The largest error obtained this way for the cases considered is 4.6 per cent.

$R_1 C_1$  does not give a good approximation to  $t_1$ . The smaller  $C_2$  compared with  $C_1$ , the better  $r_1 c_1$  approximates the value  $t_1$ . In any case  $t_2$  and  $t_1$  will lie within limits given by the relations

$$r_1 c_1 \leq t_1 \leq r_1 (c_1 + c_2) \quad (8)$$

$$\infty \geq t_2 \geq r_1 (c_1 + c_2) \quad (9)$$

For the case of identical stages Eqs. (4) and (5) become

$$e_2 = 1.17 E_0 e^{-\frac{0.382t}{rc}} - 0.17 e^{-\frac{2.611t}{rc}} \quad (10)$$

$$e_1 = 0.724 E_0 e^{-\frac{0.382t}{rc}} + 0.275 E_0 e^{-\frac{2.611t}{rc}} \quad (11)$$

### Applications

The principal application of resistance-capacitance filters is in conjunction with rectifiers, where the purpose is to obtain a current proportional to the envelope or rectified value of a current of higher frequency. The most common case is the detection or demodulation of an r-f carrier, but in this instance the problem of filtering out the carrier without appreciably distorting the a-f waves is generally made comparatively easy by the large ratio of carrier to modulation frequency.

In practically all these applications, the rectifier, with comparatively low conducting resistance, charges a capacitor. When the modulation falls, the rectifier resistance is practically infinite for reverse current. Thus the speed of response of the system must be separately calculated for charge and discharge.

If the rectifier impedance may be assumed to be infinite during the discharge period, the circuit is simple and its timing easy to calculate. When the rectifier is conducting, a number of circuit elements enter into the net charging

resistance. For simplicity, the rectifier and its associated circuit may be represented by means of equivalent circuits.

For estimating the time constant of a capacitor that is being charged through some supply circuit, or for making calculations involving power transfer from one circuit to another, the impedance of both circuits, as measured from the connecting terminals, must be known. This may call for arbitrarily separating the entire network into two parts, one of which is considered to be the load or receiving, and the other, the supply circuit. Frequently the supply circuit will then consist of the branch from which the power comes, plus one or more others that are loads across the actual supply branch.

For example, if a tube is supplying a-f power, it may be loaded by a plate resistor or other impedance, but the entire combination constitutes the supply circuit furnishing power to the load. Under such conditions, the impedance of the circuit is that of all the branches in multiple, regardless of which are in fact supplying and which are absorbing power. This assumes that such passive branches have impressed across them the full voltage developed across the terminals of the active branch.

In Fig. 6A the total current  $I_1$  will be  $I_3 + (E_2/R_2)$  and total supplied voltage

$$E_1 = E_2 + I_1 R_1 = E_2 + \left( \frac{E_2}{R_2} \right) R_1 + I_3 R_1$$

whence  $E_2 \left( 1 + \frac{R_1}{R_2} \right) = E_1 - I_3 R_1$   
or

$$E_2 = \frac{E_1}{1 + \frac{R_1}{R_2}} - I_3 \frac{R_1}{1 + \frac{R_1}{R_2}} = \frac{E_1 R_2}{R_2 + R_1} - I_3 \frac{R_2 R_1}{R_2 + R_1} \quad (12)$$

These equations indicate that the voltage  $E_2$  across the terminals of the supply circuit is the same as would result from supplying a voltage  $E_1 R_2 / (R_1 + R_2)$  through a resistance  $R_2 R_1 / (R_2 + R_1)$  as shown in Fig. 6B.

It is obvious that a third resistance can be added in similar manner, or that the same principle can be extended to as many branches as desired. Thus a vacuum tube with plate resistor and with a loading resistance such as shown in Fig. 7A would have the impedance corresponding to all three resistances in multiple as indicated in Fig. 7B.

Making use of the foregoing principle, the driving tube plate resistance  $R_p$  and plate supply resistance  $R_b$  may be com-

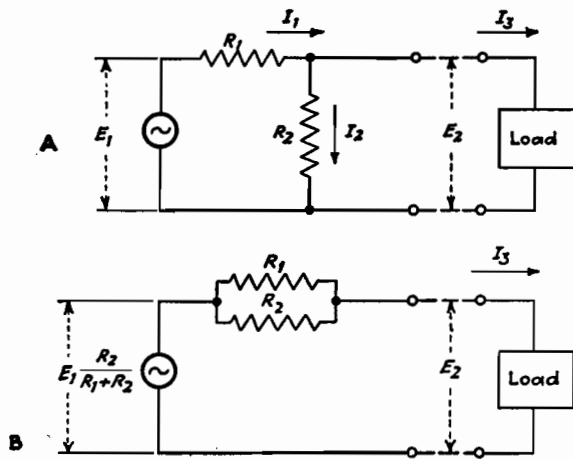


Fig. 6.—Loaded supply circuit A and its equivalent B.

bined into a single resistance  $R_1$ . With this simplification, the resistance-coupled rectifier in Fig. 8A may be represented by Fig. 8B.

For an approximate analysis of the action of the circuit shown in Fig. 8B, it seems simplest to assume that the impressed voltage and current are square waves. We shall make the further assumption that the reactance of the block-

ing capacitor is zero, and the capacitance is so large as to have negligible reactance. For working out the voltage and current relations, it is necessary to consider only what happens during one or two cycles, at any stage of the operation of charging the capacitor. If, as is usually the case, a large number of cycles are required to charge the capacitor, the back emf during such a small interval will be substantially

constant. The voltage across the capacitor at the time under consideration is designated by  $E_3$ .

Assuming a voltage  $E_3$  across the condenser and a d-c charging current  $I_3$  is being supplied, we can calculate the magnitude of the alternating voltage at the source  $E_1$ , and the expression for the relationship between  $E_1$ ,  $I_3$ , and  $E_3$  will show the effective resistance of the circuit

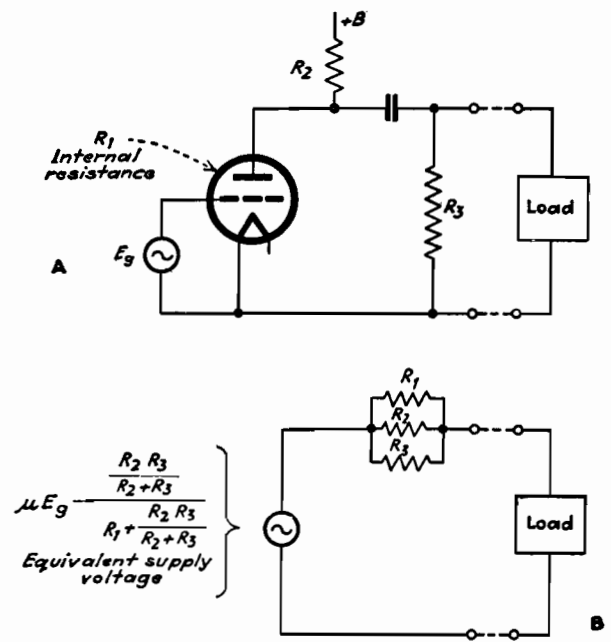


Fig. 7.—Loaded tube circuit A and its equivalent B.

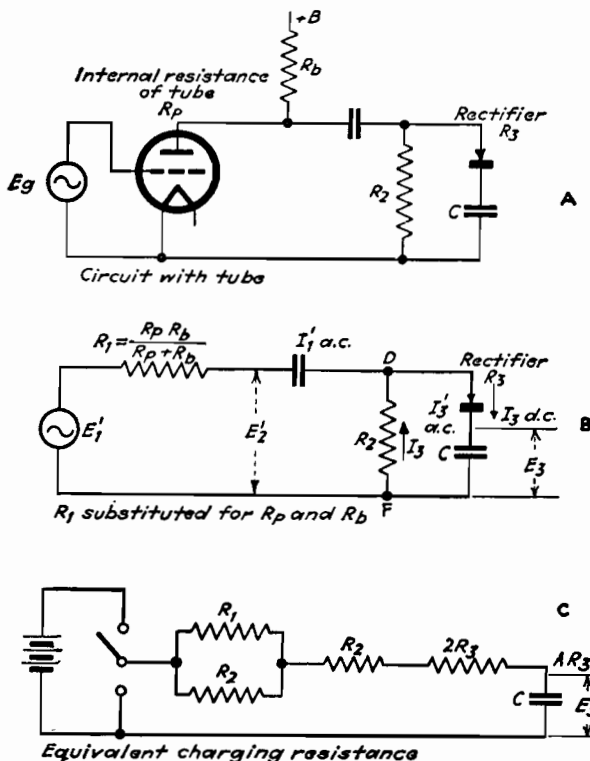


Fig. 8.—Rectifier circuit and charging circuit having same impedance.

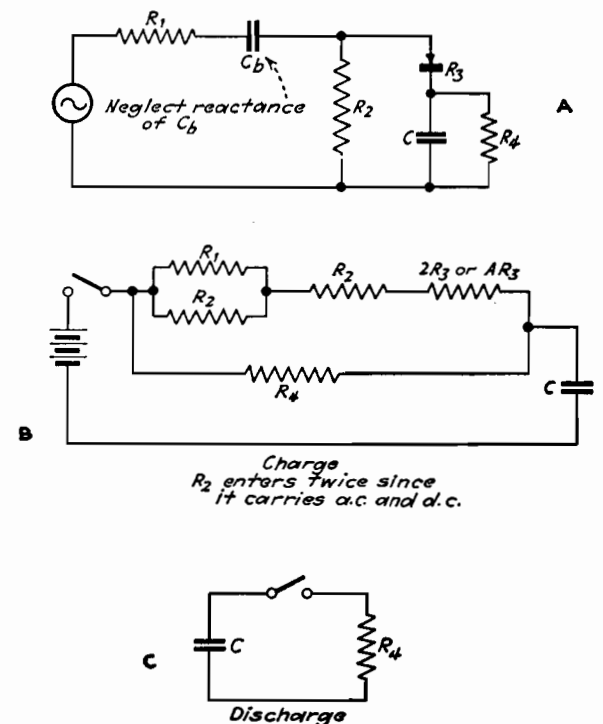


Fig. 9.—Resistance-capacitance coupled rectifier with capacitor and discharge resistances.

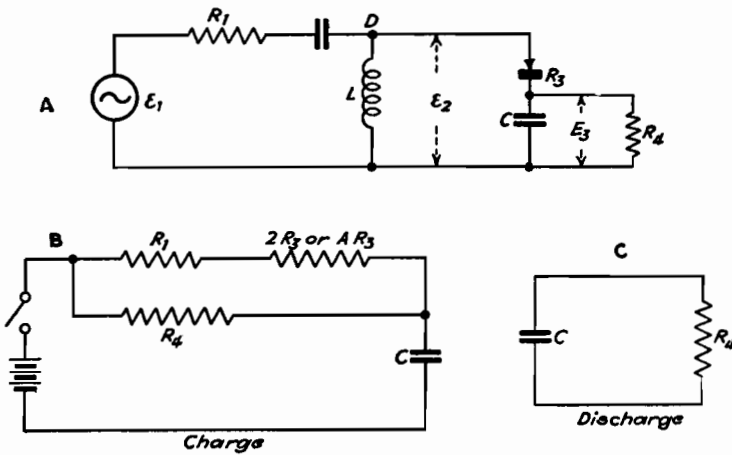


Fig. 10.—Capacitance-coupled rectifier with inductance by-pass.

including the rectifier, through which the capacitor is being charged.

The assumption of a square-wave alternating current plus the condition that for a half cycle there is no current through the rectifier means that the direct current  $I_3$  and alternating current  $I_3$  at this point are equal, giving a total current of  $I_3 + I_3' = 2I_3$  for the positive half cycle, and  $I_3 - I_3' = 0$  for the negative half cycle. While the current  $2I_3$  is flowing through the rectifier, the voltage across the rectifier and load  $C$  will be  $E_3 + R_3 \times 2I_3$ . The direct current,  $I_3$  must return to the point  $D$  through the resist-

ance  $R_2$ , and this requires that the point  $D$  be maintained at an average potential equal to  $I_3R_2$  negative with respect to  $F$ , which voltage is built up across the blocking capacitor. The alternating voltage at the point  $D$  (referred to  $F$ ) is determined from this average potential ( $-I_3R_2$ ) and the maximum positive value  $E_3 + 2I_3R_3$ . The alternating voltage is therefore

$$E_2' = E_2 + 2I_3R_3 + I_3R_2 \\ = E_3 + I_3(R_2 + 2R_3) \quad (13)$$

In addition to the direct current  $I_3$  which flows through  $R_2$ , the voltage  $E_2'$

will cause an alternating current  $E_2/R_2$  through  $R_2$ . Then the total alternating current that the generator must supply will be

$$I_1' = I_3' + \frac{E_2'}{R_2} = I_3 + \frac{E_2'}{R_2} \\ = I_3 + \frac{E_3 + I_3(R_2 + 2R_3)}{R_2} \\ = \frac{E_3}{R_2} + I_3 \left( 1 + \frac{R_2 + 2R_3}{R_2} \right) \quad (14)$$

The voltage that the generator must supply is

$$E_1' = E_2' + I_1'R_1 = E_3 + I_3(R_2 + 2R_3) \\ + R_1 \left[ \frac{E_3}{R_2} + I_3 \left( 1 + \frac{R_2 + 2R_3}{R_2} \right) \right] \\ = E_3 \left( 1 + \frac{R_1}{R_2} \right) \\ + I_3 \left[ R_1 + (R_2 + 2R_3) \left( 1 + \frac{R_1}{R_2} \right) \right] \quad (15)$$

or dividing by  $1 + \frac{R_1}{R_2}$  and solving for  $E_3$

$$E_3 = E_1' \frac{R_2}{R_1 + R_2} \\ - I_3 \left[ \frac{R_1 R_2}{R_1 + R_2} + R_2 + 2R_3 \right] \quad (16)$$

The effective supply circuit resistance is

$$\frac{R_1 R_2}{R_1 + R_2} + R_2 + 2R_3$$

The equivalent circuit is shown in Fig. 8C.

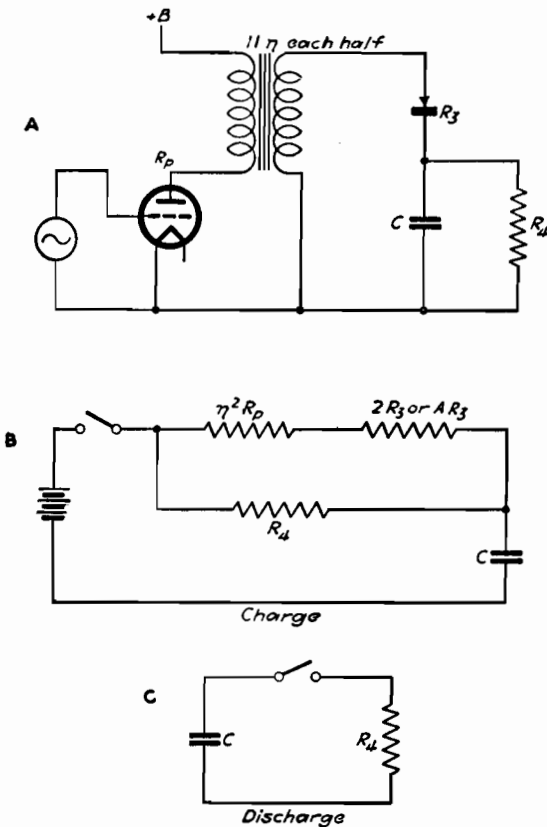


Fig. 11.—Transformer-coupled rectifier.

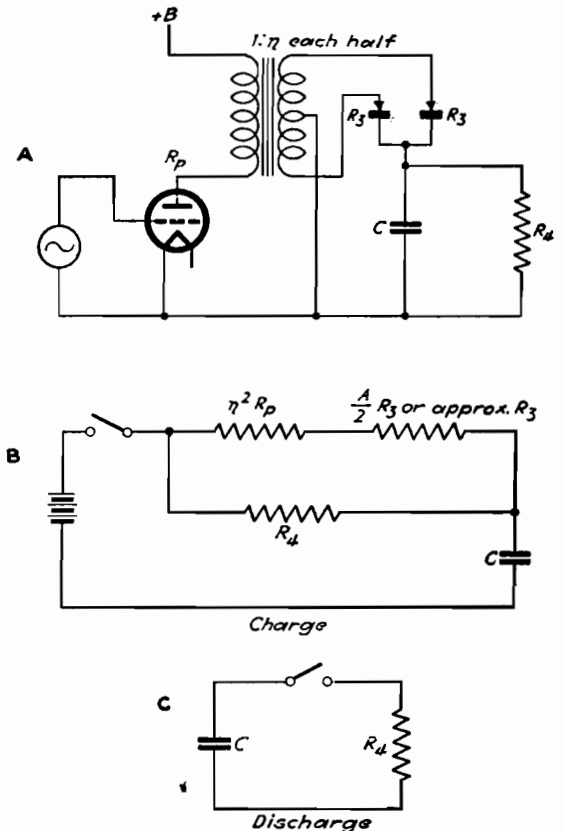


Fig. 12.—Full-wave rectifier.

For determining the time constant of a capacitor charged through a resistor, it is usual to consider that the voltage applied to the resistor is suddenly changed from 0 to  $E_1$ , or vice versa. The equivalent assumption when a rectifier is included in the circuit is that the alternating voltage is suddenly changed from 0 to  $E_1$ , or vice versa. Since in circuit 8B the rectifier does not appear as such, the capacitor charging is to be calculated on the basis of a suddenly applied direct voltage, but it is evident from Fig. 8A or B that the rectifier will prevent the capacitor discharging through the same path. It is usual to provide a discharge resistance  $R_4$  of Fig. 9.

The equivalent of Fig. 9A is Fig. 9B while the condenser is being charged. When the rectifier is inactive and the capacitor is discharging, the equivalent is simply the one discharge path  $R_4$ , indicated in Fig. 9C.

Again for simplicity, assume a square wave of impressed voltage. During the positive half cycle the alternating and direct currents add, and, since again they are equal, the current through the rectifier is  $I_3 + I_3' = 2I_3$ , and  $A$  is positive with respect to  $B$  by  $E_3 + 2I_3R_3$ . Since

there can be no steady voltage difference between  $A$  and  $B$ , the negative swing of  $A$  must be the same as the positive swing, so that

$$E_2' = E_3 + 2I_3R_3 \quad (17)$$

Since the choke takes no alternating current, the current through the blocking capacitor is  $I_1' = I_3' = I_3$ . Then the generator must supply a voltage

$$\begin{aligned} E_1' &= E_2' + I_1'R_1 = E_3 + 2I_3R_3 + I_1R_1 \\ &= E_3 + 2I_3R_3 + I_3R_1 \\ &= E_3 + I_3(R_1 + 2R_3) \quad (18) \end{aligned}$$

Again combining the discharge resistance  $R_4$  with the net resistance during charge of the rectifier circuit, we have Fig. 10B for the equivalent of Fig. 10A during charge, while, as before, the discharge equivalent includes only  $R_4$ , as indicated in Fig. 10C.

If the rectifier is fed through a transformer whose resistance to the flow of direct current in the secondary is negligible, the case is practically equivalent to that just considered, of a reactor and blocking capacitor, except that if the transformer is of some ratio, instead of unity, the primary circuit resistance must be multiplied by  $n^2$ . The circuit and equivalents are illustrated in Fig. 11.

If a full-wave rectifier is employed as indicated in Fig. 12, the factor 2 by which the rectifier resistance  $R_3$  has been multiplied in the previous cases is omitted, since one or the other of the rectifiers is working for each half wave of the applied voltage.

In the foregoing, the assumption that the rectifier carries current half the time resulted in the rectifier resistance being multiplied by 2 in the equivalent circuit. If the total rectified current must be passed in a smaller fraction of the time, the momentary current must be higher and the voltage drop correspondingly greater. Therefore, as previously explained, the rectifier resistance is multiplied by a factor  $A$  which may be as low as 2 but is in general higher depending on what fraction of time conduction is taking place.

### Bibliography

- (1) SINNETT, C. M., "Practical Volume Expansion," *Electronics*, November, 1935.
- (2) The application of such systems is discussed in papers by R. H. Townsend, H. McDowell, and L. E. Clark, *Acad. Motion Picture Arts & Sci.*, February, 1931; B. Kreuzer, *Jour. Soc. Motion Picture Engrs.*, June, 1931; E. W. Kellogg and C. N. Batsel, *Jour. Soc. Motion Picture Engrs.*, August, 1931; and H. C. Silent, *Jour. Soc. Motion Picture Engrs.*, May, 1932.

## SECTION V

# CAPACITORS

	Page
Rounded-edge Capacitor Plate Design.....	73
V-h-f Behavior of Capacitors.....	76
Capacitor Discharge Chart.....	80
Capacitor Charge-discharge Nomograph.....	82
Capacitor-lead Resonance Chart.....	83
Resonance Chart for Mica Capacitors.....	85
Power-factor Correction Charts.....	86
Temperature Compensation of Tuned Circuits.....	88
Determining Frequency Stability of Tuned Circuits.....	89

## Rounded-edge Capacitor Plate Design

By SAMUEL SABAROFF

Optimum conditions in a parallel-plate air-dielectric capacitor involve consideration of relationships between thickness and spacing of plates as well as the effect of rounded edges and corners on corona and spark-over phenomena

**B**ETWEEN two oppositely charged parallel plates of infinite extent the field is said to be uniform. It is known, however, that the field between two finite plates is *not* uniform, tending to greater gradients at the edges.

Stress at a point in a dielectric is determined by the gradient at that point, and stresses above certain critical values lead to the formation of corona and spark-over. A knowledge of the factors determining maximum gradient assists in proper design of a capacitor.

### Approach Is Analytical

In this discussion, the dielectric will be taken as air. Plate thickness is assumed to be small, compared with any other linear dimension, except where otherwise noted. Plates with corners are assumed to have them rounded so that their radii of curvature will be large compared with the plate thickness.

It is an easily demonstrable fact that the gradient at a sharp edge is greater than at a rounded surface. Application of a sufficiently high voltage to a conductor will make corona stream from sharp edges while there is very little evidence of it on the flat surfaces. It would seem advantageous to construct a capacitor with edges having a maximum radius of

curvature. Disregarding the possibility of curling the edges over to increase curvature, the plates should be as thick as possible up to a certain point. This lessens the gradient at the edges.

Now suppose the spacing between the two plates is very small compared with plate thickness. For sufficiently small spacing, breakdown will occur between the plates and the edge effect becomes relatively minor.

There may be a relation between plate spacing and thickness that will give a minimum gradient for a fixed voltage and a given plate spacing. This is the basic design problem.

### Spacing-thickness Relation

This may be pictured as follows, with plate spacing identified as  $S$  and thickness as  $T$ . For large values of  $S/T$ , the radius of the plate edge is small and a high gradient exists there. As plate thickness is increased—keeping plate center-to-center spacing and applied voltage constant—the radius of edge curvature is increased. This decreases the edge gradient. Inside the capacitor, however, the gradient increases because of the reduced spacing. The best value of  $S/T$  can be located at the crossover point between these two opposing effects. At

this point the maximum gradient that can occur becomes a minimum. Such critical values have been calculated and observed for other electrode shapes.<sup>1</sup>

It has been suggested by Ekstrand<sup>2</sup> that the best value of  $S/T$  may be between the values of 2 and 3. This investigation seems to corroborate his figures by fixing the optimum  $S/T$  at 2.77.

### What Constitutes Breakdown?

It has become somewhat of a habit to consider breakdown as coincidental with spark over. Actually, breakdown has occurred at the first sign of corona, and corona may become evident at a considerably lower voltage than spark over.

When a conductor is raised beyond a certain critical potential, the air adjacent to it becomes ionized, forming corona. The ionized air, being itself a conductor, can be considered to increase the size of the original conductor. If this effect is accompanied by an increase of gradient, the condition becomes unstable and spark over occurs. If there is a decrease in gradient, the condition is stable and corona remains as such.

Application of this concept to our capacitor is almost obvious. Suppose that  $S/T$  is greater than the critical



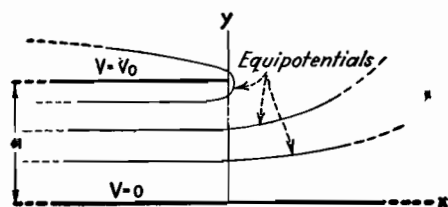


Fig. 1.—Situation adjacent to one infinite and one semi-infinite capacitor plate in space. Note that equipotential contours tend toward a curved-edge plate above.

value. Now, as we apply a gradually increasing voltage, corona will commence. If we consider the corona as part of the plate, then in effect the plate thickness has been increased, thus reducing the value of  $S/T$ . Spark over should then take place when the value of  $S/T$  is less than the optimum.

If we start applying voltage when  $S/T$  is less than the best value, then the transition from corona to spark over is almost instantaneous, since an increase in plate thickness will increase the gradient. There are irregularities in the practical manifestation of this principle. One reason is that corona will not form uniformly on the plates, being most evident where the gradient is maximum.

In the case of wires, spheres, and concentric cylinders,<sup>3</sup> corona appears for a constant gradient at a distance proportional to  $\sqrt{r}$  from the surface, where  $r$  is the radius. It may therefore be expected that experiment will show the existence of a similar factor in the formation of corona at the edges of a capacitor.

The microcosmic picture of air breakdown is complex and even of a somewhat metaphysical nature,<sup>4</sup> but breakdown characteristics have, in general, been determined by experiment.

This discussion concerns, in the main, a calculation for the best value of  $S/T$ . The derivations and approximations are guided by existing physical conditions. Results must be tested by experiment and qualified where necessary.

#### Basic Assumptions

Assume that the plates are semi-infinite in extent and that the radius of curvature of an edge is equal to half the plate thickness. Because of symmetry, thus applying the theory of images, it only will be necessary to consider the field between one semi-infinite plate and an infinite plate. This latter is placed midway between the semi-infinite plates and has a potential equal to half their sum.

First, consider a pair of plates that are of extreme thinness. The solution for

this case is well known.<sup>5</sup> An approximate plot of the equipotentials is shown in Fig. 1, in which it is assumed that the semi-infinite plate has a potential of  $V_0$  volts with respect to the infinite plate and is spaced  $a$  in. from it.

Along an equipotential, the gradient will depend entirely on concentration of the lines of force. In order to find the point of maximum gradient for any potential, it will be necessary to maximize  $E$  partially with respect to force function

Plate-dimension Ratios and Voltages of Capacitors at Various Frequencies

T, in.	S, in.	$\frac{S}{T}$	Spark over, kv			Max gradient (calculated), kv/in.		
			60 cycles	700 kilo-cycles	1,500 kilo-cycles	60 cycles	700 kilo-cycles	1,500 kilo-cycles
0.128	0.218	1.705	14.0	13.5	13.7	89.1	85.8	87.1
0.04	0.192	4.8	8.4	7.59	6.82	80.2	72.5	75.1
0.064	0.719	11.24	24.0	14.28	11.7	82.0	48.8	40.0

Any equipotential can be replaced by a conductor (of the same shape and charged to the same potential) without disturbing the external field in any way. Thus, if the equipotentials are replaced by equivalent plates, they will tend to an ordinary thin plate with rounded edges as the potential of the semi-infinite plate is approached. The procedure will now be to match, as far as possible, an actual plate to one of these equipotentials and thus obtain an expression for the maximum gradient at its edge. A somewhat arbitrary extension will then be made to indicate the maximum gradient on a plate of any thickness.

Potential around an infinitely thin plate, semi-infinite in extent, can be expressed in the following parametric form:

$$\left. \begin{aligned} x &= \frac{a}{\pi} \left( 1 + e^{-\frac{\pi U}{V_0}} \cos \frac{\pi V}{V_0} - \frac{\pi U}{V_0} \right) \\ y &= \frac{a}{\pi} \left( e^{-\frac{\pi U}{V_0}} \sin \frac{\pi V}{V_0} - \frac{\pi V}{V_0} \right) \end{aligned} \right\} \quad (1)$$

where  $V$  is potential at any point having the coordinates  $xy$ .  $U$  is the force or stream function.

In complex form Eq. (1) is

$$Z = \frac{a}{\pi} \left( 1 + e^{\frac{j\pi W}{V_0}} + \frac{j\pi W}{V_0} \right) \quad (2)$$

$$\begin{aligned} \text{where } Z &= x + jy \\ W &= V + jU \\ j &= \sqrt{-1} \end{aligned}$$

#### Finding the Gradient

At any point, the gradient is found by

$$E = \left| \frac{dw}{dz} \right| = \frac{V_0/a}{\sqrt{1 + e^{-\frac{2\pi U}{V_0}} + 2e^{-\frac{\pi U}{V_0}} \cos \frac{\pi V}{V_0}}} \quad (3)$$

where  $E$  is gradient in volts per inch.

$U$ . Thus  $\delta E / \delta U = 0$  when

$$e^{-\frac{\pi U}{V_0}} = \cos \frac{\pi(V_0 - V)}{V_0} \quad (4)$$

Substituting Eq. (4) in Eqs. (1) and (3)

$$\left. \begin{aligned} x_m &= \frac{a}{\pi} \left[ \sin^2 \frac{\pi(V_0 - V)}{V_0} + \log \cos \frac{\pi(V_0 - V)}{V_0} \right] \\ y_m &= \frac{a}{\pi} \left[ \frac{\pi V}{V_0} + \sin \frac{\pi(V_0 - V)}{V_0} \cos \frac{\pi(V_0 - V)}{V_0} \right] \end{aligned} \right\} \quad (5)$$

and

$$E_m = \frac{V_0/a}{\sin [\pi(V_0 - V)/V_0]} \quad (6)$$

As  $V$  approaches  $V_0$ , Eqs. (5) and (6) become

$$\left. \begin{aligned} x_m &= \frac{a\pi(V_0 - V)^2}{2V_0^2} \\ y_m &= a \end{aligned} \right\} \quad (7)$$

and

$$E_m = \frac{V_0^2}{a\pi(V_0 - V)} \quad (8)$$

#### Selecting the Curvature

At this point it becomes necessary to determine the manner in which an actual plate should be matched to an equipotential. A reasonable condition is that the radius of curvature of the actual plate and the radius of curvature of the equipotential at the point of maximum gradient be made equal.

For the radius of curvature, the formula is

$$R = \left[ 1 + \left( \frac{dy}{dx} \right)^2 \right]^{3/2} \left( \frac{d^2y}{dx^2} \right)^{-1} \quad (9)$$

At any point on an equipotential the radius of curvature, as found from Eqs. (1) and (9), is



$$R = \frac{a \left[ 1 + 2e^{-\frac{\pi U}{V_0}} \cos \left( \frac{\pi V}{V_0} \right) + e^{-\frac{2\pi U}{V_0}} \right]^{\frac{3}{2}}}{\pi e^{-\frac{\pi U}{V_0}} \sin \left( \frac{\pi V}{V_0} \right)} \quad (10)$$

On any equipotential, at the point of maximum gradient, the radius of curvature is found by substituting Eq. (4) in (10), thus

$$R_m = \frac{a \sin^2 [\pi(V_0 - V)/V_0]}{\pi \cos [\pi(V_0 - V)/V_0]} \quad (11)$$

As  $V$  approaches  $V_0$ , the radius of curvature becomes

$$R_m = \frac{a\pi(V_0 - V)^2}{V_0^2} \quad (12)$$

Let  $S$  equal the actual plate spacing and  $T$  equal the plate thickness. An approximate match can be assumed when  $(y_m - R_m)$  is identified with  $S/2$  and  $R_m$  is assumed equal to  $T/2$ . It is not necessary to consider  $x_m$ , and it is now ignored.  $V$  is made equal to  $v/2$  where  $v$  is the actual potential between the plates. When  $a$  and  $V_0$  are eliminated from Eqs. (7), (8), and (12),

$$S = \frac{v}{E} \left( \frac{v}{\pi ET} + \frac{2}{\pi} \right) - \frac{T(\pi - 1)}{\pi} \quad (13)$$

where the subscript has been omitted from  $E_m$ .

Since  $T$  is assumed small with respect to  $S$ , the right-hand term can be omitted in Eq. (13), resulting finally in

$$S = \frac{v}{E} \left( \frac{v}{\pi ET} + \frac{2}{\pi} \right) \quad (14)$$

Up to this point a small value of  $T$  has been assumed with respect to  $S$ . Now disregard the derivation and consider Eq. (14) alone. If we allow the plate thickness to approach infinity in Eq. (14), it becomes

$$S = \frac{2}{\pi} \frac{v}{E} \quad (15)$$

Compare this with the relation

$$S = \frac{v}{E} \quad (16)$$

which holds for two plates in which the edge effect is negligible. This is equivalent to the condition when  $T$  equals infinity.

#### Condition Generalized

Similarity between Eqs. (15) and (16) suggests the possibility of Eq. (14)

being adjusted so that it would hold for  $T$  large as well as small. This can be done approximately by replacing the constant  $2/\pi$  in Eq. (14) by unity, thus

$$S = \frac{v}{E} \left( \frac{v}{\pi ET} + 1 \right) \quad (17)$$

Equation (17) is admittedly approximate. Assuming for the moment that its accuracy has been established, let us examine it for the presence of a best value for  $S/T$ . This best value is, of course, the one that makes  $E$  a minimum.

Adding  $T$  to both sides of Eq. (17) gives

$$S + T = \frac{v}{E} + \frac{v^2}{\pi E^2 T} + T \quad (18)$$

Differentiating Eq. (18) with respect to  $T$ , remembering that  $(S + T)$  is constant, and then equating  $dE/dT$  to zero results in the condition

$$\frac{v}{ET} = \sqrt{\pi} \quad (19)$$

Substituting Eq. (19) in (17) results in

$$\frac{S}{T} = 1 + \sqrt{\pi} = 2.77 \quad (20)$$

as the best ratio of plate spacing to plate thickness. Note that the best value of  $S/T$  as found above falls within the limits suggested by Ekstrand.

#### Alternate Forms

Equation (17) may be made more symmetrical by dividing through by  $T$ .

$$\frac{S}{T} = \frac{v}{ET} \left( \frac{v}{\pi ET} + 1 \right) \quad (21)$$

Another useful form is

$$\frac{E}{E_{av}} = \frac{1}{2} \left( 1 + \sqrt{1 + \frac{4S}{\pi T}} \right) \quad (22)$$

where  $E_{av} = v/S$ .

The form of Eq. (21) suggests that it may be generalized into

$$\frac{S}{T} = \frac{v}{ET} + \sum_{n=0}^{\infty} K_n \left( \frac{v}{ET} \right)^n \quad (23)$$

where  $K_n$  is to be determined by experiment.

Ekstrand<sup>2</sup> published some measurements on the spark-over voltages of three capacitors with rounded edges at frequencies of 60 cycles, 700 kc, and 1,500 kc. The table lists calculated

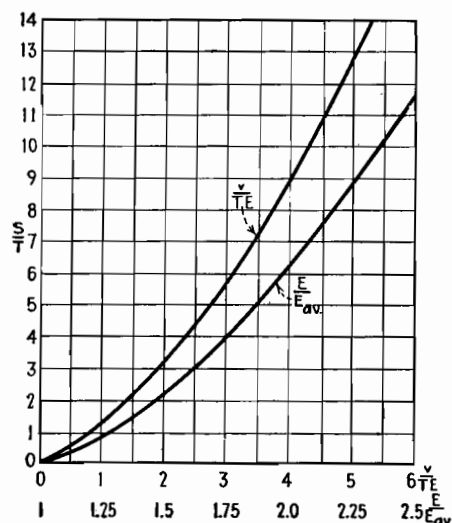


Fig. 2.—Values of capacitor-plate spacing-thickness ratio are plotted against potential and gradient relationships.

values of maximum gradients on these capacitors as determined by means of Eq. (22). Any modification by corona of effective plate thickness has been neglected.

#### Frequency-independent Spark Over

At 60 cycles, the calculated maximum gradients at spark over do not vary more than about 10 per cent, with a mean value of 83.8 kv per in. This value for the spark-over gradient is of the expected order for low frequencies. Only one capacitor, with a ratio of  $S/T$  equal to 1.705, approximates this value for 700 and 1,500 kc. The other two give breakdown gradients progressively lower for increasing frequencies. These facts seem to indicate that a critical value may exist for  $S/T$ , below which spark over becomes relatively independent of frequency.

Note that the spark-over performance of these three capacitors at 60 cycles can be predicted from Eq. (22), at least to common engineering accuracy. For use in testing this relationship further, Eqs. (21) and (22) are plotted in Fig. 2.

#### References

- (1) PEEK, F. W., "Dielectric Phenomena in High Voltage Engineering," 3d ed., pp. 30-31, McGraw-Hill Book Company, Inc., New York, 1929.
- (2) EKSTRAND, P. A., "Radio-frequency Spark-Over in Air," *Proc. IRE*, 28, No. 6, 262-266, June, 1940.
- (3) Same as (1), chapters 4 and 5.
- (4) DARROW, K. K., "Electrical Phenomena in Gases," Chap. 9, Williams & Wilkins Company, Baltimore, 1932.
- (5) OLLENDORF, R. R., and POHLHAUSEN, K., "Theory of Functions," pp. 138-140, Technology Press, Massachusetts Institute of Technology, Cambridge, Mass., 1942.

# V-h-f Behavior of Capacitors

By E. L. HALL

Measurements of power factor and apparent capacitance for several makes of capacitors, sockets, tubes, and concentric cables over a frequency range of 27.5 to 200 Mc, using a h-f Q meter. Apparent capacitance increases greatly as leads are lengthened

CONSIDERABLE experimental and development work of the past few years has been accomplished without much thought as to whether the given radio components yielded the maximum performance possible. The chief requisite was to get results quickly.

A technician might be assigned a specific project involving the design of apparatus to operate at 150 Mc, for example. The design would involve some tubes, sockets, capacitors, coils, etc. Use of the first components at hand might result in very poor operation of the device and consequent delay of an important project, because components unsuitable for this frequency were used. Since the radio frequencies within the circuits found tubes, sockets, and capacitors<sup>1</sup> all with relatively low-impedance paths across them, wherein much of the r-f energy was wasted, only a small amount arrived at the output terminals for useful work. If a much lower frequency had been selected, with appropriate changes in  $L$  and  $C$  values, the device probably would have operated satisfactorily with those components.

## V-H-F Measuring Technique Used

A number of measurements were made on several types of components to determine their comparative suitability for use at frequencies from 27.5 to 200 Mc. These measurements were made with a type 170-A Boonton Q meter.<sup>2</sup> This instrument gives a measurement of voltage at resonance across a variable capacitor before the unknown component is connected and again after it is connected in the circuit. Readings of Q-meter voltage and tuning capacitance are taken for both conditions, from which other characteristics can be calculated. The power factor in per cent was calculated from the following:

$$\text{Per cent power factor} = \frac{100C_1(Q_1 - Q_2)}{(C_1 - C_2)Q_1Q_2}$$

where  $C_1$  and  $Q_1$  are capacitance and Q

readings at resonance before adding the capacitor to be tested, and  $C_2$  and  $Q_2$  are capacitance and Q readings at resonance after adding the capacitor to be tested. The values of  $C$  were read directly in micromicrofarads, and the values of  $Q$  were read from two vacuum-tube voltmeters.

apparatus. The power factor was calculated and is given in Table I.

## Twelve 10-μuf Capacitors

Power factor measurements were made at six frequencies upon twelve varieties of 10-μuf capacitors. Considerable change was noted in apparent capacitance.

Table I.—Double Plugs

Double plug No.	Description	Power factor in per cent at frequency in Mc							
		27.5	50	75	100	125	150	180	220
1	Exposed terminals, black molded phenolic resin	4.51	2.92	2.98	2.98	2.54	2.85	3.07	3.02
2	Enclosed terminals, black molded phenolic resin	5.00	4.15	4.16	3.86	4.71	4.90	5.18	4.86
3	Enclosed terminals, orange molded low-loss	0.94	0.84	0.82	0.76	0.91	1.21	1.25	1.16
4	Enclosed terminals, chocolate molded polystyrene	0.11	0.12	0.19	0.27	0.12	0.45	0.49	0.50
5	Enclosed terminals, yellow molded phenolic resin	1.38	1.00	1.12	1.11	0.64	1.30	1.43	1.68
6	Exposed terminals, transparent methacrylate resin	1.00	0.66	0.44	1.13	0.47	0.59	0.90	0.96

While the results presented below were usually made on only one of a make of components, the variation in results among the various units is such as to emphasize the need for knowledge of the electrical characteristics of components to be used at very high frequencies. These measurements were all made at room temperature. Change of characteristics of components with temperature and humidity and for frequencies above 200 Mc were not determined.

The type 170-A Q meter is particularly useful in measurements involving small capacitances up to 25 μuf, although not limited to this range. It therefore lends itself to measurements in which the capacitance is small.

To determine relative losses in several kinds of insulating materials, measurements were made on a number of double plugs of the kind supplied by General Radio Co. for connecting circuits and

Tables of power factor and apparent capacitance values are given in Table II, and corresponding curves for four of the capacitors are shown in Fig. 1. It will be noted from the table of power factors that the curve for the No. 4 silver-mica midget capacitor, if shown, would be similar to the curve for No. 12, the variable air capacitor with ceramic insulation; also that the No. 4 silver-mica capacitor has about half the loss of No. 3, a silver-mica capacitor of another make.

## 25-μuf Mica Capacitors

The importance of keeping all components for use at ultrahigh frequencies physically as small as possible and keeping connecting wires as short as possible will be shown in the following data. Two 25-μuf mica capacitors were selected. One was a midget type about 5/8 in. long not counting leads, and the other was 1 1/4

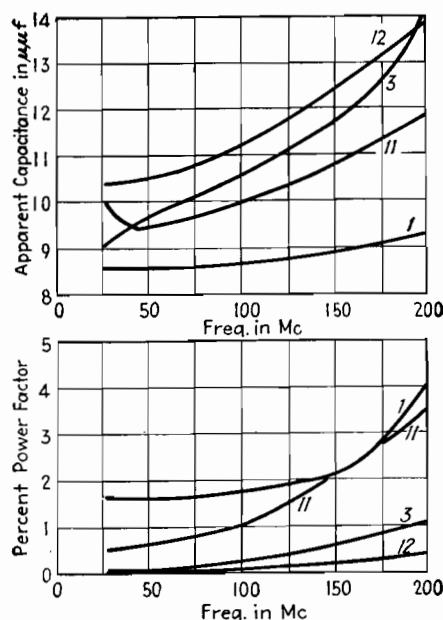


Fig. 1.—Curves showing how power factor and apparent capacitance for four of the small capacitors for which v-h-f data is given in Table II change with frequency.

in. long. The  $Q$  meter was used in the measurements, with leads on the capacitors as short as possible. The apparent capacitance was measured at frequencies from 27.5 Mc to as high a frequency as could readily be obtained. The larger capacitor required longer leads than the smaller in order to fasten on to the binding posts of the  $Q$  meter. Taking the capacitance at 27.5 Mc as a basis, the percentage change in capacitance was calculated for the different frequencies for the two capacitors, and the results are given in Table III. Curves A and H in Fig. 2 are plotted from these data and

show that the apparent capacitance of the small capacitor was about 6 per cent larger at 100 Mc, while the large capacitor was 50 per cent higher in apparent capacitance.

Table III.—25- $\mu\mu f$  Mica Capacitors

Freq., Mc	Small capacitor		Large capacitor	
	C, $\mu\mu f$	% change in C	C, $\mu\mu f$	% change in C
27.5	24.9	0	24.8	0
50	25.0	0.4	25.6	3.2
75	25.7	3.2	27.7	11.7
90	...	...	32.8	32.2
103	26.4	6.0	...	...
115	...	...	45.5	83.5
125	30.5	22.5	...	...
180	45.5	82.7	...	...

In the following tests, the small 25- $\mu\mu f$  mica capacitor of the previous test was provided with two leads 11.6 cm long. These leads were much longer than would probably ever be employed at the frequencies used in the test, but it was desired to exaggerate the effect produced. The apparent capacitance was measured for several frequencies for a number of leads of different lengths, down to the minimum length required to connect to the terminals of the  $Q$  meter. The percentage change in apparent capacitance, based on the capacitance with minimum-length leads at 27.5 Mc, is given for the different leads in Table IV and in curves A to G in Fig. 2.

The measured values of Table IV are plotted in Fig. 3 to show the percentage change in apparent capacitance with

leads of different lengths at four frequencies from 27.5 to 103 Mc. It will be evident from Figs. 2 and 3 that if the apparent or effective capacitance of a capacitor is to remain within, say, 10 per cent of its low-frequency value, connecting leads must be short or the capacitor must be used at lower frequencies. These curves explain why calculations involving inductance and capacitance at ultrahigh frequencies often fail to check experimental data.

#### Tubes and Sockets

Power-factor measurements were made on three miniature sockets at seven frequencies and on two ceramic sockets at four frequencies, using the  $Q$  meter. The measurements on a polystyrene socket gave an apparent zero power factor because this material was used in the construction of the  $Q$ -meter capacitor. The results on the other sockets are given in Table V. For sockets 1, 2, and 3 the seven contacts were connected together to form one terminal of the test capacitor, and the center metal sleeve formed the other terminal. For sockets 4 and 5, the grid terminal and the adjacent heater terminals were used.

Since considerable variation was found in the losses in small capacitors and sockets of different types, it was decided to make similar measurements on several types of vacuum tubes. Black phenolic compound has been long known to have higher losses than some other materials, yet it has been employed for the base of many types of vacuum tubes. It has been customary to remove the base of tubes used in some h-f applications, or

Table II.—10- $\mu\mu f$  Capacitors

Capacitor No.	Description	Power factor in per cent at frequency, Mc								Apparent capacitance in $\mu\mu f$ at frequency, Mc							
		27.5	45	50	75	100	150	200		27.5	45	50	75	100	150	200	
1A*	Mica midget capacitor molded in brown Bakelite	1.64	1.61	...	1.65	1.77	2.12	4.09		8.6	8.6	...	8.5	8.8	9.1	9.0	
2B	Mica midget capacitor molded in brown Bakelite	0.50	...	0.48	0.47	0.56	0.69	0.98		11.0	...	10.8	11.0	11.2	12.0	11.6	
3B	Silver mica midget capacitor molded in low-loss red Bakelite	0.07	0.10	...	0.17	0.24	0.61	1.13		8.8	9.8	...	10.1	10.6	11.7	14.1	
4C	Silver mica midget capacitor molded in low-loss red Bakelite	0.06	...	0.05	0.12	0.14	0.25	0.45		9.9	...	9.3	9.4	9.5	10.0	9.7	
5D	Mica midget capacitor molded in brown Bakelite	1.09	...	1.13	1.03	1.15	1.40	1.92		9.0	...	8.5	9.0	8.9	9.7	9.8	
6E	Mica midget capacitor molded in yellow Bakelite	0.57	0.71	...	1.08	1.40	2.79	...		9.2	9.0	...	9.3	9.7	10.2	...	
7F	Zero temperature coefficient tubular ceramic capacitor	0.04	0.05	...	0.06	0.07	0.11	0.10		9.7	9.6	...	9.8	9.7	9.7	9.1	
8F	Negative temperature coefficient tubular ceramic capacitor	0.00	...	0.00	0.01	0.01	0.03	0.00		9.2	...	9.5	9.6	9.3	9.4	8.6	
9	Trimmer capacitor, mica on bakelite base (old design)	0.86	...	0.86	0.83	0.88	0.98	1.16		9.8	...	9.5	9.5	9.7	9.9	9.1	
10	Trimmer capacitor, mica on ceramic base	0.04	...	0.04	0.08	0.09	0.15	0.21		9.0	...	9.0	9.1	9.5	9.5	9.1	
11F	Trimmer capacitor, ceramic	0.54	0.59	...	0.85	1.03	2.43	3.56		10.0	9.4	...	9.8	10.0	10.8	11.9	
12G	Variable air capacitor, ceramic insulation	0.02	...	0.02	0.07	0.09	0.23	0.40		10.4	...	10.5	10.9	11.1	12.4	13.9	

\* Letters represent manufacturers. Capacitors 1A, 2B, 3B, 5D, and 6E are of same physical dimensions and 4C is  $\frac{1}{4}$  in. longer than these.

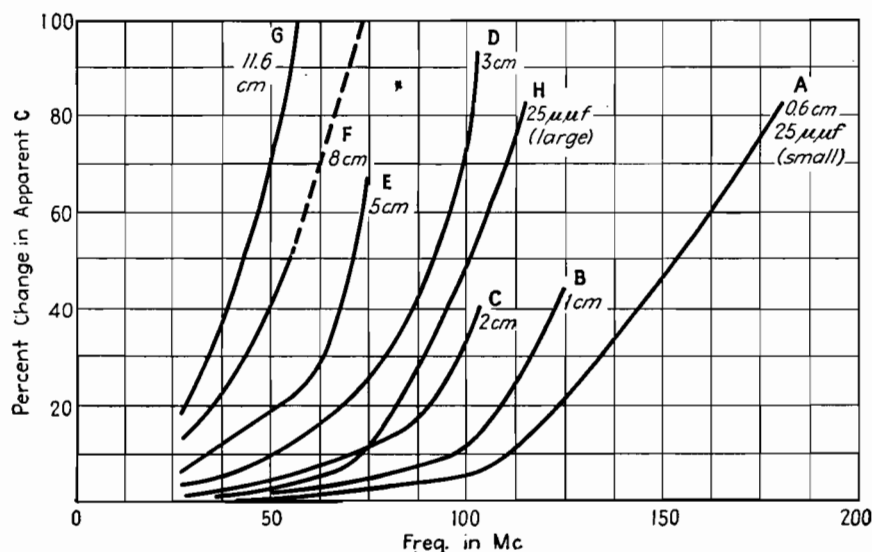


Fig. 2.—Per cent changes in apparent capacitance with frequency for a midjet 25- $\mu$ mf capacitor A and a 25- $\mu$ mf unit with physical dimensions twice as large B. These curves are based on data in Table III. Curves A to G show per cent changes in apparent capacitance with frequency for a 25- $\mu$ mf midjet capacitor used with leads from 0.6 to 11.6 cm long, as given in Table IV.

bring out the r-f terminals through the glass away from the phenolic base, but nevertheless some tubes are employed at fairly high frequencies where such expedients are neglected.

for six of the tubes listed in Table VI. All tubes but the types 9003 and 3A5 were measured without a socket. The polystyrene socket previously mentioned was used in the tests on these two tubes.

Table IV.—25- $\mu$ mf Capacitor with Various Lead Lengths

Test frequency Mc	Per cent change in capacitance for various lead lengths						
	0.6 cm	1 cm	2 cm	3 cm	5 cm	8 cm	11.6 cm
27.5	0	0	1.2	3.2	6.8	12.8	18.9
50	0.4	1.2	4.8	9.6	19.6	41.0	81.1
56	....	....	....	....	22.5	53.0	91.5
75	3.2	5.2	12.0	25.6	69.0	100+	100+
103	6.0	14.0	40.5	93.2			
125	22.5	44.6					
180	82.7						
Plotted (Fig. 2) in curve	A	B	C	D	E	F	G

Table VI gives power factor and capacitance for a number of types of tubes, measured between grid and cathode with the Q meter. Figure 4 gives curves of power factor and apparent capacitance

The first five tubes in Table VI presumably have a base made of the same black molded material. There may, however, be a difference in the glass used in the seal, or in the coating or deposit

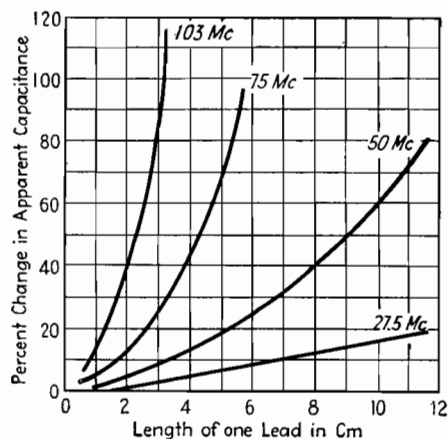


Fig. 3.—Curves for four frequencies of Table IV showing per cent change in apparent capacitance for different length capacitor leads.

within the tube, which would account for the rather large differences in the results on these tubes.

Tube 807(M) used a yellow molded material called Micanol for the base. Tube 807(C) had a ceramic base. The glass of the 954 tube was the only solid

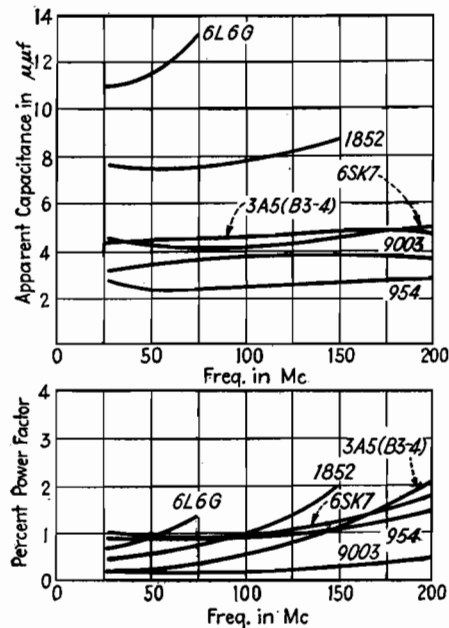


Fig. 4.—Curves showing power factor in per cent and apparent capacitance for six types of vacuum tubes in Table VI.

Table V.—Tube Sockets

Socket	Description of socket	Per cent power factor at frequency, Mc							Capacitance in $\mu$ mf at frequency, Mc						
		27.5	35	50	75	100	150	200	27.5	35	50	75	100	150	200
1	Black molded miniature.....	3.6	3.4	3.2	3.1	3.1	3.7	4.0	3.0	3.0	3.0	3.0	2.9	2.7	2.8
2	Miniature wafer; mica-filled insulation.....	0.25	0.26	0.24	0.22	0.22	0.15	0.22	1.9	1.9	1.9	1.9	1.8	1.7	1.8
3	Miniature molded; clear polystyrene.....	...	...	...	...	...	...	...	2.7	2.6	2.2	2.2	2.4	2.3	2.4
4	Five-prong ceramic.....	0.67	...	0.84	0.72	0.74	...	...	1.6	...	1.2	1.3	1.4	...	...
5	Five-prong ceramic.....	0.29	...	0.70	0.55	0.76	...	...	1.0	...	0.9	0.7	0.7	...	...

### Table VI.—Vacuum Tubes

Tube type	Per cent power factor at frequency, Mc						Apparent capacitance, $\mu\text{mf}$					
	28	50	75	100	150	200	28	50	75	100	150	200
6L6G.....	0.68	0.89	1.36	.....	Too large	.....	10.9	11.4	13.2	.....	.....	.....
1852.....	0.46	0.54	0.78	0.94	2.04	.....	7.6	7.5	7.8	7.7	8.8	.....
6SK7.....	1.00	0.97	0.94	0.99	1.33	1.80	4.5	4.2	4.0	4.5	4.5	5.0
76.....	1.08	1.24	1.84	3.38	.....	Too large	7.5	7.7	8.3	9.2	.....	.....
6C5.....	0.82	0.78	0.73	0.83	1.29	1.86	3.8	3.6	3.8	3.8	3.9	4.3
807(M).....	1.30	1.60	1.96	.....	Too large	.....	13.7	13.6	14.9	.....	.....	.....
807(C).....	1.09	1.41	1.95	.....	Too large	.....	13.2	13.9	15.1	.....	.....	.....
954.....	0.92	1.05	0.99	0.94	1.13	1.51	2.7	2.3	2.3	2.5	2.7	2.8
9003.....	0.20	0.19	0.18	0.19	0.30	0.50	3.2	3.4	3.6	3.7	3.8	3.7
3A5(A3-4).....	0.25	0.36	0.50	0.69	1.14	2.31	4.2	4.3	4.2	4.5	4.8	4.7
3A5(B3-4).....	0.19	0.28	0.42	0.60	1.08	2.14	4.3	4.4	4.5	4.6	4.9	4.7
3A5(A4-5).....	0.14	0.20	0.28	0.40	0.74	1.64	3.2	3.2	3.2	3.2	3.4	3.2
3A5(B4-5).....	0.62	0.51	0.50	0.55	0.86	1.90	2.8	3.1	3.4	3.2	3.4	3.1

dielectric involved in the measurements on this tube as it had no phenolic base and connections were made directly to the tube terminals. Comparing the results on the 954 tube with those on the 9003 tube and socket, it appears that the former used glass having a higher loss than that in the 9003 tube, or some coating within the tube increased the loss. Two 3A5 tubes were tested, and are designated *A* and *B*. The numbers 3-4 and 4-5 indicate the base pins to which connections were made.

### Concentric Cables

Power-factor measurements were made with the *Q* meter on three 6-in. lengths of concentric cable having solid insulation, a 6 in. length of line consisting of a  $\frac{5}{8}$ -in. copper tube with a No. 12 AWG copper wire supported by six ceramic spacers, and a length of shielded twisted pair with rubber and cotton insulation. The capacitances of the samples tested ranged

between 10 and 16  $\mu\text{mf}$  at 27.5 Mc. The percentage change in apparent capacitance from the value at 27.5 Mc was calculated. Table VII gives the data taken, and Fig. 5 gives curves of power factor and percentage change in apparent capacitance. Considerable change in apparent capacitance is not surprising since the capacitance is distributed along 6-in. conductors.

The data presented on several types of components are comparative and show that there is a wide range in the power factor or losses in many of these parts at frequencies up to 200 Mc.

A given component may be unsuited for use at ultrahigh frequencies and yet be entirely satisfactory at low frequencies. Likewise, it would usually be extravagant to use a ceramic or polystyrene socket in an a-f application, when a cheaper socket would suffice and the h-f types are so scarce. In further work<sup>3</sup> of this kind, similar information taken at other tem-

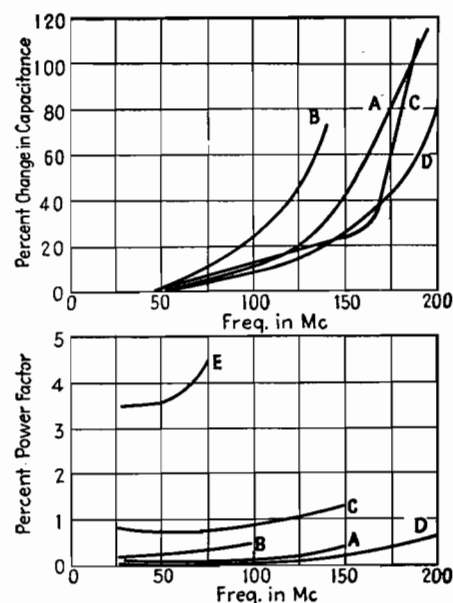


Fig. 5.—Curves showing power factor and per cent change in apparent capacitance for concentric cables in Table VII.

peratures and humidities would be of value.

No limiting value of power factor can be stated for radio components intended for use at very high frequencies. This is because other factors such as frequency, power considerations, position of use in the circuit, physical and mechanical considerations, and availability of desired types of components must be considered.

## References

- (1) Radio Instruments and Measurements, *Nat. Bur. Standards Circ.* 74, p. 111.
- (2) BROWN, H. A., "Radio-frequency Electrical Measurements," p. 70, McGraw-Hill Book Company, Inc., New York, 1938; RAO, V. V. L., *Proc. IRE*, 30, p. 502, 1942; TERMAN, F. E., "Radio Engineers' Handbook," p. 916, McGraw-Hill Book Company, Inc., New York, 1943.
- (3) MATTHEWS, A. C., Characteristics of Radio Electronic Components, *Radio*, July, 1943, pp. 24-28.

Table VII.—Samples of Concentric Conductors and a Twisted Pair

[illegible]

# Capacitor-discharge Chart

By LOUIS HANOPOL

**D**ETERMINATION of the voltage characteristic of a capacitor in a state of charge or discharge through a resistor is one of the most common electrical problems. The advent of the grid-controlled vacuum tube has increased the utility of capacitance-resistance networks as time controls. This function has been extended to timing relays, welders, and relaxation oscillators. The fundamental circuits are given in the figure.

The chart offers a convenient method of carrying out computations of the solution of the differential equation of a capacitor shunted by a resistance.

This solution takes the form

$$\frac{e}{E} = e^{-\frac{t}{RC}}$$

where  $E$  = voltage of the capacitor at full charge

$e$  = voltage of the capacitor at partial charge

$t$  = elapsed time in seconds from the initiation of the discharge

$R$  = resistance, ohms

$C$  = capacitance, farads

The chart can be interpreted in terms of the voltage of the capacitor when it is being discharged through a series resistor. The chart has as ordinates  $e/E$ , the percentage of the voltage at full charge; and covers the range from 100 to 0.1 per cent of maximum voltage. There are four overlapping curves that cover the time range from 0.01 to 100 sec. All these curves satisfy the equation for  $RC$  equal to one. These together with the simple relation

$$t_{\text{for any } RC} = t_{RC=1} \times RC$$

yield the solution for the large majority of problems.

Thus, to find the elapsed time interval from maximum voltage to any percentage of the maximum voltage, one merely reads from the chart the time interval for a given  $e/E$  and  $RC$  equal to one. This value of time is multiplied by the value of  $RC$  of the circuit being studied, and thus the latter's time constant is obtained.

Again, if for any circuit the time  $t$  and  $e/E$  are known, the chart can be read to give the time for a circuit with  $RC$  equal to one. For example, let the circuit be actuated at two points,  $E$  and  $0.5E$ . Let  $RC$  be equal to 6.

$$t_{RC=1} = 9.1 \text{ sec} \\ t = 9.1 \times 6 \text{ sec} = 54.6 \text{ sec}$$

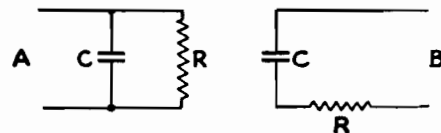
If the capacitor is being charged, its voltage becomes  $[E - (e/E)]$ ; i.e., its voltage is  $(1 - e/E)$  of the maximum. In the series case, the voltage across the resistor is  $(e/E) \times E$ .

The applications of the chart are many, from the calculation of the size of a protective discharge resistor across a high-voltage capacitor, to relaxation and bypass computations. Most electronic circuits use the  $RC$  nets to drive the vacuum tube whose output is to have two values separated by a given time interval, corresponding to that of the  $RC$  network. Control from the first vacuum tube may be extended to other tubes, transformers, and rectifiers as in welding systems. Relaxation oscillators are, from this point of view, timing systems in which the  $RC$  net biases the tube grid in the time interval  $\frac{1}{2} \times \text{frequency}$ , i.e.,  $RC$  is such that the voltage change from zero to  $e$  or  $e$  to maximum has an interval of  $\frac{1}{2} \times \text{frequency}$ , and the circuit oscillates at a frequency  $f$ .

Direct-current filter systems can be treated by using the timing approach. Here, it is required that the ripple voltage across a resistor have a given value. For a simple capacitance across a resistive load, the problem becomes that of maintaining  $e/E$  greater than some predetermined minimum percentage in the time interval  $\frac{1}{2} \times \text{frequency}$ . If  $e/E$  is never less than 99 per cent, the ripple never exceeds 1 per cent.

Attacking bypass problems in the same manner, the percentage of alternating current in a shunt resistor is that which discharges into it in the time interval  $\frac{1}{2} \times \text{frequency}$ . Thus cathode bypassing can be treated in the method above.

The use of practical time control

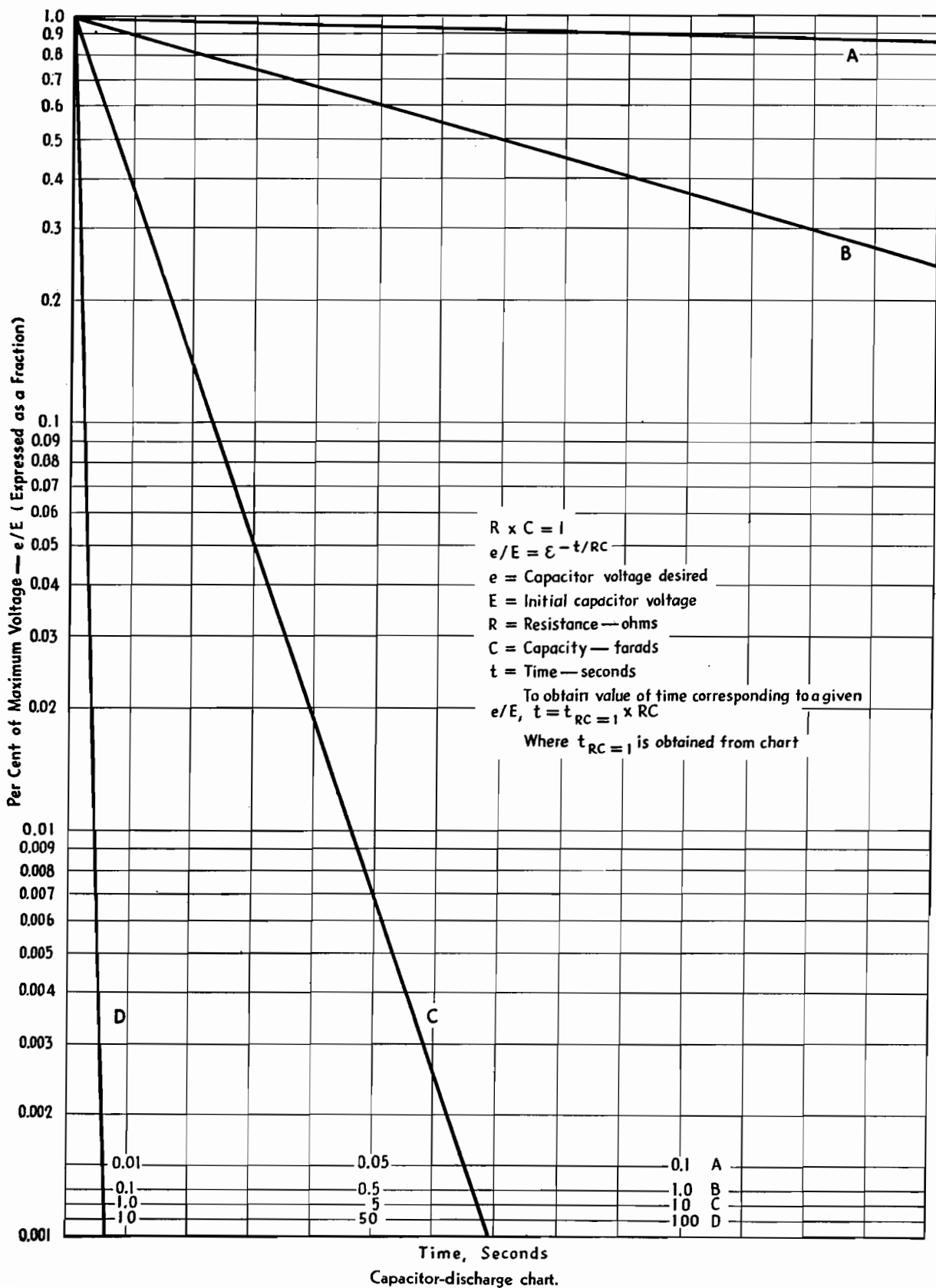


Fundamental capacitor discharge circuits.

requires that some consideration be given nonidealized circuit components. Manufactured capacitors have losses inherent in the dielectric and insulation. These are interpreted in terms of an equivalent shunt resistance. Both the capacitor and the resistor have variations in their characteristics with temperature and frequency, and these cannot be neglected when their magnitude approaches the nominal ratings of the components.

Resistors of the metallized or carbon-bakelite type have been developed to a state where the residual inductance and temperature variations are small. Large errors are not introduced from these sources until frequencies of 1,000 cycles and temperatures of 80°C are reached.

The limitations of capacitors are most obvious from their characteristics. Frequency does not affect them to about 10 to 20 kc. The initial resistance, or shunt resistance of a capacitor at 20°C, 2 to 10 megohms per  $\mu\text{f}$ , for electrolytic capacitors, 2,000 to 4,000 megohms per  $\mu\text{f}$  for paper halowax type capacitors, and 8,000 to 15,000 megohms per  $\mu\text{f}$  for mineral-oil impregnated types. The resistance gradient with temperature is steep and negative. If the shunt circuit resistor is not to be affected by the variation of the equivalent resistance, the latter must be at least one hundred times the former. The value of the equivalent capacitor resistance at its lowest value because of temperature ambients limits the value of  $RC$  obtainable with any given type of capacitor. Oil-filled capacitors can be designed for  $RC$  as high as 50 to 100 for small temperature variations. Electrolytic and some vegetable- and synthetic-oil capacitors have positive capacitance coefficients with temperature at temperatures below 0°C.

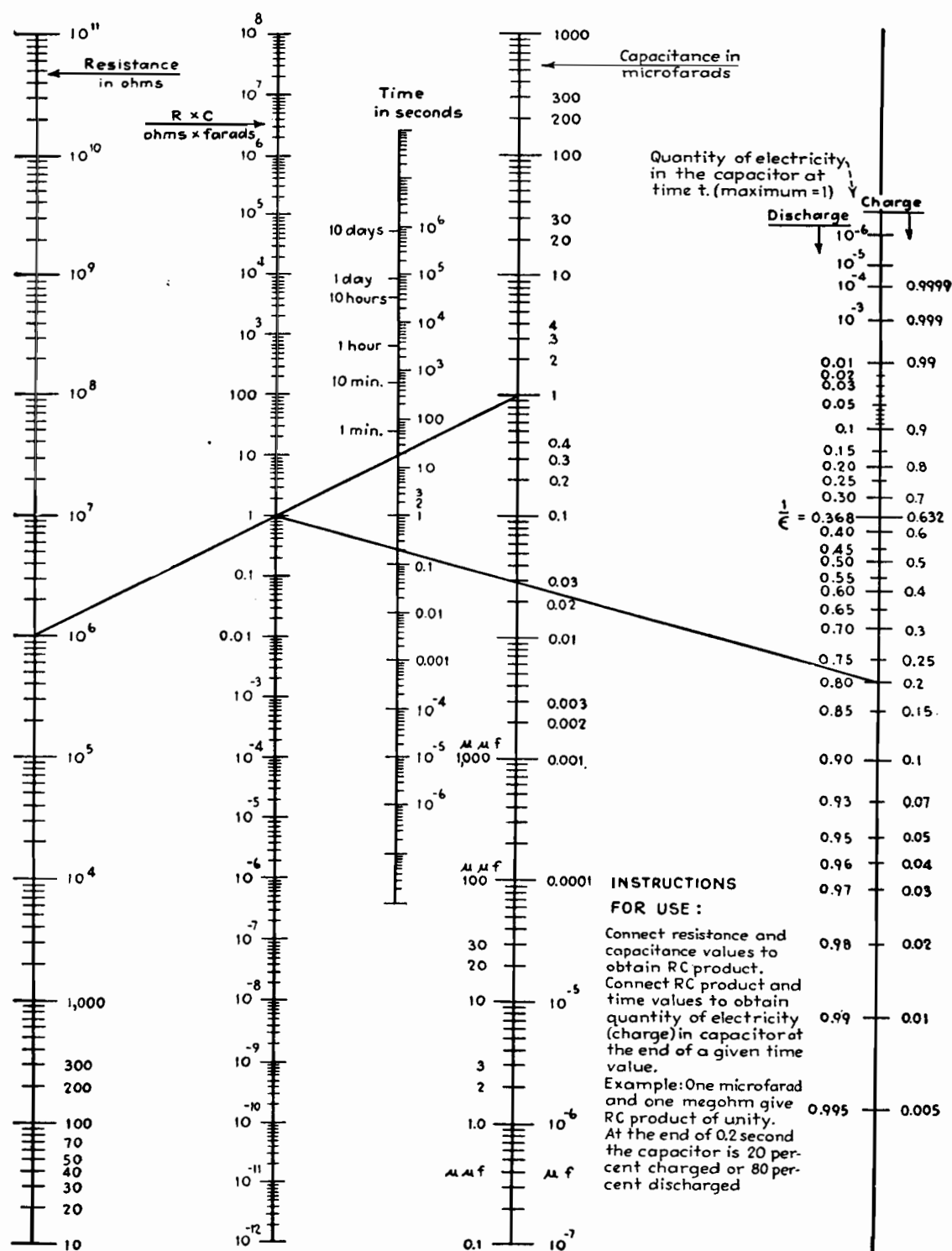




# Capacitor Charge-discharge Nomograph

By J. B. HOAG

A chart for computing the charge or discharge of a capacitor through a series resistor, in terms of time and the  $RC$  product





# Capacitor-lead Resonance Chart

By R. L. HASKINS

More effective use of capacitors in r-f circuits may be made if the series resonance of the units with their leads is taken into account.

The chart shows measured values of such resonance frequencies

MEANS of applying well-known but hitherto little used principles to the selection of capacitors for r-f circuits is suggested by the data graphically presented in Fig. 1. The principle involved is that for any frequency there is a series combination of inductance and capacitance that will provide minimum impedance and, consequently, maximum filtering or bypassing effect and that the inherent inductance of a capacitor and of its connecting leads may be utilized to secure series resonance at the desired frequency. The data from which the curves of Fig. 1 were plotted were secured by measuring the resonant frequency of a quantity of commercially constructed noninductively wound tubular capacitors with various lengths of No. 18 bare tinned copper connecting lead.

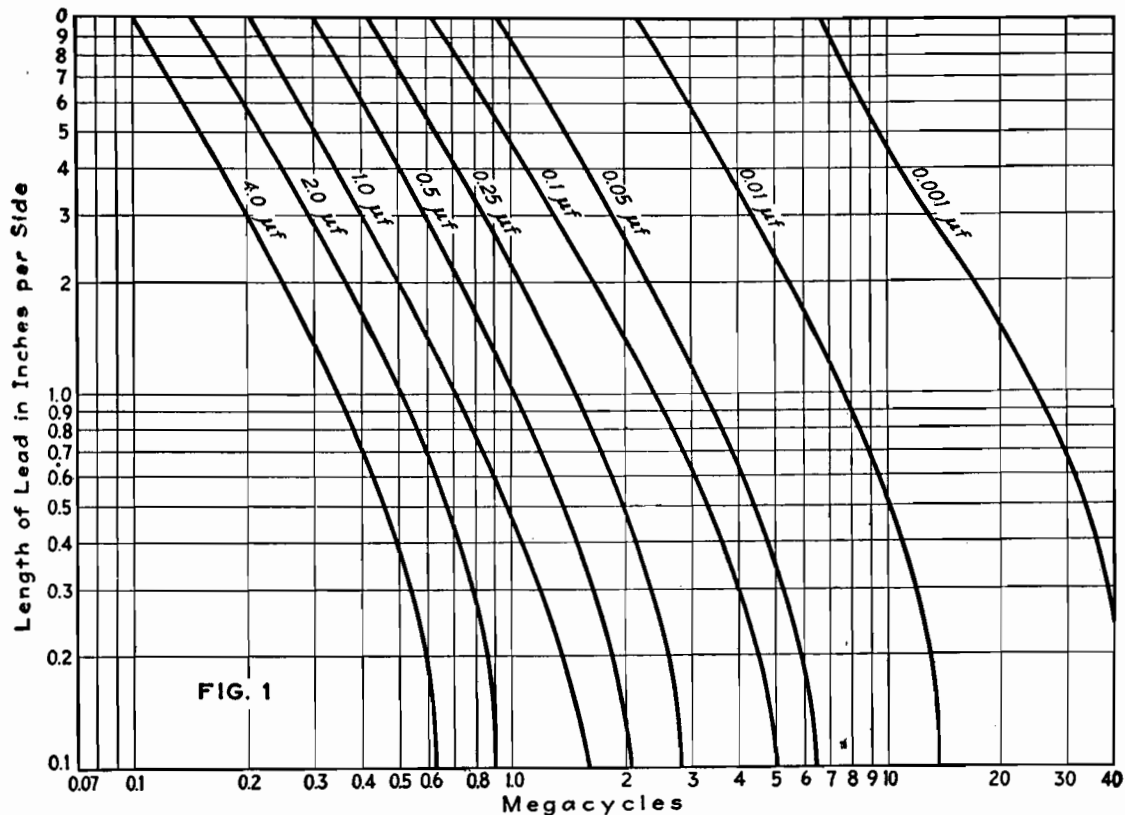
Tests on paper capacitors of standard

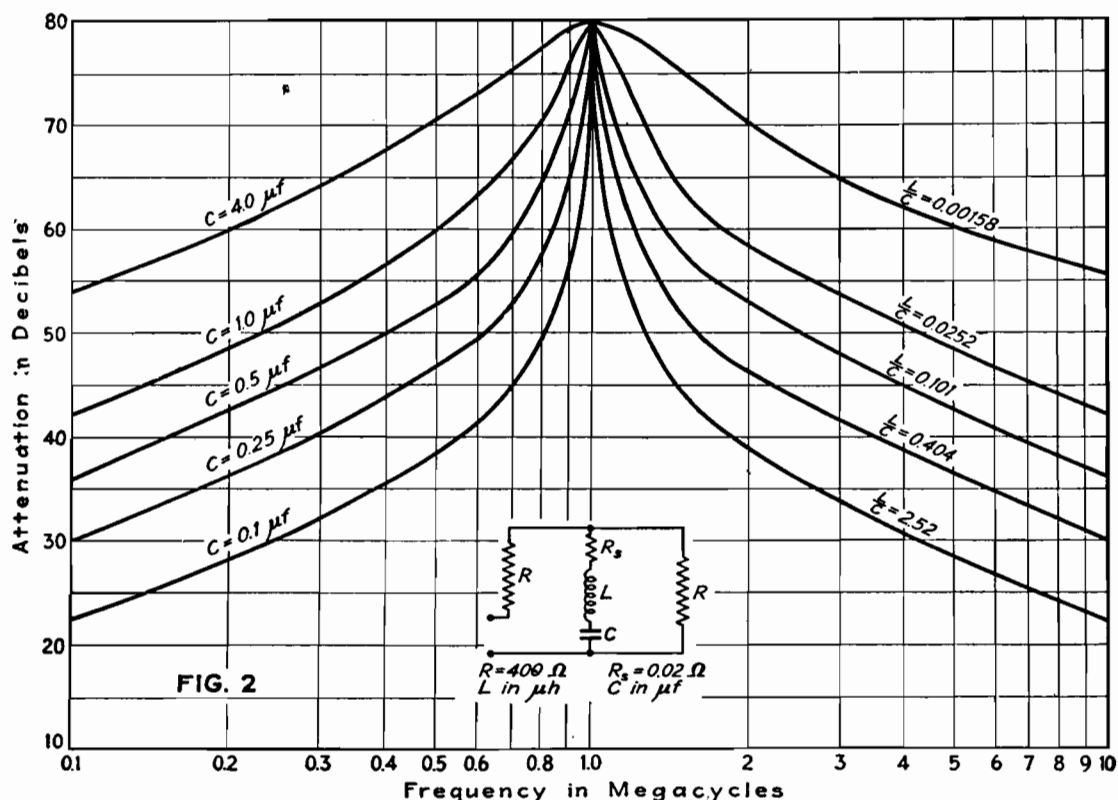
construction indicate that the residual inductance of such capacitors is approximately the same regardless of the voltage at which the unit is designed to operate. For capacitors with ratings of 200 to 800 volts, tests show residual inductance in the order of 7 to 10 millimicrohenrys. Since this inductance is usually small in comparison to the inductance of the leads, the accompanying curves may be considered practical for use in connection with capacitors of any normally employed voltage rating.

Through the use of these graphs, it is possible to choose the value of capacitance vs. lead length that will provide maximum LC ratio and thus secure maximum width of frequency band in which effective filtering or bypassing is secured. For example: Series resonance at 1 Mc results from the use of a 0.05- $\mu$ f capacitor with

10-in. leads on each side or from the use of a 0.5- $\mu$ f capacitor with 1-in. leads on each side. Obviously, the selectivity of the former circuit will be much greater than that of the latter, so that if mechanical considerations permit the use of the shorter lead, better performance will result.

This point is graphically illustrated by the curves given in Fig. 2. It will be seen that, although capacitances of 0.1 and 1.0  $\mu$ f provide the same peak attenuation when each is adjusted for resonance at the same frequency, the effective band width covered by the 1.0- $\mu$ f section is much greater than that covered by the 0.1- $\mu$ f section. This allows more effective filtering through the desired range of frequencies. Although the 4.0- $\mu$ f curve shows good filtering characteristics at frequencies between 500 and 2,000 kc, in





practice it is difficult to resonate this value of capacitance at 1,000 kc owing to the extremely low value of residual inductance necessary for resonance. Analysis of Fig. 1 shows that a 4.0- $\mu$ f capacitor has a resonant frequency of approximately 620 kc.

In utilizing these graphs in design work, it is important to note that the capacitor leads must be of equal length for each side of the capacitor, because the use of unequal lead lengths will materially alter the resonant frequency. Although the test specimens with which the data were secured had bare wire leads, the use of insulated wire or of wire differing considerably in cross-sectional area does not seriously affect the performance of the capacitor.

To determine the effectiveness of a capacitor as a filter unit, the circuit shown in Fig. 3 is employed. This provides a convenient method of determining not only the capacitor's resonant

frequency, but also its attenuation characteristics. In this circuit the attenuation becomes

$$\text{Atten. (db)} = 20 \log_{10} \left( 1 + \frac{R_g}{2Z} \right) \quad (1)$$

$$= 20 \log_{10} \left\{ 1 + \frac{R_g R_g \omega^2 C^2}{2[R_g^2 \omega^2 C^2 + (\omega^2 LC - 1)^2]} - j \frac{R_g \omega C (\omega^2 LC - 1)}{2[R_g^2 \omega^2 C^2 + (\omega^2 LC - 1)^2]} \right\} \quad (2)$$

when  $j\omega L = \frac{-j}{\omega C}$  and  $R_g > R_c$

$$\text{Atten.} = 20 \log_{10} \frac{R_g}{2R_c} \quad (3)$$

If  $R_g$  is chosen at approximately 400 ohms, the peak attenuation frequency can be easily determined and attenuations up to 80 db can be measured.

Another application for this circuit is in the calculation of effective series resistance at resonance. The formula for this calculation is

$$R_c = \frac{R_g E_2}{2E_1}$$

Attenuation tests on high-grade commercially manufactured noninductive capacitors indicate an average series resistance value of approximately 0.02 to 0.05 ohms. Since it has been found in practice that any loss in filtering efficiency is usually the result of high contact resistance between the lead and the capacitor itself, the importance of measuring effective series resistance is apparent.

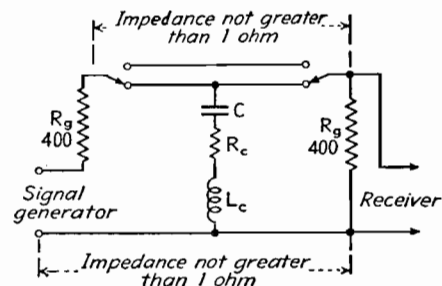


Fig. 3.—Circuit for measuring effectiveness of filter action.

# Resonance Chart for Mica Capacitors

By A. P. GREEN and C. T. McCOMB

The chart gives lead lengths and capacitance values for series resonance at any frequency from 5 to 800 Mc, for postage-stamp mica bypass capacitors with No. 20 tinned copper leads

**I**N numerous h-f electronic applications, the requirement exists that several physically separated points in a circuit be established at a common potential. To satisfy this condition most efficiently, it is necessary to operate bypass capacitors in a series-resonant condition.

The simple capacitor element is composed of an effective capacitance in series with an inductance; this inductance is composed not only of the inductance of the associated leads but also of the inherent inductance of the foil or plates of the capacitor itself. For any particular capacitor size or shape there will be associated with the capacitance an absolute minimum of effective series inductance. At low frequencies, the magnitude of the inductive component of reactance is so small that it is negligible in comparison to the capacitive component. As the frequency is increased, the capacitor element behaves as an ordinary series-resonant circuit.

For the most efficient application of a bypass capacitor to function at a given frequency or band of frequencies, the best unit will be the largest practical capacitance that will meet both the physical and resonance requirements. The physical requirement will be fixed by the space available and the necessary lead length. With the lead length factor being determined by circuit requirements, the size of capacitor for resonance is then fixed by the frequency.

An experimental determination of the resonant frequency variation as a function of lead length has been carried out using mica capacitors with leads of No. 20 tinned copper wire. The chart gives

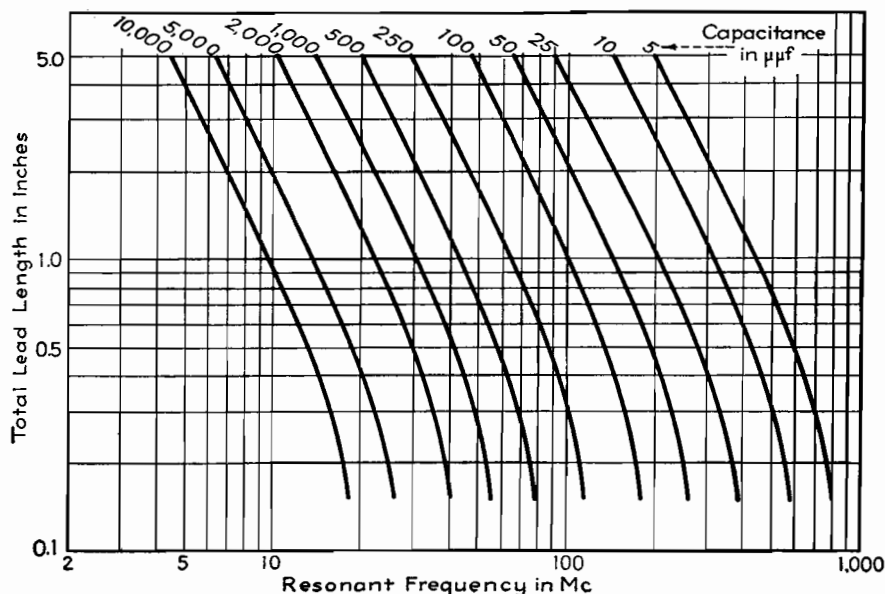
the results of measurements conducted over the practical range of lead lengths for numerous sizes of mica capacitors. The characteristic shape of the curves demonstrates the existence of the above-discussed inherent inductance of the capacitor element. Since the functional variation of resonant frequency is plotted with respect to actual lead length, the residual inductance of the unit manifests itself as an asymptotic maximum resonant frequency for any particular capacitor.

## Example of Use of Chart

A bypass capacitor is desired for 100 Mc. Reference to the chart shows that there are four capacitor sizes that exhibit a usable resonance at this point, these being represented by the four curves that

intersect the vertical 100-Mc line. The largest capacitance is most desirable as discussed above, but the choice of unit will be determined partially by the lead length requirement. It is seen from the chart that the range of available capacitances varies from 250  $\mu\text{f}$  with a total lead length of 0.31 in. to 25  $\mu\text{f}$  with a lead length of 4.0 in. Assuming that a lead length of 1.0 in. would be most desirable for the circuit, a 100- $\mu\text{f}$  capacitor would be chosen.

An examination of the chart reveals an interesting yet expected relationship. It is seen that for a constant lead length the resonant frequency varies inversely as the square root of the capacitance. Thus for a 1.0-in. lead length, 500  $\mu\text{f}$  is resonant at 43.5 Mc and 5  $\mu\text{f}$  is resonant at 435 Mc.



# Power-factor Correction Charts

By HARRY HOLUBOW

Charts for determining how much leading reactive power is needed to secure a desired amount of improvement in power factor, with practical data on the use of capacitors and auto transformers for correction purposes and on effects of harmonics

THE expression  $EI \cos \theta$  for the power taken by a-c electrical equipment may be represented in vector form as in Fig. 1a. Inasmuch as voltage  $E$  is more or less constant in any given system, the same vector diagram may be used to express power relations, as in Fig. 1b.

If the real power or the apparent power alone is known, the other may be found from the relation: real power = apparent power  $\times$  power factor. The reactive power may be found from the relation: reactive power = apparent power  $\times \sin \theta$ .

If from the right-angle triangle in Fig. 1b we designate real power as  $A$ , reactive power as  $B$ , apparent power as  $C$ , the necessary leading power for correction as  $Y$ , the new power factor as  $\cos \beta$ , and the resultant apparent power as  $X$ , as shown in Fig. 1c, the following relations hold for the calculation of improved power factor:

$$B = \sqrt{C^2 - A^2} \quad (1)$$

$$X = \sqrt{A^2 + (B - Y)^2} \quad (2)$$

$$\cos \beta = \frac{A}{X} = \frac{A}{\sqrt{A^2 + (B - Y)^2}} \quad (3)$$

The charts in Figs. 2 and 3 are based on the above equations and a unit kva of power. They may be used for any load by multiplying the value of leading kva by the value of kva involved.

## Use of Charts

Let us assume that we have a load of 5 kva, 45 per cent power factor, and it is desired to correct the load to 90 per cent power factor. A straight line, in Fig. 2,

drawn through 0.45 on the existing load power-factor scale from 0.90 on the desired load power-factor scale will intersect the capacitance in kva scale at approximately 0.675. That means that for each kva we need 0.675 kva of leading reactive power to correct to 90 per cent power factor. For 5 kva, 3.375 kva will be needed.

Drawing a straight line through 0.45 and 0.90 on the outside scales in the alignment chart in Fig. 3, we find that the kva ratio is 0.5; i.e., instead of having 5 kva before correction, the load is now only 2.5 kva.

There are, in general, two methods of correcting a poor power factor: synchronous machines and static capacitors.

## Methods of Power-factor Correction

Several types of synchronous machines are used in correcting load power factor, the most important being the so-called synchronous capacitors and synchronous motor. The synchronous capacitor is a rotating device that carries no mechanical load and draws a leading current. This device requires separate d-c excitation for the fields, and the amount of leading current may be controlled by varying the field excitation. Synchronous capacitors are available in large sizes only and are used to a great extent by the electrical utilities in their distributing substations.

The synchronous motor is similar to the synchronous capacitor in its operation, and usually requires a separate d-c excitation. It differs from a synchronous capacitor in that it is able to carry a

mechanical load, but power-factor correcting ability is comparatively small as the power factor of a synchronous motor itself is between 80 and 100 per cent leading.

The most commonly employed method of power factor correcting, especially in the case of relatively small amounts of power, is by means of static capacitors. The capacitor takes a 90-deg leading current; hence all its current is useful for correction. Capacitor losses usually being small, this method is especially economical for the small consumer. Commercial capacitors are available in capacitances ranging from 1 to 40  $\mu\text{f}$  and higher, for voltage ratings of 110, 220, 440, 660, and 2,300 volts. Parallel combinations of capacitors can be used to give almost any desired capacitance.

The reactive power of a capacitor may be expressed by the relation: reactive kva =  $E^2C/2.65 \times 10^6$ , where  $C$  is in microfarads. Where the voltage is low, capacitors have the disadvantage that the capacitance required becomes large. If the voltage is 100 volts in the example previously cited, where 3.375 kva is required, the required capacitance as given by this formula is 740  $\mu\text{f}$ . This is rather a large capacitance, and here an auto transformer can be used to advantage. If a 660-volt capacitor is connected across the high-voltage terminals of a 1:6 transformer, the capacitance value as viewed from the primary will appear as the square of the transformer ratio, or thirty-six times as large. Correction for 3.375 kva will then require only a little over 20  $\mu\text{f}$ .

Several transformer manufacturers have available as stock items power-factor correctors embodying this principle, in capacities ranging from  $\frac{1}{4}$  to  $1\frac{1}{2}$  kva. With them, power factor may be corrected right at the device, thus obtaining a saving in copper.

## Limitations in Power-factor Correcting

It is not always possible to correct a system to unity power factor. Several

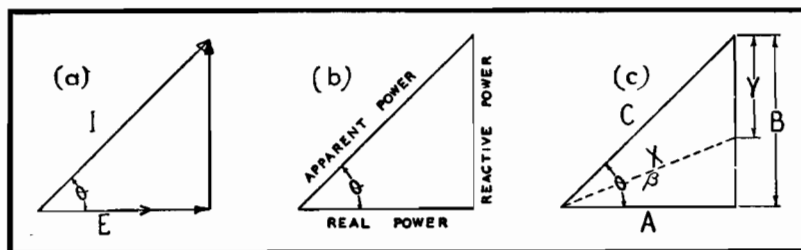


Fig. 1.—Vector diagrams representing voltage and power relations upon which the accompanying power-factor correction charts are based.

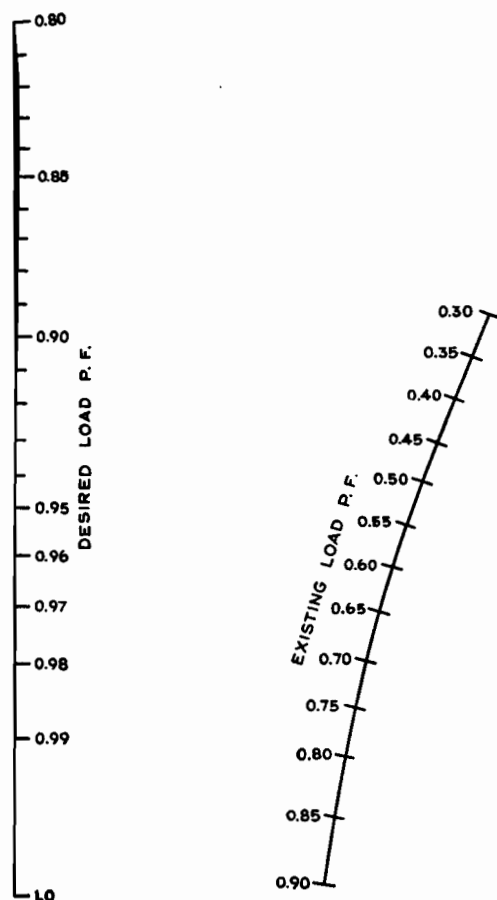


Fig. 2.—Power-factor correction chart based upon a unit kva of power. To use, draw a straight line connecting known values on left and center scales. The intersection of this line with right-hand scale gives leading kva required per unit kva.

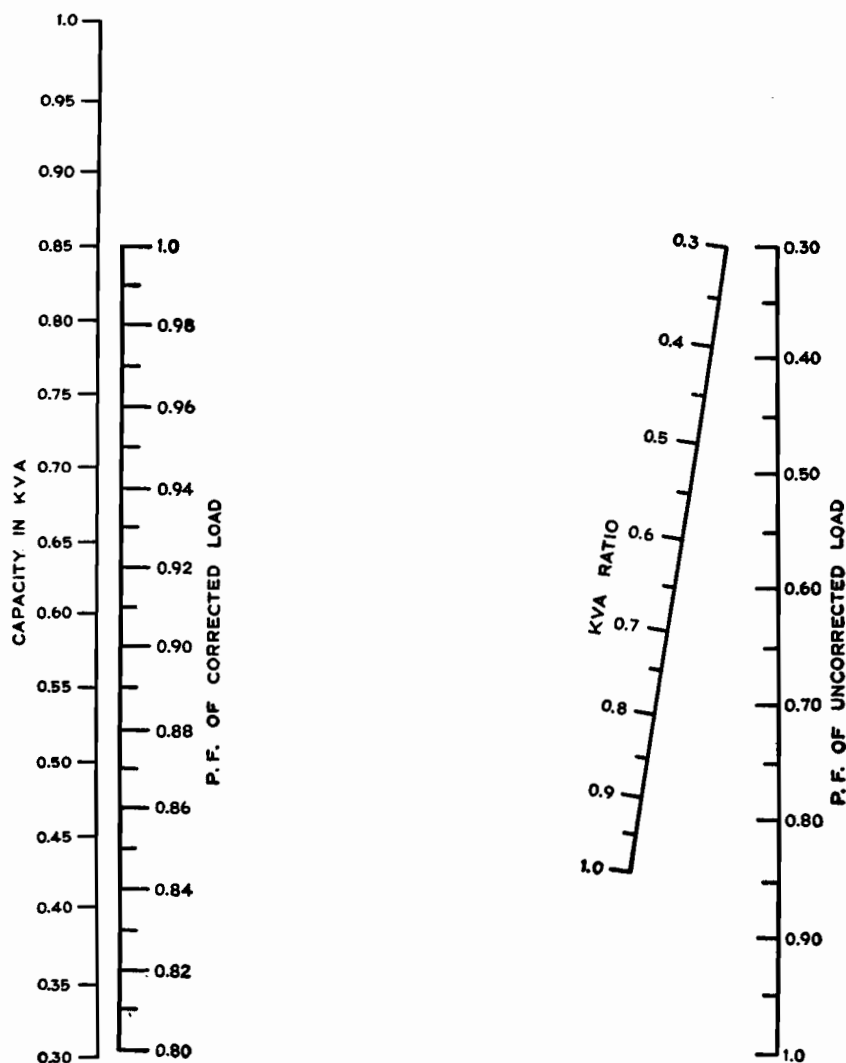


Fig. 3.—Chart giving corrected load kva per unit kva. To use, draw a straight line between known values on the two outside scales. The intersection of this line with the middle scale gives the ratio of the kva of the corrected load to that of the uncorrected load.

types of equipment, such as unloaded transformers, gaseous discharge tubes, and welding equipment, take a current that has a high percentage of harmonics. The instantaneous power in an electric circuit is the product of the voltage and current of the same angular velocity (the same frequency); hence the harmonic content of the current does not produce

any power and cannot be corrected unless by a leading current of the same frequency.

Another source of trouble is the presence of harmonics in the supply voltage when capacitors are used to correct the power factor. It is not uncommon to have the supply voltage contain as high as 15 per cent of the third harmonic, and as the

impedance of a capacitor to the third harmonic is only 33 per cent of that for the fundamental, the third harmonic current taken by the capacitor is nearly 45 per cent of the current for the fundamental component. Such conditions would produce at least about 10 per cent of uncorrectable rms current, and the best that could be hoped for is 90 per cent power.

# Temperature Compensation of Tuned Circuits

By HERBERT SHERMAN

An analysis of an uncompensated temperature error occurring in variable-frequency tank circuits employing ceramic capacitors for compensation

IN A fixed-frequency circuit, the temperature coefficient of a ceramic padding capacitor across the tank capacitor may be chosen so as to compensate for the change in capacitance of the tank capacitor or the change in inductance of the tank coil, subject to the present limitations of temperature coefficients of ceramic capacitors and the type of variation of tank capacitance and inductance with temperature.

In a variable-frequency circuit, it is well known that lumped changes in inductance or capacitance have varying effects over the frequency band covered by the circuit. For example, consider a 20- to 40-Mc capacitor-tuned circuit. Assume that a padding capacitor is added which causes a frequency change of 100 kc at 20 Mc. It can be shown that this padding capacitor will cause a change of frequency of 800 kc at 40 Mc, a ratio of 8:1, although the band coverage is 2:1.

Let  $\Delta f_1$  be the change in frequency at frequency  $f_1$ , due to the change in the lumped constants, and let  $\Delta f_2$  be the change in frequency at frequency  $f_2$ , due to the same change in the lumped constants. Then, it may be easily shown that in the following variable-frequency circuits where variable capacitance is used and

1. Lump capacitance is changed, the change in frequency is

$$\Delta f_2 = \frac{\Delta f_1 f_2^3}{f_1^3} \quad (1)$$

2. Lump inductance is changed, the change in frequency is

$$\Delta f_2 = \frac{\Delta f_1 f_2}{f_1} \quad (2)$$

Where variable inductance is used and

1. Lump inductance is changed, the change in frequency is

$$\Delta f_2 = \frac{\Delta f_1 f_2^3}{f_1^3} \quad (3)$$

2. Lump capacitance is changed, the change in frequency is

$$\Delta f_2 = \frac{\Delta f_1 f_2}{f_1} \quad (4)$$

## Inductance vs. Capacitance Compensation

Let us now consider a capacitor-tuned circuit, operating at frequency  $f_1$ , which is temperature compensated by a ceramic capacitor having a specified temperature coefficient. Assume that a temperature change causes a change in the fixed inductance of the circuit and that the ceramic capacitor temperature coefficient has been chosen so as to vary the lumped capacitance to compensate for this inductance change. At any other frequency  $f_2$ , the frequency drift due to these changes in the lumped constants is

$$\Delta f_2 = \Delta f_c - \Delta f_L \quad (5)$$

where  $\Delta f_c$  is the change in frequency at frequency  $f_2$  due to the change in lumped capacitance as defined in Eq. (1), and  $\Delta f_L$  is the change in frequency at frequency  $f_2$  due to the change in lumped inductance as defined in Eq. (2) (which

is of opposite sign to  $\Delta f_c$  since  $\Delta f_c$  was arranged to compensate for  $\Delta f_L$ ). Substituting Eqs. (1) and (2) in (5),

$$\Delta f_2 = \frac{\Delta f_1 f_2^3}{f_1^3} - \frac{\Delta f_1 f_2}{f_1} \quad (6)$$

$$\Delta f_2 = \Delta f_1 \frac{f_2}{f_1} \left( \frac{f_2^2}{f_1^2} - 1 \right) \quad (7)$$

It may be shown that the change in frequency  $\Delta f_1$  at the frequency  $f_1$ , due to a small change in lumped inductance  $\Delta L$ , is given by

$$\Delta f_1 = \frac{1}{2} \frac{\Delta L}{L} f_1 \quad (8)$$

Substituting Eq. (8) in (7),

$$\Delta f_2 = \frac{f_2}{2} \frac{\Delta L}{L} \left( \frac{f_2^2}{f_1^2} - 1 \right) \quad (9)$$

Equation (9) indicates that only at a single frequency is it possible to compensate for a change in lumped inductance with a lumped capacitance. At all other frequencies, complete compensation is not possible, and the resultant error will become more serious as the frequency of the circuit increases, or as the percentage change in lumped inductance increases, or as the frequency changes from the corrected frequency. Thus, a circuit that has been capacitance compensated at 500 kc for a 0.1 per cent change in inductance will have a frequency error of 0.15 per cent at 1,000 kc.

This discussion does not take into account the error due to the dependence of the temperature coefficient of a variable capacitor on the degree of mesh of plates.

# Determining Frequency Stability of Tuned Circuits

By G. V. ELTGROTH

Data on the performance of coils tuned by air-dielectric capacitors, during variations in air density and humidity such as are encountered when equipment is operated over a wide range of altitudes. The effect of varying carbon dioxide content, encountered in dry-ice test chambers, is also discussed

THERE are three characteristics of air as a dielectric that may affect the resonant frequency of a tuned circuit situated in this dielectric. (The effects of mechanical variation of components with varying conditions will not be considered.) They are:

1. *Density*.—The dielectric constant of air varies with pressure and, therefore, with altitude. The dielectric constant also varies with temperature, since this too affects the density of a gas.

2. *Composition*.—The relative humidity of air is constantly changing and has a decided effect on the dielectric constant at higher temperatures (above 10°C). In tests where dry ice is used, the carbon dioxide content of the surrounding medium also may rise to 60 or 70 per cent as compared with its normal value of 0.03 per cent. This will increase the dielectric constant.

3. *Saturation*.—Air almost saturated with water vapor will deposit thin films on objects situated in it. This should not be confused with condensation, which occurs when the air becomes supersaturated at the temperature of the body with which it is in contact.

We shall first develop a few simple required relations

$$\begin{aligned} C &= He \\ dC &= H de \\ \frac{dC}{C} &= \frac{de}{e} \end{aligned}$$

where  $C$  = capacitance of capacitor

$H$  = constant determined by mechanical construction

$e$  = dielectric constant of dielectric medium

Thus the per cent change in  $C$  = per cent change in  $e$ .

$$f = \frac{a}{\sqrt{C}}$$

$f$  = resonant frequency of circuit being investigated

$$\begin{aligned} df &= -\frac{1}{2} \frac{A}{\sqrt{C}} \frac{dC}{C} \\ \frac{df}{f} &= -\frac{1}{2} \frac{dC}{C} \\ A &= \frac{1}{2\pi\sqrt{L}} \end{aligned}$$

Thus the percentage change in  $f = \frac{1}{2}$  the percentage change in  $C$ , and is negative, signifying that an increase in  $C$  decreases  $f$ .

## Density

The dielectric constant of dry air for pressures below 1,000 lb per sq in. is given by  $e = 1 + 18.25P \times 10^{-6} \times \frac{292}{t}$ , where  $P$  is expressed in in. Hg and  $t$  in °K.

$$\left. \begin{aligned} \frac{\delta e}{\delta P} &= 18.25 \times 10^{-6} \times \frac{292}{t} \\ \text{Assuming } t &= 292^\circ\text{K} (19^\circ\text{C}) \\ \text{we have} \\ \frac{\delta f}{\delta P} &= -9.125 \times 10^{-6} \end{aligned} \right\} \begin{array}{l} \text{for constant} \\ \text{relative humidity and} \\ \text{temperature} \end{array}$$

The frequency will drop 9.125 cycles per Mc per in. Hg pressure increase.

Reducing the pressure from 30 in. to 10 in. Hg (equivalent to an altitude of 27,500 ft) will increase the frequency  $20 \times 9.125$  or 182.5 cycles per Mc, which is 0.01825 per cent.

Let  $P = 20$  in. Hg, and let the temperature vary over a narrow range about 292°K.

$$\begin{aligned} e &= 1 - 547.5 \times 10^{-6} \times \frac{292}{t} \\ \frac{\delta e}{\delta t} &= -\frac{547.5 \times 10^{-6} \times 292}{t^2} \\ \frac{\delta e}{\delta t} &= -1.875 \times 10^{-6}, \text{ for constant relative} \end{aligned}$$

humidity and pressure

From this it is evident that the frequency will increase 0.9375 cycles per Mc per °C rise in air temperature for dry air. This is negligible in comparison with other changes.

## Composition

*Humidity*.—If the relative humidity is held constant at various values, and the temperature of air varied, it will be found

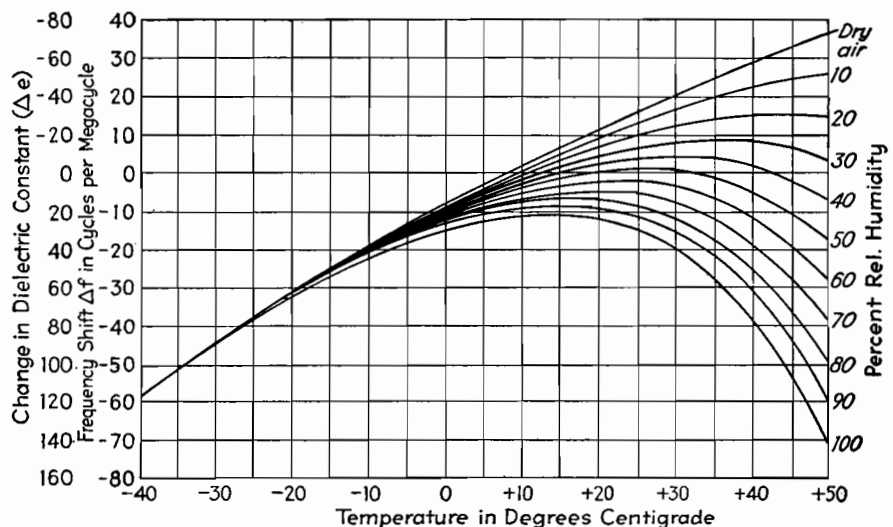


Fig. 1.—Change in frequency and dielectric constant with temperature, using various values of relative humidity as a parameter. The air reference is air at 20°C and 50 per cent relative humidity ( $e = 1.00056565$ ).

Table I.—Values of  $V$  for Air at Various Humidity and Temperature Values  
(Dielectric constant  $\epsilon = 1 + V \times 10^{-6}$ )

Temp., °C	Relative humidity											
	0%	10%	20%	30%	40%	50%	60%	70%	80%	90%	100%	$\Delta V$
-40	682	682	682	682	682	682	682	682	682	682	682	0
-30	655	655.08	655.16	655.24	655.32	655.4	655.48	655.56	655.64	655.72	655.8	0.8
-20	629	629.232	629.464	629.696	629.928	630.16	630.392	630.624	630.856	631.088	631.32	2.32
-10	605	605.56	606.12	606.68	607.24	607.81	608.37	608.93	609.49	610.05	610.61	5.61
0	583	584.27	585.54	586.81	588.08	589.35	590.62	591.89	593.16	594.43	595.7	12.7
+10	562	564.46	566.92	569.38	571.84	574.3	576.76	579.22	581.68	584.14	586.6	24.6
+20	543	547.53	552.06	556.59	561.12	565.65	570.18	574.71	579.24	583.77	588.3	45.3
+30	525	532.95	540.9	548.85	556.8	564.75	572.7	580.65	588.6	596.55	604.5	79.5
+40	508	521.4	534.8	548.2	561.6	575	588.4	601.8	615.2	628.6	642	134
+50	493	514.7	536.4	558.1	579.8	601.5	623.2	644.9	666.6	688.3	710	217
+60	478	512	546	580	614	648	682	716	750	784	818	340
+70	464	515.5	567.0	618.5	670	721.5	773	824.5	876	927.5	979	515

that the curve  $\epsilon$  vs. temperature will vary in form.

$$\epsilon_{\text{air}} = 1 + 209.66 \frac{P}{t} \times 10^{-6} \quad \left\{ \begin{array}{l} P \text{ is here expressed in} \\ \text{mm Hg, } t \text{ in deg K} \end{array} \right.$$

$$\epsilon_{\text{vapor}} = 1 + 966.83 \frac{P}{t} \times 10^{-6}$$

From these equations was derived the equation  $\epsilon = 1 + (209.66 \times 760/t + 757.174 V.P./t) \times 10^{-6}$ . Setting the portion in brackets equivalent to  $V$  gives  $\epsilon = 1 + V \times 10^{-6}$ . This relation was used in calculating the values of  $V$  in Table I for different values of temperature and relative humidity. The right-hand column labeled  $\Delta V$  contains values of the total change in  $V$  in going from 0 to 100 per cent relative humidity. Values of vapor pressure  $V.P.$  in millimeters of mercury corresponding to the indicated values of temperature and relative humidity are found in meteorological tables.

Allowance for water-film deposit on

electrodes is not included. Such deposits will add to the shift in capacitance.

A curve interpreting the data in Table I in terms of change in dielectric constant in parts per million, and resonant frequency shift in cycles per megacycle, is shown in Fig. 1.

**Carbon Dioxide Content.**—When cold tests are run with dry ice as the cooling agent, the air in the cooling chamber will have its carbon-dioxide content materially increased. The dielectric constant for carbon dioxide differs materially from that of air, the values at 19°C and 762 mm mercury pressure being 1.0005475 for air and 1.000921 for carbon dioxide.

Table II gives the variations in  $\epsilon$  and  $f$  with varying carbon dioxide content, for a constant temperature of 19°C and a pressure  $P$  of 30 in. (762 mm) of Hg.

From this table it is seen that the presence of  $\text{CO}_2$  in the air dielectric of

capacitors may produce frequency shifts up to 0.0186 per cent, a very appreciable

Table II.—Variations in  $\epsilon$  and  $f$  with Varying Carbon Dioxide Content

% $\text{CO}_2$ by vol.	$\epsilon$	$\Delta\epsilon$ (mult. by $10^{-6}$ )	$\Delta f$ , cycles per Mc
0	1.0005475	0	0
10	1.00058485	37.35	-18.68
20	1.0006222	74.7	-37.35
30	1.00065955	112.05	-56.03
40	1.0006969	149.4	-74.7
50	1.00073425	186.75	-93.38
60	1.0007716	224.1	-112.05
70	1.00080895	261.45	-130.73
80	1.0008463	298.8	-149.4
90	1.00088365	336.15	-168.08
100	1.000921	373.5	-186.25

amount in a transmitter being designed for an accuracy of 0.03 to 0.05 per cent. The figures apply to dry air, at 19°C (292°K) and 762 mm Hg. Values of  $\Delta\epsilon$  and  $\Delta f$  may be readily obtained for any other temperature or pressure by multiplying by the factor  $292P/762t$ , where  $P$  is in mm Hg and  $t$  is in °K.

A graph of the data in Table II is shown in Fig. 2. With 60 per cent carbon dioxide content, the frequency shift is over 0.01 per cent. At -40°C, when the carbon dioxide content is only 50 per cent, the frequency will be 0.0117 per cent lower than with air.

#### Saturation

Recent experimental work has shown that moisture films form on objects situated in moist air even though conditions may be such that no condensation takes place. We shall derive the effect of water-film formation on a capacitor formed by two or more parallel plane surfaces.

The capacitance of such a capacitor may be expressed as  $C = \epsilon e/S$ , where

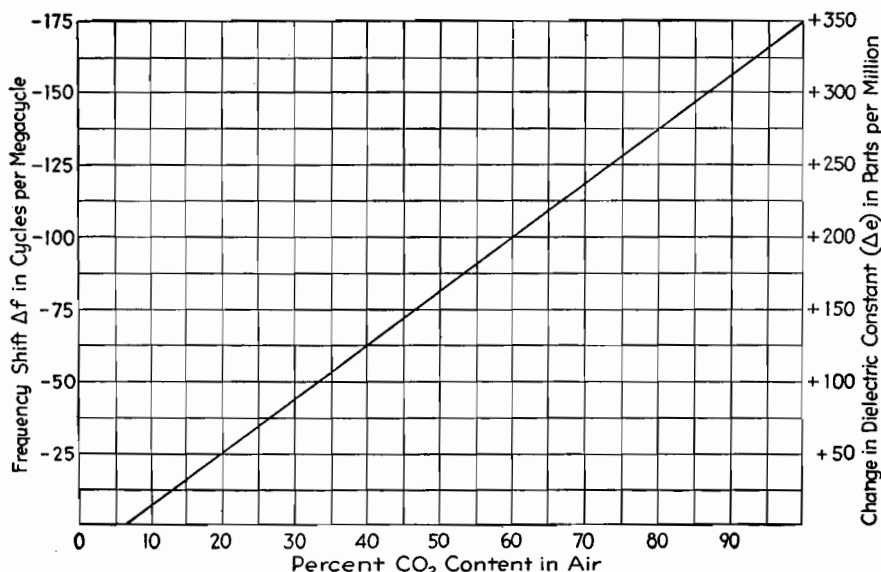


Fig. 2.—Variation of dielectric constant and frequency with volume percentage of  $\text{CO}_2$  in air. Here  $P$  is 762 mm Hg and  $t$  is 292°K (19°C).



$H$  is a constant depending on size of plates and system of units employed,  $e$  is the dielectric constant of the medium, and  $S$  is plate spacing.

Let the dielectric constant for the normal dielectric be  $e_1$ , and let that for the material in the film formed on the plates be  $e_2$ . Also, call  $C_0$  the normal capacitance,  $C'$  the capacitance with film on plates, and  $y$  the film thickness. Now, with plane plates and a uniform film thickness, the film-air interface will correspond to an equipotential surface, and

$$C_1 = \frac{He_1}{S - 2y} \quad C_2 = \frac{He_2}{2y}$$

These relations are set up by assuming a metal surface of infinitesimal thickness, at the equipotential surface of the water-air interface, and then calculating the effective capacitance on each side thereof.

The two capacitances are effectively connected in series, so we may obtain  $C'$  from the series capacitance relationship:

$$C' = \frac{C_1 C_2}{C_1 + C_2}$$

$$\text{i.e.,} \quad C' = \frac{He_1 e_2}{2y(e_1 - e_2) + e_2 S}$$

The fractional change in capacitance will then be

$$\frac{C' - C_0}{C_0} = \frac{e_2 S}{2y(e_1 - e_2) + e_2 S} - 1$$

and

$$\frac{\delta C' - C_0}{\delta y} = - \frac{2e_2 S(e_1 - e_2)}{[2y(e_1 - e_2) + e_2 S]^2}$$

We are interested in the action of thin films of foreign dielectric and will therefore confine our calculations to the region where  $y$  is less than or equal to  $0.01S$ . This permits the use of the following simplified equation:

$$\frac{\delta C' - C_0}{\delta y} = \frac{2}{S} \left( 1 - \frac{e_1}{e_2} \right)$$

On the basis of this assumption, the fractional change in capacitance is

$$\frac{C' - C_0}{C_0} = \frac{2y}{S} \left( 1 - \frac{e_1}{e_2} \right)$$

Now, for a practical application of this expression, assume a spacing between plates of  $S = 0.05$  cm (0.020 in.) and a downward frequency shift  $\Delta f$  of  $-100$  cycles per Mc, which corresponds to  $200 \times 10^{-6}$  for  $\Delta C'$ . The normal dielectric is air ( $e_1 = 1$ ) and the foreign dielectric is water ( $e_2 = 81$ ). Let us find the required film thickness for the given frequency shift.

Solving the foregoing equation for  $y$ , substituting in it the known values, and simplifying give a value of  $5.06 \times 10^{-6}$  cm for the film thickness  $y$ .

Thus, a film thickness of  $5.06 \times 10^{-6}$  cm, or 0.00001285 in., produces a frequency shift downward of 0.01 per cent. This is a film approximately 120 molecules in depth, and is quite undetectable by ordinary methods since its thickness is only about one-tenth the wavelength of green light. It is obvious at once that the formation of actual visible condensation on the plates of a tuning capacitor will result in shifts very many times this in magnitude.

For a given film thickness, the frequency shift is inversely proportional to the spacing of the plates.

Experiments have shown that on a clean polished metal surface, films up to 30 or 40 molecules thick may be formed at 98 per cent relative humidity with a temperature around  $30^\circ\text{C}$ . On a good dielectric material, the films formed under the same conditions were up to 180 molecules in depth. Since oils and greases are dielectrics, capacitor plates should be kept scrupulously free of them.

In view of the fact that moisture films have such large effects when compared with their dimensions, it is interesting to note here that if by some means the interior of a device being tested were maintained  $5^\circ\text{C}$  above the external temperature, then the interior relative humidity could not exceed 80 per cent even though the external temperature might range up to  $60^\circ\text{C}$  at 100 per cent relative humidity.

## Conclusions

Listed below are the effects on resonant frequency of each of the variables which are due to dielectric changes only.

1. *Pressure*.—For air at  $19^\circ\text{C}$  the coefficient is  $-9.125$  cycles per Mc per in. Hg, or 0.01825 per cent change in frequency for altitude change from sea level to 27,500 ft.

2. *Temperature*.—For air at  $19^\circ\text{C}$ , 30 in. Hg., the coefficient is  $+0.9375$  cycles per Mc per  $^\circ\text{C}$ . (This is negligible and need not be considered in design.)

3. *Relative Humidity*.—We give below the total frequency shift in cycles per megacycles, as air at the specified temperature and 760 mm Hg pressure is varied from 0 to 100 per cent relative humidity.

$^\circ\text{C}$ .	Cycles per Mc
-40.....	-0
-30.....	-0.4
-20.....	-1.16
-10.....	-2.8
0.....	-6.35
+10.....	-12.3
+20.....	-22.65
+30.....	-39.75
+40.....	-67.00
+50.....	-108.5
+60.....	-170.00
+70.....	-257.5

4. *Carbon Dioxide*.—Mixed with air at  $19^\circ\text{C}$  and 30 in. Hg pressure, the coefficient is  $-1.868$  cycles per Mc per per cent of carbon dioxide. Also 53.5 per cent of carbon dioxide is required to shift the frequency downward 0.01 per cent. This effect becomes greater at lower temperatures.

5. *Moisture Film Deposits*.—Deposits at 98 per cent relative humidity and  $30^\circ\text{C}$  on perfectly clean capacitor plates (0.020-in. spacing) are sufficient to lower the frequency 0.0025 per cent. The presence of oil or grease films may increase this to 0.015 per cent.

6. Wherever wax is used for sealing against moisture, wax-air interfaces must be kept out of strong electric fields.

## SECTION VI

# CATHODE-RAY TUBES

	Page
Characteristics of Phosphors for Cathode-ray Tubes.....	92
Photographing Patterns on Cathode-ray Tubes.....	93

## Characteristics of Phosphors for Cathode-ray Tubes

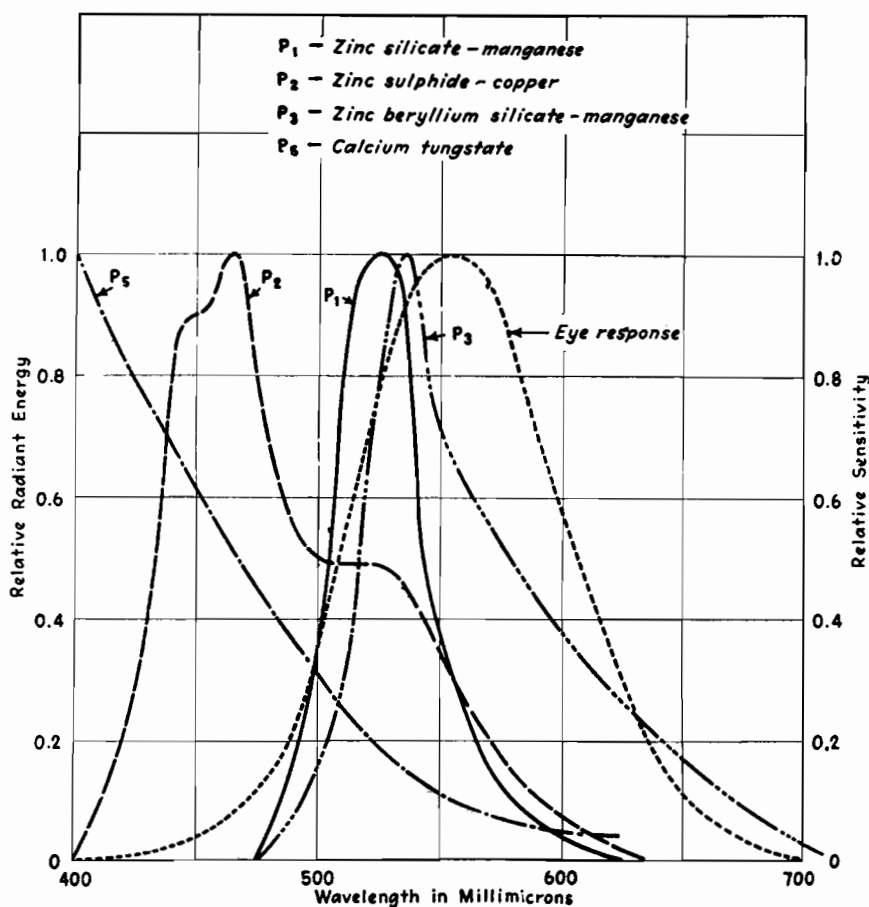
By L. B. HEADRICK

Characteristics of screen materials commonly used in cathode-ray tubes summarized in convenient form. Spectral curves given for the most commonly used screen materials

THE table and the set of curves summarize the more important characteristics of phosphors used as screen materials

in cathode-ray tubes for oscillography and television. All the data apply to

bombardment of the fluorescent screen by means of an electron beam.



Spectral distribution of relative energy for various phosphors (left ordinates) and sensitivity response of the human eye (right ordinates).

**Data on Phosphors in General Use, Subjected to  
Electron Bombardment in Cathode-ray Tubes**

Material	Formula	Color	Spectral maximum, Å	Efficiency cp/watt 1-6 kv 1 $\mu$ a/sq cm	Persistence time in seconds for the light to fall to the following fractions of its initial value			Principal uses
					10%	1%	0.1%	
Zinc sulphide.....	ZnS	Light blue	4700	1-3	.....	*10 <sup>-3</sup>	.....	Television
Zinc sulphide-silver.....	ZnS-Ag	Blue violet	4500-4700	1-3	.....	*10 <sup>-3</sup>	.....	Television
Zinc sulphide-copper.....	ZnS-Cu	Blue green	4700-5250	0.5-5	10 <sup>-3</sup>	5 × 10 <sup>-2</sup>	5 × 10 <sup>-1</sup>	Oscilloscope
Zinc cadmium sulphide-silver.....	ZnS,CdS-Ag	Blue to red	4600-7500	1-5	.....	*10 <sup>-3</sup>	.....	Television
Zinc-silicate-manganese.....	ZnO + SiO <sub>2</sub> -Mn	Green	5230	1-3	2 × 10 <sup>-2</sup>	5 × 10 <sup>-2</sup>	10 <sup>-1</sup>	Television, Oscilloscope
Zinc beryllium silicate-manganese.....	ZnO + BeO + SiO <sub>2</sub> -Mn	Green to orange	5250-6000	0.5-3	2 × 10 <sup>-2</sup>	5 × 10 <sup>-2</sup>	10 <sup>-1</sup>	Indicator and Illumination
Magnesium tungstate.....	MgWO <sub>4</sub>	Light blue	4800	Less than 1	.....	*10 <sup>-5</sup>	.....	Illumination
Calcium tungstate.....	CaWO <sub>4</sub>	Violet	4100	Less than 1	.....	*10 <sup>-5</sup>	.....	Oscilloscope
Cadmium tungstate.....	CdWO <sub>4</sub>	Blue white	4900	Less than 1	.....	*10 <sup>-5</sup>	.....	Television

\* Rough approximate values of persistence.

# Photographing Patterns on Cathode-ray Tubes

By RUDOLPH FELDT

Comprehensive investigation of the photography of transient traces on common types of cathode-ray tubes indicates that writing speeds up to 1,000 km per sec can be recorded. Procedures for obtaining maximum writing speed are outlined, with alignment charts to simplify calculation and data on the photographic efficiency of various films

IT is the purpose here to give data on maximum writing speeds which can be recorded photographically with commercial tubes operated at low and medium accelerating potentials. These data are based on the light output of the fluorescent screen, which, in combination with the color of the screen radiation, determines the photographic efficiency of a cathode-ray tube.

Photographic density (logarithm of opacity) and exposure (product of light intensity and time) are not related in a linear manner, but by the Hurter and Driffield or  $D \log E$  curve in which the density, plotted against the logarithm of the exposure, results in an S-shaped curve. Any satisfactory method of comparing films must employ a method that permits comparison over the entire range of their sensitivity response or  $D \log E$  curve. This evaluation may be accomplished quite simply and accurately by the use of calibrated gray scales, which was the method used in this investigation.

## Comparison of Films

Certain emulsions behave in a very different manner at low and high densities.

Therefore, the values obtained at both ends of the scales are of interest and are presented in Table I. The density of the film base and the residual fog are

**Table I.—Comparison of Relative Film Speeds at High and Low Densities for Various Emulsions and Fluorescent Screens**

Film	Relative exposure required					
	P1 medium-persistence green; $B = 7.5$ ft-L		P2 long-persistence green; $B = 1.55$ ft-L		P5 short-persistence blue; $B = 0.9$ ft-L	
	Low density	High density	Low density	High density	Low density	High density
Agfa Triple S Ortho.....	1.0	1.0	1.0	1.0	1.25	1.6
Eastman Ortho X.....	3.2	1.25	1.6	1.6	2.0	2.5
Eastman Superpan Press.....	5.0	1.25	1.6	1.6	3.2	3.2
Defender Ortho X-F.....	3.2	2.0	1.6	1.6	1.6	2.0
Eastman Super XX.....	3.2	2.0	2.0	1.6	4.0	4.0
Defender X-F Pan.....	4.0	2.0	2.0	2.0	4.0	4.0
Agfa Triple S Pan.....	4.0	2.5	2.0	2.0	4.0	4.0
Agfa Fluorapid Blue.....	40	.....	5.0	4.0	1.0	1.0
Eastman X-ray Blue.....	64	.....	5.0	5.0	2.0	1.6

eliminated by this method, and only densities above fog are compared.

Table I shows the relative film speeds of nine different film emulsions when exposed by the three most common types of screens employed in cathode-ray oscillography: P1 medium-persistence green, P2 long-persistence green, and P5 short-persistence blue. The films with a relative speed of 1.0 have the greatest sensitivity and serve as a reference basis. The figures shown, with relation to other film types, are the factors by which the exposure must be increased to produce the same density on the negative as was produced on the emulsion used as the basis of reference. Agfa Triple S Ortho film gives excellent results for all screen colors, while Agfa Fluorapid Blue gives slightly better results for the P5 screen.

### Effect of Intensifier Electrode

Table III indicates the extent to which the visual brightness and photographic efficiency can be increased by means of an additional electrode intensifier located between the deflecting plates and the screen. It is held at a positive potential with respect to the second anode so as to impart additional kinetic energy to the electron beam after deflection. Tube types such as the 5CP1 and 5LP1 are constructed with this additional electrode. It can be seen that the increase of efficiency corresponds to the increase of visual brightness.

To summarize the results of the initial investigation the following conclusions may be made:

1. Agfa Triple S Ortho Film is desirable for recording the radiation from P1, P2,

graphic efficiency five-fold, compared with results obtained without an intensifier.

The maximum photographic writing speed is the maximum speed of the luminescent spot that produces a recording of density 0.1 above fog at an object-image ratio of 1:1 with a lens aperture of  $F/1$  on an unspecified high-sensitivity emulsion developed with high-contrast developer.

The relation between illumination intensity on the photographic film,  $I'$ , the light radiation of the object,  $I$ , the transmission of the lens system  $T$ , the object-image ratio  $M$ , and the lens aperture  $F$  can be expressed by the formula

$$I' = \frac{IT}{4F^2(1+M)^2} \quad (1)$$

The artifice of recording oscillograms reduced in size permits securing higher writing speeds. If  $V_1$  is the writing speed at the screen, recorded for an object-image ratio  $M = 1$  and  $V$  is the writing speed on the screen at any reduction ratio  $M$ , it follows that

$$\frac{V}{V_1} = \frac{4}{(1+M)^2} \quad (2)$$

This equation shows that photographic writing speed cannot be increased by more than a factor of 4 even with extreme reduction in size. The values appearing in this discussion for maximum writing speeds always refer to  $M = 1$  and  $F = 1$ .

The manufacture of sensitive photographic emulsions is far from stabilized, and no standard emulsion has been established.

The data concerning the photographic writing rates of cathode-ray tubes should be presented in such a manner that it becomes possible to determine immediately whether a given photographic problem in cathode-ray tube oscillography can be solved through the use of a given tube operated in accordance with given electrical conditions. The writing speed is determined by the brightness and color of the screen, which in turn are determined by the screen material, its thickness, and the amount of power dissipated per unit area of the screen. Table IV gives a tabulation of dynamic ratings for films.

Film-development time and temperature must be carefully checked and maintained constant. Fresh developer must be used for each development. By means of these precautions (and others not described), it is possible to develop each negative in a large series of films under practically identical conditions.

**Table II.—Photographic Light-producing Efficiency of Common Screens (Assuming P5 Screen Is Unity)**

Type of fluorescent screen	P1 medium-persistence green	P2 long-persistence green	P5 short-persistence blue
Visual brightness (ft lamberts).....	7.5	1.55	0.9
Relative brightness.....	8.3	1.7	1.0
Relative film speed (from recorded density scales).....	0.63	0.25	1.0
Test film.....	Agfa Triple S Ortho	Agfa Triple S Ortho	Agfa Fluorapid Blue
Photographic efficiency $K$ .....	0.076	0.15	1.0
$1/K$ (ft-L for equal photographic effect).....	13.2	6.7	1.0

Table II presents a summary of the photographic efficiency of the three screens, under conditions usually found in commercial equipment (Du Mont Type 175-A). The tubes were operated at medium voltages and brightness. The photographic efficiency  $K$  is obtained by dividing relative film speed by relative brightness. Note that for the P1 screen more than 13 ft-L are required to secure the same photographic effect as is produced by 1 ft-L using the P5 screen.

**Table III.—Ratio of Increase of Photographic Efficiency and Visual Brightness through Use of Intensifier**

Screen	Photog. eff. ratio	Visual brightness ratio
P1 Medium-persistence green.....	5:1	4.7:1
P2 Long-persistence green.....	6.3:1	7:1
P5 Short-persistence blue.....	5:1	4.5:1

and P5 screens, while Fluorapid Blue gives slightly better results with the P5 screen. For high-speed recording, Triple S Ortho is somewhat superior to Fluorapid Blue.

2. Using the film most suitable for each fluorescent screen, the P1 screen requires more than thirteen times the visual brightness (as measured with the illumination meter) of the P5 screen to produce equivalent photographic effects on the negative.

3. Blue-sensitive emulsions such as Fluorapid Blue and X-ray Blue are not desirable for recording radiation from a P1 screen.

4. Comparisons were made using a single standard condition for development. However, once the most suitable emulsion has been selected (from Table I) it is possible to improve results by employing film-development procedures that make possible the attainment of maximum speed for the emulsion selected.

5. Proper use of the intensifier electrode increases visual brightness and photo-

**Table IV.—Film Sensitivity Rating under Dynamic Conditions**

Light source: P5 tube on 175-A with intensifier. Maximum brightness  $B = 0.9$  ft-L (same conditions as for Table I) Development: D76, 10 min. Signal amplitude:  $\pm 1$  cm constant

Emulsion	Photographic density		
	$f = 1$ kc, $F = 4.5$	$f = 10$ kc, $F = 1.5$	$f = 100$ kc, $F = 1.5$
Agfa Fluorapid Blue.....	0.36	0.34	0.02
Agfa TSO.....	0.36	0.37	0.04
Agfa SPP.....	0.30	0.30	*
Agfa TSP.....	0.23	0.25	*
Eastman Ortho.....	0.21		
Eastman Ortho X.....		0.23	*
Eastman SPP.....	0.20	0.22	*
Eastman Super XX.....	0.18		*
Defender KF Panchro.....	0.06		
Eastman SXX.....		0.21	
Defender XF Ortho.....		0.14	

\* Too weak to be measured accurately.

It can be seen that a frequency of 100 kc appears to be the recording limit at low voltages. The best results are obtained with Triple S Ortho film. The density can be further increased by using a more active developer, but the fog increases simultaneously with increase of density, and a compromise must be made.

A satisfactory compromise can be made by developing films for 8 min at 65°F in formula D72, other conditions remaining the same. A density  $D = 0.07$  was obtained for Triple S Ortho at  $f = 100$  kc, which compares with the value of  $D = 0.04$  obtained with the former development method under the same development conditions. Fluorapid Blue produces a very high fog and must be eliminated.

Agfa Triple S Ortho seems to be the most sensitive emulsion for all the screen materials investigated, so long as low exposures are considered, resulting in a record density less than 0.3 regardless of the duration of the exposure. Table V

shows the recorded density for different exposures.

Table V indicates that when the exposure (i.e., the product of light intensity and time) is sufficiently high, Super Pan Press gives higher recorded density and should be substituted for Triple S Ortho. It is shown that this holds true for a range from 1 kc to 1 Mc and probably beyond. It can be seen how the same pattern, recorded by lenses of different aperture, can produce results that are in favor of one or the other of both films, according to the total amount of exposure. The importance of using high-speed lenses is emphasized.

The graph of Fig. 1 has been used to determine the maximum writing speed  $V_{max}$  corresponding to density of 0.1 above fog. The values of  $V_{max}$  are referred to a lens aperture of  $F = 1$  and to an object-image ratio  $M = 1$  according to the definitions outlined. The values at highest brightness (9.7 kv) have been obtained with beam modulation.

**Table V.—Density Recorded for Different Conditions of Exposure**

Screen	Freq.	Lens aperture	Film	Recorded density	Total acceleration pot., kv
P5.....	1 kc	1.5	TSO	0.60	2.7
			SPP	0.75	
P5.....	1 kc	16	TSO	0.12	2.7
			SPP	0.06	
P5.....	100 kc	1.5	TSO	0.06	2.7
			SPP	0.03	
Experimental.....	100 kc	1.5	TSO	0.60	9.7
			SPP	0.75	
Experimental.....	1 Mc	1.5	TSO	0.26	9.7
			SPP	0.16	

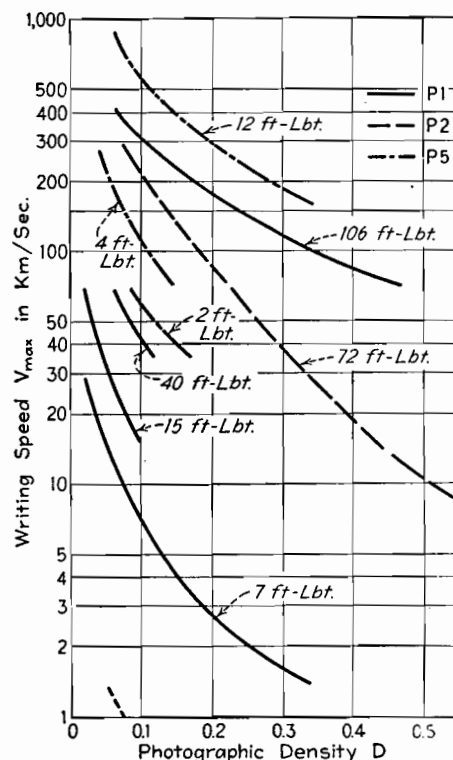


Fig. 1.—Graph of writing speed plotted against photographic density for various screens and various screen brightness values in foot-lamberts.

#### Maximum Writing Speed

In Fig. 2 the maximum writing speed  $V_{max}$  is given as a function of brightness for different screen materials. The lowest values at which the curves start are measured with 2.7 kv accelerating potential and maximum brightness, while the highest values are obtained at nearly

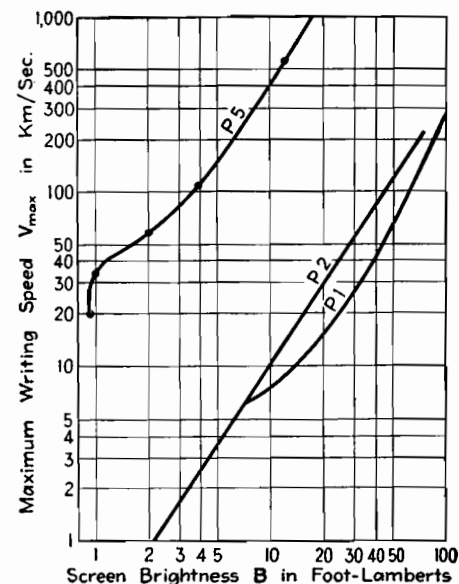


Fig. 2.—Maximum photographic writing speed, plotted as a function of brightness of fluorescent screen for three common types of cathode-ray tube screens.

10 kv total accelerating potential and with beam modulation.

It is interesting to note that at low voltages the values of the maximum writing speeds are widely different for the various screens, the minimum being 0.7 and the maximum 20 km per sec, which represents a ratio of about 1:29. At high voltages all the screen materials investigated produced high recording speeds with only slight variations. The maximum speed was 560 and the minimum 210 km per sec, giving a ratio of 1:2.7.

This result obtained for different screens is also valid for individual tubes of the same type. While at low voltages the efficiency of a tube depends to a high degree on the quality of the electron gun, at high accelerating voltages only the total accelerating potential appears important, and a number of tubes of the same type show nearly the same results.

The increase of efficiency with accelerating voltage is shown in Table VI where brightness increase (and corresponding increase of writing speed) is given for the various screens. The figures of the table are based on data plotted in Fig. 2. Table VI shows that, at low voltages,

**Table VI.—Brightness and Writing Speed Increase from Medium to High Accelerating Potentials (2.7-9.7 kv)**

Screen	Brightness increase	Increase in writing speed
P1.....	14.2	43
P2.....	46.5	300
P5.....	13.4	26.5

screens with a high photographic efficiency (such as the P5) display relatively little increase in photographic effectiveness as the accelerating voltage is increased. On the other hand, the photographic effectiveness of the P2 screen, which has a very low over-all efficiency at low voltages, increases rapidly and becomes excellent at high accelerating potentials. The fact that the photographic efficiency increases so much more than the visual brightness can be explained only by a considerable change in color at higher voltages—the light becomes richer in blue actinic radiation.

With this information available and considering the tubes selected as representing each type, the following conclusions are apparent:

1. The P5 screen produces the highest photographic writing speed.
2. P2 screens should not be employed

at low voltages, but give very satisfactory results at high voltages.

Ratings of photographic efficiency of various screens at medium and high voltages, referred to voltage on the tube using a P5 as reference, are given in Table VII.

**Table VII.—Photographic Efficiency Rating**

Medium voltage (2.7 kv)		High voltage (9.7 kv)	
Screen	Relative photog. eff.	Screen	Relative photog. eff.
P5	1.0	P5	1.0
P1	0.35	P1	0.53
P2	0.035	P2	0.38

#### Practical Applications

When the brightness of the tube that is to be used for photographic recordings is measured by means of a standard 2-in. raster and an illumination meter equipped with Viscor filter, the corresponding

maximum photographic writing speed  $V_{\max}$  can be found on the graph of Fig. 2. Most cathode-ray tube manufacturers are in a position to provide information concerning the minimum screen brightness for any standard type of tube in cases where the user does not have access to a suitable illumination meter. Certain manufacturers have expressed willingness to provide more accurate brightness data on any single tube that is to be used for photographic recording applications. Such brightness values will change throughout the life of the tube.

Once the maximum brightness for a tube is known, this data serves as a standard of calibration with which an ordinary exposure meter with photocell may be used to adjust the brightness level to a value desired for any particular application.

For all practical purposes it is advisable to divide the maximum writing speed  $V_{\max}$  by 2 to provide a sufficient margin of safety and to obtain recordings of higher density than 0.1. The values of the

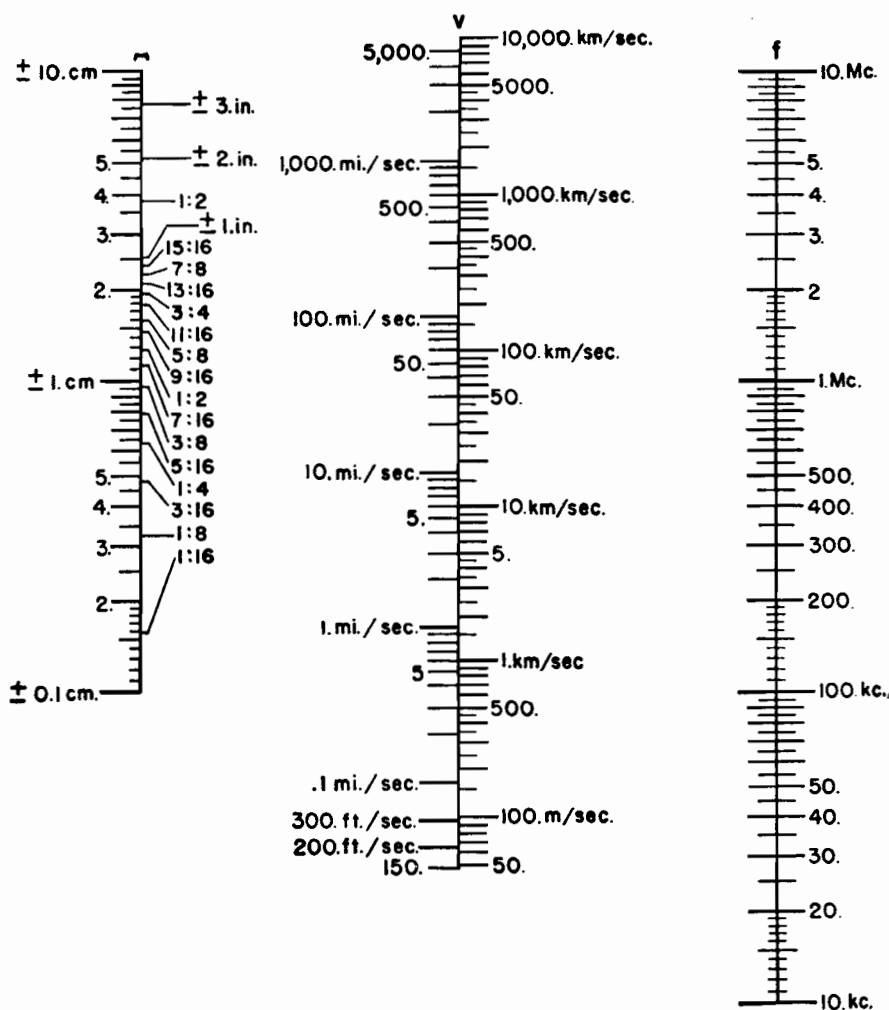


**Fig. 3.—Alignment chart relating amplitude, frequency, and maximum writing speed for sinusoidal traces.**

graph of Fig. 2 are valid for a lens with an aperture of  $F = 1$ , an object-image ratio of 1:1, and for Agfa Triple S Ortho Film with development formula Eastman D72, 8 min. at 65°F.

Figures 3 and 4 are nomographs designed to facilitate solving practical problems. Figure 3 demonstrates the relation between amplitude, frequency, and maximum writing speed for sine waves; Fig. 4 gives the photographic writing speed  $V$  as a function of  $V_{\max}$ , lens aperture  $F$ , and object-image ratio  $M$ .

#### Nomographs

Suppose it is desired to record a sine-wave transient having a peak-to-peak amplitude of approximately 6 cm ( $A = \pm 3$  cm) and a frequency  $f$  of 5 kc. The tube may have a P5 screen with a raster brightness of 2 ft-L. From Fig. 1,  $V_{\max}$  is determined to be 60 km per sec for  $D_1 = 0.1$ . Half of this is taken for safety purposes as explained above, so  $V = 30$  km per sec.

The speed of the phenomenon that is to be recorded can be found from Fig. 3 by considering a frequency of 50 kc and dividing the result by 10 to give the required frequency of 5 kc. A value of approximately 1 km per sec is obtained for  $V'$ .

By means of the nomograph in Fig. 4, we find that recording this speed at  $V_{\max} = 30$  km per sec permits the use of an aperture of  $F = 5.6$  for  $M = 1$ . If a different ratio of object on screen to image on film is desired, perhaps  $M = 10:1$ , a line drawn from this value to 1 km per sec on the  $V'$  scale crosses the  $V$  scale at 3.3 km per sec. Use of  $M = 10:1$  permits the recording of speeds 3.3 times higher than with  $M = 1$ . To confirm this, locate 3.3 km per sec on the  $V'$  scale and draw a line to the previous determined aperture  $F = 5.6$ . The cross point on the  $V_{\max}$  scale establishes the corresponding increase in  $V_{\max}$  to 102 km per sec. Since the recorded speed is only 1 km per sec, a line can be drawn from 102 km per sec on the  $V_{\max}$  scale through  $V' = 1$  km per sec, which shows an aperture between  $F = 9$  and  $F = 11$ . Consequently, the phenomenon can be recorded with an aperture  $F = 5.6$  for  $M = 1$ , with  $F = 10$  for  $M = 10:1$ , or with any intermediate values.

Assume a rectangular wave is to be recorded with a maximum rise of 5 cm per  $\mu$ sec. The maximum speed to be recorded is therefore  $5 \times 10^6$  cm per sec, or 50 km per sec.

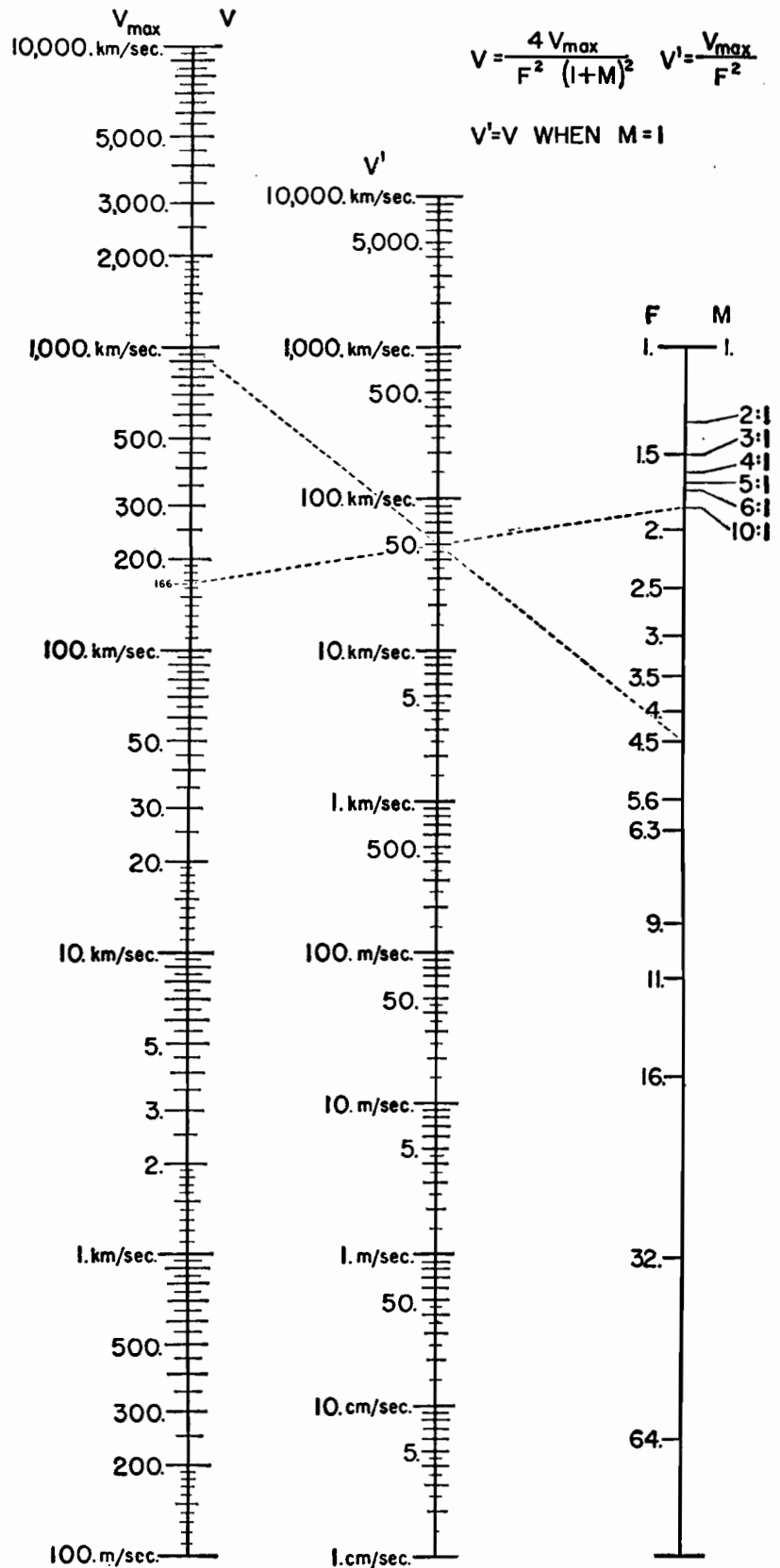


Fig. 4.—Alignment chart for determining writing speed in terms of lens aperture  $F$ , object-image ratio  $M$ , and maximum writing speed  $V_{\max}$ .



### Recording of Transient Rectangular Wave

The available lens has a maximum aperture of  $F = 1.9$ . The nomograph of Fig. 4 shows that  $V_{\max} = 180$  km per sec. Figure 2 indicates that a P5 screen with  $B = 5.6$  ft-L would be satisfactory. Assuming that in this case only 4 ft-L are available from the cathode-ray tube under the given operating conditions, it would probably be advisable to increase the exposure by raising the object-image ratio. For  $M = 8:1$  the apparent writing speed is increased threefold and a recording of satisfactory density would be secured.

### Recording of Recurrent Phenomena

As another example of the use of data here, assume the exposure time for the recording of recurrent phenomena is to be determined.

Let us assume that an amplitude of  $\pm 2$  cm and a sine wave of 1,000 cycles, with a sweep frequency of 100 cycles, appears on a P1 screen yielding a brightness,  $B$  of 7.5 ft-L. If  $n$  is the number of images per second appearing on the screen,  $t$  is the exposure time, and  $V$  is the maximum writing speed of the phenomenon which has to be recorded, then  $V = tnV_{\max}$  or  $t = V/(nV_{\max})$ . Referred to a lens with aperture  $F$ ,  $t = VF^2/(nV_{\max})$ .

In this case  $n = 100$ , and  $V = 2\pi \times 10^3 \times 2 = 12.6 \times 10^3$  cm per sec. From the graph of Fig. 2,  $V_{\max} = 6 \times 10^5$  cm per sec, and it can then be calculated that  $t = 2.1 \times 10^{-4} F^2$  sec. If an aperture of  $F = 7$  is employed,  $t = 1/100$  sec.

### Conclusions

As a result of a comprehensive survey of the technique of producing photographic records at maximum writing

speed, we may draw the following conclusions:

1. For high-speed recording, Agfa Triple S Ortho film gives the best results of the films tested for P1, P2, and P5 screens. Recommended development procedure: develop 8 min at 65°F in D72.

2. The P5 screen has the highest photographic efficiency.

3. The maximum photographic writing speed plotted against tube brightness gives an accurate means for determining the exposure time. With standard tubes and high accelerating potentials, phenomena of more than 1,000 km per sec have been recorded.

4. At high accelerating voltages (9.7 kv) all the screens previously mentioned became very efficient for photographic recordings, and the differences, which are quite important at low voltages, become relatively small. At high voltages the brightness differences between individual tubes of the same type seem to diminish.

5. Type P2 screens, which give very poor results at low voltages, show a tremendous increase in efficiency at high voltages, and it is desirable to employ this screen at high voltages.

6. It has been shown that by using synchronized high-speed shutters ( $1/100$  sec) undesirable fogging of the film by background light of the screen can be minimized up to accelerating potentials of about 6 kv. Beam modulation eliminates the necessity for synchronizing the shutter and permits the use of high accelerating potentials and strong beam currents, without danger of screen burning.

### Bibliography

(1) ARDENNE, M. V., "Cathode-ray Tubes," English edition, pp. 294-346 (German ed. pp. 215-250).

(2) PARR, G., "The Cathode-ray Tube and Its Applications," 2d ed., Appendix, pp. 157-160.

(3) RIDER, J., "The Cathode-ray Tube at Work," pp. 316-317.

(4) HENNEY, K., and DUDLEY, B., "Handbook of Photography," McGraw-Hill Book Company, Inc., New York.

(5) MEES, "The Theory of the Photographic Process."

(6) Choosing Film for Your Camera, *Film Catalog*, Edited by Agfa Ansco, 1941.

(7) CRAWFORD, J. D., Photography of Transients with Cathode-ray Oscillograph, *General Radio Experimenter*, May, 1934.

(8) LAMSON, H. W., A New Moving Film Camera, *General Radio Experimenter*, November and December, 1934.

(9) BORRIES, V. and KNOLL, The Blackening of Photographic Emulsions by Electrons and Electron-excited Fluorescence, *Z. Physik*, 35, 1934.

(10) Exposure Meter for Cathode-ray Oscillographs, *RCA Application Note* 70, Feb. 17, 1934.

(11) MCGILWIE, D. L., The Use of the High-vacuum Cathode-ray Tube for Recording High-speed Transient Phenomena, *Jour. IEE*, November, 1938.

(12) KAISER, H., Theory of the Photographic Recording, *Z. Physik*, No. 10, 1938.

(13) BIGALKE, A., A Post-acceleration Oscillograph, *Z. Physik*, No. 6, 1938.

(14) BLOK, L., An Apparatus for the Measurement of the Scanning Speed of Cathode-ray Tubes, *Philips Tech. Rev.*, July, 1938.

(15) ROGERS, T. A., and ROBERTSON, B. L., Cathode-ray Tube Photography, *Electronics*, July, 1939.

(16) CUSTERS, J. F. H., The Recording of Rapidly Occurring Electric Phenomena with Aid of the Cathode-ray Tube and the Camera, *Philips Tech. Rev.*, May, 1939.

(17) BIGALKE, A., Four-beam Cathode-ray Tube of High Recording Speed, *Arch. Elektrotech.*, No. 2, 1939.

(18) ROGOWSKI, W., and THIELSEN, H., Post-Acceleration in Cathode-ray Tubes, *Arch. Elektrotech.*, 1939, No. 6.

(19) KATZ and WESTENDORF, Obtaining High Recording Rates by Means of an Electro-static Cathode-ray Tube of Constant-vacuum, *Z. Physik*, No. 7, 1939.

(20) BIGALKE, A., Electron-ray Oscillograph, Part I, *Arch. tech. Messen*, J834-27, August, 1939.

(21) BORRIES, V., and RUSKA, E., Proposal for the Standardization and the Objective Comparison of the Measuring Efficiency of Cathode-ray Oscillographs, *Arch. Elektrotech.*, No. 3, 1940.

(22) ANGELINI, A. M., Voltage Dividers and Delay Cables for the Oscillographic Recording of Rapid Transit Phenomena, *Bull. assoc. suisse des electriciens*, July 18, 1941.

(23) BAXTER, H. W., A Concise Report on a High-speed Camera for Simultaneous Photographic Records, *Jo. Sci. Instruments*, pp. 183-184, 1942.

(24) FOLKERTS, H. F., and RICHARDS, P. A., Photography of Cathode-ray Tube Traces, *RCA Rev.*, October, 1941.

(25) ROBERTS, H. C., An Auxiliary Circuit for Cathode-ray Photography, *Electronics*, September, 1942.

## SECTION VII

# COAXIAL LINES

	Page
Design of Terminations for Concentric Lines.....	99
Q-factor Charts for Unloaded Concentric Transmission Lines.....	103
Impedance Determinations of Eccentric Lines.....	105
Graph of Impedance of Eccentric-conductor Cable.....	106
Measurement of H-f Lines.....	107

# Design of Terminations for Concentric Lines

By CARL G. DIETSCH

A presentation of both theory and practice of coupling low-impedance concentric transmission lines to antennas of various characteristics for maximum efficiency

THE use of transmission lines, especially those of the concentric tube or coaxial type, affords a convenient and efficient means for conveying r-f power. An important element to be considered in the design of such a line, whether it is to convey the power output of a transmitter to its antenna or from one stage to another of any r-f system, is the line termination of the circuit. Best results, insofar as reliability and efficiency are concerned, are secured when the termination circuit presents to the output end of the line an impedance equivalent to the characteristic impedance of the line. This impedance, being for all practical purposes equal to  $\sqrt{L/C}$ , resembles a real quantity in the form of an effective resistance equal to  $Z_0$ . Unless the line "looks into" an impedance equivalent to  $Z_0$ , stationary waves will form along the line, provided that the length of the line is long compared with the wavelength of the power being transferred, as in the case of a line feeding power to an antenna. As a result of these standing waves, high potentials exist across the line in the vicinity of the voltage anti-nodes, which tend to break down the insulation at these points. Although the shielding of a concentric line usually prevents radiation from these waves, the presence of voltage and current anti-nodes tends to produce rather serious dielectric and conductor losses and to prevent a most efficient transfer of power.

In a previous paper\* information is given concerning transmission line terminations for the condition where the characteristic impedance of the transmission line is greater than the resistance of the antenna circuit. The reader is referred to this paper for the treatment of this case and for the simple case where the antenna resistance and characteristic impedance are equal ( $Z_0 = R_A$ ).

The growing use of concentric lines of the low-impedance type, however, has led to cases where the characteristic impedance of the transmission line is lower than that of the antenna resistance. It is these cases that will be discussed here. In general, there are three cases to consider: (1) when the antenna impedance contains a resistive component only; (2) when the antenna impedance contains a resistive component and a reactive component, either capacitive (2a) or inductive (2b); and (3) when the antenna impedance contains resistive and reactive components, the latter being partially compensated by the insertion of an extra reactance of opposite sign. These three cases are considered in order.

### Examples

*Example 1. Antenna Impedance Purely Resistive.*—Refer to Fig. 1. The con-

\* DIETSCH, CARL G., *Antenna Terminations*, *Electronics*, September, 1935.

centric line, characteristic impedance  $Z_0$ , is terminated by a network consisting of  $C_B$ ,  $L_C$ , and the antenna impedance  $Z_A$ . For Example 1 the reactance of the antenna impedance is zero, and  $Z_0 < Z_A = R_A$ . Then the complex impedance  $Z_L$  presented to the end of the transmission line is

$$Z_L = \frac{R_A[X_3X_1 - X_1(X_3 - X_1)]}{R_A^2 + j[X_3X_1^2 + R_A(X_3 - X_1)] + X_1^2} \quad (1)$$

where  $R_A$ ,  $X_1$ , and  $X_3$  are as given in Fig. 1. For proper termination  $Z_0$  must equal  $Z_L$ , hence  $Z_L$  must be real, and the imaginary term is zero. Then  $Z_L = Z_0$  becomes

$$Z_0 = \frac{R_AX_1^2}{R_A^2 + X_1^2} \quad (2)$$

from which  $X_1$ , the reactance of capacitor  $C_B$ , becomes

$$X_1 = R_A \sqrt{\frac{Z_0}{R_A - Z_0}} \quad (3)$$

and  $X_3$  (calculated by equating the  $j$  term to zero), the reactance of inductance  $L_C$ , is

$$X_3 = \frac{R_A^2X_1}{X_1^2 + R_A^2} \quad (4)$$

Since  $C_B = 1/(2\pi fX_1)$  and  $L_C = X_3/(2\pi f)$ , their values in microfarads and microhenrys are then readily calculable from  $f$ , the frequency of operation. Figure 2

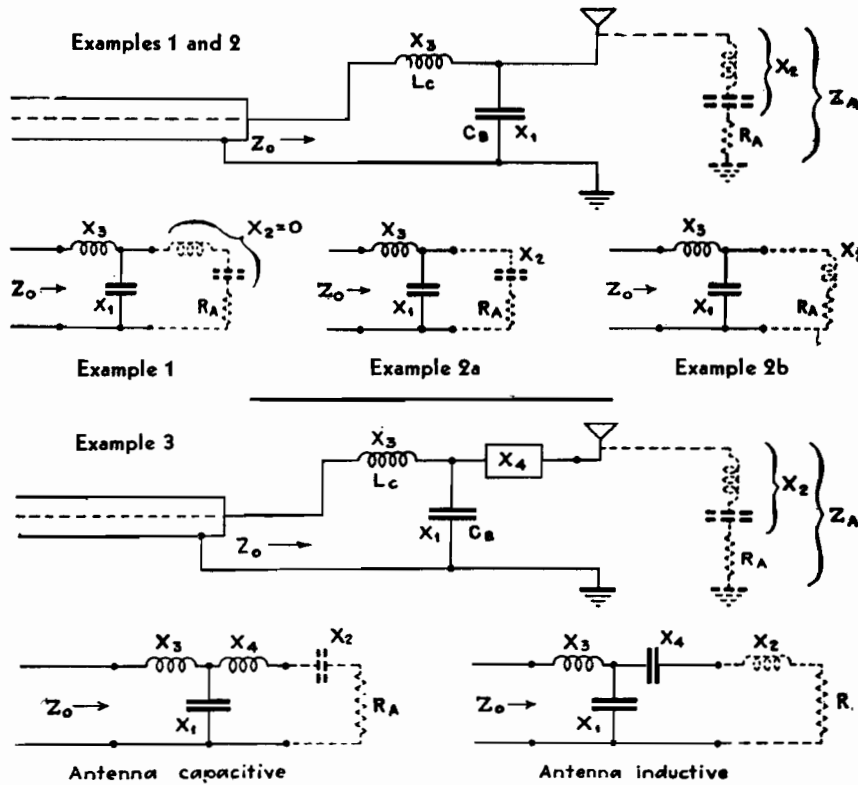


Fig. 1.—Connection diagrams and equivalent circuits for terminating concentric lines when antenna is reactive or nonreactive.

gives various values of  $X_1$  and  $X_3$  in terms of values of  $Z_0$  and  $R_A$ .

**Example 2a. Antenna Impedance with Capacitive Reactance.**—Refer again to Fig. 1. It will be noted that the equivalent diagram for Example 2a is the same as Example 1, except that the antenna impedance is now  $Z_A = R_A - jX_2$ . In this case the complex impedance  $Z_L$  presented to the concentric line is

$$Z_L = \frac{R_A X_1^2 + j[R_A^2(X_3 - X_1) + X_3 X_2^2]}{R_A^2 + (X_2 + X_1)^2} + 2X_1 X_2 X_3 + X_3 X_1^2 - X_2^2 X_1 - X_2 X_1^2 \quad (5)$$

If the line is to be terminated by a real impedance equal to  $Z_0$ , the imaginary part of this equation must be zero, as in Example 1. Then  $Z_L = Z_0$  becomes

$$Z_0 = \frac{R_A X_1^2}{R_A^2 + (X_2 + X_1)^2} \quad (6)$$

from which

$$X_1 = \frac{Z_0}{R_A - Z_0} \left[ X_2 \pm \sqrt{\frac{R_A}{Z_0} (R_A^2 + X_2^2 - Z_0 R_A)} \right] \quad (7)$$

Also, equating the imaginary term to zero, as before

$$X_3 = \frac{X_1 (R_A^2 + X_2 X_1 + X_2^2)}{R_A^2 + (X_1 + X_2)^2} \quad (8)$$

Hence, with  $Z_0$ ,  $R_A$ , and  $X_2$  given,  $X_1$

and  $X_3$  can be calculated by the above equations. From the values of  $X_1$  and  $X_3$ ,  $L_C$  and  $C_B$  can be calculated, exactly as in Example 1. Values of  $X_1$  and  $X_3$  for various values of  $R_A$  and  $X_2$ , for the cases where  $Z_0$  is 80 and 100 ohms are given in Fig. 3.

**Example 2b. Antenna Impedance Inductively Reactive.**—Reference to Fig. 1 for Example 2b shows that it is the same as Example 1 except that  $Z_A = R_A + jX_2$ . By a similar process to that used for

Example 2a we obtain formulas for  $X_1$  and  $X_3$  as follows:

$$X_1 = \frac{Z_0}{R_A - Z_0} \left[ -X_2 \pm \sqrt{\frac{R_A}{Z_0} + (R_A^2 + X_2^2 - Z_0 R_A)} \right] \quad (9)$$

and

$$X_3 = \frac{X_1 (R_A^2 + X_2^2 - X_2 X_1)}{R_A^2 + (X_2 - X_1)^2} \quad (10)$$

from which  $L_C$  and  $C_B$  are calculated as in the previous cases. Figure 4 shows various values of  $X_1$  and  $X_3$  in terms of  $R_A$  and  $X_2$ , for  $Z_0$  values of 80 and 100 ohms.

**Example 3. Added Reactance to Antenna Impedance.**—When the transmission line impedance “looks into” a complex antenna impedance, it is possible to simplify the adjustment of the circuit greatly by adding a reactance  $X_4$  as shown in Fig. 1 for Example 3. This reactance  $X_4$  may be either inductive or capacitive, as shown. If the sum of  $X_1$  and  $X_2$  is inductive, then  $X_4$  is made capacitive, and vice versa. The value of  $X_4$  is such that the algebraic sum of  $X_1$ ,  $X_2$ , and  $X_4$  is equal to zero. Since  $X_4$  is in series with the antenna impedance, it adds directly with the reactive part of the antenna impedance. The effect of the presence of  $X_4$  can then be taken into account by applying the formulas of Example 2a or 2b. It is found by so doing that the values for both  $X_1$  and  $X_3$  are expressed by a very simple equation

$$X_1 = X_3 = \sqrt{Z_0 R_A} \quad (11)$$

This occurs only, however, if  $X_4$  is so chosen that

$$\pm X_4 - X_1 \mp X_2 = 0 \quad (12)$$

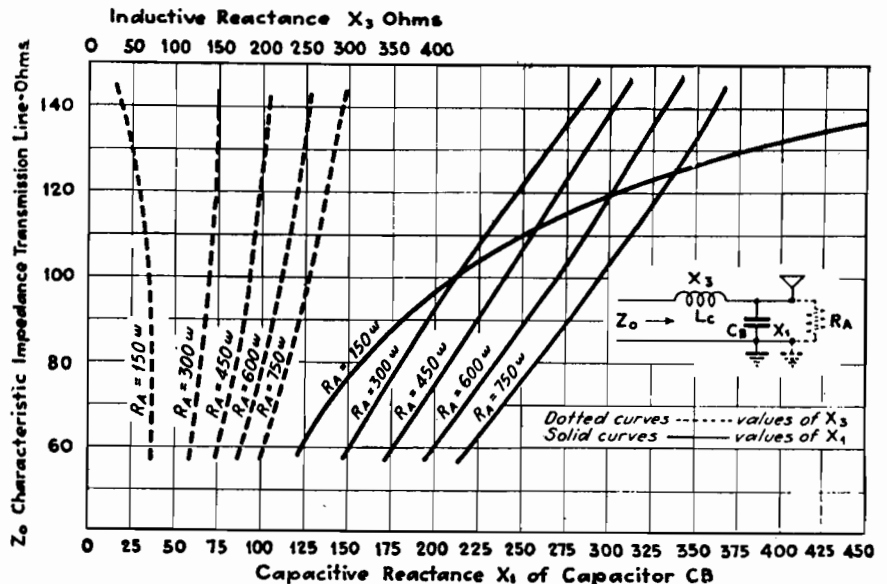


Fig. 2.—Values of terminating reactors for Example 1.

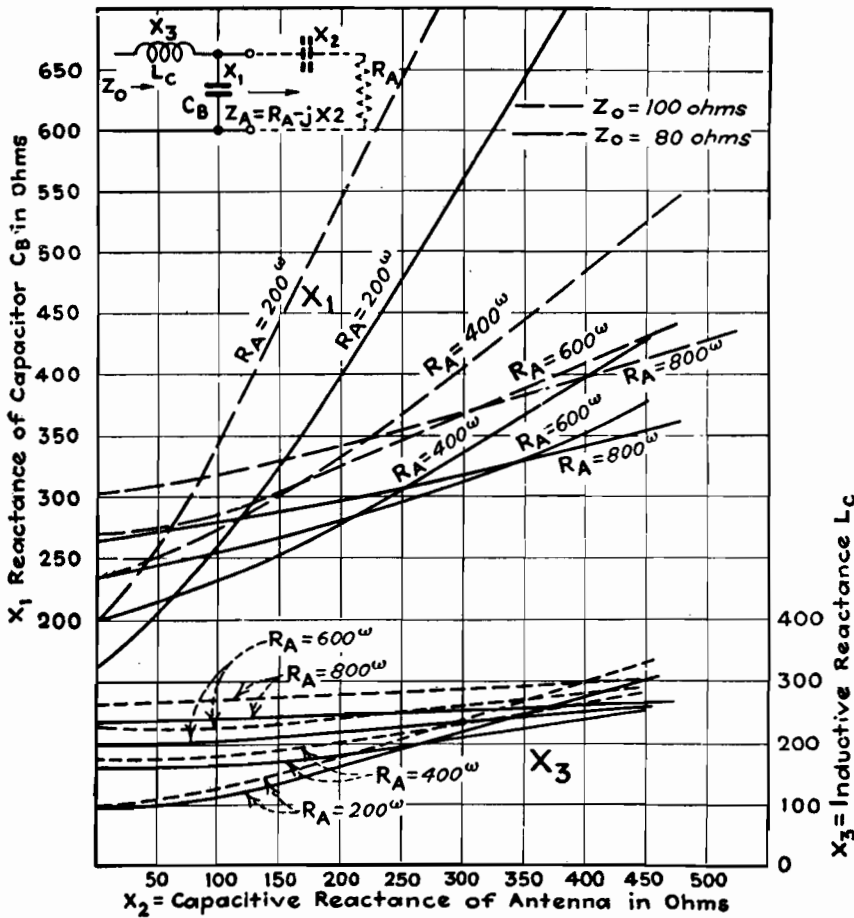


Fig. 3.—Values of terminating reactors for Example 2a.

The reactance  $X_4$  must always have the opposite sign from  $X_2$ , as indicated by the plus-or-minus signs in the equation. When  $X_4$  is so chosen, the reactance  $X_1$  and  $X_3$  may be obtained for various values of  $Z_0$  and  $R_A$  by reference to Fig. 5. Note that these values apply regardless of whether  $R_A$  is larger than, equal to, or greater than  $Z_0$ .

#### Practical Procedure in Designing Matching Circuits

In making suitable adjustments on the impedance matching circuits to provide a correct termination for a given transmission-line characteristic impedance, under Examples 2a and 2b above, where  $R_A > Z_0$ , the following procedure is recommended:

1. The transmission-line characteristic impedance should be calculated and the results checked by actual measurements if possible, such as by means of an r-f impedance bridge.

2. The antenna base resistance should be measured\* over a frequency bandwidth covering at least 100 kc on each side of the operating frequency. A curve

should then be constructed with values of antenna resistance as a function of frequency. A smooth curve drawn through the points of measurements will assist in checking their accuracy.

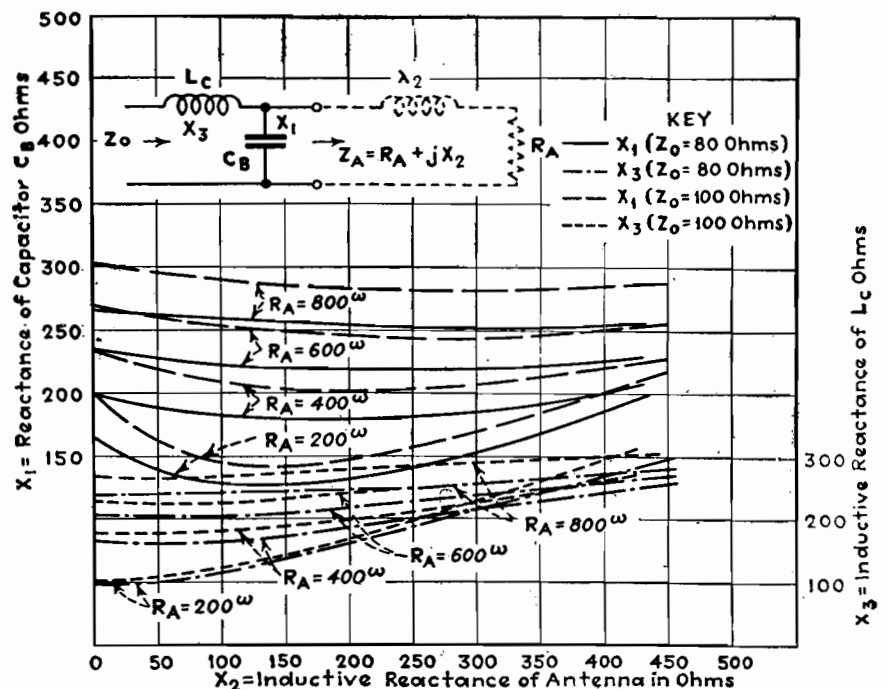


Fig. 4.—Values of terminating reactors for Example 2b, in terms of antenna resistance and reactance.

3. Together with antenna resistance measurements, the antenna reactance should be measured, either by means of an r-f impedance bridge or in a manner shown in Fig. 6, over a wide frequency range, and a curve constructed with antenna reactance as a function of frequency.

4. With the values of antenna resistance and reactance known, values of capacitance  $C_B$  and inductance  $L_C$  may be calculated for Example 2a or 2b as the case may be, and connected into the circuits as shown in Fig. 1.

5. With the transmission line connected, correct termination may be checked by measuring the transmission-line currents at the ends, if its length is equal to a quarter wavelength or odd multiples thereof. For a very long line, it is good practice to make these measurements at a number of points along the line. The existence of stationary waves of current or voltage of the fundamental frequency along the line are an indication of incorrect termination. In such a case, slight adjustments may be necessary in  $L_C$  and  $C_B$  to correct for stray capacitance of leads and tuning equipment or slight errors in measurements. If an r-f impedance bridge is available, its measuring terminals may be connected across the input to the matching circuit in place of the transmission line and the termination circuit checked for an effective resistance equivalent to the characteristic impedance of the line without the line attached.

\*Brown, Hugh A., "Radio Frequency Electrical Measurements," pp. 177-187. McGraw-Hill Book Company, Inc., New York.

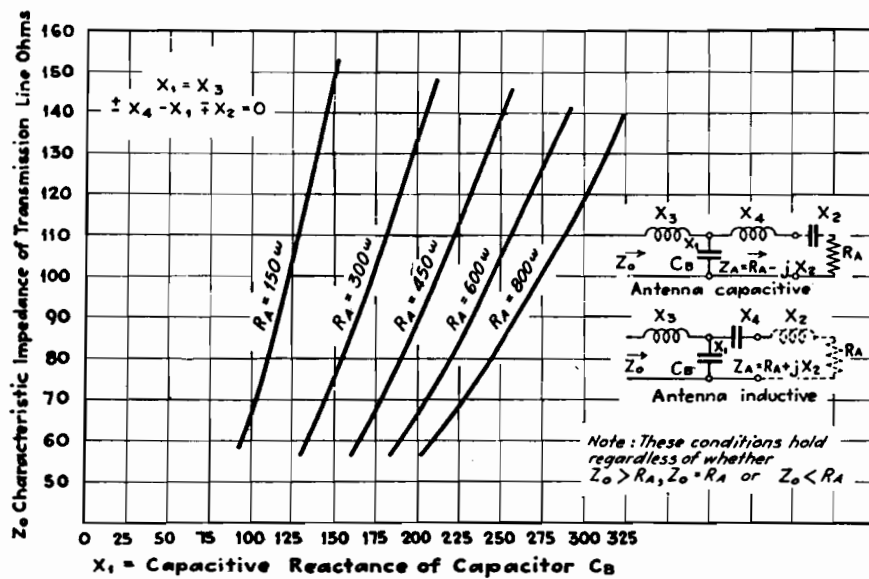


Fig. 5.—Values of terminating reactors for Example 3, when antenna reactance is compensated.

Although Example 3 requires the addition of another piece of apparatus in the form of an inductance or capacitance in the antenna lead, which may be rather expensive, the adjustment procedure is less difficult and is as follows:

1. With values of the line characteristic impedance, antenna resistance and reactance obtained by measurement, the value of  $C_B$  is calculated from Eq. (11) which gives the reactance  $X_1$  necessary.
2. With  $L_C$  disconnected from  $C_B$ , reactance  $X_4$  (inductive or capacitive) is added in the antenna circuit in series with

$X_1$ . By means of  $X_4$ , the antenna circuit is tuned to resonance as indicated by maximum current through a thermogalvanometer, when the antenna circuit is excited by means of an external oscillator loosely coupled to it.

3. A sufficient value of inductance  $L_C$ , having a value  $X_3$  equal to  $X_1$ , is then connected into the circuit as shown in Fig. 1.

4. The line is then checked for stationary waves, the absence of which indicates a condition of correct termination.

The mechanical properties of long

concentric-tube transmission lines makes the measurement of current in the center conductor rather difficult. In some cases, removable plugs are placed in the outside tube at various intervals along the line. These plugs, which when inserted make the outer tube airtight, permit connections from an antiresonant circuit across the line. Such an antiresonant circuit, when tuned to the fundamental frequency, presents a very high impedance to the line when bridged across it, and therefore does not affect its characteristic impedance at the fundamental frequency. With low power of about 10 watts flowing through the line, the galvanometer reading is an indication of the voltage at the points measured along the line. This method permits measurement for stationary waves of voltage along the line.

#### Method Used in Measuring Antenna Characteristics

Refer to Fig. 7. The procedure used is as follows: Value of capacitor  $C_0$  (usually about  $0.0005 \mu f$ ) is selected to provide sufficient series capacitive reactance to make the antenna appear capacitive over the frequency range measured. Then with the antenna excited by driver oscillator at a frequency indicated by the wave meter, and the switch at position 1, adjust  $C_1$  and  $L_2$  for resonance, as indicated by a maximum reading of  $G$ . Resistance  $R$  is then adjusted until the  $G$  reading is the same as before. This reading of  $R$  is the antenna resistance.

For antenna reactance measurements, the circuit is first calibrated for stray capacitance in a shielded resistance box by resonating the circuit (switch in position 2) first with the box in the circuit and then entirely removed. Difference in reading of capacitor  $C_2$  between the two conditions equals the capacitance of the box. This value should be added to each reading of  $C_2$ , when the circuits are resonated, which is done as above for resistance measurement. The antenna reactance  $X_2$  is equal to capacitive reactance value of  $C_2$  minus capacitive reactance of  $C_0$ . When the reactance of  $C_0$  is greater than that of  $C_2$ , then the antenna reactance is positive.

When it is found desirable to apply the matching circuits described above and illustrated in Fig. 1 to balanced lines, such as those of the open-wire or double-concentric types, the value of  $X_3$  derived by the particular formula for Examples 1 and 2 is halved and placed on each side

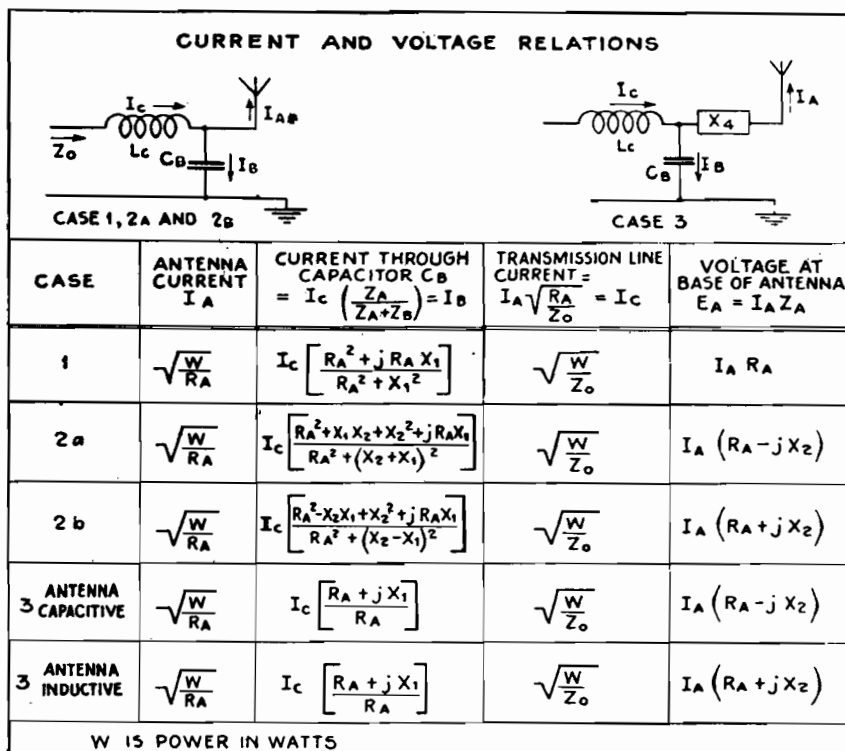


Fig. 6.—Current and voltage relations in terminating circuits.

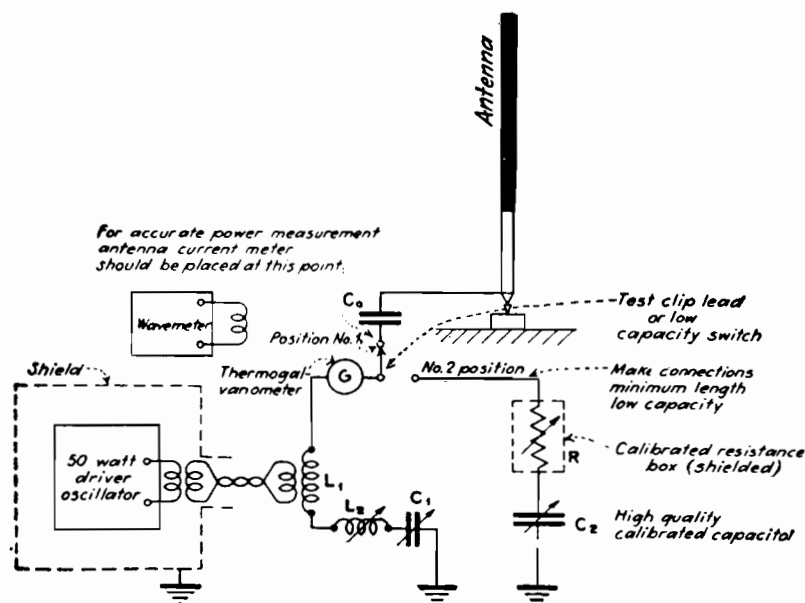


Fig. 7.—Setup for measuring antenna characteristics by substitution method as described in text.

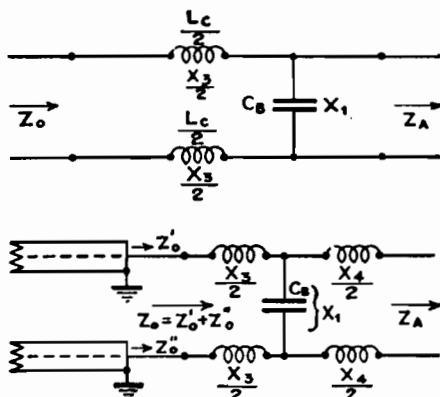


Fig. 8.—Balanced circuits.

of the circuit (see Fig. 8), while the value of  $X_4$  is halved and placed on each side of the circuit for Example 3. Under these conditions, the formulas given above

apply to the respective cases mentioned. The systems become quite useful in matching a given balanced transmission line or r-f circuit into another having entirely different input impedance characteristics.

### Conclusion

In the foregoing analysis of antenna matching circuits, they were considered as providing for a given transmission line a termination impedance equivalent to an ohmic resistance at the fundamental frequency. An analysis of the input impedance that such a line "looks into" at various harmonic frequencies discloses that it may assume an infinite number of different impedances containing resistance and positive or negative reactance components, the values of which depend on the termination circuit constants as well as those of the antenna. The values of antenna resistance and reactance may vary widely with frequency. It is apparent, therefore, that, for harmonic frequencies, stationary waves of current and voltage will form on the transmission line as well as in the antenna circuit, unless suitable harmonic filtering is provided either within the vacuum-tube transmitter or at the input to the transmission line.

The effectiveness of a given filter design for various harmonic frequencies depends on its position in the line with respect to the positions of current and voltage antinodes of the harmonic frequencies along the line.\*

\* DIETRICH, CARL G., Suppression of Transmitter Harmonics, *Electronics*, June, 1933; also HENNEY, K., "Radio Engineering Handbook," p. 655, 2d ed., McGraw-Hill Book Company, Inc., New York.

## Q-factor Charts for Unloaded Concentric Transmission Lines

By R. C. MIEDKE

An alignment chart makes possible the rapid determination of  $Q$  and sending-end impedance for copper concentric cables of optimum conductor ratios. A supplementary chart extends the results for use with concentric transmission lines having any ratio of conductor diameters

THE charts permit easy determination of the sending-end impedance  $Z_s$ , as well as the value of  $Q$  for unloaded concentric-conductor transmission lines, in terms of the resonant frequency and

the conductor sizes. The charts may be applied to the usual concentric transmission lines used as transformers, filters, or transmission networks, which are either an odd number of wavelengths

long and short-circuited at the receiving end, or an even number of wavelengths long and open at the receiving end.

Figure 1 has been drawn to apply to a concentric line of copper conductors of

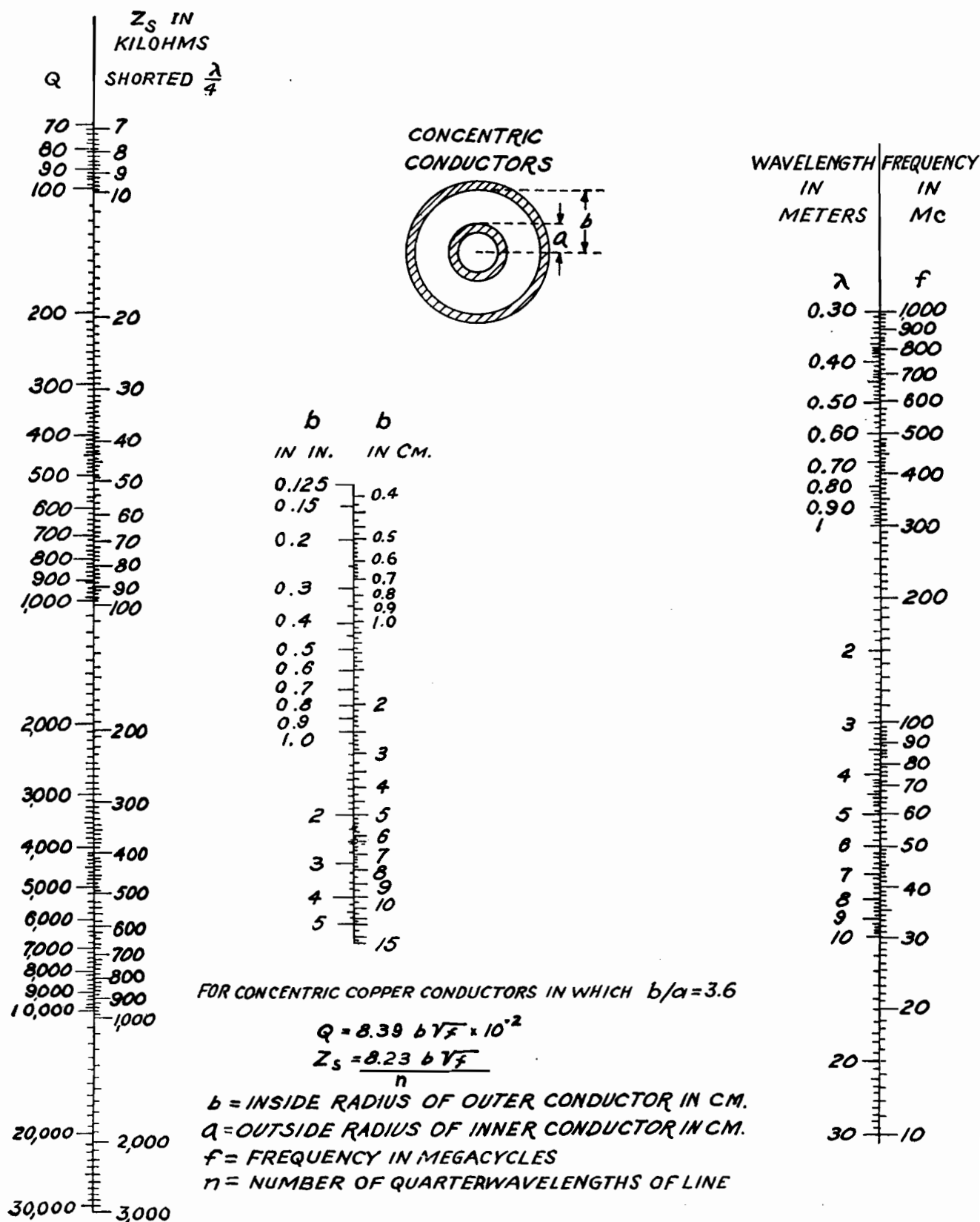


Fig. 1.— $Q$  for unloaded concentric resonant lines for optimum ratio of conductor dimensions,  $b/a = 3.6$ .



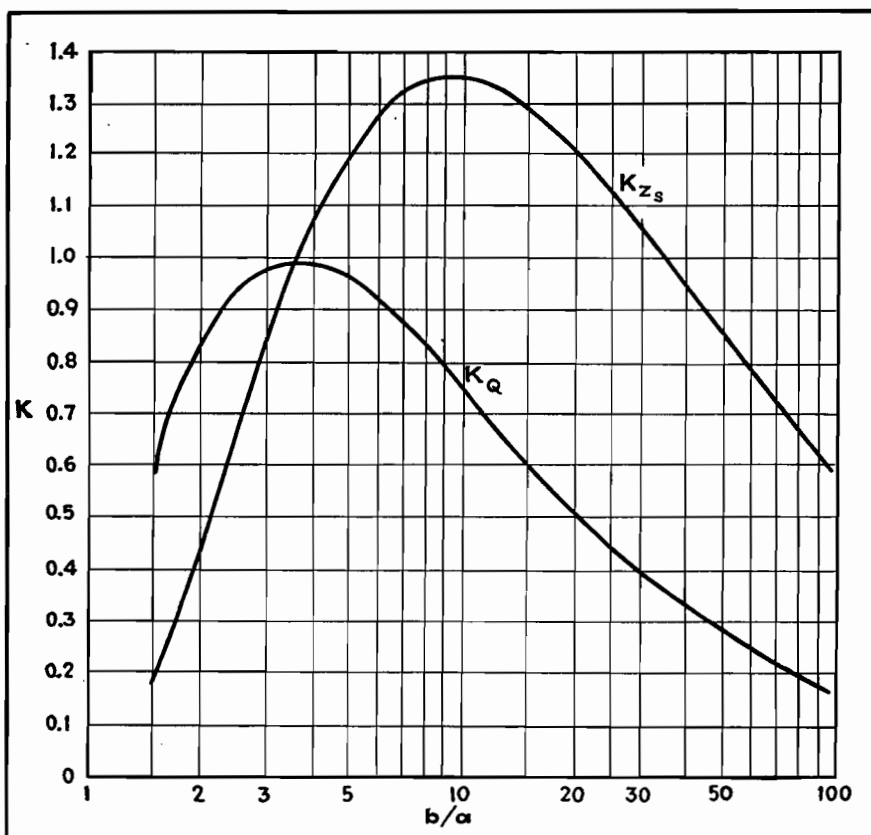


Fig. 2.—Plot of multiplying factor,  $K$ , for concentric transmission lines having various values of inner and outer conductor diameters.

such dimensions ( $b/a = 3.6$ ) as to produce maximum  $Q$ . The value of  $Q$  is independent of the number of quarter wavelengths of line length. To use Fig. 1 for a line of optimum dimensions, it is

necessary to know the inner radius of the outer conductor,  $b$ , in inches or centimeters, and either the frequency in megacycles,  $f$ , or the wavelength in meters,  $\lambda$ , at which the line is operated.

A straight line connecting either  $f$  or  $\lambda$  (on the scales at the right) with the appropriate value of  $b$  (center scale) and extended to the scales at the left will indicate the values of  $Q$  and  $Z_s$  for the line.

The value of  $Z_s$  given in Fig. 1 applies only to a line for which  $b/a = 3.6$  and for a line only one-quarter wavelength long.

To extend the use of Fig. 1 to lines for which  $b/a$  may have any value from 1 to 100, it will first be necessary to determine  $Q$  or  $Z_s$  for a line for which  $b/a = 3.6$ , as indicated above. The values of  $Q$  and  $Z_s$ , thus determined must then be multiplied by the factors  $K_Q$  or  $K_{Z_s}$ , respectively, determined from Fig. 1 for the desired value of  $b/a$ . Maximum value of  $Z_s$  occurs for  $b/a = 9.2$ .

An example will help to illustrate the use of these charts. Assume that we have a transmission line whose inner conductor has a radius of  $\frac{1}{4}$  in. and whose outer conductor has a radius of  $\frac{1}{2}$  in., and that the line is operated at a frequency of 100 Mc. From this data we have  $a = \frac{1}{4}$  in.,  $b = \frac{1}{2}$  in.,  $b/a = 2$ , and  $f = 100$  Mc. Connect the points,  $f = 100$  Mc and  $b = 0.5$  in., and read  $Q = 1,080$  and  $Z_s = 105,000$  from Fig. 1.

From Fig. 2 relating  $K$  with  $b/a$ , for  $b/a = 2.0$  we find that  $K_Q = 0.83$  and  $K_{Z_s} = 0.44$ . The correct line constants are then

$$\begin{aligned} Q' &= K_Q Q = 0.83 \times 1,080 = 896 \\ Z_s' &= K_{Z_s} Z_s = 0.44 \times 105,000 \\ &= 46,200 \text{ ohms} \end{aligned}$$

## Impedance Determinations of Eccentric Lines

By GEORGE H. BROWN

An examination of the effect on the characteristic impedance of displacing the inner conductor somewhat from its central or coaxial position

### Calculation of Characteristic Impedance

IN A well-constructed transmission line, which has low leakage conductance and low conductor resistance, the characteristic impedance is

$$Z_0 \text{ (ohm)} = \sqrt{\frac{L}{C}} \quad (1)$$

where  $L$  is the inductance per centimeter length, measured in henrys, and  $C$  is the capacitance per centimeter length, measured in farads.

Since the velocity of a wave on the line is

$$v \text{ (cm per sec)} = \frac{1}{\sqrt{LC}} \quad (2)$$

the characteristic impedance may be written

$$Z_0 = \frac{1}{vC} \quad (3)$$

If there is no insulation present in the transmission line, we may use  $v = 3 \times 10^{10}$  cm per sec, and compute  $C$  from the static capacitance between conductors. The configuration in which we are

interested is shown in Fig. 1. The radius of the outer conductor is  $b$ , the radius of the inner conductor is  $a$ , while the axis of the inner conductor is displaced an amount  $x$  from the axis of the outer conductor. The capacitance of this configuration is\*

$$C \text{ (farads per cm)} = \frac{2\pi\epsilon_0}{\cosh^{-1} \left( \frac{b^2 + a^2 - x^2}{2ba} \right)} \quad (4)$$

\* SMYTHE, WILLIAM R., "Static and Dynamic Electricity," p. 76, Eq. (5), McGraw-Hill Book Company, Inc., New York, N. Y.

where  $p_0$  (permittivity of free space) =  $8.85 \times 10^{-14}$ .

Then from Eq. (3), the characteristic impedance becomes

$$Z_c = 60 \cosh^{-1} \left( \frac{b^2 + a^2 - x^2}{2ba} \right) \quad (5)$$

The characteristic impedance may thus be calculated directly from tables of hyperbolic functions. The expression may also be transformed into the logarithmic form, by making use of the relation\*

$$\cosh^{-1}(y) = \log(y + \sqrt{y^2 - 1}) \quad (6)$$

$$\text{Let } y = \frac{b^2 + a^2 - x^2}{2ba} \quad (7)$$

$$\begin{aligned} \text{and } y^2 - 1 &= \frac{(b^2 + a^2 - x^2)^2}{4b^2a^2} - 1 \\ &= \frac{(b^2 + a^2)^2 + x^4 - 2x^2(b^2 + a^2) - 4b^2a^2}{4b^2a^2} \\ &= \frac{(b^2 - a^2)^2 + x^4 - 2x^2(b^2 + a^2)}{4b^2a^2} \quad (8) \end{aligned}$$

$$\begin{aligned} \text{Then } y + \sqrt{y^2 - 1} &= \frac{b^2 + a^2 - x^2}{2ba} + \frac{\sqrt{(b^2 - a^2)^2 + x^4 - 2x^2(b^2 + a^2)}}{2ba} \\ &= \frac{b^2 + a^2 - x^2 + \sqrt{(b^2 - a^2)^2 + x^4 - 2x^2(b^2 + a^2)}}{2ba} \quad (9) \end{aligned}$$

so that the impedance is given by

$$Z_c = 60 \log \left[ \frac{b^2 + a^2 - x^2 + \sqrt{(b^2 - a^2)^2 + x^4 - 2x^2(b^2 + a^2)}}{2ba} \right] \quad (10)$$

\* PEIRCE, B. O., "A Short Table of Integrals," 2d ed., p. 82, Eq. (680), Ginn and Company, Boston.

When the conductors are arranged to have exactly the same axis, i.e., when  $x = 0$ , Eq. (10) becomes

$$Z_c(x = 0) = Z_0 = 60 \log \left( \frac{b}{a} \right) \quad (11)$$

When  $x = b - a$ , the conductors are touching, so that the capacitance per unit length is infinite and the characteristic impedance is zero.

The parameter  $x$  may then vary between zero and  $b - a$ . In Fig. 2, the abscissa is  $x/(b - a)$ , while the ordinate is  $Z_c/Z_0$ , i.e., the ratio of eccentric characteristic impedance to the perfectly concentric impedance is shown, for a number of ratios of  $b/a$ .

When the transmission line is filled with

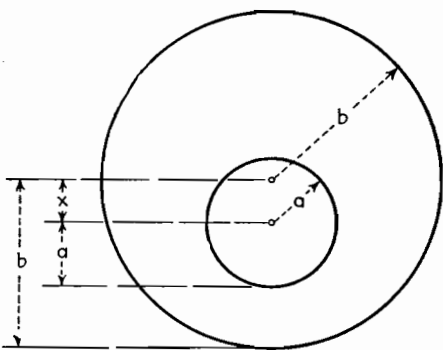


Fig. 1.—Configuration of eccentric transmission line with inner conductor displaced by amount  $x$ .

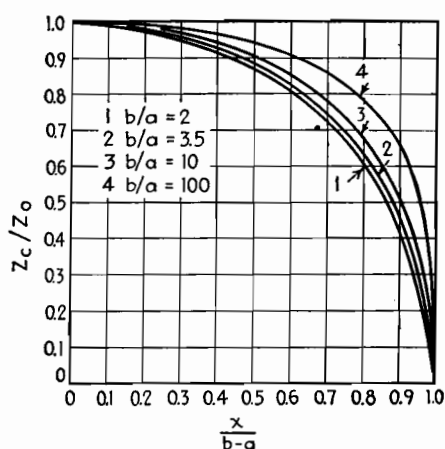


Fig. 2.—The effect of eccentricity expressed in ratio of eccentric to concentric impedance.

a solid dielectric that has a dielectric constant greater than unity, both Eqs. (10) and (11) should be divided by the square root of the dielectric constant. This leaves the ratios shown in Fig. 2 unchanged.

Figure 2 shows that the ratio of eccentric to concentric characteristic impedance, when expressed in terms of percentage of total possible shift, is very nearly independent of the ratio of the radii of the two conductors. When the inner conductor is shifted 50 per cent of the total possible amount, the characteristic impedance is dropped about 10 per cent.

## Graph of Impedance of Eccentric-conductor Cable

By WILLIAM J. BARCLAY and KARL SPANGENBERG

THE characteristic impedance of a transmission line composed of cylindrical conductors, concentrically spaced with regard to their common axis, depends on the ratio of the inner radius of the outer conductor and the outer radius of the inner conductor for a given dielectric. For such a transmission line, the impedance is constant if the construction is uniform throughout its length.

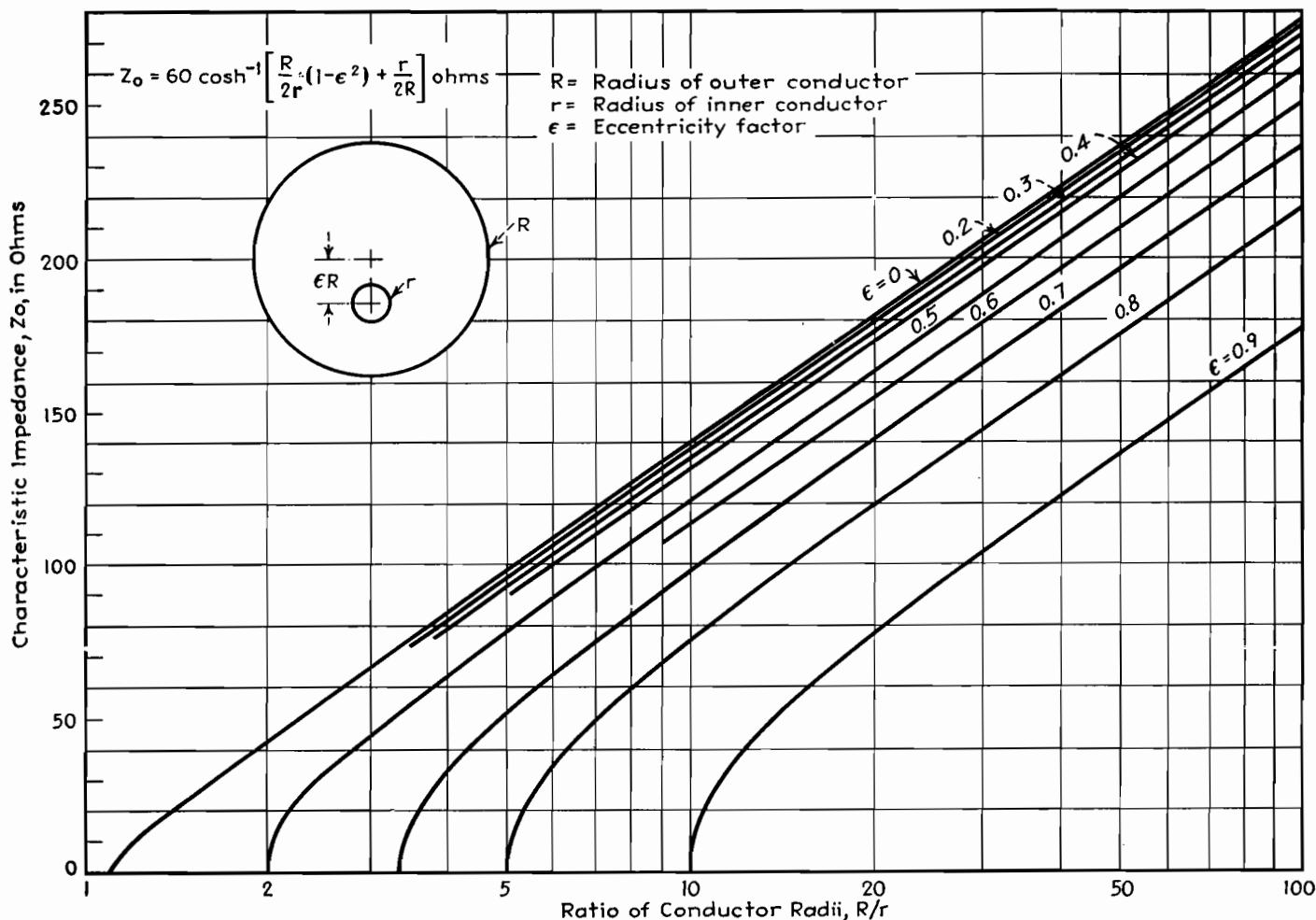
It is sometimes desirable to vary the characteristic impedance for impedance-matching purposes. While this could be accomplished by altering the relative sizes of the conductors, this procedure is not always advisable since it introduces discontinuities and manufacturing difficulties. Another method of varying the

impedance is to make the interior conductor eccentric, rather than concentric. This method has the advantage of permitting the impedance to be varied without altering the size or shape of either conductor. Furthermore, since the characteristic impedance decreases as the eccentricity factor is increased, any reasonable characteristic impedance less than that for the equivalent concentric case can be obtained.

A graph showing the characteristic impedance of a conductor cable for various degrees of eccentricity is shown above. The eccentricity factor  $\epsilon$  is expressed as a fraction of the inner radius of the outer conductor,  $R$  and  $\epsilon R$  is the displacement of

the inner conductor from the axis of the outer conductor. The graph may be used in the design of conductor-cable transmission lines, or to determine the impedance of an existing cable provided the eccentricity factor  $\epsilon$  and the ratio,  $R/r$  are both known. The graph is also useful in indicating what variations in impedance are to be expected from slight deviations of centering of the inner conductor of conductor cables.

If a straight line is drawn through  $R/r = 1$ ,  $Z_0 = 30$  and through  $R/r = 60$ ,  $Z_0 = 120$ , the portion of the impedance curves above this pencil line can, for all practical purposes be regarded as straight lines.



## Measurement of H-f Lines

THE characteristics of h-f transmission lines of most interest to the engineer are (1) the surge impedance, (2) the attenuation factor, and (3) the wave velocity. In many cases, these quantities are difficult to calculate and must be determined by measurement. The measurement procedure to be described has been found convenient and rapid and is based on the use of a  $Q$  meter.

The method consists in measuring the input impedance of a short sample section of the transmission line with the remote end of the line short-circuited, then measuring the input admittance with the remote end of the line open-circuited. If the specimen of the line is electrically short, the components of these impedances have values that are conveniently measured by the  $Q$  meter.

### Theory

The mathematical basis of the method can be briefly outlined as follows, all detailed steps being omitted:

Let  $Z$  = surge impedance of the line  
 $Z_o$  = input impedance with output end open  
 $Z_s$  = input impedance with output end shorted  
 $a$  = attenuation factor per unit length  
 $b$  = phase factor per unit length  
 $P = a + jb$  = propagation factor  
 $L$  = series inductance per unit length  
 $R$  = series resistance per unit length  
 $C$  = shunt capacitance per unit length  
 $g$  = effective shunt conductance per unit length  
 $L_s$  = input inductance with output end shorted  
 $R_s$  = input resistance with output end shorted  
 $C_o$  = input capacitance with output end open  
 $g_o$  = input conductance with output end open  
 $l$  = length of line  
 $\omega = 2\pi \times \text{frequency}$

The fundamental line equations are as follows: for the propagation factor

$$P = a + jb = \sqrt{(R + j\omega L)(g + j\omega C)} \quad (1)$$

At radio frequencies

$$a = \frac{R}{2} \sqrt{\frac{C}{L}} + \frac{g}{2} \sqrt{\frac{L}{C}} \quad (2)$$

$$\text{and} \quad b = \omega \sqrt{LC} \quad (3)$$

For the surge impedance

$$Z = \sqrt{\frac{R + j\omega L}{g + j\omega C}} \quad (4)$$

At radio frequencies

$$R \ll j\omega L \quad (5)$$

$$g \ll j\omega C \quad (6)$$

$$Z = \sqrt{\frac{L}{C}} \quad (7)$$

The impedances  $Z_o$  and  $Z_s$  at the input end of the line, which are to be measured, are related to the line constants as follows:

$$Z_o = \frac{Z}{\tanh Pl} \quad (8)$$

$$Z_s = Z \tanh Pl \quad (9)$$

$$\text{or} \quad Z = \sqrt{Z_o Z_s} \quad (10)$$

$$\text{and} \quad \tanh Pl = \sqrt{\frac{Z_s}{Z_o}} = \sqrt{(R_s + j\omega L_s)(g_o + j\omega C_o)} \quad (11)$$

Equations (10) and (11) express the desired line constants in terms of the measured quantities. For practical lines at radio frequencies, certain approximations are permissible. We shall also suppose that the length of the piece of line on which measurements are made does not exceed certain limits which will be specified later. In these circumstances, we have, with good approximation

$$Z = \sqrt{\frac{L_s}{C_o}} \quad (12)$$

$$\tanh al = \frac{R_s \sqrt{C_o/L_s} + g_o \sqrt{L_s/C_o}}{2(1 + \tan^2 bl)} \quad (13)$$

$$\tan bl = \omega \sqrt{L_s C_o} \quad (14)$$

The attenuation of a short section of a practical line is such that  $al$  can be substituted for  $\tanh al$ , giving

$$a = \frac{1}{2l} \left[ \frac{1}{1 + \omega^2 L_s C_o} \left( \frac{R_s}{Z} + g_o Z \right) \right] \quad (15)$$

$$\text{or } a = \frac{4.34}{l} \left[ \frac{1}{1 + \omega^2 L_s C_o} \right] \left[ \frac{R_s}{Z} + g_o Z \right] \text{ db per unit length.} \quad (16)$$

It is customary to express the attenuation in decibels per 1,000 ft. To do this, measure  $l$  in feet and multiply Eq. (16) by 1,000. The wave velocity is given by

$$v = \frac{1}{\sqrt{LC}} \quad (17)$$

or from Eq. (12)

$$v = \frac{\omega l}{\tan^{-1} \omega \sqrt{L_s C_o}} \quad (18)$$

and is usually expressed as a percentage of the light velocity.

The four line constants  $L$ ,  $C$ ,  $R$ , and  $g$  can be determined as follows:

$$L_s = lL \frac{\tan bl}{bl} \quad (19)$$

$$C_o = lC \frac{\tan bl}{bl} \quad (20)$$

$$R_s = \frac{Rl}{2} \left( 1 + \tan^2 bl + \frac{\tan bl}{bl} \right) + \frac{glZ^2}{2} \left( 1 + \tan^2 bl - \frac{\tan bl}{bl} \right) \quad (21)$$

$$g_o = \frac{gl}{2} \left( 1 + \tan^2 bl + \frac{\tan bl}{bl} \right) + \frac{Rl}{2Z^2} \left( 1 + \tan^2 bl - \frac{\tan bl}{bl} \right) \quad (22)$$

If measurements are made at a frequency low enough so that  $\tan bl/bl$  does not differ much from unity, then  $L = L_s/l$  and  $C = C_o/l$ . Or if  $C_o$  and  $L_s$  are plotted against frequency, the curves will be found to have horizontal asymptotes, which if divided by  $l$ , give  $L$  and  $C$ . (see Fig. 1). In the same way from Eqs. (21) and (22), if  $\tan bl$  is not too large  $R = R_s/l$  and  $g = g_o/l$ . The as-

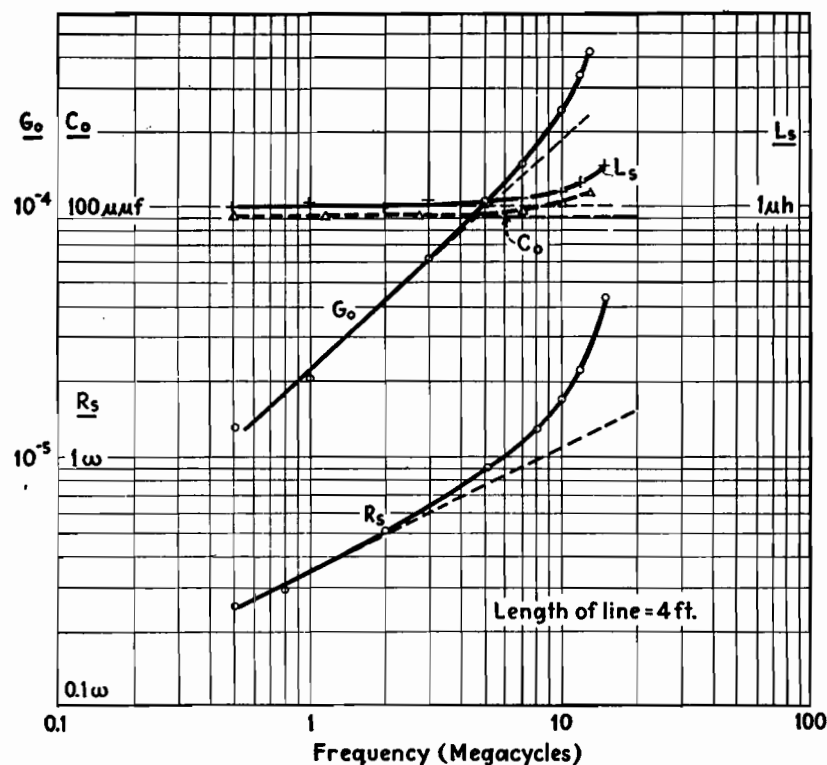


Fig. 1.—Variation in measured quantities in line having rubber insulation.

ymptotic method can be used here also, but in this case the asymptotes are not horizontal. It is of advantage to plot  $R_s$  and  $g_o$  on logarithmic paper, since  $R_s$  will vary as the square root of the frequency and the asymptotes will be a straight line. The asymptote of  $g_o$  will be a straight line of slope unity if the phase angle of the dielectric loss is constant.

The length of line to be chosen for measurement will depend on the highest frequency at which measurements are to be made and on the wave velocity, or phase factor, of the line. As a good practical rule  $bl$  should not exceed 0.9 at the highest frequency. Transmission lines may be divided roughly into two classes: (1) copper lines having very little dielectric between conductors, such as coaxial and open-wire lines, and (2) lines having a considerable amount of dielectric between conductors, such as twisted-pair lines and coaxials in which the space between conductors is entirely filled with insulation. The wave velocity of the latter is about half that of light, as compared with that of the first group, in which the velocity is substantially equal to the light velocity. As a practical guide in this matter the following empirical rules may be employed: For non-

$$l = \frac{140}{f} \text{ (ft, Mc)} \quad (23)$$

and for lines containing dielectric,

$$l = \frac{70}{f} \text{ (ft, Mc)} \quad (24)$$

The table shows the best length of line for measurements at various frequencies.

Frequency range, Mc	Length of line, ft.	
	Non-dielectric	Dielectric
0.1–1	140	70
1–10	14	7
1–50	2.8	1.4

The components  $C_o$  and  $g_o$  of the open-circuit admittance are first measured with the remote end of the line open. Connect the line across the capacitor terminals on the  $Q$  meter. If coaxial, the outer conductor should be connected to the ground terminal. Resonate the main tuning capacitor of the  $Q$  meter, and observe  $C_2$  and also  $Q_2$  of the circuit. Then disconnect the line, resonate the  $Q$  meter, and observe the new tuning capacitance  $C_1$  and new  $Q_1$  of the circuit. The desired quantities may then be computed by

$$C_o = C_1 - C_2 \quad (25)$$

$$g_o = 6.3 \times 10^{-6} f C_1 \left( \frac{Q_1 - Q_2}{Q_1 Q_2} \right) \quad (26)$$

where  $C$  is in microfarads and  $f$  is in

megacycles. This procedure should be repeated at several frequencies in the desired range up to the limit expressed roughly by Eq. (23) or (24).

Quantities  $R_s$  and  $L_s$  are measured next with the remote end of the line short-circuited. This short should be of the lowest possible resistance and inductance, and preferably soldered. For these measurements, the line is connected in series with the inductance coil used with the  $Q$  meter. If coaxial, the outer conductor should be connected to the low coil terminals of the  $Q$  meter. First resonate the main tuning on the  $Q$  meter and observe  $C_2$  and also  $Q_2$ . Then short the line directly at its input terminals by means of a heavy copper bar of the lowest possible resistance and inductance. In some cases (at low frequencies or with low-resistance lines), the bar must be soldered in place for accurate results. Then reresonate the  $Q$  meter and observe the new  $C_1$  of the new  $Q_1$ . The desired quantities are then given by

$$L_s = \frac{2.54 \times 10^4}{f^2} \left( \frac{C_1 - C_2}{C_1 C_2} \right) \quad (27)$$

$$R_s = \frac{1.59 \times 10^5}{f} \left( \frac{1}{Q_2 C_2} - \frac{1}{Q_1 C_1} \right) \quad (28)$$

where  $L_s$  is in microhenrys,  $R_s$  in ohms, the  $C_s$  in micromicrofarads and  $f$  in megacycles. The measurements should be

repeated at the same frequencies at which  $C_s$  and  $g_s$  were measured.

The surge impedance  $Z$  may be computed from Eq. (12) which, if  $L_s$  is in microhenrys and  $C_s$  in micromicrofarads, becomes

$$Z = 1,000 \sqrt{\frac{L_s}{C_s}} \quad (29)$$

The attenuation factor  $a$  may be computed from Eq. (16) which, if  $L_s$  and  $C_s$  are expressed in the above units, may be written

$$a = \frac{4,430}{l} \left[ \frac{1}{1 + 3.94 \times 10^{-5} f^2 L_s C_s} \left( \frac{R_s}{Z} + g_s Z \right) \right] \text{ db per 1,000 ft.} \quad (30)$$

where  $l$  is in feet. The values of  $R$ ,  $g$ ,  $L$ , and  $C$  may be obtained as described above.

Representative results of measurements on practical lines are shown in Figs. 1 and 2. The rise of the quantities (in Fig. 1) at the higher frequencies due to the line becoming electrically "long" is in evidence and also the method of determining the values of the line constants from the asymptotes is shown. Figure 2 shows the attenuation in decibels per 1,000 ft. for several lines as follows:  $A$  is a twisted-pair line resembling lamp cord.  $B$  is a twisted-pair line of solid No. 12 conductors, covered with waterproof insulation.  $C$  is a coaxial comprising a

central No. 12 (0.080 in.) conductor and an outer flexible braid  $\frac{1}{2}$  in. in diameter, the space between being completely filled with soft rubber. Line  $D$  is a rubber-insulated line of the same general dimensions as  $C$ . Lines  $B$  and  $C$  are commercial products widely advertised as low-loss lines. Line  $E$  is a flexible coaxial containing interlocking beads of low-loss insulating material. Line  $F$  is a solid coaxial of 73 ohms surge impedance,  $\frac{5}{16}$  in. in diameter and insulated by Isolantite beads spaced 2 in. The calculated values for this line, based on copper loss, are shown in curve  $G$ . It will be seen that the twisted-pair and rubber-insulated lines have relatively high losses and are suitable only for short runs or the lower frequencies. A type  $F$  line is quite suitable for outdoor use in conjunction with the flexible type  $E$  line for indoor use and for patching purposes.

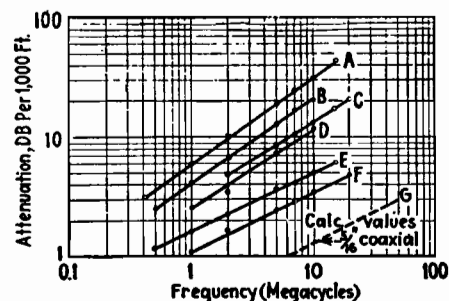


Fig. 2.—Attenuation for typical lines.

## SECTION VIII

# ELECTRONIC HEATING

	Page
Electronic Heating Design Chart.....	110
Surface Hardening of Metals.....	112
Power Equations for Dielectric Heating.....	114
Design Chart for R-f Heat-treatment Generators.....	116
Design Data for Induction Heating Coils.....	117
Magnetic Field Equations for Induction Heating Coils...	123

## Electronic Heating Design Chart

By C. V. FIELDS

Choice of over-all circuit constants for induction and dielectric heating applications can be made directly from the chart. Their limitations and dependencies are visualized

**D**ESIGNERS of induction heating, dielectric heating, and other apparatus of relatively high a-f and r-f power can choose appropriate circuit constants, in accordance with operating requirements, by the relations conveniently arranged in Fig. 1. By this method, such relations can be easily held within physical, electrical, and economic limitations.

The seven parameters covered by the chart are (1) current, (2) voltage, and (3) kva, correlated by the upper section; and (4) inductance, (5) capacitance, and (6) frequency, in the lower section; with (7) reactance having its scale as a common coordinate between the two sections in the construction of the chart as a whole.

The horizontal lines are ordinates of kva, in the upper section, and of frequency, in the lower section. The 45-deg diagonals are cross coordinates of voltage and current, in the upper section, and inductance and capacitance, in the lower. The vertical lines are of constant reactance, common to both sections; their values are shown along the abscissa.

There is no set order of operations in arriving at a desired solution, since any point represents a set of values for each of the four parameters, and naturally satisfies any equations involving them. It is necessary only to familiarize oneself with the directions of increase and decrease, and with the calibration of the

scales so that correct interpolation may be made, to obtain a commensurate set of values.

### Induction Heating

In the usual case of induction-heating-equipment design, three factors have been established and it is necessary only to ascertain the remaining values on the chart. The voltage and frequency are set by the power characteristics in the example shown in Fig. 1, namely, 400 volts and 10 kc. The current required was calculated to be 500 amp. The intersection of the known voltage and current gives the corresponding kva (200) at the left, and the 0.8-ohm inductive or capacitive reactance is read on the abscissa directly above or below the intersection. Interpolating between the two sets of diagonal lines, where the 0.8-ohm vertical line crosses the 10-kc horizontal line in the lower half of the chart, we find the inductance to be 13  $\mu$ h and the capacitance 20  $\mu$ f.

### Dielectric Heating

Physical and electrical properties of specimens to be heated by the dielectric loss method establish the capacitance, power factor, and permissible voltage. From the desired temperature and rate of heating, one computes the required kilowatts, which is divided by the power

factor to get the kva burden of the load. In the example shown in Fig. 2, the 1,000- $\mu$ f specimen requires 100 kva at a maximum of 2,500 volts, and the oscillator covers the 1,500- to 5,000-kc range.

Before proceeding to use the chart, it is necessary to change the decimal points of the  $L$ ,  $C$ , and  $f$  scales according to Fig. 2. This change does not affect the upper section of the chart, because the reactance values remain unchanged. The range of all other scales may be shifted by similarly shifting decimal points.

The fixed capacity-kva- and maximum-voltage lines are drawn in Fig. 2. The available frequency range is shaded, as is the resulting reactance spread of 32 to 105 ohms. The desired kva obviously may be obtained at 1,800 to 2,500 volts depending on the frequency used. Since the maximum permissible stress of 2,500 volts is within the shaded range, the implied 62 ohms and 2,500 kc would be used, giving a current of 40 amp.

### Capacitor Application

Assume that a certain 0.1- $\mu$ f 10-kv d-c blocking capacitor may have a 2 per cent superimposed alternating voltage of 200 volts at 200 kc, and that it is desired to know at what alternating voltage the capacitor may be operated at other frequencies. Referring to Fig. 1 or to Fig. 3 the 0.1- $\mu$ f lines cross at 8.0 ohms



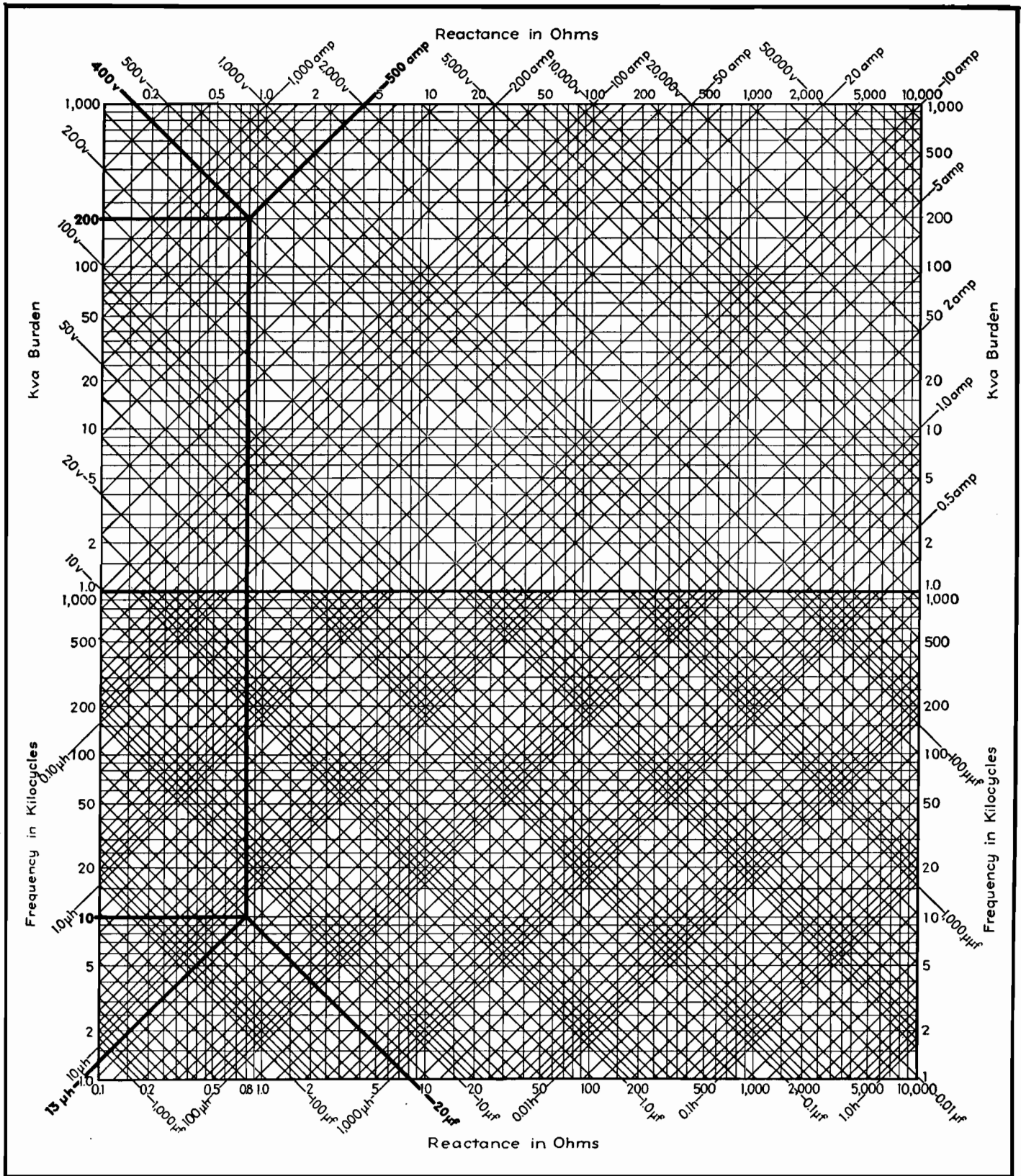


Fig. 1.—Electronic heating design chart.

in the lower half; this 8-ohm reactance line, followed up to the 200-volt line, gives 5 kva and 25 amp. These last two values establish the thermal limits of the capacitor, neither of which are to be exceeded.

At some new frequency, say 500 kc, the

intersection with 0.1  $\mu$ f occurs at 31.5 ohms, which, at 25 amperes, gives 2 kva and 80 volts alternating current.

At 50 kc the capacitor's reactance is 31.5 ohms, resulting in a 20-kva burden at 25 amp. So the 31.5-ohm line must not

extend beyond its intersection with 5 kva, which corresponds to 13 amp. and 400 volts alternating current.

It is apparent, therefore, that the intersection of any reactance line with those of current and kva, shown heavy in



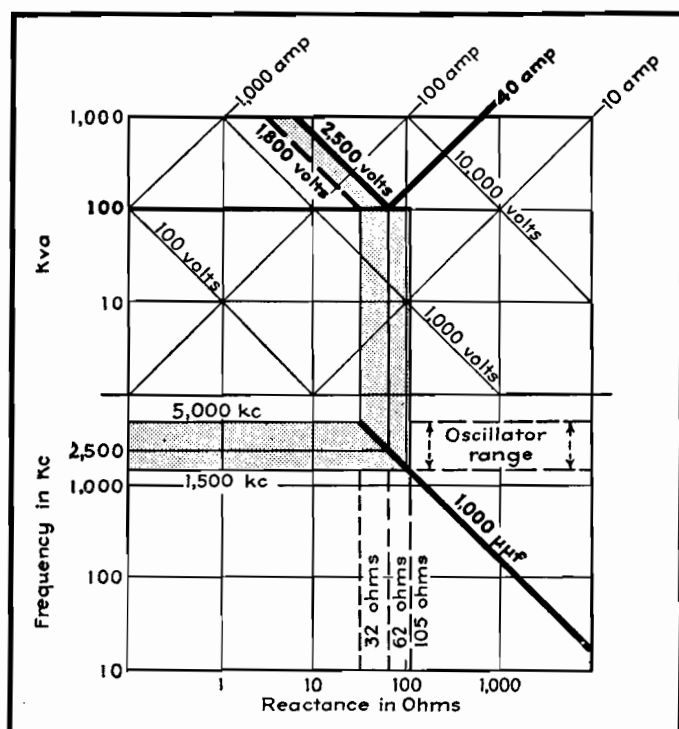


Fig. 2.—Skeleton form of the chart, illustrating procedure for shifting decimal point for inductance and capacitance values, as required for the case of dielectric heating.

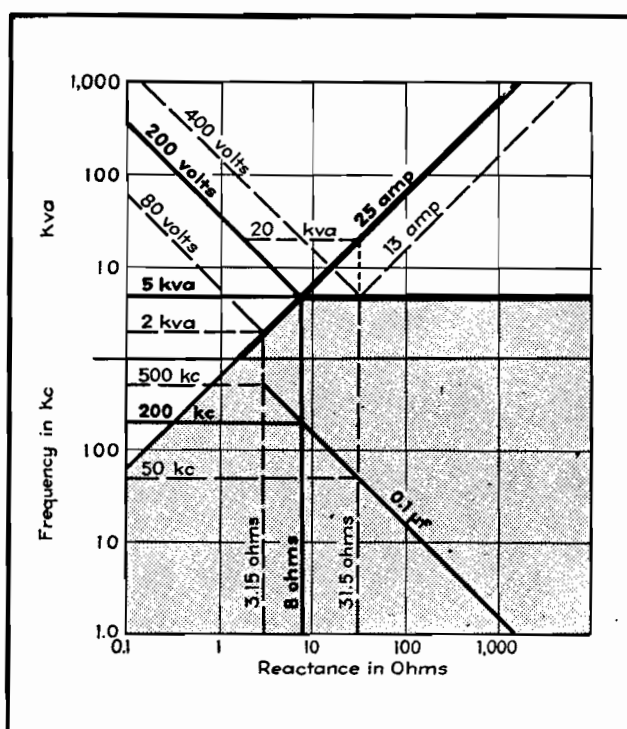


Fig. 3.—Skeleton form of the chart, indicating operating boundaries of current and kva, determined by original rated conditions when an adjustment in frequency is desired.

Fig. 3, will determine the maximum permissible alternating voltage at the frequency desired, provided of course that the combined alternating and direct

voltage do not exceed the rating for dielectric strength.

The same procedure could be followed in ascertaining permissible working con-

ditions at various frequencies for power-factor correction, or for tuning capacitors used with induction-heating coils or furnaces.

## Surface Hardening of Metals

By H. C. GILLESPIE

Effect of frequency on depth of penetration of heat during processing of plain and alloy steels by induction at radio frequencies above 10 kc, analysis of power requirements, and design data on suitable inductors

**H** EATING by electromagnetic induction delivers large amounts of power in concentrated form to the surface to be heated for hardening purposes. Surface concentration of power may be as high as 30 kw per sq in. to secure sharp delineation of the hardened layer.

If the concentration of power is increased to the point where the temperature gradients in the material are steep enough to cause a rapid flow of heat from the surface into the metal behind it, it becomes possible to accomplish the whole hardening operation of localized heating and quenching in a single step. The

process is thereby simplified and made more reliable by the elimination of the separate quench, and the hardened layer is more sharply defined.

A process that depends on steep temperature gradients in the heated zone necessarily is limited as to the thickness of the case that can be produced. The outside surface should not, of course, be melted, and the inner edge of the layer to be hardened must be at some temperature above the Curie point. The temperature distribution required in the region between these two layers is a complicated function of power, time, frequency, and the tem-

perature it is necessary to attain. It has been established, however, that cases 5 to 50 mils thick can be produced on steels of moderately high hardenability, and thicker ones on steels having qualities approaching those of air-hardening alloys. It is believed that this range fills an important gap between the relatively thin cases of the carburizing and nitriding processes, and the thicker ones obtained with low-frequency induction heating.

As indicated, the factors involved enter in a complicated manner. An experimental approach has therefore been used almost exclusively in determining

the operating parameters. It will be useful, however, to examine the effect of one of the parameters, namely, frequency, to determine its importance from theoretical considerations.

### Function of Frequency

The depth of heat penetration is determined by the attenuation suffered by alternating magnetic flux as it progresses through conducting materials. This attenuation is due to the shunting action of the conducting metal in conjunction with the inductive reaction of the medium, as affected by the permeability of the metal. For flux fields without divergence, this attenuation has exactly the form of the attenuation of a wave progressing down a transmission line.

The complete propagation constant of a line consisting of  $L$  henrys per unit length in series and  $G$  mhos conductance per unit length in shunt is

$$\nu = \sqrt{j\omega LG} = \sqrt{\frac{\omega LG}{2}} + j \sqrt{\frac{\omega LG}{2}} = \alpha + j\beta \quad (1)$$

on rationalization of the  $\sqrt{j}$ . Since we are interested in heating effects only, the phase shift factor is not of interest, the attenuation factor telling us all we need to know. In terms of the properties of the material it becomes

$$\alpha = \sqrt{\frac{\omega\mu\sigma}{2}} \text{ nepers per meter} \quad (2)$$

$$\alpha = 8.7 \sqrt{\frac{\omega\mu\sigma}{2}} \text{ db per meter} \quad (3)$$

$\mu$  and  $\sigma$  being in mks units of permeability and conductivity, respectively. The depth at which the flux, or current, is attenuated by 1 neper is defined as the penetration depth and is equal to

$$d = \frac{1}{\alpha} = \sqrt{\frac{2}{\omega\mu\sigma}} \quad (4)$$

Since we usually want to know the depth of penetration in thousandths of an inch and use cycles per second rather than radians per second, and since the handbook tables list the permeabilities of materials relative to that of space and the conductivity in cgs units, a composite form of Eq. (4) will be given

where  $\mu_1$  = relative permeability  
 $\sigma_1$  = conductivity, mhos per cm  
 $f$  = frequency, Mc

$$d = 1.98 \sqrt{\frac{1}{f_1 M_1 \sigma_1}} \text{ mils} \quad (5)$$

The values of  $\mu_1$  and  $\sigma_1$  that should be used require some examination before

inserting them in the formula.  $\sigma_1$  is a function of temperature, decreasing about nine times as the temperature rises from room to hardening temperature. The relative permeability of steel is a function of temperature, becoming unity above the Curie point (about 1425°F for plain carbon steels). It is also dependent on the strength of the magnetic field in which the steel is placed, being effectively unity if saturation values of magnetization are greatly exceeded.

A chart presented in Fig. 1 shows the penetration depth in steel as a function of frequency for room temperature and for temperatures just above the Curie point. Copper is also shown for comparison. With this as a guide, frequencies can be chosen that will (1) ensure efficient operation and (2) confine the heating to a zone within that which is to be hardened. The first requirement is met by using a frequency that is high enough so that the penetration depth is less than about a third of the thickness of the piece; the incident energy is then nearly completely attenuated, i.e., absorbed, by the metal. The second is met by use of a frequency high enough so that most of the power is absorbed well within the thickness of the case desired.

### R-f Power Requirements

Power requirements, as indicated, are high. For SAE 1095 steel (drill rod) the power required to secure cases of varying thickness by the self-quenching method is shown in Fig. 2. The power

referred to on the chart is that actually delivered to the steel.

These data were obtained on 1¼-in. diameter rods, which are considered to have enough metal behind the heated zone to yield a maximum quenching rate at the beginning of the cooling cycle. That is, further increase in diameter does not affect the slope of this part of the cooling curve, because there has been no time for increase in the temperature at the center of the rod during the short heating cycle. It is the rate of cooling above 1000°F that is most important to the hardening process.

On a rod of this diameter the surface area per inch length is  $\pi \times 1\frac{1}{4} = 3.9$  sq in. For power outputs within the range of generating equipment of a reasonable

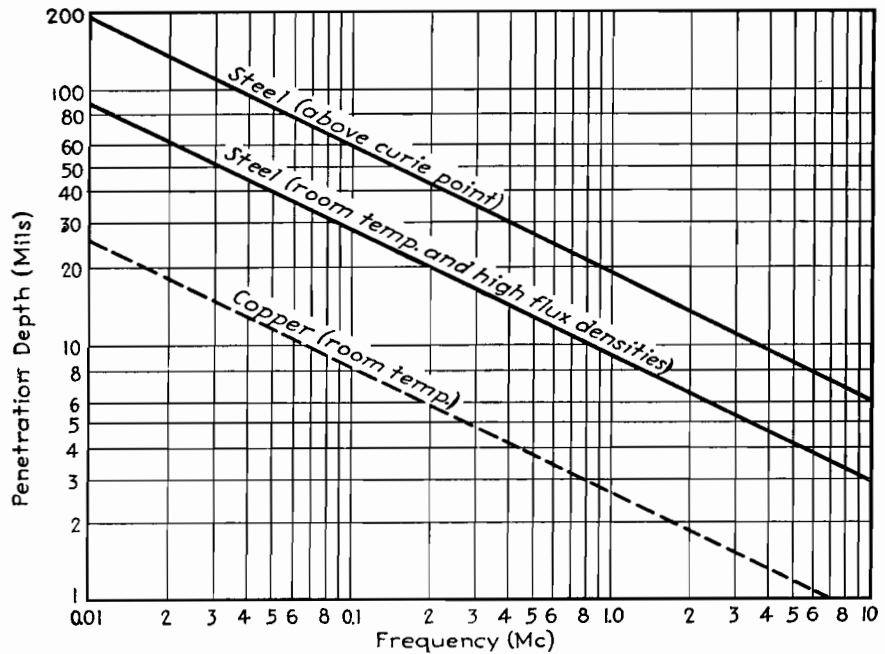


Fig. 1.—Penetration depth vs. frequency for steel in the process of being hardened. A curve for copper is shown for reference.

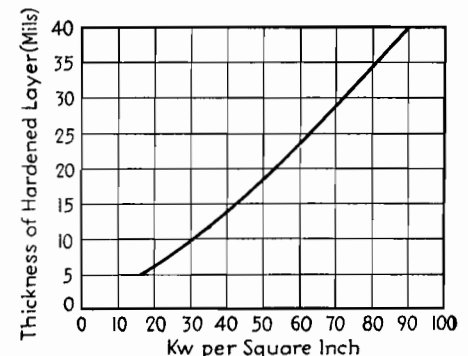


Fig. 2.—Power required to produce cases of varying depth, for self-quenching hardening. This curve applies to steel requiring a relatively low quenching rate for full hardening. Steels of low hardenability require more and steels of high hardenability less power per square inch.

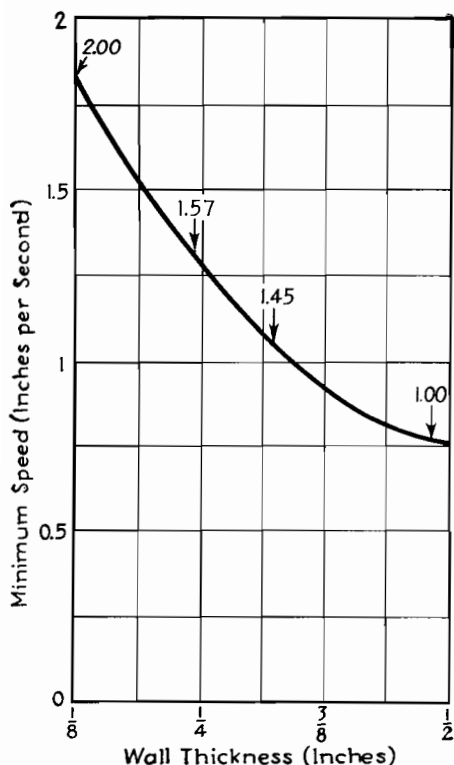


Fig. 3.—Scanning speed required for hardening various wall thicknesses by self-quenching, down to  $\frac{1}{8}$  in. Numbers on curve refer to power requirement relative to lowest.

size (below 100 kv), it is necessary to limit the length of rod treated at one time. For this reason it becomes necessary to heat a piece progressively, with only a narrow band being heated at any one time. This "scanning" method can be applied only lengthwise of pieces of regular section; if it is attempted to scan around the circumference, or in any pattern that returns the heating coil to the starting point, a softened area will be produced there.

It is often desired to harden the surface of a hollow cylindrical piece, such as the wall of an engine cylinder. Here the thickness of the material becomes an important factor in determining the speed with which the heating must be accomplished. This is shown in terms of scanning speed in Fig. 3, for wall thicknesses down to  $\frac{1}{8}$  in. A considerable increase will be noted for the smaller thicknesses, but at the same time there is an economy of energy. At the higher speeds less power is lost by heat conduction in from the surface, as indicated by the relative power figures associated with each curve.

The data presented so far apply to SAE 1095 steel. Power requirements are higher and range of permissible operating conditions wider for steels of higher hardenability, such as alloys containing large amounts of nickel, manganese, chromium, and the like.

#### Design of Suitable Inductors

The inductors used for this kind of work must be accurately contoured to suit the workpiece, of small cross-section to concentrate the power as much as possible, and provided with a channel for 1 to 5 gpm of cooling water. The configuration of an inductor placed within 0.050 in. of the work and carrying current of such a frequency that the penetration depth is less than a similar figure is more properly thought of in terms of its length rather than of the area enclosed by it, which is usually taken to calculate inductance. The inductance and resistance per unit length looking into such a coil is of the order of  $0.01 + j0.1$  ohms at 0.5 Mc at room temperature. The problem of coupling between impedances

of the level of the usual tank circuit reactance (50 to 100 ohms) and impedances of less than 1 ohm is most satisfactorily solved by making the coupling as tight as possible. This makes it possible to transfer power to the inductor circuit without tuning the secondary and without an excessive amount of kva in the tank circuit proper.

The amount of inductive reactance in the inductor circuit is a determining factor in the ultimate choice of operating frequency. Take, for example, the case where it is desired to deliver 100 kw to a 3-in. diameter cylinder at 0.5 Mc. The length of the inductor is approximately 10 in., exclusive of leads. Its total impedance is then  $0.1 + j1.0$  ohms. To deliver 100 kw to the load, approximately 105 kw must be delivered to the inductor coil, so that

$$1.05 \times 10^5 = I^2 \times 0.1$$

$$I = 1.03 \times 10^3 \text{ amp}$$

$$IX = E = 1,030 \text{ volts}$$

across the ends of the coil. At higher frequencies the voltage for similar powers would be proportionally higher. If we are working with  $\frac{1}{32}$ -in. spacing between the coil and the workpiece, the total air gap at the ends of the coil is only  $\frac{1}{16}$  in. and dangerously high-voltage gradients exist.

#### Bibliography

- (1) SOMES, H. E., Hardening of Inside Diameters by Inductive Heat Treatment, *Iron Steel Engr.*, July, 1941.
- (2) SCHELKUNOFF, S. A., The Impedance Concept and Its Application to Problems of Reflection, Refraction, Shielding and Power Absorption, *Bell System Tech. Jour.*, January, 1938.
- (3) WHEELER, H. A., Formulas for the Skin Effect, *Proc. IRE*, September, 1942.
- (4) Nat. Bureau Standards, *Research Paper*, Jour. Research, 23, 1220, July, 1939.

## Power Equations for Dielectric Heating

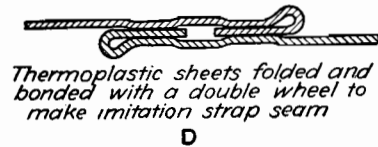
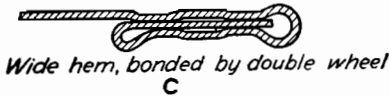
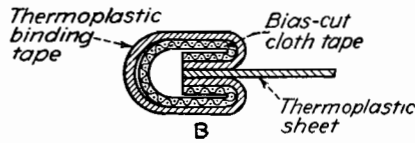
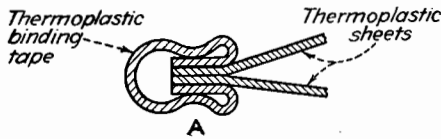
By CYRIL N. HOYLER

Theoretical analysis of dielectric electronic heating as used in bonding thermoplastic sheets of the type used to make raincoats, tobacco pouches, food packages, and inflatable articles. Rotating electrodes and h-f currents make firm moistureproof seams

TO ACCOUNT for the heat conducted into cold electrodes, G. H. Brown has developed a theoretical solution for

dielectric heating by r-f power, based on an analogy between the solution of a transmission line with series inductance

and shunt leakage conductance and the solution of the heat-flow equation. The following expression gives the temperature



Special thermoplastic sheet bonds which may be made by using binding, hemming, and other electronic sewing machine attachments.

at the center of the dielectric material being heated. Values used in the accompanying example apply to dielectrics of glue and wood:

$$u_c = \frac{4Hb^2}{\pi^3 k} \left[ \left(1 - \epsilon^{-\frac{\pi^2 a^2 t}{b^2}}\right) - \left(\frac{1 - \epsilon^{-\frac{9\pi^2 a^2 t}{b^2}}}{3^3}\right) + \left(\frac{1 - \epsilon^{-\frac{25\pi^2 a^2 t}{b^2}}}{5^3}\right) - \dots \right] \quad (1)$$

where  $u_c$  = temperature increment at the center, °C (150 - 20 = 130°C)  
 $H$  = gram-cal/(sec)/(cu cm)  
 $b$  = total thickness of material between plates (0.02 cm)  
 $k$  = thermal conductivity: 0.0004 gram-cal/(sec)(sq cm) (°C per cm)  
 $t$  = time (0.125 sec)  
 $c$  = specific heat, 0.4 cal/(°C) (per gram)  
 $\rho$  = density, 1.5 grams per cu cm  
 $a^2$  = thermal diffusivity  
 $= k/c\rho$  (0.00067 sq cm per sec)

Solving Eq. (1)

$$130 = 0.13H \left[ \left(1 - \epsilon^{-2.06}\right) - \left(\frac{1 - \epsilon^{-18.54}}{27}\right) + \left(\frac{1 - \epsilon^{-51.50}}{125}\right) \right]$$

or,  $H = 1,180$  gram-cal/(sec)/(cu cm)

Since power in watts = 4.187 × gram-cal per sec and the volume actually to be heated is 0.002 cu cm, the power required for this volume is

$$4.187 \times 1,180 \times 0.002 = 9.88 \text{ watts}$$

On the basis of similar calculations, curves have been drawn in Fig. 1 showing power requirements for various thicknesses of Vinylite at several bonding speeds. It is assumed that power is confined to a cylindrical volume having a cross-sectional area of 0.1 sq cm and a height of  $b$  cm ranging, in this case, from 0.01 to 0.08 cm. There is an optimum thickness, for a given rate of speed, at which the power requirement is a minimum.

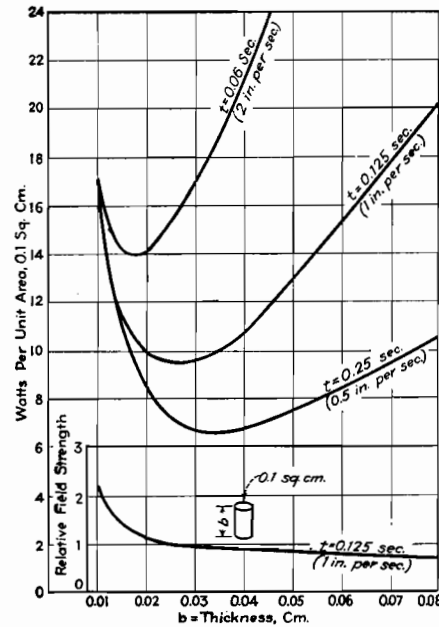


Fig. 1.—Curves showing power requirements and field strength as functions of Vinylite thickness and speed of bonding.

### Heat-conduction Losses

Inspection of the calculations for power requirements with and without heat-conduction loss may lead the casual observer to an erroneous conclusion. Since the cold electrodes require nearly twice the power that is needed when no conduction losses are entailed, it appears inefficient to use a method that conducts so much heat away. But the fact that the outside layers of the material being fused are kept cool prevents the surface from becoming gummy and thus the distortion that would otherwise appear is greatly reduced.

The power dissipated in a cylindrical volume of unit cross-section is expressed by the relation

$$P = \frac{E^2 G}{b} \text{ watts} \quad (2)$$

where  $E$  = voltage  
 $G$  = conductivity  
 $b$  = thickness

In terms of voltage, Eq. (2) becomes

$$E = \sqrt{b} \sqrt{\frac{P}{G}} \text{ volts} \quad (3)$$

Since the field strength  $F = E/b$ , Eq. (3) may be written

$$F = \frac{1}{\sqrt{b}} \sqrt{\frac{P}{G}} \text{ volts per unit thickness} \quad (4)$$

Using a subscript 1 to designate the values that apply to the minimum ordinate in the curves in Fig. 1 and a subscript 2 for values at any other point, Eq. (4) yields this relationship

$$\frac{F_2}{F_1} = \sqrt{\frac{b_1 P_2}{b_2 P_1}} \quad (5)$$

which is plotted in Fig. 1 by the curve showing relative field strength vs. thickness at a sealing rate of 1 in. per sec. Note that as the thickness becomes less than that at the minimum ordinate the power rises rapidly and the possibility of electrical breakdown becomes great.

# Design Chart for R-f Heat-treatment Generators

By EUGENE MITTELMAN

Many vacuum-tube generators for dielectric electronic heating do not produce expected power output because of improper coupling to the load and because of insufficient information about the load impedance. By using the chart, the power absorbed by the load can be quickly determined for normal operating conditions

**T**HE principal difficulty in the design of generators for dielectric heating is due to the characteristic potential distribution in the output circuit of such generators. The actual r-f potential across the object itself is a small fraction of the total h-f voltage across the electrodes. The potential distribution is a rather complicated function of a great number of variables including the wavelength, the capacitance between the electrodes and the object (which in turn is a function of the size of the electrodes, their distance from the object, and the dielectric constant of the space between the electrodes), and the conductivity and dielectric constant of the object itself.

In general, both in the industrial and medical fields of application, the load impedance represented by the object is small compared with the reactances of the coupling capacitances between object and electrodes. Hence the necessity for an excessive h-f voltage across the electrodes for the achievement of a certain required power absorption by the object.

## Chart Design

The chart is designed to give the h-f voltage  $E$  across the electrodes as a function of the distance  $D$  between the object and electrodes for any arbitrary values of the other variables as parameters. The chart may also be used to determine the power dissipated in the load when the area of the electrodes and the load impedance are known. It shows up the limitations of the electrostatic method, especially when large spacing is required. On the other hand, it demonstrates that under favorable conditions considerable power absorption may be obtained even with relatively low values of the h-f voltage across the electrodes. This latter fact is of special importance in the design of some special-purpose generators.

As the maximum available h-f voltage in the tank circuit of an oscillator is about 0.9 of the plate voltage, or 1.8 in

the push-pull type generators, the chart will prove helpful in the proper choice of the oscillator tubes.

## Use of the Chart

Select the lines of desired power absorption and load impedance at the lower left corner of the chart. From their intersection, erect a vertical line and extend upward to the 30-deg line corresponding to the correct electrode area. From this intersection, project horizontally to an intersection with a vertical line drawn through the proper wavelength on the wavelength scale. Through this last intersection point, a 45-deg line extending into the grid of logarithmic scales will give the r-f potential as a function of the electrode spacing. For dielectrics between object and electrodes having constants greater than unity, the readings on the horizontal scale that give the distances between object and electrodes must be divided by the dielectric constant.

## Examples

The correct use of the chart can be best explained by solving several examples.

1. Given a generator with a wavelength of 6 meters and a pair of electrodes 15 sq in. in area, determine the voltage across the electrodes for a 70-ohm load to absorb 50 watts, provided the spacing between object and electrodes is 1 in. on both sides. From line 1 corresponding to this case, we read off 1,600 volts rms. The voltages for other spacings may be taken from the same line.

2. Given the same wavelength and the same geometrical conditions, a load impedance of 8.5 ohms and a desired power absorption of 50 watts, find the r-f voltage across the electrodes. From line 2 we find the voltage must be increased to 3,700 volts rms.

3. The power absorption can be greatly increased even with less r-f voltage across the electrodes if the area of the electrodes is increased. Line 3 corresponds to a 6-meter generator yielding 200 watts

power absorption in a 8.5-ohm load between two electrodes whose area is 45 sq in.

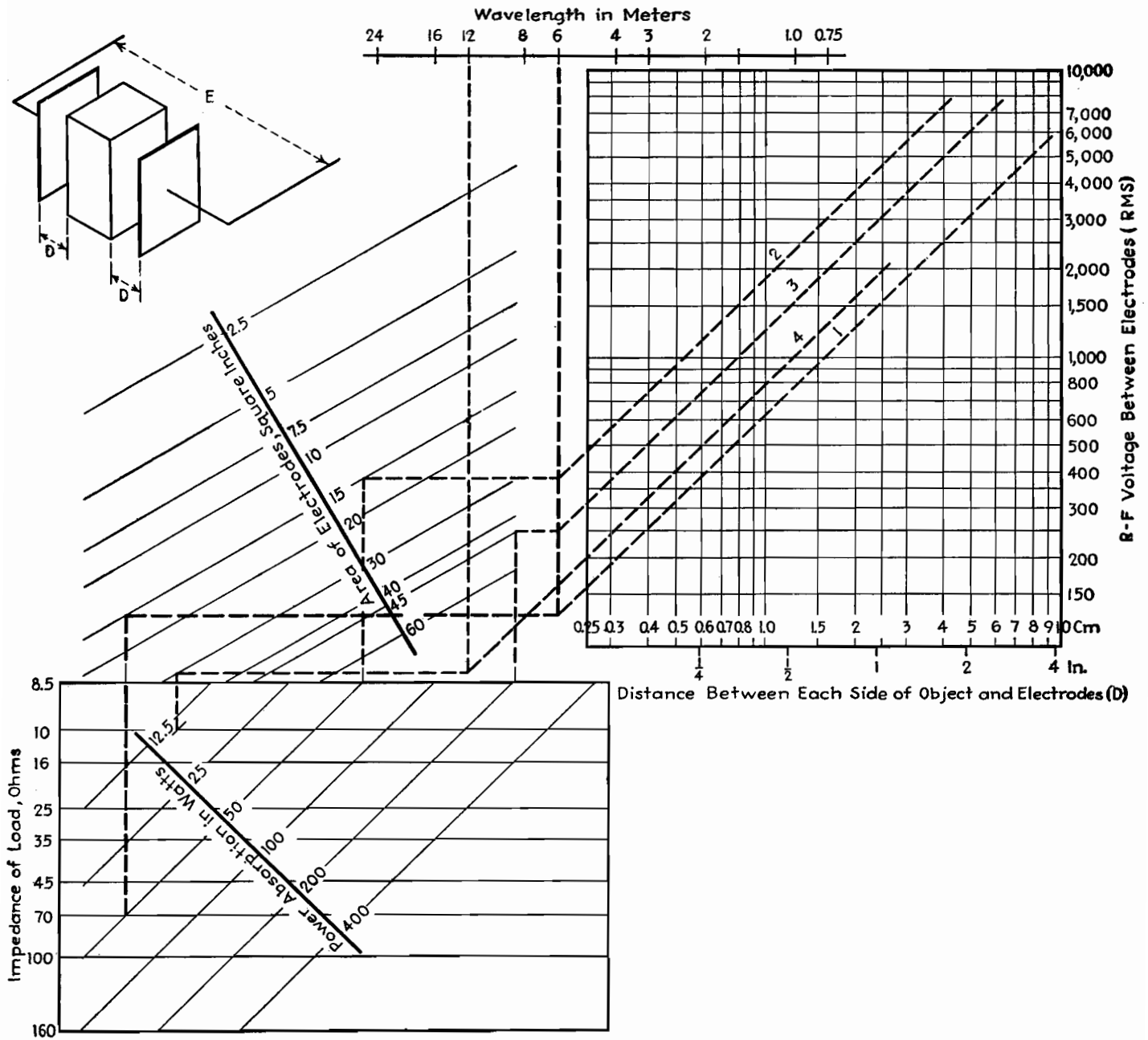
4. With a 12-meter generator, the maximum available r-f voltage with electrodes whose area is 30 sq in. shall be 2,000 volts rms. What power absorption can be expected if a load of 10 ohms equivalent impedance is placed between the electrodes separated by 2.5 cm (1 in.) air spacing on each side of the electrodes?

We find the answer by drawing a straight line at 45 deg through the point corresponding to 2,000 volts and 2.5 cm (1 in.) on the graph (line 4) until it intersects the vertical 12-meter line. From here draw a horizontal to the 30-sq in. line and project down to the 10-ohm line. The power absorption will not exceed about 14 watts.

The physical arrangement of the chart is such that any of the variables can be taken as the independent factors by entering the chart at the right place. This feature is of particular advantage when the exact operating conditions are not known, and when several factors may be varied to obtain the desired power absorption. The manner in which the various factors influence the power absorption is also immediately apparent from the geometry of the chart.

Thus, for example, increasing the area of the electrodes increases the power absorption (all other factors remaining constant) in proportion to the increase in electrode area. Likewise, by halving the wavelength, the power absorption is doubled, if this is the only change in operation. Doubling the distance between electrodes and the object means that the voltage must be doubled to maintain the same power absorption, or, conversely, for a given impedance and power absorption, the voltage of the generator must be doubled if the spacing  $D$  is doubled.

As a result of many actual measurements on practical generators, it has been found that the chart gives results in good agreement with practice.



Nomograph for determining operating conditions of high-frequency generators using capacitor electrodes.

## Design Data for Induction Heating Coils

By GEORGE H. BROWN

Examination of the action occurring in induction heating of metals, including analysis of current distribution in work coil and load, relation between frequency and coupling efficiency, impedance considerations, and discussion of factors affecting choice of frequency

IN INDUCTION heating of metals, the object to be heated is placed in the field of a suitably designed coil that is carrying an alternating current. Cur-

rents are then induced in the object, generating heat without contact. The action is that of a transformer with the secondary short-circuited.

### Equivalent Circuit for Induction Heating

In the circuit of Fig. 1, a coil of inductance  $L_1$  and resistance  $R_1$  is placed across the terminals of a generator that



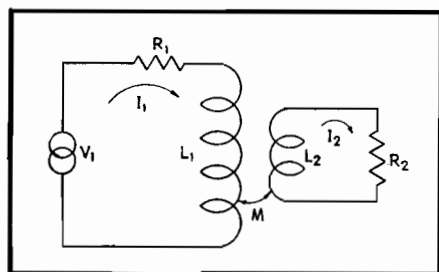


Fig. 1.—Equivalent circuit for induction heating. This is the circuit treated briefly by C. B. Kirkpatrick, "Magnetic Induction Field of Air-core Coils," *Wireless Engr.*, 20, Nos. 239, 378, August, 1943.

is developing a voltage  $V_1$ . The generator may be a rotating machine, a spark-gap oscillator, or a vacuum-tube oscillator. A piece of metal to be heated may be represented as the shorted secondary turn with a resistance  $R_2$  and an inductance  $L_2$ . The circuit equations are

$$V_1 = (R_1 + j\omega L_1)I_1 + j\omega M I_2 \quad (1)$$

$$\text{and } 0 = j\omega M I_1 + (R_2 + j\omega L_2)I_2 \quad (2)$$

where  $f$  is the frequency in cycles per second,  $\omega$  equals  $2\pi f$ , and  $M$  is the mutual inductance in henrys. Elimination between these two equations gives the impedance presented to the terminals of the generator.

$$\begin{aligned} \frac{V_1}{I_1} &= R_1 + j\omega L_1 + \frac{(M)^2}{R_2 + j\omega L_2} \\ &= R_1 + \frac{(\omega M)^2 R_2}{R_2^2 + (\omega L_2)^2} \\ &\quad + j\omega \left[ L_1 - \frac{(\omega M)^2 L_2}{R_2^2 + (\omega L_2)^2} \right] \quad (3) \end{aligned}$$

Thus we see that the primary resistance is increased by the presence of the load or shorted turn, while the inductance of the work coil has decreased.

Let  $Q = \omega L_2 / R_2$ . Then the increase in resistance due to the presence of the metal to be heated is

$$\Delta R_1 = \left( \frac{M}{L_2} \right)^2 R_2 \frac{Q^2}{Q^2 + 1} \quad (4)$$

$$\text{and } \Delta L_1 = - \left( \frac{M}{L_2} \right)^2 L_2 \frac{Q^2}{Q^2 + 1} \quad (5)$$

#### Equations for Efficiency

The efficiency of the heating circuit, i.e., the ratio of the power transferred to

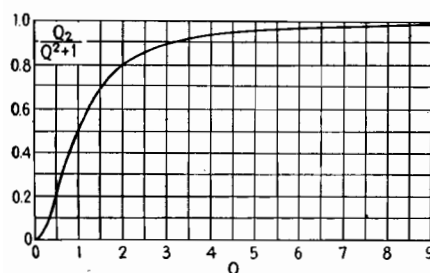


Fig. 2.—Variation of factor in Eq. (6) with  $Q$  of induction-heating secondary circuit.

the work to the total power supplied is

$$\begin{aligned} \text{Efficiency} &= \frac{\Delta R_1}{R_1 + \Delta R_1} \\ &= \frac{\left( \frac{M}{L_2} \right)^2 R_2 \frac{Q^2}{Q^2 + 1}}{R_1 + \left( \frac{M}{L_2} \right)^2 R_2 \frac{Q^2}{Q^2 + 1}} \quad (6) \end{aligned}$$

The  $Q$  of the secondary circuit is generally much larger than unity for most of the frequencies used for induction heating. The variation of the factor  $Q^2 / (Q^2 + 1)$  as a function of  $Q$  is shown in Fig. 2. It is seen that as  $Q$  becomes large, the factor in question approaches unity. If we make this limiting assumption, Eq. (6) becomes

$$\text{Efficiency} = \frac{\left( \frac{M}{L_2} \right)^2 R_2}{1 + \left( \frac{M}{L_2} \right)^2 \frac{R_2}{R_1}} \quad (7)$$

At high frequencies, the current flowing in a conductor tends to concentrate near the surface. The current density drops off exponentially with the depth. A depth  $s$  may be defined as the thickness of a layer of metal which, if it carried uniform current, would present the same resistance as the total metal sheet carrying the exponentially decaying current. Then

$$s \text{ (cm)} = \frac{1}{2\pi \sqrt{10^{-9} \mu_r \sigma f}} \quad (8)$$

where  $\mu_r$  = relative permeability of metal  
 $\sigma$  = conductivity of the metal, mhos for a centimeter cube  
 $f$  = frequency, cycles

Since this layer varies inversely as the square root of the frequency, it may be shown that the resistance varies directly as the square root of the frequency. The preceding statements are predicated on the assumption that the metal in question has a thickness several times greater than the skin thickness  $s$ .

Now, if the metal that is placed in the work coil has a thickness or a diameter that satisfies these requirements, the resistance  $R_2$  which appears in Eq. (7) will vary as the square root of the frequency. However, the same statement holds true for the resistance of the work coil  $R_1$ . In this case, the ratio  $R_2/R_1$  will be simply a constant which is independent of frequency, and the efficiency also becomes independent of frequency.

It should be remembered that we have assumed that  $Q$  is large and that the skin thickness is small compared with the thickness or diameter of the conductors in question. Also, it should be noted that this reasoning cannot be extrapolated

into the extremely high frequencies where capacitance effects must be taken into account.

#### Factors Affecting Choice of Frequency

Since the efficiency is independent of frequency, it is interesting to examine other factors that may influence the choice of frequency. In a vacuum-tube oscillator, the power is limited by the characteristics of the particular vacuum tubes used in the oscillator. Then, for a fixed power and large values of  $Q$ , the current in the primary is

$$\begin{aligned} I_1 &= \sqrt{\frac{P}{R_1 + \Delta R_1}} = \sqrt{\frac{P}{R_1 + \left( \frac{M}{L_2} \right)^2 R_2}} \\ &= \frac{1}{\sqrt{R_1}} \sqrt{\frac{P}{1 + \left( \frac{M}{L_2} \right)^2 \frac{R_2}{R_1}}} \quad (9) \end{aligned}$$

If  $R_2/R_1$  is a constant ratio independent of frequency, the current in the primary for a constant power is inversely proportional to the square root of the primary resistance. But this resistance is directly proportional to the square root of the frequency, so that

$$I_1 \propto \frac{1}{f^{0.25}} \quad (10)$$

Under the assumption we have been making, the inductance at the input terminals is independent of frequency. Also, the reactance at these terminals is generally large compared with the resistance, so that the voltage at the terminals is

$$V_1 = \omega(L_1 + \Delta L_1)I_1 \quad (11)$$

Taking Eq. (10) into consideration, we see that

$$V_1 \propto f^{0.75} \quad (12)$$

We may thus sum up our observations, remembering the assumptions that have been made during the course of the development:

1. The efficiency of power transfer is independent of frequency.
2. The reactance at the input terminals of the work coil varies directly with frequency.
3. The resistance at the terminals of the work coil varies with the square root of the frequency.
4. The current in the work coil, for a constant power input, varies inversely as the one-fourth power of the frequency.
5. The voltage in the work coil, for a constant power input, varies directly as the three-fourths power of the frequency.

To test the foregoing conclusions, experimental data were assembled con-



cerning a coil placed around a vacuum tube. The coil in question was a helix or solenoid, consisting of copper tubing that had a diameter of  $\frac{5}{32}$  in., wound to form 11 turns that were  $2\frac{1}{2}$  in. in diameter. The length of the coil was  $3\frac{1}{4}$  in. The work or object to be heated was an RCA-6A6 vacuum tube.\*

### Experimental Verification

Measurements were first made of coil resistance and reactance with the vacuum tube out. The coil was found to have an inductance of  $2.76 \mu\text{h}$ , which remained essentially constant over the range of frequencies at which measurements were made. The resistance  $R_1$  varied with frequency as shown in Fig. 3. Then the vacuum tube was inserted in the coil and the measurements repeated. The inductance decreased only about  $0.01 \mu\text{h}$ . The new resistance  $R_1 + \Delta R_1$  is shown in Fig. 3.

Efficiency of power transfer is also shown in Fig. 3. This curve was computed directly from the measured values of resistance. We see that the efficiency lies between 72.0 and 78.5 per cent for all frequencies between 1 and 15 Mc.

The current in the coil under load conditions and the voltage across the terminals of the coil are shown in Fig. 4 for the case where the available power is 1,000 watts. The coil current is approximately 50 amp at a frequency of 1 Mc, and decreases to about 20 amp when the frequency has increased to 15 Mc. Since

\* An RCA-6A6 tube was chosen as a convenient load for obtaining these data, but this heating operation was simply a laboratory experiment which had no connection with the manufacture of this type of tube.

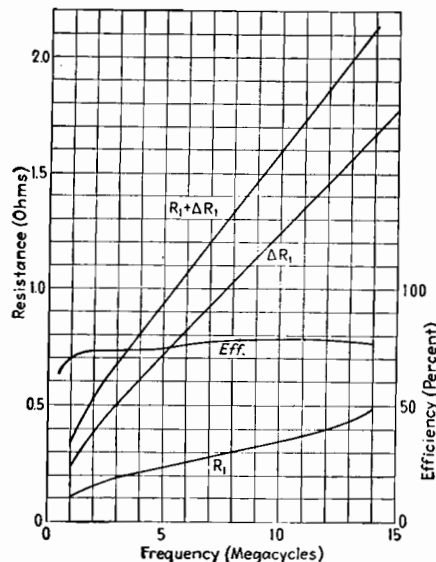


Fig. 3.—Resistance and efficiency data for a work coil used in inductively heating an RCA-6A6 vacuum tube.

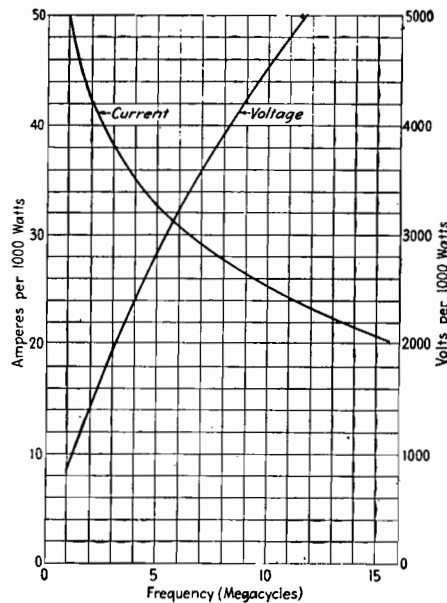


Fig. 4.—Current and voltage values on the work coil used to heat the RCA-6A6 vacuum tube when coil power is 1,000 watts.

Fig. 3 shows that the efficiency is approximately the same at the two frequencies, the coil will not get any hotter with the increased current at the low frequency than it will at the higher frequency with less current. On the other hand, the voltage is less than 1,000 volts at the low frequency while it rises to more than 5,000 volts at 15 Mc.

### Heating a Steel Cylinder

The high voltages shown here are due to the loose coupling. Closer coupling to the work will make  $\Delta L_1$  have a greater numerical value, so that the total reactance will be decreased. This important effect of close coupling will be illustrated by means of another example. The work coil was very similar to the one used for coupling to the RCA 6A6 tube. Copper tubing which had a diameter of  $\frac{5}{32}$  in. was wound to form 11 turns. The total length of the coil was  $3\frac{1}{4}$  in., and the inside diameter of the coil was 4.92 cm. This coil was placed around a steel cylinder which had a diameter of 4.76 cm. Thus the spacing between the coil and the steel cylinder was 0.08 cm.

The measured values of  $R_1$  and  $R_1 + \Delta R_1$  are shown in Fig. 5, together with the calculated value of  $\Delta R_1$ . The efficiency calculated from Eq. (6) is exactly 90 per cent over the range of frequencies at which measurements were made so there is no need to show the results in curve form.

The measured values of reactance with and without the steel cylinder are shown in Fig. 6. Because of the close coupling, the reactance drops a great deal when

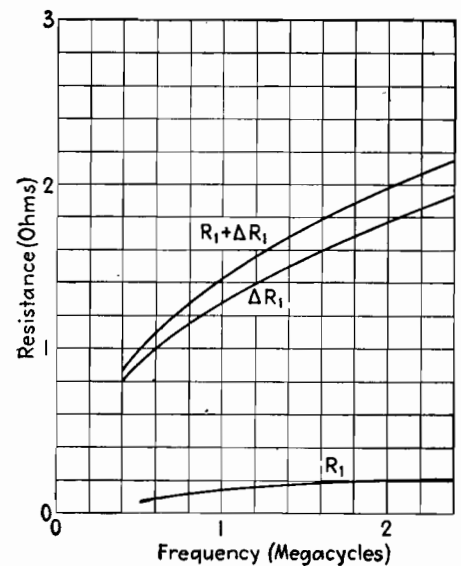


Fig. 5.—Resistance values of multiturn work coil closely coupled to steel load.

the cylinder is inserted. The effect of this is remarkable when the voltage across the coil is considered. Figure 6 shows that this voltage lies between 80 and 160 volts when the operating frequency is between 0.5 and 2.4 Mc. The current in the coil as a function of frequency is also shown in Fig. 6.

### Analysis of Single-turn Coupling Coil

At times, it becomes necessary to couple to a cylinder of metal with a single-turn coil closely spaced to the work. Then the coil impedance is very low and transformers must be used to obtain efficient operation. This is true in many soldering operations and in the practice of scanning for casehardening of steel by self-quenching. Before considering the

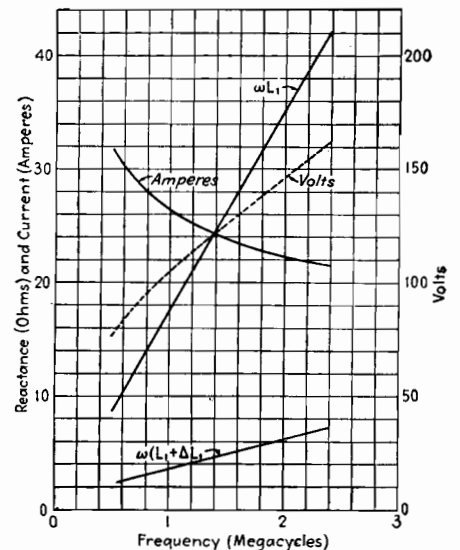


Fig. 6.—Reactance, voltage, and current of multiturn work coil closely coupled to steel load.

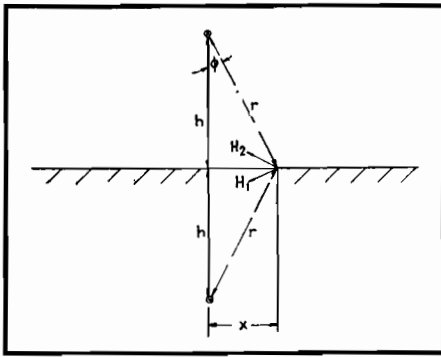


Fig. 7.—Current-carrying conductor above and parallel to a conducting sheet.

transformers that may be used in this operation, it seems desirable to examine the action of the single-turn coupling coil. If the cylinder to be heated is of large diameter, the case may be simplified by treating the problem as a straight conductor parallel to a flat sheet of metal of great thickness.

In Fig. 7, we see a long conductor parallel to a conducting layer and  $h$  units above the layer. This filamentary conductor is carrying current into the paper. For the purpose of computing fields above the metal layer, we place another conductor or image  $h$  units below the surface of the layer. This image is effectively a conductor carrying current out of the paper. At a point  $x$  units along the conducting layer, as shown in Fig. 7, the current-carrying conductor above the metal sheet sets up a magnetic intensity vector  $H_1$  which is at right angles to the line  $r$  drawn from the conductor to the point in question. The magnitude of this magnetic intensity is

$$H_1 = \frac{I}{2\pi r} \quad (13)$$

where  $r = \sqrt{h^2 + x^2}$ . The magnetic intensity due to the image is  $H_2$  and is exactly equal to  $H_1$  in magnitude but

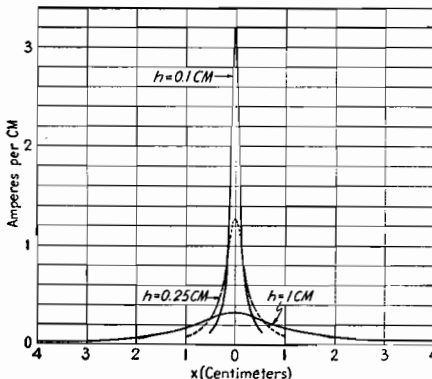


Fig. 8.—Current distribution in a sheet for a filamentary conductor at various heights above the sheet

points in the direction shown in Fig. 7. The vector sum of these two vectors is parallel to the surface of the layer and has a magnitude that is

$$H = 2H_1 \cos \phi = 2h \frac{H_1}{r} \quad (14)$$

Now if the layer is a good conductor, the current in the layer will be concentrated near the surface. Then the current density  $J$  in amperes per centimeter in the little patch shown in Fig. 7, where the patch is of unit width and  $x$  and  $h$  are in centimeters, is

$$J = H = \frac{1}{\pi} \frac{h}{h^2 + x^2} = \frac{I}{\pi h} \frac{1}{1 + \left(\frac{x}{h}\right)^2} \quad (15)$$

#### Current Distribution in Metal Sheet

Figure 8 shows the current distribution in the sheet for a number of values of  $h$ , with the current  $I$  in the conductor, and flowing out of the paper, equal to 1 amp. We see that as the conductor is placed closer to the layer or sheet, the current density increases directly below the conductor, but drops off quickly in a lateral direction.

To sum up all the current in the sheet, integrate Eq. (15) from  $x = -\infty$  to  $x = +\infty$ . Then

$$\begin{aligned} \int_{x=-\infty}^{x=+\infty} J dx &= \frac{2hI}{\pi} \int_{x=0}^{x=\infty} \frac{dx}{h^2 + x^2} \\ &= \frac{2}{\pi} hI \frac{1}{h} \tan^{-1} \left( \frac{x}{h} \right) \Big|_{x=0}^{x=\infty} = I \quad (16) \end{aligned}$$

The total current flowing in the sheet is thus equal to the current assumed to be flowing in the single conductor.

We shall now proceed with a consideration of the losses in the sheet. The current density  $J$  flows out of the paper in a small patch of unit lateral width and of thickness  $s$ . This dimension  $s$  (Fig. 9) is the skin thickness given by Eq. (8). The current flowing out of the patch shown in Fig. 9 is  $J dx$ . The resistance of the patch shown, with a length of 1 cm into the paper, is

$$dR = \frac{1}{\sigma s} dx \quad (17)$$

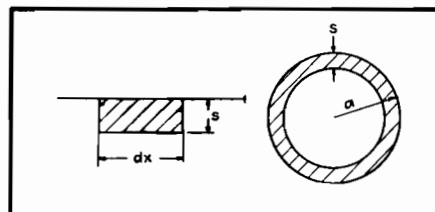


Fig. 9 (left).—Current-carrying patch on the surface of a conducting sheet.

Fig. 10 (right).—Current distribution on a cylindrical conductor far removed from sheet.

The watts lost ( $I^2 R$ ) in this small element is

$$(J dx)^2 dR = \frac{J^2 dx}{\sigma s} \quad (18)$$

If we now substitute Eq. (15) in (18) and integrate from  $x = -\infty$  to  $x = +\infty$ , we have the power lost in the sheet in a slice taken at right angles to the cylindrical conductor, where the thickness of the slice in the direction along the conductor is 1 cm. If  $P_m$  equals the power lost in a 1-cm slice of the metal sheet,

$$\begin{aligned} P_m &= \frac{1}{\sigma s} \int_{x=-\infty}^{x=+\infty} J^2 dx \\ &= \frac{2h^2 I^2}{\pi^2 \sigma s} \int_{x=0}^{x=+\infty} \frac{dx}{(h^2 + x^2)^2} \quad (19) \end{aligned}$$

But

$$\begin{aligned} \int_{x=0}^{x=\infty} \frac{dx}{(h^2 + x^2)^2} &= \frac{1}{2h^3} \tan^{-1} \left( \frac{x}{h} \right) \Big|_{x=0}^{x=\infty} = \frac{\pi}{4h^3} \quad (20) \end{aligned}$$

so that

$$P_m = \frac{I^2}{2\pi \sigma s h} = \frac{I^2}{h} \sqrt{\frac{10^{-9} \mu_m f}{\sigma}} \quad (21)$$

#### Finite Cylindrical Conductor

Since the cylindrical conductor generally has a conductivity and relative permeability different from the metal sheet, we should distinguish between the quantities.

- Let  $\sigma_m$  = conductivity of the metal sheet
- $\sigma_c$  = conductivity of the current-carrying conductor placed parallel to the sheet
- $\mu_m$  = relative permeability of the metal sheet
- $\mu_c$  = relative permeability of the current-carrying conductor

Then Eq. (21) should be

$$P_m = \frac{I^2}{h} \sqrt{\frac{10^{-9} \mu_m f}{\sigma_m}} \quad (22)$$

If the conductor of radius  $a$  is placed far enough from the sheet so that the presence of the sheet does not alter the current distribution on the conductor, the current on the conductor will flow in a thin layer  $s$  equal to the skin thickness (Fig. 10). Then the power lost in a centimeter of conductor is

$$P_c = \frac{I^2}{2\pi a s \sigma_c} = \frac{I^2}{a} \sqrt{\frac{10^{-9} \mu_c f}{\sigma_c}} \quad (23)$$

and the ratio of the power spent in the metal sheet to the power lost in the conductor is

$$\frac{P_m}{P_c} = \frac{a}{h} \sqrt{\frac{\mu_m \sigma_c}{\mu_c \sigma_m}} \quad (24)$$

Before interpreting Eq. (24), examine the effect of the altered current distri-

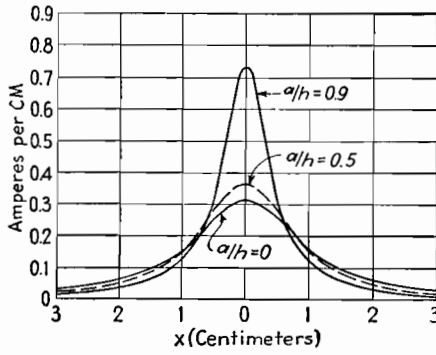


Fig. 11.—Current distribution in the conducting sheet when the conductor has a finite radius and  $h = 1.0$  cm.

bution on the sheet and on the conductor due to close spacing.

When the conductor has a finite radius  $a$  with the axis of the conductor a distance  $h$  above the metal sheet, the fields external to the conductor may be computed by replacing the cylindrical conductor by a filament carrying the current  $I$  at a new height  $h'$  where

$$h' = \sqrt{h^2 - a^2} = h \sqrt{1 - \left(\frac{a}{h}\right)^2} \quad (25)$$

The effect on the current density in the metal sheet may be studied by substituting  $h'$  for  $h$  in Eq. (15). Then

$$J \text{ (amp per cm)} = \frac{I}{\pi h} \frac{\sqrt{1 - \left(\frac{a}{h}\right)^2}}{1 - \left(\frac{a}{h}\right)^2 + \left(\frac{x}{h}\right)^2} \quad (26)$$

The current density distribution is shown in Fig. 11 for a number of values of the radius, where the height of the conductor is equal to 1 cm. Increasing the radius of the cylinder has the same effect as bringing a thin filament closer to the metal sheet.

The power loss in the metal sheet may be obtained by substituting  $h'$  for  $h$  in

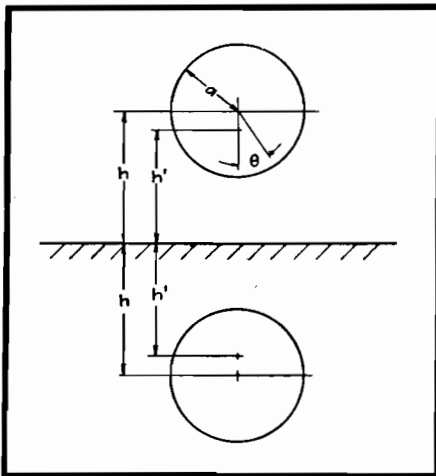


Fig. 12.—Cross-section of cylindrical conductor and image in the sheet.

Eq. (22), with the result that

$$P_m = \frac{I^2}{h} \sqrt{\frac{10^{-9} \mu_m f}{\sigma_m}} \frac{1}{\sqrt{1 - \left(\frac{a}{h}\right)^2}} \quad (27)$$

#### Current Distribution in the Cylinder

The current distribution around the surface of the cylindrical conductor may be obtained by using the construction of Fig. 12. By means of a tedious algebraic construction, it may be shown that the current density on the surface of the conductor, confined to a layer  $s_c$  cm in thickness, is

$$J \text{ (amp per radian)} = \frac{I}{2\pi} \frac{\sqrt{1 - \left(\frac{a}{h}\right)^2}}{1 - \frac{a}{h} \cos \theta} \quad (28)$$

By substituting 360 deg for  $2\pi$  radians in Eq. (28), we may express the current density in amperes per degree. This has been done in constructing the curves of Fig. 13. The current-density distribution depends only on the ratio of radius to height. When the conductor is brought very close to the metal sheet, the current on the conductor crowds around to the side closest to the sheet.

The power loss in the conductor is found by integrating the  $I^2 R$  loss around the circumference of the conductor. Then

$$\begin{aligned} P_c &= 2 \int_{\theta=0}^{\theta=\pi} \frac{(J d\theta)^2}{\sigma_c s_c a d\theta} \\ &= \frac{I^2}{2\pi^2 a \sigma_c s_c} \left[ 1 - \left(\frac{a}{h}\right)^2 \right] \int_{\theta=0}^{\theta=\pi} \frac{d\theta}{\left[ 1 - \frac{a}{h} \cos \theta \right]^2} \quad (29) \end{aligned}$$

The integral itself is equal to

$$\frac{\pi}{1 - \left(\frac{a}{h}\right)^2} \frac{1}{\sqrt{1 - \left(\frac{a}{h}\right)^2}}$$

so that

$$\begin{aligned} P_c &= \frac{I^2}{2\pi a s_c \sigma_c} \frac{1}{\sqrt{1 - \left(\frac{a}{h}\right)^2}} \\ &= \frac{I^2}{a} \sqrt{\frac{10^{-9} \mu_c f}{\sigma_c}} \frac{1}{\sqrt{1 - \left(\frac{a}{h}\right)^2}} \quad (30) \end{aligned}$$

If we now divide Eq. (27) by Eq. (30), we obtain

$$\frac{P_m}{P_c} = \frac{a}{h} \sqrt{\frac{\mu_m \sigma_c}{\mu_c \sigma_m}} \quad (31)$$

It is a somewhat surprising fact that this result is identical with the result shown in Eq. (24) which was deduced from simple assumptions that did not take into account the redistribution of current due to the finite conductor size.

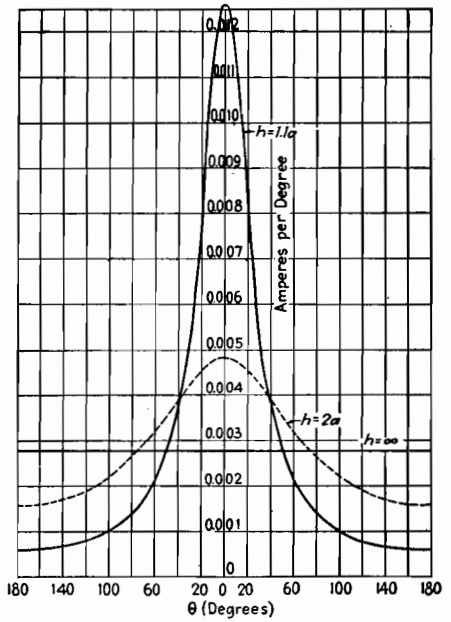


Fig. 13.—Current distribution on the cylindrical conductor occasioned by the presence of the metal sheet.

Since in inductive heating the coupling coil is usually made of copper, the relative permeability  $\mu_c$  may be set equal to unity for simplicity. The efficiency is obtained from Eq. (31) in the following manner:

$$\begin{aligned} \text{Efficiency} &= \frac{P_m}{P_m + P_c} = \frac{1}{1 + \frac{P_c}{P_m}} \\ &= \frac{1}{1 + \frac{h}{a} \sqrt{\frac{\sigma_m}{\mu_m \sigma_c}}} \quad (32) \end{aligned}$$

#### Efficiency Curves

Figure 14 shows the variation of efficiency with the ratio  $a/h$ . The need for close conductor spacing is readily seen. Figure 15 shows the efficiency curves replotted as a function of  $\mu_m \sigma_c / \sigma_m$ . The conductivity of the conductor is important in determining the coupling

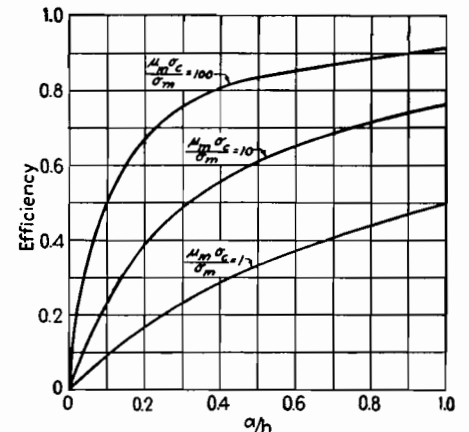


Fig. 14.—Coupling efficiency of cylindrical conductor parallel to a metal sheet.

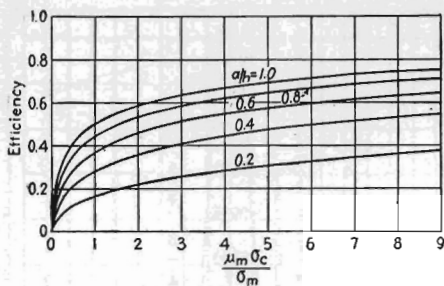


Fig. 15.—Coupling efficiency as a function of conductivity.

efficiency. Where a copper conductor is used to couple to iron, the coupling efficiency may become high. However, it is sometimes necessary to heat a copper article by induction. At the start of the heating cycle, the ratio  $\sigma_c/\sigma_m$  is unity ( $\mu_m = 1$  for copper). From Fig. 15, we see that the best possible efficiency is 0.5 when the radius of the conductor is equal to the height above the sheet. However, for practical purposes  $a/h$  is less than unity, so that the coupling efficiency will be less than 50 per cent at the start of heating. Fortunately, the picture does not continue to be so gloomy. The coupling coil or conductor is usually hollow tubing through which cooling water flows, so that the conductivity of the conductor does not change as time passes. The load begins to heat so that its conductivity decreases. This results in an improvement in efficiency so that the conductivity decreases still faster, and soon the efficiency assumes reasonable proportions.

If the heating coil is wrapped around a cylindrical load that has a radius many times larger than the diameter of the conductor that makes up the coil and is large compared with the spacing between the coil and the work, we may use these results obtained for a conductor parallel to a flat sheet. If the circumference of the load is  $C$  cm, the resistance of a single-turn coil may be obtained from Eqs. (27) and (30). This resistance is

$$R = \frac{C}{a} \frac{\sqrt{10^{-9}f/\sigma_c}}{\sqrt{1 - (a/h)^2}} \left(1 + \frac{a}{h} \sqrt{\frac{\mu_m \sigma_c}{\sigma_m}}\right) \quad (33)$$

#### Characteristic Impedance of Load

To obtain the reactance, we must first have available the expression for the characteristic impedance of the conductor over the flat sheet. This is

$$Z_c = 60 \log_e \left\{ \left(\frac{h}{a}\right) \left[1 + \sqrt{1 - \left(\frac{a}{h}\right)^2}\right] \right\} \quad (34)$$

This characteristic impedance as a function of  $a/h$  is shown in Fig. 16.

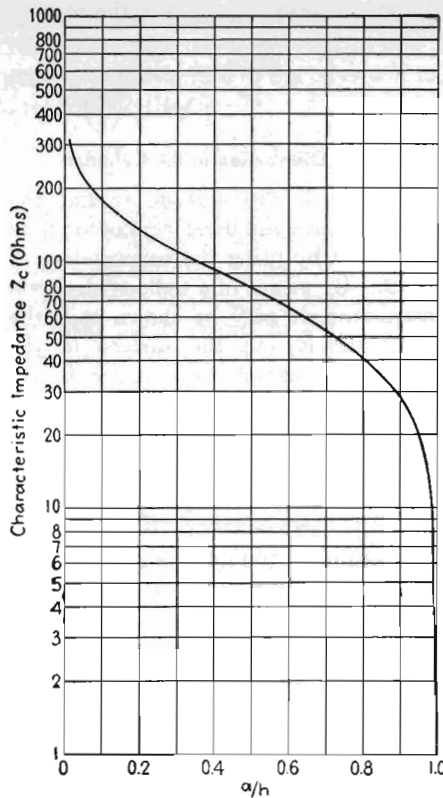


Fig. 16.—Characteristic impedance of cylinder parallel to metal sheet.

#### Summary of Data in Example for Three Values of $h$

$h$ , cm.....	0.44	0.54	0.64
Efficiency, %.....	84.2	81.4	78.5
$R$ , ohms.....	0.0195	0.0156	0.0131
$Z_c$ , ohms.....	73	87	97
$X$ , ohms.....	0.23	0.273	0.304
$I$ , amp for 1,000 watts.....	226	253	276
$V$ , volts for 1,000 watts.....	52	69	84
$I$ , amp for 100,000 watts.....	2,260	2,530	2,760
$V$ , volts for 100,000 watts.....	520	691	840

The single-turn coil around the load is usually fed in push-pull. Then the mid-point of the coil is at ground potential. The reactance between one terminal of the coil and the work is then the characteristic impedance multiplied by the tangent of the electrical length of the semi-circumference. The total reactance is twice this value. That is,

$$X = 2Z_c \tan \left( \frac{2\pi C}{\lambda} \frac{C}{2} \right) \cong \frac{2\pi CZ_c}{\lambda} = \frac{2\pi f Z_c C}{3 \times 10^{10}} \quad (35)$$

Thus we have at hand the necessary formulas for computing the efficiency, resistance, reactance, current, and voltage. A casual inspection of these equations will reveal that the five conclusions

reached early in the paper are sustained, within the limits of the restrictions placed on dimensions.

#### Example

The magnitude of values encountered when a single-turn coil is used will be shown by means of an example. The following constants will be used:

- $C = 15.0$  cm
- $a = 0.24$  cm
- $h = 0.44$  cm
- $\sigma_c$  = conductivity of copper coil = 580,000 mhos for a cm cube
- $\sigma_m$  = conductivity of hot steel—6,000 mhos for a cm cube
- $\mu_m$  = unity for steel above the Curie point
- $f = 10^6$  cycles

From Eq. (32), we find that the efficiency is 84.2 per cent. Substituting the numerical values in Eq. (33) gives a resistance of 0.0195 ohm, with a current of 226.0 amp for a power of 1,000 watts.

Since  $a/h$  is 0.545, Fig. 16 gives 73 ohms for the characteristic impedance. Then Eq. (35) shows that the reactance is 0.23 ohm. This reactance multiplied by the current gives a voltage across the terminals of the coil of 52 volts.

The table gives a summary of these data for a few values of  $h$ . It may be seen that increasing  $h$  results in a slight increase in the current to be handled and a sharp increase in the voltage appearing at the terminals of the coil. Values of current and voltage for an operating power of 100,000 watts are also shown in this table. The current is far in excess of the values of tank circuit current that may be obtained so that it is virtually

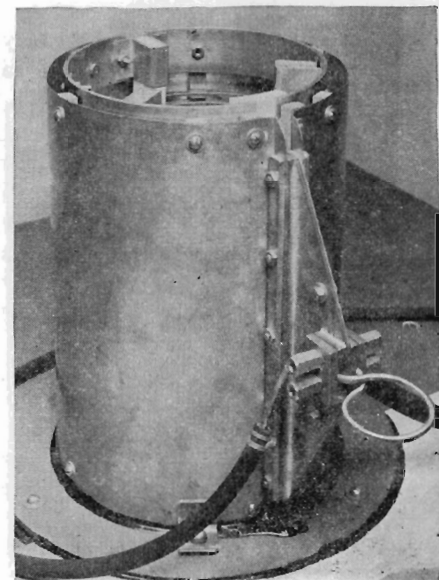


Fig. 17.—A current transformer which is useful for inductive heating.

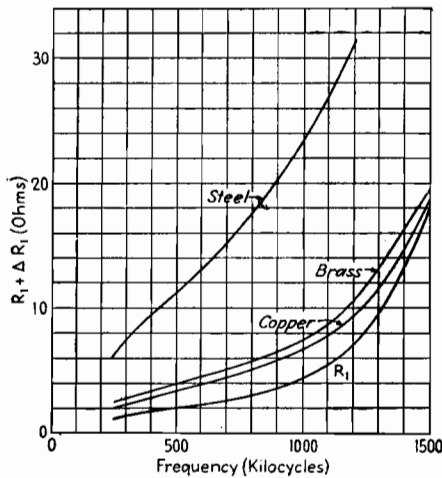


Fig. 18.—Input resistance of transformer with copper, brass, and steel loads. The curve marked  $R_1$  is the no-load resistance.

impossible to place this coil directly in the tank circuit.

#### Output Transformer

A transformer that has been extremely useful in working into low-impedance loads of the type being considered here is pictured in Fig. 17. This transformer consists of a multiturn primary which is part of the tank circuit and a single-turn secondary which is really a sheet of copper wrapped around the primary with as close a spacing to the primary as is consistent with voltage requirements. Where the single-turn coil presents resistance values of the order of a few hundredths of an ohm and reactance values of a few tenths, the resistance looking into the primary of

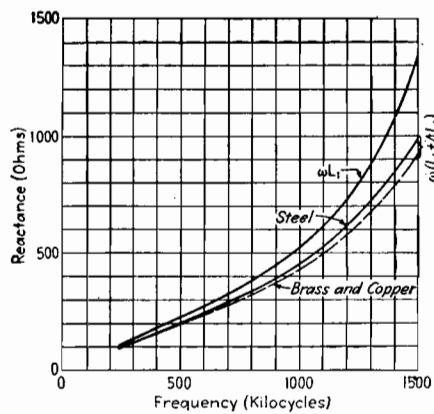


Fig. 19.—Input reactance of transformer with copper, brass, and steel loads. The curve marked  $\omega L_1$  is the no-load reactance.

the transformer may be several ohms, while the input reactance may be several hundred ohms.

Measurements of input resistance and reactance as well as efficiency were made on a transformer similar to the one shown in Fig. 17. The primary consisted of 31 turns. The secondary copper sheet fed into a single-turn coil which encircled a cylinder. Copper, brass, and steel cylinders were used. Figure 18 shows the values of resistance for the three cylinders as well as the resistance measured when no cylinder was in the single-turn coil. The accompanying reactance values are shown in Fig. 19, while the efficiency curves are given in Fig. 20. The efficiency into a steel load is very good, while the efficiencies with copper and brass loads approach the maximum values that

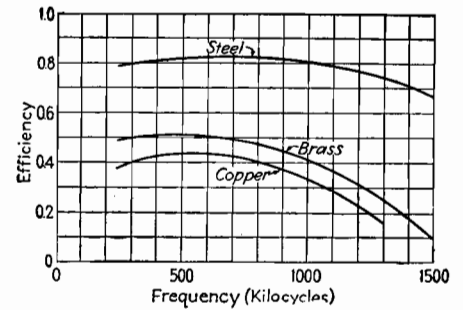


Fig. 20.—Efficiency of coupling to copper, brass, and steel by means of a transformer.

may be expected. The dropping off in efficiency at the higher frequencies is due to resonance effects in the transformer, brought about by distributed capacitance. The efficiency at the higher frequencies can be improved by the proper change in the design of the transformer. However, there is really very little need for this redesign because of the fact that in most metal heating applications there is no point in using frequencies higher than a few hundred kilocycles.

In conclusion, it may be well to restate that, while the simplifying assumptions made here show that the efficiency of coupling to metal loads is independent of frequency, factors such as distributed capacitance come into play at the higher frequencies. At the lower frequencies, the skin thickness may be of the same order of magnitude as the dimensions of the object to be heated, with a consequent sharp reduction in efficiency. This latter effect is partially explained by a consideration of Eq. (6) and Fig. 2.

## Magnetic Field Equations for Induction Heating Coils

By GEORGE H. BROWN

An abstract of the most important parts of Kirkpatrick's paper,\* with some of the equations modified to make them more generally useful. Thus, magnetic intensity is expressed in ampere-turns per centimeter rather than the flux density in gauss

IN THE practice of induction heating, the coils that are used to induce cur-

\* KIRKPATRICK, C. B., The Magnetic Induction Field of Air Core Coils and Its Application to High-frequency Heating in Valve Manufacture, *A.W.A. Tech. Rev. (Australia)*, 5, No. 6, pp. 229-250, December, 1941. Reprinted in *Wireless Engr.*, August, 1943, pp. 372-382.

rents in the work are, in general, small compared with the wavelength. In this restricted case, it is then possible to neglect the radiation term in the magnetic field distribution. That is, in formulating the magnetic field intensity from the well-

known vector potential, it is not necessary to retard the potential; the phase delay due to the finite velocity of propagation of the waves may be neglected. Then the magnetic field intensity distribution expressions are independent of frequency.

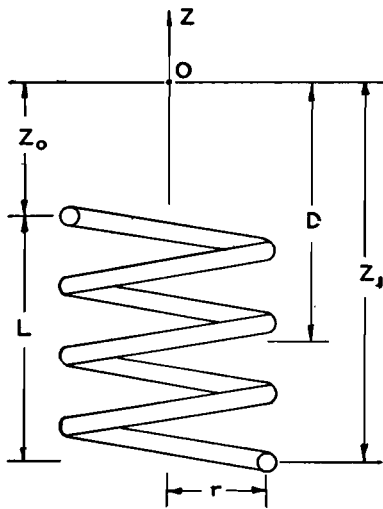


Fig. 1.—Helical heating coil.

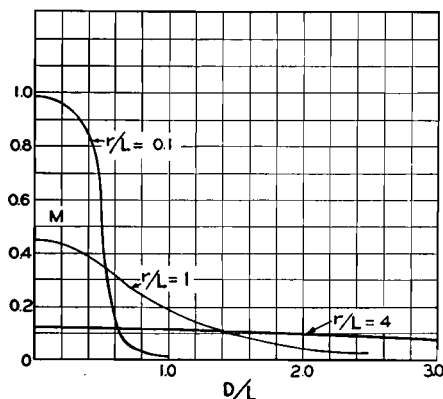
Kirkpatrick has made use of this fact to develop expressions for the magnetic field intensities along the axis of a number of coils which are of interest in induction heating of vacuum-tube parts.

First, consider the circular helix of Fig. 1. On the axis of the coil, at the point *O*, the strongest component of magnetic intensity is along the axis. This component of magnetic intensity is along the axis. This component is

$$H_z \text{ (ampere-turns per cm)} = \frac{nI}{2} \left( \frac{Z_1}{\sqrt{Z_1^2 + r^2}} - \frac{Z_0}{\sqrt{Z_0^2 + r^2}} \right) \quad (1)$$

where *n* = pitch of the coil in turns per cm  
*N* = total number of turns on coil  
*L* = length of coil, cm  
*N* = *nLr* = radius of coil, cm  
*Z*<sub>0</sub> = distance from near end of coil to point *O*, cm  
*Z*<sub>1</sub> = distance from far end of coil to point *O*, cm  
*I* = current in coil amp

(It should be noted that *Z*<sub>0</sub> should be regarded algebraically. When the point *O* moves into the coil, *Z*<sub>0</sub> becomes negative.)

Fig. 2.—Variation of the factor *M*, given in Eq. (5).

If we measure distance from the center of the coil to point *O* and call this distance *D*, Eq. (1) may be rewritten in a more useful form

$$H_z = \frac{nI}{2} \left[ \frac{\left(D + \frac{L}{2}\right)}{\sqrt{\left(D + \frac{L}{2}\right)^2 + r^2}} - \frac{\left(D - \frac{L}{2}\right)}{\sqrt{\left(D - \frac{L}{2}\right)^2 + r^2}} \right] \\ = \frac{NI}{2L} \times \left[ \frac{\left(D + \frac{L}{2}\right)}{\sqrt{\left(D + \frac{L}{2}\right)^2 + r^2}} - \frac{\left(D - \frac{L}{2}\right)}{\sqrt{\left(D - \frac{L}{2}\right)^2 + r^2}} \right] \quad (2)$$

The product *NI* has been introduced because of the fact that, with loose coupling to the load, the total ampere-turns in the coil are determined by the particular vacuum tubes used in the oscillator. That is, the current in the primary tank circuit of the oscillator depends on tube characteristics, but this current may be stepped up in the work coil by means of suitably designed transformers.

The magnetic intensity at the exact center of the helix may be determined from Eq. (2) by setting *D* equal to zero. Then

$$H_z = \frac{NI}{\sqrt{L^2 + 4r^2}} \quad (3)$$

To examine the variation of magnetic intensity as we move along the axis, we need only investigate the behavior of a factor *M* where

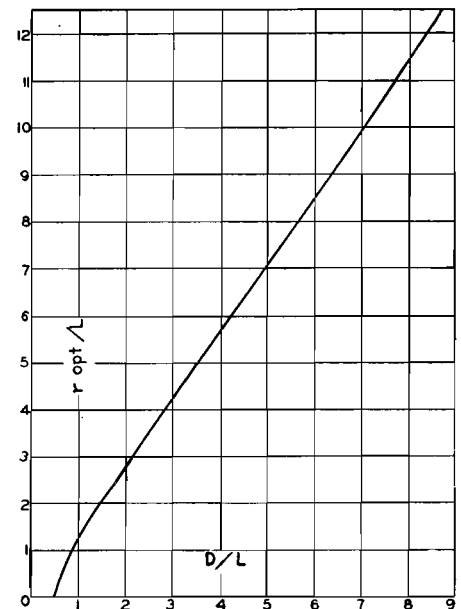
$$H_z = M \times \frac{NI}{L} \quad (4)$$

and

$$M = \frac{1}{2} \left[ \frac{\left(\frac{D}{L} + \frac{1}{2}\right)}{\sqrt{\left(\frac{D}{L} + \frac{1}{2}\right)^2 + \left(\frac{r}{L}\right)^2}} - \frac{\left(\frac{D}{L} - \frac{1}{2}\right)}{\sqrt{\left(\frac{D}{L} - \frac{1}{2}\right)^2 + \left(\frac{r}{L}\right)^2}} \right] \quad (5)$$

The variation with *M* as a function of *D/L* is shown in Fig. 2, for a number of values of *r/L*. We see from these curves that a large coil radius results in low values of magnetic intensity within the coil, with a slow falling off as we move away from the coil, while a coil of small radius yields high intensities within the coil with a sharp decline as we move out of the coil.

It is interesting to examine Eq. (5) to determine an optimum value of the radius

Fig. 3.—The optimum value of the radius of a helical coil as a function of the dimension *D*, with the coil length fixed.

*r* when the distance *D* is fixed. Equation (5) is then differentiated with respect to *r* and the result set equal to zero. This yields the optimum value of *r*

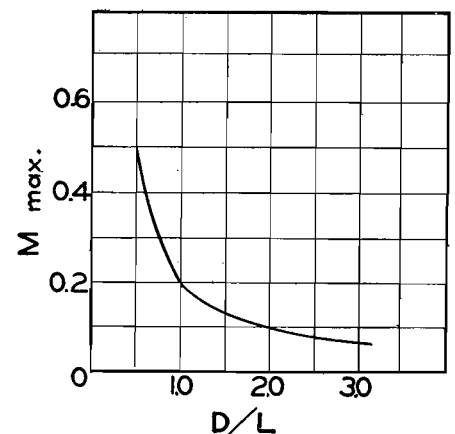
$$r_{\text{opt}}/L = \left[ \left(\frac{D}{L} - \frac{1}{2}\right) \left(\frac{D}{L} + \frac{1}{2}\right) \right]^{1/4} \left[ \left(\frac{D}{L} - \frac{1}{2}\right)^{3/4} + \left(\frac{D}{L} + \frac{1}{2}\right)^{3/4} \right]^{1/2} \quad (6)$$

The optimum value of *r/L* as a function of *D/L* is shown in Fig. 3. It is seen that for values of *D/L* greater than 2, the optimum value of *r/L* is

$$\frac{r}{L} = \sqrt{2} \frac{D}{L} \quad (7)$$

Figure 4 shows the maximum values of *M* that may be obtained, when the conditions of Eq. (6) prevail.

At times, when a metal part inside a vacuum tube is to be heated, the limiting

Fig. 4.—Maximum values of the factor *M*, when the optimum radii shown in Fig. 3 are used.



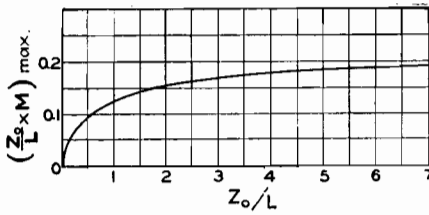


Fig. 5.—Maximum field factor when spacing to work is fixed.

factor in coil spacing is determined by the location of the metal part in the glass envelope. This fixes the dimension  $Z_0$  in Fig. 1. Then we may rewrite Eq. (4) as

$$H_z = \frac{NI}{Z_0} \frac{Z_0}{L} M \quad (8)$$

Remembering that  $Z_0/L$  equals  $(D/L) - 0.5$  and making use of the maximum of  $M$  shown in Fig. 4, Fig. 5 was constructed, which shows the maximum value of the factor  $(Z_0/L)M$  where the radius has been made to be optimum in accordance with Fig. 3. This curve shows that the maximum intensity is obtained by making  $Z_0/L$  as large as possible. Since  $Z_0$  is fixed, we must make  $L$  very small. This indicates that a single-turn coil with a radius equal to  $\sqrt{2} Z_0$  is the proper choice for maximum intensity. In this limiting case, the magnetic intensity is

$$H_z = \frac{0.1925I}{Z_0} \quad (9)$$

The action of a single-turn coil may be studied by setting  $N$  equal to unity in Eq. (2) and placing  $L$  equal to zero in the same equation. This makes the equation indeterminate, but differentiating numerator and denominator results in the following expression:

$$H_z = \frac{I}{2D} \frac{(r/D)^2}{[1 + (r/D)^2]^{3/2}} \quad (10)$$

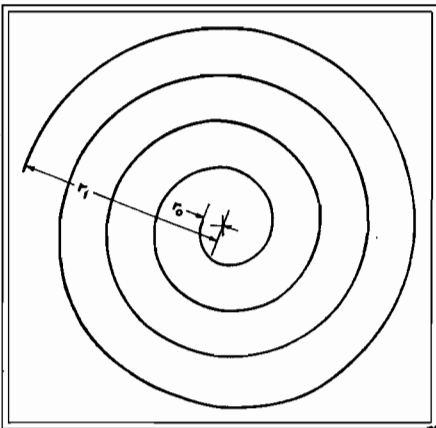


Fig. 6.—An equidistant spiral, sometimes called the spiral of Archimedes, for the special case  $r_0/r_1$  equal to 0.1 and  $N$  equal to 4.

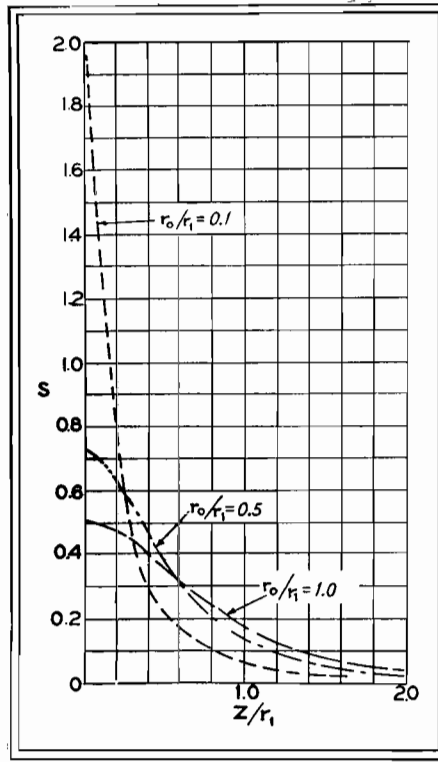


Fig. 7.—Variation of the factor  $Q$  of an Archimedes spiral as a function of  $Z/r_1$  for a number of values of  $r_0/r_1$ .

We have seen that the single-turn coil may be useful for getting close to the work. There are, however, applications in which the field should be spread over a surface where the single turn may afford too much concentration. Also, where adequate transformers are not available, it may be desirable to use a flat multiturn coil to provide the necessary number of ampere-turns. A coil of this type which lends itself to analysis is the equidistant spiral or the spiral of Archimedes. Here a point moving on the coil travels so that the radial distance to the center is linearly proportional to the angle of rotation.

Let  $r_1$  = maximum radius of outer turn,  $r_0$  = minimum radius of inner turn,

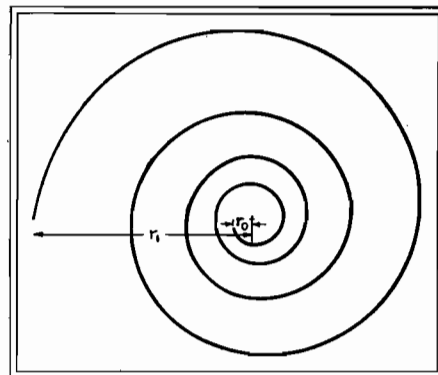


Fig. 8.—An equiangular spiral for the special case  $r_0/r_1$  equal to 0.1 and  $N$  equal to 4.

$N$  = total number of turns, and  $r$  = radius at angle  $\theta$  where  $\theta$  is measured in radians. Then

$$\frac{r}{r_1} = \frac{\theta}{2\pi N} \left(1 - \frac{r_0}{r_1}\right) \quad (11)$$

Figure 6 shows a spiral of Archimedes where  $r_0/r_1 = 0.1$  and  $N = 4$ . The magnetic intensity in the  $Z$  direction on the  $Z$  axis is given by

$$H_z = \frac{NI}{r_1} \frac{1}{2 \left(1 - \frac{r_0}{r_1}\right)} \times \left\{ \log_e \left[ \frac{1 + \sqrt{1 + \left(\frac{Z}{r_1}\right)^2}}{\frac{r_0}{r_1} + \sqrt{\left(\frac{Z}{r_1}\right)^2 + \left(\frac{r_0}{r_1}\right)^2}} \right] - \frac{1}{\sqrt{1 + \left(\frac{Z}{r_1}\right)^2}} + \frac{\frac{r_0}{r_1}}{\sqrt{\left(\frac{r_0}{r_1}\right)^2 + \left(\frac{Z}{r_1}\right)^2}} \right\} \quad (12)$$

When  $r_0/r_1$  is not zero, and  $Z$  is equal to zero,

$$H_z = \frac{NI}{r_1} \frac{1}{2 \left(1 - \frac{r_0}{r_1}\right)} \log_e \left(\frac{r_1}{r_0}\right) \quad (13)$$

When  $r_0$  is zero, but  $Z$  is not equal to zero,

$$H_z = \frac{NI}{r_1} \times \frac{1}{2} \left\{ \log_e \left[ \frac{1 + \sqrt{1 + \left(\frac{Z}{r_1}\right)^2}}{\left(\frac{Z}{r_1}\right)} \right] - \frac{1}{\sqrt{1 + \left(\frac{Z}{r_1}\right)^2}} \right\} \quad (14)$$

It is convenient to write Eq. (12)

$$H_z = Q \times \frac{NI}{r_1} \quad (15)$$

where

$$Q = \frac{1}{2 \left(1 - \frac{r_0}{r_1}\right)} \left\{ \log_e \left[ \frac{1 + \sqrt{1 + \left(\frac{Z}{r_1}\right)^2}}{\frac{r_0}{r_1} + \sqrt{\left(\frac{Z}{r_1}\right)^2 + \left(\frac{r_0}{r_1}\right)^2}} \right] - \frac{1}{\sqrt{1 + \left(\frac{Z}{r_1}\right)^2}} + \frac{\frac{r_0}{r_1}}{\sqrt{\left(\frac{r_0}{r_1}\right)^2 + \left(\frac{Z}{r_1}\right)^2}} \right\} \quad (16)$$

The variation of  $Q$  as a function of  $Z/r_1$  for a number of values of  $r_0/r_1$  is shown in Fig. 7. It should be noted that setting  $r_0/r_1$  equal to unity is the equivalent of a single closed turn of constant radius.

The equiangular spiral is a flat coil so wound that the conductor at any point makes a constant angle  $\beta$  with the radius vector. Under this condition,

$$r \frac{d\theta}{dr} = \tan \beta \quad (17)$$



where  $\theta$  is the reference angle. Integration of Eq. (17) yields

$$r = K\epsilon^{\theta \cot \beta} \quad (18)$$

At  $\theta = 0$ , the start of the coil  $r = r_o$ , where  $r_o$  is the minimum radius of the inner turn.

Therefore

$$K = r_o \text{ and } r = r_o \epsilon^{\theta \cot \beta} \quad (19)$$

The greatest value of  $\theta$  is at the outer end of the coil. Here  $\theta = 2\pi N$ , where  $N$  is the total number of turns on the coil. At this point  $r = r_1$ . Then Eq. (19) becomes

$$r_1 = r_o \epsilon^{2\pi N \cot \beta} \quad (20)$$

$$\text{and } \cot \beta = \frac{1}{2\pi N} \log \epsilon \frac{r_1}{r_o} \quad (21)$$

Under these boundary conditions, Eq. (18) becomes

$$\frac{r}{r_1} = \frac{r_o}{r_1} \epsilon^{\frac{\theta}{2\pi N} \log \epsilon \frac{r_1}{r_o}} \quad (22)$$

$$\text{or } \frac{r}{r_1} = \frac{r_o}{r_1} \left( \frac{r_1}{r_o} \right)^{\frac{\theta}{2\pi N}} \quad (23)$$

A spiral of this type, with  $r_o/r_1 = 0.1$  and  $N = 4$ , is shown in Fig. 8.

Then the magnetic intensity on the  $Z$  axis is

$$H_z = S \times \frac{NI}{r_1} \quad (24)$$

where

$$S = \frac{1}{2 \log \epsilon \left( \frac{r_1}{r_o} \right)} \left[ \frac{1}{\sqrt{\left( \frac{Z}{r_1} \right)^2 + \left( \frac{r_o}{r_1} \right)^2}} - \frac{1}{\sqrt{\left( \frac{Z}{r_1} \right)^2 + 1}} \right] \quad (25)$$

When  $Z = 0$ , Eq. (25) becomes

$$S = \frac{1}{2 \log \epsilon \left( \frac{r_1}{r_o} \right)} \left( \frac{r_1}{r_o} - 1 \right) \quad (26)$$

For large values of  $Z$ , a good approximation for Eq. (25) is

$$S = \frac{1 - \left( \frac{r_o}{r_1} \right)^2}{4 \log \epsilon \left( \frac{r_1}{r_o} \right)} \left( \frac{r_1}{Z} \right)^3 \quad (27)$$

When  $r_o/r_1 = 1$ , the spiral becomes a single-turn coil of constant radius, and Eq. (25) reduces to Eq. (10).

The variation of  $S$ , in Eq. (25), as a function of  $Z/r_1$  is shown in Fig. 9. Comparison with Fig. 7 shows that there is no striking difference between the field from an Archimedes spiral and an equiangular spiral. Both of these figures show that if high field concentration is desired on the axis close to the plane of the coil, small

values of  $r_o/r_1$  should be used, while values of  $r_o/r_1$  close to unity give the greatest field at large distances from the plane of the coil. Actually in practice, a spiral coil would not be used unless it could be placed close to the work.

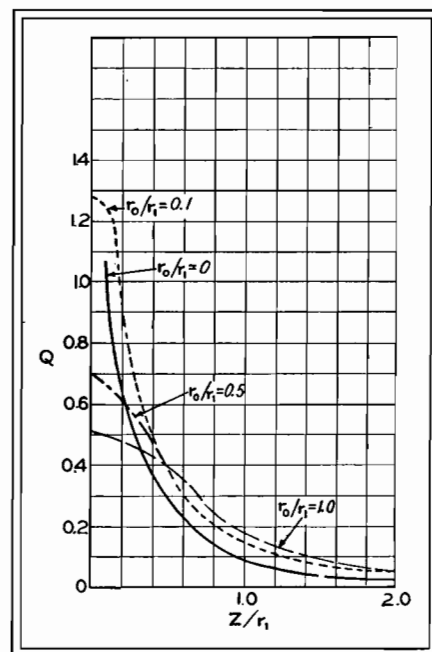


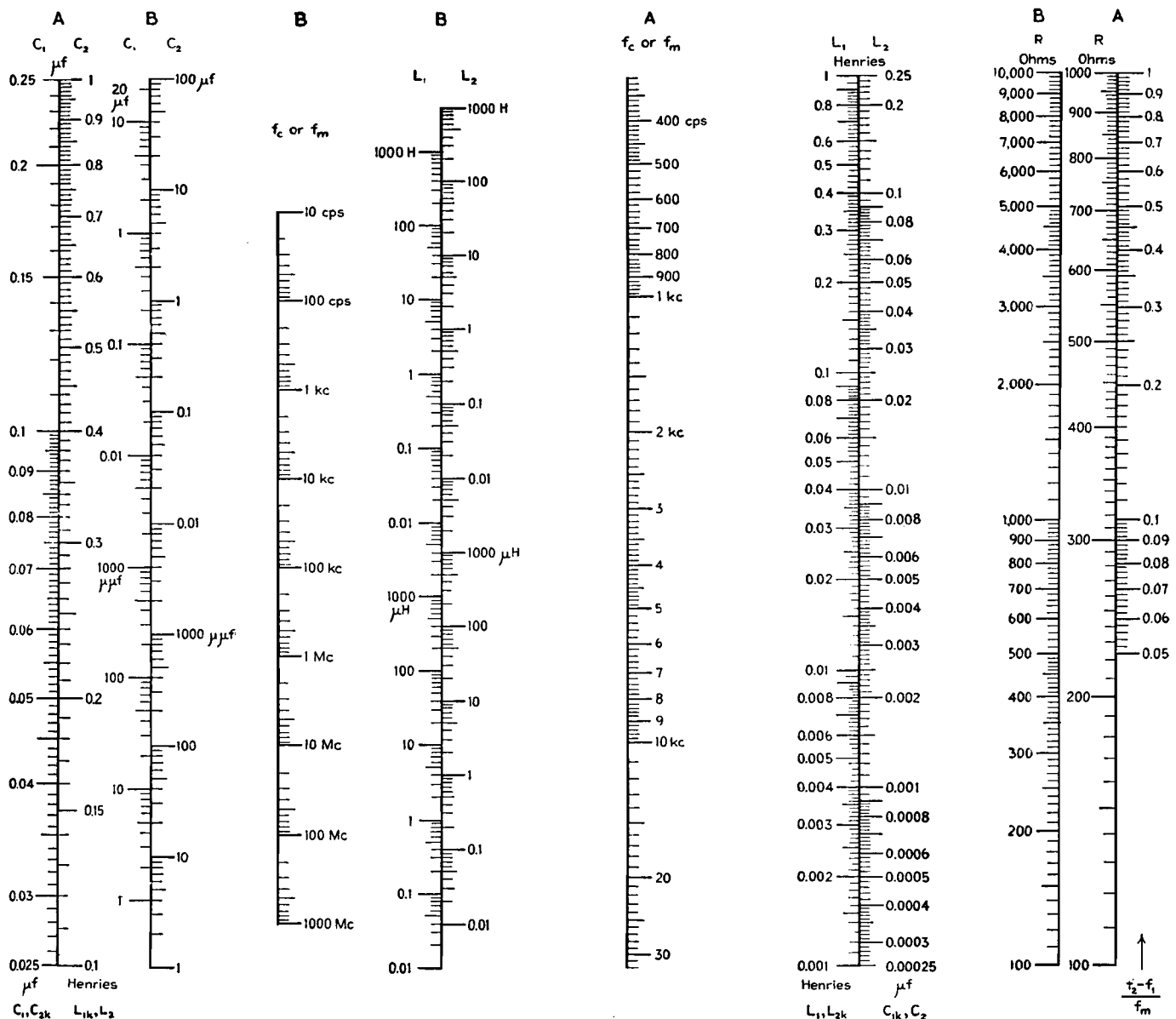
Fig. 9.—Variation of the factor  $S$  of an equiangular spiral as a function of  $Z/r_1$  for a number of values of  $r_o/r_1$ .

## SECTION IX FILTERS

	Page
Constant- $k$ Filter-design Chart.....	127
M-derived Filter-design Chart.....	129
Filter-conversion Chart.....	130

# Constant-K Filter-design Chart

By JOHN BORST



Constant-k filter-design chart.

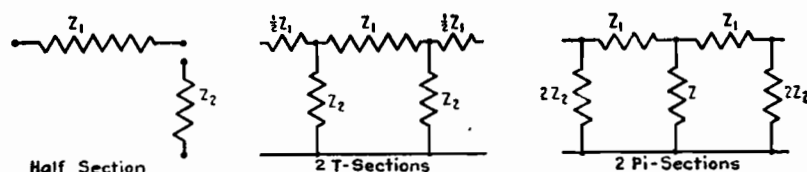


Fig. 1.—T and pi filter sections.

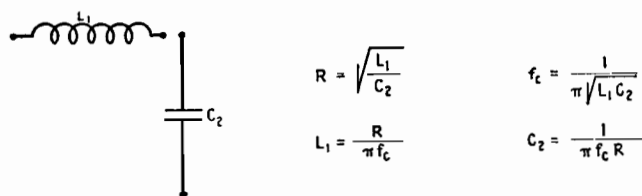


Fig. 2.—Equations for low-pass filter.

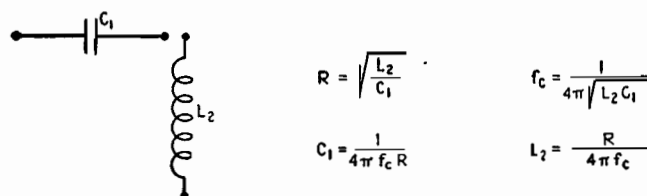


Fig. 3.—Equations for high-pass filter.

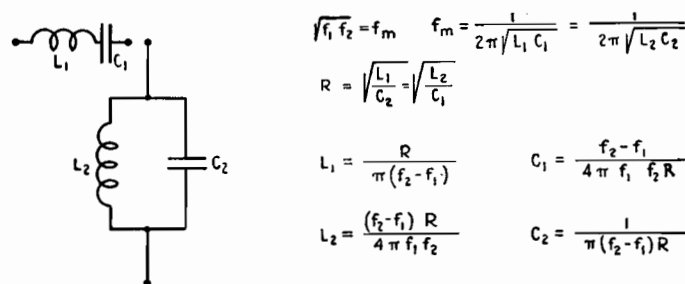


Fig. 4.—Equations for band-pass filters.

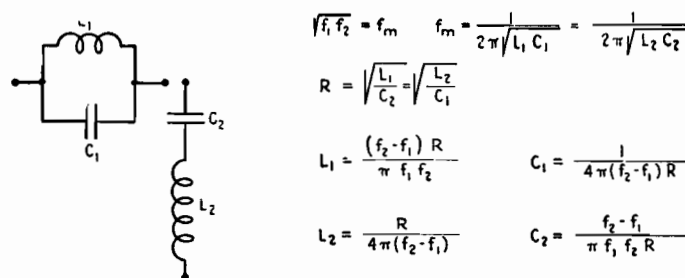


Fig. 5.—Equations for band-suppression filter.

THE values of the elements of various types of constant- $k$  filter sections are easily and quickly determined by the use of the chart. It is applicable to low-pass, high-pass, symmetrical band-pass, and band-suppression filters.

Figure 1 shows the configuration of  $T$  and  $\pi$  filter sections which can be built up from the full series impedance  $Z_1$  and the full shunt impedance  $Z_2$ .

The equations and diagrams (Figs. 1 to 5) refer to the full series and the full shunt impedances in all cases. Elements in the series arm are indicated by the subscript 1, while those in the shunt arm are denoted by the subscript 2. The equations used here are found in the work of T. E. Shea, "Transmission Networks and Wave Filters," as well as in other textbooks on the subject.

In the chart there are two sets of four logarithmic scales, one set marked  $A$ , the other  $B$ . These two sets serve to solve the same equation and differ only in the ranges covered. For the sake of accuracy, the  $A$  scales cover only a very narrow range so that the significant figures of the element values may be obtained. The placing of the decimal point is then most easily accomplished by using the scales marked  $B$ . A single straight line will connect corresponding values of all variables on the four scales.

#### Use of the Chart

To obtain the values for low-pass filters, the illustrative diagram and equations of which are given in Fig. 2, the scales  $L_1$ ,  $C_2$ ,  $f_c$ , and  $R$  are used. When a straight line connects any two to these variables on the scales mentioned, the intersection of that line and the other two scales will determine the other two values. Note that  $L_1$  is read at the left of the  $L_1/L_2$  scale and  $C_2$  at the right of the  $C_1/C_2$  scale. High-pass filter values (see Fig. 3) are obtained in the same manner, using scales  $C_1$ ,  $L_2$ ,  $f_c$ , and  $R$ .

Band-pass filters are shown in Fig. 4. Knowing the midfrequency  $f_m$  which is the geometric mean between the two cutoff frequencies, and knowing the desired characteristic impedance  $R$ , draw a line through the two desired values on the  $f_m$  scale and the  $R$  scale and read at the other intersections all four values:  $L_1$ ,  $L_2$ ,  $C_1$ , and  $C_2$ . These figures are for a filter with a band width  $(f_2 - f_1)/f_m$  equal to unity. When this factor has any other value, the proper size of the desired elements  $L_{1k}$ ,  $L_{2k}$ ,  $C_{1k}$ , and  $C_{2k}$  can be found on the chart using  $L_1$ ,  $L_2$ ,  $C_1$ , and  $C_2$ . For this purpose use the three scales with the designations at the bottom. Employing the values found for unity band width, a straight line is drawn to connect corresponding values on the scales  $L_1$ ,  $L_{1k}$ , and  $(f_2 - f_1)/f_m$ ; also,  $L_2$ ,  $L_{2k}$ , and  $(f_2 - f_1)/f_m$ , etc.

For band suppression (Fig. 5), using four times the desired value of  $R$ , find values of  $L_{2k}$  and  $C_{2k}$  as for a band-pass filter; also using  $R/4$ , find  $L_{1k}$  and  $C_{1k}$ . Then interchange subscripts  $1k$  and  $2k$  to obtain the corresponding elements of the band-suppression filter.

# M-derived Filter-design Chart

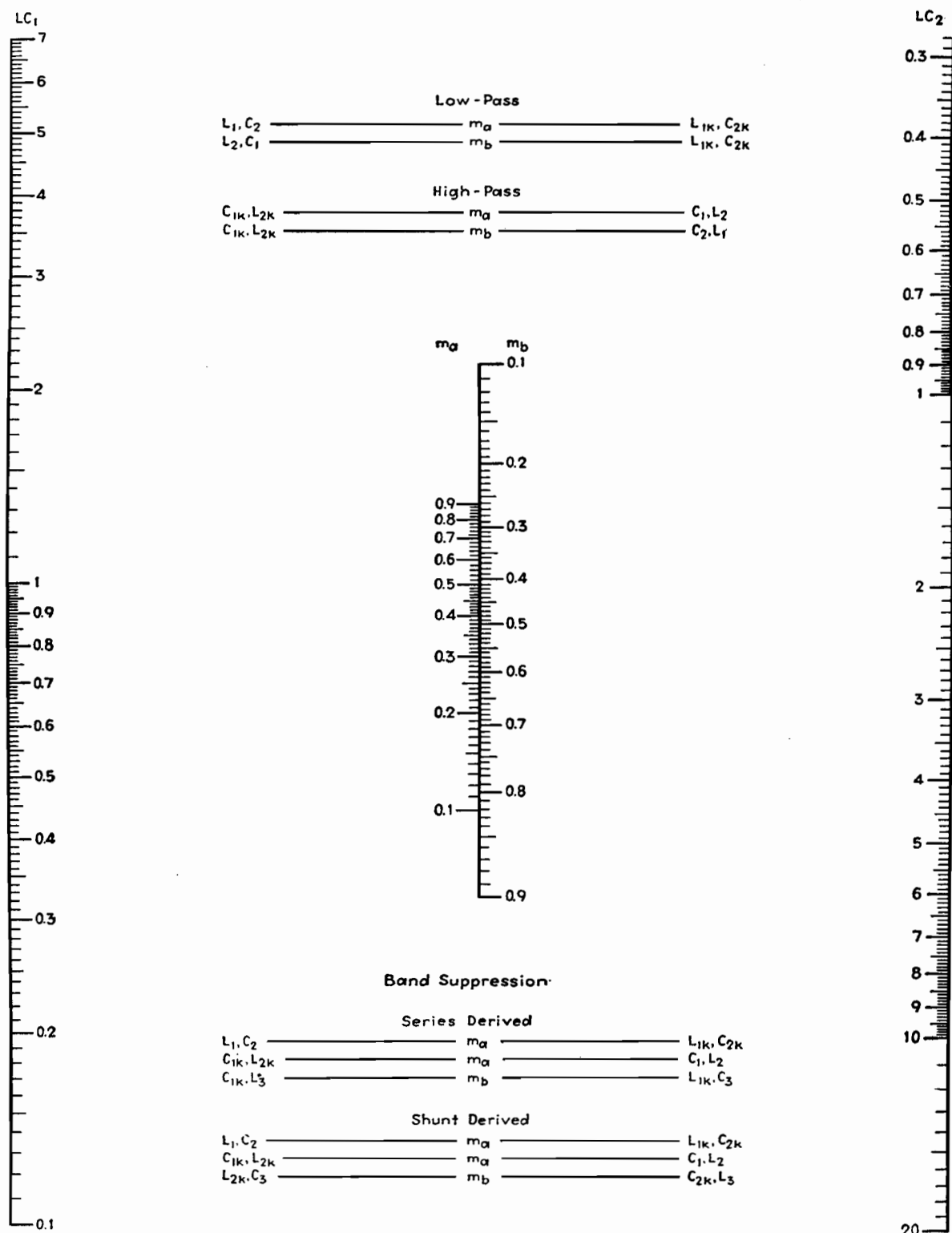
By JOHN BORST

**T**HE chart permits the user to find the elements of m-derived sections for low-pass, high-pass, and band-suppression filters, when the values of the correspond-

ing constant- $k$  sections are known. The chart applies to series-derived as well as shunt-derived sections.

The range of the m-derived section

chart has been purposely made short so as to permit accurate determinations of the  $L$  and  $C$  values. The scales marked  $LC_1$  and  $LC_2$  may be multiplied by any



M-derived filter design chart.

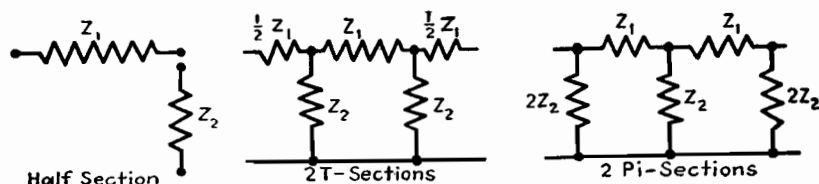


Fig. 1.—T and pi filter sections.

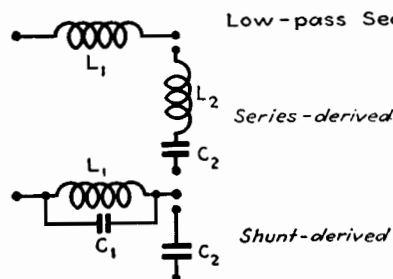


Fig. 2.—Equations for low-pass m-derived filter sections.

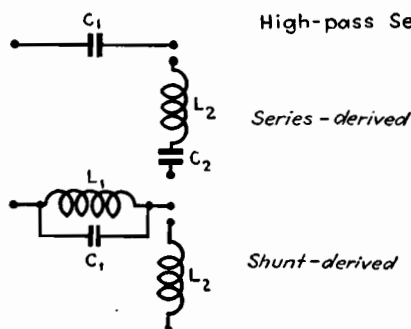


Fig. 3.—Equations for high-pass m-derived filter sections.

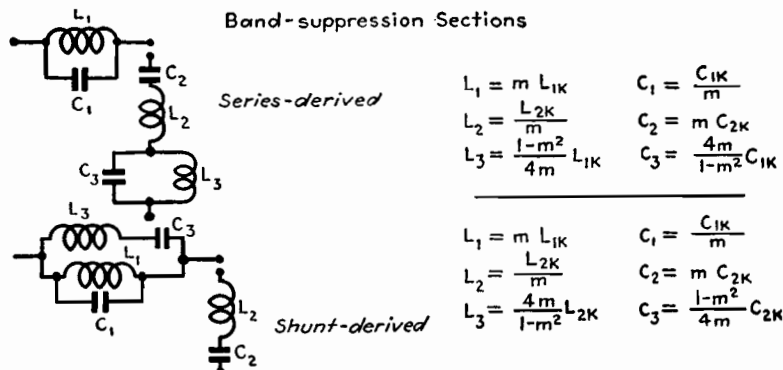


Fig. 4.—Equations for band-suppression m-derived filter sections.

convenient factor when necessary, so long as the same factor is applied to each.

The chart is based on the fact that the m-derived elements are derived from the constant- $k$  elements by multiplying or dividing by one of two factors:  $m$  or

$4m/(1 - m^2)$ . For this reason, two scales of  $m$  are employed. The given value of  $m$  is read on  $m_a$  (the left-hand scale in the center of the chart) for use when the equation contains  $m$  only. The value of  $m$  is read on  $m_b$  when the equation con-

tains the factor  $4m/(1 - m^2)$ . The outer scales are marked  $LC_1$  and  $LC_2$  since they serve either as  $L$  and  $C$  scales. In using the chart, the same units are used in reading the  $LC_1$  or  $LC_2$  scales (for example, both microfarads or both millihenrys). Corresponding values of the constant- $k$  element and the m-derived element are found by connecting the given value of the constant- $k$  element and the given value of  $m$  (read on  $m_a$  or  $m_b$ ) with a straight line. This straight line intersects the corresponding m-derived value on the opposite scale. The corresponding equations and diagrams of the sections are given in Figs. 1 to 4.

In the following, values with the subscript  $k$  are the constant- $k$  values, whereas values with the subscript 1, 2, or 3 are the m-derived values.

For low-pass filters, series-derived, connect  $L_{1k}$  on the  $LC_2$  scale with  $m$  on  $m_a$ , read  $L_1$  on  $LC_1$ . Similarly, connect  $C_{2k}$  on  $LC_2$  with  $m$  on  $m_a$ , read  $C_2$  on  $LC_1$ . Connect  $L_{1k}$  on  $LC_2$  with  $m$  on  $m_b$ , read  $L_2$  on  $LC_1$ .

For low-pass filters, shunt-derived, use  $m$  on  $m_a$ ,  $L_{1k}$  and  $C_{2k}$  on  $LC_2$ , read  $L_1$  and  $C_2$  on  $LC_1$ , respectively. Using  $m$  on  $m_b$ ,  $C_{2k}$  on  $LC_2$ , read  $C_1$  on  $LC_1$ .

For high-pass filters, series-derived, use  $m$  on  $m_a$ ,  $C_{1k}$  and  $L_{2k}$  on  $LC_1$ , read  $C_1$  and  $L_2$  on  $LC_2$ . Using  $m$  on  $m_b$ ,  $C_{1k}$  on  $LC_1$ , read  $C_2$  on  $LC_2$ .

For high-pass filters, shunt-derived, use  $m$  on  $m_a$ ,  $C_{1k}$  and  $L_{2k}$  on  $LC_1$ , read  $C_1$  and  $L_2$  on  $LC_2$ . Using  $m$  on  $m_b$ ,  $L_{2k}$  on  $LC_1$ , read  $L_1$  on  $LC_2$ .

For band-suppression filters, series-derived, use  $m$  on  $m_a$ ,  $L_{1k}$  and  $C_{2k}$  on  $LC_2$ , read  $L_1$  and  $C_2$  on  $LC_1$ . Using  $m$  on  $m_a$ ,  $C_{1k}$  and  $L_{2k}$  on  $LC_1$ , read  $C_1$  and  $L_2$  on  $LC_2$ . Using  $m$  on  $m_b$ ,  $L_{1k}$  on  $LC_2$ , read  $L_3$  on  $LC_1$ . Using  $m$  on  $m_b$ ,  $C_{1k}$  on  $LC_1$ , read  $C_3$  on  $LC_2$ .

For band-suppression filters, shunt-derived, find  $L_1$ ,  $C_2$ ,  $L_2$ ,  $C_1$  as in band-suppression, series derived. Using  $m$  on  $m_b$ ,  $L_{2k}$  on  $LC_1$ , read  $L_3$  on  $LC_2$ . Using  $m$  on  $m_b$ ,  $C_{2k}$  on  $LC_2$ , read  $C_3$  on  $LC_1$ . The operations are indicated on the chart.

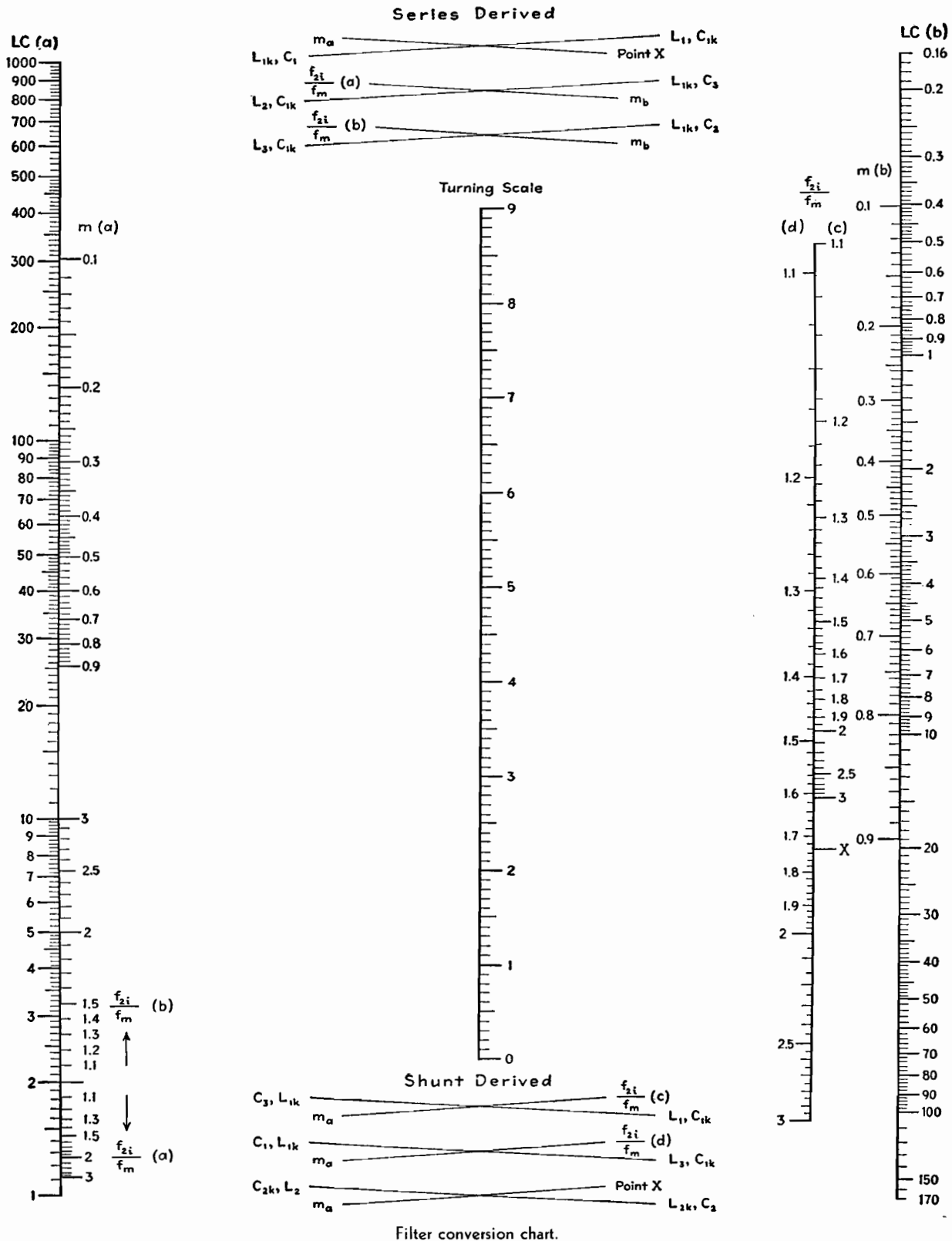
## Filter-conversion Chart

By JOHN BORST

THE chart may be used to determine the elements of m-derived band-pass filter sections from the corresponding constant- $k$  sections. The constant- $k$  values

are marked with the subscripts 1k or 2k, whereas the corresponding m-derived values have the subscripts 1, 2, or 3. The relationship between the two sets

of values depends on two variables, the assigned value of  $m$  (from 0.1 to 0.9), and the ratio  $f_{2i}/f_m$ , where  $f_{2i}$  is the frequency of infinite attenuation above the pass



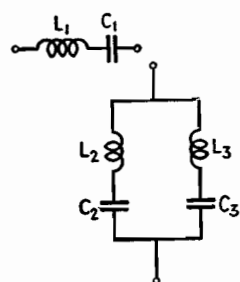
band and  $f_m$  is the mid-band frequency (the geometric mean of the cutoff frequencies). As the equations in Figs. 1 and 2 show, the  $m$ -derived values are found by multiplying the constant- $k$  value by two factors, one a function of  $m$ , the other a function of the frequency ratio.

Hence two alignments are necessary in using the chart, the two having a common point on the turning scale. The operations are shown schematically at the top and bottom of the chart. Two scales for the variable  $m$ , marked  $m(a)$  and  $m(b)$ , are provided, as well as four scales

marked  $f_{2i}/f_m$ , (a), (b), (c), (d) since these variables enter into the equations in two and four different ways, respectively.

#### Instructions for Series $m$ -derived Sections

For the series-derived band-pass filter (see Fig. 1), to find  $L_1$  align the given



$$f_m = f_1 f_2 = f_{1i} f_{2i}$$

$$L_1 C_1 = \sqrt{L_2 C_2 L_3 C_3}$$

$$L_1 = m L_{1K}$$

$$L_2 = L_{1K} \frac{1-m^2}{4m} \left[ 1 + \left( \frac{f_m}{f_{2i}} \right)^2 \right]$$

$$L_3 = L_{1K} \frac{1-m^2}{4m} \left[ 1 + \left( \frac{f_{2i}}{f_m} \right)^2 \right]$$

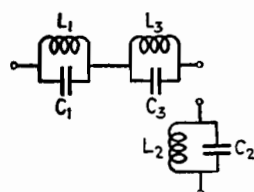
$$m = \sqrt{1 - \frac{\left( \frac{f_2}{f_m} - \frac{f_m}{f_2} \right)^2}{\left( \frac{f_{2i}}{f_m} - \frac{f_m}{f_{2i}} \right)^2}}$$

$$C_1 = \frac{C_{1K}}{m}$$

$$C_2 = \frac{C_{1K}}{1 + \left( \frac{f_{2i}}{f_m} \right)^2} \cdot \frac{4m}{1-m^2}$$

$$C_3 = \frac{C_{1K}}{1 + \left( \frac{f_m}{f_{2i}} \right)^2} \cdot \frac{4m}{1-m^2}$$

Fig. 1.—Equations for series-derived band-pass filter.



$$f_m = f_1 f_2 = f_{1i} f_{2i}$$

$$L_2 C_2 = \sqrt{L_1 C_1 L_3 C_3}$$

$$L_1 = m L_{1K} \frac{\left( \frac{f_{2i}}{f_m} - \frac{f_m}{f_{2i}} \right)^2}{1 + \left( \frac{f_{2i}}{f_m} \right)^2}$$

$$L_2 = \frac{L_{2K}}{m} \frac{\left( \frac{f_{2i}}{f_m} - \frac{f_m}{f_{2i}} \right)^2}{1 + \left( \frac{f_m}{f_{2i}} \right)^2}$$

$$L_3 = m L_{1K} \frac{\left( \frac{f_{2i}}{f_m} - \frac{f_m}{f_{2i}} \right)^2}{1 + \left( \frac{f_m}{f_{2i}} \right)^2}$$

$$m = \sqrt{1 - \frac{\left( \frac{f_2}{f_m} - \frac{f_m}{f_2} \right)^2}{\left( \frac{f_{2i}}{f_m} - \frac{f_m}{f_{2i}} \right)^2}}$$

$$C_1 = \frac{C_{1K}}{m} \cdot \frac{1 + \left( \frac{f_m}{f_{2i}} \right)^2}{\left( \frac{f_{2i}}{f_m} - \frac{f_m}{f_{2i}} \right)^2}$$

$$C_2 = m C_{2K}$$

$$C_3 = \frac{C_{1K}}{m} \cdot \frac{1 + \left( \frac{f_{2i}}{f_m} \right)^2}{\left( \frac{f_{2i}}{f_m} - \frac{f_m}{f_{2i}} \right)^2}$$

Fig. 2.—Equations for shunt-derived band-pass filter.

value of  $m$  on  $m(a)$  with the point  $X$  on the scale  $f_{2i}/f_m$ , and note the intersection with the turning scale. Then align the given value of  $L_{1K}$  on the scale  $LC(a)$  with the same point on the turning scale and read  $L_1$  on the scale marked  $LC(b)$ . To find  $C_1$  align  $C_{1K}$  on  $LC(b)$  with the same intersection of the turning scale and read  $C_1$  on  $LC(a)$ . To find  $L_2$ , align the given value of the frequency

ratio  $f_{2i}/f_m$  on the scale marked  $f_{2i}/f_m(a)$  with the given value of  $m$  on  $m(b)$ , and read the intersection on the turning scale. Then align the given value of  $L_{1K}$  on  $LC(b)$  with the same point on the turning scale, and read  $L_2$  on  $LC(a)$ . To find  $C_2$  align the frequency ratio on the scale marked  $f_{2i}/f_m(b)$  with the given value of  $m$  on  $m(b)$ , and note the intersection with the turning scale. Then align the given

value of  $C_{1K}$  on  $LC(a)$  with the same point on the turning scale and read  $C_2$  on  $LC(b)$ . To find  $L_3$  use the intersection on the turning scale found for  $C_2$  and align it with the given value of  $L_{1K}$  on  $LC(b)$ , finding  $L_3$  on  $LC(a)$ . To find  $C_3$  use the intersection on the turning scale found for  $L_2$ , align it with the given value of  $C_{1K}$  on  $LC(a)$ , and find the required value of  $C_3$  on  $LC(b)$ .

#### Shunt-derived Band-pass Sections

To find  $L_1$  (see Fig. 2), align the given value of  $m$  on  $m(a)$  with the given value of the frequency ratio on  $f_{2i}/f_m(c)$ , and note the intersection on the turning scale. Then align this intersection point with the given value of  $L_{1K}$  on  $LC(a)$ , and find the required value of  $L_1$  on  $LC(b)$ . To find  $C_1$ , align the given value of  $m$  on  $m(a)$  with the given value of the frequency ratio on  $f_{2i}/f_m(d)$ , and note the intersection. Then align the intersection point with the given value of  $C_{1K}$  on  $LC(b)$  and read the required value of  $C_1$  on  $LC(a)$ . To find  $L_2$ , align the given value of  $m$  on  $m(a)$  with the point  $X$  on the frequency ratio scale, and note the intersection. Then align the intersection with the given value of  $L_{2K}$  on  $LC(b)$ , and find  $L_2$  on  $LC(a)$ . To find  $C_2$ , use the same intersection point found for  $L_2$  and align it with the given value of  $C_{2K}$  on  $LC(a)$ , finding the required value of  $C_2$  on  $LC(b)$ . To find  $L_3$ , use the intersection on the turning scale found for  $C_1$ , align it with the given value of  $L_{1K}$  on  $LC(b)$ , finding  $L_3$  on  $LC(a)$ . To find  $C_3$ , use the intersection with the turning scale found for  $L_1$ , align it with the given value of  $C_{1K}$  on  $LC(b)$ , and find the required value of  $C_3$  on  $LC(a)$ .



## SECTION X

# INDUSTRIAL CONTROL

	Page
Design of Electronic Control Circuits.....	133
Capacitor-discharge Welding Systems.....	136
Grid Control of Industrial Gas-filled Tubes.....	140

## Design of Electronic Control Circuits

By WARREN A. SCHWARZMANN

For many industrial applications, amplifiers can be operated advantageously from an a-c source of power. Graphical methods of determining the power output of a-c operated triode and pentode amplifiers are given

IN THE industrial application of electron tubes, it is frequently possible and convenient to operate the tubes from an a-c source of power. Such operation is not suitable for those applications which require the instantaneous and continuous flow of plate current, but it is suitable for

those control operations which need not take place more quickly than every cycle of the a-c supply.

The prediction of the power output of a-c operated amplifiers is usually of major consideration in this method of operation. Methods for calculating the output power

of a-c operated amplifiers using tubes having triode or pentode characteristics will be outlined here. The results presented here are based on theoretical calculations as well as on laboratory measurements, using either a purely resistive load or a plate load consisting of a resistor and capacitor in parallel. The methods given here are intended to provide approximate results quickly, using the average plate characteristics of the tubes as given in any tube manual.

The schematic diagrams for which the data given in this article apply are shown in Figs. 1 and 2. In these diagrams and in the analysis to follow, the following symbolic notation has been used:

$E_{bb}$  = rms value of alternating plate supply voltage

$e_c = E_{c0} + E_g$  rms value of cathode-grid voltage

$E_{c0}$  = steady grid bias voltage

$E_g$  = rms value of alternating component of cathode-grid voltage;  $E_g$  is considered to be positive when in phase with  $E_{bb}$ , and negative when 180 deg out of phase with  $E_{bb}$

$E_L$  = rms value of voltage across RC load for triode or pentode

$e_L$  = rms value of voltage across resistive load of triode

$E_0$  = value of plate voltage (on plate voltage-plate-current family) obtained at the axis  $I_b = 0$  when the straight portion of the curve  $E_c = 0$  is extended to intersect this axis

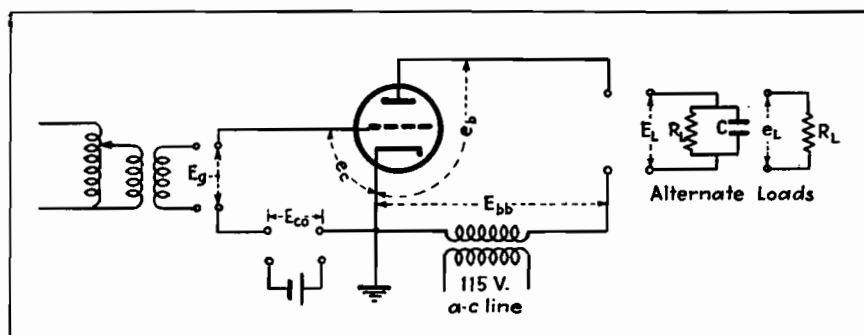


Fig. 1.—Schematic diagram for triode, for two different types of loads, illustrating the notation with respect to voltage and load.

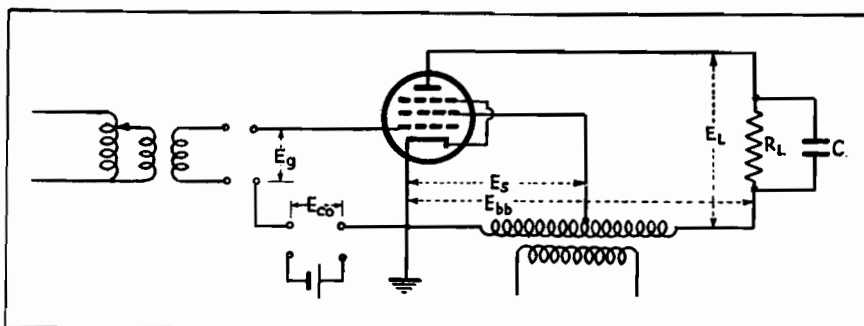


Fig. 2.—Connections for pentode and load for which the graphical diagram of power output is determined.

$E_{sg}$  = screen grid voltage for which tube ratings or static characteristic curves of tube are available

$E_{sg}'$  = actual screen grid voltage at which tube is to be operated

$I_L$  = average value of the current flowing through load resistor  $R_L$

$I_0$  = calculated plate current at zero grid bias and zero plate voltage and for screen voltage for which static curves or tube ratings are available, obtained by projecting the saturated curves to left axis

$I_s$  = calculated plate current at zero bias, zero plate voltage, and for screen grid voltage at which tube is operated

$P$  = power delivered by tube to its load

$R_L$  = resistance of external plate load resistor

$r_p$  = internal plate resistance of tube

$\mu$  = amplification factor

The behavior of a triode can be predicted with reasonable accuracy from relatively simple equations which express the load current in terms of tube parameters and operating voltages. In the case of tubes having pentode characteristics, investigations have shown that graphical methods are more convenient and accurate than the mathematical equations.

It can be shown that, for a triode with a pure resistance load, the average plate current is

$$I_L = \frac{1.35(E_{bb} + \mu E_g) + \mu E_{c0} - E_0}{3r_p + 3R_L} \quad (1)$$

This equation expresses the average value of the plate current when the tube parameters and operating voltages are known. It should be observed that  $r_p$  and  $\mu$  are to be determined in the usual manner for the rms values of the operating voltages. Of course, these values will vary throughout the cycle, but the published values can usually be used for engineering purposes.

If the resistance load is shunted by a capacitor of sufficient capacitance so as to keep the load voltage essentially constant throughout a complete cycle, then the average load current may be obtained from the expression

$$I_L = \frac{1.35(E_{bb} + \mu E_g) + \mu E_{c0} - E_0}{(3r_p + R_L)} \quad (2)$$

where the symbols have the values previously given.

Equations (1) and (2) are based on the assumption that the alternating components of the grid and plate voltage are in phase. If there is a phase shift between the plate supply voltage and the sinusoidal component of grid voltage, the

numerators of Eqs. (1) and (2) become

$$1.35(E_{bb}^2 + 2E_{bb}\mu E_g \cos \phi + \mu^2 E_g^2)^{1/2} + \mu E_{c0} - E_0 \quad (3)$$

where  $\phi$  is the angle of phase shift and  $E_g$  is considered to be positive.

If  $\mu E_g$  is much less than  $E_{bb}$ , the numerator simplifies to

$$1.35(E_{bb} + \mu E_g \cos \phi) + \mu E_{c0} - E_0 \quad (4)$$

#### Maximum Ratings for 6G6-G Connected as Pentode

Plate voltage.....	180 max volts
Screen voltage....	180 max volts
Plate dissipation..	2.75 max watts
Screen dissipation	0.75 max watts

#### Typical Operation and Characteristics, Class A<sub>1</sub> Amplifier

Plate voltage.....	135	180	volts
Screen voltage.....	135	180	volts
Grid voltage.....	-6	-9	volts
Peak a-f grid voltage.....	6	9	volts
Zero-signal plate current.....	11.5	15	ma
Zero-signal screen current.....	2.	2.5	ma
Plate resistance....	0.170	0.175	megohm
Transconductance..	2,100	2,300	μmhos
Load resistance....	12,000	10,000	ohms
Total harmonic distortion.....	7.5	10	%
Maximum signal power output....	0.6	1.1	watts

Once the average value of the plate current and the resistance of the load are shown, the average voltage across the load can be determined as can also the power dissipated in the load resistor, provided the resistor is a linear device. Experience has indicated that these equations can usually be used to produce results that are accurate to within 5 or 10 per cent, although occasionally errors as high as 25 per cent may be encountered. The equations are derived on the following assumption:

1. The static plate characteristics are straight, parallel, equidistant lines, which assumes that the amplification factor is constant. If high negative grid bias is used, the approximation is not too good because of the curvature of the plate characteristic.

2.  $E_0$  is the value of the plate voltage when  $E_g = 0$  and no plate current flows. For constant- $\mu$  triodes,  $E_0 = -\mu E_c$ , where  $E_c$  is the negative bias voltage.

#### Output of A-c Operated Pentode Amplifier

The power output of tubes having pentode characteristics are most conveniently and accurately determined

through the use of the graphical chart. This chart can be used with any pentode type of tube once its static characteristics are known. The results have been applied only for a load consisting of a resistor and capacitor combination in parallel as the load circuit.

It will be noted that the coordinates are given either as a current ratio or as a voltage ratio; hence the diagram is applicable to any voltage and current at which the tube can be operated. For example, in order to obtain the load current, the ordinates shown must be multiplied by  $I_0$ ; likewise to obtain the load voltage, the abscissa must be multiplied by  $E_{bb}$ .

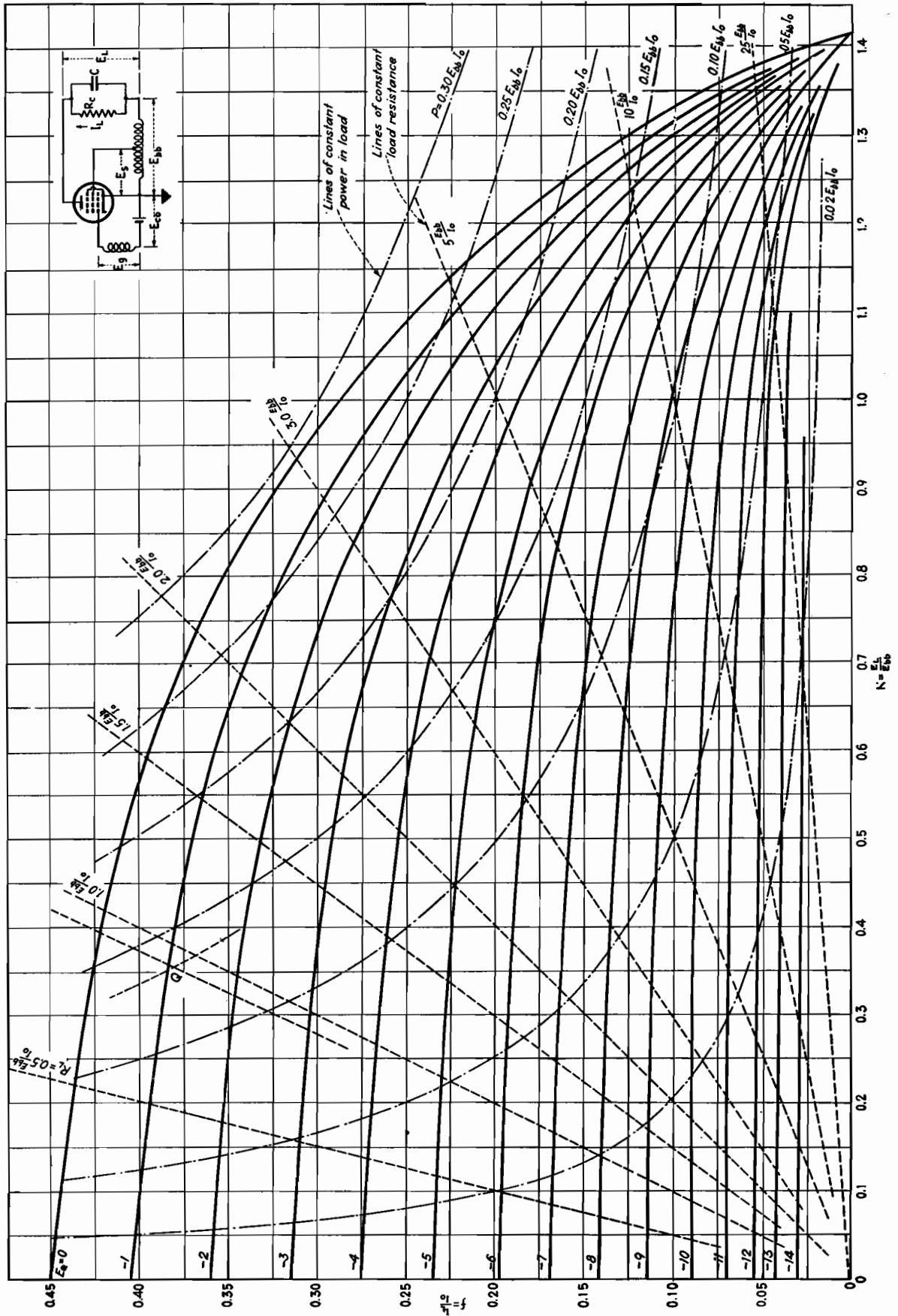
Let us take a specific problem. We have a relay that we desire to open and close. A capacitor will be used across it to prevent chattering. The current required to close the relay is 8 ma, the release current is 7 ma, and the relay resistance is 5,000 ohms. A voltage of 2 volts is available for actuating the relay (or its amplifying tube), and a 115-volt 60-cycle power source is available.

The power required to close the relay is  $P = I^2 R = (8 \times 10^{-3})^2 \times 5 \times 10^3 = 0.32$  watt. The voltage required is  $E_L = I_L R = 8 \times 10^{-3} \times 5 \times 10^3 = 40$  volts. Since only 2 volts are available for control of the relay, an amplifying tube is required, and one capable of operating from the 115-volt line should be selected. A 6G6 pentode will be selected since this has more than adequate power output at its rated voltages, and gives promise of producing sufficient power output at electrode voltages of 115 volts. For purposes of illustration, the problem will be worked out on the assumption that only the tube ratings are available; if the static curves are available, more precise results could be obtained.

To use the chart shown, it is necessary to determine the scales for the chart. The load voltage on the abscissa is found by multiplying the scale factor  $K$  by  $E_{bb}$ . This gives us a new voltage scale for the abscissa, representing the voltage across the load  $E_L$ .

To find the scale for the ordinate  $f$ , we must determine  $I_0$ , the current that would flow when no grid bias is applied, when the plate voltage is zero, and when the screen voltage is at its operating value. If the tube characteristic curves are available, we can determine this current (for the screen voltage for which the curves are plotted) by extending the linear portion of the  $E_{c1} = 0$  curve to the left axis for which  $E_p = 0$ .

ALTERNATING CURRENT OPERATED AMPLIFIER LOAD CURRENT-LOAD VOLTAGE CHART FOR PENTODES



The published ratings of the 6G6 used as a pentode show that for plate and screen voltage of 135 volts and a control grid bias of -6 volts, the plate current is 11.5 ma. To obtain operating conditions for a 115-volt supply, it is necessary to assume that the pentode characteristics are horizontal, and equally spaced. If we assume that the plate current is independent of plate voltage, we can say as an approximation that 11.5 ma of plate current flows at zero plate voltage, when the screen voltage is 135 volts and the control grid voltage is -6 volts.\* The plate current at zero control grid voltage can then be calculated as  $11.5 + g_m \Delta E_c$ , where  $g_m$  is the published transconductance and  $\Delta E_c$  is the change in grid voltage, in this case from -6 or +6 volts. Thus, the plate current at zero control grid voltage is

$$I_z = 11.5 \times 10^{-3} + 2100 \times 10^{-6} \times 6 \\ = 24.1 \times 10^{-3} = 24.1 \text{ ma}$$

If a value of screen voltage different from that for which the tube data are given is to be used, the current  $I_z$  will have to be modified to take account of the new screen grid voltage. If  $E_{sg}'$  is the actual screen grid voltage and  $E_{sg}$  is the screen grid voltage for which the tube data apply, the desired current is  $I_0 = I_z E_{sg}' / E_{sg}$ .

\* This fictitious plate current is determined by extrapolating the curves of saturation to the zero plate voltage abscissa. It is a value that is convenient for purposes of calculation rather than a value actually encountered in tube operation.

In our particular case

$$I_0 = 24.1 \frac{115}{135} = 20.53 \text{ ma}$$

This current  $I_0$  multiplied by the scale factor  $f$  gives the load current  $I_L$ . Whereas we ordinarily find the third or  $E_c$  scale graphically, it is necessary to make some assumptions as to the characteristics of the tube in the absence of static curves. The chart shown gives grid bias values necessary to cause a 10 per cent reduction in plate current. For this reason, it is necessary to determine the bias necessary to reduce the plate current to 90 per cent of its value at  $E_c = 0$ . If the value of  $I_0$  is put in the equation  $E_g = I_p / g_m$ , and the difference in  $E_g$  between  $I_0 = 20.53 \text{ ma}$  and  $0.9I_0 = 0.9 \times 20.53 = 18.5 \text{ ma}$  is found, this will be the bias required to produce a 10 per cent change in plate current. Thus,

$$E_{cz}' = \frac{I_0 - 0.9I_0}{g_m} = \frac{20.5 - 18.5}{2.1} = 0.953 \text{ volts}$$

This calculation takes into account the compensation required by virtue of the fact that the actual plate voltage is 115 volts instead of the rated value of 135 volts, since the current  $I_0$ , rather than  $I_z$ , was used in this calculation. If the scale  $E_Q$  of Fig. 3 is multiplied by  $E_{cz}'$ , the bias for tube operation is also determined.

The resistance of the relay is  $R_L = E_L / I_L$ , or, in terms of the operating

voltage and current,  $R_L = nE_{bb}/I_0$ , where  $n$  is the scale factor for the resistance lines. In this example,  $R_L = 5,000 \text{ ohms}$ ,  $E_{bb} = 115 \text{ volts}$ , and  $I_0 = 0.0205 \text{ amp}$ . The scale factor is

$$n = \frac{I_0 R_L}{E_{bb}} = 0.0205 \times \frac{5,000}{115} = 0.892$$

We interpolate on the load resistance curves between  $R_L = 0.5E_{bb}/I_0$  and  $R_L = 1.0E_{bb}/I_0$  and determine the line of operation at 5,000-ohm load.

The power required is 0.32 watt. This power may be expressed as

$$P = E_L I_L = m E_{bb} I_0$$

where  $m$  is a scale factor

$$m = \frac{P}{E_{bb} I_0} = \frac{0.32}{115 \times 0.0205} = 0.134$$

Interpolating between the hyperbolic curves  $P = 0.1E_{bb}/I_0$  and  $P = 0.2E_{bb}/I_0$ , we can determine the intersection of the resistance and power curves. This is the point of operation for the relay, and is designated by the letter  $Q$  on the chart.

For these operating conditions, the grid voltage change which is required to operate the relay is

$$E_Q = \frac{E_c}{E_{cz}'} = \frac{2}{0.953} = -2.20 \text{ volts}$$

Since we are at about -0.8 volt already, relay operation will occur for  $E_Q = -3 \text{ volts}$ .

## Capacitor-discharge Welding Systems

By H. KLEMPERER

Voltage, current, and time relations for the successive phases in capacitor-discharge welding are developed for shunt and inverse tube circuits, and a quick method is given for determining whether undesirable saturation exists in the welding transformer

A METHOD is presented which allows a quick determination of the maximum incremental flux density occurring in the welding transformer under various conditions. In addition, formulas and graphs are developed to show voltages, currents, and duration of the successive phases of the capacitor-discharge welding current.

### Wave Shape of Welding Current

Welding circuits of the type under consideration generally consist of the

capacitor bank, the welding transformer (with electronic tubes as switching elements), and the secondary loop with the welding load. This circuit is shown in Fig. 1. The discharge is initiated by the series tube and is terminated by the shunt tube, or in some systems by the inverse tube.

The coupled circuits can be simplified to the equivalent circuit shown in Fig. 1 by transposing the secondary inductance and resistance values  $L_s$  and  $R_s$  into the primary circuit according to the relations

$$R = n^2 R_s \quad (1)$$

$$L = n^2 L_s \quad (2)$$

where  $n$  is the turns ratio of the welding transformer. It has been shown by direct measurements that the reflected resistance  $R$  and inductance  $L$  by far outweigh the resistance and inductance of the primary circuit, including leakage inductance and the resistance of the transformer primary.

The attenuation of the welding circuit is expressed by the attenuation angle  $\delta$  as follows:

$$\sin \delta = \frac{R}{2} \sqrt{\frac{C}{L}} \quad (3)$$

Using Eqs. (1) and (2), the attenuation angle is obtained from the original circuit constants  $L_s$ ,  $R_s$ ,  $C$ , and  $n$ , which are known to the transformer designer.

$$\sin \delta = n \frac{R_s}{2} \sqrt{\frac{C}{L_s}} \quad (4)$$

With increasing turns ratio, the attenuation of the welding discharge increases, until, when  $n$  is equal to the critical turns ratio  $n_c$ , the circuit is critically damped. The corresponding critical turns ratio is therefore defined as

$$n_c = \frac{2}{R_s} \sqrt{\frac{L_s}{C}} \quad (5)$$

Having determined the critical turns ratio  $n_c$  from the circuit constants, it is possible to draw the attenuation triangle for any turns ratio of the welding transformer. That construction will allow a simple scaling of the constants of the current equation.

The attenuation triangle is a right triangle with the base and hypotenuse drawn in proportion to  $n$  and  $n_c$ , respectively, as in Fig. 2. The top angle is  $\delta$ , the attenuation angle of the welding circuit, and the complementary base angle is  $\phi$ , the phase angle between voltage and current in the weld circuit.

If the base is scaled in proportion to  $R/2L$ , which is the inverse oscillation time constant of the welding circuit (dimension  $\text{sec}^{-1}$ ), the altitude will read the natural frequency  $v/2\pi$  of the welding circuit.

Thus, reading  $\delta$  and  $v$  from the attenuation triangle, the current equation

$$i = \frac{E_0}{\sqrt{L/C} \cos \delta} e^{-\frac{tR}{2L}} \sin vt \quad (6)$$

is easily evaluated. The value  $\sqrt{L/C}$  can be read from the attenuation triangle,

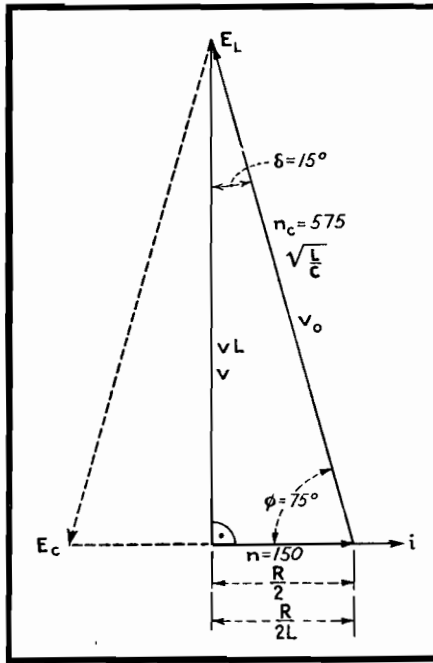


Fig. 2.—Attenuation triangle expressing relations in a capacitor-discharge welding circuit, worked out here for the circuit constants given in the example at the end of the circle.

since it is the hypotenuse if the base is made equal to  $R/2$  ohms.

From Eq. (6), the time in seconds, counting from the beginning of the weld, at which the welding current reaches its peak is

$$T_M = \frac{\varphi}{v} \quad (7)$$

This current maximum has a value in amperes equal to

$$I_M = \frac{E_0}{\sqrt{L/C}} e^{-\varphi \tan \delta} \quad (8)$$

#### Systems with Shunt Tube

In welding systems using a shunt tube, the welding energy is prevented from oscillating back into the primary circuit. Neglecting tube drops, the current commutates from series tube to shunt tube at

the time when the capacitors are fully discharged. This time in seconds is

$$T_K = \frac{\pi - \varphi}{v} \quad (9)$$

The commutating current in amperes at this time has the value

$$I_K = \frac{E_0}{\sqrt{L/C}} e^{-(\pi - \varphi) \tan \delta} \quad (10)$$

After this commutation, the welding circuit is changed; the capacitor being disconnected, the current decays exponentially according to

$$i_s = I_K e^{-\frac{tR}{L}} \quad (11)$$

This current  $i_s$  reaches its end abruptly at the moment when it is too small to support the cathode spot in the shunt tube. This extinction usually takes place somewhere between 5 and 3 amp. Calling the extinction value of the current  $I_F$ , the time of extinction in seconds is

$$T_F = T_K + \frac{L}{R} \log_e \frac{I_K}{I_F} \quad (12)$$

which also designates the duration of the weld.

Considering the welding circuit as a coupled system (Fig. 1), it is evident that a residual current in the secondary keeps on flowing after the primary current thus has ceased to flow. This residual current has an initial amplitude  $nI_F$  of several hundred amperes and dies out with the time constant  $L_s/R_s$ . Unless suppressed by additional means, this residual current may cause excessive sparking at the moment when the electrodes are opened.

#### System with Inverse Tube

In the capacitor-discharge welding system, using an inverse tube instead of the shunt tube, the series tube stays conducting until the current wave has gone to zero. At this time, while the capacitor voltage passes its negative peak, the current commutates from series to inverse tube. Through the inverse tube, the former half cycle is repeated with decreased amplitudes and in the opposite direction, and at the end of the full period the capacitors carry a residual charge of the original sign.

The inverse voltage peak in volts is

$$-E_M = E_0 e^{-\pi \tan \delta} \quad (13)$$

The inverse current in amperes rises to

$$-I_M = \frac{E_0}{\sqrt{L/C}} e^{-(\pi + \varphi) \tan \delta} \quad (14)$$

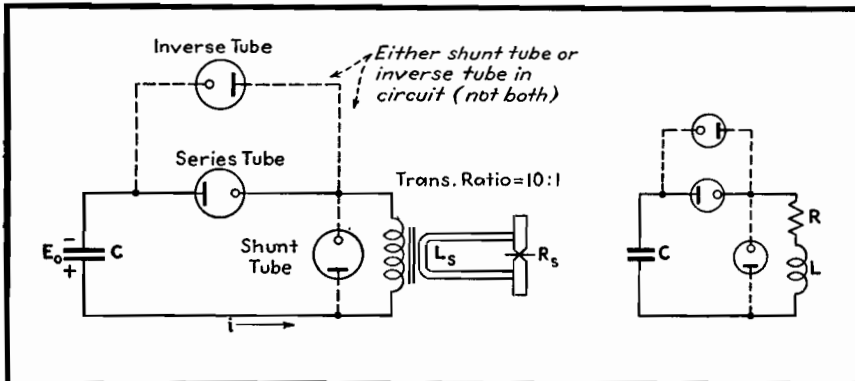


Fig. 1.—Basic capacitor-discharge welding circuit (left), and simplified equivalent circuit (right).

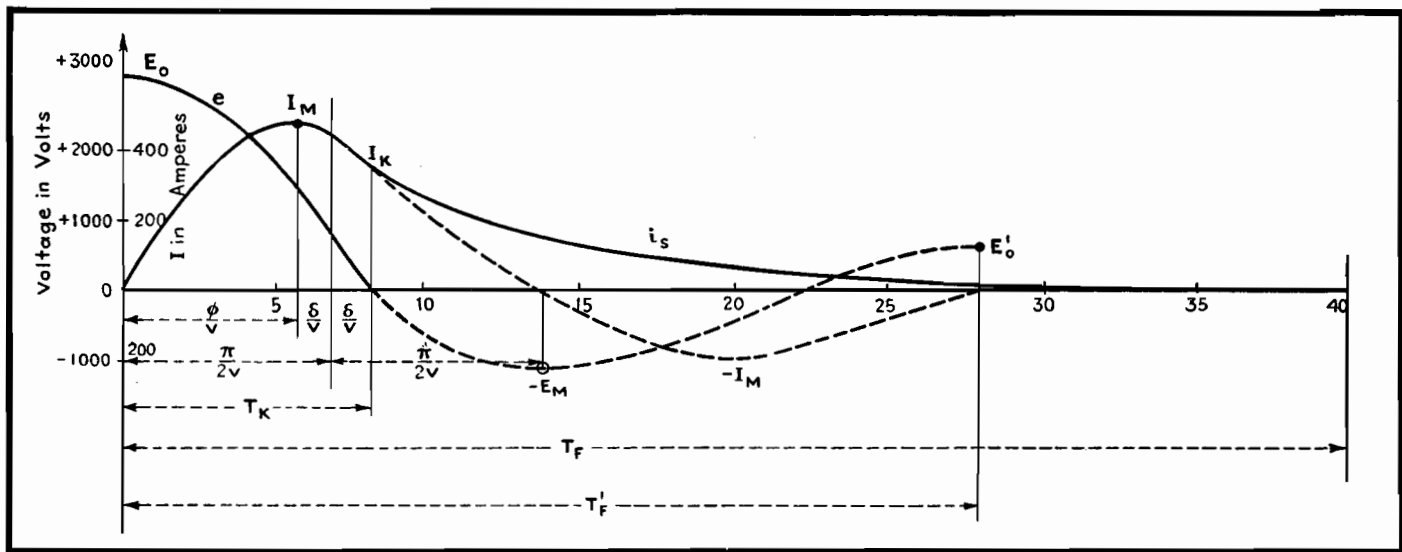


Fig. 3.—Welding current and voltage as calculated for the two-circuit versions of Fig. 1. Solid lines are for system with shunt tube; dash-dash lines for system with inverse tube.

and the residual capacitor voltage at the end of the welding period is

$$E_F = E_o e^{-2\pi \tan \delta} \quad (15)$$

Finally, the time in seconds of the welding period is

$$T_F' = \frac{2\pi}{v} \quad (16)$$

#### Example

In a typical welding equipment, the measured secondary resistance value  $R_s$  was  $1.14 \times 10^{-4}$  ohm. This resistance value is much larger than the resistance of the actual weld, which in the case of aluminum is of the order of  $10^{-5}$  to  $10^{-6}$  ohm. The secondary inductance  $L_s$  was  $9 \times 10^{-7}$  henry. (The inductance varies mainly with throat depth and height.) The machine was run at  $C = 840 \mu\text{f}$  and  $E_o = 3,000$  volts. The turns ratio of the welding transformer was  $n = 150$ .

From these data and Eq. (5) the critical turns ratio is determined to be  $n_c = 575$ . The time constant  $L/R$  is  $7.9 \times 10^{-3}$  sec.

The attenuation triangle is drawn as shown in Fig. 2. The following data are scaled from the triangle:  $\delta = 15^\circ$ ;  $\phi = 75^\circ$ ;  $v = 222$ , which corresponds to a natural frequency of 35.4 cycles. With these data substituted into the above equations, the following results are obtained:

$$T_M = 5.9 \times 10^{-3} \text{ sec}; I_M = 475 \text{ amp}$$

$$T_K = 8.2 \times 10^{-3} \text{ sec}; I_K = 406 \text{ amp}$$

In the system with the shunt tube, commutation takes place at this moment  $T_K$ . An exponentially decaying current

$i_s$  flows from here on and comes to an end after a total duration of the weld of approximately  $T_F = 40 \times 10^{-3}$  sec.

If the same system is operated with an inverse tube instead of the shunt tube, energy flows back from the secondary circuit through the series tube into the capacitors, which swing negative to  $-E_{\text{max}} = 1,300$  volts. There the inverse tube picks up, the inverse current rises

to  $-I_{\text{max}} = 200$  amp, and the residual positive capacitor voltage at the end of the weld is  $E_F = 565$  volts. The duration of the welding period is  $T_F' = 28 \times 10^{-3}$  sec.

#### Flux Density in Welding Transformer

If the transformer saturates, the above equations do not apply any more because  $L$  becomes a function of  $i$ . The magnetiz-

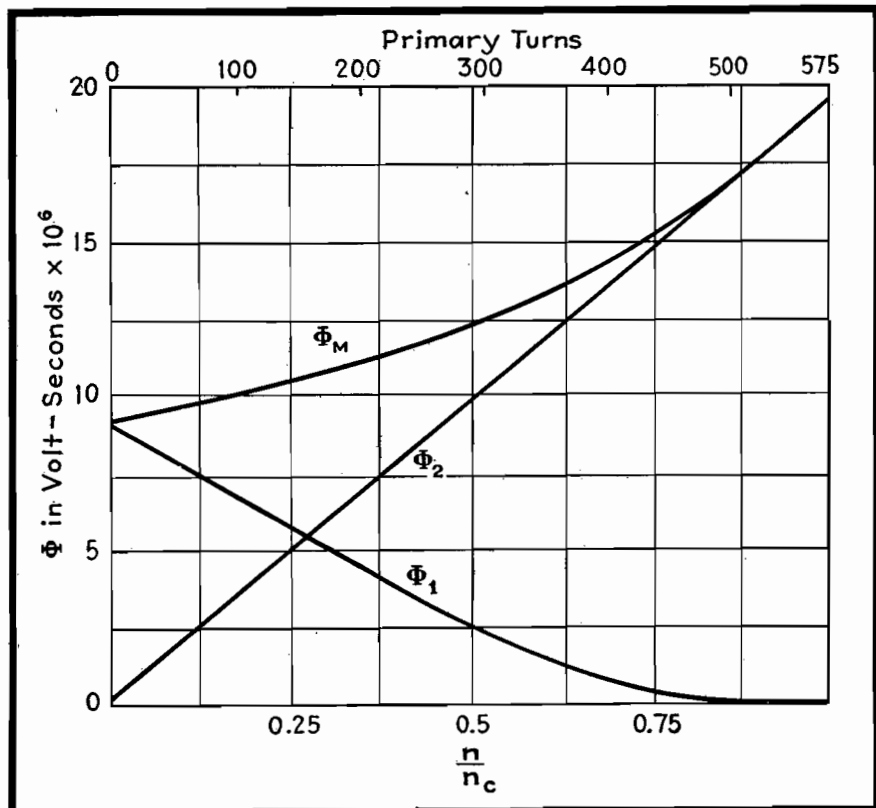


Fig. 4.—Maximum flux in the welding transformer of a capacitor-discharge circuit, plotted as a function of the turns ratio. Circuit constants employed are those of the example.

ing current, which was neglected, grows to a substantial value; primary and secondary current wave shapes do not agree any more. Briefly, the primary current grows in peak value and in tail length, and its energy is largely wasted in the iron. Subsequent welds get weaker and weaker, and a danger point is reached if the tail is so long that the transformer is still energized when the next weld is started.

For these reasons, a check of the maximum flux in the welding transformer is desirable. A relation between this maximum flux and the transformer turns ratio can be developed from the fundamental flux equation

$$\frac{d\phi}{dt} \left( L \frac{di}{dt} + Ri \right) \frac{10^8}{n} \quad (17)$$

$$\phi_{\max} = \frac{10^8}{n} \left( Li + Rit \right)_{E=E_0}^{E=0} \quad (18)$$

$$\phi_{\max} = \frac{10^8}{n} (LI_K + RCE_0) \quad (19)$$

Here  $I_K$  is the commutating current of Eq. (10). Since  $I_K$  flows at zero voltage, which is the time when the capacitors have transferred their total energy into the welding circuit, these equations hold for circuits using an inverse tube as well as a shunt tube. Substituting Eq. (10) into Eq. (19), we get

$$\phi_M = E_0 \times 10^{-8} (\sqrt{LsC} e^{-(\pi-\varphi)\tan\delta} + nR_sC) = \phi_1 + \phi_2 \quad (20)$$

Thus  $\phi_M$  can be readily figured when  $\delta$  and  $\phi$  are taken from the attenuation triangle (Fig. 2).

The maximum flux in capacitor impulse welding transformers is composed of two terms  $\phi_1$  and  $\phi_2$ . Only  $\phi_2$  is linearly growing with the turns ratio  $n$ ;  $\phi_1$  is decreasing in a somewhat exponential manner from an initially high value, and disappears at the approach of critical damping. The sum  $\phi_M$  rises very slowly

at low turns ratios and, in fact, does not change too much under practical conditions.

Flux conditions for a transformer in the above calculated welding circuit are plotted in Fig. 4 over the transformer turns ratio. The total flux rises only about 60 per cent for a change of turns ratio from 100 to 450 turns.

While the maximum flux rises in proportion to the applied capacitor voltage, it also increases in an almost linear manner, though not in proportion, with the capacitor size. To illustrate this relation, the flux conditions in the welding transformer are plotted in Fig. 5 under constant voltage and turns ratio as a function of the capacitor size. Again, as Eq. (20) shows, the two flux components rise in a different manner: one is proportional to the capacitance, and the other, except for very low values, is almost constant. The resulting maximum flux line is fairly straight for practical capacitor sizes. The flux scale of Fig. 5 applies to the above calculated welding circuit and a turns ratio of 150:1.

Some welding systems operate with such a high transformer turns ratio that the capacitor discharge is aperiodically damped ( $n > n_c$ ). In these circuits, the welding discharge is carried by the series tube alone, and, since there is no reversal in the direction of power flow, the series tube may be replaced by a contactor. Disadvantages of this system are long duration of the welding discharge and a high flux in the transformer.

In all welding circuits using capacitor-discharge power of substantially unidirectional flow, precautions have to be taken against saturation of the transformer resulting from incomplete demagnetization after subsequent impulses. To overcome this effect in some systems the primary transformer connections are reversed after each weld. This is done either by means of mechanical contactors or by a double set of discharge tubes. In other systems, electronic flux reset arrangements are used to counteract or reverse the residual transformer flux in the time between the welds. In systems handling small amounts of power only, sometimes an air gap in the welding transformer is provided.

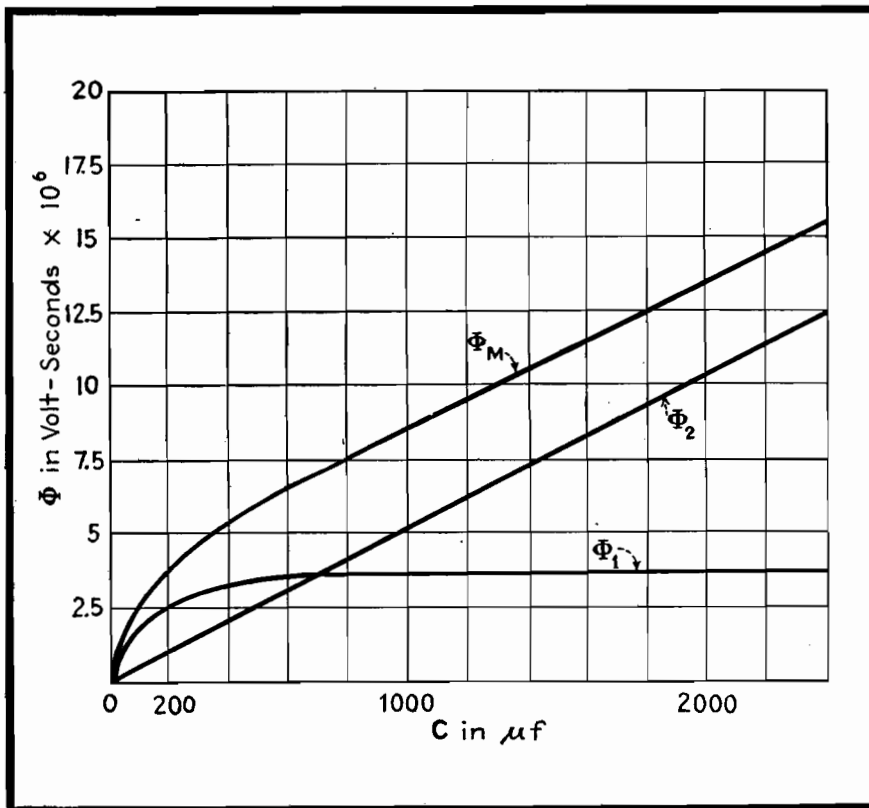


Fig. 5.—Curves for maximum flux in the welding transformer as a function of capacitor size, with a constant turns ratio value  $n$  of 150. Circuit constants for these curves are those of the example in the article. The two lower curves are for the components that make up the maximum flux at each instant.



# Grid Control of Industrial Gas-filled Tubes

By W. D. COCKRELL

Summary of typical phase-shifting circuits which enable smooth control of thyratrons and ignitrons to be obtained in industrial electronic systems

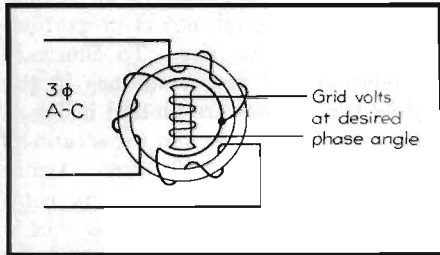


Fig. 1.—Use of selsyn for grid control by which any desired phase may be applied to the grid.

THE usefulness of the gas-filled electron tube lies in its low constant internal voltage drop and the resulting high circuit efficiency for large currents. However, the ionization of the gas that permits this low drop also prevents the control grid from stopping the current flow when it has once begun. Hence, the most usual application of thyratrons is on an a-c system where the periodic reversal of the anode voltage permits deionization and a chance for the grid to regain control. After the current has ceased flowing, a negative grid will prevent its restarting even though the anode has again become positive. It is by retarding the application of the tripping voltage to the grid until the desired time in the positive cycle that the average current in the thyatron is controlled.

For some simple "on-off" actions, it is possible to operate the grid from a d-c supply, but to obtain a smooth control of the grid-firing angle throughout the required part of the positive cycle, it is necessary to use firing circuits that operate wholly or partially from the same a-c supply used for the anode circuit.

## Three Fundamental Methods of Obtaining Phase Shift

If a three-phase supply is available, we may use a form of transformer wound with a three-phase stator and a rotatable secondary by means of which we can apply any desired phase to the grid circuit. This is the familiar selsyn or autosyn device, as shown in Fig. 1.

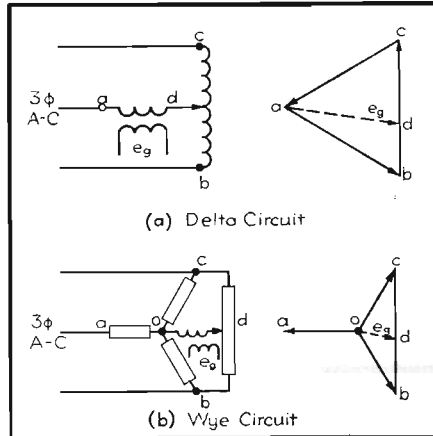


Fig. 2.—Autotransformer or potentiometer to add a fixed voltage to a variable out-of-phase voltage for limited degree of phase shift.

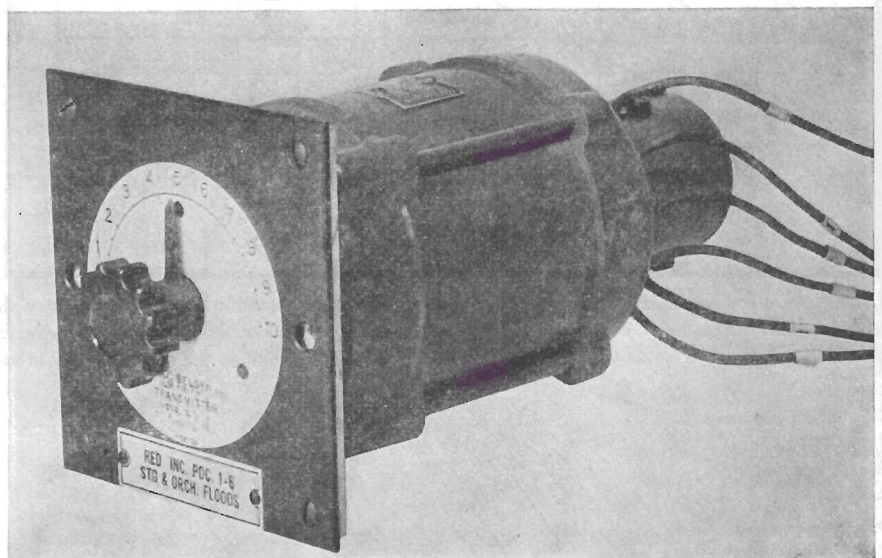
For limited phase shift, we may add a constant voltage of fixed phase to a variable out-of-phase voltage by means of an autotransformer or potentiometer placed across the second phase winding as in Fig. 2. The vectors show that this method will change the amount as well as the phase of the grid voltage, but, since the thyatron critical firing voltage is usually very near zero, this change in the amount of grid voltage is not detrimental.

## Grid-shift Circuits Obtained from Single-phase Alternating Current

However, three-phase often is not available and it is necessary to obtain our phase shift from a single-phase circuit by means of resistance-reactance bridges and such devices. These may be divided into (1) those which change components of the bridge circuit to obtain a definite phase shift of a constant amplitude voltage (Fig. 3), and (2) circuits which combine a fixed phase shift obtained from the a-c supply, with a variable d-c voltage (Fig. 4).

First to be considered are the bridge type of phase-shift circuits. These usually are composed of a transformer having a midtap and reactance and resistance legs to form the other two sides of the bridge.

The circuit of Fig. 5a combines a resistor and a capacitor. The values of capacitance required for reasonable impedances at the normal commercial frequencies, such as 60 cycles, are usually so large that variation of the capacitance is not practical. Therefore, the resistive element is varied. This usually consists of a small rheostat which may be operated by hand or by automatic mechanical control means of conventional design.



Selsyn transmitter for obtaining phase shift from three-phase power.



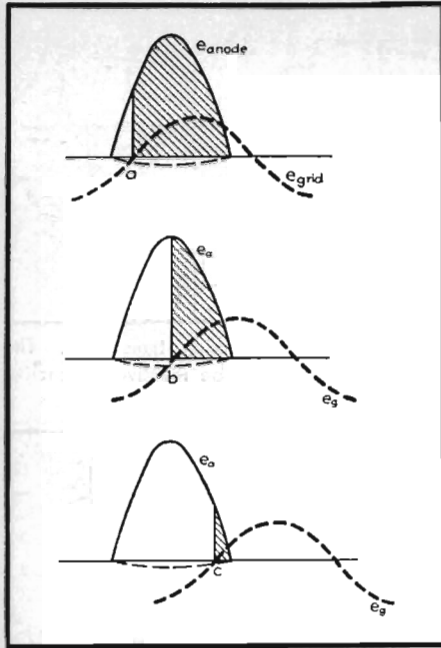


Fig. 3.—Grid control by phase shift. Shaded area indicates tube conduction; dotted line is critical grid-firing curve.

If the bridge consists of a resistor and a reactor, as in Fig. 6, we have a greater freedom of action, since either the resistor or the inductance of the reactor may be varied. For instance, the reactor may consist of a solenoid whose core may be withdrawn, or a small induction regulator in which the rotor and stator may be moved with respect to each other. Or the inductance may be of the saturable reactor type in which direct current supplied to one winding of the reactor will saturate the core and thus vary the a-c reactance of the other winding. This has the added advantage that the direct current is insulated from the thyatron grid circuit.

#### Grid-circuit Wave Form

Because of the rather severe third harmonic that appears in the a-c circuit

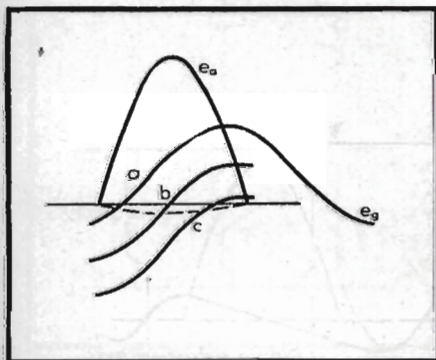


Fig. 4.—Grid control by fixed, alternating, and variable direct voltages. Compare this with Fig. 3.

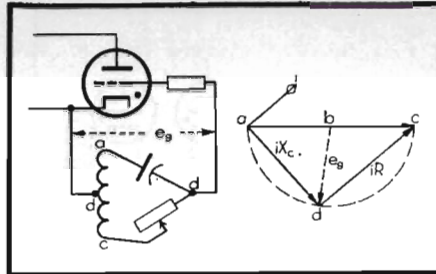


Fig. 5.—Resistor-capacitor phase-shift network.

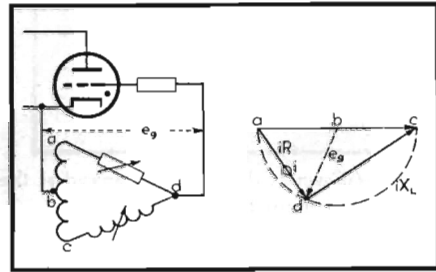


Fig. 6.—Resistor-reactor phase-shift network.

of a saturable reactor, the grid-circuit wave form will no longer be sinusoidal, but becomes more of a square wave form. This, however, is quite desirable for a grid-tripping circuit.

A bridge circuit using only one variable element cannot fully swing the output vector (since one leg cannot be reduced to zero). But, by combining capacitors and inductances in one leg, it is possible to obtain a phase shift of almost 360 deg as the inductance of the reactor is varied past the resonant point.

The variable resistance for the bridge may be obtained directly or may be reflected through a transformer placed in one leg. A number of interesting electronic circuits have been developed to supply this resistance element.

Two circuits are shown (Figs. 7a and

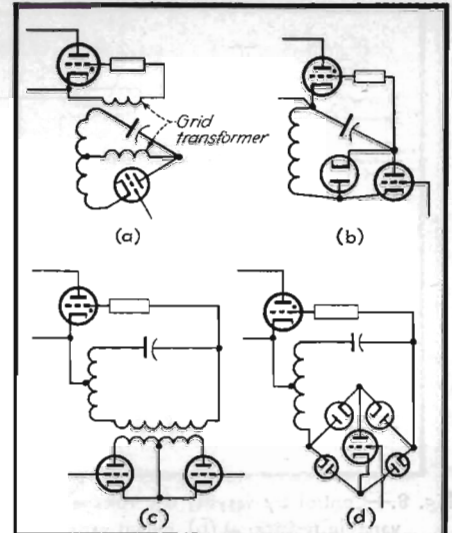


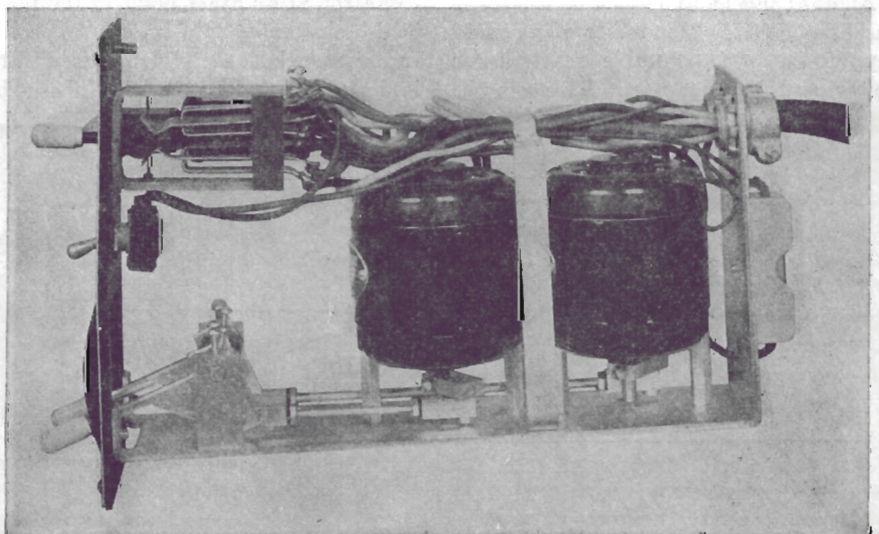
Fig. 7.—Vacuum tubes replacing resistor of Fig. 5.

7b) in which electronic tubes replace the resistance directly. There is also a certain amount of rectification in Fig. 7b which changes the d-c component of the grid voltage.

Circuits that reflect the resistance through a transformer are particularly useful because this permits insulation of the control circuit from the thyatron circuit. The simplest of these are the biphas half-wave rectifier (Fig. 7c) and the bisected rectifier square in which one tube does the work of the two tubes of the previous circuit. This last circuit is sometimes used directly in the bridge, as in Fig. 7d.

#### Grid Shift Using Fixed Phase and Variable Direct Current

One of the most used forms of this type of control is that of Fig. 8, using a



Two rotary-control inductors with switches in a control unit used as in Fig. 6.

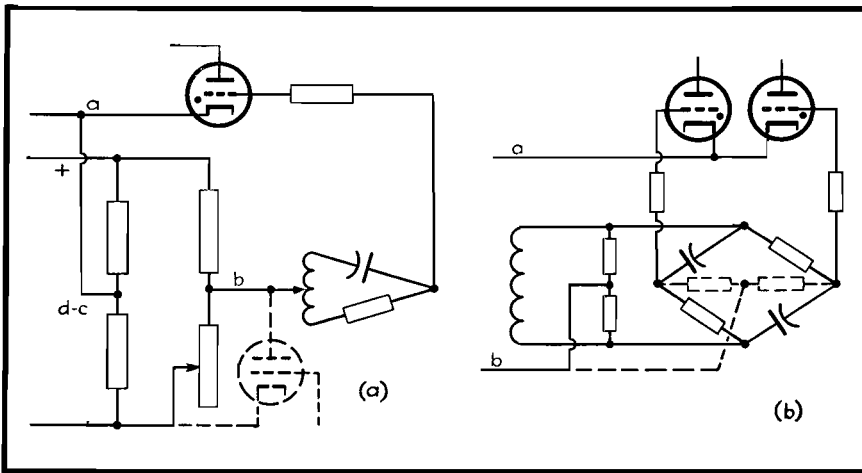


Fig. 8.—Control by varying d-c voltages. At (a), a tube (shown as dotted) is employed as the variable resistor; at (b), circuit variation to control two thyatrons and to obtain midtap.

90-deg phase shift on which is superimposed direct voltage which may be varied from the positive peak voltage to the negative peak voltage of the a-c component. Theoretically, this permits the transmission of an integrated voltage proportional to the d-c control voltage. Under practical consideration, however, the load is rarely a pure resistive load, but is inductive or contains a back emf so that the actual relation of power output is not so linear.

Because there is no inductance in the grid circuit, and the incidental capacitances are small, this system is capable of extremely high-speed operation. But, for the same reason, it is susceptible to h-f transients, and the small angle of intersection between the controlled voltage and the critical grid voltage at the beginning and end of the cycle makes it somewhat critical to tube characteristics and temperature unless it is used in some self-balancing over-all control circuit.

Another ingenious circuit of this type has been used for a number of years to supply the d-c saturable reactors for power and heating uses. This circuit,

shown in Fig. 9, combines a long time constant  $e_a$  and a short time constant  $e_b$  capacitor-resistor timing circuit and a twin-diode rectifier.

A feed-back transformer from the load supplies the excitation for the short time-constant network, tending to force the grid negative; and the long time-constant network, which tends to turn the thyatron on, is supplied from a control voltage which may be of any frequency or phase. Only a few milliamperes are drawn from the control circuit, so that this control, although somewhat slow in operation, lends itself very well to controls requiring much preliminary switching and superimposed control signals such as the preselected and preset lighting effects required for theater lighting control. The voltage feed-back feature compensates to a great extent for changes in load.

#### Peaking Transformers

For greatest accuracy in firing a thyatron at an exact point in the phase, it is customary to insert a peaking transformer in the grid firing circuit after it has passed through the phase-shift

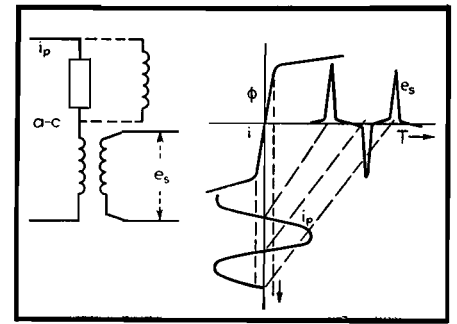


Fig. 10.—Use of peaking transformer. The series impedance may be resistive or reactive (shown as dotted).

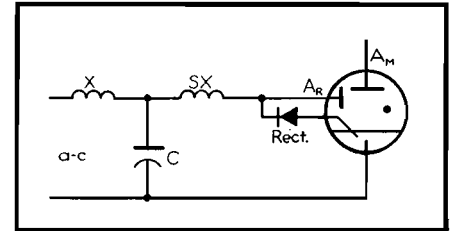


Fig. 11.—Ignition firing by saturable reactor, SX. X is a current limiting reactor; C is an energy storage capacitor,  $A_m$  and  $A_r$  are main and relieving anodes, respectively.

network. This peaking transformer is a type of saturated transformer permitting a very sharp sliver of voltage, only a few electrical degrees wide, to be generated once each half cycle. Thus, the thyatron is fired during these few degrees if it is to be fired at all during the cycle. Figure 10 shows a typical peaking transformer and the output voltage wave shape.

#### Ignitron Firing

Another similar form of peaking action may be produced by means of a saturating reactor made of some magnetic material having a very sharp bend to the saturation curve, such as Nicaloi. This saturating reactor, in the circuit shown in Fig. 11, will permit a sudden surge of current to be passed through an ignitron igniter which is similar in action to the surge of voltage

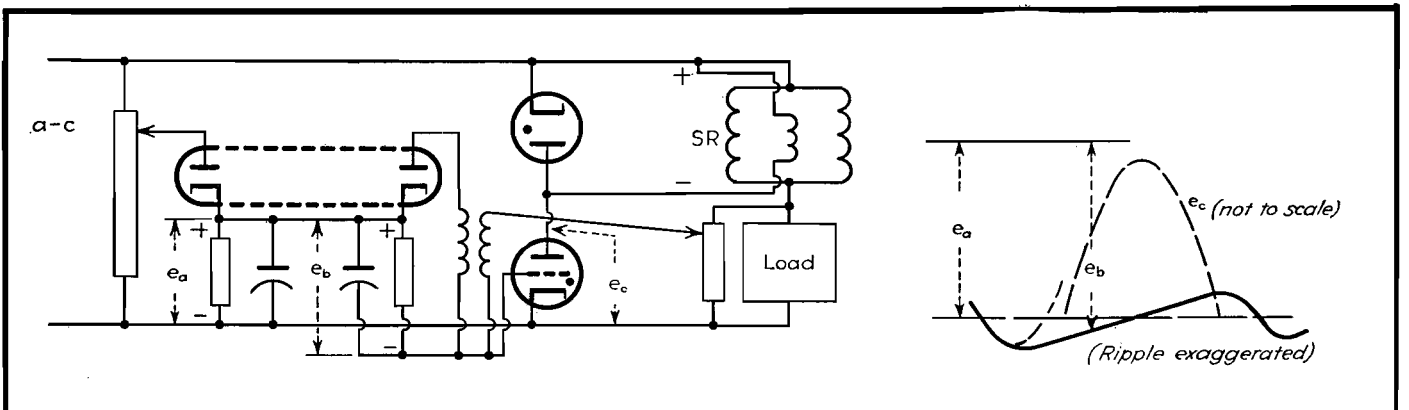
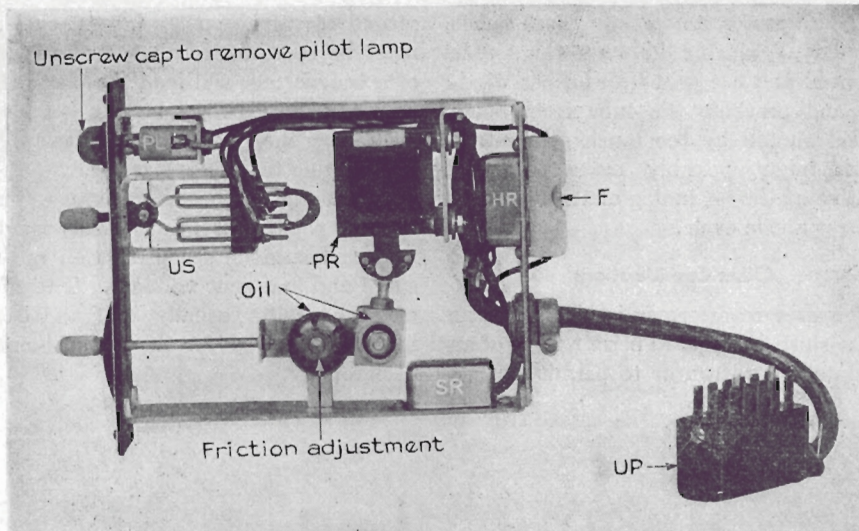


Fig. 9.—Grid control for saturable reactor excitation, with curves of wave form.





Small solenoid with adjustable core PR in a unit control panel.

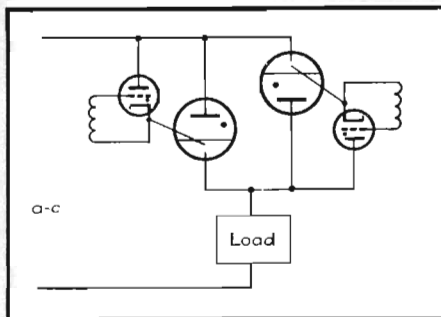


Fig. 12.—Anode firing of ignitrons by thyatrons acting as single-phase a-c switches.

from a peaking transformer. This type of circuit is often used in the large pumped type of ignitron rectifier. When the arc has started, the igniter current is transferred to a relieving electrode which protects the starter from excess current and heating. A blocking layer rectifier is placed in series with the igniter to prevent damage due to reverse current.

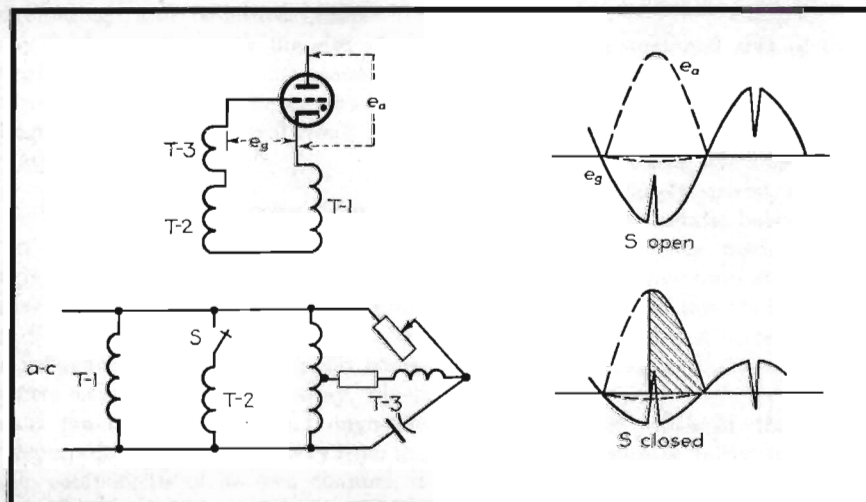


Fig. 13.—Three-transformer grid circuit for thyatron used to fire on ignitron as in Fig. 12. T-1 supplies hold-off voltage; T-2 supplies turn-on voltage; and T-3 supplies peaking voltage, adjustable phase. S is a control switch.

#### Anode Firing

An ignitron tube for control circuits, such as resistance welding, is usually fired by the principle known as anode firing (Fig. 12). In this circuit, a firing thyatron is connected between the ignitron anode and the igniter. When the thyatron grid is fired in the usual way, the igniter is thus connected to the ignitron anode, but as soon as the ignitron is ionized and becomes conducting, the voltage across the thyatron and igniter drops to the interelectrode potential of the ignitron (below 20 volts), and the thyatron is extinguished, thus protecting the igniter.

Because the thyatron cathode is floating except for its connection to the igniter, it is necessary that it be fired through a grid transformer. Its grid circuits (Fig. 13) often consist of three transformer secondaries. The first T-1

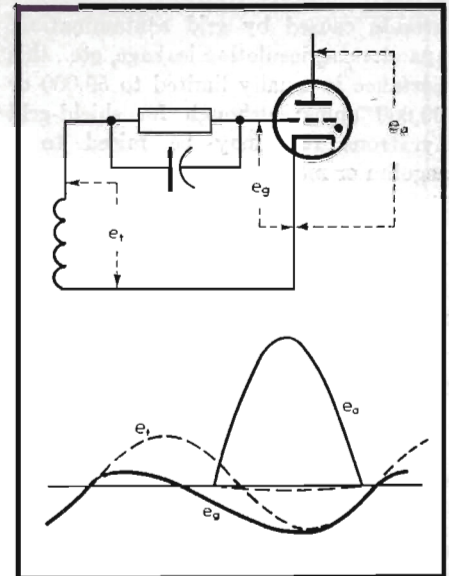


Fig. 14.—Phase advance obtained by grid rectification.

is an out-of-phase voltage which holds the grid quite negative. The second T-2 is an in-phase voltage not quite equal to the first out-of-phase voltage, which is energized when the thyatron is to conduct. The third T-3 is the secondary of a peaking transformer which may be phase shifted and which, combined with the second "turn-on" voltage, permits the thyatron to fire when the second transformer is energized.

Since resistance welders are inherently low power-factor lagging loads in which the thyatron is fired somewhere between 45 and 135 electrical degrees, this circuit is quite satisfactory for this operation.

#### Cautions to Be Observed

It must be remembered that each time the grid of an electron tube goes positive, it tends to draw grid current. This current is usually minimized by inserting a resistor in series with the grid. From a theoretical standpoint, this should be as high as possible, but from a practical standpoint, owing to small parasitic

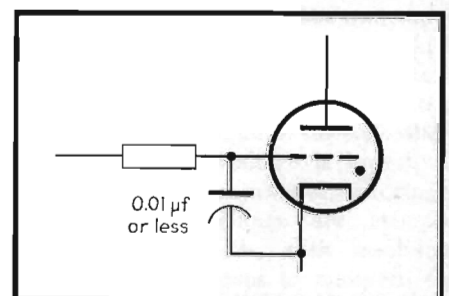


Fig. 15.—Grid-cathode capacitor for protection against surge or transient voltages.

currents caused by grid contamination, capacitances, insulation leakage, etc., this resistance is usually limited to 50,000 or 100,000 ohms; although for shield-grid thyratrons this may be raised to a megohm or more.

#### Grid Rectification

Sometimes, a small capacitor is placed in parallel with this grid resistor (Fig. 14) to be charged by grid rectification on the inverse cycle and thus force the grid slightly more negative than usual. This

compensates for any small phase shifts that have occurred between the anode potential and the grid transformer winding, and prevents the tube from being turned on full by too much grid retard which might possibly make the grid positive at the beginning of the following positive anode cycle.

#### Other Considerations

If a grid transformer is placed in the phase-shifted circuit to permit firing of an insulated thyatron or to permit firing a

second thyatron on the inverse cycle, it must be remembered that the reactance of a transformer will load the phase-shift circuit, and this must be allowed for in computing the vectors. This also applies if a peaking transformer is used.

It is customary in some circuits to place a small capacitor (Fig. 15) between the grid and cathode for protection against surge and transient voltages. The effect of this capacitor, usually less than  $0.01 \mu f$ , must be allowed for in the grid-circuit design.

## SECTION XI

# IRON-CORE TRANSFORMERS AND CHOKES

	Page
Notes on Iron-core Transformer Design.....	145
Design of Audio Reactors for D-c Service.....	147

## Notes on Iron-core Transformer Design

By E. B. HARRISON

---

Power transformers and filter reactors designed to minimize stray fields are described. Comparable audio types attenuate external fields about 90 db

---

ONE of the greatest sources of noise in an amplifier is the complex field created by power transformers and filter reactors. Perhaps the most effective method of eliminating this noise is the reduction of fields at their source.

For a transformer of conventional shell-type design with a given load rating, the shape and magnitude of the stray field depends on several factors, among which are the size of the transformer, the flux density at which the transformer core is operated, the geometry of the core structure, and the magnetic shielding surrounding the structure. Since the stray field increases with the size of the transformer and with increased flux density, there is an optimum size, other things being equal, that will result in the lowest stray field.

### Reducing Power-transformer Fields

In any shell-type design utilizing a single coil, the lowest stray field may still be large enough to modulate the program in adjacent audio transformers and tubes. Its influence can extend to audio transformers as much as 3 to 4 ft away, which means practically that even though the power equipment is located away from the audio components of its own channel, it may affect other channels in adjacent racks. It has been found desirable, therefore, to produce transformers designed for operation in crowded racks. These transformers are built on a core-

type magnetic circuit, having two coils astatically balanced, occupy less space than the conventional design, and operate at high efficiencies, *i.e.*, with low temperature rise.

Figure 1 is a sketch of the core structure around which this type of transformer is built. It can be shown that for the most efficient designs the following approximations hold:

1. The core loss in watts is equal to the copper loss in watts.
2. The mean length of the magnetic circuit is equal to the mean length of the copper circuit.
3. The cross-sectional area of the core is equal to the cross-sectional area of the window.

The geometry of the structure is such that the coils are long solenoids with their magnetic axes closely spaced, resulting in an almost perfect astatic balance of their fields. Measurements made on transformers built to these proportions indicate that the field is so low that moderately shielded low-level input transformers may be operated next to them without hum pickup.

The narrow width of the core was chosen to ensure a fairly uniform flux distribution, and this flux distribution is enhanced by the method of stacking, reducing the usual areas of high flux density and resulting high loss.

In a fully interleaved core assembly (*i.e.*, 1 and 1) as shown in Fig. 2, the

reluctance of the air gap at the lamination joint causes a portion of the flux to seek a path through the adjacent laminations, raising the flux density and losses therein. Now, when the extent of the interleaving is reduced by stacking the laminations in pairs (2x2), the reluctance of the leakage path through the adjacent laminations is increased, because the length is effectively increased, forcing a greater portion of the flux to flow across the joint air gap. The reduction of high-flux-density areas, by this method of stacking, increases the permeability of the total core structure as shown in Fig. 3, where the solid line represents the permeability of the 1 by 1 stack, and the dotted line that of the 2 by 2 stack.

### Filter-reactor Design

Since their fields generally are of the most vicious type, being made up of not one but many frequencies, the companion power filter reactors were built around the same principles of design. The astatic balance is carried to the point of locating the air gap in the center of the coils where the possibility of leakage is lowest, as shown in Fig. 4. In practice, two stacks of U-shaped punchings are clamped together in the coils, with insulating spacers in the air gaps to maintain the correct gap separation.

The clamps and bolts are so located that very little magnetic flux passes through them. The removal from the

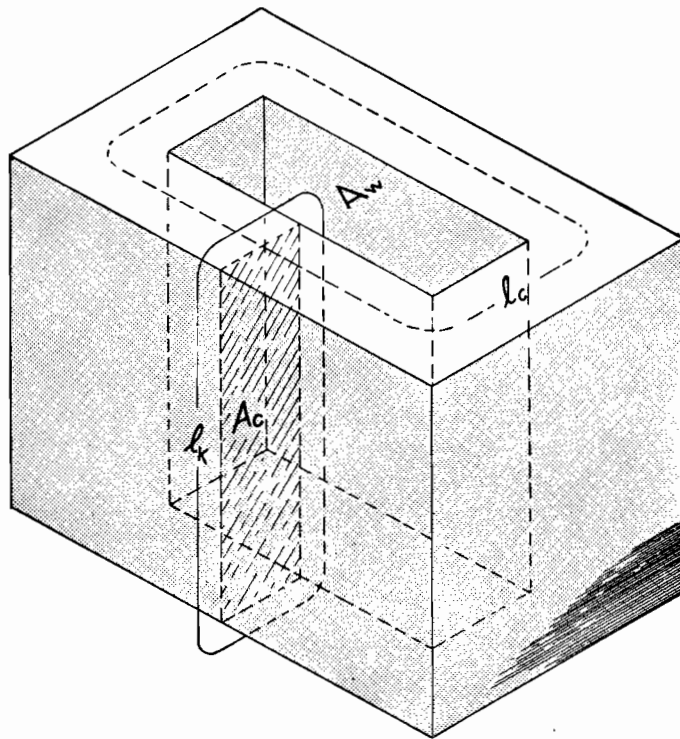


Fig. 1.—Core structure of the type of power transformer discussed by the author.  $A_c$  is area of core;  $A_w$  is area of window and is equal to  $A_c$ ;  $l_c$  is length of magnetic circuit;  $l_k$  is length of copper circuit and is equal to  $l_c$ .

magnetic circuit of this relatively high-coercive-force steel eliminates all the harmonics generated by the common commercial type of filter choke which is clamped together between steel frames secured by bolts passing through the core, all of which carry magnetic flux. The  $Q$  of the choke is raised appreciably so that a substantially better filtering action is obtained for a given inductance. Incidentally, audio chokes designed on these principles have shown a  $Q$  of 70 at 1,000 cycles.

#### Audio-transformer Design Factors

Audio transformers operate at low inductions, ranging from several thousand gauss in a high-level output transformer

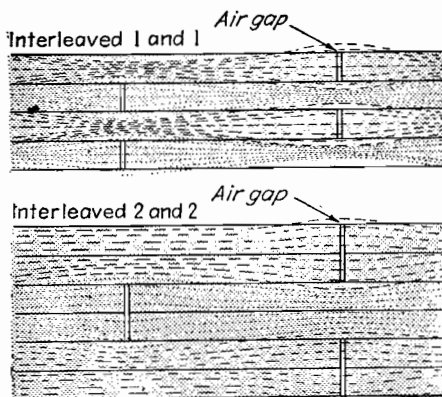


Fig. 2.—Lamination joints of two types of interleaved-core assemblies.

down to 1 gauss and less in low-level input and interstage transformers. The hysteresis and eddy-current losses at low induction must be small, and the initial permeability should be high. Since eddy-current losses vary inversely with the resistivity of the core material, and as the square of the thickness of the laminations, the core stock must also have high electrical resistivity and must be used in thin sheets.

The presence of eddy currents in the core results in a phenomenon known as skin effect or shielding effect. This effect is merely the observed result of the loading caused by the secondary currents circulating around the individual laminations. The cemf generated by these currents prevents the penetration of flux to the center of the plate or lamination. This means that as the frequency is increased the effective core area decreases, the total flux is less, the permeability is less, and the inductance of the winding goes down.

To take full advantage of the high initial permeability, the core should be laid out with as short a path as possible, having a minimum of high-reluctance joints, best located actually within the windings surrounding parts of the core. It is fortunate that the requirements for small-size high-inductance transformers lay in the low-level field where the trans-

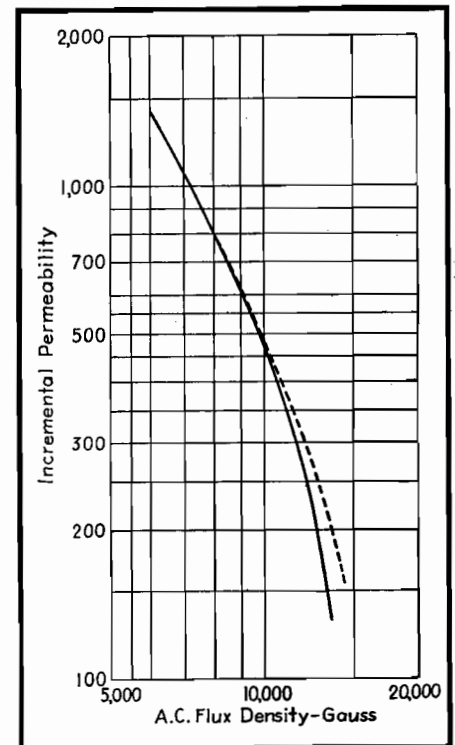


Fig. 3.—Relationship between flux density and incremental permeability of total core structure of a power transformer.

former has nothing to do but present to the tube grid a considerably enlarged facsimile of the input signal voltage, because it is frequently the case that high copper-insertion losses are built into such a design.

The windings surrounding the core, of necessity, have distributed capacitance across themselves, between themselves, and to the core and the case. These capacitances are nearly always unequal; i.e., the effective capacitances across the two ends of a coil are unlike, which in the case of a push-pull transformer will, as the frequency increases, cause increasingly unequal voltages to be impressed on the tube grids. The deviation usually is quite pronounced well below the frequency of resonance, and the point at which a measurable difference is found should be taken as the upper limit of the range that the transformer can cover.

#### Shielding Improves Balance

The capacitive balance between the windings can be improved, or at least controlled, by the introduction of shield windings or sheets. Sometimes the shield is connected to a section of the winding; more often it is tied to ground. Frequently, windings are placed in a coil at a place where they act as shield windings, because, in the circuit in which they are



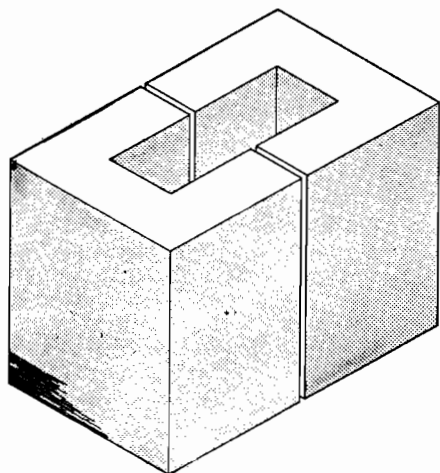


Fig. 4.—To obtain minimum flux leakage, the air gap of a filter reactor is located in the center of the coils.

used, they are connected externally to ground.

When the shield is introduced between the primary and secondary windings and connected to ground, electrostatic shielding, which prevents the transmission of incoming longitudinal currents past the barrier thus set up, is also obtained.

Since magnetic flux is not only in the core, but also linking every part of the winding, leakage links are present, causing the induction of a lesser voltage in some coils than in others with equal turns. For this reason, each winding must be

symmetrically located with respect to the other windings. In the case of a push-pull transformer, both secondary windings must cut the same amount of leakage flux, and the leakage flux around the start of the primary must be the same as the leakage flux around the end of the primary winding. It is this leakage flux, which does not thread all the windings of all the coils, that is responsible for the leakage reactance in a transformer, resulting in a drooping response at high frequency. Many transformers have had designed into them just the proper amount of leakage reactance to resonate with the high distributed capacitance across the secondary windings at a predetermined high frequency. Such a transformer will show an excellent frequency-response characteristic, but will not have the same time constant for all frequencies. Neither will it reflect a constant load to the line. These faults can be only partially corrected by secondary loading, as a loss of high frequencies is sure to result.

The windings on each side of a balanced transformer must have equal resistance. In the case of a symmetrical coil arrangement, this usually follows as a matter of course. However, in some designs of a special nature where one part of a coil is wound on top of another, it may be necessary to change the wire size to accomplish the desired result.

In an effort to keep the over-all size of a transformer small, very fine wires are used in the high-impedance windings. The wires are also reduced in size because the spacing between winding layers must be large to keep the distributed capacitance low. The presence of any moisture in the coil or in the paper insulation would seriously impair the balance between the coils and the h-f response of the transformer. This moisture would also facilitate electrolytic action between the bare coil ends where they are attached to the lead wires. It is necessary, therefore, that the coil be thoroughly desiccated and then sealed.

This may be accomplished by a vacuum impregnation system in which the coils are heated under pressure and then maintained in a heated condition at a high vacuum for 12 to 16 hr. While still heated and under vacuum, the transformers are immersed in a high-melting-point amorphous wax which has been highly refined to remove impurities. Pressure is then applied to the surface of the hot fluid wax to force it into the coil and between the laminations. The paper layer becomes framework to support an insulating layer of wax. Each individual wire is fully coated, and the individual laminations are insulated from each other by a coat of wax.

## Design of Audio Reactors for D-c Service

By REUBEN LEE

Methods, applicable to small units as well as large, for designing and rating iron-cored audio reactors in terms of the steady direct current they must carry

THE design of reactors carrying direct current, i.e., the selection of the right number of turns, air-gap, etc., can be done directly and simply from a magnetic data curve such as that in Fig. 1, plotted between  $LI^2/V$  and  $NI/l_c$ . The various symbols comprised in the coordinates are

$L$  = a-c inductance, henrys

$I$  = direct current, amp

$V$  = volume of iron core, cu cm =  $A_c l_c$  (ref. Fig. 2)

$A_c$  = cross-section of core, sq cm

$l_c$  = length of core, cm

$N$  = number of turns in winding

$a$  = air gap, cm

An example will show how easy it is to make a reactor according to this method. Assume a stack of iron having a cross-section  $\frac{7}{8}$  by  $\frac{3}{8}$  in., and suppose the iron fills 92 per cent of this space. The measured length of the flux path in this core is  $7\frac{1}{2}$  in. It is desired to know how many turns of wire and what air gap are necessary to produce 70 henrys when 20 ma direct current are flowing in the winding.

This problem is solved as follows:

$$A_c = (0.875)^2 \times (2.54)^2 \times 0.92 = 4.55 \text{ sq cm}$$

$$l_c = 7.5 \times 2.54 = 19.05 \text{ cm}$$

$$\frac{LI^2}{V} = \frac{70 \times 4 \times 10^{-4}}{4.55 \times 19.05} = 3.23 \times 10^{-4}$$

From Fig. 1 it is seen that  $NI/l_c$  is 7.5, and the air gap is between 0.001 and 0.0012 times the core length.

$$\frac{NI}{l_c} = 7.5$$

$$N = \frac{7.5 \times 19.05}{0.020} = 7,150 \text{ turns}$$

The total air gap per leg is between  $0.001 \times 7\frac{1}{2}$  and  $0.0012 \times 7\frac{1}{2}$ , or 7.5 to 9 mils; the exact value is not of material

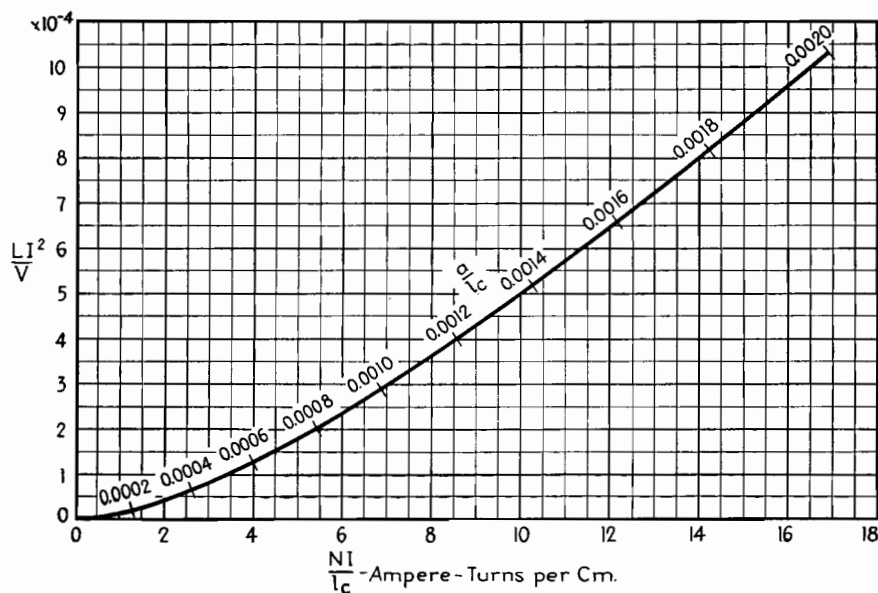


Fig. 1.—Fundamental reactor design chart for silicon steel. Dimensions used are shown in Fig. 2.

consequence. The reason for this statement will appear later.

The curve of Fig. 1 is the envelope of a family of fixed air-gap curves such as those shown in Fig. 3. These curves are plots of calculations based on the assumption that the a-c flux in the iron core has a negligibly small value compared with the d-c flux. Each curve has a region of optimum usefulness, beyond which saturation sets in, and its place is taken by a succeeding curve having a larger air gap. A curve tangent to the series of fixed air-gap curves is that of Fig. 1, and the regions of optimum usefulness are indicated by the scale  $a/l_c$ . Hence Fig. 1 is a curve determined by the d-c flux conditions in the iron and represents the most  $LI^2$  or energy content for a given amount of a given material.

Figure 3 illustrates how the exact value of air gap is of little consequence in the final result. The dotted curve connecting curves B and C is for an inter-

mediate value of gap, 6 mils. Point  $Y'$  represents the maximum inductance that could be obtained from a given core at this point by using a 6-mil gap. Point  $Y$  is the inductance obtained if a gap of either 4 or 8 mils is used. The difference in inductance between  $Y$  and  $Y'$  is 4 per cent, for a difference in air gap of 33 per cent.

It should be realized here that the length of the path of magnetic flux through the coil has two components: the air gap  $a$ , and the length of the core  $l_c$ . In Fig. 1 these two components are handled separately,  $l_c$  in the scale of abscissas and  $a$  in the scale plotted along the curve. The two components do not add directly because their permeabilities are different. In the air gap, of course, the permeability is unity, while in the core it has a value depending on the degree of saturation of the iron. Figure 4 shows the permeability for a typical high-grade silicon steel. The effective length of the magnetic path is  $a + l_c/\mu$ , for the steady or d-c component of flux.

The curve in Fig. 4 marked  $\mu$  is the normal permeability of the iron for a steady value of flux—in other words, for the d-c flux in the core. It is quite different, however, from the permeability for small alternating fluxes superposed upon this steady value. The latter is marked  $\mu_\Delta$  in Fig. 4, and it is known as incremental permeability. The a-c inductance of the reactor is determined by the length of the a-c flux path and hence, to a large extent, by the incremental permeability.

The distinction between  $\mu$  and  $\mu_\Delta$  is

made clear by referring to Fig. 5, which shows the top half of a typical hysteresis loop. The direct current in the winding fixes the steady magnetizing force  $H_{d-c}$ , to which corresponds a flux density  $B_{d-c}$ . A small alternating voltage across the reactor causes a superposed increment of flux  $\Delta B$  to alternately add to and subtract from  $B_{d-c}$ , following the small hysteresis loop which touches the large loop at point  $E$  and the normal magnetization curve at point  $F$ . The incremental permeability is  $\Delta B/\Delta H$  and is represented by the slope of the line  $AA'$ . It will be seen that  $AA'$  has a slope much less than that of the normal magnetization curve at point  $O$ . Also, the smaller  $\Delta B$  is, the flatter the line  $AA'$  becomes, and consequently the smaller the value of permeability  $\mu_\Delta$ .

Because of this low value of  $\mu_\Delta$  for minute alternating voltages, the effective length of magnetic path  $a + l_c/\mu_\Delta$  is considerably greater for alternating than for steady flux. But the inductance varies inversely as the length of a-c flux path. If, therefore, the incremental permeability is small enough to make  $l_c/\mu_\Delta$  large compared with  $a$ , it follows that small variations in  $a$  do not affect the inductance much. This is the reason that the exact value of the air gap is not important.

The conditions assumed by the foregoing method of design are met in most radio applications. In receivers and amplifiers working at low audio levels, the a-c voltage is small and hence the alternating flux is small compared with the d-c flux. Even if the a-c voltage is on the same order as the d-c voltage, the a-c flux may be small. This is true if a large number of turns are necessary to produce the required inductance; for a given core, the a-c flux is inversely proportional to the number of turns.

#### Use with Large Reactors

With the increasing use of higher audio power, necessitating larger sizes of reactors and transformers, it often happens that that a-c flux is no longer small compared with the direct current. This is especially true in high-impedance circuits, where the direct current has a low value and the alternating voltage has a high value.

To illustrate the effect of these latter conditions, assume a reactor has already been designed for negligibly small alternating flux (i.e., according to Fig. 1), and operates as shown by the small loop of Fig. 5. Without changing anything else, suppose the alternating voltage across the reactor is greatly increased, so that

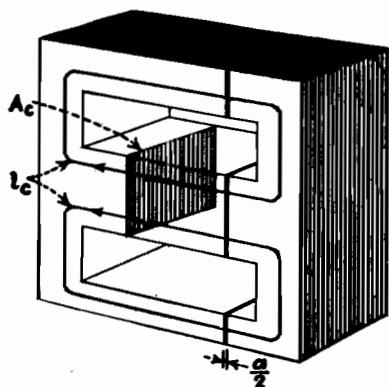


Fig. 2.—Typical core structure, showing dimensions used in reactor design.

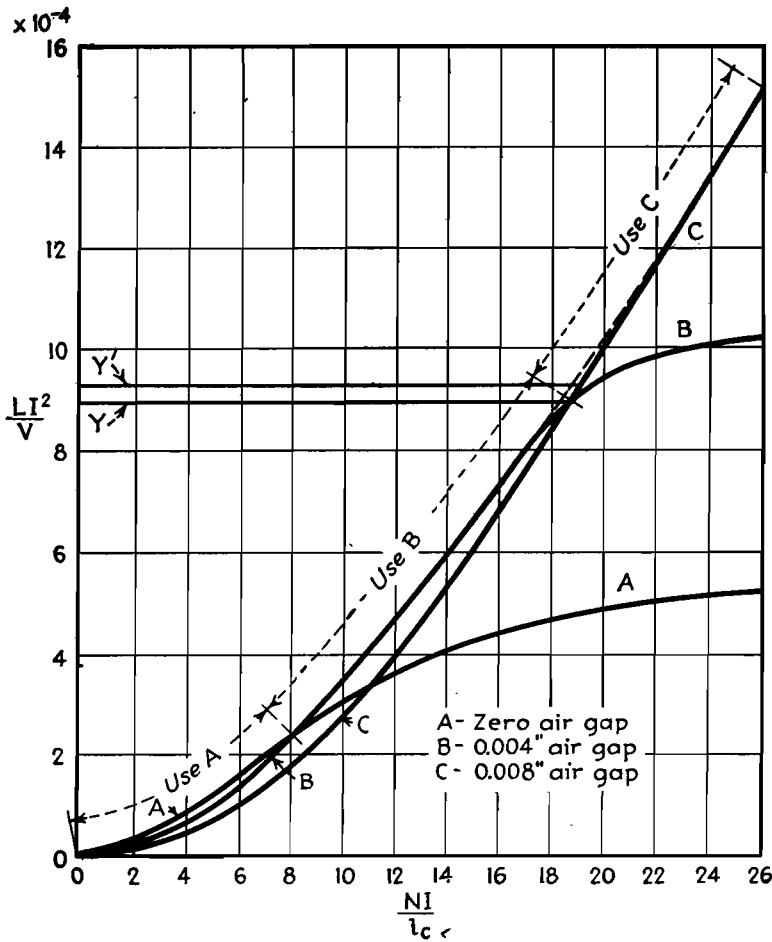


Fig. 3.—The envelope of several magnetization curves for different air gaps gives the maximum energy per unit volume (cf. Fig. 1).

the total a-c flux change is from  $B_1$  to  $B_2$ . The reactor still operates about point  $O$ . The hysteresis loop, however, becomes the unsymmetrical figure  $CFDEC$ . The average permeability during the positive flux swing is represented by the line  $OC$ , and during the negative flux swing by  $OD$ . The slopes of both  $OC$  and  $OD$  are greater than that of  $AA$ ; hence, the first effect exhibited by the reactor is an increase of inductance.

The increase in inductance is nonlinear, and this has a decided effect on the performance of apparatus. An inductance bridge measuring such a reactor at the higher a-c voltage would show an inductance corresponding to the average slope of lines  $OD$  and  $OC$ . But if the reactor were put in the filter of a rectifier, the measured ripple would be higher than a calculated value based on the bridge value of inductance. This is because the positive peaks of ripple have less impedance presented to them than do the negative peaks; hence they create a greater ripple at the load. Suppose, for example, that the ripple output of the rectifier is 500 volts, and this would be

attenuated to 10 volts across the load by a linear reactor having a value of inductance corresponding to the average slope of lines  $OC$  and  $OD$ . With the reactor working as indicated by Fig. 5, the slope of  $OD$  is five times that of  $OC$ . Conse-

quently, the expected average ripple attenuation of 50:1 actually becomes 16.7:1 for positive flux swings, and 83.3:1 for negative, and the load ripple is  $1/2(500/16.7 + 500/83.3) = 18$  volts, or an increase of nearly 2 to 1 over what would be anticipated from the measured value of inductance.

Turning to modulation chokes and transformers, assume that in Fig. 5 curve  $CFDEC$  represents the operation of such a component. The reactive current drawn from the modulator tubes at low audio frequencies may be well within reasonable bounds for negative peaks of modulation, but may be high enough at positive peaks to cause an excessive amount of low-frequency distortion. This may be confirmed by comparing the change in  $H$  (which is a measure of reactive current) on both sides of point  $O$ ; the positive peak current is five times as great as the negative peak current.

This high positive peak current could be reduced to a value approaching the negative peak by increasing the air gap somewhat, and thereby reducing  $H_{a-c}$  so that it passes through point  $O'$ . Now  $B_1$  and  $B_2$  drop down so as to intersect  $D'$  and  $C'$ , respectively. Moreover, the average permeability has increased, and so has the inductance. It will be apparent that to decrease  $H_{a-c}$  further means another increase in a-c permeability—approaching in value the d-c or normal permeability. As a matter of fact, this is what a good design of modulation reactor involves: keeping the a-c permeability high for both positive and negative modulation peaks. This can be done only if the maximum flux density is kept

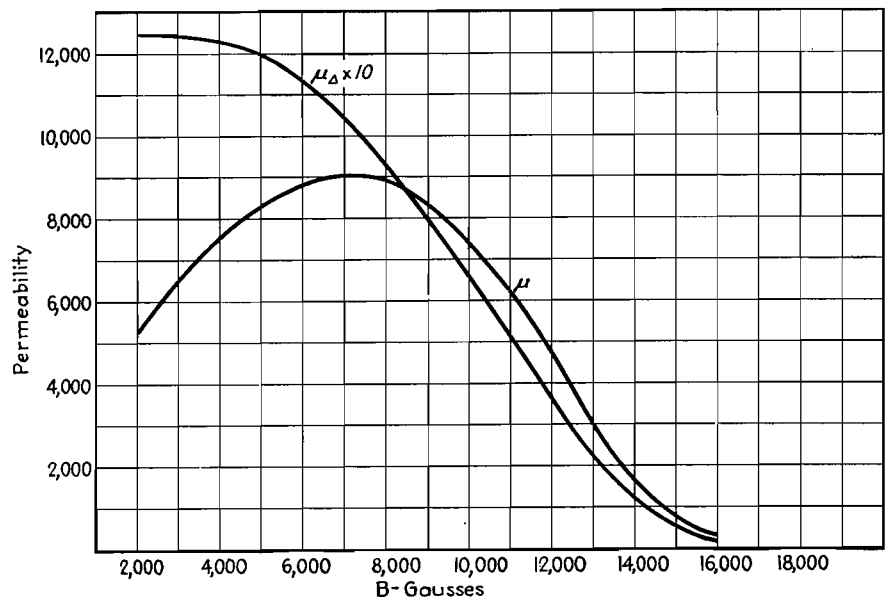


Fig. 4.—Normal and incremental permeabilities for silicon steel.

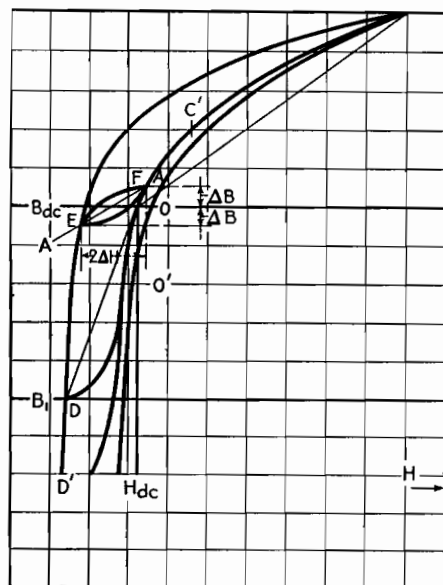


Fig. 5.—Hysteresis loops for d-c reactors.

low enough to avoid the saturating effects represented by point *C* in Fig. 5. Conversely, it follows that if saturation is present in a reactor, it is manifested by a decrease in inductance as the direct current through the winding is increased from zero to full load value.

In a reactor having high a-c permeability, the equivalent length of core  $l_c/\mu$  is likely to be small compared with the air gap  $a$ . Hence, it is vitally important to keep the air gap close to its proper value in modulation components. This is in marked contrast to reactors not subject to high a-c voltages.

If a modulation choke is to be checked to see that no distortion-producing saturation effects are present, access must be had to an inductance bridge. With the proper values of alternating voltage across the reactor, measurements of inductance can be made with various values of direct current through it. If the inductance remains nearly constant up to normal direct current, no saturation is present, and the reactor is suitable for the purpose. If, on the other hand, the inductance drops considerably from zero direct current to normal direct current,

the reactor very probably is a distortion producer. Increasing the air gap slightly may improve it, otherwise it should be discarded in favor of a reactor that has been correctly designed for the purpose.

The fact that the inductance is greater with no direct current in the reactor is taken advantage of in the design of swinging chokes. These chokes are used in rectifier filters to improve the regulation. The higher the inductance of the choke, the less rise in voltage there is at light d-c loads. If, then, the choke is allowed to saturate considerably at full load, the inductance rises as the load is decreased, and the regulation is improved, without necessitating the use of a large choke having high inductance at full load. Part of the advantage is lost because saturation prevents the reactor from performing well on positive ripple peaks at full load, but the over-all result is a smaller choke for the same regulation and ripple.

Besides this quality of linearity, it is necessary that the reactor or transformer have the proper amount of inductance. The latter can be found from Fig. 6, which represents the low-frequency end of three audio response curves. Instead of having frequency for abscissas, these curves have

$X_n/R_1$ , where  $X_n$  is the reactance at low audio frequencies and  $R_1$  is the resistance of the source, such as a transmission line or vacuum tube. The remaining variable  $R_2$  is the load resistance, and the three curves are for three common relations between  $R_2$  and  $R_1$

$$R_2 = R_1 \text{ (line matching)}$$

$$R_2 = 2R_1 \text{ (load for triodes to give undistorted power output)}$$

$$R_2 = \infty \text{ (open grid load)}$$

In the case of a transformer, the load resistance  $R_2$  is referred to the primary side by the square of the transformer ratio.

A final example will serve to illustrate the use of the curves. Let a transformer be required to deliver the maximum undistorted power output of a triode having a plate resistance of 5,000 ohms into a 500-ohm load, with not more than 1-db drop in response at 30 cycles.

For maximum undistorted power output, the primary load resistance should be 10,000 ohms, and so the turns ratio is  $\sqrt{10,000/500}$ , or 4.46. The proper curve in Fig. 6 is  $R_2 = 2R_1$ , and for 1 db down we see that  $X_n/R_1 = 1.3$  or  $X_n = 6,500$  ohms at 30 cycles. This corresponds to 34.5 henrys primary inductance.

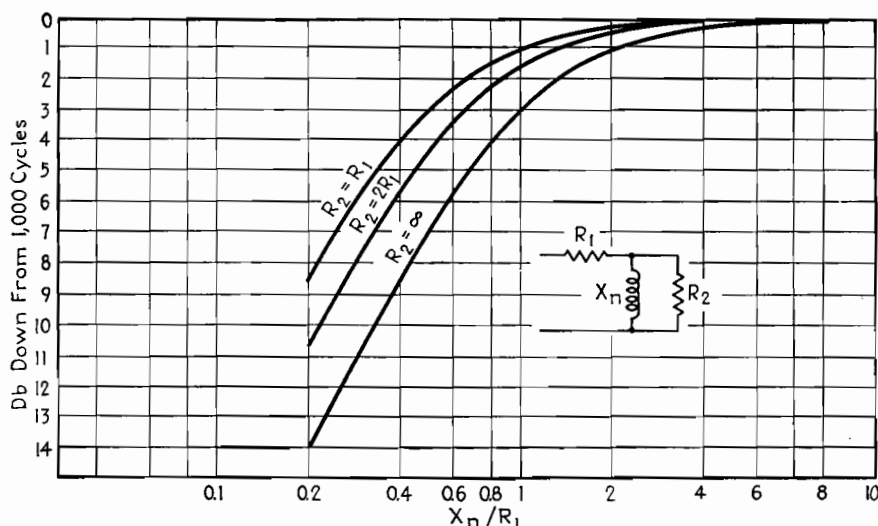


Fig. 6.—Transformer characteristics at low audio frequencies.

## SECTION XII

# MATHEMATICS

	Page
Amplification Factor Chart.....	151
Polar-rectangular and Rectangular-reciprocal Vector Charts.....	153
Impedance-conversion Chart.....	155
Impedance-magnitude and Phase-angle Charts.....	156
Impedance-combining Chart.....	158
Chart for Equivalent Series and Parallel Circuits.....	161
Equivalent Resistance Chart.....	163
Chart for Determining Square Root of a Complex Number	165

## Amplification Factor Chart

By E. R. JERVIS

A method of determining the amplification factor of a receiving tube from its geometrical construction by means of a graphical solution of the Vodges and Elder formula

ONE of the most important parameters in the design of radio receiving tubes is the amplification factor, and there are almost as many methods of calculating it as there are tube engineers. The reason for this multiplicity of solutions is that no formula has yet been found which is completely satisfactory.

The most widely used formula is probably that of Van der Bijl. It is very useful for quick computations, and its accuracy is quite sufficient for practical purposes after its constant for the particular structure in question has been determined. The formulas of Miller and King are certainly more accurate, but the increase in accuracy is not sufficient to compensate for the large increase in complexity of computation. A more accurate version of the formulas, given by Vodges and Elder, is rather involved.

To enable the engineer to compute the amplification factor as accurately as possible with computations kept to a minimum, this formula was put in nomogram form. The chart gives the value of the amplification factor for both cylindrical and plane structures.

The Vodges and Elder formula for cylindrical triode electrodes is

$$\mu = \frac{2\pi NR_g \log_e R_p/R_g - \log_e \cosh \pi NW}{\log_e \coth \pi NW}$$

and for plane electrodes it is

$$\mu = \frac{2\pi ND - \log_e \cosh \pi NW}{\log_e \coth \pi NW}$$

where  $\mu$  = amplification factor  
 $N$  = pitch of grid winding  
 $W$  = diameter of grid wire  
 $R_p$  = radius of plate (cylindrical structure)  
 $R_g$  = radius of grid (cylindrical structure)  
 $D$  = distance between grid and plate (plane structure)

In order that the chart will consist of straight-line scales, two new variables have been introduced. The screening factor of the grid, given by the product  $NW$ , is used instead of the grid wire diameter  $W$ , while the ratio of plate radius to grid radius  $R_p/R_g$  is used instead of the plate radius.

The amplification factor is determined in the following manner. On scale I a point is located that represents the actual grid pitch. On scale II a point is located that represents the screening factor of the grid or the product  $NW$ . A straight line connecting these two points is extended to intersect scale III at a reference point. At this point a discrimination must be made between plane and cylindrical structures. For a plane structure, a point corresponding to  $D$  is located on scale V and a straight line drawn connecting it and the reference point on scale III. This line intersects scale IV at the value of amplification factor for the structure in question.

For a cylindrical structure, points are located on scales VI and VII correspond-

ing to  $R_p/R_g$  and  $R_g$ , respectively, and connected by a straight line extended to intersect scale V at a reference point. A line connecting the reference points on scales III and V intersects scale IV at the value of amplification factor for the structure in question.

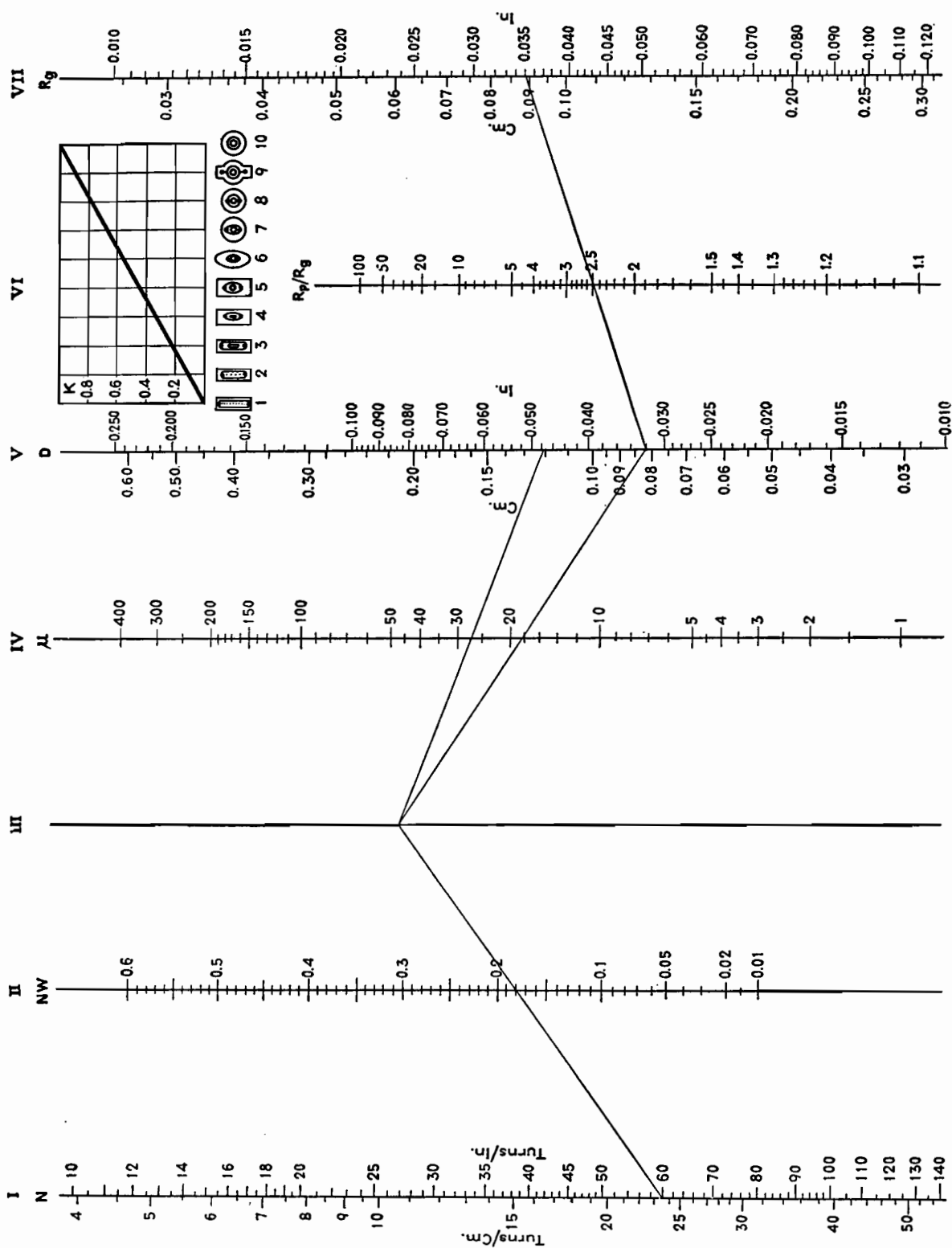
**Comparison between Calculated and Measured Values of Amplification Factor**

Tube type	Structure number	Form factor	Calculated values of			Measured $\mu$
			$\mu_p$	$\mu_c$	$\mu$	
2A3.....	1	00	4.2	...	4.2	4.2
31.....	2	0.11	4.0	2.2	3.9	3.8
45.....	2	0.11	4.0	3.2	3.8	3.5
26.....	5	0.44	8.5	5.8	7.3	8.3
76.....	6	0.55	16	11	13.1	13.8
75.....	7	0.66	148	69	95.8	100
6K5.....	8	0.77	92	47	66.5	70
6B5.....	9	0.88	5.6	4.1	4.24	4.20

The most serious discrepancies from theory result from the presence of grid supports and the fact that tube structures are generally a combination of shapes rather than plane or cylindrical. The general procedure is to determine the value of  $\mu$  considering the structure to be both plane and cylindrical and to take an intermediate value. A fairly close evaluation of the effect of electrode shape can

# AMPLIFICATION FACTOR CHART

By  
E. R. JERVIS



be made by the use of the following formula:

$$K = \frac{\mu_p - \mu}{\mu_p - \mu_c}$$

where  $K$  = form factor

$\mu_p$  = amplification factor for plane structure

$\mu_c$  = amplification factor for cylindrical structure

$\mu$  = amplification factor for actual structure

The insert shows an attempt to evaluate the form factor for various practical

constructions. The diameter of the grid supports is kept constant. A few typical results are given in the table.

An exhaustive discussion of the discrepancies would be too long, because of the complexity of the problem. However, a few cases might well be pointed out. For instance, the 12 per cent error shown for type 45 is due to the abnormal structure of this tube. The plate is very close to the grid, and the grid has a relatively large diameter and a coarse pitch. Therefore, the values of  $\mu_p$  and  $\mu_c$  are close together and their approxi-

mation is poor because of the nonuniformity of the field at the surface of the plate.

In cylindrical structures the most common cause of error is that due to the variation in size and position of the grid supports. A change in diameter or in the center-to-center distance will change the form factor. The relative position and size of the supports have been omitted in the diagram so as not to complicate the problem any further. An average value that has proved to be quite accurate in practical cases has been taken.

# Polar-rectangular and Rectangular-reciprocal Vector Charts

By PAUL W. KLIPSCH

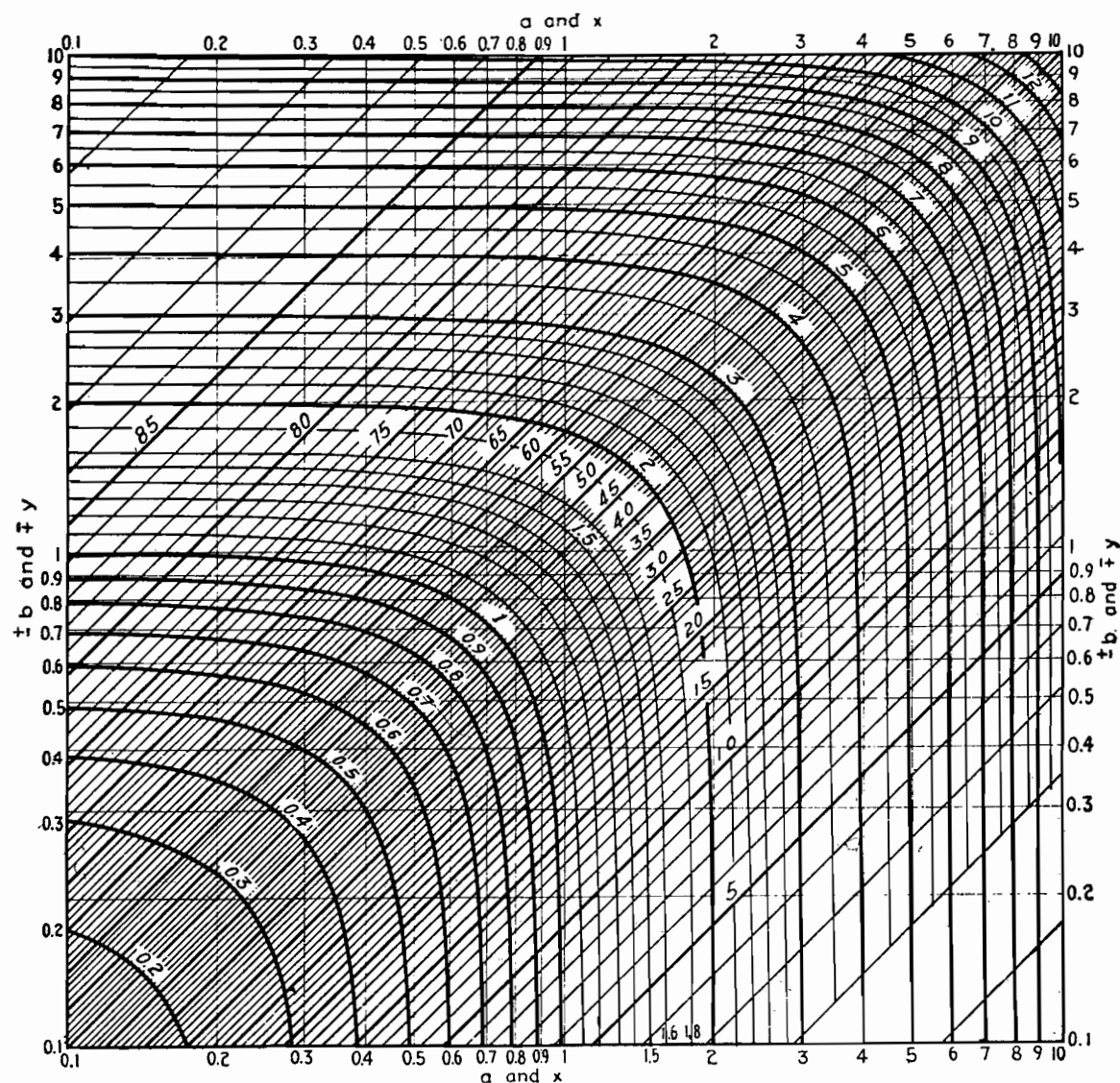


Fig. 1.—Graph for converting between rectangular and polar coordinates to solve equations of the form  $z = x + jy = a \angle b$ . The  $x$  and  $y$  axes are logarithmically spaced, while the curves represent the argument  $a$ . The straight lines from lower right to upper left give the phase angle  $b$ .



Two charts are given here for performing two vector operations, namely, transforming from rectangular to polar coordinates (or the reverse) and determining the reciprocal in rectangular coordinates.

The first of these operations, determining the vector sum or absolute value, together with the phase angle, can be done by means of a slide rule.

Consider the problem of finding  $z$  in the equation

$$x + jy = z$$

The absolute value of  $z$  (written  $|z|$ ) is readily found in two operations on a slide rule as follows: On the  $C$  and  $D$  scales take the ratio of  $x$  and  $y$  such that the ratio, greater than unity, appears on the  $D$  scale at the index mark on the slide. Opposite this ratio, find its square on

the  $A$  scale, add 1, run the slide up to this new point, and under  $x$  or  $y$ , whichever is the smaller, on the  $C$  scale will be found  $|z|$  on the  $D$  scale. For example, take  $3 + j4$ . Set 3 on the  $C$  scale opposite 4 on the  $D$  scale which places the slide index at 1.333 on the  $D$  scale and 1.778 on the  $A$  scale. Add 1 and run the slide index up to 2.778 on the  $A$  scale. Under 3 on the  $C$  scale find the answer 5 on the  $D$  scale. This is in effect a solution of the equation

$$|z| = (x^2 + y^2)^{1/2} = y \left[ \left( \frac{x}{y} \right)^2 + 1 \right]^{1/2}$$

Finding the phase angle involves the additional operation of determining the value of the impedance angle  $\angle z = \tan^{-1} y/x$ .

This method is as simple and fast as the same determination on the vector slide rule.

An alternative of the slide-rule method is the use of the chart of Fig. 1 in which a transformation from rectangular to polar coordinates is performed in a single operation. The modulus and argument (absolute value and phase angle) can be found from the  $x$  and  $y$  components, or the reverse operation can be performed. For example, locating the point  $(3, 4)$  on the rectangular system gives  $|z| = 5$  on the curved coordinates and  $\angle z = 53^\circ$  on the diagonal coordinates.

The second vector manipulation is that of finding the reciprocal. For a series of operations in solving a multimesh network, the multiplicity of slide-rule steps becomes tedious, but the chart of Fig. 2 gives each reciprocal in a single operation. The vector reciprocal is the solution of the equation

$$x + jy = (a + jb)^{-1}$$

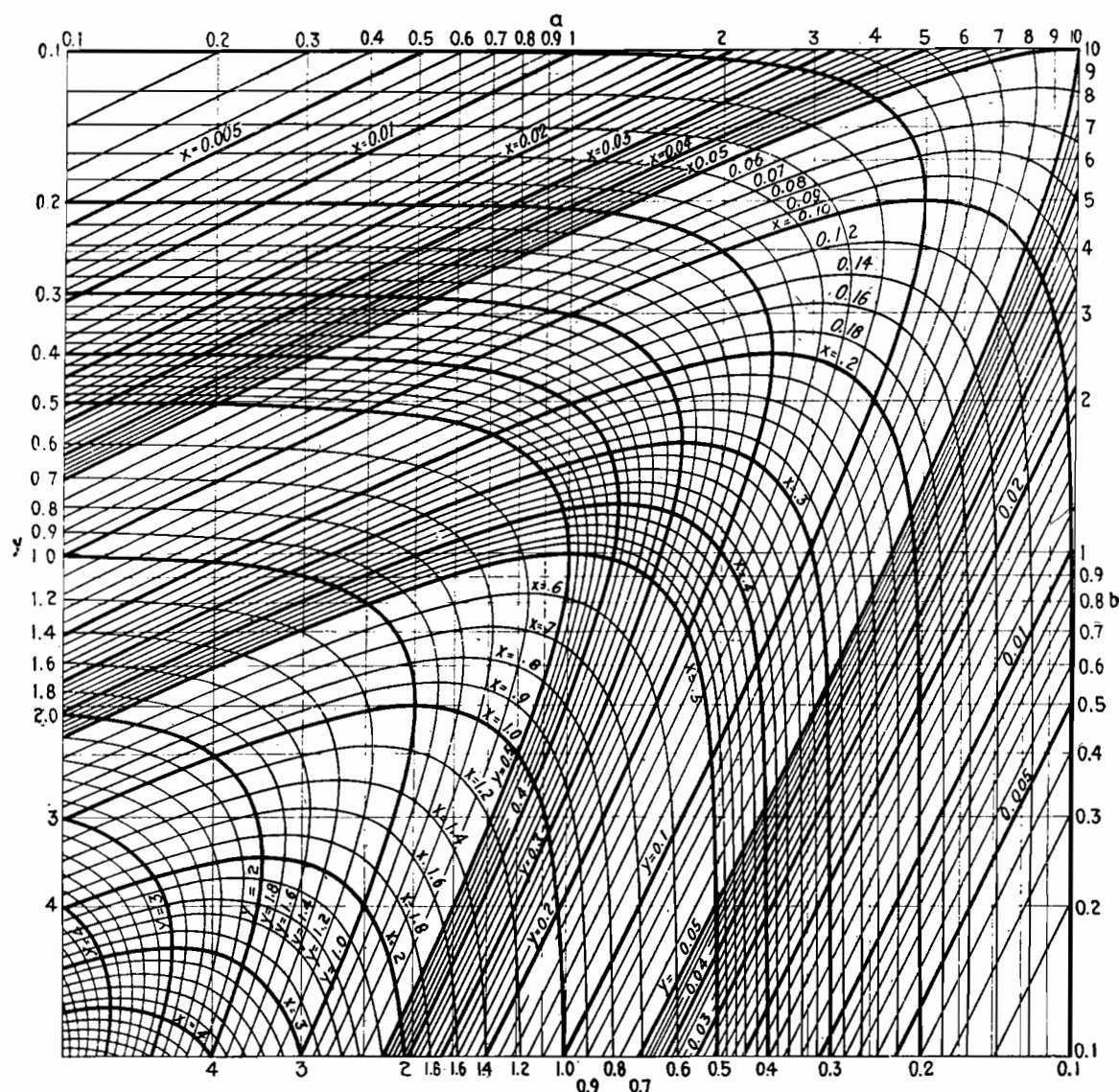


Fig. 2—Graph for determining reciprocal of complex number. The reciprocal of  $z = a + jb = 3 + j4$  on the  $a$  and  $b$  scales (top and right) is found to be  $z^{-1} = x - jy = 0.12 - j0.16$  on the  $x$  and  $y$  scales (bottom and left).

and the solution by means of the chart of Fig. 2 is simply that of looking up the numbers  $a$  and  $b$  on the rectangular system and then finding the coordinates of the same point  $(a, b)$  on the curvilinear system which are  $x$  and  $y$ , the sign of  $y$  being reversed with respect to the sign of  $b$ .

When the ratio of  $a$  to  $b$  lies outside the range  $1/10$  to  $10$ , a simple approximation may be used, and when the numbers are

otherwise off the chart a factor of  $10$  or power of  $10$  may be applied to the number to arrive at a value locatable on the chart, looking up the converted value on the chart and applying the same factor to the answer. To use the  $3 + j4$  example again, the reciprocal is found to be  $0.12 - j0.16$ . As an example of a complex number outside the scale of the chart, take  $30 + j40$ . Using a factor

$1/10$ ,  $(30 + j40)/10 = 3 + j4$ , and the reciprocal is  $1/10 \times (0.12 - j0.16) = 0.012 - j0.016$ . For the case in which the ratio of  $a$  to  $b$  is greater than  $10$ , the chart is not needed to arrive at a close approximation. For example, let  $a + jb = 3 + j40$ . The reciprocal is  $3/40^2 - j1/40 = 3/1,600 - j1/40 = 0.00188 - j0.025$  within less than 1 per cent, the true value being close to  $0.00187 - j0.0249$ .

## Impedance-conversion Chart

By PERRY H. WARE

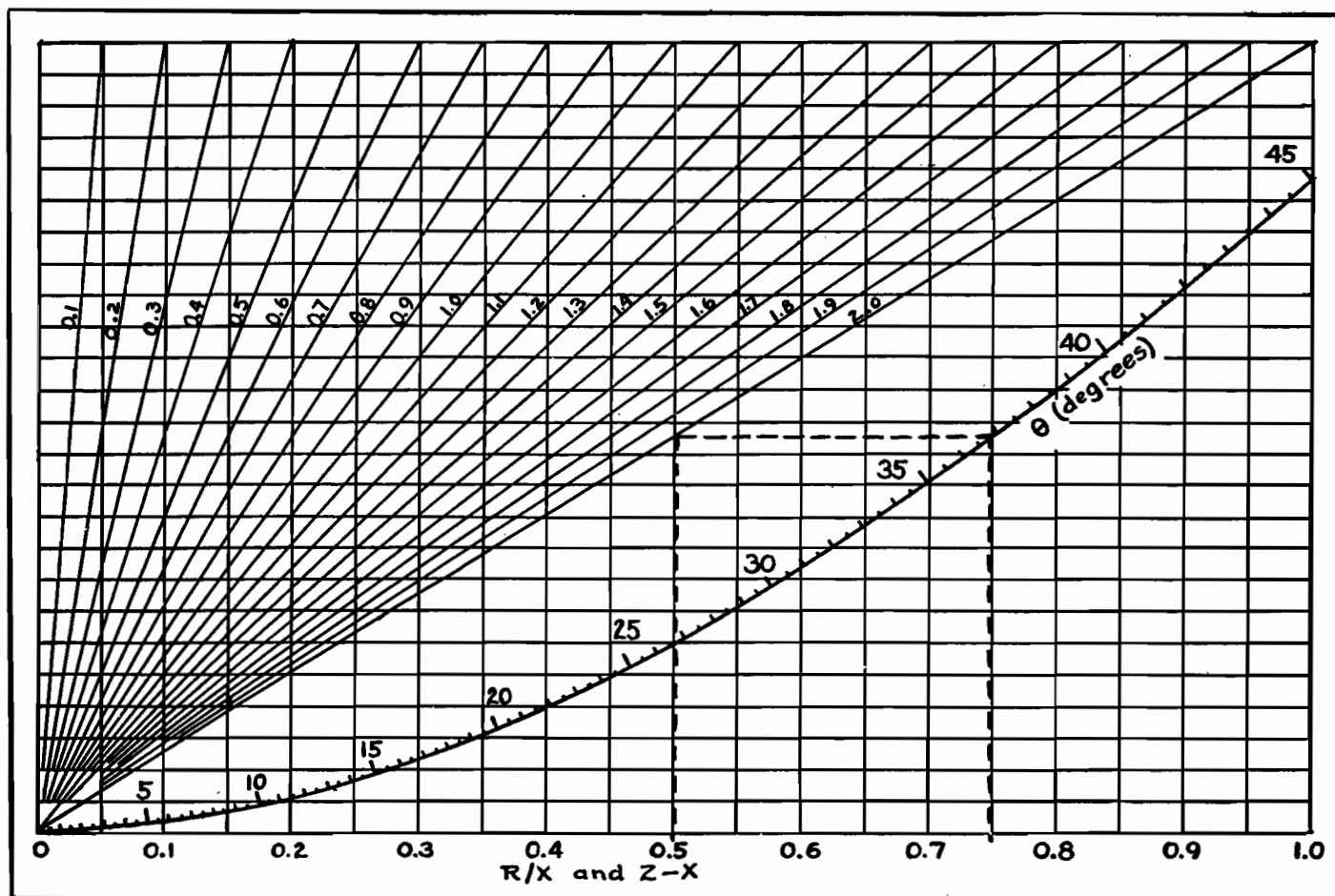
Conversion of complex quantities from rectangular to polar form, or vice versa, is readily accomplished, using only a straightedge. When reactance and resistance are known, the magnitude and phase angle of the impedance may be quickly determined

IN THE course of impedance calculations, it often becomes necessary to transfer the form of an impedance from rectangular coordinates to polar coordinates ( $R + jX = Z/\phi$ ). The accompanying chart pro-

vides a simple and timesaving means of making this transformation.

As an example, suppose that bridge measurements yield an impedance of  $1.5 + j2.0$  ohms. The value of  $R/X$  is

in this case equal to  $0.75$ . Drawing a vertical line (shown as a dashed line on the chart) through  $0.75$  on the horizontal scale, it will be seen that this line intersects the phase-angle curve on the chart



at a value of 36.9 deg. This angle  $\theta$  is the complement of the true phase angle, 53.1 deg. Drawing a horizontal line to the left from 36.9 on the phase-angle curve until it intersects the diagonal line 2.0 corresponding to the value of  $X$ , then dropping a perpendicular to the horizontal scale, we obtain a correction  $Z - X$  of 0.5, which when added to the value of  $X = 2.0$ , yields the impedance,  $Z$  equal to 2.5; therefore  $1.5 + j2.0 = 2.5 \angle 53.1$  deg.

If  $R$  is larger than  $X$ , the ratio  $X/R$  is used as the original argument, and  $\theta$  is the phase angle directly as read. The diagonal line corresponding to  $R$  rather than  $X$  is used, and the correction is added to  $R$ .

The chart will work with any values of  $X$  and  $R$ , by moving the decimal point in the scales of  $X$  (on the diagonal lines) and correction term  $Z - X$  (on the scale of abscissas) the same number of places, leaving the  $R/X$  scale as marked. For

example,  $20 + j15$  yields a value of  $X/R = 0.75$ , giving phase angle equal to 36.9 deg. Considering the line  $R = 2.0$  as  $R = 20$ , the correction term is 5.0, rather than 0.50, and the impedance is  $25 \angle 36.9^\circ$ .

The inverse operation ( $Z \angle \phi = R + jX$ ) may also be carried out by means of estimated values, and practice will enable the user of the chart to carry out the computations quite rapidly.

## Impedance-magnitude and Phase-angle Charts

By T. C. BLOW

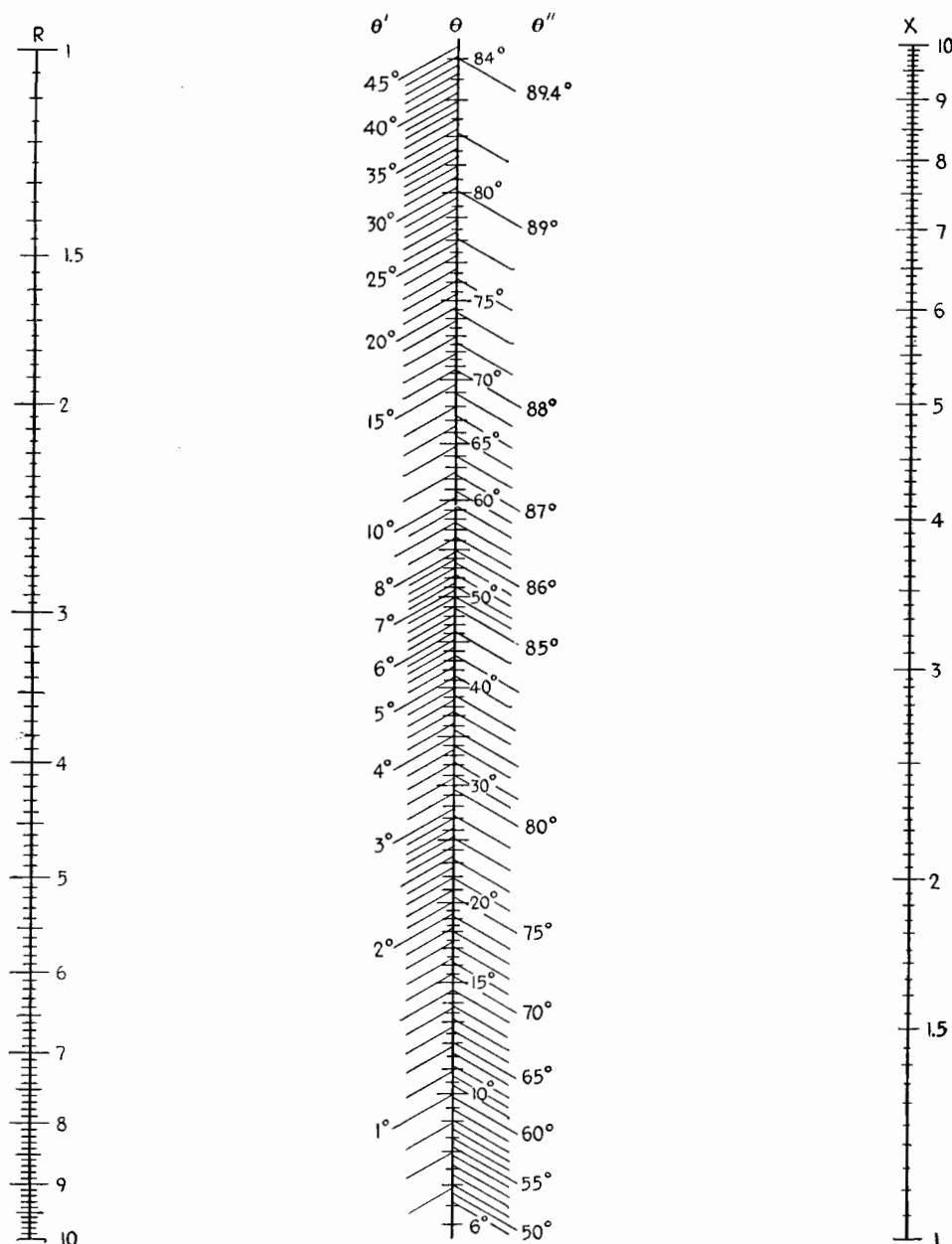


Fig. 1.—Impedance-angle alignment chart.

**T**HE alignment chart (Fig. 2) permits graphical solutions of equations of the type represented by the equation  $Z = (R^2 + X^2)^{1/2}$  for values of  $X/R$  from 0.1 to 10. It is thus useful for determining the magnitude of an impedance.

To determine the impedance magnitude, connect the selected values of  $X$  and  $R$  with a straight line (neglecting decimal points) and read the impedance on the

appropriate  $Z$  scale. If the values of  $R$  and  $X$  are in the same decade, read the center scale  $Z$ . If  $R$  and  $X$  are in adjacent decades, read the  $Z$  scale nearest the larger component. Thus, the scale  $Z'$  is read if  $R$  is larger than  $X$ ; the  $Z''$  scale is read if  $X$  is larger than  $R$ .

*Example.*—To determine  $Z = (8.5^2 + 60^2)^{1/2}$ , in which  $X$  is in the decade beyond  $R$ , connect 8.5 on the  $R$  scale with

6.0 on the  $X$  scale and read 60.5 on the  $Z''$  scale, which is nearer the larger component  $X$ .

The impedance angle chart (Fig. 1) is designed to determine the vector angle of any impedance made up of  $X$  and  $R$  components for values of  $X/R$  between 0.01 and 100.

To determine the phase angle  $\theta$ , connect the selected values of  $X$  and  $R$

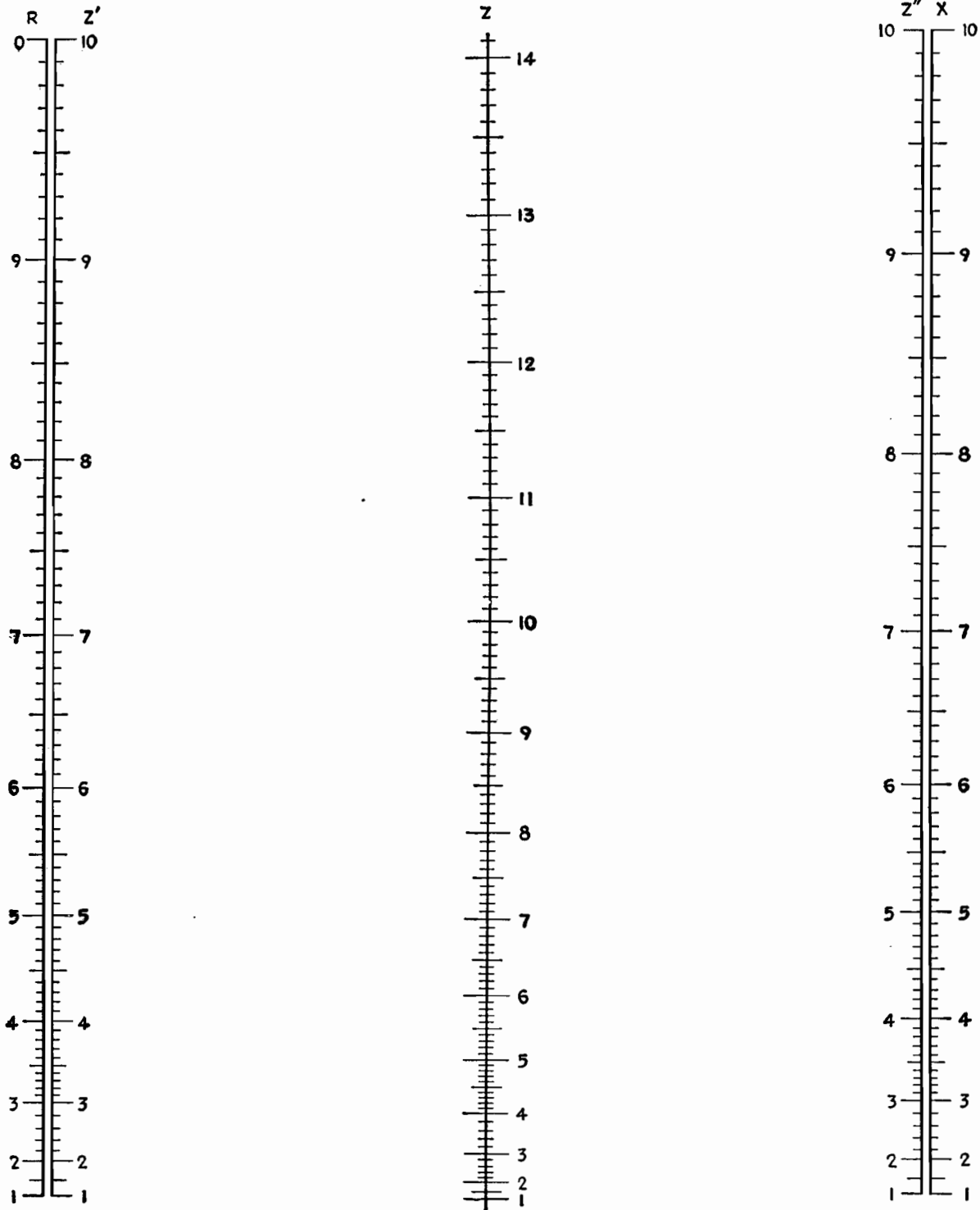


Fig. 2.—Impedance-magnitude alignment chart.

with a straightedge (neglecting decimal points) and read the angle on the proper  $\theta$  scale. If  $X$  and  $R$  are in the same decade, read the center scale  $\theta$ . If  $X$  and  $R$  are in adjacent decades, read the scale nearest the larger component.

*Example.*—To determine the angle of an impedance composed of  $R = 20$  ohms and  $X = 50$  ohms, connect 20 on the  $R$  scale with 50 on the  $X$  scale. The angle is  $\theta = 68.2$  deg., read from the center scale.

*Example.*—To determine the angle of an impedance,  $R = 24$  and  $X = 850$ , connect 24 on the  $R$  scale with 850 on the  $X$  scale. Since these values are not in the same decade and since  $X$  is larger than  $R$ , read  $\theta = 88.3^\circ$  on the  $\theta''$  scale.

## Impedance-combining Chart

By GARY MUFFLY

Timed tests indicate that impedance combined in series or parallel may be computed several times faster with the accompanying chart than with a vector slide rule. Accuracy is better than usually required for practical problems, regardless of the impedance values involved

COMPUTATION of a-c circuits involving complex parallel impedances has always been a laborious process. The graphical method presented here is fast and accurate under all conditions, and is applicable to series as well as parallel combinations of impedances.

All that is required for the method is the chart in Fig. 1, a slide rule, and pencil and paper to tabulate results. Impedance values are kept in polar form. This allows multiplication and division to be performed readily in solving complex-number equations of some of the more involved types of circuits (such as bridges).

### Dual Application

The combining of series and parallel data on one chart is based on the selection of a parameter  $N$  which applies to both cases as shown below:

$$Z_s = Z + z \quad (1)$$

$$Z_p = \frac{Zz}{Z + z} = \frac{Zz}{Z_s} \quad (2)$$

where  $z$  = smaller given impedance

$Z$  = larger given impedance

$Z_s$  = series combination of  $Z$  and  $z$

$Z_p$  = parallel combination of  $Z$  and  $z$

Let us now define a complex number  $N$  equal to  $Z_s/Z$ , making

$$Z_s = ZN \quad (3)$$

It then follows that

$$Z_p = \frac{Zz}{ZN} = \frac{z}{N} \quad (4)$$

Thus we have a number  $N$  that relates the series or parallel impedance combi-

nation very simply to the larger or smaller given impedance. It is for determining this value  $N$  that we use the chart. The entire principle of the graphic solution is based on this operation.

Substituting Eq. (3) in Eq. (1) gives

$$N = \frac{z}{Z} + 1 \quad (5)$$

Since  $N$  is a complex number, we may express it in polar form and call its angle  $\beta$ . If the given impedance vectors are also expressed in polar form, the determination of their series or parallel combination is a matter of multiplying or dividing one of the given impedances by  $N$  and adding or subtracting  $\beta$  from its angle.  $N$  and its angle  $\beta$  depend on  $z/Z$ , as Eq. (5) shows.

The ratio  $z/Z$  of the given impedances is another complex quantity, having an angle  $\alpha$  which is simply the angular difference between the given impedance vectors.  $N$  and  $\beta$  are determined simultaneously from the chart by applying the values of  $z/Z$  and  $\alpha$ , which will be found along the axes of ordinates and abscissas.

### Method of Using Chart

In using the chart, it follows from Eqs. (3) and (4) that the  $N$  and  $\beta$  values are referred to a reference impedance  $Z$  in series combinations, and to a reference impedance  $z$  in parallel combinations. The angle  $\beta$  taken from the chart may add to the reference impedance (either  $Z$  or  $z$ ) in some cases and subtract from it in others, in determining the angle of the resultant. Since the sign of this

angle depends on several other signs, it is best to ignore the signs of all angles and insert the proper sign for  $\beta$  at the last moment. This is easily done by inspection, simply remembering that the resultant must lie between the given vectors, and taking  $\beta$  in the proper direction from the reference impedance to satisfy this rule.

The abscissa and ordinate scales of the chart are expanded arbitrarily to enlarge the upper-right corner, and make the curves become nearly polar in form at the corner. This part of the chart corresponds to resonant conditions. When  $N$  drops to 0.05 or thereabout, and the corresponding circuit  $Q$  becomes about 20, the circuit may be computed to better advantage by standard methods of approximation, which become very accurate in this region, while the accuracy of the chart falls off.

The  $N$  values on the chart are plotted with solid lines and the  $\beta$  lines are broken. The lines are also weighted so that an experienced computer learns to find the desired coordinates with a minimum amount of eye work.

### Vector Relations

To consider a method of combining impedances by geometric construction will help in visualizing the steps taken in the chart method. Figure 2 illustrates the relationship between the series and parallel combinations of two given impedances. It also includes lines for solution by geometric construction. This type of method is of little or no practical value for quantitative results, but is

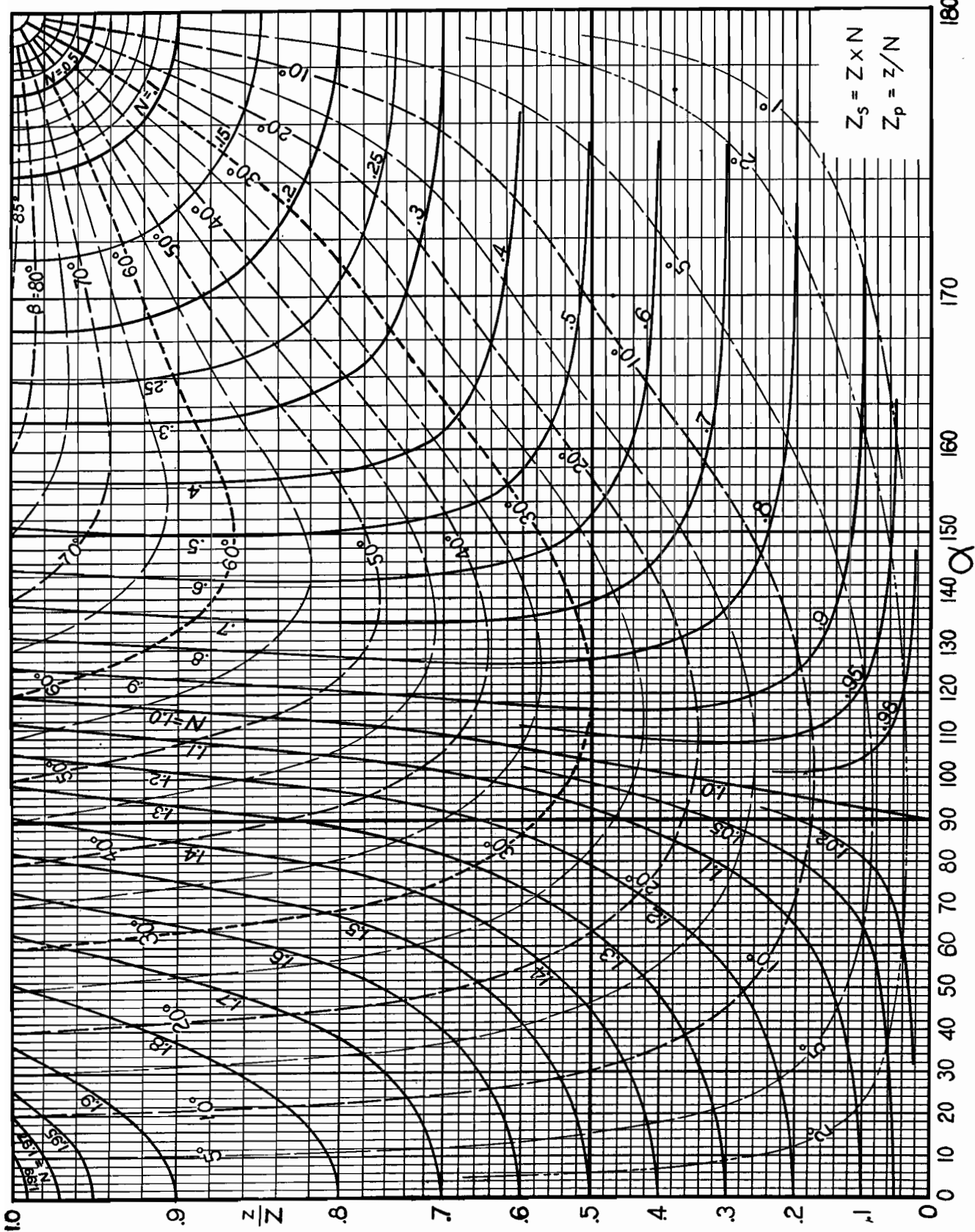


Fig. 1.—Impedance-combining chart for solving complex networks. Procedure for use: (1) Divide the smaller impedance value  $z$  by the larger impedance value  $Z$  to get  $z/Z$ . (2) Find the difference angle  $\alpha$  between the given impedance vectors  $z$  and  $Z$ . (3) Apply these values of  $z/Z$  and  $\alpha$  to the chart to get the values of  $N$  and  $\beta$ . (4) If combining impedance in series, multiply  $N$  by  $Z$  to get  $Z_s$ , and add or subtract  $\beta$  from the angle of  $Z$  (so the resultant lies between the given vectors) to get the angle of the resultant impedance. (5) If combining impedances in parallel, divide  $z$  by  $N$  to get  $Z_p$ , and add or subtract  $\beta$  from the angle of  $z$  (so the resultant lies between the given vectors) to get the angle of the resultant impedance.

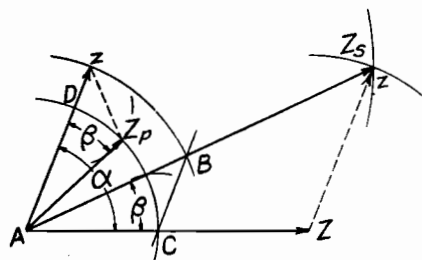


Fig. 2.—Geometric method of combining two impedances in series or parallel.

often helpful in analyzing the effect of combining impedances.

In Fig. 2,  $Z_s$  is obtained by the well-known method of completing a parallelogram. From Eq. (2),  $Z_p/z = Z/Z_s$ . By laying off the length of  $z$  on  $Z_s$ , drawing  $BC$  parallel with the original  $z$ , and completing the construction shown (remembering that  $\beta$  is a common angle between  $Z_p$  and  $z$  as well as between  $Z$  and  $Z_s$ ), the validity of this construction in satisfying Eq. (2) is evident from the similar triangles thus formed. That the angles  $\beta$  are equal follows from Eq. (2) as given immediately above. Since this is a complex-number equation, the angular relationships of  $Z_p$  to  $z$  and of  $Z$  to  $Z_s$  must be equal.

### Examples

The examples below should help in learning to use the chart and in tabulating the resulting circuit data efficiently.

**Example 1.**—What are the series and parallel impedance combinations of a resistance of 30 ohms and a capacitive reactance of 40 ohms?

The given impedances may be written:  $z = 30/0^\circ$ ,  $Z = 40/-90^\circ$ . By division and subtraction,  $z/Z = 0.75$ , and  $\alpha = 90^\circ$ . From the corresponding point on the chart,  $N = 1.25$ , and  $\beta = 37^\circ$ . The resultants are determined as follows:  $Z_s = NZ = 1.25 \times 40/-90^\circ + 37^\circ = 50/-53^\circ$ ;  $Z_p = z/N = 30/1.25/0^\circ - 37^\circ = 24/-37^\circ$ .

The solution would ordinarily be abbreviated as follows, using numbers or letters in parentheses in the text (corresponding numbers on diagrams are encircled) to identify the four impedances:

It should be recalled here that the angle  $\beta$  (37 deg here) is sometimes added

Solution	Explanation
(1) 30/0	This is $z$
(2) 40/-90	This is $Z$
0.75, 90	$\{ z/Z = 30/40 = 0.75;$ $\alpha = 0 - (-90) = 90$
1.25, 37	Get $N$ and $\beta$ from chart
(s) 50/-53	$Z_s = NZ$
(p) 24/-37	$Z_p = z/N$

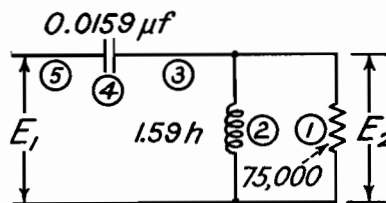
to, and sometimes subtracted from, the reference impedance to get a resultant lying between the given angles. Thus, 37 deg from  $-90$  deg toward  $0$  deg gives  $-53$  deg for the series combination above, and the same 37 deg taken from  $0$  deg toward  $-90$  deg gives  $-37$  deg for the parallel combination.

**Example 2.**—Determine  $E_2/E_1$  for the circuit of Fig. 3 at frequencies of 250, 800, 1,000, and 2,000 cycles.

The first step is to number all the impedances and their combined values, preferably in the order in which they will appear in the solution. Thus, impedance (1) of Fig. 3 combines with (2) in parallel to get (3), which in turn combines in series with (4) to get (5), the input impedance. Next, the given impedances for the proposed frequencies of solution are computed and entered in the incom-

plete table shown directly under the circuit diagram. The values may be kept in thousands of ohms or megohms, to avoid carrying unnecessary digits through the tabulation. The  $p$  and  $s$  at the left are to remind us whether parallel or series combination is to be made. Blank spaces are left for the chart parameters and the unknown impedances. These are filled in by the method of Example 1 in a systematic manner, preferably carrying the slide rule or chart work as far as possible at one time to avoid switching back and forth more than necessary.

The tabulation as completely filled in at the bottom of Fig. 3 provides for easy checking and contains complete data that can be used to compute any of the relative phases or amplitudes within the circuit.



FREQ.	250	800	1000	2000
(1)	75 $\angle$ 0	75 $\angle$ 0	75 $\angle$ 0	75 $\angle$ 0
(2)	2.5 $\angle$ 90	8 $\angle$ 90	10 $\angle$ 90	20 $\angle$ 90
$p \ z/Z, \alpha$ $N, \beta$				
(3)				
(4)	40 $\angle$ -90	12.5 $\angle$ -90	10 $\angle$ -90	5 $\angle$ -90
$s \ z/Z, \alpha$ $N, \beta$				
(5)				
FREQ.	250	800	1000	2000
(1)	75 $\angle$ 0	75 $\angle$ 0	75 $\angle$ 0	75 $\angle$ 0
(2)	2.5 $\angle$ 90	8 $\angle$ 90	10 $\angle$ 90	20 $\angle$ 90
$p \ z/Z, \alpha$ $N, \beta$	.033, 90 1.00, 2	.107, 90 1.006, 6	.133, 90 1.01, 7.5	.267, 90 1.04, 15
(3)				
(4)	2.5 $\angle$ 88 40 $\angle$ -90	7.95 $\angle$ 84 12.5 $\angle$ -90	9.9 $\angle$ 82.5 10 $\angle$ -90	19.2 $\angle$ 75 5 $\angle$ -90
$s \ z/Z, \alpha$ $N,$	.062, 178 .938, 2	.635, 174 .375, 10	99, 172.5 .13, 82	.26, 165 .75, 5
(5)				
$E_2/E_1 = (3)/(5)$	37.5 $\angle$ -89.8	4.69 $\angle$ -80	1.3 $\angle$ -8	14.4 $\angle$ 70
$Z_s - Z_s$	.0666	1.7	7.61	1.33
	177.8°	164°	90.5°	5°

Fig. 3.—Circuit for Example 2 in text, and tabulated solution for four different frequencies. Impedances are numbered in the order of their appearance in the solution.



# Chart for Equivalent Series and Parallel Circuits

By R. TOOMBS

Semicircle diagram permits rapid conversion of series values of an impedance to the equivalent of an impedance composed of parallel elements, and vice versa. Chart may be applied over wide range of impedance values

**I**N DEALING with circuits containing resistance and reactance, the need often arises for a quick and easy method of converting the series values of an impedance to the equivalent parallel values. The possibility of a graphical process appeared most useful, and the semicircle diagram has been devised as a graphical method of meeting these requirements.

Any point on this diagram represents an impedance whose series resistance and reactance are indicated by its rectangular coordinates, while the equivalent parallel components are given by the values where the corresponding circular coordinates cut the resistance and reactance axes, remote from the origin.

For finding the equivalent series components of an impedance expressed as parallel quantities, the resistance and reactance circles corresponding to the parallel values are followed round to their point of intersection. The rectangular coordinates of this point indicate the equivalent series components of the impedance. As the chart is symmetrical about the diagonal  $X_1 = R_1$ , either axis may be used for resistance as long as the other axis is used for reactance.

Values at which the circles would meet their respective axes have been marked against some of the circles. The range of the diagram may be increased by applying a common multiplication factor to the scales of both axes and the figures marked on the circles.

The chart is particularly useful in the design of networks for matching two

circuits of different impedances. Where a resistance load of  $R_A$  is to be built out to match a circuit of higher resistance  $R_B$  without any power loss, this can be done by adding a series reactance  $j_s X_A$  and then shunting the combination by a parallel reactance  $j_p X_B$  of opposite sign. The resistance circle corresponding to the value of  $R_B$  is followed until it cuts the rectangular resistance ordinate of the value of  $R_A$ . The other rectangular and circular ordinates of this point immediately give the respective values of the series and parallel reactances  $j_s X_A$  and  $j_p X_B$  which are required to effect the matching. These, of course, must be of opposite sign.

## Examples

*Example 1.*—Find the equivalent parallel components of an impedance expressed as 19 ohms resistance in series with 9 ohms positive reactance. The impedance point on the chart is determined by the rectangular coordinates from 19 on the horizontal (resistance) axis and 9 on the vertical (reactance) axis. The circles that intersect at this point would cut these two axes, respectively, at 23.25 and 49. Therefore, a resistance of 23.25 ohms shunted by a reactance of 49 ohms is equivalent to the given impedance expressed as a resistance of 19 ohms in series with a reactance of 9 ohms.

*Example 2.*—Match an antenna of 19 ohms resistance and 142 ohms series reactance to a 100-ohm transmission line. For convenience of operation on the chart,

half the above values are considered, and an impedance of  $9.5 - j.71$  converted to a pure resistance of 50 ohms. This is also a case where it is advantageous to use the vertical axis for resistance and the horizontal axis for reactance. The rectangular ordinate from 9.5 on the vertical axis cuts the 50 resistance circle (*i.e.*, which would meet the vertical axis at 50) at the point whose other rectangular and circular ordinates meet the horizontal axis at 19.62 and 24.25, respectively. Thus we have

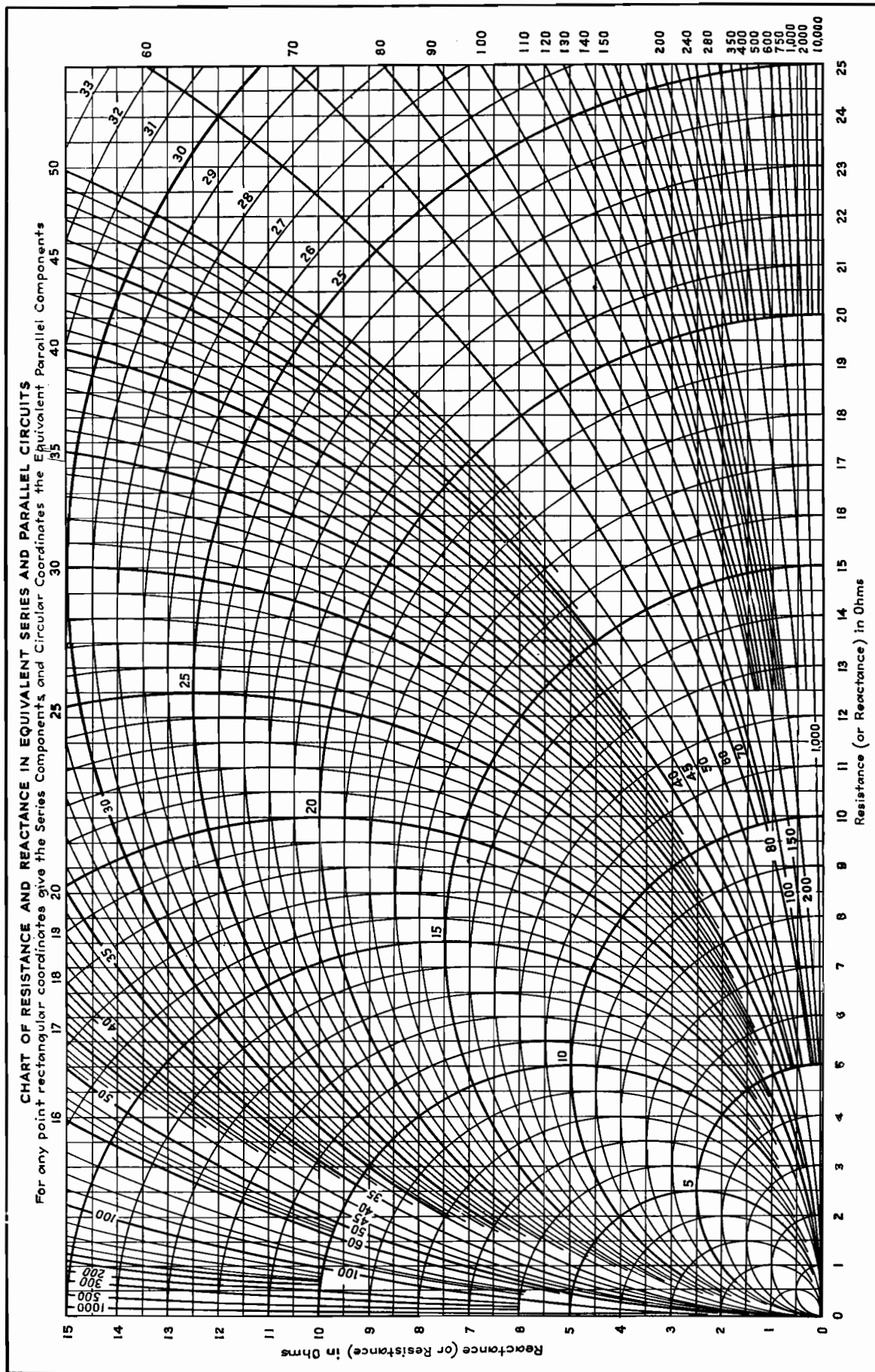
$$9.5 \pm j.19.62 = 50 \pm j.24.25$$

and multiplying by 2

$$19 \pm j.39.24 = 100 \pm j.48.5$$

Therefore, if the antenna reactance of  $-j142$  ohms is reduced to  $-j.39.24$  ohms by the addition of a series coil having a reactance of 102.8 ohms, the circuit will be equivalent to 100 ohms resistance in parallel with a negative reactance of 48.5 ohms. This reactance is then tuned out by a shunt coil of  $+48.5$  ohms reactance, thus leaving the equivalent pure resistance of 100 ohms to match the feeder.

If the added series coil had a reactance of 181.24 ohms (*i.e.*,  $142 + 39.24$ ), the effective series reactance of this, together with the antenna, would be  $+j.39.24$  ohms. The equivalent parallel reactance would also be positive and would have to be tuned out by a shunt condenser of 48.5 ohms reactance to leave the same pure resistance of 100 ohms.



# Equivalent Resistance Chart

By ALFRED E. TEACHMAN

An alignment chart for computing equivalent parallel resistances in circuits containing reactance and series resistance. Applicable also for determining the impedance of tuned circuits at resonance and the  $Q$  values of reactive elements

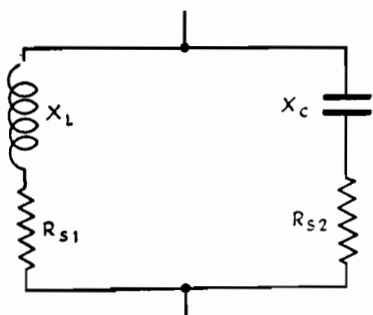


Fig. 1.—Parallel tuned circuit containing resistance in each arm.

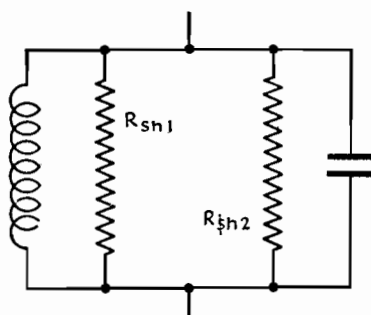


Fig. 2.—Series resistances of Fig. 1 converted to equivalent shunt resistances.

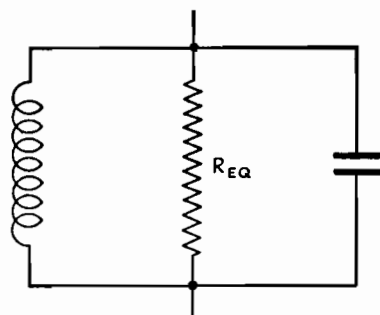


Fig. 3.—Shunt resistances of Fig. 2 combined to give equivalent resistance of circuit.

AN imperfect capacitor may be represented by a perfect capacitor having a series or shunt resistance producing equivalent losses. The relationship of the equivalent series or shunt resistance is expressed by the formula

$$\text{Shunt resistance} = \frac{(\text{capacitive reactance})^2}{(\text{series resistance})}$$

Thus it is possible to have an imperfect capacitor with internal series resistance shunted by an external resistance and by easy computation to combine and express the resultant as the equivalent series or shunt resistance. This simplification is a great aid in the solution of many problems.

The same proposition, though not so commonly noted, applies equally well to coils having series or shunt resistance. In the formula given above, the capacitive reactance is replaced by the inductive reactance.

The alignment chart makes easy work of conversions. For problems of this type, the scales  $A$ ,  $B$ , and  $X$  are used. As an example, take the dotted line  $A$ . This represents a capacitor or coil having a reactance of 2,000 ohms with a shunt resistance of 1,000,000 ohms across the terminals. The intercept on scale  $A$  gives an equivalent series resistance of 4 ohms which may be added to the known series resistance, and the combined value is then carried through the problem as a single term.

Of particular interest are the appli-

cations that may be made to parallel tuned-circuit calculations at resonance. Most simple parallel tuned circuits may be represented by the equivalent circuit of Fig. 1 in which  $X_L$  and  $X_C$  are equal. Were these elements without losses, the circuit would possess the properties of infinite impedance and zero phase angle. However, series resistance is usually present in one or both arms of the circuit, and as a result the circuit behaves as though consisting of a perfect coil and capacitor shunted by a high resistance which is the equivalent resistance of the parallel circuit. At resonance, the resultant current is in phase with the supply voltage and behaves as a pure resistance.

By use of the conversion scales  $A$  and  $B$  of the alignment chart, the series resistance of the branch arms may be converted to the equivalent parallel resistances as illustrated by Fig. 2, and by combining these resistances, in parallel, we derive the parallel resistance of the circuit as in Fig. 3.

Most often the capacitor used in a parallel tuned circuit has so little loss that it is neglected, and the principal resistance residing in the coil determines the parallel resistance. When making such an assumption, it is only necessary to convert the series coil resistance to the equivalent shunt resistance which becomes the parallel resistance of the tuned circuit. The results obtained by this method are exactly the same as by the formula:  $Z_o = X_L^2/R$ .

As an example: the dotted line  $B$  is for a coil having a reactance of 1,000 ohms and a series resistance of 5 ohms. The equivalent parallel resistance is 200,000 ohms, which is also the resistance of the parallel tuned circuit.

The term  $Q$ , the ratio,  $X/R$  represents a very convenient factor which may be used as a figure of merit in rating coils and capacitors. Since resistance is more commonly associated with coils, the term generally refers to them, although the  $Q$  of a tuned circuit may be given as the ratio of reactance in one arm to the total series resistance in the circuit. When so used, the quantity of  $Q$  also represents the voltage gain of the circuit, which means that a voltage induced in the circuit will appear across the coil or capacitor terminals multiplied  $Q$  times owing to the resonance properties of the circuit. The  $Q$  of a coil does not vary directly with frequency as might be expected from inspection, but changes rather slowly with frequency due to the compensating effect of the coil resistance which generally increases with frequency. Coils are often rated as having an average  $Q$  for a band of frequencies, and, when used with a nearly perfect capacitor, the circuit  $Q$  is approximately the same as the coil.

When working with  $Q$ ,  $X$ , and  $R$ , the corresponding lettered scales are to be used. The dotted line  $C$  shows that a coil or tuned circuit having a series resistance of 5 ohms and a reactance of 1,000 ohms will have a  $Q$  of 200. Using

a coil having a known average  $Q$  value in conjunction with a good capacitor, the average parallel resistance of the circuit can be found by placing a straightedge

intercepting the  $Q$  and reactance values and reading series resistance on the  $R$  scale. Then, by transferring the  $R$  scale value to scale  $A$  and retaining the re-

actance value, a straight line passing through these points will give the parallel resistance of the tuned circuit as read on the  $B$  scale.

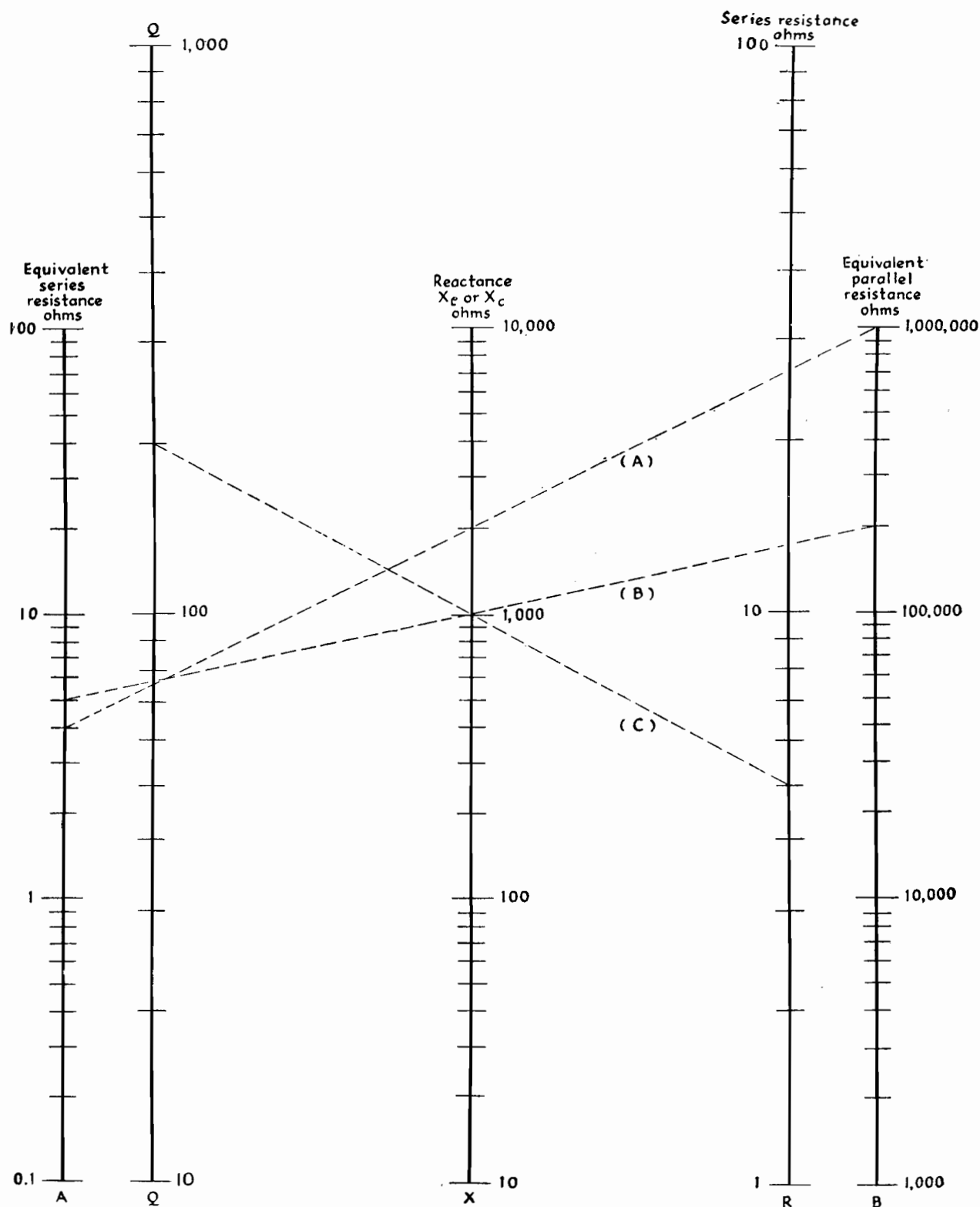


# Chart for Determining Square Root of a Complex Number

By ROBERT G. NISLE

The tedious and time-consuming calculations required in finding the square root of a complex number in transmission-line and filter calculations can be greatly simplified through the use of the graph

IN designing certain types of electrical networks, and particularly in making transmission-line or filter calculations, the need frequently arises for evaluating the square root of a complex number such as an impedance. If the impedance is expressed in polar coordinates, any root can be quickly and easily found, but if the expression is originally given in rectangular coordinates, the required operations are tedious and time consuming. The impedance must first be converted from rectangular to polar form, the square root is then determined, and finally the result is reconverted into rectangular coordinates, thereby requiring three separate and distinct operations. It is the purpose here to present a method by which the square root of any complex number that is expressed in rectangular coordinates can be easily and quickly determined, also in rectangular coordinates.

The errors that may be expected are simply those which would be expected in reading any graph, and these may be considered to be negligible for most engineering purposes.

The range of variables covers those quantities usually encountered in practical engineering work. However, if it is necessary to consider ranges outside that covered by the graph, this can be done by multiplying the original complex number by some suitable scale factor (such as 0.01 or 100) so that the problem may be fitted into the range for which the chart is drawn. The final result will then have to be multiplied by the reciprocal of this original scale factor (e.g., 100 or 0.01, respectively).

If the original complex number is

$$Z = a + jb$$

the problem before us is to determine

$$Z^{1/2} = x + jy$$

The double set of coordinates relate the quantities  $x$ ,  $y$ ,  $b$ , and  $K = a/b$  so that, when any two are known, their intersection determines a position or point on the chart from which the remaining two quantities may be determined. To use the chart, first determine  $K = a/b$ . Then, knowing  $K$  and  $b$ , find the intersection of these two coordinates on the vertical and horizontal axes. The point of intersection thus found will also be the point of intersection for the desired values of  $x$  and  $y$ , read off from the slanting scale.

It should be noted that  $Z^{1/2}$  has two roots, a positive root and a negative root. Geometrically, these two possibilities are indicated in graphical form by means of vectors which are directed in opposite directions, or are 180 deg apart. The physical requirements of the problem must be considered when deciding which of the two roots is to be used.

The use of the chart can be best illustrated through the solution of several representative examples.

## Examples

*Example 1.*—Assume that we have an impedance

$$Z = a + jb = 15 + j20$$

and that it is required to determine

$$Z^{1/2} = x + jy$$

First determine  $K = a/b = 0.75$ . Locate the intersection of the coordinates  $K = 0.75$  and  $b = 20$ . At this point, read  $x = 4.46$  and  $y = 2.25$ . The desired result is then

$$Z^{1/2} = x + jy = 4.46 + j2.25$$

or its negative value

$$Z^{1/2} = -x - jy = -4.46 - j2.25$$

*Example 2.*—If the complex number is

$$Z = -15 + j20$$

the result is

$$Z^{1/2} = x + jy = 2.25 + j4.46$$

or, alternatively,

$$Z^{1/2} = -x - jy = -2.25 - j4.46$$

*Example 3.*—If the impedance is

$$Z = -15 - j20$$

the final result is

$$Z^{1/2} = -2.25 + j4.46$$

or

$$Z^{1/2} = 2.25 - j4.46$$

*Example 4.*—If the impedance is

$$Z = 15 - j20$$

the final result is

$$Z^{1/2} = -4.46 + j2.25$$

or

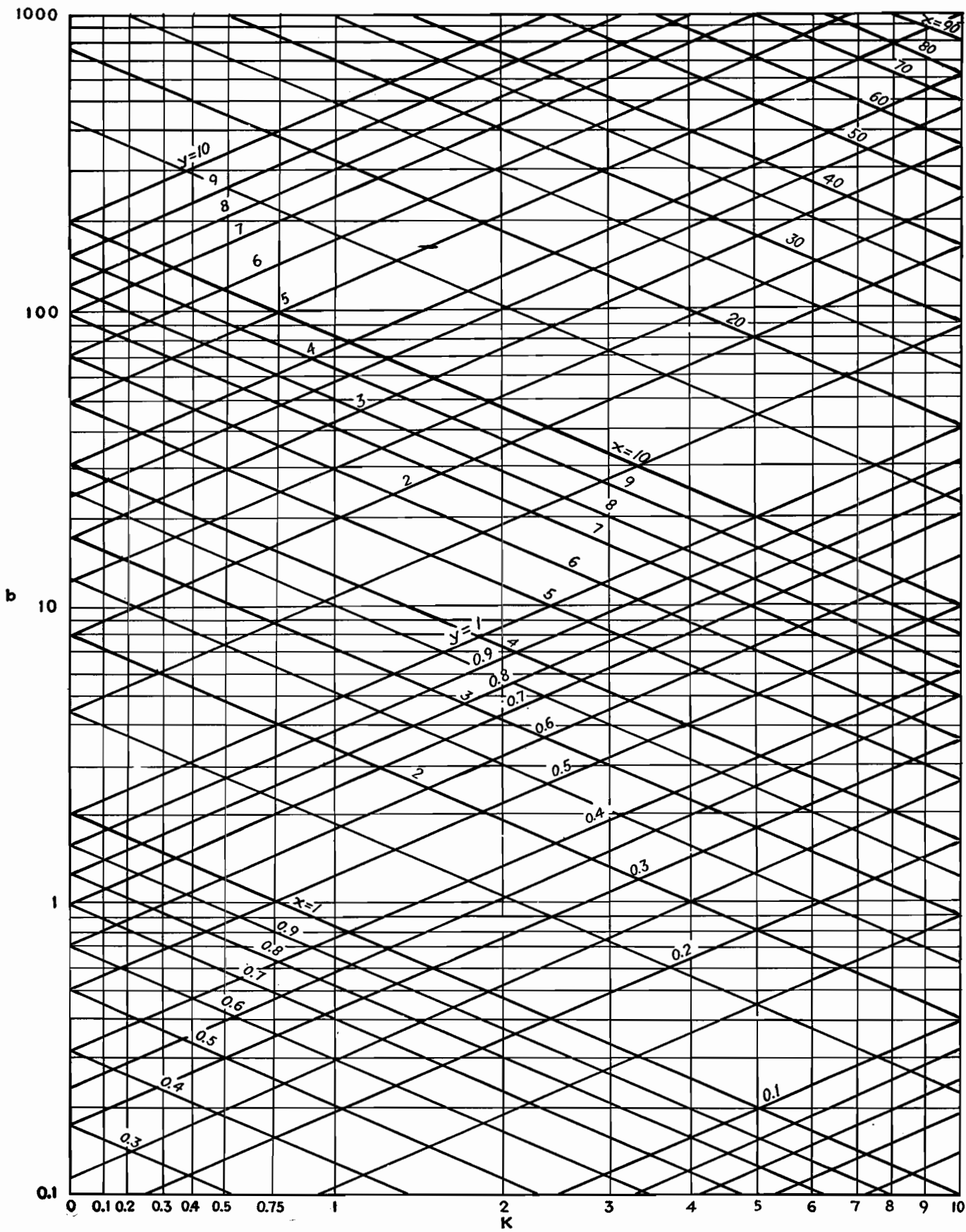
$$Z^{1/2} = 4.46 - j2.25$$

*Example 5.*—If the impedance is

$$Z = 150 + j200$$

we find that  $K = 0.75$ ,  $b = 200$ ,  $x = 14.2$ , and  $y = 7.1$ . The result is

$$Z^{1/2} = 14.2 + j7.1$$



## SECTION XIII NETWORKS

	Page
Pi Networks as Coupled Tank Circuits.....	167
Impedance-magnitude and Phase-shift Curves for Linear Networks.....	171
Equalizer Design.....	174
Evaluating Performance of Symmetrical Four-terminal Networks.....	177
Reactance Networks with Resistance Terminations.....	181
Low- and High-pass Wave Filter Units.....	185
Band-pass Wave Filters.....	189

# Pi Networks as Coupled Tank Circuits

By FREDERIC D. SCHOTTLAND

A development of the theory of pi networks as they apply to r-f output circuits of transmitters. A design procedure is outlined and curves are given to simplify matching the output stage directly to the transmission line or antenna, without an output transformer

THE use of a  $\pi$  configuration of reactances to couple a class C power amplifier to its load is not new. However, the proper handling of such a network in this application is far from being common knowledge to engineers who design or operate transmitting equipment. This lack of knowledge generally results in a circuit containing few of the obtainable advantages, and one whose harmonic attenuation leaves much to be desired.

### New Approach Needed

Unfortunately for the transmitter engineer, design information on  $\pi$  networks is to be found principally in texts concerning themselves with filter and transmission-line theory. As a consequence, the subject is not approached in such a manner as to apply directly to the problem at hand. When following the customary design procedure, an infinite number of solutions are indicated. Cut-and-try methods of adjustment are extremely laborious, and modifications appear to give totally uncorrelated results. The underlying theory as presented in texts is in such form as to give little help, since the means for imposing the further conditions necessary to obtain the single desired solution are by no means apparent.

If the  $\pi$  network is to replace the coupled tank circuit, obviously it must perform the same functions. In general, the basic requirements of the circuit are as follows:

1. It must transform the load to some predetermined impedance.
2. It must deliver a prescribed amount of energy at some maximum or required efficiency.
3. It must provide a preselected degree of harmonic attenuation.

### Review of Matching Problem

Figure 1a is a simplified schematic of a vacuum tube coupled through a plate-

tuned transformer to a load that may be an antenna at resonance or a properly terminated transmission line. Figure 1b accomplishes the same coupling through the use of a  $\pi$  network. Both will perform the functions listed above.

In the coupled tank circuit of Fig. 1a, the first function is controlled by correctly choosing the turns ratio of  $L_1$  and  $L_2$  and the amount of mutual inductance. The second function is accomplished by having the proper ratio of  $L_1$  to  $C$ . Finally, we obtain sufficient harmonic attenuation by keeping the circuit above some minimum value of  $Q$ . In other words, we couple in a resistance with a definite relationship to either reactance.

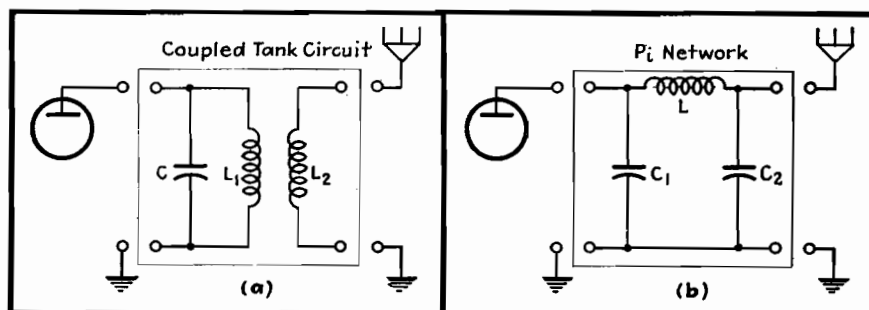


Fig. 1.—Simplified representation of a class C r-f output stage feeding a transmission line or antenna at resonance through a coupled tank circuit (a) and through an equivalent pi network (b).



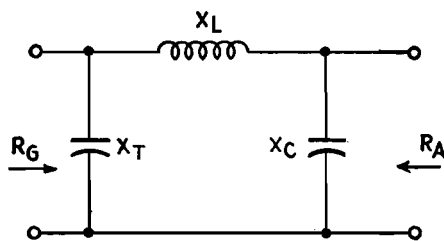


Fig. 2.—Pi section used as a low-pass coupling network.

Inspection of the  $\pi$  network of Fig. 1b does not immediately reveal how all this is accomplished. We know that a  $\pi$  network will transform impedances and act as a coupling device, but how to control the efficiency and the  $Q$  of the circuit is not indicated, nor is this design information available in convenient form.

#### Reduction of $\pi$ to L

In any actual circuit we are not concerned with the internal impedance of our tubes as such, but rather with the impedance into which it must work. As a limiting case it becomes that impedance which will give the maximum transfer of r-f power under the specific operating conditions of grid bias, excitation, and plate voltage employed, without exceeding the rated plate dissipation of the tube. In the circuit of Fig. 2, therefore,  $R_G$  will be taken to mean the impedance with which we wish to terminate our generator, and not the internal impedance of the generator itself.

The values of  $X_T$  and  $X_C$  to match  $R_A$  to  $R_G$  are obtained from the relations\*

$$X_T = \frac{-R_G X_L}{R_G \pm \sqrt{R_G R_A - X_L^2}} \quad (1)$$

$$X_C = \frac{-R_A X_L}{R_A \pm \sqrt{R_G R_A - X_L^2}} \quad (2)$$

To avoid an imaginary value for  $X_T$  or  $X_C$ ,

$$X_L^2 \leq R_G R_A \quad (3)$$

To make  $X_C$  infinite in value so the output capacitor will drop out, we must choose the negative sign for the radical and use a value of  $R_G$  such that

$$R_A = \sqrt{R_G R_A - X_L^2} \quad (4)$$

This in no way changes the performance of the network, but the circuit simplifies to the L network of Fig. 3, which may be more easily analyzed.

The L network shown in Fig. 3 is of extreme interest. It is not only the equivalent circuit of a  $\pi$  network, but if  $R_A$  is taken as the reflected resistance of

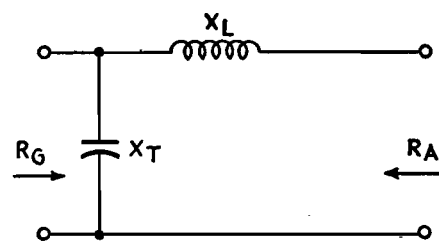


Fig. 3.—Equivalent circuit of pi-coupling network.

the load, it is the equivalent circuit of a coupled tank network as well. Here, then, is common ground and a means of correlating the two circuits. At resonance,  $X_T$  is equal to  $X_L$ .  $R_G$  was defined as the impedance into which we are to work. That is, it is the image impedance of the network, so

$$X_L = X_T = \frac{R_G}{Q} \quad (5)$$

$$R_A = \frac{X_L}{Q} \quad (6)$$

From Eq. (5), at any desired  $Q$  the value of  $X_L$  is fixed, and consequently the value of  $X_T$  is also fixed. The value of  $R_A$  is given by Eq. (6). From Eqs. (5) and (6), we see that

$$R_G = \frac{X_L^2}{R_A} \quad (7)$$

#### Limitations of L Network

We formerly intended to find a network that would match  $R_G$  to whatever antenna we had. Because of the restriction of Eq. (4), however, we must now match our antenna to our network. This by no means destroys the usefulness of the network, for the value of  $R_A$  that has been obtained is the minimum impedance into which we may work under the given operating conditions. This minimum is entirely independent of the restrictions of Eq. (4).

If the actual load has an impedance greater than  $R_A$ , it can be made to look like  $R_A$  so far as its resistance is concerned, by shunting it with the proper value of reactance. Naturally we shall choose a capacitance for this purpose, since it will act to increase the harmonic attenuation. If the actual antenna has an impedance smaller than  $R_A$ , there is nothing we can do about it. Obviously, to increase the impedance we must insert a reactance in series with  $R_A$ . If this is a capacitance, it will subtract from  $X_L$ , and if an inductance, it will add. We may, therefore, view the addition of a series reactance as a change in the value of  $X_L$ . If we reduce  $X_L$  to obtain the required  $Q$ , the  $QX_L$  is reduced and  $R_G$  is

not matched. Similarly, if  $X_L$  is increased, we again obtain a mismatch.

Fortunately, it is seldom necessary to couple into an antenna whose impedance is much below that usually found to be the proper terminating impedance of the network. At low radio frequencies, of course, this difficulty may very well be encountered. Although the normal antenna in this case may be so short electrically as to have low resistance, its capacitance in general will also be quite low. To resonate such an antenna, considerable inductance will be required in the loading coil. The resistance of such a coil will be comparable to the antenna itself, and, added to it, will bring the resistance into which the network is coupled to a higher value. Of course, this added resistance represents a loss, but that loss was inherent in the circuit and not added by the coupling network. The whole matter may be resolved as follows:

At low frequencies (such as radio beacon frequencies below the broadcast band), it is desirable to use a class C amplifier whose generator impedance is as low as possible, such as a low-voltage high-current tube or tubes in parallel. This will make  $R_G$  and, consequently,  $R_A$  lower. If  $R_A$  is still greater than the effective antenna resistance, the resulting circuit would have a higher  $Q$  than required, and would, in effect, be undercoupled.

When the actual load, which we shall call  $R_L$ , is greater than  $R_A$ , the problem has a complete solution. A reactance in parallel with  $R_L$  will give a circuit whose impedance is lower than  $R_L$ . By properly choosing this reactance, the resistive component may be made equal to  $R_A$ , something which was impossible to do with additions of series reactances. This reactance should be capacitive, to increase harmonic suppression.

#### Development of $\pi$ Circuit

It is interesting to note that we are throwing off the yoke of Eq. (4), since we are now resynthesizing the original  $\pi$  network of Fig. 2. However, for simplicity, and to maintain the analogy to coupled tank circuits, we shall continue to use the L network of Fig. 3. We shall treat this newly formed parallel circuit as an entity in terms of its series equivalent.

Figure 4a shows this parallel circuit, where  $R_L$  is a load greater than  $R_A$ , and  $X_C$  is the compensating capacitive reactance necessary to make the total circuit resistance look like  $R_A$ . Figure 4b is the series equivalent, where  $X_E$  becomes the effective series reactance of Fig. 4a. It

\* EVERITT, W. L., "Output Networks for Radio Frequency Power Amplifiers," *Proc. IRE*, 19, No. 5, 725-737, May 1931.

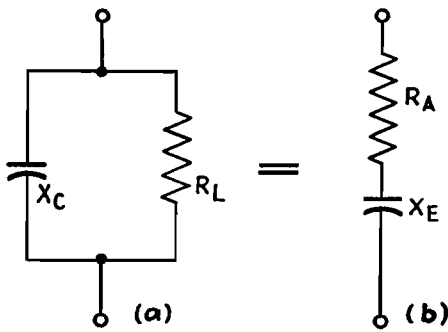


Fig. 4.—Load with reactance in parallel (a), and its equivalent series circuit (b).

will be as though  $X_L$  had been reduced. To compensate, either  $X_L$  or the tuning capacitance must be increased. To maintain the original conditions, we shall naturally increase  $X_L$ .

From Fig. 4b,

$$R_A = jX_E = \frac{-jR_L X_C}{R_L - jX_C} \quad (8)$$

Clearing  $j$  from the denominator,

$$R_A - jX_E = \frac{R_L X_C^2 - jR_L^2 X_C}{R_L^2 + X_C^2}$$

$$R_A = \frac{R_L X_C^2}{R_L^2 + X_C^2} \quad (9)$$

$$X_E = -\frac{R_L^2 X_C}{R_L^2 + X_C^2} \quad (10)$$

Solving Eq. (9) for  $X_C$  now gives

$$X_C = -R_L \sqrt{\frac{R_A}{R_L - R_A}} \quad (11)$$

Equation (11) gives the value of compensating capacitive reactance  $X_C$  which will transform  $R_L$  into  $R_A$ . Figure 5 is a family of curves for this relationship, where  $R_L$  is plotted vs.  $X_C$  for selected values of  $R_A$ .

In using Fig. 5, the range may be extended by multiplying all the quantities by the same factor. For example, assume that it is required to find the reactance that will transform an actual resistive load  $R_L$  of 60 ohms into one of 20 ohms. Since there is no curve in the range of  $R_A = 20$ , we shall use the  $R_A = 2$  curve and assume that  $R_L$  and  $X_C$  are also ten times their given values. We enter the graph from the left at the point  $R_L = 6$ . Traveling to the right, we find that the intersection with  $R_A = 2$  occurs at  $X_C = 4.2$ . Multiplying by 10, our answer is 42 ohms.

Equation (10) gives the series equivalent reactance introduced by  $X_C$ , this being the value by which  $X_L$  will have to be increased to compensate. Figure 6 is a family of curves for this relationship. This curve is also used in extended ranges by multiplying all the quantities by the same factor. Proceeding with the above example, we enter the curve at  $X_C = 42$ ,

and find the intersection with  $R_L = 60$  at  $X_E = 28$  ohms. No factor was involved, and the answer is read directly.

Since the design procedure for a coupled tank circuit holds for the equivalent circuit of Fig. 3, any calculations the engineer is accustomed to make to determine the proper reactances to use for a coupled tank circuit hold equally well for the  $\pi$  network. Of course, in most cases only  $X_C$  would remain the same, while  $X_L$  would have to be increased by an amount equal to the value of  $X_E$ . Knowing  $X_C$  and  $Q$ ,  $R_A$  could be readily obtained.

#### Terminating Impedance

At best, the calculation of the generator impedance of a class C power amplifier is only an approximation. An actual measurement under operating conditions is much to be preferred. While we cannot do precisely that, we are able to do what is even more to the point. The circuit lends itself admirably to a measurement of  $R_G$ , the resistance with which we

actually wish to terminate the vacuum tube.

The circuit of Fig. 3 is set up with sufficient metering to obtain plate current, plate voltage, and load current. In place of  $R_A$  we may use any convenient value which we shall call  $R_X$ . The circuit is then tuned by means of  $X_T$  and the output and input powers calculated. If we have not exceeded or equaled the rated power dissipation capabilities of the tube,  $X_L$  is reduced and the circuit retuned. This procedure is continued until, at resonance, either maximum or required power output is obtained within the limitations of tube power dissipation. In the case of pentodes, the screen as well as plate dissipation must be watched, particularly if the ratio of  $X_L$  to  $R_X$  is large. Having adjusted the circuit, we have terminated it with the proper  $R_G$ . Since we know  $R_X$  or can measure it, by measuring  $X_L$  or  $X_T$  we are able to calculate  $R_G$ . From this data  $R_A$  is fixed according to the circuit  $Q$  which is to be used.

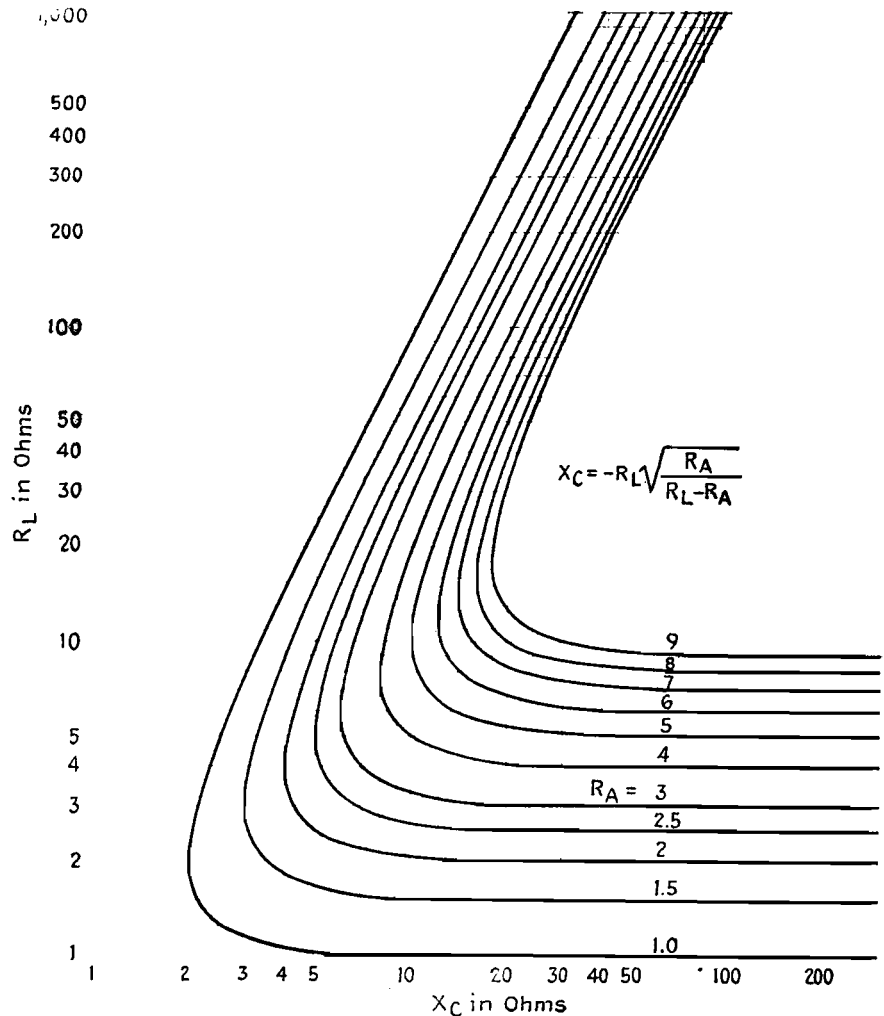


Fig. 5.—Chart giving value of compensating capacitive reactance  $X_C$  required to make load circuit have correct resistance for matching purposes.

If  $R_X$  is much different from  $R_A$ , it is necessary to repeat the adjustments and measurements using some value of  $R_X$  nearer to the calculated  $R_A$ . Just when it is necessary to repeat the measurements may easily be determined. If  $R_X$  is quite large, upon adjusting the circuit for proper impedance, the resulting  $Q$  will be a low value. If it becomes much below 10, the conditions of maximum impedance and unity power factor will not occur simultaneously, and the harmonic generation will be appreciable. Consequently, erroneous measurements will result. If, on the other hand,  $R_X$  is too low,  $X_L$  will be large in order to bring  $R_G$  to its proper value. This will result in a condition of undercoupling. The tube will be delivering full output possible under the conditions, but that output will be low as will be the input power. Since the internal impedance of a vacuum tube is a function of the operating conditions,  $R_G$  will be different from that under the required load conditions.

#### Antenna Measurement

In many cases, the actual antenna resistance  $R_L$  is not known. This too may be found experimentally. Since we already know  $R_G$ , by replacing  $R_X$  with the actual antenna, adjusting for the required power, and measuring  $X_L$  or  $X_T$ , we have sufficient data to calculate the unknown load resistance. Here again we should have comparable values of load, and the first measurement will generally have to be repeated using a value of  $R_X$  more nearly the same as  $R_L$ . Of course, if equipment is available, the measurement may be made by the substitution method. This means, in most cases, having available power resistors, continuously variable, and with negligible or tunable reactance. The first method is quite accurate and more adaptable to the equipment of the normal laboratory or transmitting plant.

Note that for the antenna measurement we are not concerned with  $R_G$  as it will finally exist, but simply wish to keep it constant for the two measurements, the one with  $R_X$  and the other with  $R_L$ . To be most accurate, therefore, all meter readings should be the same for both measurements. Low power may, of course, be used in this antenna resistance measurement.

#### Design Summary

The following outline summarizes the procedure to be followed in the design of a  $\pi$  coupling network.

1. Set up the circuit of Fig. 3 with any value of  $R_A$ , such as  $R_X$ . Adjust  $X_L$  until when tuned by  $X_T$  the required power output within dissipation limits is obtained. Measure  $R_X$  and  $X_L$  or  $X_T$ . The required load impedance  $R_G$  is given by Eq. (7).
2. Select a value of  $Q$  for the required harmonic attenuation, and calculate  $X_L$  and  $X_T$  from Eq. (5).
3. Find the value of  $R_A$  from Eq. (6).
4. Replace  $R_X$  by  $R_L$ , the actual load, and adjust the circuit for the required power output. Measure  $X_L$  or  $X_T$ , and using the value of  $R_G$  found in step 1, calculate  $R_L$  from Eq. (7) solved for  $R_A$ , which in this case is  $R_L$ .
5. Replace this value of  $R_L$  by an  $R_X$  of approximately the same value, and repeat steps 1 and 4.
6. If neither the value of  $R_X$  used in step 1 nor the value in step 5 is approximately equal to  $R_A$ , repeat steps 1, 2, and 3 using an  $R_X$  more nearly the same as that of  $R_A$  as found in step 3.
7. Find  $X_C$  from Fig. 5 or from Eq. (11).

8. Find  $X_E$  from Fig. 6 or from Eq. (10).
9. Increase  $X_L$  by  $X_E$ .

If reasonable care has been exercised, the circuit will be found to tune within a small percentage of the calculated  $X_T$ , and the final adjustments will be easy to make.

If  $X_T$  was varied very much in achieving tuning, this will alter the  $Q$  and should be corrected. Let us examine the case where  $X_T$  was increased for tuning, knowing that if it were decreased the reverse procedure would hold. In order to decrease  $X_T$  (increase the capacitance), either  $X_E$  must be increased or  $X_L$  decreased. The effect on the power output will clearly indicate which is required. An examination of Fig. 6 will show whether  $X_C$  is to be increased or decreased to cause the proper change in  $X_E$ . It will be seen that up to the point where  $X_C$  is equal to  $R_L$  an increase in  $X_C$  will cause an increase in  $X_E$ . When the value of  $X_C$  is greater than  $R_L$ , a decrease in  $X_C$  is needed to cause an increase in  $X_E$ . Incidentally, it is just this effect that makes the

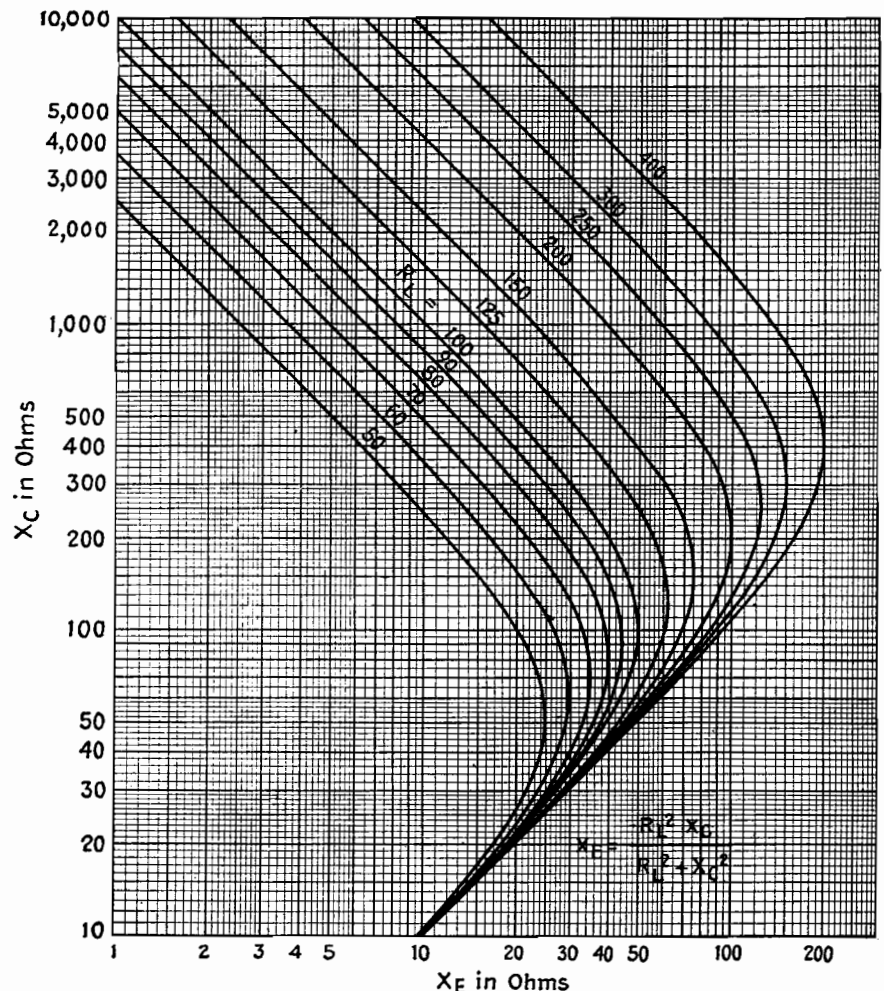


Fig. 6.—Chart giving reactance value  $X_E$  by which the inductive reactance  $X_L$  in the network must be increased to give correct tuning.

adjustment of a  $\pi$  network by cut-and-try methods so confusing to the uninitiated. Not only can tuning be accomplished by any of the three reactances, but the change in the direction of the effect of changes in  $X_C$  produces apparently uncorrelated results.

### Example

Probably the best method of explaining the design procedure is to work out a typical design. The following example is actual observed data.

1. The circuit of Fig. 3 is set up, choosing initially for  $R_A$  the value  $R_x = 60$  ohms.  $X_L$  is adjusted for maximum power output, then measured and found to be 308 ohms. From this,  $R_G = X_L^2/R_x = 94,900/60 = 1,580$  ohms.

2. Using a  $Q$  of 12,  $X_L = X_T = R_G/Q = 1,580/12 = 132$  ohms.

3.  $R_A = X_L/Q = 132/12 = 11$  ohms.

4. Inserting the actual antenna and readjusting for maximum power output,  $X_L$  is found to be 413 ohms. From this,  $R_L = X_L^2/R_G = 171,000/1,580 = 108$  ohms.

5. Steps 1 and 4 are repeated using  $R_x = 108$  ohms. On readjustment,  $X_L$  is found to be 425 ohms, and  $R_G = X_L^2/R_x = 181,000/108 = 1,660$  ohms.

Replacing  $R_x$  by  $R_L$  and again readjusting,  $X_L$  is measured as 417 ohms, and  $R_L = X_L^2/R_G = 174,000/1,660 = 105$  ohms.

6. Since  $R_A$  and both values of  $R_x$  are quite different, we shall repeat steps 1, 2, and 3 using  $R_x = 15$ . When adjusted now,  $X_L = 149$  ohms, and  $R_G = X_L^2/R_x = 22,200/15 = 1,480$  ohms. At a  $Q$  of 12,  $X_L = X_T = 1,480/12 = 123$  ohms, and  $R_A = X_L/Q = 123/12 = 10$  ohms.

7. Using Fig. 5, we enter at  $R_L = 10.5$  ohms, and the intersection with  $R_A = 1$  occurs at  $X_C = 3.4$ . Since a factor of 10 has been used,  $X_C = 34$  ohms.

8. Using Fig. 6 we enter the curve at  $X_C = 340$  and, assuming a curve  $R_L = 105$  to exist slightly above  $R_L = 100$ , we can estimate the intersection to occur at  $X_E = 30$ . Since a factor of 0.1 was used,  $X_E = 3$  ohms.

9.  $X_L$  is, therefore, increased to 126 ohms.

Our final circuit has  $X_T = 123$  ohms,  $X_L = 126$  ohms, and  $X_C = 34$  ohms. It properly terminates our tube when loaded by a resonant antenna of 105 ohms, yielding a circuit  $Q$  of 12. In actual practice, this tuned almost perfectly as calculated, and the change in  $X_T$  to produce exact tuning was too slight to warrant any further changes.

### Conclusion

The foregoing assumes that means for making reactance and resistance measurements are at hand. In the field, particularly using emergency equipment, this will not be so. However, it is hoped that sufficient light has been thrown on the subject to enable "blind" tuning to be accomplished logically and rapidly.

As a suggestion, start with an L network, resonate the antenna, and then add output capacitance as required. Up to a point, increases in capacitance and inductance will bring up the antenna current. Thereafter, the current will start to drop off. In other words, at first  $R_L$  is too large to achieve a low enough  $R_G$ . As  $X_C$  reduces the effective  $R_L$ , the current will increase to the point of overcoupling and excessive power output, as evidenced by excessive plate current. Further reduction of  $R_L$  or increase in  $X_L$  will be in the direction of low coupling and high  $Q$ , which is, of course, more desirable. For safety, then, adjustment is continued in this direction until the plate meter indicates that not too great a plate input is being delivered to the tube. With a little experience, one will easily learn the "feel" of  $\pi$  network adjustments, and will work out rapid and surprisingly accurate methods of tuning without any equipment other than the transmitter meters.

# Impedance-magnitude and Phase-shift Curves for Linear Networks

By VITOLD LEOPOLD EDUTIS

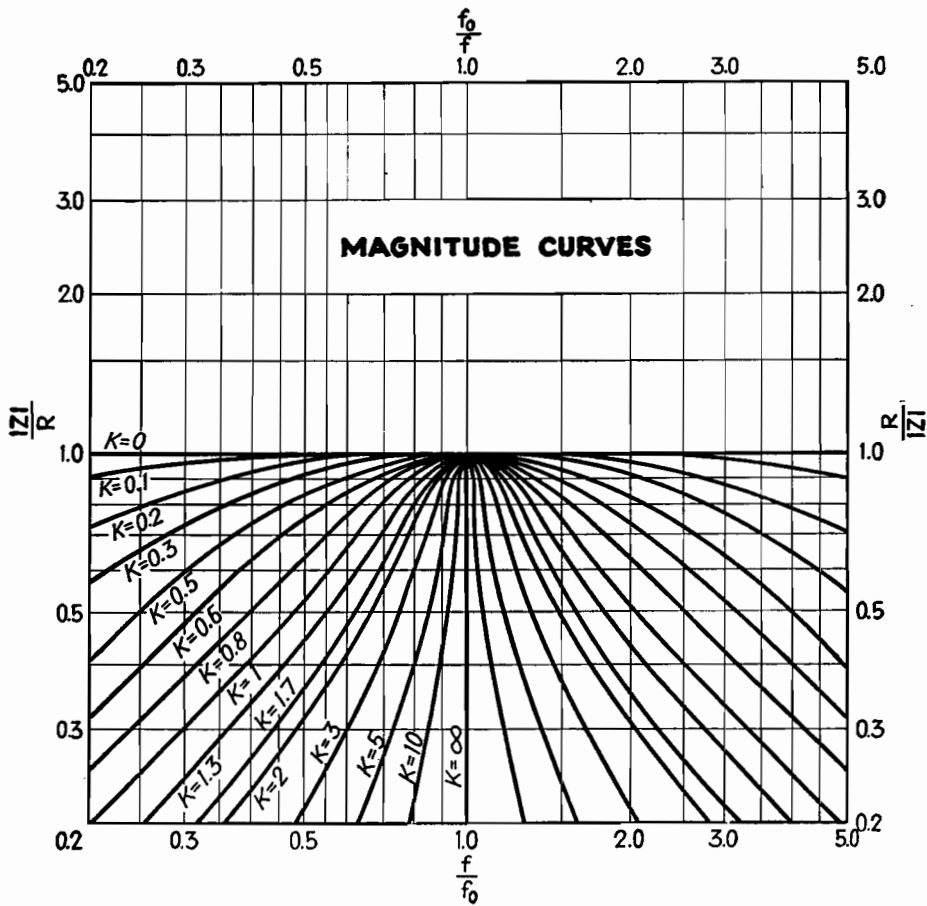
THE charts show the magnitude and phase shift of resonant circuit impedances composed of lumped  $L$ ,  $R$ , and  $C$  constants connected in a two-terminal network. The curves represent a selection from a wide range of two-terminal networks prepared and calculated as a result of a systematic examination of two-terminal networks. For the circuit networks shown in the tables, the curves show the magnitude of the impedance, and the phase shift for various values of the parameter  $K$ , which is defined in the table. The curves are plotted as normalized impedances, so that the true impedance in ohms may be determined from the graph for any value of resistance  $R$ . The curves are also

generalized to apply for any frequency over a wide range in the vicinity of the natural resonant frequency by plotting the abscissa in terms of  $f/f_0$ , where  $f$  is the frequency at which the circuit is operated, and  $f_0$  is the resonant frequency of the circuit defined by  $f_0 = \frac{1}{2\pi} \sqrt{LC}$ . Because of the general manner in which the curves are plotted, the graphs are applicable to six types of three-element resonant circuits instead of only to two.

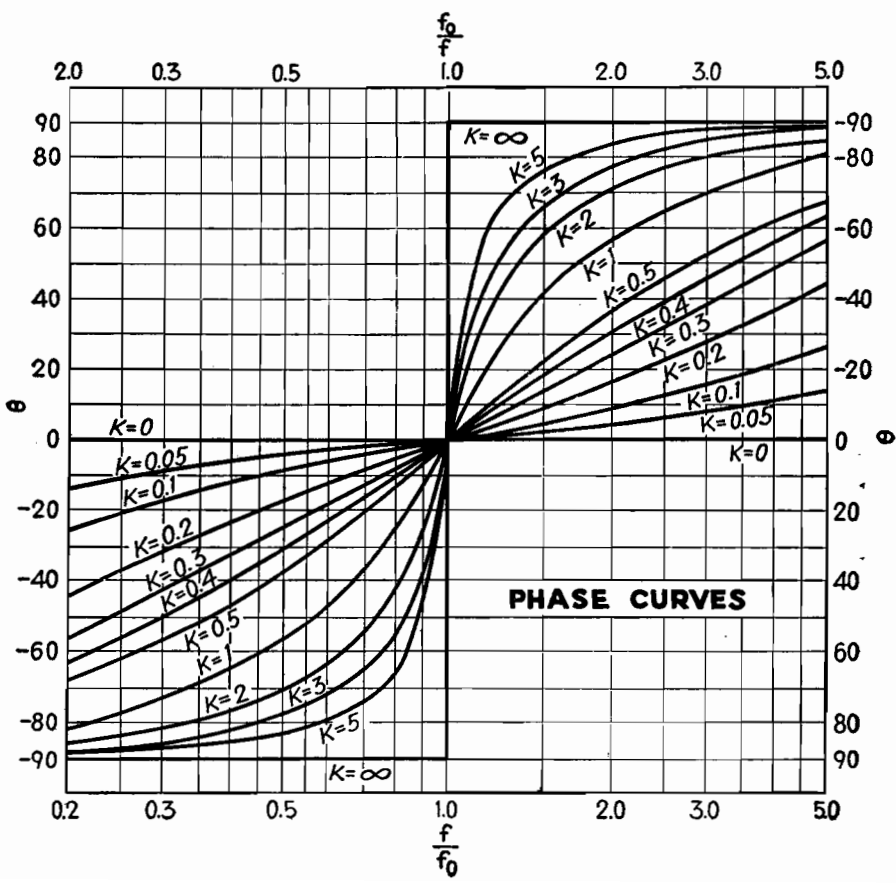
The table accompanying each graph shows the circuit of the appropriate network, indicates the correct set of axes to be used in determining the impedance magnitude and phase shift, indicates the value of the parameter  $K$  for the various curves of any family, and designates the

inverse and reciprocal network of the selected circuit. Two networks are said to be inverse if their magnitude and phase-angle characteristics vary with frequency in a mutually inverse manner and if definite ratios exist between corresponding elements in the two networks. Two networks are said to be reciprocal if the impedance of one is conjugate to the impedance of the other when the frequency of one is the reciprocal of the frequency of the other.

The graphs may be used to determine the magnitude and phase of the impedance of any of the six selected circuits, or, conversely, for the magnitude and phase curves selected, any of two or more networks may be selected to provide the



Phase axes	$f, f_0$	$\theta, \theta'$
Magnitude axes	$\frac{ Z }{R}, \frac{f}{f_0}$	$\frac{R}{f}, \frac{ Z }{f_0}$
Parameter K	$\sqrt{\frac{R^2 C}{L}}$	$\sqrt{\frac{L}{R^2 C}}$
Resonant frequency $f_0$	$\frac{1}{2\pi \sqrt{LC}}$	$\frac{1}{2\pi \sqrt{LC}}$
Reciprocal network	1	2
Inverse network	2	1
No.	1	2
Network		



desired impedance characteristic within the range of the graphs.

With the characteristic curves of magnitude and phase shift presented, it is possible to find the impedance magnitude and phase angle of a network graphically. This eliminates many long and tedious calculations. Although the method is not so accurate as the method of calculation, it is extremely useful because in most cases the accuracy is sufficient for engineering purposes. The impedance magnitude can be obtained to within approximately 1 per cent of the exact value. The phase shift can be read to within 1 deg. The graphs are drawn to apply to values of  $R$ ,  $L$ , and  $C$ , in ohms, henrys, and farads, respectively, while  $f$  is of course determined in cycles.

Two examples will suffice to illustrate the method of using these graphs. Suppose we have a series  $LRC$  circuit consisting of an inductance of 100  $\mu\text{h}$  and a capacitance of 100  $\mu\text{mf}$  so that the resonant frequency is 1.592 Mc. What resistance will be required if the circuit

impedance is to be maintained to 3 db (ratio of 0.5) below its resonant impedance at 2.4 Mc? What will be the phase shift?

From the data above,  $ZR = 0.5$  and  $f/f_0 = 1.5$  from which we find  $K = 2$ . From these data, and transposing the formula for  $K$ , we find the value of the required resistance to be

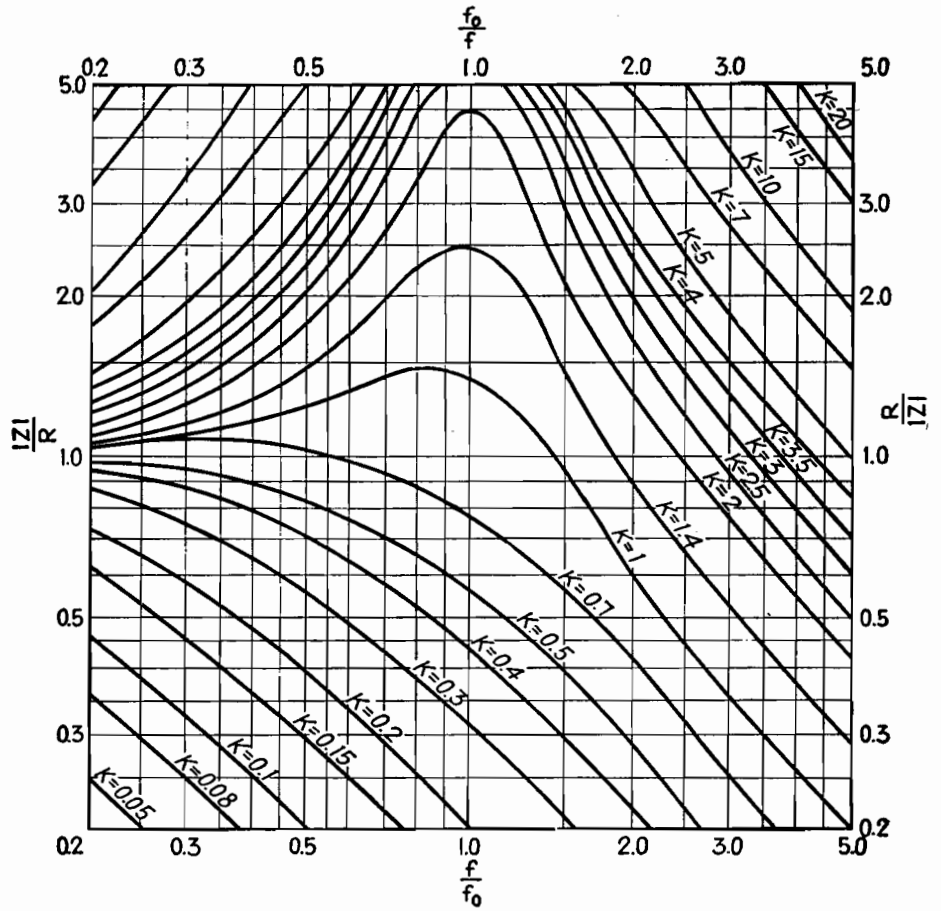
$$R = \frac{1}{K} \sqrt{\frac{L}{C}} = \frac{1}{2} \sqrt{\frac{100 \times 10^{-6}}{100 \times 10^{-12}}} = \frac{1}{2} \sqrt{\frac{1}{10^{-6}}} = \frac{1}{2} \sqrt{10^6} = \frac{1,000}{2} = 500 \text{ ohms}$$

The phase angle will be 58 deg.

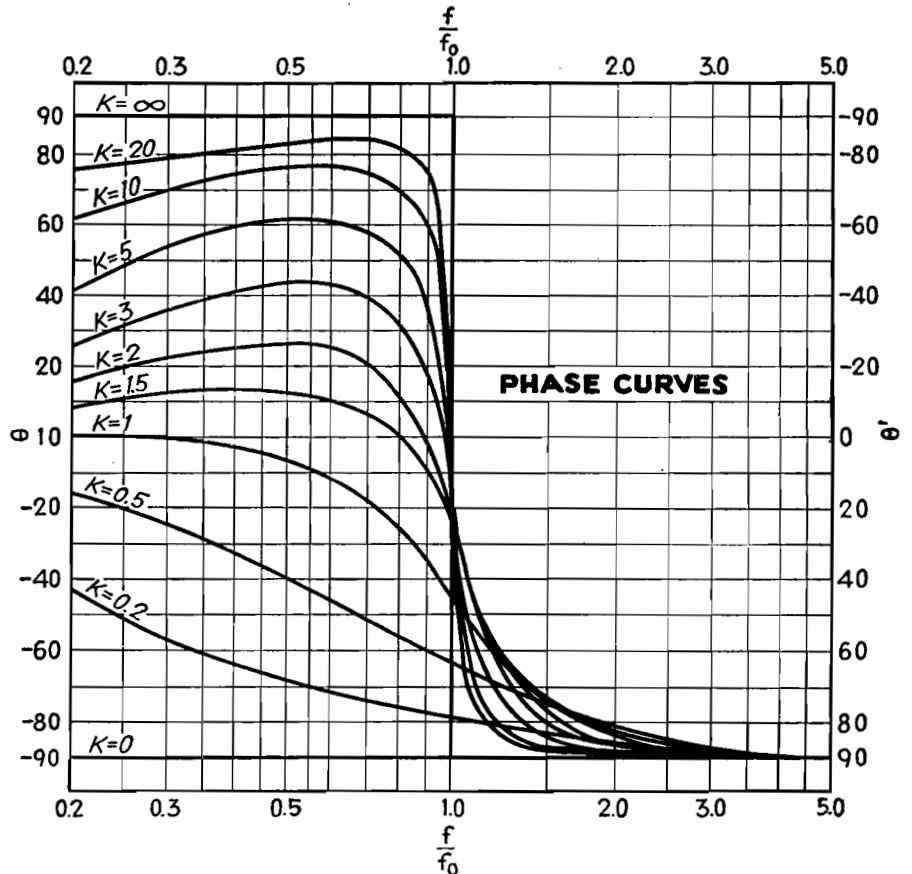
The same problem may be applied to a circuit consisting of a capacitance in parallel with an inductance (circuit 3). Assume, for simplicity, that the same values and circuit constants are employed. What value of resistance of the coil is required?

For  $f/f_0 = 1.5$  and  $ZR = 0.5$ , we find  $K = 0.62$ , from which  $R = 1,620$  ohms.

The phase angle is  $-73$  deg.



Network	No.	Inverse network	Reciprocal network	Resonant frequency $f_0$	Parameter $K$	Magnitude axes	Phase axes
	3	4	6	$\frac{1}{2\pi\sqrt{LC}}$	$\sqrt{\frac{L}{R^2C}}$	$\frac{ Z }{R}, \frac{f}{f_0}$	$\theta, \frac{f}{f_0}$
	4	3	5	$\frac{1}{2\pi\sqrt{LC}}$	$\sqrt{\frac{R^2C}{L}}$	$\frac{f}{f_0}, \frac{R}{ Z }$	$\frac{f}{f_0}, \theta'$
	5	6	3	$\frac{1}{2\pi\sqrt{LC}}$	$\sqrt{\frac{R^2C}{L}}$	$\frac{R}{ Z }, \frac{f_0}{f}$	$\theta', \frac{f_0}{f}$
	6	5	4	$\frac{1}{2\pi\sqrt{LC}}$	$\sqrt{\frac{L}{R^2C}}$	$\frac{f_0}{f}, \frac{ Z }{R}$	$\frac{f_0}{f}, \theta$





# Equalizer Design

By MICHAEL J. DI TORO

Attenuation and phase functions of frequency-transmission characteristics are given in circle diagrams, for determining performance and selecting circuit constants of "constant-resistance" and other conventional types of audio and r-f equalizers

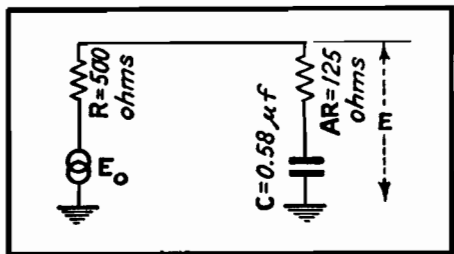


Fig. 1a.—Low-pass equalizer network.

THE use of circle diagrams for facilitating the solution of various problems in engineering is well known.<sup>1,2</sup> A chart that may be used in determining the characteristics of a large number of electrical circuits used in audio and r-f systems will be described.

The attenuation, phase, and impedance functions of various corrective networks may be determined directly from the chart by following the circular loci of constant  $A$  and constant  $X$ . Here  $A$  is the ratio of two resistances, while  $X$  is the product of radian frequency and an inherent time constant of the circuit. As soon as particular values of  $A$  and  $X$  are determined from given specifications, the behavior for all other values of  $X$  or  $A$  is read directly from the chart. Examples showing both methods of application will be considered.

Suppose it is desired to design a simple low-pass network satisfying the following specifications:

1. As the frequency increases, the attenuation introduced by the network is to increase gradually from zero to not more than 14 db, while at the pivoting or crossover frequency of 1,000 cycles the attenuation should be 7 db.

2. The network is to work from a signal source having 500 ohms internal resistance.

A circuit having these general characteristics is shown in Fig. 1a, and in the fourth-quadrant group of circuits shown on the chart. The problem is to determine the values of the resistances  $R$  and  $AR$ , and the capacitance  $C$ , which satisfy the specifications. Since the source

internal resistance is to be 500 ohms, it is possible to let  $R$  be this internal resistance, 500 ohms. For purposes of analysis, let the signal-source voltage be a sine wave of frequency  $f$ , represented by the complex quantity  $E_0$ . Let the output voltage be another complex quantity  $E$  which differs from  $E_0$  in both magnitude and phase.

Certain facts are evident on inspection of Fig. 1a. For direct current, or zero frequency, the ratio  $E/E_0 = 1$ , or  $E$  and  $E_0$  are equal both in magnitude and phase. As the frequency increases and approaches infinity, the reactance of the capacitance  $C$  and the voltage across  $C$  approach zero together. Hence, at infinite frequency,  $E$  is again in phase with  $E_0$  and should be 14 db below  $E_0$ , or  $E/E_0 = 0.2$ . But  $E/E_0 = AR/(R + AR) = A/(1 + A) = 0.2$ , or  $A = 0.25$ . This determines  $AR$  to be equal to  $0.25 \times 500 = 125$  ohms. For intermediate frequencies, a little consideration will show that the voltage  $E$  lags  $E_0$  and has a magnitude somewhere in the range between  $E = E_0$  and  $E = 0.2 E_0$ .

Consider now the use of the chart in determining quantitatively the manner in which the ratio  $E/E_0$  varies with frequency. Reference is first made to Fig. 1b, since it is a simplified but partial duplication of the portions of the circular loci chart which pertain to the problem.

The end of the heavy arrow indicates the complex quantity  $E/E_0$ . The magnitude of this ratio is equal to the length of the arrow, while a clockwise or counter-clockwise arrow rotation indicates a respective phase-angle lag or lead of  $E$  relative to  $E_0$ . As the frequency increases from zero to infinity, this arrow starts from a horizontal position where  $E/E_0 = 1$ , then rotates clockwise, decreasing in magnitude. The rotation indicates that  $E$  lags in phase relative to  $E_0$ . After the arrow reaches a point of  $-42^\circ$  maximum lag, it continues in reverse rotation, while decreasing further in magnitude. At infinite frequency, the arrow is again horizontal, where  $E$  and  $E_0$  are again in phase, and the length of the arrow (the magnitude of  $E/E_0$ ) is

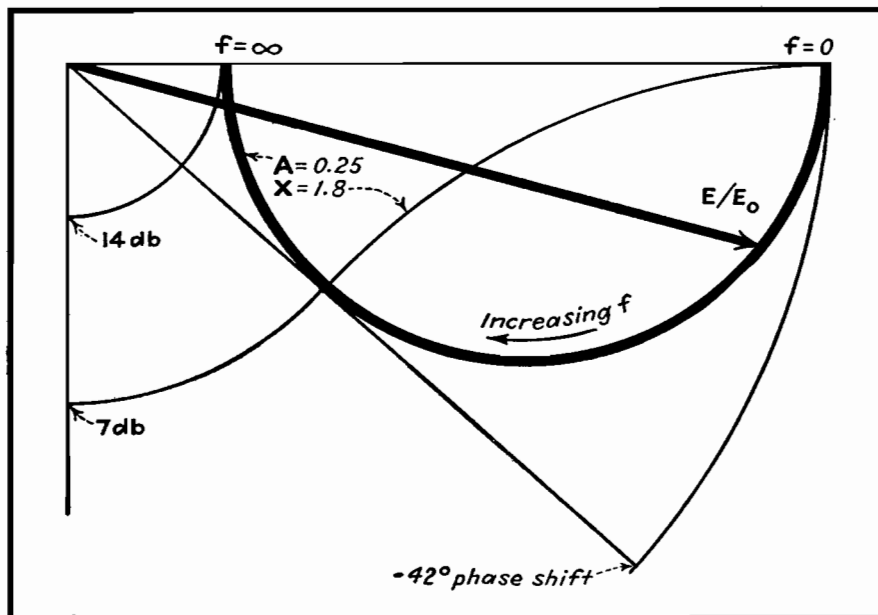


Fig. 1b.—Simplified, partial duplication of the design chart used in solution of the network of Fig. 1a.



f (cps)	X	Atten. (db)	Phase Shift
295	0.53	1.5	-27°
520	0.94	3.5	-37°
1,000	1.8	7.0	-42°
1,950	3.5	10.5	-36°
3,900	7.0	12.5	-25°

Fig. 1c.—Table of computed values of  $X$  for corresponding selected frequencies  $f$  and readings of values for the attenuation and phase-shift functions taken from the chart.

0.2. As the frequency varies, the locus of  $E/E_0$  is a circle. This is shown in Fig. 1b by the heavy circular line, which is obtained from the chart in the following manner:

It is recalled that a 14-db maximum attenuation is desired at infinite frequency. Thus, on the vertical amplitude linear decibel scale, locate the circle of constant 14-db attenuation. Follow this circle in a counterclockwise direction, and note the point where it intersects the horizontal line. The circle of constant value of  $A$  which also intersects this point is the circle for which  $A = 0.25$ . This circle is the desired locus of  $E/E_0$ .

The chart and Fig. 1b also show that orthogonal to the circles of constant  $A$  are those of constant relative frequency  $X$ . As indicated in the fourth quadrant of the chart,  $X = 2\pi fCR$ , i.e.,  $X$  is proportional to the frequency and equals unity at the frequency where the magnitude of the reactance of capacitance  $C$

is equal to  $R$ . It is now recalled that at 1,000 cycles the specifications require an attenuation of 7 db. Figure 1b and the chart show that the circle of constant 7-db attenuation intersects the circle of constant  $A = 0.25$  at the value of  $X = 1.8$ . Hence,  $C$  is determined by noting that  $X = 1.8 = 2\pi fCR = 2\pi \times 1,000 \times C \times 500$ , or  $C = 0.58 \mu f$ .

### Complete Transmission Function

If desired, the amplitude and phase frequency characteristics of the network, for frequencies other than 1,000 cycles, are easily determined. Following the procedure outlined above, it is found, for example, that the attenuation is 3.5 db at  $X = 0.94$ , or  $f = X/2\pi CR = 0.94/2\pi \times 0.58 \times 500 = 520$  cycles, and the phase angle is  $-37$  deg. Both the attenuation and phase characteristics are tabulated in Fig. 1c. It should be noticed particularly that the chart gives a physical picture of the way in which the ratio  $E/E_0$  varies with frequency.

The circuit chosen is the simplest that will fulfill the specifications, but it has the disadvantage of presenting to the 500-ohm source an impedance that is not solely resistive and that varies with frequency. If a constant resistive impedance of 500 ohms is desired, as one looks from the source into the network, then the circuit may be elaborated to the bridged-T type shown on the chart and in Fig. 1d. This is one of a series of constant-resistance networks<sup>3</sup> whose solution may be obtained by using the chart.

### Phase-shifting Network Example

Suppose a simple phase-shifting circuit is to be designed using the circuit shown in Fig. 2. At the frequency of 1,000 cycles, it is desired to control the phase of  $E$  relative to that of  $E_0$  by the setting of

the variable resistance  $AR$ . The total phase shift should not be less than 35 deg, and there should occur a minimum change in the magnitude of  $E$  as its phase is varied. The problem now is to determine  $C$  and  $AR$ ,  $R$  being given equal to 500 ohms.

Studying the chart, it is seen that, inasmuch as the frequency is now constant, the locus of  $E/E_0$  is again circular but now follows the circles of constant relative frequency  $X$ . It is desired to choose a circle for some value of  $X$  such that, as  $A$  varies, a maximum phase shift occurs in  $E/E_0$  together with a minimum change of magnitude. By choosing the circle for which  $X = 2$ , a phase shift of  $-65$  to  $-28$  deg, or a difference of 37 deg, is obtainable with only about a 0.6-db change in magnitude. Hence  $X = 2 = 2\pi fCR = 2\pi \times 1,000 \times 500 \times C$ , or  $C = 0.64 \mu f$ . The value of  $A$  at  $-65$  deg is zero, while at  $-28$  deg the value of  $A$  is 0.48. Thus  $AR$  should vary from 0 to 0.48, so the resistance  $AR$  of Fig. 2 should vary from zero to  $0.48 \times 500 = 240$  ohms.

The table in Fig. 2 gives values of phase shift vs. settings of  $AR$ .

The use of the chart is not limited to examples of the types just described. For example, it is possible to solve also for the magnitude and phase of the input impedance or admittance of the networks shown in the first and fourth quadrants of the charts. Application to other circuit problems not given here are also possible.

### References

- (1) SELETZKY, A. C., "Cross Potential of a 4-arm Network," *Elec. Eng.*, **52**, No. 12, 861, December, 1933.
- (2) HAZELTINE, A., "Current Loci in the General Linear A. C. Network," *Elec. Eng.*, **56**, No. 3, 325, March, 1937.
- (3) TERMAN, F. E., "Radio Engineers' Handbook," p. 245, McGraw-Hill Book Company, Inc., 1943.

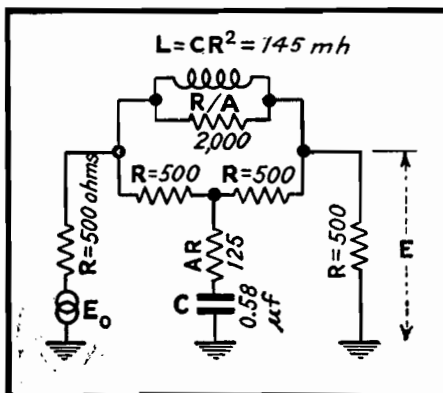


Fig. 1d.—Bridged-T network derived for constant-resistance impedance match at both its input and output terminals with attenuation characteristics for the circuit of Fig. 1a.

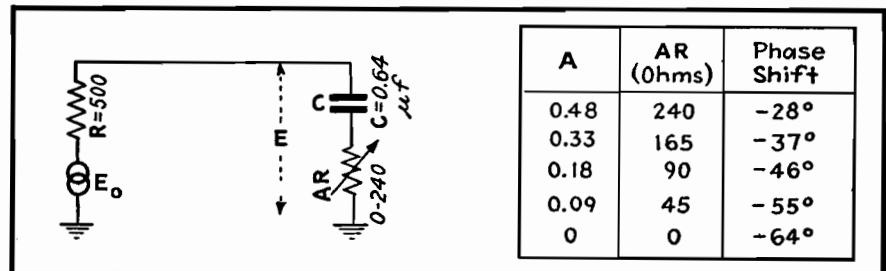
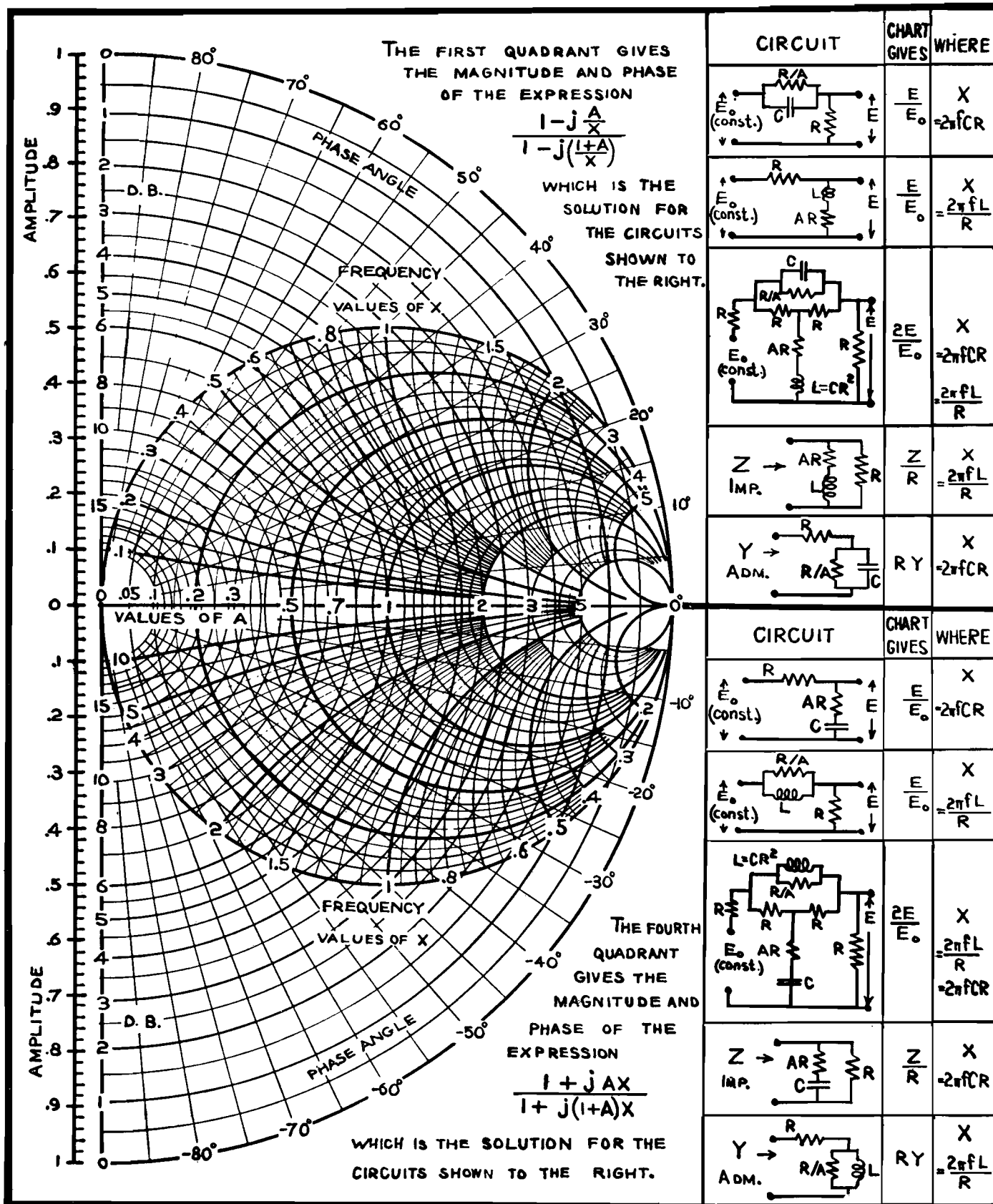


Fig. 2.—Phase-shifting network for constant-amplitude phase correction discussed in the text. Values of  $AR$ , adjusted for the desired condition, are given in the table.



# Evaluating Performance of Symmetrical Four-terminal Networks

By E. S. PURINGTON

A special method of evaluating the transmission characteristics of four-terminal networks that possess electrical and structural symmetry. This method saves considerable labor and time compared with conventional solutions. Basic theory is given, with application to the Wien bridge

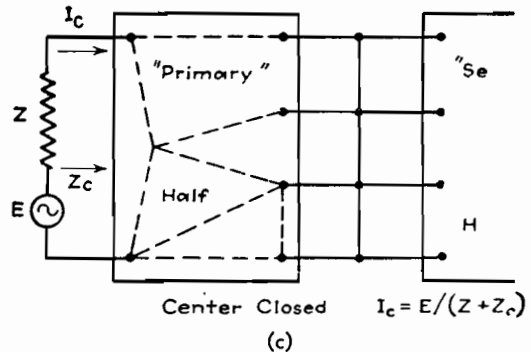
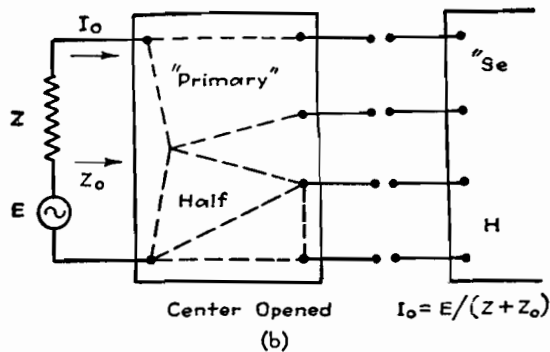
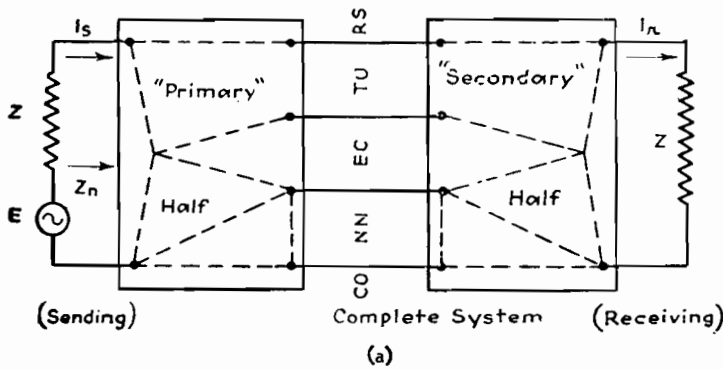


Fig. 1.—To determine the characteristics of a symmetrical electrical, four-terminal network, the sending and receiving currents are determined by shorting and then opening the connections between sending and receiving halves of the network.

Two methods of evaluating the transmission performance of four-terminal networks are well recognized. Firstly and fundamentally, mesh equations may be set up and solved to determine the terminal currents. Secondly and more abstrusely, the performance of the network may be first determined on the basis of image impedance terminations, and then reflection and interaction factors applied to determine the performance with the actual terminations.

If the network possesses electrical symmetry (this is not unusual), and especially when the network together with its terminations possesses structural symmetry, a special method of treatment is available. It possesses the advantage of the mesh equation method of yielding

explicit instead of tabular performance information, and the advantage of the image impedance termination method of dealing with assemblies of impedance elements instead of with currents and voltages at and between network junction points.

While nothing can be determined by the special-purpose method that cannot also be determined by the other procedures, it has the important advantage of usually yielding the required information with the smallest effort. It can be advantageously applied in studies of resistor-capacitor and resistor-inductor networks, wave filter units, composite wave filters made up of a chain of related filter units, and transmission-line phenomena.

This special-purpose method is based on a theorem recorded in Fig. 1. The symmetrical electrical system of Fig. 1a involves a structurally symmetrical network separated into two mirrored half portions analogous to a primary and a secondary circuit. These two portions are joined by electrical connectors, through which power can pass from the primary to secondary portion. No mutual inductance exists between any inductor of the first portion and a corresponding inductor of the second portion. Power transfer is therefore measurable by the currents through and the voltages between the connectors. Major interest is in the received current  $I_r$  in the receiving termination  $Z$  due to a sinusoidal driving voltage  $E$  in the sending arm which is also

of impedance  $Z$ . Of minor interest may be the sending current  $I_s$  or the impedance  $Z_n$  looking into the network from the sending arm during the circuit operation.

The currents  $I_r$  and  $I_s$  can be most readily determined by evaluating the currents in the sending arm when the secondary is isolated from the primary, in one case by making the connectors voltageless by closing them together as in Fig. 1c, and in another case by making them currentless by opening them as in Fig. 1b. In these figures, the impedances  $Z_c$  and  $Z_o$  looking into the network from the sending arm are not dependent on elements beyond the connectors, but depend on the structural make-up of the first half portion only. In terms of the currents  $I_c$  and  $I_o$ , which are readily evaluated from  $E$ ,  $Z$ ,  $Z_c$ , and  $Z_o$ , the currents of interest in Fig. 1a are known and can be shown to be

$$I_s = \frac{1}{2} (I_c + I_o) \quad (1)$$

$$I_n = \frac{1}{2} (I_c - I_o) \quad (2)$$

This simple theorem relating the terminal currents of the network as a whole to the sending currents under the conditions of the network being closed and opened at the center of symmetry is a generalization from information on symmetrical electrical coupled circuits previously published.\* Its value is merely to provide a short cut in solving problems of the type to which it applies. If the difficulty of solving network problems for an explicit solution is roughly as the square or the third power of the number of elements, then there will be a time saving of 50 to 75 per cent by evaluating first  $I_c$  and  $I_o$ , then  $I_s$  and  $I_r$ .

It is usually preferable to express the circuit performance on a comparative rather than an absolute basis, so that the expressed performance is not dependent on the magnitude of the driving force  $E$ . A convenient reference condition is the system with the network absent, i.e., with  $E$  and the sending and receiving impedances  $Z$  in a series arrangement. Then the current in the receiving arm would be  $I_r' = E/2Z$ . Performance may be expressed by an insertion ratio, defined as the ratio of the reference current  $I_r'$  in the receiving termination with the network absent to the actual current  $I_r$  in the receiving termination with the network present. In general this is a vector function, say  $(M + jN)$  of the three impedances  $Z$ ,  $Z_c$ , and  $Z_o$ , which

are readily found to be

$$\text{Insertion ratio} = \frac{E/2Z}{I_r} = (M + jN) = \frac{(Z + Z_o)(Z + Z_c)}{Z(Z_o - Z_c)} \quad (3)$$

The insertion ratio is set up in this manner to make it numerically equal to or greater than unity for the important case of the terminations being equal pure resistors, for which no inserted network can possibly increase the received current.

In place of the vector insertion ratio, the performance may be more conveniently expressed by the insertion loss, decibel, in combination with the insertion phase lag due to the presence of the circuit. These are derivable from the vector insertion ratio  $(M + jN)$  by

$$\text{Insertion loss db} = 10 \log_{10} (M^2 + N^2) \quad (4)$$

$$\text{Insertion phase lag} = \tan^{-1} \frac{N}{M} \quad (5)$$

Inspection of the insertion ratio equation yields only the general information that the insertion loss is infinite for any frequency making  $Z_o = Z_c$ . This is equivalent to saying that  $I_r$  is zero provided  $I_c = I_o = I_n$ .

The insertion ratio expresses the effect of insertion of the network upon the output circuit of the system. For the input branch, the performance, if of interest, may be expressed in terms of the relative loading on the sending arm, given by the ratio of the load impedance  $Z_n$  upon the source to the load  $Z$  which would exist with the network absent

$$\text{Loading effect} = \frac{Z_n}{Z} = \frac{\frac{Z_o Z_c}{Z^2} + \frac{(Z_o + Z_c)}{2Z}}{1 + \frac{(Z_o + Z_c)}{2Z}} \quad (6)$$

From Eq. (6) it can be deduced that the loading and therefore the sending current is unchanged for any frequency making  $Z_o Z_c = Z^2$ , or for any frequency making one of  $Z_o$  and  $Z_c$  infinite and the other zero, with a finite product. At such frequencies, the source delivers the same amount of power regardless of whether the network is absent or present. Zero insertion loss can exist for such a frequency only if the inserted network contains no current-carrying dissipative impedance.

Therefore the complete performance of the system of Fig. 1 may be determined, relative to the performance with the network absent, by Eqs. (3) to (6), involving the impedance  $Z$  representing the terminations, and the impedances  $Z_c$  and  $Z_o$  looking into the network closed and opened at the center of

symmetry as representing the complete inserted network.

### Application of Method to Wien Bridge

As a specific example, consider the parallel  $T$  equivalent of the Wien bridge, made up of resistor and capacitor elements, and terminated by equal resistors, as in Fig. 2a. The entire system involves eight arms, with three independently choosable elements  $R$ ,  $R_1$ , and  $C_1$ , and has the known property of not transmitting at the frequency for which  $C_1$  and  $R_1$  are of equal numerical impedance. The system rearranged for evaluation of  $Z_c$  and  $Z_o$  is shown in Fig. 2b.

Now if the transconductance  $(I_n/E)$  of the system were plotted as a function of frequency, there would be a threefold infinitude of curve shapes, since the magnitudes of  $R$ ,  $R_1$ , and  $C_1$  independently influence the performance so expressed. But in putting the performance on a relative basis, the insertion ratio would not be changed if the impedances of each of the three independently choosable elements were all modified by the same factor. Therefore the insertion performance as a function of frequency would require a twofold infinitude of curve shapes. But further, the abscissa representing frequency as well as the ordinate representing power transfer can be put on a relative basis by establishing a reference frequency, as for example  $F_o$ , the frequency of infinite loss for which  $R_1$  and  $C_1$  are of equal numerical impedance. The actual abscissa, then, will be  $x = f/F_o$ , the ratio of any frequency  $f$  to the reference frequency  $F_o$ . Under these conditions, a single infinitude of curves will relate an insertion effect to the frequency ratio. That is, the insertion loss and the insertion phase lag will be a function of the frequency ratio  $x$ , and of a single other independent variable or parameter that will be the same for all points on representative curves. This is most conveniently an impedance-level parameter relating to the ratio of the numerical impedance of  $R_1$ , and therefore of  $C_1$  at  $F_o$ , to the terminating resistance of  $R$ . These relations are fully summarized in Fig. 2, together with the evaluation of  $Z$ ,  $Z_c$ , and  $Z_o$  in terms of  $R$ ,  $h$ , and  $x$ .

The balance of the problem involves a routine algebraic process of substituting  $Z$ ,  $Z_c$ , and  $Z_o$  in Eq. (3) to determine  $M$  and  $N$  in terms of  $x$  and  $h$ , with  $R$  dropping out because all impedances are on a relative basis. Thereupon the insertion loss and insertion phase lag,

\* Proc. IRE, June, 1930, pp. 996-998.

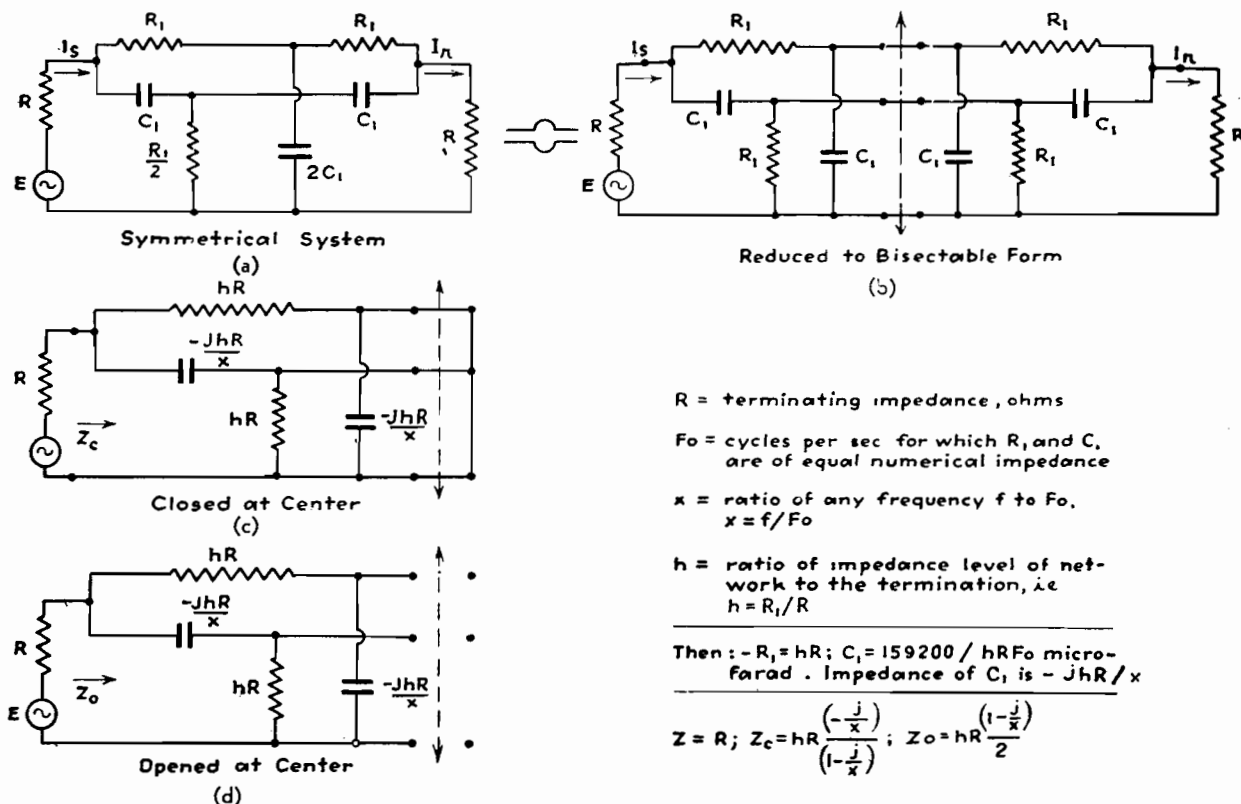


Fig. 2.—Typical problem, that of the Wien bridge, solved by the method of closing and opening the structure at its center of symmetry.

also functions solely of  $x$  and  $h$ , are determined by Eqs. (4) and (5). In dealing with resistor-capacitor systems, the routine will be found less tedious upon making a change of variable  $y = -1/x$ , for the duration of the main algebraic manipulation. In any event, the routine algebraic work for the particular problem of Fig. 2 yields

$$\text{Insertion loss db} = 10 \log_{10} \left\{ \frac{[x^2 + (1+h)^2][(1+2h^{-1})^2 x^2 + 1]}{(x^2 - 1)^2} \right\} \quad (7)$$

$$\text{Insertion phase lag} = \tan^{-1} \left\{ \left[ \frac{2+4h+h^2}{h+h^2} \right] \left[ \frac{x}{1 - \left( \frac{2+h}{h+h^2} \right) x^2} \right] \right\} \quad (8)$$

In Fig. 3 is shown the insertion loss as a function of  $x$  for three values of impedance level  $h$ , namely, 0.2,  $\sqrt{2}$ , and 10. For the value  $h = \sqrt{2}$ , the insertion loss is the same function of  $x$  as of  $1/x$ , and would be symmetrical if the abscissas were plotted logarithmically. For low values of  $h$ , the structure has low-pass properties, with infinite loss at  $x = 1$ ; and for high values of  $h$ , it has similar high-pass properties.

In addition to the usual use of the circuit as a frequency-metering device, it may be also used for filtering purposes. For example, suppose the network is to be used to supply filtering for a power supply. If  $R$ , the load resistance

is to be 50,000 ohms,  $h$  is chosen 0.2, and  $F_o$  is desired to be 120 cycles. Then application of the equations of Fig. 2 indicates the parts required for such a filter are one 5,000- and two 10,000-ohm resistors and one 0.266- and two 0.133- $\mu$ f capacitors.

#### Uses of the Wien Bridge

In Fig. 3, values of the insertion phase lag are indicated at various points on the

curves, and in each case at  $x = 1$  corresponding to infinite insertion loss, there is a discontinuity of 180 deg. This is not predictable of Eq. (8) since any angle has the same tangent as the same angle plus or minus any integer times 180 deg. The location of the quadrant of the phase lag angle can be determined by knowing the algebraic senses of both  $M$  and  $N$ , or in simple cases physical checks are useful. This may be at zero

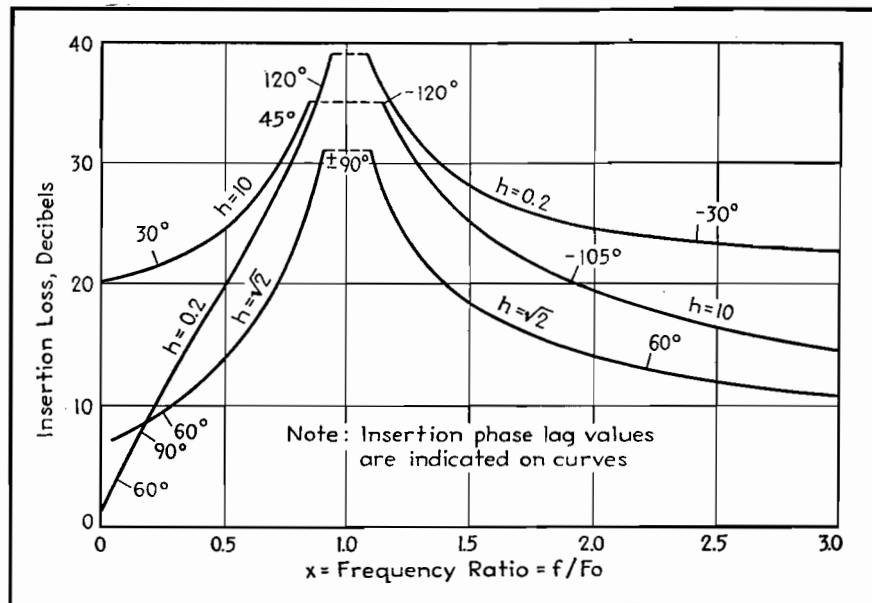


Fig. 3.—Insertion loss curves of Wien bridge for three values of impedance level,  $hR_1/R$ .

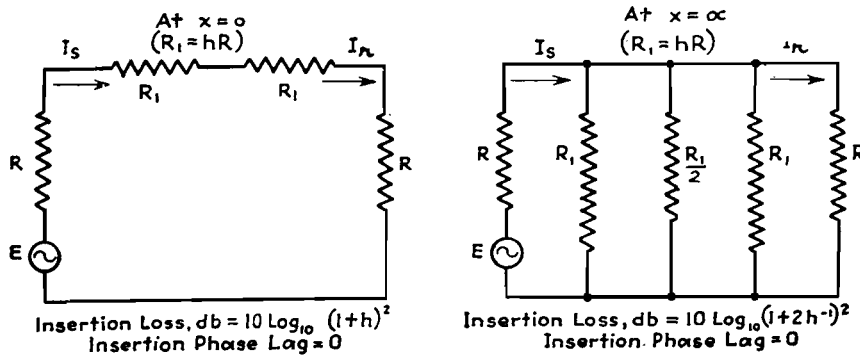


Fig. 4.—Equivalent circuit of Wien bridge at zero and infinite frequencies.

frequency for which any capacitor becomes an open circuit of infinite impedance, and at infinite frequency for which any capacitor is a short circuit of zero impedance.

Figure 4 shows how Fig. 2 appears at zero and infinite frequencies, as pure resistance networks, with the network producing an insertion loss in both cases but with no phase shift. On the curves, 180 deg must be subtracted in passing through  $x = 1$  from the low side to the high, to make the insertion phase lag the same at  $x = 0$  and  $x = \infty$ . It would be only for mathematical convenience to assert the lag as zero at zero frequency, and 360 deg at infinite frequency, with the lag increasing continuously on the two legs of the curves, and increasing discontinuously between them. There is of course no physical discontinuity involved, because the phase-lag discontinuity occurs simultaneously with infinite insertion loss value. Physically, the received current  $I_r$  is in one direction before becoming zero, and in the reverse direction after becoming zero. This suggests an impedance bridge at the condition of balance, with the received current in the detector arm of

the bridge, and in fact such an interpretative arrangement is possible.

#### Application of Method to Impedance B

The general equations for the currents in all six arms of a simple impedance bridge due to a driving force in the power arm are a matter of record. In Fig. 5a, the general type of structure under consideration is shown in block, with the network specified by  $Z_c$  and  $Z_o$ , the impedances looking into the network closed and opened at the center of symmetry. With the network bisectable,  $Z_c$  and  $Z_o$  represent physically realizable combinations of reactor and resistor

elements. If now an impedance bridge is made up as in Fig. 5b, using the same driving force and terminations as in Fig. 5a, and the bridge arms are made  $Z_c$  and  $Z_o$  derived from Fig. 5a and arranged as indicated, then it will be found that identical sending currents and identical received currents occur for the two figures. That is, except for internal arrangement, any bisectable four-terminal network may be replaced by a symmetrical but nonbisectable network in the form of an impedance bridge. When used for transmission purposes, any impedance bridge with opposite arms equal as in the present case is termed a symmetrical lattice network. Such networks are of especial importance because not all lattice networks are capable of being replaced by simple bisectable equivalents, since the two terminal impedances  $Z_c$  and  $Z_o$  in the bridge structure in general need not correspond to  $Z_c$  and  $Z_o$  obtained by bisection of a four-terminal impedance.

Accordingly, the basic treatment of structurally bisectable networks here presented automatically extends itself to cover one important type of network which although not bisectable is nevertheless electrically symmetrical.

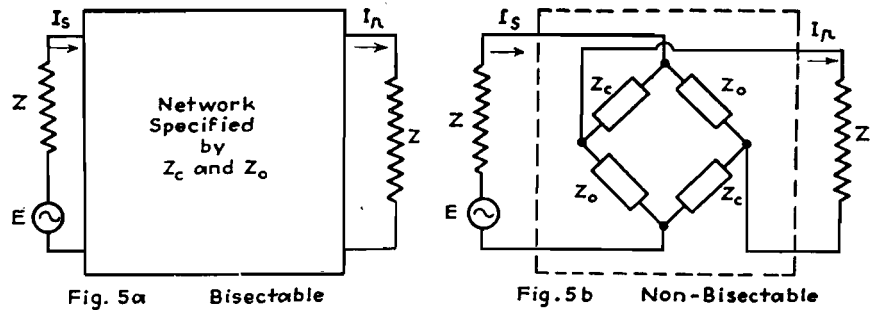


Fig. 5.—Method of replacing a bisectable network by a nonbisectable bridge.

# Reactance Networks with Resistance Terminations

By E. S. PURINGTON

A general treatment of bisectable reactance networks with equal resistance terminations, especially with the reactors ideal, illustrated by working out the detailed performance of four-element networks commonly used for simple low-pass purposes. Illustrative curves and numerical examples are given for determining the reactor elements required to produce a specified curve, and for determining the curve corresponding to a given set of elements

MANY electrical circuits consist of a bisectable symmetrical network of reactor elements inserted between two equal resistance terminations. These are exemplified by the simple but important arrangement of Fig. 1A, where the network comprises the reactor elements  $L_1$ ,  $C_1$ , and  $C_2$ , and the driving voltage  $E$  in the sending arm  $R$  produces an output current  $I_r$  in the receiving arm which is also a resistor  $R$ . Also indicated is the first half portion of the system resulting from bisection, and the electrical connectors by which power can be transferred to the second half portion. With the reactor elements dissipative, the insertion properties of the network are most readily derivable from the termination impedance  $R$ , and the impedances  $Z_o$  and  $Z_c$  looking from the termination  $R$  into the first half portion, first with the connectors opened, then closed by shorting them together, using

$$\text{Insertion ratio} = \frac{E/2R}{I_r} = \frac{(1 + Z_o/R)(1 + Z_c/R)}{(Z_o/R - Z_c/R)} = M + jN \quad (1)$$

This equation becomes greatly simplified if ideal conditions are stipulated, with the terminations  $R$  of pure ohmic resistance independent of frequency, with each reactor element free from dissipative loss, and with the numerical impedance of each inductor proportional to frequency and of each capacitor inversely proportional to frequency. By reference to Fig. 1B,  $Z_o$  and  $Z_c$  become pure reactance impedances  $jX_o$  and  $jX_c$ , and simple right-angle triangle-type vector diagrams, showing the circuit relation for the open and closed conditions, result. The ratio  $X_o/R$  is the tangent of the phase angle by which voltage  $E$  leads the current  $I_o$ , and  $X_c/R$  is the tangent of the angle by which

voltage  $E$  leads the current  $I_c$ . These angles  $\theta_o$  and  $\theta_c$  cannot differ from zero by more than 90 electrical degrees, but can be positive or negative. For the case illustrated,  $\theta_o$  is negative for all frequencies, but  $\theta_c$  is positive for low frequencies and negative for high frequencies. The ratios  $X_o/R$  and  $X_c/R$  will be here termed  $q_o$  and  $q_c$  from analogy to the quality factor  $Q$  expressing the reactance-resistance ratio for coils or capacitors. These  $q$  values in general are complex functions of frequency, with values ranging from negative infinity to positive infinity. The vector diagrams of Fig. 1B depict conditions for a combination of elements which for some frequency make  $\theta_o = -45^\circ$ ,  $\theta_c = 30^\circ$ , for which the tangents are  $q_o = -1.0$  and  $q_c = 0.577$ .

With this stipulated simplification, Eq. (1) becomes

$$\text{Insertion ratio} = \frac{E/2R}{I_r} = \frac{(1 + jq_o)(1 + jq_c)}{j(q_o - q_c)} = M + jN \quad (2)$$

This simplifies to

$$\text{Insertion ratio} = \left( \frac{q_o + q_c}{q_o - q_c} \right) + j \left( \frac{q_o q_c - 1}{q_o - q_c} \right) = M + jN \quad (3)$$

so that  $M$  and  $N$  are directly computable. For the sample values given above,  $M = 0.268$ ,  $N = 1.0$ , and since  $M$  and  $N$  are both positive, the insertion ratio vector is in the first quadrant, with the termination current  $I_r$  lagging behind the reference current  $E/2R$  and therefore behind  $E$  itself by less than 90 electrical degrees. The insertion loss in decibels,  $10 \log_{10} (M^2 + N^2)$  is 0.3 db, and the insertion lag,  $\tan^{-1} (N/M)$  is  $+75^\circ$  deg. In general,

$$\text{Loss} = 10 \log_{10} \left[ 1 + \left( \frac{1 + q_o q_c}{q_o - q_c} \right)^2 \right] \quad (4)$$

$$\text{Lag} = \tan^{-1} \left( \frac{q_o q_c - 1}{q_o + q_c} \right) \quad (5)$$

These equations are especially useful if the loss and lag are to be computed after expressing values for any specific circuit as algebraic functions of frequency. For

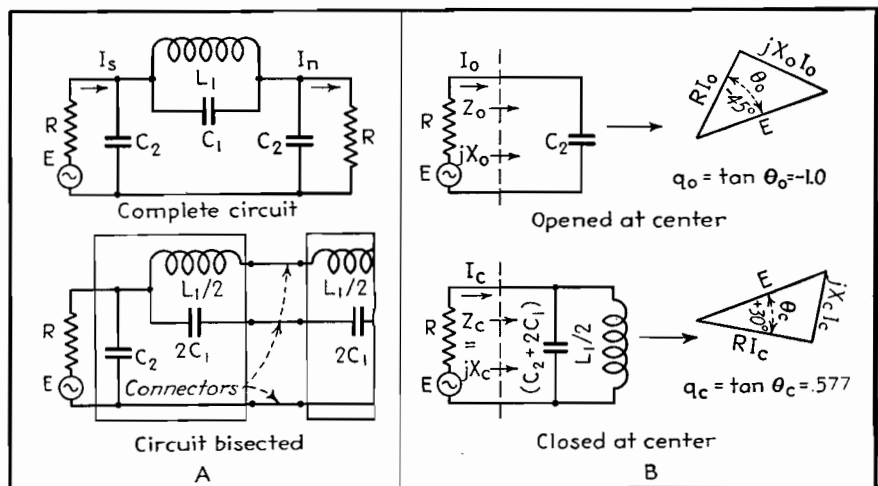


Fig. 1.—Bisectable reactance networks with equal resistance terminations.



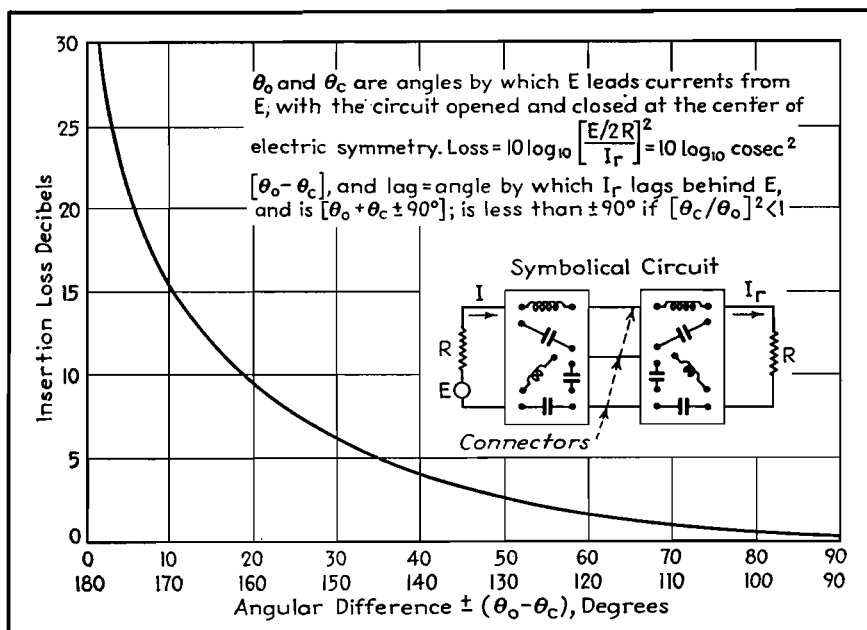


Fig. 2.—Loss and lag characteristics for bisectable R-X circuits.

single-point computations, especially simple equations, result by substituting  $q_o = \tan \theta_o$  and  $q_c = \tan \theta_c$  in Eqs. (4) and (5), and simplifying to yield

$$\text{Loss} = 10 \log_{10} \text{cosec}^2 (\theta_o - \theta_c) \quad (6)$$

$$\text{Lag} = (\theta_o + \theta_c) \pm 90^\circ \quad (7)$$

In Fig. 2 are given a chart and explanatory matter for quickly evaluating the insertion loss by Eq. (6), applying to any bisectable symmetrical network with equal resistance terminations. By its use, the insertion loss for any specific choices of elements such as  $L_1$ ,  $C_1$ , and  $C_2$  of Fig. 1a inserted between specified resistance terminations  $R$  can be most rapidly evaluated. Substantially all that is required is computation of the angles  $\theta_o$  and  $\theta_c$  by which the driving voltage  $E$  leads the current produced by that voltage for the two conditions, with the circuit as a whole opened and closed at the center of symmetry.

The more important problem usually is to predetermine what values must be assigned to the elements to be inserted between specified terminations  $R$  so that the loss and possibly the lag will be a suitable function of frequency. For this purpose it is desirable to use equations in terms of the  $q$  values, survey the entire possibilities of curve shapes afforded by a given network arrangement, choose the shape that is most satisfactory, and evaluate the reactor elements which for the specified  $R$  will yield that shape. Before carrying through the necessary routine using Fig. 1, it will be helpful to study Eqs. (4) and (5) in greater detail.

Quick inspection of Eq. (4) shows the

loss is zero for any frequency making the product of the  $q$  values negative unity, and the loss is infinite for any frequency making the  $q$  values equal. Less obviously, zero loss is approached for any condition making one of the  $q$  values a very large value and the other a very small value. Such is the case in the cited example of Fig. 1B for frequencies near zero, making  $q_o$  highly negative and  $q_c$  only slightly positive. Less obviously also the loss is very great for any condition making both of the  $q$  values very small, as is the case in Fig. 1B for very high frequencies with the  $q$  values only slightly negative. Inspection of the circuit configuration often reveals conditions of zero and infinite loss. In Fig. 1A, the loss is of necessity infinite for the frequency of antiresonance of elements  $L_1$  and  $C_1$ , corresponding in fact to the  $q$  values of Fig. 1B being algebraically equal. Inspection of a circuit configuration will always fail to disclose the condition of zero loss due to the product of the  $q$  values being negative unity, since not all combinations of elements will result in such a condition existing.

It is noteworthy that the loss equation involves the product and the difference of the  $q$  values, while the lag equation involves the product and the sum. The quotient of the  $q$  values is not as yet specifically involved, but for the present has the hidden value of clearing up the equational ambiguity as to the quadrant location of the phase angle. In Eq. (5), if the tangent of the phase lag angle is positive, the angle may be in the first or third quadrant, but if negative, in

the second or fourth. Referring back to Eq. (2),  $M = (q_o + q_c)/(q_o - q_c)$  is positive provided the quotient  $(q_c/q_o)$  is within the limits  $-1$  to  $1$ . Therefore if  $(q_c/q_o)^2$  is less than unity, or correspondingly  $(\theta_c/\theta_o)^2$  is less than unity, the lag angle must be located in the first or fourth quadrant for which  $M$  is positive, otherwise it must be located in the second or third quadrant for which  $M$  is negative.

Absolute determination of the lag angle must be based on agreement as to lag for some specified frequency. Since in Fig. 1A all the network currents for very low frequencies are in the inductor  $L_1$  directly connecting the two terminations, so that the network produces no effect at zero frequency, it will be agreed that the lag is zero at zero frequency, and not, for example,  $360^\circ$ . But at infinite frequency the loss approaches infinity and the lag angle approaches the boundary between the first and second quadrants. Absolute lag, as for example,  $90^\circ$ ,  $450^\circ$ , or  $-270^\circ$ , can be found only by applying the physical doctrine of continuity and integrating the phase changes as the frequency progresses from zero to infinity. Unfortunately Eq. (3) points out that as frequency changes in such a way as to make  $(q_o - q_c)$  change sign, the vector  $(M + jN)$  changes by  $180^\circ$ . No physical discontinuity is involved, because at the same time the insertion loss is infinite. What happens is a reversal of the load current  $I_r$  as it passes through a condition of zero magnitude, analogous to the change of direction of current in the galvanometer arm of a bridge in passing through a condition of balance. Nevertheless there is no short method of checking whether  $180^\circ$  must be added or subtracted when the frequency passes through the critical value. Apparently the only satisfactory procedure to clear up this point, if important, is to compute the performance at least once with an element such as  $L_1$  of Fig. 1A slightly dissipative, using the more general Eq. (1), useful when  $Z_c/R$  is a complex imaginary. The lag performance under this condition will serve as a guide to what should be done in the limiting case with the element  $L_1$  mathematically free from loss.

#### Solution of Specific Problem

The procedure necessary to develop loss and lag equations for any network to which the preceding theory applies will be illustrated by working out the complete

solution for Fig. 1A. Here is a circuit with four differently choosable electrical elements, the terminations  $R$ , and the network reactors  $L_1$ ,  $C_1$ , and  $C_2$ . It is required to develop the insertion performance equations covering all possible combinations, survey the possible curve shapes, and tabulate information as to how any selected curve shape may be realized.

If a set of values is randomly assigned to the circuit elements, the performance as here defined will not be modified by multiplying the impedance of each element by a given factor, as for example by doubling  $R$ , doubling  $L_1$ , and halving the capacitances of  $C_1$  and  $C_2$ . But the performance will be altered if the terminations  $R$  are held constant while the impedances of the network elements are doubled, since the  $q$  values will be doubled. To provide for various impedance levels of the network elements with respect to the terminations, an impedance level parameter  $h$  is introduced to which in the equations the  $q$  values will be proportional.

With a fixed specified value for  $R$ , the only way that the elements of the network may be modified without curve shape changes is by multiplying the network reactor values  $L_1$ ,  $C_1$ , and  $C_2$  all by the same factor, as by doubling. What previously happened at frequency  $f$  will subsequently happen at a frequency  $f/2$ , thereby shrinking the curve if plotted on a frequency basis. If, however, some significant reference frequency  $F_0$  is set up, as for example, the cutoff frequency of the curve shape if used for filtering purposes, and the curve is plotted in terms of the ratio of any frequency to the reference frequency, change of the reference frequency will not change the curve shape. In the present example, the significance of  $F_0$  as the cutoff frequency is chosen to give the simplest possible loss equation, but its cutoff significance appears only after specific curve shapes are plotted. The ratio  $f/F_0$  will be here given the designation  $x$  customarily applied to the abscissa in curve plotting.

With a fixed  $R$ , and choices of  $h$  and  $F_0$  which must be held constant, variations in elements  $L_1$ ,  $C_1$ , and  $C_2$  are still possible.  $L_1$  and  $C_1$  determine a finite frequency for infinite insertion loss. The ratio of this frequency to  $F_0$  will be termed  $k$ , the infinite loss parameter. Changing  $k$  requires modification of  $L_1$ ,  $C_1$ , or of both, and with the requirement that  $h$  and  $F_0$  will not be changed, it develops that all three reactor impedances

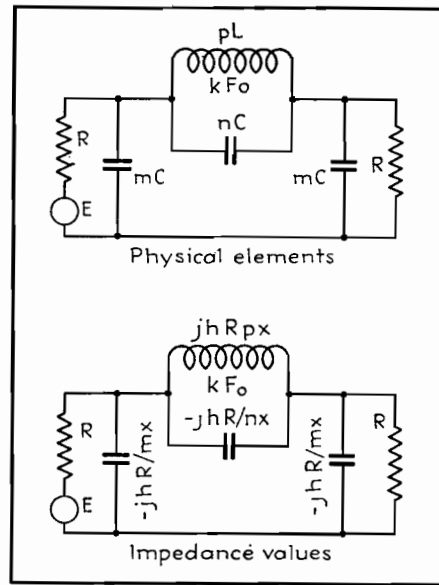


Fig. 3.—Circuit designations showing relation between physical elements and impedance values.

must be altered, but not in a proportionate manner.

In place of the three physical elements  $L_1$ ,  $C_1$ , and  $C_2$  it becomes necessary, therefore, to deal with three abstract elements  $F_0$ ,  $h$ , and  $k$  to yield performance equations in terms of  $x$ ,  $h$ , and  $k$ . It must be possible to evaluate the reactors for the specified  $R$ , the value desired to represent  $F_0$  corresponding to  $x = 1$ , and the values chosen for the parameters  $h$  and  $k$  determining and identifying the curve shape to be duplicated.

It works out most advantageously to designate reactor values as functions of  $R$ ,  $F_0$ ,  $h$ , and  $k$  in two steps. Basic values of inductance and capacitance designated  $L$  and  $C$  are defined as those having numerical impedances  $hR$  at  $F_0$ , thereby involving everything except  $k$ . The various inductor and capacitor elements in the network are then these basic values multiplied by factors  $m$ ,  $n$ , and  $p$ , for example, which involve only  $k$ . In terms of inductance, element  $L_1$  of Fig. 1A is replaced in Fig. 3 by element  $pL$ , for example, but because of the definition of  $L$  on an impedance basis, the element is also capable of being assigned an impedance designation  $pL = jhRpx$ . Similarly, for example,  $C_2$  can be designated  $mC = -jhR/mx$ , and  $C_1 = -jhR/nx$ . Designations here used for basic values of  $L$  and  $C$  differ from other practices in standard texts, but this seems justifiable because of the greater simplification of results and because of the direct physical significances in terms of impedances. The general equations uni-

versally useful for computing basic  $L$  and  $C$  values, together with the various combinations of units with which they may be used, are

$$L = \frac{0.1592hR}{F_0}$$

$$C = \frac{159,200}{hRF_0}$$

$F$	$R$	$L$	$C$
cycle	ohms	henry	$\mu f$
kc	ohms	mh	$m\mu f$
Mc	ohms	$\mu h$	$\mu\mu f$

For example, to be at an impedance level of  $h = 4$  with respect to a 500-ohm termination at 200 cycles, the basic value of  $L$  must be 1.592 henrys. Or a 100- $\mu f$  capacitor operating at  $F_0 = 10$  Mc may be considered to be at an impedance level of  $h = 2.2$  with respect to a 72-ohm resistive impedance.

For determining what functions of  $k$  the multiplying factors  $m$ ,  $n$ , and  $p$  of Fig. 3 must be, one requirement is that  $pL$  and  $nC$  must be of equal numerical impedance for the special frequency value  $kF_0$  for which  $x = k$ . This requires the relation  $pn = 1/k^2$ . Two other relations must be found. Inspection of Eq. (4) indicates the desirability of making  $q_0$   $q_c$  as simple an algebraic function as possible. Using the impedance designations of Fig. 3, routine algebraic procedure yields for the  $q$  values and their product

$$q_0 = \frac{-h}{mx}; q_c = \frac{-hpx}{[(m + 2n)px^2 - 2]}$$

$$q_0q_c = \frac{h^2}{[m(m + 2n)x^2 - 2m/p]}$$

The product function  $q_0q_c$  will take on the simplest possible form  $h^2/(x^2 - 1)$  provided the relations  $m(m + 2n) = 1$  and  $p = 2m$  are met as well as the previously established relation  $pn = 1/k^2$ . These three relations are met if  $m$ ,  $n$ , and  $p$  are the following function of  $k$ :

$$m = \sqrt{1 - k^{-2}}$$

$$n = \frac{1}{2k} \sqrt{k^2 - 1} = \frac{1}{2mk^2}$$

$$p = 2\sqrt{1 - k^{-2}} = 2m \quad (8)$$

With these functions of  $k$  now replacing  $m$ ,  $n$ , and  $p$ , the  $q$  values become

$$q_0 = \frac{-h}{\sqrt{1 - k^{-2}}}$$

$$q_c = \frac{-h\sqrt{1 - k^{-2}}(x)}{(x^2 - 1)} \quad (9)$$

The four combinations of the  $q$  values that,

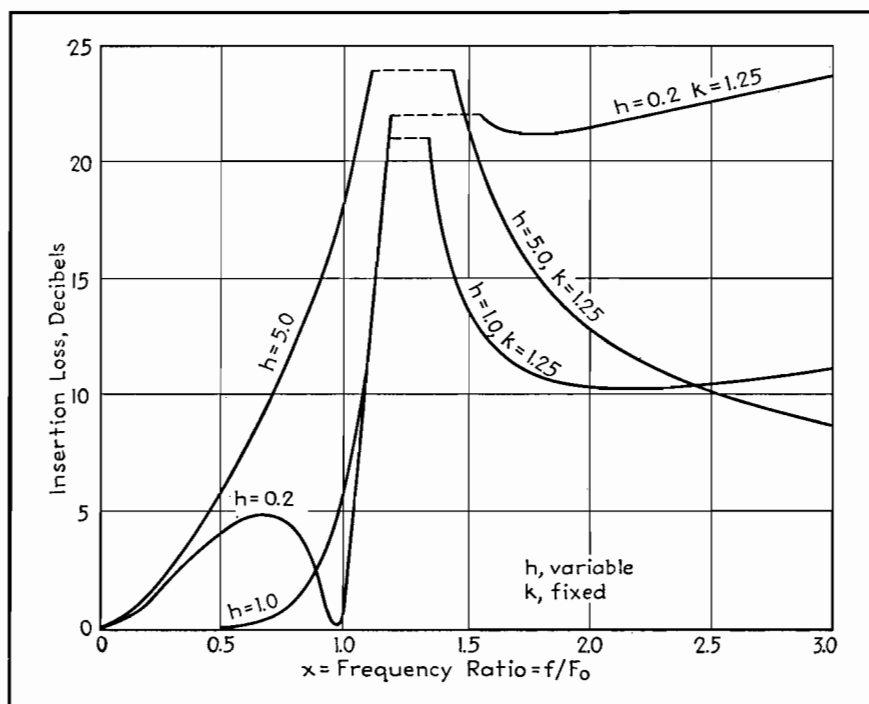


Fig. 4.—Low-pass filter characteristics, effect of changing impedance level.

determine the circuit performance are

$$\begin{aligned} q_o q_c &= \frac{h^2}{(x^2 - 1)} \\ (q_o - q_c) &= \frac{h(k^2 - x^2)}{k \sqrt{(k^2 - 1)} (x)(x^2 - 1)} \\ \frac{q_c}{q_o} &= \frac{(1 - k^2)x^2}{(x^2 - 1)} \\ (q_o + q_c) &= \frac{h[k^2 - (2k^2 - 1)x^2]}{k \sqrt{(k^2 - 1)} (x)(x^2 - 1)} \end{aligned} \quad (10)$$

Substitution of the product, difference, and sum functions of the  $q$  values in Eqs. (4) and (5) yields the loss and lag equations which when reduced to simplest form are recorded as part of the chart in Fig. 6. These permit loss and lag curve shapes to be computed and plotted as functions of  $x = f/F_0$  for all possible combinations of  $h$  and  $k$  within the allowable ranges of these parameters. The loss is zero db for any condition making  $F_{loss}$  zero, including the two conditions  $x = 0$  and  $x = a = \sqrt{1 - h^2}$ , the latter of which occurs only if  $h$  is less than unity for this type of circuit. This condition is a function of the network and of the termination. Infinite loss requires the loss function to be infinite, including the two conditions  $x = k$  and  $x = \infty$ , which are determined by the network only. Information is included also to enable the network elements to be computed corresponding to any specified value of  $R$ , any frequency  $F_0$  desired to correspond to  $x = 1$ , and any curve shape specified by numerical values of  $h$  and  $k$ .

Included with the chart are loss curves

for  $h = 0.6$  and  $k = 1.1, 1.5$ , and infinity, illustrating choices of parameters that give circuit element values suitable for low-pass filter purposes. With the sharpest cutoff curve ( $k = 1.1$ ) there is only 6 db difference between maximum loss in the pass range and the minimum loss in the attenuation range. For higher values of  $k$ , greater filtering effect in the two ranges is accompanied by lesser sharpness of cutoff. At  $k = \infty$ , factor  $n$  becomes zero, and the element  $nC$  is therefore not required. The other limiting condition with  $k = \text{unity}$  results in the network being entirely absent with the

two terminations direct connected to give zero loss and lag at all frequencies.

Figure 4 shows the effect of changing the impedance level using a fixed value of  $k = 1.25$ , and three choices of  $h$ . Values of  $h$  less than unity, say in the vicinity of  $h = 0.6$  are most desirable if low loss is desired over the greatest possible frequency range.

Figure 5 gives more detailed information for parameter values  $h = 0.6$  and  $k = 1.25$  and includes information for a dissipative case computed by the more complex equations required, based on Eq. (1). Various loss and lag points cover an assumed case with inductor element  $pL$  including in series a resistor sufficient to make the  $Q$  of the inductor arm the reasonable value of 20. The effect of dissipation is of most importance just below cutoff. Comparison of the loss curve for the dissipative case with the curve of Fig. 4 for  $h = 1$  will serve to emphasize that choice of impedance level of the network with respect to the terminations may be of more practical importance than choice of kind and amount of material necessary to give extreme values of quality factors of reactor elements. In Fig. 5, the lag points for the dissipative case justify the phase reversal for the limiting non-dissipative case at  $x = k$  being interpreted as a decrease of lag with increasing frequency, thereby making the lag for infinite frequency 90 instead of 450 deg. This should not be considered to rule out the possibility of other and more complex networks yielding integrated lag changes of more than 360 deg. over the entire frequency range.

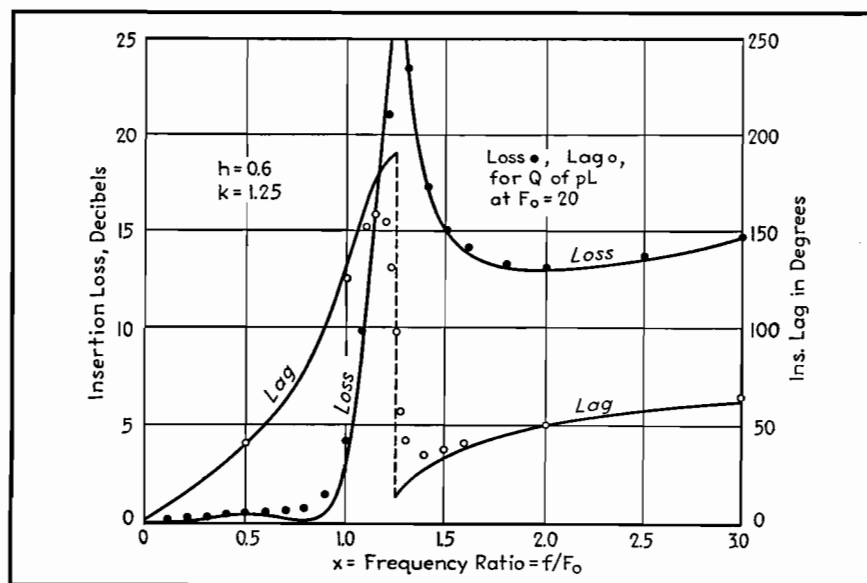


Fig. 5.—More detailed data for parameter values  $h = 0.6, k = 1.25$ .

The information of the chart is arranged for ready evaluation of reactor elements corresponding to any curve shape and specified values of terminations and cutoff frequency. For example, for terminations 5,000 ohms, impedance level  $h = 0.6$ , and  $F_o = 10$  kc, the basic values of  $L$  and  $C$  are 47.7 mh and 5.31  $\mu\text{f}$ . Values of the multiplicative factors for values of  $k$  greater than unity here mentioned are given below.

$k$	$m$	$n$	$p$
1.1.....	0.416	0.99	0.832
1.25.....	0.600	0.533	1.200
1.50.....	0.745	0.298	1.490
Infinite.....	1.000	0.000	2.000

Noting that the sum of all three capacitors ( $n + 2m$ )  $C$  is practically independent of  $k$ , and that over a limited range of inductance the amount of material is practically independent of  $pL$  provided the coil quality  $Q$  is kept constant, it follows that economics does not enter into the choice of  $k$ . For the choices of  $R$ ,  $F_o$ , and  $h$  given above and the additional choice  $k = 1.25$ , the network is found to require an inductor  $pL = 55.3$  mh, two capacitors,  $mC = 3.19$   $\mu\text{f}$ , and one capacitor  $nC = 2.84$   $\mu\text{f}$ .

The inverse problem of determining the curve shape and cutoff frequency for a specified set of circuit values is somewhat more complex, but will be carried through to indicate that all combinations are cared for in the general solution here given. Given, for example,  $R = 500$  ohms,  $mC = 0.1\mu\text{f}$ ,  $nC = 0.2\mu\text{f}$ ,  $pL = 2h$ , it is required to determine  $R$ ,  $F_o$ ,  $h$ , and  $k$ . Knowing that  $pL$  and  $nC$  resonate at  $kF_o$ , it follows that  $kF_o = 159.2/\sqrt{(pL)(nC)} = 252$  cycles. Study of Eq. (8) shows that  $k$  can be determined from the two capacitor values  $mC$  and  $nC$ , since

$k = \sqrt{1 + mC/2nC}$ , i.e.,  $k = 1.12$ . Therefore  $F_o = 225$ . Also from Eq. (8), values of  $m$ ,  $n$ , and  $p$  for  $k = 1.12$  are 0.447, 0.894, and 0.894, respectively. Therefore from the known values of the circuit elements,  $L = 2.24$  henrys and  $C = 0.224$   $\mu\text{f}$ . Using the formulas for

$L$  or for  $C$  in terms of  $h$ ,  $R$ , and  $F_o$ ,  $h$  in either case is 6.31. Therefore,  $R = 500$ ,  $F_o = 225$ ,  $h = 6.31$ , and  $k = 1.12$ . For this combination, the curves could be plotted if desired, but the loss curve would not be radically different in nature from Fig. 4,  $h = 5$ ,  $k = 1.25$ .

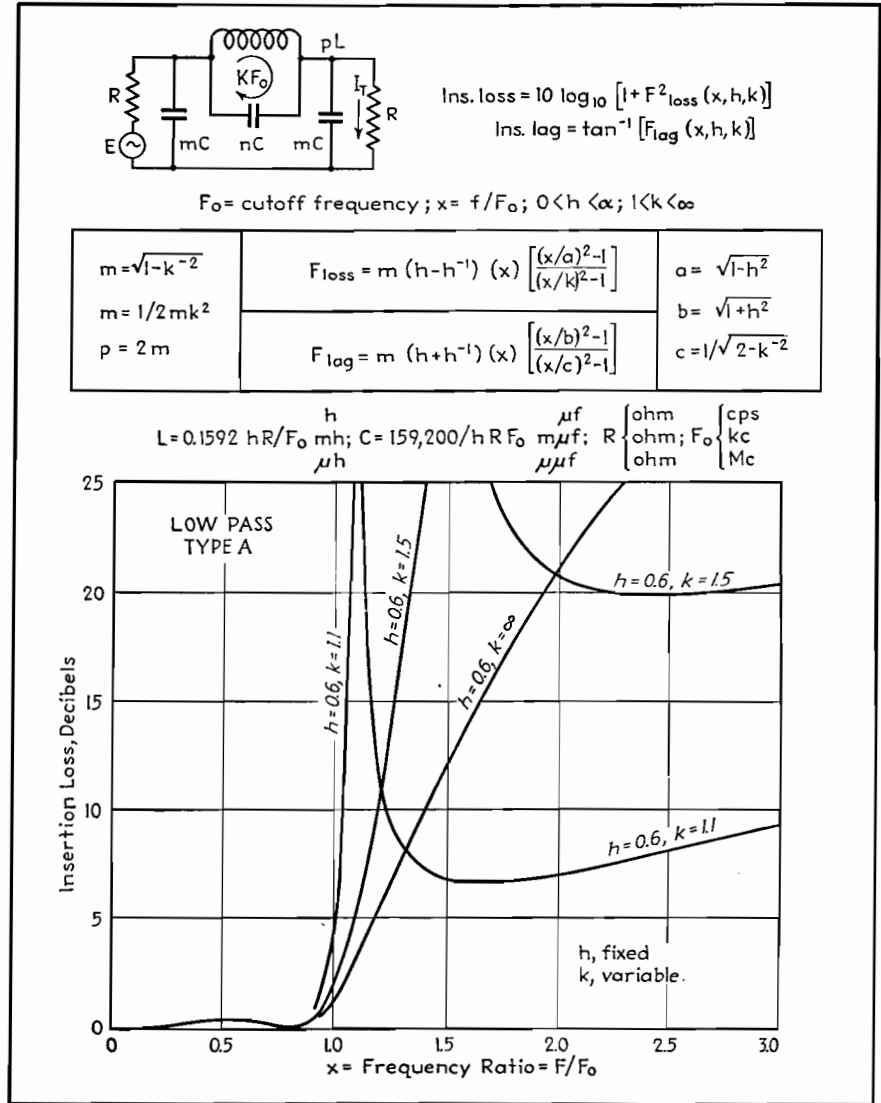


Fig. 6.—Characteristics of low-pass filter unit with several values of  $h$ .

## Low- and High-pass Wave Filter Units

By E. S. PURINGTON

Treatment of electric wave filters on the basis of considering them as bisectable symmetrical circuits

IN THE symmetrical bisectable network of Fig. 1, the sending current  $I_s$  and the received current  $I_r$  due to the driving

force  $E$  can be evaluated from the currents  $I_o$  and  $I_c$ , which would flow from  $E$  with the network opened and closed at the

center of symmetry, by using

$$I_s = \frac{1}{2}(I_o + I_c) \quad (1)$$

$$I_r = \frac{1}{2}(I_o - I_c) \quad (2)$$

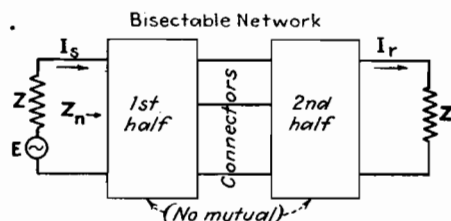


Fig. 1.—Combination block and schematic diagram of symmetrical bisectable network.

With the impedances looking into the network from the sending impedance  $Z$  (termed  $Z_o$  for the center opened condition, and  $Z_c$  for the center closed condition), the values of the terminal currents in terms of  $Z$ ,  $Z_o$ , and  $Z_c$  are

$$I_s = \frac{E}{2} \left[ \frac{2Z + (Z_o + Z_c)}{(Z + Z_o)(Z + Z_c)} \right] \quad (3)$$

$$I_r = \frac{E}{2} \left[ \frac{(Z_o - Z_c)}{(Z + Z_o)(Z + Z_c)} \right] \quad (4)$$

The effect of the presence of the network upon the sending termination may be expressed by the loading ratio, defined as the ratio of the impedance  $Z_n$  by which the sending arm is loaded with the network present to the impedance  $Z$  by which it is loaded with the network absent, given by

$$\text{Load ratio} = \frac{Z_n}{Z} = \frac{[Z_c Z_o / Z^2] + [(Z_o + Z_c) / 2Z]}{1 + [(Z_o + Z_c) / 2Z]} \quad (5)$$

The effect of the presence of the network on the receiving termination is expressed by the ratio of the current  $E/2Z$  which would flow in the receiving termination if the network were absent, to the current  $I_r$  which flows with the network present. This is the insertion ratio given by

$$\text{Insertion ratio} = \frac{E/2Z}{I_r} = \frac{(Z + Z_o)(Z + Z_c)}{Z(Z_o - Z_c)} = M + jN \quad (6)$$

In general the impedances  $Z$ ,  $Z_o$ , and  $Z_c$  involve resistor and reactor elements so that the insertion ratio is a complex imaginary  $M + jN$  which can be evaluated for any specific circuit under consideration. The loss in decibels and the phase shift of the received current due to the presence of the network are

$$\text{Loss} = 10 \log_{10} (M^2 + N^2) \quad (7)$$

$$\text{Lag} = \tan^{-1} \frac{N}{M} \quad (8)$$

Whenever the circuit is made up of a bisectable reactance network terminated with resistances  $R$ , the impedances  $Z_o$  and  $Z_c$  become reactive impedances  $jX_o$  and  $jX_c$ . Upon abbreviating  $X_o/R$

$= q_o$  and  $X_c/R = q_c$ , the insertion ratio becomes more explicitly

$$\text{Insertion ratio} = \frac{E/2R}{I_r} = \left( \frac{q_o + q_c}{q_o - q_c} \right) + j \left( \frac{q_o q_c - 1}{q_o - q_c} \right) \quad (9)$$

and the loss and lag equations in terms of the  $q$  values become

$$\text{Loss} = 10 \log_{10} (1 + F_{\text{loss}}^2) \quad (10)$$

$$\text{where } F_{\text{loss}} = \left( \frac{1 + q_o q_c}{q_o - q_c} \right) \text{ and} \quad (11)$$

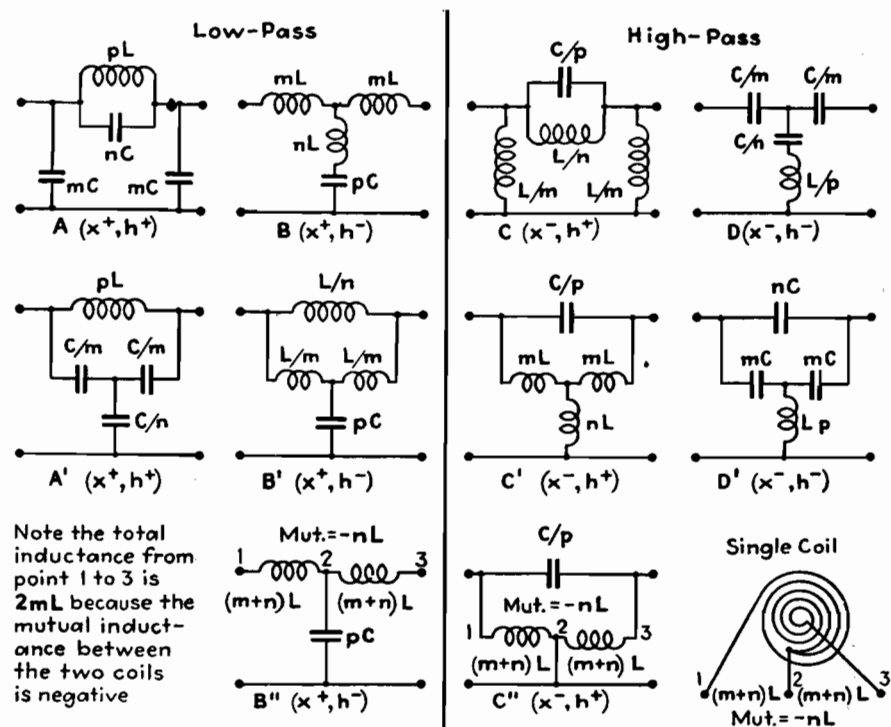
$$\text{Lag} = \tan^{-1} (F_{\text{lag}})$$

$$\text{where } F_{\text{lag}} = \left( \frac{q_o q_c - 1}{q_o + q_c} \right)$$

For illustrating the operation of this complete theory of symmetrical circuits,

a study was made of a four-element network which under proper conditions is suitable for low-pass filter work. The performance of this network together with that of nine other related networks is summarized in Table I. It is understood that each network is terminated with resistances  $R$ . Listed are the four ladder networks  $A$  to  $D$ , most commonly used in low- and high-pass filter work, their bridged  $T$  equivalents  $A'$  to  $D'$  derived by making  $\Delta$  to  $Y$  conversions of inductor and capacitor combinations, and two mutual-inductance-type equivalents  $B''$  and  $C''$ . The performances of all these 10 networks when terminated by resistances  $R$  are expressed by a single loss and a single lag equation. When a

Table I. Standard Low- and High-Pass Wave Filter Units



For terminations  $R$ ,  $\text{Loss} = 10 \log_{10} (1 + F_{\text{loss}}^2)$ ;  $\text{Lag} = \tan^{-1} (F_{\text{lag}})$

$$\begin{aligned} m &= \sqrt{1 - k^2} & F_{\text{loss}} &= m(h - h^{-1}) \quad x \pm 1 \left[ \frac{(x \pm 1/a)^2 - 1}{(x \pm 1/k)^2 - 1} \right] & a &= \sqrt{1 - h \pm 2} \\ n &= 1/2 mk^2 & & & b &= \sqrt{1 + h \pm 2} \\ p &= 2m & F_{\text{lag}} &= \pm m(h + h^{-1}) \quad x \pm 1 \left[ \frac{(x \pm 1/b)^2 - 1}{(x \pm 1/c)^2 - 1} \right] & c &= 1/\sqrt{2 - k^2} \end{aligned}$$

Where required, choose exponents of  $x$  and  $h$  in accordance with the notation adjacent to networks. In the lag equation, use  $+$  sign before  $m$  for low-pass units, and  $-$  for high-pass units.

$L = 0.1592 hR/F_o$  ( $h$ , ohm, cps) or ( $mh$ , ohm, kcs) or ( $\mu h$ , ohm, mcs)

$C = 159200/hR F_o$  ( $\mu f$ , ohm, cps) or ( $m\mu f$ , ohm, kcs) or ( $\mu\mu f$ , ohm, mcs)

choice is to be made of an exponent of  $h$  or  $x$ , it should be in accordance with the notation adjacent to the type designation. For the lag equation, the sign before  $m$  is to be plus for  $A$  and  $B$  types, but minus for  $C$  and  $D$  types. Parameter  $k$  which determines  $m$ ,  $n$ , and  $p$  applied to  $L$  and  $C$  to evaluate network elements must universally be chosen greater than unity, but the sign of the exponent of  $x$  provides automatically that infinite loss occurs at  $x = k$  for  $A$  and  $B$  types and at  $x = 1/k$  for  $C$  and  $D$  types. Universal equations provide for computation of the circuit elements for use with a specified  $R$ , after a choice has been made of the value of  $F_o$  desired to correspond to unity value of the frequency ratio  $x = f/F_o$ , and of the curve shape parameters  $h$  and  $k$ . Simplicity of expression of performance and design results because the basic inductance and capacitance values  $L$  and  $C$  were selected to be of equal numerical impedance  $hR$  at  $F_o$ , which unfortunately is not the case with the usual terminologies.

Types  $A$  and  $B$ , likewise  $C$  and  $D$ , may be termed impedance-level complementaries. For a given set of values of  $x$  and  $k$ , the loss for one unit at impedance level  $h$  is the same as for its impedance level complementary at  $1/h$ . Correspondingly, types  $A$  and  $C$ , likewise  $B$  and  $D$ , may be termed frequency complementaries. For a given set of values of  $h$  and  $k$ , the loss for one unit at frequency ratio  $x$  is the same as for its frequency complementary at  $1/x$ . All five  $A$  and  $B$  units therefore can give the same insertion performance suitable for low-pass work, and all five  $C$  and  $D$  units are similarly suitable for high-pass work. Performance information is most easily obtained for the  $B$  unit, and this is readily convertible into information for the other three units. Graphical information for impedance complementaries is the same, except that curves labeled with a given value of  $h$ , such as  $5/3$ , when they represent type  $B$  should be relabeled  $h^{-1}$  such as  $3/5$  when they represent type  $A$ . Information for type  $A$  is convertible to information for  $C$  by plotting ordinate values at  $x$  for  $A$  and  $1/x$  for  $C$ .

#### Network Parameters Tabulated

To assist in the understanding of the relations of the various types of units, functional values of the  $q$  values and their products are given in Table II.

Considering first the simpler related frequency complementaries such as units

Table II.—Network Parameters

Type of network	$q_o$	$q_c$	$q_o q_c$
A, A'	$-h/mx$	$-hm(x/x^2 - 1)$	$h^2/(x^2 - 1)$
B, B', B''	$h(x^2 - 1)/mx$	$hm x$	$h^2(x^2 - 1)$
C, C', C''	$hx/m$	$hm/x(x^2 - 1)$	$h^2/(x^2 - 1)$
D, D'	$-hx(x^2 - 1)/m$	$-hm/x$	$h^2(x^2 - 1)$

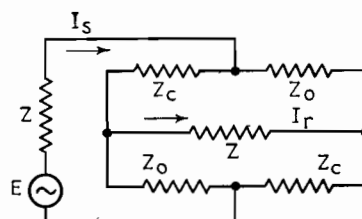
$A$  and  $C$ , reactor elements involving like multiplicative and divisive factors such as  $pL$  of  $A$  and  $C/p$  of  $C$  are related elements, with the universal property that the related elements are of the same numerical impedance at frequency of reciprocation  $F_o$ , such as  $phR$ , but one represents an inductance and the other a capacitance. As a result, the impedance of any element is the same function of  $x$  as its related element is of  $-1/x$ . This is true also of all similar combinations of elements, such as the parallel resonance impedance of elements involving  $p$  and  $n$  in the type  $A$  and  $C$  structures. As a result, the  $q$  functions of  $A$  and  $C$  are frequency reciprocally related and also the loss and lag functions. Because the loss function is to be squared, it is irrelevant as to whether the sign before  $m$  is plus or minus, but it is of importance in the determination of lag.

For the impedance level complementaries, the related elements are also one an inductor and the other a capacitor, but the universal property is that under the conditions of equal network performance the products of the impedances of related elements is  $R^2$ . Thus the impedance of  $pL$  of  $A$  at level  $h$  is  $jphRx$ , while the impedance of the related element  $pC$  of  $B$  at level  $h^{-1}$  is  $-jR/phx$ , and the product is  $R^2$ . This is also true of related network arms, with the product of the impedance of the series arm involving  $p$  and  $n$  in  $A$  and the impedance of the

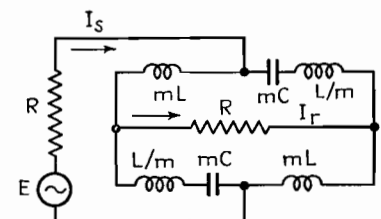
shunt arm involving  $p$  and  $n$  in  $B$  also equal  $R^2$ . As a result,  $q_o$  of  $A$  is  $-1/q_c$  of  $B$ , and  $q_c$  of  $A$  is  $-1/q_o$  of  $B$ , provided  $A$  and  $B$  are at reciprocal levels. By referring back to Eq. (9), the insertion-ratio equation is unchanged upon substituting  $-1/q_c$  for  $q_o$  and also  $-1/q_o$  for  $q_c$ . Functionally expressed, insertion ratio ( $q_o$ ,  $q_c$ ) equals insertion ratio ( $-1/q_c$ ,  $-1/q_o$ ). Therefore the insertion ratio loss and lag are the same for a set of values of  $x$  and  $k$ , provided  $h$  for the  $A$  unit is  $h^{-1}$  for the  $B$  unit.

#### Bridge and Lattice Networks

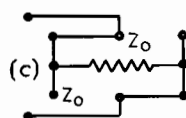
Less used types of networks for low-and high-pass purposes are the bridge or lattice types, and also what may be termed the reversed types. The bridge type, separately shown in Fig. 2a, is not bisectable, but if the terminal currents  $I_s$  and  $I_r$  are determined in terms of  $Z$ ,  $Z_o$ , and  $Z_c$  by setting up the mesh equations, the solution will be found to be identical with  $I_s$  and  $I_r$  for Fig. 1 given in Eqs. (3) and (4). Therefore any bisectable network as in Fig. 1 may be replaced by setting up a bridge as in Fig. 2a, with the arms of the bridge structurally identical with  $Z_o$  and  $Z_c$  produced by bisecting Fig. 1, then opening and closing at the center. The equivalent of the type  $B$  unit is shown for example in Fig. 2b, but this would be little used in practice because of the superior practical advantages of the  $B$  unit. In the bridge



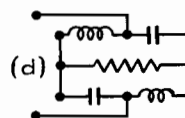
(a) Equivalent of Fig 1



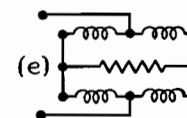
(b) Equivalent of type B



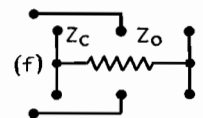
(c)  $X=0$ , Loss=0



(d)  $X=\sqrt{1-h^{-2}}$ , Loss=0



(e)  $X=K$ , Loss= $\alpha$



(f)  $\lambda=\alpha$ , Loss= $\alpha$

Fig. 2.—Schematic diagram of various types of bridge networks.



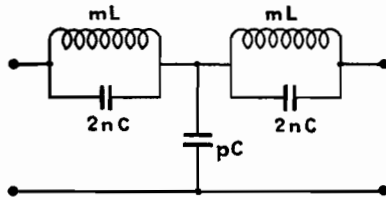


Fig. 3.—Reversed A unit.

form it is however somewhat simpler to visualize the network performance. Smaller figures (Figs. 2c to 2f) illustrate the impedances of the bridge arms for the value of  $x$  corresponding to zero and infinite loss. For  $x = 0$ , arm  $Z_c$  is of zero impedance and arm  $Z_o$  of infinite impedance. Therefore, regardless of the circuit constants  $I_s$  passes through the network to become  $I_r$  without loss or phase shift. For  $x = \sqrt{1-h^2}$ , a condition is met with  $q_o q_c = -1$  corresponding to  $Z_o Z_c = R^2$ , which by Eq. (5) makes the load ratio upon the source arm unity. The same power flows from the source termination with the network present as would flow with the network absent, and since the network is not dissipative, all the power received by the network flows to the load termination, making the insertion loss zero. For the value  $x = k$ , all the bridge arms are of the same inductive impedance value and the bridge is balanced, resulting in infinite insertion loss. It will be noted that the bridge may be balanced if  $Z_o$  and  $Z_c$  are equally dissipative at the balance frequency. Therefore infinite insertion loss at  $x = k$  and  $x = 1/k$  is possible for some units of Table I, even when the terminations are not pure resistors and the network elements are not pure reactors. This property of networks is the basis of using the type  $A'$  unit for checking the departure of an inductor  $pL$  from standard inductance and quality values, using a capacitor  $C/n$  with variable capacitance and loss properties. The final condition of interest at  $x = \infty$  makes all the bridge arms of infinite impedance, thereby disconnecting the sending arm from the receiving arm completely and making the loss infinite.

Bridge networks are more flexible than the other types. Interchanging the arms  $Z_o$  and  $Z_c$  reverses the phase of the received current without changing the loss. A greater variety of choices of elements is possible. In Fig. 2b, there is no restriction on the value of  $m$ , so that element  $mL$  if desired could be of greater inductance than element  $L/m$ . This is not possible with the type  $B$  unit, because a real value of  $k$ , corre-

sponding to the frequency of resonance of shunt arm  $nL$  in series with  $pC$ , makes  $m$  less than unity. A bridge structure with  $m$  greater than unity corresponds to a circuit with  $k$  a pure imaginary such as  $1.25\sqrt{-1}$ , so that the bridge cannot be represented by a  $B$  or  $B'$  unit. Furthermore, with  $m$  greater than unity, the factor  $n$  is a negative quantity. With  $m$  greater than unity, the bridge can however be replaced by the  $B''$  unit, with the factor  $n$  negative instead of positive calling for a mutual inductance between the two inductors in an additive sense. The performance of the bridge structure or its mutual inductance equivalent is covered by the same loss and lag equations as given in Table I. All that is required is that  $k$  be assigned a value not in the real range 1 to infinity, but rather in the range of pure imaginaries. The equations will properly express the performance with  $k$  imaginary, just as they will for the value of  $x = \sqrt{1-h^2}$  for zero loss for a  $B$  unit being a pure imaginary, when  $h$  is chosen less than unity. Therefore the particular bridge of Fig. 2b is seen to be no more general than the simpler networks of Table I except as to the possibility of changing the phase-lag equation by 180 electrical degrees.

In contrast with the bridge types of low- and high-pass filter units, the reversed types have a limited amount of practical value. If, for example, the  $\pi$  type  $A$  unit is bisected, the resulting half sections reversed and the unit reassembled, a five-element  $T$  unit results as in Fig. 3. By inspection, it yields zero loss at  $x = 0$ , and infinite loss at  $x = k$  and  $x = \infty$ , and therefore qualifies as being potentially useful as a low-pass unit. Usually the

unit of Fig. 3 is used at  $h = 1$ ,  $k = 1.25$ , or else half the unit is attached, at the beginning or end or both, to a chain otherwise made up of an integral number of type  $A$  units. The broad purpose is to make the loss for the range  $x = 0$  to  $x = 1$  more uniform than possible with the  $A$  unit also operating at level  $h = 1$ . It is interesting to compare the performance of Fig. 3 under the usual conditions  $h = 1$ ,  $k = 1.25$  with the performance of a type  $A$  unit, without restriction of the parameters that may be used. For the  $A$  reversed unit, as in Fig. 3, the loss function in general is

$$F_{\text{loss}} = mx \left\{ h^{-1} + \frac{h(x^2 - 1)}{[(x/k)^2 - 1]^2} \right\}$$

and for the parameters  $h = 1$ ,  $k = 1.25$ ,

$$F_{\text{loss}} = 0.168x^3 \left\{ \frac{(x/0.826)^2 - 1}{[(x/1.25)^2 - 1]^2} \right\}$$

In Fig. 4 is shown in heavy lines the loss in accordance with this equation, using two scales of ordinates to permit the loss for the range  $x = 0$  to  $x = 1.125$  to be shown with enlarged ordinates. For comparison, the loss curve for a type  $A$  unit with  $h = 0.6$ ,  $k = 1.14$  is shown in dotted lines. The parameter  $h$  was chosen to give reasonably uniform loss in the low-loss range, and parameter  $k$  was chosen to match the solid curve as to the 8-db difference between maximum loss in the low-loss range and minimum loss in the high-loss range. The slopes of the curves in the transitional region are very closely the same. If a figure of merit could be established, based on the uniformity of loss in the low-loss range, the useful difference of losses in the two ranges, and the speed of transition from

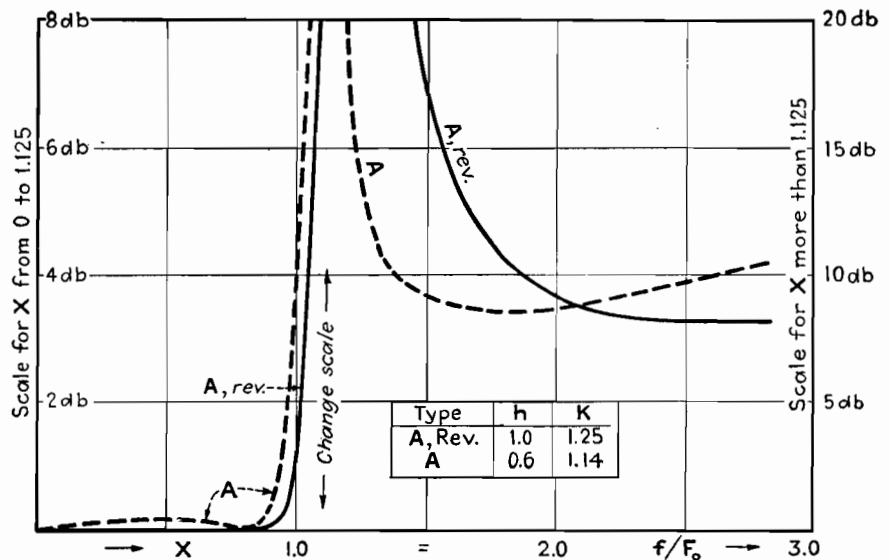


Fig. 4.—Comparison of behavior of network A and A, reversed.



one range to the other, then presumably the five-element unit would not receive a much higher rating than the four-element unit.

While this method of treating low- and high-pass electric wave filter units is

somewhat different from the conventional methods of analysis, it is hoped that the point of view expressed here may be found useful by the reader in the design and construction of his own filter elements. It is believed that the analysis on the

basis of bisectable networks has certain advantages over those analytical approaches which are more frequently encountered in the technical literature and with which the average engineer is more familiar.

# Band-pass Wave Filters

By E. S. PURINGTON

Analysis of wave filters of the band-pass type on the basis of bisectable symmetrical circuit arrangements

THE insertion loss and lag for bisectable reactance networks with respect to equal resistance terminations are derivable from  $q$  functions as defined in Fig. 1. The function  $q_o$  is determined by the circuit involving the sending termination  $R$  and the first portion of the network with the connectors to the second portion opened, and  $q_c$  is similarly determined by the same arrangement but with the connectors closed together. These  $q$  values are the tangents of the phase angles by which the driving voltages  $E$  lead the circuits  $I_o$  and  $I_c$ , respectively, for the opened and closed conditions. To provide for coverage of the performance with varying ratio of the impedances of all the network elements with respect to the terminations, an impedance level parameter  $h^*$  was introduced to which the reactances  $X_o$  and  $X_c$  of the figure and, consequently, the  $q$  values are proportional.  $Q_o$  and  $Q_c$  may now be defined as the values of the  $q$  functions at unity impedance level; i.e.,  $Q_o = q_o/h$  and  $Q_c = q_c/h$ . Further, it is convenient to abbreviate for the product, sum, and difference of the  $Q$  values;  $P = Q_o Q_c$ ,  $S = (Q_o + Q_c)$ , and  $D = (Q_o - Q_c)$ . With these additional nomenclatures, the circuit loss and lag equations are

$$\text{Loss} = 10 \log_{10} (1 + F_{\text{loss}}^2),$$

$$F_{\text{loss}} = \left( \frac{h^2 P + 1}{h D} \right) \quad (1)$$

$$\text{Lag} = \tan^{-1} (F_{\text{lag}}), F_{\text{lag}} = \left( \frac{h^2 P - 1}{h S} \right) \quad (2)$$

In addition, the lag angle is to be placed in the second or third quadrant provided  $(Q_c/Q_o)^2$  is greater than unity. Therefore the performance is entirely expressible

for any network combination when the four simple arithmetical combinations of the  $Q$  values and the impedance level are known.

Occasionally it is required to know the impedance  $Z_n$  of Fig. 1 relating to the impedance load on the sending arm  $R$  which includes the driving force  $E$ , due to the network with the receiving arm  $R$  attached. This is given by the readily derived equation

$$Z_n = \left( \frac{E}{I_s} - R \right) = R \left[ \frac{h^2 D^2 + j 2 h S (1 + h^2 P)}{4 + h^2 S^2} \right] \quad (3)$$

This is a pure resistance of value  $R$

when  $P = -h^{-2}$  corresponding to a zero-loss condition; it is also a pure resistance but of value  $R h^2 D^2 / 4$  when  $S = 0$  corresponding to a 90-deg phase-shift condition, and can be a pure reactance only when  $D = 0$  corresponding to an infinite insertion-loss condition.

The general theory of which the above summary is the simplest equational expression has been illustrated by a detailed study of low- and high-pass wave filter units. The performance was expressed in terms of the ratio  $x$  of any frequency  $f$  to a reference frequency  $F_o$ , which preferably has some physical significance. For the low-pass and high-pass units, types A to D of Fig. 2,  $F_o$  corresponded to theoretical cutoff. Sim-

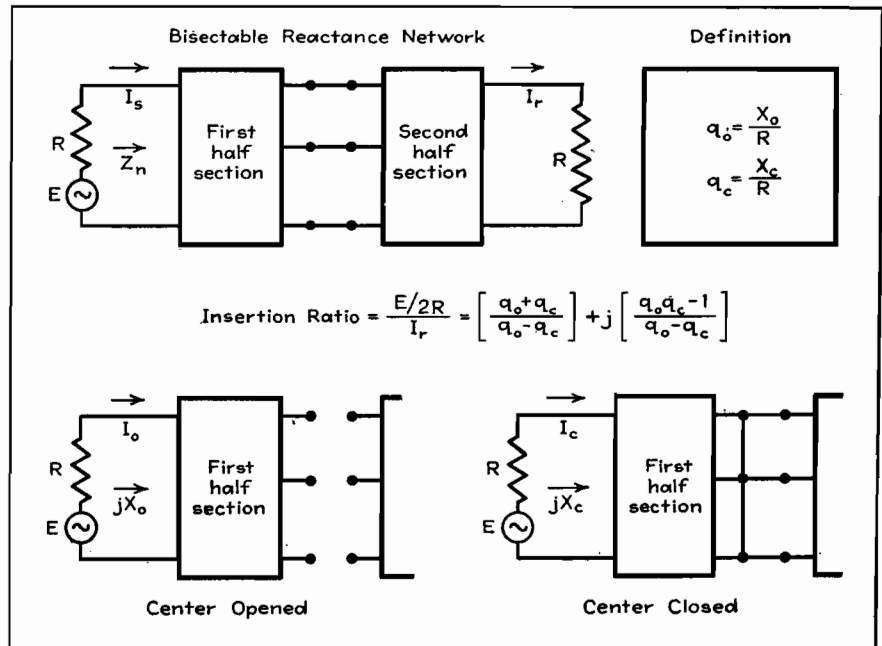


Fig. 1.—Bisectable reactance networks with equal resistance terminations.

\*  $h = R_1/R$ , where  $R_1$  = impedance level of network and  $R$  = filter termination.

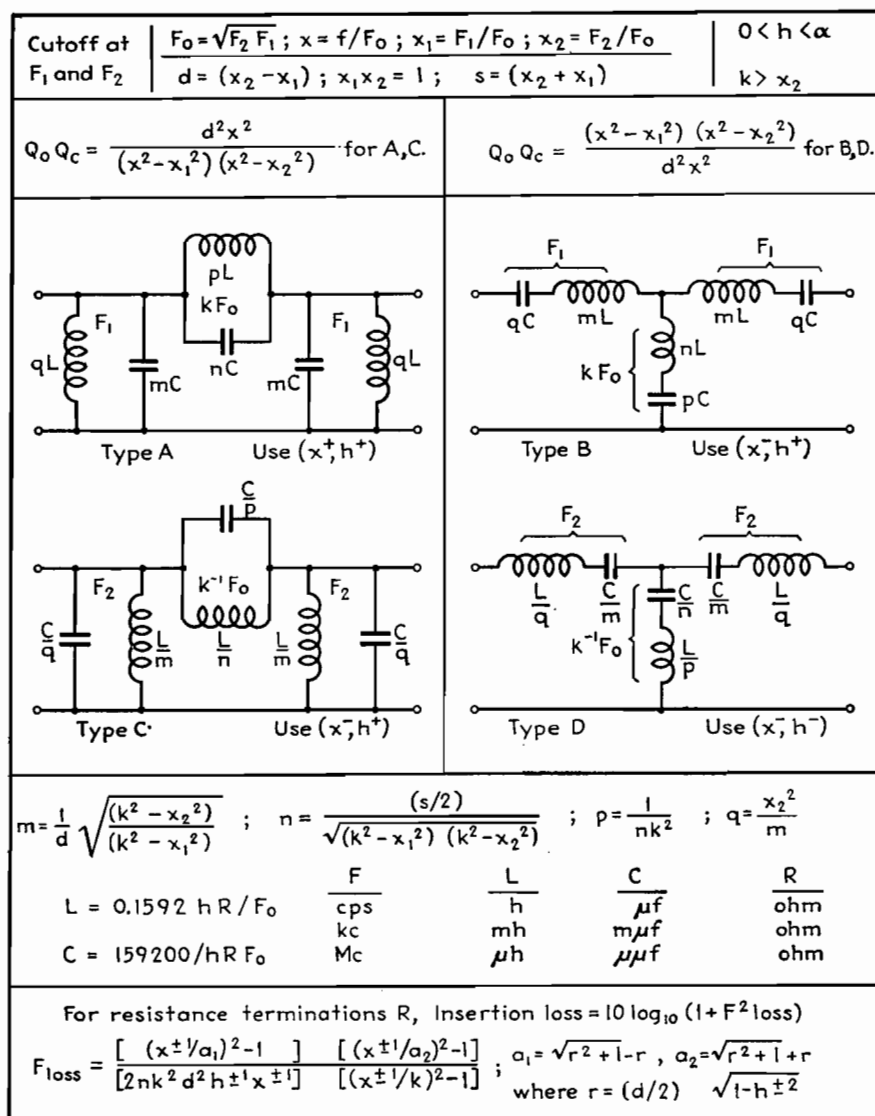


Fig. 2.—Circuits and parameters of fundamental band-pass filters built up from low- and high-pass structures.

plexity of equations resulted by properly setting up the circuit elements to make the product function  $P = Q_o Q_c$  a simple algebraic function, such as  $(x^2 - 1)$  for the type B unit. The functions  $Q_o$  and  $Q_c$  involved  $x$  and also a parameter  $k$ † relating to a value of  $x$  corresponding to infinite insertion loss. For all types, one of the  $Q$  values corresponded to an inductor and a capacitor in series or in parallel and resonating at  $x = 1$ , and the other  $Q$  corresponded to an inductor or a capacitor only. Low- and high-pass filters are two-band filters, with the cutoff frequency  $F_0$  the transition point between low- and high-loss values.

### Three-Band Filter Units

Next in the order of complexity are the three-band filter units of which the band-

† Thus  $k = F_{00}/F_0$ , where  $F_{00}$  is the frequency of which the insertion loss is infinite and  $F_0$  is the geometric mean of the two cutoff frequencies.

pass units are the more important. Band-pass filters are desired to produce high insertion loss for both low and high frequencies, but to produce low loss in the range between a lower cutoff frequency  $F_1$  and a higher cutoff frequency  $F_2$ . The present discussion is limited to the elementary units useful for this purpose.

One simple method of approach is to consider the minimum structural change in low- and high-pass units necessary to make them yield high loss at both low and high frequencies, leaving the possibility of low loss in the mean frequency range. The four resulting structures are shown in Fig. 2, where elements identified by multiplicative or divisive factors  $m$ ,  $n$ , and  $p$  applied to basic inductance value  $L$  and capacitance value  $C$  correspond to similarly designated elements for low- and high-pass purposes. Elements involving the next alphabetical letter  $q$  operate to

provide the loss band not provided by the other elements.

The chart provides full information for determining the possible insertion loss characteristics when any unit is terminated by equal resistances, and for evaluating the network elements required to yield a loss characteristic specified by values of parameters  $h$ ,  $k$ , and  $d$ , for a specified choice of  $R$  and  $F_0$ . It will be noted that the newly introduced parameter  $d$  relates to the relative difference of the two cutoff frequencies. This is a bandwidth parameter and is determinable from the cutoff frequency ratio value  $x_1$  and/or  $x_2$ , or from either. Choice of reference frequency  $F_0$  as the geometric mean of the two cutoff frequencies is in the interest of equational simplicity and, further, results in the product function  $P = Q_o Q_c$  being the same for any unit as for its frequency complementary. These product functions are set up to be in conformity with the structural arrangements, and also to make them negative in the range  $x_1$  to  $x_2$ , and negative unity at the geometric center of the range at  $x = 1$ . Some of the threefold infinitude of possible insertion-loss curve shapes are shown in Fig. 3, for a choice of bandwidth parameter  $d = 0.409$  making  $F_2$  50 per cent greater than  $F_1$ . The impedance level parameter in each case is chosen to make the insertion loss nearly as uniformly low as possible in the pass band, and the infinite insertion loss parameter is given values to make infinite loss occur for A and B units at  $F_2$  multiplied by 1.25, 1.5, and infinity, respectively. A rough comparison is therefore possible between the performance of band-pass units A and B and the corresponding performance of low-pass units A and B previously considered. The shunting effect of  $qL$  and blocking effect of  $qC$  in these two units are mainly operative at low frequencies to modify the characteristics below  $F_2$ , providing an additional frequency for zero loss, and providing for infinite loss at zero frequency. From inspection of the curves, it is evident that A and B units will be used whenever the emphasis is to be on sharpness of cutoff above  $F_2$ , and C and D units whenever the emphasis is to be on cutoff below  $F_1$ .

These band-pass units may be replaced by a wide variety of structural equivalents owing to the number of ways that T and delta arrangements of inductors and capacitors occur, but these will not be covered here. In general, these basic band-pass filter arrangements are characterized by both of the  $Q$  values corre-

sponding to similarly tuned circuits, one resonant at  $F_1$  and the other at  $F_2$ . For  $A$  and  $C$  units, these are parallel resonant circuits, and for  $B$  and  $D$ , they are series resonant circuits. The end circuits involving  $m$  and  $q$  represent one of the tuned circuits, and regardless of the nature or complexity of the coupling circuit between them, these end circuits are of themselves sufficient to make the loss infinite at both zero and infinite frequencies. Consequently, band-pass units are readily possible with any number of reactor elements in the coupling arms, here involving only two elements in an arrangement similar to the end circuits which they couple.

### Coupled Circuit Application

The information recorded here covers the simpler case in which the coupling element is a single reactor. For the special case of the infinite-loss parameter becoming infinity, the four factors become  $m = 1/d$ ,  $n = 0$ ,  $p = 2/s$ , and  $q = dx_2^2$ , so that elements involving  $n$  are not required. Types *A* and *D* then become simple inductively coupled types, and *B* and *C* become simple capacitively coupled. When the three inductors of such a type *A* unit are replaced by two inductors with mutual inductance between them, the unit takes on the important form of Fig. 4, with which loss, lag, and design information is included. This is the familiar coupled circuit system with each circuit  $mC$  and  $wL$  tuned very closely at the geometric center of the transmission band, and connected in parallel with the terminations, with mutual inductance  $gL$  between the inductors  $wL$ .

Because of its extensive use it is important to record here Fig. 5, a brief method of treatment when each tuned circuit is dissipative with  $Q$  designating the combined quality factor of the elements  $mC$  and  $wL$ . This will hold sufficiently well for practical purposes when the bandwidth parameter is a small quantity, making  $mw = 1$  very closely. Under these conditions, the reactances of both  $mC$  and  $wL$  are numerically  $h dR$  at  $F_0$ . It is irrelevant for practical purposes whether the dissipative effect is represented by a resistance  $h dR$  divided by  $Q$  in series with  $mC$  or  $wL$ , or by a resistance  $h dR$  multiplied by  $Q$  in parallel with these elements. By making the latter choice, the middle circuit of Fig. 5 indicates the performance is the same as if the two terminations  $R$  were shunted by resistances  $R_Q = h dRQ$ . By the application of Thévenin's theorem, the performance

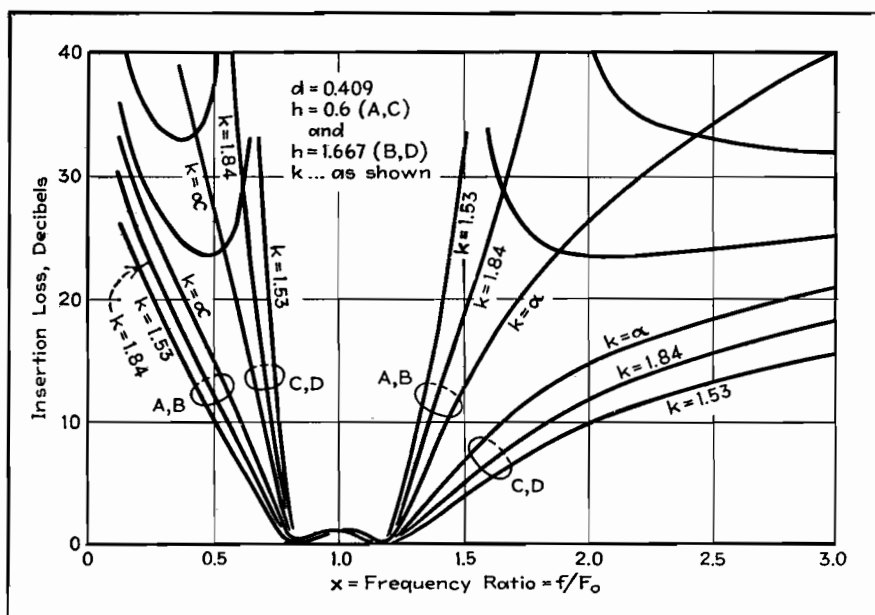


Fig. 3.—Loss curves for band-pass filter units for band-width parameter  $d = 0.400$ .

of this dissipative circuit is precisely the same as if the network were nondissipative, but with  $E$  and  $R$  replaced by lower values  $E'$  and  $R'$  for which the formulas are given. As a result, for narrow-band dissipative cases the performance of the dissipative circuit as to loss and lag is to a close approximation determinable from the nondissipative equations. Because of the lowered effective terminations, it is required that the actual impedance level parameter  $h$  be replaced in the performance equations by a greater value  $h' = h(1 + 1/h dQ)$ . Owing to the lowered effective driving voltage  $E'$ , it is required that the loss computed using  $h'$  be increased by  $20 \log_{10} (1 + 1/h dQ)$  db at all frequencies. In both cases, the modification of the performance due to the dissipative effect is determined by the product of the three parameters  $h$ ,  $d$ , and  $Q$ . Obviously, the practical need for

low-loss coils and capacitors is not so great for wide-band units of this type as for narrow-band units.

### A 5-Mc Interstage Transformer

As a practical example, consider the design and performance of an intertube i-f transformer, specified to have a nominal bandwidth of 200,000 cycles centered at  $F_o = 5$  Mc, for use with 1-megohm terminations. The bandwidth parameter is therefore  $d = 0.04$ , and if an impedance level parameter  $h = 0.60$  were chosen to yield a good approach to uniform transmission in the pass band, the value of the input and output capacitors  $mC$  would be the impossibly low value of  $1.33 \mu\text{f}$ . If these capacitors are assigned a lowest practical value, say  $25 \mu\text{f}$ , the coil  $wL$  must be correspondingly  $40 \mu h$ , making both elements of reactance 1,260 ohms at 5 Mc. On this basis, the impedance

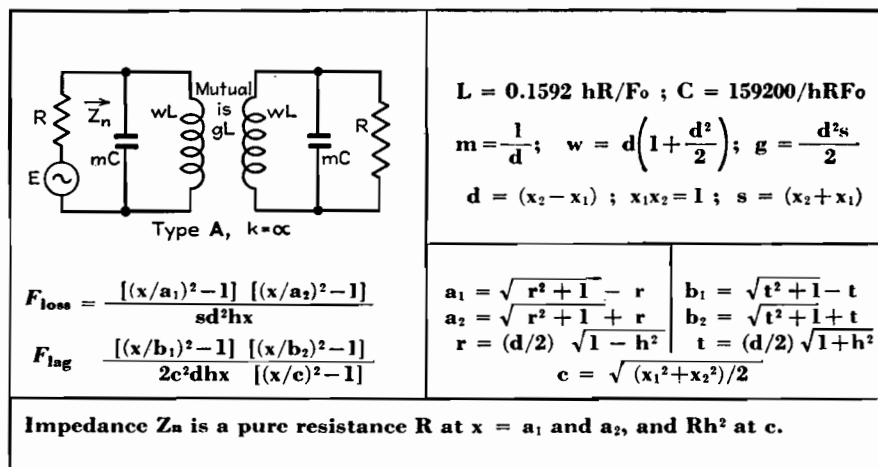


Fig. 4.—Type A ( $k = \infty$ ) inductively coupled band-pass filter.

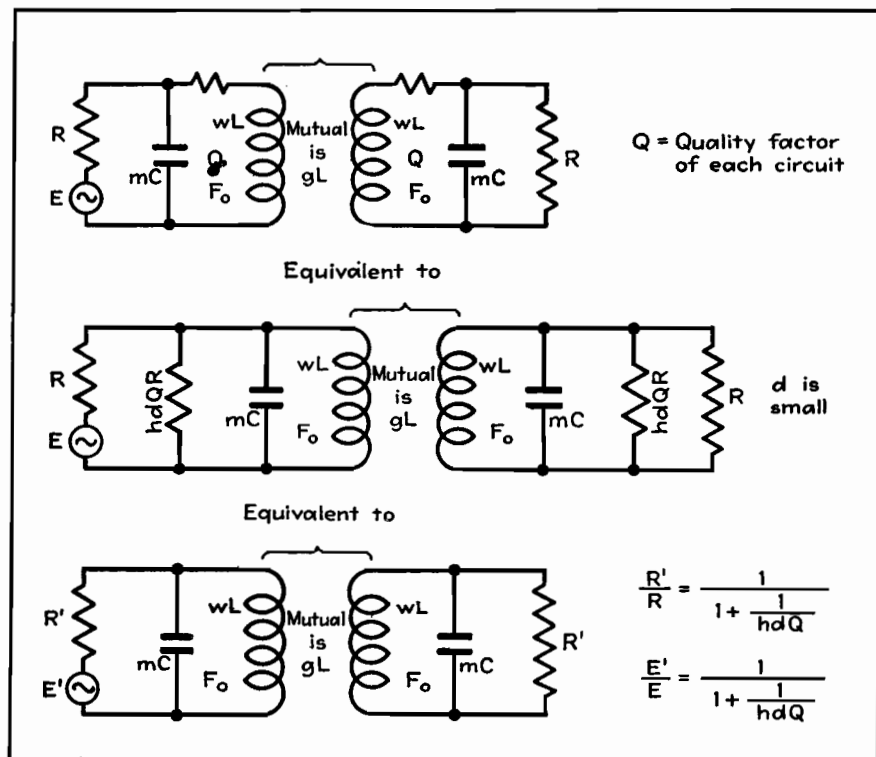


Fig. 5.—Treatment of narrow-band dissipative symmetrical coupled circuits.

level is  $h = 0.031$ , and dissipative loss is necessary in order that the transmission curve may be satisfactory. For  $h = 0.031$ ,  $d = 0.04$ , a value of circuit quality factor  $Q = 44$  will make  $h' = 0.6$ . As far as performance is concerned, it is irrelevant as to whether this quality factor is obtained by smallness of coils, closeness of shield, or by resistance artificially introduced. In any event, the effective termination is cut from  $R = 1$  megohm to about 50,000 ohms, and the effective voltage in the termination is cut to  $E' = E/19.4$  corresponding to 25.7 db added insertion loss. Since the dissipative effect is represented by resistors

of 55,000 ohms across each  $mC$ , the actual load  $Z_a$  upon the sending termination of impedance 1 megohm is about 27,000 ohms at the frequencies of minimum loss.

#### Correlation between Loss and Lag

Computed curves for loss and lag corresponding to the example given are shown in Fig. 6, illustrating the correlation between loss and lag performance that occurs in conventional transformers. In the transmission band, the loss is uniform to within about 0.5 db between the cutoff frequencies. For frequencies equally above and below the center of the

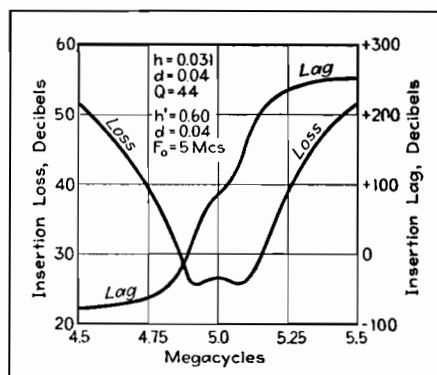


Fig. 6.—Loss and lag curves of typical intermediate-frequency 5-Mc transformer described in text.

band, and differing by twice the nominal bandwidth, the loss is about 9 db greater than in the transmission band. The lag is an increasing function of frequency, changing by 360 deg throughout the entire frequency range, and by approximately 180 deg in the transmission band. For the central frequency, the phase shift here shown as a 90-deg lag can be made a 90-deg advance by changing the sense of the coupling. If the driving voltage  $E$  represents an amplitude-modulated wave form, side frequencies are shifted differently than the central frequency, so that shifts of the phase of modulation occur amounting to 90 deg for the highest frequency of modulation.

It will be understood that the present discussion is limited to the symmetrical units directly related to the previously discussed low- and high-pass units. Other band-pass units may in turn be related to the basic band-pass units here considered. Especially complete information is given for symmetrical coupled-circuit units as a special case of the more general type A band-pass unit.

## SECTION XIV OSCILLATORS

	Page
Phase-shift Oscillator Design Charts.....	193
Determining Temperature Coefficient of Quartz Crystals..	195

# Phase-shift Oscillator Design Charts

By WALTER W. KUNDE

The simple one-tube phase-shift oscillator offers frequency stability and good wave form at low cost. With the nomograms given here, its design reduces to simple arithmetic

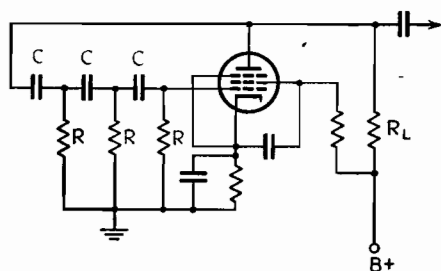


Fig. 1.—Basic circuit of the phase-shift oscillator. The output frequency is determined by the values of  $R$  and  $C$ , and these are given in the accompanying nomograms. Other circuit values follow conventional practice. In a variable-frequency audio oscillator, a three-gang variable capacitor can be used for  $C$  or ganged rheostats can be used for  $R$ .

IN DESIGNING various types of test equipment, a voltage source operating at a fixed frequency other than 60 cycles is often desired. The single-tube phase-shift oscillator has found wide application in this field, because of its simplicity, excellent stability, and good wave form. When followed by an amplifier designed to furnish the required output voltage, it can be used to supply power for a-c bridge measurements, insulation tests, testing aircraft transformers and their associated equipment, and many other purposes.

The basic circuit for an oscillator of this type is shown in Fig. 1. When using ordinary resistors and capacitors, the actual frequency obtained may differ slightly from the computed value, owing to manufacturing tolerances of the components used. Any one of the resistors

or capacitors in the phase-shift network may be varied slightly to compensate this effect. This is accomplished very nicely by making one of the resistors semivariable.

The constants used in the phase-shift network to obtain a desired frequency are determined by the formula

$$f = \frac{1}{2\pi\sqrt{6RC}} \quad (1)$$

The alignment charts shown in Figs. 2 and 3 were developed to minimize errors and give a rapid visual indication of possible  $RC$  combinations that would give the desired frequency.

It was shown by Ginzton and Hollingsworth\* that the circuit gain must equal a minimum of 29 for oscillation to take place. This condition is readily met provided that  $R \gg R_L$ , where  $R_L$  is the equivalent parallel value of the plate resistor and the grid resistor of the following amplifier tube. This is apparent when we consider the equation

$$A = 29 + 23 \frac{R_L}{R} + 4 \left( \frac{R_L}{R} \right)^2 \quad (2)$$

where  $A$  is the gain required for oscillation to start.  $A$  is independent of frequency when  $R \gg R_L$ . For example, let  $R = R_L$  for some given frequency. One can readily see that the required gain for oscillation to start is approximately

double that required when  $R$  is much greater than  $R_L$ .

The chart shown in Fig. 2 is used primarily for fixed low-frequency oscillators when a high-gain tube such as the 1851 is used. Lower values of  $R_L$  are used for a tube of this type, consequently  $R$  can be made smaller for a given frequency and  $C$  is in the range of the more commonly available values.

Figure 3 is a more universal chart and is used for both fixed and variable-frequency oscillators. Note that the values of  $C$  correspond closely to the values of variable capacitors considered to be common. For variable-frequency oscillators, either the resistors  $R$  or the capacitors  $C$  may be variable and ganged together. In a laboratory oscillator requiring more than one frequency range, variable capacitors with a 10-to-1 range may be used with a switch that changes the entire set of resistors in decade steps.

### Examples

**Example 1.**—The desired frequency is 1 kc. Assume  $R_L = 50,000$  ohms. Using either Fig. 2 or 3, determine suitable values for  $R$  and  $C$  as follows: Remembering that  $R$  must be very much greater than  $R_L$ , assume a value of 650,000 ohms for  $R$ . Place a straightedge on 1 kc and on  $R = 650,000$  ohms, and read 0.0001  $\mu\text{f}$  as the required capacitance.

**Example 2.**—To design a variable-frequency oscillator using variable capacitors whose range is 20 to 500  $\mu\text{f}$ , assume  $R = 1,000,000$  ohms for the middle

\* GINZTON, E. L., and HOLLINGSWORTH, L. M., Phase-shift Oscillators, *Proc. IRE*, February, 1941, p. 43.

range of frequencies, and use Fig. 3 as follows to determine suitable values of  $R$  and  $C$ : Using the assumed value of  $R$  as

a pivot point, allow the straightedge to slide between the maximum and minimum values of  $C$ . The frequency range

is determined immediately without any lengthy calculations, being approximately 130 to 3,200 cycles.

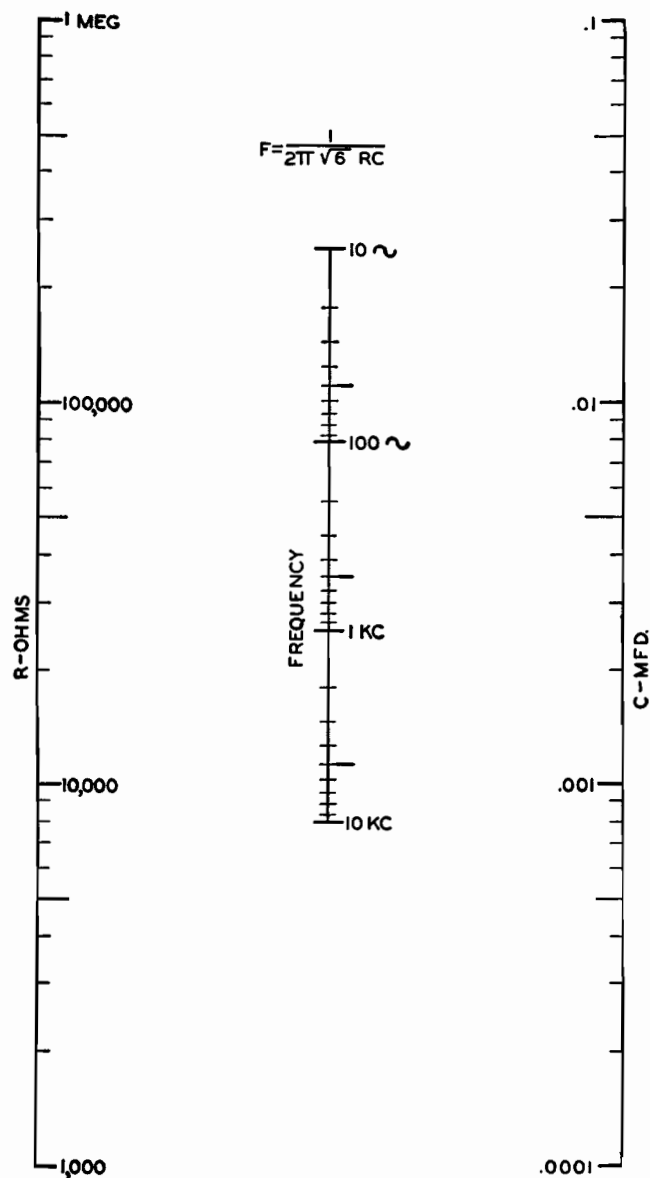


Fig. 2.—Nomogram for determining values of  $R$  and  $C$  in the phase-shift oscillator circuit of Fig. 1. The ranges of values are appropriate for a fixed-frequency oscillator, permitting a choice of convenient values for the fixed resistors and capacitors.

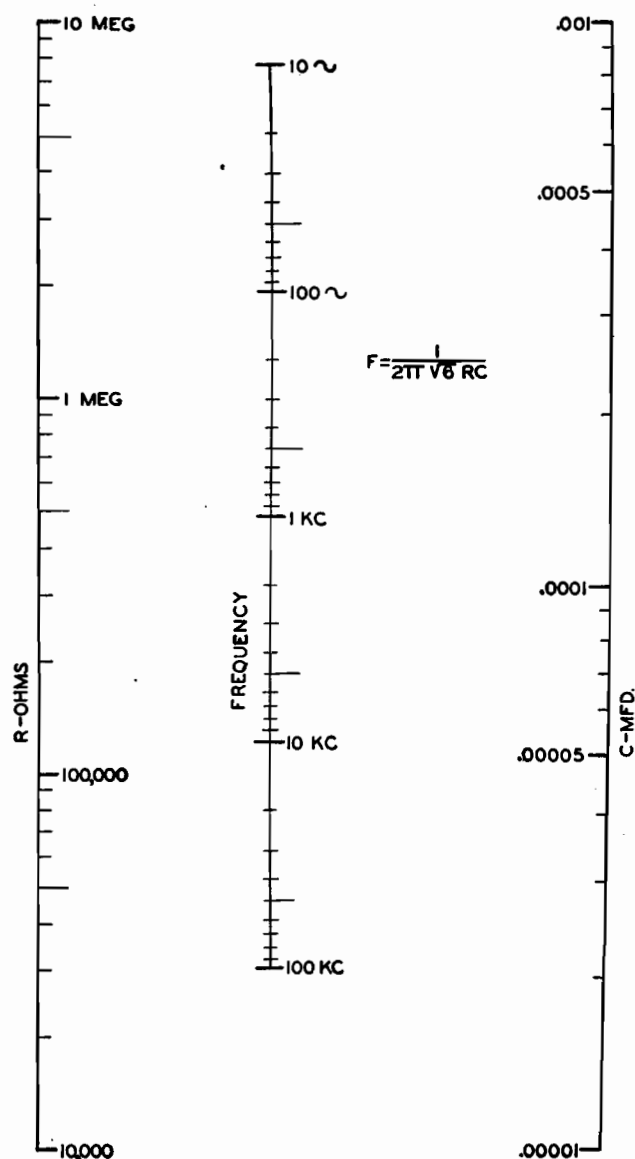


Fig. 3.—Nomogram for the same conditions as Fig. 2 but with a range of capacitance values more appropriate for a variable-frequency oscillator in that it covers variable capacitor ranges that are readily obtainable. The frequency can go up to 100 kc.

# Determining Temperature Coefficient of Quartz Crystals

By NORMAN L. CHALFIN

Two charts are presented for determining the temperature coefficient of frequency for quartz crystals when the nominal operating frequency and the frequency change for a given temperature are known. One chart applies to only one crystal frequency, but is readily set up for any desired frequency. The other chart is universal, for all frequencies

THE temperature coefficient of frequency for any quartz plate of nominal frequency  $f_o$  is given by the expression

$$\text{Temp. coeff.} = \frac{\Delta f}{f_o(t_{\max} - t_{\min})} \quad (1)$$

where temp. coeff. = cycles per Mc per °C

$\Delta f$  = change in frequency in cycles between the temperatures  $t_{\max}$  and  $t_{\min}$

$t_{\max}$  = highest temperature in °C at which the frequency is measured

$t_{\min}$  = minimum temperature in °C at which the frequency is measured

$t_{\max} - t_{\min} = \Delta t$  = temperature change in °C for which the change in frequency  $\Delta f$  is observed

$f_o$  = nominal frequency of the quartz plate in Mc

When a large number of calculations must be made for crystals having the same rated frequency, the direct-reading chart (Fig. 1) saves a great deal of time. The crystal frequency is the only value needed to set up a chart of this type, and individual charts can readily be prepared for any desired frequencies.

The chart is based on Eq. (1). For convenience, a temperature coefficient of 1.0 is assumed to permit converting the equation to the form  $\Delta f = f_o \Delta t$ , which follows the expression  $y = ax$  for a straight line passing through the origin of  $xy$  coordinates.

To prepare a chart for a desired temperature change value  $\Delta t$ , set up horizontal and vertical reference scales much as in Fig. 1. Substitute the rated crystal frequency value  $f_o$  and the desired value for  $\Delta t$  and solve for  $\Delta f$ . Now plot this value against a temperature coefficient value of 1.0 on the graph, and draw a straight line from zero through this point.

The procedure can be repeated for as many other values of  $\Delta t$  as are desired. The example is drawn for  $f_o = 1$  Mc.

The alignment chart (Fig. 2) is essentially a combination of an infinite number of different direct-reading charts; hence the one chart serves for all crystal frequencies.

To use the universal chart, determine the frequency change  $\Delta f$  in cycles between the temperature limits  $t_{\max}$  and  $t_{\min}$ . With a straightedge, align the value of  $t_{\max} - t_{\min}$  on scale E with the proper value of  $\Delta f$  on scale D. On scale B read the value  $\Delta f/(t_{\max} - t_{\min})$ . Align  $f_o$  on A

with  $\Delta f/(t_{\max} - t_{\min})$  originally found on scale B but now transferred to scale C, and read on scale F the temperature coefficient.

If the coefficient and the nominal crystal frequency are known, the chart may be used to indicate either the temperature change in which a given frequency change will occur, or the frequency change allowable in a given temperature range for the known temperature coefficient.

An example will illustrate the use of this chart. A change in frequency of 210 cycles is observed when the tem-

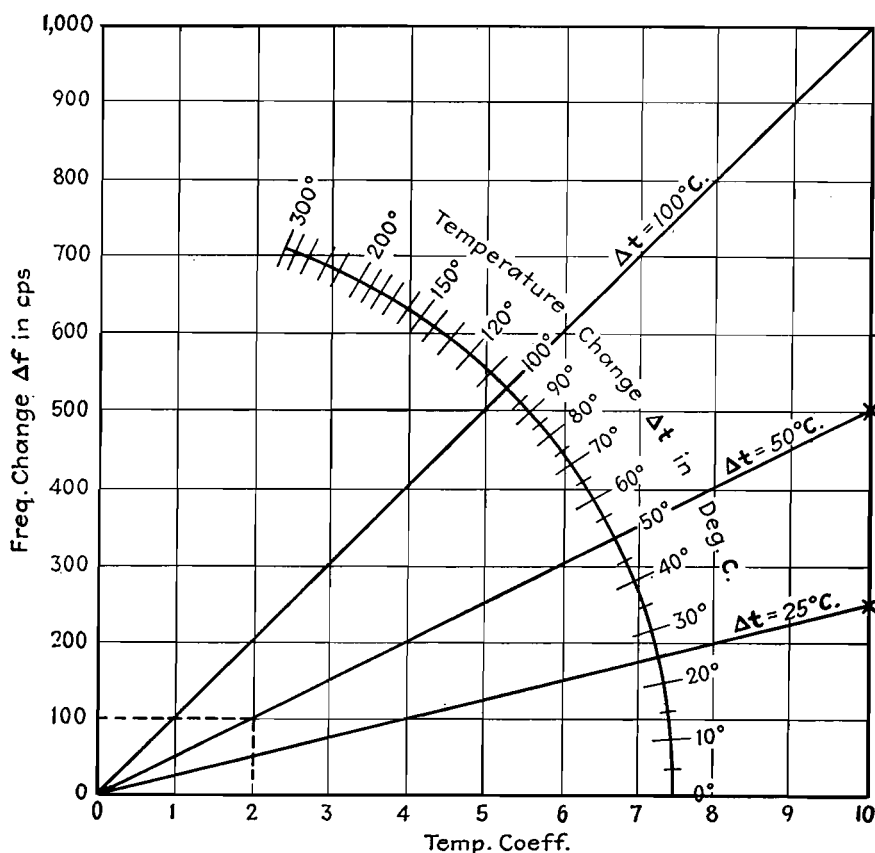


Fig. 1.—Example of a direct-reading temperature coefficient chart for a 1-Mc quartz-crystal unit.



perature changes from 20 to 50°C and the nominal frequency is 3.0 Mc. The temperature change is 50 – 20 = 30°C. If this value on scale *E* is aligned with

210 on scale *D*, the frequency change per degree temperature change is found, from scale *B* to be 7 cycles. Transfer this value to scale *C* and connect 7 on

scale *C* with the operating frequency (3.0 Mc) on scale *A*, and read the temperature coefficient of frequency on scale *F* as 2.33 cycles per Mc per °C.

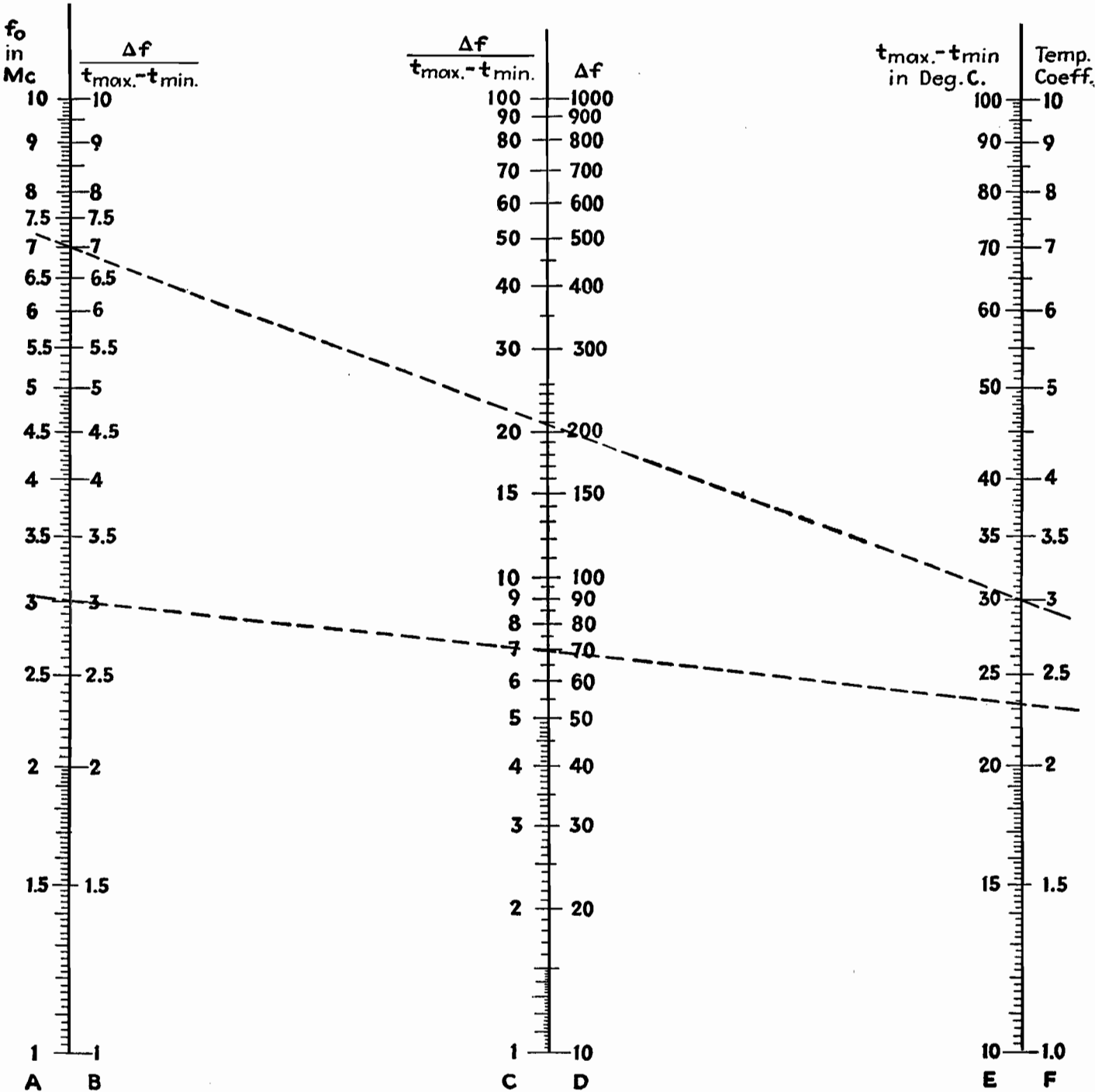


Fig. 2.—Temperature coefficient of quartz crystals in cycles per Mc per degree C.

## SECTION XV

# PERMANENT MAGNETS

Permanent-magnet Design.....	Page 197
Designing Stabilized Permanent Magnets.....	203
Mechanical Problems of Permanent-magnet Design.....	207

## Permanent-magnet Design

By EARL M. UNDERHILL

Empirical data based on practical experience and fundamental equations, taking into account the many variables involved in the design of a permanent magnet for a particular job. The procedure given here often provides required characteristics in the first trial design

IN THE design of permanent magnets, we are interested in the demagnetization curve of the particular magnet steel at hand and not in any other portion of the hysteresis loop. In the complete hysteresis loop shown in Fig. 1a, the demagnetization curve is in the second quadrant, and is reproduced by itself in Fig. 1b. It is important that the reason for this concentration of interest be understood clearly.

Any permanent magnet that is supplying useful flux to an air gap, within which is located an object requiring this flux, is working somewhere on its demagnetization curve. A moment's reflection and a glance at Fig. 2 will show why this must be.

Let us assume that the horseshoe magnet shown in Fig. 2a has been saturated and the magnetizing field removed. The flux path is closed by the soft steel bar (usually called a keeper) across its poles, and there exists no demagnetizing influences on the magnet. Since  $H$  is zero, the flux density in the magnet is at the point  $B_R$  of Fig. 1.

If a slot is cut through the keeper as shown in Fig. 2b, the magnetic poles thus exposed on the cut surfaces will exert a demagnetizing effect upon the magnet. Putting this in different words—a negative value of  $H$ , the value of which depends on

the size of the cut, will have been applied to the magnet, and  $B$  in the magnet will lie somewhere on the demagnetization curve between  $B_R$  and  $H_C$ .

The value of  $B$  can never be less than zero in a working magnet, since the only demagnetizing force exerted is that of the air gap, which would be zero when  $B$  is equal to zero. In other words, the only demagnetizing influence on the magnet is a sort of self-inflicted one which weakens

as the flux density in the magnet approaches zero, and which could never reverse the polarization of the magnet.

The intersection of the demagnetization curve with the  $B$  ordinate, which we have designated as  $B_R$ , is usually called the residual flux density, while the intersection of the curve with the  $H$  ordinate, which we have designated  $H_C$ , is usually called the coercive force of the material in question.

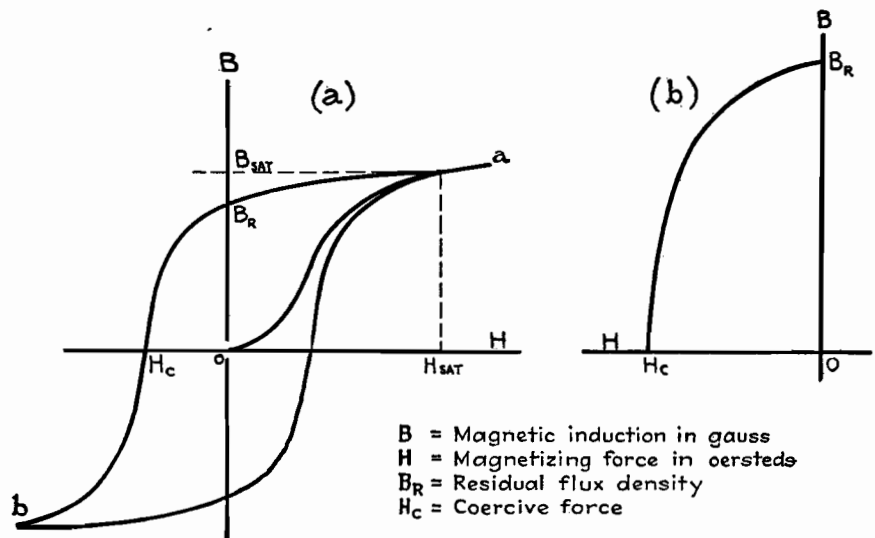


Fig. 1.—(a) Complete hysteresis loop. (b) Second-quadrant demagnetization curve reproduced by itself.

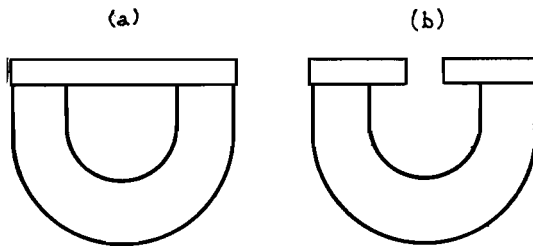


Fig. 2.—(a) Horseshoe magnet with flux path closed. (b) With slot cut through keeper exposing poles and exerting a demagnetizing effect upon the magnet.

### Design Equations

Now, consider the magnetic circuit shown in Fig. 3, consisting of a permanent magnet, a pair of soft iron pole pieces, and an air gap.

The magnet has a certain length designated by  $l_m$ , and a certain area  $A_m$ . The area (which we are, for the moment, assuming to be constant throughout the length of the magnet) is that of a section taken perpendicularly to the length. Likewise, the air gap has a certain length  $l_g$  and a certain area  $A_g$ . Let us also assume for the moment that  $A_g$  is equal to the area of the exposed soft iron pole face; although we shall see later that this is not necessarily so in this general case.

For the purposes of the following discussion, let us disregard leakage and assume that all the flux lines in the magnet cross the air gap. This assumption permits us to write that the flux in the gap is equal to the flux in the magnet, or  $\phi_g = \phi_m$ . Since  $\phi = BA$  when the flux density is uniform over the area, we get

$$B_g A_g = B_m A_m \quad (1)$$

Now, again referring to Fig. 3 and still assuming no leakage, the total work done by a unit north pole moving through the length of the magnet is exactly equal to the total work done on the pole moving through the gap. If this were not true, we should have in a magnet a source of energy capable of continual dissipation with no change in original value—an infinite reservoir of magnetic energy.

Since field strength  $H$  is defined as the force exerted on a unit pole (and still

assuming no leakage), we may write  $H_g l_g = H_m l_m$ . In air,  $B = H$ ; hence our expression becomes

$$B_g l_g = H_m l_m \quad (2)$$

### Leakage Constants

Equations (1) and (2) are the complete design equations for a permanent-magnet system operating without leakage. The factors determining the amount of leakage that will exist in any given magnetic circuit are numerous but are concerned mostly with the geometry of the circuit and the number and reluctance of leakage paths.

Leakage may be computed quite accurately by tedious and painful methods, but, in general, this is unnecessary and is seldom done by design engineers. Instead, a constant is added to each of the design equations to take care of the leakage flux, and the final design equations become

$$FB_g A_g = B_m A_m \quad (3)$$

$$fB_g l_g = H_m l_m \quad (4)$$

These are two simple equations universally used by magnet engineers in their work. Usually, but not always, the problem involved is the determination of the correct magnet area and length to

supply a given flux density  $B_g$  to a given gap of dimensions  $A_g$  and  $l_g$ .

Assuming that the leakage constants  $F$  and  $f$  are known, it is obvious that  $A_m$  and  $l_m$  cannot be solved for until  $B_m$  and  $H_m$  are known. We may choose  $B_m$  and  $H_m$  to make the magnet operate at any point on the demagnetization curve we wish. The question naturally arises: Is there some particular operating point on the curve which is more advantageous than any other point? The answer is, yes. Rearrange Eqs. (3) and (4) to make them appear as follows:

$$A_m = \frac{FB_g A_g}{B_m}$$

$$l_m = \frac{fB_g l_g}{H_m}$$

Now multiply them together

$$\text{Volume}_m = \frac{FfB_g^2 \text{volume}_g}{B_m H_m} \quad (5)$$

### Energy Product Curve

It is evident from Eq. (5) that the volume of magnet material used to supply the flux density  $B_g$  to the gap in question is inversely proportional to the product of the  $B$  and  $H$  of the magnet at its operating point, and that this volume will be a minimum when the product is a maximum. For this reason, a so-called energy product curve invariably accompanies every demagnetization curve.

An energy-product curve is similar to that shown accompanying the demagnetization curve of Fig. 4, and consists merely of the product of  $B$  and  $H$  at each point along the demagnetization curve, plotted against  $B$ . The point at which this product is a maximum (namely,  $B_o, H_o$ ) is selected and the value  $B_o$  and  $H_o$  substituted into Eqs. (3) and (4).

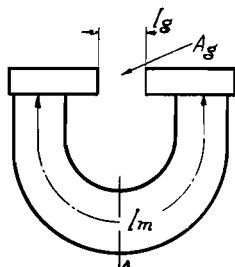


Fig. 3.—Simple magnetic circuit consisting of a permanent magnet, a pair of pole pieces, and an air gap.

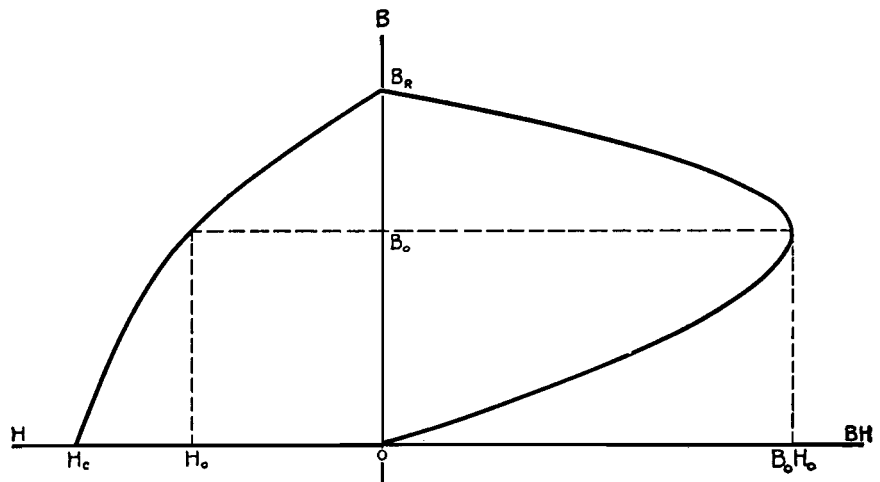
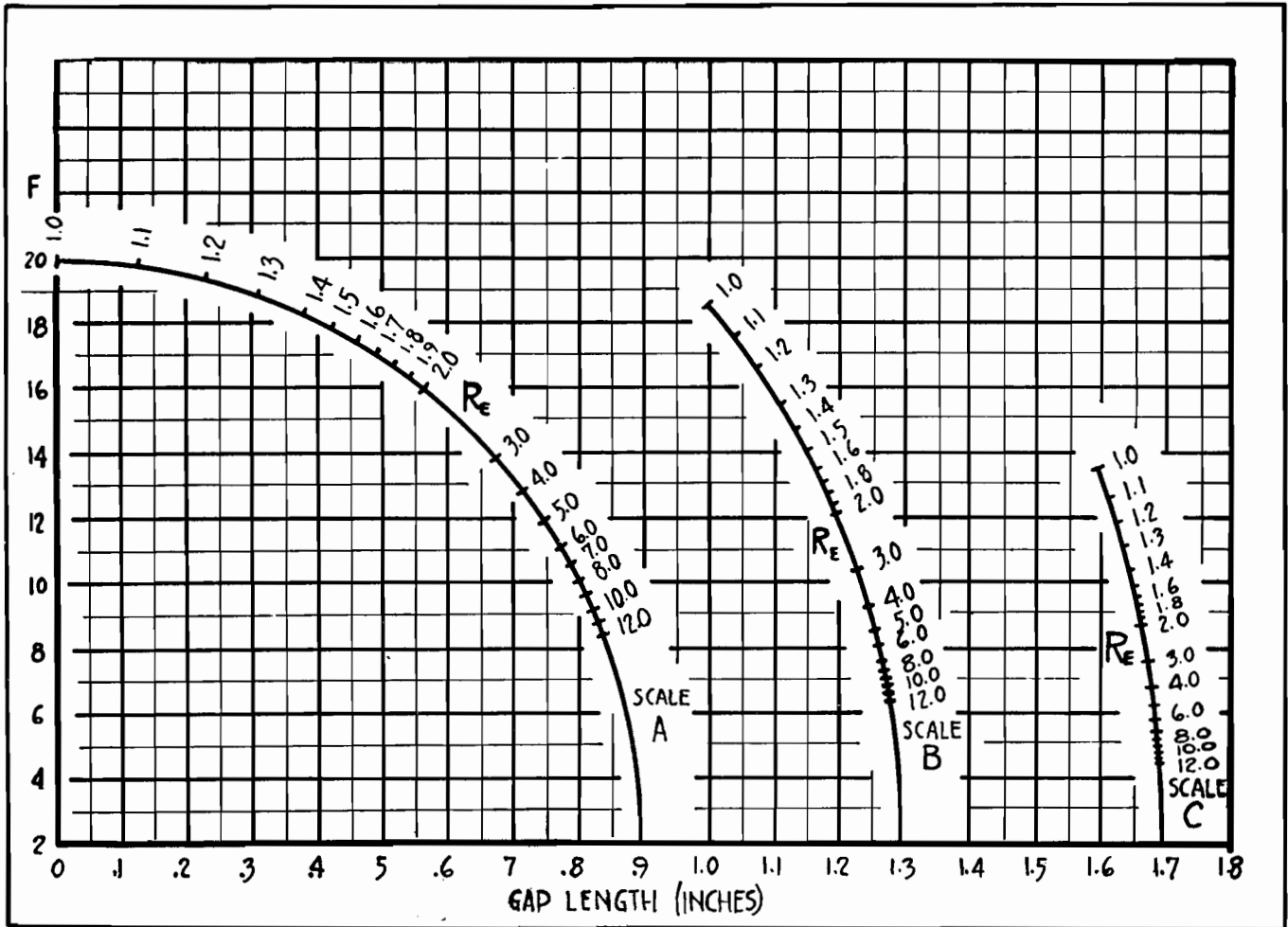


FIG. 4

Fig. 4.—Energy-product curve shown in conjunction with demagnetization curve.

Fig. 5.—Graph for determining design factor  $F$ .

The magnet designer is thus provided with all the factors necessary to solve his two design equations. Since it has been assumed that  $F$  and  $f$  are known,  $B_o$  and  $H_o$  may be obtained from the demagnetization curve of the material he intends using, and  $B_o$ ,  $l_o$ , and  $A_o$  he sets for himself as the independent requisites of the circuit.

#### Estimating Leakage Constants

But  $F$  and  $f$  have only been assumed to be known. Determination of their values is one of the most difficult of all problems in permanent-magnet design work.

Since  $f$  is the simpler of the two, let us look at it first. The value of  $f$  varies only over a relatively small range, usually from a minimum of 1.2 to a maximum of 1.5, and the extremes are seldom met in practice. A value of  $f$  equal to 1.35 is a good engineering guess for this constant for almost any permanent-magnet circuit.

The value of  $F$  has a much greater range. Its lower limit is approximately 2.0, while its upper limit is nonexistent. Theoretically,  $F$  may be infinitely large,

but in practice it usually varies between 2.5 and 10.0.

While it is a fact that theoretically the designer knows only the size of the working gap and the flux density that he wishes to establish in this gap, he usually has some idea of the size of the rest of the circuit because of space considerations in his equipment.

The first step in determining  $F$  is to lay out at full scale on a piece of paper the closest guess it is possible to make as to the actual size of the completed circuit. Next, draw a pair of complete circles in such a way that, when they are placed over the outline of the estimated circuit, the inner circle will conform roughly with the inside contour of the circuit and the outer circle will conform roughly with the outside contour of the circuit. Designate by  $R_E$  ( $R_E > 1.0$ ) the ratio of the diameter of the two circles, and spot this point on the proper scale in Fig. 5.

#### Use of Graphs

It may be determined from Fig. 6 whether scale  $A$ ,  $B$ , or  $C$  is to be used in

Fig. 5. If the designer plans to make his circuit with the pole faces of the magnet parallel to the faces of the gap but with the direction of magnetization of the magnet opposite in sense to that of the gap as shown in Fig. 6a, he should use scale  $A$ . If the pole faces of the magnet are to be perpendicular to those of the gap as shown in Fig. 6b, he should use scale  $B$ . If the pole faces of the magnet are parallel to the gap and with the direction of magnetization of the magnet in the same sense as that of the gap as shown in Fig. 6c, he should use scale  $C$ .

With the proper value of  $R_E$  located on the proper scale of Fig. 5, it is then necessary only to draw a straight line between this point and the point (0, 2) located at the intersection of the heavy abscissa and ordinate. From the straight-line graph thus formed, the value of  $F$  may be picked for the proper value of gap length.

#### Testing a Sample

Having empirically arrived at a suitable design and having made up a sample

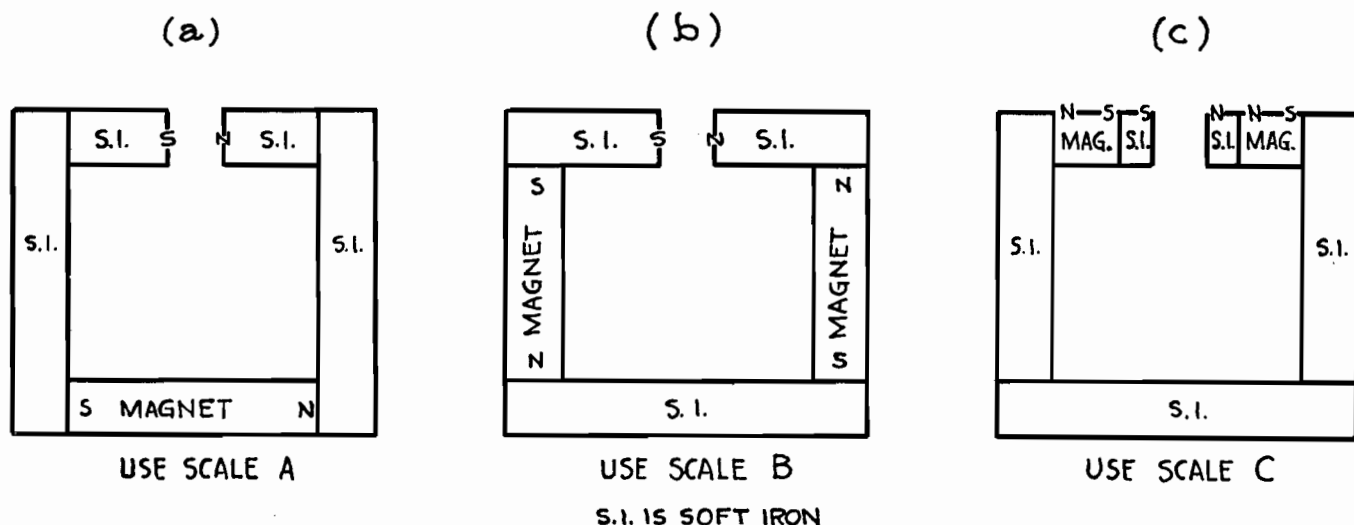


Fig. 6.—Chart of magnet types, for determining proper scale to use on Fig. 5.

magnet assembly, it is a simple matter, by measuring the total flux in the gap and in the neutral section of the magnet, to obtain an accurate value of  $F$  [Eq. (3) shows that  $F$  is the simple ratio of these two quantities]. At the same time, since the areas of the gap and magnet are known, the flux densities are known, and  $f$  may then be calculated accurately with the aid of design equations and a

demagnetization curve of the magnet material used.

At this point an accurate redesign of the magnet is possible, if necessary, to give the designer something extremely close to the exact circuit he wants.

Typical demagnetization and energy product curves for various alloys are given in Fig. 7 for use in connection with this magnet design procedure.

#### Use of Nomograph

The nomograph in Fig. 8 makes possible a mechanical solution of the design equations superimposed on the demagnetization curves of Fig. 7.

Related problems such as the following may be easily solved with the aid of this figure: (1) Given the magnet size, alloy and gap size, what will be the flux density

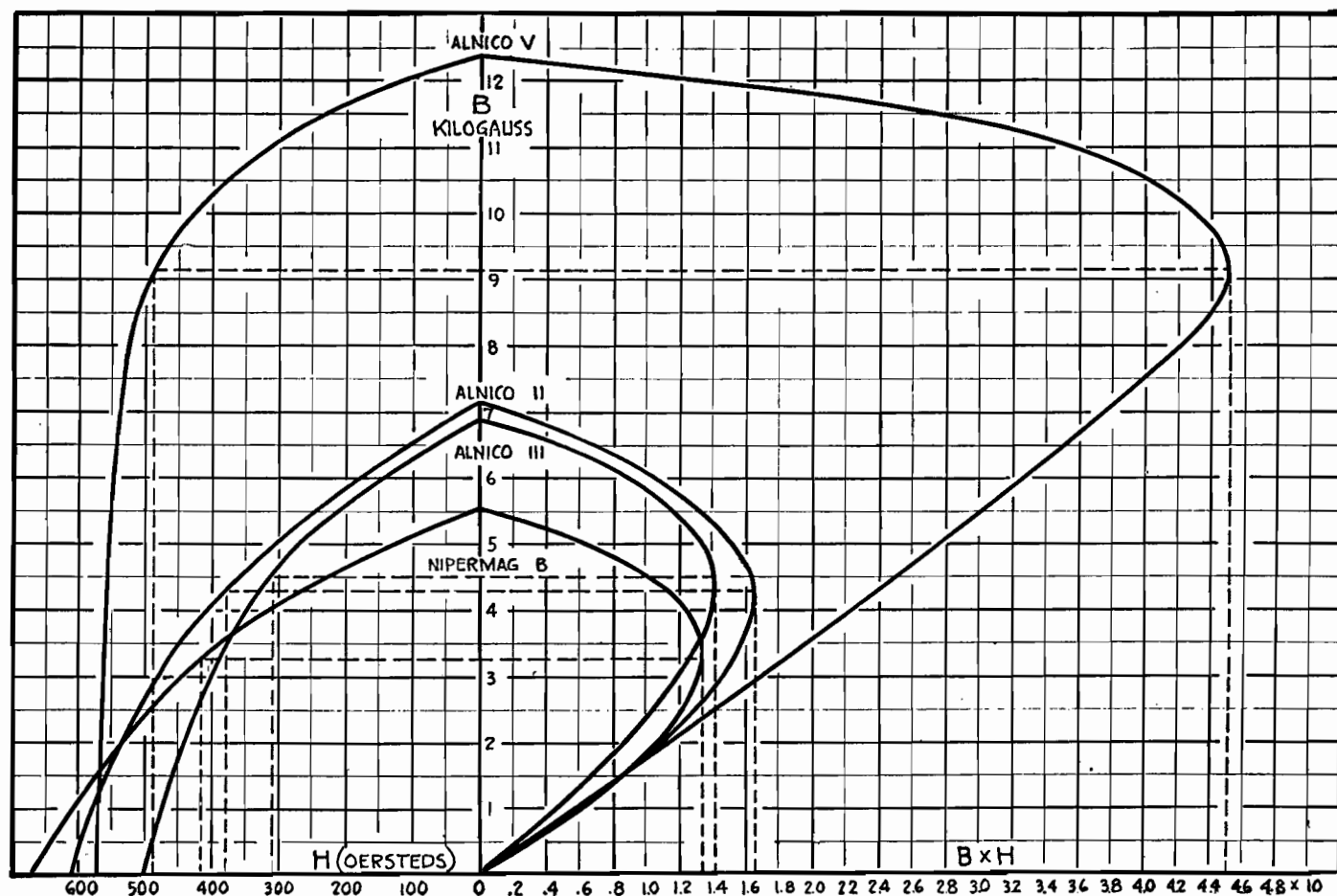


Fig. 7.—Typical demagnetization and energy-product curves for various alloys.

in the gap? (2) Given the magnet size and gap size, what will be the best alloy to use to give maximum flux density in the gap?

When using the nomograph, a straightedge must be laid across from  $X$  to  $X'$  or from  $Y$  to  $Y'$ . When this is done, the three quantities marked by the intersection of the straightedge with the three scales involved all bear the correct relationship to each other.

### Meter Magnet Design

To illustrate the procedure presented here, some typical problems in permanent magnet design for meters will now be given.

Let us suppose that an instrument manufacturer, desirous of doubling the sensitivity of one of his instruments and redesigning to take advantage of the latest improvements in permanent magnet steels, decides to obtain the doubled sensitivity by leaving the sizes of the gap and the moving coil as they were and simply doubling the flux density in the gap. Let us suppose, furthermore, that the old model had a 0.500-in. core, a 0.125-in. gap, and a flux density of 1,750 gauss. The problem is to design a permanent magnet to supply the above-mentioned gap with 3,500 gauss.

The first step is to lay out the air gap to scale and guess as to what the rest of the circuit will look like. This has been done in Fig. 9. Figures for the magnet size have been picked "at random" and may or may not be close to the eventual size. Two circles have been drawn on the figure to conform approximately with the inside and outside contours of the circuit. (When drawing a circle to conform to an irregular contour, the area of the circle should be made approximately equal to that enclosed by the irregular contour.)

The ratio of the diameters of these circles turns out (by measurement) to be equal to  $R_g = 2.25$ . Since this is a type A circuit (refer to Fig. 6), the value  $R_g = 2.25$  is marked off on scale A of Fig. 5 and a straight line drawn between this point and the point (0, 2). Figure 5 has thus become a straight-line graph, and a value of  $F = 4.7$  is picked from it, corresponding to the gap length of 0.125 in.

Let us suppose that we have decided to choose Alnico II as our magnet material. We have then, with the aid of Fig. 7, all the factors necessary to the solution of our design equations:  $F = 4.7$ ;  $f = 1.35$ ;  $B_g = 3,500$ ;  $B_m = 4,300$ ;  $H_m =$

380;  $l_g = 0.125$  in. = 0.3175 cm;  $A_g = 112.8 \pi 0.550 \times 0.500/360 = 0.270$  sq in. = 1.742 sq cm.

These values are now substituted in Eqs. (3) and (4), giving  $A_m = 4.7 \times 3,500 \times 1.742/4,300 = 6.66$  sq cm = 1.033 sq in., and  $l_m = 1.35 \times 3,500 \times 0.3175/380 = 3.948$  cm = 1.554 in.

These values may also be obtained with the aid of the nomograph of Fig. 8. If a ruler is laid between the points 4,300 on the  $Y'$  scale and 3,500 on the  $B_g$  scale, we read on the  $Y$  scale a value of 1.23 for the quantity  $FA_g/A_m$ . Similarly, a ruler laid between the points 380 on the  $X$  scale and 3,500 on the  $B_g$  scale yields on the  $X'$  scale a value of 0.109 for the quantity  $fl_g/l_m$ .  $A_m$  and  $l_m$  may thus be easily determined.

### Correcting First Estimates

As we look at the values of  $A_m$  and  $l_m$  just determined, we discover that our original guesses for these two quantities were greatly in error. The length, we see, has to be increased by about 50 per cent and the area by about 100 per cent. However, the 1-in. dimension previously assigned as the width of the magnet still

looks pretty good, so we maintain this dimension when we redraw the circuit as shown in Fig. 10.

Running through the calculations for the circuit of Fig. 10, we find  $R_g = 2.0$  and  $F = 5.2$ . Consequently,  $A_m = 5.2 \times 3,500 \times 1.742/4,300 = 7.37$  sq cm = 1.143 sq in., and  $l_m = 1.35 \times 3,500 \times 0.3175/380 = 3.948$  cm = 1.554 in. (as before).

These values of  $A_m$  and  $l_m$  are entirely consistent with the dimensions of Fig. 10, used to determine our value of  $F$ . Consequently, a third calculation is unnecessary, and we may consider these values as the specifications for the required magnet.

The final circuit is shown in Fig. 11. It is to be borne in mind that this is for a magnet of Alnico II, and no other alloy. If the magnet size for Alnico III or a tungsten or cobalt-steel magnet is required (in order to study the economics of the situation, for instance), these calculations must be repeated, using in each case the  $B_g$  and  $H_g$  for the magnet alloy under study.

Incidentally, the magnet of Fig. 11 need not necessarily be 1.070 in. square as shown. It might, for instance, be 1.000

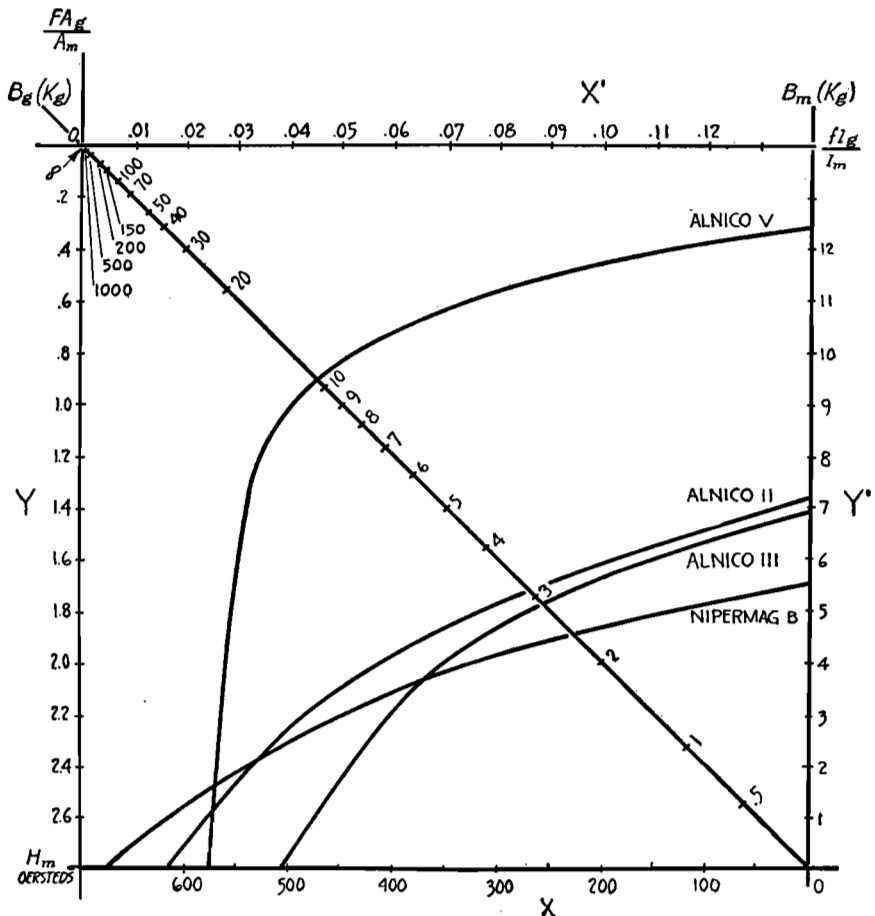


Fig. 8.—Nomograph permitting mechanical solution of design equations superimposed upon Fig. 7.

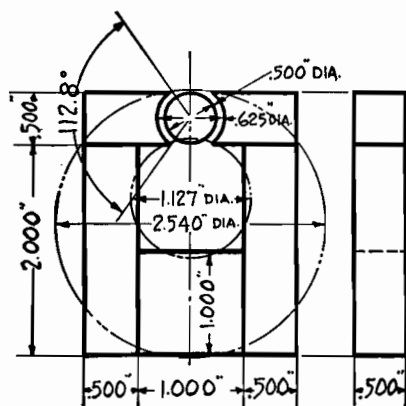


Fig. 9.—Layout of proposed meter magnet to scale, the first step in redesign.

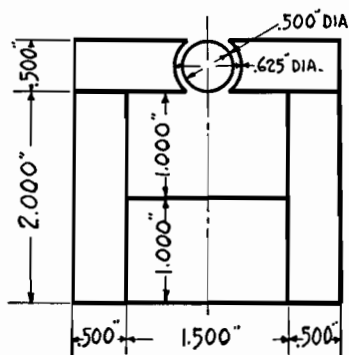


Fig. 10.—Meter magnet circuit redrawn to correct initial errors.

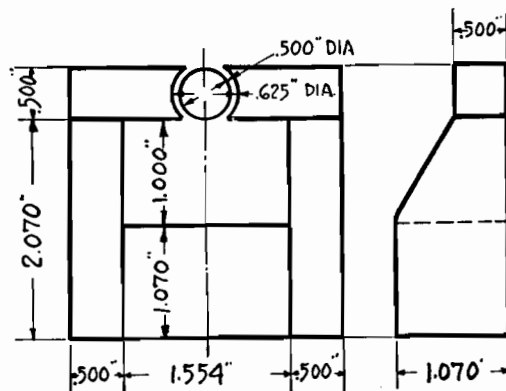


Fig. 11.—Final meter magnet circuit as redesigned to take advantage of new steels.

$\times 1.143$  in. or any two dimensions that give a cross-section of 1.143 sq in. and that do not cause the circuit to depart materially from the dimensions of Fig. 10.

#### Selecting Magnet Material

Just one more problem: Suppose the above-mentioned instrument manufacturer, because of a sudden shift in demand just as his new instrument is starting through production, decides that perhaps he ought to reduce the flux density in the gap of this instrument from 3,500 gauss to 3,200, or possibly even to 3,000 gauss. Assume that all the parts for the original design have been purchased or manufactured and assembly work has been started.

Obviously, it would involve a severe loss to redesign at this point and scrap all finished parts. So the manufacturer might wonder if it would not be more economical in the long run to scrap his stock of Alnico II magnets and to replace it with magnets of the same size but of smaller energy content.

The problem, then, is to take the circuit of Fig. 11 exactly as it stands and determine what alloy or alloys, if any, may be used to replace the Alnico II magnet and give the desired results.

The nomograph of Fig. 8 is most helpful in this type of problem. Using the

values we determined earlier ( $l_g = 0.3175$  cm;  $A_g = 1.742$  sq cm;  $l_m = 3.948$  cm;  $A_m = 7.37$  sq cm;  $F = 5.2$ ;  $f = 1.35$ ), we get

$$\frac{fl_g}{l_m} = 1.35 \times \frac{0.3175}{3.948} = 0.109$$

$$F \frac{A_g}{A_m} = 5.2 \times \frac{1.742}{7.37} = 1.23$$

Marking these two points off on the appropriate scales, i.e., the  $X'$  and the  $Y$  scales, respectively, and laying a straightedge between these points and the point 3,200 on the  $B_g$  scale, we arrive at the values 340 and 3,900 on the  $H_m$  and  $B_m$  scales, respectively.

Now, erect a perpendicular to the  $H_m$  scale at 340 and another perpendicular to the  $B_m$  scale at 3,900. These two lines intersect at a point that is just inside the demagnetization curve for Alnico III, indicating that if Alnico III is used as the alloy for the permanent magnet in question the flux density in the air gap will just slightly exceed 3,200 gauss. Alnico III will therefore satisfactorily fulfill the conditions stipulated.

Since the intersection of these perpendiculars lies outside the curve for Nipermag B, this alloy would give less than 3,200 gauss in the gap and hence would be unsatisfactory.

Repeat the above process using the

point 3,000 on the  $B_g$  scale. This gives us values of 325 on the  $H_m$  scale and 3,700 on the  $B_m$  scale. The intersection of the perpendiculars at these points occurs inside the Nipermag B curve. Hence, Nipermag B is a satisfactory alloy to produce 3,000 gauss in the air gap. Alnico III may also be used to produce 3,000 gauss but would require more demagnetization than Nipermag B. Neither of these alloys would be working at its  $B_o, H_o$  point under the conditions of this problem. This is to be expected since the circuit was designed to make Alnico II operate at its maximum efficiency.

Figure 8 makes an excellent summary of this initial paper, and shows graphically that no one of the alloys under consideration would give a higher flux density than any of the others in all types of gaps.

If both gap and magnet size are fixed, it should be readily apparent that for certain relationships of these factors both Nipermag B and Alnico II are sometimes better even than Alnico V. Nipermag B, cutting as it does all the Alnico curves shown, changes (for low values of  $H_m$ ) from the alloy producing the lowest flux density in a gap to (for high values of  $H_m$ ) the alloy producing the highest flux density in a gap.



# Designing Stabilized Permanent Magnets

By EARL M. UNDERHILL

In motor, generator, magneto, and similar applications of permanent magnets, demagnetizing influences exist and provide stabilization of flux density in air gaps

THE design of permanent magnets for motors, generators, magnetos, and similar devices involves the necessity of becoming familiar with minor hysteresis loops in general, and with the phenomenon of stabilization in particular. The operation of these devices imposes demagnetizing influences (in addition to the influence of the gap) on the magnet.

## Minor Hysteresis Loop

Suppose that the magnet of Fig. 1a has just been magnetized, fully saturated, and then removed from the influence of the magnetizing field. This procedure is performed with a soft iron keeper in the gap of the magnet, and the flux density in the magnet is now at the point  $B_r$  of Fig. 1b. When the keeper is removed, the magnet operating point will move down the curve to the point  $x$  in accordance with the laws developed in the previous article.

Now, what happens if the keeper is put back into the gap? The operating point does not move back up to the  $B_r$  point as might be expected, but starts off on a new curve as indicated by the arrows of Fig. 1b, and arrives at the point  $y$ . Thus, in the single removal and replacement of the keeper, the magnet has suffered in flux density the difference between  $B_r$  and  $y$ . When the keeper is again removed, the operating point travels back to  $x$  over the upper curve as

indicated. The loop thus formed by the two curves between  $x$  and  $y$  is known as a minor hysteresis loop.

In handling minor hysteresis loops, two approximations are usually made, both of second-order effect. First, it is assumed, as stated above, that the loop closes itself at the points  $x$  and  $y$ . This is not strictly the case. The operating point, on its return trip from  $y$  toward  $x$ , actually crosses its outbound path (near  $x$ ) and intersects the major hysteresis loop slightly below  $x$ .

Theoretically, also, this same phenomenon happens to a smaller and smaller extent each time the keeper is replaced and removed. Actually, however, the difference becomes almost entirely unmeasurable after about two or three cycles. For the purposes in mind we can forget this and assume, as above, that the loop closes itself at the points  $x$  and  $y$ .

The second approximation made relative to this type of minor hysteresis loop

is that it is not a loop at all, but rather a straight line. This approximation is permissible because of the extreme narrowness of the loop, and inaccuracies thus introduced into our calculations are negligible. Henceforth, therefore, we shall think of and handle the minor hysteresis loop as a single straight line (between the points  $x$  and  $y$  of Fig. 1b, for instance) which acts as the path of the magnet operating point in both directions.

## Effect of Demagnetizing Field

Let us now take our two design equations and write them in the form

$$B_g = \frac{A_m}{F A_g} B_m \quad (1)$$

$$B_g = \frac{l_m}{f l_g} H_m \quad (2)$$

If these two equations are plotted against coordinates  $B_g$  and  $H_m$ , as in Fig. 2, Eq. (1) will be identical in shape to the demagnetization curve ( $B_m$  vs.  $H_m$ ) but

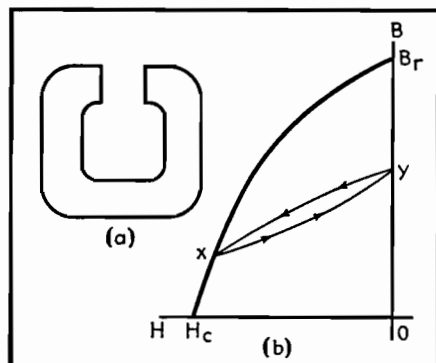


Fig. 1.—Basic magnet shape considered in this article, and demagnetization curve showing minor hysteresis loop between  $x$  and  $y$ .

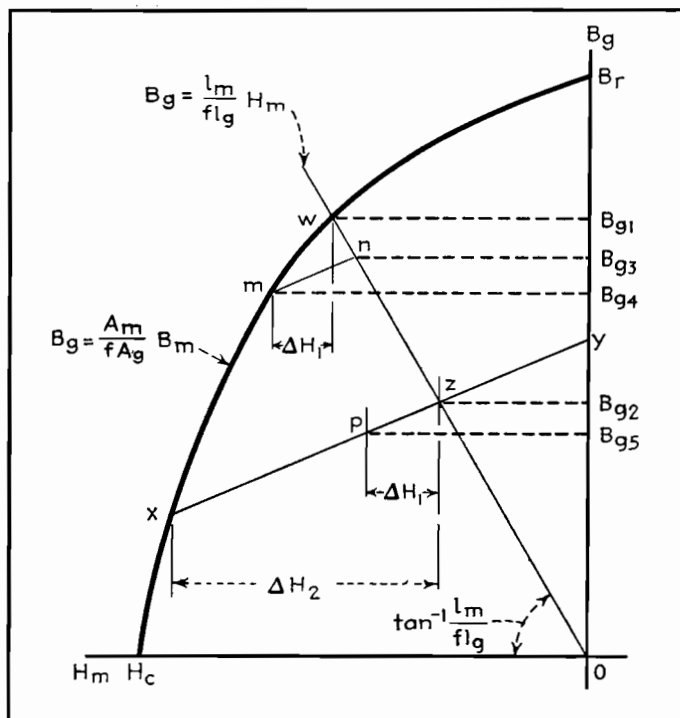


Fig. 2.—Plot of Eqs. (1) and (2), with minor hysteresis loops represented by straight lines  $x$ - $y$  and  $m$ - $n$ . This type of graph permits determining stabilizing effect of a demagnetizing field.

multiplied by the constant factor  $A_m/F A_g$ , and Eq. (2) will be a straight line passing through the origin and of slope  $l_m/f l_g$ . Obviously, the intersection of these two curves at the point  $w$  is the graphical solution for  $B_g$  of the two simultaneous equations. This, of course, is the flux density in the gap (of size  $l_g$ ,  $A_g$ ) of a magnet (of size  $l_m$ ,  $A_m$ ) having leakage constants  $f$  and  $F$  and having been completely saturated and its keeper withdrawn.

If an additional demagnetizing influence is applied to the magnet in question, it forces the operating point down the curve to the point  $x$ . (This additional demagnetizing field may be an a-c field, a d-c field in opposition to the magnetization of the magnet, heat, etc.) When the additional demagnetizing field is removed, the operating point will run up the minor hysteresis loop  $xy$  until it reaches the point  $z$ , the intersection of  $xy$  with the straight line of Eq. (2).

This process has resulted in the loss of flux density in the air gap of amount  $B_{g1} - B_{g2}$ , but it has given us a stable magnet. To show this, let us imagine that the magnet we have just stabilized is put into service and that in the field it encounters a demagnetizing field of strength  $\Delta H_1$ . The operating point will run down the minor hysteresis loop  $xy$  till it reaches the point  $p$ . Here a state of balance is again reached, and, as long as  $\Delta H_1$  persists, the magnet will supply a flux density of  $B_{g5}$  to the air gap. Of course, as soon as  $\Delta H_1$  is removed, the operating point returns to  $z$  and the flux density in the gap again becomes  $B_{g2}$ .

Suppose that we had not stabilized the magnet before putting it into operation and that the magnet was again subjected to the demagnetizing field  $\Delta H_1$ . The operating point would move down the major hysteresis loop from  $w$  to  $m$ , where it would remain for the duration of the demagnetizing influence. The flux density in the gap would change from  $B_{g1}$  to  $B_{g4}$ , a far greater change than  $B_{g2}$  to  $B_{g5}$ . Furthermore, when  $\Delta H_1$  is removed, the operating point will not return to its original position, but will move up the minor hysteresis loop  $mn$  to the point  $n$ , its intersection with the straight line of Eq. (2). Thus, the unstabilized magnet not only suffered more during the application of  $\Delta H_1$ , but, on its removal, presented the air gap with a permanent change  $B_{g1} - B_{g3}$  in flux density.

It is evident, then, that any apparatus requiring a gap flux of constant cali-

bration must employ a stabilized magnet. There are limits to the demagnetizing field that any stabilized magnet can stand, and the limit in the case under discussion is shown by  $\Delta H_2$ . If the demagnetizing field exceeds this limit, the operating point will drop further down the major hysteresis loop and, on removal of the demagnetizing field, come back up on a different minor hysteresis loop.

The more a magnet is demagnetized from the point  $w$  (Fig. 2), the more stable it becomes. The designer must take into consideration the maximum adverse field his magnet has to stand before specifying the amount of stabilization it is to receive.

### Demagnetization Curves

In design considerations for a motor or magneto magnet, the first job is that of writing an equation for the demagnetization curve. Perhaps the two most useful methods of expressing  $B$  as a function of  $H$  are either by a power series or an equation of a parabola. (It must be borne in mind that although the demagnetization curve is in the second quadrant of the major hysteresis loop we shall refer to  $H$  as positive, not negative.) At the moment we are interested in the parabolic relation between  $B$  and  $H$ . Within very close limits the following equation may be made to approximate the demagnetization curve of any properly heat-treated alloy:

$$B = \frac{B_r(H_c - H)}{H_c - aH} \quad (3)$$

where  $B$  = dependent variable

$H$  = independent variable

$B_r$  = residual flux density, gauss

$H_c$  = coercive force, oersteds

$a$  = a constant for the particular curve under consideration

This equation may also be written

$$\beta = \frac{1 - \theta}{1 - a\theta} \quad (4)$$

where  $\beta = B/B_r$

$\theta = A/H_c$

In this,  $\theta$  may also be expressed as

$$\theta = \frac{1 - \beta}{1 - a\beta} \quad (5)$$

Now, multiplying Eqs. (4) and (5), differentiating with respect to  $\theta$ , and setting  $d(\beta\theta)/d\theta = 0$ , we get

$$\frac{d\beta}{d\theta} = -1 \quad (6)$$

Differentiating Eq. (4) with respect to  $\theta$  and substituting Eq. (6) into the result,

we get

$$\beta = \theta \quad (7)$$

This establishes a very important point, namely, that  $B/B_r = H/H_c$  at the point of maximum energy product  $B_g H_g$ .

The form of Eq. (3) shows that only three points are necessary to establish fully the complete demagnetization curve. These points may be any three points along the course of the curve, but upon occasion it may be desirable to specify a curve by the three cardinal points,  $B_r$ ,  $H_c$ , and the point of  $B_g H_g$ .  $B_r$  and  $H_c$  fit directly into Eq. (3), and the point of  $B_g H_g$  is introduced through the constant  $a$ . Transposing Eq. (4)

$$a = \frac{\beta + \theta - 1}{\beta\theta} \quad (8)$$

At the point of  $B_g H_g$ ,  $\beta = \theta$ . Hence, combining Eq. (7) with Eq. (8), we have

$$a = \frac{2\beta - 1}{\beta\theta} = \frac{2\theta - 1}{\beta\theta}$$

Multiplying these two equations together and taking the square root of the result

$$a = \frac{2\sqrt{\beta\theta} - 1}{\beta\theta} = \frac{2}{\sqrt{\beta\theta}} - \frac{1}{\beta\theta}$$

And thus we obtain a value for  $a$ , in terms of  $B_g H_g$ .

$$a = 2\sqrt{\frac{B_r H_c}{B_g H_g}} - \frac{B_r H_c}{B_g H_g} \quad (9)$$

### Stabilization of Magnets

The primary difference (from a design standpoint) between a magneto magnet and, let us say, a loudspeaker magnet is the fact that the former is subject to heavy demagnetizing influences over and beyond the demagnetizing influence of the air gap itself. The magneto manufacturer long ago discovered that if he assembled his instrument completely and then magnetized the magnet (which would be the proper procedure in the case of the loudspeaker), the instrument when placed on test would deliver an output that would be high initially but would fall off rapidly at first and then asymptotically approach some much lower value. This phenomenon is due, of course, to the demagnetizing effect of the current in the coils of the magneto, and the only possible practical remedy is the use of a stabilized magnet right from the beginning.

The next question, then, is: How much shall the magnet be stabilized in order that the magneto's initial output shall remain constant with time? This question, of course, is related to the magnitude

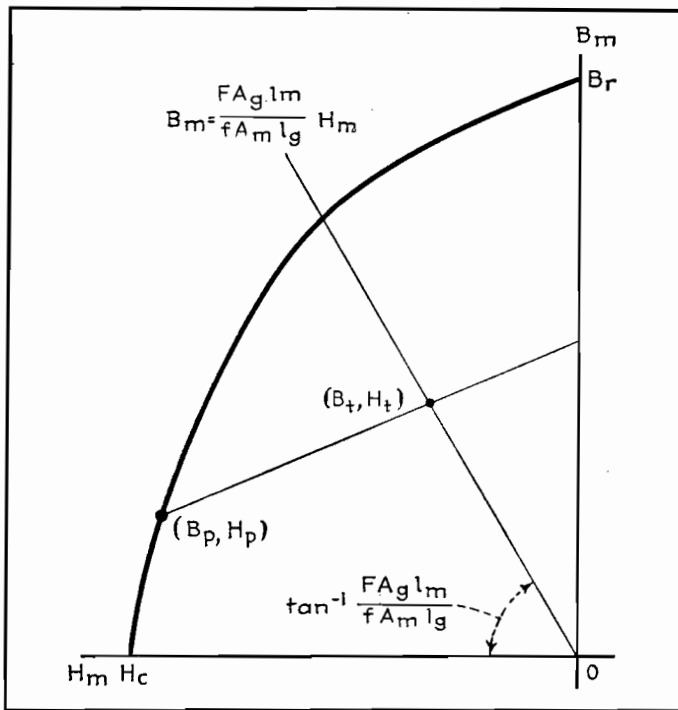


Fig. 3.—Graph showing open-circuit condition for same problem as in Fig. 2.

of the demagnetizing forces present in the operation of the machine. These forces may be computed, if necessary, on the basis of the machine's maximum load or even on the basis of short-circuit (if a generator or magneto) or stalled (if a motor) conditions. Most manufacturers, however, have found this computation to be unnecessary. They have learned from experience that, in general, a machine magnet is sufficiently stabilized if it is fully magnetized prior to inserting it in its magnetic circuit. This is true whether the magnet is part of the stator or the rotor.

Figure 3 is similar to Fig. 2 except that we now have  $H_m$  plotted against  $B_m$  instead of against  $B_g$  as previously. This means that the slope of the straight line of Eq. (2) is multiplied by the factor  $F A_g / A_m$ , and the equation of this line becomes

$$B_m = \frac{F A_g l_m}{f A_m l_g} H_m \quad (10)$$

When our magnet is magnetized to (or beyond) its saturation point, the operating point runs up the normal magnetization curve (not shown on Fig. 3) to some point high up on the major hysteresis loop and remains there until the current in the magnetizer is turned off, at which time it drops to the point  $B_r$  of Fig. 3. When the magnet is removed from the magnetizer, it is open-circuited, i.e., operating in no magnetic circuit other than that formed of itself and a return

path of unit permeability. This condition is invariably one in which the pole faces of the magnet exert a self-imposed and very severe demagnetizing influence.

Of course, the severity of this demagnetizing force is a function of the dimensions and shape of the magnet, being much greater for short fat straight rods than for long thin horseshoes, for instance. But for practical magneto and motor magnets made of a practical alloy (such as one of the Alnicos), the demagnetizing influence of the open-circuit condition is large, and the operating point of Fig. 3 will run down the demagnetization curve from  $B_r$  to some point  $B_p, H_p$ .

If the magnet (regardless of whether it is part of the rotor or stator) is encased in its housing, and the magnetic circuit completed (working air gaps in such machines run of the order of 0.010 in. in total length), the severe demagnetizing influence of the open-circuit condition will have been removed, and the only demagnetizing influence then exerted on the magnet (until the machine starts operating) is that of the working air gap itself.

As the demagnetizing influence on a magnet is decreased, its operating point moves back toward the  $B$  ordinate along a minor hysteresis loop. As the demagnetizing influence on the magnet is decreased from the open-circuit condition to the working gap condition, the operating point moves up the minor hysteresis loop from the point  $B_p, H_p$  to the point

$B_t, H_t$  which is the intersection of this loop with the straight line of Eq. (10).

#### Final Operating Point

The point  $(B_t, H_t)$  is the final operating point of the magnet. As the machine is put into operation and additional magnetizing and demagnetizing influences, due to the current in its coils, are brought to bear on the magnet, the operating point will oscillate back and forth along the minor hysteresis loop about the point  $B_t, H_t$ . (The influences referred to in the previous sentence are not steady and constant in magnitude, but are instead influences that vary in magnitude with a frequency equal to the speed of the machine or some integral fraction or multiple of that speed.) The final flux density in the working air gap of the machine may be readily computed from the magnet operating point  $(B_t, H_t)$  and the fundamental design equations for magnets.

#### Flux Density in Air Gap

In the analytical process, the first question is: After the magnet is saturated and removed from the magnetizer, how far down the demagnetization curve does its operating point travel? This question is answered by an empirical equation giving the value of the quantity  $B/H$  for an open-circuited magnet as a function of the quantity  $l/D^*$

$$\frac{B}{H} = (1.89 - a) \left( \frac{l}{D} + a \right)^{1.82} \quad (11)$$

where  $l$  = mean length of magnet along path of magnetization

$D$  = effective diameter of magnet  
 $= 2 \sqrt{\text{area of magnet}/\pi}$

$a$  = alloy constant as defined by Eq. (9)

From the above equation, together with a demagnetization curve for the alloy we are using, we can determine the point  $B_p, H_p$  of Fig. 3.

We now have everything we need to determine the point  $B_t, H_t$  if we but have the slope of the minor hysteresis loop connecting the two points. Minor hysteresis loops sometimes accompany demagnetization curves of standard alloys,

\* Equation (11) is not accurate for very small values of  $l/D$ . There exists a more complicated equation which is accurate even at small values of the argument, but because of the greater simplicity of Eq. (11) and because it is accurate at practical values of  $l/D$ , it is to be preferred. Equation (11) is for straight magnets. It may be used with fair accuracy for four-pole rotors, but a correction factor is necessary if it is to be used in connection with horseshoe magnets.

but, in general, technical publicity on permanent magnets disregards them entirely, and the information is often difficult to obtain.

Although the slopes of the minor hysteresis loops connected with any one demagnetization curve vary as a function of the point on the curve at which they originate, all of them are very closely approximated by the slope of the demagnetization curve itself at the point  $B_r$ . This means that we may obtain very easily the slope of a minor hysteresis loop for any demagnetization curve in terms of the  $B_r$ ,  $H_c$ , and  $a$  for that particular curve. Referring to Eq. (3) and differentiating  $B$  with respect to  $H$ , we get

$$\frac{dB}{dH} = \frac{-B_r H_c (1-a)}{(H_c - aH)^2} \quad (12)$$

Setting  $H = 0$  in the above equation, we get the slope of the demagnetization curve at  $B_r$  and, consequently, the slope of the minor hysteresis loops connected with that particular demagnetization curve

$$\frac{dB}{dH}_{H=0} = m = -\frac{B_r}{H_c} (1-a) \quad (13)$$

The slope  $m$  in the above equation is negative even though in the ordinary convention a minor hysteresis loop has a positive slope. This is due to the fact that for convenience we have reversed the convention and are treating  $H_c$  and  $H$  in general as positive rather than negative values.

It is now possible to write the straight-line equation for the minor hysteresis loop connecting the points  $B_p, H_p$  and  $B_t, H_t$  of Fig. 3

$$B = B_p - m(H_p - H) \quad (14)$$

where  $m$  is as defined in Eq. (13).

The final operating point  $B_t, H_t$  of the magnet may be determined by the simultaneous solution of Eqs. (10) and (14). Performing this operation, we get

$$B_t = \frac{B_p - mH_p}{1 - \frac{mfA_m l_g}{FA_g l_m}} \quad H_t = \frac{B_p - mH_p}{\frac{FA_g l_m}{fA_m l_g} - m} \quad (15)$$

From the above and either one of the two

fundamental design equations, namely,  $FB_g A_g = B_m A_m$  and  $fB_g l_g = H_m l_m$ , we obtain the gap flux density:

$$B_g = \frac{B_p - mH_p}{\frac{FA_g}{A_m} - \frac{mf l_g}{l_m}} \quad (16)$$

Thus the problem—given the magneto and the magnet, determine the flux density in the working air gap—is solved. This problem was deliberately chosen first because the steps of its solution and the actual workings of the physical entities involved have a chronological parallelism that enhances the understanding of both.

#### Finding Size of Magnet

Although presented first, the preceding problem for obvious reasons is by no means so important as the following problem: given the magneto and the required gap flux density, determine the size of the magnet. At first glance it may seem silly to make a special problem out of a case involving three general factors when the only change is between the dependency and independency of the factors. But further thought will reveal that when the size of the magnet is the required factor, it is really two factors, the length and the area of the magnet, that are required. As a consequence, to obtain a unique solution to the problem, we must impose one more condition.

The first problem may be broken down to its essentials in the following way: given  $l_m$ ,  $A_m$ ,  $l_g$ ,  $A_g$ ,  $F$ ,  $f$ ,  $B_r$ ,  $H_c$ , and  $a$ , determine  $B_g$ . With these specifications there is no control over the point  $B_t, H_t$  and it lands wherever it happens to land. Now, since it is necessary to add a further condition to the already established requirements of our second problem, what more natural requirement could we choose than that of working the magnet material at its best possible efficiency under the circumstances, in other words, at the highest possible value of the product  $B_t H_t$ ? The essentials of the second problem now become: given  $l_g$ ,  $A_g$ ,  $F$ ,  $f$ ,  $B_r$ ,  $H_c$ , and  $a$ , and the require-

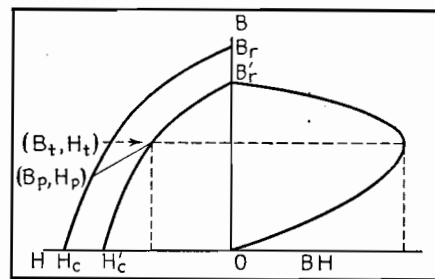


Fig. 4.—Final graph from which the operating point can be determined.

ment that the magnet be the smallest possible and still fulfill all other conditions, determine  $l_m$  and  $A_m$ .

Referring to Fig. 4, we see that the final magnet operating point  $B_t, H_t$  must lie on some minor demagnetization curve such as  $B_r', H_c'$ . This would be the demagnetization curve obtained if initially the magnet material were not saturated. Obviously, an infinite number of such curves lie between the demagnetization curve itself and the origin, and  $B_t, H_t$  must lie on one of them. The curve  $B_r', H_c'$  has accompanying it an energy product curve, and it is our job to make sure that the point  $B_t, H_t$  coincides with the point of maximum energy product of  $B_r', H_c'$ . Since  $B_r', H_c'$  is a proportionately reduced curve, we may write

$$\frac{B_r'}{B_r} = \frac{H_c'}{H_c} \quad \text{or} \quad \frac{B_r'}{H_c'} = \frac{B_r}{H_c}$$

We know from Eq. (7) that if  $B_t, H_t$  is located at the maximum energy product point, then

$$\frac{B_t}{B_r'} = \frac{H_t}{H_c'} \quad \text{or} \quad \frac{B_r'}{H_c'} = \frac{B_t}{H_t}$$

Consequently,

$$\frac{B_t}{H_t} = \frac{B_r}{H_c} \quad (17)$$

This is the one additional necessary condition to the solution of the second problem, and we find ourselves armed with six equations (Eqs. 3, 11, 16, 17, and two in 15) to determine four incidental unknowns  $B_p$ ,  $H_p$ ,  $B_t$ , and  $H_t$  plus the two desired unknowns  $l_m$  and  $A_m$ .

# Mechanical Problems of Permanent-magnet Design

By EARL M. UNDERHILL

Alnico machining tolerances, casting allowances, choice of alloys, cost factors, methods of mounting, and other mechanical problems related to electrical design of permanent magnets are taken up, with emphasis on practical data obtained through actual experience

**M**ANY factors usually influence the choice of magnet material. Among the more important the following may be mentioned:

1. Space considerations.
2. Weight.
3. Economy. Here the cost of the magnet is only one factor. The designer must determine whether or not the use of a better alloy will enable compensating savings in other materials in his device.
4. Availability. This is a particularly important consideration today.
5. Machinability and workability.
6. Calibration stability and resistance to stray fields.
7. Resistance to heavy demagnetizing fields.
8. Physical strength.

Having determined the proper magnet size and alloy, the designer is obliged to make a drawing of his magnet, to specify just how it shall be mounted, and to make provision for the fastening of the magnet to the rest of the magnetic circuit. This phase of the design introduces the problems of hole size and location and the methods by which the holes are formed, shaft mounting of rotors, brazing and soldering, etc. These problems as well as those influencing the choice of an alloy will be considered here. Only the aluminum-nickel-iron alloys (popularly known as Alnico and Nipermag) will be discussed here, and we shall refer to these alloys in the general sense simply as Alnico for the sake of simplicity.

## Alnico Tolerances

Alnico is a very hard, brittle, and (in the generally accepted sense of the word) nonmachinable alloy. It cannot be turned, milled, or drilled with ordinary tools, but it can be ground fairly easily with any common abrasive. The alloy is cast, usually in h-f induction furnaces, to a size slightly greater than that to

which it is to be finished, and then taken down to finished size by grinding. All holes and slots in any given piece must be cast in. If a close tolerance is required on holes in Alnico, the common procedure is to cast the holes somewhat undersize and then finish to correct size by grinding. Tables I and II list some of the known physical properties of the various grades of Alnico and Nipermag.

deg, and a parallelism tolerance between opposite ground faces of 0.002 in. per linear inch across either ground face.

## Casting Allowance

These factors all add up to the following very rough but fairly accurate rule: Allow, for clean finish grinding, approximately 0.015 in. per 1.5 sq in. of each surface to be ground. If, for example, we

Table I.—Physical Properties of Alnico Alloys and Nipermag

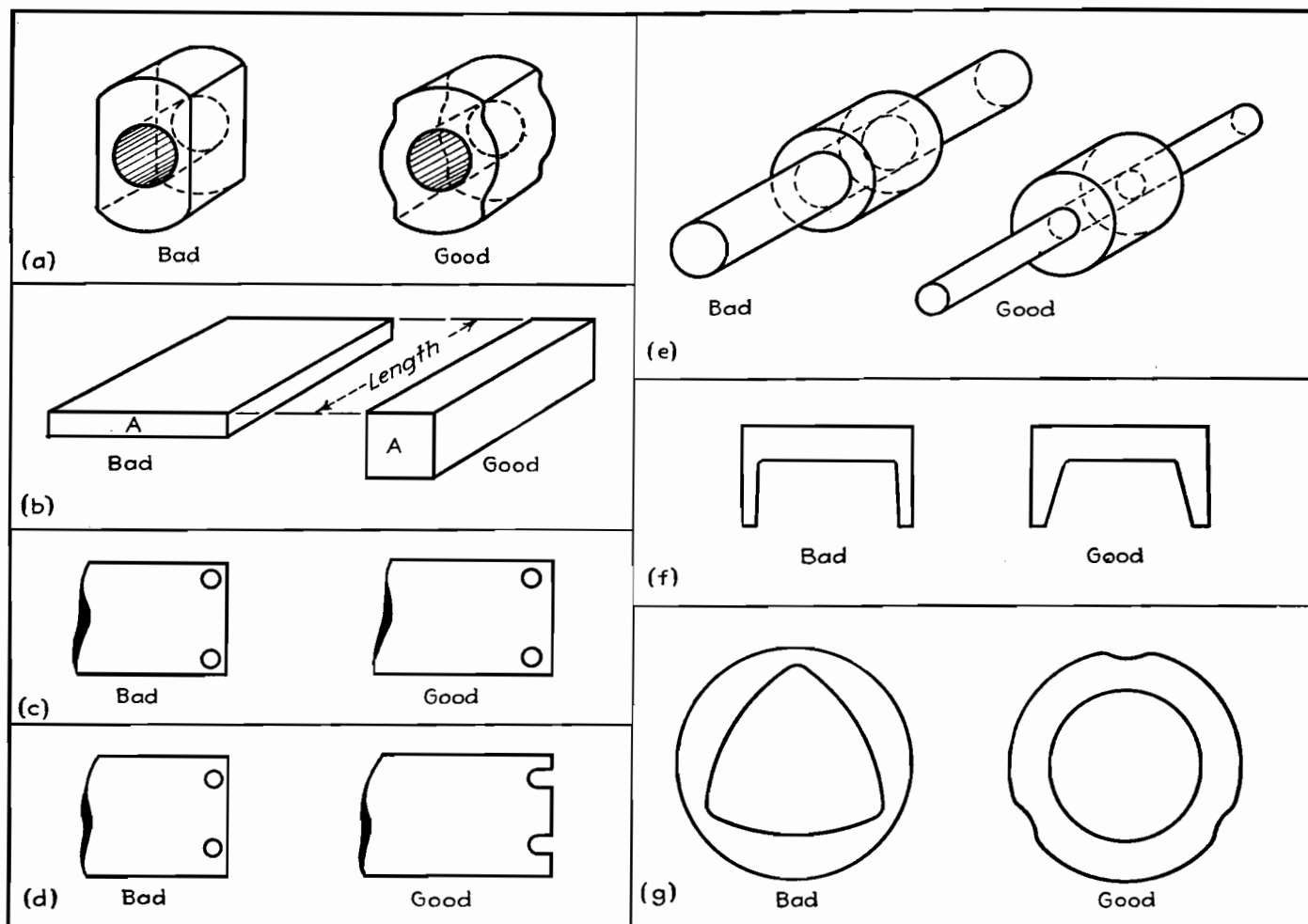
Property	Alloy					
	Alnico I	Alnico II	Alnico III	Alnico IV	Alnico V	Nipermag
Specific gravity	6.9	7.1	6.9	7.0	7.3	6.9
Electrical resistivity at 25°C, ohm-cm/sq. cm.	$75 \times 10^{-6}$	$65 \times 10^{-6}$	$65 \times 10^{-6}$	$75 \times 10^{-6}$	$47 \times 10^{-6}$	$66 \times 10^{-6}$
Tensile strength, lb./sq. in.	4,000	2,500	12,000	9,000	5,450	
Transverse modulus of rupture, lb./sq. in.	13,900	7,000	22,500	24,000	10,200	
Hardness, Rockwell "C"	42-55	45-57	40-55	45-55	45-55	40-55

Since Alnico magnets are cast, it is impossible to form these magnets initially with a high degree of precision. Barring unusual features, a good commercial tolerance for a cast dimension of less than 2 in. is  $\pm \frac{1}{64}$  in., from 2 to 4 in.,  $\pm \frac{1}{32}$  in. These dimensions may be ground to as small a tolerance as the user may wish, and, if desired, Alnico may be made to take a mirrorlike polish. However, the designer must bear in mind, where price is a consideration, that commercial tolerances obtain. Tight tolerances entail substantial price increases. Plus or minus 0.005 in. is a commonly specified limit between two finish-ground faces of cast permanent magnets, although much closer ones can be held. The same applies to a perpendicularity tolerance between a finish ground face and the center plane of the as-cast magnet of plus or minus  $1\frac{1}{2}$  deg, a perpendicularity tolerance between two finish ground faces of plus or minus  $\frac{1}{2}$

have a casting that is just 3.0 sq in. in section and that we wish to finish to a length of, say, 1.500 in. by grinding its two end surfaces, we should have to make this piece 1.560 in. long to allow it to clean up properly.

Actually, it would be necessary to put our casting tolerance on top of this in order to assure that, even though the casting came minimum size, we should still have enough stock to clean up. Consequently, the cast length dimension for this piece should be specified as 1.576 in.  $\pm \frac{1}{64}$  in.

A magnet casting is usually made by means of a sand mold, and a mold, in turn, by means of a pattern. Provision must be made, when making the pattern, to enable its withdrawal from the mold without disturbing the sand. This is accomplished by providing the pattern with a slight taper, or draft. This same draft is inherited by the casting



Examples of good and bad mechanical design of cast permanent magnets: (a) widening the thinnest parts of a permanent-magnet rotor adds greatly to strength; (b) the closer a magnet approaches a square or circle in cross-section, the fewer the cracks during production; (c) for success in casting holes, leave ample metal between holes and outer surfaces; (d) whenever possible, use slots in place of holes to avoid cracks; (e) when casting a magnet around an insert like this shaft, keep the magnet area large in relation to the insert area, to prevent cracks during casting; (f) avoid sudden changes in cross-section by tapering as shown here; and (g) strain is less when there are indentations in the outer surface than when they are on inner surfaces.

itself, and the designer must be prepared for it. Fortunately, it is not large, usually amounting to about 1 deg. (This means 1 deg between a surface and the axis of the casting, or 2 deg between two opposite surfaces.) For emphasis and reference convenience, the important points of the preceding few paragraphs are tabulated in Table III.

#### Cost per Gauss

Economic considerations are frequently most important in the determination of the proper alloy and the proper size and shape of casting. Actual prices cannot be given, as price is a function not alone of the grade of the Alnico in question but also of the weight and size of the casting, its intricacy, the amount and type of grinding, tolerances required, quantity on order, etc. Even the price relationship among the various alloys is subject to change as improvements in product and production manifest themselves.

Frequently, too, it may happen that a casting of Alnico V, for example, which has been designed to do the same job as another casting of, let us say, Alnico II is so utterly different from the latter in size and shape that production technique of the two items is also entirely different. In such cases, any general comparison between the two alloys on a dollars-per-pound basis will be obviously misleading.

In general, it is necessary for the magnet designer to calculate a size and shape of casting for each alloy he has in mind to do a particular job, lay it out in detail and

include all mounting holes, inserts, etc., and submit it to the magnet manufacturer for quotation. He will then be able to calculate the cost of a gauss in his working air gap for each alloy in which he is interested.

The designer must ask himself such questions as: Can I, by using a better alloy and thus increasing the flux density in my working air gap, more than effect compensating savings by using fewer turns of larger sized wire on the coil which is to operate in this gap? Or: Can I, by using a better alloy and thus

Table II.—Operating Temperature Ranges and Expansion Data for Magnet Alloys

Temperature range, °C	Mean coefficient of temperature expansion, in./in./°C × 10 <sup>6</sup>					
	Alnico I	Alnico II	Alnico III	Alnico IV	Alnico V	Nipermag
20-120	11.9	11.5	13.2	12.3	11.6	11.0
20-220	12.1	12.1	13.2	12.7	11.3	
20-300	12.6	12.4	13.0	13.1	11.6	



reducing the weight of my magnet, more than effect compensating saving by reducing shaft, bearing, and housing sizes? Also, will this reduced weight make possible entirely new applications of my device?

#### Factors Affecting Cost

Many factors influence the cost of a magnet. In the following tabulation is a listing of the more important factors and their qualitative effects on cost.

1. *Alloy.*—Alloy affects price in several ways. (1) There are the raw material costs. The higher the cobalt and nickel content of an alloy, the higher its raw material cost. (2) There are heat-treating costs. All alloys are about on a par in this respect except Alnico V. This alloy must be heat-treated in a magnetic field and hence is more costly to produce. (3) There are spoilage costs. Certain alloys, notably those high in nickel content and low in cobalt content, require a very fast quench during heat-treatment to establish properly their magnetic characteristics. Castings made of these alloys frequently develop bad cracks, and rejections during production are sometimes high.

2. *Size or Weight.*—This is the prime basis of cost estimation. The heavier the piece (in any one alloy), the higher its cost.

3. *Quantity.*—As in nearly any other field, the larger the quantity on order (up to 15,000 pieces), the lower the cost.

4. *Grinding.*—The larger the surface to be ground, the higher the price.

5. *Grinding Tolerances.*—The smaller the tolerances (below  $\pm 0.005$  in.), the higher the price.

6. *Parallelism and Perpendicularity Tolerances.*—The smaller the tolerances required (below good commercial tolerances), the higher the price.

7. *Ease of Production.*—Certain magnets are of such size and shape that they may be cast as a bar of uniform cross-section and the magnets cut from the bar (by means of an abrasive cutting disk) after the pouring or heat-treating operation. This procedure leads to obvious savings in production, and consequent lower prices.

8. *Shape.*—Certain shapes tend to crack badly and others not at all. Production rejections due to cracks from this source seriously affect prices.

9. *Coring and Inserts.*—The greater the diameter and length of the cored hole or insert, the higher the cost. In cases where the pattern is capable of forming its own core, there is no extra charge.

#### Mounting Magnets

The most common method of mounting an Alnico magnet is by means of one or more holes or slots cast into the magnet during the pouring process. These holes usually act as clearance holes through which bolts of some sort pass and serve to clamp the magnet, usually to a plastic or nonmagnetic metallic base. Such holes are usually quite small in relation to the over-all size of the casting. Much larger in this respect is the hole cast in a magneto, motor, or generator rotor magnet for accommodation of the shaft on which the magnet is mounted.

Again, this mounting hole may be a clearance hole for the shaft. If it is, the magnet may be securely fastened to the shaft by means of end pieces, or the shaft may be cast into the magnet with the aid of aluminum or other suitable material such as Cerro-Matrix, a low-melting alloy similar to type metal which possesses the property of expanding upon solidification and cooling. Sometimes a shaft hole is not made as a clearance hole, but instead is cast somewhat undersized and then ground to the size of the shaft. The shaft is then pressed into the magnet. This is not an advisable procedure because of the physical weakness of Alnico.

during the pouring process. If the length of the hole to be formed is too great with respect to its diameter, a special core of baked sand, carbon, or other materials must be placed in the mold, and later removed from the casting. Such holes tend, a good deal more frequently than the first type, to be mislocated, curved, or out of line.

#### Use of Inserts for Mounting

A second common method of mounting Alnico magnets is to cast soft iron inserts into the magnet (during the pouring process) and to drill and tap or ream these inserts. The inserts are usually coarse knurled to allow the Alnico to grip them tightly. In the case of magneto, motor, or generator magnets, the shafts are sometimes cast directly into the magnets during the pouring process. Such shafts are rough knurled and/or keyed where the magnet material grips them. All finishing operations on the shaft are done after pouring and heat-treatment.

Still a third method of mounting magnets is to cast them into a housing wall. (We are not talking now of the pouring process of the magnets themselves, but rather of a process in which

Table III.—Alnico Casting Tolerances and Allowances

Item	Good commercial tolerance
Cast dimensions $\begin{cases} \text{Less than 2 in.} \\ \text{2-4 in.} \end{cases}$	$\pm \frac{1}{64}$ in. $\pm \frac{1}{32}$ in.
Finish ground dimensions (plane surfaces)	$\pm .005$ in.
Parallelism between ground parallel faces	.002 in./linear inch across face
Perpendicularity $\begin{cases} \text{Between ground face and center plane of} \\ \text{"as cast" magnet.} \\ \text{Between two ground faces.} \end{cases}$	$1\frac{1}{2}^\circ$ $\frac{1}{2}^\circ$
Casting draft	$1^\circ$
Grinding allowance	Rule: .015 in./1.5 sq. in. of each surface to be ground

In all foundry work, the mold is the negative of the casting. Consequently, a hole in a casting is represented in the mold by some solid matter. In a sand mold, the core that forms the hole of a casting can sometimes be formed by the pattern itself when it makes its impression in the sand. This is the case where the hole has a diameter-to-length ratio great enough to allow the column of sand in the mold that forms this hole to support itself against the inrush of the molten metal

the finished magnets are used as inserts in a casting made of a nonmagnetic, usually much softer and more easily handled material.) Aluminum and Cerro-Matrix are both suitable for this operation. Other and less frequently used methods of mounting magnets include the use of straps and brackets, clamps, certain cements, and bolts or rods welded to the magnet. (The welding process destroys the magnet's characteristics in the vicinity of the weld.)



### Mounting the Pole Pieces

Methods of attaching soft-iron pole pieces and return members to Alnico magnets are listed briefly below.

1. A clearance hole with a shoulder may be provided in the Alnico, through which a screw engages a tapped hole in the soft-iron member.

2. A counterbored clearance hole may be provided in the soft-iron member, through which a screw engages a hole drilled and tapped in a soft-iron insert cast into the magnet.

3. The soft-iron member may be brazed to the Alnico magnet. Care must be exercised here to see that the temperature of the magnet is not raised too high. The safe maximum limit for this temperature is 1100°F, although a temperature value as high as 1200°F may be used if it affects only a small portion of the casting and is not maintained for more than 2 or 3 min.

4. The soft-iron member may be soft soldered to the magnet. There are

several known methods for doing this, most of them involving a preparation of the surfaces to be soldered by means of an acid.

5. The soft-iron member may be cemented or clamped to the magnet.

6. The soft-iron member may be welded to the magnet. This is not recommended.

### Heat-treating Precautions

The heat-treatment of Alnico puts it through a rather rough temperature cycle. The metal is quenched, sometimes very rapidly, from temperatures that exceed 2000°F. One direct consequence of this is the development of severe cracks in magnets of certain shapes or sizes. It is not always possible to set up design principles from the standpoint of avoiding these cracks, and it is not always possible to predict ahead of time just which designs will crack and where. Certain aspects of the situation are known and are listed below:

1. The more closely a magnet ap-

proaches in design a solid sphere or cube, the less likely it is to develop bad cracks.

2. Inserts, large in comparison to the section of the magnet into which they are cast, are very apt to cause cracking of the magnet.

3. Through holes or inserts placed too close to a surface other than the two they connect are apt to cause cracks through to this surface.

4. Rapid changes of section through the magnet should be avoided.

This discussion has been centered about cast Alnico. There is, however, another method of making Alnico magnets of small sizes (less than approximately two ounces in weight) and that is through the process of sintering. The sintering process is one of compressing metal powders under pressure and temperature in a permanent metal mold. In general, magnets having a dimension of less than approximately  $\frac{3}{16}$  in. are difficult to cast and should be made by the sintering process.

## SECTION XVI

# PULSES

	Page
Determining Shape and Magnitude of Amplified Pulses...	211
Computing Circuit Response to Pulses.....	213
Circuit Response to Nonsinusoidal Wave Forms.....	216
Square-wave Harmonic Amplitude Table.....	219
Square Waves for Impedance Measurements.....	220

# Determining Shape and Magnitude of Amplified Pulses

By ERIC A. WALKER

IN CALCULATING the gain of an amplifier stage, defined as the ratio of the voltage on the second stage to the voltage on the first stage, no reference is usually made to the shapes of the two voltage waves, for it is tacitly assumed that both are sinusoidal. In fact, if the plate resistance  $R_p$  and the amplification factor  $\mu$  are assumed to be constant, no distortion is accounted for and the output must have the same shape as the sinusoidal input voltage.

The solution is not so simple if the input voltage is a complex wave, for the various harmonics are amplified disproportionately and the shape of the input and output voltages are quite different. For instance, an instantaneous pulse of voltage, such as is required in some television circuits, may become quite distorted. There are two methods by which the shape as well as the magnitude may be determined.

To illustrate the first method, suppose that the input signal is the periodic pulse shown in Fig. 1. Let us further suppose that this pulse recurs 13,230 times each second, and that it is 1  $\mu$ sec wide. The Fourier series of this wave is found to be

$$f(x) = \frac{Eb}{2\pi} + \sum_{n=1}^{\infty} \frac{E}{\pi n^2} (1 - \cos nb) \sin(2\pi nft) + \sum_{n=1}^{\infty} \frac{E}{\pi n^2} (\sin nb) \cos(2\pi nft)$$

where  $f = 13,230$   
 $E$  = height of the pulse

$n$  = number of the harmonic to be found  
 $b$  = duration of the pulse

If one begins to substitute values of  $n$  in the above equation, it is soon evident that many terms will be required before their effect on the resultant wave becomes negligible, or before the series begins to approximate the square-topped pulse. Then to find out how much each harmonic is amplified it is necessary to extend the gain-frequency curves much further than is usually done.

A simpler method of finding both the shape and the magnitude of an amplified pulse requires the use of simple operational methods. The solution is usually in three steps:

1. Determine the operational impedance of the circuit.
2. Find the operational expression for the driving function, in this particular case the voltage pulse.
3. Find the solution in a table of operators or by any other method necessary or available. The methods of the operational calculus are found in many textbooks.\*† Only the necessary steps will be given here.

To find the operational impedance of a circuit, the circuit is redrawn replacing the inductances with impedances equal to  $pL$  and replacing the capacitances with impedances equal to  $1/pC$ . Then the

\* BUSH, V., "Operational Circuit Analysis," John Wiley & Sons, Inc., New York.  
 † BERG, E. J., "Heaviside's Operational Calculus," McGraw-Hill Book Company, Inc., New York.

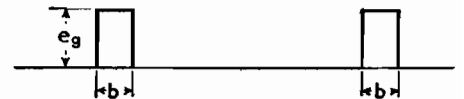


Fig. 1.—Periodic pulse on which analysis is based.

input impedance is found in the ordinary manner. The entire process will be carried through for several circuits.

Figure 2a shows a circuit consisting of a tube and a resistance load. Figure 2b shows the equivalent circuit neglecting all inductance and capacitance. The impedance is

$$Z_{12} = R_p + R_L \quad (1)$$

Figure 3 shows the method by which the voltage function is put into the equation. The pulse can be considered as made up of two voltages (often called

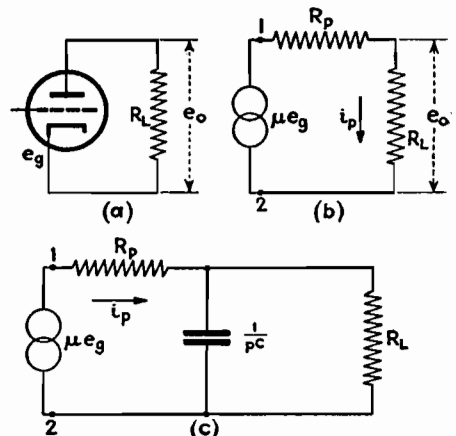


Fig. 2.—Actual, equivalent, and operational circuits for h-f response.

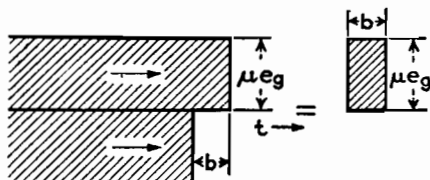


Fig. 3.—Derivation of pulse from two unit voltages.

Heaviside unit functions)  $+\mu e_g$  and  $-\mu e_g$ , the second applied at a time  $b$  later than the first. This method can be used for periodic functions if the two or more transients that are caused by the pulse have decayed to negligible values before the next pulse is impressed.

If one first impresses the positive unit pulse on the impedance  $Z_{12}$ , one gets

$$e_o = \frac{+\mu e_g R_L}{R_p + R_L} \quad (2)$$

The solution is obviously a continuous positive voltage. Add to this a solution with  $-\mu e_g$  as the driving voltage, lagging in time by  $b$ , and the amplified pulse is obtained.

Figure 2c is the same circuit including a shunt capacitance  $C$ . In this circuit

$$Z_{12} = \frac{R_p + R_L + pR_p R_L C}{1 + pR_L C} \quad (3)$$

$$\text{and } e_o = \frac{\mu e_g}{R_p C} \left( \frac{1}{p + \frac{R_p + R_L}{R_p R_L C}} \right) \quad (4)$$

The solution is

$$e_o = \frac{\mu e_g R_L}{R_p + R_L} \left[ 1 - e^{-\left( \frac{R_p + R_L}{R_p R_L C} \right) t} \right] \quad (5)$$

This equation shows that the maximum amplification that can be attained is

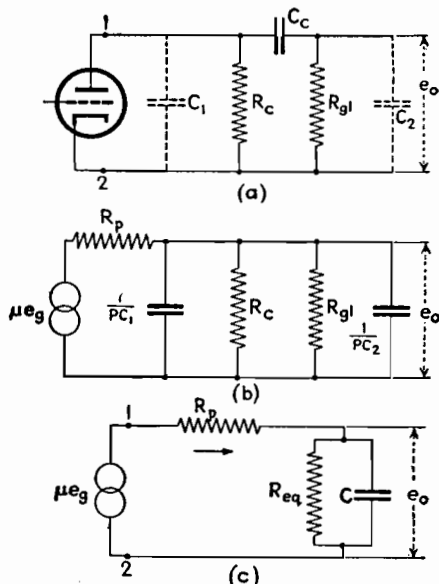


Fig. 4.—Actual and equivalent circuits for low-frequency response.

$\mu R_L / (R_p + R_L)$ . Add to this a solution lagging in time by  $b$  and with a negative sign and the resulting pulse is obtained.

Many circuits include a coupling capacitor, as shown in Fig. 4a. If an attempt is made to solve the complete circuit as shown, an equation with four roots is obtained. Its solution is laborious. Much information can be obtained by studying two simpler circuits. These are the case where  $C_c$  is so large it can be neglected and the case where the stray capacitances  $C_1$  and  $C_2$  are so small they can be neglected.

Figure 4b shows the circuit of Fig. 4a with  $C_c$  replaced by a short circuit. This circuit yields exactly the same equation as the circuit of Fig. 2c if the  $C$  and the  $R_L$  of Eq. (5) are replaced by

$$C = C_1 + C_2 \quad R_L = \frac{R_c R_g}{R_c + R_g}$$

as shown in Fig. 4c. Equation (5) then becomes

$$e_o = \frac{\mu e_g R_c R_g}{R_p R_c + R_p R_g + R_c R_g} \left[ 1 - e^{-\left( \frac{R_p R_c + R_p R_g + R_c R_g}{C R_p R_c R_g} \right) t} \right] \quad (6)$$

If one uses a type 954 tube and assumes the following values:  $\mu = 1,100$ ;  $C_1 + C_2 = 11 \mu\text{f}$ ;  $R_c = 10^4$  ohms,  $R_g = 10^6$  ohms, and  $R_p = 10^6$  ohms, this equation becomes

$$e_o = 10.78 e_g (1 - e^{-0.903 \times 10^7 t}) \quad (6a)$$

Some idea of the effect of the coupling capacitor that has been neglected can be obtained by considering  $C_1$  and  $C_2$  as sufficiently small so that they can be ignored in a trial solution. Then

$$e_o = \frac{\mu e_g R_c R_g C_c p}{p C_c (R_c + R_g)(R_p + R_c) - R_c^2 + R_p + R_c} \quad (7)$$

$$e_o = \frac{\mu e_g R_c R_g}{R_p R_c + R_p R_g + R_c R_g} \left( \frac{p}{p + a} \right) \quad (7a)$$

where

$$a = \frac{R_p + R_c}{C_c (R_p R_c + R_p R_g + R_c R_g)}$$

The solution then is

$$e_o = \frac{\mu e_g R_c R_g}{R_p R_c + R_p R_g + R_c R_g} \left[ 1 - e^{-\left( \frac{R_p + R_c}{C_c (R_p R_c + R_p R_g + R_c R_g)} \right) t} \right] \quad (8)$$

The decrement factor, found by evaluating  $a$  for this circuit, is 9.9. The effect of this term is negligible for the

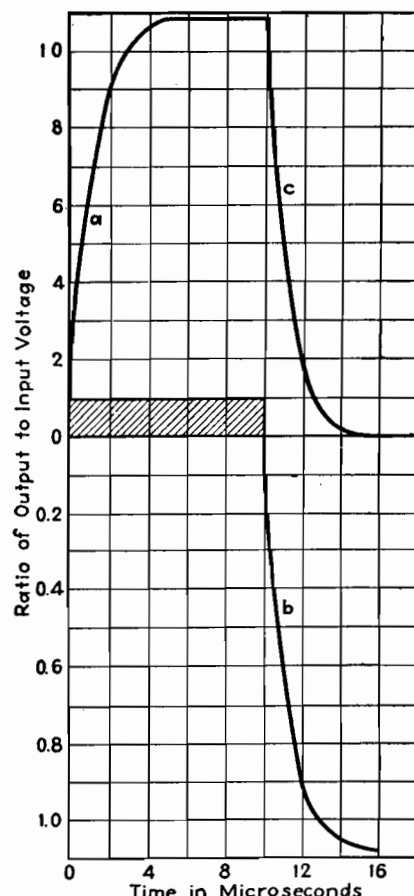


Fig. 5.—Pulse (crosshatched) and response of amplifier. The response is the superposition of the two portions a and b corresponding to positive and negative voltages.

microsecond pulse that we have been considering, and therefore this capacitance can be safely neglected.

A common circuit is one in which inductive compensation is used, as shown in Fig. 6. A solution of this circuit is given by

$$e_o = \mu e_g \left[ \frac{R_c R_g}{R_p} + \frac{1}{2b R_p L C} \left( \frac{R_c - L(a+b)}{b+a} e^{-(a+b)t} + \frac{R_c - L(a-b)}{b-a} e^{-(a-b)t} \right) \right] \quad (9)$$

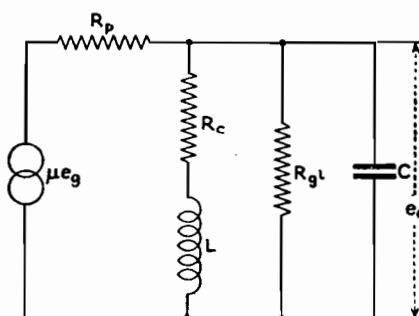


Fig. 6.—Compensated amplifier circuit for wide-band response.

where  $R_T = R_p R_{gl} + R_c R_{gl} + R_p R_c$

$$a = \frac{R_c}{2L} + \frac{1}{2R_p C} + \frac{1}{2R_{gl} C}$$

$$b = \sqrt{\frac{1}{4} \left( \frac{R_c}{L} + \frac{1}{R_p C} + \frac{1}{R_{gl} C} \right)^2 - \frac{1}{LC} \left( 1 + \frac{R_c}{R_p} + \frac{R_c}{R_{gl}} \right)}$$

The two decrement factors  $a + b$  and

$a - b$  may be real or complex depending on the values of the constants. If they are complex, the circuit will oscillate. For the critical case a value of  $L$  can be chosen which will make the constant  $b$  equal to zero. Because  $b$  also appears in the denominator of the equation, this makes the transient theoretically infinite in magnitude but of very short duration.

If one recalls that  $\mu$  and  $R_p$  are constants only as long as the path of operation is on a linear portion of the tube characteristics, it is evident that the output voltage peaks will not actually become infinite. There are two values of inductance that will make the constant  $b$  equal to zero. For the above circuit, they are  $L = 11.165$  and  $L = 0.272 \times 10^{-3}$  henry.

# Computing Circuit Response to Pulses

By JOHN B. TREVOR, Jr.

A method is outlined for computing the voltage across a particular element of a network at any desired cycle after application of a repetitive discontinuous wave form, such as a rectangular pulse. General equations are given and a numerical example is worked out

IF A wave form consists of a number of cycles that cannot be expressed by a limited number of harmonically related sinusoidal terms, and yet successive cycles are identical, we have a repetitive discontinuous wave form. An example of such a voltage wave form is a train of rectangular pulses.

A method will be outlined here for the computation of circuit responses to repetitive discontinuous voltage wave forms. As compared with alternative methods,<sup>1,2</sup> the mathematical development is simpler and a clearer physical picture is obtained. A general description of the method will be given, illustrated by working out a specific application.

## General Statement of Problem

In Fig. 1a a source of voltage  $e$  is connected to a load  $Z$ . The voltage wave form is as shown in Fig. 1b. During the interval  $0 \leq t \leq \tau$ , the voltage can be expressed by the function  $f(t)$ . At  $\tau$  there is a discontinuity, and from  $\tau$  to  $T$ , the end of the cycle, the voltage is expressed by the function  $\rho(t - \tau)$ , where  $t$  has any value between  $\tau$  and  $T$ . It is required to find a circuit response  $e'$  where  $e'$  is the voltage across a particular element of the network, during the  $n$ th cycle. In the case shown in Fig. 1b, there is a single discontinuity in the voltage wave form at  $t = \tau$ . It may happen that there is more than one discontinuity, or it may happen that  $\rho(t - \tau)$  is zero.

With  $\rho(t - \tau)$  zero, if the interval  $(T - \tau)$  is sufficiently long so that

the response is effectively zero before the commencement of the next cycle, the problem reduces to one that can be solved by conventional methods. This is done by setting up two equations, one for the period when the emf has a finite value, and the second for zero applied emf. The first of these equations will have initial conditions corresponding to rest conditions for the circuit, while the initial conditions for the second equation will be found from the value of the first equation at the instant  $t = \tau$ .

## First Step in Solution

The general case, where at the end of the cycle the response is not zero, will now be investigated. The first step consists in finding the response for the first cycle. At the instant before the

start of the first cycle, there is zero response, hence the initial conditions will be given by, in the notation of Fig. 1, the response to  $f(t)$  at  $t = 0$ . Now  $f(t)$  expresses the emf until some time  $\tau$ , where  $\tau \leq T$ . If  $\tau = T$ ,  $e'$  for the first cycle has been evaluated. In case  $\tau < T$ , the response over the interval  $\tau \leq t \leq T$  must be found. The equation for the response over the second interval is obtained by solving for the response to  $\rho(t - \tau)$ , with initial conditions appropriate to the value of the energy stored in the network at  $t = \tau$  due to  $f(t)$ . The first step in the solution for the response to the  $n$ th cycle of emf is then the solution for the response to the first cycle.

The steps in the solution will be illustrated by solving an actual example. The network of Fig. 2 is excited by a source of d-c potential which is connected to the network through switch  $S$ . This switch is closed cyclically for an interval  $\tau$  and opened for an interval  $(T - \tau)$ . The switch may be a rotating commutator or some type of relay that is repetitively energized and de-energized. The resist-

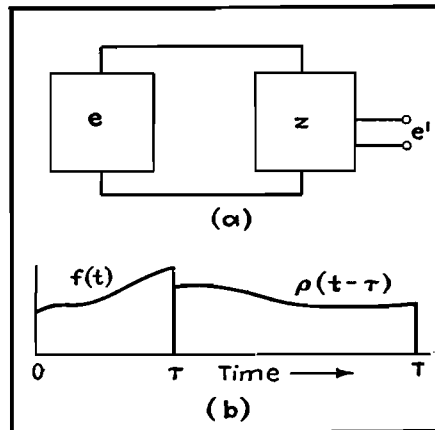


Fig. 1.—Block diagram (a) and voltage wave-form (b) for the problem under consideration.

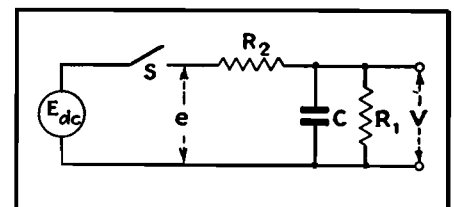


Fig. 2.—Network used as actual example in illustrating the various steps involved in solution of the problem.

ance of the voltage source is lumped with series circuit resistance in  $R_2$ . It is required to find  $V_n$ , the voltage across  $C$  during the  $n$ th cycle. The applied emf will have the following form:

$$e = f(t) = E \quad (1)$$

$$\text{where } 0 \leq t \leq \tau$$

$$e = \rho(T - \tau) = 0$$

$$\text{where } \tau \leq t \leq T$$

The emf is then a pulse of period  $T$  and of length  $\tau$ . The fact that  $\rho(t - \tau)$  is zero simplifies the equations of the example, but does not result in any loss of generality since it is assumed that at  $T$  the response is not virtually zero.

It can be shown<sup>3</sup> that, for the first cycle,

$$i_1 = E \left( \frac{1}{R_1 + R_2} \right) \left( 1 + \frac{R_1}{R_2} e^{-\frac{R_1 + R_2}{R_1 R_2 C} t} \right) \quad (2)$$

where  $0 \leq t \leq \tau$ .

Here  $i_1$  is the current through  $R_2$ , the subscript of  $i$  referring to the first cycle.

From Eq. (2), since  $V = E - iR_2$ , where  $0 \leq t \leq \tau$ ,

$$\alpha_1 = \frac{R_1 + R_2}{R_1 R_2 C} \quad (3)$$

$$\beta = \frac{R_1}{R_1 + R_2} \quad (4)$$

Now  $V$  is given by

$$V_1 = E\beta(1 - e^{-\alpha_1 t}) \quad (5)$$

where  $0 \leq t \leq \tau$ .

The subscript of  $V$  again indicates the first cycle.

Equation (5) gives  $V_1$  for the first part of the cycle only. The value of  $V_1$  for the second part of the cycle will now be found. At  $t = \tau$ , from Eq. (5)

$$V_1 = E\beta(1 - e^{-\alpha_1 \tau}) \quad (6)$$

With  $S$  open, it is evident that  $C$  discharges through  $R_1$  alone and we can write

$$V_1 = E\beta(1 - e^{-\alpha_1 \tau}) e^{-\alpha_2(t-\tau)} \quad (7)$$

where  $\tau \leq t \leq T$

$$\text{and } \alpha_2 = \frac{1}{R_1 C}$$

Equations (5) and (7) give  $V_1$  for the entire first cycle from  $t = 0$  to  $t = T$ . This completes the first step in the solution.

#### Evaluation of Response for Following Cycles

At the end of the first cycle the response has a finite value different from zero. It is therefore to be expected that the response to the second cycle will not be identical with the response to the first cycle. The superposition theorem is an important aid in evaluating the response

to the second and following cycles. In brief,<sup>4</sup> this theorem states that the response of a network to a number of voltages is equal to the sum of the responses to the individual voltages, if the network is linear.

The superposition theorem allows the response to the  $n$ th cycle to be expressed as the sum of the response to the external emf, which is found for the first cycle, plus the response to the energy stored in the circuit at the end of the  $(n - 1)$  cycle. Beginning with the start of the first cycle, when no energy is stored in the circuit, the response equation or equations are found for the applied emf. These equations are solved for the response at  $t = T$ . Then the response during the second cycle is equal to the sum of the response to the applied emf and the response due to the energy stored in the circuit at  $t = T$  for the first cycle. A similar process yields the response to the third and following cycles. Thus, a general expression for the  $n$ th cycle can be set up. It is of advantage to regard  $t$  as zero at the start of the  $n$ th cycle, and  $(n - 1)$  cycles to the left of the zero point.

This step in the solution will also be illustrated by the example of Fig. 2. As shown previously,

$$V_1 = E\beta(1 - e^{-\alpha_1 t}) \quad (5)$$

where  $0 \leq t \leq \tau$ .

$$V_1 = E\beta(1 - e^{-\alpha_1 \tau}) e^{-\alpha_2(t-\tau)} \quad (7)$$

where  $\tau \leq t \leq T$ .

At the end of the first cycle, from Eq. (7),

$$V_1'' = E\beta(1 - e^{-\alpha_1 \tau}) e^{-\alpha_2(T-\tau)} \quad (8)$$

where  $V_1'' = V_1$  at the end of the first cycle.

But  $V_1'' = V_2'$  (8a)

where  $V_2' = V_2$  at the start of the second cycle. During the interval  $0 \leq t \leq \tau$  of the second cycle, capacitor  $C$  discharges through  $R_1$  and  $R_2$  in parallel, giving rise to a voltage term

$$V_2' e^{-\alpha_1 t}$$

According to the superposition theorem,  $V_2$ , the value of  $V$  for the second cycle, is given by adding this term to Eq. (5)

$$V_2 = E\beta(1 - e^{-\alpha_1 t}) + V_2' e^{-\alpha_1 t} \quad (9)$$

where  $0 \leq t \leq \tau$

and from Eqs. (8) and (8a)

$$V_2 = E\beta[(1 - e^{-\alpha_1 t}) + e^{-\alpha_2(T-\tau)}(1 - e^{-\alpha_1 \tau}) e^{-\alpha_1 t}] \quad (10)$$

where  $0 \leq t \leq \tau$ .

For the remainder of the cycle, where  $\tau \leq t \leq T$ ,  $V_2$  is found by substituting

$t = \tau$  in Eq. (9), and, recalling that the discharge is through  $R_1$  only over this portion of the cycle,

$$V_2 = E\beta[(1 - e^{-\alpha_1 \tau})(1 + e^{-\gamma})] e^{-\alpha_2(t-\tau)} \quad (11)$$

where  $\tau \leq t \leq T$

$$\text{and } \gamma = \alpha_1 \tau + \alpha_2(T - \tau) \quad (11a)$$

In a similar way  $V_3$  can be found. From Eq. (11), letting  $t = T$ ,

$$V_2'' = V_3' = E\beta(1 - e^{-\alpha_1 \tau}) (1 + e^{-\gamma}) e^{-\alpha_2(T-\tau)}$$

Then, from the same considerations used in the derivation of Eq. (10)

$$V_3 = E\beta[(1 - e^{-\alpha_1 t}) + (1 - e^{-\alpha_1 \tau}) e^{-\alpha_2(T-\tau)}(1 + e^{-\gamma}) e^{-\alpha_1 t}]$$

where  $0 \leq t \leq \tau$ , and over the rest of the cycle

$$V_3 = E\beta[(1 - e^{-\alpha_1 \tau})(1 + e^{-\gamma} + e^{-2\gamma})] e^{-\alpha_2(t-\tau)}$$

where  $\tau \leq t \leq T$ .

It is convenient to generalize the results for the second cycle, found in Eqs. (10) and (11), from the superposition theorem, to similar equations for the  $n$ th cycle

$$V_n = E\beta(1 - e^{-\alpha_1 t}) + V_n' e^{-\alpha_1 t} \quad (12)$$

where  $0 \leq t \leq \tau$  and  $1 \leq n \leq \infty$

$$V_n = [E\beta(1 - e^{-\alpha_1 \tau}) + V_n' e^{-\alpha_1 \tau}] e^{-\alpha_2(T-\tau)} \quad (13)$$

where  $\tau \leq t \leq T$  and  $1 \leq n \leq \infty$

Here  $V_n'$  is the initial voltage across  $C$  at the start of the  $n$ th cycle.

#### Expansion and Solution of the General Equations

Having found a general expression for the response during the  $n$ th cycle, it is necessary to expand this equation and solve it in closed form. This solution takes the form of a summation. If there is a discontinuity in the applied emf during the cycle, then there will be two equations, each covering part of the cycle.

Returning to the example of Fig. 2, Eqs. (12) and (13) can be expanded for the  $n$ th cycle. By comparison with the equations for the second and third cycles, the equations for the  $n$ th cycle are

$$V_n = E\beta[(1 - e^{-\alpha_1 t}) + (1 - e^{-\alpha_1 \tau}) e^{-\alpha_2(T-\tau)}(1 + e^{-\gamma} + e^{-2\gamma} + \dots + e^{-(n-2)\gamma}) e^{-\alpha_1 t}]$$

where  $0 \leq t \leq \tau$  and  $\phi \leq n \leq \infty$ .

$$V_n = E\beta(1 - e^{-\alpha_1 \tau})(1 + e^{-\gamma} + e^{-2\gamma} + \dots + e^{-(n-1)\gamma}) e^{-\alpha_2(t-\tau)}$$

where  $\tau \leq t \leq T$  and  $1 \leq n \leq \infty$ .

The terms in the brackets are geometric progressions with the sums

$$\frac{e^{-\gamma(n-1)} - 1}{e^{-\gamma} - 1} \quad \text{and} \quad \frac{e^{-\gamma n} - 1}{e^{-\gamma} - 1}$$

Hence  $V_n$  can be written

$$V_n = E\beta(1 - e^{-\alpha_1\tau}) \left( \frac{e^{-\gamma n} - 1}{e^{-\gamma} - 1} \right) e^{-\alpha_2(t-\tau)} \quad (14)$$

where  $\tau \leq t \leq T$  and  $1 \leq n \leq \infty$

$$V_n = E\beta(1 - e^{-\alpha_1 t}) + E\beta(1 - e^{-\alpha_1\tau}) e^{-\alpha_2(T-\tau)} \left[ \frac{e^{-\gamma(n-1)} - 1}{e^{-\gamma} - 1} \right] e^{-\alpha_1 t} \quad (15)$$

where  $0 \leq t \leq \tau$  and  $1 \leq n \leq \infty$ .

Equations (14) and (15) are a complete solution of the illustrative problem. There are, however, a number of other results which are of some interest.

### Steady-state Solution

Having found equations that give the response for all portions of the  $n$ th cycle, it is convenient to let  $n \rightarrow \infty$  and derive equations equivalent to the steady-state equations for sine-wave emf's.

In the case of Eqs. (14) and (15), the steady-state equations, found by letting  $n \rightarrow \infty$ , are

$$V_\infty = E\beta(1 - e^{-\alpha_1\tau}) \left( \frac{1}{1 - e^{-\gamma}} \right) e^{-\alpha_2(t-\tau)} \quad (16)$$

where  $\tau \leq t \leq T$

$$V_\infty = E\beta(1 - e^{-\alpha_1 t}) + E\beta(1 - e^{-\alpha_1\tau}) e^{-\alpha_2(T-\tau)} \left( \frac{1}{1 - e^{-\gamma}} \right) e^{-\alpha_1 t} \quad (17)$$

where  $0 \leq t \leq \tau$  and the subscript  $\infty$  for  $V$  indicates  $n \rightarrow \infty$ .

### Time-constant Formulas

In the example of Fig. 2, the time constant for charging  $C$  may be defined as the number of cycles, multiplied by  $T$ , which it takes for  $V$  to rise to  $(1 - e^{-1})$  of its final value at  $\tau$  as given by Eq. (16). Letting  $N$  be the particular value of  $n$  which gives this result, from the ratio of Eqs. (16) and (14)

$$\frac{V_N}{V_\infty} = (1 - e^{-1}) = \frac{E\beta(1 - e^{-\alpha_1\tau}) \left( \frac{e^{-\gamma N} - 1}{e^{-\gamma} - 1} \right) e^{-\alpha_2(t-\tau)}}{E\beta(1 - e^{-\alpha_1\tau}) \left( \frac{-1}{e^{-\gamma} - 1} \right) e^{-\alpha_2(t-\tau)}} = 1 - e^{-\gamma N}$$

From which

$$N = \frac{1}{\gamma} \quad \text{and} \quad NT = \frac{T}{\gamma} = \frac{R_1 R_2 C}{R_2 + R_1 \tau / T}$$

The time constant for decaying  $V$  when excitation is removed is  $1/\alpha_2 = R_1 C$ .

### Example

The circuit of Fig. 2 will now be solved for the voltage  $V$  across capacitor  $C$  for specific values of  $R_1$ ,  $R_2$ ,  $C$ , and  $E_{d.c.}$ ,

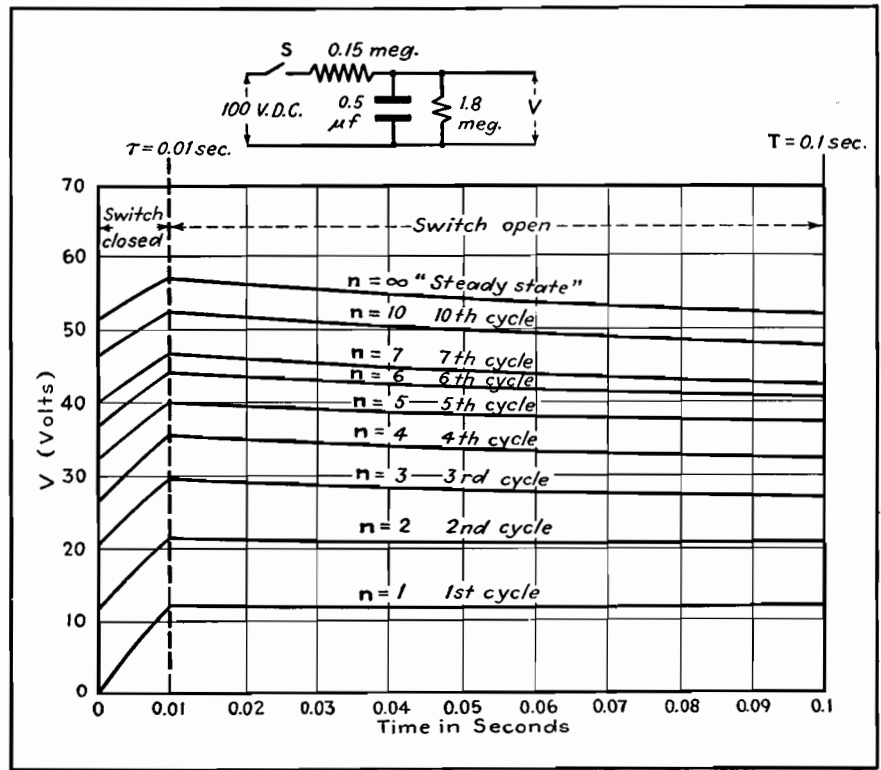


Fig. 3.—Output voltage plotted against time for the first seven cycles, the tenth cycle, and the final steady-state condition in the circuit shown, and for the numerical values and waveform assumed in the example.

where the open-closed cycling of switch  $S$  is specified. Let  $R_1 = 1.8$  megohms,  $R_2 = 0.15$  megohms,  $C = 0.5 \mu f$ , and  $E_{d.c.} = 100$  volts.

Switch  $S$  opens and closes in a cyclic manner such that the period of closure is 0.01 sec and the open period is 0.09 sec. In the notation used previously, this corresponds to  $\tau = 0.01$  sec and  $T = 0.10$  sec.

Let it be required to find the voltage  $V$  of Fig. 2 from the first closure of switch  $S$  until steady-state conditions are established.

From Eq. (8),

$$\alpha_2 = \frac{1}{R_1 C} = 1.11$$

From Eq. (3),

$$\alpha_1 = \frac{R_1 + R_2}{R_1 R_2 C} = 14.45$$

From Eq. (4),

$$\beta = \frac{R_1}{R_1 + R_2} = 0.925$$

and from Eq. (11a),

$$\gamma = \alpha_1 \tau + \alpha_2 (T - \tau) = 0.2444$$

Since the time constant of the circuit of Fig. 2, with a rectangular pulsed wave form, has been shown equal to  $T/\gamma = 0.41$  sec, the fourth cycle will just fail to bring  $V$  up to 0.63 of its final value.

By plotting the first seven cycles, the tenth cycle, and the steady state, the value of  $V$  from the start of the first cycle to the steady state can be shown reasonably well. Substituting the values of  $\alpha_1$ ,  $\alpha_2$ ,  $\beta$ , and  $\gamma$  just found in Eqs. (14) and (15), the transient state is found

$$V_n = 57.1(1 - e^{-0.2444n})e^{-1.11(t-0.01)}$$

where  $0.01 \leq t \leq 0.1$  and  $1 \leq n \leq \infty$

$$V_n = 92.5 - (40.7 + 51.8e^{-0.2444(n-1)})e^{-14.45t}$$

where  $0 \leq t \leq 0.01$  and  $1 \leq n \leq \infty$

The steady-state equations, from Eqs. (16) and (17), are

$$V = 57.1e^{-1.11(t-0.01)}$$

where  $0.01 \leq t \leq 0.1$

$$V = 92.5 - 40.7e^{-14.45t}$$

where  $0 \leq t \leq 0.01$

Figure 3 shows, in graphical form, the value of these equations for the first seven cycles, the tenth cycle, and the steady state.

### References

- (1) GARDNER and BARNES, "Transients in Linear Systems," Vol. I, p. 308.
- (2) CARNAHAN, C. W., The Steady State Response of a Network to a Periodic Driving Force of Arbitrary Shape, *Proc. IRE*, **23**, No. 11, 1393, November, 1935.
- (3) BERG, E. J., "Heaviside's Operational Calculus," p. 19, McGraw-Hill Book Company, Inc., New York.
- (4) THERMAN, F. E., "Radio Engineer's Handbook," p. 198, McGraw-Hill Book Company, Inc., New York.

# Circuit Response to Nonsinusoidal Wave Forms

By P. T. CHIN

Short-cut method of determining the current response either graphically or analytically in circuits energized by square, saw-tooth, repeated exponential, and similar waves, by decomposing into components starting at different instants, then adding responses

FOURIER's analysis<sup>1</sup> is a general method for evaluating the circuit response to nonsinusoidal periodic waves. But it is not always the most convenient method for evaluating the transient response, especially to those nonsinusoidal periodic waves which are discontinuous in the wave itself or its derivative with respect to time. The actual solution of a problem by means of this method is sometimes tedious and time consuming.

Another method, possibly first used by Poisson and later by Duhamel<sup>2</sup> and based on the superposition of step functions, decomposes any kind of waves, periodic or not, into so-called Heaviside unit functions<sup>3</sup> which start at different instants. This method has been used more extensively in treating nonperiodic waves. In fact, it is a very powerful tool for evaluating the circuit response to some types of commonly encountered nonsinusoidal waves that are discontinuous in the wave itself or its derivative

with respect to time, such as square waves, saw-tooth waves, trapezoidal waves, repeated exponential waves, and output voltage waves of controlled rectifiers.

Owing to the geometry of the nonsinusoidal wave, an easier solution can often be obtained; instead of being decomposed into Heaviside unit functions, the wave can be decomposed into waves of other types which have the same wave form but start at different instants. This short-cut method (based on an extension of superposition of step function, generally known as Duhamel's integral) permits determining the transient response easily by either analytical or graphical methods.

## Decomposition of Square Waves

Square waves are used in the communications field for testing the frequency response of electric circuits<sup>4</sup>. A symmetrical square wave having an amplitude

$A$  and a period of  $2t_1$  can be decomposed into a number of different constant-amplitude components starting at different time intervals, as shown graphically in Fig. 1. The first component starts at  $t = 0$  and has an amplitude of  $+A$ . The second starts  $t_1$  later and has an amplitude of  $-2A$ . At interval  $t_1$  after this, the third component starts with an amplitude of  $+2A$ . Thereafter, components of  $-2A$  and  $+2A$  in amplitude start alternately at successive intervals of  $t_1$ .

The decomposition of an unsymmetrical square wave, having unequal positive and negative amplitudes of  $A_1$  and  $A_2$ , respectively, is shown in Fig. 2. The duration of  $A_1$  is  $t_1$ , and that of  $A_2$  is  $t_2$ .

## Saw-tooth and Trapezoidal Waves

Saw-tooth waves can also be used to test frequency response of electrical circuits. In some respects, these waves are superior to square waves, as suggested

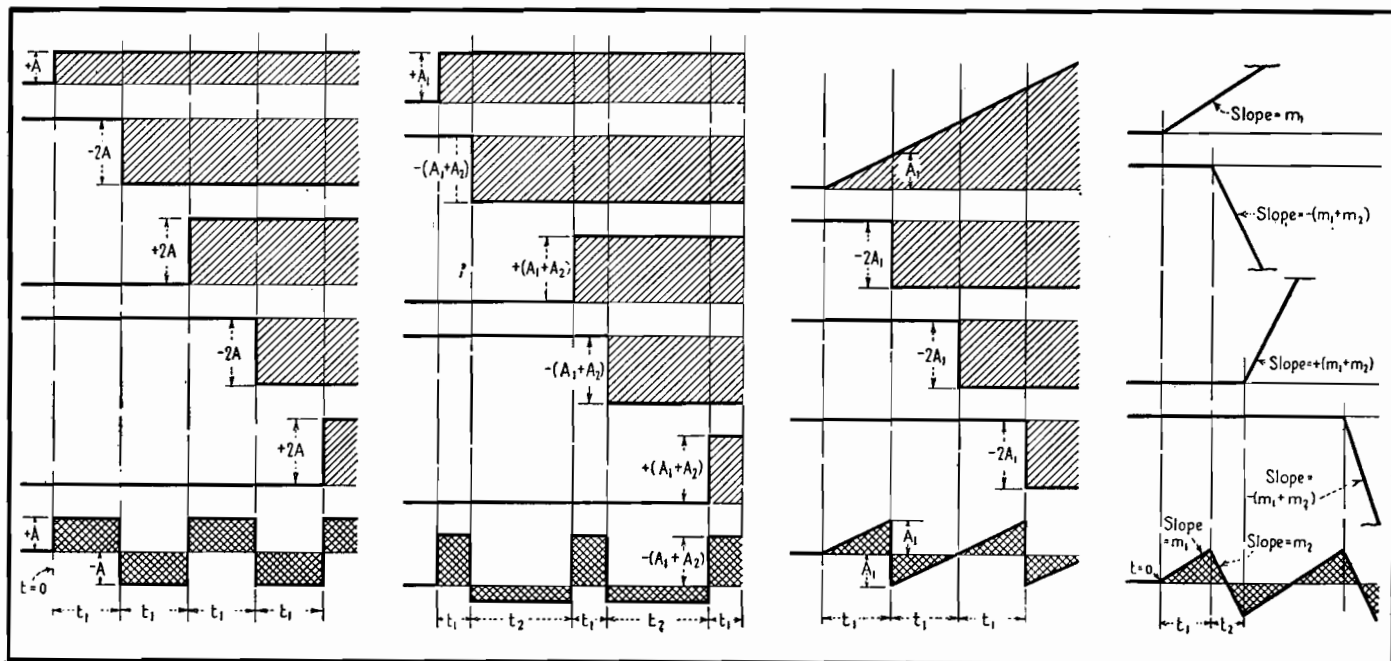


Fig. 1.—Decomposition of symmetrical square waves shown at bottom with double shading.

Fig. 2.—Decomposition of unsymmetrical square wave into components shown above.

Fig. 3.—Decomposition of ideal saw-tooth wave into two types of components.

Fig. 4.—Decomposition of saw-tooth wave into rising and falling components.



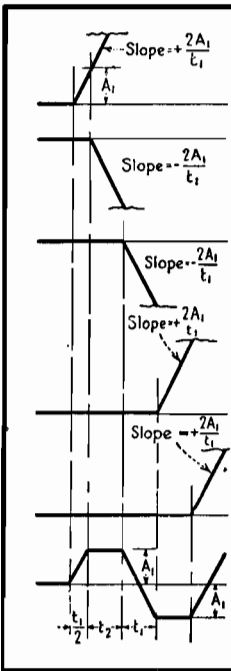


Fig. 5.—Decomposition of trapezoidal waves. Components are cut off here to conserve space.

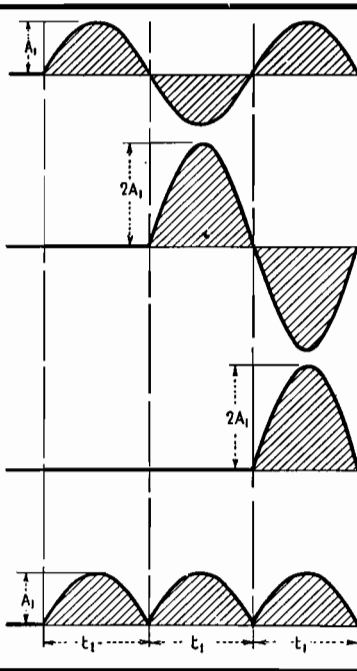


Fig. 6.—Decomposition of output voltage of biphas uncontrolled rectifier; no phase retard.

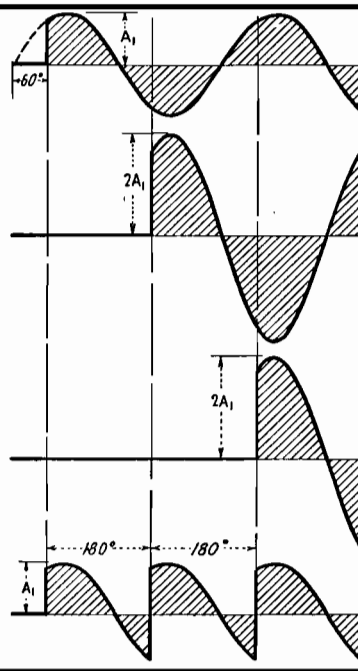


Fig. 7.—Decomposition of output voltage of biphas rectifier, phase retarded 60 deg.

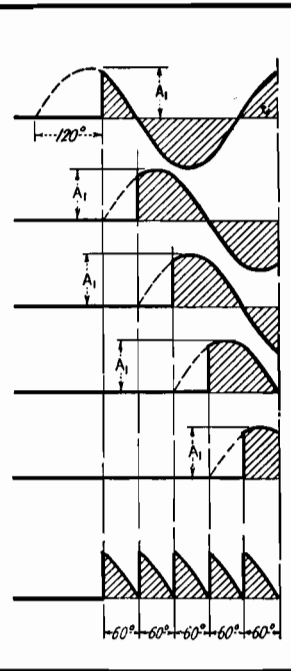


Fig. 8.—Decomposition of output voltage of six-phase rectifier, phase retarded 60 deg.

by Waidelich.<sup>5</sup> An ideal saw-tooth wave, having a slope  $A_1/t_1$  and a period of  $2t_1$ , can be decomposed into a linearly rising voltage having a slope of  $A_1/t_1$  and starting to occur at  $t = 0$ , plus constant driving forces of  $-2A_1$  starting to occur at succeeding intervals of  $t_1$  as shown in Fig. 3.

The saw-tooth waves of Fig. 3 can hardly be produced by practical means, since it takes some time for the saw-tooth wave to fly back to its original position. Figure 4 shows more practical saw-tooth waves which can be produced by some electronic circuits.<sup>6</sup> These waves can be decomposed into a linearly rising wave of slope  $m$ , starting at  $t = 0$ ; a linearly rising wave of slope  $-(m_1 + m_2)$ , starting  $t_1$  later; a wave of slope  $+(m_1 + m_2)$ , starting at  $t_1 + t_2$ ; a wave of slope  $-(m_1 + m_2)$ , starting at  $2t_1 + t_2$ , etc. (The linearly rising waves in Fig. 4 should continue to rise, but in order to save space they are not shown beyond the broken lines.)

Figure 5 shows the decomposition of trapezoidal waves. The procedure is more or less similar to that for saw-tooth waves.<sup>7</sup>

#### Output Voltage Waves of Gaseous Rectifiers

When gaseous-discharge type rectifiers, such as thyatrons and ignitrons, supply an inductive load with continuous conduction of current, the geometry of the

output voltage wave depends on the number of phases of the rectifier circuit and the angle of phase retard.<sup>8</sup>

Figure 6 shows the decomposition of the output voltage wave of a biphas uncontrolled rectifier circuit having no phase retard. It can be decomposed into a continuous sine wave having a peak value  $A_1$ , starting in a positive direction at  $t = 0$ , followed by a series of sine waves each having a peak value of  $2A_1$ , and starting in a positive direction every half-cycle later.

Figure 7 shows the decomposition of the output voltage wave of a biphas rectifier with a phase retard of 60 electrical degrees. It is evident that the decomposition is similar to that shown in Fig. 6 except that each sine wave starts with a magnitude corresponding to the value  $A_1 \sin 60^\circ$  instead of zero.

Figure 8 shows the decomposition of the output voltage wave of a six-phase rectifier. The continuous sine waves are spaced at 60 deg, and all the sine waves have the same peak value  $A_1$ .

#### Repeated Exponential Waves

Repeated exponential waves sometimes occur in television circuits.<sup>9</sup> The period of the waves is  $2t_1$ , and each wave has the expression  $A_1 e^{-at}$ . Figure 9 shows that repeated exponential waves can be decomposed into a exponential wave which starts at  $t = 0$  and has the expres-

sion  $A_1 e^{-at}$ , followed by component waves having the expressions  $-A_1(1 + e^{-at_1})e^{-at}$  and  $+A_1(1 + e^{-at_1})e^{-at}$ , occurring alternately at intervals of  $t_1$ .

Once a nonsinusoidal periodic wave has been decomposed into component waves, the over-all circuit response can be obtained by superimposing the individual circuit responses on the component waves. These responses are similar in their wave form but start at different instants. Two examples, one for a square-wave voltage applied to  $R$  and  $C$  in series and the other for the output current of a biphas controlled rectifier supplying an inductive load, will be used to show the procedure used in both the analytical and graphical versions of this short-cut method of determining circuit response.

#### Circuit Response to Square Waves

Suppose it is required to find the transient response of a circuit to a symmetrical square-wave voltage having a magnitude  $A$  and a period  $2t_1$ . This involves finding the response during the existence of the  $n$ th square wave after the square-wave voltage is applied.

#### Analytical Solution

Taking the analytical solution first, assume that time is zero at the beginning of the  $(n + 1)$ th square wave,  $n$  being an even number. The component waves are as follows:

Component wave	Magnitude	Instant at which wave starts
$n + 1$	$+2A$	0
$n$	$-2A$	$-t_1$
$n - 1$	$+2A$	$-2t_1$
$n - 2$	$-2A$	$-3t_1$
...	...	...
3	$+2A$	$-(n - 2)t_1$
2	$-2A$	$-(n - 1)t_1$
1	$+A$	$nt_1$

Let  $i_{n+1}, i_n \dots i_2, i_1$  be the current responses to the  $(n + 1)$ th,  $n$ th ... 2d and 1st component waves, respectively. Now, since the response of the circuit is a function of time [written  $f(t)$ , with its significance depending on the particular combination of circuit elements in the circuit], the individual circuit responses to the component waves may be specified as follows in the general analytical solution where time is defined as  $t_1 \geq t \geq 0$ :

$$\begin{aligned} i_{n-1} &= 2Af(t) \\ i_n &= -2Af(t + t_1) \\ i_{n-1} &= 2Af(t + 2t_1) \\ &\dots \\ i_2 &= -2Af[t + (n - 1)t_1] \\ i_1 &= Af(t + nt_1) \end{aligned} \quad (1)$$

The total current response is

$$\begin{aligned} i &= i_1 + i_2 + i_3 + \dots + i_n + i_{n+1} \\ &= 2A \sum_{s=1}^n (-1)^{s-1} f(i + st_1) - Af(t + nt_1) \end{aligned} \quad t_1 \geq t \geq 0 \quad (2)^*$$

where  $s$  is any integral number between 1 and  $n$ .

\* Equation (2) is also true when  $n$  is odd.

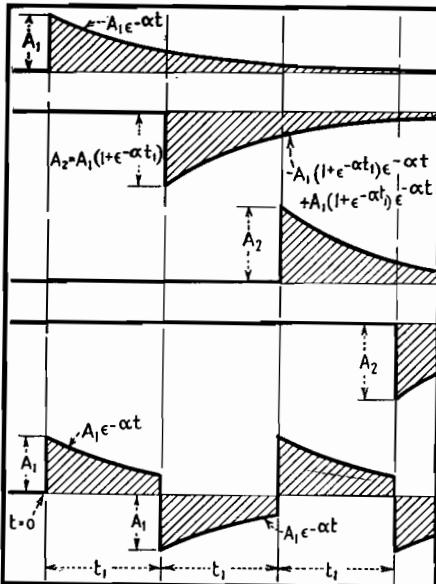


Fig. 9.—Decomposition of repeated exponential waves.

Equation (2) is a general solution of the circuit response to a square wave from its known response to a Heaviside unit function. The steady-state solution can be obtained by making  $n$  approach infinity.

As an example of the analytical solution, suppose the circuit is made of a resistance  $R$  and a capacitance  $C$  in series. The circuit response to a Heaviside unit function  $f(t)$  will be  $(1/R)e^{-t/CR}$ , and the total current response will be

$$i = \frac{2A}{R} e^{-t/CR} \left[ \sum_{s=1}^n (-1)^{s-1} e^{-st/CR} \right] - \frac{A}{R} e^{-\frac{(t+nt_1)}{CR}} \quad t_1 \geq t \geq 0 \quad (3)$$

The expression in brackets is a familiar geometric series. When its sum is substituted in Eq. (3), the total current response becomes

$$i = \frac{2A}{R} e^{-t/CR} \left[ \frac{1 - e^{-\frac{(n+1)t_1}{CR}}}{1 + e^{-\frac{t_1}{CR}}} \right] - \frac{A}{R} e^{-\frac{(t+nt_1)}{CR}} \quad t_1 \geq t \geq 0 \quad (4)$$

The steady-state solution can be obtained by letting  $n$  approach  $\infty$

$$i = \frac{2A}{R} e^{-t/CR} \left( \frac{1}{1 + e^{-\frac{t_1}{CR}}} \right) \quad t_1 \geq t \geq 0 \quad (5)$$

The graphical solution for the current response during the first four square

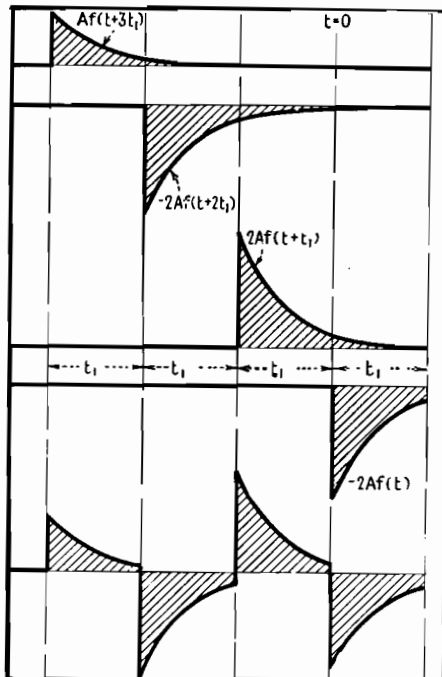


Fig. 10.—Current response where square-wave voltage is applied to  $R$  and  $C$  in series.

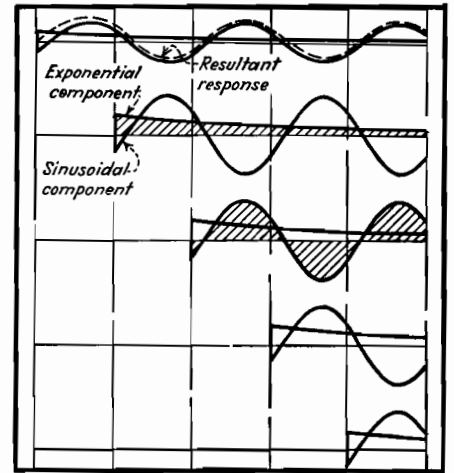


Fig. 11.—Current responses to component voltage waves of a controlled gaseous rectifier for an inductive load.

waves is summarized in Fig. 10. It is performed by plotting the circuit responses to component waves that have a magnitude of  $A$  for the first component and  $-2A$  and  $+2A$  alternatively for the successive components, spaced at a time interval of  $t_1$ . Superimposing all the responses gives the resultant current response, shown at the bottom in Fig. 10. The graphical method is convenient in obtaining the transient response during the first few cycles, but as time goes on, the manipulation becomes more and more tedious and the result less and less accurate.

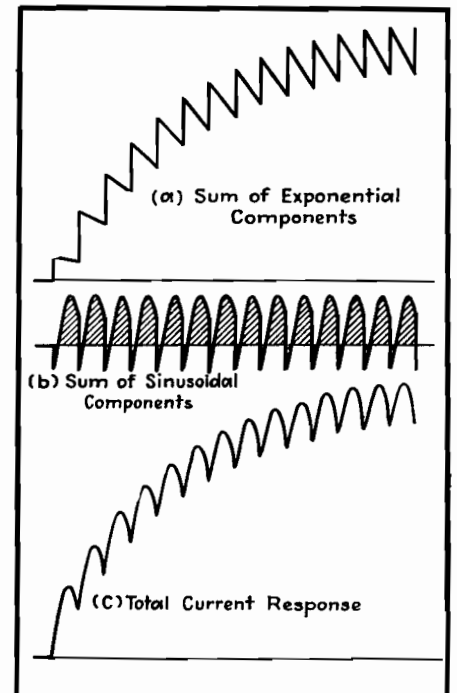


Fig. 12.—Total current response for arrangement of Fig. 11 is obtained by combining each type of component voltage separately then combining the two resultant wave forms.

## Current Response of Biphase Controlled Rectifier

With an inductive load consisting of a resistance and an inductance in series supplied by a controlled rectifier of the gaseous-discharge type, the current during successive conduction periods will be different after the closing of the switch if the conduction is continuous. It is required to find the transient current response at any instant during the existence of the  $n$ th rectified voltage wave after the closing of the switch.

Again starting with the analytical solution, the peak value of the anode voltage is  $A$ . The phase retard of the controlled rectifier can be expressed as  $\theta_f$  electrical degrees. The time interval equivalent to 180 electrical degrees is  $t_1$ , and is equal to  $\pi/\omega = 1/2f$ . The beginning of  $n$ th rectified wave is taken as the zero axis of time.

Component wave	Magnitude	Time at which wave starts	
		Elec. deg.	Sec.
$n$ th	$2A$	0	0
$(n-1)$ th	$2A$	$2\pi$	$-t_1$
$(n-2)$ th	$2A$	$2\pi$	$-2t_1$
.....	.....	.....	.....
2	$2A$	$(n-2)\pi$	$-(n-2)t_1$
1	$A$	$(n-1)\pi$	$-(n-1)t_1$

The transient current response of an inductive load consisting of  $R$  and  $L$  in series to a unit sinusoidal wave closing at  $\sin(\omega t + \theta_f)$  is<sup>10</sup>

$$i = \frac{1}{Z} \sin(\phi - \theta_f) e^{-\alpha t} + \frac{1}{Z} (\omega t - \phi + \theta_f) \quad (6)$$

where  $Z = [(\omega L)^2 + R^2]^{0.5}$

$$\theta = \tan^{-1} \frac{\omega L}{R}$$

$$\alpha = \frac{R}{L}$$

Then the current responses to component waves are

$$i_n = \frac{2A}{Z} \sin(\phi - \theta_f) e^{-\alpha t} + \frac{2A}{Z} \sin(\omega t - \phi + \theta_f)$$

$$i_{n-1} = \frac{2A}{Z} \sin(\phi - \theta_f) e^{-\alpha(t+t_1)} + \frac{2A}{Z} \sin(\omega t - \phi + \theta_f + \pi)$$

$$\dots\dots\dots$$

$$i_2 = \frac{2A}{Z} \sin(\phi - \theta_f) e^{-\alpha[t+(n-2)t_1]} + \frac{2A}{Z} \sin[\omega t - \phi + \theta_f + (n-2)\pi]$$

$$i_1 = \frac{A}{Z} \sin(\phi - \theta_f) e^{-\alpha[t+(n-1)t_1]} + \frac{A}{Z} \sin[\omega t - \phi + \theta_f + (n-1)\pi]$$

$$t_1 \geq t \geq 0 \quad (7)$$

The total current response is

$$i = i_1 + i_2 + \dots + i_{n-1} + i_n$$

$$= \frac{2A}{Z} \sin(\phi - \theta_f) e^{-\alpha t} \left( \frac{1 - e^{-n\alpha t_1}}{1 - e^{-\alpha t_1}} \right) - \frac{A}{Z} \sin(\phi - \theta_f) e^{-\alpha[t+(n-1)t_1]} + \frac{A}{Z} \sin(\omega t - \phi + \theta_f)$$

$$t_1 \geq t \geq 0 \quad (8)$$

The steady-state solution, with  $n \rightarrow \infty$ , is

$$i = \frac{2A}{Z} \sin(\phi - \theta_f) \frac{e^{-\alpha t}}{1 - e^{-\alpha t_1}} + \frac{A}{Z} \sin(\omega t - \phi + \theta_f)$$

$$\pi \geq \omega t \geq 0 \quad (9)$$

Figure 11 shows the current responses to the component waves graphically. The exponential and sinusoidal components for each component wave are plotted separately. The resultant of exponential components, which is in the form of stepped exponential waves, is shown in Fig. 12a. The sum of all sinusoidal components, which is a discontinuous

periodic wave consisting of 180 electrical degrees of sine wave starting from  $\sin(\phi - \theta_f)$ , is shown in Fig. 12b. The total response is the sum, shown in Fig. 12c.

## Conclusions

The principle of decomposing some types of nonsinusoidal waves into waves of the same wave form but starting at different instants can be utilized as a short-cut method to obtain both the transient and the steady-state circuit responses to these waves.

The mathematical analysis involved in this method is comparatively simple and fundamental. It can be performed by those who do not have an adequate training in higher engineering mathematics, such as Laplacian transformation often used as a tool in solving problems of this nature.

The graphical analysis is very convenient for evaluating the transient response during the first few cycles, but may become more tedious and less accurate for evaluating the steady-state response, especially for circuits with large time constants.

## References

- (1) KARMAN and BIOT, "Mathematical Methods in Engineering," p. 382, McGraw-Hill Book Company, Inc., New York, 1940.
- (2) GARDNER and BARNES, "Transients in Linear Systems," p. 364, John Wiley & Sons, Inc., New York, 1942.
- (3) Reference (1), p. 394.
- (4) BARTELINK, E. H. B., A Wide Band Square Wave Generator, *Elec. Eng.*, **60**, No. 6, 371, June, 1941.
- (5) WAIDELICH, D. L., Steady-State Testing with Saw-tooth Waves, *Proc. IRE*, **32**, No. 6, 339, June, 1944.
- (6) PUCKLE, O. S., Time Bases, *Jour. Inst. Elec. Engrs. (London)*, **89**, Part III, No. 6, 100, June, 1942.
- (7) Reference (1), p. 435.
- (8) COBINE, "Gaseous Conductors," McGraw-Hill Book Company, Inc., New York, 1941.
- (9) CLARKE, A. C., More Television Waveforms, *Electronic Eng.*, **15**, No. 177, 245, November, 1942.
- (10) KURTZ and CORCORAN, "Introduction to Transients," p. 151, John Wiley & Sons, Inc., New York, 1935.

# Square-wave Harmonic Amplitude Table

By DONALD L. HERR

A tabular compilation of the relative amplitudes of the harmonic components of square waves of unity amplitude computed to the thirtieth harmonic, for pulse widths from 10 to 90 per cent of the total period

IN THIS table are tabulated the first 30 harmonics in square waves of zero to 100 per cent pulse width, in steps of

10 per cent pulse width. The harmonics have been computed on the basis of unit pulse amplitude and  $x$  per unit pulse

width, as shown in Fig. 1. For pulse widths up to and including 50 per cent ( $x \leq 0.50$ ) the harmonic amplitudes,

Order of harmonic	Pulse width, per cent of total period of the wave				
	(90) 10	(80) 20	(70) 30	(60) 40	50
(Fundamental) 1	0.197	0.374	0.515	0.605	0.637
2	0.187	0.302	0.302	0.187	0
3	0.172	0.202	0.0656	-0.125	-0.213
4	0.150	0.0936	-0.0936	-0.151	0
5	0.127	0	-0.127	0	0.127
6	0.101	-0.0635	-0.0624	0.101	0
7	0.0738	-0.0866	0.0281	0.0471	-0.0910
8	0.0468	-0.0758	0.0758	-0.0468	0
9	0.0218	-0.0416	0.0573	-0.0675	0.0707
10	0	0	0	0	0
11	-0.0179	0.0341	-0.0469	0.0551	-0.0578
12	-0.0312	0.0504	-0.0504	0.0312	0
13	-0.0397	0.0281	-0.0152	-0.0288	0.0490
14	-0.0432	0.0267	0.0267	-0.0432	0
15	-0.0424	0	0.0424	0	-0.0424
16	-0.0378	-0.0234	0.0234	0.0378	0
17	-0.0303	-0.0356	-0.0116	0.0220	0.0374
18	-0.0208	-0.0336	-0.0336	-0.0208	0
19	-0.0104	-0.0197	-0.0271	-0.0318	-0.0335
20	0	0	0	0	0
21	0.00936	0.0178	0.0245	0.0288	0.0303
22	0.0170	0.0275	0.0275	0.0170	0
23	0.0224	0.0263	0.00853	-0.0162	-0.0277
24	0.0252	0.0156	-0.0156	-0.0252	0
25	0.0255	0	-0.0255	0	0.0255
26	0.0233	-0.0144	-0.0144	0.0233	0
27	0.0190	-0.0224	0.00728	0.0139	-0.0236
28	0.0134	-0.0216	0.0216	-0.0134	0
29	0.00681	-0.0129	0.0178	-0.0208	0.0220
30	0	0	0	0	0

with proper signs, are obtained directly from the table. The harmonic amplitudes for a square wave with pulse width greater than 50 per cent ( $x > 0.5$ ) are numerically equal but opposite in sign to those of the square wave with per unit pulse width  $1 - x$ .

The amplitudes of the sinusoidal components form the group

$$\frac{2}{\pi} \left[ \frac{1}{m} \sin(m\pi x) \right]$$

where  $m$  is the order of the harmonic. Values of  $m$  that are integral multiples of  $1/x$  correspond to harmonics of zero amplitude. For  $0 < x < 1$ , the amplitudes of the higher order harmonics approach zero in value. For  $x$ , very

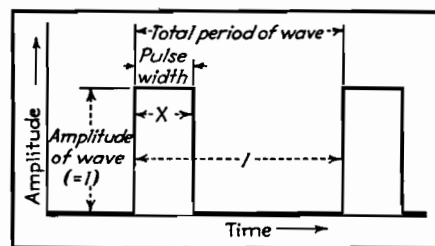


Fig. 1.—Basic pulse.

small (corresponding to very narrow pulses), the amplitudes of the lower order harmonics all approach the same value,  $2x$ . The values are obtained from a Fourier expansion throughout the interval  $t = 0$  to  $t = 1$ .

For the wave form of Fig. 1, using the base line as reference,

$$f(t) = \begin{cases} 1, & 0 < t < x \\ 0, & x < t < 1 \end{cases} \quad (1)$$

In general, for a Fourier expansion throughout the interval  $c$ ,

$$f(t) = \frac{1}{2} b_0 + b_1 \cos \frac{\pi t}{c} + b_2 \cos \frac{2\pi t}{c} + \dots + b_m \cos \frac{m\pi t}{c} + \dots \quad (2)$$

where

$$b_m = \frac{2}{c} \int_0^c f(t) \cos \frac{m\pi t}{c} dt \quad (3)$$

By virtue of Eq. (1) the expression for the coefficients becomes

$$b_m = 2 \int_0^x \cos m\pi t dt \quad (4)$$

from which  $\frac{1}{2} b_0 = x$

$$b_m = \frac{2 \sin m\pi x}{\pi m}$$

From Eq. (2), therefore,

$$f(t) = x + \frac{2}{\pi} \sum_{m=1}^{\infty} \frac{1}{m} \sin m\pi x \cos m\pi t \quad (5)$$

using the base line as reference.

## Square Waves for Impedance Measurements

By FRANK ROCKETT

Description of equipment and procedures for determining capacitance and inductance, as well as natural frequency, distributed capacitance, resistance, and  $Q$  of inductors, by oscilloscopic observation of square-wave decay rates. Results of actual measurements are given, showing accuracy

INTEREST in square waves has centered around their utility in indicating the transient reaction and wide-band response of circuits. In addition, square waves can be used to measure impedances by

the following method. It employs a minimum of calibrated equipment, is simple in circuit and operation, rapid, and, with the precautions described below, highly accurate.

Advantages of square waves for testing lie in their multiple-frequency content. For example, in determining resonant frequency of a circuit, square-wave response indicates where the resonant

frequency lies, irrespective of what square-wave test frequency is being used.

On the other hand, the sine-wave response of the circuit will not give an indication until the test frequency has been adjusted approximately to the resonant frequency. Where the resonant frequency is altogether unknown, positive indication obtained from a square wave of any frequency eliminates the time-consuming necessity of hunting for the unknown frequency as in sine-wave testing.<sup>1</sup>

### Apparatus Requirements

Equipment needed for square-wave impedance measurements includes a square-wave generator of known frequency, a calibrated or standard impedance, and a cathode-ray oscilloscope. Either the square-wave frequency or the calibrated impedance must be variable (preferably the frequency if it must be one and not the other), but the range over which measurements can be made is greatly extended if both are made variable. Output impedance of the square-wave generator should be at most one-tenth the smallest impedance to be measured. If it is not low enough, a cathode follower<sup>2</sup> can be added, as in Fig. 1. The input impedance of the oscilloscope should be at least ten times larger than the largest impedance to be measured. As will be shown, this impedance can be as high as the grid input of a vacuum tube. If inductance or capacitance is to be measured, the calibrated impedance is a resistance. To measure resistance, a calibrated capacitor is the more useful, although an inductor can be used if necessary.

Consider the circuit of Fig. 2a. It can be shown by operational analysis that if the generator provides a square wave of frequency  $F = 1/(2\pi RC)$  the voltage developed across  $R$  is of the form in Fig. 2b. This voltage across  $R$  decays during a half cycle to 0.043 of its initial value. An oscilloscope across  $R$  is used to observe this decay of resistor voltage.

When the square-wave frequency or the resistance, as the case may be, has been adjusted so that the output voltage decays to 4.3 per cent of its maximum value, the impedance  $X_C$  equals the resistance  $R$ , or  $C = 1/(2\pi fR)$ . If the square-wave frequency is that frequency at which information is required, the measurement directly gives  $X_C = R$ . Because of this relation, the technique is referred to as equal-impedance measurement.

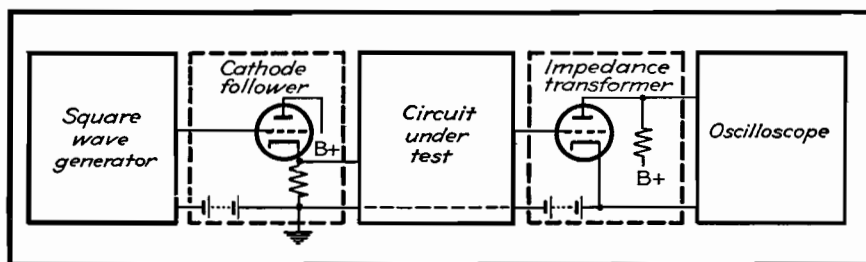


Fig. 1.—Cathode follower decreases output impedance of generator while impedance transformer increases input impedance of oscilloscope in the general setup of equipment used for square-wave testing.

That the specified condition has been reached can readily be observed from the scale on the face of the oscilloscope. If the time base of the oscilloscope is used and it is the frequency that is being varied, it is necessary simultaneously to readjust the sweep rate of the oscilloscope. The oscilloscope trace will be as shown in Fig. 2b. However, if no sweep is used—just vertical deflection—the trace will be as shown in Fig. 2c. In addition, the trace can be located on the oscilloscope screen by means of the vertical centering control so as to eliminate most of the lower half of the trace, thereby taking full advantage of the screen size as illustrated in Fig. 2d.

If resistance is to be measured, the calibrated capacitor is inserted for  $C$  and the unknown resistor for  $R$ . Resistance is given by  $R = 1/(2\pi fC)$ .

If inductance is to be measured, the procedure is the same except that the voltage developed across the inductor is applied to the oscilloscope. To make use of the voltage developed across the resistor in measuring inductance, it is necessary to compare it with the applied square-wave voltage in order to observe the equal-impedance condition of Fig. 3b. This procedure requires an arrangement such as an electronic switch. It has given less reliable results than the preceding method—doubtless because of this added complication. Inductance is given by  $L = R/(2\pi f)$ .

### Time-constant Method

An alternative to the preceding is to use a square wave with a repetition period of  $2T$  where  $T$  is the time constant of the  $RL$  or  $RC$  circuit under study. That is, the period of a half cycle of the square wave is adjusted to equal the time constant of the circuit, with the result that by the end of each half cycle the output wave has fallen to 36.8 per cent of its initial value (see Fig. 3a). Capacitance is given by  $C = 1/(2\pi fR)$ , and inductance by  $L = R/(2\pi f)$ .

This choice of repetition rate has the advantage of interrupting the decay voltage at a point of greater slope than in the equal-impedance method. Dimensions of the image on the oscilloscope are more sensitive to changes in circuit parameters, and hence, as a measuring method, the time-constant repetition rate has an advantage. However, the amplitude of the initial output voltage, as well as the final decay value, changes rapidly with circuit changes—which is not the case if frequencies near the equal-impedance frequency are in use.

Aside from being a source of annoyance during adjustments—it can be compensated for by continuous manipulation of the oscilloscope gain—this is no drawback. As a matter of technique the equal-impedance method may be preferred; it is quicker. But for higher accuracy,

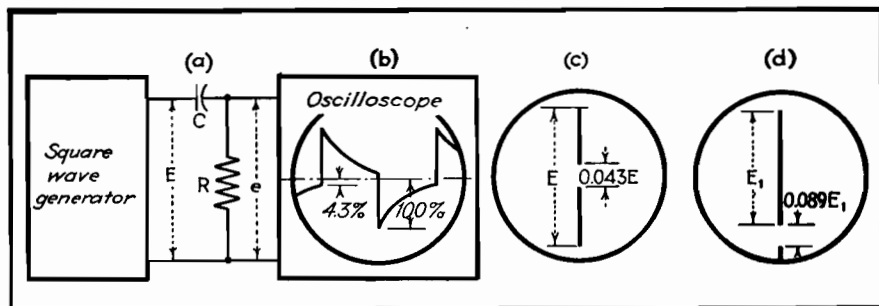


Fig. 2.—Circuit response to a square wave of frequency  $1/(2\pi RC)$  follows the law  $e = Ee^{-t/RC}$  decaying from an initial value of 100 per cent to a final value of 4.3 per cent as at (b). Without sweep the trace appears as in (c). Moving the trace off center (d) increases the accuracy.

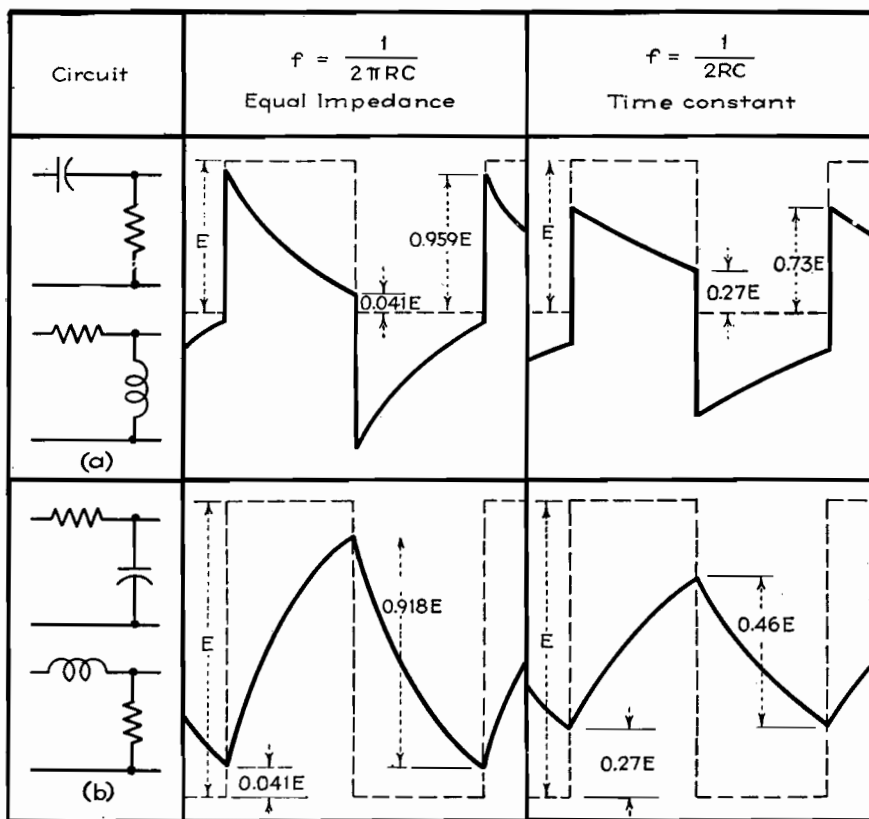


Fig. 3.—High-pass (a) and low-pass (b) circuit outputs and inputs are compared for square-wave frequencies of equal impedance and time-constant conditions.

justifiable only if the precautions described previously are observed, the time-constant method is superior.

With a particular set of equipment, the two methods can be used interchangeably to extend the range over which measurements can be made. For example, if the h-f response of the equipment is limited and the calibrated resistance fixed, use of the time-constant method will permit measuring capacitors  $\pi$  times as large as could be measured by the equal-impedance rate.

#### Extensions of the Method

It is conceivable that other repetition rates could be used. The two frequencies mentioned have been chosen because of their particular significance in circuit analysis. One extension of the response analysis to a square wave of the equal-impedance frequency, which indicates the reason for making measurements at this particular frequency, is in determining the cutoff frequencies of filters or amplifiers.

Cutoff frequencies of communication circuits are often taken in sinusoidal analysis as those at which the output is half the mid-frequency power. This condition occurs at the equal-impedance frequency in simple  $RL$  and  $RC$  networks.

Because of the cascading of impedances

and the use of compensation networks, the decay curves of communication circuits will no longer be simple exponentials, as in Fig. 3. However, the square-wave frequency at which the output decays to 4.3 per cent of its initial value can still be taken as the low cutoff frequency. Thus the equal-impedance method can be used to measure low cutoff frequencies of complex circuits. A similar extension of the method can be made to measure high cutoff frequencies.

Caution must be used in making this extension because it is the deviation from the exponential curve which reveals most about communication circuits. This method considers only the information obtainable from the end points of the circuit response to square waves. Similar use can, with reservations, be made of the time-constant method, and to measure h-f cutoff.

#### Measurement of Q Factor

Inductors, because of their distributed capacitances, have self-resonant frequencies above which they behave as capacitors. In choosing chokes and transformers, it is necessary to know not only their inductances, but also the frequency ranges over which they are inductive. By square-wave measurement, the self-reso-

nant frequency of an inductor and its resonant  $Q$  can be determined.

The reactance of the inductor is measured by the previous technique. The inductor is then connected between the high sides of the square-wave generator and the oscilloscope; the low sides of the instruments are directly connected as in Fig. 4a.

When excited by the multiple-frequency transient of the square wave, the inductor oscillates at its natural period with the result that there is a damped sine wave superimposed on the square wave which is being applied to the oscilloscope through the inductor (Fig. 4b). The number of oscillations per cycle of the square wave, times the square-wave frequency, gives the natural frequency ( $f_0$ ) of the inductor.

The square-wave frequency should be adjusted so that a whole number of cycles appears on each cycle of the square wave, because counting fractions is difficult. Also, the square-wave frequency should be considerably lower (one-tenth is a convenient ratio) than the natural frequency of the inductor. This is partly because, as the square-wave frequency approaches the self-resonant frequency of the inductor, it forces the oscillations to the extent of changing their frequency, and partly because, with

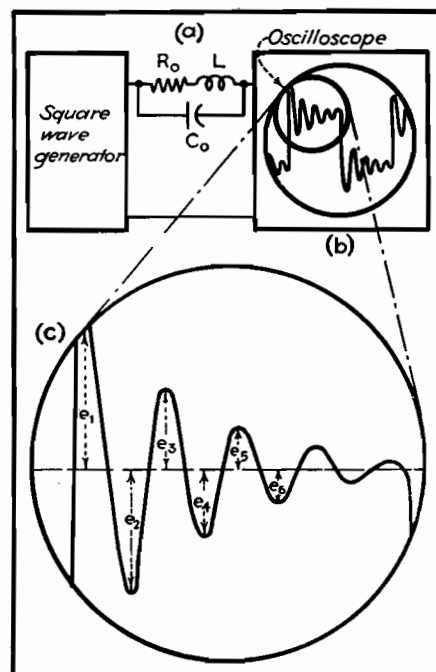


Fig. 4.—Equivalent inductor circuit (a) and square-wave response (b) enlarged in (c) from which come values for determining natural frequency  $f_0 = nF$ , where  $n$  is the number of cycles per cycle of square wave and  $F$  is the square-wave frequency  $R_0 = 2Lf_0 \log_e(e_3/e_5)$ ;  $C_0 = 1/(2\pi f_0)^2 L$ ; and  $Q_0 = \pi/\log_e(e_3/e_5)$ .

but a few cycles of oscillation per cycle of square wave, errors in estimating fractions or in observing when there are none, increase.

There is no gain in using a square-wave frequency lower than one-twentieth  $f_0$  because of the large number of cycles per square wave that must then be counted. The half period of the lowest square wave that can be used must be no longer than the oscillation decay time of the self-resonant inductor.

The rate of decay of the oscillation is used to measure the a-c resistance of the inductor at its natural frequency. Because the impedance of the inductor at its resonant frequency is more dependent on the  $Q$  of the inductor in this range than it is on the simple inductance, the coil resistance at the natural frequency ( $R_0$ ) is of greater significance at the upper frequency limit of usability.

This method is illustrated in Fig. 4c. Transformers can be treated as combinations of self- and mutual inductances, each having its own natural frequency and apparent a-c resistance. Critical damping can be quickly determined by this same method. Resonant circuits of all types can likewise be measured.

### Neutralizing Impedance Effects

The input impedance of the oscilloscope reduces the shunt-arm impedance, while the output impedance of the square-wave generator increases the series-arm impedance of the test circuit. Rather than attempt to correct analytically for these impedances, which can well be complex, it is better to remove their effect, especially since to do so is easy.

Reducing the output impedance of the square-wave generator by means of a cathode follower has been discussed. If the output impedance of the square-wave generator has a d-c path, as it will if a cathode follower is used, all the foregoing circuits provide d-c grid returns. Therefore, an impedance transformer can be placed ahead of the oscilloscope, presenting to the test circuit merely the grid loading of a vacuum tube (Fig. 1).

With the input and output impedance effects minimized, the only remaining limitation on the range of utility of this method is that of frequency. The percentage deviation of the wave produced by the generator from an ideal square wave is the minimum percentage of error to which impedance measurements can be made. The amplitude and phase shift

response of the oscilloscope must be linear from at least ten times the highest square-wave frequency at which tests are to be made, to one-tenth the lowest.

To determine the frequency range within which the equipment is reliable, the generator output should be observed on the oscilloscope to be used. This procedure does not indicate which of the instruments is at fault but, because distortion in either one is equally detrimental to accuracy, it does indicate the usable range for the combined equipment.

Stray shunt capacitances to ground must be kept small. Such strays are most likely to appear from the unknown impedance to surrounding metal such as the cases of the generator and oscilloscope. Even at moderately high frequencies, lead inductance distorts square waves, and therefore it is necessary to hold all lead lengths to a minimum. Because of the wide frequency response of the oscilloscope, the circuit must be shielded from stray fields.

### References

- (1) BRAILSFORD, H. D., Measuring Coil Characteristics without an Impedance Bridge, *Electronics*, May, 1943.
- (2) RICHTER, WALTHER, Cathode Follower Circuits, *Electronics*, November, 1943.



## SECTION XVII RECTIFIERS

	Page
Behavior of Half-wave Rectifiers.....	224
Half-wave Gas Rectifier Circuits.....	226
Full-wave Rectifier Analysis.....	229
Filter Performance Charts for Half-wave Rectifiers.....	233
Rectifier Filter Design.....	236
Filter Design for Grid-controlled Rectifiers.....	239

# Behavior of Half-wave Rectifiers

By M. B. STOUT

The wave forms of the output voltage and current of a half-wave single-phase rectifier with various types of load are analyzed by means of Fourier's series. The d-c fundamental frequency and some harmonic terms are computed for the circuits discussed

THE analyses presented here are made by means of a Fourier series representation of voltage and current wave forms. The series method is a convenient way to express recurring wave forms. Also, if the voltage at the input terminals of the rectifier load circuit is expressed properly by a series, the corresponding current series can be obtained by applying to each voltage term the impedance of the circuit for that frequency.

The series method can be applied to multisection filters for which the differential equation or the operational method is difficult; moreover, it has the virtue of showing directly the harmonic components. The analyses given here show the wave form and the series terms for the circuit input voltage, as well as for the current, as the input voltage takes many forms with a half-wave rectifier, depending on the type of load.

Curves are presented to show the behavior of a half-wave rectifier with several types of load.<sup>1</sup> The results shown here are computed on the basis of a perfect rectifier, i.e., a rectifier having zero voltage drop across it for conduction periods and zero reverse current for nonconduction periods. A power supply of sinusoidal wave form and negligible impedance is also assumed. The perfect rectifier is used here as it is desired to

show general circuit characteristics rather than the peculiarities of any particular type of rectifier. However, rectifier imperfections can be taken into account approximately in particular cases. A gaseous rectifier may be approximated by a constant voltage drop for the conduction periods. A vacuum rectifier may be replaced by a perfect rectifier plus a resistance to a fair degree of approximation if the tube drop is small compared with the load voltage.

### Discussion of the Curves

Figure 1 shows the case of a purely resistive load. The current and the voltage  $e'$  follow the sinusoidal pattern for

the half cycle from 0 to 180 deg, and then are zero from 180 to 360 deg. The equations show the first few terms of the series for  $e'$  and  $i$  to represent this form of variation. We see a constant or d-c term, a very large term of line (or fundamental) frequency, and smaller amounts of various multiples of this frequency. The difference between  $e$  and  $e'$  shown by the curves during the nonconduction period is significant physically as the inverse voltage across the rectifier.

Figure 2 shows the current in a circuit consisting of resistance and inductance in series. It will be seen that conduction continues beyond the 180-deg point owing to the induced emf of the inductance.

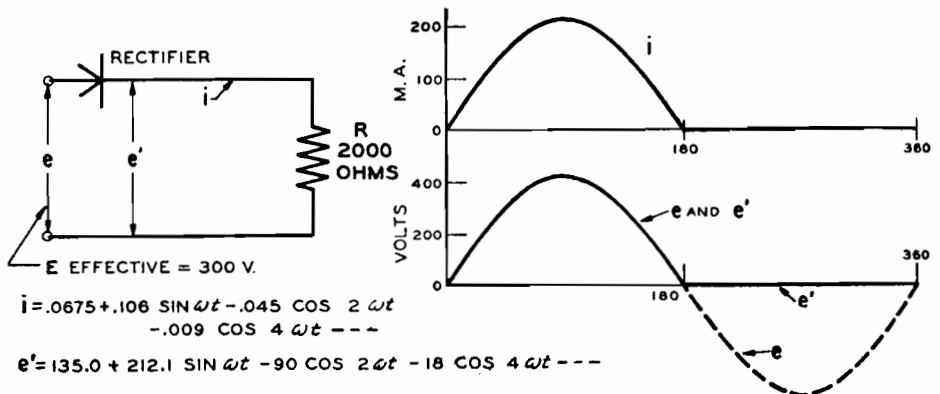


Fig. 1.—Curves for the case of a pure resistance load. The equations give the d-c, fundamental, and harmonic terms.

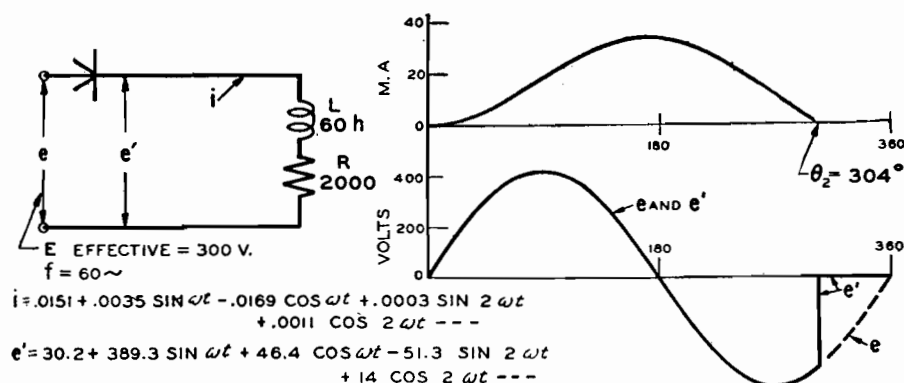


Fig. 2.—The effect of inductance in the load circuit is to increase the period of conduction.

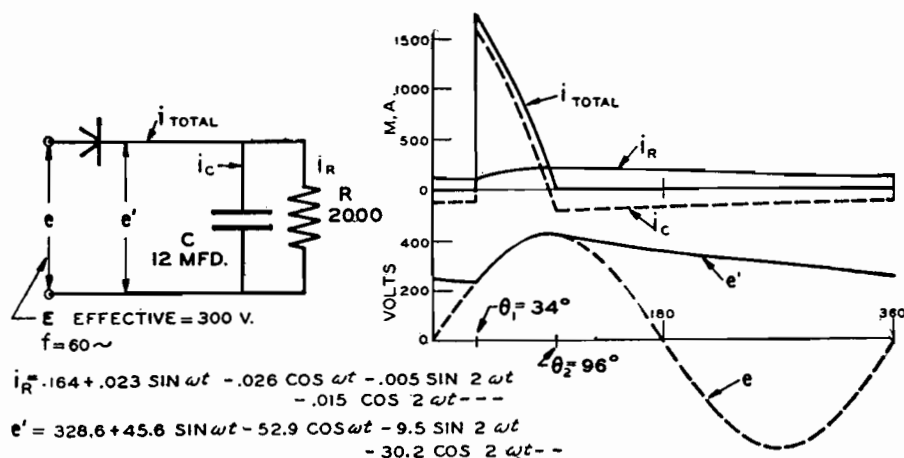


Fig. 3.—When a capacitance is in parallel with a resistance, the conduction period is decreased, but there is a continuous flow of current through the resistance.

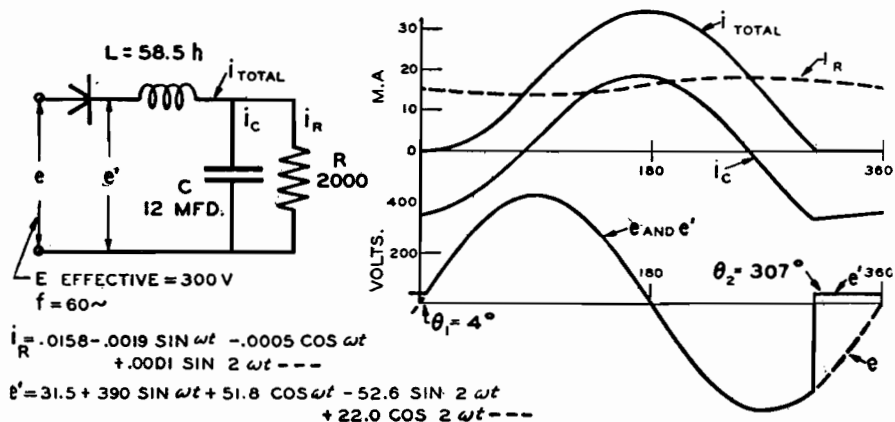


Fig. 4.—A simple filter circuit causes the conduction period to continue to beyond the 300-deg point.

For the constants used in this case the switch opens at about 304 deg, so  $e'$  follows the sinusoidal form until that point is reached, and is zero for the remainder of the cycle. The average value of the  $e'$  curve (which is the d-c voltage component) is much smaller than in the first case, as may be checked by inspection of the curve. The average value of  $i$ , which is equal to the average value of  $e'$  divided by  $R$ , is also much less than in Fig. 1. Another striking difference, compared with Fig. 1, is the great

increase of the fundamental frequency component of  $e'$ .

Figure 3 shows the effect of placing a capacitor in parallel with a resistance. Conduction through the rectifier ceases at the point  $\theta_2$ , where the total current tends to reverse. After  $\theta_2$ ,  $e'$  follows an exponential decrease until it meets the sinusoidal  $e$  at  $360^\circ + \theta_1$ . In this case  $e'$  has a much greater average value than in Fig. 1, and a smaller harmonic content, as might be expected from its smaller range of fluctuation. The conduction

period in this case is about 62 deg. The current  $i_R$  shows rather poorly in the graph; it is of course similar in form to  $e'$ .

Figure 4 shows a simple form of filter circuit. Here, as in Fig. 2, the inductance causes conduction to continue far beyond the 180-deg point. After  $\theta_2$  there is an exponential section, for the same reason as in Fig. 3. The smoothing effect of the circuit on the load ( $i_R$ ) is shown by both the equation and the curve; the capacitor takes the major part of the alternating current through  $L$ . The voltage  $e'$  has a small d-c component and a very large fundamental frequency term (85 per cent greater than in Fig. 1).

The constants of the circuit in Fig. 5, with  $S$  open, are the same as in Fig. 2; so the effect of closing the switch may be found by comparison of Figs. 2 and 5. The circuit as a whole gives a more nearly resistive effect with  $S$  closed and conduction lasts only to 186 deg. After 186 deg,  $e'$  has a negative exponential section, owing to the decreasing current through the coil and  $R_2$ . In this case,  $e'$  has an average value nearly four times as great as in Fig. 2, and the total circuit resistance is lower, so that the total current (average value) is about five times as great. The average coil current is half of the total, or about 2.5 times as great as in Fig. 2. It is also much smoother in form. The observed increase of coil current upon closing  $S$  seems unreasonable if  $R_2$  is considered only as a shunt that diverts current from the coil. The influence of  $R_2$  on wave forms is of greater importance in this circuit, as becomes evident on studying the change in conducting period of the rectifier. Physically,  $R_2$  might be visualized as providing a discharge path for the inductance, thus enabling the rectifier to shut off near the 180-deg point, and so not subject  $L$  to the negative supply-line voltage during the half cycle from 180 to 360 deg, as in Fig. 2.

The table gives a summary of the harmonic components of the circuit input voltage  $e'$  for the five cases presented. In this table the sine and cosine terms of each frequency are combined to show the total amplitude. All components show great differences between the various cases, but the greatest interest attaches, in general, to the d-c and the fundamental frequency parts. The d-c term ranges from 30 to 328 volts, and the fundamental from 70 to 392 volts. This table illustrates the point that no one set of harmonic values can be given as representative of conditions on a half-wave

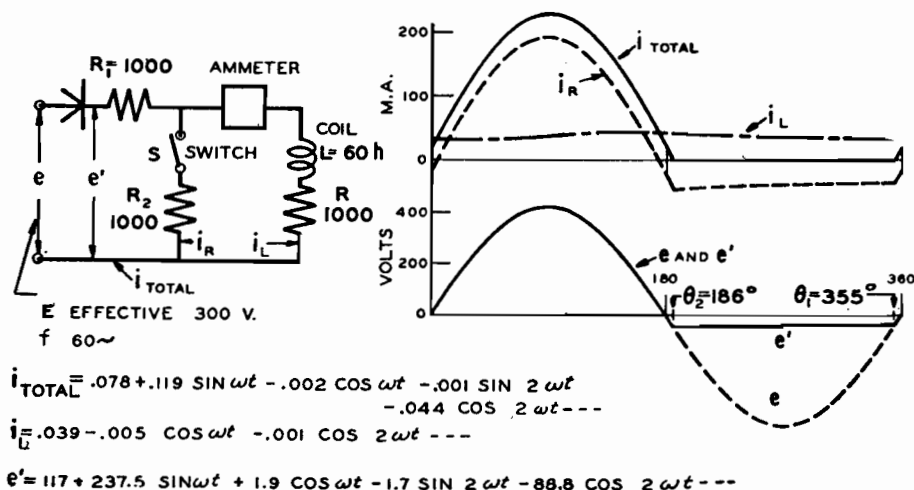


Fig. 5.—Resistance  $R_2$  provides a discharge path for the inductance, confining the conduction period to the range between zero and 186 deg.

rectifier. The voltage equation of Fig. 1 is the one usually referred to in textbooks as the voltage of a half-wave rectifier; it should be used, however, only in the special case of a resistive load.

The procedure followed in deriving the equations is, in general, a modification of

that presented for full-wave rectifiers in a previous article.<sup>2</sup> The circuit behavior can be determined qualitatively from general circuit considerations and a voltage series derived by the necessary combination of sinusoidal sections, exponential sections, etc. In case

Amplitudes of the Harmonic Components of the Circuit Input Voltage,  $e'$  (Maximum Values), of Figs. 1 to 5. The Supply Voltage Is 300 Volts (Effective)

Harmonic	Fig. 1 Load = $R$	Fig. 2 $L, R$	Fig. 3 $C, R$	Fig. 4 $L, C, R$	Fig. 5 $R, L$ shunted
D-c term.....	135.0	30.2	328.6	31.5	117.0
1 (fundamental).....	212.1	392.1	69.8	393.4	237.5
2.....	90.0	53.3	31.7	57.0	89.9
3.....	0	46.4	17.7	49.3	8.5
4.....	18.0	37.9	10.2	40.0	16.8
5.....	0	29.8	5.8	30.2	5.0
6.....	7.7	20.8	3.3	21.6	6.5
Conduction period.....	180°	304°	62°	303°	191°

the point of transition from one section to another is not known, it can be found by a trial solution, or by other methods. The current series is derived from the voltage series, and checked to see that the total current is zero during the nonconducting period.

#### Applications of the Method

The series form of representation of the circuit input voltage is useful in many ways, as it shows not only the d-c component, but also the frequencies and amplitudes of the harmonics that are present. A major use is in the study of filter circuits in which the load, or output, ripple can be computed for any harmonic, knowing the input ripple and the circuit constants. However, it must be emphasized again that the input ripple differs for practically every load connected to a half-wave rectifier, as indicated by the table, and that accuracy of output ripple is obtained only when the correct input value is used.

#### Conclusions

1. The wave form and the harmonic make-up of the voltage from a half-wave rectifier depend on the load connected to it.

2. The effect of circuit changes, as in Fig. 5, can be understood only by a study of the wave-form changes.

3. Filter ripples based on the harmonic terms of Fig. 1 are incorrect for actual filter circuits.

#### References

- (1) WALLIS, C. M., Half-wave Gas Rectifier Circuits, *Electronics*, October, 1938, p. 12 (reprinted in this book).
- (2) STOUT, M. B., Analysis of Rectifier Filter Circuits, *Elec. Eng.*, September, 1935, p. 977.

## Half-wave Gas Rectifier Circuits

By C. M. WALLIS

Current and voltage wave forms for half-wave rectifier circuits having various types of plate loading and employing gaseous conduction tubes

FREQUENTLY it is desirable to pre-determine the current and voltage wave forms that may occur in a circuit using the low-pressure gas-filled rectifier tube. The following analytical discussion presents a method, employing operational

calculus in its simpler form, for determining in an exact manner these functions in circuits utilizing such an ionic device. The analysis is rigorous insofar as the circuit problem is concerned, though certain basic assumptions have been made.

One distinguishing feature of the low-pressure gas-filled tube is that tube voltage drop during its conducting period is small and practically independent of current magnitude. This constancy of tube drop is assumed in the following

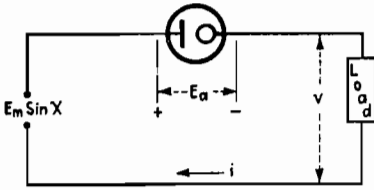


Fig. 1.—Fundamental half-wave rectifier circuit using gaseous rectifier for which analysis is carried out.

analysis. It is considered also that the circuit is fed from an a-c power source having a sinusoidally varying voltage of constant effective value.

First consider the circuit shown in Fig. 1. The voltage impressed is  $e = E_m \sin X$ .  $E_a$  denotes the constant tube drop and  $v$  the instantaneous voltage across the load. During the period of current flow, the following equation expresses the voltage relationships in the circuit

$$0 = E_m(\sin X) - v - E_a \quad (1)$$

**Example 1. Pure Resistive Loads.**—As the simplest example, let it be assumed that the load consists of a resistance in series with a battery on charge (Fig. 2). The load voltage is  $v = Ri + E_B$ . Hence Eq. (1) becomes

$$i = \frac{E_m}{R} [(\sin X) - k] \quad (2)$$

where  $k = (E_a + E_B)/E_m$ .

This equation gives the instantaneous value of the circuit current during the period of current flow, i.e., when the bracketed term is positive. The time angle of firing,  $\alpha$ , is  $\sin^{-1} k$ . The angle of cutoff,  $\beta$ , is  $(\pi - \sin^{-1} k)$ . Figure 3 illustrates the nature of the current function. It may be seen that the current flows in impulses which are portions of sine waves. The average or d-c value of the anode current is

$$I_{d-c} = E_m \left[ \frac{2 \cos \alpha - k (\pi - 2\alpha)}{2\pi R} \right] \quad (3)$$

**Example 2. Inductive Load.**—Assume now that an inductance of  $L$  henrys is placed in the circuit of Fig. 2, as shown in Fig. 4. The load voltage  $v$  must now

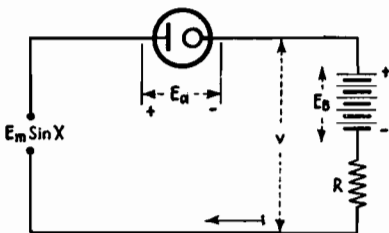


Fig. 2.—Half-wave rectifier circuit with resistance plate load.

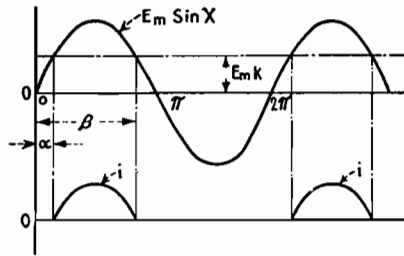


Fig. 3.—Voltage and current wave forms for half-wave circuit using gaseous conduction rectifier.

be expressed as

$$v = Ri - L\omega \frac{di}{dx} + E_B$$

which may be written in the form

$$v = L\omega(p + \eta)i + E_B$$

where  $\eta = R/L\omega$  and  $p$  is the differential operator  $d/dx$ . Substituting the above expression for the load voltage into Eq. (1), and transposing terms yields the result

$$i(p + \eta) = \frac{E_m}{L\omega} [(\sin X) - k] \quad (4)$$

which is the differential equation of the circuit current expressed in operational form.

Since Eq. (4) indicates that the current  $i$  is the result of the voltage functions  $(E_m/L\omega) \sin X$  and  $-(E_m/L\omega) k$  acting in the circuit, its complete solution includes the complementary function plus the particular integral for each voltage function. Hence the general solution may be carried out in the following manner:

$$\text{Let } i = i_1 + i_2 + i_3 \quad (5a)$$

$$\text{where } i_1(p + \eta) = 0 \quad (5a)$$

$$i_2(p + \eta) = \frac{E_m}{L\omega} \sin X \quad (5b)$$

$$i_3(p + \eta) = -\frac{E_m}{L\omega} k \quad (5c)$$

The complementary function is obtained from Eq. (5a) which is the homogeneous equation. Since it is a differential equation of the first order, its solution is of the form

$$i_1 = A e^{-\eta x}$$

The particular integral for each voltage

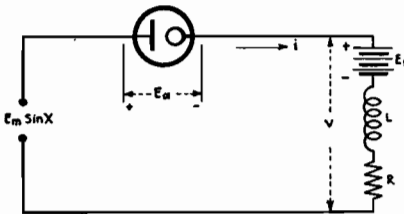


Fig. 4.—Schematic diagram of half-wave rectifier having inductive and resistive plate loading.

function is obtained from Eqs. (5b) and (5c). They are the steady-state solutions of these equations. Thus the steady-state solution of Eq. (5b) is obtained by letting  $p = j = \sqrt{-1}$ , and the steady state of Eq. (5c) is found by letting  $p = 0$ . Carrying through these operations and simplifying, the complete solution of Eq. (4) may be written

$$i = \frac{E_m}{L\omega} \left[ \frac{\sin(X - \delta)}{\sqrt{1 + \eta^2}} - \frac{k}{\eta} + A e^{-\eta x} \right] \quad (6)$$

where  $\delta = \cot^{-1} \eta$ .

The constant  $A$  is evaluated from the condition at the point of firing, i.e., when  $X = \alpha = \sin^{-1} k$ , and  $i = 0$ . Hence

$$A = e^{+\eta \alpha} \left[ \frac{k + \eta \sqrt{1 - k^2}}{\eta(1 - \eta^2)} \right] \quad (7)$$

The voltage across the inductance is  $e_L = L\omega (di/dx)$  or

$$e_L = E_m \left[ \frac{\cos(X - \delta)}{\sqrt{1 + \eta^2}} - A \eta e^{-\eta x} \right] \quad (8)$$

It is now possible to determine the exact nature of the current and voltage wave forms by assuming values of  $X$  starting at  $X = \alpha$ . The angle of cutoff  $\beta$  is that value of  $X$  which makes the bracketed term of Eq. (6) equal to zero.

Figure 5 illustrates the voltage and current wave forms obtained in such a circuit. Note that the current rise is delayed owing to the inductive property of the circuit. In addition, the period of current flow is extended, cutoff occurring at a point further along in the cycle than if the circuit were noninductive.

The following example illustrates the ease with which the above equations may be handled: A 60-cycle voltage of  $320 \sin \omega t$  is impressed across a circuit containing a gas-filled rectifier tube, a 90-volt battery on charge, a resistance of 37 ohms, and an inductance of 0.218 henry. The tube drop is 7 volts.

$$k = \frac{(E_a + E_B)}{E_m} = 0.303$$

$$A = e^{+\eta \alpha} \left[ \frac{k + \eta \sqrt{1 - k^2}}{\eta(1 - \eta^2)} \right] = 1.55$$

$$\eta = \frac{R}{L\omega} = 0.45 \quad \delta = \cot^{-1} \eta = 65.77^\circ$$

$$\alpha = \sin^{-1} k = 17.64^\circ \quad \frac{E_m}{L\omega} = 3.89$$

The current equation between values of  $X = \alpha$  and  $X = \beta$  is

$$i = [3.54 \sin(X - 65.77^\circ) + 6.03 e^{-0.45x} - 2.62] \text{ amp}$$

The equation for voltage across  $L$  is

$$e_L = [291.5 \cos(X - 65.77^\circ) - 223.5 e^{-0.45x}] \text{ volts}$$

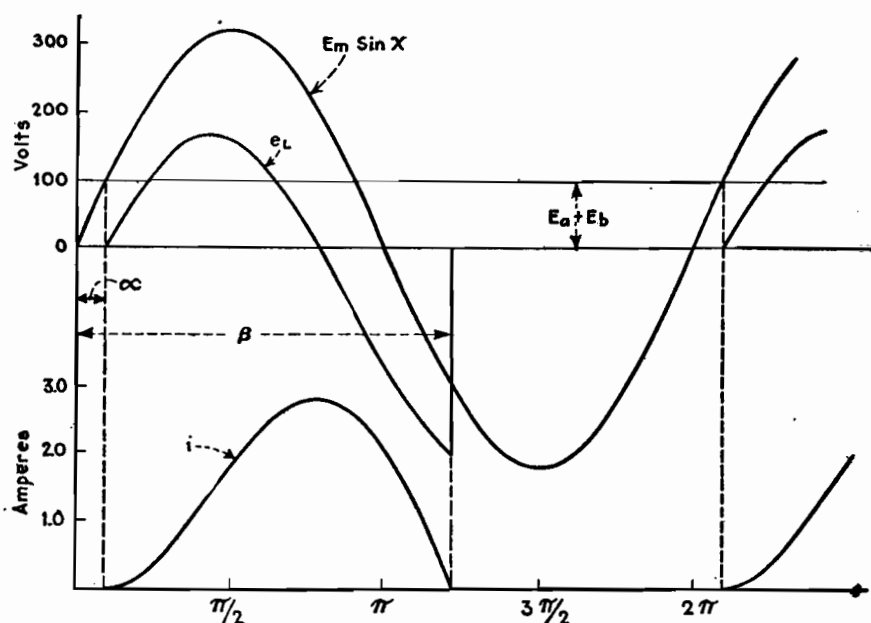


Fig. 5.—Voltage and current wave forms for rectifier with inductive and resistive load.

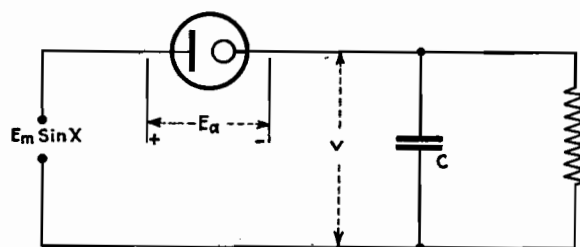


Fig. 6.—Gas-tube rectifier circuit having resistive- and capacitive-plate loading.

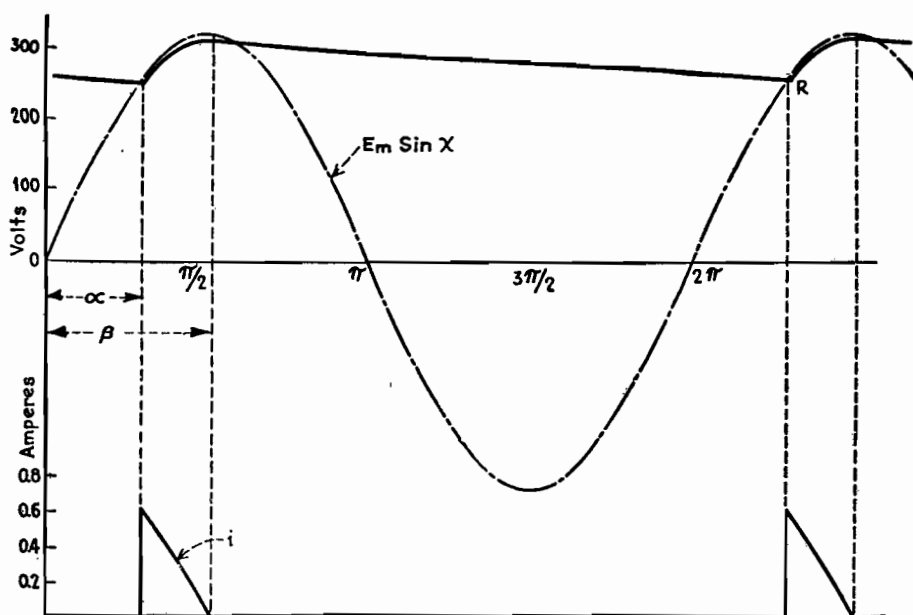


Fig. 7.—Current and voltage wave forms for resistance- and capacitance-loaded rectifier circuit of Fig. 6.

Curves computed from the above equation are shown in Fig. 5.

**Example 3. Capacitive Load.**—The third type of circuit to be considered is the one shown in Fig. 6 where the load is capacitive in character. When in oper-

ation the capacitor  $C$  is charged during the period of tube current flow. During the period that the tube is not conducting, the capacitor discharges through the resistance  $R$ . The nature of the load voltage  $v$  is illustrated in Fig. 7.

During the period of discharge

$$v = V' e^{-\frac{X-\beta}{RC\omega}} \quad (9)$$

where  $V'$  is the value of the load voltage at the instant of rectifier cutoff. During the charging period  $v = Z(p)i$  where  $Z(p)$  is the impedance of the load in operational form. Hence during this period the rectifier current  $i$  may be expressed as

$$i \Big|_{\alpha \text{ to } \beta} = \frac{E_m(\sin X) - E_a}{Z(p)} \quad (10)$$

The load impedance is

$$Z(p) = \frac{R/C\omega p}{R + 1/C\omega p} = \frac{R}{RC\omega p + 1}$$

which when substituted into Eq. (10) results in the following:

$$i \Big|_{\alpha \text{ to } \beta} = E_m \left( \frac{\sqrt{1 + R^2 C^2 \omega^2}}{R} \right) \sin(X + \delta) - \frac{E_a}{R} \quad (11)$$

where  $\delta = \tan^{-1} RC\omega$ .

The angle of tube current cutoff  $\beta$  may be determined from the above equation, since when  $X = \beta$ ,  $i = 0$ . Consequently

$$\beta = 180^\circ - \delta - \sin^{-1} \left( \frac{E_a}{E_m \sqrt{1 + R^2 C^2 \omega^2}} \right) \quad (12)$$

The value of  $V'$  is then

$$V' = E_m(\sin \beta) - E_a \quad (13)$$

It should be noted that  $\alpha$  cannot be determined from Eq. (11) since there is a discontinuous rise of current at the point of firing (Fig. 7). However, it may be found from the load voltage condition at the point  $R$  where  $X = (2\pi + \alpha)$ . At this point

$$E_m \sin(2\pi + \alpha) - E_a = V' e^{-\frac{(2\pi + \alpha - \beta)}{RC\omega}} \quad (14)$$

Equation (14) contains the unknown  $\alpha$  which cannot be solved directly. The easiest method is to plot values of the right- and left-hand members against assumed values of  $\alpha$  and determine the correct value from the intersection of the two curves. The angle of firing  $\alpha$  having been found, the current function may be determined by Eq. (10) between the limits of  $X = \alpha$  and  $X = \beta$ .

Generally it is of major interest to know the d-c value of the load voltage  $v$ . This may be found from the following equation

$$V_{d-c} = \frac{1}{2\pi} \left\{ \int_{\alpha}^{\beta} [E_m(\sin X) - E_a] dx + \int_{\beta}^{2\pi + \alpha} V' e^{-\frac{X-\beta}{RC\omega}} dx \right\}$$

or

$$V_{d-c} = \frac{1}{2\pi} \left[ E_m(\cos \alpha - \cos \beta) - E_a(\beta - \alpha) + RC\omega V'(1 - e^{-\frac{2\pi + \alpha - \beta}{RC\omega}}) \right] \quad (15)$$

One characteristic of such circuits is the high peaked current impulse that results and the low average or zero-frequency current. Knowledge of the maximum instantaneous current is important, of course, in the selection of the rectifier tube to supply such a circuit.

The following example illustrates how the above equations may be handled:

A voltage of  $320 \sin \omega t$  at 60 cycles is impressed across a half-wave rectifier circuit. The load consists of an 8,430-ohm resistance in parallel with a 8.2- $\mu$ f capacitor. The tube drop is 7 volts.

$$\begin{aligned} RC\omega &= 26.08 & \delta &= \tan^{-1} RC\omega = 87.8 \\ \beta &= 180 - \delta - \sin^{-1} \left( \frac{E_a}{E_m \sqrt{1 + R^2 C^2 \omega^2}} \right) \\ &= 92.2^\circ \\ V' &= [E_m(\sin \beta) - E_a] = 313 \text{ volts} \end{aligned}$$

The angle  $\alpha$  is determined from the equation

$$320 \sin(2\pi + \alpha) - 7 = 313 e^{-\frac{2\pi + \alpha - 92.2^\circ}{26.08}}$$

By solution  $(2\pi + \alpha) = 414^\circ$ ;  $\alpha = 54^\circ$ .

$$\begin{aligned} V_{d-c} &= \frac{1}{2\pi} [320(\cos 54^\circ - \cos 92.2^\circ) \\ &\quad - E_a(1.61 - 0.945) \\ &\quad + (26.08)(313)(1 - e^{-0.2115})] \\ V_{d-c} &= 279 \text{ volts} \\ I_{d-c} &= \frac{279}{8,430} = 0.033 \text{ amp} \end{aligned}$$

The equation for the rectifier current during the charging period is

$$i = 0.001 \sin(X + 87.8^\circ) - 0.0083 \text{ amp}$$

Figure 7 shows the voltage  $v$  and the current  $i$  as determined for the above equations.

## Full-wave Rectifier Analysis

By C. M. WALLIS

IN THE following analysis of the full-wave rectifier circuit, equations for the current and voltage wave forms are derived for inductive and capacitive loads. In case of inductive loads, an equation in terms of the load circuit parameters, which enables one to predetermine whether current cutoff does or does not occur, is given. The use of operational calculus in the analysis simplifies the solution a great deal. Sinusoidal impressed alternating voltages of constant effective value are assumed. The analysis deals primarily with circuits using gas-filled tubes, which have an anode-to-cathode voltage drop that is practically constant and independent of the tube current magnitude.

Consider the single-phase full-wave circuit shown in Fig. 1. If the transformer is mid-tapped as indicated, the rectifier circuit has balanced anode voltages of  $e_1 = E_m \sin x$  and  $e_2 = E_m \sin(x - \pi)$ . The type of voltage wave that the rectifier impresses upon the load circuit is of the pulsating type shown in Fig. 2C. This type of voltage function may be considered as a product wave, i.e., it is the result of multiplying two functions of  $x$  together: one, the sinusoidal function  $E_m \sin x$ , shown in Fig. 2A, and the other,

a unit rectangular wave function, which is shown in Fig. 2B, and designated as  $S'$  function. That is,  $S' = +1$  from  $x = 0$  to  $x = \pi$ ,  $S' = -1$  from  $x = \pi$  to  $x = 2\pi$ , etc. Consequently,  $S'E_m \sin x$  designates a completely rectified sine wave since the negative loops are made positive.

The general voltage equation for the rectifier load circuit during the period of current flow in either the first or second half cycle may be written as

$$0 = S'E_m(\sin x) - v - E_a \quad (1)$$

where  $v$  is the instantaneous value of the voltage across the load and  $E_a$  is the tube drop.

### Inductive Loads

If the load is sufficiently inductive in character, continuous flow of load current occurs. Let it be assumed that the load has  $L$  henrys inductance,  $R$  ohms resistance, and an emf of  $E$  volts acting in circuit opposition to the current flow as indicated in Fig. 3. The instantaneous load voltage may be expressed as

$$v = Ri + L\omega \frac{di}{dx} + E$$

$i$  being the instantaneous value of load current. The above equation may be written in the form

$$v = L\omega(p + \eta)i + E \quad (2)$$

where  $\eta = R/L\omega$  and  $p$  is the differential operator  $d/dx$ . Equation (1) for this particular case, by substitution of  $v$ ,

becomes

$$i(p + \eta) = \frac{E_m}{L\omega} S'(\sin x) - k \quad (3)$$

which is the differential equation of the load current, and  $k = (E_a + E)/E_m$ . The complete solution of Eq. (3) may be written in the form\*

$$i = \frac{E_m}{L\omega} \left[ \frac{S' \sin(x - \delta)}{\sqrt{1 + \eta^2}} - \frac{k}{\eta} + A e^{-\eta x} \right] \text{ amp} \quad (4)$$

where  $\delta = \cot^{-1} \eta$  and  $A$  is a constant for any one half cycle.

### Non-cutoff Case

Equation (4) gives the instantaneous load current as a function of the time

\* For the mechanics of solution of this equation the reader is referred to a previous paper by the author entitled Half Wave Gas Rectifier Circuits, *Electronics*, October, 1938 (reprinted in this book).

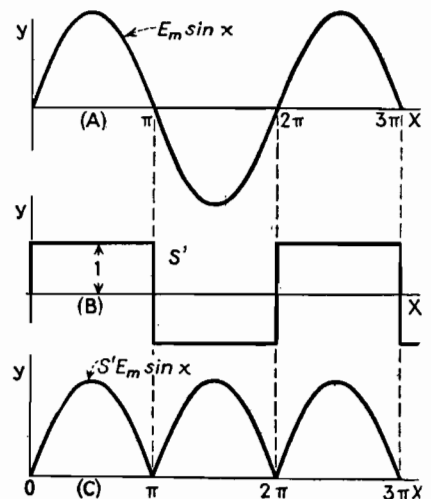


Fig. 2.—Typical voltage curves of the full-wave rectifier.

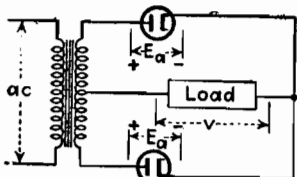


Fig. 1.—Circuit diagram of typical full-wave rectifier.

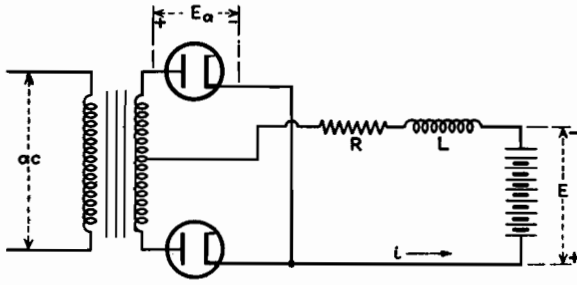


Fig. 3.—Rectifier with an inductive load and a direct voltage in opposition to the rectified voltage.

angle  $x$ . It should be noted, however, that the term  $S' \sin(x - \delta)$  is a discontinuous function, with an abrupt change in its value occurring at  $x = \pi$ ,  $x = 2\pi$ , etc. If load current cutoff does not occur then, the latter must vary continuously from one half cycle to the next. Consequently, the quantity  $A$  must be discontinuous in a manner such as to make  $i$  continuous. Hence  $A$  is constant for any one half cycle, varying however from half cycle to half cycle. For the steady-state condition, where  $i$  is periodic,  $A$  may be evaluated by setting the current at the beginning of a half cycle, where  $x = 0$  and  $S' = +1$ , to the current at the end of the half cycle, where  $x = \pi$  and  $S' = +1$ . By so doing, through the use of Eq. (4)

$$A = \frac{2}{(1 + \eta^2)(1 - e^{-\eta\pi})} \quad (5)$$

$A$  may be determined for successive half cycles in a like manner. However, since the current function is the same over each half cycle, this need not be done. The type of current wave occurring

in the non-cutoff case is shown in Fig. 4A, or in more detail in Fig. 5.

The d-c component of load current, obtained by integration of the current equation between limits of  $x = 0$  and  $x = \pi$ , is

$$I_{dc} = \frac{E_m}{R} \left( \frac{2}{\pi} - k \right) \quad (6)$$

#### Cutoff Case

If the load circuit parameters are such as to cause load current cutoff in each half cycle, as shown in Fig. 4C, then Eq. (4) may be written as

$$i \Big|_{\alpha \text{ to } \beta} = \frac{E_m}{L\omega} \left[ \frac{S' \sin(x - \delta)}{\sqrt{1 + \eta^2}} - \frac{k}{\eta} + A e^{-\eta x} \right] \quad (7)$$

where  $\alpha$  is the angle of firing and  $\beta$  is the angle of current cutoff. The former angle is of course equal to  $\sin^{-1} k$  (refer to Fig. 4C). The value of the constant  $A$  over the first half cycle is evaluated from the boundary conditions at the point of firing, namely, at  $x = \alpha$ ,  $S' = +1$ , and  $i = 0$ . Therefore, from Eq. (7)

$$A_1 = \frac{k + \eta \sqrt{1 - k^2}}{\eta(1 + \eta^2)e^{-\eta\alpha}} \quad (8)$$

Should the current pulse continue over into the second half cycle, the constant  $A$  is re-evaluated from the boundary condition at the beginning of the second half cycle, namely, at  $x = \pi$  and  $S' = -1$ , and  $i = i_{x=\pi}$ . Hence

$$A_2 = \left[ \frac{(i_{x=\pi})L\omega}{E_m} + \frac{1}{(1 + \eta^2)} + \frac{k}{\eta} \right] e^{\eta\pi} \quad (9)$$

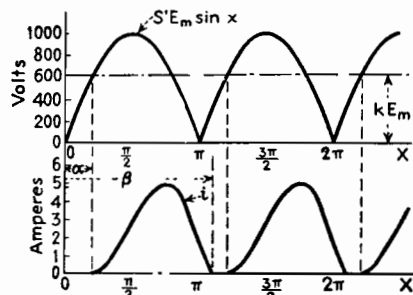


Fig. 5.—The same curves as in Fig. 4A but in greater detail.

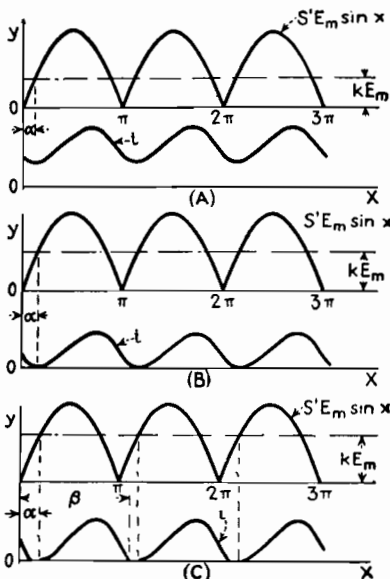


Fig. 4.—Voltage and current curves of the rectifier shown in Fig. 3 for the condition of no current cutoff.

#### Test for Cutoff

The constants  $A$  and  $A_1$  over the first half cycle for the non-cutoff case and the cutoff case are given by Eqs. (5) and (8), respectively. The criterion for non-cutoff of load current is that  $A \geq A_1$ , or that

$$\frac{2}{(1 - e^{-\eta\pi})} \geq \frac{k + \eta \sqrt{1 - k^2}}{\eta e^{-\eta\alpha}} \quad (10)$$

For a given set of load circuit constants the above equation determines readily whether the load current flows continuously or in pulses. Where the equality relationship exists in the above equation, the instantaneous value of load current just reaches zero value at  $x = \alpha$ . This is shown in Fig. 4B.

**Example 1.**—A single-phase full-wave rectifier utilizing a gas-filled tube supplies power to a d-c system. The voltage of the d-c system is 500 volts. The rectifier anode voltages are  $\pm 1,000 \sin x$ . A smoothing inductance of 0.2 henry and a resistance of 20 ohms are inserted in the d-c side of the rectifier. Assume tube drop  $E_a = 15$  volts

$$k = \frac{(E_a + E)}{E_m} = 0.515$$

$$\eta = \frac{R}{L\omega} = 0.265$$

$$\delta = \cot^{-1} \eta = 75.15^\circ$$

$$\alpha = \sin^{-1} k = 31.0^\circ$$

$$\frac{k}{\eta} = 1.94 \quad \frac{E_m}{L\omega} = 13.26$$

$$\frac{2}{(1 - e^{-\eta\pi})} = 3.54 \quad \frac{k + \eta \sqrt{1 - k^2}}{\eta e^{-\eta\alpha}} = 3.23$$

$$\text{Since } \frac{2}{(1 - e^{-\eta\pi})} > \frac{k + \eta \sqrt{1 - k^2}}{\eta e^{-\eta\alpha}}$$

load current cutoff does not occur and there is continuous current flow.

By Eq. (5)

$$A = \frac{2}{(1 + \eta^2)(1 - e^{-\eta\pi})} = 3.30$$

The current equation for the first half cycle ( $S' = +1$ ) is

$$i = 13.26 \left[ \frac{(+1) \sin(x - 75.15^\circ)}{1.035} - 1.94 + 3.30 e^{-0.265x} \right] \text{ amp}$$

or

$$i = [12.80 \sin(x - 75.15^\circ) - 25.7 + 43.75 e^{-0.265x}] \text{ amp}$$

Values of load current computed from the above equations are given in Table I.

The d-c value of the load current is

$$I_{dc} = \frac{1,000}{20} \left( \frac{2}{\pi} - 0.515 \right) = 6.05 \text{ amp}$$

The current curve is shown in Fig. 5.



Table 1.—Load Currents Computed from Above Equations

$x$	$i$	$x$	$i$
0°	5.68	100°	7.23
20°	3.59	120°	8.41
40°	3.23	140°	8.75
60°	4.11	160°	7.85
80°	5.58	180°	5.68

**Example 2.**—Suppose that the voltage of the d-c system is 600 volts, other factors remaining the same as in Example 1.

$$k = \frac{E + E_a}{E_m} = 0.615$$

$$\alpha = \sin^{-1} k = 37.95^\circ$$

$$\frac{2}{(1 - e^{-\eta\pi})} = 3.54 \frac{k + \eta \sqrt{1 - k^2}}{\eta e^{-\eta\alpha}} = 3.71$$

$$\text{Since } \frac{2}{(1 - e^{-\eta\pi})} < \frac{k + \eta \sqrt{1 - k^2}}{\eta e^{-\eta\alpha}}$$

load current cutoff occurs and the current flows in pulses. By Eq. (8),

$$A_1 = \frac{k + \eta \sqrt{1 - k^2}}{\eta(1 + \eta^2)e^{-\eta\alpha}} = 3.47$$

The current equation over the first half cycle ( $S' = +1$ ) is

$$i \Big|_{\alpha \text{ to } \pi} = [12.8(+1) \sin(x - 75.15^\circ) - 30.79 + 46.0 e^{-0.265x}] \text{ amp}$$

By solution  $ix = \pi = 1.55$  amp, and therefore the current pulse lasts over into the second half cycle. Hence

$$A_2 = \left[ \frac{(i_\pi) L \omega}{E_m} + \frac{1}{(1 + \eta^2)} + \frac{k}{\eta} \right] e^{\eta\pi} = 7.76$$

The current equation for the remaining portion of the current pulse is

$$i \Big|_{\pi \text{ to } \beta} = [12.8(-1) \sin(x - 75.15^\circ) - 30.79 + 102.7 e^{-0.265x}] \text{ amp}$$

Values of load current computed from the two above equations are given below:

$x$	37.95°	40°	60°	80°	110°
$i$	0	0.02	0.72	2.04	3.59
$x$	120°	140°	160°	180°	190°
$i$	4.60	4.86	3.86	1.55	0.49

The current curve is shown in Fig. 6.

#### Capacitive Loads

To supply a d-c plate voltage to electronic equipment, a rectifier circuit similar to that shown in Fig. 7 is frequently used.  $R_1$  represents the equivalent d-c load resistance.  $R_2$  and  $C$  represent a resistance-capacitance filter arrangement. When in operation, the

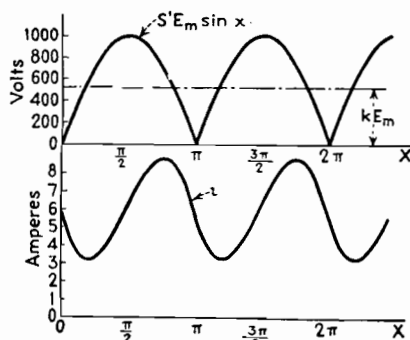


Fig. 6.—The same curves as in Fig. 4C but in greater detail.

capacitor  $C$  is charged during periods of current flow. When neither tube is conducting, the capacitor discharges through the load resistance  $R_1$ . The character of the load-voltage variation is shown in Fig. 9.

During the period of discharge, the value of the load voltage  $v$  may be expressed as

$$v = V e^{-\frac{x-\beta}{R_1 C \omega}} \quad (11)$$

where  $V$  is the load voltage at the instant of tube current cutoff, i.e., where  $x = \beta$ .

During the period of tube-current flow,  $v = E_m S' (\sin x) - E_a - R_2 i$ . Taking the load circuit impedance, expressed in operational form as  $Z(p)$ , the tube current during this period is

$$i \Big|_{\alpha \text{ to } \beta} = \frac{E_m S' (\sin x) - E_a}{Z(p)} \quad (12)$$

The load impedance in terms of the circuit parameters is

$$Z(p) = \left( R_2 + \frac{R_1}{R_2 C \omega p + 1} \right) = \frac{K + B(p)}{1 + A(p)}$$

where  $K = (R_1 + R_2)$ ,  $B = R_1 R_2 C \omega$ , and  $A = R_1 C \omega$ . Substituting the value of  $Z(p)$  in Eq. (12) and performing the indicated operations,

$$i \Big|_{\alpha \text{ to } \beta} = \frac{E_m \sqrt{1 + A^2} S' [\sin(x + \phi)] - E_a}{K + B(p)}$$

The above equation is of the same form as Eq. (3), and hence its solution may be

written as

$$i \Big|_{\alpha \text{ to } \beta} = \left[ E_m M S' \sin(x + \phi - \theta) + P e^{-\frac{K}{B} x} - \frac{E_a}{K} \right] \text{ amp} \quad (13)$$

$$\text{where } M = \sqrt{\frac{1 + A^2}{K^2 + B^2}}$$

$$\theta = \tan^{-1} (B/K)$$

$$\phi = \tan^{-1} A$$

It now remains only necessary to set up the relationships from which the constant  $P$  and the angles  $\alpha$  and  $\beta$  may be found. These may be determined from the boundary conditions at the points of firing and cutoff in the following manner.

Referring to Fig. 9 it may be seen that at the instant of firing in the second half cycle, where  $x = \alpha + \pi$  and  $S' = -1$ , that

$$(-1) E_m \sin(\pi + \alpha) - E_a = V e^{-\frac{\pi + \alpha - \beta}{A}}$$

Likewise, at the point of current cutoff in the first half cycle, where  $x = \beta$  and  $S' = (+1)$ ,

$$(+1) E_m (\sin \beta) - E_a = V$$

Eliminating  $V$  from the above two equations yields the result

$$e^{-\frac{\pi + \alpha - \beta}{A}} [E_m (\sin \beta) - E_a] = [E_m (\sin \alpha) - E_a] \quad (14)$$

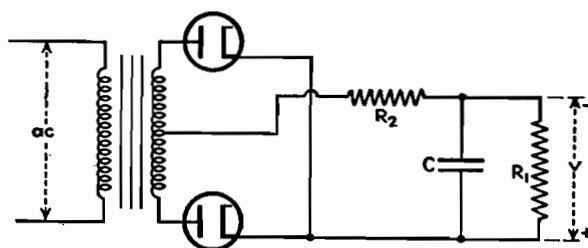
Again at the point of tube current cutoff, where  $x = \beta$ ,  $S' = +1$ , and  $i = 0$ , Eq. (13) becomes

$$0 = M E_m (+1) [\sin(\beta + \phi - \theta)] + P e^{-\frac{K}{B} \beta} - \frac{E_a}{K}$$

Similarly, at the point of firing, where  $x = \alpha$ ,  $S' = +1$ , and  $i = 0$ ,

$$0 = M E_m (+1) [\sin(\alpha + \phi - \theta)] + P e^{-\frac{K}{B} \alpha} - \frac{E_a}{K}$$

Eliminating the constant  $P$  from the two

Fig. 7.—A typical rectifier power supply.  $R_1$  is the load and  $C$  and  $R_2$  make up the filter.

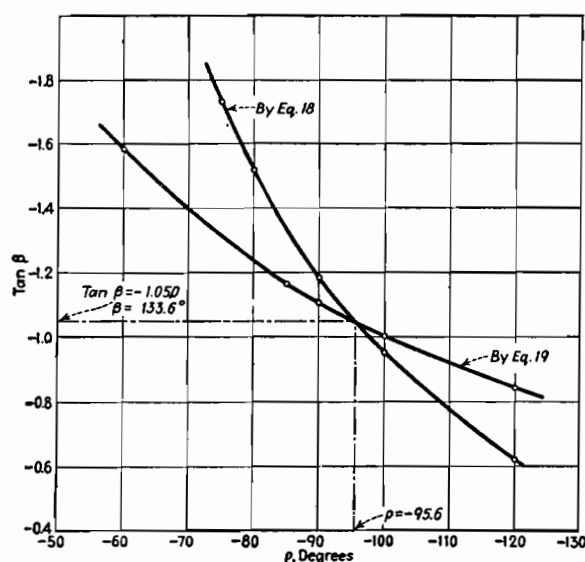


Fig. 8.—Curves that determine the duration of current flow through the rectifier elements of Fig. 7 as calculated in Example 3.

preceding equations gives the result

$$\begin{aligned} \frac{K}{\epsilon B^{\beta}} \left[ \frac{E_a}{K} - ME_m \sin(\beta + \phi - \theta) \right] \\ = \frac{K}{\epsilon B^{\alpha}} \left[ \frac{E_a}{K} - ME \sin(\alpha + \phi - \theta) \right] \quad (15) \end{aligned}$$

If the terms involving the arc drop voltage  $E_a$  are neglected in Eqs. (14) and (15), the angles  $\alpha$  and  $\beta$  may be determined. Negligible error results by this omission since the arc drop  $E_a$  is usually a very small fraction of  $E_m$ . By so doing, Eqs. (14) and (15) reduce to

$$\frac{\frac{K}{\epsilon B^{\alpha}}}{\frac{K}{\epsilon B^{\beta}}} = \frac{\sin \beta}{\sin \alpha} \quad (16)$$

$$\frac{K}{\epsilon B^{\alpha}} = \frac{\sin(\beta + \phi - \theta)}{\sin(\alpha + \phi - \theta)} \quad (17)$$

By letting  $(\alpha - \beta) = \rho$ , Eqs. (16) and (17) can each be solved for  $\beta$  in terms of the angle  $\rho$ . Thus, from Eq. (16)

$$\tan \beta = \frac{\sin \rho}{\epsilon^{-\frac{\pi + \rho}{A}} - \cos \rho} \quad (18)$$

and from Eq. (17)

$$\begin{aligned} \tan \beta \\ = \frac{\sin \rho + [\tan(\phi - \theta)](\cos \rho - \epsilon^{\frac{K}{B^{\rho}}})}{\frac{K}{\epsilon B^{\rho}} + (\sin \rho)[\tan(\phi - \theta)] - \cos \rho} \quad (19) \end{aligned}$$

The values of  $\beta$  and  $\rho$  that satisfy the above two equations can be found graphically by plotting  $\tan \beta$  in each case against assumed values of  $\rho$ . The intersection of the two curves gives of course the correct values of  $\rho$  and  $\tan \beta$ . These angles being determined,  $\alpha$  and  $P$  may be calculated from preceding equations. The current and voltage functions may next be determined.

The d-c component of the load voltage  $v$  is

$$V_{d-c} = \frac{1}{x} \left\{ \int_{\alpha}^{\beta} [E_m(\sin x) - E_a - R_2 i] dx + \int_{\beta}^{(\pi + \alpha)} V \epsilon^{-\frac{x - \beta}{A}} dx \right\}$$

Substituting in the value of  $i$ , integrating the result and simplifying, the above expression becomes

$$\begin{aligned} V_{d-c} = \frac{1}{\pi} \left\{ E_m(\cos \alpha - \cos \beta) - R_2 E_m M [\cos(\alpha + \phi - \theta) - \cos(\beta + \phi - \theta)] - \frac{E_a R_1}{R_1 + R_2} (\beta - \alpha) - \frac{R_2 P B}{K} \left( \epsilon^{-\frac{K}{B^{\alpha}}} - \epsilon^{-\frac{K}{B^{\beta}}} \right) + V A (1 - \epsilon^{-\frac{\pi + \alpha - \beta}{A}}) \right\} \quad (20) \end{aligned}$$

The d-c value of load current is

$$I_{d-c} = \frac{V_{d-c}}{R_1} \quad (21)$$

The following problem is worked out to exemplify the use of the preceding equations.

**Example 3.**—The full-wave rectifier shown in Fig. 7 has an anode voltage of  $\pm 500 \sin X$ . The resistance-capacitor filter used is composed of a 1,000-ohm resistance and a 4- $\mu$ f capacitor. The equivalent load resistance  $R_1$  is 6,000 ohms. Assume  $E_a = 10$  volts

$$K = (R_1 + R_2) = 7,000 \text{ ohms}$$

$$\phi = \tan^{-1} A = 83.7^\circ$$

$$\frac{E_a}{K} = 0.00143$$

$$B = R_1 R_2 C \omega = 9,050.$$

$$\theta = \tan^{-1} \left( \frac{B}{K} \right) = 52.3^\circ$$

$$K/B = 0.774$$

$$A = R_1 C \omega = 9.05$$

$$\tan(\phi - \theta) = 0.612$$

$$M = \sqrt{\frac{1 + A^2}{K^2 + B^2}} = 7.97(10^{-4})$$

$$E_m M = 0.3980$$

The curves obtained by plotting Eqs. (18) and (19) for assumed values of  $\rho$  are shown in Fig. 8. By graphical solution  $\alpha = 38.0^\circ$  and  $\beta = 133.6^\circ$ . From the boundary condition at  $x = \beta$  and  $i = 0$ ,

$$P = \left[ \frac{E_a}{K} - E_m M \sin(\beta + \phi - \theta) \right] \epsilon^{\frac{K}{B^{\beta}}} = -0.622$$

The equation of the current pulse in the first half cycle is, by Eq. (13),

$$\begin{aligned} i \Big|_{\alpha \text{ to } \beta} &= [0.398 \sin(X + 31.4^\circ) - 0.622 \epsilon^{-0.744x} - 0.00143] \text{ amp} \\ V &= E_m(\sin \beta) - E_a = 352 \text{ volts} \end{aligned}$$

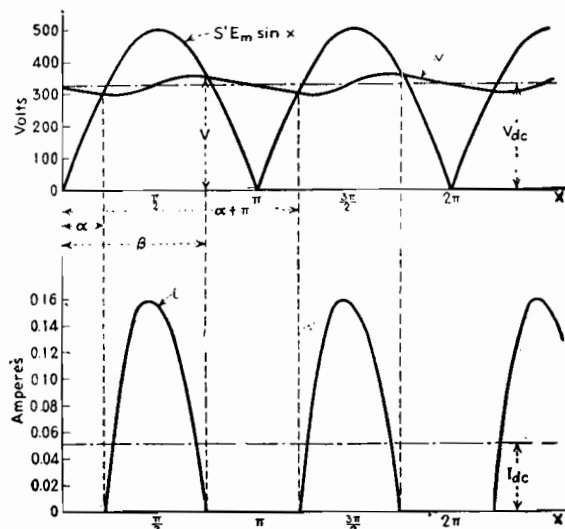


Fig. 9.—Voltage and current curves of the circuit in Fig. 7 as determined in Example 3.

The value of the d-c output voltage, by Eq. (20), is

$$V_{d-c} = \frac{1}{\pi} [(500)(1.477) - (398)(1.318) - (8.51)(1.67) + (804)(0.4343) + (3185)(0.15)] = 331 \text{ volts}$$

The equation for the instantaneous load

voltage between the limits of  $x = \alpha$  and  $x = \beta$  is

$$v = [500(\sin x) - 398(\sin(x + 31.4^\circ)) + 622e^{-0.744x} - 8.37] \text{ volts}$$

Between the limits of  $x = \beta$  and  $x = (\pi + \alpha)$

$$\rho^* = 352e^{\frac{x-133.6^\circ}{9.05}}$$

Current and voltage curves computed from the above equation are plotted in Fig. 9 for the first and successive half cycles. Since they are repeating functions, only those for the first half cycle need be computed.

## Filter Performance Charts for Half-wave Rectifiers

By W. K. H. PANOFSKY and CHARLES F. ROBINSON

A practical, simplified method of computing the output voltage, percentage ripple, and regulation of choke-input or capacitor-input half-wave rectifier and filter power supplies, which takes into account the leakage reactance of the power transformer as well as the filter and load circuit constants

IN THE design of rectifier power supplies it is essential that the performance characteristics shall be accurately predictable. In particular, in the design of high-voltage rectifying equipment, such as is encountered in X-ray and television work, this requirement is especially important, since the transformers used in such work have a necessarily high leakage reactance and the effect of this reactance must be known in advance.

In using the results of previous investigations<sup>2,3</sup> on this subject, it is necessary for the designer to make a graphical solution of a rather involved transcendental equation, or to rely on charts that have been computed for circuit parameters only commonly encountered in receiving tube power supplies.<sup>1</sup> It is the purpose here, within the range of validity of the approximations made, to remove these restrictions. The approximations are as follows:

1. The load current is considered to be essentially constant. This is justified in the following cases: (a) where the input capacitor is followed by a choke of reasonable size, (b) where the load consists of the plate circuits of pentodes and tetrodes, (c) if the load current is small enough that a quantity  $S$ , to be described later, is less than 25 per cent, and (d) where the load consists of X-ray and other tubes operating under conditions of voltage saturation. It will be noted that these conditions are practically always fulfilled.

2. The resistive component of the rectifier circuit impedance is small compared with the inductive component. Although the exact solution is based on the supposition that  $R = 0$ , a simple approximate correction given later enables the results to be applied with satisfactory accuracy to cases where  $R$  is comparable to  $\omega L$ .

Figure 1 shows the conventional half-wave single-phase rectifier circuit. The notation used in this diagram and in the remainder of this paper is as follows:

$$L = L' + n^2 L_p$$

$L'$  = inductance of filter input choke, if present

$n$  = turns ratio of transformer

$L_p$  = equivalent primary leakage inductance

$C$  = input capacitance

$\omega$  = angular frequency of power source

$$\omega' = 1/\sqrt{LC}$$

$$\rho = 1/(\omega \sqrt{LC}) = \omega'/\omega$$

$i$  = load current

$q$  = charge on capacitor

$E_0$  = peak no-load transformer voltage

$S = 2\pi i/(E_0 \omega C)$  (twice the approximate fractional ripple voltage amplitude)

$\alpha$  = starting phase angle (see Fig. 2)

$\theta$  = conduction angle

$R$  = total power supply resistance, including equivalent tube resistance.

The differential equation for  $q$ , the charge in the first capacitor, valid in the range  $0 < \omega t < \theta$  and subject to the above approximations, is

$$L \frac{d^2 q}{dt^2} + \frac{q}{C} + \frac{1}{C} \int_0^t i dt = E_0 \sin(\omega t + \alpha) \quad (1)$$

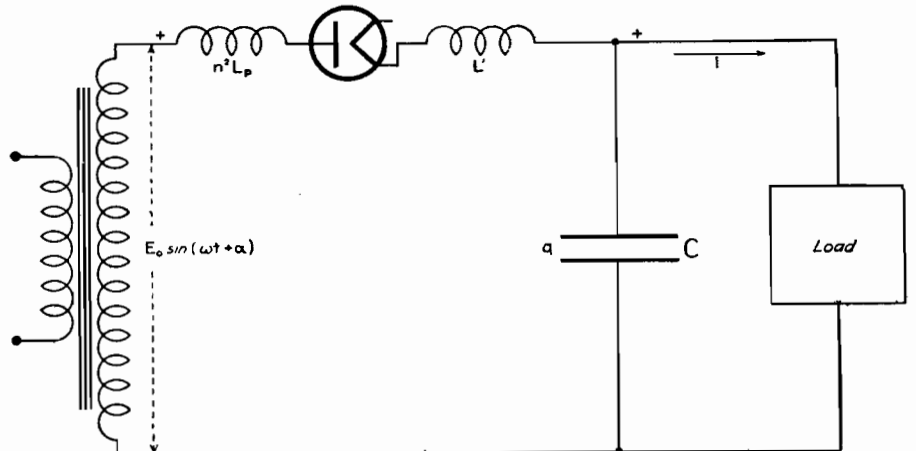


Fig. 1.—Single-phase half-wave rectifier circuit on which the solution is based.

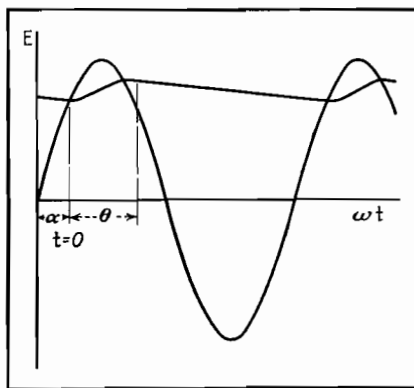


Fig. 2.—Input and output voltages of the rectifier showing starting phase angle and conduction angle. The series choke prolongs the capacitor charging interval.

the solution of which is

$$q = -it + \frac{E_0 C \sin(\omega t + \alpha)}{1 - (1/\rho^2)} + A \cos \omega t + B \sin \omega t \quad (2)$$

The boundary conditions determining  $A$  and  $B$  are

- (1) at  $t = 0$ ,  $q = CE_0 \sin \alpha$
- (2) at  $t = 0$ ,  $\frac{dq}{dt} = -i$  (i.e., the current through the inductance is zero)

On applying these conditions, the solution becomes

$$q = -it + \frac{CE_0}{1 - \frac{1}{\rho^2}} \left[ \sin(\omega t + \alpha) - \frac{1}{\rho} \sin \alpha \cos \omega t - \frac{1}{\rho} \cos \alpha \sin \omega t \right] \quad (3)$$

The rectifier will stop conducting at an angle  $\theta$  given by the condition

$$\frac{dq}{dt}(\theta) = -i \quad (4)$$

On substituting this condition into Eq. (3), there results

$$\cot \alpha = \frac{\sin \theta - \frac{1}{\rho} \sin \rho \theta}{\cos \theta - \cos \rho \theta} \quad (5)$$

A second condition, resulting from conservation of charge over the entire cycle, is

$$q(\theta) - q(0) = \frac{i}{\omega} (2\pi - \theta) \quad (6)$$

Substituting this expression into Eq. (3) and simplifying, we obtain

$$S \csc \alpha = -1 + \frac{1}{1 - \frac{1}{\rho^2}} \times \left[ \left( \cos \theta - \frac{1}{\rho^2} \cos \rho \theta \right) + \left( \sin \theta + \frac{1}{\rho} \sin \rho \theta \right) \cot \alpha \right] \quad (7)$$

where  $\cot \alpha$  is given by Eq. (5).

Equations (5) and (7), being independent, may be solved simultaneously to determine  $\alpha$  and  $\theta$ , and the values of these two angles provide complete determination of any functions of current or voltage. In the case  $\rho = 1$ , the equations are indeterminate in form. However, the solution shows no peculiar behavior in the neighborhood of  $\rho = 1$ ; in fact, it is not to be expected that this case would give rise to any singular behavior, since the current is interrupted during each cycle and resonance in the usual sense of the term cannot occur.

It will be observed that in Eqs. (5)

and (7) the circuit constants are combined in such a way that the equations contain only the parameters  $S$  and  $\rho$  explicitly. This fact and the form of the equations make it possible to obtain a graphical solution in the following way: If  $\log \csc \alpha$  is computed from Eq. (5) and  $\log(S \csc \alpha)$  from Eq. (7) for various values of  $\rho$ , and plotted as a function of  $\theta$  on transparent paper, the values of  $\alpha$  and  $\theta$  satisfying the two equations simultaneously may be obtained by simply superposing the two graphs with their  $\theta$  axes separated by  $\log S$  and the ordinate axes collinear, and then reading the coordinates of inter-

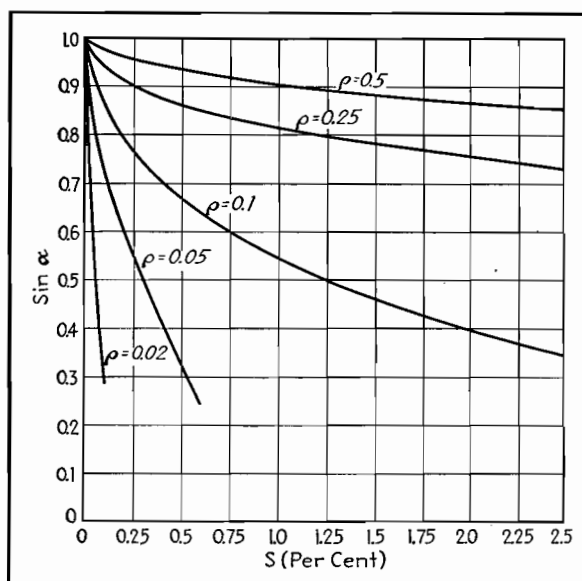


Fig. 3.—Chart of the sine of the starting angle vs. twice the fractional-ripple voltage for low-ripple voltages.

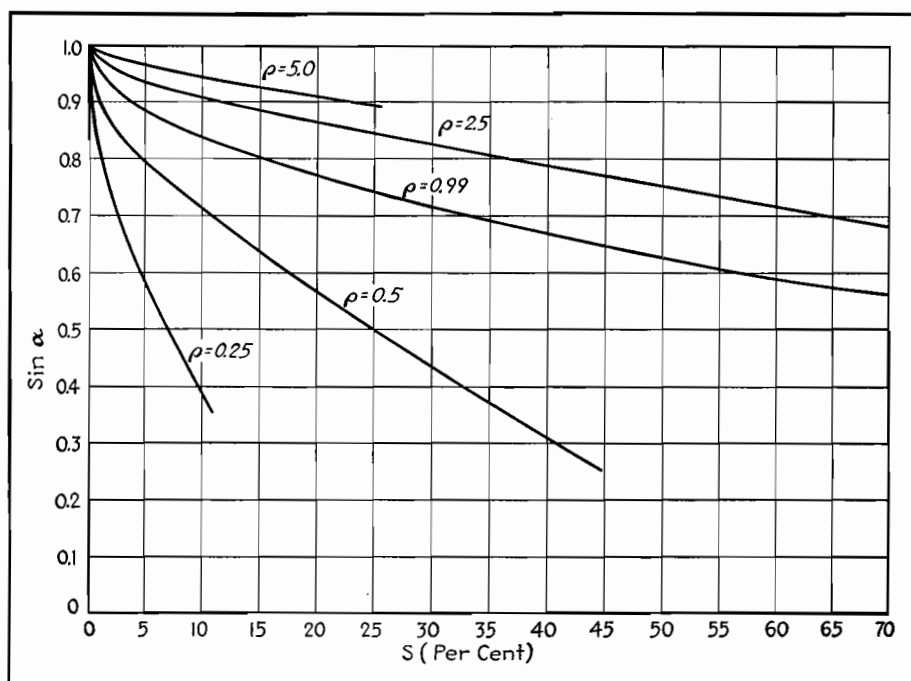


Fig. 4.—Chart of the sine of the starting angle vs. ripple voltage for large ripple voltages.

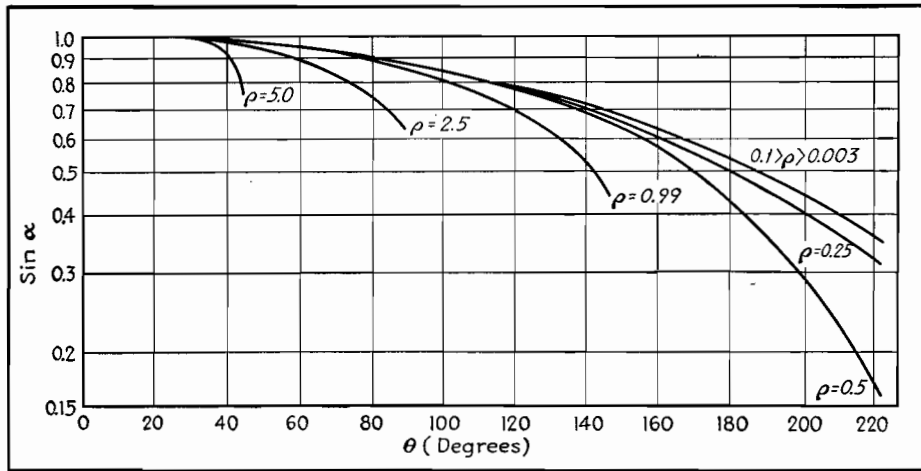
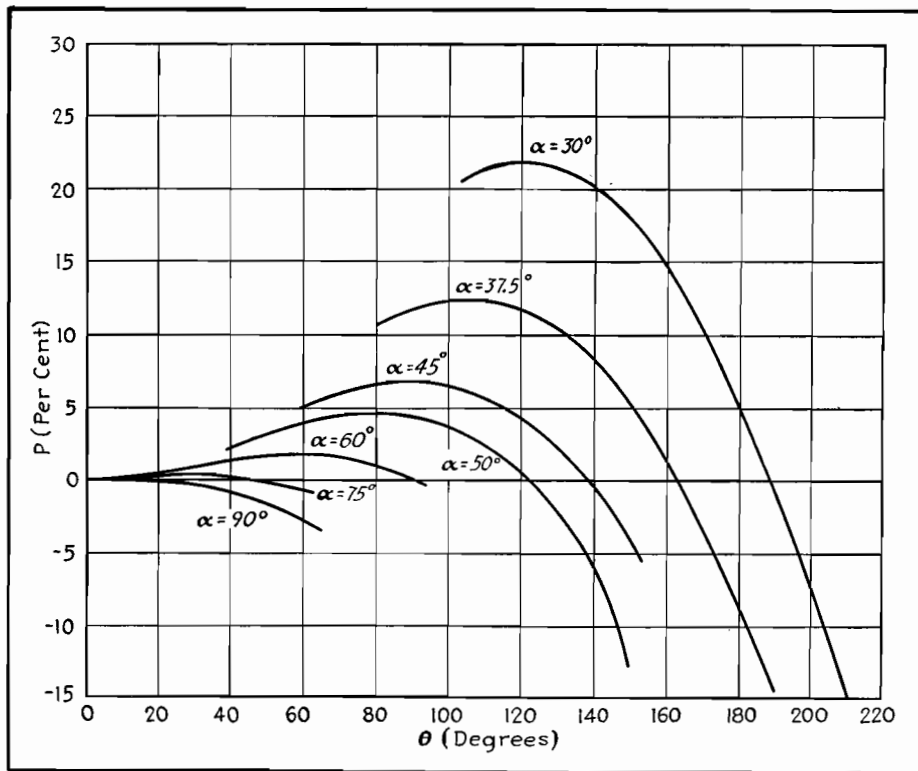


Fig. 5.—The sine of the starting angle vs. conduction angle.

Fig. 6.—The output voltage correction factor  $P$  vs. the angle of conduction.

section of curves corresponding to the same value of  $\rho$ . In this way, the values shown in Figs. 3, 4, and 5 were obtained, and from these figures the angles  $\alpha$  and  $\theta$  can be read directly as functions of arbitrary design parameters.

From Fig. 2 it is evident that for small ripple voltages the d-c output voltage is given to sufficient accuracy by

$$E_{d-c} = E_0 \left( \sin \alpha + \frac{S}{2} \right) \quad (8)$$

and hence Figs. 3 and 4 give directly the voltage-regulation curves of the rectifier. An exact expression, applicable to any ripple voltage, is obtained by integration

of Eq. (3) and elimination of the variable  $\alpha$  by means of Eq. (5). The result is

$$E_{d-c} = E_0 \left[ \sin \alpha (1 + P) + S \left( \frac{1}{2} - \frac{\theta}{2\pi} \right) \right] \quad (9)$$

Figure 6 shows the values of  $P$  for various values of  $\theta$  and  $\alpha$ . It will be noted that  $P$  is usually very small, and since  $\theta$  is usually much less than  $2\pi$ , Eq. (8) will be accurate enough for most applications.

These results may be applied directly to full-wave rectifiers provided that  $\theta < (\pi - \alpha)$ , and provided that half the load current is substituted for  $i$ . If the filter input inductance is very large

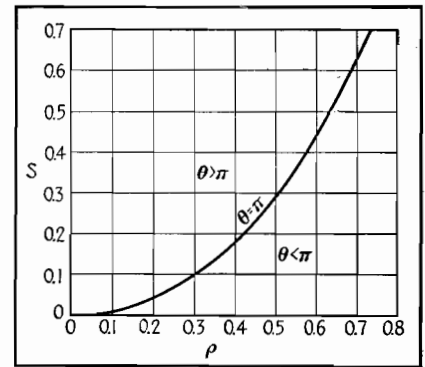


Fig. 7.—Conditions of conduction greater or less than a half cycle.

compared with  $n^2 L_p$ , the restriction becomes  $\theta < \pi$ . The case  $\theta > \pi$ , current flowing continuously, has been treated by Prince and Vodges<sup>1</sup> and, neglecting leakage reactance, by Wallis.<sup>2</sup> The results may be applied to voltage-doubling circuits with the single restriction  $\theta < \pi$ . Figure 7 shows this condition graphically.

These results may also be extended to circuits in which the effect of the rectifier circuit resistance is not negligible, by the following considerations:

The average current flowing in the conducting part of the cycle is  $2\pi i / \theta$ ; hence, if the wave form could be assumed to be entirely unaffected by circuit resistance, the voltage would be lowered by the amount  $2\pi i R / \theta$ . However, any decrease in average voltage results in an increased charging interval, and the voltage loss mentioned above is partly compensated for by the fact that a larger charge is delivered to the capacitor during the conduction time. Empirically, good agreement with the data of Freeman<sup>1</sup> is obtained by using half this correction; namely, by subtracting a quantity  $\Delta V$  given by

$$\Delta V = \frac{i R \pi}{\theta} \quad (10)$$

from the d-c output voltage computed by Eq. (8) or (9). The error in the correction in this form has been found to be not more than 25 per cent of the correction itself, so long as  $i R \pi / \theta$  is not greater than 20 per cent of  $E_0 \sin \alpha$ . Actually, the voltage loss due to the resistance is always somewhat less than predicted by the above expression. The final equation is

$$E_{d-c} = E_0 \left[ \sin \alpha (1 + P) + S \left( \frac{1}{2} - \frac{\theta}{2\pi} \right) - \frac{i R \pi}{\theta} \right] \quad (11)$$

The large range of usefulness of this method and of the charts presented here

is shown by the following widely different applications:

### Examples

**Example 1.**—Consider a half-wave choke-input rectifier for a receiving tube power supply.

$C = 8\mu\text{f}$   
 $L = 10$  henrys  
 $\omega = 377$  (60 cycles)  
 $\omega' = 111.5$   
 $\rho = 0.296$   
 $i = 20$  ma  
 $S = 6.95$  per cent  
 $R = 400$  ohms  
 $E_0 = 600$  volts

From Fig. 4, we find  $\sin \alpha = 0.59$ ,  
 $\alpha = 36^\circ$ . From Fig. 5,  $\theta = 162^\circ$ .

$iR\pi/\theta = 8.9$  volts,  $P$  is less than 1 per cent and therefore neglected, and hence the d-c output voltage is  $E_{d-c} = 600 \times 0.59 - 8.9 + 600 \times 0.069(1/2 - 1/3 \times 60) = 348$  volts.

**Example 2.**—Consider a voltage-doubling X-ray power supply intended for high-current experimental work at 100 kv.

$E_0 = 67.9$  kv  
 $C = 0.2 \mu\text{f}$   
 $n^2 L_p = 70$  henrys  
 $L' = 0$   
 $\omega = 377$  (60 cycles)  
 $\omega' = 277$   
 $\rho = 0.735$   
 $i = 100$  ma  
 $R = 13,500$  ohms  
 $S = 0.12$

From Fig. 4, we find  $\sin \alpha = 0.78$ , and from Fig. 5,  $\theta = 112^\circ$ . From Fig. 6,  $P = 4$  per cent. From Eq. (11), we have

$$\begin{aligned} E_{d-c} &= 67.9 [0.12(1/2 - 1/3 \times 60) + 1.04 \\ &\quad \times 0.78] - 0.1 \times 13,500 \times 180/112 \\ &= 56.5 - 2.17 \\ &= 53.33 \text{ kv per section} \end{aligned}$$

### References

- (1) FREEMAN, R. L., Thesis, Stanford University, 1934.
- (2) WALLIS, C. M., *Electronics*, March, 1940 (reprinted in this book).
- (3) WALLIS, C. M., *Electronics*, October, 1938 (reprinted in this book).
- (4) PRINCE and VODGES, "Principles of Mercury Arc Rectifiers and Their Circuits," McGraw-Hill Book Company, Inc., New York, 1927.
- (5) Terman, "Radio Engineering," 2d ed. McGraw-Hill Book Company, Inc., New York, 1937.

## Rectifier Filter Design

By HERBERT J. SCOTT

Design of low-pass L-section smoothing filters for six different rectifier connections.  
 Graphs facilitate economic choice of  $LC$  values for specified ripple voltage in the output

THE types of rectifiers most generally met with in practice are

Single-phase full-wave  
 Single-phase full-wave bridge  
 Three-phase half-wave  
 Three-phase distributed Y  
 Three-phase double Y  
 Three-phase full-wave

These are illustrated in Fig. 1.

The output of any rectifier circuit contains, in addition to the desired d-c voltage, undesired a-c voltage components. For a given d-c output voltage, the magnitude and frequency of these a-c voltage components is a function of the particular rectifier connection employed. These unwanted a-c components constitute a ripple voltage superimposed on the desired d-c voltage. This ripple voltage may be reduced until it is within tolerable limits by the use of an appropriate filter placed electrically between the rectifier output and the load.

Except for small power supplies, the filter practically always consists of a low-pass L-section filter consisting of a series-inductance element followed by a shunt-capacitance element, as illustrated in Fig. 2. In this figure, let

$E = E_{d-c} + E_{a-c}$  from the rectifier output  
 $I = I_0 + I_1$   
 $I_0$  = d-c component of current from the rectifier  
 $I_1$  = peak value of the a-c component of current from the rectifier  
 $E_0$  = d-c voltage across the load  
 $E_1$  = peak value of the a-c voltage across capacitor  $C$   
 $R$  = load resistance =  $E_0/I_0$

If, as is usually met in practice, the assumptions are made that  $R \gg R_L$  and  $X_c \ll R$ , where  $R_L$  is the resistance of the inductance and  $X_c$  is the reactance of the capacitance  $C$  at the ripple frequency, then to a very good degree of approximation

$$E_0 = E_{d-c}$$

and  $I_1$  may be considered as flowing only through the capacitance  $C$ . The d-c load current flowing through the load  $R$  is  $I_0$ .

The ripple fraction  $r$  may be expressed as the ratio

$$r = \frac{E_1}{E_0}$$

and the per cent ripple is  $r \times 100$ .

Examination of the table shows that the magnitude of the main ripple frequency voltage is very much greater

than the magnitudes of the voltages of the second and third harmonics of this ripple frequency. This, together with the fact that the filter is much more effective in its filtering action at these higher harmonic frequencies, makes it possible to ignore all but the main ripple voltage in the determination of the ripple fraction  $r$  and the determination of the proper values for  $L$  and  $C$ .

Assuming that  $I_1$  flows entirely through  $C$ ,

$$I_1 = \frac{E_{a-c}}{\omega L - 1/\omega C}$$

and

$$E_1 = \frac{I_1}{\omega C}$$

The ripple voltage across the load in terms of the ripple fraction and the d-c voltage is

$$E_1 = rE_0$$

and the a-c input voltage to the filter may be written as

$$E_{a-c} = FE_0$$

where  $F$  is a factor obtained from the table and expresses the ratio of the peak value of the a-c component of voltage (main ripple voltage) in the rectifier output to the d-c component of voltage

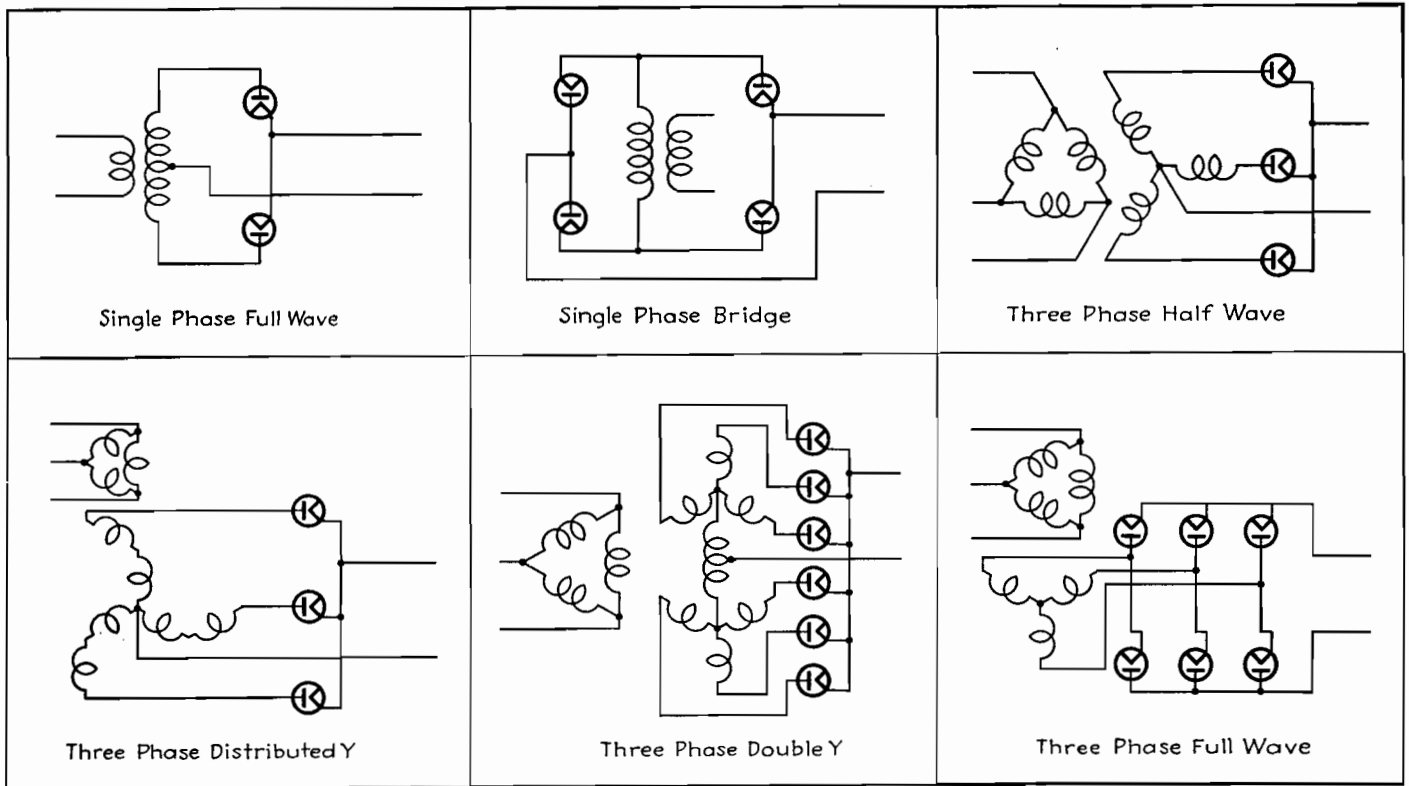


Fig. 1.—Six rectifier circuits for which smoothing filter design data are given.

in the rectifier output for the particular type of rectifier used. For a three-phase half-wave rectifier,  $F$  is seen to be equal to 0.25. Upon elimination of  $I_1$  from the above equations, there results

$$\frac{FE_0}{\omega L - 1/\omega C} = \omega r CE_0$$

from which

$$LC = \frac{F - r}{\omega^2 r} = \frac{1}{\omega^2} \left( \frac{F}{r} - 1 \right) \quad (1)$$

This is the value that the product  $LC$  must have if the ripple appearing across the load is to be the value determined by  $r$ .

There is a further condition that must be imposed on the filter, arising from the fact that at no time during the normal operation of the rectifier must the current delivered to the load become discontinuous. For this condition to be met, the peak value of the a-c current  $I_1$  flowing through inductance  $L$  must not exceed the d-c load current  $I_0$  which is also flowing through the inductance. In the limiting case these two values of current may be just equal to each other. Furthermore, this condition must be met for the minimum load current  $I_{\min}$  that the rectifier will be called on to supply. The magnitude of  $I_1$  remains essentially constant regardless of normal variations in load current, so that if  $I_1$  is maintained at a value equal to or less than  $I_{\min}$  for the minimum load point it will auto-

matically remain less than the d-c current for larger values of load. For the limiting case, then,

$$I_1 = I_{\min} \\ I_1 = \frac{FE_0 - rE_0}{\omega L}$$

but

Let the ratio of full-load current  $I_0$  to the minimum value of load current  $I_{\min}$  be  $k$ . Then

$$I_{\min} = \frac{I_0}{k} \\ I_{\min} = \frac{E_0}{kR}$$

or

Equating the expressions for  $I_1$  and  $I_{\min}$

$$\frac{FE_0 - rE_0}{\omega L} = \frac{E_0}{kR}$$

which gives\*

$$L = \frac{(F - r)kR}{\omega} \quad (2)$$

as the minimum value that  $L$  may have and meet the condition that  $I_1$  shall not be greater than  $I_{\min}$ .

If the value of the product  $LC$  is determined as in Eq. (1), in which the ripple voltage appearing across the load is limited to a certain fraction  $r$  of the d-c output voltage, the ratio of the two quantities  $LC/L$  gives the maximum value that  $C$  may have. It must be remembered that the values of  $L$  and  $C$  so obtained are limiting values only, i.e.,

\* Terman, "Radio Engineering," 2d ed., p. 488, McGraw-Hill Book Company, Inc., New York, 1937.

Relative Magnitudes of Fundamental and Harmonics for Various Types of Rectifiers

	Single-phase full-wave	Single-phase full-wave bridge	Three-phase half-wave	Three-phase distributed Y	Three-phase double Y	Three-phase full-wave
Fundamental ripple frequency $f$ , (frequency of power supply = 60 cycles).	120	120	180	180	360	360
Peak value of fundamental ripple voltage in rectifier output, $\dagger F$ .....	0.667	0.667	0.25	0.25	0.057	0.057
Peak value of second harmonic ripple voltage in rectifier output $\dagger$ .....	0.133	0.133	0.057	0.057	0.014	0.014
Peak value of third harmonic ripple voltage in rectifier output $\dagger$ .....	0.057	0.057	0.025	0.025	0.006	0.006

$\dagger$  The d-c component of voltage in the rectifier output is considered as unity.



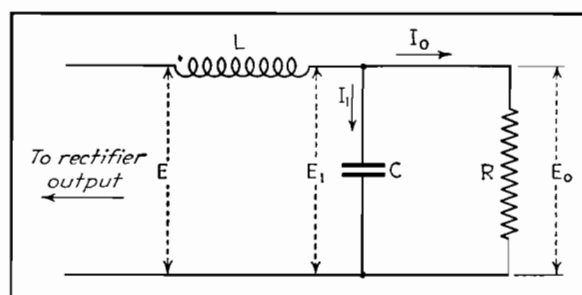


Fig. 2.—Schematic diagram of the L-section filter upon which the filter design is based.

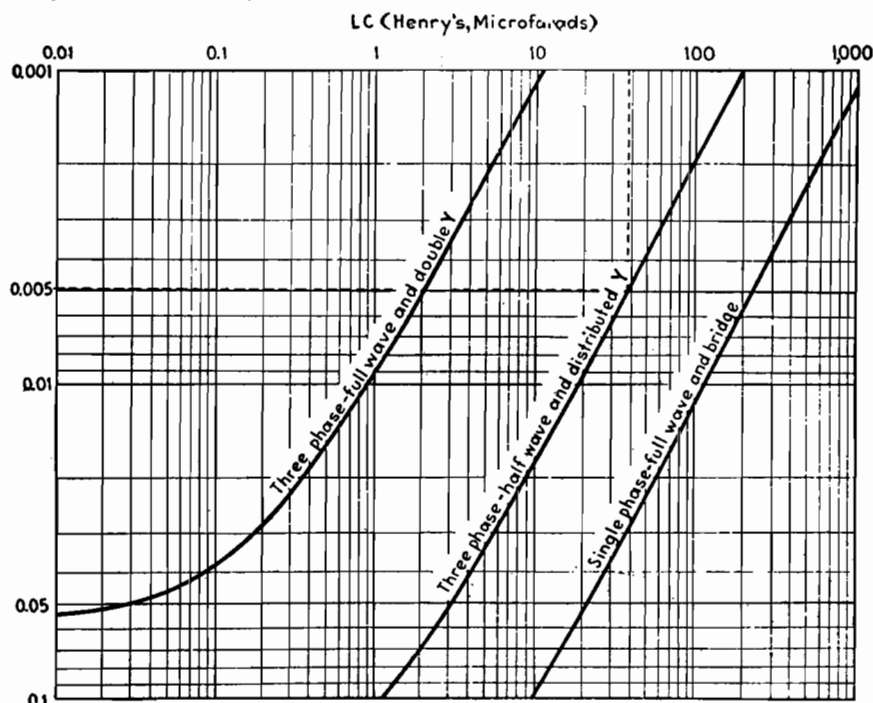


Fig. 3.—LC product for various types of rectifiers shown in Fig. 1 for specified ripple voltage in output.

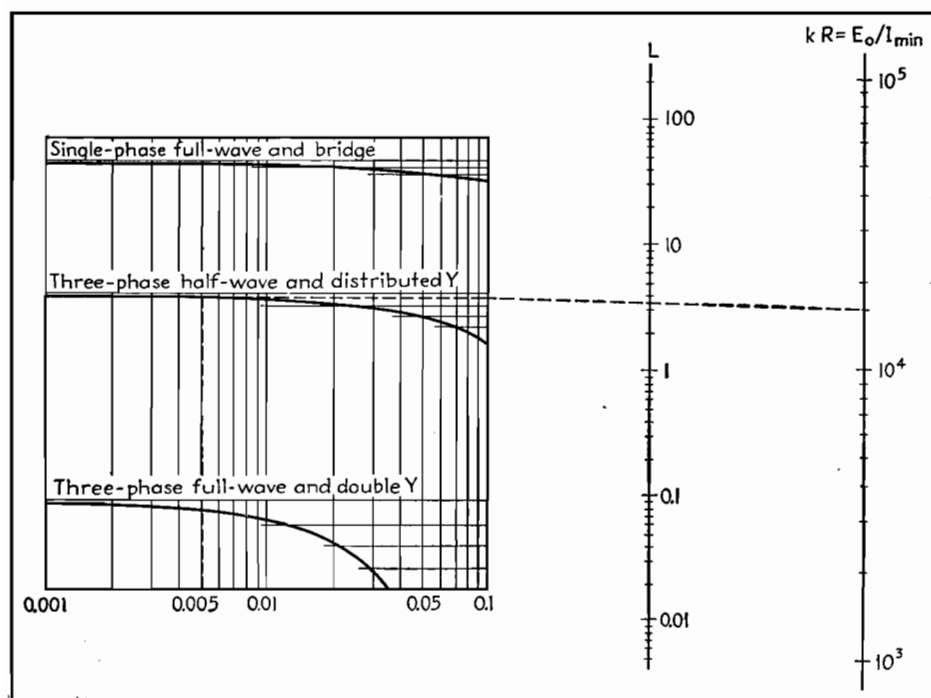


Fig. 4.—Alignment chart for determining minimum inductance required for given ripple voltage.

$LC$  = a certain quantity as determined from Eq. (1)

$L \geq$  a certain quantity as determined from Eq. (2)

$C \leq$  a certain quantity as determined above

In general, this ratio  $LC/L$  results in an unsatisfactory size for  $C$  from a standpoint of economic choice. The final choice of  $L$  and  $C$  must depend on economic considerations and the necessity of utilizing components in sizes available from the manufacturer. It makes no difference in the performance of the filter section if  $L$  is chosen  $n$  times as large as given by Eq. (2) and the value of  $C$  is  $1/n$ th as large as determined above, so long as the product of these remains equal to the value of  $LC$  as determined from considerations of allowable ripple, and so long as the value of  $X_c$  remains small with respect to  $R$ . A further condition is sometimes imposed on the value of  $C$  by stating that the filter capacitor shall have an impedance not to exceed a certain amount at some specified minimum frequency.\* Such a criterion then would establish a minimum value for  $C$ .

To facilitate computation, two charts have been prepared, one giving the product of  $LC$  as a function of the ripple fraction  $r$  and the type of rectifier employed (Fig. 3), and the other giving the minimum value of  $L$  as a function of the ripple fraction  $r$ , the type of rectifier, and the value of  $kR = E_0/I_{\min}$ . (These charts are based on a frequency of 60 cycles for the power-supply system.)

As an example of the application of the above discussion to a typical design problem, consider a three-phase half-wave rectifier which is to supply a load with 4,000 volts direct current and a full-load current of 1 amp. The filter is to be designed so that the ripple appearing across the load is to be limited to 0.5 per cent. What must be the values of  $L$  and  $C$  to give the desired performance?

Assume  $I_{\min}$  to be one-fourth full-load current, then  $k = 4$  and  $kR = E_0/I_{\min} = 4,000/0.25 = 16,000$ . The chart of Fig. 3 shows that for a rectifier of this type and a ripple fraction  $r = 0.005$ , the product  $LC = 38.4$ . For  $kR = 16,000$  and  $r = 0.005$ , the chart of Fig. 4 gives the minimum value of  $L$  as 3.5 henrys. The maximum value that  $C$  may have then is  $LC/L = 38.4/3.5 = 11 \mu\text{f}$ . The value of  $C$  thus obtained is larger than would be used in practice and represents simply a limiting value.

\* EASTMAN, A. V., "Fundamentals of Vacuum Tubes," p. 66. McGraw-Hill Book Company, Inc., New York.

If the criterion previously mentioned is applied by stating that at 40 cycles the impedance represented by  $C$  shall not exceed 1,000 ohms, a capacitor of at least 4  $\mu$ f must be used. This would

necessitate an inductance of  $L = 38.4/4 = 9.6$  henrys. A filter section then composed of an inductance of 9.6 henrys and a capacitance of 4  $\mu$ f would result in an entirely satisfactory filter that meets the

requirements of minimum  $L$ , ripple of 0.5 per cent, and  $X_c$  less than 1,000 ohms at 40 cycles, and always very much less than  $R$ .

## Filter Design for Grid-controlled Rectifiers

By HAROLD A. THOMAS

Analysis of voltage waves in single-phase thyatron rectifier circuits with inductive-input filters, taking into account the variations in harmonic content with conduction angle. Basic equations are developed into a practical design procedure, and examples are given

**S**INGLE-PHASE full-wave rectifiers employing gas triodes (thyatrons) have been used in numerous applications where accurate and smooth control of the d-c output is required. In some of these applications, adequate filtering is necessary to reduce the output ripple voltage below some specified value. The usual filter-design equations used in the case of the high-vacuum or gas-diode rectifiers are not suitable because the magnitudes of the harmonic components to be filtered vary with the conduction angle of the tube.

Grid-controlled gas-tube rectifiers are usually controlled by means of a phase-shifting circuit that controls the point on the anode voltage wave at which the tube starts to conduct.

### Rectifier with Resistance Load and No Filter

In Fig. 1 is shown a typical grid-controlled rectifier and phase-shifting circuit

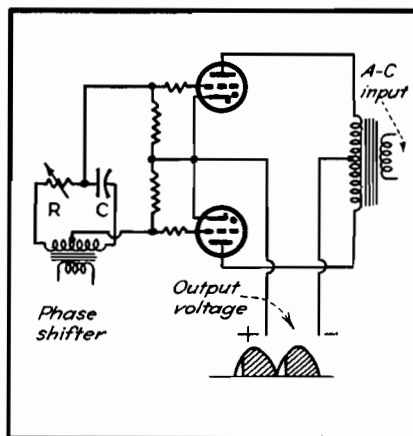


Fig. 1.—Basic circuit of grid-controlled rectifier with phase-shift control.

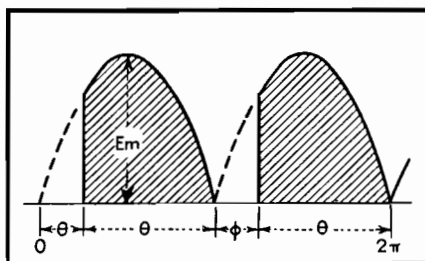


Fig. 2.—Wave form for grid-controlled rectifier with no filter.

for controlling the conduction angle, with an illustration of the type of output voltage wave to be expected for a given angle of delay if the load is pure resistance. The action of the gas triodes and phase shifter circuit will not be discussed further as this is usually dealt with in most texts on electronics, but, rather, an analysis of the voltage waves and the design of filters for these waves will be considered.

In Fig. 2 is shown a typical output voltage wave in which the firing of the tube has been delayed for an angle  $\phi$  and tube conduction takes place through an angle  $\theta = \pi - \phi$  if the arc drop is assumed negligible. This recurring wave may be expressed by a Fourier series in the usual manner

$$e = E_{d-c} + \sum_{n=1}^{\infty} A_n \cos nx + \sum_{n=1}^{\infty} B_n \sin nx \quad (1)$$

where

$$E_{d-c} = \frac{1}{2\pi} \int_{\theta}^{2\pi} f(x) dx \quad (2)$$

$$A_n = \frac{1}{\pi} \int_{\theta}^{2\pi} f(x) \cos nx dx \quad (3)$$

$$\text{and } B_n = \frac{1}{\pi} \int_{\theta}^{2\pi} f(x) \sin nx dx \quad (4)$$

In the case of the wave shown in

Fig. 2,  $f(x) \Big|_0^{\phi} = 0$  and  $f(x) \Big|_{\phi}^{\pi} = E_{\max}$

$\sin x$  where  $x = \omega t$  and  $E_{\max}$  is the crest value of the transformer voltage from one end to center tap. In determining the coefficients  $A_n$ ,  $B_n$ , and  $E_{d-c}$ , it will be necessary to integrate only through the limits from  $\phi$  to  $\pi$  and multiply the result by 2 since the half-cycles are identical. Then

$$E_{d-c} = \frac{E_{\max}}{\pi} \int_{\phi}^{\pi} \sin x dx = \frac{E_{\max}}{\pi} (1 + \cos \phi) \quad (5)$$

The d-c component of the voltage wave thus varies from zero to the value  $2E_{\max}/\pi$  as the delay angle is varied from  $\pi$  to zero. Figure 3 shows how the ratio  $E_{d-c}/E_{\max}$  varies with  $\phi$ .

Since it is usually necessary to know only the magnitude of the harmonic terms present, a complete Fourier series for the wave is not necessary. Inspection of Eq. (1) will show that the  $n$ th harmonic is given by  $(A_n \cos nx + B_n \sin nx)$ , and therefore the magnitude of the  $n$ th

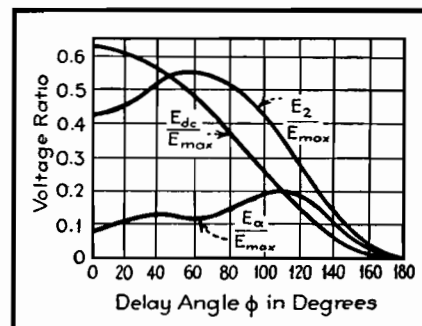


Fig. 3.—Output components of a grid-controlled rectifier with no filter.

harmonic voltage is

$$E_n \max = A_n + jB_n \quad (6)$$

Substituting Eqs. (3) and (4) in Eq. (6)

$$E_n \max = \frac{1}{\pi} \int_0^{2\pi} f(x) (\cos nx + j \sin nx) dx \\ = \frac{1}{\pi} \int_0^{2\pi} f(x) e^{jnx} dx \quad (7)$$

Putting in for  $f(x)$  its value for the particular wave under study and changing the limits, we get

$$E_n \max = \frac{2E_{\max}}{\pi} \int_{\phi}^{\pi} \sin x e^{jnx} dx \\ = \frac{-2E_{\max}}{\pi} \left[ \frac{e^{jnx} (\cos x - jn \sin x)}{1 - n^2} \right]_{\phi}^{\pi} \quad (8)$$

By applying the principle of symmetry to the wave, it may be seen that  $f(x) = f(\pi + x)$ , for which it can be shown that no odd harmonics can exist. If  $n$  is given only even values, the limits substituted and the resulting equation expanded, the following expression for the crest value of the  $n$ th harmonic voltage results:

$$E_n \max = \frac{2E_{\max}}{\pi(1 - n^2)} \\ \frac{\sqrt{(1 + \cos \phi \cos n\phi + n \sin \phi \sin n\phi)^2} + (n \sin \phi \cos n\phi - \cos \phi \sin n\phi)^2} \quad (9)$$

Figure 3 shows the variation of the second and fourth harmonic terms with the angle  $\phi$ . It must be stressed that the curve shown in Fig. 3 can be used only with a nonreactive load as the presence of a filter changes the output voltage wave of the rectifier considerably. This fact is commonly overlooked, as has been pointed out by M. B. Stout.<sup>1</sup>

#### Rectifier with Inductive-input Filter

It was noticed in Fig. 2 that current flows for only a portion of each half-cycle if the load is noninductive. If a series inductance is added, the current will tend to flow for a longer period of time but with a corresponding decrease in the peak value. If the inductance is made large enough, current will flow through the load circuit continuously. A critical value of inductance  $L_{cr}$  may be defined as that value which will just prevent the current from dropping to zero at any portion of the cycle.

If a grid-controlled rectifier with delayed firing angle has an inductive-input filter (Fig. 4) with the value of the inductance less than critical, damped oscillatory waves are set up as shown in Fig. 5a, and the circuit in general becomes very unstable. This type of operation is

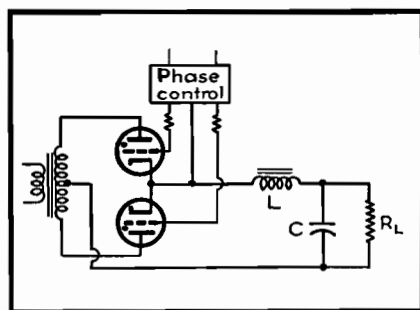


Fig. 4.—Grid-controlled rectifier circuit with inductive-input filter.

very undesirable and should be avoided by making  $L > L_{cr}$  for all values of load current and delay angle.

If  $L > L_{cr}$ , the tube that is conducting will continue to conduct until the second tube fires, even though the anode potential swings negative with respect to the transformer center tap over a portion of the cycle as shown in Fig. 5b. This effect is produced by the induced emf of the input filter choke.

Since for this case the tube drop is constant throughout the whole cycle, it will not enter into the calculation of the harmonic terms and can be subtracted from the d-c component.

A study of the wave in Fig. 5b will show that  $f(x) = E_{\max} \sin x - E_D$  Substituting this in Eq. (2) gives

$$E_{d-c} = \frac{E_{\max}}{\pi} \int_{\phi}^{\pi+\phi} \sin x dx - \frac{E_D}{\pi} \int_{\phi}^{\pi+\phi} dx \\ = \frac{2E_{\max}}{\pi} \cos \phi - E_D \quad (10)$$

A plot of Eq. (10), neglecting tube drop, is shown in Fig. 6. It is seen that the complete range of output voltage may be covered with only a 90-deg variation of delay angle. Values from this curve

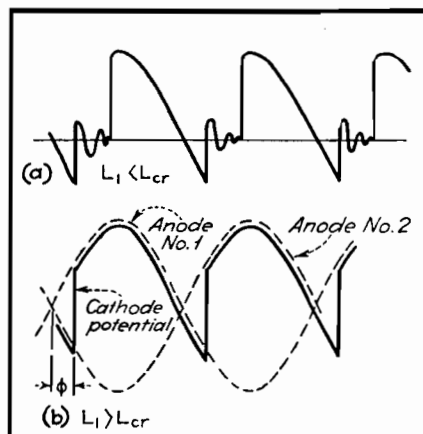


Fig. 5.—Voltage waves for grid-controlled rectifier with inductive-input filter. At (a) the inductance is less than the critical value, and at (b) it is greater than the critical value.

should be multiplied by  $E_{d-c}/(E_D + E_{d-c})$  to correct for tube drop.

Substituting  $f(x)$  into Eq. (7) gives for the  $n$ th harmonic

$$E_n \max = \frac{2E_{\max}}{\pi} \int_{\phi}^{\pi+\phi} \sin x e^{jnx} dx \quad (11)$$

which when integrated, limits substituted, and reduced as before (with  $n = 2, 4, 6 \dots$ ) gives

$$E_n \max = \frac{4E_{\max}}{(1 - n^2)} \\ \frac{\sqrt{(\cos \phi \cos n\phi + n \sin \phi \sin n\phi)^2} + (\cos \phi \sin n\phi - n \sin \phi \cos n\phi)^2} \quad (12)$$

Since any filter designed to reduce the second harmonic voltage to a specified value will be at least four times more effective for the next higher harmonic, it is necessary to consider only the second harmonic in the design of the filter. Figure 6 shows the variation of the second harmonic voltage at the input to the filter with the delay angle  $\phi$ .

The usual procedure for determining the critical value of inductance required in single-phase full-wave diode rectifier circuits is to neglect all the harmonic terms except the second and solve the resulting equivalent circuit for the direct and alternating components of current through the input choke. The critical value of inductance  $L_{cr}$  which will just keep a current flow at all times through the choke can then be determined from the critical condition of  $I_{d-c} = I_{a-c \max}$ . This solution<sup>2</sup> gives  $L_{cr} = R_T/1,130$  for a 60-cycle impressed voltage, where  $R_T$  is the total d-c resistance that the direct component of current must flow through. This equation is correct within about 10 per cent for the diode rectifiers except when operating at low voltages, but will give an error of 25 to 50 per cent, depending on the delay angle, for the grid-

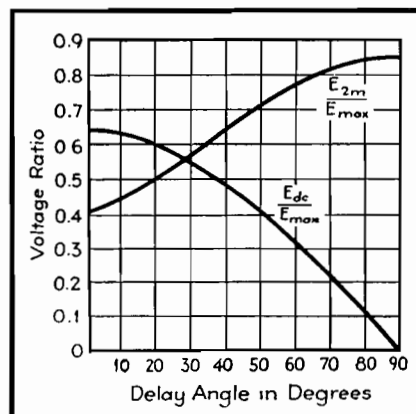


Fig. 6.—Output components of grid-controlled rectifier with inductive-input filter.

controlled rectifier. The correct value of critical inductance for grid-controlled rectifiers for different firing angles has been determined in an analysis by Overbeck.<sup>3</sup> The results of this investigation are shown in the curve of  $L_{cr}/R_T$  vs.  $\phi$  in Fig. 7. The values of  $L_{cr}/R_T$  should be multiplied by  $(E_D/E_{d-c}) + 1$  to correct for tube drop.

As mentioned before, the a-c voltages of higher order are not only much smaller initially than the second harmonic but also are attenuated by the filter to a much higher degree, and therefore the percentage output ripple voltage of the filter may be defined as the rms value of the second harmonic output voltage expressed as a percentage of the d-c output voltage. Then

$$\% \text{ ripple} = 100 \times \frac{E_2}{E_{d-c \text{ output}}} \quad (13)$$

$$E_2 = 4E_{\max} K_\phi \frac{S}{3\pi \sqrt{2}} \quad (14)$$

where

$$K_\phi = \frac{\sqrt{(\cos \phi \cos n\phi + n \sin \phi \sin n\phi)^2 + (\cos \phi \sin n\phi - n \sin \phi \cos n\phi)^2}}{2}$$

and  $S$ , the smoothing factor of the filter, is in accordance with the usual filter-design equation

$$S = \frac{1}{(2\omega)^{2a} (L_1 L_2 L_3 \dots L_n) (C_1 C_2 C_3 \dots C_n)} \quad (15)$$

$\omega$  being  $2\pi$  times the original supply frequency and  $a$  the number of sections in the filter.

The direct output voltage is the direct input voltage to the filter minus the voltage drop in the filter

$$E_{d-c \text{ out}} = \left( \frac{2E_{\max}}{\pi} \cos \phi - E_D \right) - I_{d-c} R_F \quad (16)$$

and

$$I_{d-c} = \frac{\left( \frac{2E_{\max}}{\pi} \cos \phi - E_D \right)}{R_L + R_F} \quad (17)$$

where  $R_L$  is the resistance of the load and  $R_F$  is the filter resistance. Substituting Eq. (17) into (16), then substituting the resulting equation along with Eq. (14) into (13) gives

$$\% \text{ ripple} = \frac{4E_{\max} K_\phi S \times 100}{3\pi \sqrt{2} \left( \frac{2E_{\max}}{\pi} \cos \phi - E_D \right) \left( 1 - \frac{R_F}{R_L + R_F} \right)} \quad (18)$$

In the case of rectifiers for voltages of the order of a few hundred volts or more and for delay angles up to 60 or 70 deg

(larger angles than this are impractical),  $E_D$  in Eq. (18) may be neglected. Further, since  $R_L \gg R_F$ , the quantity  $1 - R_F/(R_L + R_F)$  of Eq. (18) will be approximately equal to 1 (this approximation can be corrected for later), then Eq. (18) can be reduced to

$$\% \text{ ripple} \cong \frac{\sqrt{2} K_\phi S \times 100}{3 \cos \phi} \quad (19)$$

For a single-section filter at 60 cycles, Eq. (19) can be expressed as

$$\% \text{ ripple} \times L_1 C_1 \times 10^{-2} = \frac{0.831 K_\phi}{\cos \phi} \quad (20)$$

and for a two-section filter

$$\% \text{ ripple} \times L_1 L_2 C_1 C_2 \times 10^{-2} = \frac{1.46 K_\phi}{\cos \phi} \quad (21)$$

A plot of Eqs. (20) and (21) which may be used for design purposes is shown in Fig. 7. If the d-c resistance  $R_F$  of the filter chokes is not small compared with  $R_L$ , then the values of per cent ripple ( $L_1 C_1$ ) should be multiplied by  $(R_L + R_F)/R_L$ .

### Practical Design Procedure

Ordinarily in the design of rectifier and filter systems the output voltage, current rating, and percentage ripple that can be tolerated are specified by the use to which the rectifier is to be put, and it is the problem of the designer to choose circuit elements that will allow the specifications to be met in the most economical way. Unfortunately, when starting with the output or load requirements, some cut-and-try calculations may be necessary, though the use of the curves in Figs. 6 and 7 will reduce the amount of work quite appreciably. Also, single-phase rectifiers are used only on relatively low-power installations where high accuracy in the design is not usually necessary.

While the equations predict that the output voltage can be varied from a maximum value down to zero, it is obvious from a study of Figs. 6 and 7 that it would require an infinite filter to do so if low percentage ripple is to be maintained. Practical limits on the maxi-

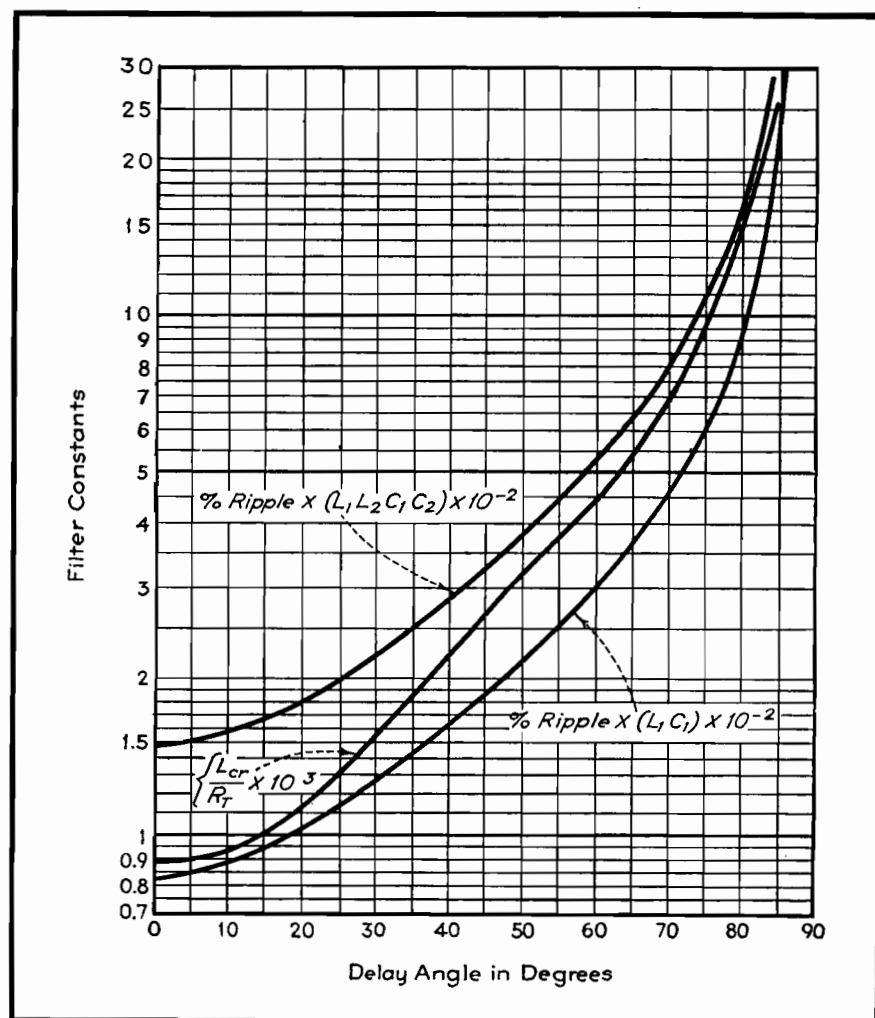


Fig. 7.—Curves for determining filter constants for grid-controlled rectifiers.

mum delay angle range between 60 to 70 deg. At 70 deg the output voltage will be reduced to about 34 per cent of the value with zero delay.

The use of a swinging choke for the input inductance will reduce the cost of the filter considerably. Also, since the percentage ripple increases with delay angle, the required  $LC$  product should be calculated for the largest delay angle. The following examples illustrate the design procedure for a typical rectifier.

### Examples

**Example 1.**—Assume the load requirements are such that the load voltage is to vary between 500 and 1,000 volts with a maximum per cent ripple of 0.5 per cent, and that the load current is to vary between 100 and 500 ma. Neglecting tube and filter voltage drop as a first approximation, we find from Fig. 6 that  $E_{d-c}/E_{max} = 0.636$  (for  $\phi = 0$ ), or  $E_{max} = 1,000/0.636 = 1,570$  volts. From Eq. (10),  $\cos \phi_{max} = 500\pi/2 \times 1,570 = 0.5$ , and  $\phi_{max} = 60^\circ$ .

From Fig. 7, for  $\phi = 0$ ,  $(L_{cr}/R_T) \times 10^3 = 0.88$ . Since  $R_T = 1,000/100 \times 10^{-3} = 10,000$  ohms, then  $L_{cr} = 8.8$  henrys. For  $\phi = 60^\circ$ ,  $(L_{cr}/R_T) \times 10^3 = 4.4$ . Here  $R_T = 500/100 \times 10^{-3} = 5,000$  ohms, and  $L_{cr} = 5,000 \times 4.4 \times 10^{-3} = 22$  henrys. Hence the input inductance should have a minimum inductance of 22 henrys at a current of 100 ma.

The amount of filtering necessary should always be calculated for the maximum delay angle. From Fig. 7, for  $\phi = 60^\circ$ , per cent ripple  $\times (L_1 L_2 C_1 C_2) \times 10^{-2} = 5.26$ . For 0.5 per cent ripple,  $(L_1 L_2 C_1 C_2) = 1,052$ . If  $L_1$  is a swinging choke having 25 henrys at 100 ma and 6 henrys at 500 ma, and if  $C_1$  and  $C_2$  are

4  $\mu$ f each, then  $L_2 = 1,052/6 \times 4 \times 4 = 11$  henrys. In this case a single-section filter would have proved impractical because of the large values of  $L$  and  $C$  required.

Since the inductance values of the chokes are now known, their resistances may be determined from the choke design. Typical values for the above chokes rated at 500 ma would be about 75 ohms each. Hence the voltage drop in the filter would be  $2 \times 75 \times 0.5 = 75$  volts. Assuming the tube drop is 10 volts, the actual transformer voltage required would be  $(1,000 + 75 + 10)/0.636 \sqrt{2} = 1,205$  volts effective each side of center tap.

In the above example the effect of ignition voltage on minimum delay angle, and two other corrections mentioned earlier in the discussion were not considered because of their small effect. However, in the case of low-voltage high-current rectifiers, these corrections would have to be made, and so, for the purpose of illustration, they will be calculated for the above rectifier.

**Example 2.**—It will be noticed from Fig. 5b that the cathode-anode potential difference is equal to twice the transformer voltage at the instant of firing, and hence the minimum value of  $\phi$  is the value that will make twice the instantaneous transformer voltage equal to the ignition voltage of the tube. If type FG-17 thyratron tubes are used in the above application, the ignition potential will be approximately 40 volts. Hence  $40 = 2E_{max} \sin \phi_{min}$ , and also from Eq. (10) (include the filter drop which was determined from the first approximate design),  $1,000 + 0.5 \times 2 \times 75 = (2E_{max}/\pi) (\cos \phi_{min}) - 10$ . Therefore  $\tan \phi_{min} = 40/1,085\pi = 0.00172$ , or  $\phi_{min} = 1^\circ$  and  $E_{max} = 1,085\pi/2 \cos 1^\circ = 1,705$  volts.

Also,  $E = 1,705/\sqrt{2} = 1,205$  volts, which is the full-load voltage rating of the transformer secondary from end to center-tap.

To calculate  $\phi_{max}$  from Eq. (10),  $500 + 0.5 \times 2 \times 75 + 10 = (2 \times 1,705/\pi) \cos \phi_{max}$ , from which  $\phi_{max} = 57.2^\circ$ . Then from Fig. 7, applying corrections,  $(L_{cr}/R_T) \times 10^3 = 4.24 (1 + 10/500) = 4.33$ , and  $R_T = (500/100 \times 10^{-3}) \times 150 = 5150$  ohms. Therefore  $L_{cr} = 4.33 \times 10^{-3} \times 5150 = 22.3$  henrys. Also from Fig. 7 for  $\phi_{max} = 57.2^\circ$ , per cent ripple  $\times (L_1 L_2 C_1 C_2) \times 10^{-2} = 4.7 (R_L + R_F)/R_L$ , and  $(R_L + R_F)/R_L = (1,000 + 150)/1,000$  since this correction should be calculated for the lowest load resistance possible for  $\phi_{max}$ , i.e., for  $R_L = 500/0.5 = 1,000$  ohms. Then  $L_1 L_2 C_1 C_2 = 1,080$  for 0.5 per cent ripple.

As before, if  $L_1$  is a 25-6 henry swinging choke and  $C_1$  and  $C_2$  are each 4  $\mu$ f, then  $L_2 = 1,080/6 \times 4 \times 4 = 11.25$  henrys.

It can be seen that in this example the more exact calculation gave practically the same solution as the approximate design based upon the curves with no corrections except that for the transformer voltage. In low-voltage power supplies, however, it would be well to make an approximate solution from the curves, find the approximate value of  $R_F$ , and then recalculate the values as was done above.

The curves and design procedure have been checked experimentally and were found to be correct within the limits of experimental error.

### References

- (1) STOUT, M. B., Wave Forms for Half-wave Rectifiers, *Electronics*, September, 1939.
- (2) EASTMAN, "Fundamentals of Vacuum Tubes," McGraw-Hill Book Company, Inc., p. 187, New York.
- (3) OVERBECK, W. P., Critical-Inductance and Control Rectifiers, *Proc. IRE*, 27, 655.

## SECTION XVIII

# RELAYS

Choosing Relays for Tube Output Circuits.....	Page 243
Design Chart for Sensitive Relays.....	246

## Choosing Relays for Tube Output Circuits

By E. E. GEORGE

Circuit conditions for developing optimum relay mmf can be rapidly determined by superimposing a relay characteristic chart on tube static curves. The effect of variations of voltage or relay and tube characteristics are easily seen

**I**F TUBE characteristics are known, it is immediately possible to determine by inspection the most suitable resistance for a standard telephone-type relay coil to operate in the plate circuit and supply the maximum magnetomotive force for operating the relay. By superimposing the two families of characteristics, the effects of variations of either the tube or the relay parameters may be more easily visualized.

The curves presented have been worked up for standard telephone-type relays, since these are used more frequently than any other type in vacuum-tube plate circuits. Figure 1 shows the ratio of turns to the coil resistance for such relays. The data given are for Automatic Electric Company's relays of the AQA or similar type, assuming copper wire, enameled cotton insulation, no slugs or other accessories that reduce the winding space, and coils full wound (except as noted) so as to get the maximum number of turns in the specified length and limiting outside diameter. Other makes of telephone relays have similar characteristics. For example, this design of relay is similar to that used in much Western Electric telephone equipment. Very few standard designs have full windings where the resistance is less than 30 ohms, and the points shown to the left end of the curve are therefore for coils  $\frac{3}{4}$  or  $\frac{7}{8}$  of full wound, since these are the maximum available below 30 ohms.

When plotted on log-log paper, the relation between the coil resistance and the number of turns in the relay may be represented by means of a straight line having a slope equal to one-half. This slope has been drawn in Fig. 1, together with the points justifying the assumption of the square-root relation connecting the relay resistance with the number of turns in the relay coil. The relays for which Fig. 1 applies have a winding length of  $2\frac{1}{16}$  in., an outside diameter of 1 in., and an inside diameter of  $\frac{3}{8}$  in.

To determine the magnetic character-

istics of the relay in terms of the operating voltages and current, the following mathematical notations will be adopted:

Let  $MMF$  = mmf developed

$T$  = number of turns on the relay

$R$  = resistance of the relay

$P$  = power consumed in the relay coil

$I_r$  = current through the relay

$I_p$  = plate current of the vacuum tube

$E_r$  = voltage across the relay coil

$E_p$  = voltage on the plate of the tube

$E_b$  = total plate supply voltage

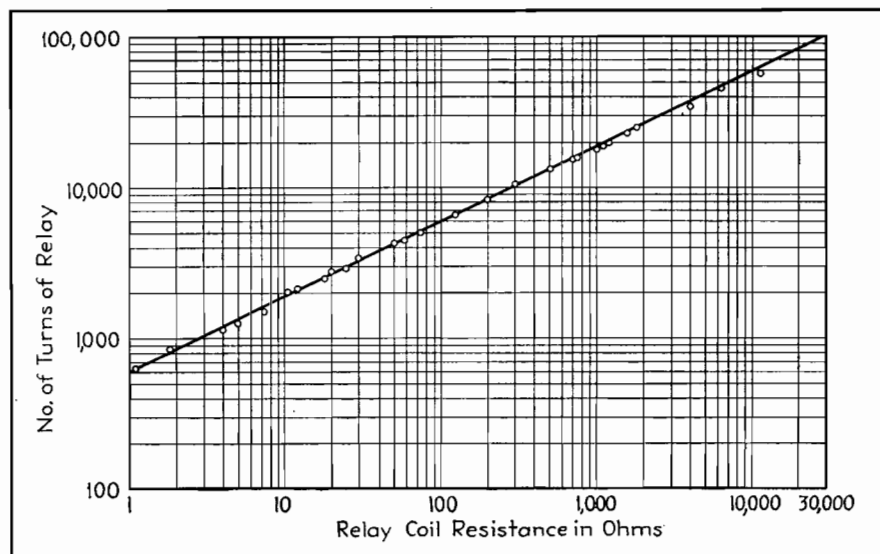


Fig. 1.—Theoretical curve and observed points showing coil resistance and number of turns for standard telephone-type relays.

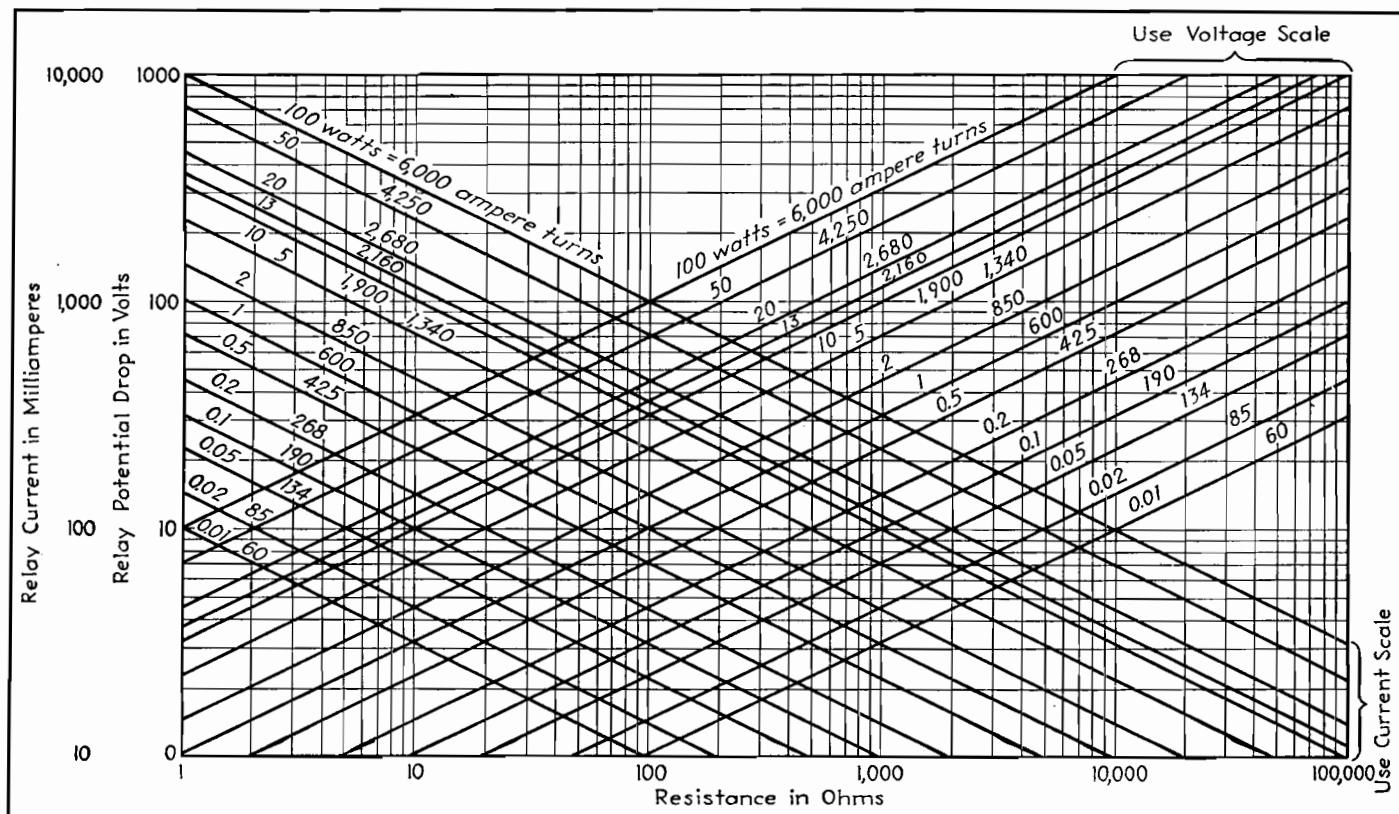


Fig. 2.—This combination chart relates five important parameters for standard telephone type relays: relay current, voltage, resistance, power consumption, and ampere turns. These curves will be useful for design work or for preparing a chart like that shown in Fig. 3.

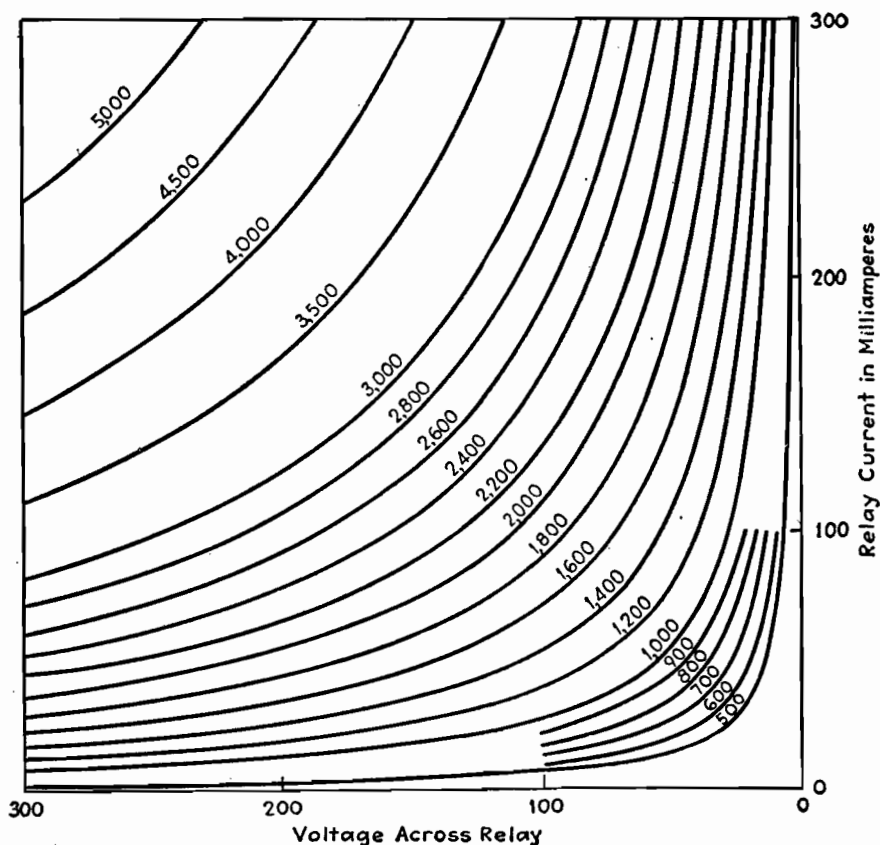


Fig. 3.—Hyperbolic curves giving telephone-relay ampere turns as a function of voltage and current.

Using this symbolic notation, we may derive from Fig. 2 the relations

$$T = 600R^{1/2} \quad (1)$$

$$P = \frac{E_r^2}{R} = I_r^2 R = E_r I_r \quad (2)$$

$$MMF = I_r T = 600 I_r R^{1/2} = 600 P^{1/2} \quad (3)$$

For a relay in the plate circuit of a vacuum tube, we have the relations

$$I_r = I_p \quad (4)$$

$$E_r + E_p = E_b \quad (5)$$

so that the mmf produced, in terms of the tube voltage and current, is

$$MMF = I_r T = 600[(E_b - E_p)I_p]^{1/2} \quad (6)$$

Equation (3) expresses the relation between the mmf in ampere turns and the power consumption of the relay, and enables us to plot ampere-turn curves with voltage, current, and resistance characteristics of the relay coil as coordinates. While the square-root relation between resistance and ampere turns is true for all types of cylindrical windings meeting closely the above-mentioned requirements of space factor and ratio of outside to inside winding diameter, the constant, 600, will vary for winding spaces of different size or shapes. Plotting data for full-wound coils of different size of wire on log-log paper enables us to deter-



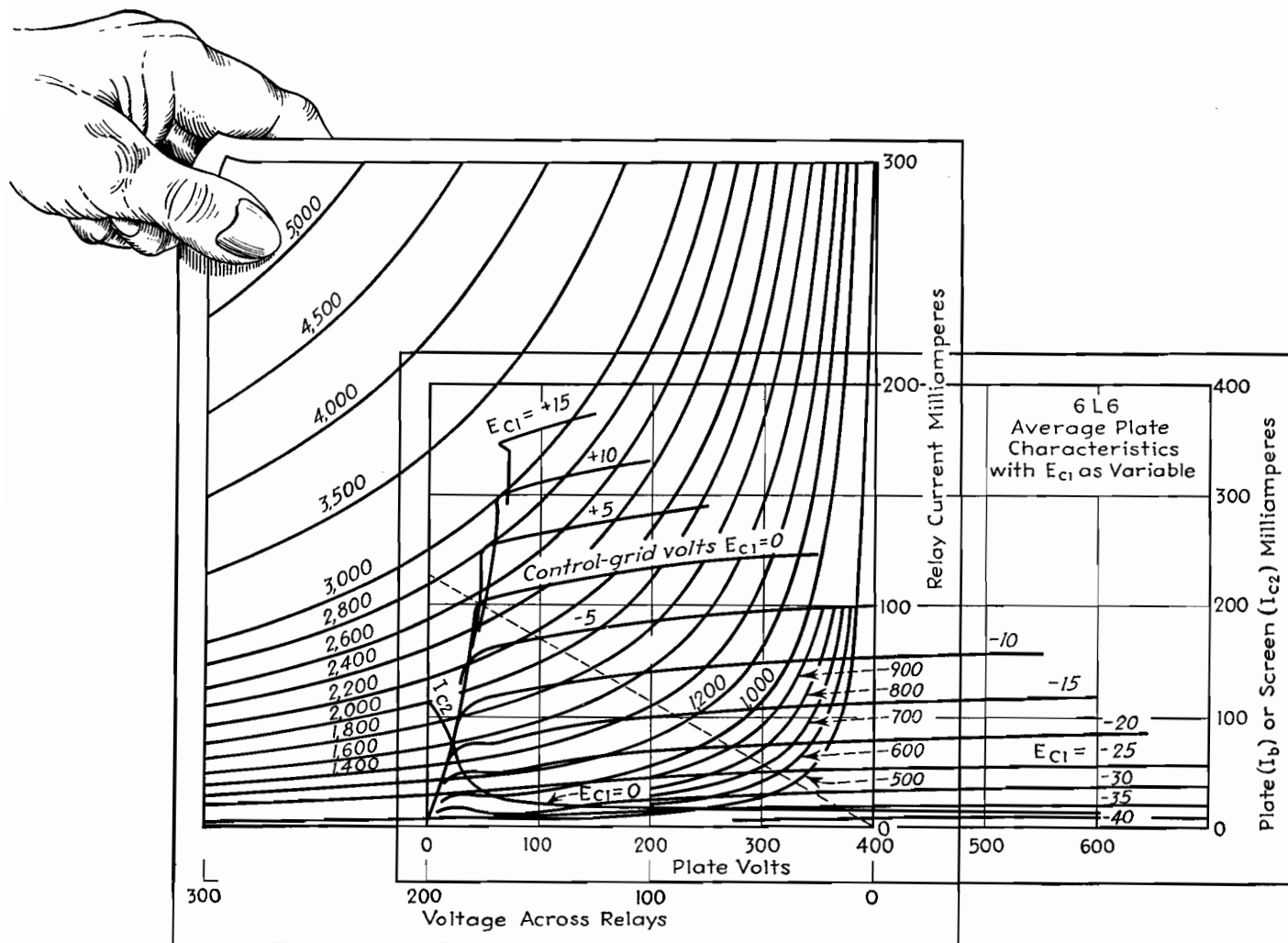


Fig. 4.—Superposition of a transparent drawing of Fig. 3 on the static characteristics of the 6L6. The origin of the relay curve corresponds to the operating point,  $E_b = 400$ ,  $I_p = 0$ . The dotted line is the load line for maximum power output, assuming the grid voltage may go to zero.

mine the proper coefficient for the square-root relation given in Eq. (3) for windings of any size, shape, or type of material.

Figure 2 shows the family of ampere-turn characteristics plotted against relay coil resistance and relay current (or relay coil voltage) as well as the power consumption for standard telephone-type relays. Since 13 watts is frequently considered a maximum continuous duty rating of telephone relays, this value is shown along with decimal and other values more convenient for graphic interpolation.

The characteristic curves of a relay, showing the mmf plotted as a function of relay current and voltage on rectangular coordinates, are rectangular hyperbolas giving loci of equal ampere turns. By changing the scale of the hyperbolas of Fig. 3, using Eq. (3) for determining the conversion ratio, the same hyperbolic curves can be used to determine the power output of the tube under operating conditions.

The method of using Fig. 3 in connection with tube static characteristics depends on having a copy of Fig. 3 to a scale suitable for use with tube characteristics, plotted on some transparent medium. It is essential that the voltage and current scales on this transparent scale be evident, since they must be compared with the equivalent scales of the tube characteristics in order to determine the proper multiplying factors. In using this chart, it has been found useful to trim close to the axes so that the transparent chart may be superimposed on tube characteristics without removing these from their binders.

To determine the scale ratio for Fig. 3 when used with any set of tube static characteristics, compare the voltage scale on the relay characteristic with the voltage scale on the tube characteristics, and the current scale of the relay chart with the current scale on the tube characteristics. If the voltage change on the tube characteristics corresponding

to a 100-volt change on the relay characteristic is  $E_v$ , and if  $I_v$  is the plate current variation of the tube characteristics corresponding to a relay current change of 100 ma, then the scale multiplying factor will be

$$F = (F_v F_i)^{1/2} = \frac{(E_v I_v)^{1/2}}{100} = 0.01 P^{1/2} \quad (7)$$

where  $F_v$  and  $F_i$  are, respectively, the voltage and current multiplying factors, and  $P$  is power in watts. An example will make this clear.

If, as shown in Fig. 4, 100 ma on the relay characteristic corresponds to 196 ma on the tube characteristic, the current scale factor will be  $F_i = 196/100$ , or 1.96. Similarly, if 198 volts on the tube characteristic corresponds to 100 volts on the relay characteristic, the voltage multiplying factor  $F_v$  is 1.98. The total multiplying factor will then be  $(1.96 \times 1.98)^{1/2}$ , or 1.972. For a given set of relay hyperbolas, the scale factor will, in general,

change with each new graph of tube characteristics.

Figure 3 shows the application of the relay characteristics, applied to a 6L6 tube. The origin of the relay characteristic curve is placed at the point on the tube characteristic corresponding to zero plate current and the operating plate voltage ( $I_p = 0$ , and  $E_b = 400$  volts in this case) with the current and voltage axes of both characteristic curves parallel. The point at which the relay characteristic becomes tangent with the tube characteristic (for any grid voltage) gives the maximum mmf that can be developed under the assumed conditions. Connecting the point of tangency thus found with the origin of the relay characteristics will give the optimum load line. Conversely, for given plate and grid bias voltages, we can determine the upper and lower limits of the mmf developed by the relay as soon as we know the signal variations of the grid voltage.

For example, with a 6L6 operating at 400 volts, the maximum mmf will be developed (assuming the grid may go to zero but not positive) when the load line connects the point of tangency of the tube and relay characteristics with the point  $E_b = 400$ ,  $I_p = 0$ . This gives a load resistance  $R_L = E_b/I_p = 400/0.225 = 1,780$  ohms. The mmf developed by the relay at zero grid voltage will be 2,500 ampere turns times the scale factor of 1.972 or 4,935 ampere turns. If the grid bias is  $-15$  volts and we superimpose a signal of 10 volts (peak) on the grid, the quiescent MMF will be  $1,250 \times 1.972$  or 2,460 ampere turns, whereas the maximum and minimum MMF will be, respectively,  $2,120 \times 1.972$ , or 4,170 ampere turns, and  $600 \times 1.972$ , or 1,180 ampere turns. The values for these latter cases are determined from the points where the relay characteristics coincide with the load line and grid voltage curves. For the load line plate voltage, grid bias,

and signal voltage we have assumed, the mmf in the relay coil will vary between 1,180 and 4,170 ampere turns, peak values.

It is desirable to make allowances for the normal variations of tube and relay characteristics as well as for voltage variations which may arise in practice. It is also desirable to operate the tube at the right of the knee of the tube characteristic curve for greatest stability.

The optimum condition for the case under consideration does not take into account any distortion in the plate circuit of the tube, so that load lines as determined by the method described may differ from those determined where high-quality a-f reproduction is a consideration. The relay characteristic can be used with other forms of tube characteristics (such as plate voltage plate current curves for given grid bias with screen voltage as parameter). The method of operation is similar to that outlined above.

## Design Chart for Sensitive Relays

By R. T. FISHER

---

Relay data that permit determination of performance under any static electrical conduction without resort to experimentation. The curves help both users and designers of relays

---

**R**EPRESENTATION of the performance of any relay of a given design, of whatever coil resistance, may be made by a single family of curves. An Ohm's-law calculator or slide rule makes their use very convenient. A complete description of the curves and their use in the design of a relay like that shown in Fig. 1 will be given.

Each curve in Fig. 2 shows, for one particular value of coil input power, the approximate magnetic force developed at the gap between armature and coil core as the length of the gap is varied.

### Graphical Analysis of Performance

If the armature is pivoted exactly halfway between gap and contacts, as it is in Fig. 1, then the contact pressure\* will always equal this magnetic force

\* As used, the term "contact pressure" does not involve the usual concept of unit area. It is used, rather than the term "contact force," to distinguish it from magnetic force, which does not involve physical contact.

less the force of the restoring spring. If this subtraction yields a negative remainder, the spring force being greater, the pressure will be on the normally closed contact *B*. The spring force is a torque, as is the magnetic force, and both must be measured at the same distance from the pivot.

In order for the method of using these curves to have general application among different relays, a convention is necessary regarding the point at which forces are to be measured. It is suggested that this point be chosen as the contact position. If so, no consideration need be given to the relative position of the pivot. In cases where it is difficult to measure the force at the contacts, it can be measured at some other point and the values corrected to equivalents at the contacts.

It will be noted in Fig. 2 that each curve is marked with two different power values, for two different types of coil construction. The reason for this is that

form-wound coils not having paper between layers of turns have a larger volume of copper and, therefore, effectively different and larger physical dimensions and more ampere turns per milliwatt.

The heavy lines and figures, superposed over the curves in Fig. 2, represent a typical relay-operation cycle.

In Fig. 1, the armature motion allows the air gap at the coil core to vary from  $G_n$  to  $G_e$ . Two vertical lines are drawn in Fig. 2 at points that represent the lengths of  $G_e$  and  $G_n$ , measured from the origin along the horizontal axis. A horizontal line has been drawn from a point on the vertical axis which represents the spring force.

Before current is applied to the coil, the spring will hold the armature in the position  $G_n$  with a force of  $A$ . As increasing current is applied to the coil, an increasing magnetic force opposes this spring force. When the coil power reaches a value of 40 mw, the graph shows

that in this particular case the magnetic force will have exceeded the spring force by a small amount above point 1. The result is, of course, that the armature rotates to the other extreme of its travel (the relay pulls on) and the pole gap becomes equal to  $G_e$ .

With the gap at this value and the coil power still 40 mw, the graph shows, at point 2, that the magnetic force exceeds the spring force by an amount equal to the distance from point 2 to point 3. This amount is, then, the contact pressure developed on the normally open contact (C in Fig. 1) when the relay has just pulled on.

If the coil power is decreased until the magnetic force becomes slightly less than the spring force, the spring will restore the armature to its original position, and the relay will have dropped out. The coil power value at which this occurs is indicated by point 3, which is a point on an interpolated curve yielding force A at a gap equal to  $G_e$ . The power value of this curve is estimated from its position with respect to given curves, and is the drop-out value for the adjustment under consideration.

When the armature drops out, restoring

the gap to the value  $G_n$ , the magnetic force will be determined by point 4, the intersection of the interpolated curve passing through point 3 with the vertical line at gap  $G_n$ . The contact pressure immediately after drop-out will then be equal to the difference between the magnetic force given by point 4 and the spring force A, shown at point 1. As the current decreases further toward zero, the contact pressure on the normally closed contact (B in Fig. 1) approaches the value of A. The cycle has now been completed.

#### Example

The curves may be used as follows:

1. From data supplied by the relay manufacturer regarding pressures and spacing necessary for good switch performance under various circumstances of electrical load and environment, coupled with an analysis of the particular problem at hand, limiting values of minimum air gap, contact spacing, and pressure are determined.

2. A trail cycle is sketched in. The problem of where to start may seem confusing at first, but is really obvious after a little familiarity is gained.

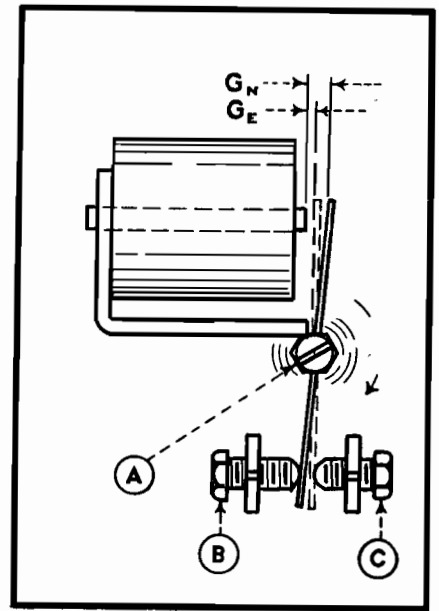
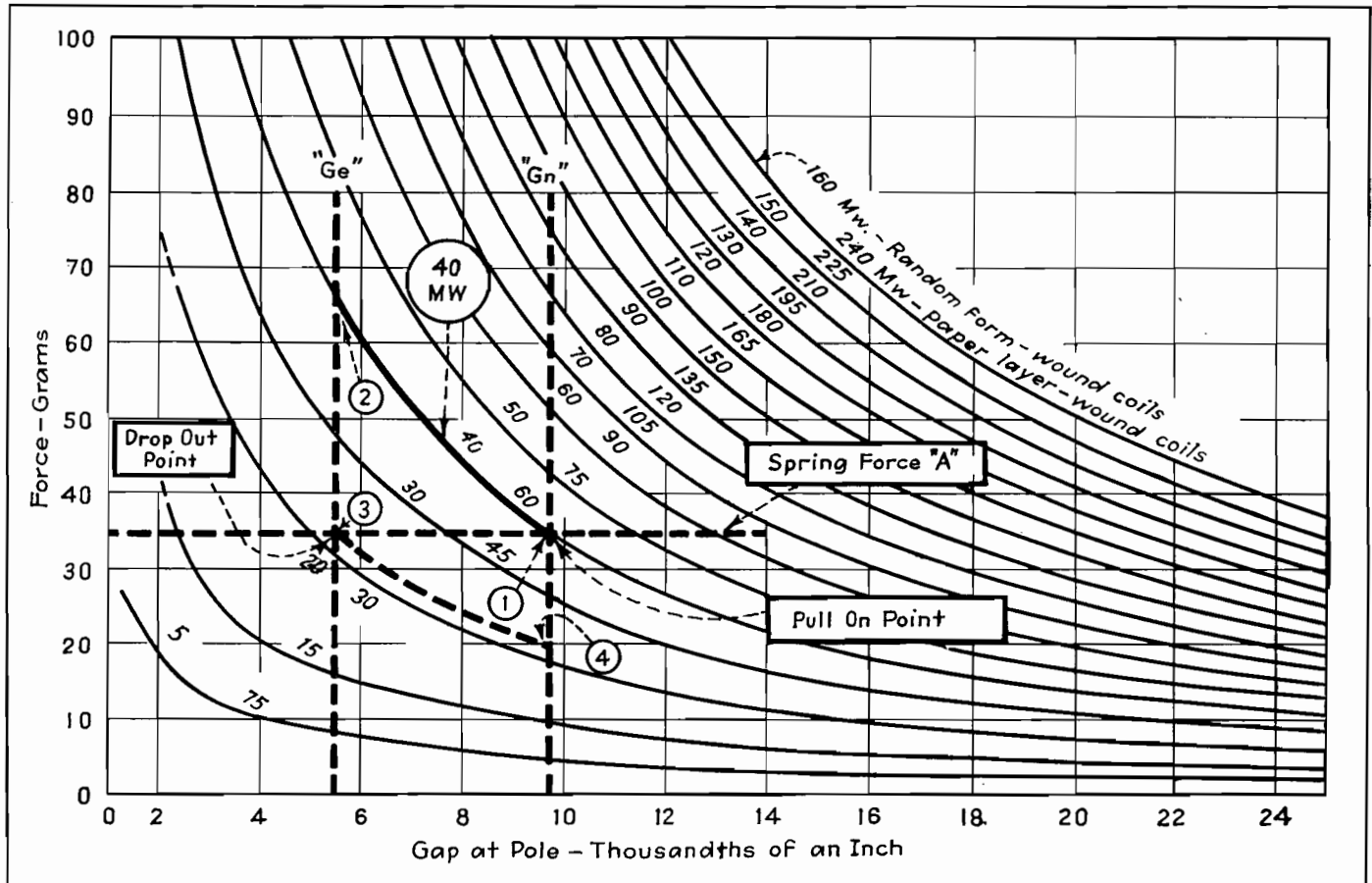


Fig. 1.—Type of relay to which the curves in Fig. 2 apply.

If the problem is expected to tax the sensitivity of the relay, it will probably be advisable to use the minimum value for  $G_e$  (the air gap when energized) recommended by the manufacturer for the conditions of the problem. The  $G_e$  line may therefore



be drawn at this point. If there is a definite requirement for drop-out, mark off on line  $G_c$  the point where it is crossed by the curve for desired drop-out power, and draw horizontally through this point the line representing the force of the spring, which will be set to this value.

Bear in mind that what we have done in drawing  $G_c$  at a particular point is to say where we shall set the normally open contact, and hence, how close to the core we shall allow the armature to travel. Further, in deciding on the drop-out value, we have said that with the armature in this particular position the spring shall be adjusted to a value such as to equal the magnetic force at the specified drop-out value, so that when the power falls below this value, the spring will restore the armature to its normal position.

$G_n$  must be far enough away from the  $G_c$  value to permit the contact separation demanded by the particular problem.

In addition, as long as the spring is not again changed, position  $G_n$  controls the value of power at which the relay pulls on. Pull-on will occur at the value of power corresponding to the curve that goes through the intersection of the spring line and  $G_n$  line.

Having drawn the  $G_n$  line, there remains only to complete the cycle by drawing in the curves corresponding to pull-on and drop-out values, in case either or both are interpolated values.

3. Inspection of this cycle will disclose whether the requirements of the problem are met. In case they are not (suppose, for example, inadequate contact pressure exists immediately after drop-out), the possible remedies will usually be obvious. The most important thing is that the exact effect of any amount of any particular adjustment can be read off the graph as soon as tentative values for some of the others are chosen.

In the adjustment of a sensitive relay, there are five main variables which may be independent. That is, any three of them that will locate two points on a cycle can be chosen independently and will fix the other two, subject to deviations of individual relays from the performance of the one for which the curves are plotted.

#### Specifying a Relay Adjustment

The five variables are: (1) pull-on, (2) drop-out, (3) spring force, (4) minimum pole gap ( $G_c$ ), (5) armature travel or contact gap ( $G_n - G_c = \text{travel}$ ).

Having specified to appropriate tolerances the values for three variables from the list, one may ask a relay manufacturer to recommend suitable values for permissible variation of the other two. In any case, he must be consulted on this point, for in adjusting the relay he can work for only three.

## SECTION XIX

# R-F COILS AND TRANSFORMERS

	Page
Distributed Capacitance Chart.....	249
Nomogram for Single-layer Coils.....	251
General-purpose Chart for Multilayer Coils.....	253
Simplified Inductance Chart for Multilayer Coils.....	256
Winding the Universal Coil.....	258
Mutual-inductance Calculations.....	261
H-f Inductance Charts .....	263
Universal Performance Curves for Tuned Transformers...	264
Double-tuned Transformer Design.....	267

## Distributed Capacitance Chart

By P. H. MASSAUT

An alignment chart based on the Palermo equation, for determining the distributed capacitance of single-layer coils in terms of wire size, spacing, and coil diameter

A PERFECT coil should present inductance only. It always shows in addition, however, resistance and capacitance. Resistance may be reduced by adequately dimensioning the coil, by making use of very low h-f loss material for the coil form and supports, and by removing from the vicinity of the coil any body liable to increase the losses.

In this connection, the quality of a coil is expressed by the well-known coefficient

$$Q_0 = \frac{\omega L_0}{R_0}$$

the value of which may vary, in practice, between 100 and 500 according to the type of coil and the frequency ( $\omega = 2\pi$  times the frequency;  $L_0$  = inductance;  $R_0$  = resistance).

The capacitance of the coil, distributed between the turns of the winding, may be replaced, as regards its reaction on the external circuit, by a lumped capacitance  $C_0$ , called the distributed capacitance of the coil, and supposed to be connected to the coil terminals (i.e., shunting the coil). This capacitance may be reduced by an appropriate choice of the coil shape and dimensions. It is impossible, even theoretically, to make it equal to zero.

It is rather difficult to find by analysis

the value of  $C_0$ , for various reasons, one of which is as follows: Suppose we know the elementary capacitance between two elements  $\Delta l$  of wire of adjacent turns; there is no difficulty in this. Let us now consider these elementary capacitances lying on the same axis of the coil: from one end to the other of the coil, they will look as if they were in series. But let us now consider them along the winding: they will look as if they were in parallel. In reality, they are neither in series nor in parallel.

As a very rough approximation, it is often admitted that the distributed capacitance  $C_0$  of single-layer coils is equal to the radius of the coil (both capacitance and radius expressed in centimeters). Palermo\* has given a much more accurate formula, which is very well verified by experiment

$$C_0 = \frac{\pi D}{3.6 \cosh^{-1} \frac{s}{d}}$$

where  $C_0$  = distributed capacitance of coil,  $\mu\text{mf}$

$D$  = diameter of coil, cm

$s$  = spacing of adjacent turns (between axes of wire)

$d$  = diameter of wire

It is noticed that  $C_0$  does not depend on the number of turns, and this is confirmed by experiment.

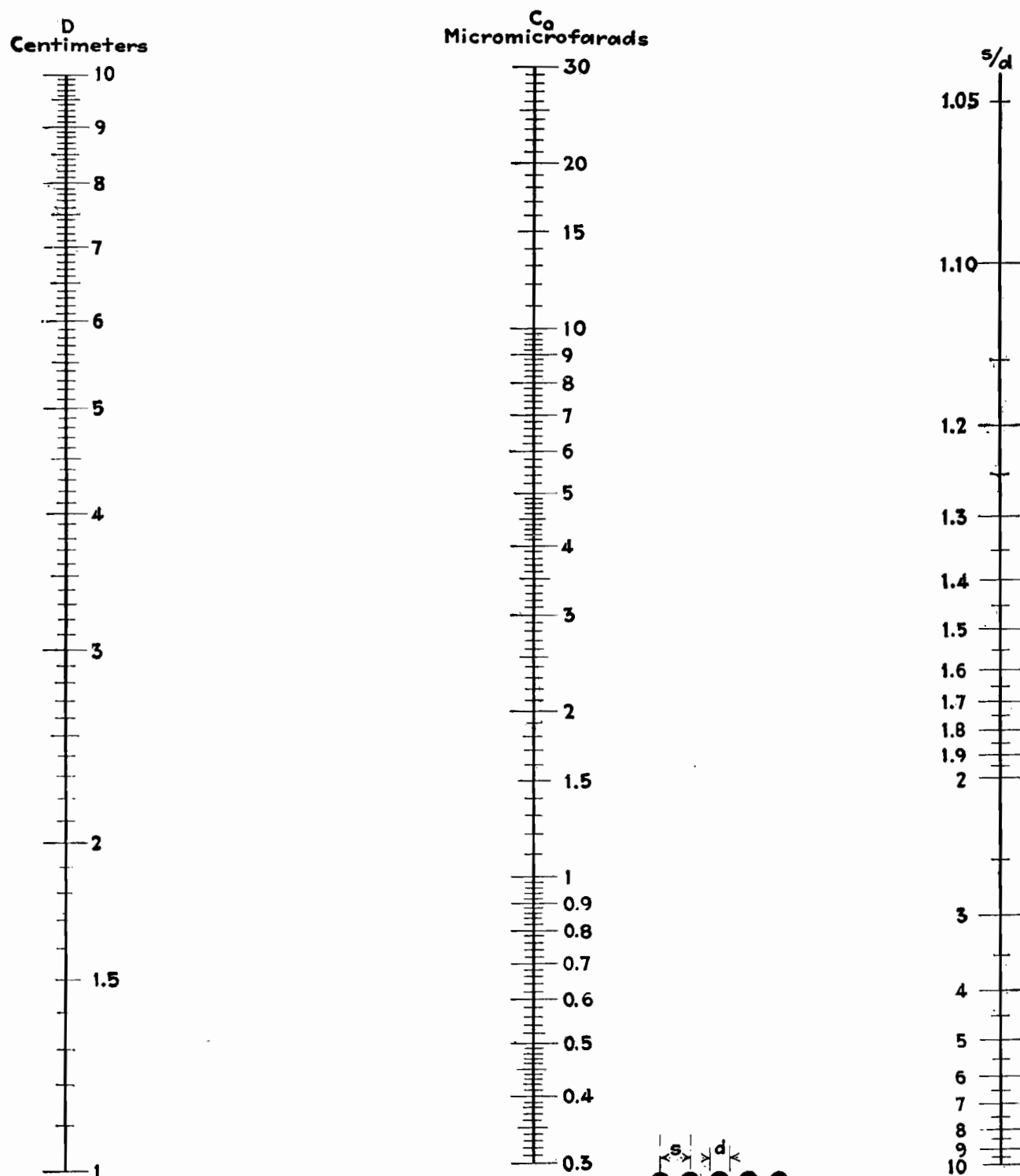
The alignment chart translates the above formula. Since  $C_0$  is proportional to  $D$ , if one has to consider a diameter lying outside the scale of the chart, it is only necessary to multiply  $C_0$  and  $D$  by the same factor. For example, if we have a coil of a diameter of 15 cm wound up with adjacent turns of enameled wire of 2 mm diameter, the enamel layer being 0.1 mm thick, we find that the distributed capacitance will be approximately  $30 \mu\text{mf}$  ( $s = 2.2 \text{ mm}$ ,  $d = 2 \text{ mm}$ ; for  $D = 1.5 \text{ cm}$ ,  $C_0 = 2.95 \mu\text{mf}$ ; consequently for  $D = 15 \text{ cm}$ ,  $C_0 = 29.5 \mu\text{mf}$ ).

It is of importance to note that the capacitance of the terminals, connecting wires, associated tube, and apparatus have to be added to this value, in order to get the total capacitance across the coil.

The knowledge of the distributed capacitance  $C_0$  is useful from various points of view. In the first place, it determines a certain natural frequency

$$f_0 = \frac{1}{2\pi \sqrt{L_0 C_0}}$$

( $f_0$  is in cycles,  $L_0$  is inductance of coil in henrys,  $C_0$  is distributed capacitance in



**Note:** When diameter "D" is ten times larger or smaller, distributed capacity " $C_0$ " will likewise be ten times larger or smaller.

Alignment chart for determining distributed capacitance of single-layer coils.

farads) beyond which it is impossible to tune a circuit of which the coil is the tuning inductance, no matter how small may be the residual capacitance of the other circuit elements. In the second place, the apparent inductance of the coil,  $L$ , as well as its apparent resistance  $R$ , at frequencies below  $f_0$ , is increased by the existence of the distributed capacitance  $C_0$ . The following approximate formulas are well known\* giving

\* Terman, F. E., "Radio Engineering," 2d ed., p. 67, McGraw-Hill Book Company, Inc., New York, 1937.

the apparent inductance and resistance  $L$  and  $R$  and holding for any frequency lower than 8/10 of the natural frequency  $f_0$ :

$$L = \frac{L_0}{1 - m^2}$$

$$R = \frac{R_0}{(1 - m^2)^2}$$

where  $m = f/f_0$  is the ratio of the frequency  $f$  at which the coil is used, to its natural frequency  $f_0$ .

The result is that the apparent factor of

quality  $Q$  is reduced in a ratio that may be considerable: it becomes  $Q = Q_0(1 - m^2)$ .

It is seen that it is important to reduce as much as possible not only the effective resistance of h-f coils, but also their distributed capacitance. The reason for this is that the value of  $Q$  is of considerable importance as well for coils used in transmitters (efficiency of circuits, stability of oscillators, reduction of harmonics) as for coils used in receivers (selectivity characteristics, amplification factor, spread of tuning range, etc.).

## Nomogram for Single-layer Coils

By CARL P. NACHOD

Chart for determining inductance-dimension data of single-layer solenoids without calculation. Based on the Nagaoka formula, and applicable especially to transmitting coils

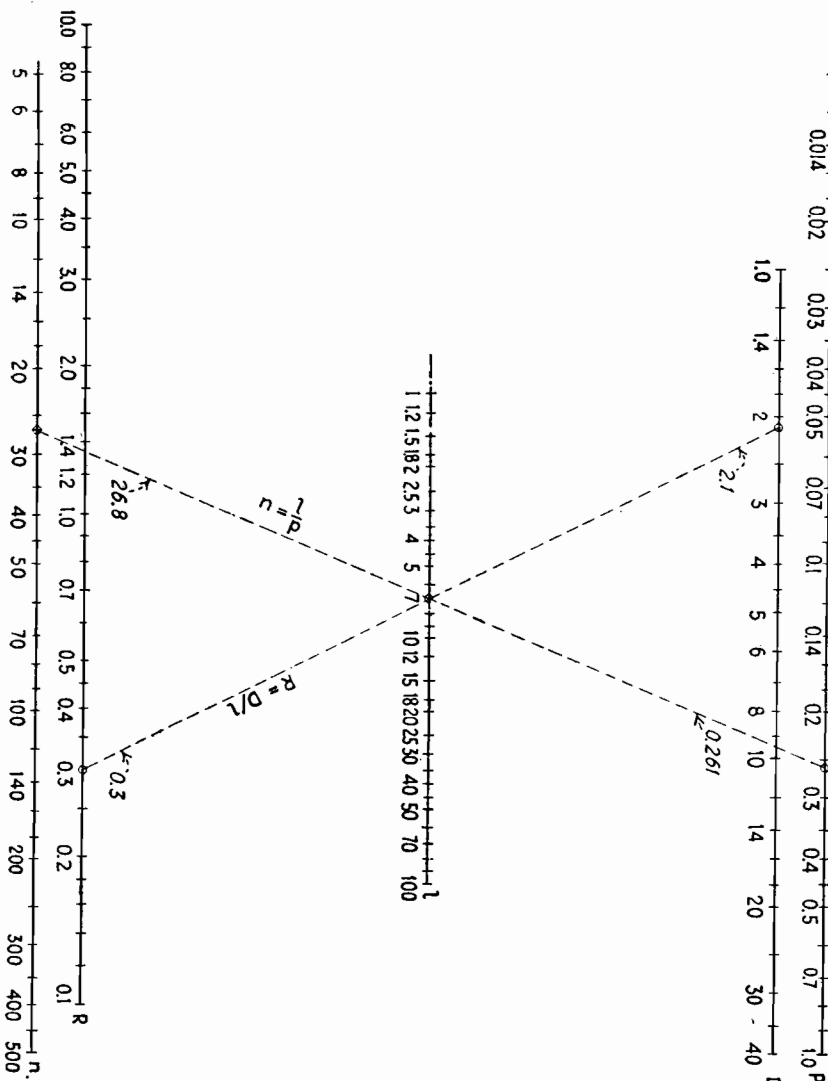


Fig. 1.—Auxiliary nomogram for determining diameter-to-length ratio and total number of turns.

THE nomogram, based on the Nagaoka formula (*Bureau of Standards Circular* 74), gives the inductance of a single-layer solenoid in terms of its length, diameter, and winding pitch. The formula is

$$L = \frac{0.025 D^2 l K}{p^2}$$

where  $L$  = inductance,  $\mu\text{h}$

$D$  = diameter of the coil, in.

$l$  = length of the coil, in.

$p$  = pitch of the coil (in. per turn)

$K$  = the Nagaoka "form factor" which is a function of  $D/l$

This ratio  $D/l$  can be calculated if desired, but it may be found also by reference to Fig. 1. By connecting the given values of  $D$  and  $l$  with a straight line, the right-hand scale marked  $R$  gives the ratio  $D/l$ . This value of  $D/l$  is then used in connection with the scale marked  $R$  in the inductance nomogram.

In the nomogram, it will be noticed that there are five vertical lines. The line at the extreme left (marked  $V$ ) is simply a turning scale and is not graduated. The inductance scale  $L$  is marked from 5 to 500  $\mu\text{h}$ . The middle scale gives the pitch  $P$  in inches and also serves as a turning scale ( $Q$ ). Values of the ratio  $R = (D/l)$  from 0.1 to 10 are given. The scale at the extreme right is graduated both in length and diameter, covering values of  $l$  from 1 to 100 in. and of  $D$  from 2 to 20 in. The use of turning scales and the combination of  $D$  and  $l$  in one scale make the nomogram highly compact without lessening accuracy.



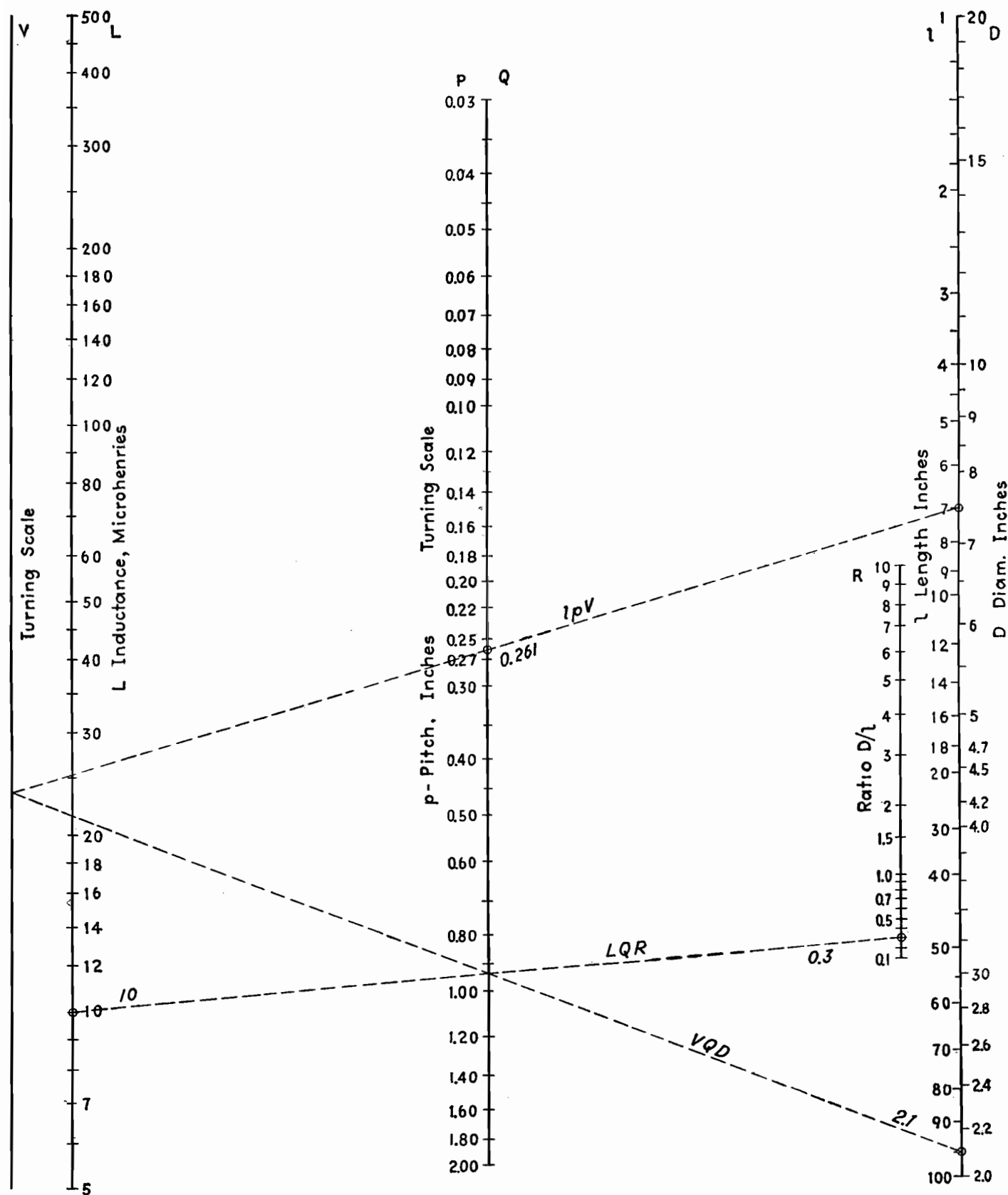


Chart for determining inductance of solenoids.

To find inductance when dimensions are given, the line  $lpV$  is drawn through the given values of length and pitch. The intersection of  $lpV$  with the  $V$  scale is then connected with the given value of diameter, in the line  $VQD$ . Finally, the intersection of  $VQD$  with the  $Q$  scale (same line as  $p$  scale) and the given value of  $R$  (as found from Fig. 1) are connected in the line  $LQR$ , intersecting the  $L$  scale in the value of inductance.

In the example given, a coil 7 in. long, with a winding pitch of 0.26 in. per turn, and a diameter of 2.1 in., is found to have an inductance of 10  $\mu$ h.

When one dimension is to be found from the given inductance and given remaining dimensions, the order of drawing the lines is changed. For example, if  $p$  is to be found when  $L$ ,  $D$ , and  $l$  are given, the intersecting lines are drawn in the order  $LQR$ ,  $DQV$ , and  $lpV$ . The values of  $l$ ,

$D$ , and  $R$  used must always be in the relation  $D/l = R$ , and the lines must always intersect the turning scales  $V$  and  $Q$ .

By making use of Fig. 1, the value of  $n = l/p$  which is the total number of turns in the coil can also be found. Since single-layer solenoids are now used principally in inductances for transmitting purposes, rather than in receiving-set applications, the dimensions included in the scales apply to coils of fairly large size.

## General-purpose Chart for Multilayer Coils

By J. E. MAYNARD

Design of multilayer inductance coils simplified through the use of families of curves relating various parameters of coil design. The form of the chart lends itself readily to the solution of many types of design problems

THE design of multilayer coils for a specified inductance presents difficulties because of the complexity of the equations derived to apply to such cases, and because of the large number of factors that must be considered since they affect the inductance. These factors include the inner and outer diameters of the coil, the thickness of the coil winding, the shape of the cross-sectional area of the windings, and the space factor of

the windings. A number of equations have been developed for the determination of inductance for multilayer windings, but a considerable saving of time may be effected through the use of the chart, which, upon measurement on a large number of coils, has been found to be accurate to within 5 per cent except in a few exceptional cases.\*

\* This chart is based on Eqs. 157 and 158, pp. 257 and 258 of *Radio Instruments and Measurements*, Nat. Bur. Standards, Circ. 74, which have been rear-

In the design of this chart, the variable factors selected are

$A = BC$  = cross-sectional area of the coil winding, sq in.

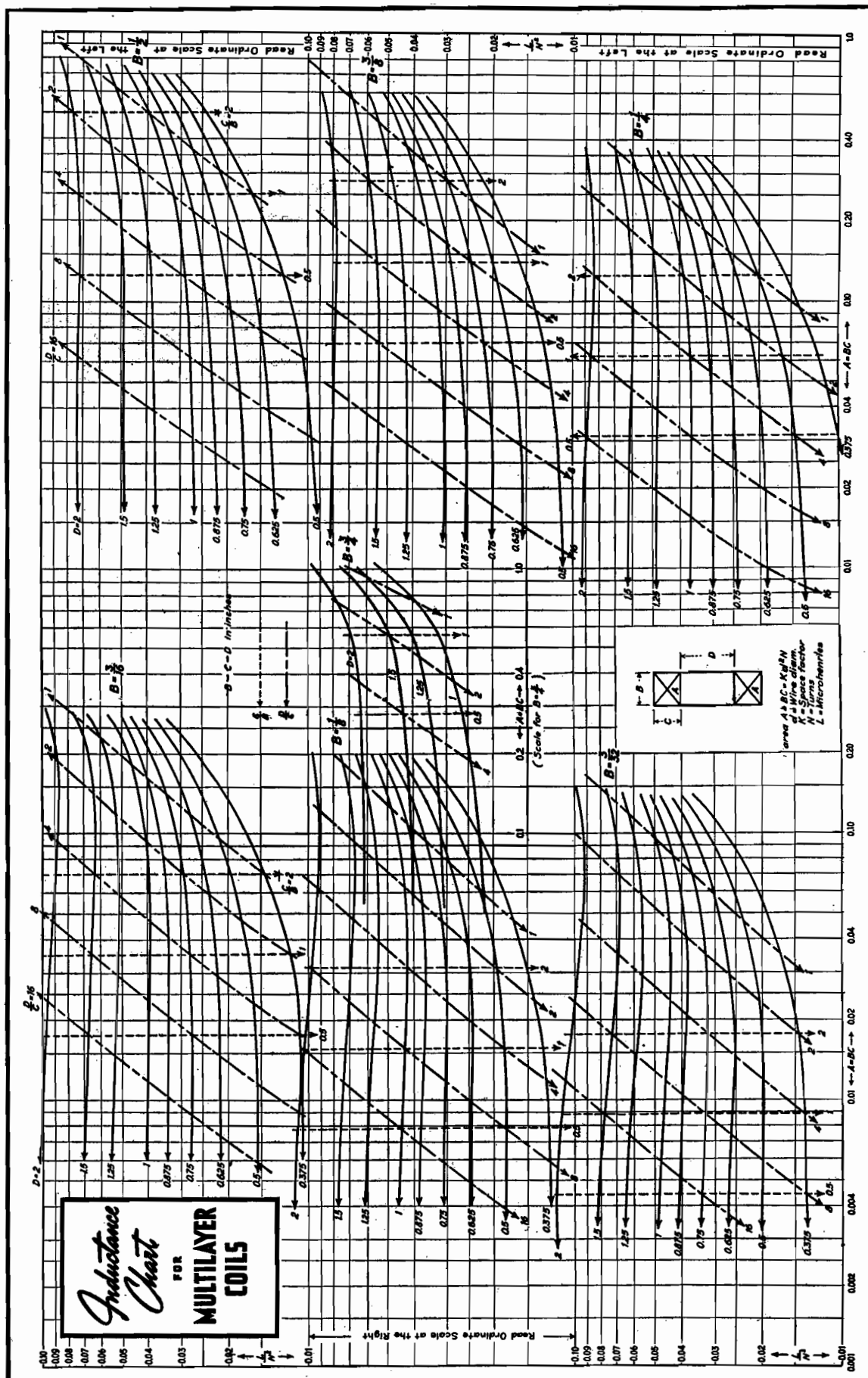
$B$  = width of coil winding, or cam width, in.

$C$  = depth of coil winding, in.

$d$  = the outer diameter of the wire plus its insulation

$N$  = the number of turns of the coil

ranged into a form more suitable for use in the design of a practical chart.



When these factors are known, the chart may be used to determine the value of  $L/N^2$ , and since  $N$  is known, the inductance in microhenrys may then be determined.

The cross-sectional area of the coil  $A$  is determined by the diameter of the wire  $d$  and the number of turns  $N$  from the relation

$$A = Kd^2N$$

where  $K$  is the space factor of the winding. The numerical value for  $K$  is usually about 1.25, but this will vary with the adjustments of the winding machine, such as the tension of the wire during winding, and the number of turns per layer. Fortunately, variations in  $K$ , and hence in  $A$ , cause much less than a proportionate variation in the inductance. Consequently, it will seldom be necessary to use a value of  $K$  other than 1.25 which has been found to be quite satisfactory.

In the above equation, the value for  $d$  for ordinary wire is merely the over-all diameter of the wire plus its insulation. For litz wire,  $d$  may be taken as the over-all diameter of a close symmetrical grouping, plus insulation. The relation between the number of strands,  $S$ , and the over-all diameter of the litz without silk or cotton insulation  $d_0$  is shown in the following table:

$S$	$d_0$
3	$2.16d_s$
5	$2.7 d_s$
7	$3.0 d_s$

where  $d_s$  is the diameter of each strand with its enamel insulation.

The inductance chart is designed in the form of several families of curves. Each family of curves corresponds to a different coil width  $B$  so that the width of the coil winding determines which family of curves is to be used in any design problem. The particular curves, in any given family, which are required for design purposes depend on the area of the coil winding,  $A$ , the inner diameter of the coil form,  $D$ , as well as on the shape factors  $D/C$  or  $C/B$ . The values of  $A$  are plotted as abscissa and the values of  $L/N^2$  as ordinates on the main set of coordinates. Values for the coil width are indicated by the letter  $B$  at the right of each family, whereas the value of the inner coil diameter  $D$  for the almost horizontal lines is given at the left of each family of curves. The shape factor  $C/B$  is given as auxiliary abscissa, while the shape factor  $D/C$  is indicated by the almost straight lines at an angle of approxi-

mately 45 deg with the main coordinate system.

Values of the parameters and contours have been indicated by arrowheads on the corresponding curves or lines to eliminate any possible confusion as to their reference. The ordinate scales for the upper and lower families of curves will be found at the left side of the chart. The abscissa scale for all the left-hand families of curves is along the lower edge, and that for the right-hand families of curves is along the right edge of the chart. The abscissa scale for the center family of curves ( $B = \frac{3}{4}$ ) is directly below these curves. Interpolation may be used within or immediately outside the range of the chart plotted.

The chart applies to coils whose inner diameter  $D$  lies between 0.375 to 2 in. in coil widths of from  $\frac{3}{32}$  to  $\frac{1}{4}$  in., and from diameters of 0.5 to 2 in. in coil widths of  $\frac{1}{4}$  to  $\frac{1}{2}$  in. One family of curves gives data for coils having values of  $D$  between 1 and 2 in., for a coil width of  $\frac{3}{4}$  in.

The flexibility of this chart provides for the solution of several types of problems. The utility of the chart may be appreciated from the following table which shows the variety of coil calculations that may be made.

Specified	Chosen	To be determined
1. Inductance Coil diameter	Wire size Coil or cam width	Depth of winding Number of turns
2. Inductance Over-all diameter	Coil or cam width Coil diameter Depth of winding Shape factors	Wire size Number of turns
3. Inductance Shape factors	Wire size Coil diameter Depth of winding	Coil or cam width Number of turns
4. Inductance Shape factors Coil diameter Coil or cam width		Number of turns Wire size

As examples of the use of this chart, several problems are given which will serve to illustrate the method of using the chart.

### Examples

**Example 1.**—We wish to obtain a given inductance using a standard winding form. Assume the desired inductance is 8,000  $\mu$ h and the coil form has an inner diameter of 0.625 in.

We begin by choosing a coil of square cross-section (so that  $C/B = 1$ ), a coil width  $B = \frac{1}{4}$  in., and select No. 35 enameled s.s.c. wire for which the diameter is  $d = 0.0083$  in. We may now determine that  $C = \frac{1}{4}$  in. and  $A = BC = \frac{1}{4} \times \frac{1}{4} = 0.0625$  sq in. Using the chart for the family of curves for which  $B = \frac{1}{4}$ , and remembering to use the left-hand coordinates, we find that  $L/N^2 = 0.021$ .

We now have two methods of determining the number of turns. By using both determinations, we may find that our chosen data are incompatible and may require some alteration. Using one method, we determine that  $N^2 = L/0.021$  from which  $N = 616$  turns. Using the other method which makes use of the equation  $A = Kd^2N$ , we have, for  $K = 1.25$  and  $d = 0.0083$ , that  $N = [0.0625/(1.25)(0.0083)^2] = 725$  turns. Since these two determinations do not check, either the wire must be made larger or the cross-sectional area must be reduced. If we choose  $A = [(616)(0.0625)/(725)] = 0.0535$  sq in., then  $N = [(0.0535)/(1.25)(0.0083)^2] = 621$  turns. From the chart we determine that  $L/N^2 = 0.0204$ . Our coil will therefore consist of 621 turns of No. 35 enameled s.s.c. wire whose depth of winding is  $C = A/B = 0.0535/0.025 = 0.214$  in., and  $L = 0.0204 \times 621^2 = 7,900 \mu$ h.

An actual coil had the following measured data:  $B = 0.242$  in.,  $D = \frac{5}{8}$  in., and  $C = 7/32$  in. = 0.219 in. There were 610 turns of No. 35 enameled s.s.c. wire, from which  $K = 1.26$ . The measured inductance was 8,050  $\mu$ h.

**Example 2.**—We wish to obtain a given inductance with a coil winding of specified over-all diameter. Assume the desired inductance to be 50,000  $\mu$ h, and that the over-all coil diameter is to be 1.25 in.

We choose a winding space such that  $B = 0.5$  in. and  $D = 0.625$  in. Then  $C = 0.5(1.25 - 0.625) = 0.3125$  in., and  $D/C = 2$ . For these dimensions we determine from the chart that  $L/N^2 = 0.017$ , and consequently  $N = (L/0.017)^{1/2} = (50,000/0.017)^{1/2} = 1,715$  turns and  $A = BC = 0.156$  sq in. We still have to determine the required wire size. From the equation  $A = Kd^2N$  we have that  $d = (A/KN)^{1/2} = (0.156/1.25 \times 1,715)^{1/2} = 0.0085$  in. We select No. 35

enameled s.s.c. wire from wire table data.

An actual coil measured as follows:  $D = \frac{5}{8}$  in.,  $B = 31/64$  in.,  $C = 5/16$  in., and  $L = 50,000 \mu\text{h}$ . There were 1,700 turns of No. 35 s.s.c. wire.

**Example 3.**—We wish to obtain a given inductance and maintain optimum shape factors for good  $Q$ . In general, for good  $Q$ ,  $C/B$  should be about 2. The ratio  $L/R_{d-c}$  is optimum for  $C/B = 1$ , but the ratio  $L/R_{r-f}$  is optimum for  $C/B > 1$ .  $D$  should be as large as may be consistent with practical requirements.

Let the desired inductance be  $3,500 \mu\text{h}$ , and let  $C/B = 2$  and  $C/D = 2.5$ . Choose a coil width  $B = \frac{1}{8}$  in., so that  $C = 2B = \frac{1}{4}$  in., and  $D = 2.5C = \frac{5}{8}$  in. We shall be able to choose the wire size more readily after determining the required number of turns. From the chart, we determine that  $L/N^2 = 0.0247$  and  $A = 0.0312$  sq in. Therefore,  $N = (3,500/0.0247)^{1/2} = 376$  turns, and  $d = (A/KN)^{1/2} (0.0312/1.25 \times 376)^{1/2} = 0.0082$  in. We may therefore use No. 35 enameled s.s.c. wire.

An actual coil measured as follows:  $B = 0.126$  in.,  $A = 0.0316$  sq in.,  $D = \frac{5}{8}$  in. and  $L = 3,450 \mu\text{h}$ . There were 386 turns of No. 35 enameled s.s.c. wire.

**Example 4.**—We have a coil whose inductance and dimensions we can measure, and we would like to duplicate it without damaging it. The measured data on the coil to be duplicated are found to be  $D = 0.5$  in.,  $B = 0.218$  in.,  $C = 0.22$  in., and  $L = 262 \mu\text{h}$ . Consequently,  $A = BC = 0.048$  sq in. Because the desired value of  $B$  does not appear on the chart, interpolation becomes necessary. For  $A = 0.048$  sq in.,  $D = 0.5$  in., and  $B = 0.25$  in., we find that  $L/N^2 = 0.0155$ . For the case in which  $A = 0.048$  sq in.,  $D = 0.5$  in., and  $B = 0.25$  in., we find from the chart that  $L/N^2 = 0.0177$ . It now becomes necessary to interpolate to determine  $L/N^2$  for the desired value of  $B$ . Interpolating, we have  $L/N^2 = 0.0155 + [(0.25 - 0.218)/(0.25 - 0.187)] (0.0177 - 0.0155) = 0.0167$ . This gives  $N = (262/0.0167)^{1/2} = 126$  turns. The wire size is  $d = (A/KN)^{1/2} =$

$(0.048/1.25 \times 124)^{1/2} = 0.0181$  in., so that No. 31 enameled d.c.c. wire may be used. The actual number of turns on the measured coil was 125.

From the character of the curves on the chart, it will be noted that this method of determining the number of turns on an unknown coil is considerably more accurate than any based on dimensional measurements, since it is largely dependent on the electrical measurement of inductance and the accuracy of the chart. The dimensional measurements determine the value of  $A$  which, as previously mentioned, is noncritical in determining the inductance per squared turn ratio. Furthermore,  $N$  is proportional to the square root of the determined data. On the other hand, the determination of turns from the measurements of the coil dimensions and wire diameter through the equation  $N = (A/Kd^2)$  involves such variables as space factor and tolerance in wire diameter as well as the difficulty of measuring accurately the dimensions  $B$  and  $C$ .

## Simplified Inductance Chart for Multilayer Coils

By E. S. PURINGTON

The inductance and  $Q$  of solenoidal or multilayer coils wound on a cylinder are readily determined from the accompanying graphs when the dimensions of the coil are known. The effect of insulation in reducing space factor is considered. Skin-effect considerations are also discussed

THE chart is useful for preliminary design of air-core coils wound on a cylindrical surface. Derived from Stefan's formula given in *National Bureau of Standards Circular* 74, it primarily covers multiple-layer coils, but as a limiting case also covers solenoids and pancakes.

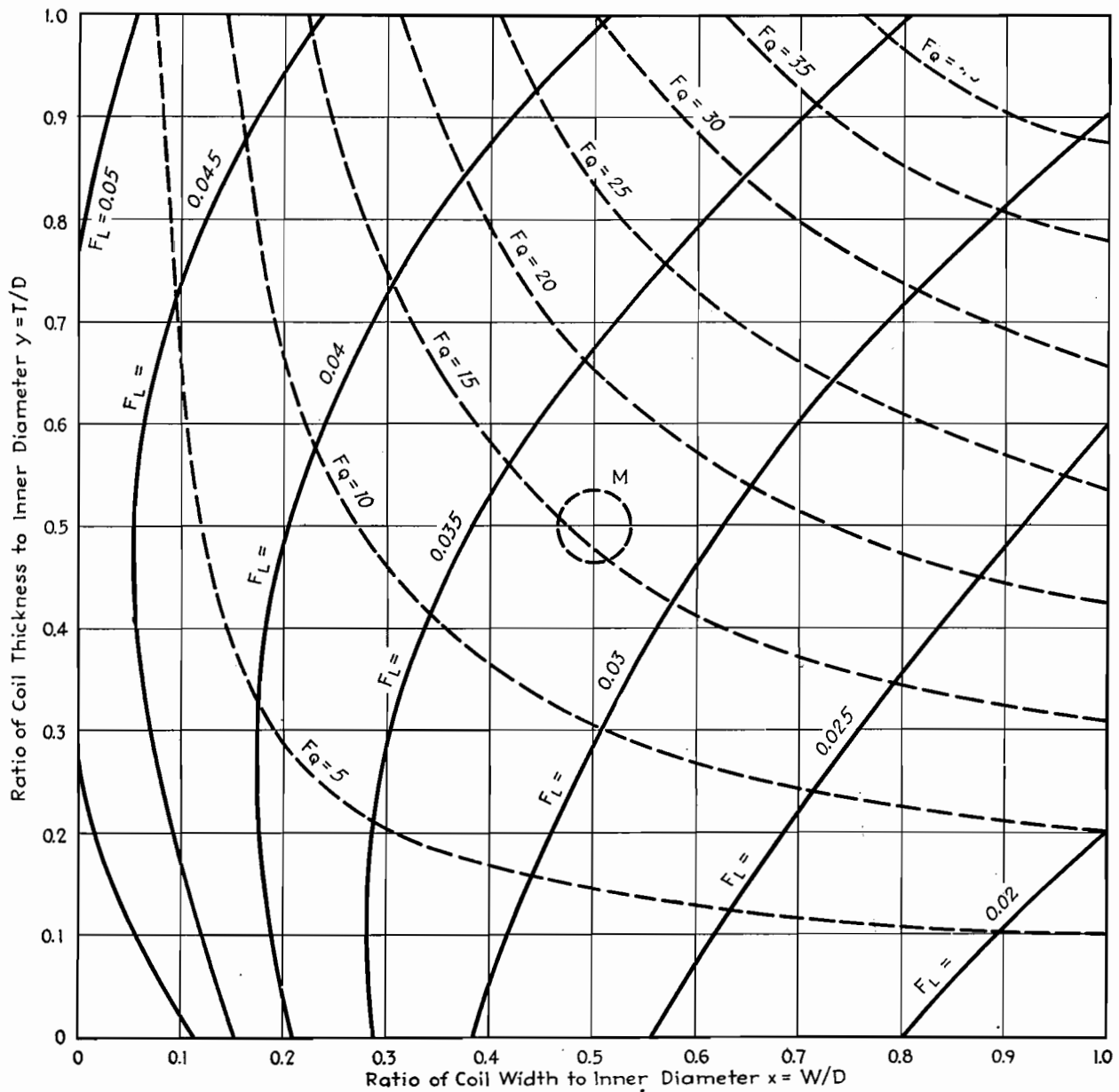
With a coil of specified shape and a uniform winding, the geometric inductance is proportional to a dimension and to the square of the total number of turns. For engineering purposes, the basic dimension may well be the inside diameter in inches, here designated  $D$ , which remains fixed as the coil is wound. Shape is expressed by the ratio of the winding space  $W$  and the thickness of the winding  $T$  to the basic dimension  $D$ . In winding solenoids,  $T/D$  remains fixed, and in winding pancakes or multiple-layer coils,

$W/D$  remains fixed. For convenience, let the two shape variables be  $x = W/D$  and  $y = T/D$ .

The geometric inductance in microhenrys, definable as the inductance at very low frequencies, is equal to the internal diameter  $D$  in inches, multiplied by the square of the total number of turns  $N^2$  and by the shape factor  $F_L(x, y)$ . On the chart, the heavy lines of constant  $F_L$  ranging from 0.02 to 0.05 enable  $F_L$  to be determined within a very few per cent for shape values of  $x$  and  $y$  up to unity. For example, at  $x = 0.75$ ,  $y = 0.50$  corresponding to the illustrated coil shape,  $F_L$  is 0.028. Thus if a coil of 0.015 henry is desired on a form  $D = 2$ ,  $W = 1.5$ , with  $T$  to be approximately but not exceed 1 in., then application of the formula shows that about 520 turns are required. Since the cross-

section of the winding space is  $S = WT = D^2(xy)$ , or 1.5 sq in., wire must be used giving about 346 turns per sq in. For example the largest d.c.c. wire which can be used is No. 18, which winds about 378 turns per square inch. Revised estimates indicate the required inductance will be reached with 524 turns of such wire at  $y = 0.46$ .

The important reference shape indicated by  $M$  at  $x = y = 0.5$  is that for which a given amount of specified wire yields the maximum possible inductance for this type of coil. For example, wire tables indicate that a pound of No. 24 d.c.c. wire occupies 7.07 cu in. and winds 1,215 turns per square inch. Using the volume formula  $V = \pi D^3(xy)(l + y)$ , the value of  $D$  for a coil with 7.07 cu in. of winding space and  $x = y = 0.5$  is 1.82 in. The cross-section of the winding



Inductance in microhenrys is given by

$$L = DN^2 F_L(x, y)$$

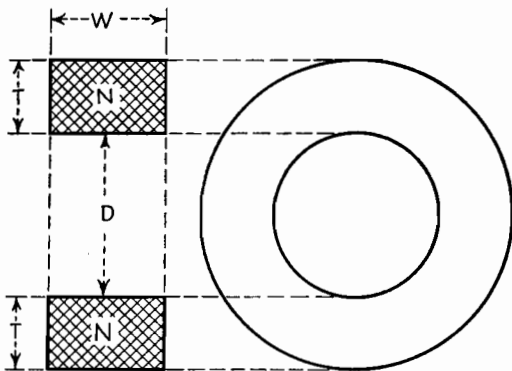
Where  $D$  is the inner diameter of the coil in inches,  $N$  is the total number of turns of the coil, and  $F_L(x, y)$  is the shape factor for inductance calculations, as given by the heavy lines of the graph

The maximum inductance for a given amount of wire is obtained for coils whose shape factor is at the region  $M$  for which  $x = 0.5$  and  $y = 0.5$

Upper limit of coil quality is given by

$$Q = D^2 f F_Q(x, y)$$

Where  $D$  is the inner diameter of the coil, in inches,  $N$  is the total number of turns of the coil, and  $F_Q(x, y)$  is the shape factor for coil  $Q$  given by the dotted lines of the graph



space  $S = D^2(xy)$  is 0.83 sq in. and will be filled by 1,010 turns. Since  $F_L = 0.035$  for this shape, the inductance is now readily found to be 0.06 henry, as the maximum possible for the specified amount of wire and the shape restrictions applying to this chart.

Since No. 24 d.c.c. wire runs about 18.4 ohms per lb, and the maximum of 0.06 henry has been established for the pound, it readily follows that the specified material cannot yield a greater value of the quality factor  $Q$  than 20 per kc. Wire economy, however, is not always the determining element influencing the choices of the coil shape. For example, a shape  $x = y = 0.75$  might be used if a l-f coil of a specified  $Q$  is desired with economy of outside diameter. Or a shape  $x = 0.7, y = 0.4$  might be preferred if the coil is to be coupled to an additional outer winding. Or a shape  $x = 0.5, y = 0.05$  might be chosen for use in a h-f application. Some general information placing an upper limit on the possible  $Q$  for coils of this type is included by use of dotted lines  $F_Q$  ranging from 5 to 40. For coils wound with commercial annealed copper, the  $Q$  at 68°F, and at  $f$  kc cannot exceed  $D^2fF_Q(x,y)$ , with  $F_Q$  as here determinable.

The upper limit for a coil with  $D = 1.82, x = y = 0.5$  as above discussed, by the formula is  $Q < 51.5$  at 1,000 cycles. This is based on the winding space being entirely occupied by conducting material. No. 24 d.c.c. wire requires 0.00082 sq in. of winding space per turn, but the cross-section of the copper is only 0.00032 sq in. That is, only 39 per cent of the winding space is effective, and for this wire, the  $Q$  at 1,000 cycles cannot exceed 0.39 times the theoretical maximum.

For reference, the cut-down space factor for circular wires with the thinnest and thickest usual types of insulation can be estimated from the following table.

Space Factors for Various Wires		
AWG size	Enameled	Double cotton
10	0.73	0.62
20	0.68	0.435
30	0.645	0.23
40	0.585	0.056

At high frequencies, the nonuniform distribution of current in the conducting material itself further reduces the effective space factor. Litz wire, made by parallelizing several small enameled wires, improves the effective space factor by reducing the

amount of copper which, because of the skin effect, does not contribute to the actual conduction. Thus a litz wire designated  $4 \times 8 \times 38$ , comprising 32 strands of No. 38 wire, has the same cross-section of copper as a No. 23 single conductor. The physical space factor of the litz is about half that of its No. 23 equivalent with double cotton insulation, and it is therefore not at all desirable for l-f purposes. But the total surface of the strands composing the litz wire is about seven times that of the equivalent single conductor. Therefore, on the assumption that only material close to the surface actually carries current, at high frequencies the effective space factor of the litz, while not large, would be about 3.5 times that of a No. 23 d.c.c. wire.

Other well-known effects also cause the actual  $Q$ , and to a lesser extent the  $L$  of practicable coils, to differ from the values computable from the coil geometry and the d-c resistivity of the conducting material. Proper allowance for these effects is largely a matter of experience or application of formulas based on experiments. What is presented here is merely graphical information based on well-established formulas, with sufficient precision for purposes of preliminary design.

# Winding the Universal Coil

By A. W. SIMON

Details of how to calculate the various factors entering into the winding of universal coils used with such great frequency in modern radio receivers

UNIVERSAL coils are wound so that, as the dowel or form on which the coil is wound rotates, the wire is guided back and forth by a shuttle, which displaces the wire in linear proportion to the angle of rotation from the last point of maximum left or right displacement. This shuttle is actuated by a cam mounted on a shaft, which is geared in a definite ratio to the shaft turning the dowel.

The wire may make one or more crossovers while the dowel makes one revolution; or the dowel may make one or more revolutions while the wire makes one crossover; and it is also possible (and often advantageous) to wind coils where

the number of crossovers per turn or the number of turns per crossover is an integer plus a simple fraction, such as  $1\frac{1}{2}, 1\frac{1}{3}, 2\frac{1}{2}$ , etc. Strictly speaking, in the case of the one crossover per turn winding, the wire does not cross over in exactly one revolution, but either in somewhat more (progressive winding) or somewhat less (retrogressive winding) than an exact revolution; and similar relations hold for multiple crosses.

In studying the universal winding, its developed diagram is of great convenience. Figure 1 represents the developed diagram for the case of a progressive winding with one crossover per turn. The trace may

be taken to represent the left-hand edge of the wire. The wire starts at  $O$ , runs across at a definite angle  $\phi$  to the axis and has reached the point  $A$  when the dowel has made a complete revolution, continues on and completes the crossover at a point  $B$ , a distance  $h$  from the starting line  $OO'$ ; then reverses its direction and has reached the point  $C$  when the dowel has made two complete revolutions, continues on and completes the second crossover at a point  $D$ , distance  $2h$  from the starting line  $OO'$ . The process is then repeated, beginning from a new starting line through the point  $D$ , and so on.



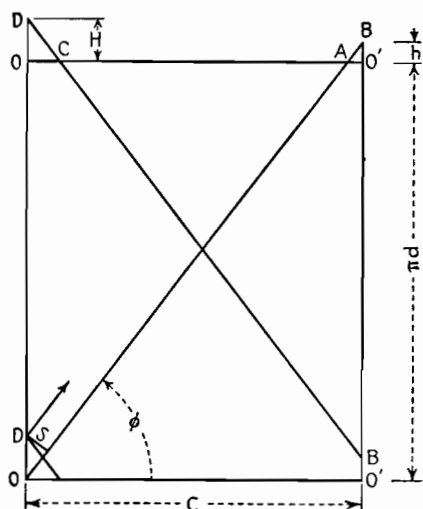


Fig. 1.—Developed diagram of progressive winding with one crossover per turn.

In the case of a retrogressive winding of one cross per turn (Fig. 2), on the other hand, the wire again starts at  $O$  and runs across at a definite angle  $\phi$  to the axis but completes the crossover before the dowel has made a complete revolution, at a point  $B$  located at a distance  $h$  on this side of the starting line  $OO'$ , reverses its direction and has reached the point  $A$  when the dowel has made exactly one revolution, continues on and completes the second crossover at a point  $D$ , a distance  $2h$  behind the starting line  $OO'$ . The whole process is then repeated, beginning with a new starting line through the point  $D$ , and so on.

It will be noted that, in the case of a retrogressive winding, the new starting line falls continually behind the preceding one; while in the case of a progressive winding it moves continually ahead. Hence if the wire is wound in a clockwise direction in both cases, in the retrogressive

winding the layering proceeds in the opposite, *i.e.*, the counterclockwise, direction; while in the progressive winding, the layering proceeds in the same, *i.e.*, also the clockwise, direction.

The distance  $O'B = h$  might be defined as the linear advance per crossover; while the distance  $OD = H$  might be defined as the advance per winding cycle or the winding space.

If we redraw the developed diagram for a complete winding cycle but ignore the slight advance  $h$  per crossover, we obtain the pattern of the winding. A knowledge of the winding pattern is really sufficient in most cases to deduce the geometrical characteristics of the coil, such as the number of crossovers per winding cycle or the number of herringbones. The winding patterns for 1,  $1\frac{1}{3}$ ,  $1\frac{1}{2}$ , and 2 crossovers per turn are given in Fig. 3.

If now we denote by  $n$  the number of crossovers per turn, where  $n$  is equal to or greater than unity, by  $q$  the number of crossovers per winding cycle (obtained from the winding pattern), by  $c$  the maximum displacement of the cam, by  $d$  the diameter of the dowel, and by  $s$  the distance between centers of two adjacent parallel wires at the dowel diameter, we have

$$s = H \cos \phi = qh \cos \phi \quad (1)$$

Also we have

$$c \tan \phi = (\pi d/n) + h \quad (2)$$

If, further, we denote by  $\theta$  the angular rotation of the cam, by  $\psi$  the angular rotation of the dowel, by  $r$  the gear ratio employed between the camshaft and the dowel shaft, by  $x$  the displacement of

the wire parallel to the axis, and by  $y$  the displacement perpendicular thereto (on the developed surface) we can put

$$x = \frac{c\theta}{\pi} \quad (3)$$

$$y = \frac{\psi d}{2} \quad (4)$$

But the ratio of  $y$  to  $x$  is equal to  $\tan \phi$ , whence we have also

$$\tan \phi = \frac{r\pi d}{2c} \quad (5)$$

Eliminating  $\phi$  between Eqs. (1), (2), and (5) we have finally

$$r = \frac{2}{n} \left[ \frac{1 \pm \sqrt{a^2 + b^2 - a^2 b^2}}{(1 - a^2)} \right] \quad (6)$$

where the upper sign is taken for a progressive winding and the lower for a retrogressive one, and where  $a$  and  $b$  are given by

$$a = \frac{s}{qc} \quad (7)$$

$$b = \frac{ns}{q\pi d} \quad (8)$$

However, since  $a$  and  $b$  are small quantities, Eq. (6) can be written with negligible error in the form

$$r = \frac{2}{n} (1 \pm \sqrt{a^2 + b^2})(1 + a^2) \quad (6a)$$

where  $a$  and  $b$  are defined as above, and  $n$  is restricted to values equal to or greater than unity.

From this equation the gear ratio required in winding a coil can be calculated, provided the cam displacement (coil width), the dowel diameter, the number of crossovers per turn, the number of crossovers per winding cycle (deduced from the number of crossovers per turn),

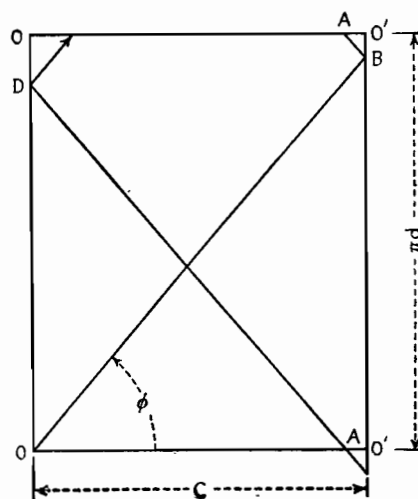


Fig. 2.—Developed diagram of retrogressive winding with one crossover per turn.

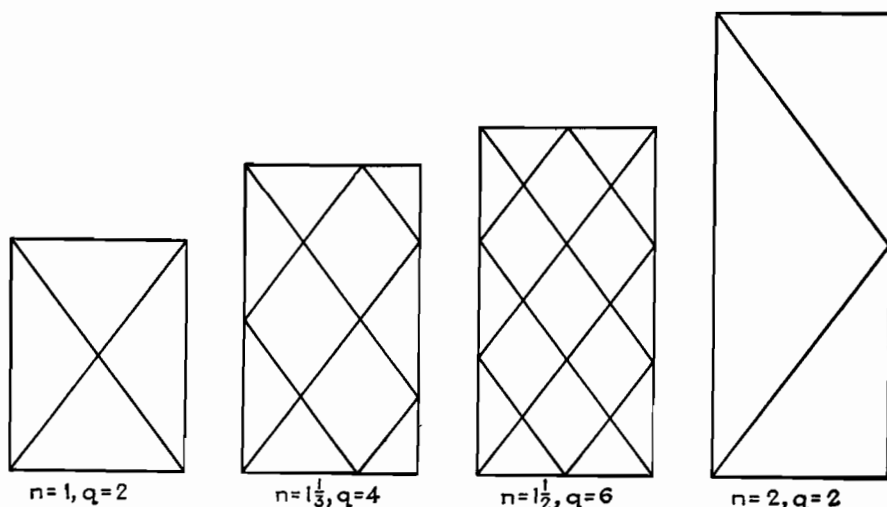


Fig. 3.—Winding patterns for 1,  $1\frac{1}{3}$ ,  $1\frac{1}{2}$ , and 2 crossovers per turn.

and lastly, the wire spacing at the dowel diameter are given.

In connection with the latter, *i.e.*, the spacing between centers of adjacent wires at the dowel diameter, it is convenient to define a spacing factor  $f$  according to the equation

$$s = f\delta \quad (9)$$

where  $\delta$  is the nominal diameter of the wire. This spacing factor can be selected on the basis of other factors such as the mechanical properties of the coil and the distributed capacitance of the winding. As regards purely the mechanical properties of the coil, it is found that a value of  $f$  equal to 1.25 produces very satisfactory results. Coils wound with this factor are very stable mechanically and have sharply defined straight walls.

We pass now to a consideration of the significance of the number of crossovers per turn and the question of the correct number to be used in a given case. This is determined purely by mechanical considerations, as follows:

In order to wind well, the winding angle  $\phi$  must be between certain limits. If it is too small, the component of the tension of the wire parallel to the axis of the dowel overcomes the frictional force holding the wire on the dowel, and the wire slides on the dowel toward the center of the winding; while if the angle  $\phi$  is too steep, the wire is not pinned down properly at the edges of the coil, resulting in a weaving of the wall. Hence, in order to build up a coil as high as possible, the number of crossovers must be so chosen that at the dowel diameter the angle  $\phi$  is near its lower limit; the coil will then build up satisfactorily until  $\phi$  attains its upper limit.

Based on the fact that the angle  $\phi$  must be near its lower limit, we see, for example (Fig. 4), that if  $\phi$  has the correct value in the case of coil 1 of one crossover per turn, coil 2, which has half the width, must be wound with two crossovers in order to maintain the same angle; while coil 3, which has double the diameter of coil 1, must be wound also with two crossovers per turn to maintain the same angle  $\phi$ . Hence the formula giving the correct number of crosses per turn must have the form

$$n = \frac{kd}{c} \quad (10)$$

where  $k$  is a constant. In practice it is found that one crossover per turn is very satisfactory in the case of a  $\frac{1}{4}$ -in. coil wound on a  $\frac{3}{8}$ -in. dowel, which, sub-

stituted in Eq. (10), gives  $k = 2/3$ , so that we can write in general

$$n = \frac{2d}{3c} \quad (11)$$

This equation holds over a considerable range of diameters and coil widths.

Coils can be wound with a number of crossovers slightly less than the formula calls for, but never with one greater, since we have chosen  $k$  so that  $\phi$  shall be at the lower limit.

The side of a universal wound coil exhibits a definite pattern in the form of a number of spokes or spirals radiating outward. The nature of this pattern and the number of spokes or spirals depends on the gear ratio employed. From a knowledge of the gear ratio, it is possible to predict whether a radial or spiral pattern will appear in a given case, as well as the actual number of spokes or spirals that make up the pattern; while, conversely, from a count of the number of spokes or spirals appearing on the side of a coil, the gear ratio employed in winding it can be deduced. (The number of spirals is, however, more difficult to count.)

Of fundamental importance in this connection is the number  $N$  of winding spaces of length  $H$  per layer of the coil, which is given by the equation

$$N = \frac{\pi d}{H} = \frac{\pi d}{qh} \quad (12)$$

Solving Eqs. (1), (2), and (5) for  $\pi d/qh$  we obtain

$$\frac{\pi d}{qh} = \frac{2n}{q(nr - 2)} \quad (13)$$

But the formula for  $r$  takes the form

$$r = \frac{2}{n} (1 + p) = \frac{2}{n} \left(1 + \frac{1}{P}\right) \quad (14)$$

where  $p$  is a small fraction and  $P$  its reciprocal, and this gives in turn

$$(nr - 2) = 2p = \frac{2}{P} \quad (15)$$

Substituting these values back in Eq. (13) we obtain finally

$$N = \frac{n}{pq} = \frac{nP}{q} \quad (16)$$

From this equation, the number of winding spaces per layer can be calculated, provided the number of crossovers per turn, the number of crossovers per winding cycle, and the gear ratio are known.

If  $N$  is integral, the points of maximum displacement of the wire for successive layers will fall on the same radius, giving rise to a radial pattern; while if  $N$  is not integral, they will be displaced in successive layers, giving rise to a spiral pattern. Two examples will make this clear:

Let us suppose one crossover per turn ( $n = 1$ ,  $q = 2$ ) and a gear ratio of 74/36 has been used. The gear ratio can be written in the form

$$r = \frac{74}{36} = 2 \left(1 + \frac{1}{36}\right)$$

from which we have, by comparison with Eq. (14),  $p = 1/36$  and  $P = 36$ , whence Eq. (16) gives  $N = 18$ . Hence a coil wound with this gear ratio should have 18 spokes in the pattern.

On the other hand, if a gear ratio 72:35 has been used, we would have  $p = 1/35$  and  $N = 17.5$ . Hence the points of maximum displacement of one layer would fall halfway between those of the preceding, thus giving rise to a spiral pattern.

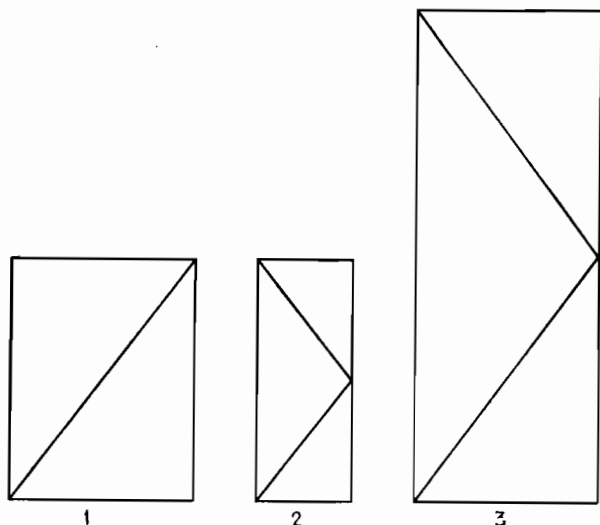


Fig. 4.—Effect of width and diameter of coil on the required number of crossovers per turn.

By changing the gear ratio by only half a tooth, a radial pattern can be changed to a spiral pattern, and vice versa.

If we are interested in determining the gear ratio employed in winding a coil from a count of the number  $N$  of winding spaces, we solve Eqs. (15) and (16) for  $r$  and have

$$r = 2 \left( \frac{1}{n} + \frac{1}{Nq} \right) \quad (17)$$

For example, if 18 spokes are observed on the side of a coil wound with one crossover per turn ( $q = 2$ ), the gear ratio was

$$r = 2 \left( 1 + \frac{1}{36} \right) = \frac{74}{36}$$

A knowledge of  $N$ , i.e., the number of winding cycles per layer, also enables us to deduce the number of turns per layer and the total number of layers on a given coil.

Since the wires cross over each other in a universal winding, it is necessary to define exactly what is to be understood by the term layer as applied to this type of winding, and we shall take the first layer to mean that portion of the winding required to cover just the area of the dowel between the lateral confines of the coil, the second layer that portion required to cover just the area of the first layer, etc. A layer then will be actually two wire diameters in thickness.

Since there are  $N$  winding spaces per layer, two crossovers for each winding space, and  $n$  crossovers per turn, we have as the number  $l$  of turns per layer

$$l = \frac{2N}{n} \quad (18)$$

If we denote by  $l$  the total number of layers in the coil (each of depth  $2\delta$ ) and by  $T$  the total number of turns in the coil, we have

$$l = \frac{T}{l} = \frac{nT}{2N} \quad (19)$$

For example, the two coils cited above will have 36 and 35 turns per layer, respectively.

## Mutual-inductance Calculations

By DALE POLLACK

A simplified method for performing one of the most involved calculations in coil practice, the determination of the mutual inductance between two coaxial single-layer coils in terms of their winding pitches, dimensions, and separation

THE calculation of the mutual inductance between two coils always presents a problem to the engineer, the usual procedure being to measure the value experimentally. Series expressions for the calculation of mutual inductance have been available for some time, but their application is in general quite

laborious. A somewhat simplified procedure has been presented by Grover,\* in which, however, some simplicity has been sacrificed in the interest of accuracy. Grover's results have been further simplified

\* GROVER, F. W., Tables for Calculation of the Mutual Inductances of Any Two Coaxial Single-layer Coils, *Proc. IRE*, 21, 1039, 1933.

here and are presented in a form designed for rapid computation with satisfactory engineering precision.

Three schedules are given for the following cases:

1. For large values of mutual.
2. For small values of mutual.
3. For concentric coils.

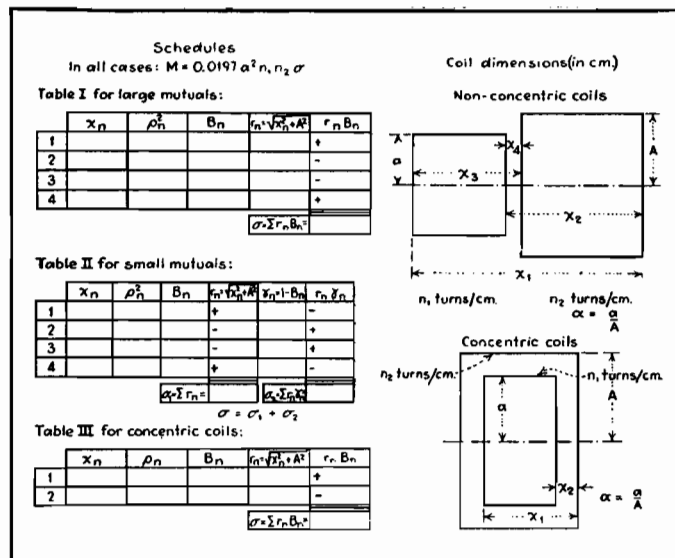


Fig. 1.—Calculation schedules and coil dimensions for determining values of mutual inductance.

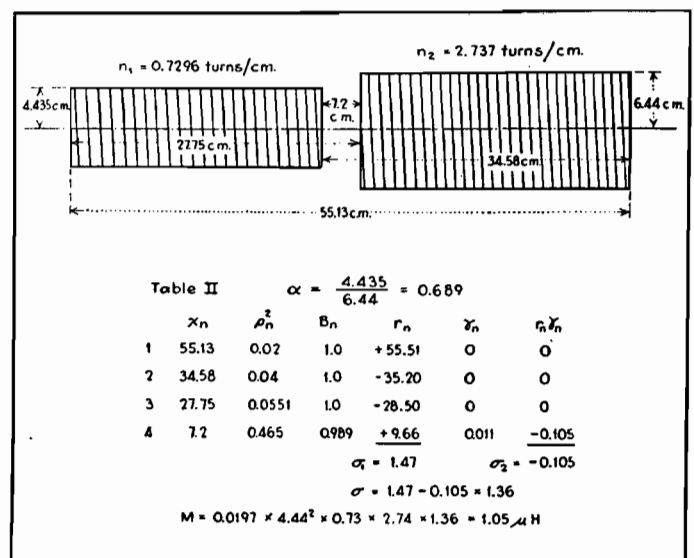
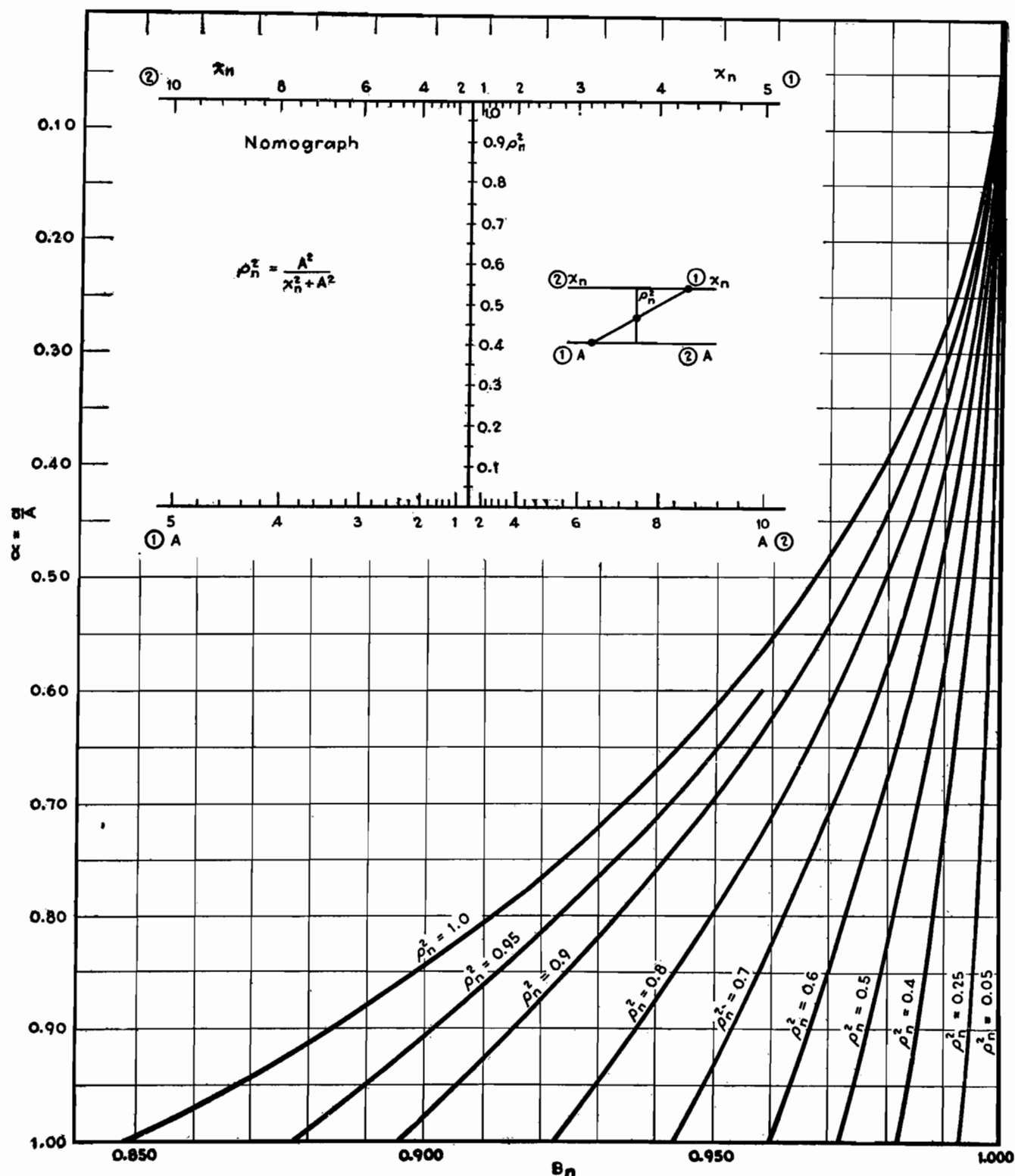


Fig. 2.—Typical example of two coils whose mutual inductance is found to be 1.05 microhenrys.



Nomograph for computing mutual inductance.

In each case, the procedure is the same. Fill in the first column  $X_n$  in the proper schedule from the coil dimensions shown in Fig. 1. The second column  $\rho_n^2$  is obtained from the nomograph or from the equation given. Two sets of scales for  $X_n$  and  $A$  are given in the nomograph, but the ranges may be extended by shifting the decimal points on either set of

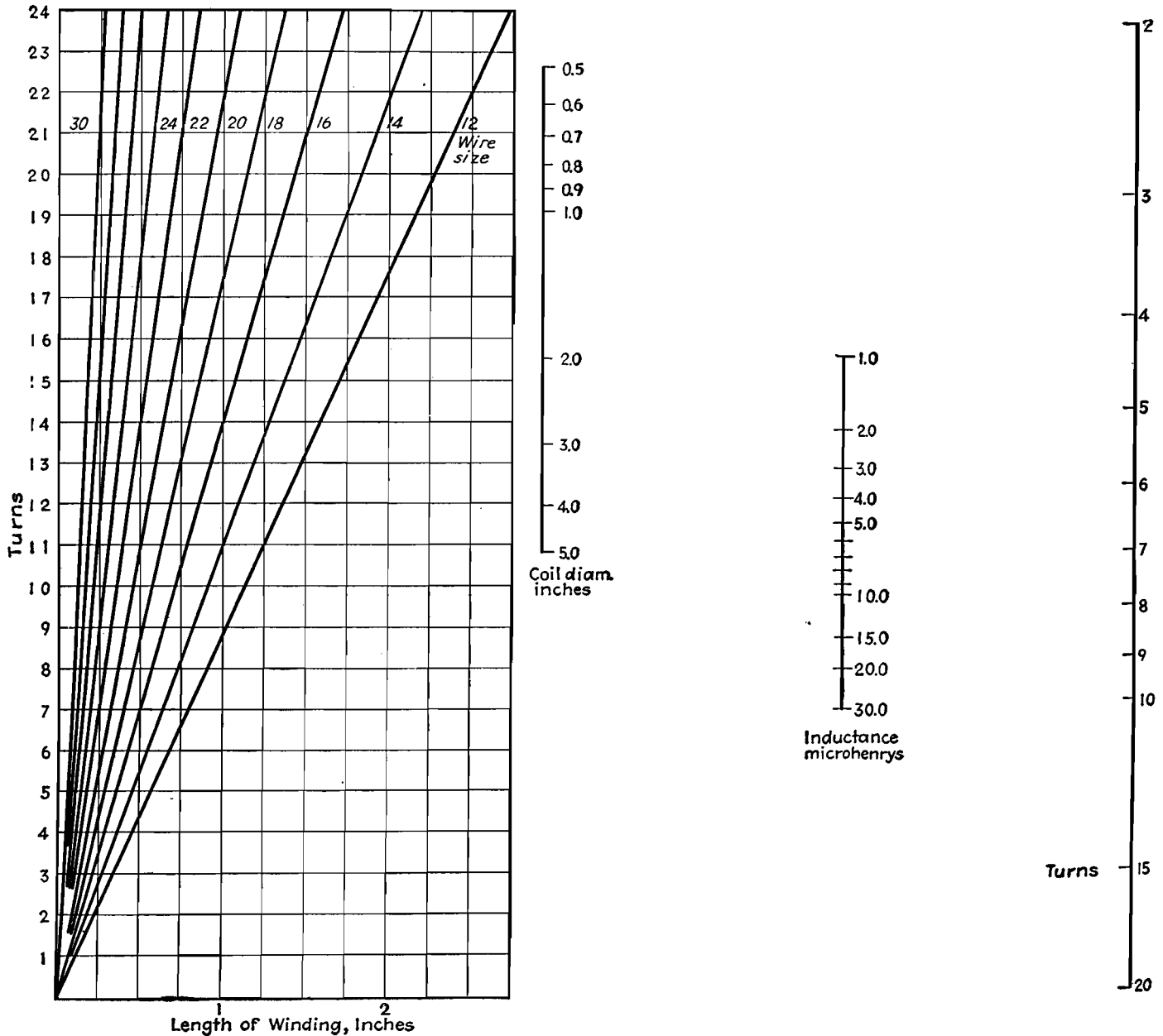
scales by the same number of places. The third column  $B_n$  is obtained from the curves on the reverse side. The  $r_n$  column is computed from  $r_n = \sqrt{X_n^2 + A^2}$ . The last column is calculated as shown. Finally, the last columns (the fourth and sixth columns, in Table II) are added algebraically, taking account of the sign indicated in the column, and a value of  $\sigma$

is thus obtained, which is used in the equation  $M = 0.0197 a^2 n_1 n_2 \sigma \mu h$ . The entire calculation takes only a few minutes.

For illustration, the example in Fig. 2 is given, in which Table II is used. The calculated value  $1.05 \mu h$  is within 3 per cent of the correct value calculated, which is  $1.0862 \mu h$ , according to Grover.

# H-f Inductance Charts

By FREDERICK C. EVERETT



Charts in various forms have been available for the design of short-wave inductances, but there has been nothing to ensure that the highest possible  $Q$  had been obtained in the design. By utilizing the information produced by Pollack\* it has been possible to make the entire computation without "cut and try."

These charts are suitable only when the length of winding is equal to half of the diameter, which is the optimum proportion. The number of turns for any desired inductance can be obtained at once from the chart on the right. Using half the diameter for the length, the optimum size of the wire can be obtained from the chart on the left. The coil should be wound so that the wire occupies the length of winding used in the computation.

\* POLLACK, DALE, Inductances for Frequencies—4 to 25 Mc. *Elec. Eng.*, September, 1937.

# Universal Performance Curves for Tuned Transformers

By J. E. MAYNARD

THE design and calculation of tuned transformers for a particular purpose can be greatly simplified through the use of two families of curves that give the attenuation and the phase displacement of the transformer as functions of a selectivity variable and a parameter. These universal performance curves may be applied to any physical situation when the proper conversion factors are used, and can be used in design work, or to determine quickly the selectivity and band-pass performance of a given set of coupled coils.

The assumptions on which the mathematical work underlying this article depend are as follows:

1. The  $Q$  of the transformer circuits over a narrow frequency range may be considered constant.
2. The  $Q$  of the circuits is sufficiently high so that parallel and series resonance occurs at the same frequency, i.e., that for which  $\omega L = 1/\omega C$ .
3. No feedback exists in the tube circuits.
4. The coupling between the two coils is purely reactive.

These assumptions may readily be accepted for most practical situations, or allowances may be made in cases for which these assumptions are violated. Assumption 3 will not always be strictly tenable.

The equivalent circuit of the transformer that was used in the analytical work is shown in Fig. 1 and closely approximates the circuits used in practice, in which both inductive and capacitive coupling exists between the coils. Under assumption 3, all circuit losses may be represented by the inclusion of these

losses in the parallel conductances  $G_1$  and  $G_2$ . For instance, the loading on the primary of the transformer due to the internal plate resistance of the driver tube will be included in  $G_1$ , or the loading on the secondary of a transformer used to drive a diode will be included in  $G_2$ . The losses in shielding and coils will also be considered as part of these conductances.

By writing Kirchhoff's equations for the various meshes of the equivalent circuit and making the proper substitutions and transformations, it can be shown that, for positive values of mutual inductance  $M$  between the transformer coils, there is a frequency of infinite attenuation  $f_\infty$  for which the inductive and capacitive coupling are equal and opposite or for which  $K_L/\omega L = K_C\omega C$ . It can also be shown that for the cases in which either type of coupling predominates (or the two types of coupling are of like sign) the resultant coupling  $K$  may be treated as a total or net coupling, the absolute value of which is constant near resonance. Under these conditions, which will be assumed hereafter, performance of the transformer near resonance is the same regardless of the type or combinations of coupling employed. This enables us to obtain a symmetrical performance curve, so that only one half of the curve need be given in the charts.

## Calculations for Determining Universal-selectivity and Universal Phase-shift Graphs

The performance of the transformer is given by

$$\frac{i_p}{e_p} = \pm \frac{jy}{A_0 n^2} \quad (1)$$

in which  $y$  is a complex expression determining the selectivity of the network near resonance,  $A_0$  is a real coefficient which is a function of resonant circuit impedance, coupling between primary and secondary, primary-to-secondary inductance ratios and circuit quality factors, and  $n$ , which we may treat as unity near resonance, is the ratio of any frequency  $f$  to the resonance frequency  $f_0$ .

It can be shown that  $i_p$ , as used, is directly proportional to the grid voltage of the tube driving the transformer. If we let the absolute magnitude of  $y$  be designated as  $Y$ , then

$$Y = [t^2(1+a)^2 + (1-at^2+aK^2Q^2)^2]^{1/2} \quad (2)$$

where  $t$  is the tangent of the phase angle between secondary voltage and current and is a function of frequency defined by

$$t = \left(n - \frac{1}{n}\right) Q$$

where  $a$  is  $Q_1/Q_2$ ,  $K$  is the total or net coupling given by  $\pm(K_L/n) - nK_C$ , and  $Q$  is the quality factor of the secondary circuit.

This equation has the advantage that it may be reduced to a form containing an independent variable associated with the circuit selectivity  $S$ , a dependent attenuation variable  $u$ , and a parameter  $b$ . In order to effect this transformation, it will be convenient to adopt a somewhat more abbreviated notation. For example, let

$$t = S \left(\frac{1+a}{2a}\right) \quad (3)$$

$$Y = u \left(\frac{1+a}{2a}\right)^2 a \quad (4)$$

and

$$aK^2Q^2 = \left[ \left(1+b^2\right) \left(\frac{1+a}{2a}\right)^2 a \right] - 1 \quad (5)$$

Substituting Eqs. (3), (4), and (5) in Eq. (2), we obtain for the attenuation, the expression

$$u = [4S^2 + (1-S^2+b^2)^2]^{1/2} \quad (6)$$

Let  $u_0$  be the attenuation at resonance, for which  $S = 0$ . The attenuation  $u$  at any frequency  $f$  compared with the attenuation at resonance  $u_0$  is then given

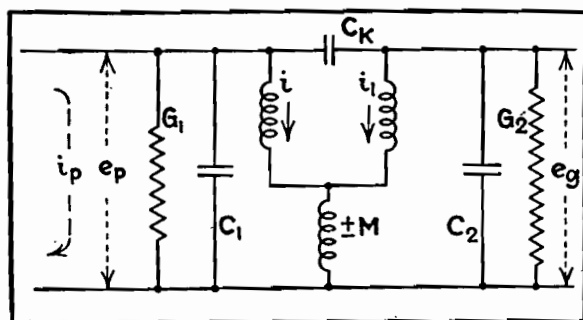


Fig. 1.—Equivalent circuit upon which the mathematical analysis is based.

by

$$\frac{u}{u_0} = \frac{[4S^2 + (1 - S^2 + b^2)^2]^{1/2}}{1 + b^2} \quad (7)$$

The values of Eq. (7) are plotted as the universal selectivity curves in Fig. 2.

It is desirable to determine the attenuation in terms of some stated bandwidth. The relation

$$\Delta f = \frac{(1 + a)f_0 S}{4aQ} \quad (8)$$

which may be derived from Eq. (3) and the definition of  $t$  permits interpretation of the selectivity curves in terms of bandwidth  $2\Delta f$ . The curves have been plotted for positive values of  $S$  only, since the assumptions that have been made lead to curves symmetrical about the resonance point.

The vector form of Eq. (6) is

$$u = (1 - S^2 + b^2) + j2S \quad (9)$$

in addition to which we have a  $\pm 90$ -deg phase rotation due to  $\pm j$  in Eq. (1), from which the phase shift of the transformer becomes

$$\theta \pm 90^\circ = \frac{\tan^{-1} 2S}{1 - S^2 + b^2} \pm 90^\circ \quad (10)$$

the polarity of the additional 90-deg rotation being positive for the negative values of  $K$  or negative for positive values of  $K$ .

A family of curves representing Eq. (10) is shown as the universal phase-shift curves in Fig. 3. The universal-selectivity and universal phase-shift curves determine the performance of a transformer, under the assumptions that have been made, and enable us to determine the attenuation and phase shift (relative to resonance) when we know  $a$ ,  $f_0$ ,  $S$ , and  $Q$ .

A convenient set of formulas that enable us to estimate quickly the selectivity and band-pass performance of a given set of transformers operated in cascade may be obtained from these universal curves. For adjacent-channel attenuation of three or more ( $u/u_0 \geq 3$ ), and for values of  $b$  between 0.2 and 1.41 (which includes most cases of usual design), Eq. (7) may be approximated by

$$\frac{u}{u_0} = \frac{S^2}{1 + b^2} \quad (\text{for } b \geq 1) \quad (11)$$

$$\frac{u}{u_0} = \frac{1 + S^2}{1 + b^2} \quad (\text{for } b < 1) \quad (12)$$

The following formulas for the nose of the curve, based on an over-all attenuation of  $u/u_0 = 2$ , may be derived from Eq. (7).

For  $u/u_0 = 2$

$$S^2 = b^2 - 1 + 2(1 + b^2 + b^4)^{1/2} \quad (13)$$

For  $u/u_0 = \sqrt{2}$

$$S^2 = b^2 - 1 + (2 + 2b^4)^{1/2} \quad (14)$$

For  $u/u_0 = \sqrt[3]{2}$

$$S^2 = b^2 - 1 + (1.59 - 0.82b^2 + 1.59b^4)^{1/2} \quad (15)$$

These equations allow calculations based on an equivalent single transformer whose attenuation, raised to a power corresponding to the number of transformers used, will provide an estimate for the over-all performance of the system. Our known quantities are an adjacent-channel attenuation figure for  $u/u_0$ , and definite bandwidths by means of which  $S$  becomes a numerical linear function of  $Q$ . The unknown quantities are then  $b$  and  $Q$ . Eliminating  $b$  between Eq. (11) and any one of the last three equations permits determination of the  $Q$  required to meet the specified performance. The corresponding value of  $b$  will then indicate the shape of curve by reference to the universal chart. The problem to be solved may be set up for any two unknowns in the above system of equations, and each transformer may be solved individually rather than assuming all transformers identical, but Eqs. (14) and (15) apply only for two or three identical transformers.

#### Single Tuned Circuit

The performance of a single tuned circuit may also be expressed by means of a universal curve. The equations for selectivity and phase shift for a single tuned circuit are given by

$$\theta' = \tan^{-1} S \quad (16)$$

for phase shift, and

$$u' = (1 + S^2)^{1/2} \quad (17)$$

for attenuation of resonance in terms of the variables already used. The phase shift and attenuation curves for the single tuned circuit are given in dotted lines on the families of curves in Figs. 2 and 3.

#### Use of Universal Selectivity and Phase-shift Curves in Practical Applications

Some numerical examples will serve to illustrate the use of these curves and formulas.

Let us take a two-stage amplifier operating at 465 kc resonant frequency for the first case. We shall assume that all three transformers are identical; tuned circuit impedances may be kept low enough so that this will be a reasonable approximation. Suppose we desire to design an amplifier to have critical curve

shape ( $b = 1$ ) with all coils identical and to obtain an adjacent-channel attenuation of 100, what  $Q$  will be required and what will be the band width at an over-all attenuation of 2?

The equivalent single transformer will have an adjacent-channel attenuation of  $\sqrt[3]{100}$  or 4.65. From the universal curve for  $b = 1$  we find, for  $u/u_0 = 4.65$ , that  $S$  is 3.02. At the adjacent channel,  $\Delta f$  is 10 kc. Since  $a = 1$ , solving Eq. (8)  $Q$  is 70 for these values of  $\Delta f$  and  $S$ . Solving Eq. (15) with  $b = 1$  we have  $S = 1.24$ . With this value of  $S$  and a  $Q$  of 70, Eq. (8) gives us  $\Delta f = 4.13$ . Our bandwidth ( $2\Delta f$ ) for  $u/u_0 = \sqrt[3]{2}$  is then 8.26 kc. This will be the bandwidth at an attenuation of 2 for three of these transformers in cascade with a  $Q$  of 70 in each circuit. We might have used Eq. (11) instead of the curve to obtain our first value of  $S$ , which would then have been  $S = 3.05$ .

Let us take a slightly different problem. Suppose we have coils of  $Q = 120$  available (in shield) and wish to design a single-stage amplifier using these coils to obtain an adjacent-channel attenuation of 50, what will be the shape of curve and bandwidth at an attenuation of 2, using a resonant frequency of 480 kc?

In single-stage design, high tuned-circuit impedances are normally used to obtain high gain. We shall assume in this case that circuits reduce the effective  $Q$  of the first transformer primary to 80 and of the second transformer secondary to 40. This leads to two transformers that are not identical. The over-all attenuation of 50 at the adjacent channel will be the product of the attenuations at this frequency in each transformer. Since the second transformer has lower  $Q$  circuits, we shall call for less attenuation in this transformer. Let us require an attenuation of the adjacent channel of 10 and 5 in the first and second transformers, respectively.

The solution for the first transformer gives  $a = Q_1/Q_2 = 80/120 = 0.667$ , and from Eq. (8) we find  $\Delta f$  to be  $2.5S$  (in kc). Then for  $\Delta f = 10$  kc, we have  $S = 4$ . Solving Eq. (12) with  $S = 4$  and  $u/u_0 = 10$ , we find that  $b^2 = 0.7$ , and substituting this value into Eq. (14) we find for  $u/u_0 = \sqrt{2}$  that  $S = 1.19$ . For this value of  $S$ , we have  $\Delta f = 1.19 \times 2.5$ , or 2.98 kc and the curve shape is defined by  $b = 0.84$ .

For the second transformer,  $Q_1 = 120$ ,  $Q_2 = 40$ , and therefore  $a = 3.0$ . From Eq. (8) we determine that  $\Delta f = 4S$  (in kc) so that for  $\Delta f = 10$  kc the value of



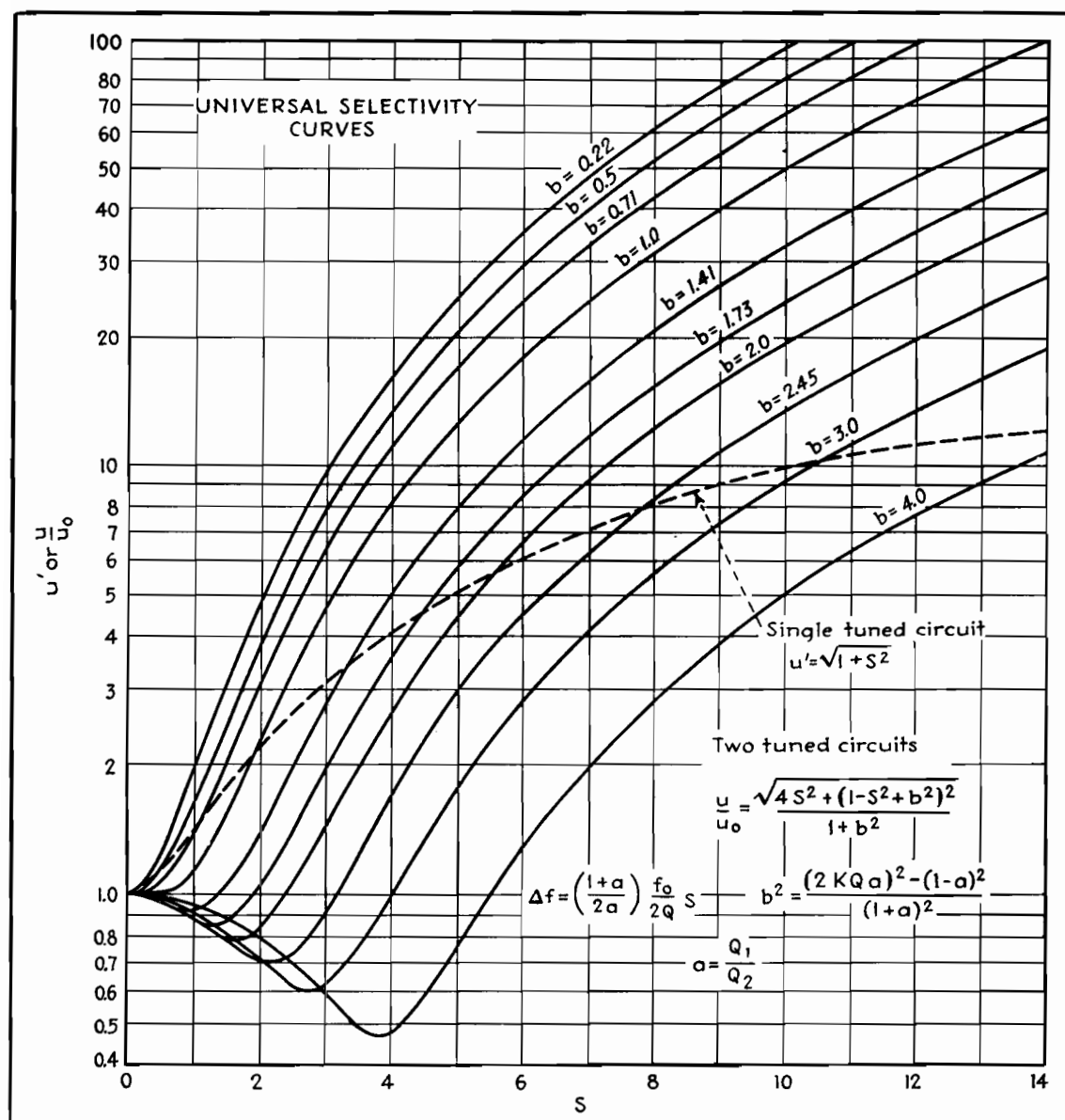


Fig. 2.—Solid curves for two tuned circuits show attenuation,  $u/u_0$ , and parameter  $b$  plotted against  $S$ . By interpolating, curves for other values of  $b$  may be determined. Dashed line shows similar information for single tuned circuit.

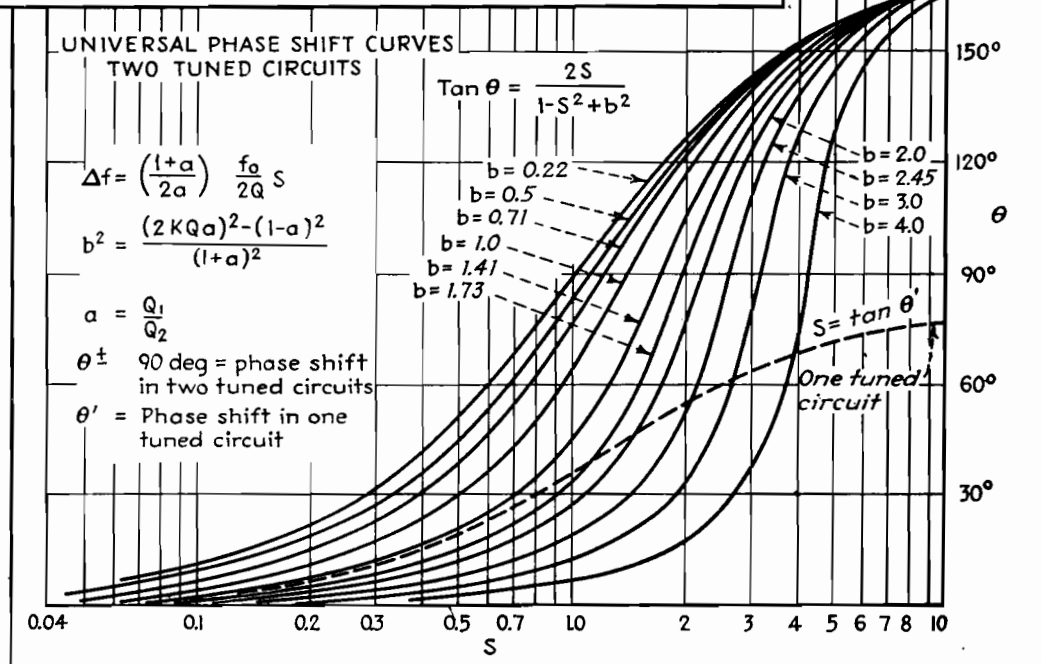


Fig. 3.—Phase-shift curves showing  $\theta$  plotted against  $S$  for various values of the parameter  $b$ . Dashed curve applies to single tuned circuit.

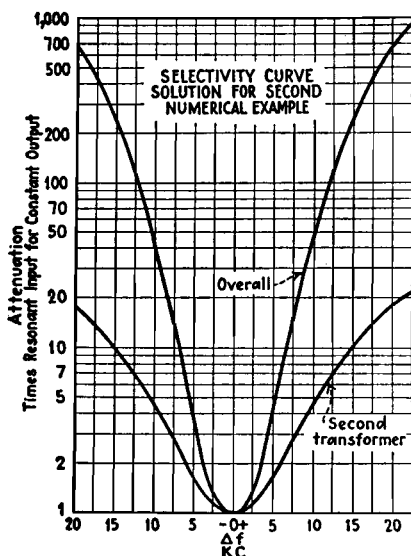


Fig. 4.—Second transformer and over-all attenuation curves for second illustrative problem.

$S$  is 2.5. Solving Eq. (12) for  $u/u_0 = 5$  and  $S = 2.5$ , we find that  $b^2 = 0.45$ . From Eq. (14), which applied for  $u/u_0$

$= \sqrt{2}$ , the value of  $S$  becomes 1.0, for which value  $\Delta f = 4.0$  kc. The curve shape is defined by  $b = 0.67$ . We may conclude from this solution that the over-all bandwidth for an attenuation of 2 will be about 7 kc and the curve shape will be somewhat less than critical, as shown in Fig. 4.

The universal curves for  $b = 0.67$  and  $b = 0.84$  may be obtained by interpolation from the universal curve chart and redrawn with a frequency scale for abscissas from the conversions  $\Delta f = 2.5S$  and  $\Delta f = 4.0S$ . The products of attenuation on these curves at discrete frequencies will then provide the over-all selectivity curve of the system as shown. It will be noted that the adjacent-channel attenuation is slightly less than 50. This is due to the approximation in Eq. (12).

For the last case, assume a single tuned circuit with  $u/u_0 = 4$ . For this attenuation we can determine from the universal selectivity curve that  $S = 4$ , and for this

value of  $S$  we determine from the phase-shift curve that  $\theta = 75^\circ$ . Actually, for  $u/u_0 = 4$ , the value of  $S$  is 3.87 and  $\theta = 75.5^\circ$ , but the results obtained graphically are sufficiently accurate for most purposes. For greater accuracy, the single tuned circuit equations may be used.

The use of these curves is not, of course, limited to i-f amplifier systems such as were used for illustration. For instance, band-pass audio filters may be designed in this manner. R-f amplifier circuits often contain preselectors consisting of tuned coupled circuits that vary in resonant frequency with the tuning of the receiver. In fact, any system in which we wish to select a relatively narrow band of frequencies from a given spectrum lends itself to treatment by tuned coupled transformers conforming to the universal curves presented herewith and within the premises on which the analysis rests.

## Double-tuned Transformer Design

By DAWKINS ESPY

Fundamental equations are plotted in general form showing the relations between  $k$ ,  $Q$ , db,  $f/f_0$ , response at resonance, and attenuation. Examples illustrate use of curves

**D**ETERMINING the performance and circuit constants of a double-tuned transformer is a problem frequently encountered. The use of the charts will greatly facilitate the calculations.

The general expression for the attenuation of two identical coupled circuits is<sup>1</sup>

$$db = 20 \log \frac{\sqrt{4 \left( Q \frac{\Delta f}{f_0} \right)^2 + \left[ 1 + (Qk)^2 - \left( Q \frac{\Delta f}{f_0} \right)^2 \right]^2}}{2Qk} \quad (1)$$

This relation is plotted in Fig. 1 so as to give the level variation of a family of  $Qk$  curves with respect to  $Q(\Delta f/f_0)$ .

The coupling between the two coils  $k$  and the  $Q$  of the coils is related to width of the pass band by<sup>2</sup>

$$\frac{\Delta f}{\sqrt{2} f_0} = \sqrt{\frac{k^2 - 1}{Q^2}} \quad (2)$$

where  $\Delta f/f_0$  is the fractional frequency deviation. The  $\sqrt{2}$  converts from peak

separation to bandwidth.<sup>3</sup> The level change in the pass band may be obtained by setting  $\Delta f/f_0 = 0$  in Eq. (1) and dividing the result by 2 in order to obtain the variation in gain from the average, as a function of coupling. This leads to

$$\Delta db = 10 \log \frac{(Qk)^2 + 1}{2Qk} \quad (3)$$

Equations (2) and (3) are plotted simultaneously in Fig. 2. This chart gives the solution of the problem involving the four variables  $k$ ,  $Q$ ,  $\Delta f/f_0$ , and  $\Delta db$ , with any two of them known. Since  $k$  is usually an adjustable variable, there are three possible cases

Known	Unknown
(1) $\Delta f/f_0$ and $\Delta db$	$Q$ and $k$
(2) $\Delta f/f$ and $Q$	$\Delta db$ and $k$
(3) $\Delta db$ and $Q$	$\Delta f/f$ and $k$

The relative response at resonance, due to variations in  $Qk$ , is obtained from the

reciprocal of the expression resulting from setting  $\Delta f/f_0 = 0$  in Eq. (1). This gives

$$\text{Gain reduction factor} = \frac{2Qk}{(Qk)^2 + 1} \quad (4)$$

The solid curve in Fig. 3 is plotted from Eq. (4). The factor used to determine the average gain in the pass band, as a function of  $Qk$ , is obtained by averaging the gain reduction factors at maximum pass-band gain and at resonance. This yields

$$\text{Gain reduction factor} = \frac{(Qk + 1)^2}{2[(Qk)^2 + 1]} \quad (5)$$

A plot of this expression for values of  $Qk \leq 1$  is shown by the dashed line in Fig. 3.

### Design Considerations

Design requirements of double-tuned r-f transformers ordinarily involve some particular attenuation at a given fre-

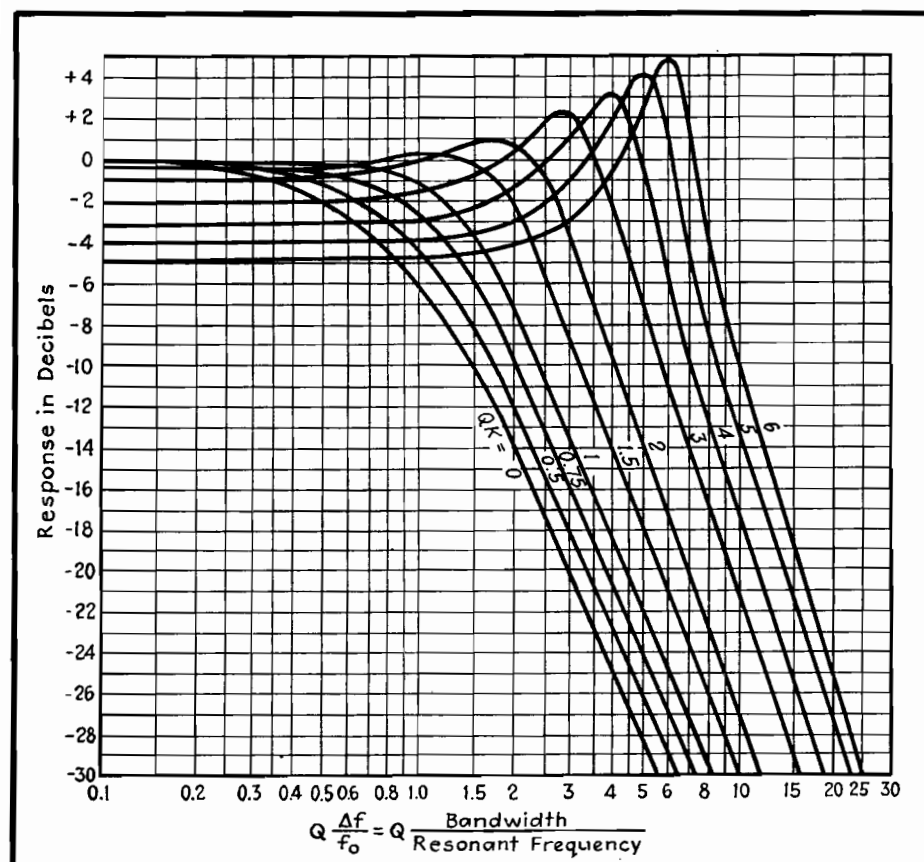


Fig. 1.—Universal selectivity curves showing deviation from average pass-band response vs. deviation from resonance.

quency-deviation from resonance. Knowing the required response in decibels  $\Delta f/f_0$  and the available  $Q$ , the required  $Qk$  is determined from Fig. 1, and thus the value of  $k$  is found. If attenuation at a specific point has been the design criterion, the resulting  $\Delta db$  can be determined from Fig. 2.

Frequently a transformer must be designed with a certain allowable response deviation from the average pass-band response. Usually the deviation, given in the charts as  $\Delta db$ , the width of the band, given as  $\Delta f$ , and the resonant frequency  $f_0$  are known. By using Fig. 2, it is possible to calculate the corresponding  $Q$  and  $k$ . The resulting attenuation at various frequencies can be determined by the use of Fig. 1.

#### Design Procedure

1. Determine  $Q$ ,  $k$ ,  $\Delta f/f_0$ , and  $\Delta db$  from Fig. 2.
2. Calculate maximum gain from  $(g_m X_L Q/2)$  where  $g_m$  is the transconductance of the tube driving the transformer and  $X_L$  is the reactance of either coil at  $f_0$ .
3. From  $Qk$  or  $\Delta db$ , find the gain-reduction factor from Fig. 3 and multiply it by the gain obtained in step 2 to obtain actual gain.
4. Determine the gain at any portion of the response curve from Fig. 1.

#### Examples

**Example 1.**—An i-f transformer operating at 456 kc with a tube having a  $g_m$  of 3,000  $\mu$ mhos is required to have a pass band of 16 kc. The response must not vary more than 1 db from the average. The inductance of each transformer winding is 250  $\mu$ h. Find  $Q$ ,  $k$ , the average gain, and the attenuation at 20 kc from resonance.

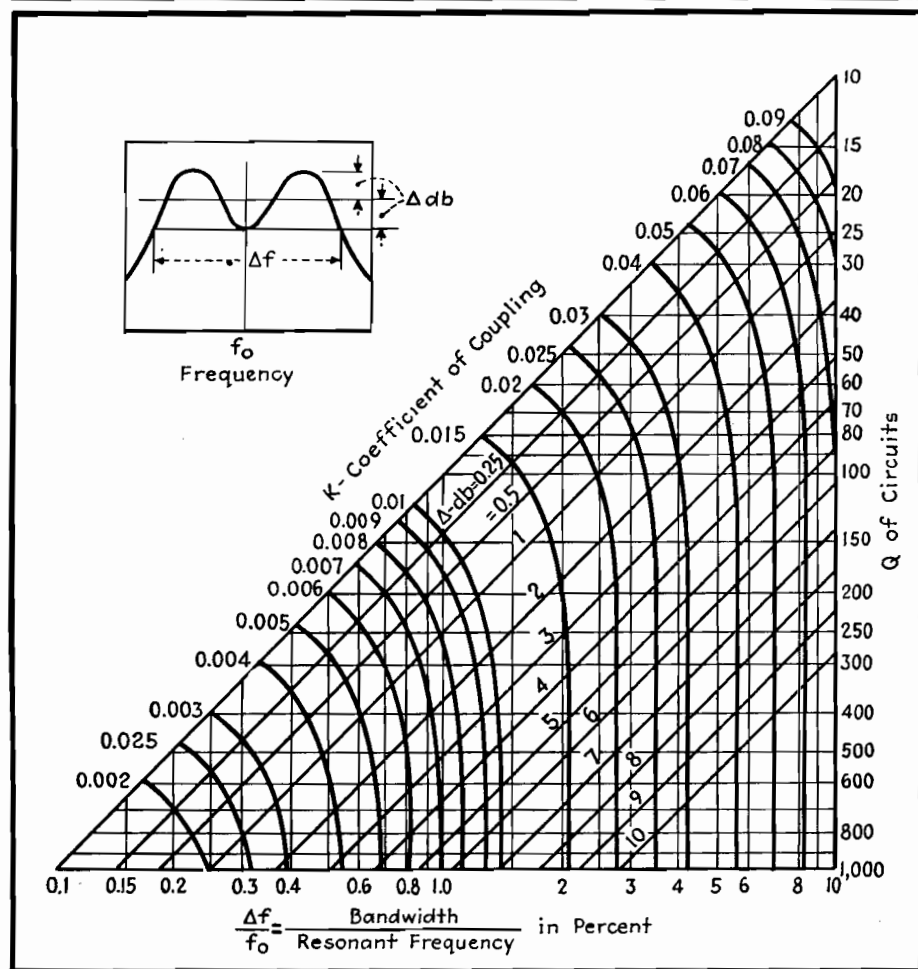
$$\text{Calculating } \frac{\Delta f}{f_0} = \frac{16}{456} = 3.51 \text{ per cent}$$

$$\text{From Fig. 2: } Q = 70, k = 0.028$$

$$\text{Max gain} = \frac{g_m X_L Q}{2} = \frac{3,000 \times 10^{-6} \times 2\pi \times 456 \times 10^3 \times 250 \times 10^{-6} \times 70}{2} = 75.2$$

$$\text{Average gain in pass band } 75.2 \times 0.9 = 67.7, \text{ where the 0.9 is read from Fig. 3.}$$

Fig. 2.—Three-parameter chart giving the relation between frequency deviation, coupling coefficient, and circuit  $Q$  for values of maximum response variation within the band.



For 20-kc deviation,  $\Delta f = 40$  kc and

$$\left(\frac{Q\Delta f}{f_0}\right) = (70 \times \frac{40}{456}) = 6.14$$

$$Qk = 70 \times 0.028 = 1.96$$

From Fig. 1 the attenuation = 18 db.

*Example 2.*—An i-f transformer is required to work at 3 Mc with a tube that has a  $g_m$  equal to 5,000  $\mu$ mhos, using a 30- $\mu$ h coil with a  $Q$  of 200. Find  $k$  and gain at resonance to give a compromise between gain and selectivity. Determine the gain at bandwidths of 10, 25, 50, and 75 kc.

A value of  $Qk = 0.5$  is a good compromise between gain and selectivity, reducing the gain to 0.8 of the value obtained at critical coupling (Fig. 3), while improving the selectivity (Fig. 1).

For  $Qk = 0.5$ ,  $k = \frac{0.5}{200} = 0.0025$

$$\text{Max gain} = \frac{g_m X_L Q}{2} = 283$$

$$\text{Gain at resonance} = 283 \times 0.8 = 226$$

$$= +7.1 \text{ db}$$

$$\frac{Q}{f} = 200/3,000 = 0.0667$$

From Fig. 1

$\Delta f$ in kc.....	10	25	50	75
$Q(\Delta f/f_0)$ .....	0.667	1.667	3.333	5.000
Attenuation in db from Fig. 1.....	2.2	9.3	19.5	26.0
Gain in db: 47.1 minus attenuation	44.9	37.8	27.6	21.1

#### References

(1) STURLEY, K. R., "Radio Receiver Design." John Wiley & Sons, Inc., New York, 1943, rearrangement of an expression on p. 300.

(2) EVERETT, W. L., "Communication Engineering," 2d ed., McGraw-Hill Book Company, Inc., 1937, modification of an equation on p. 502.

(3) AIKEN, C. B., Two-Mesh-Tuned Coupled Circuit Filters, *Proc. IRE*, 25, February, 1937.

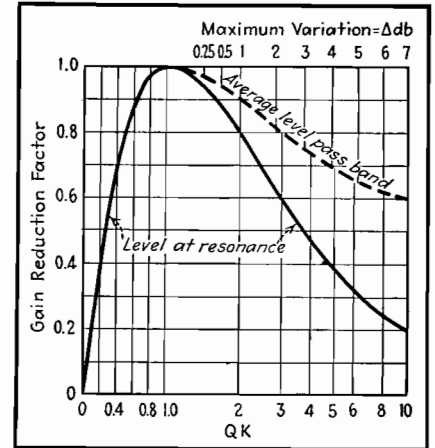


Fig. 3.—Output level plotted as a function of product of coupling coefficient and circuit  $Q$ .

## SECTION XX

# R-F IMPEDANCE-MATCHING NETWORKS

R-f Impedance-matching Networks.....	Page 270
Charts for L-type Impedance-transforming Circuits.....	272
Computing R-f Transition Losses.....	278

## R-f Impedance-matching Networks

By RALPH P. GLOVER

Data for the design of pi-section networks used in matching transmitters to antennas and in similar problems where r-f transition losses are to be minimized

**T**HE problem of efficiently connecting two circuits of different impedances arises frequently in r-f transmission design. At radio frequencies the impedance match can be accomplished with high efficiency by means of a network of inductive and capacitive elements.

The pi-section low-pass network is preferable in most cases because of its harmonic reducing properties; the most efficient design is obtained by making the network a symmetrical structure which is the equivalent of a quarter-wave line.

Such a network is shown in Fig. 1. It consists of an inductance in series with the line, and shunt capacitors at input and output. The inductor is preferably adjustable by means of a clip or taps. The input and output capacitors should be variable over a range above and below the computed value to take care of normal terminal impedance variations and to allow exact adjustment under operating conditions. In practical design problems, it is obviously important to determine the network voltages.

### Example

Design a network to couple a 500-ohm transmitter output to a 70-ohm concentric transmission line. The power is 1,000 watts at 1,000 kc.

**Example 1.**—Determine the network branch reactances. For the quarter-wave type, all three branches have numerically the same reactance. In Fig.

2, the intersection of a 70-ohm load with a 500-ohm source gives a reactance of 187 ohms.

**Example 2.**—Compute the inductance and capacitance necessary to give this reactance at carrier frequency.

$$L_B = \frac{X}{\omega} = \frac{187}{2\pi \times 1 \times 10^6} = 29.8 \mu\text{h}$$

$$C_A = C_C = \frac{1}{\omega X} = \frac{1}{2\pi \times 1 \times 10^6 \times 187} = 852 \mu\text{mf}$$

It is good practice to make  $L_B$  about 25 per cent larger than the computed value, say 35  $\mu\text{h}$ , and adjust to the exact value required by means of a short-circuiting clip. The shunt capacitor elements should have an available total capacitance of approximately 1,000  $\mu\text{mf}$  each.

**Example 3.**—Determine the current and voltage ratings of the capacitors and the current in the inductive branch.

The impedance looking into the input terminals of the network under working conditions is a resistance of 500 ohms. For a power of 1,000 watts, the corresponding rms voltage is obtained from Fig. 2 at the intersection of the line for 500 ohms. Thus  $E_0 = 707$  volts, rms. Assuming 100 per cent efficiency (approached in well-designed networks at moderate frequencies)  $E_L$  is similarly determined from Fig. 2 by interpolation as 270 volts rms for an impedance of 70 ohms.

$$I_A = \frac{E_0}{X} = \frac{707}{187} = 3.78 \text{ amp rms}$$

$$I_C = \frac{E_L}{X} = \frac{265}{187} = 1.42 \text{ amp rms}$$

$$I_B = \sqrt{I_A^2 + I_C^2} = 4.04 \text{ amp rms}$$

It is important to remember that the voltages and currents given above are rms carrier values; components with adequate safety factors for peak modulation conditions should be selected.

**Example 4.**—Design of high harmonic-attenuation shunt branch. Suppose it is desired to produce very high attenuation at the second harmonic without altering the properties of the network at carrier frequency. We can replace  $C_A$  by a series combination resonating at second harmonic but presenting a net capacitive reactance of  $X$  ohms for carrier frequency. Referring to Fig. 3 and the table for  $K_1$  and  $K_2$ ,

$$L_{AS} = K_1 L_B = 0.333 \times 29.8 = 9.93 \mu\text{h}$$

$$C_{AS} = K_2 C_A = 0.75 \times 852 = 639 \mu\text{mf}$$

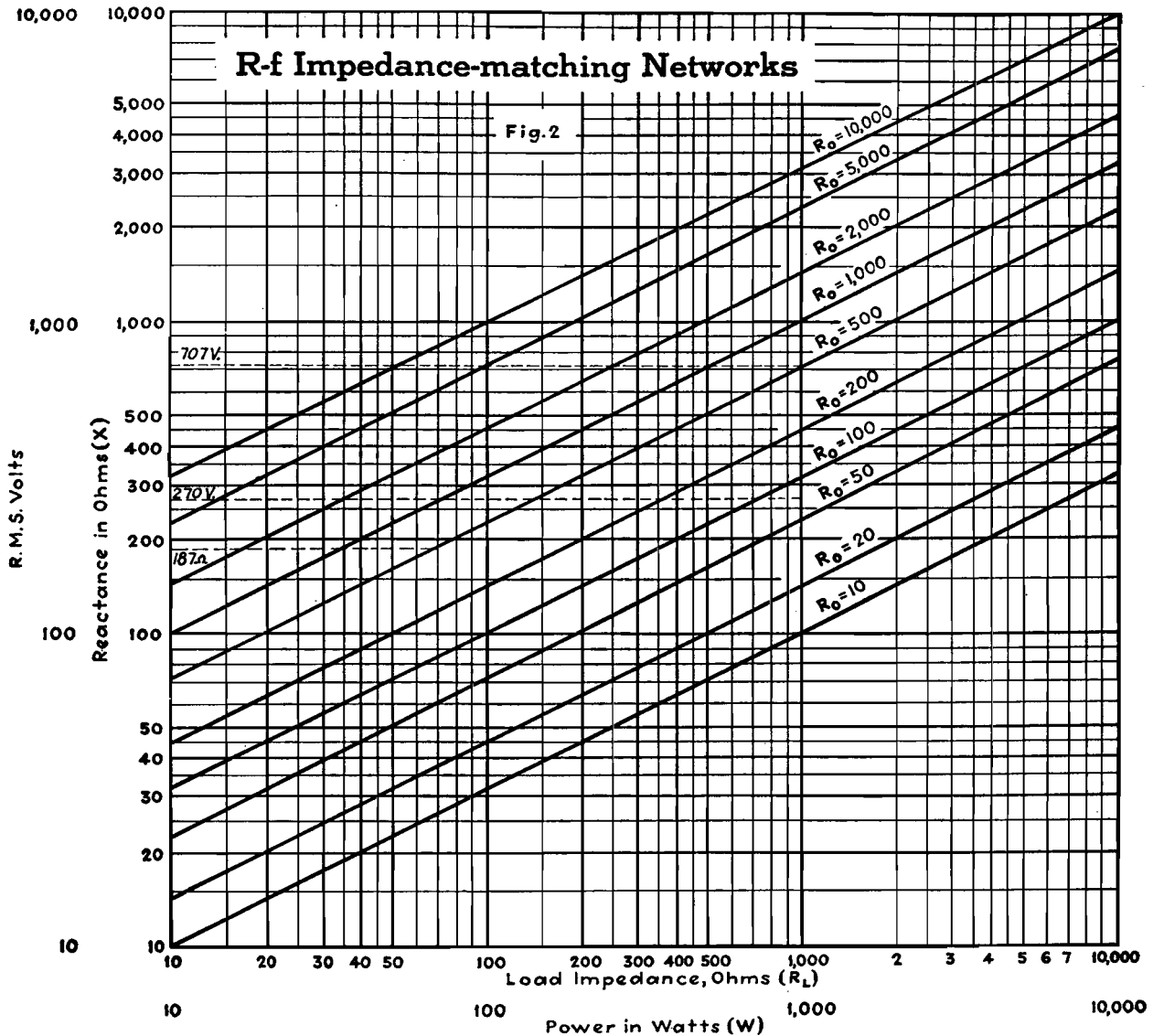
The carrier component of current through the composite branch is the same as that already computed for the simple shunt capacitor case. The carrier component voltage across  $C_{AS}$  is therefore

$$E_C = I_A X_{CS} = \frac{I_A}{\omega C_{AS}}$$

$$= \frac{3.78}{6.28 \times 1 \times 10^6 \times 639 \times 10^{-12}}$$

$$= 943 \text{ volts rms}$$

It is usually sufficient to base the design on carrier frequency conditions



## Summary of Formulas

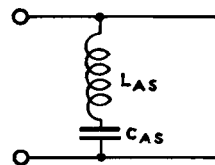
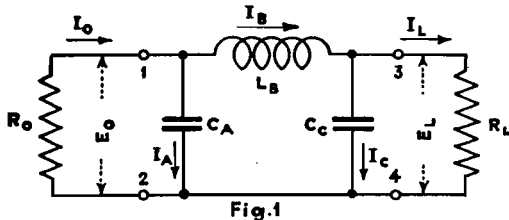


TABLE 1

Harmonic	$K_1$	$K_2$
2nd	0.333	0.75
3rd	0.125	0.889

$$K_1 = \frac{1}{1-N^2} \quad K_2 = \frac{1-N^2}{N^2}$$

Where N is the order of the harmonic (2 for 2nd, 3 for 3rd etc.)

- ①  $X = \sqrt{R_0 R_L}$  (Fig. 2) then compute;  
 $C_A = C_C = \frac{1}{\omega X}$  farads;  $L_B = \frac{X}{\omega}$  henries  
 Where  $\omega = 2\pi f$ ;  $f$  = carrier frequency
- ②  $E_0 = \sqrt{R_0 W}$  &  $E_L = \sqrt{R_L W}$  where  $W$  = network input in watts (Fig. 2)
- ③  $I_A = \frac{E_0}{X}$ ;  $I_C = \frac{E_L}{X}$  r.m.s. amperes (compute) (For carrier peak values, multiply  $E$  &  $I$  by 1.414)  
 (For 100 per cent mod. peak values, multiply  $E$  &  $I$  by 2.828)  
 $I_B = \sqrt{I_A^2 + I_C^2}$  (compute)  $\left[ \begin{array}{l} I_B = \sqrt{I_L^2 + I_C^2} \\ I_L = I_A; I_0 = I_C \end{array} \right]$

- ④ For very high harmonic attenuation, replace  $C_A$  or  $C_C$  or both by series inductance and capacity, resonant at the harmonic, but presenting a capacitive reactance of  $X$  ohms at carrier frequency as shown in Fig. 3

and allow a generous factor of safety (for peak conditions) in determining the ratings of components.

If it is desired to make the network balanced to ground, this may readily be accomplished by dividing  $L_B$  into two equal inductors and inserting one inductor in each side of the line.

The possibilities of short and open-

circuit conditions should be considered and appropriate protective measures adopted where required.

It has been assumed that both generator and load impedances are pure resistances, a condition closely approached in many practical problems. Where the terminating impedances involved have reactive components, these components can often

be neutralized by inserting series reactance of opposite sign.

When the network is used for coupling an electronic amplifier to its load, the network is designed exactly as indicated in the chart, except that  $R_0$  is taken as the impedance required for proper loading of the amplifier output.

## Charts for L-type Impedance-transforming Circuits

By PHILLIP H. SMITH

One of the simplest and most effective impedance-transforming networks for radio-frequency applications is the half-section L-type circuit employing two essentially pure reactances. Design charts and practical examples of their use are presented

At a single frequency and, for most practical purposes, embracing at least the side-band frequencies of a radiotelephone transmitter, the simple L circuit may be used effectively to transform any load impedance to any desired pure input resistance value. Conversely, the L circuit may be employed to accomplish the reverse transformation, i.e., to transform any load resistance to any desired complex input impedance value. It is necessary to consider only the former type of trans-

formation, however, if one bears in mind that the circuit can always be reversed to make the transformation in the opposite direction. This simplifies the presentation of design information.

In Fig. 1 there are a total of eight possible combinations of reactance types (i.e., inductive and capacitive) in an L circuit. Each of these eight circuits is capable of transforming a restricted range of complex load impedance values to a given pure resistance value. The transformable impedance values associated with each circuit can conveniently be represented as an area on an impedance vector diagram. A set of eight such impedance vector diagrams will therefore completely outline the capability and limitations of the eight possible reactance combinations, and will furnish a comprehensive outline of the impedance-transforming capability of each reactance combination.

For r-f applications, the losses in an L circuit will usually be small in comparison to the power that is being conducted through the circuit. The circuit losses will generally not limit to any serious extent the range of load impedance values that can be transformed successfully to a desired resistance, nor will they ordinarily have a major effect on the reactance values for the circuit elements that are theoretically required on the assumption that they are lossless. The

design charts to be described are, therefore, plotted for the idealized case of lossless circuits. Having selected a suitable lossless circuit and having obtained the reactance values required in such a circuit from the charts, one is in a better position to determine the probable resistance of the circuit elements that he must use and what the losses will be. In some cases, there will be a choice available between two or more L-circuit configurations. In these cases, one may select the circuit more suitable to one's needs either because it may introduce the lesser loss or because the circuit components may be more readily available.

### Choice of Reactance Combination

The eight vector diagrams, shown in Fig. 2, provide a convenient method of selecting a suitable L circuit for any particular impedance transformation.

Each of the eight diagrams in Fig. 2 is plotted on rectangular coordinates, and, according to the usual procedure, the series resistance component of the load impedances is indicated along the horizontal coordinates marked  $R_i$ , and the series reactance component  $X_i$  is indicated along the vertical coordinate, either up or down from the  $R_i$  axis, depending on whether it is an inductive or a capacitive reactance component, respectively. Both coordinates of these diagrams are measured in the same units, namely, ohms, but

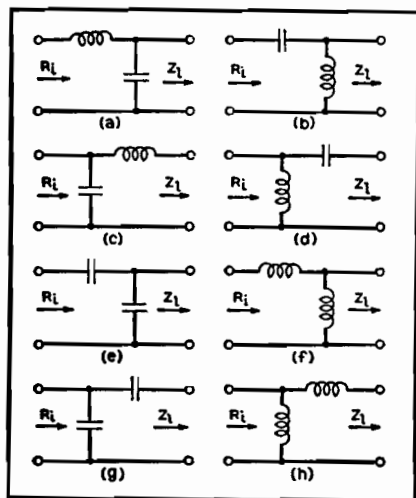


Fig. 1.—L-type impedance-matching circuits for transforming a complex load impedance  $Z_L$  to a pure resistance  $R_i$ . There are eight possible circuit combinations of reactances as shown above.



Construction Data for L Circuit Design Curves

Fig.	Family of circular lines labeled:	Position of center of each circular line (coordinates)		Radius of each circular line	Family of straight vertical lines labeled:	Position of each straight vertical line along $R_i$ axis
		$R_i/R_i =$	$X_i/R_i =$			
3A	$X_C/R_i$	$\frac{1}{2}(X_C/R_i)^2$	$-X_C/R_i$	$\frac{1}{2}(X_C/R_i)^2 R_i$		
3B	$X_L/R_i$	$\frac{(X_L/R_i)^2 + 1}{2}$	0	$\frac{(X_L/R_i)^2 + 1}{2} R_i$		
4A	$X_L/R_i$	$\frac{1}{2}(X_L/R_i)^2$	$-X_L/R_i$	$\frac{1}{2}(X_L/R_i)^2 R_i$		
4B	$X_C/R_i$	$\frac{(X_C/R_i)^2 + 1}{2}$	0	$\frac{(X_C/R_i)^2 + 1}{2} R_i$		
5	.....	.....	.....	.....	$X_C/R_i$	$\frac{(X_C/R_i)^2}{1 + (X_C/R_i)^2}$
5	$X_L/R_i$	0.5	$-X_L/R_i$	$0.5 R_i$		
6	.....	.....	.....	.....	$X_L/R_i$	$\frac{(X_L/R_i)^2}{1 + (X_L/R_i)^2}$
6	$X_C/R_i$	0.5	$-X_C/R_i$	$0.5 R_i$		
7	$X_{C1}/R_i$	0	$-\frac{1}{2}(X_{C1}/R_i)$	$-\frac{1}{2}(X_{C1}/R_i) R_i$		
7	$X_{C2}/R_i$	$\frac{(X_{C2}/R_i)^2 + 1}{2}$	0	$\frac{(X_{C2}/R_i)^2 + 1}{2} R_i$		
8	$X_{L1}/R_i$	0	$-\frac{1}{2}(X_{L1}/R_i)$	$\frac{1}{2}(X_{L1}/R_i) R_i$		
8	$X_{L2}/R_i$	$\frac{(X_{L2}/R_i)^2 + 1}{2}$	0	$\frac{(X_{L2}/R_i)^2 + 1}{2} R_i$		
9	.....	.....	.....	.....	$X_{C1}/R_i$	$\frac{(X_{C1}/R_i)^2}{1 + (X_{C1}/R_i)^2}$
9	$X_{C2}/R_i$	0.5	$-X_{C2}/R_i$	$0.5 R_i$		
10	.....	.....	.....	.....	$X_{L1}/R_i$	$\frac{(X_{L1}/R_i)^2}{1 + (X_{L1}/R_i)^2}$
10	$X_{L2}/R_i$	0.5	$-X_{L2}/R_i$	$0.5 R_i$		

NOTE: For  $X_C$ ,  $X_{C1}$ , or  $X_{C2}$  use a minus (-) sign, and for  $X_L$ ,  $X_{L1}$ , or  $X_{L2}$  use a plus (+) sign ahead of its numerical value.

are labeled as a function of the desired input resistance value,  $R_i$ , as  $1R_i$ ,  $2R_i$ ,  $3R_i$ , etc., rather than directly in ohms, to make the diagrams of more general application. Thus, for example, the desired input resistance  $R_i$  may be 100 ohms. In this event the scale intervals along the coordinates designated as  $1R_i$ ,  $2R_i$ ,  $3R_i$ , etc., would simply be 100, 200, 300, etc., ohms, respectively. If the desired input resistance  $R_i$  were, for example, 60 ohms, the scale intervals designated as  $1R_i$ ,  $2R_i$ ,  $3R_i$ , etc., would be 60, 120, 180, etc., ohms, respectively. The desired input resistance may have any chosen value, but for a given problem

the value will be known, and will be a fixed constant throughout the problem, thus establishing numerically the scale intervals, in ohms, along the coordinates of the vector diagrams in Fig. 2.

It will be noted that a shaded area is shown on each of the eight diagrams in Fig. 2. This is to indicate that any load impedance vector whose extremity falls anywhere within this "forbidden" region cannot be transformed to  $R_i$ , the desired input resistance value, with the specific L circuit to which the diagram applies. In this case one of the other seven L circuits must be selected. If the extremity of the load impedance vector falls

anywhere inside the unshaded area, the circuit is capable of performing the desired impedance transformation. Where either the unshaded (transformable) or the shaded (forbidden) area exists at the outer limits of the diagram, it may be regarded as continuing, if the diagram were sufficiently large, to infinity.

In cases where the impedance-transforming capability of two or more L-type circuits overlap, the particular circuit that results in the more practical circuit constants should, of course, be chosen. It is of interest to note that the circuits shown on diagram *e* and diagram *g* (Fig. 2) are each capable of transforming the same range of load impedances although each accomplishes a given transformation with different reactance values. The circuits on diagram *f* and diagram *h* are also both capable of making the same impedance transformations. Note also that either of these circuits is capable of transforming only a small portion of the range of impedance values that may be transformed by the circuit of diagram *a* or *b*.

#### Graphical Concept of Impedance Transformation

On each of the eight impedance vector diagrams, shown on Fig. 2, an example of the function of each element of the circuit is illustrated, using an assumed load impedance vector  $Z_L$ . The influence of each of the circuit elements on the load impedance vector  $Z_L$  may be regarded as forcing the latter to move along an impedance path from its initial position to a position along the  $R$  axis, with its extremity at position  $1R_i$ . This impedance path followed by a single vector is illustrated on each of the eight diagrams of Fig. 2 by a zigzag line (and arrows to show its direction of movement). More specifically, for example, refer to diagram *a* of Fig. 2. Here, any load impedance, as  $Z_L$ , may be selected whose extremity falls in the unshaded area, which it is desired to transform, with an L circuit of the type indicated on this diagram, to a chosen value of pure resistance  $1R_i$ . In this case, it will be noted that the effect on the impedance vector  $Z_L$  of the shunt capacitive reactance is to rotate its extremity clockwise around a circular zigzag path leading to the point  $Z_1$ . This path is always along a circle tangent to the  $X$  axis and centered on the  $R$  axis.  $Z_1$  represents the extremity of a second impedance vector, the resistance component of which is equal to  $1R_i$ . (To simplify the diagrams, only the extremity of the vector  $Z_1$  is indicated.)

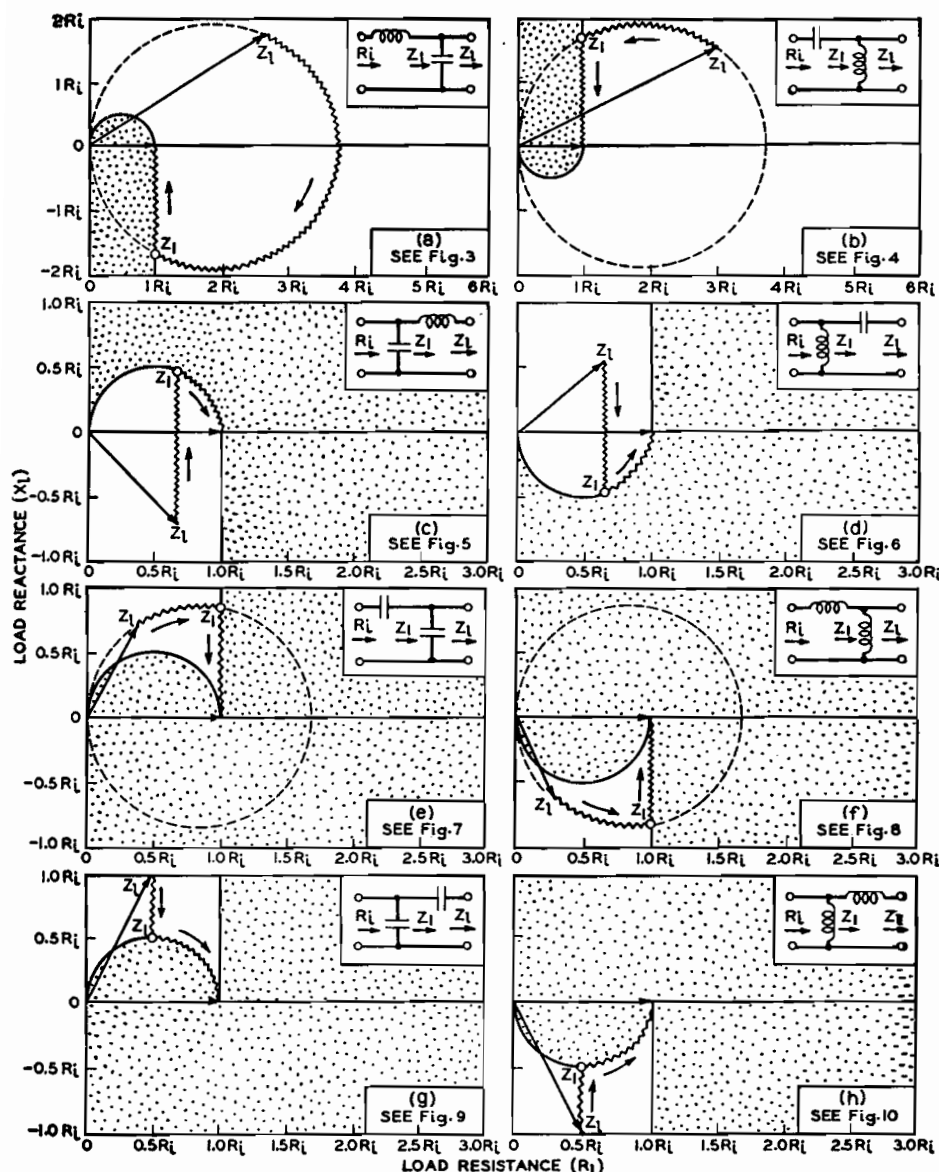


Fig. 2.—Any impedance,  $Z_L$ , whose vector terminates within an unshaded area on the above diagrams is transformable to a pure resistance,  $R_L$ , by means of the circuit to which the diagram applies.

The capacitive reactance component of the impedance vector  $Z_L$  is then canceled by the reactance of the series inductance element of the L circuit which moves the vector vertically along the zigzag path to position  $1R_L$ , thus completing the transformation.

$Z_L$  is, of course, the parallel resultant of the complex load impedance  $Z_L$  chosen and a definite value of shunt capacitive reactance, and impedance vectors whose extremities lie at intermediate points along the indicated circular "path" would, of course, have been obtained only if an intermediate shunting reactance value (between infinity and the value which is required to move the vector  $Z_L$  to the position  $Z_1$ ) had been selected.

If, in the limit, the shunting reactance were of infinite capacitance (0 reactance),

the circular path that  $Z_L$  follows would, of course, continue along this same circular path all the way to the origin. A specific capacitive load-shunting reactance is therefore required to stop the rotation of the vector at the desired point  $Z_1$ . Similarly, a specific inductive series reactance is required to continue the path of the vector from  $Z_1$  exactly to position  $1R_L$ . The required reactances of the capacitor and coil are not shown on this key diagram (Fig. 2), which, as explained, is intended only to outline the capabilities of the particular circuit to which the diagram refers.

#### Determination of L-Circuit Constants

After having selected an L circuit for a given impedance transformation with the

aid of Fig. 2, it will next be required to determine the reactance values in the circuit. To obtain the proper value of the inductive and capacitive reactances required in a given L-circuit arrangement to transform a given complex load impedance ( $R_L + jX_L$ ) to a given pure resistance  $1R_L$ , select the family of design curves that have been plotted for the particular circuit chosen. These are plotted on Figs. 3 to 10, for each reactance element of each of the eight possible circuits. The appropriate design curves from which the circuit constants can be obtained may be identified by referring to the small schematic circuit diagram associated with each family of design curves or by the notation given in connection with each diagram of Fig. 2.

The load impedance point (extremity of the load impedance vector) should be spotted on the appropriate design chart. The proper circuit reactance value is then determined by interpolating between the nearest reactance curves plotted. If, for example, the load impedance point is midway between a curve labeled  $X_L = 3R_L$  and a curve labeled  $X_L = 3.5R_L$ , the correct reactance value for  $X_L$  would be  $3.25R_L$ , and so on.

#### Examples

**Example 1a.**—Select an L-type circuit that will transform a load impedance of  $150 + j75$  ohms to a pure resistance of 50 ohms.

**b.** Determine the reactance value for each branch of the circuit selected.

**Solution:**

a. From the above example

$$R_L = 50$$

$$Z_L = 150 + j75 = 3R_L + j1.5R_L$$

Refer to key diagram Fig. 2, and observe that the extremity of the above load impedance vector ( $3R_L + j1.5R_L$ ) falls within the unshaded (transformable) area of diagrams a and b, and within the shaded (forbidden) area of diagrams c to h. A choice of two circuits is therefore available for this transformation. Select one—say that of diagram b.

b. Refer to Fig. 4A as directed on diagram b, and determine the correct reactance value for  $X_L$  by noting that the extremity of the load impedance vector ( $3R_L + j1.5R_L$ ) will fall at a point approximately midway between the curves labeled  $X_L = 3.5R_L$  and  $X_L = 3.0R_L$ ; therefore  $X_L$  is approximately  $3.25R_L$ , i.e.,  $X_L = 3.25 \times 50 = 162.5$  ohms. From

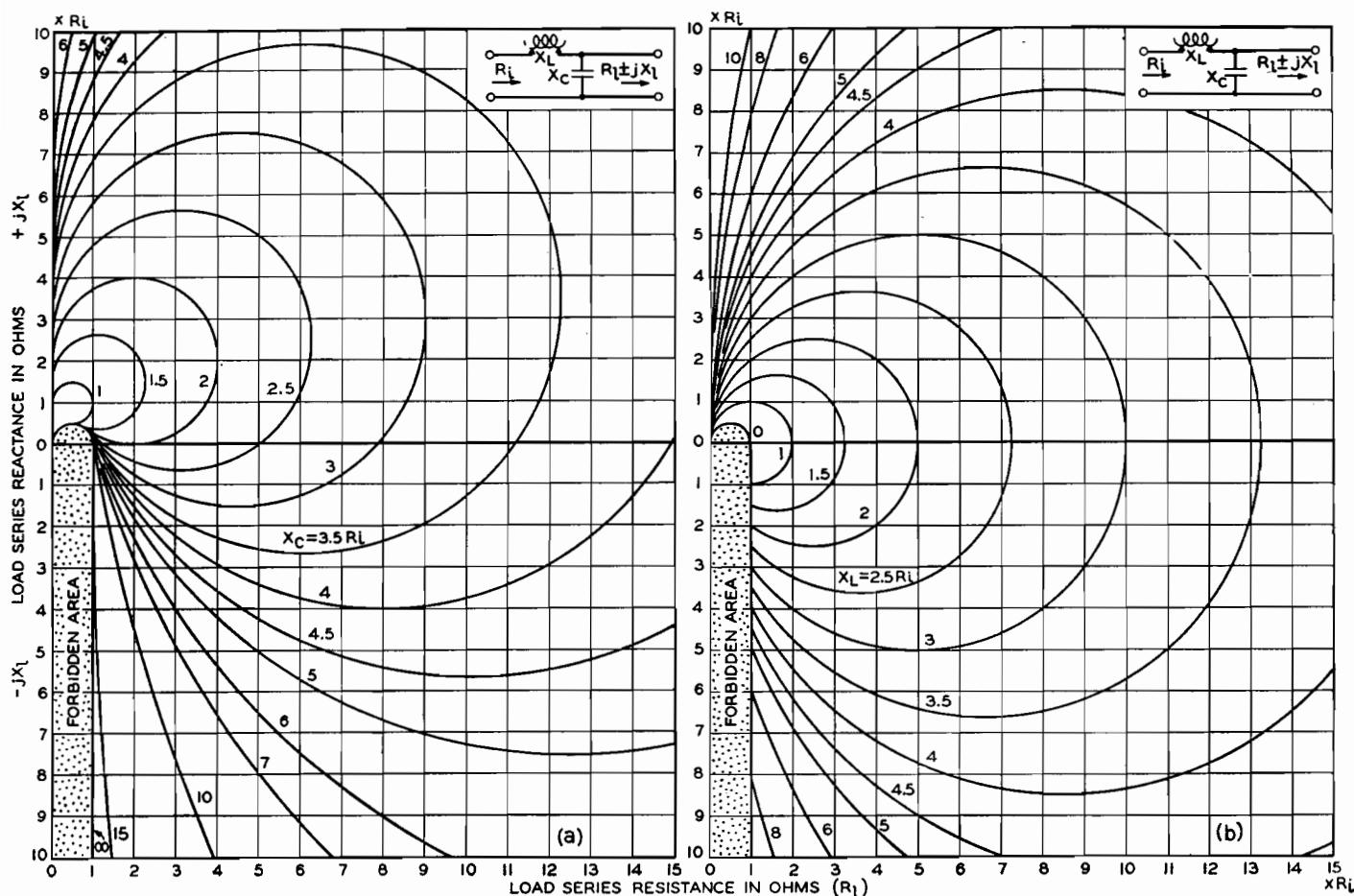


Fig. 3.—Shunt reactance  $X_C$  (left) and series reactance  $X_L$  (right) required to transform load impedance  $R_L \pm jX_L$  to a pure resistance  $R_L$ .

Fig. 4B observe in a similar manner that  $X_C = 1.65R_L$ , i.e.,  $X_C = 1.65 \times 50 = 82.5$  ohms.

If a complex load impedance is not known exactly but can be estimated within certain limits, these limits may be blocked out directly on the design charts, and the range of circuit reactances required can thus be bracketed at a glance. This feature will be most appreciated when an L circuit must be designed to accommodate any one of a range of possible load impedance values. The design of a circuit to match the base impedance of a radio antenna, which is usually not definitely known, to the characteristic impedance of a concentric transmission line is readily accomplished with this type of diagram. In such cases, it will be found of great value to be able to visualize the limitations of a given circuit and thereby establish limiting requirements for the circuit elements. Example 2a, which follows, illustrates this case.

**Example 2a.**—Select an L circuit that can be adjusted to match any load impedance falling within the range 25 to 75 ohms resistance and 0 to 50 ohms

positive reactance to a pure resistance of 100 ohms.

b. Give the limiting reactance values of each of the two circuit elements.

**Solution:**

a. From the above example

$$R_L = 100$$

$$Z_L = (25 \text{ to } 75) + j(0 \text{ to } 50) \text{ ohms} \\ = (0.25R_L \text{ to } 0.75R_L) + j(0R_L \text{ to } 0.5R_L) \text{ ohms}$$

From Fig. 2 select a diagram upon which the above "block" of impedance values falls within an unshaded (transformable) area. The L circuit of Fig. 2 diagram is found to be the only suitable circuit for this case. The answer to the first part of this problem is, therefore, the circuit of Fig. 2 diagram.

b. Refer to Fig. 6 as directed on diagram, and block out the above square of impedance values and observe the limiting values for  $X_L$  and  $X_C$  by noting the curves which just touch the edges of the blocked-out area. The following limiting values will be observed:

$$X_L = 0.58R_L \text{ to } 1.73R_L = 58 \text{ to } 173 \text{ ohms} \\ X_C = 0.43R_L \text{ to } 1.0R_L = 53 \text{ to } 100 \text{ ohms}$$

### Complex Input Impedance

By the addition of a third reactance element in series with the chosen input resistance obtained with an L impedance matching circuit, any complex load impedance value can, of course, be transformed to any desired complex input impedance value. The charts are applicable in this case also. The reactance required in the third element, in series with the input, of course, depends on the value of input reactance desired. If a circuit is chosen that already includes a series-reactance element in the input side of the circuit such as shown on Fig. 1, diagrams a, b, e, and f, the third reactance required would add algebraically with the former, resulting in a single net reactance value in this position.

### Balanced Circuits

If the input impedance must be balanced with respect to ground, the L circuit design curves can be used to design a suitable impedance matching circuit by treating the problem as an unbalanced one. The required series reactance thus obtained from the diagrams is then divided into two parts, each having

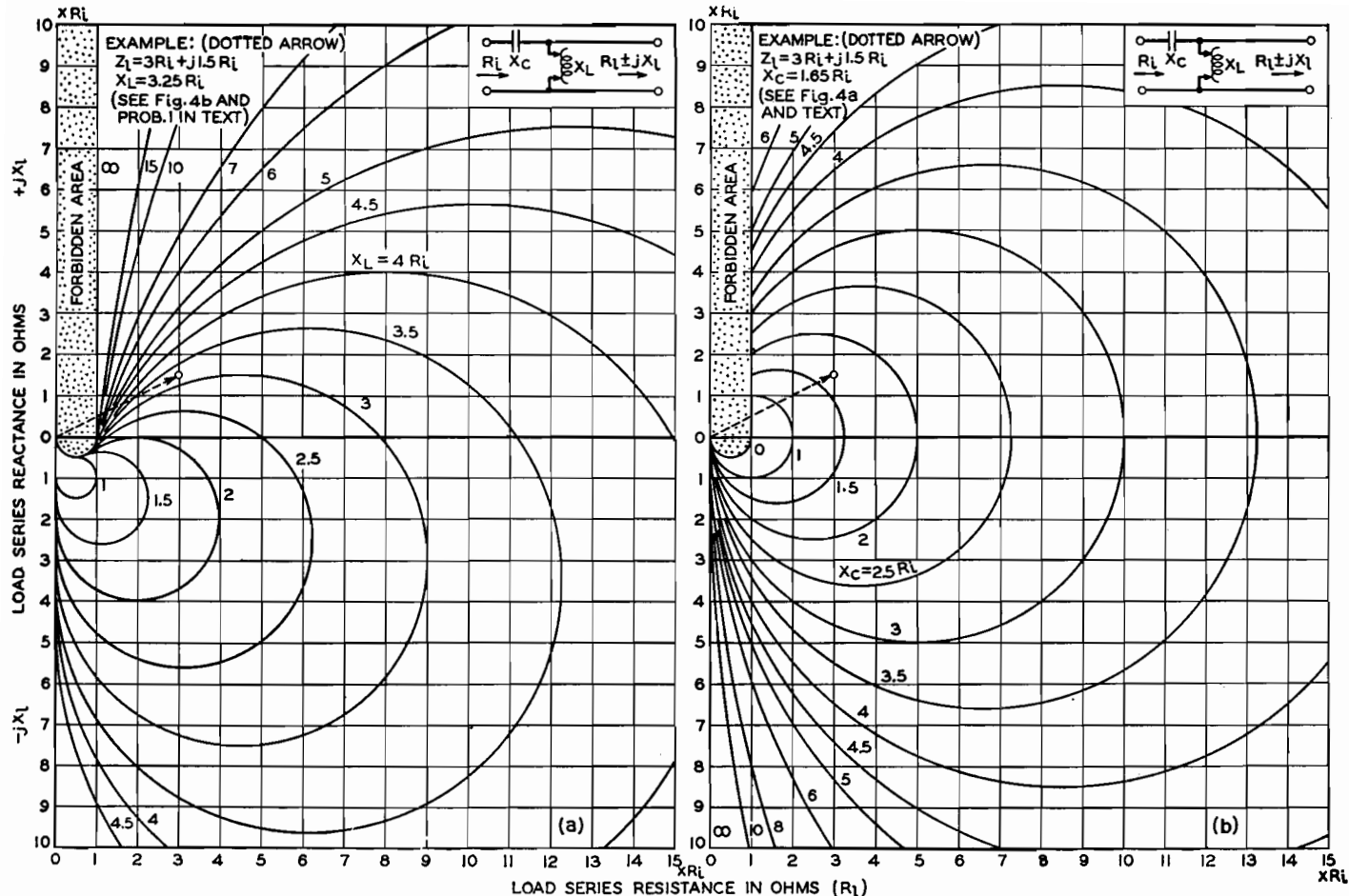


Fig. 4.—Shunt reactance  $X_L$  (left) and series reactance  $X_C$  (right) required to transform load impedance  $R_L \pm jX_L$  to pure resistance  $R_i$ .

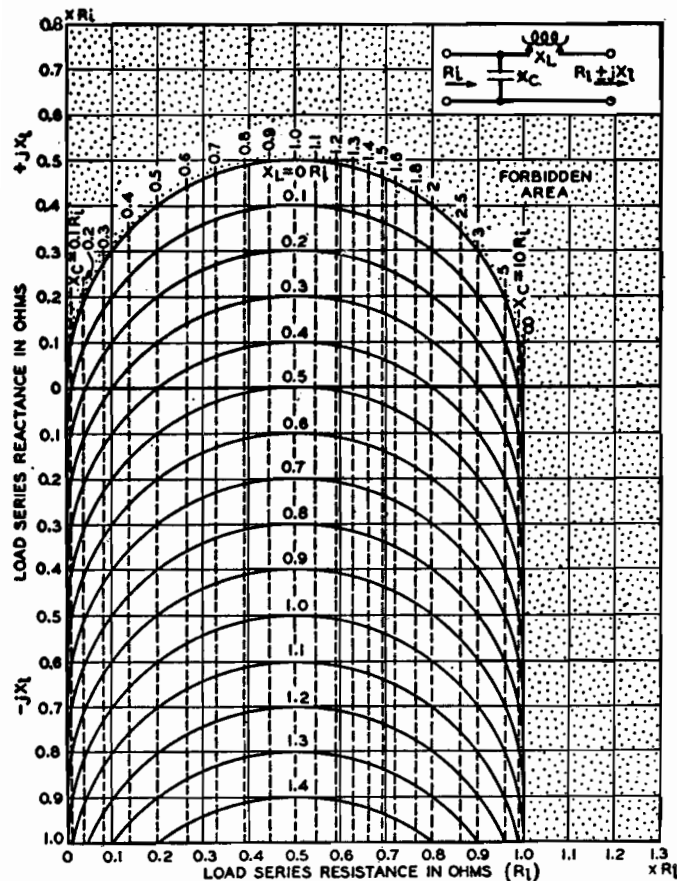


Fig. 5.—Series reactance  $X_L$  and shunt reactance  $X_C$  required to transform load impedance  $R_L \pm jX_L$  to pure resistance  $R_i$ .

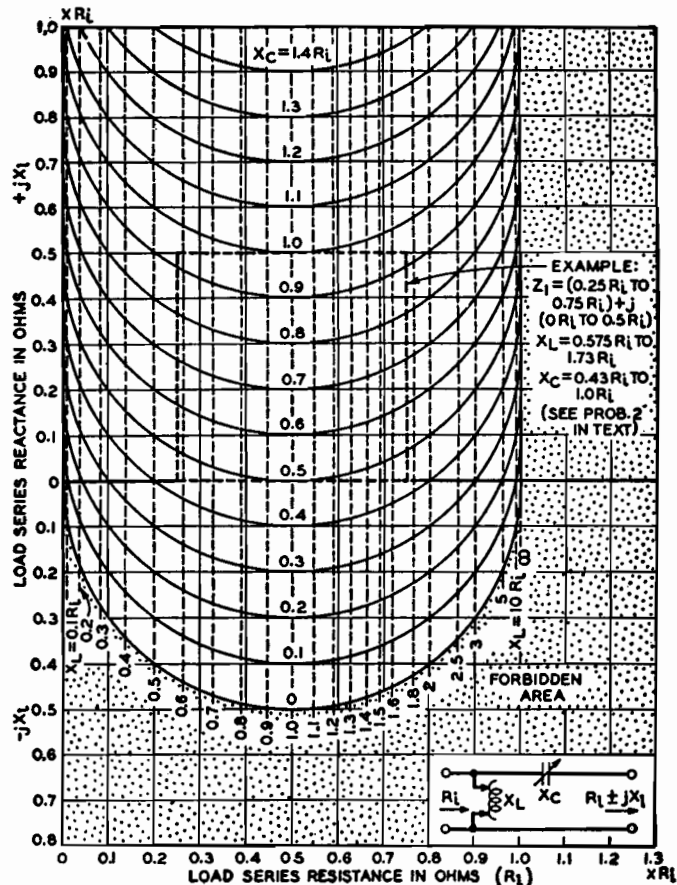


Fig. 6.—Shunt reactance  $X_L$  and series reactance  $X_C$  required to transform load  $R_L \pm jX_L$  to pure resistance  $R_i$ .

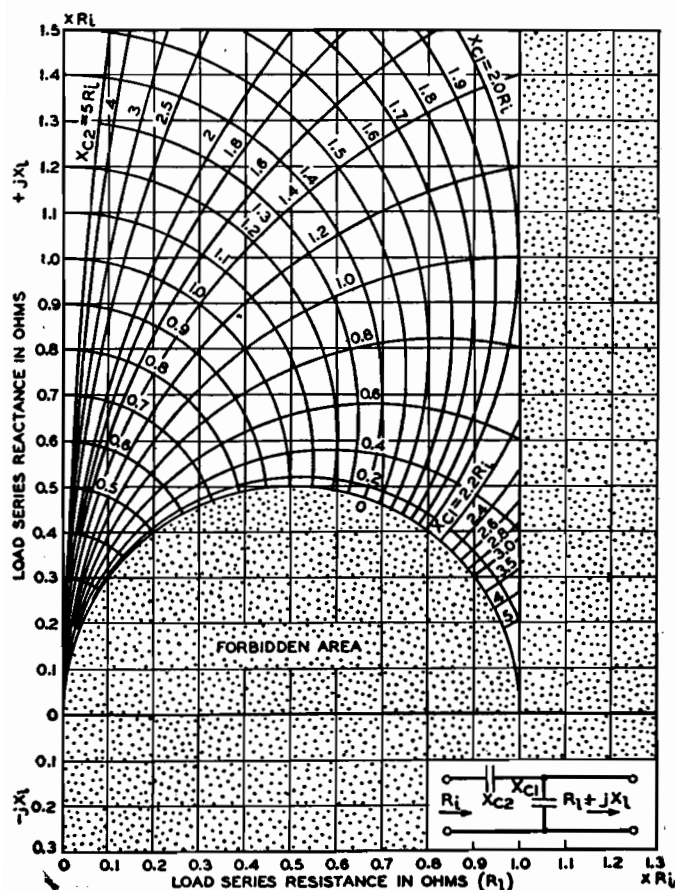


Fig. 7.—Shunt and series capacitive reactances required to transform load impedance  $R_L + jX_L$  to pure resistance  $R_L$ .

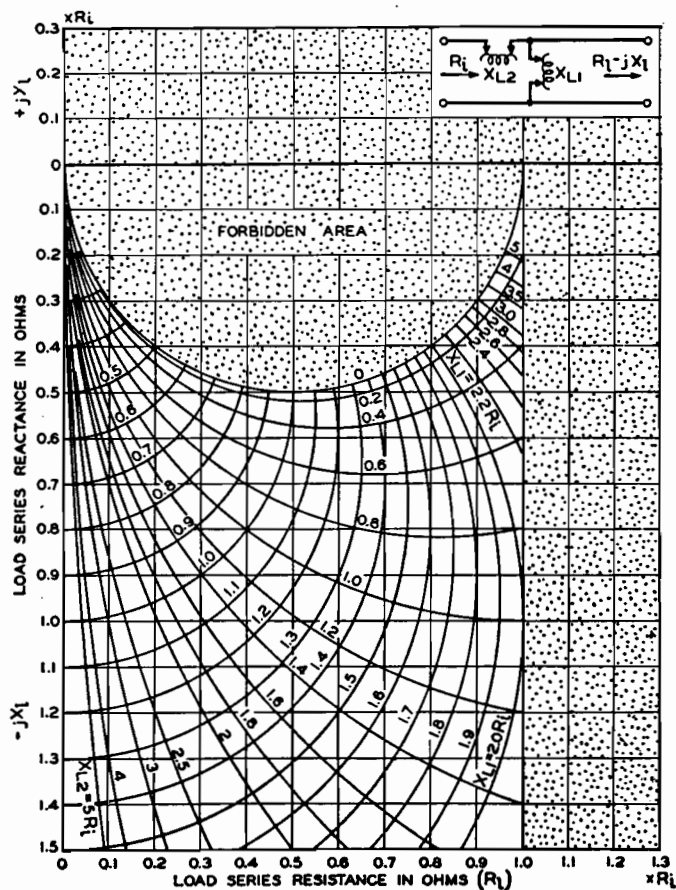


Fig. 8.—Series and shunt inductive reactances required to transform load impedance  $R_L - jX_L$  to pure resistance  $R_L$ .

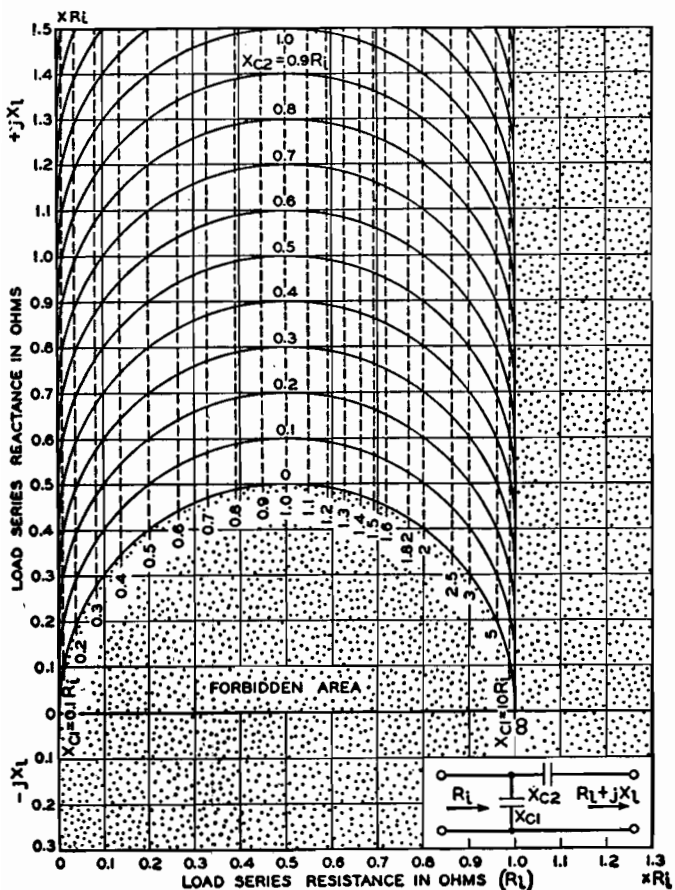


Fig. 9.—Shunt and series capacitive reactances required to transform load impedance  $R_L + jX_L$  to pure resistance  $R_L$ .

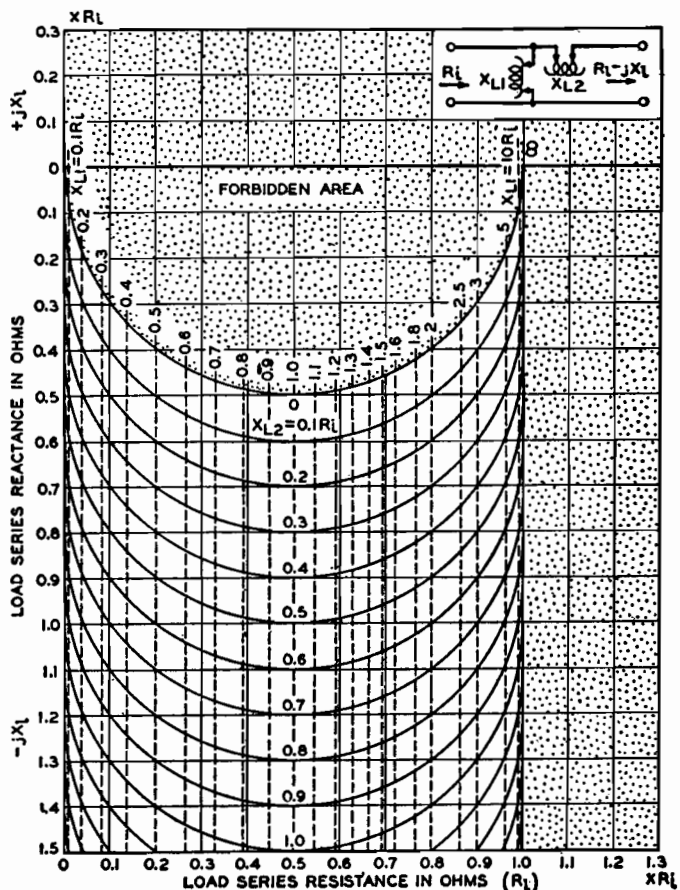


Fig. 10.—Shunt and series inductive reactances required to transform load impedance  $R_L - jX_L$  to pure resistance  $R_L$ .



one-half of the value called for on the charts. These two halves of the necessary total series reactance are then connected in series with each side of the circuit to preserve the balanced-to-ground arrangement.

#### Construction of Design Curves for L Circuits

All the design charts are drawn with either circular or straight lines on rectangular coordinate paper. If it is desired to reproduce a larger, more accurate set of charts, it is necessary to

know only the center point and radius of each curve. The formulas in the table give the construction information for the design charts on Figs. 3 to 10, which apply to all L-type impedance-transforming circuits shown in Fig. 1. To avoid a confusion of intersecting curves, the design charts plotted in Fig. 3 (Fig. 3A and 3B) and Fig. 4 (Fig. 4A and 4B) show only individual families of curves, each family applying to one of the reactance elements of the circuit. Since in all other cases, namely, Figs. 5 to 10, no

confusion results by superimposing two families of curves that apply to the two circuit elements of a given circuit, this has been done to reduce the number of charts required.

The correct algebraic sign for the numerical value of reactances  $X_C$ ,  $X_{C1}$ ,  $X_{C2}$ ,  $X_L$ ,  $X_{L1}$ , and  $X_{L2}$  in the construction-data formulas should be used, i.e., for  $X_C$ ,  $X_{C1}$  or  $X_{C2}$ , use a minus (-) prefixed ahead of its numerical value, and for  $X_L$ ,  $X_{L1}$ , and  $X_{L2}$ , which are inductive reactances, use a plus (+) prefix.

## Computing R-f Transition Losses

By HAROLD A. WHEELER

R-f losses due to impedance mismatching may be evaluated by the graphical method presented here, in preparation for the design of an r-f impedance-matching network for minimizing the loss thus incurred

IN THE design of transmission lines, filters, amplifiers, and other communication networks, there is always the problem of matching impedances at the junction of sending and receiving circuits. The maximum power transfer occurs when the two circuits have equal resistance and zero (or equal and opposite) reactance. Any departure from this condition is said to cause a transition loss relative to the maximum power transfer. This article presents formulas and a simple chart for determining the transition loss at the junction of two impedances, caused by the mismatching of resistance and the presence of reactance.

The table gives the meaning of two parameters  $U$  and  $V$  as applied to the mismatching of two impedances, one of which is a pure resistance. See diagrams A and B in the chart. The real component of the impedance ratio is  $U$ , and the imaginary component is  $V$ . Perfect matching is indicated when  $U = 1$  and  $V = 0$ . Otherwise the power transfer is less than the maximum in the ratio

$$\frac{1}{A} = \frac{4U}{(1+U)^2 + V^2} \quad (1)$$

This power ratio is a loss preferably expressed in decibels.

Any given value of the power loss can be caused by various combinations of

$U$  and  $V$ . All such combinations form a curve on the  $UV$  plane, one curve for every value of  $A$ . The family of curves is represented by the above equation, which may be rewritten

$$[U - (2A - 1)]^2 + V^2 = (2A - 1)^2 - 1 \quad (2)$$

For each value of  $A$ , this equation represents a circle whose center is at the point

$$U = (2A - 1), \quad V = 0 \quad (3)$$

and whose radius is

$$\sqrt{(2A - 1)^2 - 1} \quad (4)$$

The maximum and minimum values of  $U$  are

$$(2A - 1) \pm \sqrt{(2A - 1)^2 - 1} \quad (5)$$

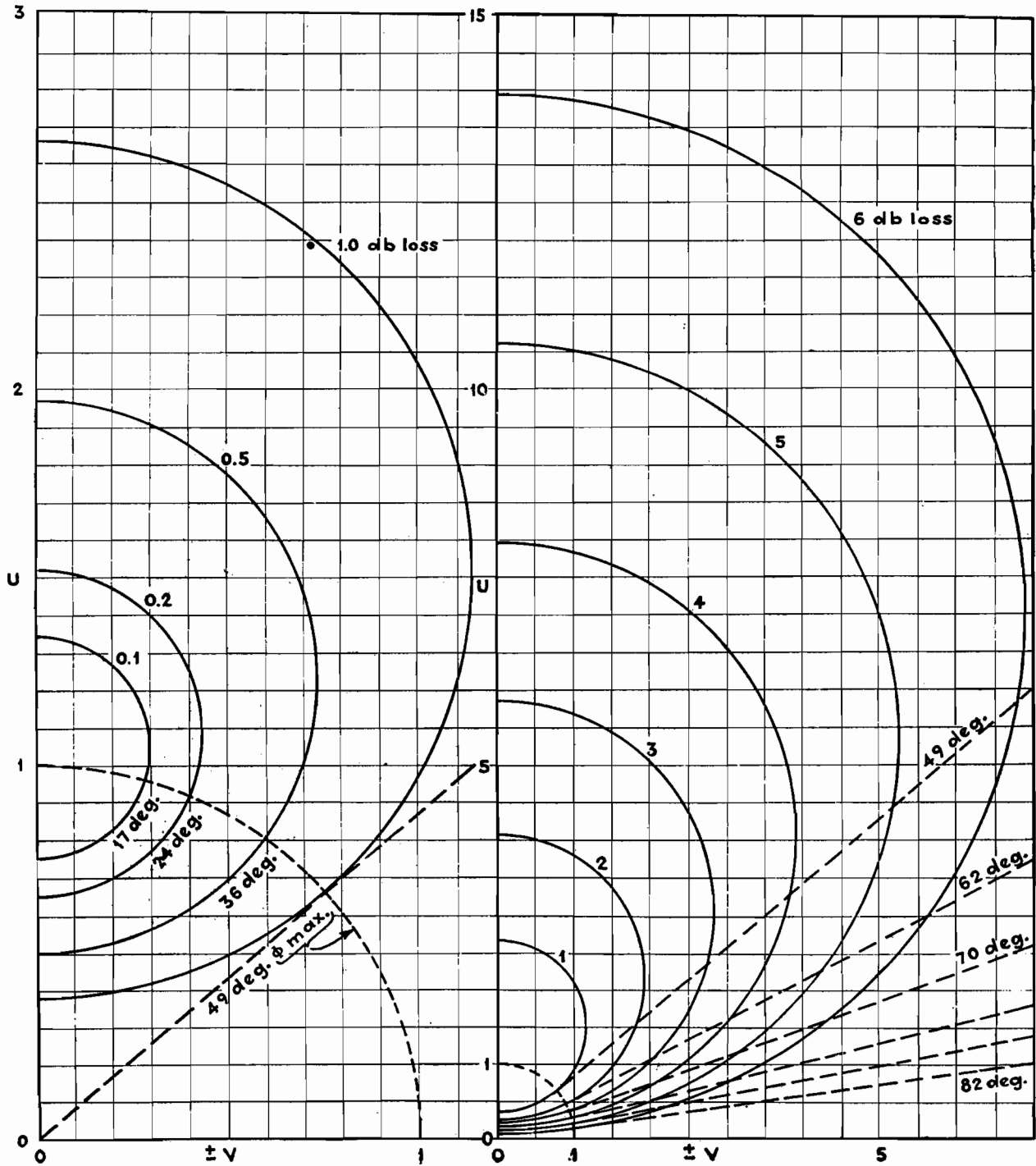
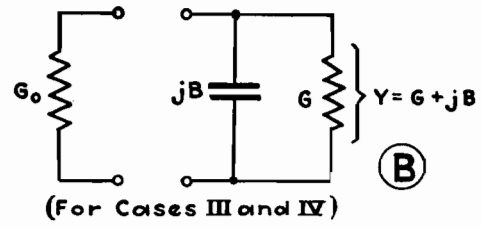
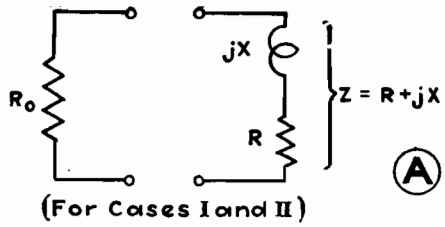
The maximum value of  $V$  is equal to the radius as given in Eq. (4).

The phase angle  $\phi$  of the reactive impedance is also defined in the table.

The table below defines the parameters  $U$  and  $V$  when a pure resistance is matched with an impedance. The loss in decibels caused by the mismatch can be found by locating the point on the chart corresponding to  $U$  and  $V$  in the particular case under consideration.

	Case I	Case II	Case III	Case IV
$U \pm jV =$	$\frac{Z}{R_o}$	$\frac{R_o}{Z}$	$\frac{Y}{G_o}$	$\frac{G_o}{Y}$
$U =$	$\frac{R}{R_o}$	$\frac{R}{R_o} \cdot \frac{R_o}{\left(\frac{R}{R_o}\right)^2 + \left(\frac{X}{R_o}\right)^2}$	$\frac{G}{G_o}$	$\frac{G}{G_o} \cdot \frac{G_o}{\left(\frac{G}{G_o}\right)^2 + \left(\frac{B}{G_o}\right)^2}$
$\pm V =$	$\frac{X}{R_o}$	$\frac{X}{R_o} \cdot \frac{R_o}{\left(\frac{R}{R_o}\right)^2 + \left(\frac{X}{R_o}\right)^2}$	$\frac{B}{G_o}$	$\frac{B}{G_o} \cdot \frac{G_o}{\left(\frac{G}{G_o}\right)^2 + \left(\frac{B}{G_o}\right)^2}$
$\pm \tan \phi =$	$\frac{X}{R}$	$\frac{X}{R}$	$\frac{B}{G}$	$\frac{B}{G}$

NOTE: Case I and II refer to diagram A in the chart. Case III and IV refer to diagram B.





For each value of  $A$ , this angle has a maximum value determined by the relations

$$U^2 + V^2 = 1; \quad \cos \phi = \frac{1}{2A - 1} \quad (6)$$

The latter expression is also the minimum value of the power factor of the reactive impedance, for a given value of the power loss.

The above values have been used in drawing the chart. Each circle is drawn about  $U$  (center) with a radius of  $V$  (max).

The chart shows graphically the relations between the transition loss and the circuit parameters. The following relations appear from the chart and the above formulas.

1. The product of  $U$  (max) and  $U$

(min) is unity, so that these values are mutually reciprocal.

2. Any straight line through the origin represents a certain phase angle of the reactive impedance. Such a line intersects any given circle (if at all) at two points whose distances from the origin are mutually reciprocal. Since the distance from the origin to a point is the absolute value of the corresponding impedance ratio, interchanging the impedances does not affect the loss.

3. For any given phase angle, the loss is a minimum when the absolute value of the impedance ratio is unity. For a phase angle of 49 deg, the minimum loss is 1 db.

Let it be required to determine the transition loss between two impedances,

in general, either or both of which may be reactive. The two impedances are represented as

$$Z_1 = R_1 + jX_1; Z_2 = R_2 + jX_2 \quad (7)$$

The net reactance is

$$X = X_1 + X_2 \quad (8)$$

The values of two parameters,  $U$  and  $V$ , are then determined by either one of the following alternative representations:

$$U = \frac{R_2}{R_1}; \pm V = \frac{X}{R_1} = \frac{X_1 + X_2}{R_1} \quad (9)$$

$$U = \frac{R_1}{R_2}; \pm V = \frac{X}{R_2} = \frac{X_1 + X_2}{R_2} \quad (10)$$

The chart is more accurately readable when the relation that gives the greater value of  $U$  is used.

## SECTION XXI

# R-F POWER AMPLIFIERS

	Page
R-f Power-amplifier Chart.....	281
Power-amplifier Plate Tank Circuits.....	283
Class B R-f Amplifier Chart.....	286
Power Efficiency of R-f Power-amplifier Stages.....	287
Graphical Determination of Power-amplifier Performance.....	291
Analysis of Self-biased Modulated Amplifiers.....	295

## R-f Power-amplifier Chart

By E. H. SCHULZ

THE following simplified approximate method of designing class B and C amplifiers gives results sufficiently accurate for most engineering work. If provision is made to vary the principal parts of the circuit (such as grid bias, driving voltage, and load coupling) by a small amount, optimum operating conditions may be obtained. The accuracy that may be expected is indicated by Table II. Although the method is outlined for class C design, it may be used for class B design by making the angle of conduction equal to or slightly larger than 180 deg.

The method is based on the following assumptions:

1. The  $E_p I_p$  curves are parallel and equidistant for equal grid-bias increments in the positive grid region.
2.  $I_p = k(e_o + e_p/\mu)$
3. The amplification factor  $\mu$  is a constant.

In addition, the grid current and the peak plate current must be approximated. The symbols are as follows:

- $I_m$  = peak plate current
- $I_1$  = peak value of fundamental component of plate current
- $I_2$  = peak value of second harmonic component of plate current
- $I_{d-c}$  = d-c plate current
- $E_b$  = plate supply voltage
- $E_c$  = grid bias voltage
- $E_i$  = peak input from driver stage
- $E_o$  = peak output voltage
- $E_{pmin}$  = minimum value of plate voltage
- $E_{pmax}$  = maximum positive value of grid voltage
- $P_i$  = d-c plate input power

- $P_o$  = r-f power output
- $\theta$  = angle of conduction in degrees of fundamental frequency

Since the allowable peak plate current is not given by the tube manufacturer, it must be approximated by multiplying the emission as given in Table I by the filament heating power in watts. Allowance should be made for grid current (usually 10 to 20 per cent), and for tetrodes and pentodes allowance should be made for screen current.

*Example 1. Class C Amplifier with Given Plate Input Power.*—1. Select tube and plate supply voltage  $E_b$  (high values give greater efficiency but require greater driving power).

2. Determine the d-c plate current  $I_{d-c} = P_i/E_b$ .

3. Select several angles of conduction between 100 and 130 deg. (Small angles give greater plate efficiency but require greater driving power.) Determine the peak plate current  $I_m$  and the fundamental component  $I_1$  from  $I_{d-c}$  and the chart for each angle.

4. Check  $I_m$  against allowable value.

5. Consult  $E_p I_p$  curves and select values of  $E_{pmax}$  and  $E_{pmin}$  to give required  $I_m$ .  $E_{pmin}$  should be as small as possible for maximum efficiency, and  $E_{pmax}$  should be less than 80 per cent of  $E_{pmin}$  for low driving power. In the case of tetrodes and pentodes,  $E_{pmax}$  should not exceed 80 per cent of the screen voltage, nor should  $E_{pmin}$  be less than the screen voltage.

Since the manufacturer's  $E_p I_p$  curves do not extend far enough into the positive

grid region, some  $E_p I_p$  curves for positive grid voltages must be sketched in by assuming that the curves for constant grid voltage increments are equidistant and parallel to the straight-line portion of the zero grid voltage curve.

6. Calculate the grid bias from

$$E_c = \frac{E_b}{\mu} + \left( \frac{E_{pmax} + E_{pmin}}{\mu} \right) \alpha$$

where  $\alpha = \cos(\theta/2)/[1 - \cos(\theta/2)]$  may be taken directly from the chart.

7. Calculate peak value of the driving voltage  $E_i = E_c + E_{pmax}$ .

**Table I.—Maximum Emission Current for Various Filament Materials, to Be Used in Choosing  $I_m$**

Type of Filament	Maximum Emission, Ma/Watt of Heating Power
Tungsten*.....	2-4
Thoriated tungsten†..	10-35
Oxide coated‡.....	10-40

\* Based on safety factor of 1. Multiply by 0.6 to 0.7 for linear amplifier or for modulated stage to ensure linearity.

† Based on safety factor of 3 to 10.

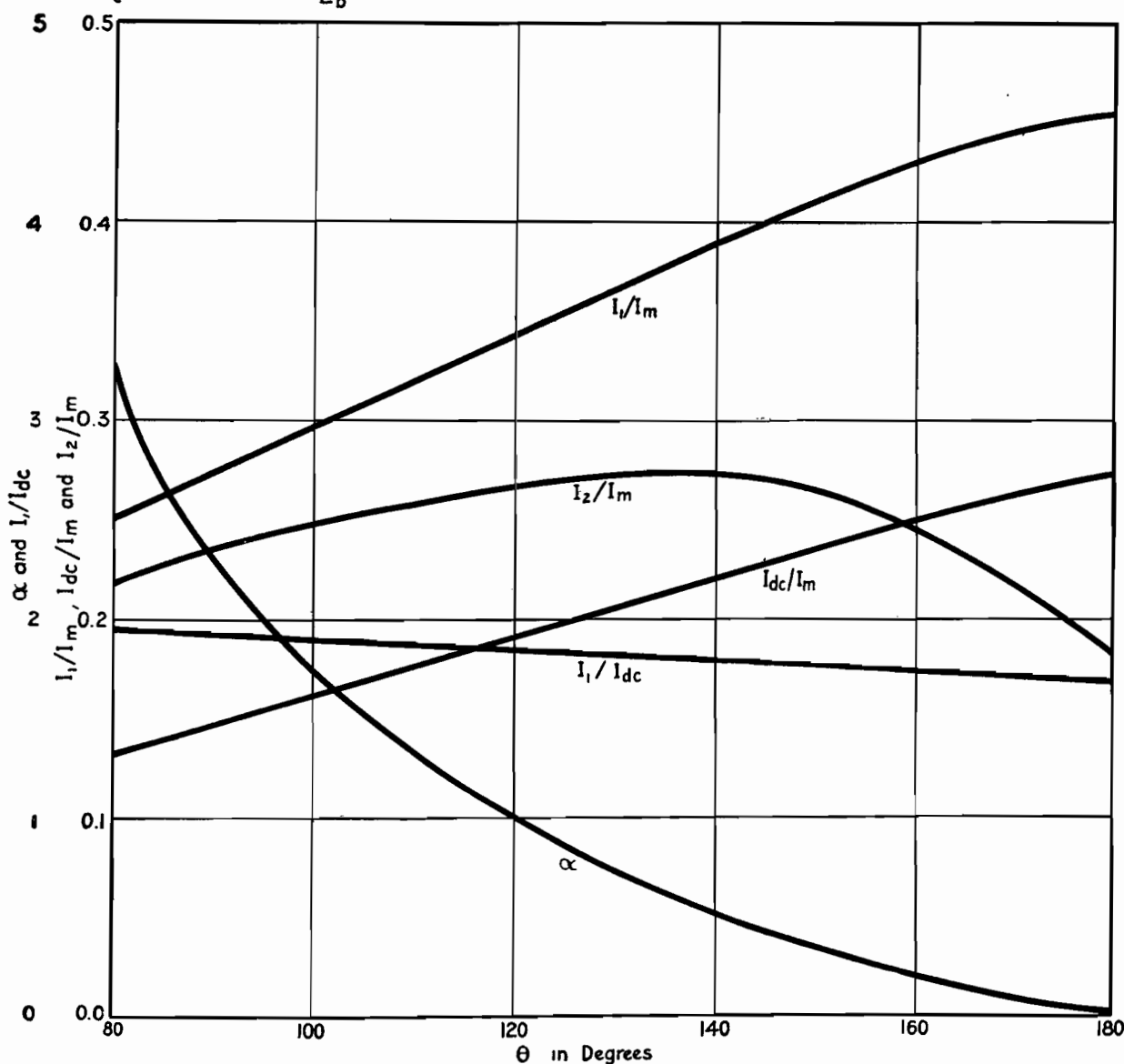
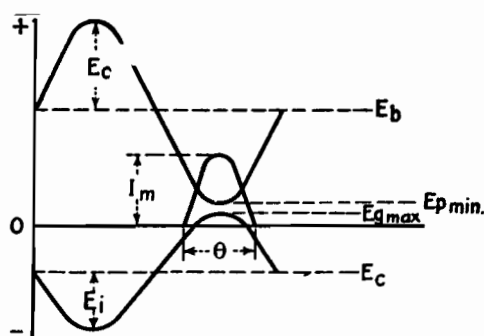
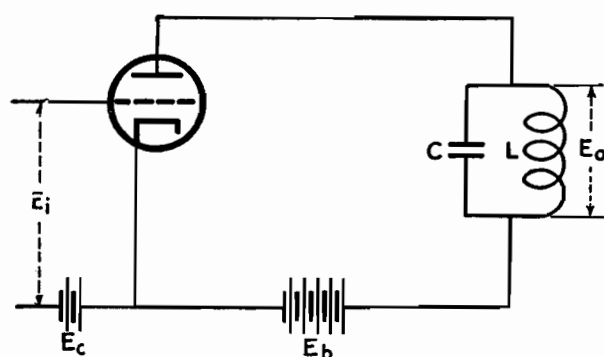
‡ Based on safety factor of 5 to 15.

8. Calculate power output  $P_o = I_1 E_o/2$ , where  $E_o = E_b - E_{pmin}$ . Also calculate plate dissipation  $= P_i - P_o$ .

9. Assuming that the grid current is 10 to 20 per cent of the plate current, determine the approximate driving power from  $E_c$  multiplied by the d-c grid current.

10. Check  $I_{d-c}$ ,  $E_c$ , driving power, and plate dissipation against maximum allowable for tube.

11. Choose the angle of conduction that gives the most desirable operation from the standpoint of output, efficiency,



and driving power. If desired, this may be repeated for several values of  $E_{pmin}$  and  $E_{o max}$ .

#### 12. Design tank circuit:

Equivalent impedance of tank  $Z_o = E_o / I_1$

$$L = \frac{Z_o}{2\pi f Q} \text{ henrys}$$

$$C = \frac{1}{(2\pi f)^2 L} \mu\text{f}$$

$Q$  may be set arbitrarily between 10 and 15 or may be established by the allowable second harmonic as follows:

$$Q = \frac{26}{\text{per cent 2d harmonic}} \times \frac{I_2}{I_1}$$

where  $I_2$  = second harmonic component of plate current for given  $\theta$ . A large  $Q$  will give a low harmonic component but

will increase the heating loss in the tank circuit.

*Example 2. Class C Amplifier with Given Power Output.*—1. Select tube and  $E_b$  as in step 1, Example 1.

2. Choose allowable  $I_m$  from Table I.

3. Select  $E_{pmin}$  and  $E_{o max}$  as in step 5, Example 1.

4. Calculate  $E_o = E_b - E_{pmin}$  and  $I_1 = 2P_o / E_o$ .

5. From the ratio  $I_1/I_m$  (see Fig. 2), determine  $\theta$  and  $I_{d-c}$ .

6. Calculate plate input  $P_i = E_b I_{d-c}$  and plate dissipation  $P_c = P_i - P_o$ .

7. Calculate  $E_c$ ,  $E_i$ , and driving power as in steps 6, 7, and 10 of Example 1.

8. Repeat for several values of  $I_m$ , or try different combinations of  $E_{pmin}$  and  $E_{gmax}$  for a given  $I_m$  to give better results from the standpoint of efficiency, tube life, driving power, etc.

9. Design tank circuit as in Example 1.

After the tank circuit has been tuned to resonance and the grid bias and plate voltage have been adjusted to the correct values, the grid excitation voltage should be adjusted so that the correct  $E_{gmax}$  is

obtained, as measured by means of a peak voltmeter. The coupling of the load to the tank circuit should then be

Table II.—Comparison of Design and Experimental Values for Class C Amplifier Using Type 10 Tube

	Design	Experimental
$I_{d-c}$	60	62.5
$P_o$	19.6	18.8
$P_i$	30	31.2
$E_{gmax}$	110	118
$E_{pmin}$	130	123
$I_g$	10-12	12

$E_b = 500$  volts     $f = 800$  kc  
 $\theta = 135^\circ$ ,  $E_c = 138$ ,  $I_m = 282$ ,  $I_1 = 106$

increased until the desired plate current is obtained. The tank circuit should be retuned each time that the coupling is changed. Small variations from the calculated values may improve the overall operating conditions. In amplifiers using tetrodes and pentodes, the tank should be tuned for maximum output rather than for minimum plate current, because the plate current is not very critical with respect to tuning.

### Bibliography

- (1) EVERITT, W. L., "Communication Engineering," 2d ed., pp. 526-595, 1937.
- (2) Terman, F. E., "Radio Engineering," 2d ed., pp. 314-315, 1937.
- (3) Analysis and Design of Harmonic Generators, *Elec. Eng.*, 57, 640, November, 1938.

## Power-amplifier Plate Tank Circuits

By ARVID B. NEWHOUSE

TIME spent on calculations of tank circuits of r-f power amplifiers can be considerably reduced by an analysis of the circuit conditions and the use of certain equations. Some aspects of the design of power-amplifier plate-tank circuits will be discussed here, particularly a-m amplifiers for broadcasting service. Equations are derived for calculating pertinent tank-circuit quantities, and methods of calculating values of inductors and capacitors to satisfy power and selectivity requirements are given. For a study of class B and C amplifier tank circuits, the reader is referred to a paper by P. H. Osborn.<sup>1</sup>

### Energy Storage

The r-f amplifier that will be studied is represented by the simplified circuit shown in Fig. 1. Although a series-fed unbalanced circuit is illustrated, the analysis will apply to other arrangements. It is assumed that the impedance of  $C_b$  is so low that substantially the full voltage developed across the tank circuit appears at the plate of the tube, and also that the excitation voltage  $E$ , the grid bias  $E_c$ , and the d-c plate voltage  $E_b$  are such as to deliver the required power with a known minimum of distortion. The inductor resistance is represented by  $R_L$ , whereas  $R_M$  represents the resistance reflected into the tank circuit from the load (succeeding amplifier, transmission line, or antenna) by the coupling system.

It is assumed that only resistance is reflected into the tank circuit by the coupling system.

The relations between plate current and plate and grid voltages during an r-f cycle are shown in Fig. 2. The instantaneous grid voltage  $e_g$  is equal to the bias voltage  $E_c$  plus the exciting voltage which has the maximum value  $E$ . Likewise, the instantaneous plate voltage  $e_p$  is the sum of the d-c plate voltage  $E_b$  and the superimposed voltage across the tank circuit, the latter reaching  $E_T$  as its maximum value. The plate current  $i_p$  flows during approximately one-half cycle in class B amplifiers, and for a shorter period in class C amplifiers. Both  $i_p$  and  $E_T$  vary in magnitude when the carrier is amplitude modulated,  $E_T$  attaining twice its carrier value when

100 per cent modulation peaks are reached.

Let  $P_i$  = power output of the tube, delivered to the tank circuit

$R = R_L + R_M$ , total series resistance in the tank circuit

$V = E_T/\sqrt{2}$ , rms voltage across the tank circuit

$I = 2\pi fCV$ , rms current flowing in  $C$

$f$  = carrier frequency

Although strictly true only for the case of an ideal parallel resonant circuit, it is sufficiently accurate for this discussion to assume that  $X_L = 2\pi fL$  is equal to  $X_C = 1/2\pi fC$ . Also, with respect to the tank current, it will be assumed that  $R^2$  is small compared with  $X_L^2$  in the expression  $I_L = V/\sqrt{X_L^2 + R^2}$ , so that  $I_L$  is substantially equal to  $V/X_L$ .

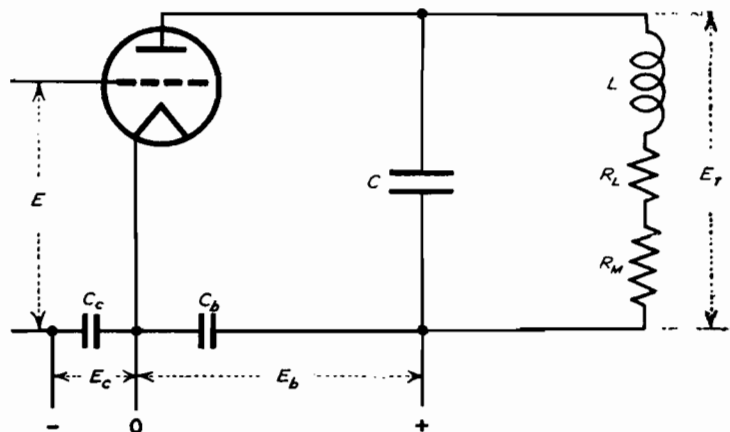


Fig. 1.—Simplified circuit diagram of a triode radio-frequency power amplifier.

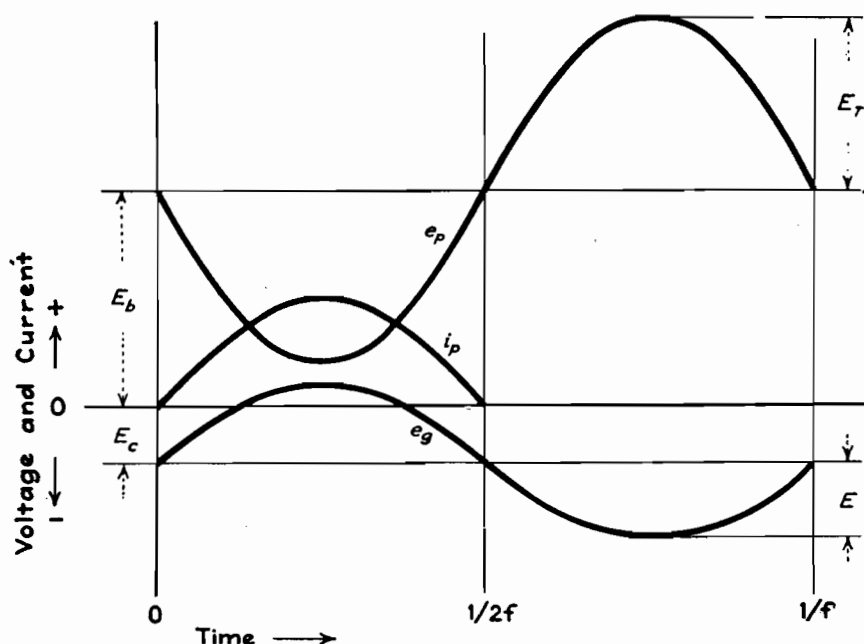


Fig. 2.—Voltage and current relations in a triode power amplifier.

Then  $I_L$  is equal to  $I = 2\pi fCV = V/X_C$ , and  $I$  may be used as the rms value of the tank current. The error introduced by these approximations is about 1 per cent. The ratio  $X_L/R$  will be designated  $Q_T$ , the figure of merit of the tank circuit, as distinguished from  $Q_L = X_L/R_L$ , the figure of merit of the inductor. In this discussion, the capacitor is assumed to have no resistance.

When tuned to resonance (unity power factor) the tank circuit will appear to the plate of the tube as a resistor having the value  $R_T = V^2/P_i$  ohms. But  $R_T$  may also be expressed in any of the following forms:<sup>2,3</sup>

$$R_T = \frac{X_C^2}{R} = \frac{X_L^2}{R} = Q_T X_C = Q_T X_L \\ = \frac{X_C X_L}{R} = \frac{2\pi fL}{2\pi fCR} = \frac{L}{CR} \quad (1)$$

Energy is received from the tube in pulses, a pulse each time plate current flows, and is delivered to the coupled load in a continuous flow. This means that the inductor and capacitor must act as a flywheel or tank for the storage of energy to maintain the flow. Let us postulate steady-state conditions. Then just sufficient energy is received by the tank circuit to maintain the oscillations at constant amplitude. Now at the instant the circulating current is zero, the voltage across the tank circuit is at its maximum and all the energy is stored in the capacitor. The amount of this energy is  $\frac{1}{2}CE_T^2$ , or  $CV^2$  joules.

The energy expended as heat in the tank circuit and that passed on to the load

each cycle is equal to that delivered by the tube each cycle or  $P_i/f$  joules. The ratio of the stored energy to the energy lost each cycle is  $fCV^2/P_i$ . Multiplying numerator and denominator by  $2\pi$ , we have  $VI/2\pi P_i$ .

Prince and Vogdes<sup>4</sup> work with self-controlled oscillators yielded results showing that, for stability and for minimizing harmonics, twice as much energy must be stored in the tuned circuit as is dissipated each cycle. The ratio  $VI/2\pi P_i$  is then about 2. However, this requirement is relaxed in the case of amplifiers, especially if they are followed by coupling systems or filters that discriminate against harmonics. In such applications, because of the external control of frequency and the reduction of harmonics passed on to the radiating system, a storage of energy equal to about 150 per cent of the loss appears ample. The ratio of circulating volt-amperes to output power may then be about  $3\pi$ , and the constants commonly used in design computations are 9 or 10.

The number and amplitude of the harmonics emitted by the radiating system depend on a number of elements other than the power amplifier plate load circuit. Generation of harmonics is reduced by carefully selecting the operating parameters for the tubes, and the harmonics generated may be prevented from reaching the output device by employing coupling systems and filter networks which discriminate against them. The relation between the amount of tank current and the second harmonic magnitude has been measured and calculated by Osborn,<sup>1</sup>

and the adjustment of the tank current to minimize harmonics has been treated by Dietsch.<sup>5</sup> Both Osborn and Dietsch show the rapid increase of the second harmonic as the tank volt-amperes is reduced below  $4\pi$  times the power output. However, the practice now prevailing of using push-pull power amplifiers minimizes the amount of second and other even harmonics in the output. In a push-pull amplifier, the tank circuit must furnish the flywheel effect for only one-half cycle, which permits the use of lower values of the ratio  $VI/P_i$ .

Obviously, the power wasted as heat in the tank inductor varies directly with the h-f resistance, while the power passed on to the load is  $I^2 R_M$ . It follows that the tank-circuit efficiency factor is  $R_M/(R_L + R_M)$ . In order to make the circuit efficiency as high as possible, it is necessary that the inductor be designed for a minimum r-f resistance at the frequency contemplated. Because of the change in the current distribution and density in the conductor, the r-f resistance varies with frequency in such a manner that the  $Q_L$  of any inductor is virtually constant over a wide frequency range. This figure of merit is used for comparing different inductors. The equivalent criterion for capacitors is  $D = R_C \omega C$ , where  $R_C$  is the r-f resistance of the capacitor. This factor is not often considered in transmitter design because, in most capacitors,  $D$  is rather small and because, for a given frequency, mode of operation, and cost, the choice of capacitors is limited. Ordinarily, there is some latitude in inductor design.

With respect to the figure of merit of the tank circuit,  $Q_T = X_L/R$ , where  $R = R_L + R_M$ , the following relations are assembled for reference:

$$R_T = \frac{V^2}{P_i} = \frac{X_L^2}{R} = Q_T X_L$$

and  $X_L = V/I$ , approximately.

$$Q_T = \frac{R_T}{X_L} = \frac{V^2}{P_i} \times \frac{I}{V} = \frac{VI}{P_i} \quad (2)$$

That is,  $Q_T$  is also the ratio of the tank current volt-amperes to the tube power output and, therefore, indicates the energy storage capability of the tank circuit.

In his paper, Osborn<sup>1</sup> described how too high a ratio of tank circuit volt-amperes to output power caused the tank circuit to discriminate against the higher side-band frequencies. He also derived a formula for calculating the distortion at

any modulating frequency for a given ratio of  $VI$  to  $P_i$ .

When it is desired to obtain a measure of the amplifier output channel width, a relationship similar to  $f/(f_2 - f_1) = Q$ , which holds for the series circuit, might be convenient. Here  $f$  is the carrier frequency and  $f_2 - f = f - f_1$  are the two side bands so related to  $f$  that the output power at  $f_1$  and  $f_2$  is one-half that at  $f$  for the same voltage  $V$ . Under these conditions,  $Q$  is then the ratio of the total inductive (or capacitive) reactance to the total resistance, including that in the generator. Hence for a given carrier frequency  $f$  and a given value for  $Q$  the channel width between the half-power (or 3 db down) frequencies can be readily computed.

However, to make use of this concept in power-amplifier plate-tank circuit design, it is necessary to take into account the equivalent series resistance in the plate circuit due to the tube resistance shunting the tank circuit. The relation of this internal resistance to the tank circuit is shown in Fig. 3, in which the tube output circuit is redrawn to place all the resistance in adjacent branches of the network.  $L$  and  $C$  are the tank inductance and capacitance  $R = R_L + R_M$ , and  $R_b$  is the apparent internal resistance of the tube plate circuit path viewed as an a-c generator. Then by the use of Thevenin's equivalent series circuit theorem we obtain the series impedance  $Z_s = R_s + jX_s$ .

$$\begin{aligned} Z_s &= \frac{R_b(R + jX_L)}{R_b + R + jX_L} \\ &= \frac{(R_b R + jX_L R_b)(R_b + R) - jX_L}{(R_b + R)^2 + X_L^2} \\ &= \frac{R_b R(R_b + R) + R_b X_L^2}{(R_b + R)^2 + X_L^2} \\ &\quad + j \frac{(R_b + R)R_b X_L - R_b R X_L}{(R_b + R)^2 + X_L^2} \end{aligned}$$

The  $Q$  of the output circuit will be designated  $Q_o$  and is equal to the reactance divided by the resistance, or  $X_s/R_s$ .

$$\begin{aligned} Q_o &= \frac{(R_b + R)R_b X_L - R_b R X_L}{R_b R(R_b + R) + R_b X_L^2} \\ &= \frac{R_b^2 X_L}{R_b R(R_b + R) + R_b X_L^2} \end{aligned}$$

Since  $R$  is small compared with  $R_b$ ,  $R_b + R = R_b$ , very nearly. Then

$$Q_o = \frac{R_b^2 X_L}{R_b^2 + R_b X_L^2} \quad (3)$$

The ratio of the channel width (between the half-power frequencies) to the carrier frequency is  $(f_2 - f_1)/f = 1/Q_o$ .

$$\begin{aligned} \frac{1}{Q_o} &= \frac{R_b R + X_L^2}{R_b X_L} = \frac{R_b R}{R_b X_L} + \frac{X_L^2}{R_b X_L} \\ &= \frac{1}{Q_T} + \frac{X_L}{R_b} \end{aligned}$$

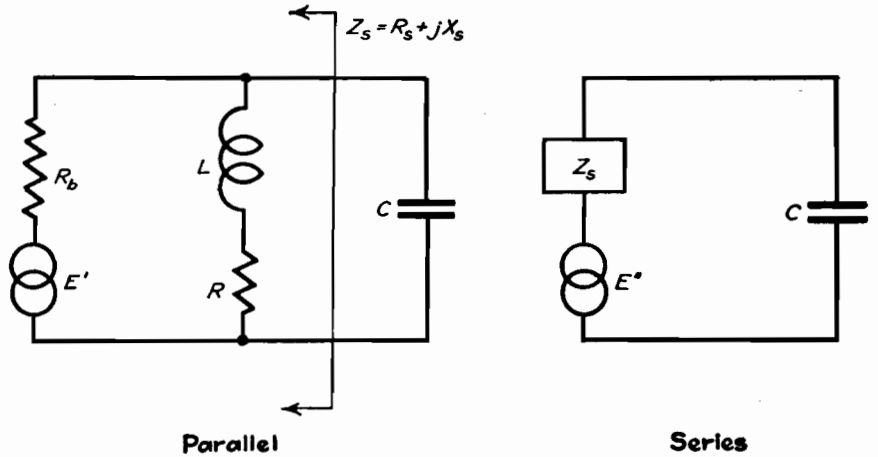


Fig. 3.—Parallel-to-series transformation of a triode amplifier output circuit network.

Equation (3) indicates the relation that exists between  $R$ ,  $X_L$ ,  $R_T$ , and  $R_b$  for the assumed 3-db distortion limit. That is, for a certain desired value of  $(f_2 - f_1)$  at a carrier frequency  $f$ , the value for  $Q_o$  determined by Eq. (3) may not be exceeded. Since  $R_T$  and  $R_b$  are fixed when the power output and the tube operating parameters are set, the limitation falls on  $Q_T$ ,  $X_L$ , and  $R$ , and determines an inferior limit for the tank reactance and the coupling to the load.

Equation (3) serves as a guide for the power-amplifier output channel width. To apply the equation, it is necessary to find the value of  $R_b$ , the apparent internal resistance of the amplifier tube plate circuit. This may be done as follows. In Fig. 4 is shown the relation of  $R_b$  to the tank circuit, the latter indicated by  $R_T$ . In this diagram  $I_a^2 R_T = P_i$ , the tube output power; and  $I_a^2 R_b = P_b$ , the power loss in the tube.

$$\frac{P_b}{P_i} = \frac{I_a^2 R_b}{I_a^2 R_T} = \frac{R_b}{R_T}$$

Hence,

$$R_b = \frac{P_b}{P_i} \times R_T \quad (4)$$

It will be noted that  $R_b$  is not the a-c plate resistance  $r_p$  included in the tube data by manufacturers or calculated from static characteristics. The tube plate resistance has a finite value only when

plate current is flowing, and increases without limit during nonconducting intervals. Further, plate current flows only during periods when the instantaneous plate voltage is low, as may be seen in Fig. 2. If  $R_b$ , the apparent resistance, is large so that  $X_L/R_b$  is small compared with  $1/Q_T$ ,  $Q_o$  will approach  $Q_T$  as a limit and the selectivity of the entire output circuit will approach that of the tank circuit alone. Usually  $X_L/R_b$  is comparatively large, making  $Q_o$  much less than  $Q_T$ .

### Conclusion

In this discussion, two limits have been found for the ratio of power-amplifier tank current to output powers, a minimum value determined by energy storage requirements, and a maximum that is determined by the tube constants and output distortion limitations. It was also noted that this ratio is  $Q_T$ , which is equal to the quotient of load resistance  $R_T$  divided by the reactance  $X_L$  or  $X_C$ , and to the quotient of the reactance divided by the total series resistance in the tank circuit.

### Appendix

To justify the approximations preceding Eq. (1), the following developments are appended.

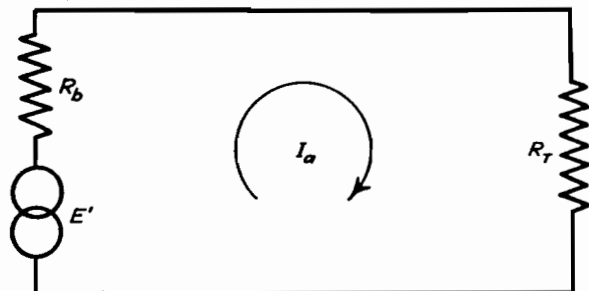


Fig. 4.—Triode-amplifier output circuit viewed as a generator with a resistive load.

Let the impedance the tank circuit presents to the plate of the tube in Fig. 1 be  $Z_T = R_T + jX_T$ . Also, for simplicity, let  $R = R_L + R_M$ .

$$Z_T = \frac{-jX_C(R + jX_L)}{R + j(X_L - X_C)} \\ = \frac{RX_C^2}{R^2 + (X_L - X_C)^2} + j \frac{X_L X_C (X_C - X_L) - R^2 X_C}{R^2 + (X_L - X_C)^2}$$

For parallel resonance (unity power factor)  $X_T = 0$ , and the numerator of the second term in the equation above must equal zero.

$$X_L X_C (X_C - X_L) R^2 X_C = 0 \\ X_L (X_C - X_L) = R^2 \\ X_L X_C - X_L^2 = R^2 \\ X_C = \frac{R^2 + X_L^2}{X_L} = X_L + \frac{R^2}{X_L}$$

A hypothetical tank circuit may have an  $R_T$  of 1,000 ohms and a  $Q_T$  of 10. Then  $X_L$  will be 100 ohms, and  $R$  will be made 10 ohms by adjustment of the coupling to the load.

$$X_C = 100 + \frac{10^2}{100} = 100 + 1 = 101 \text{ ohms}$$

Hence, equating  $X_C$  to  $X_L$  in this case introduces an error of only 1 per cent. When  $Q_T$  is greater than 10,  $X_C$  will approach closer to  $X_L$  in size, and would coincide, of course, if  $R$  could be made zero. The error introduced by this approximation will be of the order of 1 per cent in most practical circuits.

To compare the current in the  $L$  and  $C$  branches, let  $I_L$  be the rms current in the inductor and  $I_C$  the rms current in the capacitor. The rms voltage across the tank circuit is  $V$ . The current flowing in each branch is equal to the voltage across the tank circuit divided by the impedance of the branch.

$$I_C = \frac{V}{X_C} \quad \text{and} \quad I_L = \frac{V}{\sqrt{X_L^2 + R^2}} \\ \frac{I_C}{I_L} = \frac{V}{X_C} \times \frac{\sqrt{X_L^2 + R^2}}{V} = \frac{\sqrt{X_L^2 + R^2}}{X_C}$$

Inserting the previously assumed values for  $X_L$ ,  $R$ , and  $X_C$ ,

$$\frac{I_C}{I_L} = \frac{\sqrt{100^2 + 10^2}}{101} = \frac{10 \sqrt{100 + 1}}{101} \\ = \frac{10 \sqrt{101}}{101} \\ \frac{I_C}{I_L} = \frac{10 \times 10.05}{101} = \frac{100.5}{101}$$

Equating  $I_C$  to  $I_L$  involves an error of only about 0.5 per cent in a circuit with a  $Q_T$  of 10, and this error becomes less for higher values of  $Q_T$ . The errors introduced by setting  $X_L$  equal to  $X_C$  and  $I_L$  equal to  $I_C$  are small compared with the inaccuracies in most of the data from which power-amplifier plate tank circuits are designed.

#### References

- (1) OSBORN, PERRY H., A Study of Class B and C Amplifier Tank Circuits. *Proc. IRE*, **20**, 813-834, May, 1932.
- (2) EVERITT, W. L., "Communication Engineering," pp. 54-60, McGraw-Hill Book Company, Inc., New York, 1932.
- (3) GLASGOW, R. S., "Principles of Radio Engineering," pp. 35-44, McGraw-Hill Book Company, Inc. New York, 1936.
- (4) PRINCE, D. C., and VOGDES, F. B., "Vacuum Tubes as Oscillation Generators," General Electric Co., pp. 37-38, 1929.
- (5) DIETSCH, C. G., Suppression of Transmitter Harmonics, *Electronics*, **6**, 167-169, June, 1933.

## Class B R-f Amplifier Chart

A method of calculating power output, plate efficiency, r-f plate current, and d-c plate current from tube characteristics and operating voltages, making use of the "perveance" of the amplifier tube

A simplified graphical and tabular method is presented for determining the performance of class B r-f amplifiers having a parallel tuned circuit coupled to the load. The results given here have been based on the analysis given in "An Analysis of Class B and C Amplifiers" by B. F. Miller, in the *Proceedings of the IRE* for May, 1935, page 496, and have been adapted to class B operation by W. Van B. Roberts.

Assume:

$E_B$  = quiescent or operating plate voltage (direct current)

$E_C = E_B/\mu$  is the grid bias voltage for class B operation

$E_g$  = amplitude of grid excitation voltage of fundamental frequency corresponding to  $\omega$

$E_p = (E_B - E_i)$  = instantaneous value of plate voltage

$E_i$  = amplitude of the voltage of fundamental frequency appearing across the tank circuit composed of  $L$  and  $C$

$K' = I_p/E_p^{3/2}$  = perveance of triode, determined from the static tube characteristics for the condition that  $E_g = E_c = 0$ ;  $I_p$  is measured in amperes and  $E_p$  in volts

$K = K'R$

$R$  = resistance of parallel resonant circuit and load when tuned to the grid exciting frequency  $\omega/2\pi$

$I_p$  = plate current flowing in tube output circuit

$\alpha = 0.457K \sqrt{\mu E_g}$

$\beta = E_i/\mu E_g$

$\mu$  = amplification factor of triode

$\omega = 2\pi f$  where  $f$  = fundamental frequency of the grid excitation voltage

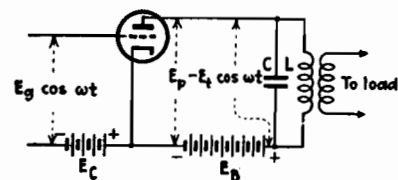
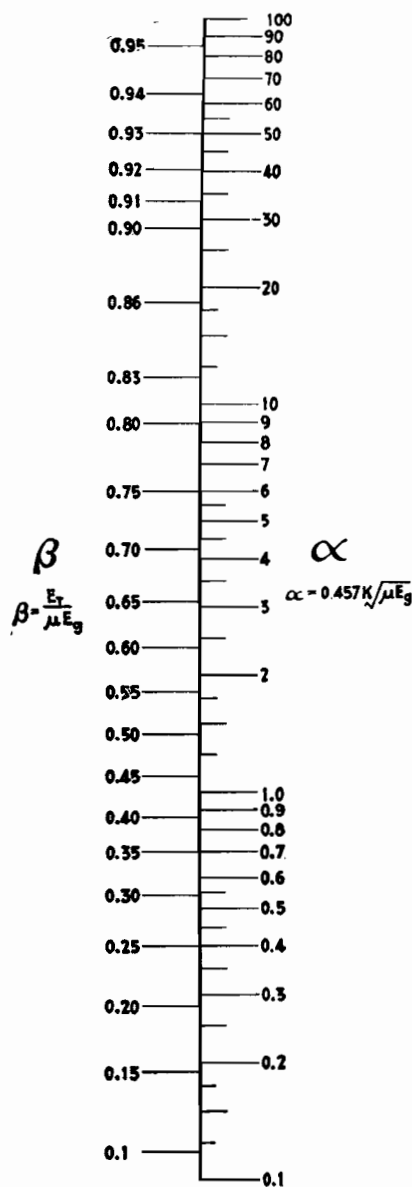
The operation of the amplifier is determined through the use of the alignment chart and the circuit factors  $\alpha$  and  $\beta$ , which require that the values of  $K'$ ,  $R$ ,  $\mu$ , and  $E_g$  be known for any given set of conditions, from which  $E_i$  can be found. The value of  $\mu$  for the tube in use can be determined from measurements or from

the manufacturers' data sheets. The value of  $K'$  is not given by the tube manufacturers but can easily be determined if the static tube characteristics are available. Following along the static curve for  $E_c = 0$ , the plate current in amperes  $I_p$  is observed for a plate voltage  $E_B$  which is high compared with the filament voltage but not sufficiently high as to produce saturation. The value of  $K'$  is then given by

$$K' = \frac{I_p}{E_B^{3/2}}$$

The value of the resonant impedance of the tank circuit,  $R$ , may be determined from methods given in such standard engineering textbooks as Terman's "Radio Engineering" or Everitt's "Communication Engineering." The grid excitation voltage  $E_g$  can be measured with a vacuum-tube voltmeter for a given set of conditions if necessary, but for analyzing





the operation of class B amplifiers, it is usually desirable to let  $E_g$  take definite values which may be arbitrarily selected.

Knowing (or assuming) a given set of values for  $K'$ ,  $R$ ,  $\mu$ ,  $E_B$ , and  $E_g$ , we calculate

$$\alpha = 0.457 K' R \sqrt{\mu E_g} = 0.457 K' \sqrt{\mu E_g}$$

and from the alignment chart determine the value of  $\beta$  corresponding to this value of  $\alpha$ . By multiplying  $\beta$  by  $\mu E_g$ , the value of  $E_t$  is determined. Knowing  $E_t$ , the operating characteristics of the amplifier can be determined for the chosen

values of  $K'$ ,  $R$ ,  $\mu$ , and  $E_g$ . Thus:

$$E_t = \beta \mu E_g$$

$I_{pw} = E_t/R$  = amplitude of the plate current of fundamental frequency

$I_{p0} = 0.605 E_t/R$  = d-c current flowing in the plate circuit

$P_o = E_t^2/2R$  = power output of the amplifier

$P_i = 0.605 E_t E_B/R$  = power input to the plate circuit

The analysis underlying this simplified

method of calculation is based on the assumption that the plate current is proportional to the  $3/2$  power of the plate voltage, which is a good approximation in practice. The analysis does not take into account the flow of grid current so that the method can be used only for those values of excitation grid voltages for which  $\mu E_g$  is less than the instantaneous plate voltage given by  $E_p = (E_B - E_t)$ .

## Power Efficiency of R-f Power-amplifier Stages

By HARRY STOCKMAN

Application of the Chaffee contour-diagram method of analysis to the determination of power efficiency in nonlinear transmission systems with tubes operating as class B or class C amplifiers. Practical examples are given

THE power efficiency of such high-power devices as class C stages in radio transmitters has for a long time been a factor of great importance. Lately, the power efficiency of such low-power devices as class C operated u-h-f converters has been given considerable thought.

Both the devices mentioned have one thing in common: an inner impedance that varies within wide limits. As the inner impedance is variable, such technical terms as conjugate match and critical coupling, used in the class A terminology, lose their conventional meaning and must be replaced by modified technical terms or new technical terms.

### Fundamental Considerations

The source connected to the transmission chain in Fig. 1 may represent an oscillating tube with its supply. In its symbolic form the source is shown to have one d-c part and one a-c part, the former delivering the d-c power  $P$  to the latter, and the latter delivering the a-c power  $P_o$  to the transmission chain.

In the general case, the a-c source is nonlinear. The emf and inner impedance of such a source cannot with advantage be expressed in simple mathematical

form, and an analytical treatment of the power relations is therefore not practical and may not even be possible.

In a special case the source is linear and may then be truly characterized by an emf  $E$  in series with an inner impedance  $Z$ , independent of amplitude. A simple analytical treatment can now be made but is not of much interest, as linear operation is mostly used when the output power is comparatively small.

As shown in Fig. 1a, the d-c/a-c generator feeds into a load  $Z_{Lu}$  via a number of transmission sections 1, 2 . . .  $n$ , which are introduced either to provide matching or to convey power from one point to another. A transmission section as shown may represent a transformer, a link coupling, a feeder, or a radiation coupling to a receiving device.

The power  $P_u$  developed in the load  $Z_{Lu}$  is the utilized power. (All power notations refer to active power.) The amount of power delivered to a particular section 1, 2 . . .  $n$  of the system, or to the load  $Z_{Lu}$ , may be calculated if the proper input impedance  $Z_{L1}$ ,  $Z_{L2}$  . . .  $Z_{Ln}$ , or  $Z_{Lu}$  is known (assuming steady-state conditions). The total power at the specified point is the sum of the component powers, a component power being the

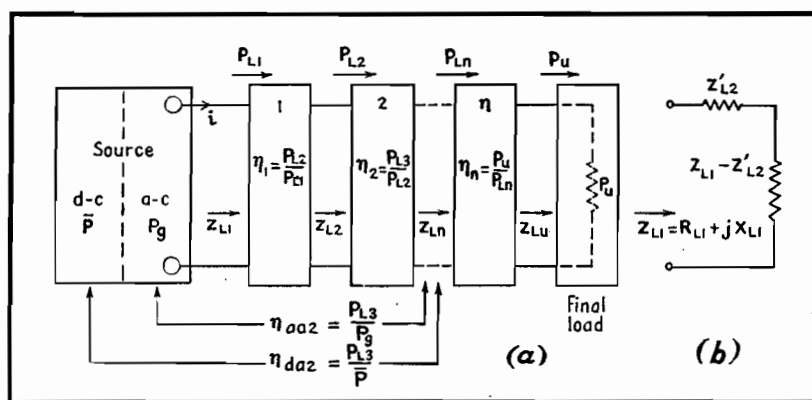


Fig. 1.—Power transfer in a transmission chain connected to a nonlinear source.

power developed by a particular frequency component.

Any specified output power  $P_{L1}$ ,  $P_{L2}$ , ...,  $P_{Ln}$ , or  $P_u$  is conveniently expressed as a fraction of any specified source power. Such a fraction is known as power efficiency and may for practical purposes be defined as

$$\eta = \frac{\text{specified active output power}}{\text{specified active input power}} \quad (1)$$

Power efficiencies may generally be classified as a-c/a-c power efficiency  $\eta_{aa}$  and d-c/a-c power efficiency  $\eta_{da}$  (and in case of rectifying devices a-c/d-c power efficiency  $\eta_{ad}$ ). For determination of the power efficiency, the nature of each one of the two powers concerned must be known. It may, for example, be necessary to know if the output power includes the fundamental component only, or if it includes all components produced. In addition it may be of interest to know how the power readings are related to various parameters.

If the input power  $\bar{P}$  is measured at small amplitudes and the output power  $P_u$  measured at large amplitudes, an error may intentionally or unintentionally be introduced which makes the measurement unreliable. In this way, boosted power efficiencies can be obtained, which even exceed the limiting values given by mathematical analysis, based on the assumption that  $\bar{P}$  and  $P_u$  refer to the same amplitude value.

Any power efficiency referring to the source and a specified load in a circuit may be termed total power efficiency. Examples of total power efficiencies are  $\eta_{aa2}$  and  $\eta_{da2}$  in Fig. 1. A total power efficiency may be broken up into one power efficiency for the source  $\eta_{aa}$ , and one power efficiency for each following transmission section  $\eta_1, \eta_2, \dots, \eta_n$ . The total power efficiencies are then computed as

$$\eta_{aa2} = \eta_{aa}\eta_1\eta_2 \dots \eta_n \quad (2)$$

$$\eta_{da2} = \eta_{da}\eta_1\eta_2 \dots \eta_n \quad (3)$$

For  $x = n$  the power efficiencies include the entire system and may be referred to as over-all power efficiencies  $\eta_{aan}$  and  $\eta_{dan}$ . This procedure is convenient as the power efficiency for each one of the transmission sections can be investigated and improved without the necessity of taking the circuit components of the rest of the transmission chain into consideration. The total power efficiency is maximum when each  $\eta$  figure involved is maximum.

It is desirable that  $\eta_1, \eta_2, \dots, \eta_n$  be expressed in network parameters for the individual section. A transformation of the load impedance on the output side of a section to the input side of the same section makes possible a treatment free from voltage and current considerations. Thus in the case of section 1, as redrawn in Fig. 1b, with the load  $Z_{L2}$  reflected to the input side as  $Z'_{L2}$

$$\eta_1 = \frac{P_{L2}}{P_{L1}} = \frac{I^2 \text{Re}(Z'_{L2})}{I^2 \text{Re}(Z_{L1})} \quad (4)$$

$$\eta_1 = \frac{\text{Re}(Z'_{L2})}{\text{Re}(Z_{L1})}$$

This method is of special importance for matching sections employing coupled circuits. An application follows.

### Class A Application

In the first case to be considered, the source in Fig. 1 is a tube operated in class A with small constant amplitude. The tube is treated as a linear device. The emf may be sinusoidal and have the form  $e = E_m \sin \omega t$ , and the constant inner impedance expressed as  $Z = R + jX$ . A simple derivation shows that conditions for maximum power transfer require  $Z_{L1}$  to be the conjugate quantity of  $Z$ . Then

$$(P_{L1})_{\max} = \frac{E^2}{4R} \quad (5)$$

where  $E = E_m/\sqrt{2}$ . For this condition

$$\eta_{aa} = \frac{P_{L1}}{P_g} = 50\% \quad (6)$$

$P$  is here the source of a-c power (fictitious) in the equivalent plate circuit for the tube concerned.<sup>1</sup> An a-c/a-c efficiency of 50 per cent is the theoretical limit for the conditions specified. The maximum d-c/a-c efficiency may be much below 50 per cent.

### Treatment of Class C Devices

The concept of conjugate match loses its significance not only for class C operated tubes, but as well for some class B and class A operated tubes, especially when the applied amplitude is comparatively large. The reason for the deviation from the conjugate-match principle may be the inconstancy of the plate resistance, or the fact that matching to a multiple or fraction of the plate resistance is desirable rather than a matching to the plate resistance itself. It is well known that for some operation of class A and class B amplifiers the introduction of an optimum load impedance solves the problem as far as the technical side is concerned. Thus the turns ratio and impedances of a transformer, when matching a loudspeaker to an output tube, may be determined with the optimum load impedance of the tube as the only known tube design data. The plate resistance (or rather average plate resistance) of the tube is of no interest.

In the more extreme case of class C operation of r-f amplifiers, the introduction of an optimum load impedance is not a sufficiently good solution. Various methods for dealing with r-f power tubes have been developed.

The following treatment is described by Chaffee.<sup>2-4</sup> Static measurements are performed to give static characteristic curves, preferably  $e_p e_g$  curves, from which may be calculated so-called contours, joining points of equal driving power, plate dissipation, output power, plate efficiency, etc. An alternative method is to measure the various operational voltages, currents, and powers and plot the contours in the  $e_p e_g$  axes system.

An example of an  $e_p e_g$  diagram, including several contours, is shown in Fig. 2. The position of the Q point in the upper left corner is determined by the applied d-c grid potential, -175 volts, and the applied d-c plate potential, 1,000 volts. For these values the plate current is zero. When a sufficiently large alternating voltage is applied to the grid, class C

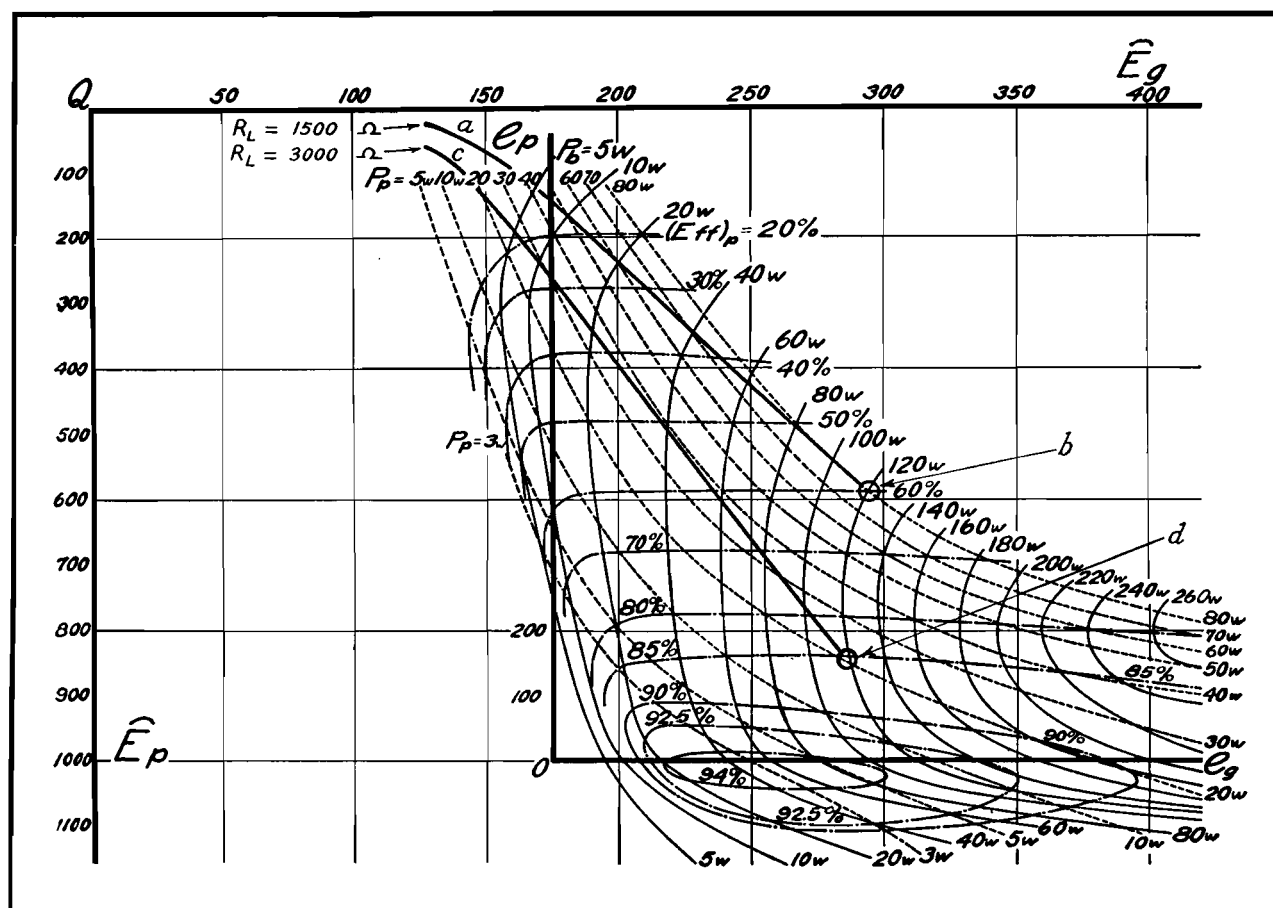


Fig. 2.—Chaffee contour diagram for accurate determination of the operating characteristics of a UV211 tube when  $E_B$  is 1,000 volts and  $E_C$  is  $-175$  volts.

operation with pulsating plate current results. The fundamental component of the plate voltage may reach an amplitude of the order of 500 to 1,000 volts, the actual value being determined by the impedance in the plate circuit. Contours are shown for the plate dissipation  $P_p$ , the output power  $P_o = P_{L1}$ , and the plate efficiency  $(Eff)_p = \eta_{da} = P_o / (P_p + P_o)$ .

### Examples

**Example 1.**—Assume  $E_{gm} = 290$  volts,  $E_{pm} = 590$  volts, and  $R_L = 1,500$  ohms. The path of operation  $Qb$  will then have its end point  $b$  located as shown, so that  $P_p = 80$  watts,  $P_o = 120$  watts, and  $(Eff)_p = 60$  per cent.\*

**Example 2.**—Assume  $E_{gm} = 280$  volts,  $E_{pm} = 840$  volts, and  $R_L = 3,000$  ohms. The path of operation  $Qd$  will now have its end point  $d$  located further down, so that  $P_p = 20$  watts,  $P_o = 120$  watts, and  $(Eff)_p = 85$  per cent. The position of the end point of the path of operation must be given proper consideration. The contours  $ab$  and  $cd$  for plate loads of

1,500 and 3,000 ohms represent loci for end points when the amplitudes are varied.

### A Practical Application

A transmission system including a class C amplifier is shown in Fig. 3a. (Neutralization and modulation circuits may be added.) The power tube, to which the diagram in Fig. 2 applies, feeds via an output transformer and a feeder a center-driven antenna of input impedance  $Z_{L3} = R_{L3} + jX_{L3}$ . It is assumed that the antenna half length  $h$  is slightly less than a quarter wavelength so that  $X_{L3} = 0$ . It may further be assumed that  $R_{L3}$  equals the characteristic impedance  $R_c$  of the feeder, so that no standing waves appear on the feeder and no reactance is reflected into the secondary of the transformer.

The main requirement on the circuit elements  $L_2$  and  $C_2$  is that they provide resonance for the fundamental transmission frequency. The ratio  $L_2/C_2$  is not critical from the point of view of matching, as the mutual impedance  $M$  will be adjusted accordingly so that the load presented to the tube will be the one required by the end point in the contour

diagram. The primary  $L_1C_1$  is tuned to resonance to secure a tube load impedance of zero phase angle and thus secure efficient operation of the tube.

The tube  $T$  with power supply represents the d-c/a-c source in Fig. 1. Leaving the grid dissipation and the grid driving power out of consideration, the power efficiency of interest will be the one indicated in Fig. 3a. The plate efficiency  $\eta_{da} = \eta_p$  is obtained from contour diagrams of the type shown in Fig. 2. The output transformer efficiency  $\eta_1$  is computed as indicated by Eq. (4), in accordance with the tuned equivalent circuits in Fig. 3b and 3c.

$$\eta_1 = \frac{Re(Z_{L2}')}{Re(Z_{L1})} = \frac{\omega^2 M^2}{R_{L2}} \frac{R_1 + \omega^2 M^2}{R_{L2}} \quad (7)$$

(The coil resistance of the secondary circuit is assumed to be negligible compared with  $R_{L2}$ .) It is important to realize that the power efficiency described by Eq. (7) refers to the transformer and its load only; the tube is in the circuit all the time, but is disregarded in this discussion.

With the tube left out of consideration, the circuit is linear and the mutual

\* In the diagram, amplitude is indicated by an eyebrow over the symbol rather than by the subscript  $m$ .

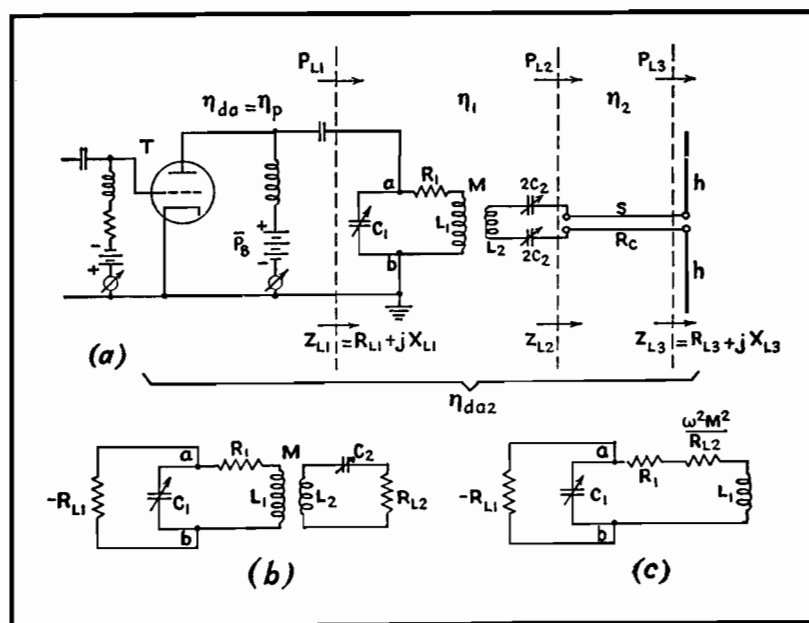


Fig. 3.—Transmission circuit with nonlinear generator (a class C r-f power tube).

inductance  $M$  and coefficient of coupling  $k = M/(L_1 L_2)^{1/2}$  can therefore be estimated in terms of critical coupling. For a transformer with both circuits tuned to resonance, critical coupling may be defined by one of the two relations

$$\omega^2 M^2 = R_1 R_{L2} \quad (8)$$

or

$$k_c^2 = \frac{1}{Q_1 Q_2} \quad (9)$$

Here  $Q_1 = \omega L_1 / R_1$  and  $Q_2 = \omega L_2 / R_{L2}$ . As this discussion of critical coupling does not have anything to do with the tube,  $Q_1$  refers to the primary circuit above with no resistance component reflected from the tube into the circuit. At critical coupling the transformer efficiency of Eq. (7) becomes

$$\eta_1 = 1/(1 + (k_c/k)^2) \Big|_{k=k_c} = 50 \text{ per cent} \quad (10)$$

#### Class A Operation

It will now be temporarily assumed that the tube is operated in class A with limited amplitude, so that the entire circuit can be considered linear. The vital question is now: what coupling in the transformer yields maximum power in the load impedance  $R_{L2}$ ? The simplest case is at hand when the plate resistance of the tube is so high that, when reflected into the primary circuit, it becomes almost negligible compared with  $R_1$ . In this case, maximum power transfer is obtained

when the critical coupling described by Eqs. (8) and (9) is maintained. This follows directly from Eq. (5), or rather from the assumed conditions under which Eq. (5) is derived. Equation (6) gives the system power efficiency as 50 per cent.

Consider next a class A tube with somewhat lower plate resistance. The reflected plate resistance  $r_p'$  in series with  $R_1$  must now be taken into account, and it is therefore necessary to increase the coupling in the transformer until the condition

$$\omega^2 M^2 = (R_1 + r_p') R_{L2} \quad (11)$$

is obtained. The power developed in  $R_{L2}$  is then maximum, and the power efficiency of the (tube, transformer, load) system is 50 per cent.

It would be permissible to say that the conditions for maximum power transfer are obtained for critical coupling in the system, but it is better to continue using the term "critical coupling" for the transformer and load only, especially as the case just discussed is of limited practical value. As far as the transformer is concerned, it is overcoupled and has an efficiency above 50 per cent.

Now consider the general case when the tube is operating in class C and the system is nonlinear. It is tempting to continue to think of the tube as represented by a reflected resistance in the

primary circuit of the transformer, as this explains why overcoupling yields increased output power. It is, however, dangerous to think in terms of class A in nonlinear circuit applications. An equation like Eq. (11) would be misleading if  $r_p'$  were used to represent a nonlinear quantity, and would not be of much use anyhow as  $r_p'$  is then a notation for something that cannot be given a simple mathematical form. There is then so much more reason to restrict the term critical coupling to the transformer part of the circuit. This does not mean, however, that the distance between the coils is to be adjusted for critical coupling. As before, considerable overcoupling is required, and the  $\eta_1$  figure may in a practical case be fairly close to 100 per cent. Thus for a high  $k$  value, such as  $k = 10k_c$ ,

$$\eta_1 = 1/(1 + (k_c/k)^2) \Big|_{k=10k_c} = 99 \text{ per cent} \quad (12)$$

If in Fig. 3 the losses in the antenna are neglected and the losses in the feeder known, the over-all d-c/a-c power efficiency is obtainable as  $\eta_{da2} = \eta_{da} \eta_1 \eta_2$ , as indicated by Eq. (3). Here the plate efficiency  $\eta_{da} = \eta_p$  is obtained from the contours as previously described.

#### Conclusion

The necessity for standard definitions of various power efficiencies and their theoretical limits has been stressed. The simplicity of a system, in which the over-all efficiency is broken up into a source efficiency and a number of section efficiencies, is brought out in the discussion. In the treatment of class C devices, reference is made to the paramount possibilities of the Chaffee contour method. A transmission system is discussed, in which the source efficiency is obtained by this method. It is suggested that for class C operation the term critical coupling be restricted to the matching device only.

#### References

- (1) STOCKMAN, H., The Validity of the E. P. C. Theorem for Power Calculations, *Proc. IRE*, **32**, No. 6, June, 1944.
- (2) CHAFFEE, E. L., The Operating Characteristics of Power Tubes, *Applied Phys.*, **9**, No. 6, June, 1938.
- (3) CHAFFEE, E. L., Power Tube Characteristics, *Electronics*, **11**, No. 6, June, 1938.
- (4) SARBACHER, R. I., Performance of Self-biased Modulated Amplifiers, *Electronics*, April, 1943.

# Graphical Determination of Power-amplifier Performance

By ROBERT I. SARBACHER

Complete performance of class B and C power amplifiers may be obtained graphically from static characteristics of a tube, through use of a plastic calculating device

WHEN it is desired to obtain the complete dynamic characteristics of a power tube, it is often more convenient to employ a method of graphical analysis to obtain this information, than to test the tube directly. A number of such methods of analysis have been developed which involve graphical integrations of the current wave form,

obtained from the static characteristic curves of the tube. The calculating device to be described here may be adapted to these various graphical analyses. By its use the calculating process may be simplified and the time required to make the calculations appreciably reduced.

In the following discussion the harmonic

analysis, developed by E. L. Chaffee, has been employed. This method of analysis, which has been discussed elsewhere,<sup>1</sup> is exceptionally accurate and is easily adapted to the calculating device.

### Design of Calculator

The calculating device consists of a sheet of clear acetate-base plastic, having

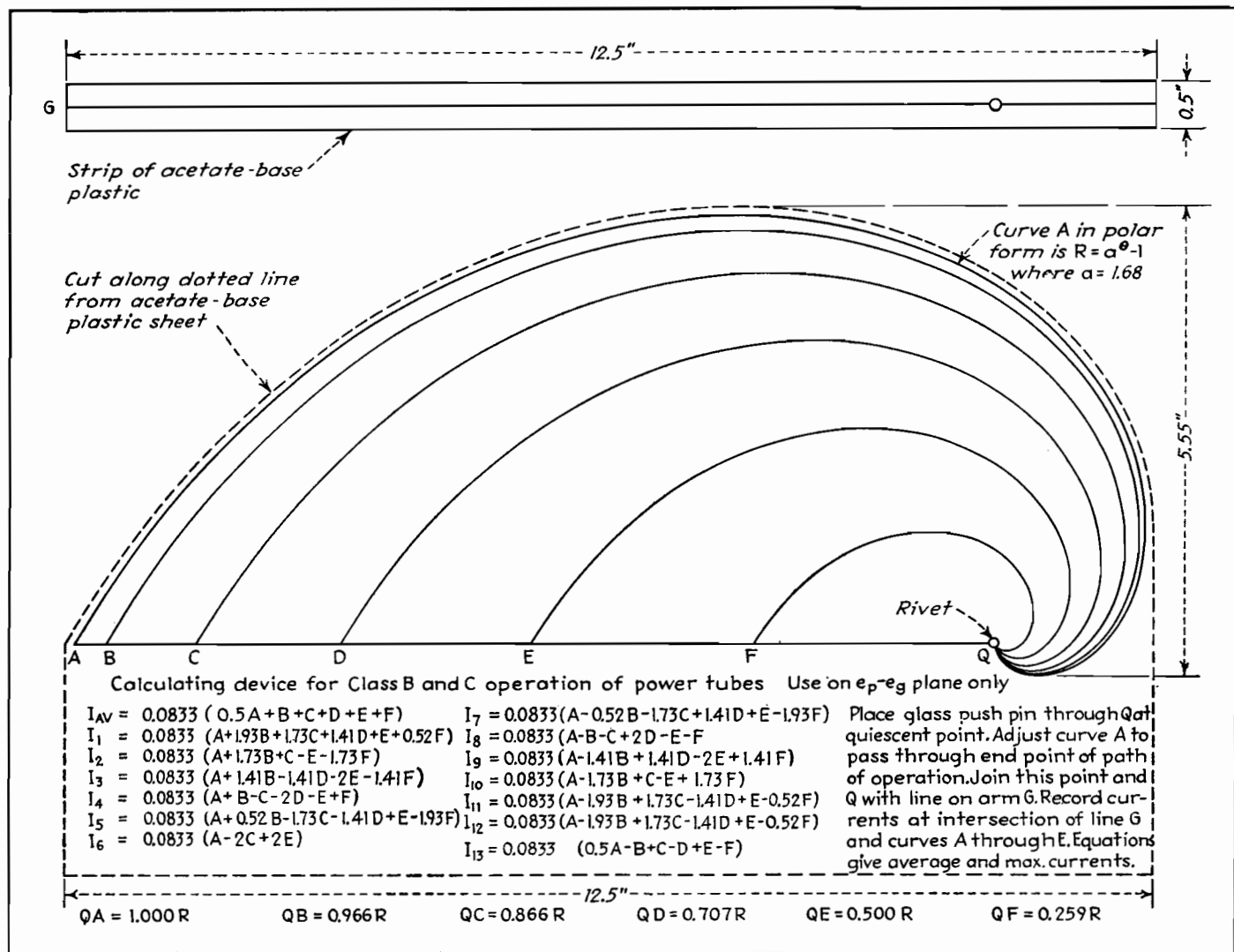


Fig. 1.—Calculating device for power tube analysis in class B and C operation consists of two pieces of plastic marked as shown and fastened together at Q by means of hollow rivet.

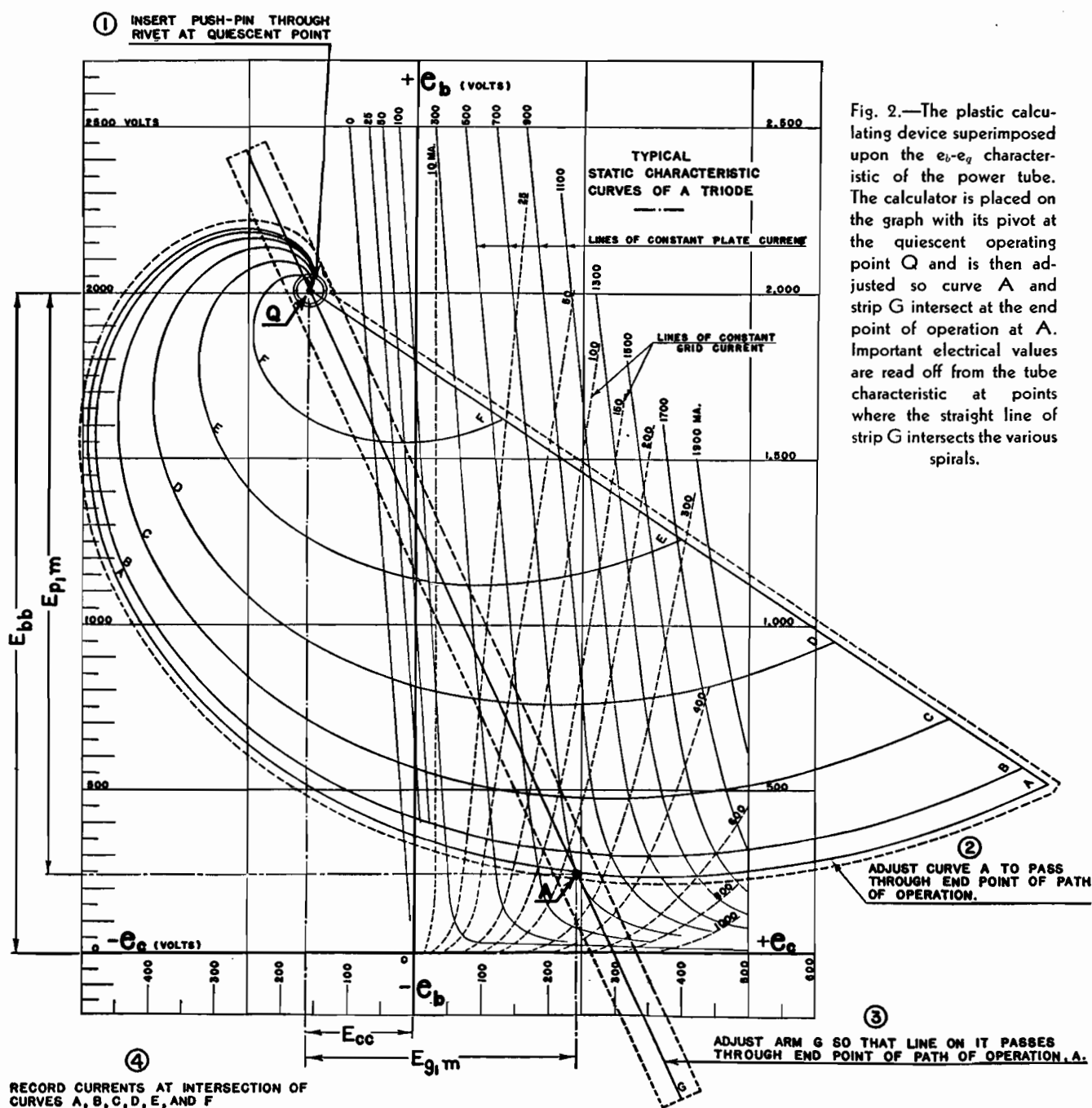


Fig. 2.—The plastic calculating device superimposed upon the  $e_b$ - $e_g$  characteristic of the power tube. The calculator is placed on the graph with its pivot at the quiescent operating point Q and is then adjusted so curve A and strip G intersect at the end point of operation at A. Important electrical values are read off from the tube characteristic at points where the straight line of strip G intersects the various spirals.

a thickness of 0.0030 or 0.0040 in. Its over-all size depends on the size of the sheet on which the static characteristic curves of the tube to be analyzed are plotted. The device is especially adapted for use on the plate voltage-grid voltage characteristics of the tube. These characteristics are often referred to as the  $e_b$ - $e_g$  plane of the tube. When this plane is not available, it may be used in a manner to be described later. If the static characteristics of the tube are plotted on conventional  $8\frac{1}{2}$  by 11 in. paper, the dimensions indicated on Fig. 1 have been found convenient. Lines that are marked A, B, C, D, E, F are drawn or

scratched with a sharp metal object on the surface of the plastic sheet. These lines are spaced in such a way as to divide a straight line passing through Q and any point on the curve A in a definite proportion, depending on the type of analysis used.

A small strip of plastic about  $\frac{1}{2}$  in. wide and 12 in. long, with a straight line ruled down its center, is pivoted to the plastic sheet at Q, as shown in the figure, in such a way that the line on the strip passes through the point Q. This strip is designated G in the figure. A hollow rivet is used in order that a thumbtack or glass push pin may be inserted through the

device at this point. The hole in the rivet should be of the proper diameter to provide a close fit with the shaft of the push pin.

The curves A through F, shown in Fig. 1, may represent any convenient spiral such as  $r = a^\theta - 1$  or  $r = A\theta$  in polar form. The data for these spirals may be calculated from tables available in a standard handbook. In the construction of the series of spirals shown in the figure, the following procedure was used. The curve A was first plotted carefully according to the equation  $R = a^\theta - 1$ , where  $a = 1.68$  for values of  $\theta$  in steps of 10 deg from  $\theta = 0$  to  $\theta = 270$  deg.

Radial lines were drawn from  $Q$  spaced 10 deg apart to facilitate the plotting. The lengths of these radial lines lying between the curve  $A$  and the point  $Q$  were then divided proportionately, in accordance with the schedule given in the figure. The remaining curves  $B$  through  $F$  were then drawn in as shown. The plastic plate was placed over the drawing, and the curves traced on the plate with a sharp pointed scribe. The scratched grooves were filled with black ink. When the thin strip  $G$  with the straight line drawn on it is riveted to the plastic plate, the calculator is ready to use.

### Application of Calculator

An example is shown in Fig. 2 of the way the calculator is used. Representative characteristics of a power tube plotted on the  $e_b e_c$  plane are shown in this figure. The first step in the process of obtaining information for the dynamic characteristics of the tube is to locate a desirable quiescent point on this diagram. This follows from the preselection of the polarizing potentials to be applied to the tube. This will, of course, be done in accordance with the particular conditions and requirements of the problem. The next step is to select several likely positions for the end point of the path of operation. Let point  $A$  of Fig. 2 represent one such end point. Then insert a glass push pin through  $Q$  on the calculator at the quiescent point, so that the calculator is hinged at this point. Adjust curve  $A$  to pass through the end point of the path of operation. Join this point and  $A$  with the line on arm  $G$ . Record both plate and grid currents under the intersection of the line  $G$  and the curves  $A$  through  $F$ . These values may be substituted in the equations of Chaffee, as illustrated in the following example.

### Examples

With the plate polarizing potential  $E_{bb} = 2,000$  volts, and the grid polarizing potential  $E_{cc} = -160$  volts (twice cutoff), the quiescent point  $Q$  is located as shown in Fig. 2. An arbitrary end point  $A^*$  for the path of operation is located as shown in this diagram. It was chosen in this case to be at the intersection of the line  $e_b = e_c = 240$  volts and the line of constant plate current, 700 ma. For this end point the maximum grid excitation voltage  $e_{g1m} = 240 - (-160) = 400$  volts,

and the maximum alternating voltage across the plate tank circuit is  $E_{p1m} = 2,000 - 240 = 1,760$  volts, peak value.

The currents recorded at the intersection of the curves  $A, B, C, D, E$ , and  $F$ , and the line  $G$  for the case shown in Fig. 2 are

Plate Circuit	Grid Circuit
$A = 700$ ma	$A = 235$ ma
$B = 675$ ma	$B = 200$ ma
$C = 575$ ma	$C = 120$ ma
$D = 400$ ma	$D = 40$ ma
$E = 165$ ma	$E = 11$ ma
$F = 2$ ma	$F = 0$ ma

Equations for the currents given by the Chaffee 13-point analysis are as follows:

$$I_{av} = 0.0833(0.5A + B + C + D + E + F) \quad (1)$$

$$I_1 = 0.0833(A + 1.93B + 1.73C + 1.41D + E + 0.52F) \quad (2)$$

$$I_2 = 0.0833(A + 1.73B + C - E - 1.73F) \quad (3)$$

$$I_3 = 0.0833(A + 1.41B - 1.41D - 2E - 1.41F) \quad (4)$$

$$I_4 = 0.0833(A + B - C - 2D - E + F) \quad (5)$$

$$I_5 = 0.0833(A + 0.52B - 1.73C - 1.41D + E + 1.93F) \quad (6)$$

$$I_6 = 0.0833(A - 2C + 2E) \quad (7)$$

$$I_7 = 0.0833(A - 0.52B - 1.73C + 1.41D + E - 1.93F) \quad (8)$$

$$I_8 = 0.0833(A - B - C + 2D - E - F) \quad (9)$$

$$I_9 = 0.0833(A - 1.41B + 1.41D - 2E + 1.41F) \quad (10)$$

$$I_{10} = 0.0833(A - 1.73B + C - E + 1.73F) \quad (11)$$

$$I_{11} = 0.0833(A - 1.93B + 1.73C - 1.41D + E - 0.52F) \quad (12)$$

$$I_{12} = 0.0833(0.5A - B + C - D + E - F) \quad (13)$$

where  $I_{av}$  = average current

$I_1$  = fundamental current

$I_k$  =  $k$ th harmonic current

By inserting in Eq. (1) the plate-current values read from the graph and tabulated above, we obtain the average plate current  $I_{ba} = 0.0833(0.5 \times 700 + 675 + 575 + 400 + 165 + 2) = 180.6$  ma. From Eq. (2) we may obtain the maximum value of the fundamental plate current by similarly inserting the appropriate current recorded above  $I_{p1m} = 0.0833(700 + 1.93 \times 675 + 1.73 \times 575 + 1.41 \times 400 + 165 + 0.52 \times 2) = 310.5$  ma.

From Eqs. (3) through (13) we may obtain in a similar manner the maximum value of any of the harmonics flowing in the plate circuit.

In the grid circuit, the average grid current is obtained through a similar procedure to give  $I_{ca} = 0.0833(0.5 \times 235 + 200 + 120 + 40 + 11 + 0) = 25.3$  ma, and the maximum value of the fundamental grid current is  $I_{g1m} = 0.0833(235 + 1.93 \times 200 + 1.73 \times 120 + 1.41 \times 40 + 11 + 0.52 \times 0) = 117$  ma. Similarly, the harmonic amplitudes in the grid circuit may be calculated.

With this information, the operating characteristics of the amplifier may be calculated as follows: The power output

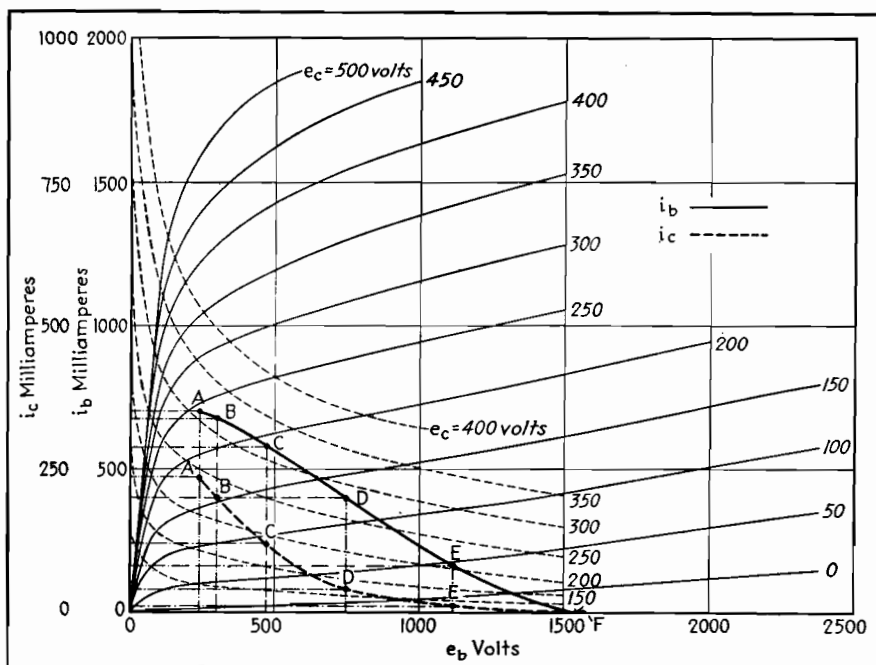


Fig. 3.—A set of static characteristics in the  $i_b$ - $e_b$  and  $i_c$ - $e_b$  planes corresponding to the  $e_b$ - $e_c$  curves of Fig. 2. This type of characteristic can be used with the calculator by converting them to the curves of Fig. 4.

\* At this point the total instantaneous current is  $i_b + i_c = 700 + 235 = 935$  ma. Since the total emission of the filament for this tube is 400 ma, the choice of this operating point represents a factor of safety for the filament of more than 4.



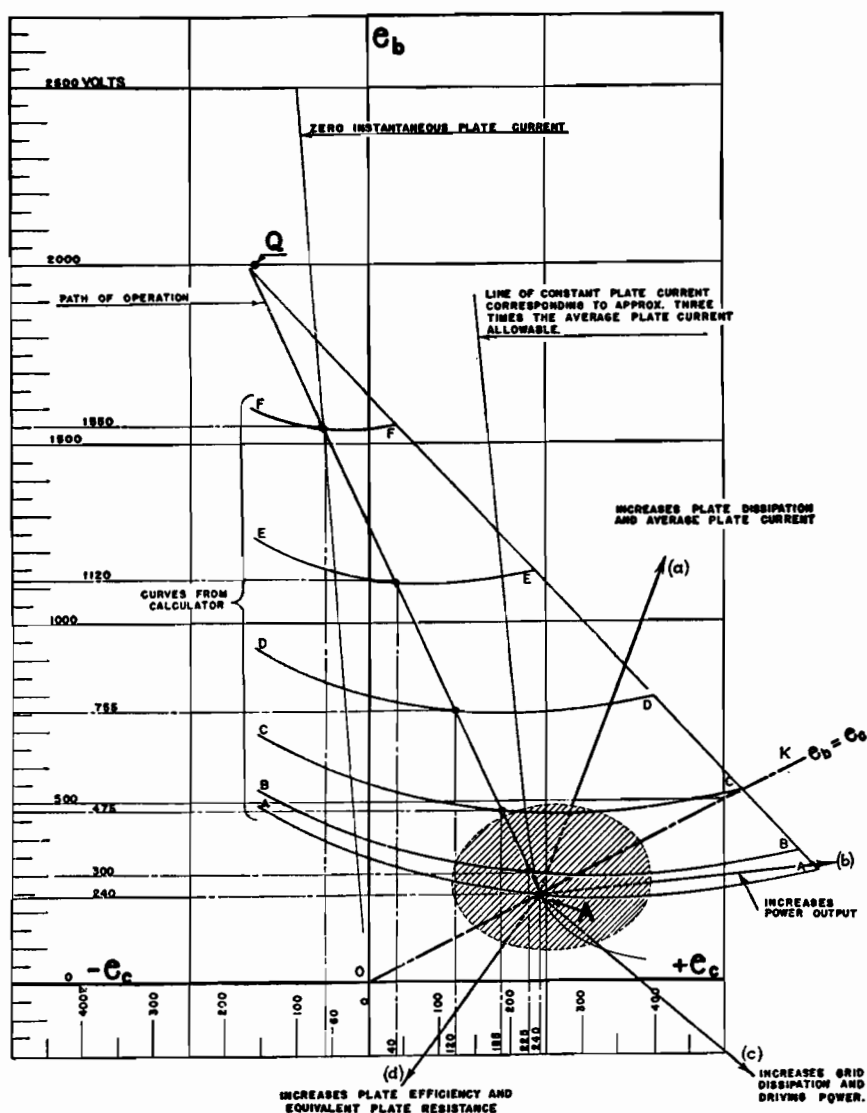


Fig. 4.—Static curves in the  $e_b$ - $e_c$  plane, constructed from Fig. 3, with calculator superimposed. Note the arrows, radiating from point A, indicating means for improving certain types of performance of power tubes.

is given by

$$P_o = \frac{1}{2} E_{p1m} I_{p1m} = \frac{1}{2} \times 1,760 \times 0.3105 = 273 \text{ watts}$$

The d-c power input to the amplifier is  $P_B = E_{bb} I_{ba} = 2,000 \times 0.1806 = 361.2$  watts.

The apparent\* plate dissipation is  $P_p = P_B - P_o = 361.2 - 273 = 88.2$  watts. This value is well within that specified by the manufacturer as the maximum allowable plate dissipation. The plate efficiency is then

$$\eta_p = \frac{P_o}{P_B} \times 100 = \frac{273}{361.2} \times 100 = 75.6 \text{ per cent}$$

The equivalent load resistance  $R_L$  may also be calculated as follows:

\* The true plate dissipation may differ from the apparent plate dissipation because of the existence of secondary emission or ion currents in the tube.

$$R_L = \frac{L_{eff}}{C R_{eff}} = \frac{E_{p1m}}{I_{p1m}} = \frac{1,760}{0.3105} \times 1,000 = 5,680 \text{ ohms}$$

This relation together with that of the effective selectivity ( $Q_{eff} = \omega L_{eff} / R_{eff}$ ) and the frequency desired enables us to calculate the constants for the tank circuit.

In the grid circuit, the driving power is given by

$$P_d = \frac{1}{2} E_{g1m} I_{g1m} = \frac{1}{2} \times 400 \times 0.117 = 234 \text{ watts}$$

The power supplied to the grid resistance to maintain the grid bias, or the power delivered to the grid polarizing source is

$$P_c = E_{cc} I_{cc} = 160 \times 0.0253 = 4.05 \text{ watts}$$

If a grid resistance is used to supply the grid bias, its value is

$$R_{cc} = \frac{160}{0.0253} = 6,320 \text{ ohms}$$

The apparent power dissipated at the grid is  $P_g = P_d - P_c = 23.40 - 4.05 = 19.35$  watts.

Other assumed positions of the end point of the path of operation may be investigated in a similar manner. When the results of these calculations are collected, it is possible to select the conditions that will best meet the requirements of the problem on hand, while keeping within the manufacturer's tube ratings. If complete dynamic characteristics are desired, they may be obtained by calculating the performance data for a number of paths of operation whose end points are evenly spaced over the entire characteristic surface. These data may be prepared as suggested by Chaffee in his discussion of the operating characteristics of power tubes.<sup>2</sup> One will then have available all the information concerning the possibilities of the tube for the given polarizing potentials chosen.

An example of how the calculator may be used when the static characteristics are not available on the  $e_b e_c$  plane, but are available on the  $i_b e_b$  and  $i_c e_b$  planes will be given. For convenience, characteristics for the same tube are used. Naturally the same final results are obtained.

Suppose it is desired to determine the performance of a tube, operating as a class C amplifier, whose static characteristics are shown in Fig. 3. The maximum variations in grid voltage shown in this figure are  $e_c = -100$  volts to  $e_c = +500$  volts, and the plate voltage variations are  $e_b = 0$  to  $e_b = 2,500$  volts. Construct the  $e_b e_c$  axes shown on Fig. 4 on suitable graph paper. The voltage scales for these axes are selected to include at least the maximum voltage variation mentioned above. It is convenient to draw on Fig. 4 the line of zero plate current. This is approximately a straight line passing through the origin of the  $e_b e_c$  plane, having a slope equal to the negative of the amplification factor of the tube.

The manufacturer's specifications for a tube usually give the maximum plate voltage that is permissible in this class of service. Using this value of voltage which is consistent with the requirements of maximum power output and efficiency for the tube, we may now select the grid polarization to be used. This voltage may be chosen as twice the cutoff value.† This establishes the quiescent point, as indicated in Fig. 4.

† The value of twice cutoff, although widely used is not an optimum. Experience with a variety of tubes indicates that 1.6 times cutoff voltage is more nearly correct.

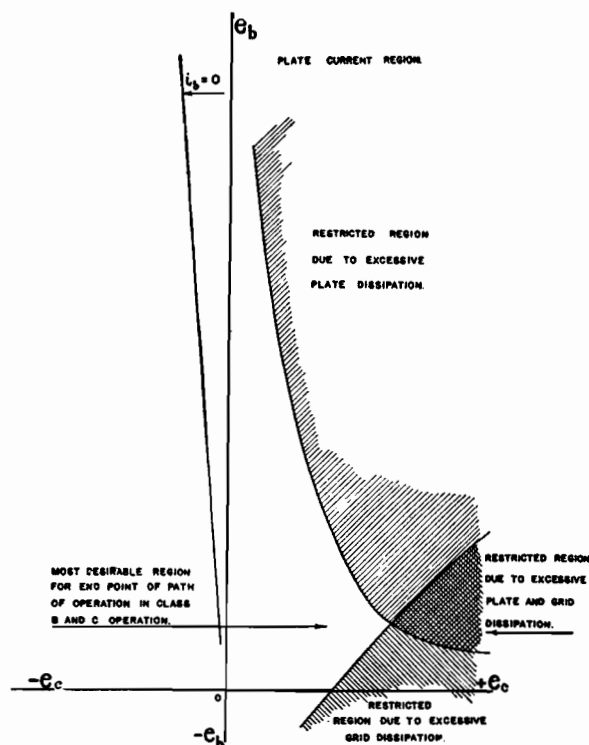


Fig. 5.—Regions of normally restricted operation due to limitations of tube rating.

Construct a line  $OAK$  on the  $e_b e_c$  plane for  $e_b = e_c$ . On this line, indicate the point at which the instantaneous plate current is approximately three times the maximum average plate current allowable. This point will now be used as the end point of the path of operation, as is indicated in Fig. 4. A numerical example will be carried through for this end point. If similar calculations are carried through for others in the neighborhood of this one, the conditions of operation that are best suited to the design requirements and that are within the manufacturer's limitations specified for safe operating conditions may be found. If the above procedure is followed, the operating conditions that will be obtained will be

very nearly the correct conditions for the tube. If, instead of using the line  $e_b = e_c$ , we use a line  $e_b = 0.8e_c$ , it is possible that the power output and efficiency may be slightly better than in the former case.

After adjusting the calculating device as indicated in the previous example, we may tabulate the voltages, both plate and grid, which lie under the intersection of the arm  $G$  and the curves  $A$  through  $F$  as follows:

	$A$	$B$	$C$	$D$	$E$	$F$
$i_b$	240	300	475	755	1120	1550
$i_c$	240	225	185	120	40	-60

At the points indicated in the  $i_b e_b$  diagram (Fig. 3), we may read the instantaneous plate current that exists at these points. Similarly, on the  $i_c e_b$  diagram we may read the instantaneous grid currents.\* For the case illustrated they are

	$A$	$B$	$C$	$D$	$E$	$F$
$i_b$	700	675	575	400	165	2
$i_c$	235	200	120	40	11	0

We may now substitute these instantaneous values of current in the equation given previously and proceed with the calculations in a similar manner to that done in the first example.

The arrow directions shown in Fig. 4 indicate the general way the operating conditions vary as the end point of the path of operation is moved within the region enclosed by the dotted lines. If, for example, efficiency is a primary consideration, we may choose to move  $A$  in the direction  $d$ . This will increase the efficiency and equivalent plate resistance required, but will reduce the power output. There will be but slight effect on the driving power or grid dissipation. If, on the other hand, power output is a primary consideration, we would move  $A$  slightly in the direction  $b$  until the plate or grid dissipation would limit operation. The possible positions that  $A$  may assume on the  $e_b e_c$  plane are restricted by excessive electrode dissipation in the manner indicated qualitatively on Fig. 5.

#### References

- (1) CHAFFEE, E. L., A Simplified Harmonic Analysis, *Rev. Sci. Instruments*, **7**, 384, 1936.
- (2) CHAFFEE, E. L., The Operating Characteristics of Power Tubes, *Jour. Applied Phys.*, **9**, 471, 1938.

\* Note that these values do not form a straight line when plotted in Fig. 3. The difference is, of course, due to the harmonic currents which flow.

## Analysis of Self-biased Modulated Amplifiers

By R. I. SARBACHER

A procedure is given for determining the dynamic characteristics and optimum performance of self-biased modulated amplifiers. The manner in which polarizing voltages vary during tube operation is determined. Improved linearity of circuit operation and reduced peak driving power are shown

THE purpose here is to present a method that is straightforward in approach and that may be extended to other types of resistance bias operation of electron

tubes. Results obtained by this method throw some light on the manner of operation of resistance-biased class C plate-modulated amplifiers.

The method of calculation to be described requires that the complete static characteristics of the tube be available. These may sometimes be

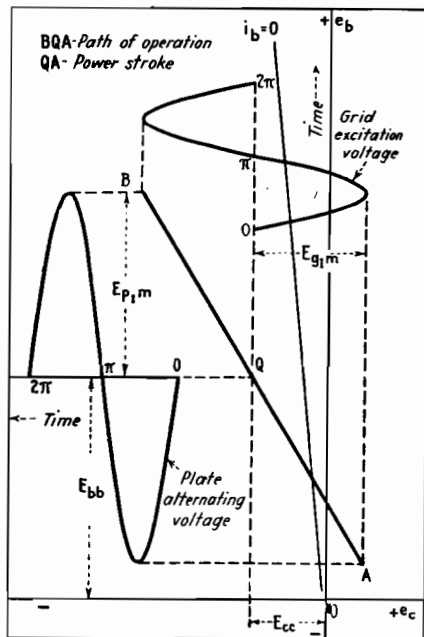


Fig. 1.—Static curves in  $e_b$ - $e_c$  plane showing quiescent point Q, path of operation A-B, and power stroke Q-A.

obtained from the manufacturer or by special techniques described elsewhere.<sup>14,15</sup>

To clarify the treatment that is to follow, it will be well to have clearly in mind what is meant by the path of operation and the power stroke as these terms are applied in class C operation of power tubes. On the  $e_b$ - $e_c$  diagram, the path of operation represents the locus of the instantaneous values of the plate and grid voltages during a complete cycle. If these voltages are sinusoidal and 180 deg out of phase, the path of operation is a straight line having a negative slope, and centered at the quiescent point Q as shown in Fig. 1. The end points for the path of operation are shown as A and B. We are concerned here only with that part of the path of operation between Q and A, called the power stroke, since it is only during this part of the path that plate and grid currents flow.

#### Plate-modulated Tube with Fixed Bias

We shall first consider the conditions that exist in the case where fixed bias is employed in the modulated amplifier. The required characteristics of the power tube, plotted on the  $e_b$ - $e_c$  diagram, are shown in Fig. 2. Under carrier conditions, with no modulation voltage applied, the quiescent point established by the application of the polarizing potentials to the tube is located arbitrarily at  $Q'$ . During the modulation cycle, when generator bias or battery bias is employed, this Q point is constrained to move

vertically up and down as the amplitude of the plate polarizing potential is being changed at an audio rate. The limiting excursions of Q are  $Q'''$  and  $Q''$  when 100 per cent modulation is employed. The calculation of the dynamic characteristics under this condition of operation is straightforward. It is necessary to determine only the end point A of the path of operation for any given position of the point Q on the line joining  $Q'''$  and  $Q''$ . When this information about the position of A is available, the shape of the plate- or grid-current pulse that exists for this path is known. By the application of any of the harmonic analysis techniques, the average or fundamental components of the current pulses may be calculated. The determination of A for any position of Q during the modulation cycle follows from the selection of the grid excitation and the equivalent resistance of the tank circuit. The selection of the grid excitation fixes

A in the horizontal direction. The vertical position of A may be found by first assuming three or four possible vertical positions as indicated by  $A_1$ ,  $A_2$ ,  $A_3$ , and  $A_4$ , as in Fig. 3, for different values of fundamental voltage across the plate tank. For each assumed position of A, we may calculate the fundamental plate current  $I_{p1m}$  by the use of an appropriate harmonic analysis. This may be plotted as a function of  $E_{p1m}$ , as indicated in the lower part of Fig. 3. On the  $I_{b1m}$ - $E_{p1m}$  diagram, lines of constant equivalent resistance of the tank circuit  $(R_b)_\omega = L/RC = E_{p1m}/I_{p1m}$  will appear as straight lines. In Fig. 3 is shown the line corresponding to the particular value of  $(R_b)_\omega = K_1$  chosen for this calculation. The intersection of this line with the curve through the various A points gives the vertical coordinate of the end point,  $A'$  of the path of operation for the particular plate load and  $Q'$  point chosen, as indicated in Fig. 2. By repeating this

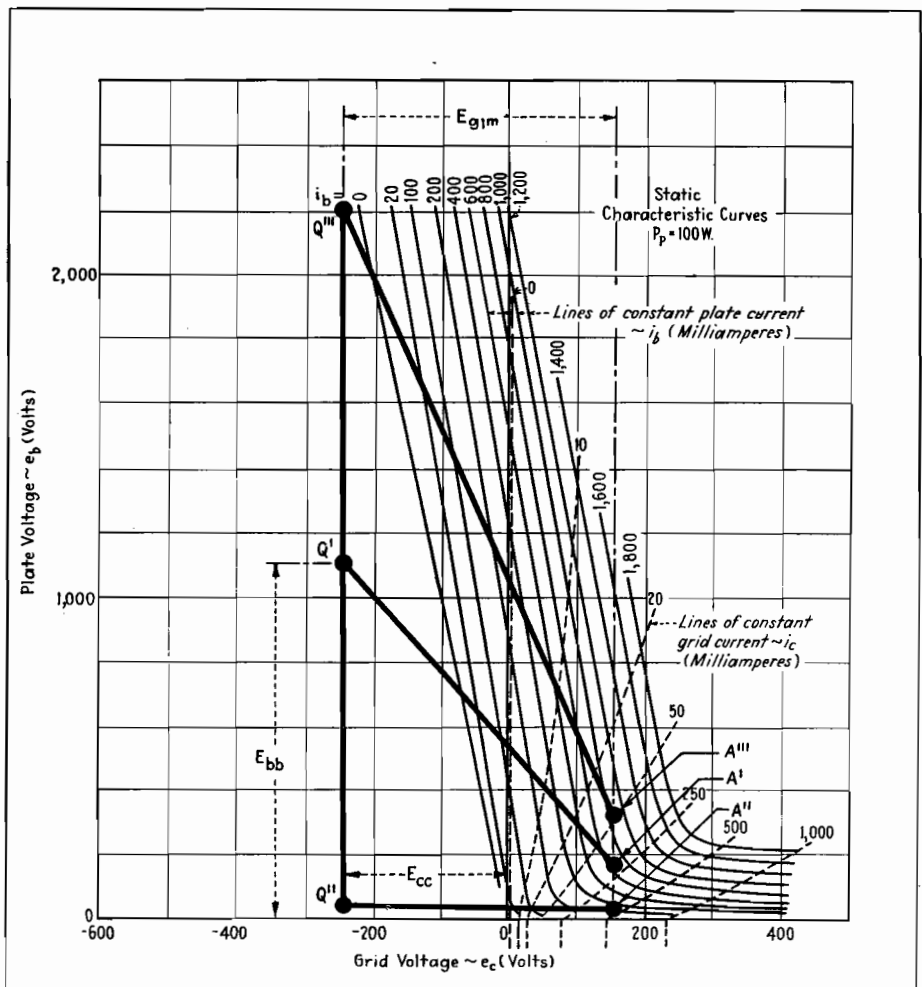


Fig. 2.—Constant plate-current and constant grid-current curves (dotted) of tube whose performance as self-biased plate-modulated amplifier is to be determined. For plate-modulated tube with constant bias, the plate operating point varies between  $Q''$  and  $Q'''$ . Only the power stroke of the path of operation is shown.

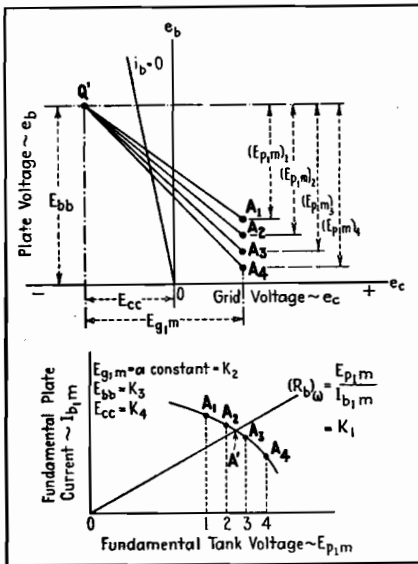


Fig. 3.—For specified plate polarizing voltage, grid bias, and grid excitation voltage, the end point of the operating path  $A'$  is determined by selecting several arbitrary end points  $A_1$  to  $A_4$  (above). These points are plotted on the  $I_{p1m}$ - $E_{p1m}$  plane and a smooth curve drawn through them. The intersection of this curve with the load line  $(R_b)_\omega$  determines the desired end point  $A'$ .

procedure, the fundamental and average currents in both plate and grid circuit may be calculated by this method for different positions of  $Q$ , and the value of  $A$  may be determined for each value of  $Q$  consistent with the requirements of the grid excitation and equivalent plate resistance. Knowing the fundamental and average currents for any  $Q$  and  $A$  points, the power output, driving power, plate efficiency, and other so-called dependent variables of the modulating system may be calculated. Hence, the dynamic characteristics may be determined.

#### Complications of Resistance Bias

When resistance bias is employed, the problem is far more complicated, for the path followed by  $Q$  during the modulation cycle is no longer known. This is because the average grid current that determines the bias is a function of the position of both  $Q$  and  $A$ . Since  $Q$  is not known,  $A$  cannot be determined. For example, if at a given carrier condition (zero modulation) we introduce a resistance of such a value as to replace the generator and supply the same bias as it does, operating conditions at this point will be identical with those obtained with the generator. But if the plate potential is increased or decreased, the movement of the  $Q$  point is dependent on the way the

grid current will vary, consistent with the limitations imposed on the tank circuit equivalent resistance and the excitation. Further, if the bias is supplied by inserting a resistance in the cathode lead, the movement of  $Q$  will depend on the variation of the average plate current in addition to the above. Obviously, the path followed by  $Q$  will be a complex function of at least four independent variables,  $E_{bb}$ ,  $E_{cc}$ ,  $E_{g1m}$ , and  $(R_b)_\omega$ , and in the case where the bias, or part of the bias, is furnished by plate current, by five independent variables, the fifth variable being the bias resistor.

The problem then is to determine the locus which the  $Q$  point takes during the excursion of the plate voltage in the modulation cycle. Once this locus is determined for the particular grid excitation, equivalent plate resistance, and biasing resistance that are chosen and fixed for this calculation, the position of  $A$  could be determined for any  $Q$  point along this path in a manner similar to that outlined above. However, in order to find the path that  $Q$  follows in the case of resistance biasing, it is necessary first to find the coordinates of  $A$  for any likely position of  $Q$  during the modulation cycle. The positions that  $A$  is likely to take can certainly be restricted to that portion of the  $e_b e_c$  plane to the right of the  $e_c = 0$  axis and above the  $e_b = 0$  axis, in Fig. 3.

When these coordinates of  $A$  are found, the problem is greatly simplified, as will be shown.

Now, for any position of  $Q$  on the  $e_b e_c$  plane (Fig. 2), the horizontal coordinate of  $A$  is fixed by the choice of the grid excitation voltage. The vertical coordinate of  $A$  can be determined for any given equivalent plate resistance in the following manner. First we select an arbitrary position for  $Q$  for a given value of plate polarizing potential  $E_{bb}$ , and a specified value of the grid polarizing potential  $E_{cc}$  the value of the grid excitation  $E_{g1m}$  remaining fixed. For this  $Q$  point we may calculate the fundamental plate current amplitude as a function of the fundamental voltage across the plate tank circuit in a manner similar to that employed in the case of generator bias. For the tube whose characteristics are shown in Fig. 2, and for operating voltages  $E_{bb} = 900$  volts,  $E_{cc} = -50$  volts, the curve obtained is that labeled  $E_{cc} = -50$  volts in Fig. 4. Other curves like this may be obtained by holding the plate polarizing potential  $E_{bb}$  fixed at 900 volts and increasing the grid polarizing potential  $E_{cc}$  negatively in steps of 50 volts. These curves take the form of the family of curves shown in Fig. 4. Lines of constant plate resistance may now be drawn on this diagram. For example, the dashed line (Fig. 4)

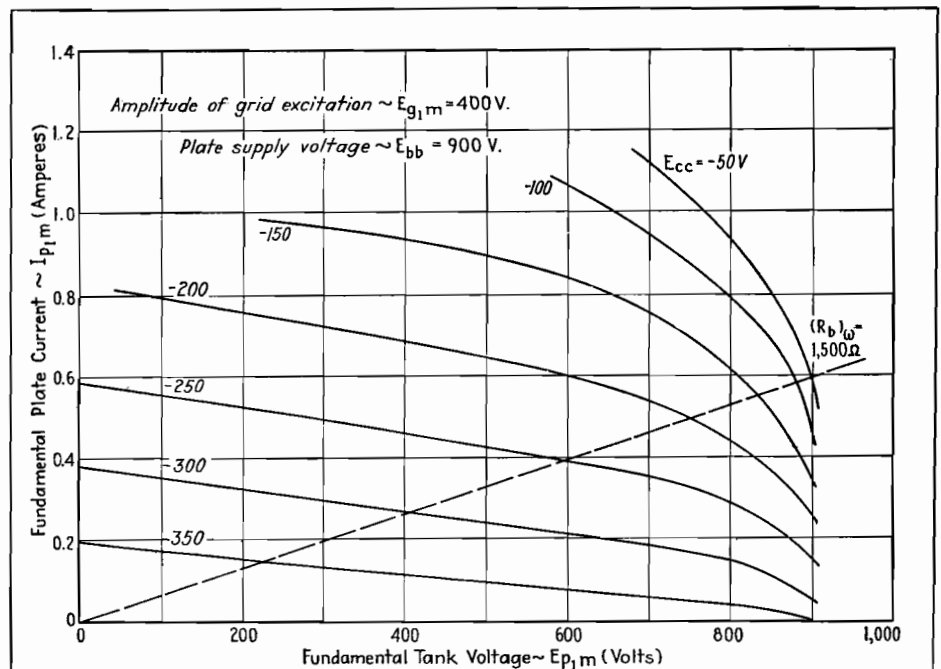


Fig. 4.—Graphical plot of end points of the path of operation. Each curve, for different value of grid bias, is determined in the same manner as the curve in the lower half of Fig. 2. The intersection of the plate load line with the family of curves permits the determination of data for one curve of those shown in Fig. 4. Several such diagrams are required, each for the same grid excitation but for different values of plate voltage.

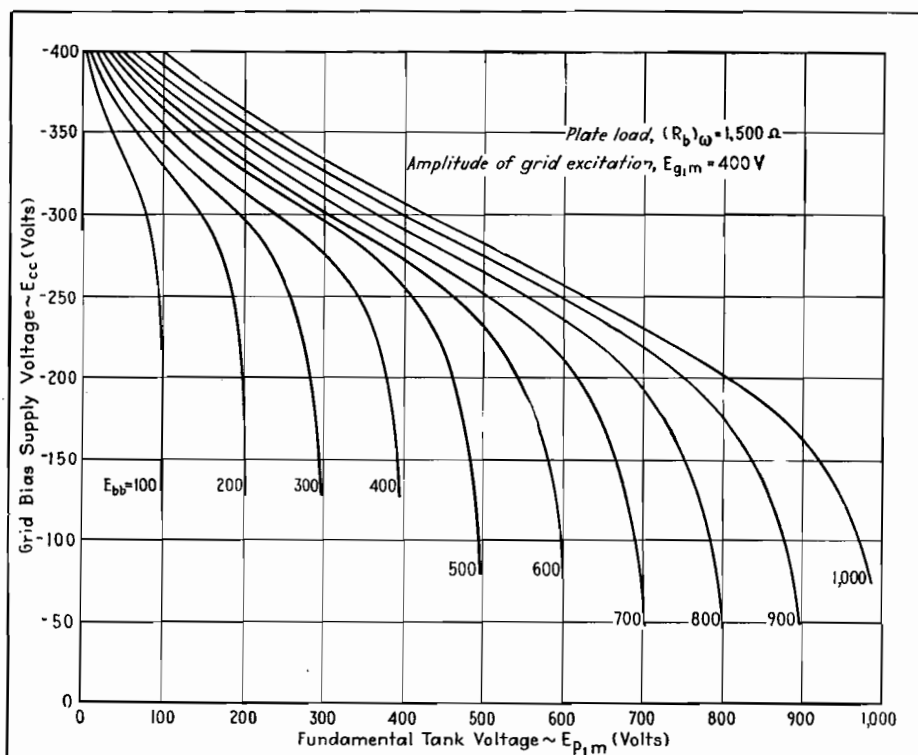


Fig. 5.—For constant plate and grid excitation, this family of curves (each one of which is derived from a family like those of Fig. 3) shows the relation between grid bias and alternating voltage across the tank circuit.

represents a constant equivalent resistance  $(R_b)_\omega = 1,500$  ohms. Diagrams similar to this one are obtained for a number of values of plate polarizing potential, and on each the same line of constant equivalent plate resistance is drawn.

For various values of plate voltage the intersection of the lines of constant grid voltage,  $E_{cc}$  with the line of constant plate resistance  $(R_b)_\omega$  may be plotted on a diagram having the coordinates of Fig. 5. These curves of Fig. 5 may, in turn, be transferred to the  $e_b e_c$  plane. When this is done, they take the form indicated by the red curves in Fig. 6. Actually Fig. 5 is only an intermediate diagram which is convenient to use in order to obtain the material represented on Fig. 6.

#### Tube Operation for Fixed-bias Plate-modulated Conditions

When the family of curves of Fig. 6 representing lines of constant  $E_{p1m}$  have been obtained and plotted on the  $e_b e_c$  diagram, the problem is almost solved. It is convenient to draw the family of curves  $E_{p1m} = \text{constant}$  on transparent or translucent paper rather than to plot them directly on the  $e_b e_c$  diagram so that they may be superimposed on the curves of Fig. 2, as shown in Fig. 6. From the

superimposed curves we know the value of  $E_{p1m}$  that must be used for any arbitrarily chosen  $Q$  point. For any  $Q$  point in the region to the left of  $e_c = 0$  and above  $e_b = 0$ , both horizontal and vertical coordinates of  $A$  are now determined, since the assumed grid excitation gives the horizontal distance of  $A$  from the  $Q$  point while the value of  $E_{p1m}$  on which the  $Q$  point falls as read from the curves gives the vertical distance.

An example will help clarify the procedure. The derived curves are superimposed on the constant current static curves. A point  $Q'$  is arbitrarily selected at  $E_{bb} = 1,200$  volts and  $E_{cc} = -250$  volts. This  $Q'$  point cuts the derived curves at  $E_{p1m} = 600$  volts, and the excitation voltage was taken as  $E_{g1m} = 400$  volts. Then, with  $Q'$  as the starting point, the coordinates of  $A'$  are  $e_b = E_{bb} - E_{p1m} = 1,200 - 600 = 600$  volts, and  $e_c = E_{cc} + E_{g1m} = -250 + 400 = +150$  volts.

#### Effect of Resistance Bias

We have not yet taken into account the effect of resistance bias, which is the final step in the analysis. The value of the bias voltage will depend on the value of the bias resistor and its location in the circuit. It will also depend on the average grid current in the case of grid

bias or on the average cathode current in the case of cathode bias. For triodes, the cathode current is the sum of the grid and plate currents. Accordingly, the next step in the analysis is to determine the average value of the grid bias voltage for the possible methods of resistance bias. To determine this bias voltage, we must first determine the average current, flowing through the bias resistance. If it is entirely in the grid circuit, we are interested in determining only the grid current, whereas if it is in the cathode circuit, both grid and plate current must be known.

To determine the average currents, we use paths of operation such as the one mapped out between  $Q'$  and  $A'$  (Fig. 6). We may select the  $Q$  points for these paths at regular intervals in the region defined by the curves of Fig. 6. In the present calculation, these points were selected at the intersection of lines drawn at 50-volt intervals through the grid axis and 100-volt intervals through the plate axis. The paths of operation for each of these  $Q$  points were drawn in accordance with the previous discussion. After the paths have been determined, the calculation of the current follows. This calculation is greatly facilitated through the use of a plastic calculating device described in another article.<sup>16</sup> After obtaining the average currents, they may be plotted as a function of the grid polarizing voltage for constant values of the plate polarizing potential. These polarizing voltages correspond, of course, to the coordinates of  $Q$  for which a given current calculation was made.

#### Bias Resistance in the Grid Circuit

When the bias resistance is in the grid circuit, it is only necessary to calculate, for the various paths of operation chosen, the average grid current  $I_{ca}$ . This is plotted as a function of  $E_{cc}$  on Fig. 7, for various values of plate polarizing potential  $E_{bb}$ . From this figure we can determine the locus followed by  $Q$  on the  $e_b e_c$  diagram for any given grid biasing resistance in the following way. Since the bias resistance is entirely in the grid circuit, the grid polarizing potential is given by

$$E_{cc} = I_{ca} R_{cc}$$

where  $R_{cc}$  is the grid resistance. This equation, when plotted on the  $I_{ca} E_{cc}$  diagram, appears as a straight line passing through the origin, having a slope equal to  $1/R_{cc}$ . Two such lines corresponding to two values of  $R_{cc}$  are

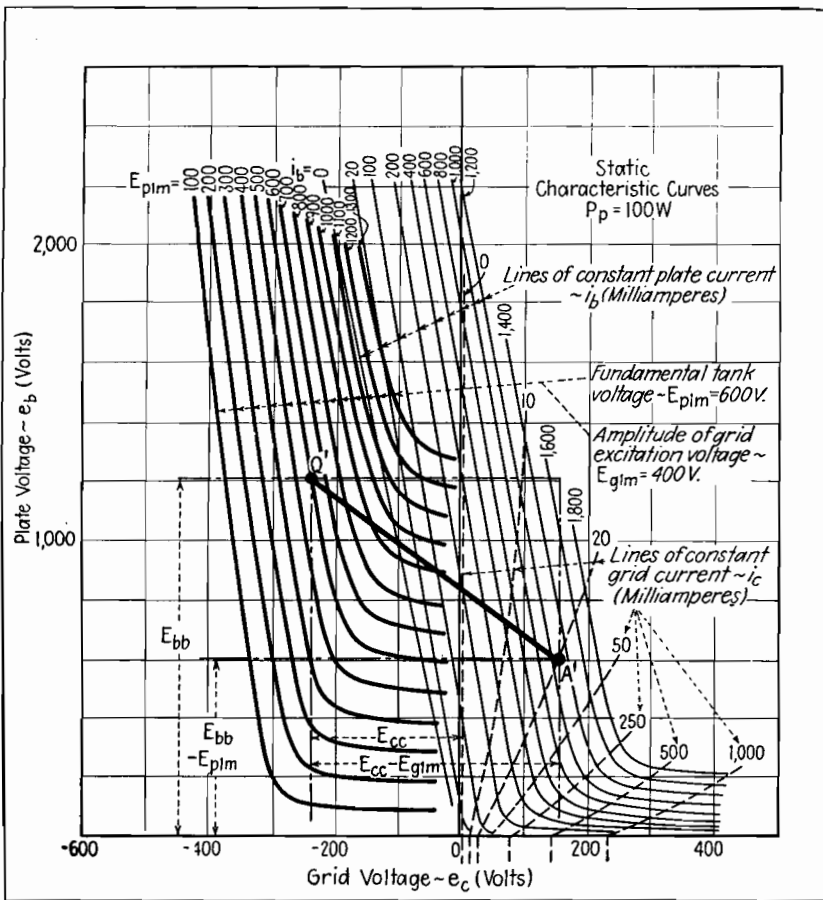


Fig. 6.—Curves of Fig. 4 replotted on the  $e_b$ - $e_c$  plane (heavier) and superimposed on the original constant current curves of Fig. 1. The composite set of curves enables the end point A' to be determined for any Q' point, for the grid excitation voltage, constant grid bias, and plate load  $(R_b)_\omega$ , assumed for this calculation.

shown on Fig. 7. The intersections of one of these lines with the lines of constant plate voltage determine the grid polarizing potentials that must be developed across  $R_{cc}$  for the given grid excitation voltage and equivalent plate resistance  $(R_c)_\omega$  which were chosen and fixed for this calculation. These intersections may be plotted on the  $e_b$ - $e_c$  plane, and thus determine the locus of the Q point during the modulation cycle for this value of grid resistance. When this locus has been obtained, the calculation of the complete dynamic characteristics may proceed directly. A number of Q points are selected, evenly spaced, along this locus. For each of these Q points the coordinates of the A points are defined. The horizontal distance from Q to A is given by the grid excitation, and the vertical distance from Q down to A is given by the curves of Fig. 6. Thus the paths of operation for any Q on the locus are obtained. For these paths the average grid current, average plate current, fundamental grid current, and fundamental plate current may be calcu-

lated, using the plastic device. Knowing these currents together with  $E_{bb}$ ,  $E_{cc}$ ,  $E_{g1m}$ ,  $E_{p1m}$ , and  $R_{cc}$ , the power relations in the modulator may be calculated from the relations:

$$\text{Driving power, } P_d = \frac{1}{2} I_{g1m} E_{g1m}$$

$$\text{Power input, } P_B = I_{ba} E_{bb}$$

$$\text{Power output, } P_b = \frac{1}{2} I_{p1m} E_{p1m}$$

$$\text{Power delivered to grid resistor,}$$

$$P_{rec} = I_{ca}^2 - I_{ca} E_{cc}$$

$$\text{Grid dissipation, } P_g = P_d - I_{ca} E_{cc}$$

$$\text{Plate dissipation, } P_p = P_B - P_b$$

Determination of these quantities for each of the Q points selected along the locus gives the complete dynamic characteristics of the modulator. Other characteristics may be obtained by selecting a different value of  $R_{cc}$ , and a family of dynamic characteristics showing the effect of a variation of this parameter may be calculated.

#### Bias Resistance in Both the Plate and Grid Circuits

When the bias resistance is in both the plate and grid circuits, it is necessary to

calculate both the average grid current  $I_{ca}$  and the average plate current  $I_{ba}$  for the various paths of operation. The sum of these currents ( $I_{ba} + I_{ca}$ ) may then be plotted as a function of  $E_{cc}$  for the various values of  $E_{bb}$  selected. Lines of constant cathode resistance  $R_{bc} = E_{cc} / (I_{ba} + I_{ca})$  may be drawn on this diagram and will appear as straight lines. The intersection of any one of these straight lines with the lines of constant plate voltage  $E_{bb}$  will determine the coordinates of the path followed by Q during the modulation cycle, on the  $e_b$ - $e_c$  diagram. When this locus of Q is found for the desired cathode resistance, the remaining problem of obtaining the dynamic characteristics for the modulator is again straightforward.

With any point on this path as a Q point, the coordinates of the end point for the path of operation passing through this Q are known as in the preceding case. That is, the horizontal coordinate of A is given by the grid excitation, as measured from Q, and the vertical coordinate of A is given by the curve passing through this Q. This vertical coordinate will be given in terms of the maximum fundamental plate voltage  $E_{p1m}$  of course, and thus will represent the vertical distance in volts below Q to the point A. Hence we may calculate for the path joining this Q and A the fundamental plate and grid currents from which may be determined, together with the average plate and grid current which we already know, all the dependent variables associated with this

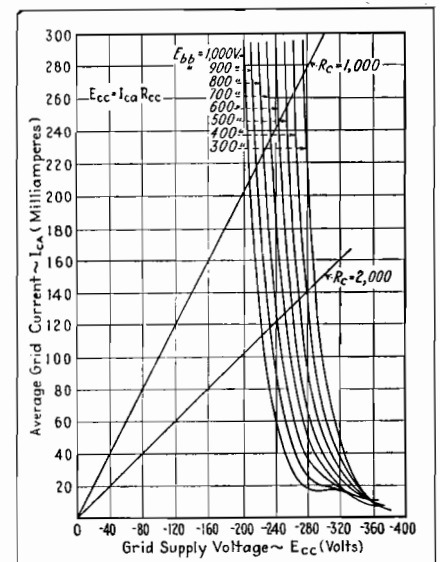


Fig. 7.—Family of curves for different values of plate polarizing voltage, plotted on grid voltage—average grid current characteristics. From this diagram on which grid resistance  $R_c$  appears on a straight line, the paths followed by Q in the  $e_b$ - $e_c$  plane can be determined.



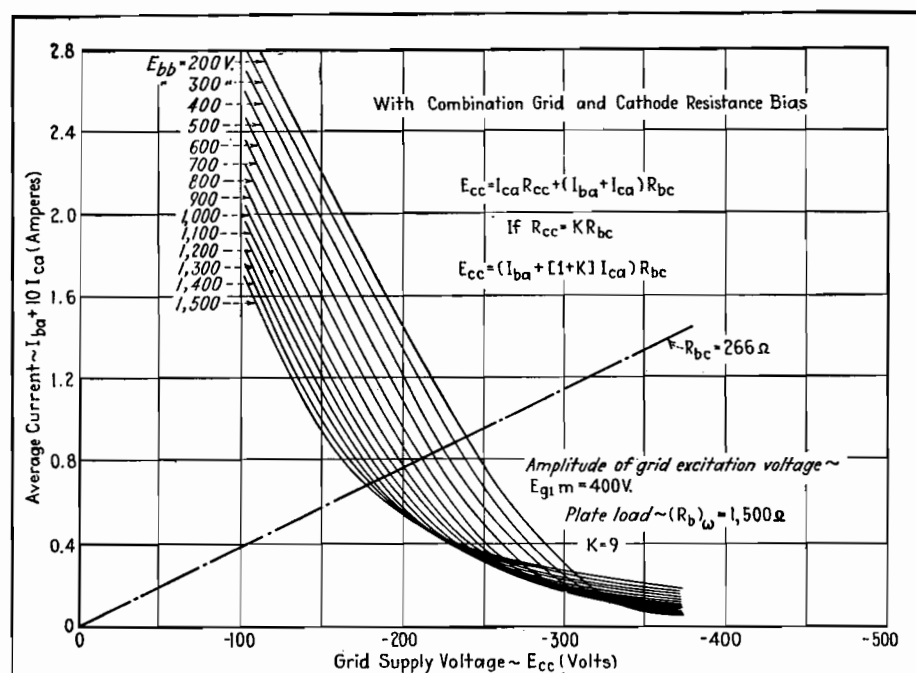


Fig. 8.—Family of plate polarizing voltages for combined grid and cathode resistance bias. In this diagram, it has been assumed that  $R_{cc} = 9R_{bc}$ .

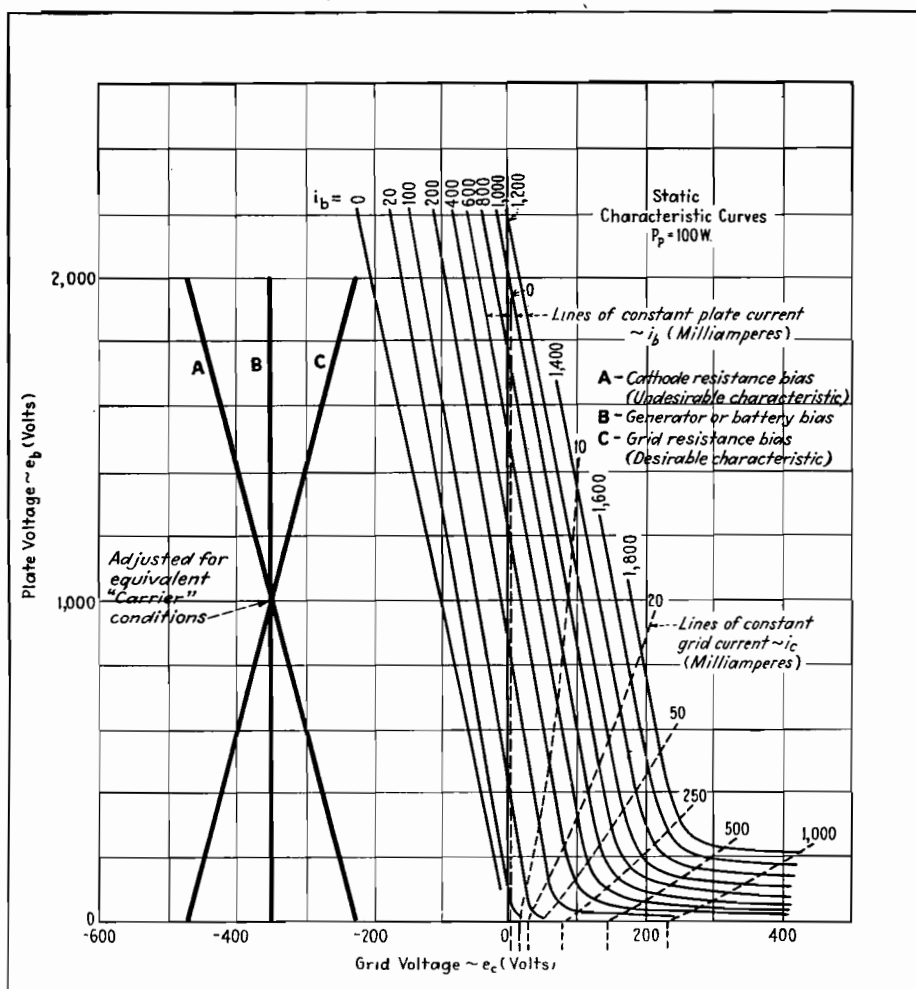


Fig. 9.—Characteristic paths of the Q point for various methods of bias. Curve A is for cathode resistance bias and is the least desirable type of resistance bias. Curve B is for constant grid voltage bias. Curve C, which represents the most desirable type of resistance bias, is for the bias resistance in the grid circuit.

condition of operation. By repeating this process for other selected  $Q$  points along this locus, the complete dynamic characteristics of the modulator are determined.

These dynamic characteristics apply, of course, only for the specific cathode resistance chosen. Families of characteristics may be obtained by choosing other values of cathode resistance, as in the case discussed previously. The power relations in the modulator are slightly modified by the cathode resistor. The quantities  $P_d$ ,  $P_b$ ,  $P_B$ , and  $P_o$  are the same but the other relations are

Power delivered to cathode resistor,

$$P_{bc} = (I_{ba} - I_{ca})^2 R_{bc}$$

Plate dissipation,

$$P_p = P_B - P_b - I_{ba}^2 R_{bc}$$

**Bias Resistance Partly in the Grid and Partly in the Plate Circuits**

If the biasing resistance is partly in the cathode circuit and partly in the grid circuit, the calculation is somewhat more involved since there are two resistances  $R_{cc}$  and  $R_{bc}$ . Here the grid polarizing voltage is given by

$$E_{cc} = I_{ca}R_{cc} + (I_{ba} + I_{ca})R_{bc}$$

Let us set

$$R_{cc} = kR_{bc}$$

where  $k$  is a positive constant greater than zero. Then

$$E_{cc} = [I_{ba} + (1 + k)I_{ca}]R_{bc}$$

and the polarizing grid voltage is again expressed in terms of only one resistor. It is, therefore, evident that if  $I_{ba} + (1 + k)I_{ca}$  is plotted as a function of  $E_{cc}$  we shall be able to determine the path followed by  $Q$  in a manner similar to that used in the case of grid bias alone or plate bias alone. An example of this plot when  $k = 9$  is shown in Fig. 8. The intersections of line  $R_{bc} = 266$  ohms with the lines of constant  $E_{bb}$  give the values of  $E_{cc}$  that will determine the locus of the  $Q$  point under this condition of operation. Families of characteristics may be obtained for various values of  $k$ .

The power relations under this condition of operation are also modified slightly from those forms as given under grid-bias operation. The quantities  $P_d$ ,  $P_b$ , and  $P_B$  remain the same, but the other relations are

Power delivered to grid resistor,

$$P_{cc} = I_{ca}^2 R_{cc}$$



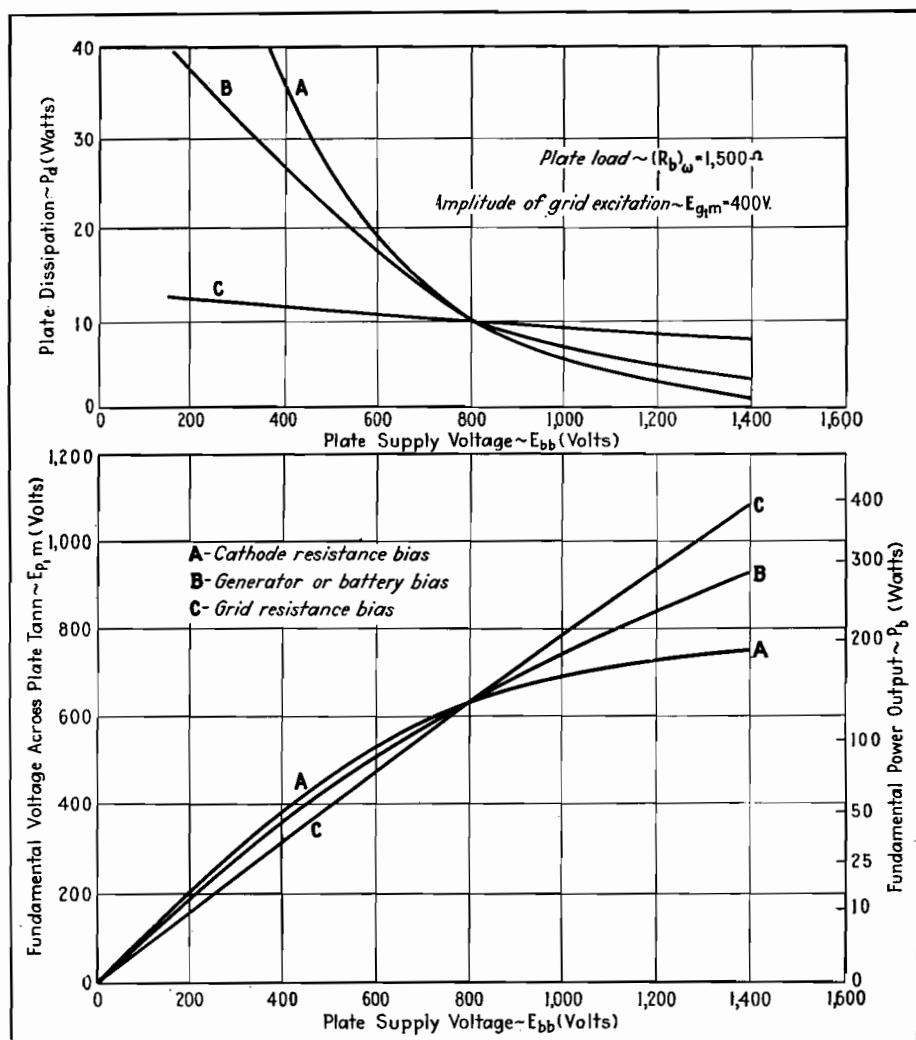


Fig. 10.—Dynamic characteristics for plate modulated amplifier, for three types of biasing conditions. Most desirable characteristic is that for which power output is linearly proportional to d-c plate voltage and maximum driving power is a minimum.

Power delivered to cathode resistor,

$$P_{bc} = (I_{ca} + I_{ba})^2 R_{bc}$$

Plate dissipation,  $P_p = P_B - P_{ba}^2 R_{bc}$

Grid dissipation,

$$P_g = P_d - I_{ca}^2 R_{cc} - I_{ca}^2 R_{bc}$$

#### Combination Bias

In the case of part-battery and part-resistance bias, the lines for constant resistance may be drawn on any of these average current vs. grid voltage diagrams depending on the location of the bias resistance. The procedure is to draw the lines of constant biasing resistance through the zero current axis at the value of  $E_{cc}$  corresponding to the battery voltage. The intersection of this line with the lines of constant plate voltage determines the path, as in the previous cases.

#### Characteristics of Various Bias Methods

Since the locus of  $Q$  can be found for any combination of self-biasing or battery and resistance-biasing combination, a complete solution of the problem is at hand. The effect on this locus of different conditions of service are shown in Fig. 9. This illustrates the paths followed by the  $Q$  point on the  $e_b e_c$  plane during the modulation cycle for three different types of biasing. Curve A is for cathode bias alone, curve B is for battery bias alone, and curve C is for grid resistance bias alone. The system is here adjusted for equivalent carrier conditions in order to make the comparison of the different types of biasing more effective. Curve C, which is shown below to be the most desirable, may be obtained by part-battery and part-grid-resistance bias, or part-cathode resistance and part-grid-resistance bias.

The effect on the dynamic modulation characteristics for these three paths is indicated in Fig. 10. We can see that the path C is by far the most desirable, since it improves the linearity of the modulation process, increases the power output, and reduces the driving power. Further, the driving power is less peaked, while the change in efficiency is but slightly effected. Hence, it is desirable to use grid resistance bias entirely. For tube protection, however, it is sometimes desirable to use a certain amount of generator or cathode resistance bias. Path A, for the case of cathode bias alone, gives most unfavorable results, reducing the linearity while, at the same time, increasing the grid driving power and reducing the power output and efficiency. However, it is found that by using an amount of cathode bias sufficient to protect the tube, and the remaining bias supplied by the grid current alone, it is possible to approximate the condition indicated in C with only a slight sacrifice in efficiency. Or if part-battery bias and part-grid-resistance bias are used, these conditions may be approximated more easily. Complete dynamic characteristics for every condition of operation are, therefore, made available.

#### Bibliography

- (1) NOYES, A., A Sixty-cycle Bridge for the Study of Radio Frequency Power Amplifiers, *Proc. IRE*, **23**, 785, 1935.
- (2) CHAFFEE, E. L. and KIMBALL, C. N., A Method of Determining the Operating Characteristics of a Power Oscillator, *Jour. Franklin Inst.*, **221**, 237, 1936.
- (3) CHAFFEE, E. L., Power Tube Characteristics, *Electronics*, July, 1937, p. 30.
- (4) CHAFFEE, E. L., The Operating Characteristics of Power Tubes, *Jour. Applied Phys.*, July, 1938.
- (5) FAY, C. E., The Operation of Vacuum Tubes as Class B and Class C Amplifiers, *Proc. IRE*, **20**, 548, 1932.
- (6) EVERITT, W. L., Optimum Operating Conditions for Class C Amplifiers, *Proc. IRE*, **22**, 152, 1934.
- (7) THERMAN, F. E., and FERNS, J. H., The Calculation of Class C Amplifier and Harmonic Generator Performance of Screen-grid and Similar Tubes, *Proc. IRE*, **22**, 359, 1934.
- (8) MILLER, B. F., An Analysis of Class B and Class C Amplifiers, *Proc. IRE*, **23**, 496, 1935.
- (9) BABITS, V. A., Les Methodes Graphiques pour Determiner les Elements des Amplificateurs de Haute Frequence Class B et C, *L'Onde Electrique*, **14**, 668, 1935.
- (10) EVERITT, W. L., Optimum Operating Conditions for Class B Radio-frequency Amplifiers, *Proc. IRE*, **24**, 305, 1936.
- (11) THERMAN, F. E., and ROAKE, W. C., Calculation and Design of Class C Amplifiers, *Proc. IRE*, **24**, 620, 1936.
- (12) WAGENER, W. G., Simplified Methods for Computing the Performance of Transmitting Tubes, *Proc. IRE*, **25**, 47, 1937.
- (13) CHAFFEE, E. L., Power Tube Characteristics, *Electronics*, July, p. 30, 1937.
- (14) KOZANOWSKI, H. N., and MOUROMTSEFF, I. E., Vacuum Tube Characteristics in the Positive Grid Region by an Oscillographic Method, *Proc. IRE*, **21**, 1082, 1933.
- (15) CHAFFEE, E. L., A Method of Obtaining the Static Characteristic Curves of Power Tubes, *Electronics*, June, 1938, p. 34 (reprinted in this book).
- (16) SARBACHER, R. I., A Mechanical Device for Calculation of Class B and C Amplifier Performance, *Electronics*, December, 1942, p. 52.

Design for Exponential Horns of Square Cross-section . . .	Page 302
Chart of VU-DB Relationships . . . . .	303
DB Ruler for Christmas-tree Patterns on Records . . . . .	304

# Design for Exponential Horns of Square Cross-section

By GEORGE H. LOGAN

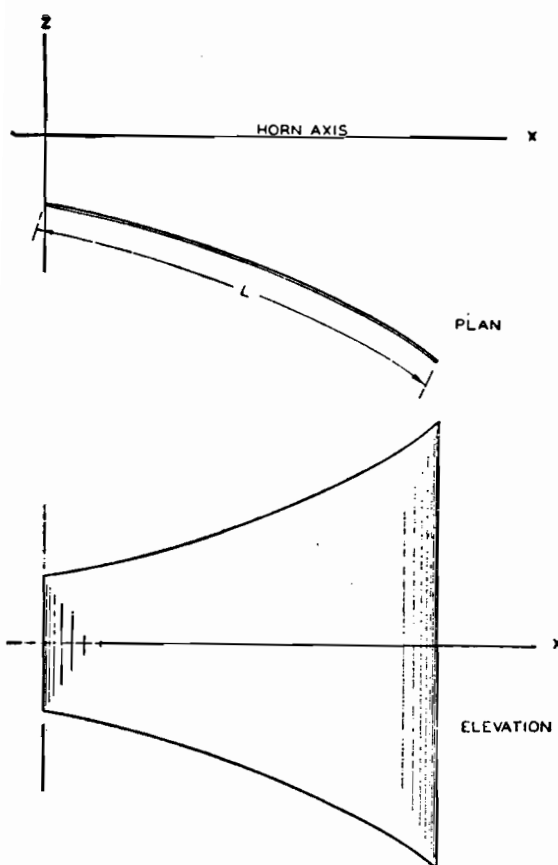


Fig. 1.—Side view and elevation of one side of exponential horn of square cross section.

THE sides of an exponential horn are commonly cut from sheet metal, the layout being effected with the aid of a cardboard template. The projected view of one side, bent into shape for assembly, is shown in Fig. 1. If the elevation view were flattened out to lie in a plane, its appearance would be identical to that of the template.

For any distance  $x$  on the horn axis, there is a corresponding length of template  $L$  and a corresponding template width  $2y$ . Hence, if we derive the expressions  $y = f_1(x)$  and  $L = f_2(x)$ , we can determine the template width and length in terms of the  $x$  dimension.

The cross-sectional area of an exponential horn, at any point on the axis

$A_x$ , is given by

$$A_x = A_0 e^{Bx} \quad (1)$$

in which  $A_0$  is the area at the throat of the horn,  $B$  is the flare constant, and  $x$  is the distance from the throat of the horn. If the horn is of square cross-section, then

$$A_x = (2y)^2 \quad (2)$$

and to obtain the relation between  $x$  and  $y$  we substitute Eq. (2) into Eq. (1), obtaining

$$y = \frac{\sqrt{A_0}}{2} e^{\frac{Bx}{2}} = k e^{bx} = f_1(x) \quad (3)$$

in which  $k = A_0^{1/2}/2$ , and  $b = B/2$ .

It now remains to determine  $f_2(x)$ , and this may be done by methods of the calculus. The general expression for the incremental length of the curve is

$$dL = [(dx)^2 + (dy)^2]^{1/2} \quad (4)$$

From Eq. (3) we find that  $dy = b k e^{bx} dx$ , and consequently the length of the horn template is given by

$$L = \int (1 + b^2 k^2 e^{2bx})^{1/2} dx \quad (5)$$

By making the proper substitutions and simplifications, it can be shown that the solution of Eq. (5) is

$$L = \frac{1}{b} \left( U + 1.1513 \log_{10} \frac{U-1}{U+1} \right) - \frac{1}{b} \left( u + 1.1513 \log_{10} \frac{u-1}{u+1} \right) = f_2(x) \quad (6)$$

in which  $U = (1 + b^2 k^2 e^{2bx})^{1/2}$ , and  $u = (1 + b^2 k^2)^{1/2}$ .

Thus, Eqs. (3) and (6) give the width and length relations, respectively, corresponding to any abscissa  $x$  on the horn axis for an exponential horn of square cross-section. The use of these equations in the making of suitable templates can best be illustrated by means of an example.

For a particular type of horn, the design constants were  $k = 7.5$  and  $b = 0.0274$ , and the maximum axial length was

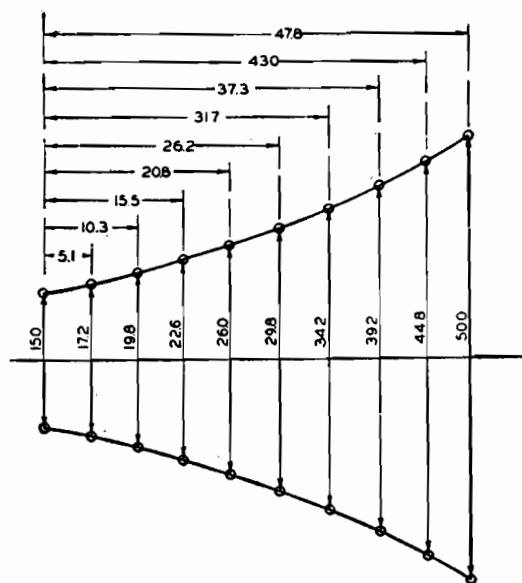


Fig. 2.—Template for exponential horn of square cross section laid out in accordance with the equations derived in this article.

$x_{\max} = 44$  in. Substituting these values in Eq. (3) gives

$$y = 7.5 e^{0.274 \times 44}$$

where  $e = 2.718 \dots$ . The solution of this equation, which gives the semi-width of the mouth of the horn, is  $y = \text{antilog}_{10} [\log_{10} (7.5) + (0.0274) (44) \log_{10} 2.718] = \text{antilog}_{10} 1.39866 = 25.0$  in. Consequently, the width of the horn at the mouth is  $2y$ , or 50.0 in.

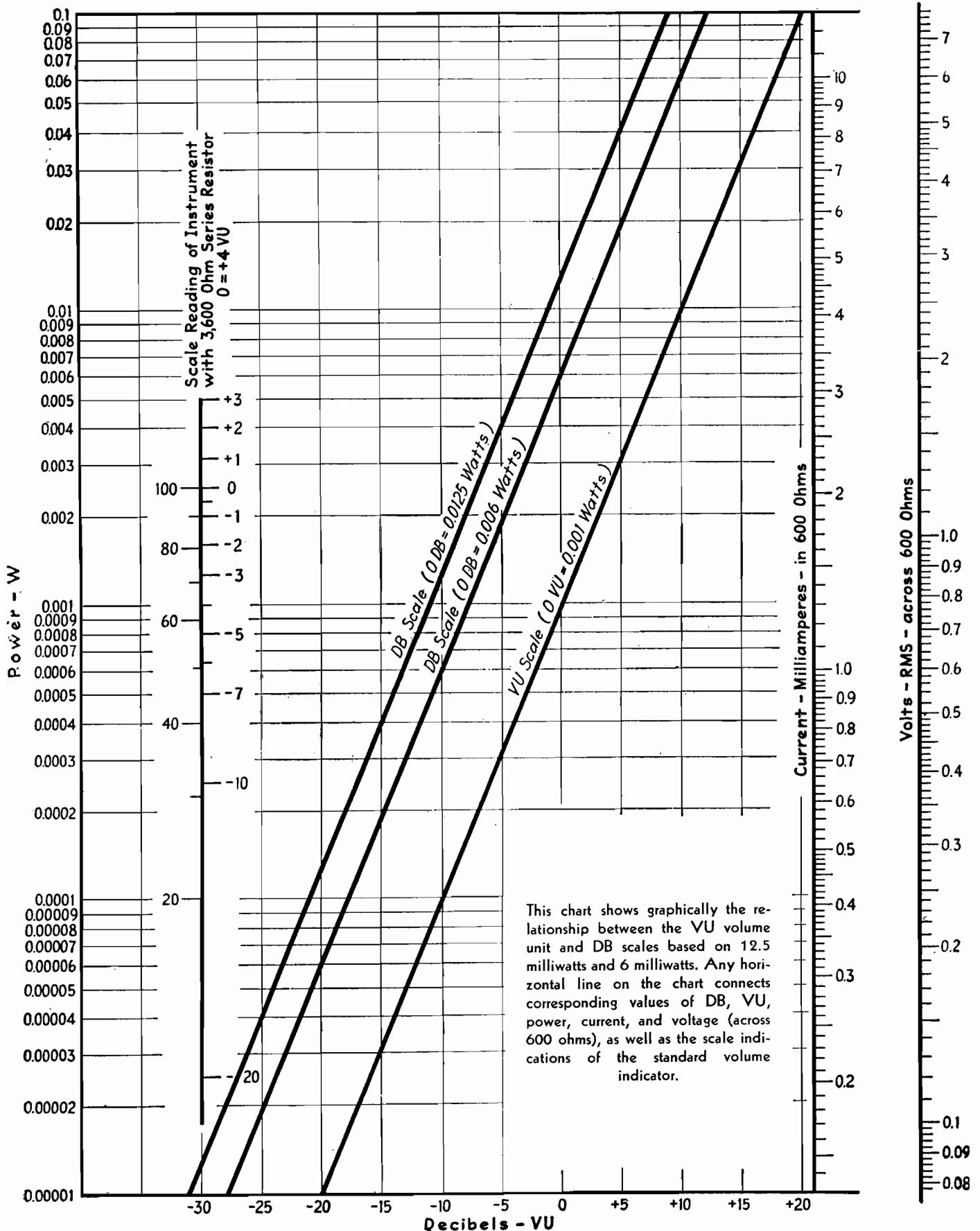
The over-all length of the template, corresponding to  $x_{\max}$ , is  $L_{\max}$  and is given by Eq. (6). Using the constants specified, we find that  $U = \sqrt{1.47039} = 1.2126$ , and  $u = \sqrt{1.0422} = 1.0208$ . Therefore,

$$L_{\max} = \frac{1}{0.0274} \left( 1.2126 + 1.1513 \log_{10} \frac{0.2126}{2.2126} \right) - \frac{1}{0.0274} \left( 1.0208 + 1.1513 \log_{10} \frac{0.0208}{2.0208} \right) = 1.569 + 46.255 = 47.8 \text{ in.}$$

In a similar manner, progressive values of  $x$  between 0 and 44 in. are chosen, and the corresponding values of  $y$  and  $L$  are computed from Eqs. (3) and (6). With a series of such values available, the template (Fig. 2) may be laid out.

# Chart of VU-DB Relationships

By FRANK B. HALES



# DB Ruler for Christmas-tree Patterns on Records

By DON R. KING

In checking the response of a recording system, it is convenient to have a measuring rule that will convert the width of the Christmas-tree diffraction pattern directly into decibels above or below a known reference. The response curve can thus be plotted quickly

IN testing instantaneous recording equipment for over-all frequency response, it has become quite a common practice to use the diffraction pattern method. In this method a record is cut, using an oscillator or other source of constant voltage input, and cutting a series of different frequencies at a constant input level. If the record thus cut is held so that parallel beams of light strike the surface at a considerable angle, the reflected light forms a pattern, the width of which is directly proportional to the velocity of the stylus at that point. The width of the pattern is also a measure of the absolute value of the velocity and thus the cutting level.

It is customary in analyzing this pattern to measure the width with a caliper or ruler at the different points of interest and to convert the resulting ratios into decibels or volume units in order to interpret the results properly. This procedure is much simplified by the use of a simple scale, which is illustrated here, on which the pattern width reads directly in decibels. By this means the frequency characteristic may be interpreted at a glance, and in addition the actual level of the cut is known.

The scale is constructed by the use of the equation

$$V = \frac{W\pi N}{60}$$

where  $V$  = velocity of the stylus, cm per sec

$N$  = number of revolutions of turntable per minute

$W$  = width of pattern, cm

The zero point of the decibel scale has been set at the point corresponding to a stylus velocity of 6.35 cm per sec (2.5 in. per sec). This figure is the generally accepted standard recording level, and the scale then indicates the variation referred to this standard.

The scale may be drawn on a heavy piece of paper, or, if a more substantial one is wanted, the graduations may be scratched on a strip of celluloid. It is possible to obtain inexpensive celluloid rules that have printed metric divisions, and the values given in the accompanying table may be scratched on the ruler, using the printed markings on the rule

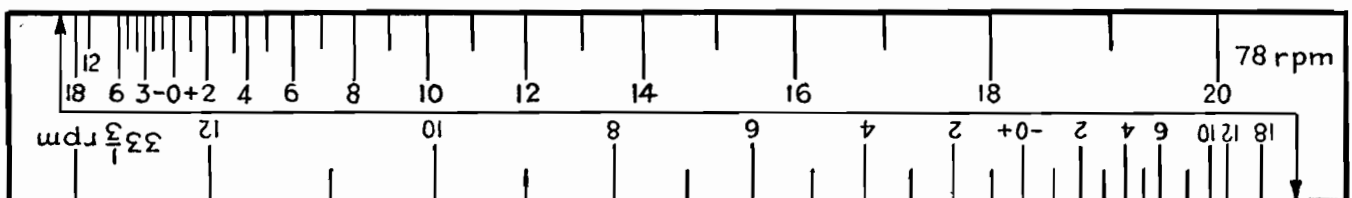
itself for measurements. The original markings may then be removed with emery cloth and the scratches filled with white wax crayon.

While the diffraction pattern method of measurement is more suited to constant-velocity records, the scale may also be applied to constant-amplitude records. In this case, it must be remembered that the velocity is directly proportional to frequency, and the pattern width, instead of being constant, should increase 6 db per octave. In using the scale, the 1,000 cycle band should measure 0 db and each octave above or below should differ by 6 db.

Values Used in Ruler Scales

Db/Vu	Velocity, cm/sec	Pattern width, cm 78 rpm	Pattern width, cm 33 $\frac{1}{3}$ rpm	Db/Vu	Velocity, cm/sec	Pattern width, cm 78 rpm	Pattern width, cm 33 $\frac{1}{3}$ rpm
-18	0.79	0.20	0.46	+ 5	11.3	2.76	6.46
-12	1.59	0.39	0.91	+ 6	12.7	3.11	7.28
-10	2.00	0.49	1.15	+ 7	14.2	3.48	8.14
- 8	2.54	0.62	1.45	+ 8	15.9	3.91	9.14
- 6	3.18	0.78	1.82	+ 9	17.9	4.39	10.3
- 5	3.57	0.88	2.05	+10	20.3	4.90	11.5
- 4	4.00	0.98	2.30	+11	22.6	5.53	12.3
- 3	4.50	1.10	2.58	+12	25.4	6.22	14.5
- 2	5.08	1.24	2.89	+13	28.4	6.95	16.3
- 1	5.65	1.39	3.24	+14	31.8	7.79	18.2
0	6.35	1.55	3.64	+15	35.7	8.75	20.5
+ 1	7.12	1.75	4.08	+16	40.6	9.82	23.0
+ 2	8.00	1.96	4.58	+17	45.0	11.0	25.8
+ 3	8.97	2.20	5.15	+18	50.8	12.4	28.9
+ 4	10.16	2.48	5.78	+19	56.5	13.9	32.4
				+20	63.5	15.5	36.4

Referred to standard recording level of 6.35 cm/sec (2.5 in./sec)



The arrow at the end of the scale is placed at one edge of the diffraction pattern. The other edge then falls opposite the recording level in db present in that portion of the pattern.

## SECTION XXIII

# TELEVISION, FREQUENCY MODULATION, AND FACSIMILE

	Page
Shunt-peaking Compensation for Video Amplifiers.....	305
Television Definitions and Design Equations.....	307
Influence of Feedback in Video Amplifiers.....	309
Single-inductor Video Coupling Networks.....	311
Frequency-deviation Measurements of F-m Transmitters.....	317
Facsimile Design Chart.....	319

## Shunt-peaking Compensation for Video Amplifiers

By WILLIAM H. FREEMAN

A graphical method of determining the shunt inductance in the plate circuit of a wide-band video amplifier, in terms of the resistance and capacitance present and the required upper frequency limit. Useful in television and similar applications

THE advent of television has brought into considerable prominence the problem of wide-band amplifiers. Other fields, such as facsimile and transient-phenomena amplifiers, however, find uses for wide-band amplifiers. Previous to the popularization of television, little was published in the way of design data for these amplifiers. The purpose of this chart is to give design data so that wide-band amplifiers having an upper cutoff frequency from 0.15 to 15 Mc may be designed with the minimum amount of time and effort.

Figure 1 shows the basic shunt-peaked circuit used for the computation of the chart data. The capacitance  $C$  is the sum of the output capacitance of tube  $V_1$ , the input capacitance of tube  $V_2$ , and the distributed capacitance of the wiring between the two tubes.

In designing a wide-band amplifier, the cutoff frequency  $f$  is known. Next, the shunt capacitance is measured or estimated, depending on the accuracy of correction desired. Then, knowing the shunt capacitance and the cutoff frequency, the value of  $R_0$  can be found from

the formula

$$R_0 = \frac{1}{2\pi fC} \quad (1)$$

where  $f$  is the cutoff frequency. Next, the peaking inductance  $L_0$  can be calculated using the formula

$$L_0 = 0.5CR_0^2 \quad (2)$$

These two formulas were used in constructing the accompanying chart.

For best time delay characteristics, Eqs. (1) and (2) should be slightly different, as follows:

$$R_0 = 0.85X_c \quad (3)$$

$$\text{and } L_0 = 0.415CR_0^2 \quad (4)$$

These equations, however, have the disadvantage that the load resistor is lower than in Eqs. (1) and (2), which means that the gain through a single stage will be reduced about 15 per cent on all frequencies.

To use the chart, proceed in the following manner. (1) Decide on the cutoff frequency. (2) Measure or in some way ascertain the shunt capacitance. With these two values, locate the corre-

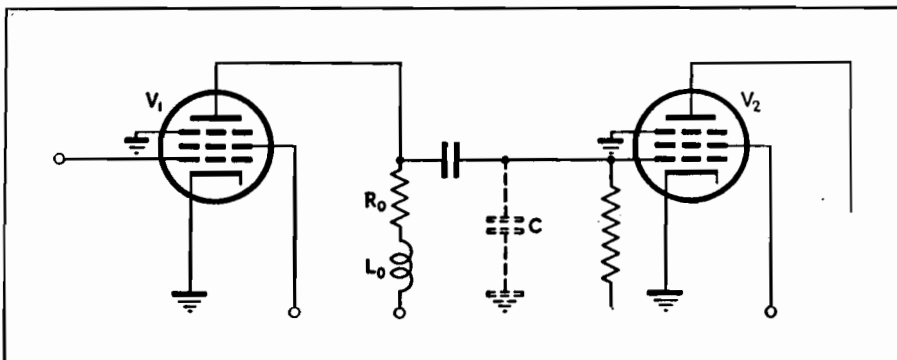
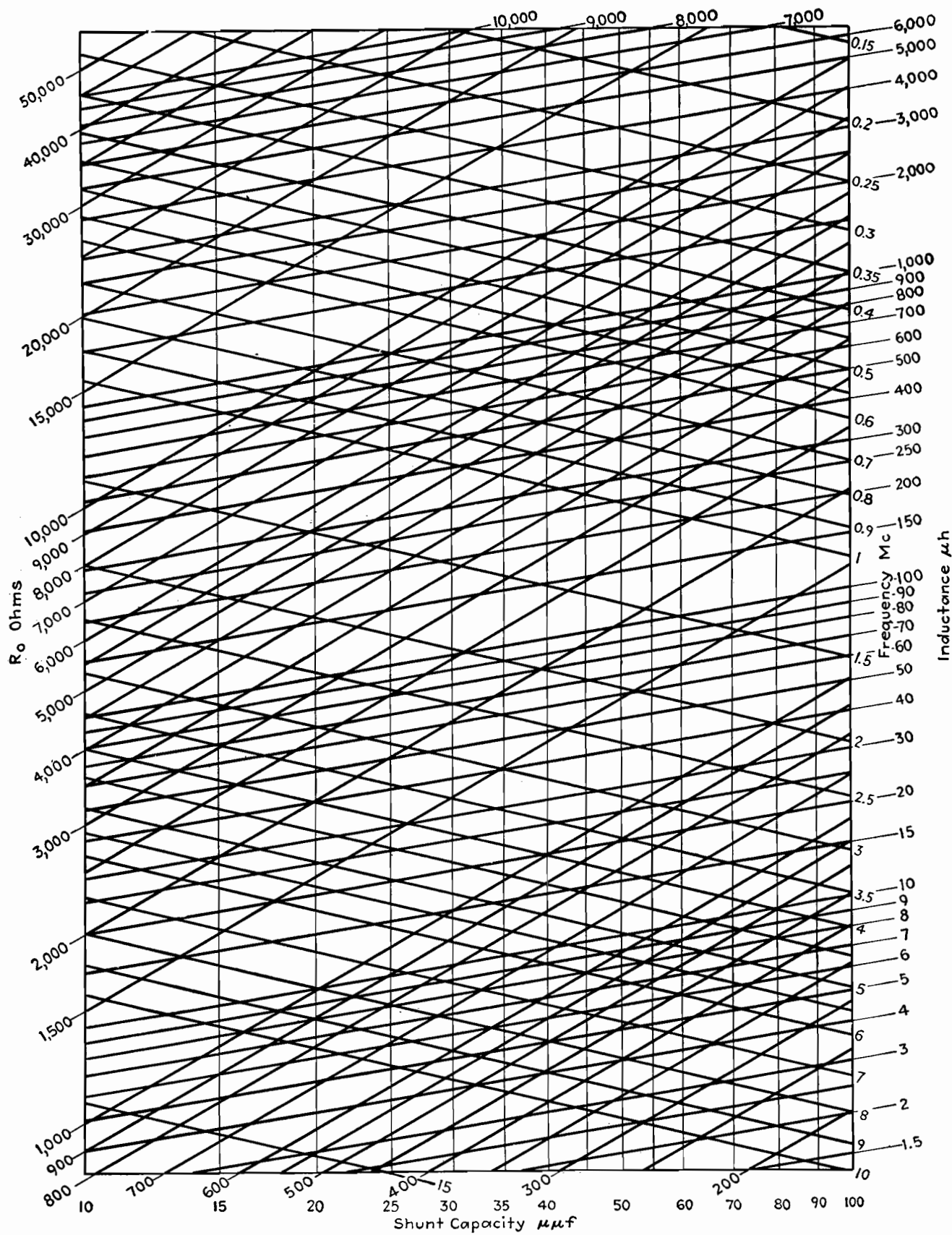


Fig. 1.—Basic shunt-peaking compensated amplifier circuit.



sponding point on the chart. From this point, by following the proper lines the values of  $R_0$  and  $L_0$  can be found. For example, let us assume some values for  $C$ , the shunt capacitance and the cutoff frequency. Let the value of  $C$  be  $35 \mu\text{f}$  and the cutoff frequency be 3 Mc. From the point on the chart we see that  $R_0$  is 1,500 ohms and  $L_0$  is  $40 \mu\text{h}$ .

The frequency range selected for the chart, 0.15 to 15 Mc, includes all video frequencies with sufficient leeway on the higher frequencies to permit its use in special applications. Although transformers can be had that will give very excellent performance up to 200,000 cycles, the price of these units sometimes limits their use. Therefore, the limit of 0.15 Mc was chosen to include uses that

might require the frequency range to hold out to 0.2 Mc, but in which transformers might either be too expensive or undesirable.

While the chart was originally made to determine  $R_0$  and  $L_0$ , it may be used in other ways. It will give directly the reactance of capacitors between 10 and  $100 \mu\text{f}$  at any frequency in the range of the chart. Also, if any two of the four values indicated on the chart  $R_0$ ,  $L_0$ ,  $C$  and frequency are known, the other two may be found.

The basis of the shunt-peaking compensation system is the effect of the tuned circuit formed by  $L_0$  and  $C$ . The resonant frequency of this combination is chosen, in accordance with Eqs. (1) and (2), at a value 1.41 times the fre-

quency  $f$  to which uniform gain is required. At this resonant frequency, the combination  $L_0$ - $C$ , being a parallel circuit, tends to produce a high impedance in the plate circuit of the tube, and consequently the gain of the stage is proportionately increased. This increase in gain offsets the loss in gain due to the shunting effect of the shunt capacitance  $C$ , and at the frequency  $f$  the two effects just balance one another.

#### Bibliography

- (1) SEELEY and KIMBALL, Analysis and Design of Video Amplifiers, *RCA Rev.*, October, 1937, p. 171.
- (2) PREISMAN, Some Notes on Video-Amplifier Design, *RCA Rev.*, April, 1938, p. 421.
- (3) SEELEY and KIMBALL, Analysis and Design of Video Amplifiers, Part II, *RCA Rev.*, January, 1939, p. 290.
- (4) FREEMAN, R. L., and SCHANTZ, Video Amplifier Design, *Electronics*, August, 1937, p. 22.

## Television Definitions and Design Equations

By DONALD G. FINK

### Image Analysis

- $d_c$  critical viewing distance, beyond which structure of picture is not evident.
- $f$  frame repetition rate, number of complete pictures per second.
- $f'$  field repetition rate, number of interlaced fields per second.
- $h$  height (in.) of the reproduced picture.
- $k$  utilization ratio, relating vertical definition to number of scanning lines (values range from 0.75 to 1.0).
- $k_h$  ratio of horizontal retrace scanning velocity to horizontal active scanning velocity.
- $k_v$  ratio of vertical retrace scanning velocity to vertical active scanning velocity.
- $N$  total number of picture elements in picture (contained in all active scanning lines).
- $n$  total number of lines in the scanning pattern, from beginning of one frame to beginning of the next frame.
- $n_a$  number of lines actively employed in reproducing the image, equal to  $n$  less the number of lines produced during vertical retrace scanning motion.
- $R$  rate (per sec) of scanning of picture elements.
- $w$  width of reproduced picture in same units as  $h$ .

Critical viewing distance

$$d_c = \frac{3,450h}{(kn_a)} \text{ in.} \quad (1)$$

NOTE: Equation based on visual acuity of 1 min of arc.

Number of picture elements per picture

$$N = \frac{w}{h} k^2 n_a^2 \quad (2)$$

Number of active scanning lines per frame

$$n_a = n \frac{1}{1 + 1/k_v} \quad (3)$$

Rate of scanning picture elements

$$R = \frac{w}{h} k f n^2 \left( \frac{1 + 1/k_h}{1 + 1/k_v} \right) \text{ elements per sec} \quad (4)$$

### Television Camera

- $A_p$  area (sq ft) occupied by a particular picture element on photosensitive camera surface, equal to picture area divided by  $N$  [Eq. (2)].
- $E_p$  illumination (foot-candles) falling on that particular picture element.
- $\Delta f$  total range of frequency (cycles) occupied by television signal [see Eq. (14)].
- $R$  resistance (ohms) across which output signal voltage is developed.
- $R_n$  signal-to-noise ratio (noise in rms volts) across resistance  $R$ .
- $S$  sensitivity ( $\mu\text{a}$  per lumen) of photosensitive surface, corresponding to color of light on picture element considered.
- $V_s$  output signal voltage, storage-type camera (iconoscope).
- $V_i$  output signal voltage, nonstorage type (image dissector).

Storage camera output

$$V_s = S N E_p A_p R \mu\text{v, for particular picture element considered} \quad (5)$$

NOTE: Assumes storage for one frame only, at 100 per cent efficiency.

Nonstorage camera output

$$V_i = S E_p A_p R \mu\text{v for particular element considered} \quad (6)$$

Signal-to-noise ratio

$$R_n = \frac{V}{\sqrt{1.6 \times 10^{-20} R \Delta f}} \quad (7)$$

NOTE:  $V$  may be  $V_s$  or  $V_i$  depending on type of camera considered. Temperature of resistor  $R$  is taken at  $20^\circ\text{C}$ .

### Electron Beams

- $c$  speed of light,  $3.0 \times 10^{10}$  cm per sec.
- $D$  distance (cm) from screen end of deflecting field to fluorescent screen.
- $d_e$  distance (cm) of deflection, measured on screen from axis of electron gun, for electric deflection.
- $d_m$  distance (cm) of deflection, measured on screen from axis of electron gun, for magnetic deflection.
- $e/m$  charge-to-mass ratio of electron,  $5.3 \times 10^{17}$  esu per gram (electric units), or  $1.7 \times 10^7$  emu per gram (magnetic units).
- $H_d$  strength of magnetic deflecting field, emu.
- $l$  length (cm) of deflecting field measured along axis of electron gun.
- $s$  separation (cm) between deflecting plates.



$v$  velocity of electrons in electron beam, component along axis of gun.  
 $V_d$  deflection voltage, volts.  
 $V_a$  accelerating (second anode) voltage, volts.

Electron velocity

$$v = c \sqrt{1 - \frac{1}{[V_a e / (300 m c^2) + 1]^2}} \text{ cm/sec} \quad (8)$$

NOTE: This equation takes into account the increase in electron mass with velocity, which cannot be neglected for  $V_a$  above 2,000 volts.  $e/m$  in electric units.

Electric deflection

$$d_e = \frac{V_{dle}}{30 s v^2 m} (D + \frac{1}{2} l) \text{ cm} \quad (9)$$

NOTE: Ratio  $e/m$  in electric units.

Magnetic deflection

$$d_m = \frac{H D l e}{m v} \text{ cm} \quad (10)$$

NOTE: Approximate equation, true when  $l$  is small compared with radius of deflection path within field. Ratio  $e/m$  in magnetic units.

#### Fourier Series of Wave Forms

$f$  fundamental frequency of the wave in cycles ( $1/f$  equals duration of 1 cycle).  
 $n$  order of the final harmonic in the series.  
 $t$  time, sec.  
 $V(t)$  the wave function; over-all peak-to-peak amplitude is unity.

Square wave:

$$V(t) = \frac{2}{\pi} \left( \frac{\sin 2\pi f t}{1} + \frac{\sin 2\pi 3 f t}{3} + \frac{\sin 2\pi 5 f t}{5} + \dots + \frac{\sin 2\pi n f t}{n} \right) \quad (11)$$

NOTE:  $n$  odd only; origin at center of wave.

Ideal saw-tooth wave (zero retrace time):

$$V(t) = \frac{1}{\pi} \left( \frac{\sin 2\pi f t}{1} - \frac{\sin 2\pi 3 f t}{2} + \frac{\sin 2\pi 5 f t}{3} - \frac{\sin 2\pi 7 f t}{4} + \dots \pm \frac{\sin 2\pi n f t}{n} \right) \quad (12)$$

NOTE: Even-order harmonics plus, odd-order minus. Origin at center.

Nonideal saw-tooth wave (finite retrace time):

$$V(t) = \frac{1}{\pi^2(p - p^2)} \left( \frac{\sin \pi p}{1} \sin 2\pi f t + \frac{\sin 2\pi p}{4} \sin 2\pi 2 f t + \frac{\sin 3\pi p}{9} \sin 2\pi 3 f t + \frac{\sin n\pi p}{n^2} \sin 2\pi n f t \right) \quad (13)$$

NOTE:  $p$  is the ratio of the duration of the forward trace to the duration of the complete cycle. Origin at center.

#### Video Amplification

$C$  (see figures for capacitance values).  
 $C_{gk}$  grid-cathode capacitance ( $\mu\text{mf}$ ) of tube.  
 $C_{pk}$  plate-cathode capacitance ( $\mu\text{mf}$ ) of tube.  
 $C_{gp}$  grid-plate capacitance ( $\mu\text{mf}$ ) of tube.  
 $f$  any frequency (cycles) within the video range.  
 $f_m$  highest frequency in the video range (constant gain and time delay required up to this frequency).  
 $G$  voltage gain of amplifier (output volts per input volts).  
 $g_m$  grid-plate transconductance (amperes per volt) of tube.  
 $L$  (see figure for inductance symbols).  
 $\mu$  amplification factor of tube.  
 $\phi_a$  phase shift (deg) in addition to 180-deg shift introduced by amplifier tube.  
 $R$  (see figure for resistance symbols).  
 $r_p$  dynamic plate resistance (ohms) of tube.  
 $\omega$   $2\pi f$ , angular frequency.

See Image Analysis for other symbols.

Highest frequency to be amplified in video range

$$f_m = \frac{(w/h) k f n^2}{2} \left( \frac{1 + 1/k_h}{(1 + 1/k_v)} \right) \text{ cycles} \quad (14)$$

NOTE:  $f$  in this equation is the frame repetition rate. See Image Analysis.

Figure-of-merit for amplifier tubes

$$\text{Figure-of-merit} = g_m / [C_{gk} + C_{pk} + C_{gp}(1 + G)] \quad (15)$$

NOTE:  $G$ , the gain per stage, may be taken as 15 for pentodes, 3 for triodes.

Total shunt capacitance per stage

$$C_t = C_s + C_{gk} + C_{pk} + C_{gp}(1 + G) \mu\text{mf} \quad (16)$$

NOTE:  $C_s$  is stray and wiring capacitance, in  $\mu\text{mf}$ .

Design formula for output load resistor,  $R_o$  (see Fig. 1)

$$R_o = \frac{1}{2\pi f_m C_t} \text{ ohms} \quad (17)$$

NOTE:  $C_t$  in farads,  $f_m$  in cycles.

Design formula for shunt compensating

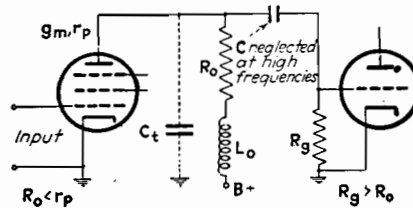


FIG. 1

Fig. 1.—Shunt-compensated video amplifier applicable to Eq. (17), (18), (19), and (20).

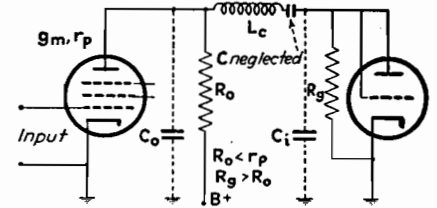


FIG. 2

Fig. 2.—Series-compensated video amplifier.  $R_o$  is determined by Eq. (17).

(peaking) inductance  $L_o$  (see Fig. 1)

$$L_o = 0.5 C_t R_o^2 \text{ henrys} \quad (18)$$

NOTE:  $C_t$  in farads,  $R_o$  in ohms.

High-frequency gain of shunt-compensated stage (Fig. 1)

$$G = \frac{g_m R_o \sqrt{1 + (1/4 f^3 / f_m^3 + 1/2 f / f_m)^2}}{(f/f_m)^2 + [f^2 / (2 f_m^2) - 1]^2} \quad (19)^*$$

Added phase shift of shunt-compensated stage

$$\phi_a = + \tan^{-1} \frac{1}{4} \left( \frac{f^3}{f_m^3} + \frac{2f}{f_m} \right) \text{ deg} \quad (20)^*$$

Design formula for series compensating (peaking) coil (Fig. 2)

$$L_c = \frac{1}{8\pi^2 f_m^2 C_o} \text{ henrys} \quad (21)^{\dagger}$$

NOTE:  $f_m$  in cycles,  $C_o$  in farads.

High-frequency gain of series-compensated stage

$$G = 1.50 G_o \quad (22)^{\dagger}$$

NOTE:  $G_o$  is gain of shunt-compensated stage (see Eq. 19) having same value of  $C_t$  and  $f_m$ .

Low-frequency gain (as a complex quantity) of RC compensated stage (Fig. 3)

$$G = \frac{g_m R_o \omega [\omega - j / (C_F R_p)]}{[\omega - j / (R_F C_F)] [\omega - j / (R_o C_o)]} \quad (23)^{\ddagger}$$

Gain of cathode-coupled stage (Fig. 4)

$$G = \frac{\mu R_k}{r_p + R_k (\mu + 1)} \quad (24)^{\ddagger}$$

Output impedance of cathode-coupled stage (Fig. 4)

$$R_o' = \frac{R_k r_p / (\mu + 1)}{R_k + r_p / (\mu + 1)} \text{ ohms} \quad (25)^{\ddagger}$$

\* SEELEY, S. W., and KIMBALL, C. N., Analysis and Design of Video Amplifiers, RCA Rev. 2, 2, 171, October, 1937.

† SEELEY and KIMBALL, Analysis and Design of Video Amplifiers, RCA Rev., 3, 3, 290, January, 1939.

‡ PREISMAN, A., Some Notes on Video Amplifier Design, RCA Rev., 2, 4, 421, April, 1938.

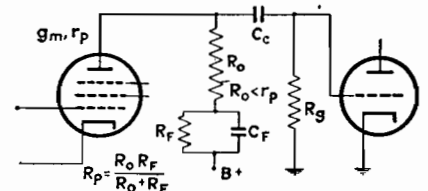


FIG. 3

Fig. 3.—Low-frequency compensation circuit for which gain may be calculated by Eq. (23).

**Coaxial Circuit Parameters**

- $A$  attenuation introduced by cable.  
 $C$  capacitance per unit length of cable, farads.  
 $d_i$  diameter of inner conductor.  
 $d_o$  diameter of outer conductor, same units as  $d_i$ .  
 $G$  conductance per unit length of cable, mhos.  
 $L$  inductance per unit length of cable, henrys.  
 $\phi$  phase shift introduced by cable, deg.  
 $R$  resistance per unit length of cable, ohms.  
 $t$  time delay introduced by cable, sec.  
 $Z$  surge impedance of cable, ohms.

**Surge impedance**

$$Z_o = \sqrt{\frac{R + j\omega L}{G + j\omega C}} = \sqrt{L/C} \text{ ohms} \quad (26)$$

NOTE: Second form applies only when  $R$  and  $G$  are small.

**Design formula for surge impedance**

$$Z_o = \frac{138.5 \log_{10} d_o}{d_i} \text{ ohms} \quad (27)$$

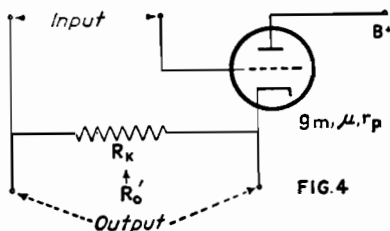


Fig. 4.—Connections of the cathode-coupled (cathode-follower) stage, used for low-impedance output applications.

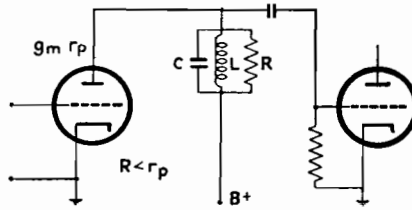


FIG. 5.—Wide-band r-f amplifier employing single, loaded, tuned circuit between stages, for Eq. (34) and (35).

**Attenuation**

$$A = \frac{0.031R}{\log_{10} (d_o/d_i)} \text{ db per unit length} \quad (28)$$

**Time delay**

$$t = \sqrt{LC} \text{ sec per unit length} \quad (29)$$

**Phase delay**

$$\phi = 2\pi f \sqrt{LC} \text{ radians per unit length} \quad (30)$$

**R-f Propagation and Amplification**

- $a$  height (meters) of receiving antenna.  
 $\Delta f$  total width of communication channel, cycles.  
 $E$  field strength at distance  $r$  (volts per meter).  
 $f_r$  resonant frequency of tuned circuit, cycles.  
 $h$  height (meters) of transmitting antenna.  
 $\lambda$  operating wavelength, meters.  
 $L$  inductance of tuned circuit, henrys.  
 $R$  resistance shunted across tuned circuit, ohms.

- $r$  distance from transmitting antenna, meters.  
 $r_h$  distance to horizon, viewed from top of antenna, meters.  
 $W$  transmitter power, watts.

**Horizon distance**

$$r_h = 1.23 \sqrt{h} \text{ miles} \quad (31)$$

NOTE:  $h$  is in feet in this equation.

**Field strength (within horizon distance)**

$$E = 88 \frac{\sqrt{W} ah}{\lambda r^2} \text{ volts per meter} \quad (32)^*$$

**Field strength (beyond horizon at 40 to 60 Mc)**

$$S = E_h \left( \frac{r_h}{r} \right)^{3.6} \text{ volts per meter} \quad (33)^*$$

NOTE:  $E_h$  is the field strength at the horizon.

**Gain of r-f stage contained single loaded tuned circuit (Fig. 5)**

$$G = g_m R \quad (34)$$

NOTE: This is the gain at the resonant frequency (middle of the communication channel). At the edges of the communication channel, the gain is 70 per cent of the above value, when the condition of Eq. (35) is fulfilled.

**Design formula for shunt loading resistance  $R$** 

$$R = (2\pi f_r L) \left( \frac{f_r}{\Delta f} \right) \quad (35)$$

NOTE: A single tuned circuit cannot offer uniform gain over the width of the communication channel. Circuits coupled either capacitively or inductively must be used to obtain "flat-top" response.

\* BEVERAGE, H. H., Some Notes on Ultrahigh Frequency Propagation, RCA Rev., 1, 3, 76, January, 1937.

# Influence of Feedback in Video Amplifiers

By RICHARD W. CRANE

Analysis of the use of negative feedback to reduce source impedance in amplifier stages and transmission lines, as required in video design and other applications where h-f response must be improved or loudspeaker hangover must be eliminated

INVERSE feedback is widely used in amplifiers today to stabilize gain, improve frequency response, and reduce distortion. One other extremely valuable feature of negative feedback is the apparent reduction of source impedance it may cause; this is not only important in itself, but may also serve as a basis for analyzing all the other features of feedback.

**Impedance Consideration**

Let us then derive a formula for the variation in source impedance with feedback. The gain of a feed-back amplifier is

$$\alpha' = \frac{\alpha}{1 - \alpha\beta} \quad (1)$$

where  $\alpha'$  = gain with feedback,  $\alpha$  = gain without feedback, and  $\beta$  = ratio of

feed-back voltage to output voltage, or the fraction of output voltage fed back (negative for degeneration).

As the load impedance approaches infinity, the equation

$$\alpha = \frac{-\mu Z_L}{Z_L + R_P} \quad (2)$$

approaches the value  $\alpha = -\mu$ , and  $\alpha'$  approaches the value  $-\mu/(1 + \mu\beta)$ , where

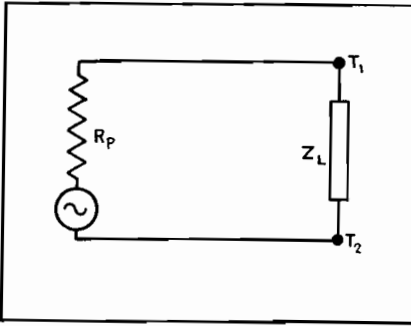


Fig. 1.—Equivalent circuit of an amplifier stage connected to a load.

$\mu$  = amplification factor of the tube,  $R_P$  = plate resistance of the tube, and  $Z_L$  = load impedance.

In Fig. 1, which is the equivalent circuit of an amplifier stage, one method of finding the source impedance would be to connect a load of such value that the voltage at  $T_1T_2$  measured exactly half the value it would have if the load impedance were infinite, in which case  $Z_L$  would equal  $R_P$ . Practically, this would mean choosing a value of  $Z_L$  such that  $\alpha = -\mu/2$ . The same reasoning holds true for an amplifier with feedback, where  $R_P = Z_L$  when

$$\alpha' = \frac{1}{2} \left( \frac{-\mu}{1 + \mu\beta} \right) \quad (3)$$

Substituting Eq. (2) in (Eq. (1),

$$\alpha' = \frac{\frac{-\mu Z_L}{Z_L + R_P}}{1 + \frac{\beta \mu Z_L}{Z_L + R_P}} \quad (4)$$

To find the apparent plate impedance we need only substitute the value of  $\alpha'$  given by Eq. (3) in Eq. (4) and solve for  $Z_L$ , which will be the value of load impedance required to make  $\alpha'$  equal one half its maximum value, and will therefore also be the source impedance of the amplifier

$$\frac{1}{2} \left( \frac{-\mu}{1 + \mu\beta} \right) = \frac{\frac{-\mu Z_L}{Z_L + R_P}}{1 + \frac{\beta \mu Z_L}{Z_L + R_P}}$$

Solving for  $Z_L$ ,

$$Z_L = R_P' = \frac{R_P}{1 + \mu\beta} \quad (5)$$

(In this equation  $\mu$  must be negative. Strictly speaking, it should always be, because of the 180-deg phase reversal in an amplifier stage.)

From this formula it can be seen that negative feedback in effect reduces the plate resistance of a tube, and in a practical case can make a pentode or beam-power tube have a source impedance as low as that of a triode, or lower.

It is well known that pentode and beam-power output stages have poor frequency response and appreciable distortion. These defects are manifested mainly in two ways.

#### Defects of Pentode and Beam Tubes

1. The speaker tends to have hangover; *i.e.*, the cone and voice coil assembly tends to vibrate at its own natural period when a transient or a steep wave-front signal is applied, and the amplifier's output will be far above normal when a signal is applied whose frequency is equal or close to the mechanical resonant frequency of the speaker. This does not occur in a triode because the low-impedance source shunts the speaker's emf and effectively damps the vibration. A pentode or beam tube with enough feedback to approximate a triode's plate resistance will behave similarly.

2. The second effect is a response that rises with increasing frequency; this happens because the primary inductance of the output transformer presents an appreciable (and, of course, varying) load to the tube throughout the audio spectrum. In a triode stage, the transformer primary's inductive reactance is high compared with the tube's plate resistance except at the very lowest audio frequencies, and thus a fairly uniform response is obtained. As in the first case, feedback will enable a beam power or pentode tube to give similar performance.

Pentode voltage amplifiers can use feedback advantageously also, for it will lessen the effect of the input capacitance of the next tube and therefore improve the h-f response.

In general, it may be said that inverse feedback will improve the action of any tetrode or pentode amplifier whose load contains shunt reactive components.

#### Current Feed-back Circuit

The foregoing discussion and derivation assume that  $\beta$  is constant regardless of changes in load impedance. This is true in the circuit of Fig. 2 or in any circuit where a portion of the output voltage is fed back. If we consider Fig. 3, however, we see a network in which a voltage is fed back which depends on the output current rather than the output voltage, and  $\beta$  is not constant but depends on  $Z_L$ . In this case,  $\beta$  is determined by the ratio of the voltage drop across  $R_F$  to the voltage drop across  $Z_L$ . Therefore,

$$\beta = -\frac{i_P R_F}{i_P Z_L} = -\frac{R_F}{Z_L} \quad (6)$$

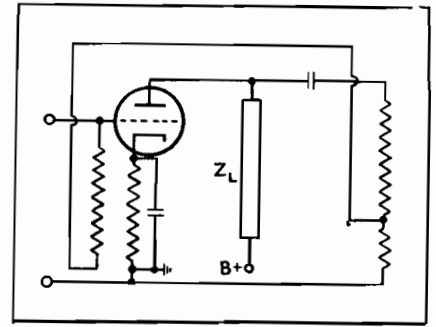


Fig. 2.—Voltage feed-back circuit using a portion of the output voltage.

In the circuit of Fig. 3, Eq. (2) becomes

$$\alpha = \frac{-\mu Z_L}{Z_L + R_P + R_F} \quad (7)$$

and Eq. (4) becomes

$$\alpha' = \frac{\frac{-\mu Z_L}{Z_L + R_P + R_F}}{1 + \frac{\beta \mu Z_L}{Z_L + R_P + R_F}} \quad (8)$$

Substituting Eq. (6) in Eq. (8),

$$\alpha' = \frac{\frac{-\mu Z_L}{Z_L + R_P + R_F}}{1 - \frac{\mu R_F}{Z_L + R_P + R_F}}$$

Simplifying,

$$\alpha' = \frac{-\mu Z_L}{Z_L + R_P + (1 - \mu)R_F} \quad (9)$$

Equation (9) is identical with Eq. (2) except that  $\alpha$  becomes  $\alpha'$  and  $R_P$  becomes  $[R_P + (1 - \mu)R_F]$ . Our formula for apparent source impedance, considering  $\mu$  negative as in Eq. (5), is

$$R_F' = R_P + (1 - \mu)R_F \quad (10)$$

Thus in Fig. 3 or in any current feed-back circuit, the tube's plate resistance is increased, and hence the output current tends to be stabilized, rather than the output voltage as in a voltage feed-back circuit. Current feedback will not improve frequency response because, if the load impedance varies with frequency,  $\beta$

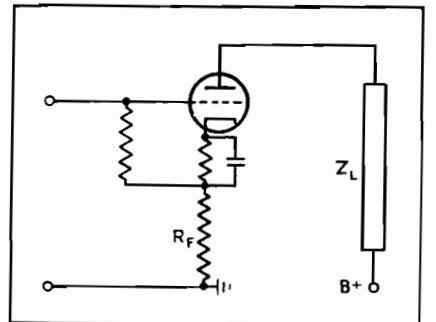


Fig. 3.—Current feed-back circuit using drop in cathode resistor.

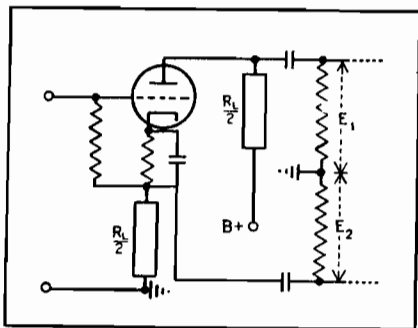


Fig. 4.—Circuit using feedback for phase inversion.

will also vary. For this type of feedback, Eq. (1) becomes

$$\alpha' = \frac{\alpha}{1 + \frac{\alpha R_F}{Z_L}}$$

Current feedback is especially undesirable in power amplifiers for it tends to stabilize the output transformer's magnetizing current (i.e., make it sinusoidal), and thus produce a distorted output voltage.

#### Phase Inverter

The circuit in Fig. 4 represents a phase inverter network that utilizes

feedback. Half the load resistance is in the plate circuit, and the other half is in the cathode circuit; hence  $\beta = -0.50$ ,  $\alpha' = 2$ , and  $E_1 = -E_2$ . This is, apparently, quite a good circuit for phase inversion; however, if we examine it in the light of the above discussion we can see an interesting problem. Looking back into the plate circuit we see a current feed-back arrangement and a high-impedance source. On the other hand, the cathode load sees a voltage feed-back circuit and a low-impedance source; thus it is apparent that the network will not give perfect phase inversion. A pentode would give especially poor results in such a circuit; however, the writer has obtained satisfactory results by using a low-mu triode with a low value of load resistance in such an arrangement.

#### Load in Cathode Circuit

Figure 5 is an interesting application of voltage feedback. The entire load is placed in the cathode circuit, so that  $\beta = -1$ , and from Eq. (5)  $R_F'$  very nearly equals  $R_P/\mu$  or  $1/G_M$ . This circuit is useful where a very low source impedance

is required, as for instance in certain video applications.

#### Conclusions

A significant fact to remember is that by using Eq. (5) and the circuits in Figs. 2 and 5 it is possible to match any tube to any load whose value is equal to or greater than  $1/G_M$ .

Inverse feedback reduces the gain of an amplifier of course, but this is no problem with present-day high-gain tubes, and the advantages of feedback offset this.

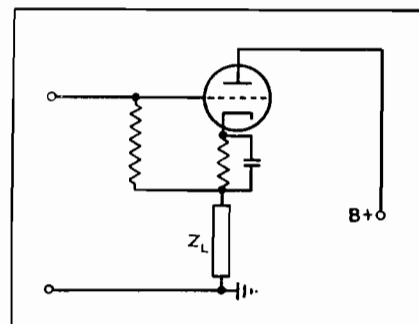


Fig. 5.—Cathode-loaded circuit with extremely low source impedance.

## Single-inductor Video Coupling Networks

By C. T. McCOMB and A. P. GREEN

Advantages over tuned interstage transformers in wide-band r-f and video amplifiers are discussed, performance is analyzed, expressions are set up for total voltage gain, bandwidth and skirt steepness ratio, and design curves are given for bandwidths up to 5 Mc

OF THE many methods of coupling between stages of tuned amplifiers, probably the simplest is the common single-inductor coupling network. While the single inductor does not possess the versatility of the tuned transformer or of other more elaborate coupling networks, neither does it entail the complexity of design, manufacture, and alignment of other types of coupling.

Consideration of the characteristics of the single-inductor coupling network is made under conditions where the center frequency and band-width requirements are such that the single inductor exhibits its most useful features. In Fig. 1 is shown a schematic circuit for use of the single inductor in a coupling network.

Variations of this circuit are possible, but they will not change the basic behavior of the network.

Figure 2 gives the fundamental equivalent network involving the inductor. The output capacitance of the preceding tube, the input capacitance of the following tube, and the distributed capacitance of the inductor and circuit are considered as a single-shunt capacitor with respect to the inductor in the equivalent circuit.

In the analysis of the network, it is assumed as a first restriction that the inductor has a sufficiently high  $Q$  so that its effective inherent shunt resistance is large compared with the size of the damping resistor used in the coupling

network. As a second restriction, the plate resistance of the preceding tube is also considered to be very large compared with the damping resistor. The first restriction is merely for the purpose of analysis so that the damping action in the network can be considered as being due solely to a lumped shunt resistor. The second restriction limits the use of this analysis to those applications where the bandwidth requirements are such that the necessary damping resistor will be small compared with the effective plate resistance of the tube. This last condition does not place a severe limitation on the usefulness of this work, because the great majority of all video

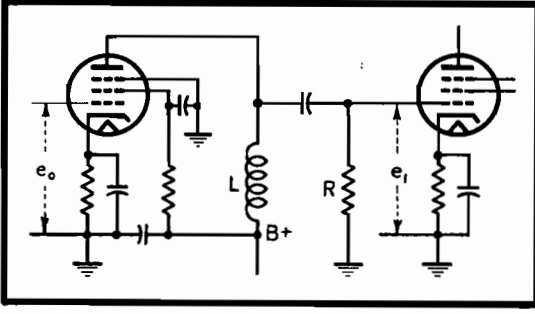
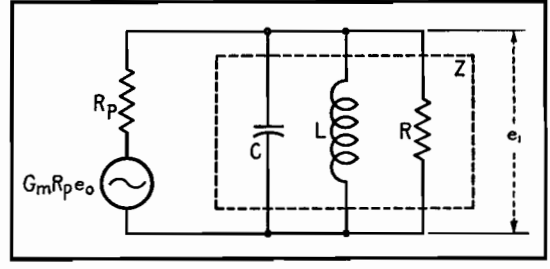
Fig. 1.—Circuit using single inductor  $L$  in coupling network.

Fig. 2.—Equivalent circuit of amplifier stage using a single-inductor coupling network.

modulation applications will fall within this range.

#### Total Voltage Gain for $N$ Stages

An examination of the equivalent network of Fig. 2 shows that the voltage gain for a single stage is given by the expression

$$\text{V.G.} = \frac{e_i}{e_o} = \frac{g_m R_P Z}{R_P + Z} \quad (1)$$

With the above-discussed second restriction that  $R$  is small compared with  $R_P$ , and since  $Z$  can never be greater than  $R$ , then for this treatment  $Z$  will be small compared with  $R_P$  and we shall have for one stage of amplification

$$\text{V.G.} = \frac{e_i}{e_o} = g_m Z \quad (2)$$

For  $N$  identical stages, as in Fig. 3, the total gain at any frequency  $\Gamma_f$  will be

$$\Gamma_f = (g_m Z)^N \quad (3)$$

From the equivalent circuit,  $Z$  can be expressed by

$$Z = \frac{1}{\frac{1}{R} + j\left(\omega C - \frac{1}{\omega L}\right)} \quad (4)$$

It is apparent that  $Z$  is a maximum and equals  $R$  when  $\omega C = 1/\omega L$ . If we let  $\omega = \omega_0$  when  $Z = R$  (at resonance), then  $\omega_0 C = 1/\omega_0 L$  or  $L = 1/\omega_0^2 C$ , we have

$$Z = \frac{1}{\frac{1}{R} + j\left(\omega C - \frac{\omega_0^2 C}{\omega}\right)} \quad (5)$$

and the total gain will be

$$\Gamma_f = (g_m Z)^N = g_m^N \left[ \frac{1}{\frac{1}{R} + j\left(\omega C - \frac{\omega_0^2 C}{\omega}\right)} \right]^N \quad (6)$$

At resonance,

$$\Gamma_{f_0} = (g_m R)^N \quad (7)$$

We can now advantageously express the total voltage gain at any frequency as a

fraction  $\alpha$  of the total voltage gain at resonance, thus:

$$\Gamma_f = \alpha \Gamma_{f_0} = \alpha (g_m R)^N \quad (8)$$

With this expression for the total voltage gain at any frequency expressed as a function of some of the known constants of the network and the determinable factor  $\alpha$ , we have a useful means for predicting the behavior of any single-inductor type tuned amplifier.

#### General Bandwidth for $N$ Stages

Since the total gain and the bandwidth are the two basic requirements for any tuned amplifier, it is necessary that an expression be obtained relating these quantities to the known constants of the network.

From Eqs. (6) and (8) for total voltage gain,

$$\Gamma_f = \alpha (g_m R)^N = g_m^N \left[ \frac{1}{\frac{1}{R} + j\left(\omega C - \frac{\omega_0^2 C}{\omega}\right)} \right]^N \quad (9)$$

We are interested only in the magnitude of the impedance at any frequency so we may reduce the complex expression on the right to a real number and cancel out  $g_m^N$ , thus

$$\alpha R^N = \left[ \frac{1}{\frac{1}{R^2} + \left(\omega C - \frac{\omega_0^2 C}{\omega}\right)^2} \right]^{\frac{N}{2}} \quad (10)$$

Taking the  $N/2$ th root of the expression, we have

$$\alpha^{\frac{2}{N}} R^2 = \frac{1}{\frac{1}{R^2} + \left(\omega C - \frac{\omega_0^2 C}{\omega}\right)^2} \quad (11)$$

Rearranging terms results in the relation

$$(\omega^2 - \omega_0^2)^2 = \frac{\omega^2(1 - \alpha^{\frac{2}{N}})}{\alpha^{\frac{2}{N}} R^2 C^2} \quad (12)$$

and since  $\omega = 2\pi f$  we can write

$$(f^2 - f_0^2)^2 = \frac{f^2(1 - \alpha^{\frac{2}{N}})}{4\pi^2 \alpha^{\frac{2}{N}} R^2 C^2} \quad (13)$$

then

$$f^2 - f_0^2 = \pm \frac{f \sqrt{1 - \alpha^{\frac{2}{N}}}}{2\pi \alpha^{\frac{1}{N}} R C} \quad (14)$$

From Fig. 4 it is seen that for any relative voltage response  $\alpha$  there are two values of  $f$ . These frequencies will be designated  $f_1$  and  $f_2$ ; since they must be positive real numbers, we have for the solutions of Eq. (14)

$$f_2^2 - f_0^2 = \frac{f_2 \sqrt{1 - \alpha^{\frac{2}{N}}}}{2\pi \alpha^{\frac{1}{N}} R C} \quad (15)$$

and

$$f_1^2 - f_0^2 = \frac{-f_1 \sqrt{1 - \alpha^{\frac{2}{N}}}}{2\pi \alpha^{\frac{1}{N}} R C} \quad (16)$$

Eliminating  $f_0$  from the above equations and using the notation for general bandwidth  $\Delta f = f_2 - f_1$ , we have

$$f_2^2 - f_1^2 = (f_2 + f_1) \frac{\sqrt{1 - \alpha^{\frac{2}{N}}}}{2\pi \alpha^{\frac{1}{N}} R C} \quad (17)$$

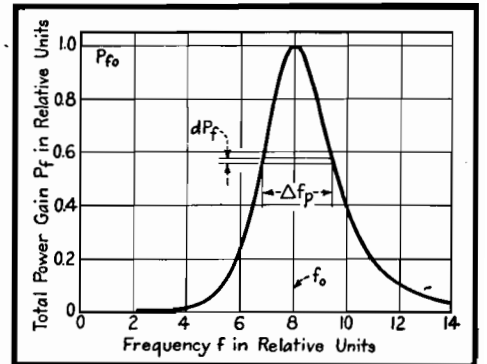


Fig. 3.—Use of single-inductor coupling networks (represented by equivalent impedance  $Z$ ) in  $N$  identical stages.

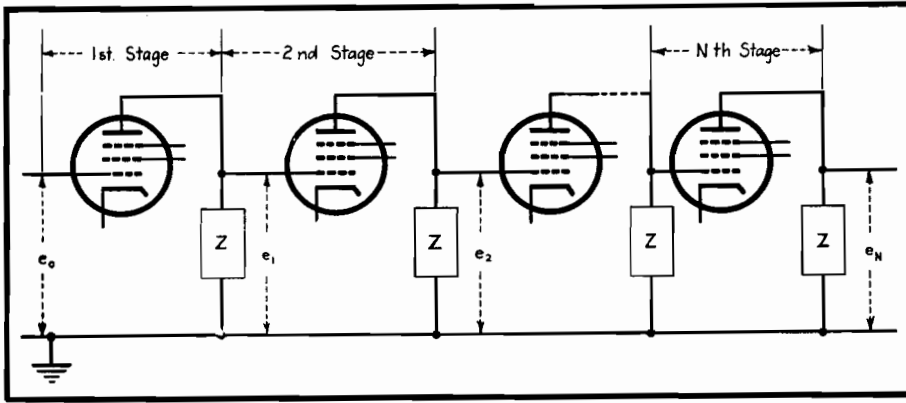


Fig. 4.—Voltage response characteristic of an amplifier stage using a single-inductor coupling network, showing significance of bandwidth for any specific value of relative voltage response off the resonant frequency.

Then, since  $f_2^2 - f_1^2 = (f_2 + f_1)(f_2 - f_1)$ ,

$$\Delta f = \frac{\sqrt{1 - \alpha^{\frac{2}{N}}}}{2\pi\alpha^{\frac{1}{N}}RC} \quad (18)$$

For convenience of analysis, this expression for general bandwidth can be given most simply as

$$\Delta f = \frac{\sqrt{\frac{1}{2} - 1}}{2\pi RC} \quad (19)$$

This relationship shows the functional variation of the bandwidth of the amplifier with respect to the circuit constants and the relative voltage response ratio at which the bandwidth is considered. It shows that, if  $R$  and  $C$  are fixed, both the bandwidth at any given relative response  $\alpha$  and the total voltage gain [since  $\Gamma_f = \alpha(g_m R)^N$ ] will remain constant, regardless of the value of the inductance  $L$  employed. Thus it is seen that any inductance variation will change only the resonant frequency and will have no effect on the bandwidth or total gain.

An important relationship exists between the high and low frequencies  $f_2$  and  $f_1$  for any relative response  $\alpha$  and the resonant frequency  $f_0$  of the coupling network. Dividing Eqs. (15) by (16), we obtain

$$\frac{f_2^2 - f_0^2}{f_1^2 - f_0^2} = -\frac{f_2}{f_1} \quad (20)$$

Solving this for  $f_0^2$  gives

$$f_0^2 = f_1 f_2 \quad (21)$$

This establishes the well-known formulation that the resonant frequency is the geometric mean of the high- and low-response frequencies at any relative response of the amplifier. It follows that

the response of an amplifier is thus geometric with respect to its resonant frequency, and a linear frequency plot of the amplifier characteristic will appear asymmetrical. For this reason a logarithmic frequency scale is usually employed so that the characteristic will appear symmetrical.

#### Skirt-steepness Ratio

An interesting characteristic of the behavior of  $N$  stages of a single-inductor coupling network can be drawn from a consideration of the expression in Eq. (19) for  $\Delta f$ . The quality of an amplifier is partially determined by its response to near signals relative to its desired bandwidth response. This characteristic is important in the signal-to-noise ratio of the amplifier since the total area under the response curve contributes to noise

energy, while only an area proportional to the signal bandwidth contributes to the signal energy. This degree of quality is expressed as a factor, skirt steepness  $S$ , which is defined as the ratio of the bandwidth at  $-60$ -db response to the bandwidth at  $-6$ -db response. This ratio is seen to be an inverse index of the quality of rejection of the amplifier in that as the ratio becomes smaller, the response to near signals will be less. From Eq. (19) for  $\Delta f$  and since for  $-60$ -db response  $\alpha = 0.001$  and for  $-6$ -db response  $\alpha = 0.5$ , we have

$$S = \frac{\Delta f_{-60\text{db}}}{\Delta f_{-6\text{db}}} = \frac{\sqrt{\frac{1}{(0.001)^{\frac{2}{N}} - 1}}}{\sqrt{\frac{1}{(0.5)^{\frac{2}{N}} - 1}}} \quad (22)$$

It is seen from this expression that the skirt steepness is dependent only on the number of stages and not on any of the other characteristics of the amplifier. The ratio  $S$  for amplifiers of one through eight stages is given in Fig. 5, along with representative response characteristics of amplifiers with different numbers of stages. A logarithmic frequency scale is used in order to obtain symmetrical curves. The three response characteristics presented are all down 6 db at a bandwidth of 2 Mc with a center frequency of 30 Mc. The difference between the characteristics is due to the number of stages used in each.

It is seen that a very great improvement in skirt steepness is obtained in going

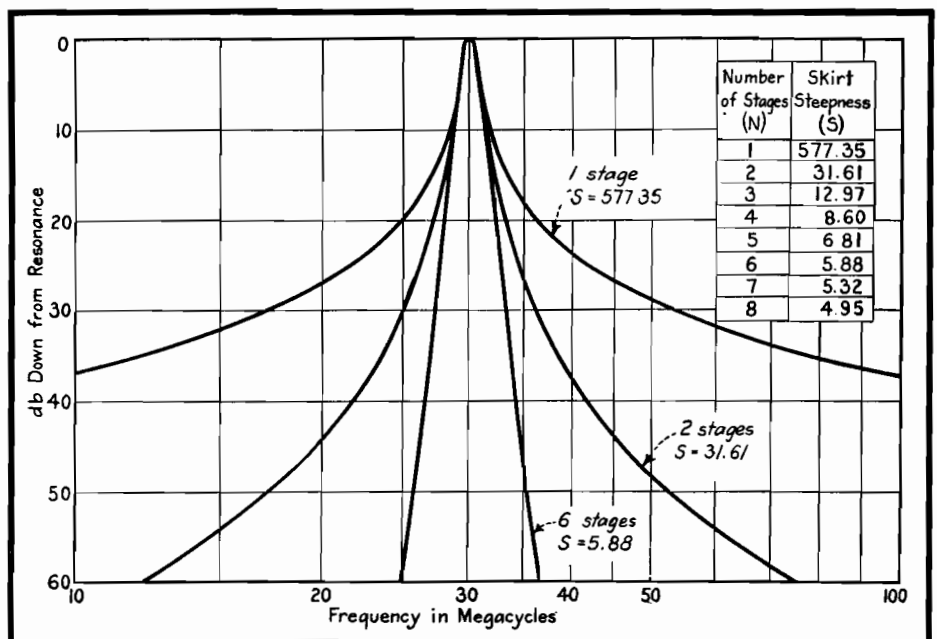


Fig. 5.—Skirt-steepness ratio values and response characteristics for amplifiers having different numbers of identical stages using single-inductor coupling.

from one stage to any greater number of stages. The much more desirable characteristic shape of the response of six stages compared with that of two stages is also evident from the curves. This decided increase in the rejection of near signals is so pronounced that in many applications the use of additional stages will be justified even though the required total gain could be obtained with a fewer number of stages.

#### Effective Bandwidth for $N$ Stages

The effective bandwidth of a resonant response characteristic is defined as the bandwidth of an assumed rectangular response of height equal to the response of the particular network at resonance and of area equal to its total integrated power response. In order to apply this definition it is necessary to treat the power gain of  $N$  stages. This is proportional to the square of the total voltage gain. From Eq. (7) for  $\Gamma_{f_0}$  we can write for the power gain at resonance

$$\text{Total power gain at } f_0 = P_{f_0} = K\Gamma_{f_0}^2 = K(g_m R)^{2N} \quad (23)$$

where  $K$  is the impedance proportionality constant for the particular general circuit under consideration. From this we have, in a manner similar to Eq. (8),

$$\text{Total power gain at } f = P_f = \beta P_{f_0} = K\beta(g_m)^{2N} \quad (24)$$

where  $\beta$  is the fractional power response factor of the total power gain at resonance. It is seen that  $\beta$  is the factor corresponding to  $\alpha$  in Eq. (8) for voltage response.

Since we are interested in obtaining a relationship in terms of the maximum power response and the bandwidth, we can write

$$K\beta(g_m R)^{2N} = K g_m^{2N} \left[ \frac{1}{\frac{1}{R} + j\left(\omega C - \frac{\omega_0^2 C}{\omega}\right)} \right]^{2N} \quad (25)$$

This becomes

$$\beta R^{2N} = \left[ \frac{1}{\frac{1}{R} + j\left(\omega C - \frac{\omega_0^2 C}{\omega}\right)} \right]^{2N} \quad (26)$$

Reducing the right side of the expression to a real number, since we are interested only in the absolute magnitude, and taking the square root of both sides of the equation gives

$$\beta^{1/2} R^N = \left[ \frac{1}{\frac{1}{R^2} + \left(\omega C - \frac{\omega_0^2 C}{\omega}\right)^2} \right]^{N/2} \quad (27)$$

Comparison of this form of the equation with the similar form obtained in the consideration of general bandwidth in Eq. (10) gives us immediately the form of the solution. We see that  $\alpha$  in Eq. (10) will be replaced by  $\beta^{1/2}$ . Using the notation  $\Delta f_P$  to indicate the bandwidth with respect to the power response curve, we have

$$\Delta f_P = \frac{\sqrt{\frac{1}{\beta^{1/2}} - 1}}{2\pi RC} \quad (28)$$

This equation now gives the necessary expression for completing the evaluation of the defined effective bandwidth. We may now write the defining integral for the total area under the power response curve. We shall take the equation for  $\Delta f_P$ , which is the expressed bandwidth at any relative response  $P_f$ , and integrate with respect to  $dP_f$  over the range of zero to  $P_{f_0}$  which is the maximum power response. This will give the total area under the curve, an example of which is given in Fig. 6.

$$\text{Area under power curve} = \int_0^{P_{f_0}} \Delta f_P dP_f \quad (29)$$

Applying the definition for effective bandwidth and noting it as  $\Delta f_e$ , we can write

$$\Delta f_e = \frac{\int_0^{P_{f_0}} \Delta f_P dP_f}{P_{f_0}} \quad (30)$$

Using Eqs. (23), (24), and (28), we can substitute in Eq. (30) as follows:

$$\Delta f_e = \frac{\int_0^{P_{f_0}} \frac{\sqrt{\frac{1}{\beta^{1/2}} - 1}}{2\pi RC} d[K\beta(g_m R)^{2N}]}{K(g_m R)^{2N}} \quad (31)$$

Noting in Eq. (31) that the variable of

relative response is  $\beta$ , we can perform the indicated differentiation, simplify the expression, and evaluate the new limits of integration for  $\beta$ . This gives

$$\Delta f_e = \frac{1}{2\pi RC} \int_0^1 \sqrt{\frac{1}{\beta^{1/2}} - 1} d\beta \quad (32)$$

which is the definite integral expression for the effective bandwidth.

Eq. (32) does not lend itself readily to integration, so we shall use a convenient substitution to reduce the expression to an easily integrated form. Letting  $\beta = \cos^{2N} \phi$ ,

$$d\beta = -2N \cos^{2N-1} \phi \sin \phi d\phi$$

and the equation becomes

Table I.—Amplifier Data

Number of stages ( $N$ )	$A_e$	$A_g$
1	0.25000	0.15915
2	0.12500	0.10243
3	0.09375	0.08114
4	0.07813	0.06923
5	0.06836	0.06137
6	0.06152	0.05570
7	0.05640	0.05135
8	0.05236	0.04788

$$\Delta f_e = \frac{-N}{\pi RC} \int_{\pi}^0 \sin^2 \phi \cos^{2(N-1)} \phi d\phi \quad (33)$$

The solution of this integral is direct, but for ease of general expression it is necessary to exclude the case of the single-stage amplifier. For this case  $N = 1$  and the integral becomes

$$\Delta f_e = \frac{-1}{\pi kC} \int_{\pi}^0 \sin^2 \phi d\phi \quad (34)$$

The solution to this is immediate, and

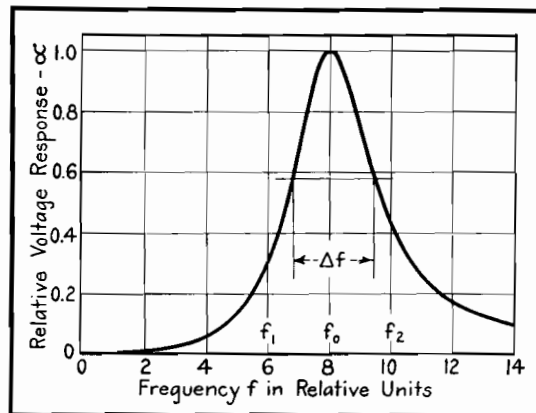


Fig. 6.—Example of power-response characteristic; the area of which is utilized in determining the effective bandwidth of a stage using a single-inductor coupling network.



for one stage we have

$$\Delta f_e = \frac{1}{4RC} \quad (35)$$

For more than one stage, the solution of the expression is obtained in the form of a series product. This is because the integration of the  $N$ th power of a trigonometric function is a repeated integral of reduced power. The general solution for the effective bandwidth for more than one stage is

$$\Delta f_e = \frac{N}{16RC} \prod_{a=4}^{a=2(N-1)} \left( \frac{a-1}{a+2} \right) \quad (36)$$

The above expression is seen to give the effective bandwidth of the amplifier in terms of the number of stages and the circuit constants  $R$  and  $C$ . The equation can be written

$$\Delta f_e = \frac{A_e}{RC} \quad (37)$$

where

$$A_e = \frac{N}{16} \prod_{a=4}^{a=2(N-1)} \left( \frac{a-1}{a+2} \right) \quad (38)$$

Now we can evaluate  $A_e$  for any number of stages and tabulate it. Then for a particular amplifier,  $C$  will be fixed by the circuit layout and type of tube used, but  $R$  must be chosen to satisfy the bandwidth requirement.

Table I gives the value of  $A_e$  for amplifiers of one to eight stages. This is seen to be extremely useful for the above-discussed application. Also tabulated in Table I are the values of  $A_g$ , which is the constant of bandwidth from Eq. (19) for general bandwidth, in which bandwidth is taken as the -3-db response width. For this case we have

$$\Delta f = \frac{A_g}{RC} \quad (39)$$

$$A_g = \frac{\sqrt{\frac{1}{\alpha^N} - 1}}{2\pi} \quad (40)$$

These values were computed directly by setting  $\alpha = 0.707$  and evaluating  $A_g$  for values of  $N$  from one through eight.

An examination of the two columns in Table I shows that as the number of stages increases, the constants become more nearly equal. This consideration leads to a desirable fact concerning the decibel down from maximum response at the effective bandwidth of a curve.

Letting  $\Delta f_e$  equal  $\Delta f_r$ , we can solve for the relative power response  $\beta$  at the

Table II.—Amplifier Response

Number of Stages ( $N$ )	Db down at $\Delta f_e$
1.....	5.399
2.....	4.163
3.....	3.886
4.....	3.757
5.....	3.683
6.....	3.633
7.....	3.605
8.....	3.570

effective bandwidth for any value of  $N$ . From Eqs. (28) and (37) we have

$$\frac{A_e}{RC} = \sqrt{\frac{1}{\beta^N} - 1} \quad (41)$$

The general expression for  $\beta$  in terms of  $A_e$  becomes

$$\beta = \left[ \frac{1}{1 + (2\pi A_e)^2} \right]^N \quad (42)$$

The decibels down at the effective bandwidth, in terms of  $A_e$  for  $N$  stages, are then

$$\text{db} = 10N \log_{10} [1 + (2\pi A_e)^2] \quad (43)$$

Table II gives the decibels-down response of the amplifier characteristic at the effective bandwidth for one through eight stages. These values are in the anticipated agreement deduced from the values of Table I; i.e., as the number of stages increases, the values of effective bandwidth and the 3-db down characteristic become more nearly equal.

The above-considered characteristics of the behavior of the single-inductor coupling network all give valuable yet simple equations for obtaining the design constants of an amplifier for a given set of conditions.

#### Composite Total Voltage Gain and Effective Bandwidth Behavior for $N$ Stages

A composite relationship can be obtained for the complete behavior of  $N$  stages of single-inductor networks in which the total voltage gain  $\Gamma_{f0}$  is functional with respect to the effective bandwidth  $\Delta f_e$  and the element constants of the networks. This relationship gives the complete design requirements for any amplifier using the two fundamental requirements of total voltage gain and effective bandwidth desired.

From Eq. (7) for total gain and Eq. (37) for effective bandwidth, we have

$$\Gamma_{f0} = \left( \frac{g_m A_e}{\Delta f_e C} \right)^N \quad (44)$$

We see that  $\Gamma_{f0}$  is expressed in terms of the effective bandwidth desired  $\Delta f_e$ ,

the effective bandwidth constant  $A_e$  (which is known and constant for any number of stages), the  $g_m$  of the tube, and the capacitance of the circuit. Thus for some independently chosen value of  $g_m$ , and with  $C$  fixed by the circuit layout and type of tube used, we have  $\Gamma_{f0}$  expressible in terms of the bandwidth desired and the number of stages.

For purposes of generalization in order to compute the desired family of curves, we shall arbitrarily assign reasonable values to  $g_m$  and  $C$ . Letting  $g_m = 5,000$   $\mu\text{mhos}$  and  $C = 25$   $\mu\text{mf}$ , we have

$$\Gamma_{f0}' = \left( \frac{200 A_e}{\Delta f_e} \right)^N \quad (45)$$

where  $\Delta f_e$  is expressed in megacycles. Figure 7 is a plot of this equation over the entire practical range of application, with  $\Delta f_e$  covering from 0.5 to 5.0 Mc and from one through eight stages considered. With this figure, one can obtain immediately the number of stages required for a particular set of design requirements.

For any other values of  $g_m$  and  $C$  in an amplifier, the total gain that will be obtained is

$$\Gamma_x = \Gamma_{f0}' \left( \frac{g_{mx}/5000}{C_x/25} \right)^N \quad (46)$$

where

$$\Gamma_x = (g_{mx} R_x)^N$$

Thus the family of curves given in Fig. 7 is perfectly general with the above equation.

With the desired total gain fixed in an amplifier and with the value of  $g_{mx}$  established to obtain that gain with the determined number of stages, the necessary value of shunt resistance  $R_x$  is obtained from Eq. (45) for  $\Gamma_x$  thus

$$R_x = \frac{1}{g_{mx}} \frac{\Gamma_x}{\Gamma_{f0}'} \quad (47)$$

#### Example of Use of Design Curves

In order to demonstrate the extreme simplicity of application of the design curves given in Fig. 7, an example will be presented.

Assume that an amplifier is desired to have a total voltage gain of 10,000 and an effective bandwidth of 2.0 Mc. The resonant frequency is not involved in the determination of either the number of stages or the shunt resistor  $R$ , as was discussed above. First, observation of Fig. 7 shows that, for the conditions required, the amplifier will have either four or five stages, with variations in  $C$  and  $g_m$  fixing the final choice. Four stages gives insufficient gain for the

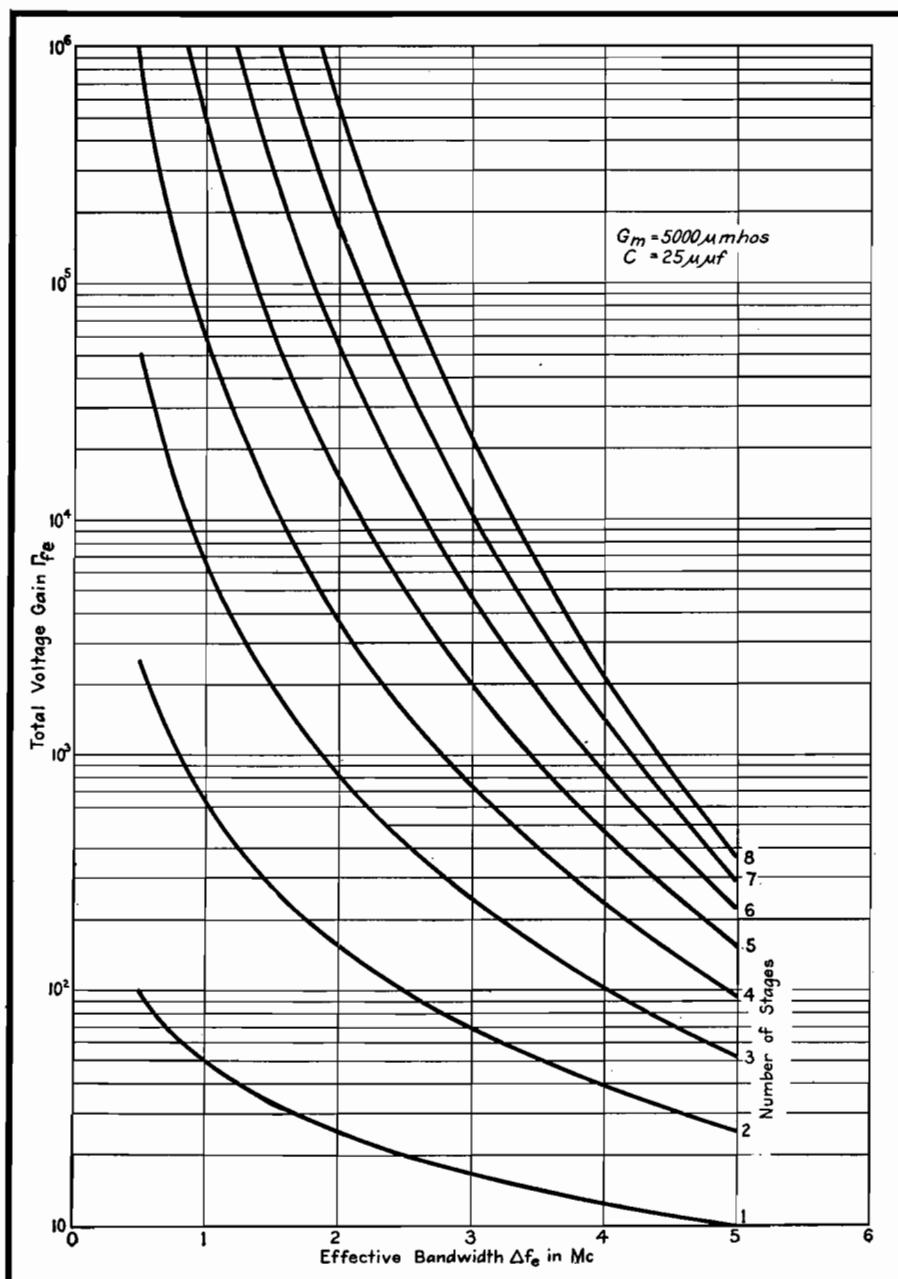


Fig. 7.—Design curves for determining the number of amplifier stages required to meet a particular set of design requirements when using single-inductor coupling networks in wide-band amplifiers.

operational conditions of  $C = 25 \mu\mu\text{f}$  and  $g_m = 5,000 \mu\text{mhos}$  that were chosen for Fig. 7, while five stages gives too much gain for these conditions. Now, assuming

that the circuit layout is such that we shall have  $22 \mu\mu\text{f}$  capacitance instead of  $25 \mu\mu\text{f}$  used in Fig. 7, from the equation for  $\Gamma_z$  this will raise the total gain.

Let us take the two cases of four and five stages and compute what the operating  $g_{mz}$  and the required shunt resistor  $R_z$  will be for our problem. For four stages, from Fig. 7 we have

$$\Gamma_z = 10,000 = 3,720 \left( \frac{g_{mz}/5,000}{22/25} \right)$$

Solving, we have

$$g_{mz} = 5,000 \times \frac{22}{25} \left( \frac{10,000}{3,720} \right)^{1/4} = 5,640 \mu\text{mhos}$$

Therefore,

$$R_z = \frac{(10,000)^{1/4}}{5,640 \times 10^{-6}} = \frac{10}{0.00564} = 1,773 \text{ ohms}$$

To get exactly the conditions set down for the amplifier of the problem when four stages are used, the operating  $g_m$  of the tubes would be raised slightly above the value used in Fig. 7. Finding this value, we can compute the value of  $R_z$ .

Now, taking our amplifier to have five stages, we obtain from Fig. 7

$$\Gamma_z = 10,000 = 15,100 \left( \frac{g_{mz}/5,000}{22/25} \right)^5$$

Solving, we have

$$g_{mz} = 5,000 \times \frac{22}{25} \left( \frac{10,000}{15,100} \right)^{1/5} = 4,055 \mu\text{mhos}$$

therefore,

$$R_z = \frac{(10,000)^{1/4}}{4,055 \times 10^{-6}} = \frac{6.3095}{0.004055} = 1,554 \text{ ohms}$$

For five stages the operating  $g_m$  of the tubes is reduced below that assumed for Fig. 7.  $R_z$  is then computed as in the previous case using the new  $g_{mz}$ .

From the above solution to the problem, the curves of Fig. 7 are completely definitive of the behavior of the general single-inductor coupling network, and for any particular amplifier the consideration of only the capacitance  $C$  that will be involved in the circuit need be determined. Then the operating  $g_m$  for the tubes and the required value of  $R_z$  can be determined directly.

# Frequency-deviation Measurement of F-m Transmitters

By L. N. HOLLAND and L. J. GIACOLETTO

The frequency deviation can be determined by increasing the a-f input of the transmitter and noting when the carrier disappears. A graph relating the frequency deviation with the modulating frequency for zero carrier simplifies this calculation

GENERATION of an f-m signal produces a carrier and side frequency terms. For a sinusoidal modulating signal, the amplitude of the carrier is directly proportional to  $J_0(Z)$  where  $J_0(Z)$  is the Bessel function of zero order and argument  $Z$ . The argument  $Z$  is usually called the modulation index and is defined by

$$Z = \frac{mf_0}{f_1} \quad (1)$$

where  $f_0$  is the carrier frequency,  $mf_0$  is the frequency deviation to either side of the carrier, and  $f_1$  is the modulating frequency. The Bessel function  $J_0(Z)$  goes through variations having a close resemblance to a damped cosinusoidal function as shown in Fig. 1. For certain values of  $Z$ , the carrier goes through zero or null points. The values of  $Z$  for which  $J_0(Z) = 0$  are denoted by  $Z_i$  and are tabulated in Table I.\* If the point at which the carrier disappears is known, the frequency deviation can be found because at this point

$$mf_0 = Z_i f_1 \quad (2)$$

There must also be known the order of the zero, i.e., the value of  $i$ .

To use this method of frequency-deviation measurement requires an audio-signal generator with a calibrated output, connected to the transmitter a-f input. A selective a-m type receiver capable of receiving c-w signals is used to ascertain the presence of the carrier. To make the measurements, reduce the transmitter a-f input to zero and tune in the carrier on the receiver, obtaining an audible beat or heterodyne note. Slowly increase the transmitter a-f input [analogous to increasing  $m$  in Eq. (1)]. The audible beat note should gradually decrease in intensity and finally disappear entirely when the amplitude of the carrier reaches zero.

\* If additional zeros are desired, note that the difference approaches  $\pi$  units as  $i$  increases.

At this point the frequency deviation is  $mf_0 = 2.405f_1$ . If the a-f input is again increased, the carrier beat note will return, increase to a maximum, decrease, and again disappear. For the second null point, the frequency deviation is  $mf_0 = 5.520f_1$ .

$i$	$Z_i$	$i$	$Z_i$
1	2.4048	11	33.7758
2	5.5201	12	36.9171
3	8.6537	13	40.0584
4	11.7915	14	43.1998
5	14.9309	15	46.3412
6	18.0711	16	49.4826
7	21.2116	17	52.6241
8	24.3525	18	55.7655
9	27.4935	19	58.9070
10	30.6346	20	62.0485

In general, the receiver will not be selective enough to admit the carrier alone, but will admit the carrier and several of the side frequencies. For this case, if the receiver is tuned to give an audible beat note  $f_a$ , it is quite possible that there will also be heard the frequencies  $f_1 \pm f_a$ ,  $2f_1 \pm f_a$ , etc. This may lead to some confusion in determining when the carrier disappears. Considerable improvement can be obtained by

introducing a low-pass audio filter between the receiver output and the speaker or head set. The filter should be designed to admit  $f_a$  and to attenuate the other frequencies. If the cutoff frequency for the filter is chosen as  $f_c$ , then  $f_1$  must be greater than  $2f_1$  in order that the other heterodyne notes fall outside the filter pass band.

To facilitate the measurement of frequency deviation, the chart has been prepared. The radial lines are a plot of Eq. (2). (The dashed curved lines are used with another method of measuring deviation, described below.) Each radial line when numbered counterclockwise corresponds to the value of  $i$  in the table. As an example of how the chart may be used, suppose that the modulating frequency is 5 kc. The deviation when the carrier disappears for the first time is found by following along the lower edge of the chart to the 5-kc ordinate and moving upward along this ordinate until it intersects the first radial line. The deviation 12 kc is read from the scale on the left. For the second null point, continue upward along the 5-kc ordinate to the second radial line, where the deviation is found to be 27.6 kc. In this manner the deviations may be determined for successive null points.

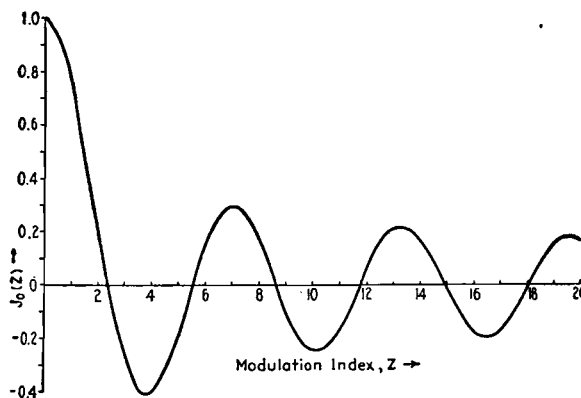


Fig. 1.—Graph of Bessel function,  $J_0(Z)$ , plotted as function of modulation index  $Z$ .

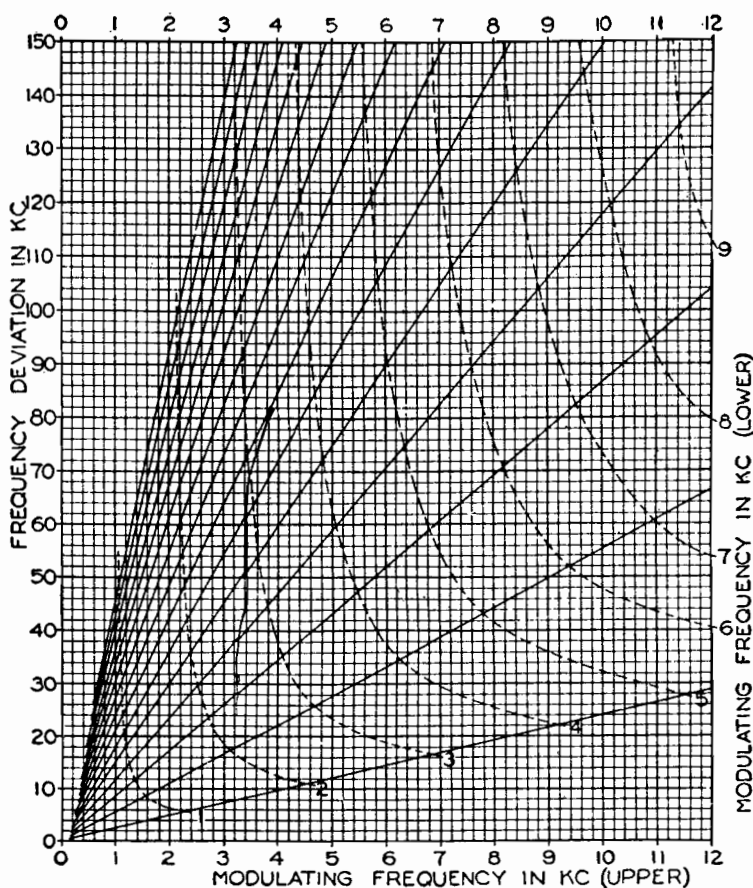


Fig. 2.—Graph relating frequency deviation of f-m transmitter and modulating frequency for zero carrier.

This method of measuring deviation follows closely the one described by M. G. Crosby.\* A slightly different method has been used by the authors with success. For this method, the a-f input is held constant and the modulating frequency varied. If this is done, the carrier will disappear for several values of  $f_1$ . Any two successive modulating frequencies that cause the carrier to disappear will uniquely determine the frequency deviation. Suppose in this method that a modulating frequency of 7.8 kc gives a carrier null, and the frequency is decreased until another null is

obtained with a modulating frequency of 5.0 kc. Then the intersection point of the ordinate at 7.8 kc (upper frequency) and the dashed curve at 5.0 kc (lower frequency) indicates a frequency deviation of 43 kc. The intersection point of the lower and higher frequency must always fall on a radial line. Also the interpolation between the dashed curves for lower frequency values is linear along any radial line.

While these methods of frequency-deviation measurement are basic in that they are independent of all circuit parameters, they have certain shortcomings that limit their usefulness. First they presuppose a linear relation between input voltage and frequency

deviation. A departure from linearity means that the carrier null points are no longer null points but minimum points. If the departure from linearity is very serious, it may be impossible to detect even a carrier minimum point. The carrier frequency must also remain reasonably constant.

If the carrier frequency changes considerably as the input level or modulating frequency is changed (depending on which method is being used), no carrier null points will be obtained. Even a small change in carrier frequency may be bothersome in that the carrier heterodyne note will change, possibly to such an extent that the heterodyne note will move outside of the filter pass band. For this reason, the filter cutoff frequency should not be too small. Also for this reason, the modulating frequency should be kept at as large a value as is feasible so that the carrier heterodyne note will never be confused with the side-band heterodyne notes. In this connection, from the nature of the carrier zeros, it will be necessary to decrease the modulating frequency for measuring smaller deviations. This factor must be given additional attention when making measurements on mobile f-m transmitters where the maximum deviation is usually only 15 kc. A filter with lower cutoff may prove useful in such cases, and the receiver should be returned to the same note if the carrier shifts.

In using the first method for making deviation measurements, care must be taken to count every null point. If a null point is overlooked, the deviation measurements will be incorrect. The second method is an improvement in this respect, since the deviation is uniquely determined. On the other hand, the second method is useless when there is appreciable variation of deviation with audio frequency. Such a situation will arise in any transmitter if either audio pre-emphasis or uncorrected phase modulation is present.

\* CROSBY, MURRAY G., A Method of Measuring Frequency Deviation, *RCA Rev.*, 4, 473-477, April, 1940.

# Facsimile Design Chart

By RAYMOND R. HAUGH

The design of the mechanical portion of a facsimile scanning unit depends on a number of factors, presented here in nomographic form. Fundamental equations are derived

**T**HE construction of a facsimile system involves the design of considerable mechanical equipment as well as electronic circuits. The characteristics of the scanning units of both the transmitter and receiver are determined by a number of factors which are listed below.

- $E$  = length of picture element, in.
- $A$  = rate of scanning, sq in. per min
- $L$  = length of scanning line, in.
- $v$  = velocity of scanning, in. per sec
- $n$  = rate of line scanning, lines per min
- $N$  = line pitch, lines per in.
- $f$  = scanning frequency, cycles

The relationship of the various factors can be expressed in three fundamental equations, as follows:

$$E = \frac{L \times n}{120 \times f} \quad (1)$$

$$A = \frac{L \times n}{N} \quad (2)$$

$$L = \frac{60 \times v}{n} \quad (3)$$

Equations (1) and (2) can be rearranged to include the factor  $v$ . They then appear as

$$E = \frac{v}{2f} \quad (4)$$

$$A = \frac{60 \times v}{N} \quad (5)$$

All three equations now include a factor for velocity of scanning. Therefore, by

selecting a definite value for the velocity of scanning, it is necessary only to assume a value for one variable in each equation and solve for the other. To reduce the work of solving these equations, the nomogram chart was constructed.

There are two general classes of equipment used in facsimile transmission. In the first class, the transmitted picture is of the same dimensions as the received picture. Here, one solution is sufficient for both transmitting and receiving scanning units. In the second class, the picture may be enlarged or reduced in the process of transmission. Here, the dimensions are different, but the proportions remain the same. Thus, the product  $LN$  and the rate of line scanning  $n$  must be equal in the transmitter and receiver.

## Use of the Chart

To illustrate the use of the chart the following examples are given: After a suitable velocity of scanning is selected as indicated above, a straightedge is placed at the proper value on scale  $v$ . The intersections of the straightedge and scales  $E$  and  $f$  indicate the solution of Eq. (4) for the length of picture element and the scanning frequency, respectively. By rotating the straightedge about the point  $v$ , and by proper interpretation, the optimum values of  $E$  and  $f$  can be obtained. Equations (3) and (5) can be solved by

following the same procedure, making use of scales  $L$  and  $n$ , and  $A$  and  $N$ , respectively.

Where the transmitted and received pictures are of different sizes, the method of solution is as follows. The characteristics of either the transmitting or receiving scanning unit are determined as described above. A straight line is established through the points on scales  $L$  and  $N$  which satisfy the first scanner. The intersection of this line and scale  $K$  gives the product  $LN$ , which must be equal in the two scanning units. The straightedge is then rotated about the point on scale  $K$  to give new values of  $L$  and  $N$ . This will now produce pictures of a different size, but of the same proportions.

A straight line between the new value of  $L$  and the value of  $n$  for the other scanning unit ( $n$  must be equal in both cases) will determine a new value of scanning velocity on scale  $v$ . The new rate of scanning is determined by the intersection of a straight line between the new values of  $v$  and  $N$  and the scale  $A$ . The remaining factor, the length of the picture element  $E$ , is determined by the intersection of the line between the new value of  $S$  and the original scanning frequency on scale  $f$  (the scanning frequency is the same in both cases), and the  $E$  scale.



## SECTION XXIV

# TRANSMISSION LINES

	Page
Transmission-line Charts.....	321
Characteristics of Resonant Transmission Lines.....	324
Transmission-line Calculator.....	326
Impedance Chart for R-f Lines.....	332
Transmission-loss Charts.....	333
R-f Matching Sections.....	335
Universal Wave Guide Chart.....	336
Skin-effect Charts and Formulas.....	338
R-f Resistance of Copper Wire.....	343

## Transmission-line Charts

By R. F. BAUM

Charts permit quick evaluation of expressions involving sines or tangents of complex numbers, speeding and simplifying the computation of voltage, current, and impedance distribution for any point on a long transmission line, and for any termination producing standing waves

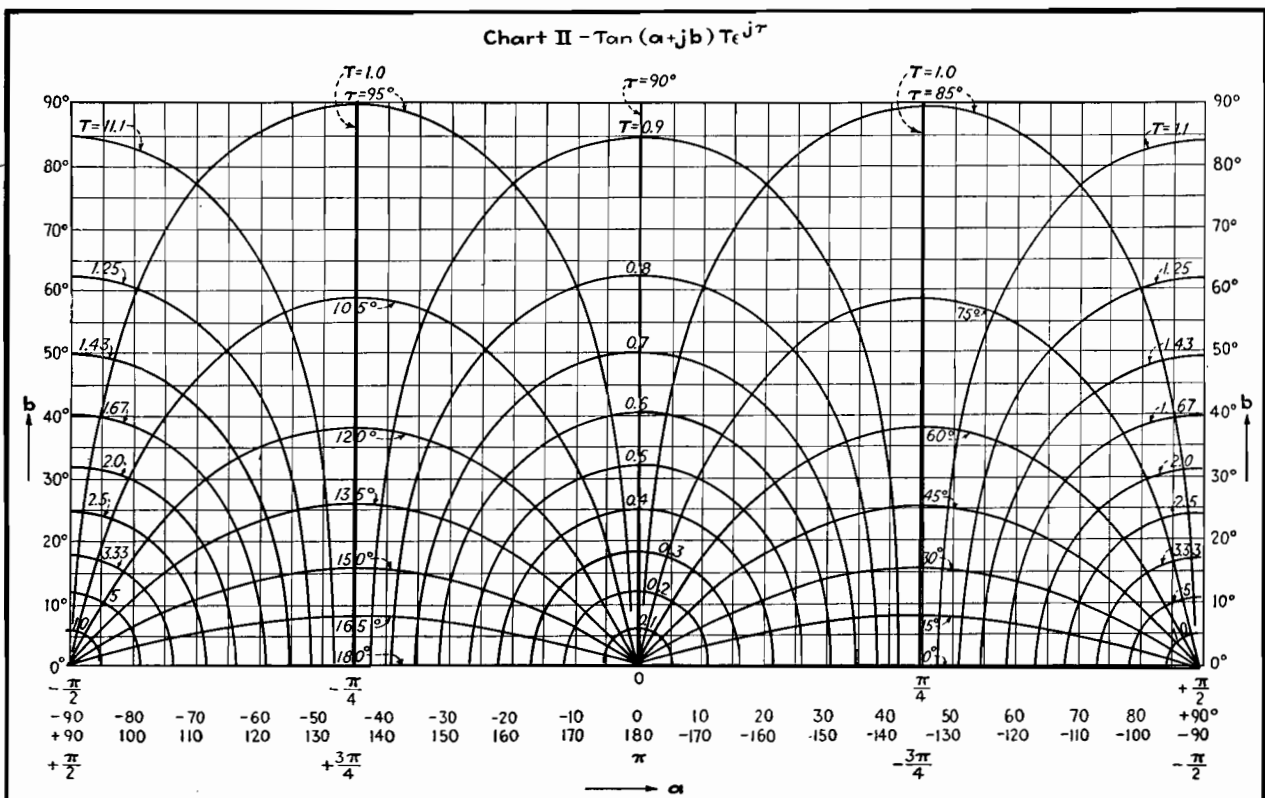


Fig. 1.—This chart enables transferring tangent of complex quantity from rectangular to polar form and vice versa.



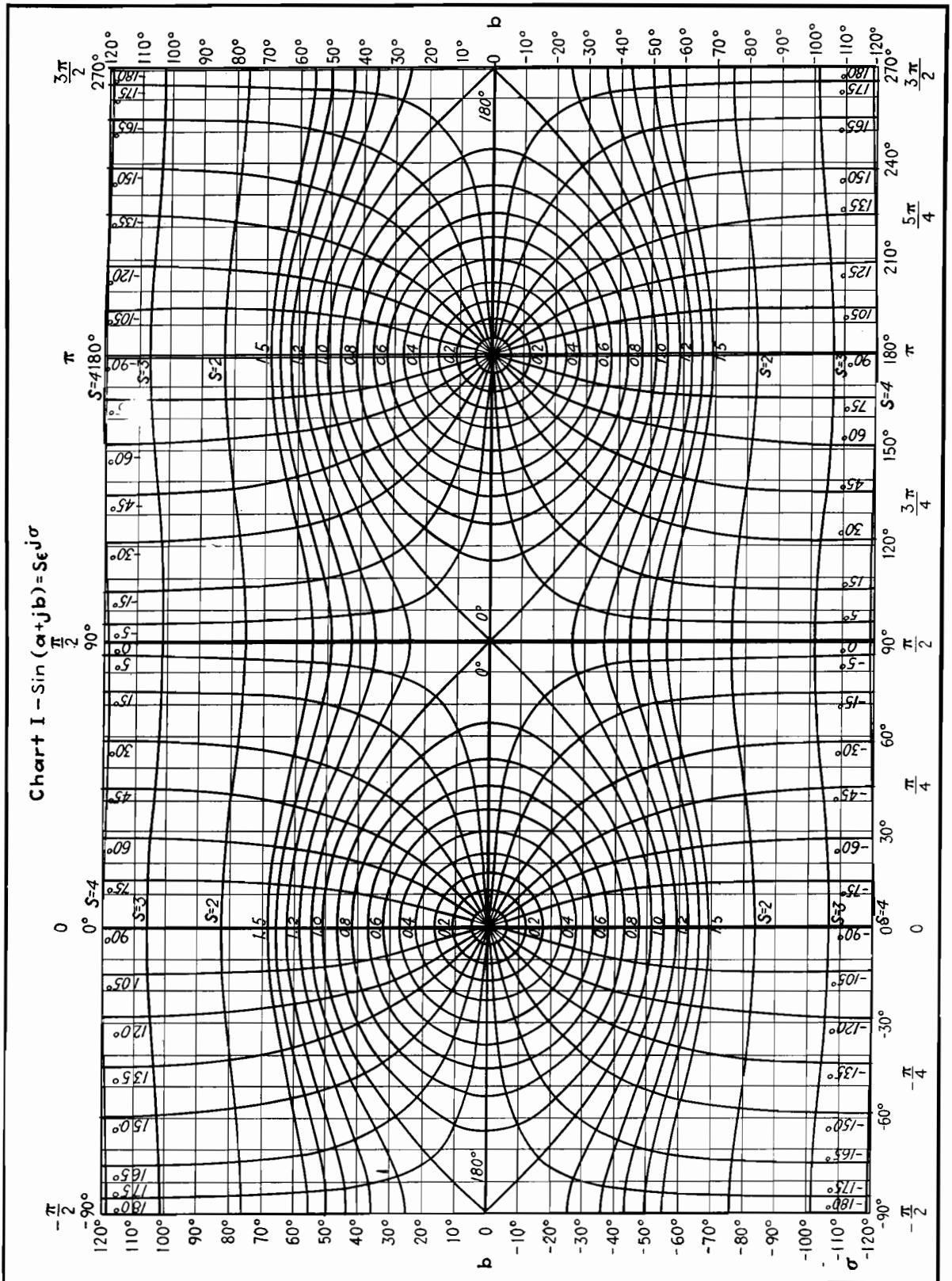


Fig. 2.—Graphical chart for transforming sine of complex quantity from rectangular to polar form and vice versa.



the error is no more than may be expected from any graphical computation.

**Example 3.**—A cable 75 meters long is fed with 10 volts applied at 1.5 Mc. The characteristic impedance is  $Z_c = 75$  ohms. The attenuation and phase constants per 100 meters of line are  $\alpha = 0.013$  and  $\beta = 3.5$ , so that  $\alpha l = 0.013 \times 0.75 = 0.0098$  radian, or 0.6 deg, while  $\beta l = 3.5 \times 0.75 = 2.63$  radians, or 151 deg. The load is given as  $Z = R + j\omega L = 55 + j125 = 136.5/66^\circ$ . From this data we find that

$$\begin{aligned}\tan Z &= \frac{jZ_c}{Z_l} = \frac{j75}{136.5/66^\circ} \\ &= 0.55/24^\circ = T e^{j\tau}\end{aligned}$$

Now, looking up in Fig. 1 the intersections  $T = 0.55$  and  $\tau = 24$  deg, we find  $Z = 28 + j10$  deg. The point  $X$  is given by

$$\begin{aligned}X &= Z + \gamma l = Z + j\alpha l - \beta l \\ &= 28 + j10 - 151 + j0.6 \\ &= -123 + j10.6^\circ\end{aligned}$$

A line connecting  $X$  with  $Z$  gives the current distribution on Fig. 2. A parallel line displaced 90 deg to the right gives

the voltage and impedance distribution. This line connects the point  $X' = -33 + j10.6$  with  $Z' = 118 + j10$ . These lines are substantially horizontal at the inclination, and  $\delta = \tan^{-1} \alpha/\beta$  is only 0.004.

Point  $X'$  in Fig. 2 reads  $S = 0.58$  and  $\sigma = 165$  deg corresponding to an input voltage  $V_o = 10/0^\circ$  volts. Therefore,

$$\begin{aligned}C_v &= \frac{\bar{V}_o}{S/\sigma} = \frac{10}{0.58/165^\circ} \\ &= 17.25/-165^\circ\end{aligned}$$

Point  $Z$  in Fig. 2 reads  $S = 0.95$ , and  $\sigma = -3$  deg and therefore the output voltage is

$$\begin{aligned}V_l &= C_v S/\sigma \\ &= [(17.25)/-165^\circ][(0.95)/-3^\circ] \\ &= 16.4/-168^\circ\end{aligned}$$

Going along the line  $X'Z'$ , the point of minimum voltage is obtained at  $0 + j10$  with  $S = 0.17$  and  $\sigma = 90$  and the point of maximum voltage at the point  $90 + j10$ , with  $S = 0.99$  and  $\sigma = 0$ . Therefore

$$\begin{aligned}V_{\min} &= 0.17 \times 17.25/90^\circ - 165^\circ \\ &= 2.95/-75^\circ \text{ volts}\end{aligned}$$

$$\begin{aligned}V_{\max} &= 0.99 \times 17.25/0^\circ - 165^\circ \\ &= 17/-165^\circ \text{ volts}\end{aligned}$$

Going along the line  $X'Z'$  in Fig. 1, we have for point  $X'$ , the values  $T = 0.58$ , and  $\tau = 157$  deg which must be multiplied by  $-jZ_c$  to obtain the input impedance. Thus

$$\begin{aligned}Z_o &= jZ_c T/\tau = (75/-90^\circ)(0.58/157^\circ) \\ &= 43.5/67^\circ \text{ ohms}\end{aligned}$$

Now point  $Z'$  must correspond to the load impedance, and at this point we find  $T = 1.75$  and  $\tau = 158$  deg. The load impedance is therefore

$$\begin{aligned}Z_l &= (75/-90^\circ)(1.75/158^\circ) \\ &= 131/66^\circ \text{ ohms}\end{aligned}$$

which differs slightly from the true value of  $136.5/66^\circ$  ohms.

Knowing the input impedance and the voltage, the input current will be

$$I_o = \frac{V_o}{Z_o} = \frac{10}{43.5/67^\circ} = 0.23/-67^\circ \text{ amp}$$

The current distribution can be followed on line  $XZ$  in Fig. 2.

## Characteristics of Resonant Transmission Lines

By J. B. EPPERSON

Elementary characteristics of ideal or low-loss transmission lines are presented in convenient graphical form. Voltage, current, and resistance along resonant lines are portrayed, together with the equivalent resonant circuit at quarter-wave sections and the reactance for other lengths of open or shorted lines

THE important part that transmission lines play in modern radio communication makes it useful to have available in compact graphical form for ready reference a graphical interpretation of the behavior of such lines. For simplicity of presentation, the curves and diagrams have been plotted on the assumption that the lines are free from losses. The presence of a slight amount of attenuation will not appreciably affect the general shape of the curves; hence the diagrams are useful for many practical applications as well as for the ideal loss-free case. If the line has appreciable attenuation, however, the curves given here must be modified slightly to apply to actual conditions.

In drawing the curves, the line is

assumed to be fed from a generator whose output impedance is equal to the characteristic impedance of the line. With this stipulation, the wave is absorbed and dissipated and is not reflected from the sending end. The curves are drawn for lines whose distant ends are open or shorted, corresponding to infinite and zero-resistance termination at the far end.

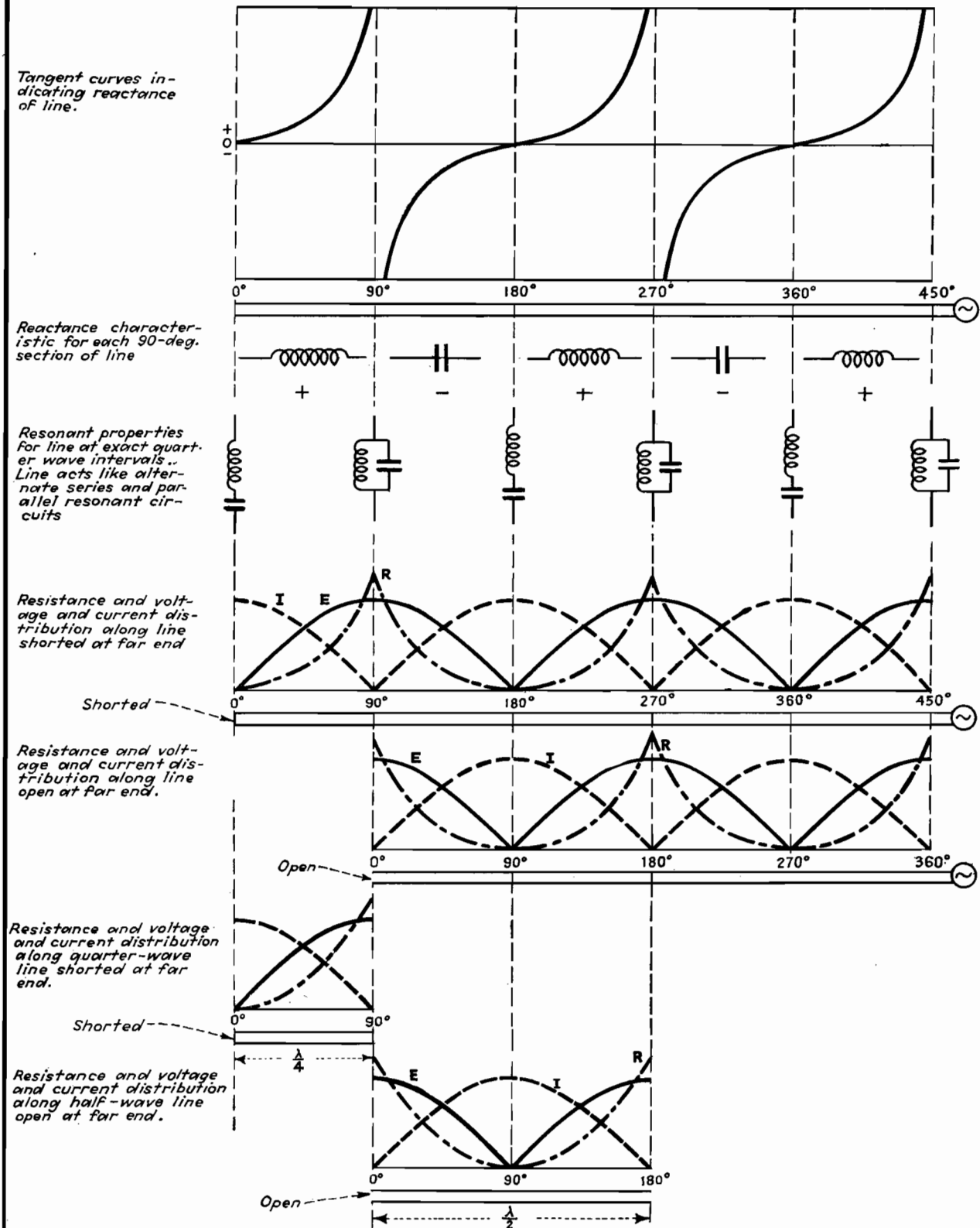
All the data for which the chart has been compiled are available at a glance. For example, the length of line required to produce a high impedance, a low impedance, an inductive reactance, or a capacitive reactance is directly evident.

Reading from top to bottom, the chart shows the following data for transmission lines:

1. The reactance curves for lines of

any length. While the curves shown apply for lines whose length is one wavelength or less, the curves are periodically repetitive, and hence may be extended to lines of any length. For lines longer than one wavelength, it is convenient to determine the line characteristics by subtracting an integral number of wavelengths from the line. The remaining length of line will then be less than one wave in length, and its characteristics may then be determined from the graphs.

2. The electrical equivalent reactance for lines of various lengths between exact multiples of a quarter-wave line. When the reactance curve is positive, the electrical equivalent reactance is inductive, whereas it is capacitive for lines of



Characteristics of resonant lines.

such length that the reactance curve is negative. The ideal line, free from attenuation, behaves either as a pure inductive reactance or as a pure capacitive reactance within any given quarter-wave section. Actual lines, in which some attenuation is present, will also show a resistive component as well as the reactive component, but this is not indicated on the diagram.

3. The resonant circuit characteristics of the line at exactly each quarter wavelength. The ideal line behaves as a series resonant circuit and as a parallel resonant circuit alternately every quarter of a wave long. In the ideal case, the line has zero resistance when the series resonant circuit is used to represent it and infinite impedance for those quarter wavelengths for which it behaves as a parallel resonant circuit. Actually, real

physical lines have more than zero and less than infinite resistance at these points. The line is resonant at 90-deg intervals for both open and shorted cases, and for quarter-wave intervals, the line behaves alternately as a series and as a parallel resonant circuit.

4. The resistance and the voltage and current distribution for open and shorted lines are given. For convenience, the resistance curve is plotted along with the voltage and current distribution along the length.

5. For the shorted line, the graphs show that, as measured from the shorted end, the line acts first as an inductance for the first quarter-wave section, then as a capacitance for the next quarter-wave section, and so on, alternately for each 90-deg interval.

6. For the open-end line, the graph

shows that, as measured from the open end, the line acts first as a capacitance and then as an inductance, alternately, for each quarter-wave section.

7. The quarter-wave diagram near the bottom of the chart is intended to show that a quarter-wave section of line may be considered as a tuned circuit. If the line is slightly less than a quarter wave, it will present inductive reactance, whereas if it is slightly longer than a quarter wave, the section will assume the characteristics of a capacitance.

8. In a similar manner, the lowest diagram is intended to show that a half-wave line may be considered as a tuned circuit element. If the line is slightly less than a half wave long, its reactance will be inductive, whereas the reactance will be capacitive if the line is slightly longer than a half wave.

## Transmission-line Calculator

By PHILLIP H. SMITH

THE calculator described here is fundamentally a special kind of impedance coordinate system, mechanically arranged with respect to a set of movable scales to portray the relationship of impedance at any point along a uniform open wire or coaxial transmission line to the impedance at any other point and to the several other electrical parameters. These other parameters are plotted as scales along the radial arm and around the rim of the calculator, both of which are arranged to be independently adjustable with respect to the main impedance coordinates. All the parameters are related to one another, and specific solutions to a given problem are obtainable through the use of an adjustable cross-hair index along the radial arm, which extends to intersect the scales around the rim. The parameters that are plotted on the calculator include the following:

1. Impedance, or admittance, at any point along the line. (a) Reflection coefficient magnitude. (b) Reflection coefficient angle in degrees.

2. Length of line between any two points in wavelengths.

3. Attenuation between any two points in decibels. (a) Standing wave loss coefficient. (b) Reflection loss in decibels.

4. Voltage or current standing wave ratio. (a) Standing wave ratio in deci-

bels. (b) Limits of voltage and current due to standing waves.

A brief discussion of each of the several parameters and the manner in which they may be evaluated from the calculator will be given.

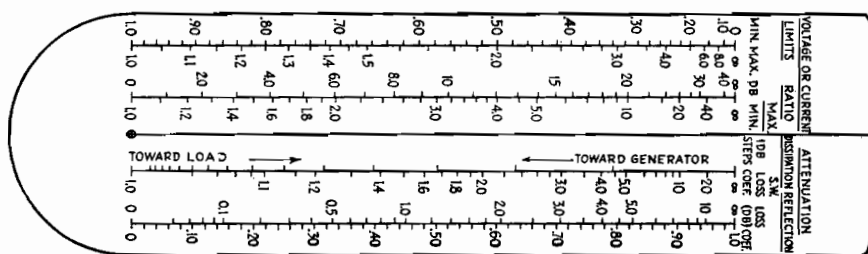
The impedance at any point along a transmission line is, unless otherwise defined, normally considered to be that impedance which would be measured if the line were cut at that point and measurements were made looking into the line section which is connected to the load.

### Impedance—General Considerations

The impedance at any point along the line and the power reaching this point from the generator completely determine the magnitude of the current and voltage and their phase relationship at that point. For a steady state, the generator imped-

ance itself, as well as the impedance looking toward the generator from any point along the line where it may have been considered to have been cut, can in no way affect the distribution of current or voltage along the transmission line to which the generator is connected.

In other words, the generator impedance can have no effect on the standing wave position or amplitude ratio or on the relation of the standing wave to the impedance distribution (locus of impedances) along the line. The generator impedance can affect only the power delivered to the transmission line and, consequently, the amplitude of the current or voltage all along the line, proportionately. The calculator relates the series components of the impedances thus considered at any point along a transmission line to a number of other parameters which will be discussed individually.



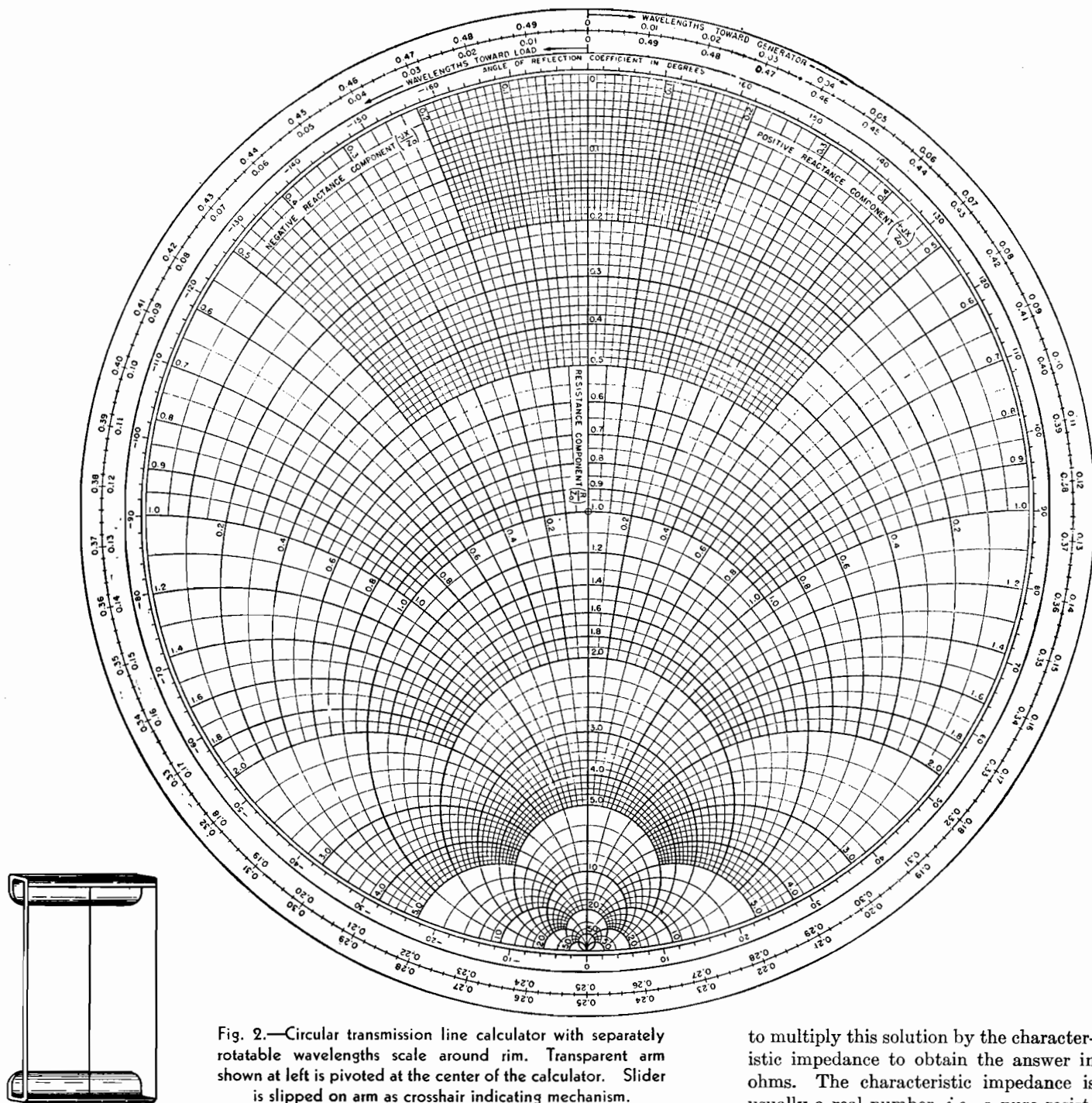


Fig. 2.—Circular transmission line calculator with separately rotatable wavelengths scale around rim. Transparent arm shown at left is pivoted at the center of the calculator. Slider is slipped on arm as crosshair indicating mechanism.

#### Impedance Coordinates—Central Area of Calculator

The series impedance components are represented on the calculator as two orthogonal families of circular curves plotted upon the central circular disk, one family of curves representing resistances and the other reactances. All impedances, both known and unknown, are read thereupon. To make the calculator of general application, these impedance coordinates are labeled as a fractional part of the characteristic impedance of the line (a fixed parameter in any given

problem which may be evaluated from the physical dimensions of the line).\*

It is therefore necessary when using the calculator for solving problems involving the impedance at any point to first divide the components of all known impedances by the characteristic impedance of the line, then obtain a solution from the calculator which, if an impedance, will be expressed as a fraction of the characteristic impedance of the line, and finally

\* MORRISON, J. F., *Transmission Lines, Pick-ups* (Western Electric Co., New York), December, 1939. See also THERMAN, "Radio Engineers' Handbook," p. 174, McGraw-Hill Book Company, Inc., New York.

to multiply this solution by the characteristic impedance to obtain the answer in ohms. The characteristic impedance is usually a real number, i.e., a pure resistance, for radio transmission lines, which makes this procedure a relatively simple one.

The relation between the impedance of the line at any point and the other parameters listed above is evaluated with the aid of the cross-hair index line on the radial arm as described later.

#### Equivalent Parallel Components of Impedance

The calculator also provides a means for converting the series components of impedances to their equivalent parallel resistance and parallel reactance com-



ponents. This is accomplished by setting the series components under the cross-hair index line on the radial arm and then moving the latter to the diametrically opposite point on the calculator and taking the reciprocal of the values read at that point as the equivalent parallel resistance and parallel reactance. (A reciprocal scale is provided along the radial arm.) The equivalent parallel component of resistance is useful in problems where it is desired to evaluate the magnitude of the voltage and to avoid converting the problem to one involving admittances.

### Admittance Coordinates

The calculator relates the series components of admittances, as well as impedances, to the various other parameters listed above and accordingly the coordinates may be considered to be admittance coordinates if preferred. In this case the coordinate axis (real) labeled Resistance Component ( $R/Z_0$ ) becomes the Conductance Component ( $a/Y_0$ ) axis, the scale units then indicating a fractional part of the characteristic admittance of the line. Likewise, the coordinate axis (imaginary) labeled Positive Reactance Component ( $+jX/Z_0$ ) becomes the Positive Susceptance Component ( $+jb/Y$ ) axis and in the negative direction the Negative Susceptance Component ( $-jb/Y$ ).

Admittance is defined as  $Y = a + jb$ , and it is important to remember that capacitance is considered to be a positive susceptance and inductance a negative susceptance. The direction of rotation indicated on the calculator in moving from one point to another is the same whether impedance or admittance coordinates are considered.

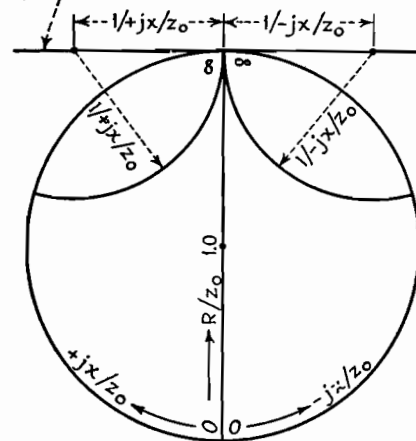
### Converting Impedances to Admittances

Impedances may be converted to admittances, or vice versa, by going to a diametrically opposite point on the calculator, as described above for obtaining the equivalent parallel resistance components, and reading the values at that point as conductance and susceptance.

### Reflection Coefficient

The impedance (or admittance) at any point along a uniform transmission line is completely defined by the amplitude and phase angle of the "reflection coefficient" at that point. It is often convenient to think of transmission-line phenomena in terms of the magnitude and phase relationship of reflected and incident

Construction line, tangent to circle at  $R/Z_0 = \infty$ . Note: Center points of all "constant reactance" circles fall on this line.



Construction of constant-reactance curves  $\pm jX/Z_0$ .

traveling waves, i.e., the reflection coefficient of the transmission line under consideration.

The magnitude of the reflection coefficient is expressed by a number between 0 and 1.0, which represents the ratio of reflected to incident voltage at the point under consideration. If the attenuation of the line is negligible, the magnitude of the reflection coefficient will be a constant at all points along the line for a given load impedance resulting in a given standing wave amplitude ratio along the line.

The magnitude of the reflection coefficient is plotted as a scale along the radial arm. The phase angle of the reflection coefficient is directly related to the impedance and accordingly is indicated on the calculator as a scale around the rim of the impedance coordinate system.

All impedances radially in line have a constant reflection coefficient phase angle. This phase angle is the angle by which the reflected wave lags the incident wave at the point along the line under consideration. Where these two waves add in phase to give a maximum voltage, the impedance is resistive and greater than the characteristic impedance of the line, and the angle of the reflection coefficient is zero degrees. Going toward the generator from this point, the departure from zero phase angle is linearly related to the distance traversed. The reflected voltage wave at first lags the incident voltage wave (having the longer path to traverse), and the phase angle of the reflection coefficient is considered to be negative for the first quarter wavelength from the voltage maximum point in the direction of the generator. The reactive com-

ponent of the impedance in this region is negative.

At the exact quarter-wavelength (90 deg) point, the incident and reflected voltage waves are exactly out of phase and the angle of the reflection coefficient is  $\pm 180$  deg. Continuing in the same direction toward the generator, the two waves become increasingly more in-phase and in this region between one-quarter and one-half wavelength from the voltage maximum point toward the generator, where the reactive component of the impedance is inductive, the reflected wave leads the incident wave, and the reflection coefficient has a positive angle.

The relationship between the magnitude of the reflection coefficient and the standing wave amplitude ratio may be derived from the fact that at the voltage maximum point the incident and reflected waves add in phase, whereas, at the voltage minimum point they are exactly out of phase, thus

$$\frac{E_{\max}}{E_{\min}} = \frac{V_I + V_R}{V_I - V_R} = \frac{1 + \frac{V_R}{V_I}}{1 - \frac{V_R}{V_I}} \quad (1)$$

Since  $V_R/V_I = k$

$$\frac{E_{\max}}{E_{\min}} = \frac{1 + k}{1 - k} \quad (2)$$

$k$  = magnitude of the voltage reflection coefficient

$V_R$  = reflected voltage

$V_I$  = incident voltage

### Length of Line—Movable Distance Scale around Rim

Impedances along a uniform transmission line vary cyclically, repeating every half wavelength if the line has negligible attenuation. Thus, for any given termination the impedance locus path in going along the line in either direction from any initial starting point will close upon itself in exactly one-half wavelength effective length. The circular calculator is arranged so that one trip around the impedance-coordinated disk at any constant distance from the center corresponds to a movement of just one-half wavelength along the transmission line. The length scale around the rim of the calculator is linear, and its zero position may be adjusted so that measurements can be started from a point radially in line with any known impedance point on the coordinates and carried in either direction, i.e., either "toward the generator" or "toward the load" to a point where it may be desired to know the impedance.



Uniform transmission lines with air dielectric and negligible attenuation have an "effective length" equivalent to the length of the wave in free space, and no correction is required for the length scale. However, any solid dielectric material in the field of the conductors causes a reduction in the length of the standing wave which is proportional to  $1/\sqrt{K}$  where  $K$  is the dielectric constant. This applies to lines where the entire field is confined to a homogeneous dielectric such as rubber-insulated coaxial lines. In coaxial lines, for example, where bead insulators are used, if the beads are spaced closer than about  $1/36$ th wavelength, the line may be considered to have a uniform effective dielectric constant. The length scale refers to the effective length of the line.

As later discussed, the relation between impedance and current distribution (standing waves), especially with respect to their position along the line, is often conveniently referred to the pure resistance points, and length measurements are often made with reference to one end or the other of the real axis, at which points the maximum and minimum current and voltage points occur.

Any line length in excess of one-half wavelength can be reduced to an equivalent shorter length to bring it within the scale range of the calculator by subtracting the largest possible whole numbers of half wavelengths therefrom.

#### Scales Along Radial Arm

A number of the parameters are uniquely related to one another as well as to the magnitude of the reflection coefficient previously described. These parameters are conveniently plotted as scales along the radial arm in nomograph form. Their relationship may be evaluated through the use of the sliding index line which permits reading any or all of the

several scales at the intersection of the slider index line. A given set of such values are also related to a given impedance locus which is traversed upon the impedance coordinates at the cross index line intersection when the radial arm is rotated once around the calculator. The several related parameters plotted along the radial arm in nomograph form include the following:

1. Attenuation in 1-db steps (due to loss resistance of line, leakage, and dielectric loss).
2. Standing wave loss coefficient (due to increased average current and voltage).
3. Reflection loss (or gain) in decibels.
4. Reflection coefficient magnitude (voltage).
5. Standing wave ratio ( $SWR$ ) of maximum to minimum current or voltage.
6. Standing wave ratio expressed in decibels ( $20 \log_{10} SWR$ ).
7. Relative voltage or current at maximum and minimum points for constant power.

#### Attenuation

Attenuation causes the impedance locus along a uniform transmission line to spiral inward toward the center of the calculator from the initial starting point when going from the load end of the line "toward the generator," and to spiral outward toward the rim when going from an initial starting point "toward the load." The rate at which this spiral locus approaches the center (or the rim) depends directly on the attenuation per unit length of line as well as on the initial starting point.

Impedances near the rim (encountered along a line bearing a large standing wave) are altered to a greater extent by a decibel unit of attenuation, for example, than impedances near the center. The attenuation scale is conveniently plotted along the radial arm since it is a measure of the rate at which the impedance locus spirals in or out.

The starting point for this nonlinear scale must be capable of being set at any impedance point on the coordinates. Also, the scale must be capable of measuring attenuation in either direction from the starting point, depending on whether conditions are to be observed in a direction from an initial starting point toward the load or toward the generator. To accomplish this, the scale is laid out, without markings, in 1-db steps. Thus, to take into account an attenuation of, say, 3 db, it is necessary to count off three 1-db intervals in the proper direction along the

attenuation scale from whatever starting point may have existed, before reading the answer on the impedance coordinates. The proper direction to go in correcting the impedance for attenuation of the line is indicated on the attenuation scale itself.

#### Standing-wave-loss Coefficient

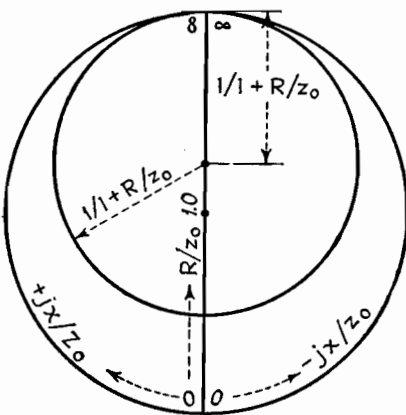
The scale along the radial arm labeled S.W. Loss Coef. shows the additional copper or dielectric loss due to the presence of standing waves in the vicinity of the standing wave measurement. This added loss coefficient, which multiplies the calculated loss in decibels for a matched line, does not affect the line impedance. This added dissipation within the line is caused by the fact that the line conducts more average current and is required to withstand more average voltage for a given transmitted power when standing waves are present than would normally be the case if the line were properly matched.

Since copper losses at any point are proportional to the square of the current and dielectric losses or leakage losses are proportional to the square of the voltage, the percentage increment in losses applies equally to either type of loss. This loss coefficient refers more accurately to the increase in losses over a half wavelength of transmission line in the immediate vicinity of the standing wave measurement. In cases where the copper and dielectric or leakage losses are approximately equal, it holds closely for any fractional part of a half wavelength. In this special case, when moving along the line, the change in copper loss due to the standing current wave is approximately compensated by an equal and opposite change in dielectric or leakage due to the reversed slope of the voltage wave, resulting in a substantially uniform increase in loss for any fractional part of a half wavelength. If, due to attenuation, the standing wave ratio and consequently the standing wave loss coefficient change in moving along the line, for example, several wavelengths, then the increased loss for the entire line section traversed lies between the coefficient limits indicated at each end.

#### Reflection Loss (or Gain)

The reflection loss may be derived from the reflection coefficient  $k$ , which, as described, is the ratio of reflected to incident voltage. The reflection loss in decibels is

$$\text{db} = 10 \log_{10} \frac{P_{\text{absorbed}}}{P_{\text{incident}}} \quad (3)$$



Construction of constant-resistance curves  $R/Z_0$ .

The absorbed power is proportional to the square of the incident voltage ( $V_I^2$ ) minus the square of the reflected voltage ( $V_R^2$ ), and the incident power is proportional to the square of the incident voltage ( $V_I^2$ ). Therefore

$$\text{db} = 10 \log_{10} \frac{V_I^2 - V_R^2}{V_I^2} \quad (4)$$

$$= 10 \log_{10} 1 - \left( \frac{V_R}{V_I} \right)^2 \quad (5)$$

$$= 10 \log_{10} (1 - k^2) \quad (6)$$

If the attenuation of the line is negligible, the reflection loss does not represent an actual loss of power, for, if an impedance match is made at the sending end of the transmission line with the generator, a reflection gain which neutralizes the loss at the load end takes place. When the attenuation is not negligible, the reflection loss at the input (which actually represents an equivalent reflection gain when the input impedance to the line is matched to the generator impedance) will be less than the reflection loss at the load. This difference between the reflection loss (which can be read on the radial arm of the calculator) at the two ends of the line represents an additional dissipation loss, which is caused by the increased average current and voltage, within the line itself.

#### Standing Wave Ratio

The standing wave ratio  $SWR$  is expressed as a number greater than 1.0. The position of the standing wave along the line is significant, and it is important to remember in using the calculator that it is always at a current maximum point that the impedance is a minimum and real, i.e., the current maximum point always falls along the  $R/Z_0$  axis (when  $Z_0$  is real) at a point between 0 and 1.0.

Likewise, it is important to remember that the current minimum point always falls along the  $R/Z_0$  axis at a point between 1.0 and  $\infty$ . The voltage standing wave is always positioned just a quarter wavelength along the line either side of the position of the current standing wave, so that a voltage minimum point on the wave will always coincide in position with a current maximum point, and likewise a voltage maximum point will always coincide in position with a current minimum point.

Thus, the relative position between impedance and current distribution (standing waves) is most conveniently referred to these pure resistances or real impedance positions along the  $R/Z_0$  axis, and stand-

ing wave measurements are made with respect to these points along the line.

A given standing wave ratio uniquely defines the locus of impedances encountered along a uniform transmission line when the latter has negligible attenuation. To determine this locus, the slider along the radial arm is set to coincide with the known standing wave ratio. The impedance locus then appears at the intersection of the cross-hair index when the arm is swung around through one complete revolution. The passage of this intersection point once around the calculator is equivalent to moving one-half wavelength along the transmission line, and it is thus seen that the impedance circle locus closes upon itself and then repeats for any two points a half wavelength apart and greater. The impedance locus passes through the resistance axis twice in one revolution of the arm about the coordinates, at which two positions the impedance is maximum and minimum, respectively, and, as described, the current and voltage, likewise, go through maximum and minimum values.

The measurement of standing waves is often accomplished through the use of sliding capacitive or inductive probes (depending on whether voltage or current waves, respectively, are to be observed). The output power taken from the probe is at a low level compared with that flowing in the main line so as not to disturb the line characteristics.

#### Standing Wave Ratio Expressed in Decibels

The probe output is amplified through a double detection receiver. The receiver includes an attenuator, in its i-f amplifier circuits, which is calibrated in decibels. The rectified output of the receiver is indicated on a reference level meter. It is convenient to adjust the meter output to an arbitrary reference mark and observe the change in attenuation required when going from a maximum to a minimum point along the standing wave. The standing wave amplitude ratio may then be expressed in decibels. Thus, a 6-db standing wave will have a ratio of maximum to minimum amplitude of 2:1. Used in this sense the term has no significance insofar as loss or power ratio is concerned. A scale is provided to permit expressing the standing-wave ratio in decibels.

#### Relative Voltage or Current at Maximum and Minimum Points

If a transmission line is conducting a given amount of power, it will do so most

efficiently when standing waves are eliminated. However, there are cases when it will be acceptable, or even desirable, to permit standing waves to exist. In this case, the line must be designed to withstand the increase in current and in voltage at the antinodes. This increase at the antinodes in both current and voltage (and decrease at the nodes) is plotted along the radial arm and refers to the increase or decrease at these points over what it would be if the line were properly terminated and were conducting the same amount of power to the load.

The voltage magnitude  $E$  at any point along the line in terms of the equivalent parallel resistance  $R_{par}$  component and the power  $P$  is

$$E = \sqrt{R_{par} \times P} \quad (7)$$

whereas the current magnitude  $I$  at any point in terms of the series resistance  $R_{ser}$  component and the power  $P$  is

$$I = \sqrt{\frac{P}{R_{ser}}} \quad (8)$$

In either case, the reactive component is not involved.

At the maximum and minimum impedance points, the series and parallel components become the same. At these points the maximum and minimum current and voltage are conveniently evaluated from the standing wave ratio, characteristic impedance, and power as follows:

$$I_{\min} = \sqrt{\frac{P}{SWR \times Z_0}} \quad (9)$$

$$I_{\max} = \sqrt{\frac{SWR \times P}{Z_0}} \quad (10)$$

$$E_{\min} = \sqrt{\frac{P \times Z_0}{SWR}} \quad (11)$$

$$E_{\max} = \sqrt{P \times Z_0 \times SWR} \quad (12)$$

where  $Z_0$  = characteristic impedance, ohms

$P$  = power, watts

$SWR$  = voltage or current standing wave ratio expressed as a number greater than unity

#### Example for Use of the Calculator

A coaxial r-f transmission line having a characteristic impedance of  $50 + j0$  ohms is terminated in an unknown impedance that causes a standing wave near the load such that  $E_{\max}/E_{\min} = 2.0$ . A voltage maximum point on the standing wave exists 0.175 wavelength from the load. The line is 2.84 wavelengths long and has 1.0-db attenuation.

1. To find the load impedance:
  - a. Set the slider on the radial arm to the position on the  $E_{\max}/E_{\min}$  scale opposite 2.0.
  - b. Rotate the radial arm until its index line coincides with the  $R/Z_o$  axis between 1.0 and  $\infty$  (where the voltage is maximum), and rotate the length scale around the rim until its zero point is aligned with the index line on the radial arm.
  - c. Rotate the radial arm 0.175 wavelength counterclockwise toward the load (from the voltage maximum point) as measured along the length scale at the rim, and read the series components of the load impedance as  $R/Z_o = 0.60$  and  $+jX/Z_o = 0.36$ . Since  $Z_o$  is  $50 + j0$  ohms, this corresponds to  $Z_L = 50(0.60 + j0.36) = 30.0 + j18.0$  ohms.
2. To find the input impedance:
  - a. As in 1a and b above.
  - b. Rotate the radial arm  $2.84 - 2.50^* = 0.34$  wavelength clockwise toward generator as measured along the length scale, and read the series input impedance components (before correcting for attenuation) as  $R/Z_o = 0.64$  and  $+jX/Z_o = 0.44$ . Since  $Z_o$  is  $50 + j0$  ohms, this corresponds to  $Z_s = 50(0.64 + j0.44) = 32.0 + j22.0$  ohms.
  - c. Correct for attenuation by moving the slider index only along the arm toward the generator one-decibel unit. The input impedance components are then read as  $R/Z_o = 0.72$  and  $+jX/Z_o = 0.37$ , which corresponds to  $Z_s = 50(0.72 + j0.37) = 36.0 + j18.5$  ohms.
3. To find the total dissipation in the line:
  - a. The attenuation as stated in the problem is 1 db, which is the nominal loss without standing waves. The increased attenuation due to standing waves (as observed at intersection of slider index with S.W. Loss Coef. scale) is 1.25 times at the load end and 1.14 times at the generator end. The slider is set, respectively, as for 2b and c above. The dissipation loss for the whole line can be shown to be increased because of standing waves by the difference read on the reflection loss scale at the two ends of the line. This is seen to be  $0.51 - 0.31 = 0.20$  db. Thus, in this case the total dissipation loss within the line is 1.20 db.
4. To find the increase in voltage or current at the maximum point due to standing waves:
  - a. With the slider index set as at 2b and c, respectively, the increase over the uniformly distributed voltage (no standing waves) due to the mismatch of impedance at the load is seen from the Limits scale to be 1.41 times at the load end and 1.31 times at the sending end of the line. At the nulls, it is reduced to 0.707 and 0.761 times, respectively. The actual magnitude of the voltage depends on the power.

#### Construction Data

It will be seen that all the circles of constant resistance are centered on the resistance ( $R/Z_o$ ) axis between the limits where  $R/Z_o = 1.0$  and  $\infty$  and that these circles are all tangent to the edge of the

coordinate system at the point when  $R/Z_o = \infty$ .

The circles of constant reactance are all centered along a straight line perpendicular to the  $R/Z_o$  axis at the point where  $R/Z_o = \infty$ .

The scales along the radial arm of the calculator are conveniently plotted as a function of the magnitude of the voltage reflection coefficient  $k$  (a linear scale running between 0 at the center and 1.0 at the rim). The formulas utilized are

Minimum voltage or current ( $N$ )

$$k = 1 - \frac{2}{1 + (1/N^2)} \quad (13)$$

Maximum voltage or current ( $X$ )

$$k = 1 - \frac{2}{1 + X^2} \quad (14)$$

Standing wave ratio (db)

$$k = 1 - \frac{2}{1 + \log^{-1} \text{db}/20} \quad (15)$$

Standing wave ratio, greater than unity ( $SWR$ )

$$k = 1 - \frac{2}{1 + SWR} \quad (16)$$

Attenuation (db)

$$k = 1 - \frac{2 \tanh(0.11512 \text{ db})}{\tanh(0.11512 \text{ db}) + 1} \quad (17)$$

Standing wave loss coefficient ( $C$ )

$$k = 1 - \frac{2}{1 + C + \sqrt{C^2 - 1}} \quad (18)$$

Reflection loss (db)

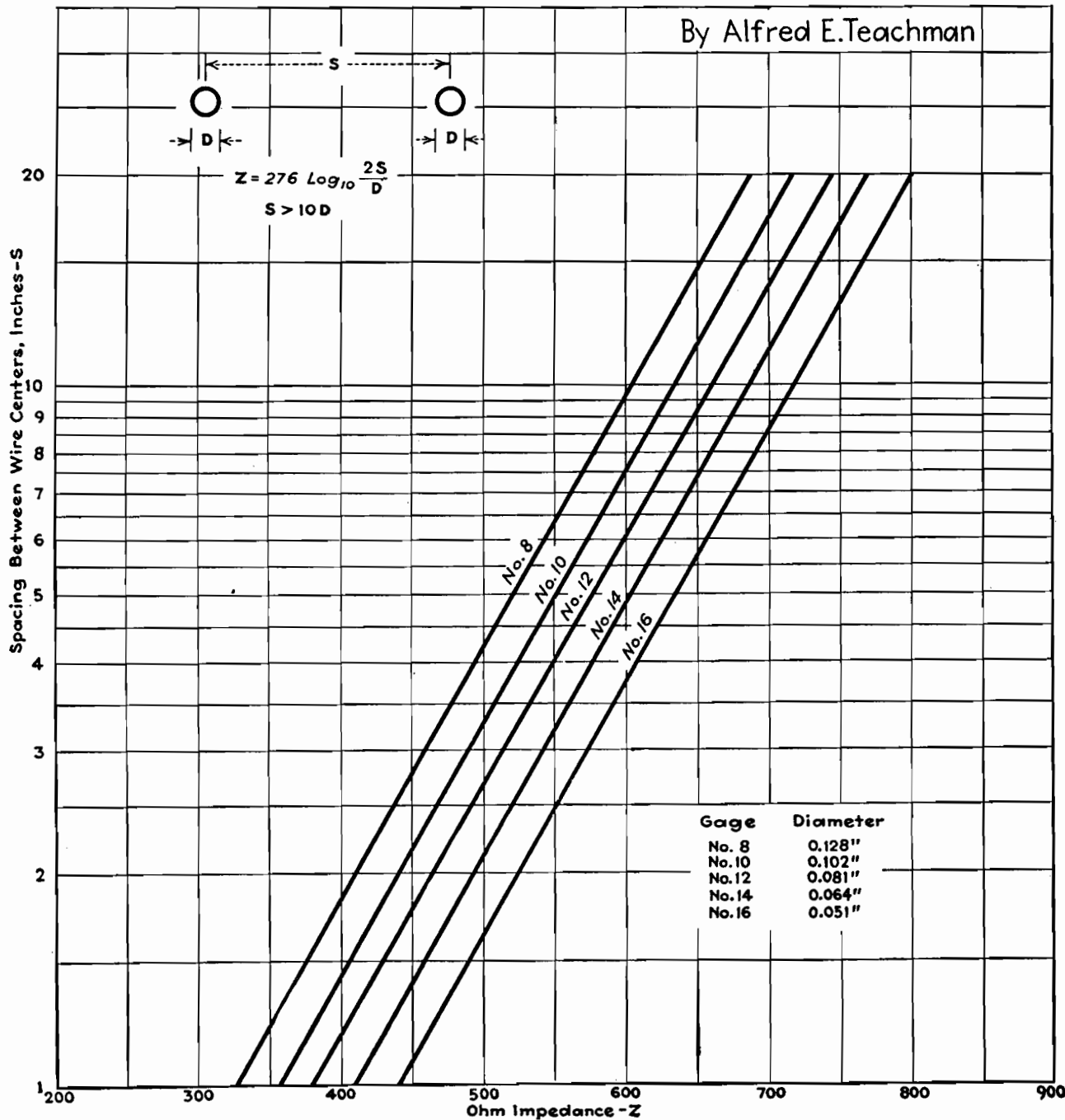
$$k = \sqrt{\frac{\left(\log^{-1} \frac{\text{db}}{10}\right) - 1}{\log^{-1} \frac{\text{db}}{10}}} \quad (19)$$

\* Subtract the largest whole number of half wavelengths to obtain equivalent length less than one-half wavelength.

# Impedance Chart for R-f Lines

By ALFRED E. TEACHMAN

Surge impedance of parallel-wire lines is given in terms of wire diameter and spacing, when the spacing is greater than ten times the wire diameter



# Transmission-loss Charts

By JACK G. ROOF

Nomographs for calculating transmission losses or gains caused by insertion of a series impedance into a line or bridging of an impedance across a line, in three ranges of values

If an emf  $E$  acts through an impedance  $Z_1$  onto an impedance  $Z_2$  in series, as in Fig. 1a, the current in  $Z_2$  is given as  $i_0 = E/(Z_1 + Z_2)$ . If a series impedance  $Z_a$  is placed between  $Z_1$  and  $Z_2$  as in Fig. 1b, the current now flowing through  $Z_2$  is  $i_a = E/(Z_1 + Z_2 + Z_a)$ . The absolute ratio of the currents in these two instances is

$$\left| \frac{i_0}{i_a} \right| = \left| \frac{Z_1 + Z_2 + Z_a}{Z_1 + Z_2} \right| = \left| \frac{1 + Z \angle \theta}{Z \angle \theta} \right|$$

where  $Z \angle \theta \equiv (Z_1 + Z_2)/Z_a$ .

Similarly, for the case of the bridged impedance of Fig. 1c,  $i_0$  is as above, and  $i_b = EZ_b/(Z_1Z_b + Z_2Z_b + Z_1Z_2)$ . The absolute value of the current ratio is

$$\left| \frac{i_0}{i_b} \right| = \left| \frac{Z_1Z_b + Z_2Z_b + Z_1Z_2}{Z_1Z_b + Z_2Z_b} \right| = \left| \frac{Z_b + \frac{Z_1}{Z_2} + 1}{\frac{Z_b}{Z_1} + \frac{Z_2}{Z_1}} \right| = \left| \frac{1 + Z \angle \theta}{Z \angle \theta} \right|$$

$$\text{where } Z \angle \theta \equiv \frac{Z_b}{Z_1} + \frac{Z_2}{Z_1}$$

Thus, in either case the same general equation results, with a necessarily different definition of  $Z \angle \theta$  in the two setups. The decibel loss due to the current decrease after insertion of the impedance is given by

$$\text{db} = 20 \log_{10} \left| \frac{i_0}{i_a} \right| = 20 \log_{10} \left| \frac{1 + Z \angle \theta}{Z \angle \theta} \right|$$

Carrying out the indicated addition of unity to  $Z \angle \theta$  and the subsequent division of this sum by  $Z \angle \theta$ , one obtains

$$\text{db} = 20 \log_{10} \sqrt{\frac{Z^2 + 2Z \cos \theta + 1}{Z^2}} = 10 \log_{10} \left( \frac{Z^2 + 2Z \cos \theta + 1}{Z^2} \right) \quad (1)$$

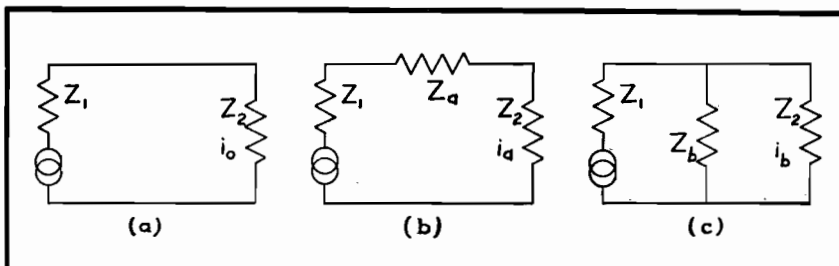


Fig. 1.—Equivalent circuit of transmission line (a), same circuit with inserted series impedance (b), and same circuit with inserted shunt impedance (c). Accompanying charts give insertion loss or gain in these circuits.

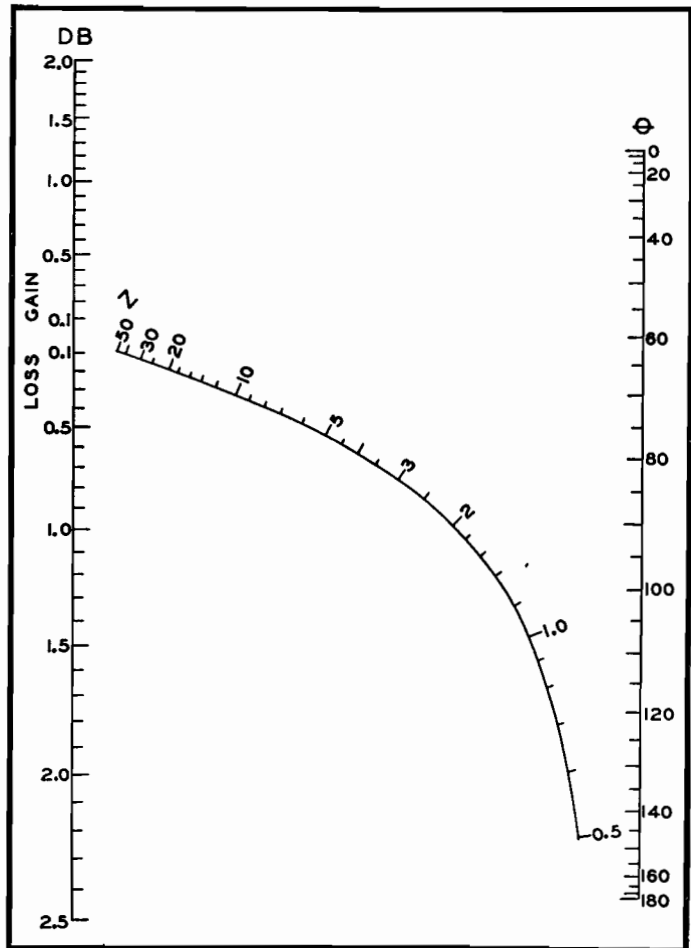


Fig. 2.—Chart for small values of impedance  $Z$  and large decibel losses and gains.

In this equation  $\text{db}$  is so defined that a positive value means a loss and a negative value means a gain in transmission. To convert Eq. (1) to a type for which a nomograph may readily be constructed, one may make the following change in form:

$$10^{db/10} = \frac{Z^2 + 1}{Z^2} + \frac{2}{Z} \cos \theta$$

which is of the form  $f(\text{db}) = \phi(Z) + \psi(Z) \cdot F(\theta)$ . This latter type of equation is known to be one for which a nomograph is calculable.<sup>1</sup>

Nomographs emphasizing two ranges of  $\text{db}$  loss (or gain) are shown in Figs. 2 and 3. The charts are labeled so as to indicate whether there is a loss or a gain

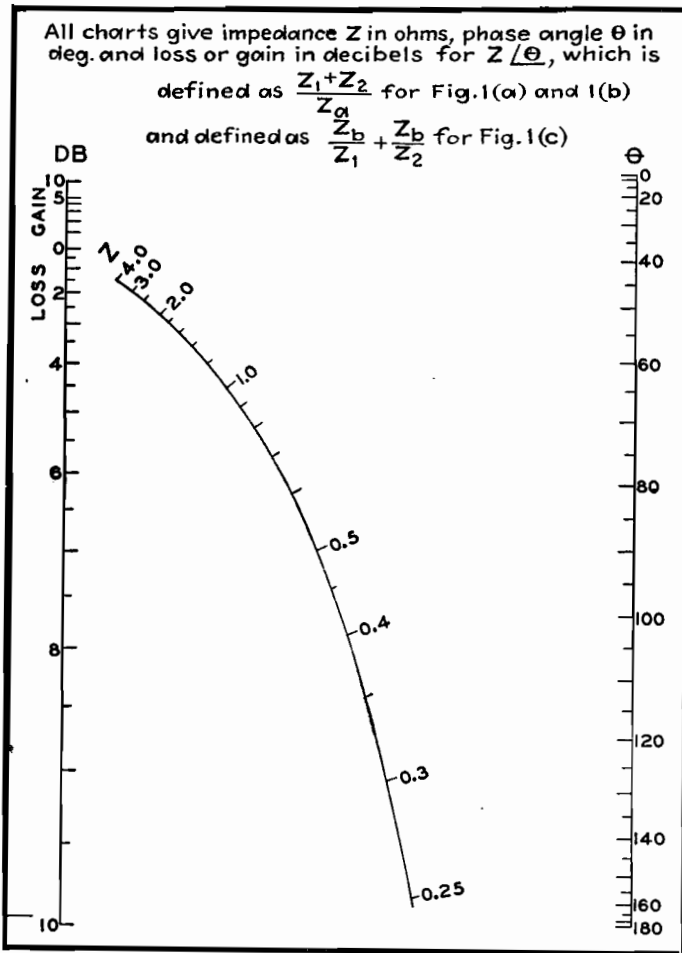


Fig. 3.—Chart for intermediate values of  $Z$  and intermediate decibel losses and gains.

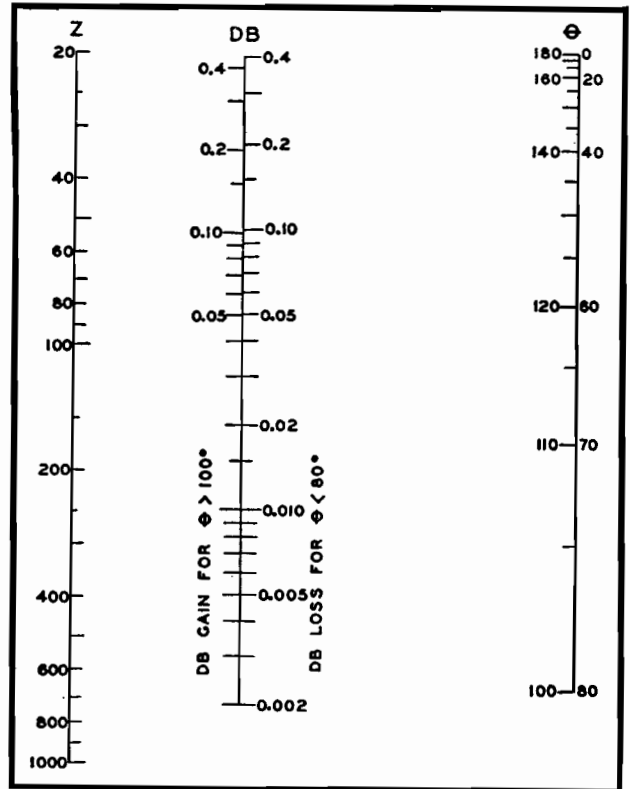


Fig. 4.—Chart for large values of impedance  $Z$  and small decibel losses and gains.

in transmission due to insertion of the new impedance. When  $\cos \theta$  is negative it is sometimes possible for db to be negative, indicating a transmission gain.

#### Improving Accuracy

Because of the particular form of Eq. (1), the accuracy at low values of db and high values of  $Z$  is not very good. However, when  $Z^2$  is large compared to unity, this equation can be simplified to give

$$10^{db/10} \approx 1 + \frac{2}{Z} \cos \theta, \text{ or}$$

$$10^{db/10} - 1 \approx \frac{2}{Z} \cos \theta \quad (2)$$

which is a good approximation if  $Z^2 \gg 1$  and if  $\theta$  is not too near 90 deg. This equation has the form  $f_2(db) = \psi(Z) \cdot F(\theta)$ , which may be represented in various forms of nomographs.

Ordinarily, because  $F(\theta)$  involves  $\cos \theta$ , which passes through zero and has negative values, the usual scheme of three parallel logarithmic scales would not be

practical. However, since the approximate Eq. (2) is not valid for values of  $\theta$  near 90 deg, this objection is of no significance. Figure 4 gives such a nomograph for high values of  $Z$  and low values of db for  $0 < \theta < 80$  deg and  $110 < \theta < 180$  deg. In this chart, use of the scale of  $\theta < 80$  deg requires reading a transmission loss; for  $\theta > 100$  deg, a gain. The maximum possible error in this chart comes with use of  $\theta = 80$  or  $100$  deg and  $Z = 20$ , in which case the absolute value of db is about 13 per cent low. This error decreases very rapidly as  $Z$  becomes larger or  $\theta$  deviates further from 90 deg, being only 3.5 per cent for  $\theta = 70$  deg and  $Z = 40$ .

The accuracy in Figs. 2 and 3 is limited only by the ability to construct, reproduce, and read the nomographs accurately. If a nomograph giving more precise values of losses and gains over a specific range of  $Z$  and  $\theta$  were needed, it could be readily constructed along the lines indicated above.

1. Suppose an impedance  $Z_a = 150 \angle 15$  deg is inserted in series between a genera-

tor of impedance  $Z_1 = 500 \angle 60$  deg and a receiver of impedance  $Z_2 = 200 \angle 90$  deg. Then

$$Z \angle \theta \equiv (Z_1 + Z_2)/Z_a$$

has a value of approximately  $4.53 \angle 53.4$  deg. Use of Fig. 3 shows for  $Z = 4.53$  and  $\theta = 53.4$  per cent a loss of approximately 1.16 db by insertion of the series impedance specified.

2. Suppose an impedance  $Z_b = 500 \angle 120$  deg is bridged across a receiver of impedance  $Z_2 = 25 \angle 15$  deg which is being powered by a generator of impedance  $Z_1 = 10 \angle 30$  deg. Then  $Z \angle \theta \equiv \frac{Z_b}{Z_2} + \frac{Z_b}{Z_1}$  has a value of approximately  $65.5 \angle 137.5$  deg. Fig. 3 shows a gain of approximately 0.10 db by use of this impedance bridge.

#### References

- (1) DAVIS, D. S., "Empirical Equations and Nomography," McGraw-Hill Book Company, Inc., New York, 1943.

# R-f Matching Sections

By A. C. OMBERG

A graphical method of computing the shunt and series elements of L-type matching sections for matching a complex impedance to a resistance, such as those of an antenna and its transmission line, in terms of the antenna and line impedances

WHEN a resistive impedance is to be matched to a complex impedance, as for example a transmission line to an antenna, a simple means of effecting a proper impedance match is the use of the L-type section, consisting of a series inductance and a shunt capacitance. A typical matching section of this type is shown in the circuit. The charts have been prepared to allow a rapid determination of the shunt and series elements in terms of the terminating impedance values.

It is assumed that the complex terminating impedance (that of the antenna) is of the form  $R + jX$ , that the reactance of the series inductance arm is  $X_s$ , and that of the shunt capacitive arm is  $X_c$ .

Then  $X$  and  $X_s$  can be combined in series to form the total inductive reactance  $X_L$ . The impedance looking into the L section, terminated by  $R + jX$ , will then be

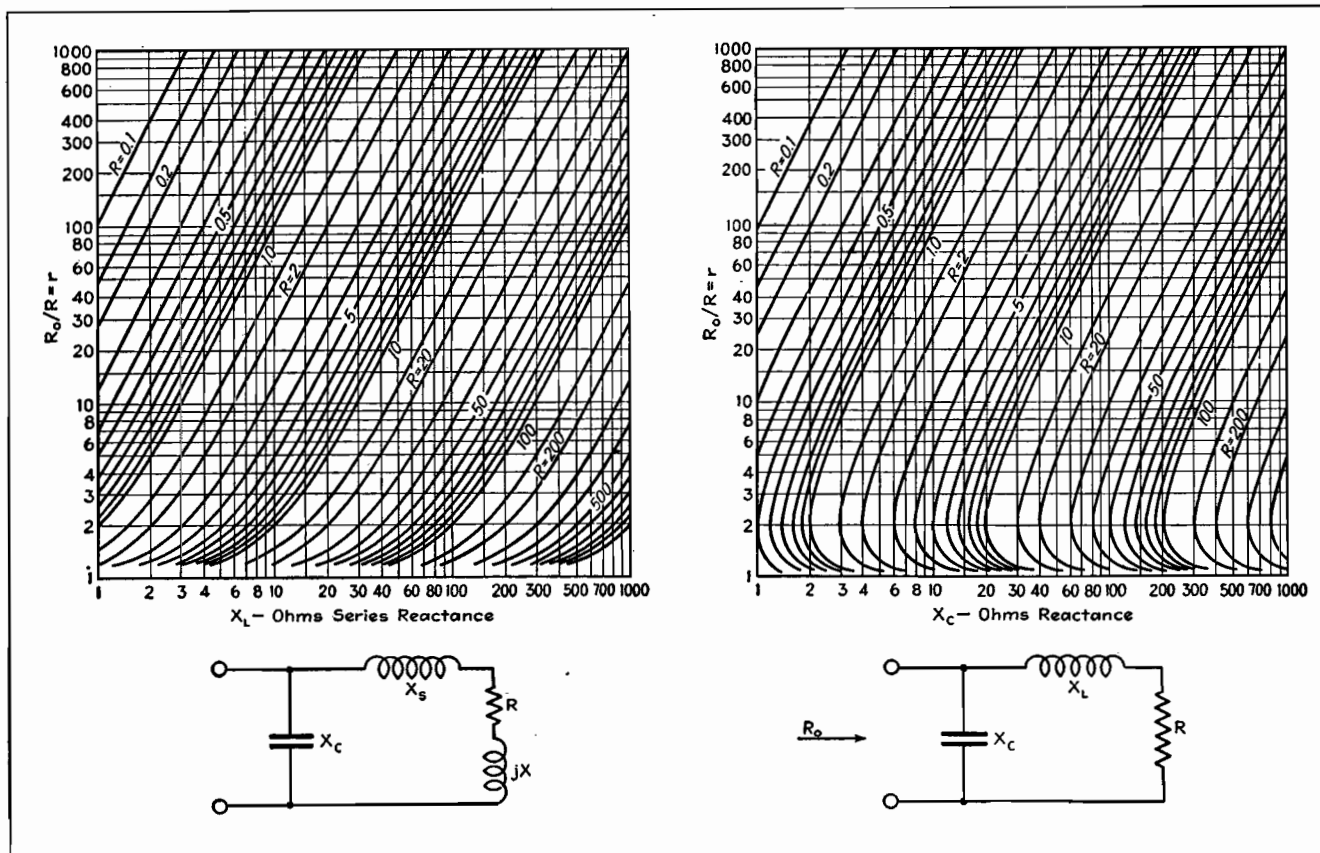
$$Z_{in} = \frac{-jX_c(jX_L + R)}{R + j(X_L - X_c)}$$

When the input of the L section is terminated in a pure resistance  $R_0$ , the surge impedance of the transmission line, a proper match is obtained when the reactive component of  $Z_{in}$  is zero, and when the resistance component is equal to  $R_0$ . With these conditions specified, the reactances  $X_L$  and  $X_c$  may be computed from

$$X_L = R\sqrt{r-1}$$

$$\text{and} \quad X_c = \frac{Rr}{\sqrt{r-1}}$$

where  $r$  is the ratio  $R_0/R$ . The curves give  $X_L$  and  $X_c$  in terms of  $r$  and  $R$ . As an example, suppose the antenna displays an impedance of  $25 + j50$  ohms, and the surge impedance of the line is 250 ohms. Then  $r = 250/25 = 10$  and  $R = 25$ . From the curves  $X_L = 75$  ohms and  $X_c = 90$  ohms. The shunt reactance is, accordingly,  $-j90$  ohms, and the total series reactance is  $+j75$  ohms,  $+j50$  ohms of which is contributed by the antenna inductance. Hence the necessary additional series inductance is  $+j25$  ohms. It should be noted that this type of network is useful only when  $r$  is greater than 1.



Charts for determining total series inductance and shunt capacitance in r-f matching sections.



# Universal Wave Guide Chart

By ARTHUR BRONWELL

Four curves on a graph give directly the phase constant, phase velocity, group velocity, attenuation constant, and wavelength for both rectangular and circular guides

It is possible to express the properties of wave guides in such a manner that the equations are identical for all rectangular and circular guides excited in either the transverse electric  $TE$  or the transverse magnetic  $TM$  modes. This makes possible the construction of a single set of curves to represent (1) phase constant  $\beta$ , (2) wavelength in the guide  $\lambda_p$ , (3) phase velocity  $v_p$ , and (4) group velocity  $v_g$  at wavelengths below cutoff, as well as (5) the attenuation constant  $\alpha$  above the cutoff wavelength. The curves are applicable to all modes of transverse electric and transverse magnetic waves in either hollow guides or dielectric filled guides. In deriving the equations from which the curves were plotted, it was assumed that the losses in the walls of the guide and in the dielectric were negligibly small, an approximation that is valid for hollow guides and approximately correct in the case of low-loss dielectric-filled guides.

The graph shows four separate quantities plotted as ordinates against the ratio of the impressed wavelength to the cutoff wavelength  $\lambda/\lambda_c$  or the corresponding frequency ratio  $f_c/f$ . To make use of the chart, it will be necessary to know both  $\lambda$  and  $\lambda_c$ . For rectangular wave guides whose cross-section dimensions are  $a$  and  $b$ , the cutoff wavelength is given by

$$\lambda_c = \frac{2\pi}{\left[\left(\frac{\pi m}{a}\right)^2 + \left(\frac{\pi n}{b}\right)^2\right]^{1/2}} \quad (1)$$

where  $m$  and  $n$  are integers expressing the mode of oscillation in the  $a$  and  $b$  directions.

For cylindrical wave guides of radius  $b$ , the cutoff wavelength is

$$\lambda_c = \frac{2\pi b}{kb} \quad (2)$$

where values of  $kb$  for various modes of excitation are given in the table. Knowing  $\lambda$  and  $\lambda_c$ , the other values can be found.

These equations are valid for either

hollow guides or metallic guides filled with a lossless dielectric medium. The wavelengths  $\lambda$  and  $\lambda_c$  also satisfy the relationship

$$f\lambda = \frac{c}{\sqrt{k}} = v \quad (3)$$

where  $c$  is the velocity of light ( $3 \times 10^{10}$  cm per sec),  $k$  is the dielectric constant, which is unity for hollow guides, and  $v$  is the velocity of propagation in unbounded dielectric having the properties of the dielectric in the guide. For hollow guides,  $v = c = 3 \times 10^{10}$  cm per sec. For given guide dimensions, the cutoff wavelength is the same for hollow or dielectric-filled guides. However, the velocity  $v$  is smaller for dielectric guides, hence the cutoff frequency is lower. These equations will be modified somewhat if the dielectric losses are taken into consideration.

As an illustration of the use of the curves, consider the special case of a hollow rectangular wave guide having the dimensions  $a = 10$  cm and  $b = 12$  cm, excited in the  $TE_{1,1}$  mode. We shall assume that the wavelength of the impressed signal is  $\lambda = 13$  cm. The cutoff wavelength then becomes

$$\lambda_c = \frac{2\pi}{\left[\left(\frac{\pi}{10}\right)^2 + \left(\frac{\pi}{12}\right)^2\right]^{1/2}} = 15.35 \text{ cm}$$

The ratio of impressed to cutoff wavelength is  $\lambda/\lambda_c = 13/15.35 = 0.847$ . From the chart we may obtain the following values:

$$\begin{aligned} \lambda_p/\lambda &= 1.89 \text{ or } \lambda_p = 1.89 \times 13 = 24.6 \text{ cm} \\ v_p/v &= 1.89 \text{ or } v_p = 1.89 \times 3 \times 10^{10} \\ &= 5.68 \times 10^{10} \text{ cm/sec}^* \\ v_g/v &= 0.525 \text{ or } v_g = 0.525 \times 3 \times 10^{10} \\ &= 1.58 \times 10^{10} \text{ cm/sec} \\ \beta\lambda &= 3.25 \text{ or } \beta = 3.25/13 \\ &= 0.250 \text{ radians/cm} \end{aligned}$$

If the impressed wavelength had been  $\lambda = 20$  cm, then  $\lambda/\lambda_c = 1.30$  and the wave would be attenuated in the guide.

\* Note that the phase velocity is greater than that of light.

The value of  $\alpha\lambda$  is then 5.1, and  $\alpha = 0.255$  neper per cm or 2.21 db per cm, since 1 neper = 8.68 db.

It should be borne in mind that the attenuation considered here is not due to power loss in the guide walls, but rather, consists of a reflection of the wave energy back to the source due to the fact that the guide dimensions are below cutoff. There is no power loss in this type of attenuation, and the attenuation constant indicates how rapidly the electric and magnetic field intensity components decrease as the wave progresses along the guide.

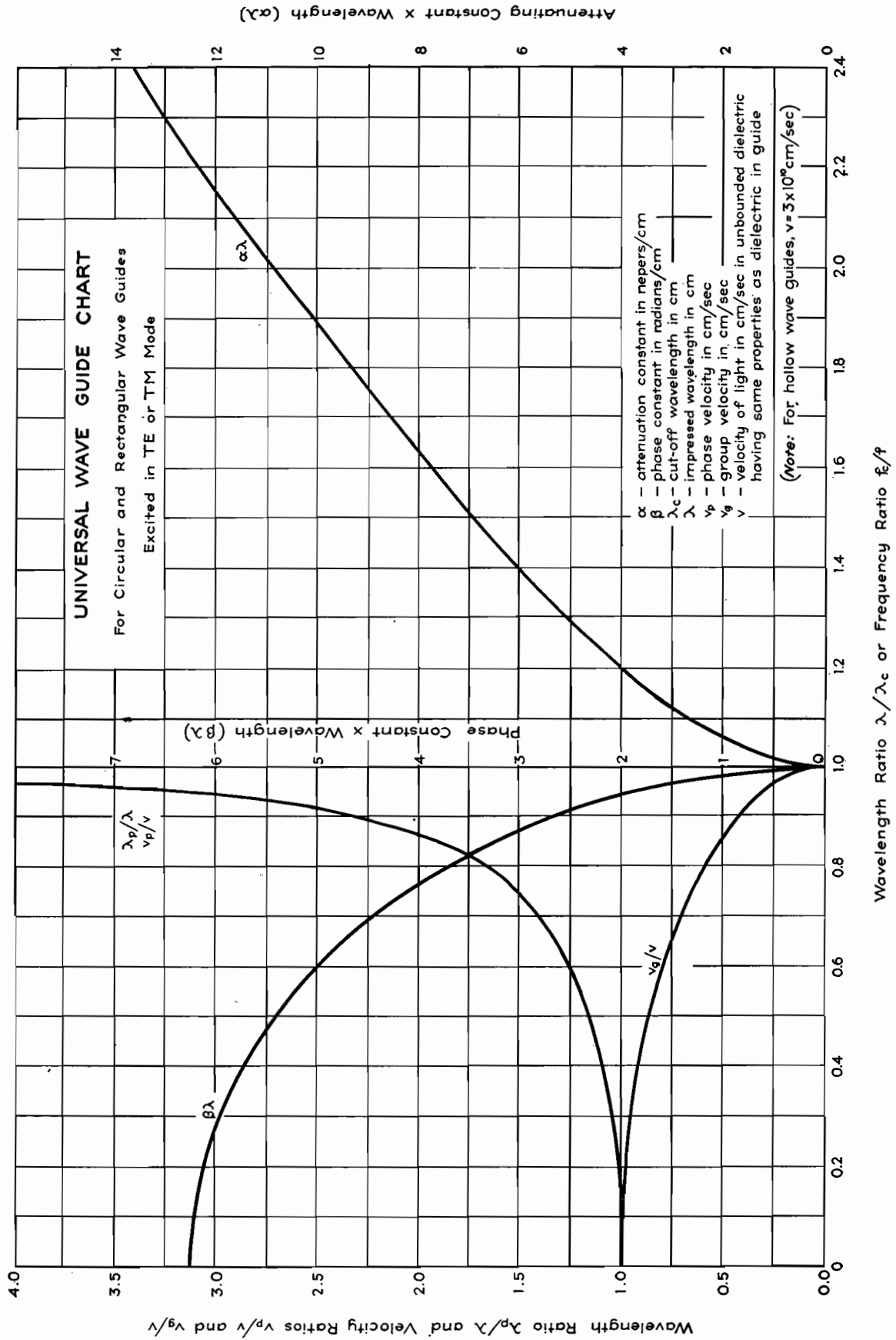
If the guide is of circular cross-section, with  $b = 5$  cm, and excited in the  $TE_{1,1}$  mode with  $\lambda = 13$  cm, the cutoff wavelength is  $\lambda_c = 2\pi b/kb = 2\pi \times 5/1.84 = 17.1$  cm. The ratio is then  $\lambda/\lambda_c = 0.761$  and, from the chart, we have the following values:

$$\begin{aligned} \lambda_p/\lambda &= 1.54 \text{ or } \lambda_p = 1.54 \times 13 = 20.10 \text{ cm} \\ v_p/v &= 1.54 \text{ or } v_p = 1.54 \times 3 \times 10^{10} \\ &= 4.64 \times 10^{10} \text{ cm/sec}^* \\ v_g/v &= 0.645 \text{ or } v_g = 0.64 \times 3 \times 10^{10} \\ &= 1.93 \times 10^{10} \text{ cm/sec} \\ \beta\lambda &= 4.0 \text{ or } \beta = 4.0/13 \\ &= 0.307 \text{ radians/cm} \end{aligned}$$

The attenuation of the circular wave guide at wavelengths above cutoff may be computed in a manner similar to that of the rectangular guide. The universal nature of this graph should make it a useful implement in wave-guide studies.

Values of  $kb$  Corresponding to Different Modes of Transmission in Cylindrical Wave Guides

$TM_{n,m}$ waves			$TE_{n,m}$ waves		
$n$	$m$	$kb$	$n$	$m$	$kb$
0	1	2.40	0	1	3.83
0	2	5.52	0	2	7.02
1	1	3.83	1	1	1.84
1	2	7.02	1	2	5.33
2	1	5.14	2	1	3.05
2	2	8.42	2	2	6.71



# Skin-effect Charts and Formulas

By J. R. WHINNERY

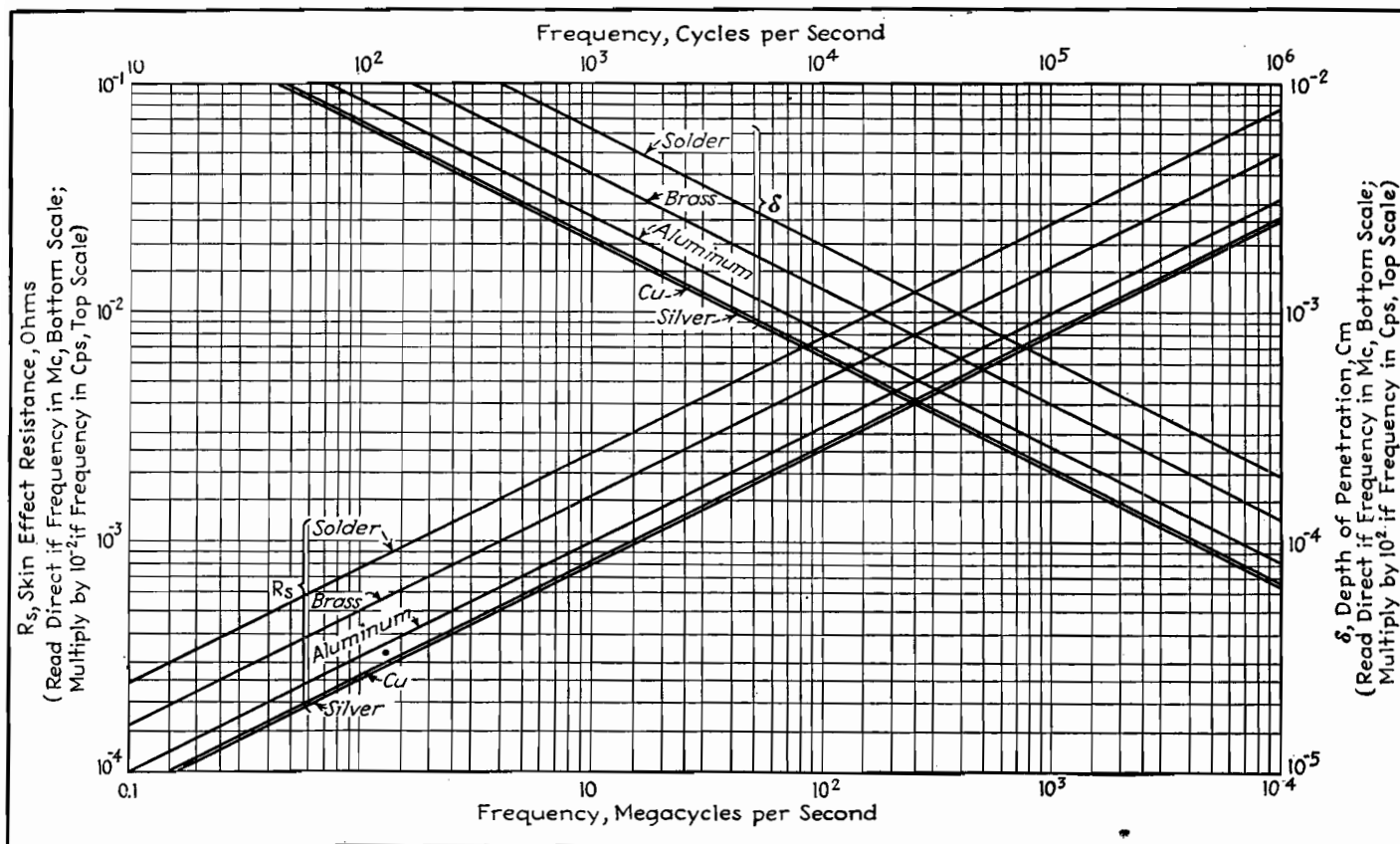


Fig. 1.—Skin-effect quantities to be used in the following curves.

ALTHOUGH skin-effect phenomena are well known, there have recently been many requests for design curves and formulas convenient for engineering use. A compilation of these formulas and curves is given here. The theoretical analysis is not included since it appears in many other references.\* The curves for coated conductors are of special interest in modern u-h-f applications. The cases treated are as follows:

1. Plane solid of infinite depth.
2. Round wire at low frequencies.
3. Round wire at very high frequencies.
4. Round wire at any frequency.
5. Tubular conductors at very low frequency.
6. Tubular conductors at very high frequency.
7. Thin-walled tubular conductors at any frequency.
8. Conductors coated with other conductors.
9. Conductors coated with thin layer of poor conductors or imperfect dielectric.

In all the following results, it has been assumed that all conductors (except the imperfect dielectric in the last section) are good enough conductors so that displacement currents in them are unimportant compared with conduction currents. It has been assumed that current does not vary along the conductor in a distance comparable to depth of penetration into the conductor. Both of these are excellent approximations for all but very poor conductors (such as earth) at any radio frequency. It is also assumed that there are no other conducting paths close enough to seriously disturb the current distributions calculated. This assumption is not good, for instance, for the wire in a closely wound coil. Other assumptions are listed in specific sections.

## Units and Nomenclature

$f$  = frequency, cycles

$\omega = 2\pi f$

$\sigma$  = conductivity in  $\frac{1}{\text{ohm cm}} = \text{mhos/cm}$

$\mu$  = permeability on the basis of unity permeability for nonmagnetic materials

$\epsilon$  = dielectric constant on basis of unity for air or space

$\delta$  = depth of penetration, cm. For a plane solid of infinite depth, this is the depth to which current density has fallen to  $1/e$  (about 37 per cent) of its value at the surface; it is also the thickness of a plane conductor having d-c resistance equal to the h-f resistance of the plane conductor of infinite depth

$R_s$  = skin effect resistance in ohms, the resistance for a unit width and unit length of the plane solid of infinite depth

$R_o$  = d-c resistance of any conductor

$r_o$  = radius of a solid round wire, or outer radius of a hollow tubular conductor, cm

$r_i$  = inner radius of a hollow tubular conductor, cm

$d$  = wall thickness of tubular conductor or coating thickness for coated conductor

$j = \sqrt{-1}$

\* See for instance A. HUND, "Phenomena in High-frequency Systems," McGraw-Hill Book Company, Inc., New York.

$\lambda$  = wavelength, measured in the dielectric coating =  $3 \times 10^{10} / f \sqrt{\mu_1 \epsilon_1}$  cm

$L_i$  = internal inductance of any conductor, or contribution to inductance of a circuit from flux inside the conductor

$(L_i)_o$  = internal inductance of a conductor at very low frequencies

### Working Formulas

1. *Plane Solid of Infinite Depth.*—Practically, this merely means any conductor whose depth and surface curvatures are large compared with depth of penetration into that conductor.

$$\delta = \frac{1}{2\pi \sqrt{f\mu\sigma} \times 10^{-9}} \text{ cm} \quad (1)$$

$$R_s = \frac{1}{\sigma\delta} = 2\pi \sqrt{\frac{f\mu \times 10^{-9}}{\sigma}} \text{ ohms} \quad (2)$$

Internal reactance  $(\omega L_i) = R_s = 1/\sigma\delta$  ohms.

$R_s$  and  $\omega L_i$  are exactly equal numerically for the plane solid of infinite depth at infinite frequency and for conductors of any size or shape at infinite frequency. This is approximately true for the other cases given below.

### Representative Values at 20°C

	Conductivity, mhos/cm ( $\sigma$ )	Depth of penetration, cm ( $\delta$ )	Skin effect resistance, ohms ( $R_s$ )
Silver.....	$6.17 \times 10^5$	$\frac{6.41}{\sqrt{f}}$	$2.52 \times 10^{-7} \sqrt{f}$
Copper.....	$5.80 \times 10^5$	$\frac{6.60}{\sqrt{f}}$	$2.61 \times 10^{-7} \sqrt{f}$
Pure aluminum.....	$3.72 \times 10^5$	$\frac{8.26}{\sqrt{f}}$	$3.26 \times 10^{-7} \sqrt{f}$
Brass.....	$1.57 \times 10^5$	$\frac{12.7}{\sqrt{f}}$	$5.01 \times 10^{-7} \sqrt{f}$
Solder.....	$0.665 \times 10^5$	$\frac{19.5}{\sqrt{f}}$	$7.70 \times 10^{-7} \sqrt{f}$

Curves of  $\delta$  and  $R_s$  as functions of frequency are given for these materials in Fig. 1.

2. *Round Wire at Low Frequencies.*—At frequencies low enough so that skin effect has not appreciably changed current from a uniform distribution, resistance and internal inductance are practically those calculated for d-c conditions. Note that resistance is inversely proportional to area, or square of radius.

$$R_o = \frac{1}{\pi r_o^2} \text{ ohms/cm length} \quad (3)$$

$$(\omega L_i)_o = \frac{\omega\mu}{2} \times 10^{-9} \text{ ohms/cm length} \quad (4)$$

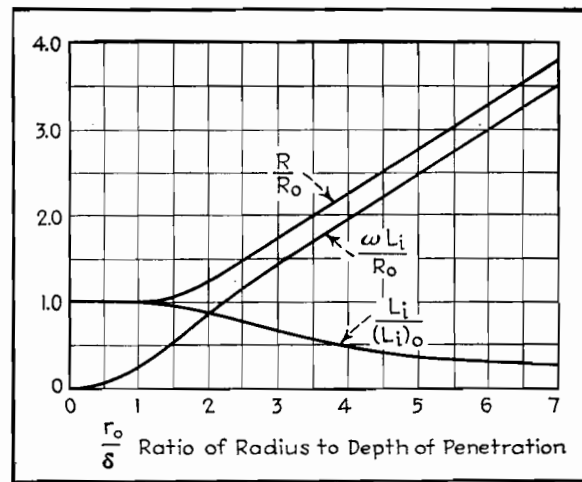


Fig. 2.—Solid round wire. Skin effect quantities compared to d-c values.  $R$  = true resistance of round wire.  $R_o$  = d-c resistance of round wire.  $L_i$  = internal inductance.  $(L_i)_o$  = internal inductance at very low frequencies.

The equation for resistance, including the first correction term that appears as the frequency increases, is

$$R_{l-f} = R_o \left[ 1 + \frac{1}{48} \left( \frac{r_o}{\delta} \right)^4 \right] \quad (5)$$

$\delta$  is given by Eq. (1) or Fig. 1.

This formula is good within 7 per cent if  $r_o/\delta < 2$  (i.e., if radius is less than twice the depth of penetration). The dividing line between low and high frequencies in this and following equations

4. *Round Wire at Any Frequency.*—Resistance and internal reactance in general may be best expressed in terms of ratios. Below are ratios to d-c resistance, and to the values of resistance and reactance calculated from the h-f formula of Eq. (6). There is also given the ratio of internal inductance to that at very low frequencies.

$$\frac{R_{l-f}}{R_o} = \frac{q}{2} \left[ \frac{\text{ber } q \text{ bei}' q - \text{bei } q \text{ ber}' q}{(\text{ber}' q)^2 + (\text{bei}' q)^2} \right] \quad (7)$$

$$\frac{\omega L_i}{R_o} = \frac{q}{2} \left[ \frac{\text{ber } q \text{ ber}' q + \text{bei } q \text{ bei}' q}{(\text{ber}' q)^2 + (\text{bei}' q)^2} \right] \quad (8)$$

$$\frac{R_{l-f}}{R_{h-f}} = \sqrt{2} \left[ \frac{\text{ber } q \text{ bei}' q - \text{bei } q \text{ ber}' q}{(\text{ber}' q)^2 + (\text{bei}' q)^2} \right] \quad (9)$$

$$\frac{(\omega L_i)}{R_{h-f}} = \sqrt{2} \left[ \frac{\text{ber } q \text{ ber}' q + \text{bei } q \text{ bei}' q}{(\text{ber}' q)^2 + (\text{bei}' q)^2} \right] \quad (10)$$

$$\frac{L_i}{(L_i)_o} = \frac{4}{q} \left[ \frac{\text{ber } q \text{ ber}' q + \text{bei } q \text{ bei}' q}{(\text{ber}' q)^2 + (\text{bei}' q)^2} \right] \quad (11)$$

$$q = \frac{\sqrt{2} r_o}{\delta} [\delta \text{ given by Eq. (1) or Fig. 1}]$$

In the above formulas,  $\text{ber } q$ ,  $\text{bei } q$ , etc., are Bessel functions tabulated widely in references, and the prime mark indicates the first derivative.\*

Equations (7) to (11) are more exact than Eqs. (3) to (6) and are plotted in Figs. 2 and 3. Eqs. (3) to (6) are approximate only, and the errors from using them are as follows:

Resistance from h-f Eq. (6)

$$\text{Error} < 10 \text{ per cent if } \frac{r_o}{\delta} > 5.5$$

$$\text{Error} < 5 \text{ per cent if } \frac{r_o}{\delta} > 10$$

Reactance from h-f Eq. (6)

$$\text{Error} < 10 \text{ per cent if } \frac{r_o}{\delta} > 2.2$$

$$\text{Error} < 5 \text{ per cent if } \frac{r_o}{\delta} > 2.8$$

Resistance from l-f Eq. (3)

$$\text{Error} < 10 \text{ per cent if } \frac{r_o}{\delta} < 1.5$$

\* See, for instance, Dwight, "Tables of Integrals and Other Mathematical Data," or McLachlan, "Bessel Functions for Engineers."

depends upon conductor size, conductivity, and permeability. The criterion is the ratio  $r_o/\delta$ .

3. *Round Wire at Very High Frequencies.*

At high frequencies, penetration into the conductor is slight, curvature of the surface is unimportant, and the round wire acts practically as a plane solid of great depth and width equal to circumference of the wire. Note that resistance is now inversely proportional to circumference, or first power of radius.

$$R_{h-f} = (\omega L_i)_{h-f} = \frac{R_s}{2\pi r_o} \quad (6)$$

$R_s$  is given by Eq. (2) or Fig. 1.

Fig. 4.—Tubular conductor. Skin-effect quantities compared to d-c values.  $R$  = resistance of tubular conductor.  $R_o$  = d-c resistance of tubular conductor.  $L_i$  = internal inductance.

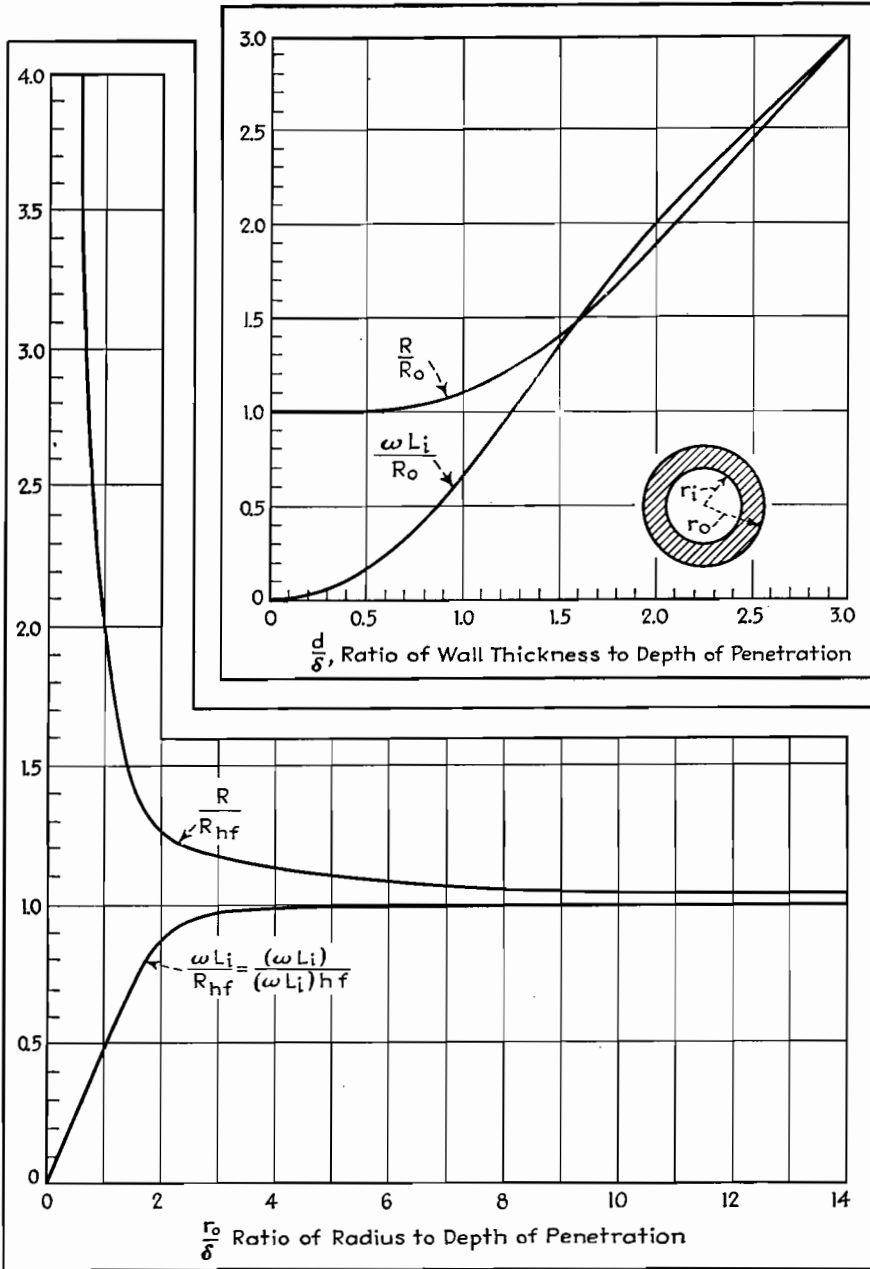


Fig. 3.—Solid round wire. Skin-effect resistance and reactance compared to values calculated from high-frequency formulas.  $L_i$  = internal inductance.  $R$  = actual resistance of round wire.  $\omega$  = frequency  $\times 2\pi$ .  $R_{hf}$  = resistance calculated from high-frequency formulas.

Error < 5 per cent if  $\frac{r_o}{\delta} < 1.2$

Reactance from l-f Eq. (4)

Error < 10 per cent if  $\frac{r_o}{\delta} < 1.9$

Error < 5 per cent if  $\frac{r_o}{\delta} < 1.5$

5. *Tubular Conductors at Very Low Frequency;  $d/\delta < 3/4$ .* 1. Voltage applied at outer radius (as for inner conductor of a coaxial line)

$$R_o = \frac{1}{\pi \sigma (r_o^2 - r_i^2)} \text{ ohms/cm length} \quad (12)$$

$$(L_i)_o = \frac{2 \times 10^{-9} \mu}{(r_o^2 - r_i^2)^2} \left[ \frac{r_o^4 - r_i^4}{4} - r_i^2 (r_o^2 - r_i^2) + r_i^4 \log_e \left( \frac{r_o}{r_i} \right) \right] \text{ henrys/cm} \quad (13)$$

2. Voltage applied at inner radius (as for outer conductor of a coaxial line)

$$R_o = \frac{1}{\pi \sigma (r_o^2 - r_i^2)} \text{ ohms/cm} \quad (14)$$

$$(L_i)_o = \frac{2 \times 10^{-9} \mu}{(r_o^2 - r_i^2)^2} \left[ \frac{r_o^4 - r_i^4}{4} - r_o^2 (r_o^2 - r_i^2) + r_o^4 \log_e \left( \frac{r_o}{r_i} \right) \right] \text{ henrys/cm} \quad (15)$$

6. *Tubular Conductors at Very High Frequency;  $d/\delta > 2$ .* 1. Voltage applied at outer radius

$$R_{h-f} = (\omega L_i)_{h-f} = \frac{R_o}{2\pi r_o} \quad (16)$$

2. Voltage applied at inner radius

$$R_{h-f} = (\omega L_i)_{h-f} = \frac{R_o}{2\pi r_i} \quad (17)$$

7. *Thin-walled Tubular Conductor at Any Frequency.*—It is assumed only that the wall thickness is small compared with the radius of the tube (say less than  $1/5$ ). Values are given again as ratios to d-c resistance calculated from Eqs. (12) and (14), or h-f resistance calculated from Eqs. (16) and (17).

$$\frac{R}{R_o} = \frac{d}{\delta} \left[ \frac{\sinh \left( \frac{2d}{\delta} \right) + \sin \left( \frac{2d}{\delta} \right)}{\cosh \left( \frac{2d}{\delta} \right) - \cos \left( \frac{2d}{\delta} \right)} \right] \quad (18)$$

$$\frac{(\omega L_i)}{R_o} = \frac{d}{\delta} \left[ \frac{\sinh \left( \frac{2d}{\delta} \right) - \sin \left( \frac{2d}{\delta} \right)}{\cosh \left( \frac{2d}{\delta} \right) - \cos \left( \frac{2d}{\delta} \right)} \right] \quad (19)$$

$$\frac{R}{R_{h-f}} = \left[ \frac{\sinh \left( \frac{2d}{\delta} \right) + \sin \left( \frac{2d}{\delta} \right)}{\cosh \left( \frac{2d}{\delta} \right) - \cos \left( \frac{2d}{\delta} \right)} \right] \quad (20)$$

$$\frac{\omega L_i}{R_{h-f}} = \left[ \frac{\sinh \left( \frac{2d}{\delta} \right) - \sin \left( \frac{2d}{\delta} \right)}{\cosh \left( \frac{2d}{\delta} \right) - \cos \left( \frac{2d}{\delta} \right)} \right] \quad (21)$$

$d$  is wall thickness.  $\delta$  is given by Eq. (1) or Fig. 1.

These ratios are plotted as curves in Figs. 4 and 5, as functions of  $d/\delta$ . The error in using the high-frequency Eqs. (16) or (17) is less than 5 per cent if wall thickness is more than two times the depth of penetration.

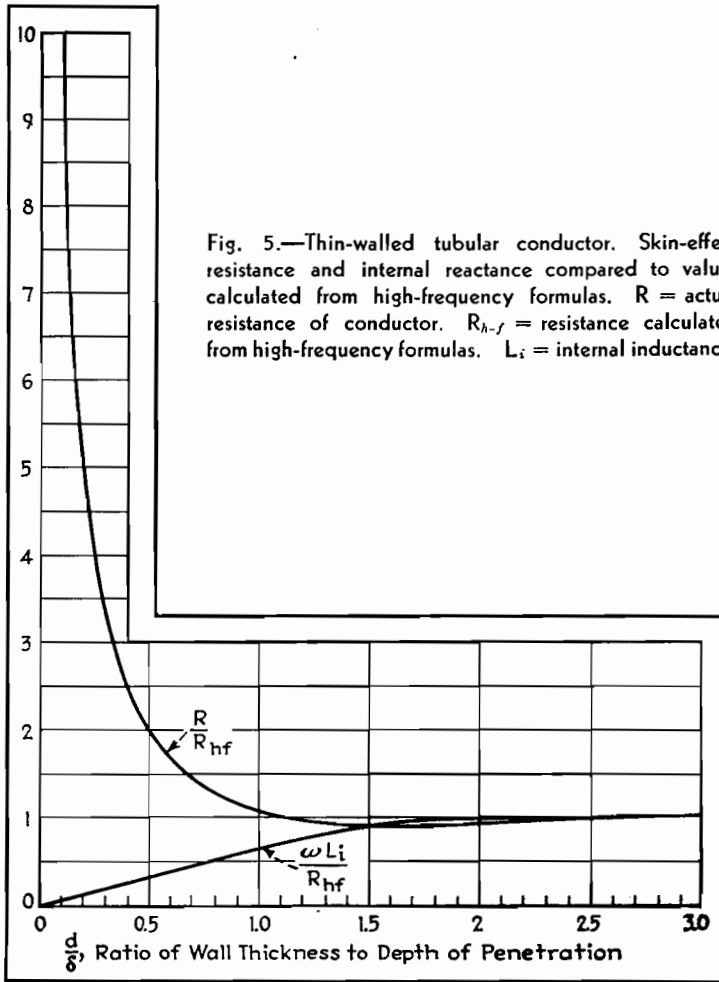
8. *Conductors Coated with Other Conductors.*—It is assumed that the coated material (but not necessarily the coating) is thick compared with depth of penetration in it, and that the coating thickness is small compared with any curvature of the surface. Results are given as ratios of resistance and reactance of the composite conductor to that of a similar conductor made entirely of the material of the coating.

$$\frac{(R + j\omega L_i)}{R_1} = (1 + j) \times \left( \frac{\sinh \gamma_1 d + \frac{R_{s2}}{R_{s1}} \cosh \gamma_1 d}{\cosh \gamma_1 d + \frac{R_{s2}}{R_{s1}} \sinh \gamma_1 d} \right) \quad (22)$$

where  $\frac{R_{s2}}{R_{s1}} = \sqrt{\frac{\mu_2 \sigma_1}{\mu_1 \sigma_2}}$  and  $\gamma_1 = \frac{(1 + j)}{\delta_1}$

$R_1$  is the resistance if the coating were of infinite depth.

$\delta_1$  is given by Eq. (1) or Fig. 1.



Curves are plotted in Figs. 6, 7, and 8 as functions of the ratio of coating thickness to depth of penetration, for values of  $R_{s2}/R_{s1} = 1.6, 0.34, \text{ and } 5$ . These corre-

spond approximately to silver coating on brass, solder coating on copper, and copper coating on iron or Fernico. It is seen that in all cases when coating thickness

is equal to or greater than the depth of penetration  $\delta_1$  for the material of the coating [obtained from Eq. (1) or Fig. 1], the composite conductor is nearly as good, or as bad, as though the conductor were made entirely of the coating material.

Note on the curves that in the neighborhood of  $d/\delta = 1.5$ , the silver-coated brass conductor has slightly lower resistance than a solid silver conductor, copper-coated iron has lower resistance than solid copper, and solder-coated copper has greater resistance than solid solder. This effect arises from the redistribution of current in the coating because of the presence of the base material.

9. *Conductor Coated with Thin Layer of Poor Conductor or Imperfect Dielectric.*—Equation (22) is applicable until the conducting coating becomes so poor that displacement currents in the conductor are appreciable compared with conduction currents. [That is,  $\omega\epsilon_1/(36\pi \times 10^{11}\sigma_1)$  is comparable to unity.] Then, writing impedance as a ratio to the resistance if the conductor had no coating at all

$$\frac{R + j(\omega L_i)}{R_2} = g \left[ \frac{g \sinh x + (1 + j) \cosh x}{g \cosh x + (1 + j) \sinh x} \right] \quad (23)$$

where 
$$g = \frac{120\pi \sqrt{\frac{\mu_1}{\epsilon_1}}}{R_{s2} \sqrt{1 - jp}}$$

$$x = j \frac{2\pi d}{\lambda} \sqrt{1 - jp}$$

$$p = \frac{\sigma_1 \times 36\pi \times 10^{11}}{\omega\epsilon_1}$$

= power factor of coating provided  $p \ll \text{unity}$

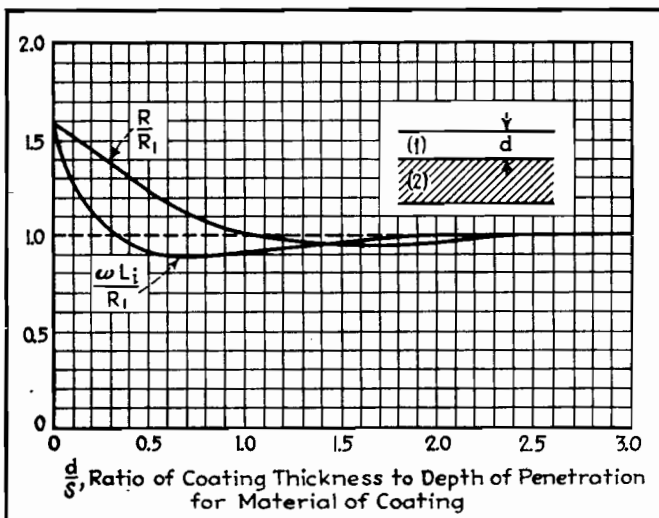


Fig. 6.—Skin-effect quantities for coated conductors.  $\sqrt{\frac{\mu_2 \sigma_1}{\mu_1 \sigma_2}} = 1.6$  corresponding approximately to silver on brass.  $\mu$  = permeability.  $\sigma$  = conductivity. Resistance and reactance are given as ratios to those of a solid conductor of the coating material.

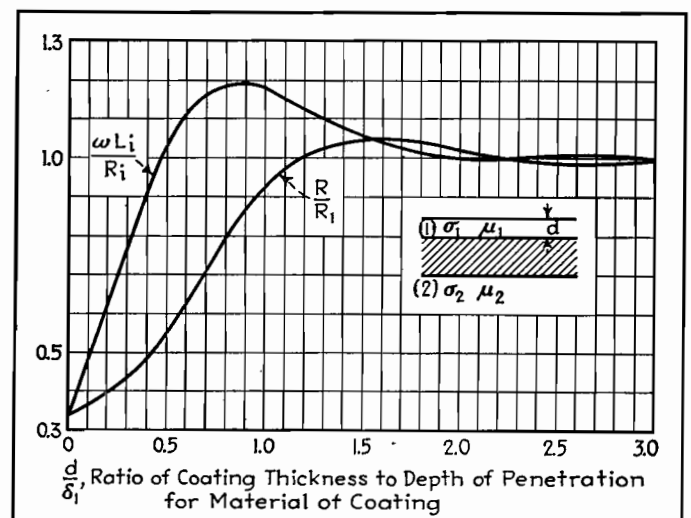
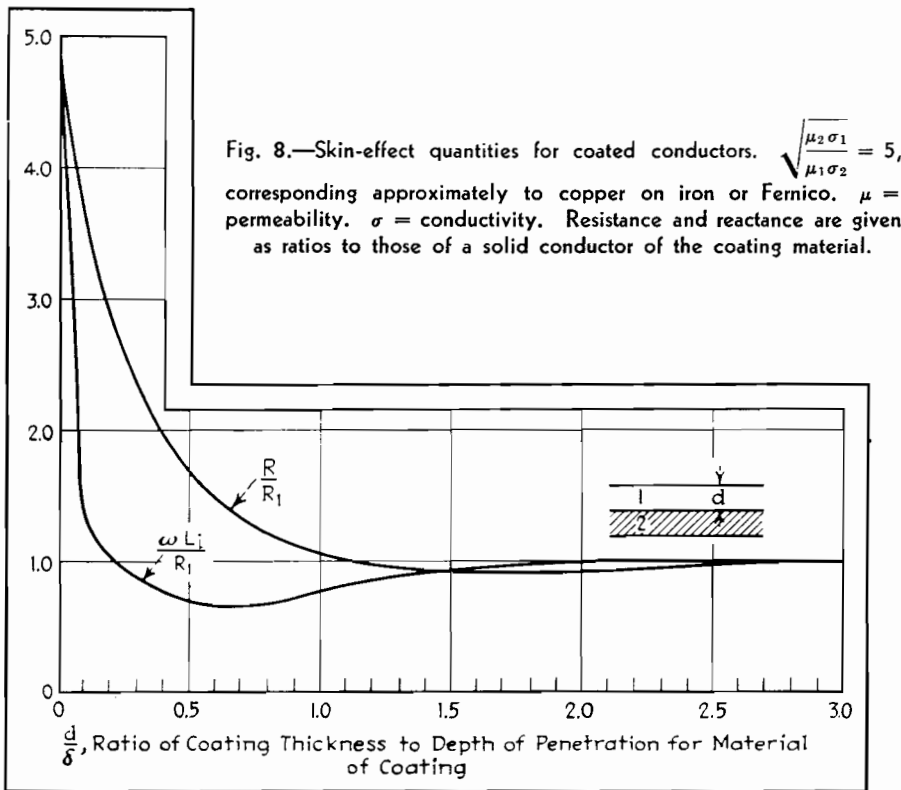


Fig. 7.—Skin-effect quantities for coated conductors.  $\sqrt{\frac{\mu_2 \sigma_1}{\mu_1 \sigma_2}} = 0.34$  corresponding approximately to solder on copper.  $\mu$  = permeability.  $\sigma$  = conductivity.



$R_{s2}$  given by  $R_s$  in Eq. (2) or Fig. 1.

$\lambda$  = wavelength in the coating =  $\frac{\lambda_o}{\sqrt{\mu_1 \epsilon_1}}$   
 $\lambda_o$  = free space wavelength  
 $d$  = coating thickness

All quantities are complex, so that calculations using Eq. (23) are not simple. Usually the coating is a small part of a wavelength in thickness. Then, if  $p$  is not large, the first-order correction terms found from an expansion of Eq. (23) are

$$\frac{R}{R_2} \cong 1 + \frac{dR_{s2}}{30\lambda} \sqrt{\frac{\epsilon_1}{\mu_1}} \quad (24)$$

$$\frac{\omega L_i}{R_2} \cong 1 + \frac{240\pi^2 d}{\lambda R_{s2}} \sqrt{\frac{\mu_1}{\epsilon_1}} \quad (25)$$

It is of interest to find that the first-order corrections are independent of conductivity of the coating. For any practical cases ( $d/\lambda$  small and  $R_{s2}$  less than one, as shown by Fig. 1), the correction to resistance is always small, but the correction to internal reactance may be very large since the coating may be much thicker than depth of penetration in the coated conductor, and so may contain much more magnetic flux than the coated conductor.

The unimportance of conductivity of the coating comes about since under the above assumptions the coating is not thick compared with  $\delta$  for the material of the coating (which is large since con-

ductivity is poor), and so most of the current is confined to the coated material. It is then the coated material, not the coating, that is important in determining the power loss, or resistance component.

If coating is comparable to  $\delta$  for the coating material, Eq. (23) should be used completely. If coating is thick and comparable to wavelength, the problem is usually one of wave matching and should be treated somewhat differently.

In Fig. 9 are plotted curves of  $R/R_2$  and  $\omega L_i/R_2$  as functions of  $d/\lambda$  for  $\epsilon_1 = 4$ ,  $\mu_1 = 1$ , and  $R_{s2} = 0.0015$  ohms and 0.015 ohms, corresponding approximately to a thin dielectric or semiconducting coating on copper at 30 and 3,000 Mc, respectively.

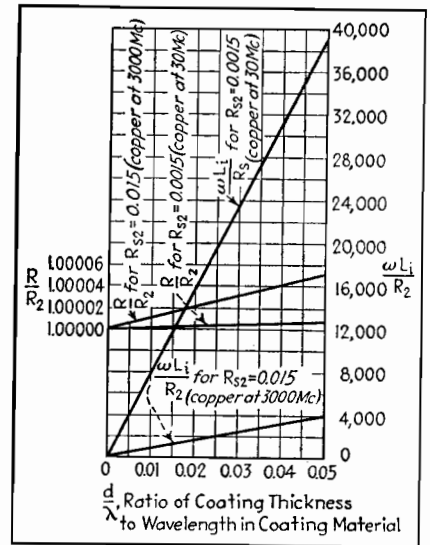


Fig. 9.—Skin-effect quantities for conductor with a coating of dielectric or poor conductor.  $R_2$  = resistance (also internal reactance) if coating were not present.  $\omega L_i$  = internal reactance of coated conductor.  $R$  = resistance of coated conductor. Dielectric constant of coating material equal to four.



# R-f Resistance of Copper Wire

By JOHN H. MILLER

THE chart shown here, prepared during an investigation of h-f measurements with the thermoammeter, covers the frequency range from 500 kc to 100 Mc. The resistance ratios indicate the well-known fact that the resistance of copper wire (or any other conductor) increases greatly over its d-c value when it is carrying h-f current. The curves may be extended to higher frequencies and larger wire sizes through the use of the following equation, which applies, how-

ever, only when the resistance ratio is greater than 8:

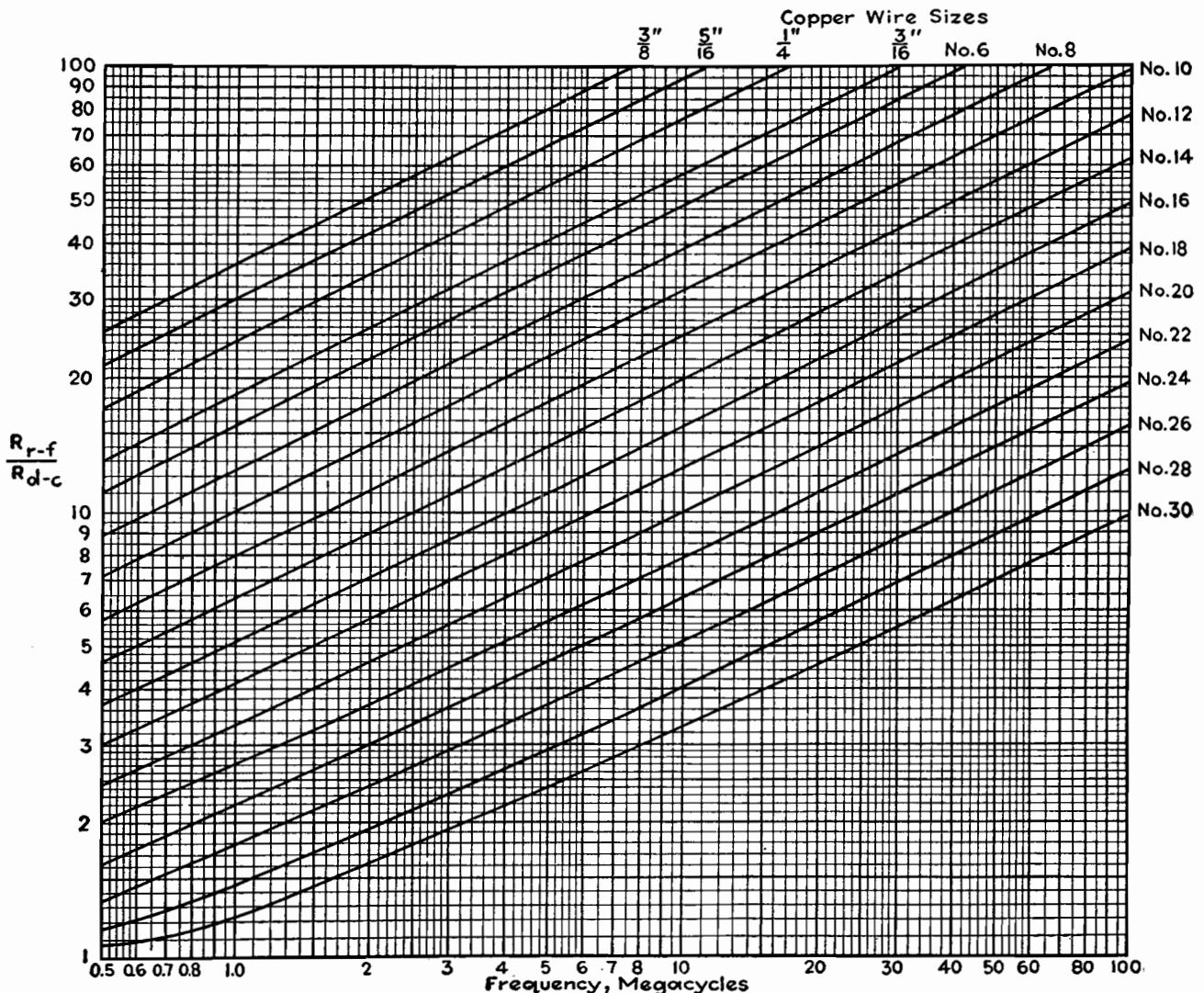
$$\frac{R_{r-f}}{R_{d-c}} = 0.25 + 0.0962d\sqrt{f}$$

where  $d$  is the diameter of the wire in inches, and  $f$  is the frequency in cycles. The ratio (in the chart and when calculated by the formula) applies for copper wire only, at room temperature.\*

It is of interest to note that No. 10 copper wire, which is very closely 0.1 in.

in diameter, has a d-c resistance of 1 ohm per thousand feet, a resistance at 100 Mc of one hundred times its d-c resistance. Other ratios may be observed from the chart which may give a better picture of the actual resistance encountered at radio frequencies.

\* The data for the curves are taken from August Hund, "High-frequency Measurements," p. 264, McGraw-Hill Book Company, Inc., New York; and also Radio Instruments and Measurements, Nat. Bur. Standards Circ. 74.



## SECTION XXV

# TUBES

Tube Filament and Heater Characteristics.....	Page 344
Secondary Electron Radiation.....	349
Open-grid Tubes in Low-level Amplifiers.....	358
28-volt Operation of Receiving Tubes.....	360

# Tube Filament and Heater Characteristics

By CECIL E. HALLER

Mathematical analysis of volt-ampere characteristics of various filament metals. Resulting equations are plotted as a reference chart that gives filament current, temperature, and wattage for any electron tube at various operating voltages with good accuracy

**F**REQUENTLY in the design and application of electron tubes, it is necessary to predict the value of filament current and possibly also the filament temperature when the applied filament voltage deviates from the normal or rated value. Such an instance occurs when two or more filaments having different volt-ampere characteristics are operated in series and it is required to predict the voltage variation across each individual filament with respect to the supply voltage variation. The solution of this problem requires a knowledge of the volt-ampere characteristic of each filament. The voltage across each filament can then be determined for any arbitrary assumed current value. If appropriate current values are chosen, a curve of each individual tube voltage vs. the supply voltage can be constructed.

A knowledge of the individual volt-ampere characteristics over the required range may not be readily available unless it has previously been experimentally determined. It is the purpose here to indicate a method of constructing the volt-ampere characteristic if the current is known for at least one operating voltage. The knowledge of this point enables the current to be predicted at a new operating voltage with good accuracy provided that the change in voltage is within approximately  $\pm 25$  per cent of the

known voltage. The same analysis will also permit the determination of the value of watts and temperature in terms of the known operating condition.

### Basic Filament Equations

In order to illustrate the method of transposing the operating condition of a filament, the two basic equations involved in the design of filaments and heaters for electron tubes will be considered.

The first equation is

$$W = K_1 T^{n_w} \quad (1)$$

where  $W$  = power radiated, watts

$K_1$  = constant of proportionality, which includes the area of the emitter

$T$  = temperature,  $^{\circ}\text{K}$

$n_w$  = an exponent that is reasonably constant for a given metal over a limited range of temperature

The second equation is

$$W = \frac{E^2}{R} = I^2 R \quad (2)$$

where  $E$  = applied filament voltage

$R$  = resistance of the filament, which is in general a function of temperature

$I$  = filament current

In order to solve Eqs. (1) and (2), let

$$R = K_2 T^{n_r} \quad (3)$$

where  $K_2$  = a constant of proportionality  
 $n_r$  = an exponent which may be regarded constant over a limited temperature range

Solutions of Eqs. (1), (2), and (3) for  $W$ ,  $I$ , and  $T$  in terms of  $E$  yield<sup>1</sup>

$$W = K_1 (K_1 K_2)^{\frac{2n_w}{n_w + n_r}} (E)^{\frac{2n_w}{n_w + n_r}} \quad (4)$$

$$I = \left( \frac{K_1}{K_2} \right)^{\frac{n_w - n_r}{2}} \left( \frac{1}{K_1 K_2} \right)^{\frac{2}{n_w + n_r}} (E)^{\frac{n_w - n_r}{n_w + n_r}} \quad (5)$$

$$T = \left( \frac{1}{K_1 K_2} \right)^{\frac{2}{n_w + n_r}} (E)^{\frac{2}{n_w + n_r}} \quad (6)$$

Thus, when using  $W_o$ ,  $I_o$ ,  $T_o$ ,  $E_o$  and  $W_x$ ,  $I_x$ ,  $T_x$ ,  $E_x$  as the known and unknown conditions, respectively, Eqs. (4), (5), and (6) may be written

$$\frac{W_x}{W_o} = \left( \frac{E_x}{E_o} \right)^{\frac{2n_w}{n_w + n_r}} \quad (7)$$

$$\frac{I_x}{I_o} = \left( \frac{E_x}{E_o} \right)^{\frac{n_w - n_r}{n_w + n_r}} \quad (8)$$

$$\frac{T_x}{T_o} = \left( \frac{E_x}{E_o} \right)^{\frac{2}{n_w + n_r}} \quad (9)$$

### Use of Average Values for Exponents

Values for  $n_w$  have been determined for some of the more common metals, and are given in Table I. The exponent  $n_w$  includes the change of total emissivity with temperature. Since the total emissivity of metals increases with tempera-

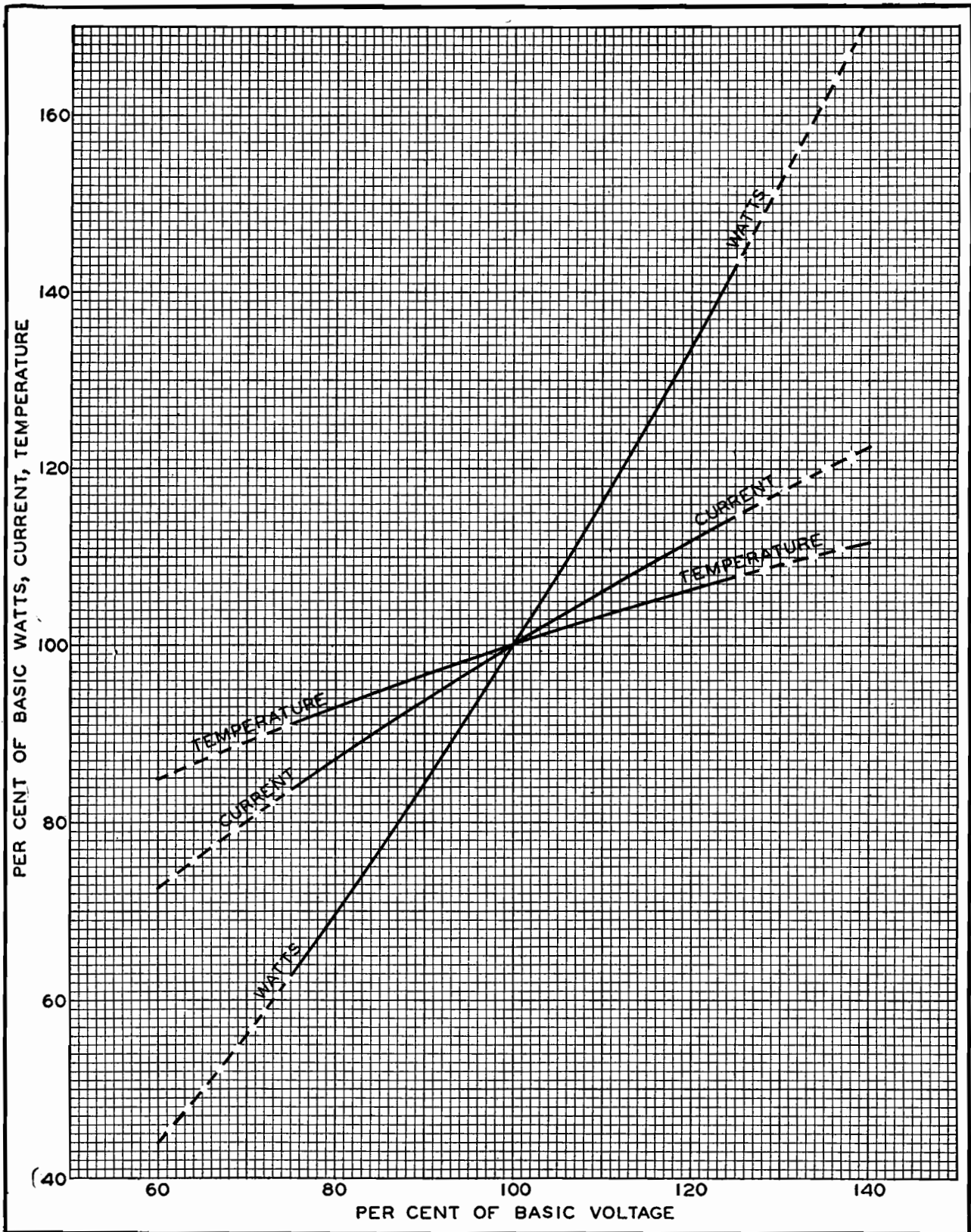


Fig. 1.—Chart giving wattage, current, and temperature of a filament or heater at operating voltages up to 25 per cent above or below basic voltage with sufficient accuracy for most engineering purposes. Accuracy drops in dotted regions.

Table I.—Values of Exponents for Four Filament Metals

Material	Temp., °K	$n_w$	$n_r$	$\frac{2n_w}{n_w + n_r}$	$\frac{n_w - n_r}{n_w + n_r}$	$\frac{2}{n_w + n_r}$
Tungsten <sup>1</sup> .....	1000	5.65	1.20	1.65	0.650	0.292
Tungsten <sup>1</sup> .....	2000	4.93	1.19	1.61	0.612	0.327
Tungsten <sup>1</sup> .....	2500	4.66	1.20	1.59	0.590	0.341
Molybdenum <sup>3</sup> .....	1000	5.32	1.15	1.64	0.645	0.309
Molybdenum <sup>3</sup> .....	2000	4.99	1.15	1.63	0.625	0.326
Tantalum <sup>3</sup> .....	1600	4.80	0.785	1.72	0.720	0.358
Tantalum <sup>3</sup> .....	2800	4.80	0.785	1.72	0.720	0.358
Nickel.....	1000	4.65†	0.62†	1.76	0.764	0.379

\* Values by different investigators range from 4.65 to 5.29.

† Estimated from experimental data on nickel.

ture,<sup>2</sup> the Stefan-Boltzmann law of radiation requires that  $n_w$  be greater than 4. For materials having an emissivity independent of temperature, the value will be 4. The value of  $n_r$  for some metals at different temperatures is also given in Table I. These limited data indicate  $n_r$  ranges from 0.6 to 1.2.

If  $W_1$  and  $W_2$ , the watts radiated at temperatures  $T_1$  and  $T_2$ , are known, then

$$n_w = \frac{\log (W_1/W_2)}{\log (T_1/T_2)}$$

In a like manner, if  $R_1$  and  $R_2$  are the resistances at temperatures  $T_1$  and  $T_2$ , then

$$n_r = \frac{\log (R_1/R_2)}{\log (T_1/T_2)}$$

These permit an experimental check of the values of  $n_w$  and  $n_r$  if two sets of operating conditions are known.

Table I also gives the value of  $(n_w - n_r)/(n_w + n_r)$ . It will be noted that it ranges from 0.59 to 0.76. It is now of interest to see what error results in using an average value of this exponent in Eq. (8). A voltage ratio  $E_x/E_0$  of 1.25 will be taken as the maximum voltage for which Eq. (8) is to be used. If the exponents 0.59 and then 0.76 are used, the respective values of current ratio  $I_x/I_0$  are 1.140 and 1.185, or a deviation of only  $\pm 1.9$  per cent from the mean value.

#### Plotting the Chart

It is evident therefore that an average exponent can be chosen which applies to all the metals in Table I and in general

$$\left(\frac{I_x}{I_0}\right) = \left(\frac{E_x}{E_0}\right)^{0.61}, \quad 0.75 < \left(\frac{E_x}{E_0}\right) < 1.25 \quad (10)$$

is true to sufficient accuracy for most engineering purposes. This equation has been drawn as the current curve for the chart in Fig. 1.

It can further be shown that the accuracy involved in assuming  $2n_w/(n_w + n_r) = 1.61$  and  $2/(n_w + n_r) = 0.327$  is even greater than for the case just discussed. Then

$$\frac{W_x}{W_0} = \left(\frac{E_x}{E_0}\right)^{1.61} \quad (11)$$

$$\frac{T_x}{T_0} = \left(\frac{E_x}{E_0}\right)^{0.327} \quad (12)$$

These equations are plotted in Fig. 1.

In order to check Eq. (8) and Fig. 1, data were taken for a wide variety of electron tubes. It will be noted from Fig. 1 and Table II that the calculated values of current deviate, in general, by less than  $\pm 4$  per cent from the measured values. We can conclude from this that Fig. 1 is generally applicable to all types of electron tubes for the specified range of  $(E_x/E_0)^5$ . Some samples of the use of this curve will now be given.

**Example 1.**—The type RCA-826 has a thoriated-tungsten filament rated at 7.5 volts and 4 amp. What will be the filament current at 5.62 volts (75 per cent of rated voltage)? Tracing up from 75 on the horizontal scale in Fig. 1 to the current curve, and then across, gives 83.8 per cent. The new filament curve is then  $0.838 \times 4 = 3.35$  amp. By actual measurement, the current was found to be 3.34 amp. While no temperature measurements were made at this voltage, one would expect the temperature to decrease to 91 per cent of its rated value in degrees Kelvin.

2. An oxide-coated cathode has a temperature of 1000°K when the heater is operated at 5 volts. What voltage will be required to increase the temperature to 1060°K? From Fig. 1, when  $T_x/T_0 = 106$ , one finds  $E_x/E_0 = 1.19$  or  $E_x = 5 \times 1.19 = 5.95$  volts. The heater voltage was found to be 6.0 volts when determined experimentally. If the voltage had been increased to 7 volts, then  $E_x/E_0 = 1.4$  and  $T_x/T_0 = 1.118$  or  $T_x =$

1118°K. Actual measurements indicated the temperature to be 1135°K.

#### Two Filaments in Series

In order to examine the operation of filaments or heaters in series, let two tubes  $T_1$  and  $T_2$ , having the same nominal voltage rating, be connected in series to a power supply  $E_s$  (see Fig. 2). In general, the filaments of tubes  $T_1$  and  $T_2$  may have different volt-ampere characteristics. Such differences may be due to the individual variation of filament current when read at a specified or rated voltage. These variations of filament currents, which are expected and normal, result from the necessary manufacturing tolerances on both materials and processes.

The usual filament-current tolerance on receiving and the smaller transmitting tubes, whose filaments or heaters might be operated in series, is generally of the order of 5 to 10 per cent. In order to ensure satisfactory operation initially and throughout the expected life of the tube, the tube manufacturer usually specifies the percentage the applied filament voltage may be allowed to deviate from normal. This voltage deviation is usually of the order of  $\pm 5$  per cent for the thoriated-tungsten type emitters and  $\pm 10$  per cent for the oxide-coated filament or heater-cathode types. It becomes apparent that for series operation of the filament or heaters the supply-voltage variation needs careful consideration in order to ensure that the individual filament-voltage tolerances are not exceeded on either  $T_1$  or  $T_2$ .

If  $T_1$  and  $T_2$  are both high or both low filament-current tubes, no problem exists since the volt-ampere characteristics are substantially identical (*i.e.*, they have the same currents for the same applied voltage). Only the combination needs to be considered, where one has the higher limit value and the other has the lower limit value of filament current.

#### Determining Permissible Filament Voltage Variations

As a specific problem, assume the filament-current tolerance to be  $\pm 5$  per cent and let it be required to determine the permissible variation of supply voltage without exceeding an individual tube voltage range of  $\pm 10$  per cent. This problem frequently arises in the design of mobile transmitters when the filament or heaters are operated in series.

The bogie or normal volt-ampere characteristic  $BKE$  of Fig. 2 may then be constructed from Eq. (10). For  $T_1$ ,

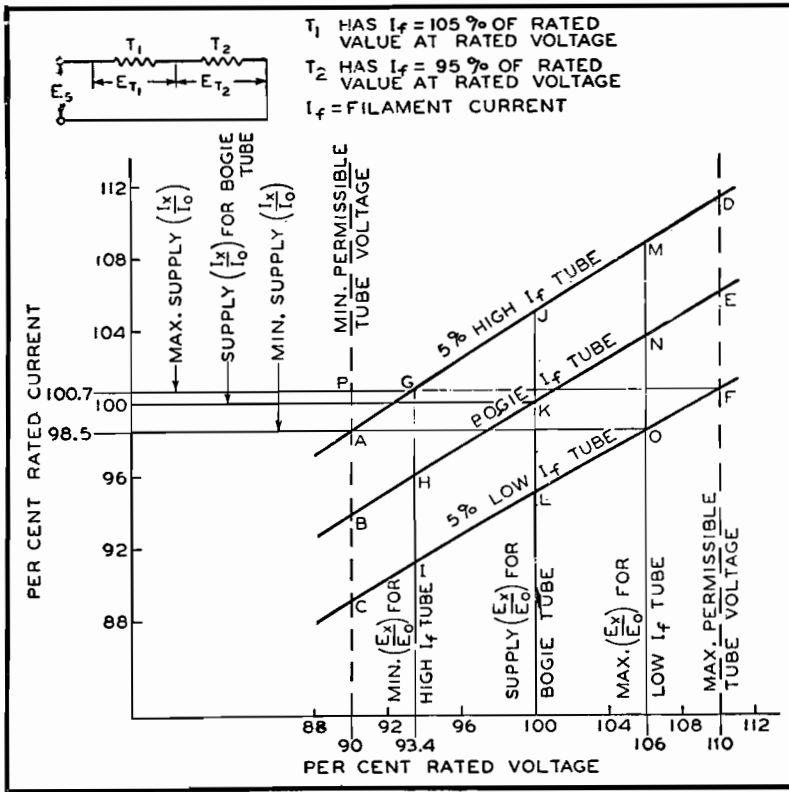


Fig. 2.—Volt-ampere characteristics for series operation of filaments or heaters having different characteristics.

the 5 per cent high filament-current tube, the equation of the volt-ampere characteristic is

$$\frac{I_x}{I_0} = 1.05 \left( \frac{E_x}{E_0} \right)^{0.61} \quad (13)$$

Curve *AJD* can be constructed from this equation.

Similarly for *T*<sub>2</sub>, the low filament-current tube, the equation is

$$\frac{I_x}{I_0} = 0.95 \left( \frac{E_x}{E_0} \right)^{0.61} \quad (14)$$

which is represented by the curve *CLF* in Fig. 2.

An arbitrary current may then be assumed in order to determine the individual voltage across tubes *T*<sub>1</sub> and *T*<sub>2</sub>. The supply voltage is represented by the sum of the voltages across *T*<sub>1</sub> and *T*<sub>2</sub>. If *T*<sub>1</sub> (the high filament-current tube) has the minimum permissible voltage 0.9 *E*<sub>0</sub> represented by point *A*, tube *T*<sub>2</sub> (the low filament-current tube) will have a voltage represented by point *O*. The sum of the two voltages at points *A* and *O* represents the minimum permissible supply voltage consistent with the previous imposed condition of  $\pm 5$  per cent filament-current tolerance

Table II.—Measured and Calculated Data on Typical Tube Samples

Type number	Filament or heater	Type of emitter	Rate voltage		Reduced voltage				Increased voltage			
			<i>E</i> <sub>x0</sub>	<i>I</i> <sub>x0</sub> observed	<i>E</i> <sub>x1</sub>	<i>I</i> <sub>x1</sub> observed	<i>I</i> <sub>x1</sub> calculated from Fig. 1	% difference	<i>E</i> <sub>x2</sub>	<i>I</i> <sub>x2</sub> observed	<i>I</i> <sub>x2</sub> calculated from Fig. 1	% difference
203A	Filament	Th-W	10.0	3.28	7.5	2.72	2.74	+0.7	12.5	3.70	3.76	+1.6
801A	Filament	Th-W	7.5	1.22	5.62	1.05	1.02	-0.3	9.38	1.42	1.40	-1.4
807	Cathode	Oxide	6.3	0.87	4.72	0.74	0.73	-1.4	7.88	0.99	1.00	+1.0
813	Filament	Th-W	10.0	5.00	7.50	4.12	4.18	+1.5	12.5	5.80	5.72	-1.4
815	Cathode	Oxide	6.3	1.65	4.72	1.39	1.37	-1.4	7.88	1.88	1.89	+0.5
826	Filament	Th-W	7.5	4.00	5.62	3.35	3.34	-0.3	9.38	4.55	4.58	+0.7
833A	Filament	Th-W	10.0	10.10	7.5	8.50	8.44	-0.7	12.50	11.60	11.56	-0.3
836	Cathode	Oxide	2.5	5.05	1.88	4.22	4.25	+0.7	3.13	5.75	5.78	+0.5
861	Filament	Th-W	11.0	10.05	8.25	8.30	8.40	+0.1	13.75	11.50	11.50	0
866	Filament	Oxide	2.5	5.00	1.87	4.03	4.18	+3.7	3.13	5.80	5.72	-1.4
913	Cathode	Oxide	6.3	0.600	4.72	0.504	0.502	-0.4	7.88	0.685	0.687	+0.3
1616	Filament	Oxide	2.5	4.90	1.87	3.97	4.10	+3.3	3.13	5.73	5.61	-2.1
1624	Filament	Oxide	2.5	1.83	1.87	1.47	1.53	+4.1	3.13	2.12	2.09	-1.4
2050	Cathode	Oxide	6.3	0.575	4.72	0.489	0.481	-1.6	7.88	0.657	0.657	0
2051	Cathode	Oxide	6.3	0.605	4.72	0.515	0.506	-1.8	7.88	0.688	0.693	+0.6
8025	Filament	Th-W	6.3	1.94	4.72	1.65	1.61	-2.4	7.88	2.19	2.22	+1.4
9001	Cathode	Oxide	6.3	0.157	4.72	0.135	1.31	-3.0	7.88	0.177	0.179	+1.1
1T4	Filament	Oxide	1.4	0.0525	1.05	0.043	0.044	+2.3	1.75	0.0613	0.0600	-2.2
6SK7	Cathode	Oxide	6.3	0.310	4.72	2.61	2.59	-0.8	7.88	0.352	0.355	+0.9
6SS7	Cathode	Oxide	6.3	0.150	4.72	0.129	1.25	-3.1	7.88	0.170	0.172	+1.2
12A6	Cathode	Oxide	12.6	0.156	9.45	0.134	1.30	-3.0	15.75	0.177	0.178	+0.6
2AP1	Cathode	Oxide	6.3	0.595	4.72	0.508	0.498	-2.0	7.88	0.668	0.680	+1.7

and  $\pm 10$  per cent individual voltage tolerance.

In a similar manner the maximum voltage  $1.1 E_0$  that can be applied to  $T_2$ , the low filament-current tube, is represented by point  $F$ , and the voltage on  $T_1$ , the high filament-current tube, by point  $G$ . The sum of the voltages at points  $G$  and  $F$  gives the maximum permissible supply voltage. The nominal supply voltage is twice the nominal tube voltage or  $2E_0$  since it was assumed that the nominal voltage ratings of  $T_1$  and  $T_2$  were identical. The maximum permissible percentage of supply voltage deviation may then be calculated directly from the graphical analysis. This solution indicates supply voltage tolerance of  $+1.7$  per cent and  $-2.0$  per cent.

It is interesting to note that the distance  $A$  to  $P$  represents the maximum permissible range of supply current. This suggests that if the supply voltage cannot be maintained within the required limits, a series ballast tube, whose current is maintained within the range  $A$  to  $P$ , might be used to permit a larger variation in the supply voltage. The use of the ballast tube would of course require an increased supply voltage in order to supply the required voltage drop of the ballast tube.

An alternative solution to permit wider supply-voltage tolerances consists in shunting the low filament-current tube with a resistor. This resistor is adjusted until both tubes have substantially the same filament voltage. This method is essentially one of shifting the operating point on the volt-ampere characteristic of the low filament-current tube and resistor until at normal supply voltage it coincides with that of the high filament-current tube. This method does not, however, make the volt-ampere characteristics identical and, therefore, never can permit a percentage supply-voltage change equal to the permitted percentage of individual filament voltages. In order to simplify adjustments, adjustable resistors are frequently used across both filaments.

#### Generalized Solution for Tubes in Series

The method of the solution of two tubes in series may be generalized for  $N_H$  tubes having high filament currents in series with  $N_L$  tubes having low filament currents, as shown in Fig. 3.

Let  $m$  = percentage filament-current tolerance

$p$  = permissible percentage tolerance of individual applied voltage

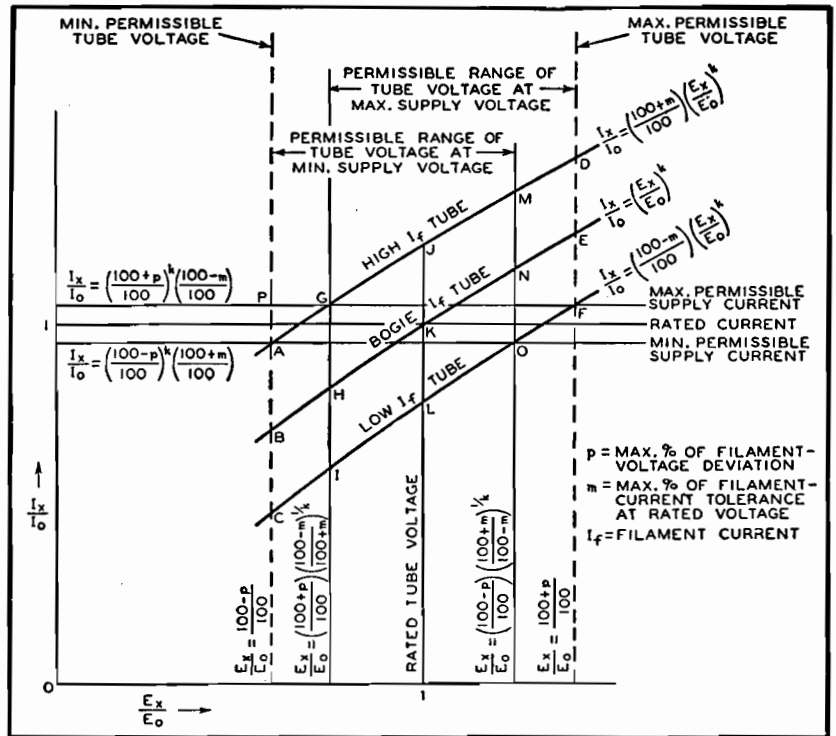


Fig. 3.—Generalized solution for any number of tubes in series, some having high and some low filament current.

The volt-ampere characteristic of a limit tube is expressed by

$$\left(\frac{I_x}{I_0}\right) = \left(\frac{100+m}{100}\right) \left(\frac{E_x}{E_0}\right)^{0.61} \quad (15)$$

But since  $E_x/E_0$  for the limiting condition of maximum voltage on a low filament-current tube is equal to  $(100+p)/100$ , Eq. (15) may be rewritten for a low filament-current tube as

$$\left(\frac{I_x}{I_0}\right)_{\max} = \left(\frac{100+p}{100}\right)^{0.61} \left(\frac{100-m}{100}\right) \quad (16)$$

where  $I_x/I_0$  is the maximum permissible supply current when at least one each of limit values of high and low filament-current tubes are operated in series. Similarly, the minimum permissible current is given by

$$\left(\frac{I_x}{I_0}\right)_{\min} = \left(\frac{100-p}{100}\right)^{0.61} \left(\frac{100+m}{100}\right) \quad (17)$$

Equations (14) and (15) form the basis for calculating the current requirements imposed on a series ballast tube should one be used.

The values of current given in Eqs. (16) and (17), when substituted in the appropriate equations for the volt-ampere characteristics, give the voltage at points  $G$  and  $O$ , respectively, as

$$\left(\frac{E_x}{E_0}\right) = \left(\frac{100+p}{100}\right) \left(\frac{100-m}{100+m}\right)^{1.64} \quad (18)$$

$$\left(\frac{E_x}{E_0}\right) = \left(\frac{100-p}{100}\right) \left(\frac{100+m}{100-m}\right)^{1.64} \quad (19)$$

The value of  $(E_x/E_0)$  given in Eq. (18) represents the voltage across a high filament-current tube at the maximum permissible supply voltage, while the value given in Eq. (19) represents the voltage across a low filament-current tube at the minimum permissible supply voltage. The sum of  $N_H$  voltages given in Eq. (18) +  $N_L$  voltages of the value  $(100+p)/100$  gives the maximum supply voltage or

$$\left(\frac{E_x}{E_0}\right)_{\max} = N_H \left[ \left(\frac{100+p}{100}\right) \left(\frac{100-m}{100+m}\right)^{1.64} \right] + N_L \left(\frac{100+p}{100}\right) \quad (20)$$

In a like manner, the minimum supply voltage is

$$\left(\frac{E_x}{E_0}\right)_{\min} = N_L \left[ \left(\frac{100-p}{100}\right) \left(\frac{100+m}{100-m}\right)^{1.64} \right] + N_H \left(\frac{100-p}{100}\right) \quad (21)$$

The percentage of supply voltage tolerance becomes

$$\% E_s \text{ above normal} = \left\{ \frac{N_H \left[ \left(\frac{100+p}{100}\right) \left(\frac{100-m}{100+m}\right)^{1.64} \right] + N_L \left(\frac{100+p}{100}\right)}{N_H + N_L} - 1 \right\} 100 \quad (22)$$



$$\% E_s \text{ below normal} = \left\{ \frac{N_L \left[ \left( \frac{100-p}{100} \right) \left( \frac{100+m}{100-m} \right)^{1.64} \right]}{N_H + N_L} + N_H \left( \frac{100-p}{100} \right) - 1 \right\} 100 \quad (23)$$

Equations (22) and (23) were derived on the premise that at least one tube of the group had a filament current  $(100 + m)/100$  times rated value and at least one other had  $(100 - m)/100$  times rated value. This premise imposes the condition that both  $N_H$  and  $N_L$  must be different from zero in Eqs. (22) and (23). If either  $N_H$  or  $N_L$  is zero, the solution is simple as all possess the same volt-ampere characteristic. The permissible supply-voltage percentage deviation is  $p$ .

#### Application to Universal Receivers

It is common practice in the design of a-c/d-c sets in which the filaments or heaters are connected in series to use tubes that have different values of rated filament voltage. The analysis of this condition can be reduced to an expression similar to Eqs. (22) and (23) except that  $N_H$  and  $N_L$  must include the equivalent number of respective tubes in terms of the lowest nominal voltage tube. For example, a 35-volt tube may be represented by 5.55 tubes of 6.3 volts nominal rating.

Substitution in Eqs. (22) and (23) of the conditions of the previously discussed

case of two tubes ( $N_H = 1$  and  $N_L = 1$ ) with  $m = 5$ ,  $p = 10$ , and  $(n_w - n_r)/(n_w + n_r) = 0.61$  gives +1.8 per cent and -2.0 per cent for the supply voltage tolerance, which is in good agreement with the graphical solution.

An examination of the case of three tubes in series where  $N_H = 2$ ,  $N_L = 1$ ,  $m = 5$ ,  $p = 10$ , and  $(n_w - n_r)/(n_w + n_r) = 0.61$  gives the tolerance on the supply voltage as -1 per cent and -4.7 per cent. In other words, the supply voltage can never be permitted to rise to normal without exceeding the maximum voltage rating on the low filament-current tube.

#### Conclusions

The curves given in Fig. 1 enable the transposition of heater or filament operating conditions within the usual desired engineering accuracy for electron-tube applications. These curves should not be used when an accuracy within  $\pm 3.5$  per cent for filament current is desired with a  $\pm 25$  per cent change in filament voltage. The percentage of error in all equations converges to zero as the ratio of  $E_s/E_0$  approaches unity, or the smaller the percentage change of voltage in the transposition, the smaller the degree of error. A limited number of types of filaments and heaters have been examined and found to give good agreement with the curves of Fig. 1. The accuracy of the volt-ampere characteristic can be estab-

lished by experimentally determining  $(n_w - n_r)/(n_w + n_r)$  for the particular application. This determination may be made from the relation

$$\frac{n_w - n_r}{n_w + n_r} = \frac{\log (E_1/E_2)}{\log (I_1/I_2)}$$

where  $I_1$ ,  $E_1$  and  $I_2$ ,  $E_2$  are currents and voltages at known operating points.

Once the value of  $(n_w - n_r)/(n_w + n_r)$  has been established over the probable application range of voltage, the operating conditions of a group of filaments in series may then be predicted for various supply voltages. This permits the supply voltage tolerance to be established so that the applied filament voltage tolerance may not be exceeded.

The solutions given here represent the steady-state conditions and do not indicate what may happen during the initial application of voltage or for short-time voltage transients.

#### References

- (1) JONES and LANGMUIR, The Characteristics of Tungsten Filaments as Functions of Temperature, *Gen. Elec. Rev.*, June, July, and August, 1927.
- (2) "Temperature—Its Measurement and Control in Science and Industry," p. 1186, American Physical Society, Reinhold Publishing Corporation, New York.
- (3) WORTHING, A. G., Physical Properties of Well seasoned Molybdenum and Tantalum as a Function of Temperature, *Phys. Rev.*, 28, No. 1.
- (4) MELLOR, JOSEPH, W., "Comprehensive Treatise on Inorganic and Theoretical Chemistry," Longmans, Green and Company, New York.
- (5) FORSYTHE, W. E., "Measurements of Radiant Energy," p. 32, McGraw-Hill Book Company, Inc., New York.

## Secondary Electron Radiation

By J. H. OWEN HARRIES

A thorough survey of existing American, British, and other information on the subject, arranged for maximum usefulness to electronic engineers engaged in designing electron multipliers, dynatrons, beam tetrodes, pentodes, and other tubes in which secondary electrons resulting from electron bombardment are either utilized or suppressed

WHEN an electron stream strikes an electrode surface, or, indeed, any surface, an emission of secondary electrons is produced. There is no known substance in which this effect does not occur. In fact, there is no substance that is known to act as a perfect absorber of any electrons that may impact onto it.

In electronic tubes, secondary radiation is sometimes useful, and sometimes un-

desirable. The phenomenon is complex, and information about it is scattered in various treatises many of which are commonly read only by those interested in pure physics. Most of these publications deal with the characteristics of secondary radiation, not from any interest in it for engineering purposes, but as a part of investigations into atomic structure.

This paper includes a survey of the

existing information on secondary radiation and is presented from the engineering standpoint. It includes references to the original papers.

#### Energy Distribution of Secondary Electrons

In most treatises on secondary radiation, the electron energies are expressed in volts. The velocity  $v$  in centimeters per second of an electron that has fallen



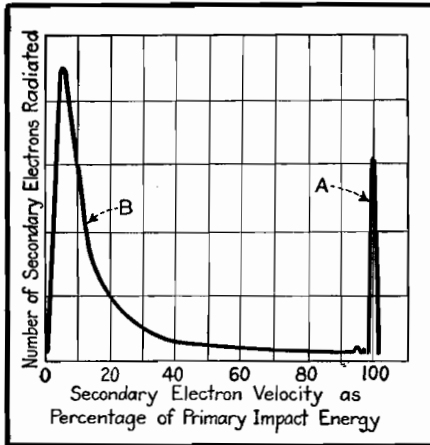


Fig. 1.—Energy distribution of secondary electrons produced by the impact of primary electrons having a kinetic energy of 155 volts. The general shape of this curve holds between 20 to 10,000 volts.

through an electrostatic potential of  $V$  volts is  $v = 5.95 \times 10^4 \sqrt{V}$ . The kinetic energy of the electron is  $\frac{1}{2}mv^2$  and is, therefore, proportional to the voltage  $V$ .

In many publications on electronic engineering, as distinct from treatises on the physics of secondary electrons, it is sometimes stated that secondary electrons are radiated almost entirely at energies very low compared with the primary impact energy. This is not so.

A typical curve of energy distribution of secondary electrons is shown in Fig. 1. In this graph the number of secondary electrons radiated is plotted against the velocity (energy) with which the secondary electrons are shot out from a radiating surface. These secondary electron energies are plotted as a percentage of the primary impact energy. The primary impact energy is 155 volts. It will be observed that an appreciable number of secondaries are radiated at energies about equal to the primary impact energy, although there are a larger number radiated at very low velocities. Very thorough researches have been made during the last two decades into this question of secondary radiation energy distribution.<sup>1-19</sup>

#### Methods of Determining Energy-distribution Curve

The general kind of energy distribution of the secondary electrons shown in Fig. 1 appears to hold over quite a wide range of primary impact velocities (20 to 10,000 volts).<sup>2</sup> It has been confirmed very carefully for most of the pure metals, and is known to hold in general for the other materials employed in radio tubes.

This kind of secondary electron energy distribution does not appear to depend

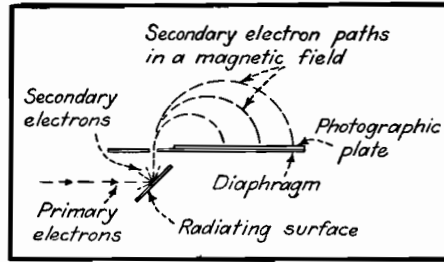


Fig. 2.—Photographic method of determining the velocity distribution of secondary electrons. A magnetic field is assumed to exist in the space above the diaphragm with a direction normal to the plane of the paper.

on the angle of incidence of the primary beam onto the emitting surface,<sup>13,20</sup> nor does it appear to depend on the angle of emergence of the secondary electrons, though this point does not appear to have been quite so conclusively demonstrated by workers in this field.

In Fig. 2 an electron gun is arranged to produce a beam of primary electrons at a known velocity. The primary electrons are arranged to collide with a surface which then radiates secondary electrons. Some of the secondary electrons can pass through an aperture in a diaphragm into a space in which there exists a homogeneous magnetic field in the direction normal to the plane of the paper. It is a well-known property of such a magnetic field that electrons traveling into it as shown will tend to describe circles the radii of which are given by

$$r = 3.37 \sqrt{V_s B} \quad (1)$$

where  $B$  is the magnetic flux density, and  $V_s$  is the secondary electron energy in volts.

A photographic plate is positioned as shown. The number of electrons of any given velocity reaching the plate will be indicated by blackening at the appropriate place. This method, however, is not very practicable, because the sensitivity of a photographic plate is rather low.

A Faraday cylinder, which has the property of trapping electrons and the

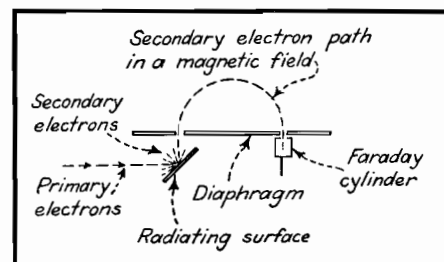


Fig. 3.—Another method of arriving at the velocity distribution of secondary electrons. The magnetic field in this case is variable.

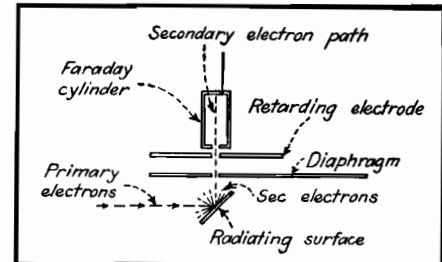


Fig. 4.—The retarding potential method of arriving at the velocity distribution of secondary electrons radiated in a specific direction.

secondaries they produce, can be substituted for the photographic plate as in Fig. 3. By varying the magnetic field, the number of secondary electrons of each velocity may be found.

Another method, shown in Fig. 4, does not use a magnetic field but, instead, employs a retarding potential to sort out the secondary electrons in terms of their energies. The primary electrons hit a secondary radiator at a known energy, and secondary electrons pass through a diaphragm into a Faraday cylinder. The amount which are able to enter depends on the potential of a retarding electrode positioned as shown and on the initial energies of the secondaries themselves.

The arrangement of Fig. 5 enables the energies to be obtained for the secondary electrons at all angles. The primary electron beam strikes a radiating surface which is at the center point of a collecting sphere. A retarding potential is applied to this sphere, and the number of electrons reaching it is measured as a function of this potential.

In the arrangements of Figs. 4 and 5, the energy-distribution curve is obtained by differentiation of the curve of current to the Faraday cylinder or collection sphere as a function of the retarding potential.

#### Interpretation of Curve

The general results of all these methods agree. The particular curve shown in

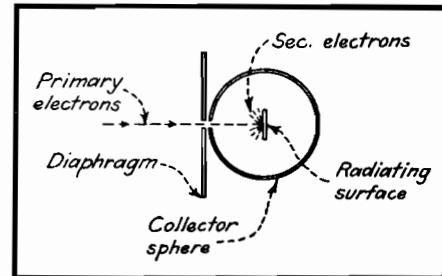


Fig. 5.—The retarding potential method of arriving at the velocity distribution of secondary electrons emitted and reflected from a radiating surface.

Fig. 1 is given by Rudberg and is obtained by the magnetic method.

It is generally agreed that the energy-distribution curve of Fig. 1 may be interpreted as follows: Peak A represents that portion of the emergent electrons which retains the full primary energy. At secondary electron velocities between about 98 and 50 per cent of the primary velocity, the number of secondary electrons radiated does not change much with the secondary electron velocity. Large quantities of secondary electrons are emitted with low velocities, as indicated by peak B, but the number emitted drops rapidly as secondary velocity approaches zero (at secondary energies of the order of tenths of a volt and less).

Peak A of the curve is produced by electrons that emerge after being elastically reflected. They result from diffraction unaccompanied by loss of energy to the atoms that are being bombarded by the primary electrons. All other parts of the curve are produced by secondary electrons that have been deflected by repeated collision accompanied by considerable energy loss.

Those secondaries contributing to parts of the curve other than A are usually referred to as emitted or true secondary electrons. Those contributing to part A of the curve are usually referred to as reflected electrons. For this reason, the phenomenon as a whole is usually referred to as secondary radiation, and the words emitted and reflected are reserved for the special meanings set out.

#### Action of Low Impact Velocities

With primary impact velocities below about 10 volts, it has been found that the energy distribution of Fig. 1 does not hold. The secondary radiation consists almost entirely of reflected electrons that retain the full primary energy, so that the whole of the radiation is contained in a peak like A on Fig. 1.

The percentage of emitted secondary electrons to reflected secondary electrons increases steadily up to primary velocities of the order of 1,000 volts, after which it falls once again. As previously mentioned, however, the general shape of Fig. 1 holds between about 20 and 10,000 volts.

#### Space Potential Considerations

It is important to realize that under electrostatic conditions the velocity of each of the secondary electrons at any point in space will be determined by the space potential  $V$  of that point. It follows that an electron emitted at a

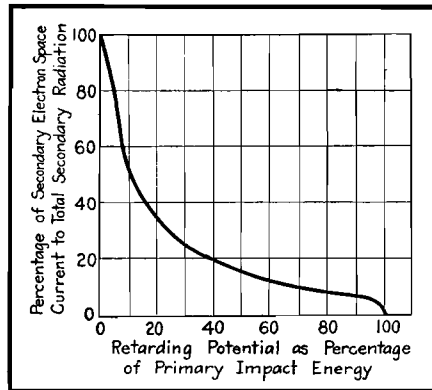


Fig. 6.—Ratio of secondary electron current traveling to a collector and the total secondary radiation, plotted as a function of the retarding potential between the radiator and the collector.

velocity which corresponds to a voltage  $V_s$  will be brought to rest at any point in space where a negative space potential  $-V$  numerically equals  $V_s$ . This is the principle by which secondary electrons are sorted into their respective velocities (or energies) by means of the retarding electrode or collecting sphere of Figs. 4 and 5, respectively. A potential that is arranged in this way to stop secondary electrons is generally referred to as a retarding potential.

Figure 6, which is obtained by integration of Fig. 1, shows the ratio of secondary electron current to any collector (such as the collector sphere in Fig. 5) to the total secondary radiation current as a function of the retarding potential. This potential is expressed as a percentage of the impact energy in volts.

In pentodes and beam tetrodes, the prevention of the flow of secondary electrons is one of the primary objects of the tube design. With reference to Fig. 5, it will be realized that if the collector sphere is at a potential (with respect to the cathode) which is 90 per cent of the impact potential of the radiator (also measured in volts with respect to the cathode), then a retarding potential of 10 per cent will exist between the collector sphere and the radiator. Figure 6 shows that under this condition the secondary radiation current flowing to the collector electrode will be 54 per cent of the total secondary radiation from the radiator.

All this, of course, assumes quasi-steady-state conditions as regards voltage (*i.e.*, that the voltage does not vary rapidly with time) and that no appreciable space charge due to the primary or secondary electrons exists in the space between the emitter and the collector sphere. The physics measurements quoted in this paper are all made under static condi-

tions, and care has been taken to avoid space-charge effects, but these effects must not be forgotten when applying the information to practical radio tubes.

Table I.—Maximum Total Secondary Radiation Coefficients

Secondary emitter	Max. value of sec. radiation coeff.	Primary impact velocity (volts) at which max. of sec. radiation coeff. occurs
Cesium (compound layer).....	8.5	400–600
Rubidium (compound layer).....	5.75	700
Beryllium.....	5.4	600
Calcium.....	4.95	520
Barium.....	2.72	530
Potassium (compound layer).....	2.5	600
Aluminum.....	2.4	400
Silicon.....	1.63	380
Platinum.....	1.52	1,000
Silver.....	1.47	800
Gold.....	1.45	780
Tungsten.....	1.33	625
Nickel.....	1.3	500
Tantalum.....	1.3	625
Copper.....	1.27	600
Iron.....	1.27	400
Molybdenum.....	1.27	375
Niobium.....	1.17	400
Carbon (lampblack).....	0.6–1	

Such tubes when in operation are seldom free from space-charge effects.

Some relationship exists between the secondary energy distribution curve and the material of the emitter. This has been found by Sharman<sup>15</sup> to be in agreement with the atomic properties of the material. At voltages of the order of 8,000 volts, however, Stehberger<sup>21</sup> failed to find any such connection. The answer to this question is rather vague at present.

#### Angular Distribution of Secondary Radiation

The relative amount of secondary radiation at various angles from a surface may be determined by apparatus such as that illustrated in Fig. 7. The Faraday collector is rotatable with respect to the radiating surface. The angle of incidence of the primary electrons to the normal of this surface is indicated by  $\alpha$  and the angle of secondary radiation by  $\beta$ . The number of secondary electrons per unit angle may thus be determined.

Measurements of angular distribution have been carried out by a number of workers.<sup>21-25</sup> While there is some experi-

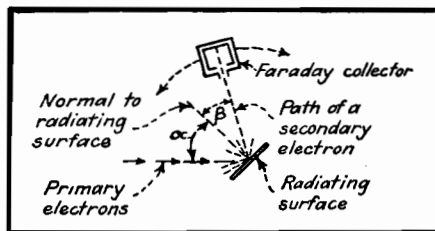


Fig. 7.—Use of an angularly adjustable collector to measure the secondary radiation coefficient of both reflected and emitted electrons as a function of the angle of emission to the normal.

mental evidence<sup>23</sup> of optical reflection of the primary electrons (i.e.,  $\alpha = \beta$ ), the evidence of this effect is by no means generally accepted. At present it seems reasonable to assume a cosine distribution of secondary radiation, as shown in Fig. 8; i.e., the intensity of the secondary radiation varies as  $\cos \beta$ , and this distribution is virtually independent of  $\alpha$ . The maximum value of the secondary radiation varies, however, with  $\alpha$ . This effect is discussed in greater detail later.

#### Total Secondary Radiation Coefficient

The arrangement of Fig. 5 may clearly be used for measuring the total radiation of secondary electrons if the collector sphere is at a slightly higher potential than the radiating surface. This measurement is in fact a summation of the curve of Fig. 1, and gives the ratio between the total number of secondary electrons and the total number of primary electrons striking the emitter. This ratio is generally referred to as the total secondary radiation coefficient. It must always be remembered, when interpreting values of this ratio, that in all cases a velocity distribution must be assumed. In the case of impact energies between about 10 volts up to the order of 10,000 volts, this distribution would be that of Fig. 1.

In practical electronic devices, the actual ratio of secondary electron current to a given electrode near the emitter to the primary electron current will depend (among other things) on this velocity distribution. Not all the secondary elec-

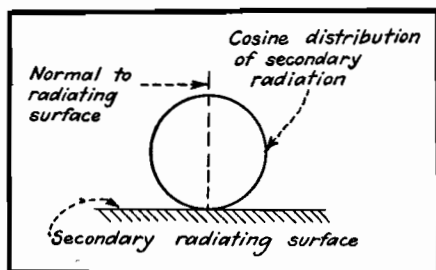


Fig. 8.—Distribution of secondary electrons as a function of the angle  $\beta$  of secondary radiation.

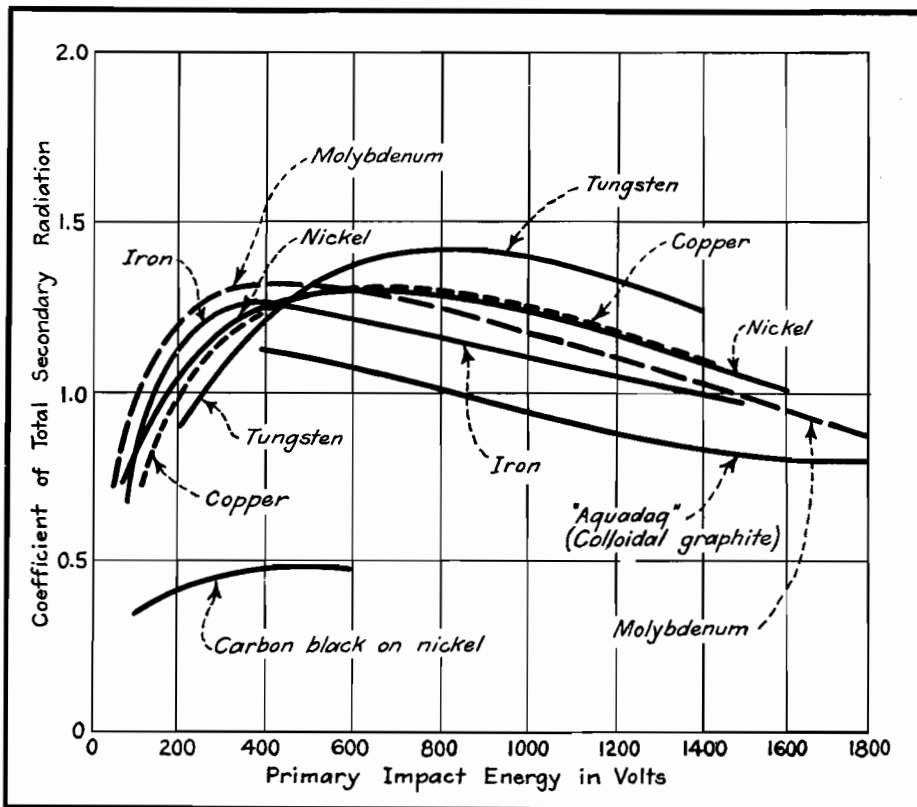


Fig. 9A.—Coefficient of total secondary radiation as a function of primary impact energy in volts for the materials commonly used in vacuum tubes.

trons necessarily contribute to the secondary electron current.

The total secondary radiation coefficient plotted against the primary electron impact energy was one of the characteristics to be investigated by the earliest workers.<sup>26-30</sup>

#### Secondary Radiation Coefficient of Pure Metals and Carbon

Typical measurements of the total secondary radiation coefficient are shown in Figs. 9A and B. These curves have been confirmed by many investigators. The curves rise to a maximum and then fall as the primary impact velocity increases still further. The maximum value of coefficient obtained lies between about 1.2 and 5.5 in the case of pure metals. Its highest value is of the order of 8 to 11 for compound surfaces of caesium of the kinds used in secondary electron multipliers and the like. Not many substances have coefficients of less than unity. That for carbon varies between 0.6 and 1.0.

Provided that the metal surfaces are clean and are completely degassed, the secondary radiation coefficient is found to be about the same by many different investigators.<sup>31-39</sup>

Table I (from Kollath<sup>40</sup>) shows typical

values of the maximum secondary radiation coefficient, and the values of primary impact energy at which it occurs, for a number of substances.

#### Secondary Radiation Coefficient of Evaporated Layers

Copeland<sup>32,35,41</sup> has obtained interesting results by evaporating various substances

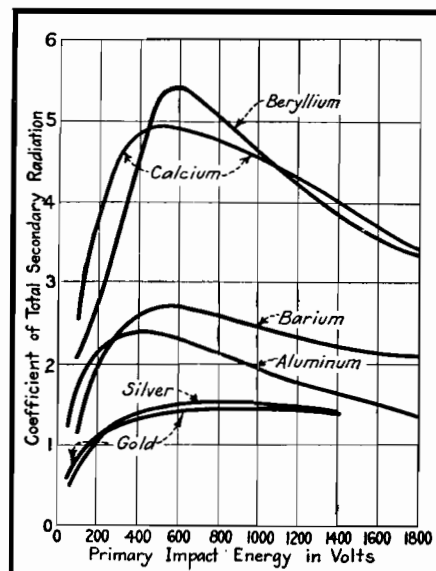


Fig. 9B.—Coefficient of total secondary radiation as a function of primary impact energy for various substances.

onto a metal foundation. Evaporating caesium onto gold increased the secondary radiation coefficient of the combination several times over that of gold alone. He also investigated other combinations of layers and foundations. The results appear to be explainable in terms of the degree of penetration of the primary electrons through the surface layer, and the varying absorption of the secondary electrons by the different substances used.

#### Secondary Electron Coefficient of Composite Surfaces

It was found<sup>35</sup> that composite materials have a high secondary radiation coefficient. For instance, evaporated deposits of calcium onto gold, and lithium onto tantalum, produce coefficients of the order of 4 to 5. It was observed that calcium and lithium belong to the alkaline-earth group of metals. They have low work functions and a high thermionic and photoelectric emission. An investigation of caesium-caesium-oxide-silver was a natural step, and high secondary electron coefficients resulted. It was discovered, however, that neither a low work function nor a high photoelectric sensitivity is the only factor concerned in producing a high secondary electron coefficient. Typical results for composite surfaces on silver are shown in Fig. 10.

Table II is given by Weiss<sup>42</sup> for various values of the maximum secondary radiation coefficient for caesium-caesium oxide deposits on various metal foundations.

The processing of the layer produced is of great importance. The deposit used as the composite surface is probably of the order of monoatomic thickness.

In detail, the production of secondary electron emissive surfaces is, like the production of coated thermionic cathodes, largely an empirical process.

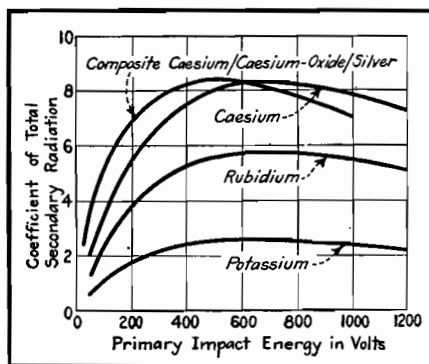


Fig. 10.—Coefficient of total secondary radiation as a function of primary energy in volts for pure metals and a composite oxidized layer on silver.

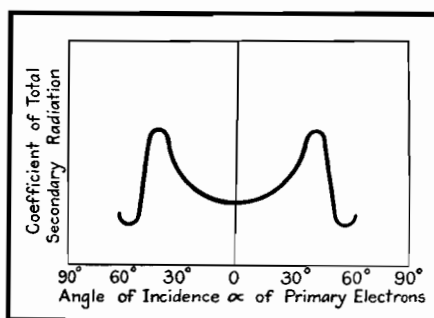


Fig. 11.—Coefficient of total secondary radiation from an insulator as a function of the angle of incidence of the primary electrons. A critical angle of incidence will be observed.

Table II.—Maximum Secondary Radiation Coefficient for Caesium Layers on Various Metal Foundations

Metal	Max. value of sec. radiation coeff.	Primary impact energy (volts) at which max. of sec. radiation coeff. occurs
Silver.....	8-11	600
Magnesium...	6.8-7.5	700
Tantalum....	4.1-5.5	600
Zinc.....	4.5-5.4	600
Nickel.....	4.6-5.2	550
Aluminum....	4.4-4.7	600
Copper.....	3.5-4.0	600
Tungsten....	3.8-3.9	600
Lead.....	2.3-3.3	650
Molybdenum..	2.5-3.1	500
Iron.....	1.9-2.7	500
Gold.....	2.3	600

#### Secondary Radiation Coefficient of Insulators

There is comparatively little information in this matter, but it seems<sup>24,25</sup> that secondary emission from insulators consists largely of electrons that have a low velocity compared with the primary electron velocity. The cosine law of distribution appears to hold, and the coefficient can exceed unity. There is, however, a difference with regard to the angle of incidence of the primary electrons impacting the radiator. In the case of conductors, the secondary radiation coefficient increases continuously with the angle of incidence, but in insulators this is not so. The coefficient increases up to a critical angle of incidence in either direction from 0 deg, beyond which the coefficient drops sharply and then again increases, as shown in Fig. 11.

This critical angle has been found to be evident only at certain levels of primary impact velocity in the range from 1,300 to 3,000 volts. The critical angle increases with increasing voltage, and eventually vanishes. It is also affected

by temperature. For example, a critical angle that is 35°C at room temperature falls to 15°C at the temperature of liquid air. It vanishes at 150°C. At this and higher temperatures, the phenomenon is the same for insulators as for conductors.<sup>24,42,44-50</sup>

Explanations<sup>21,51,52</sup> assume that a surface layer of negative space charge is produced on the insulator and affects the emission of secondary electrons. An insulating surface does not necessarily have a negative charge, however. The charge will depend on the conditions of the experiment and on the secondary radiation coefficient of the material.

#### Variation of Secondary Radiation Coefficient with Primary Angle of Incidence

In general, at low primary impact energies (up to about 100 volts or so), the secondary radiation coefficient is the same for all angles of incidence.

At higher voltages this is not so. A typical result due to Müller<sup>55</sup> is for a primary impact energy of 2,500 volts, and is shown in Fig. 12. It is interesting to note (Kollath<sup>40</sup>) that if the coefficients for various metals are plotted in order of increase of coefficient with incidence they will then be arranged more or less in descending order of their specific gravities. The secondary radiation coefficient, as a function of the angle of primary incidence to the normal, rises with decreasing specific gravity.<sup>53-56</sup> The results previously described apply to angles of incidence in the neighborhood of the normal unless otherwise specified.

#### Secondary Emission at High Primary-impact Velocities

Primary impact energies have been investigated which are very much greater than the few thousand volts to which the previous remarks have been confined, but

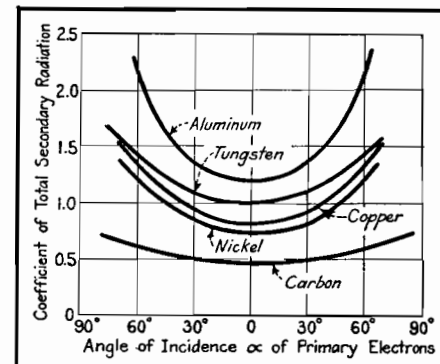


Fig. 12.—Coefficient of total secondary radiation from various conductors as a function of the angle of incidence  $\alpha$  of the primary electrons.

The primary impact energy is 2,500 volts.

high-voltage results differ little. The velocity distribution curve of Fig. 1 is affected only insofar as peak A increases in relative area (i.e., the reflected electrons increase in number).<sup>20,21,23,57,58</sup>

The secondary radiation coefficient as a whole falls with increasing primary impact energies. The increased penetration of the primary electrons of high velocity into the metal results in the secondary electrons being reabsorbed in the surface layers of the material. This fall in secondary radiation coefficient is to some extent counteracted by primary electrons which emerge in a direction different from the normal to the surface, and cause secondary electrons to be emitted from the surface layer of the material. In fact, this latter effect predominates in producing secondary radiation at very high values of primary impact velocity.<sup>21</sup> The angular distribution of the radiation follows the cosine law.

Consideration of the depth at which emission is produced is of considerable importance where radiation is obtained from both sides of a thin foil through which primary electrons are arranged to pass.<sup>3</sup>

Many investigators<sup>7,16,59-63</sup> have shown that the structure of the radiating surface has considerable effect on the coefficient. No effect on it is noted by Hayakawa<sup>61</sup> at the magnetic transformation points of ferromagnetic materials, but sudden changes have been shown to occur at the points of allotropic modification of the surface structure. An abrupt variation in the secondary radiation coefficient of iron at the Curie point has, on the other hand, been recorded by another worker.<sup>62</sup>

#### Further Investigation Needed

According to Rao,<sup>63</sup> a nickel monocrystal gives a lower secondary radiation coefficient than an ordinary polycrystalline nickel surface. An opposite result is obtained by H. E. Farnsworth<sup>7</sup> with respect to copper. His result appears to agree with the experimental fact that the secondary radiation coefficient of finely precipitated carbon or platinum black has a particularly low coefficient of secondary radiation.

Further investigation seems to be needed. In the meantime it seems that either monocrystal surfaces of different materials have different effects on the coefficient, or that there is perhaps some optimum size of crystal which gives a maximum coefficient.

#### Effect of Temperature on Secondary Electron Coefficient

As far as can be ascertained, there is no temperature effect. According to Kollath<sup>40</sup> this point might, however, be worth further investigation, particularly with regard to the complex surface coatings now commonly used in commercial practice.

#### Effect of Gas on Secondary Radiation Coefficient

All materials contain a certain amount of gas before they have been heat-treated by the usual valve (tube) manufacturing processes which are necessary to produce a high vacuum. Occluded gas has a considerable effect on the secondary radiation coefficient, and, until the radiator is completely degassed, repeatable results are not obtained. Measurements on the effect of gas have been made by Farnsworth,<sup>7</sup> Warnecke,<sup>36</sup> and Ahearn.<sup>64</sup> In general, the presence of gas increases the secondary radiation coefficient, often several times.

#### Mechanism of Secondary Electron Radiation

The quantitative analysis of the atomic mechanism of the phenomenon is in a very rudimentary state. In fact, a survey of the subject reduces itself largely to an unsatisfactory recital of disjointed experimental facts rather than to a coherent statement of theory. Kollath's paper<sup>40</sup> gives an excellent outline of the situation up to 1937. The relationship between secondary radiation phenomenon and the atomic structures of various metals gives no very conclusive result, nor has the work function any very useful relationship, though there has been shown to be some proportionality between the secondary radiation coefficient and this quantity. The depth of penetration of the primary electrons has been estimated, and Becker<sup>14</sup> arrives at a calculated depth of penetration of about 30 Å (about 15 to 20 atomic layers) at primary impact velocities of the order of 500 volts.

#### Emission Time of Secondary Electrons

As far as the author is aware, no measurements, or computations of this quantity have yet been made. It may prove, however, to be very important in view of the increasing use of extremely high frequencies in electronics. So far, the only conclusion appears to be—and this is a unanimous one<sup>65,72</sup>—that the time of emission is less than  $10^{-9}$  sec. This is as much as several times the periodic time at the highest radio fre-

quencies now being brought into use. Modern u-h-f technique might enable the time to be measured. A suggestion due to Kollath<sup>40</sup> involves comparing the times of arrival of electrically reflected primary electrons with those of secondary electrons. Experimental difficulties appear, however, to be considerable.

#### Secondary Emission Transit Times

In view of the initial velocity spectrum (Fig. 1) common to all secondary radiation (the fact that secondary electrons are not all emitted at the same velocity), secondary electrons traveling from the emitter to another electrode do so with differing transit times. This effect is of substantial importance to the operation of vacuum tubes at very high frequencies, and is dealt with later.

#### Secondary Radiation in Electronic Engineering

In electronic engineering, secondary radiation is sometimes found to interfere with the desired operation of the radio tube in which it occurs. Sometimes, on the other hand, it is utilized as an essential part of the mechanism of operation.

#### The Dynatron

In a tetrode, when the screen grid is at a higher potential than the anode, secondary radiation from the anode may travel to the screen grid and produce a negative resistance characteristic in the anode circuit over a range of anode voltages. Hence the valve can be made to generate oscillations. This effect was first described by Hull.<sup>72</sup> In considering these results with respect to modern radio techniques, due regard must be paid to secondary radiation transit angle effects.

#### Secondary Electron Multipliers

Secondary electron multipliers<sup>74</sup> of both the magnetic and electrostatic types are so well known that it is unnecessary to describe them in detail. In multipliers, the primary electrons strike an emissive surface which is of such a kind as to produce a high ratio (usually between 8 and 11) of total secondary radiation coefficient. Secondary electrons thus radiated are caught by another plate from which further secondaries are again radiated. This process is repeated several times in order to produce a very high total magnification of the original primary-electron-beam current.

The primary electron beam can be controlled either by photoelectric effects<sup>75</sup> or by voltage control. Greater importance appears to attach to the amplifica-



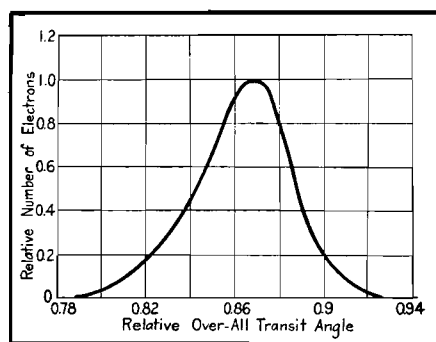


Fig. 13.—Variation of transit angle of secondary electrons in a secondary electron multiplier. This variation is due to the distribution of secondary electron energies illustrated in Fig. 1. Note that this graph ignores peak A of Fig. 1.

tion of photoelectric currents than to voltage control, as the limitations of the latter type cause it to be rather specialized in application.<sup>76</sup> An interesting and comparatively recent example of voltage control has been described by Wagner and Ferris.<sup>77</sup> Control of the primary electrons in secondary multipliers by deflecting them instead of using a control grid appears to have been first described by Hopkins.<sup>78</sup> The composite cesium-cesium-oxide-silver curve in Fig. 10 shows the ratio of secondary emission current to primary current obtained from one of the radiating surfaces in a multiplier.

Since secondary electrons are not emitted with a single velocity, but with a spectrum of velocities, the transit angle between the radiators in the multiplier also has no single value.

In Fig. 13, the ordinates represent the relative number of secondary electrons emitted at each of various relative over-all transit angles of the secondary electrons in a three-stage electron multiplier. The relative over-all transit angle is expressed as a fraction of the transit angle that would exist if the secondary electrons were emitted with zero velocity. It will be observed that the transit angles of the individual secondary electrons vary over a

wide range. Furthermore, secondary electrons are radiated from different parts of the radiator, and have to travel along paths of different lengths to reach the next electrode.

The result of these combined effects has been shown by Malter<sup>87</sup> to produce an h-f cutoff in the response of the multiplier as a whole. The resulting frequency cutoff of a typical multiplier is shown in Fig. 14.

#### Farnsworth Multipactor

Another application of secondary electron multiplication involves the utilization of transit time to produce h-f oscillations. This idea was first put forward by Philo T. Farnsworth.<sup>78</sup>

#### Reduction of Screen Grid Current

In many screen-grid radio tubes, the anode is maintained during operation at a potential higher than that of the screen grid. Secondary radiation of quite a considerable amount is produced at the points of impact on the screen grid of the primary electrons that constitute the space current. The secondary electrons travel from the screen grid to the anode and so decrease the screen grid current and increase the anode current, very considerably. This results in an increase in the static transconductance of the tube. It must not be forgotten that, owing to the varying transit angles of the secondary electrons, this increase will not hold at very high frequencies. The phenomena produced will be somewhat similar to that exemplified above with respect to secondary electron multipliers. There seems to be no published information in this matter.

#### Secondary Radiation from Cathodes

In certain tubes—notably the magnetron—the cathode may be bombarded by primary electrons which return to it at considerable velocities. By adding to the emission, the resulting secondary radiation may have an appreciable effect on the operating characteristics of the valve.

#### The Pentode

In the great majority of electronic tubes, secondary radiation is a nuisance and elaborate steps have to be taken to prevent it from interfering with the operation of the tubes. It will be clear from Fig. 5 and the associated text, however, that attempts to prevent the radiation of secondary electrons from the electrodes of radio tubes are foredoomed

to failure. In fact, quite early engineering experiments confirmed this.<sup>89</sup>

Since secondary radiation itself cannot be prevented, the only remaining thing to do is to prevent the secondary electrons traveling from one electrode to another. This is the idea behind the pentode.

It is almost unnecessary to describe this well-known tube in detail.<sup>81</sup> The traverse of secondary electrons from the anode to the screen grid when the anode is at a lower potential than the screen grid during operation is prevented partly by the use of a retarding potential. A grid (called the suppressor grid) is interposed between the screen grid and the anode and is maintained at a low potential.

Primary electrons pass through the spaces between the suppressor grid wires. A retarding potential exists between these spaces and tends to reduce the secondary radiation current from the anode to the screen grid to a fraction of the primary electron current (see Figs. 4 and 6). At the same time, owing to the cosine law of distribution (Fig. 8), only a small number of the secondary electrons are directed toward the gaps in the suppressor grid. This results in a still further reduction of the total secondary electron current.

A further effect that tends to reduce the adverse flow of secondary electrons is the addition to the retarding potential caused by space charge effects. Both primary and secondary electrons contribute to the space charge potential. The combination of all these effects (and possibly others) operates in a very complex manner, and the author is not aware of a satisfactory quantitative theory, but pentode valves may readily be designed by empirical means.

Remembering that the potential of the spaces between the wires of the suppressor grid cannot be zero (or the primary electrons themselves would be prevented from arriving at the anode), it is untrue to say that the operation of a pentode is explained merely by the interposition of a retarding potential between the anode and screen grid. A retarding potential that did not reduce the potential between the wires of the suppressor grid to zero would still leave a considerable amount of secondaries flowing. This is clear from Fig. 6. Curves A in Fig. 15 shows the familiar dynatron characteristic which is produced in the absence of a suppressor grid. Curve B shows the characteristic found in a pentode, and curve C shows the type of characteristic that might perhaps be expected if the suppressor

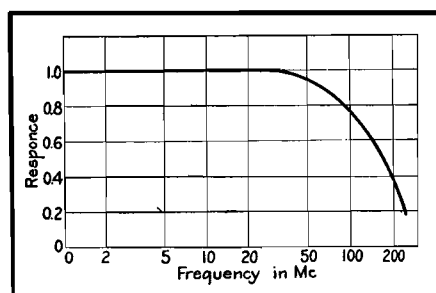


Fig. 14.—Frequency response of an electron multiplier, showing fall off at very high frequencies due to the transit angle effect illustrated in Fig. 13.

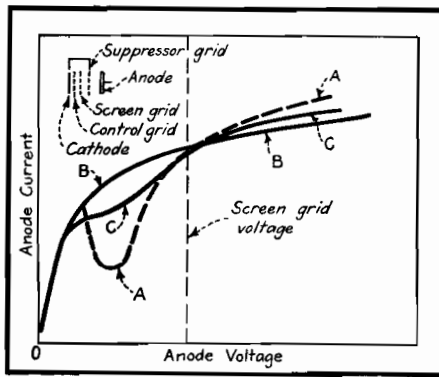


Fig. 15.—Curve A is the anode characteristic of a dynatron valve. Curve B is that of a pentode. Curve C is the approximation to the kind of curve that might be expected if a suppressor grid is assumed to operate solely by producing a retarding potential.

grid retarding potential alone were the only operative factor in preventing the flow of secondary electrons.

### Secondary Electron Traps

Owing to the cosine distribution of secondary radiation (Fig. 8), if a beam of primary electrons enters an enclosed metal cavity (at a positive potential) through a small aperture as in Fig. 16, only a very small part of the resulting secondary radiation will succeed in leaving the cavity. This is the principle of the Faraday cylinder previously referred to (Figs. 3, 4, and 7). Attempts have been made and suggested<sup>80</sup> to utilize such cylinders as the anodes or collector electrodes of practical radio tubes. Since in such radio tubes the effective anode area for the collection of primary electrons must usually be considerably greater than the small aperture illustrated in Fig. 16, these attempts have not been very successful as far as the author is aware.

### Critical-distance Beam Tetrodes

In 1931 the author, working on the production of the then novel idea of producing beams of electrons of appreciable fractions of an ampere at a few hundred volts, found that if the space

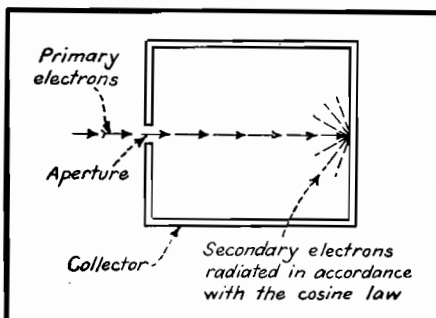


Fig. 16.—A Faraday cylinder or electron trap.

current in a dynatron type of tetrode is confined into a beam, an optimum value exists for the distance of the anode from the screen grid (accelerating grid; he named this distance the critical distance) at which the passage of secondary electrons from the anode to the accelerating grid is prevented. The anode characteristic then obtained is of the kind illustrated in Fig. 17.<sup>82-86</sup> The sharp knee at the left-hand side of the curve is characteristic of this type of tube and results in a considerably lower distortion level<sup>82,86</sup> than the more rounded knee of the pentode (Fig. 15).

Tubes of this kind were made in 1931 and were put on the market in England by a commercial firm in 1935. They came into wide use, under the name of beam tetrode when this tube was first marketed (in America) in 1936; yet, like the pentode (the invention of which dates from 1926), there is again no satisfactory published theory. The straight part of the anode characteristic of this valve (Fig. 17) can be accounted for only by the reduction of the traverse of secondary radiation to a very small fraction indeed of the total radiation. By reference to Fig. 6, it will be seen that this appears to infer a retarding potential virtually equal to the primary impact velocity itself.

Attempts have been made to explain this critical-distance characteristic in terms of the potential minimum produced by space charge,<sup>88,89</sup> but the author has shown<sup>86</sup> that the magnitude of the retarding potentials predicted by this theory is not sufficient (by a factor of several times) to prevent the occurrence of the dynatron kink in the anode characteristics. Moreover, the problem is not merely one of preventing the passage of secondary radiation at one set of values of anode current, anode voltage, and screen voltage. It is, on the contrary, that of maintaining a flat working surface of the characteristic over a wide variation

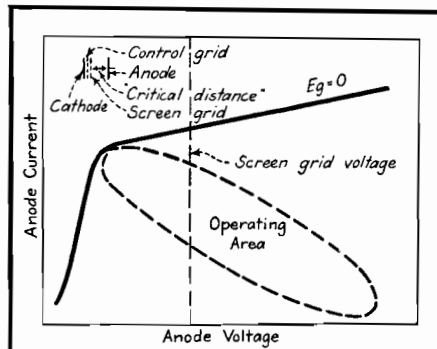


Fig. 17.—A critical-distance beam-tetrode characteristic.

area (Fig. 17). A purely space-charge retarding potential theory leads to no such range of working currents and voltages.

A complete formulation of the problem must include the effects of the formation of the primary electrons into a beam (without which the effect seems not to take place in practice), the variation of the density of this beam with control grid voltage, the energies of the secondary electrons, the angular distribution of the secondary radiation, the end effects, and the depression of space potential due to the presence of low-potential conductors near the screen grid-anode space.

It has been pointed out by the author some time ago<sup>83</sup> that if the accelerating voltage is higher than a few hundred volts, the critical-distance effect is not produced satisfactorily. This appears to have a relationship to the increase in the area of peak A in the secondary radiation energy distribution curve (Fig. 1) at the higher primary impact velocities.

### Secondary Emission from Grids

Grids and other electrodes in electronic tubes that are struck by electrons will emit secondaries which, particularly in tubes where optical images are to be formed, may be very undesirable. Such effects may be minimized, though not eliminated, by treating the surfaces involved. Coating with carbon black or like methods are used (Fig. 9A).

### Secondary Radiation from Insulated Electrodes and Insulators in Vacuum Tubes

If an insulated conductor is positioned in the path of a beam of primary electrons, its potential will depend on the impact energy of the primary electrons and on the secondary electron coefficient of the conductor.

For instance, referring (Fig. 9A) to the curve for nickel, it will be seen that it becomes unity at a primary impact velocity of approximately 1,750 volts. The initial potential of a clean insulated electrode made of nickel will, in the absence of a flow of primary electrons, be that of the space in which it is situated. If this potential and the impact energy of the primary electrons on the nickel electrode are both above 1,750 volts, then, from Fig. 9A, the total secondary radiation coefficient will be less than unity. The insulated nickel electrode will therefore charge negatively until its potential reaches 1,750 volts, when the secondary radiation coefficient is unity, and the



number of electrons leaving the electrode will be equal to those reaching it. This, of course, assumes space-charge-free conditions, and assumes further that all the secondary electrons emitted by the nickel are collected by other electrodes in the tube.

If, again, the space potential of the insulated nickel electrode and the initial energy are between about 160 and 1,750 volts, then, from Fig. 9A, the secondary radiation coefficient will be greater than unity, and the electrode will tend to charge positively until an equilibrium potential of about 1,750 volts is again reached.

If, however, the space potential and the primary impact energy are below 160 volts, then, from Fig. 9A, the total secondary radiation coefficient is less than zero. The insulated electrode will charge up negatively until it reaches zero potential, at which no primary electrons strike it. Therefore, in general, an insulated conductor upon which electrons impinge tends to take up either a potential tending to zero, or a high positive potential. It has been suggested to employ this effect to maintain a suppressor grid in a pentode at the order of zero potential. Clearly, if the electrode is contaminated, or otherwise has a greater secondary radiation coefficient than the pure material (and this may very easily occur in a practical radio tube), the impact potential at which the total secondary radiation coefficient is unity may well become very high.

The equilibrium potentials of insulators (such as the glass walls of a vacuum tube) due to secondary radiation may vary discontinuously and profoundly affect the space potential in the tube as a whole, and therefore in many instances upset the operation of the device. In the absence of more information on the secondary radiation coefficients of insulators, and because of the complicated nature of their behavior, it is not possible to state any

useful theory. In radio tubes, care is taken to minimize the results of bulb charging. This is done by causing the electrode assembly to be self-shielding (i.e., semi-enclosed as far as the operative part of the electron beam is concerned) or by putting a conductive film (such as colloidal graphite) on the walls of the glass envelope and connecting it to a suitable part of the electrode system. This is found to be necessary in cathode-ray oscilloscope tubes where the beam is not enclosed by the metal electrodes.

### References

- (1) RUDBERG, E., *Phys. Rev.*, **50**, 138, 1936.
- (2) BECKER, A., *Ann. Physik*, **78**, 228, and 253, 1925.
- (3) BECKER, A., *Ann. Physik*, **84**, 779, 1927.
- (4) BRINSMAD, J. B., *Phys. Rev.*, **30**, 494, 1927.
- (5) CAMPBELL, N. R., *Phil. Mag.*, **24**, 783, 1912.
- (6) DADOURIAN, H. M., *Phys. Rev.*, **14**, 434, 1919.
- (7) FARNSWORTH, H. E., *Phys. Rev.*, **26**, 41, 1925.
- (8) FARNSWORTH, H. E., *Phys. Rev.*, **31**, 405-413, March, 1928.
- (9) HAWORTH, L. J., *Phys. Rev.*, **37**, 93, 1931.
- (10) HAWORTH, L. J., *Phys. Rev.*, **42**, 906, 1932.
- (11) HAWORTH, L. J., *Phys. Rev.*, **48**, 88, 1935.
- (12) HAWORTH, L. J., *Phys. Rev.*, **50**, 216, 1936.
- (13) LANGENWALTER, H. W., *Ann. Physik*, **24**, 273, 1935.
- (14) RUDBERG, E., *Proc. Roy. Soc. (London)*, **127**, 111, 1930.
- (15) SHARMAN, C. F., *Proc. Cam. Phil. Soc.*, **23**, Part 5, 523 to 530, January, 1927.
- (16) SOLLER, T., *Phys. Rev.*, **36**, 1212, 1930.
- (17) WELLS, D. A., *Phil. Mag.*, **5**, 367, 1928.
- (18) DAVISSON and KUNSMAN, *Phys. Rev.*, **22**, 242 and 256, September, 1923.
- (19) DAVISSON and KUNSMAN, *Science*, **54**, 404, 522 to 524, Nov. 25, 1921.
- (20) FUCHTBAUER, C., *Physik. Z.*, **7**, 748, 1906.
- (21) STEHBERGER, K. H., *Ann. Physik*, **86**, 825, 1928.
- (22) SEITZ, W., *Ann. Physik*, **6**, I, 1901.
- (23) TATE, J. T., *Phys. Rev.*, **17**, 394, 1921.
- (24) DAENE, H., and SCHMERWITZ, G., *Z. Physik*, **53**, 404, 1929.
- (25) FARNSWORTH, H. E., *Phys. Rev.*, **31**, 414, 1928.
- (26) BAAYER, O. v., *Physik. Z.*, **10**, 168, 1909.
- (27) BAAYER, O. v., *Verh. deut. physik. Ges.*, **10**, 96 and 935, 1908.
- (28) BAAYER, O. v., *Physik. Z.*, **10**, 176, 1909.
- (29) CAMPBELL, N. R., *Phil. Mag.*, **25**, 803, 1913.
- (30) GEHRTS, A., *Ann. Physik*, **36**, 995, 1911.
- (31) COPELAND, P. L., Thesis in the Department of Physics, State University of Iowa, July, 1931.
- (32) COPELAND, P. L., *Jour. Franklin Inst.*, **215**, 435, 1933.
- (33) COPELAND, P. L., *Jour. Franklin Inst.*, **215**, 593, 1933.
- (34) COPELAND, P. L., *Phys. Rev.*, **46**, 167, 1934.
- (35) COPELAND, P. L., *Phys. Rev.*, **48**, 96, 1935.
- (36) WARNECKE, R., *Jour. phys. radium*, **5**, 267, 1934.
- (37) WARNECKE, R., *Jour. phys. radium*, **7**, 270, 1936.
- (38) FARNSWORTH, H. E., *Phys. Rev.*, **20**, 358, 1922.
- (39) FARNSWORTH, H. E., *Phys. Rev.*, **27**, 413, 1926.
- (40) KOLLATH, R., *Physik. Z.*, **38**, 202-224, 1st Apl., 1937.
- (41) COPELAND, P. L., *Phys. Rev.*, **35**, 293, 1930.
- (42) WEISS, G., *Fernsehen und Tonfilm*, **41**, 1936.
- (43) KALCKHOFF, G., *Z. Physik*, **80**, 305, 1933.
- (44) WEHNELT, A., *Ergeb. exakt. Naturw.*, **4**, 417, 1928.
- (45) SCHMIDT, W., Diss. Berlin, 1923.
- (46) NICKEL, G., Diss. Berlin, 1922.
- (47) BEYSLAG, B., Diss. Berlin, 1926.
- (48) UREDAT, E., Diss. Berlin, 1930.
- (49) WEHNELT, A., *Z. Physik*, **48**, 165, 1928.
- (50) KNOLL, M., *Z. tech. Physik*, **16**, 467, 1935.
- (51) JOFFE, A., *Z. Physik*, **48**, 737, 1928.
- (52) KLEMPERER, O., *Z. Physik*, **47**, 417, 1928.
- (53) STRÜBIG, H., *Physik. Z.*, **37**, 402, 1936.
- (54) BRUNING, H., *Physica*, **3**, 1046, 1936.
- (55) MÜLLER, H., *Z. Physik*, im Druck.
- (56) BALTRUSCHAT, M., and STARKE, H., *Physik. Z.*, **23**, 403, 1922.
- (57) CHYLINSKI, S., *Phys. Rev.*, **28**, 429, 1926.
- (58) CHYLINSKI, S., *Phys. Rev.*, **42**, 393, 1932.
- (59) FARNSWORTH, H. E., *Phys. Rev.*, **31**, 419, 1928.
- (60) FARNSWORTH, H. E., *Phys. Rev.*, **34**, 679, 1929.
- (61) HAYAKAWA, K., *Soc. Rep. Tohoku Imp. Univ.*, **1**, 22, 934, 1933.
- (62) TARTAKOWSKY, P., and KUDERJAWZEWA, W., *Z. Physik*, **75**, 137, 1932.
- (63) RAO, S. R., *Proc. Roy. Soc. (London)*, **128**, 57, 1930.
- (64) AHEARN, A. J., *Phys. Rev.*, **38**, 1858, 1931.
- (65) ALDOUS, W. A., and CAMPBELL, N. R., *Proc. Roy. Soc.*, **151**, 694, 1935.
- (66) HAYNER, L. J., *Physics*, **6**, 323, 1935.
- (67) HAYNER, L. J., and HULL, A. W., *Phys. Rev.*, **33**, 281, 1929.
- (68) MOULLIN, E. B., *Proc. Roy. Soc. (London)*, **147**, 100, 1934.
- (69) PENNING, F. M., and KRUTHOF, A. A., *Physica*, **2**, 793, 1935.
- (70) ZIEGLER, M., *Physica*, **2**, 415, 1935.
- (70a) ZIEGLER, M., *Physica*, **3**, I, 1936.
- (71) ZIEGLER, M., *Physica*, **3**, 307, 1936.
- (72) HULL, British patent 1555, 1915.
- (73) ZWORYKIN and REJCHMAN, *Proc. IRE*, **27**, 558 and 566, September, 1939.
- (74) IAMS and SALZBERG, *Proc. IRE*, **23**, 55-64, January, 1935.
- (75) THOMPSON, *Proc. IRE*, **29**, 583-587, November, 1941.
- (76) WAGNER and FERRIS, *Proc. IRE*, **29**, 598-602, November, 1941.
- (77) HOPKINS, U. S. patent 1,920,863 (1932).
- (78) FARNSWORTH, P. T., U. S. patent 2,071,515, U. S. patent 2,174,488.
- (79) HULL and WILLIAMS, *Phys. Rev.*, **27**, 423, 1926.
- (80) TELLEGHEN, British patent 287,958.
- (81) HARRIES, *Wireless World*, Aug. 2d, 1935.
- (82) HARRIES, British patents 380, 429, and 385, 968, 1931; and *Wireless Eng.*, **13**, 190-199, April 1936.
- (83) HARRIES, *Wireless Eng.*, **15**, 212, April 1938.
- (84) HARRIES, *Electronics*, May, 1936, p. 33-35.
- (85) HARRIES, *Wireless Eng.*, **14**, 63, February, 1937.
- (86) HARRIES, *Electronic Eng.*, January, 1942, 586-587.
- (87) MALTER, *Proc. IRE*, **29**, 587-598, November, 1941.
- (88) SALZBERG, and HAEFF, *RCA Rev.*, **2**, 336-374, January, 1938.
- (89) DOW, "Fundamentals of Engineering Electronics," Chapman & Hall, Ltd., London.

# Open-grid Tubes in Low-level Amplifiers

By ROBERT J. MEYER

Omission of the grid leak in a conventional low-level amplifier, leaving only surface leakage paths between the grid and cathode, reduces the noise due to shot effect and thermal agitation. A cathode resistor of proper size gives further lowering of noise level

FOR certain applications in amplifiers requiring a high input resistance and low noise level, it has been found desirable to eliminate the grid leak. Examples of such applications are amplifiers operating from a low-level high-impedance source, amplifiers that must present the smallest possible load to the preceding stage, and amplifiers that must handle signal voltages of the same order as the noise level. Operation of a tube with an open grid was found to be less noisy than operation with a grid leak.

## Noise in Amplifier Circuits

The three principal types of noise in an amplifier circuit are flicker, shot effect, and thermal agitation. These noises can be considered as being developed by equivalent generators in the grid circuit of a noise-free tube.

The flicker voltage, which is produced by irregularities in the temperature of the heating element, is inversely proportional to the square of the frequency.

Shot noise is uniformly distributed throughout the frequency spectrum, independent of the electron velocity and independent of the manner in which the total current divides between the electrodes. The values of the shot voltage  $E$  for triodes can be calculated from the formulas

$$|E| = 2 \times 10^{-10} \sqrt{\frac{\Delta F}{g_m}} \quad (1)$$

For pentodes, the formula is

$$|E| = \frac{2 \times 10^{-10}}{g_m} \sqrt{\frac{I_b}{I_b + I_{c2}} (g_m + 8I_{c2}) \Delta F} \quad (2)$$

The thermal agitation voltage developed by a resistor is

$$E^2 = 4KTR \Delta F \quad (3)$$

where  $R$  = resistance

$\Delta F$  = frequency band passed

$T$  = temperature, °K

$K$  = Boltzmann's constant ( $1.39 \times 10^{-23}$ ).

If the impedance in the grid circuit is not a pure resistance, the resistive component is a function of the frequency, and the voltage can be obtained from

$$E^2 = 4KT \int_{F_1}^{F_2} R(f) df \quad (4)$$

These formulas apply only to wire-wound resistors or to carbon resistors in which no current is flowing.

There is always some capacitance across a resistor, and this parallel combination forms a low-pass filter that affects the thermal agitation voltage  $e$  as follows:

$$e = 1.28 \times 10^{-10}$$

$$\sqrt{RF_0 \left( \tan^{-1} \frac{F_2}{F_0} - \tan^{-1} \frac{F_1}{F_0} \right)} \quad (5)$$

where  $F_0 = 1/2\pi RC$  and  $F_2$  and  $F_1$  are the upper and the lower frequency limits, respectively, being considered. It can be seen from Eq. (5) that the thermal agitation voltage output of an  $RC$  combination is independent of the value of  $R$ , because  $F_1 = 0$  and  $F_2 = F_0$ , reducing  $e$  from a function of  $R$  and  $C$  to a function of  $C$  only.

If the noise voltage from an  $RC$  combination is applied to an amplifier, some of this voltage may be in a part of

the frequency spectrum which is not passed by the amplifier. In this case, the voltage passed by the amplifier would be a function of  $R$  as expressed in Eq. (5), where  $F_1$  and  $F_2$  would now be the frequency limits of the amplifier, and  $R$  and  $C$  would be the grid leak and the input capacitance in the amplifier circuit. If  $F_1$  is very much less than the upper frequency limit of the amplifier, Eq. (5) reduces to

$$e = 1.28 \times 10^{-10} \sqrt{\frac{1}{2\pi C} \cot^{-1} \frac{F_1}{F_2}} \quad (6)$$

The form of Eq. (5) can be changed to show more clearly the relation between the thermal noise and the value of  $R$ .

$$e = 1.28 \times 10^{-10}$$

$$\sqrt{\frac{1}{2\pi C} (\tan^{-1} 2\pi F_2 CR - \tan^{-1} 2\pi F_1 CR)} \quad (7)$$

$$\tan \left[ \frac{2\pi C e^2}{(1.28 \times 10^{-10})^2} \right] = \frac{2\pi C (F_2 - F_1) R}{1 + 4\pi^2 F_1 F_2 C^2 R^2} \quad (8)$$

Equation (8) shows that the noise increases as the value of  $R$  increases from zero, reaches a maximum at some finite value of  $R$ , and decreases as the value of  $R$  is increased beyond this value. This equation shows that operation of a tube with an open grid would be less noisy than operation with a grid leak. In an amplifier circuit, to obtain minimum noise, the grid leak is sufficiently high if the thermal noise is less than the shot effect.

Another source of noise is the flow of leakage current between the cathode and the grid. This noise would be at a minimum when the cathode-to-grid voltage is at a minimum. The tube would thus be quietest with a proper value of bias, and the open-grid tube automatically biases itself to this bias voltage.

Experimental results confirmed that noise is less with an open grid than with a grid leak, and less with a cathode resistor than without one. This result is to be expected, for the cathode resistor voltage

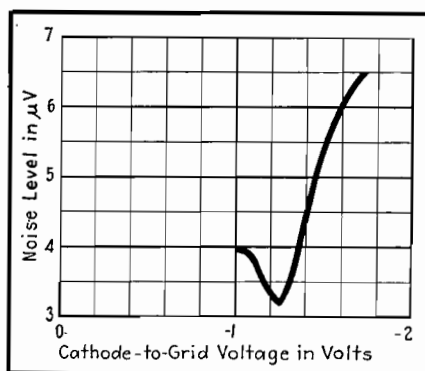


Fig. 1.—Noise level vs. cathode-to-grid voltage for a 6SJ7 tube connected as a triode, with 40  $\mu\mu\text{f}$  in the grid circuit to simulate a high-impedance crystal pickup having no short resistance.

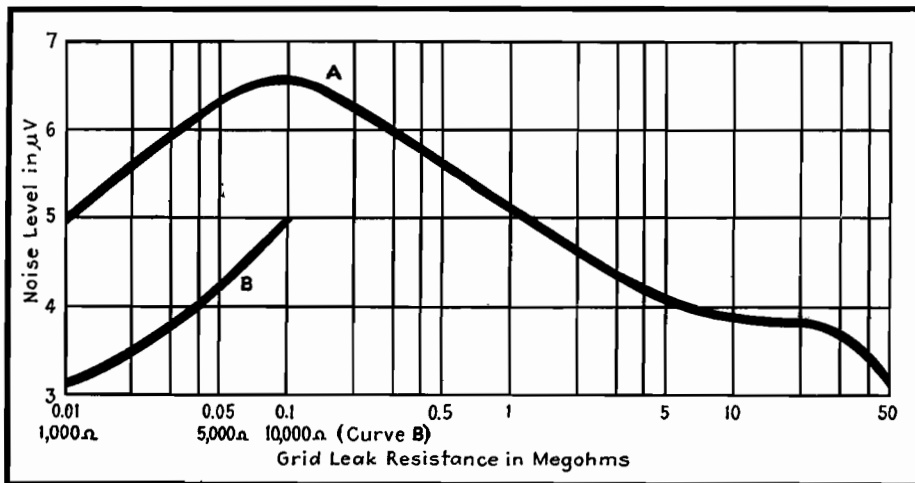


Fig. 2.—Noise level vs. grid-leak value for a triode-connected 6SJ7 tube. Curve B is for very low values of grid-cathode resistance.

drop reduces the voltage between the cathode and the grid, reducing the leakage current and the noise resulting from it. The value of noise obtained with a grid leak and no cathode resistor is exceptionally high, probably because the zero bias allows a comparatively high value of grid current to flow through the carbon grid leak, greatly increasing the noise across the resistor.

The curve of noise level vs. cathode-grid voltage is given for a 6SJ7 tube in Fig. 1. Least noise is obtained for that value of cathode resistor which gives a cathode-grid voltage of  $-1.2$  volts. The open-grid tube seems automatically to bias itself approximately to that value which gives the least noise. The effect of electron flow to the grid (which tends to make the grid negative) and the effects of emission from the grid and gas current to the grid (which tend to make the grid positive) balance each other to give the grid a small negative bias.

#### Effect of Grid Leak Value

Figure 2 shows the relation between the noise level and the value of grid leak. These readings were taken with a 750-ohm cathode resistor. Except for a shorted or nearly shorted grid, the best signal-to-noise ratio is obtained with an open grid. For the constants in this test, i.e., amplifier frequency response and input capacitance, the worst ratio is obtained for a grid leak around 100,000

ohms. For a different amplifier the worst ratio would occur at a different value of grid leak, but the general shape of the curve would be the same. These results are in agreement with Eq. (8) and the discussion following it.

#### Effect of Plate Voltage

The relation between the plate voltage on a tube and the noise level at the grid is given in Fig. 3. Again there is less

noise without a grid leak than with a grid leak, but in both cases the best signal-to-noise ratio is obtained for a plate voltage of about 90 volts.

It would be expected from Eq. (1) that the noise would continue to decrease as the plate voltage is increased because the  $g_m$  is increasing. However, the larger number of positive ions and secondary electrons present in the tube at higher plate voltages tends to make the tube slightly noisier.

Operation of a tube without a grid leak seems practical in applications involving low-level operation, with no d-c potentials in the preceding stage, and a negative grid bias of not more than about 2 volts.

#### Bibliography

- (1) REICH, H. J., "Theory and Applications of Electron Tubes," p. 184, McGraw-Hill Book Company, Inc., New York, 1939.
- (2) EVERITT, W. L., "Communications Engineering," p. 241, McGraw-Hill Book Company, Inc., New York, 1937.
- (3) HARRIS, W. A., "Fluctuations in Vacuum Tube Amplifiers and Input Systems," *RCA Rev.*, **5**, 505, April, 1941.
- (4) KING, RONALD, "A Screen Grid Voltmeter Without External Leak," *Proc. IRE*, **22**, 771, June, 1934.
- (5) MOULLIN, E. B., "Spontaneous Fluctuations of Voltage," Oxford University Press, New York, 1938.
- (6) TERMAN, F. E., "Radio Engineering," p. 228, McGraw-Hill Book Company, Inc., 1937.

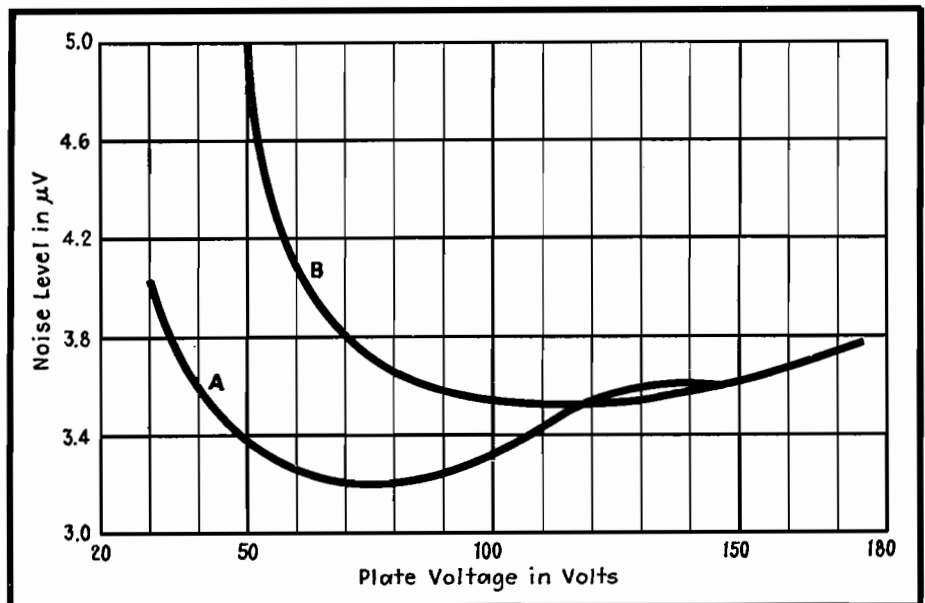


Fig. 3.—Noise level vs. plate voltage for a triode-connected 6SJ7 tube with two different grid-circuit arrangements. Curve A, 40  $\mu\text{F}$  in grid circuit; curve B, 40  $\mu\text{F}$  in parallel with 35 megohms in grid circuit.

# 28-volt Operation of Receiving Tubes

By C. R. HAMMOND, E. KOHLER and W. J. LATTIN

Performance of pentodes and triodes operated directly from an aircraft battery as B supply. Grid leak bias is recommended to minimize effects of grid contact potential and  $G_m$  variations. Tables show performance of RC-coupled amplifiers in 28-volt service.

THE application of receiving tubes at plate and screen voltages of 28 volts enables the designer of aircraft radio and related equipment to effect substantial simplifications. The direct use of the aircraft primary battery for the B supply permits elimination of high-voltage generating components with consequent reduction in size, weight, cost, maintenance, and power requirements of the equipment. Improved reliability and efficiency are also obtained.

Data are given here for typical operation of standard r-f pentodes, triodes, and voltage-amplifier types from a 28-volt B supply. Single-ended 12-volt metal types were chosen mainly because they have been the accepted standard of the Services and of the majority of leading aircraft radio manufacturers. Miniature tube types are included because they will exhibit advantages in v-h-f equipment. Data on several GT double-triode types are given, since it is thought they may find application as phase inverters, multi-vibrators, or oscillators.

## Operating Problems at 28 Volts

Operation of electron tubes with plate and screen voltages obtained directly from the primary 28-volt aircraft battery offers a few difficulties that must be recognized in establishing design practices, equipment performance tolerances, and choice of tube types. These difficulties are principally the following:

1. Variation of grid contact potential between tubes of a given type.
2. Greater percentage variation of transconductance and other characteristics, for certain types (tube-to-tube) than is experienced with the same tubes at maximum voltage ratings.
3. The wide range of battery voltage (occurring in the aircraft) over which satisfactory tube performance must be obtained.

Tube operation at 28 volts plate and screen supply makes it necessary to employ the lowest possible bias. At zero

bias with low grid circuit resistance, an obvious difficulty with grid current loading of tuned circuits arises. At low orders of fixed or cathode bias, difficulty is experienced with many tubes of a large lot drawing grid current because the bias is not high enough to overcome the contact potential. If the bias is made high enough that no tubes draw grid current, the average gain for all tubes is at an undesirable low level. A good compromise is to employ grid-leak bias which evens out the variations of gain from tube to tube. Tubes that tend to run high in grid contact potential also tend to run high in transconductance, and vice versa, so that tubes with high  $G_m$  will bias themselves back further than tubes with low  $G_m$ .

## Effective Grid Bias

We define grid contact potential, as employed in this discussion only, to be that grid potential at which the grid current characteristic (in the absence of gas or positive ion current) intercepts the zero grid current axis. The grid current characteristics of several type 9003 tubes are shown in Fig. 1. The grid contact potential values are approximately  $-0.7$  volt for tube 1 and  $-1.0$  volt for tube 3. The values are usually found to lie between  $-0.2$  and  $-1.2$  volts for most vacuum tubes of the classes discussed

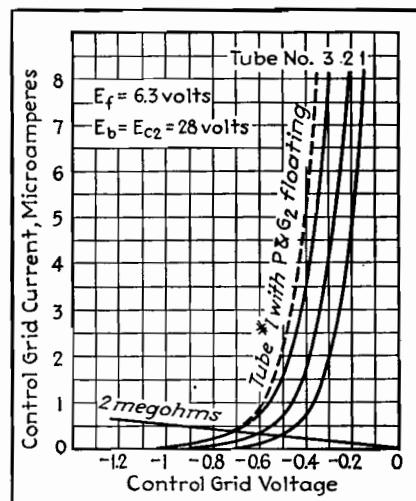


Fig. 1.—Typical grid current characteristics of type 9003 pentode in contact potential region.

here. Since the potential depends on such items as the work functions of emitting materials, mean velocity of emitted electrons, area of effective electron emission, cathode temperature, grid-cathode spacing, potentials on other tube elements, etc., it is impossible to hold the value to that degree of uniformity achieved in the control of other parameters during the manufacture of vacuum tubes.

When a grid leak resistor is used, the value of bias for the tube under consideration will be found at the point at which the load line for the resistor inter-

Table I.—Characteristics of R-f Pentode Amplifier Types with 28-volt B Supply

Type	Trans-conductance, $\mu$ mhos	Plate resistance, megohms	Plate current, ma	Screen current, ma	Cutoff bias, * volts
6AG5	1300	Over 1	0.40	0.10	-2
12SF7	1075	Over .4	2.0	0.60	-9
12SG7	1325	Over .75	0.75	0.35	-5
12SH7	1200	Over 2	0.35	0.15	-2
12SJ7	1350	Over .75	1.0	0.30	-3
12SK7	1350	Over .3	2.0	0.60	-10
9001	1150	Over .7	0.65	0.30	-3
9003	1250	Over .3	1.6	0.70	-10

\* Cutoff bias for transconductance of  $10 \mu$ mhos. Data in this table were obtained with rated heater voltage, plate and screen voltage of 28 volts, and grid bias of zero volts through 2 megohms.

Table II.—Typical Audio Amplifier Operation of Triodes at 28 Volts

Tube type	12AH7GT		12J5GT		12SN7GT		12SR7		9002	
Heater voltage.....	12.6		12.6		12.6		12.6		6.3	
Heater current, amp.....	0.15		0.15		0.30		0.15		0.15	
Transformer or Choke-fed A-f Amplifier										
	(Per section)				(Per section)					
	28		28		28		28		28	
Plate voltage.....	0	-1	0	-1	0	-1	0	-1	0	-1
Grid bias voltage.....	10	0	10	0	10	0	10	0	10	0
Grid resistor, megohms.....	1.25	1.0	1.2	1.0	1.2	1.0	1.0	0.75	0.50	0.50
Plate current, milliamperes.....	1200	1100	1625	1450	1625	1450	1150	1000	1150	1100
Transconductance, $\mu$ mho.....	14,000	15,000	12,250	14,500	12,250	14,500	15,750	18,000	17,750	21,000
Plate resistance, ohms.....	16.8	16.5	20	21	20	21	18	18	20.5	23
Amplification factor.....										
Resistance Coupled A-f Amplifier										
	(Per section)				(Per section)					
	28		28		28		28		28	
Plate supply voltage.....	0	0	0	0	0	0	0	0	0	0
Grid bias voltage.....	10	10	10	10	10	10	10	10	10	10
Grid resistor, megohms.....	0.05	0.10	0.05	0.10	0.05	0.10	0.05	0.10	0.05	0.10
Plate load resistor, megohms.....	0.10	0.22	1.0	0.10	0.22	1.0	0.10	0.22	1.0	0.10
Following grid resistor, megohms.....	0.10	0.22	1.0	0.10	0.22	1.0	0.10	0.22	1.0	0.10
Plate current, $\mu$ amp.....	275	150	75	225	150	75	225	150	75	175
Amplification.....	9.5	11	12	11	12	13	11	12	13	10
Max output (5% dist), rms volts.....	3	3.5	5	2.5	3	4	2.5	3	4	1.5

sects the grid current characteristic of the tube, as illustrated in Fig. 1. Thus tube 1 will assume a bias of about  $-0.5$  volt and tube 3 about  $-0.7$  volt with a 2-megohm grid resistor. If both of these tubes were operated with a common 2-megohm grid resistor, they would both have a bias of  $-0.7$  volt determined by the higher contact potential tube. Therefore, it may be desirable in many cases of 28-volt operation to use separate isolating resistors for each tube in the a-v-c system unless the effects of higher contact potential tubes in increasing bias on all tubes of the a-v-c system are acceptable. Of course, in some instances where a very high value of d-c diode load is employed, the diode contact potential may establish the bias for the tubes on the a-v-c line and the use of separate isolating resistors would not be important.

#### Minimizing Effects of $G_m$ Variations

Since the minimum bias for maximum gain for each tube of a lot is established by the grid leak, this method of bias is recommended instead of cathode bias for 28-volt operation. While cathode bias tends to smooth out tube variations, it can be shown that cathode bias will not minimize  $G_m$  variations except when the bias is so large that the average  $G_m$  is reduced more than can be tolerated in

28-volt operation. Grid leak bias is almost as effective for smoothing tube variations and is inherently available in most a-v-c systems. For this reason all tube ratings given here are made with a 2-megohm grid leak (with the exception of voltage amplifiers that employ a 10-megohm leak) at zero external bias. The grid signal employed is 0.10 volts rms.

This signal is standard on the  $G_m$  test line of the tube plant and is employed in the laboratory so that data are directly useful for translation into test limits. For the condition of zero grid circuit resistance at 28 volts B supply, the value of  $G_m$  observed varies negligibly as the

grid signal is reduced from 0.1 volt. For the condition of 2 megohms grid circuit resistance, some grid current rectification occurs and biases the grid back somewhat. Therefore higher measured values of  $G_m$  will be observed for grid signals less than 0.1 volt.

High  $G_m$  types show more change in  $G_m$  with signal level than medium  $G_m$  types. Low  $G_m$  tubes of a given type tend to show more change than high  $G_m$  tubes. For example, when the grid signal is reduced from 100 mv to 50 mv for type 12SH7, the highest tubes increase their observed  $G_m$  about 5 per cent, while the lowest tubes increase it about 9 per cent. For

Table III.—Typical Resistance-coupled Audio Amplifier Operation of Pentodes at 28 Volts

Tube type	12SF7		12SJ7		9001	
Heater voltage, volts.....	12.6		12.6		6.3	
Heater current, amp.....	0.15		0.15		0.15	
Plate supply voltage, volts.....	28		28		28	
Grid bias voltage, volts.....	0		0		0	
Grid resistor, megohms.....	10		10		10	
Screen grid resistor, megohms.....	0.33	0.82	0.22	0.47	0.068	0.27
Plate load resistor, megohms.....	0.10	0.22	0.10	0.22	0.10	0.22
Following grid res., megohms.....	0.22	1.0	0.22	1.0	0.22	1.0
Plate current, $\mu$ a.....	180	90	180	95	170	70
Screen grid current, $\mu$ a.....	60	25	60	35	90	35
Amplification.....	23	35	34	47	36	52
Max output (5% dist.) volts.....	3	4	4	4.5	3.5	4

type 12SG7, the respective differences are 3.5 per cent and 5 per cent, and for type 12SK7 they are 1.2 per cent and 1.5 per cent. Thus the following data indicate slightly lower values and less uniformity than might be obtained in circuit practice.

The average characteristics of several pentode types for 28-volt operation are shown in Table I. The mutual conductance curves for remote cutoff pentodes are given in Fig. 2, and for sharp cutoff pentodes in Fig. 3. These curves are for the condition of zero grid circuit resistance, and the high value of  $G_m$  shown for some types at bias values less than about  $-0.75$  volt will not be realized in r-f amplifier applications with 2-megohm grid leak bias (see Table I).

#### Transconductance Variations at 28-volt Design Center

It is of practical interest to note the percentage variation in transconductance which occurs as the B supply voltage is varied. Some aircraft radio equipments must operate over a range of 22 volts minimum to 32 volts maximum, or  $-21$  per cent and  $+14$  per cent from a design center of 28 volts. From a cathode temperature standpoint, tubes cannot be rated for supply voltage variations greater than  $\pm 10$  per cent for continuous operation. However, if equipments are to

be measured for performance at extremes of voltage variation, Figs. 4 and 5 show the order of variation in stage gains to be expected for each tube type as the B voltage is varied (heater voltage constant). The disadvantage of high  $G_m$  tubes such as types 6AG5, 12SG7, and 12SH7 is apparent.

Typical transconductance variations as a function of heater voltage (B voltage constant) are illustrated in Fig. 6. Both effects must be tolerated and allowed for in equipment performance test specifications. Figure 6 also demonstrates that contact potential bias is to be preferred over fixed or cathode bias if variation in transconductance over a range of heater voltage is an important consideration.

There is one point that should be emphasized in connection with 28-volt operation of standard receiving tubes. It is that a tube rated for a very high transconductance at higher voltages will not necessarily exhibit a higher transconductance at 28 volts than the medium transconductance tubes such as the types 12SJ7, 12SK7, etc. The curves of Figs. 4 and 5 demonstrate this fact. Furthermore, many of the very high transconductance types are rated with  $-1.0$  volt bias at maximum plate and screen voltage ratings, and no appreciable reduction in bias is obtained with grid

leak bias. For tubes like types 12SJ7 and 12SK7 which are rated with  $-3.0$  volts bias at maximum voltage ratings, it is possible to reduce the bias sufficiently for 28-volt operation that a value of transconductance is obtained equal to or better than that of the high  $G_m$  types. In addition, the medium  $G_m$  types exhibit tube-to-tube uniformity at 28 volts comparable to that obtained at maximum voltage ratings, while the high  $G_m$  types do not.

#### Selection of Tube Types

The comparative average transconductance and the typical range of variation between tubes of a given lot are illustrated in Fig. 7 for several types. This figure should assist the designer who is critical of product variations in the selection of types to be used. Figures 2 and 3 should be useful in the choice of types for a particular application. For most r-f and i-f applications with automatic volume control the 12SK7 appears to be a good selection both from the standpoint of average characteristics and minimum tube-to-tube variations. For v-h-f use, the 9003 should prove very satisfactory.

The types most satisfactory for resistance-coupled voltage amplifiers with 28-volt B supply are pentodes and low- $\mu$  triodes. High- $\mu$  triodes cannot be used

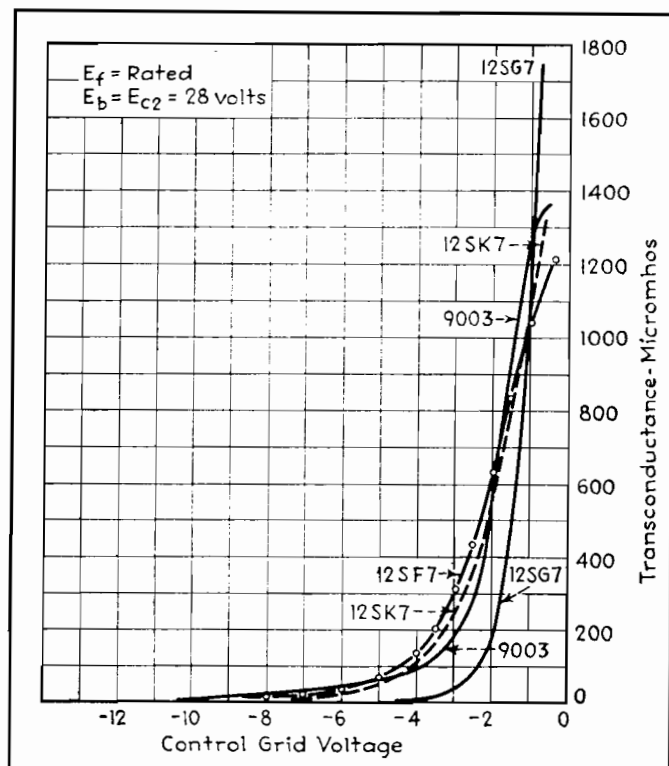


Fig. 2.—Transconductance vs. control-grid bias for remote cutoff pentodes.

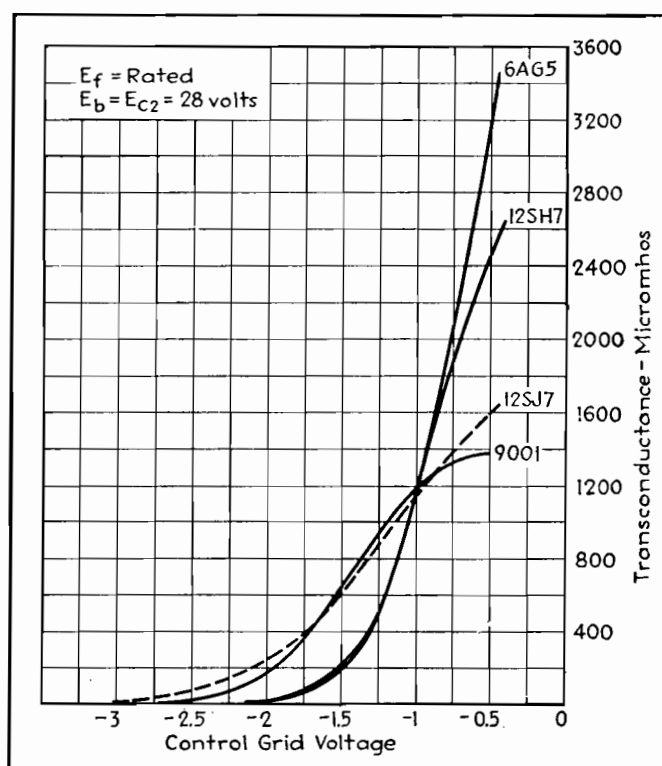


Fig. 3.—Transconductance vs. control-grid bias for sharp cutoff pentodes.



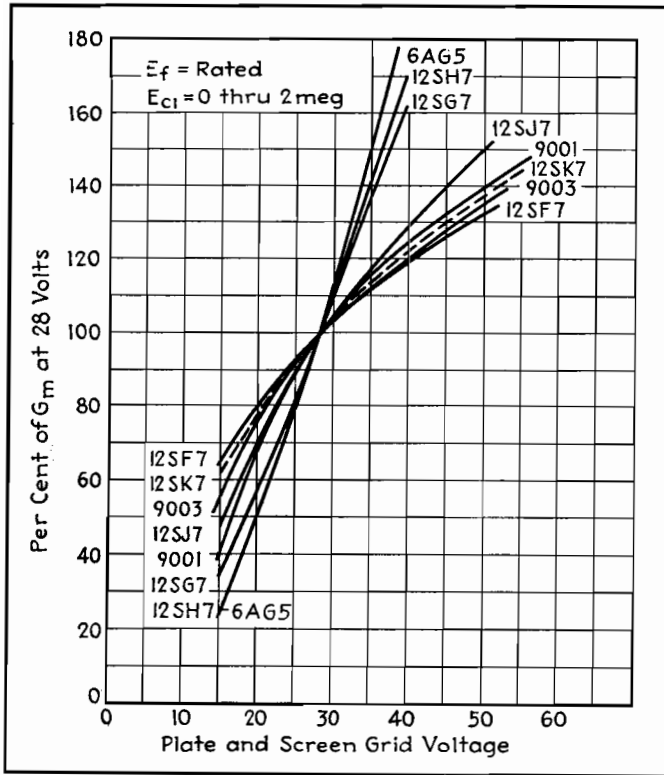


Fig. 4.—Percentage variation of transconductance of r-f pentodes with B supply voltage.

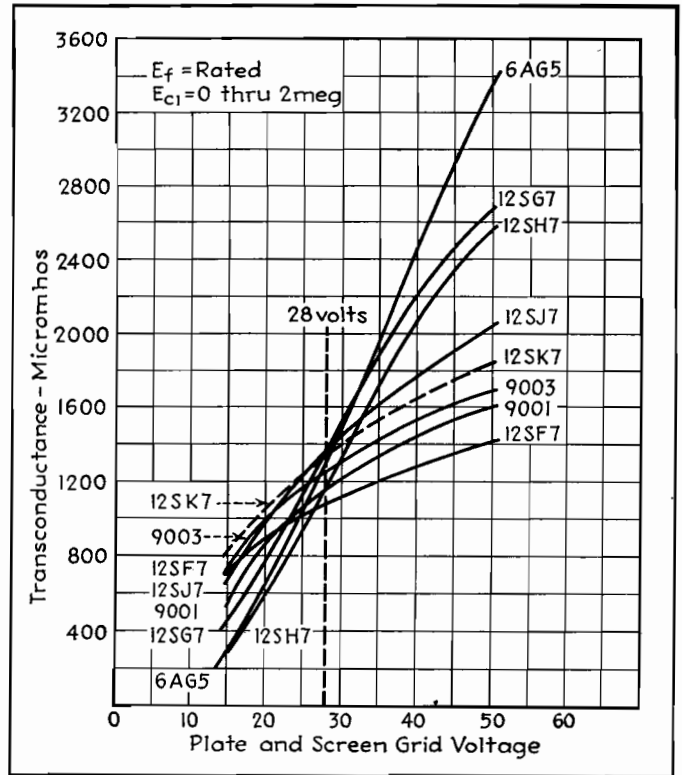


Fig. 5.—Transconductance of r-f pentodes vs. B supply voltage, for eight different tube types.

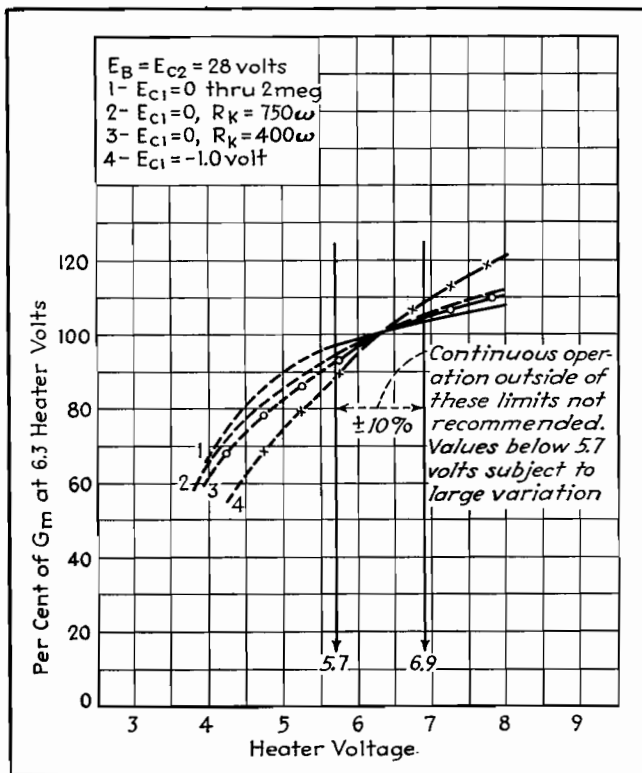


Fig. 6.—Percentage variation of transconductance of type 9003 pentode heater voltage.

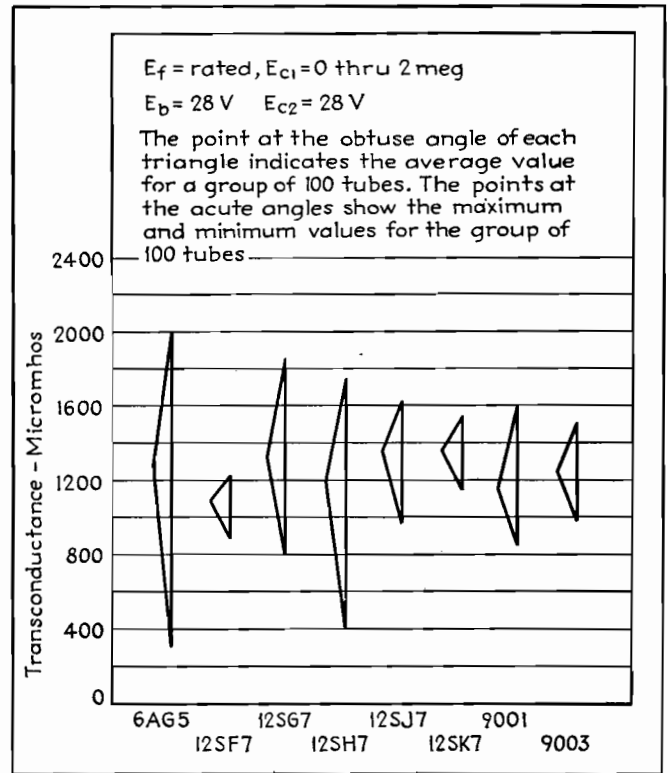


Fig. 7.—Transconductance variation of r-f pentodes with 28-volt B supply.



successfully because the bias developed in the grid resistor by the grid contact potential will cause the tubes to operate at or near plate current cutoff. The cutoff bias of a triode is approximately the ratio of plate voltage to  $\mu$ . For the type 12SQ7, which has a  $\mu$  of 100, the approximate cutoff bias would be  $28/100$ , or  $-0.28$  volts. Since the bias developed by contact potential in the grid resistor may vary from  $-0.2$  to  $-1.2$  volts, the impracticability of using high- $\mu$  triodes

is apparent. They will not only produce less amplification than a low- $\mu$  triode at 28-volt B supply, but will produce much less maximum voltage output, with large gain variations between tubes of a given type.

#### 28-volt Amplifier Performance

Data on resistance-coupled audio amplifier gain and maximum output voltage (for 5 per cent distortion) are given for triodes in Table II, for three different

values of plate load and following grid resistor. Information on transconductance, plate resistance, and  $\mu$ , which will be applicable in the case of transformer or choke-fed amplifier stages, is also given. Resistance-coupled amplifier data for several pentodes is presented in Table III. Any of the tubes shown in these tables should prove very satisfactory in 28-volt service, the selection depending on the gain requirements and use of auxiliary diode or triode sections.

## SECTION XXVI TUNED CIRCUITS

Bandwidth Factors for Cascade Tuned Circuits.....	Page 365
Frequency Response of Parallel Resonant Wave Traps...	367
Narrow Band-pass Filter Performance.....	369
Attenuation Charts for Band-pass and Band-rejection Filters.....	372
Band-pass Characteristics.....	375
Superheterodyne Oscillator Tracking Chart.....	377

# Bandwidth Factors for Cascade Tuned Circuits

By C. E. DEAN

**C**ALCULATIONS of bandwidth at a given deviation from resonance for cascade tuned circuits may be quickly and conveniently carried out by means of the table and equations given here. A pair of graphs, providing the same data as that of the tables, but which may be useful for interpolated values not contained in the table, is also included.

From the data, the engineer may determine the bandwidth for a specified attenuation if the resonant frequency, the  $Q$  of the circuits, and the type of tuned circuits are known. Likewise, the required circuit  $Q$  can be obtained when the degree of coupling, attenuation, and bandwidth are specified for a given resonant frequency.

In Fig. 1, representing a typical resonance curve,

- let  $f_0$  = resonant frequency of all circuits
- $f_w$  = over-all bandwidth in the same units as  $f_0$
- $E_0$  = voltage at resonance
- $E_w$  = voltage at the extremities of the desired bandwidth
- $A$  = attenuation, expressed as the voltage ratio,  $E_0/E_w$
- $a$  = attenuation expressed in db, i.e.,  $= 20 \log_{10} A$
- $n$  = total number of resonant circuits
- $W$  = bandwidth factor obtained from the table or graphs
- $Q$  = circuit quality, defined by

$$Q = \frac{\omega L}{R} = \frac{W f_0}{f_w}$$

The equations that are the basis for the table are

$$f_w = \frac{W f_0}{Q} \quad (1)$$

and for circuits of very loose coupling

$$W = (A^n - 1)^{1/2} \quad (2)$$

$$A = (1 + W^2)^{1/n} \quad (3)$$

For circuits of optimum coupling

$$W = \sqrt{2} (A^n - 1)^{1/4} \quad (4)$$

$$A = \left(1 + \frac{W^4}{4}\right)^{1/n} \quad (5)$$

The method of using the tables and the graphs in Figs. 2 and 3 can best be illustrated by considering a few typical examples.

### Examples

*Example 1.*—Given a tuned r-f amplifier of one stage with input and output circuits

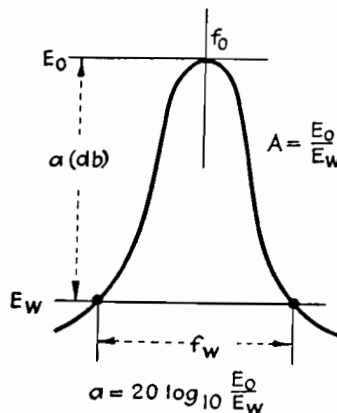


Fig. 1.—Typical resonance curve with voltages, frequencies, and attenuations indicated.

each with a  $Q$  of 100, determine the bandwidth 20 db down if the resonant frequency is 1,000 kc and circuits are loosely coupled.

From the table or graph for loosely coupled circuits and an attenuation  $a = 20$  db, we find that  $W = 3$ . Then, from Eq. (1) we have  $f_w = 3 \times 1,000/100 = 30$  kc.

*Example 2.*—Given an i-f amplifier with four tuned circuits in two pairs, all tuned to 455 kc and having a  $Q$  of 90, determine the bandwidth 40 db down for optimum coupling.

From the table or graph for optimum coupled circuits,  $W = 4.5$ , and from Eq. (1) we find the bandwidth to be  $f_w = 4.5 \times 455/90 = 22.7$  kc.

*Example 3.*—It is required that one pair of optimum-coupled i-f circuits have a bandwidth of 18 kc at 20 db down when the resonant frequency is 455 kc. What is the required  $Q$ ?

From Eq. (1),  $Q = W f_0 / f_w = 4.5 \times 455/18 = 113$ .

*Example 4.*—It is required that an amplifier have a bandwidth of 10 kc at 6

Circuits	$W_6$	$W_{60}$	$W_{60}/W_6$
5 separate, loosely coupled	0.57	3.9	6.8
6 separate, loosely coupled	0.51	3.0	5.9
4 in pairs, optimum-coupled	1.4	8.0	5.7
6 in pairs, optimum-coupled	1.2	4.5	3.8

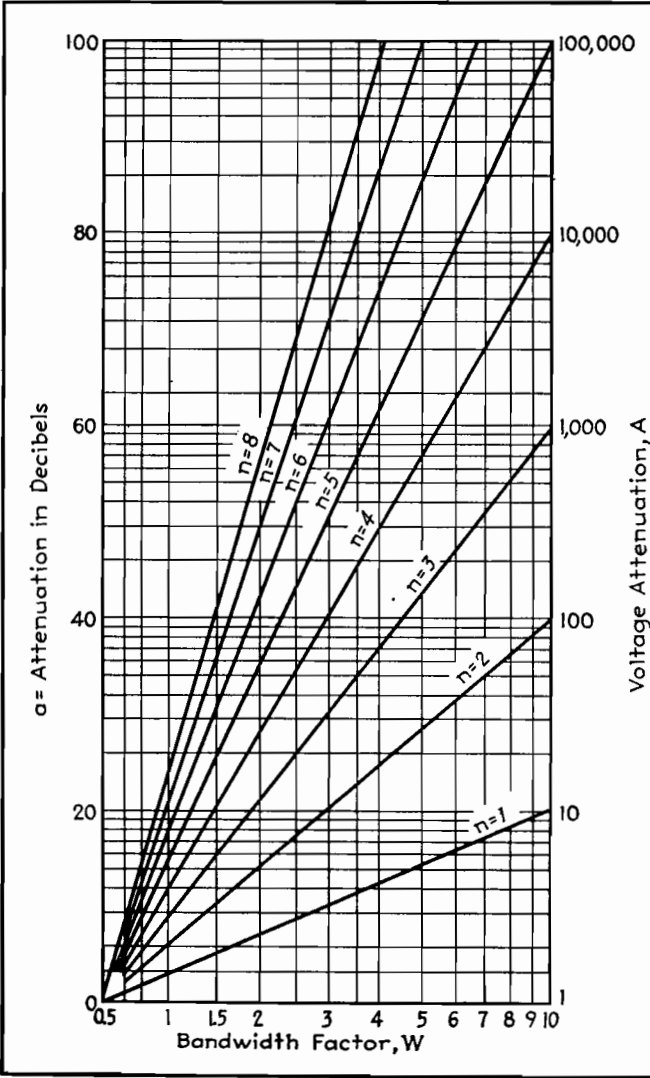


Fig. 2.—Attenuation and bandwidth factors for loosely coupled cascaded tuned circuits.

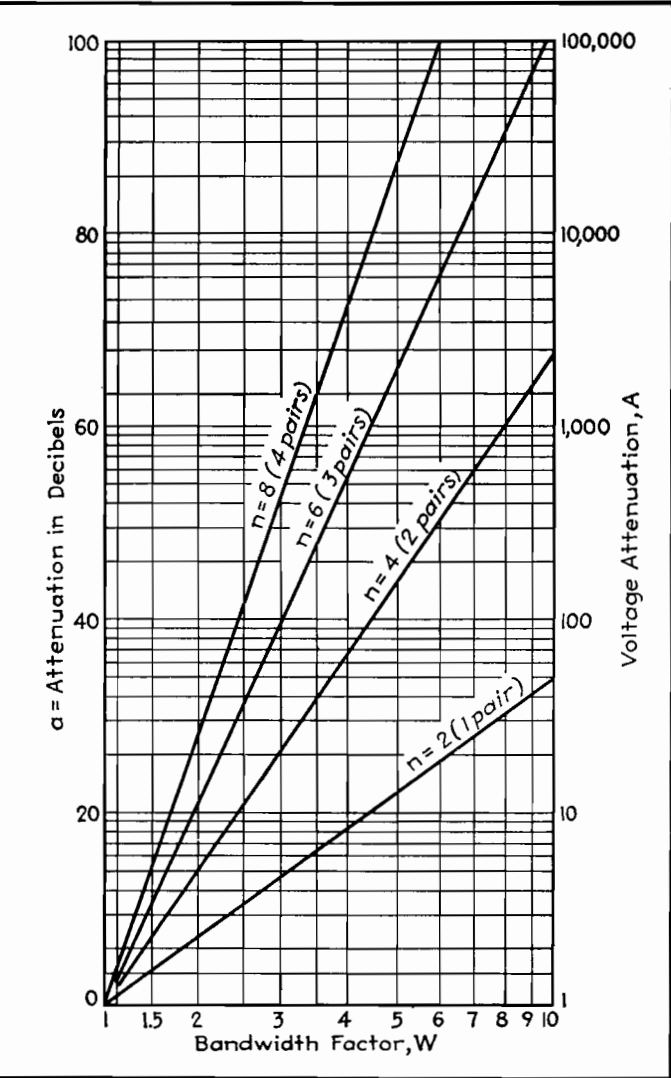


Fig. 3.—Attenuation and bandwidth factors for cascaded circuits, optimum coupled, in pairs.

Total number of circuits $n$	Bandwidth factor, $W$												
	$A = 1.12$ $a = 1$ db	$A = 1.26$ $a = 2$ db	$A = 1.41$ $a = 3$ db	$A = 2$ $a = 6$ db	$A = 4$ $a = 12$ db	$A = 7$ $a = 17$ db	$A = 10$ $a = 20$ db	$A = 20$ $a = 26$ db	$A = 40$ $a = 32$ db	$A = 70$ $a = 37$ db	$A = 100$ $a = 40$ db	$A = 1000$ $a = 60$ db	$A = 10^4$ $a = 80$ db

Circuits of Equal Individual Selectivity Very Loosely Coupled or Cascaded in Successive Stages of an Amplifier

1	0.51	0.77	1.00	1.73	3.9	6.9	10						
2	0.35	0.51	0.64	1.00	1.7	2.2	3	4.4	6.3	8.3	10		
3	0.28	0.41	0.51	0.77	1.2	1.7	1.9	2.5	3.3	4.0	4.5	10	
4	0.24	0.35	0.44	0.64	1.0	1.3	1.5	1.9	2.3	2.7	3.0	5.5	10
5	0.22	0.31	0.39	0.57	0.86	1.1	1.2	1.5	1.8	2.1	2.3	3.9	6.3
6	0.20	0.28	0.35	0.51	0.77	0.96	1.1	1.3	1.6	1.8	1.9	3.0	4.6
7	0.18	0.26	0.32	0.47	0.70	0.86	0.96	1.16	1.4	1.54	1.65	2.5	3.6
8	0.17	0.24	0.30	0.44	0.64	0.79	0.88	1.06	1.23	1.38	1.47	2.2	3.0

Circuits of Equal Individual Selectivity Optimum-coupled in Pairs

2 (1 pair)	1.01	1.24	1.4	1.9	2.8	3.7	4.5	6.2	9.0				
4 (2 pairs)	0.84	1.01	1.1	1.4	1.9	2.2	2.5	3.0	3.5	4.1	4.5	8.0	
6 (3 pairs)	0.75	0.90	1.0	1.2	1.6	1.8	2.0	2.3	2.6	2.8	3.1	4.5	6.6
8 (4 pairs)	0.70	0.84	0.93	1.13	1.4	1.6	1.7	1.9	2.2	2.3	2.5	3.5	4.5

db and an attenuation of at least 60 db for a bandwidth of 60 kc. Determine the circuit arrangement and required  $Q$  for operation at 455 kc.

In terms of bandwidth,  $(f_w)_{60} \leq 6(f_w)_6$ , or  $W_{60}f_0/Q \leq 6W_6f_0/Q$ , where the new

subscripts indicate the attenuation in decibels. It is seen that  $f_0$  and  $Q$  cancel, leaving the requirement  $W_{60}/W_6 \leq 6$ . From the table or graph we obtain the data as shown on page 365.

Six separate circuits would be required,

but four circuits in pairs are adequate and might be chosen.

For this problem, the necessary  $Q$  is determined by the required 10-kc bandwidth at 6 db from Eq. (1),  $Q = Wf_0/f_w = 1.4 \times 455/10 = 64$ .

## Frequency Response of Parallel Resonant Wave Traps

By MYRIL B. REED

THE two-branch parallel circuit in Fig. 1, commonly called a wave trap, is very widely used in both communication and power networks, for power factor and voltage control in power systems, and for tuning and filtering in communication systems.

The results of a complete mathematical study of the current-frequency response of the wave trap are given here in a readily usable form.

A mathematical analysis of the total current as a function of frequency may be carried out, for constant generator voltage  $E$ , by studying the admittance expression

$$Y = \sqrt{\left(\frac{R_L}{R_L^2 + 4\pi^2 f^2 L^2} + \frac{R_C}{R_C^2 + \frac{1}{4\pi^2 f^2 C^2}}\right)^2 + \left(\frac{2\pi f L}{R_L^2 + 4\pi^2 f^2 L^2} - \frac{2\pi f C}{R_C^2 + \frac{1}{4\pi^2 f^2 C^2}}\right)^2}$$

Also of interest is the phase angle between the generator voltage and the current flowing into the parallel circuit. This angle, given by

$$\theta = \tan^{-1} \frac{X_C Z_L^2 - X_L Z_C^2}{R_C Z_L^2 + R_L Z_C^2}$$

is positive if current leads voltage.

A graphical representation of the behavior of the wave trap is shown in Fig. 2. As shown, there are five general forms of the admittance or current-frequency relation. In addition to the well-known constant and minimum value relations (curves  $Y_5$  and  $Y_4$  and the corresponding  $\theta_5$  and  $\theta_4$  curves) there are the maximum value ( $Y_3$ ), decreasing ( $Y_2$ ), and increasing ( $Y_1$ ) admittance functions with the corresponding phase functions  $\theta_3$ ,  $\theta_2$ , and  $\theta_1$ . As may be

shown mathematically, these five pairs of curves constitute all possibilities. The relative frequencies at which the maximum or minimum values of  $Y$  and unity power factor resonance occur are shown on the curves and in the tabulation below.

It is ordinarily difficult to determine which one of the five admittance-frequency responses a particular wave trap will have. However, by means of the following system of inequalities, it is easy to determine such features of a wave trap as: whether it will resonate, whether resonant frequency, if it exists, is at a higher or lower frequency than that at maximum or minimum admittance, whether the admittance function has a maximum or minimum, and whether the angle  $\theta$  is lead or lag.

In the following table, let

$f_r$  = resonant frequency (current and voltage in phase)

$f_m$  = frequency at which minimum current occurs

$f_M$  = frequency at which maximum current occurs

$L$  = inductance in the inductive branch

$C$  = capacitance in the capacitive branch

$R_L$  = resistance of the inductive arm

$R_C$  = resistance of the capacitive arm

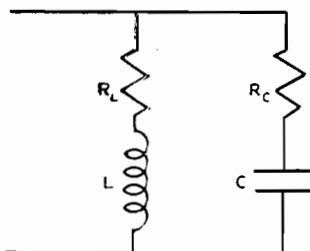


Fig. 1.—Circuit diagram of parallel resonant circuit with resistance in both arms, for which the accompanying analysis applies.

Then, depending on the relative magnitude of  $R_C R_L$  with respect to that of  $L/C$ , there are three possible cases to be analyzed, as shown in the table. By proper selection of the appropriate circuit conditions, the table may be used to determine the circuit response for any possible physical condition that may be encountered.

The use of this system of relations can best be illustrated by an example. Assume  $R_C = 2,000$  ohms,  $R_L = 100$  ohms,  $L = 1$  henry, and  $C = 10^{-5}$  farad. Then

$$R_C R_L = 2 \times 10^5 > 10^5 = \frac{L}{C}$$

$$R_C^2 = 4 \times 10^6 > \frac{L}{C}, \text{ and } R_L^2 = 10^4 < \frac{L}{C}$$

$$\left(R_L^2 + \frac{L}{C}\right)^2 = 121 \times 10^8 > 42 \times 10^8$$

$$= 2R_L^2(R_L^2 + R_C R_L)$$

From the third from the last row of case III the admittance equation is a decreasing function (see  $Y_2$  of Fig. 2) which will never be resonant, and, since  $R_C < R_L$ , from case III,  $\theta < 0$ , or the circuit power factor is lagging for all frequencies as shown in curve  $\theta_2$  of Fig. 2.

If  $R_C = 1$  ohm,  $R_L = 100$  ohms,  $C = 10^{-5}$  farad, and  $L = 1$  henry

$$R_C R_L < \frac{L}{C}; R_C^2 < \frac{L}{C}; \text{ and } R_L^2 < \frac{L}{C}$$

hence from case I the admittance has a minimum,  $f_m$  at 50.2 cycles, as shown by curve  $Y_4$  of Fig. 2. Also, since  $R_C < R_L$ , the minimum admittance is at higher frequency than resonance,  $f_r = 45.3$  cycles. Also, from case I,  $\theta > 0$  or leading for frequencies above resonance and  $\theta < 0$  or lagging for frequencies below resonance.

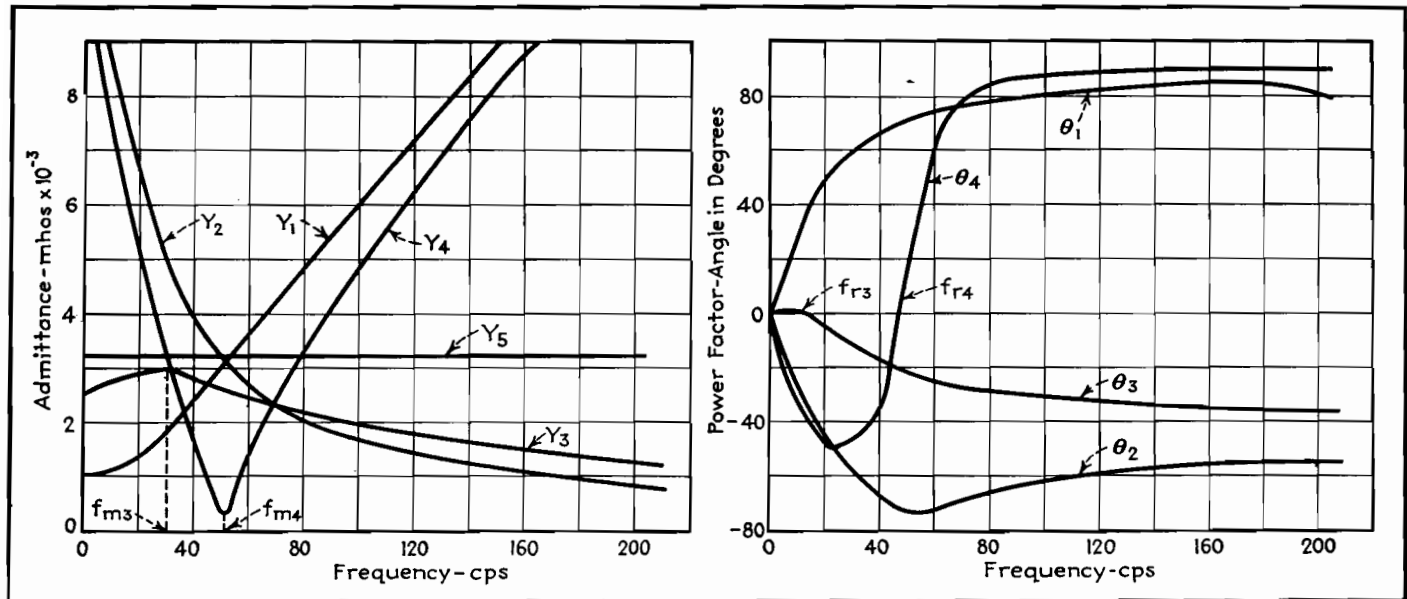


Fig. 2.—Admittance- and phase-angle curves used in example but typical of all possible operating conditions of LC circuit. For all frequencies,  $\theta_s = 0$ .

#### Admittance, Resonance, and Phase Relations for Parallel Circuit

Circuit element relations	Response-frequency relation	Resonance and phase relations
<p>Case I: <math>R_c R_L &lt; L/C</math></p> $\left. \begin{array}{l} R_L^2 < L/C \\ R_c^2 < L/C \end{array} \right\} \begin{array}{l} R_L > R_c; f_m > f_r \\ R_L = R_c; f_m = f_r = \frac{1}{2\pi \sqrt{LC}} \\ R_L < R_c; f_m < f_r \end{array}$ $\left. \begin{array}{l} R_L^2 = L/C; R_c^2 < L/C \\ R_L^2 < L/C; R_c^2 = L/C \\ R_L^2 < L/C \end{array} \right\} \begin{array}{l} (R_c^2 + L/C)^2 > 2R_c^2(R_c^2 + R_c R_L) \\ (R_c^2 + L/C)^2 \leq 2R_c^2(R_c^2 + R_c R_L) \\ (R_c^2 + L/C)^2 \geq 2R_c^2(R_c^2 + R_c R_L) \end{array}$ $\left. \begin{array}{l} R_L^2 > L/C \\ R_c^2 < L/C \end{array} \right\} \begin{array}{l} (R_L^2 + L/C)^2 \leq 2R_L^2(R_L^2 + R_c R_L) \\ (R_L^2 + L/C)^2 \geq 2R_L^2(R_L^2 + R_c R_L) \\ (R_L^2 + L/C)^2 > 2R_L^2(R_L^2 + R_c R_L) \end{array}$	<p>Curve has a minimum at <math>f_m</math></p> <p><math>Y</math> decreases; curve has no maximum or minimum</p> <p><math>Y</math> increases; curve has no maximum or minimum</p> <p>Curve has a minimum at <math>f_m</math></p>	<p>Circuit is resonant</p> <p><math>f &lt; f_r; \theta &lt; 0</math></p> <p><math>f = f_r; \theta = 0</math></p> <p><math>f &gt; f_r; \theta &gt; 0</math></p> <p>Circuit is not resonant</p> <p><math>R_L &gt; R_c; \theta &gt; 0</math></p> <p><math>R_L &lt; R_c; \theta &lt; 0</math></p>
<p>Case II: <math>R_c R_L = L/C</math></p> $\left. \begin{array}{l} R_L^2 < L/C \\ R_c^2 > L/C \\ R_L^2 > L/C \\ R_c^2 < L/C \end{array} \right\} \begin{array}{l} R_L^2 = L/C \\ R_c^2 = L/C \end{array}$	<p><math>Y</math> decreases; curve has no maximum or minimum</p> <p><math>Y</math> increases; curve has no maximum or minimum</p> <p><math>Y = \sqrt{C/L}</math>, and curve is constant for every frequency</p>	<p>Circuit is not resonant</p> <p><math>R_L &lt; R_c; \theta &lt; 0</math></p> <p><math>R_L &gt; R_c; \theta &gt; 0</math></p> <p>Circuit is resonant at every frequency</p> <p><math>\theta = 0</math> always</p>
<p>Case III: <math>R_c R_L &gt; L/C</math></p> $\left. \begin{array}{l} R_L^2 > L/C \\ R_c^2 > L/C \end{array} \right\} \begin{array}{l} R_L > R_c; f_m > f_r \\ R_L = R_c; f_m = f_r = \frac{1}{2\pi \sqrt{LC}} \\ R_L < R_c; f_m > f_r \end{array}$ $\left. \begin{array}{l} R_L^2 = L/C; R_c^2 > L/C \\ R_L^2 > L/C; R_c^2 = L/C \end{array} \right\} \begin{array}{l} (R_L^2 + L/C)^2 < 2R_L^2(R_L^2 + R_c R_L) \\ (R_L^2 + L/C)^2 \geq 2R_L^2(R_L^2 + R_c R_L) \\ (R_L^2 + L/C)^2 \leq 2R_L^2(R_L^2 + R_c R_L) \end{array}$ $\left. \begin{array}{l} R_L^2 > L/C \\ R_c^2 < L/C \end{array} \right\} \begin{array}{l} (R_c^2 + L/C)^2 < 2R_c^2(R_c^2 + R_c R_L) \\ (R_c^2 + L/C)^2 \geq 2R_c^2(R_c^2 + R_c R_L) \\ (R_c^2 + L/C)^2 > 2R_c^2(R_c^2 + R_c R_L) \end{array}$	<p>Curve has a maximum at <math>f_m</math></p> <p><math>Y</math> decreases; curve has no maximum or minimum</p> <p><math>Y</math> increases; curve has no maximum or minimum</p> <p>Curve has a maximum at <math>f_m</math></p>	<p>Circuit is resonant</p> <p><math>f = f_r; \theta = 0</math></p> <p><math>f &gt; f_r; \theta &lt; 0</math></p> <p><math>f &lt; f_r; \theta &gt; 0</math></p> <p>Circuit is not resonant</p> <p><math>R_L &gt; R_c; \theta &gt; 0</math></p> <p><math>R_L &lt; R_c; \theta &lt; 0</math></p>

# Narrow Band-pass Filter Performance

By HARRY HOLUBOW

Charts enabling one to design quickly a filter of desired characteristics. For given cutoff frequencies and coil  $Q$ , the minimum attenuation, attenuation at cutoff frequencies and the actual curve may be obtained. Time spent in trial design is reduced to a few minutes

FOR control or experimental purposes, filters of the type that pass only narrow bands are often used. These filters may be symmetrical (constant  $K$ ) or unsymmetrical in general type; the characteristics of the two types differ somewhat, and it is to the advantage of the engineer to be able to determine quickly which type he should employ. By means of certain simplifications in method, it is possible to use the nomograms given and derived here without too much loss in accuracy.

In addition to symmetrical band-pass filters with constant  $K$ , unsymmetrical filter types III<sub>1</sub> and III<sub>4</sub>\* shown in Fig. 1 are of considerable importance. Although the attenuation characteristics of these two types are not so steep as those of the constant- $K$  type, their inherently lower insertion loss at the mid-band frequency makes their use desirable for certain applications. This is especially true in the very narrow band-pass filters where the insertion losses at the mid-band frequency of the symmetrical filter become too large. The attenuation of

either of the two types of filters is not symmetrical, the attenuation being much greater at frequencies above the pass band with type III<sub>1</sub>, and below the pass band with type III<sub>4</sub>. Because of the higher impedance at frequencies away from the pass band, type III<sub>1</sub> is used in preference to type III<sub>4</sub>.

The performance of these filters may be predetermined either from the relation

$$\cosh \alpha = 1 + \frac{Z_1}{Z_2}$$

or graphically from  $Z_1/4Z_2$ . It is, however, felt that both of these methods are too lengthy, and much quicker methods can be used.

Considering filter type III<sub>1</sub>, and neglecting dissipation in the capacitors, the following relation may be obtained for the series arm impedance  $Z_1$  at any frequency  $F$

$$Z_1 = j2\pi FL_1 - j \frac{1}{2\pi FC_1} + \frac{2\pi FL_1}{Q}$$

where  $Q = 2\pi FL/r = 1/d$ ,  $d$  is the dissipation factor, and  $r$  is the resistance of the coil.

Inserting the expressions for  $L_1$  and  $C_1$  from Fig. 1, and simplifying, the following

is obtained

$$Z_1 = j \frac{2R(F^2 - F_1^2)}{F(F_2 - F_1)} + \frac{2RF}{Q(F_2 - F_1)}$$

Similarly, the shunt arm impedance is

$$Z_2 = -j \frac{(F_2 + F_1)R}{2F}$$

Then

$$\frac{Z_1}{2Z_2} = - \frac{2(F^2 - F_1^2)}{(F_2 - F_1)(F_2 + F_1)} + j \frac{2F^2}{Q(F_2 - F_1)(F_2 + F_1)}$$

or

$$\frac{Z_1}{2Z_2} = - \frac{2(F^2 - F_1^2)}{F_2^2 - F_1^2} + j \frac{2F^2}{Q(F_2^2 - F_1^2)} \quad (1)$$

## Filter Performance

The theoretical attenuation of the filter may now be determined from the relation

$$\cosh \alpha = 1 + \frac{Z_1}{2Z_2} = 1 - \frac{2(F^2 - F_1^2)}{F_2^2 - F_1^2}$$

The relation

$$\begin{aligned} \frac{Z_1}{2Z_2} &= - \frac{2(F^2 - F_1^2)}{F_2^2 - F_1^2} = -2 \frac{(F/F_1)^2 - 1}{(F_2/F_1)^2 - 1} \quad (2) \\ &= -2 \frac{(F/F_2)^2 - (F_1/F_2)^2}{1 - (F_1/F_2)^2} \\ &= -2 \left[ 1 + \frac{(F/F_2)^2 - 1}{1 - (F_1/F_2)^2} \right] \quad (3) \end{aligned}$$

\* SHEA, T. E., "Transmission Networks and Wave Filters," p. 316, D. Van Nostrand Company, Inc., New York, 1929.

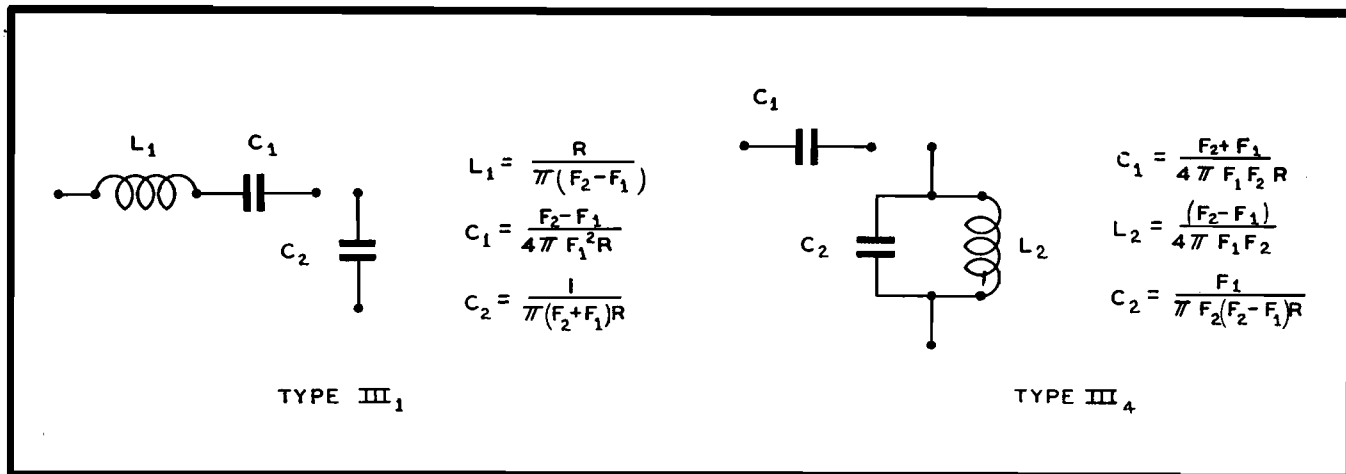


Fig. 1.—Types of unsymmetrical band-pass filters; type III<sub>1</sub> has greater attenuation above pass band; type III<sub>4</sub> has higher attenuation below pass band. Type III<sub>1</sub> has higher impedance at frequencies away from pass band.  $R$  equals terminating resistance;  $F_2$  equals upper cutoff and  $F_1$  equals lower cutoff frequency.

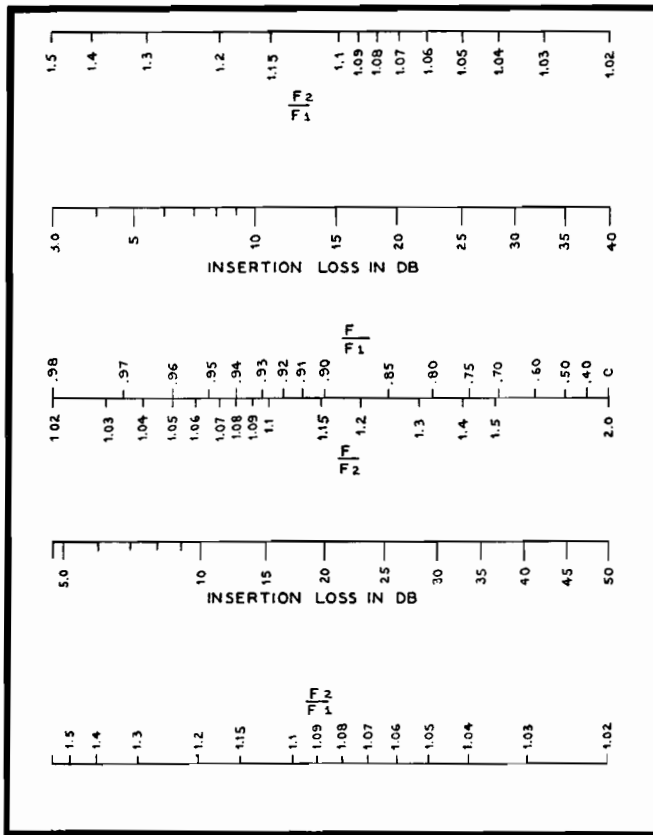


Fig. 2.—Alignment chart giving insertion loss in filters described.  $F_1$  and  $F_2$  are the cutoff frequencies;  $F$  is any frequency inside the pass band. Upper three scales are for region below  $F_1$ ; lower scales are for region above  $F_2$ .

The two alignment charts in Fig. 2 are constructed using relations (2) and (3) for  $Z_1/2Z_2$  in the formula

$$\cosh \alpha = 1 + \frac{Z_1}{2Z_2}$$

and may be used for a quick determination of the theoretical performance of type III<sub>1</sub> filters since Fig. 2 gives the attenuation at any frequency in the pass band and Fig. 3 gives the minimum insertion loss.

Unlike the constant- $K$  section, the lowest insertion loss for this type of filter does not occur exactly at mid-band, but takes place when

$$-2 \frac{F^2 - F_1^2}{F_2^2 - F_1^2} = -1$$

for in this case

$$\cosh \alpha = 1 + \frac{Z_1}{2Z_2} = j \frac{2F^2}{Q(F_2^2 - F_1^2)}$$

and  $\alpha$  is a minimum. Solving,

$$-2 \frac{F^2 - F_1^2}{F_2^2 - F_1^2} = -1$$

We have

$$F^2 = 0.5(F_2^2 + F_1^2)$$

or the point of minimum insertion loss

takes place for a frequency

$$F = 0.707 \sqrt{F_2^2 + F_1^2} \quad (4)$$

At the point of minimum attenuation

$$\cosh \alpha = \frac{F_2^2 + F_1^2}{Q(F_2^2 - F_1^2)} = \frac{(F_2/F_1)^2 + 1}{Q[(F_2/F_1)^2 - 1]} \quad (5)$$

The nomogram shown in Fig. 3 is based on this equation. At the cutoff point where  $F = F_1$ ,

$$\frac{Z_1}{2Z_2} = j \frac{2F_1^2}{Q(F_2^2 - F_1^2)}$$

$$\text{and } \cosh \alpha = 1 + j \frac{2F_1^2}{Q(F_2^2 - F_1^2)} \quad (6)$$

while at the cutoff point  $F = F_2$  the attenuation may be expressed as

$$\cosh \alpha = -1 + j \frac{2F_2^2}{Q(F_2^2 - F_1^2)} \quad (7)$$

Alignment charts in Fig. 4 may be used to find the insertion loss at the cutoff points.

Now the entire response curve of the filter may be found by using Fig. 2 to determine the attenuation within the pass band. The minimum attenuation and the attenuation at the cutoff frequencies can be found by using Figs. 3 and 4, respectively. The approximate performance is found by drawing a curve through these points.

### Characteristics of Filter Having Antiresonant Shunt Arm

Similarly, for the band-pass filter type III<sub>4</sub> shown in Fig. 1, it may be shown that

$$\frac{Z_1}{2Z_2} = \frac{-j2F_1^2[F^2 + jQ(F^2 - F_2^2)]}{(Q - j1)F^2(F_2^2 - F_1^2)}$$

After eliminating the imaginary in the denominator

$$\frac{Z_1}{2Z_2} = \frac{2F_1^2(F^2 - F_2^2)}{F^2(F_2^2 - F_1^2)} + \frac{2F_1^2}{Q^2(F_2^2 - F_1^2)} - j \frac{2F_1^2}{Q(F_2^2 - F_1^2)} + j \frac{2F_1^2(F^2 - F_2^2)}{QF^2(F_2^2 - F_1^2)}$$

The expression of  $Z_1/2Z_2$  is much more complicated than the one obtained for type III<sub>1</sub>. It may be simplified, however, by neglecting

$$\frac{2F_1^2}{Q^2(F_2^2 - F_1^2)}$$

The error introduced by this omission is slight even if  $Q$  is only 25 and  $F_2/F_1$  is 1.02. Then

$$\frac{Z_1}{2Z_2} = \frac{2F_1^2(F^2 - F_2^2)}{F^2(F_2^2 - F_1^2)} - j \frac{2F_1^2}{Q(F_2^2 - F_1^2)} + j \frac{2F_1^2(F^2 - F_2^2)}{QF^2(F_2^2 - F_1^2)} \quad (8)$$

While the equation for  $Z_1/2Z_2$  still seems somewhat complicated, it can be handled quite easily. In the method just outlined, the imaginary part of the expression  $Z_1/2Z_2$  is used mainly to calculate the performance at  $F_1$  and  $F_2$ , and the minimum insertion loss from Eq. (8). When  $F = F_1$ ,

$$\frac{Z_1}{2Z_2} = -2 - j \frac{2F_1^2}{Q(F_2^2 - F_1^2)} \quad (9)$$

and when  $F = F_2$ ,

$$\frac{Z_1}{2Z_2} = -j \frac{2F_2^2}{Q(F_2^2 - F_1^2)} \quad (10)$$

Equations (9) and (10) are the same as (6) and (7) except that the insertion loss at  $F_1$  for type III<sub>4</sub> is the same as at  $F_2$  for type III<sub>1</sub> and at  $F_2$  the same as  $F_1$ . The alignment chart in Fig. 4 may then be used for both types except that the values for  $F_2$  and  $F_1$  are interchanged when applying to a type III<sub>4</sub> filter.

In the same manner, the real part of Eq. (8),

$$\frac{2F_1^2[1 - (F_2/F)^2]}{F_2^2 - F_1^2}$$

compares with the real part of Eq. (1) which can be written as

$$\frac{2F_1^2[1 - (F/F_1)^2]}{F_2^2 - F_1^2}$$

From these relations it can be seen that the theoretical performance of type III<sub>4</sub>



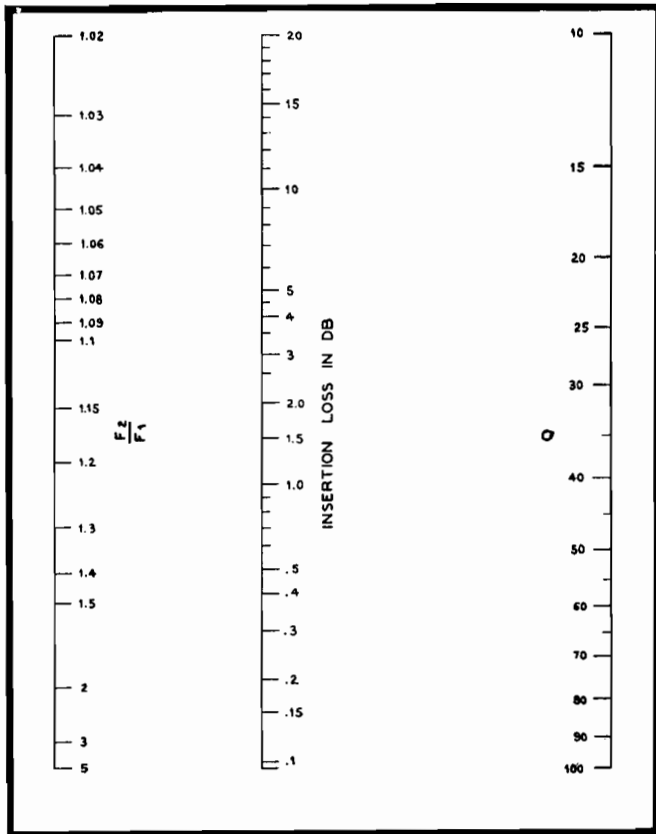


Fig. 3.—Charts giving minimum loss in using an unsymmetrical filter of the types described. This occurs at the frequency which is equal to  $0.707 \sqrt{F_2^2 + F_1^2}$ .

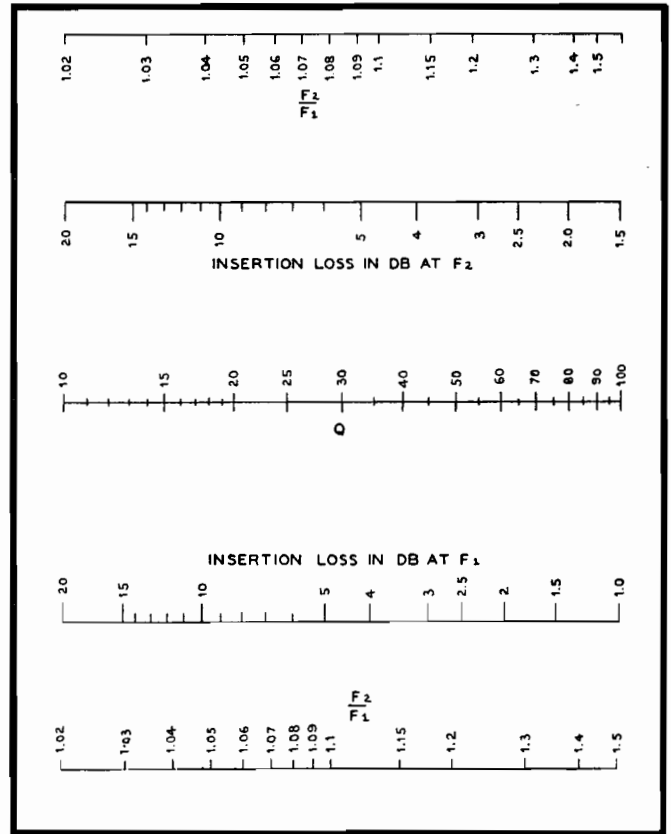


Fig. 4.—Insertion loss at the cutoff frequencies in unsymmetrical type III<sub>1</sub> band-pass filters. This chart may be used for a type III<sub>4</sub> filter if the values of  $F_1$  and  $F_2$  are interchanged.

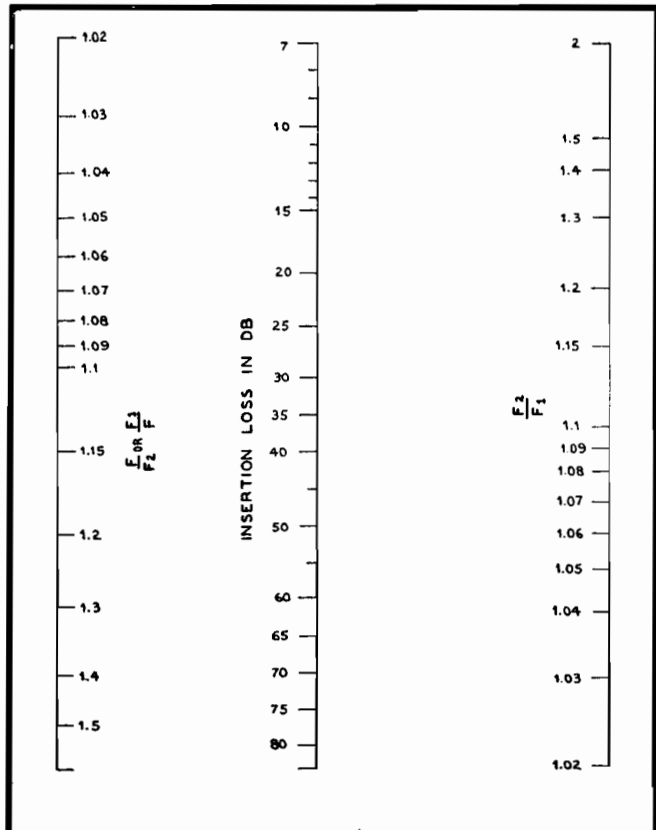


Fig. 5.—Alignment chart of insertion loss in symmetrical constant-k band-pass filters.

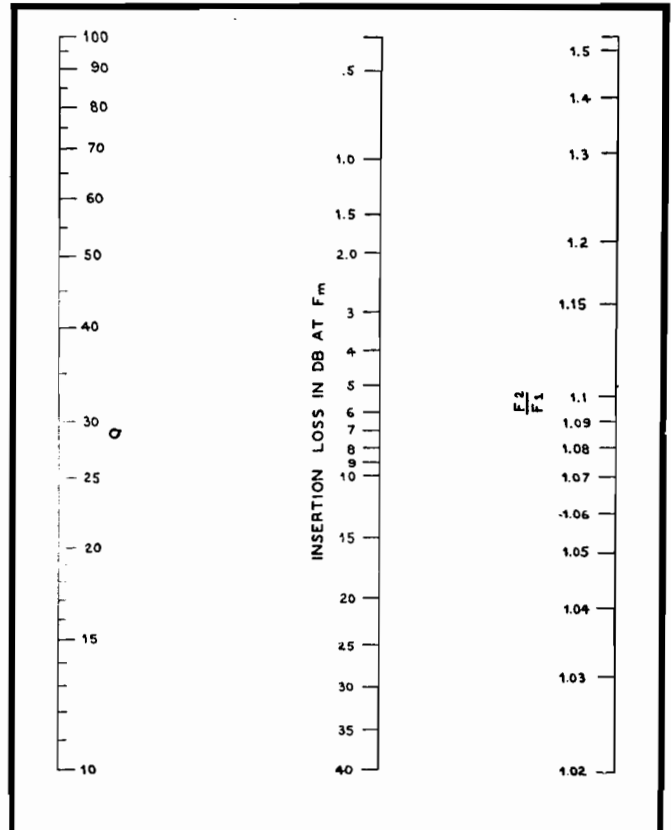


Fig. 6.—Insertion loss at the midband in constant-k band-pass filter. Reflection losses do not appreciably affect these values.

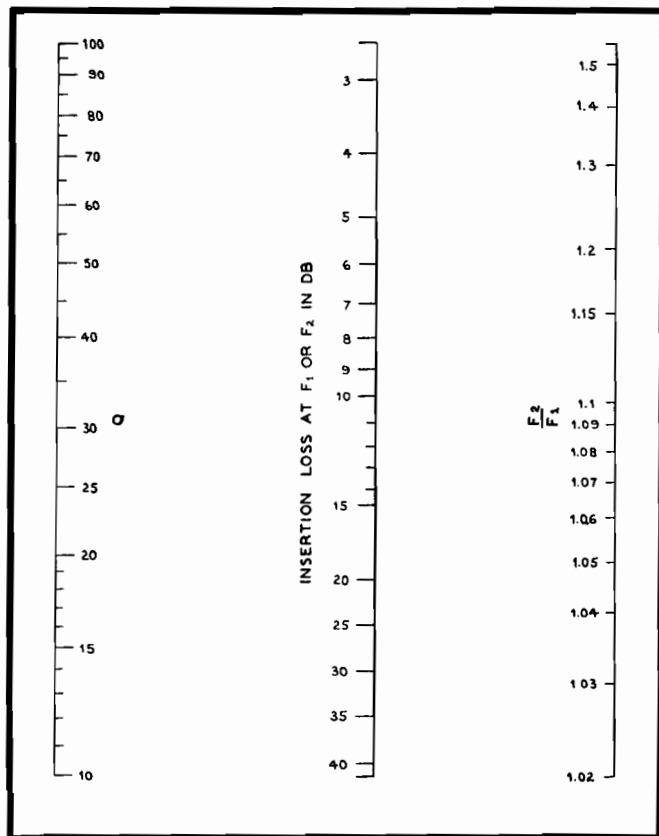


Fig. 7.—Insertion loss of cutoff points in constant- $k$  filter. Actual attenuation will be greater due to reflection losses.

filters may be obtained from the alignment charts in Fig. 2 if for values of  $F_2/F$  the values of  $F/F_1$  are used; similarly,  $F/F_2$  of type III<sub>1</sub> are used to calculate  $F/F_1$  of type III<sub>4</sub>.

The point of minimum insertion loss in this type of filter occurs where

$$F = \frac{\sqrt{2F_1F_2}}{\sqrt{F_2^2 + F_1^2}} \quad (11)$$

Substituting this value for  $F$  in Eq. (10), the expression at minimum insertion loss is

$$\cosh \alpha = \frac{F_2^2 + F_1^2}{Q(F_2^2 - F_1^2)}$$

This is similar to Eq. (5), and the nomogram in Fig. 3 may be used.

Thus we see that the performance of both filter types may be obtained from the same set of alignment charts.

#### Application to Constant- $k$ Filters

The charts in Figs. 5, 6, and 7 are obtained in the same manner for use with the constant- $k$  type filter, and are especially applicable in calculating the performance of narrow-band filters. None of these charts takes into account reflection losses. The actual attenuation in the constant- $k$  type and type III<sub>1</sub> will be greater than obtained at points away from the mid-band. The performance near the mid-band will not depart greatly from

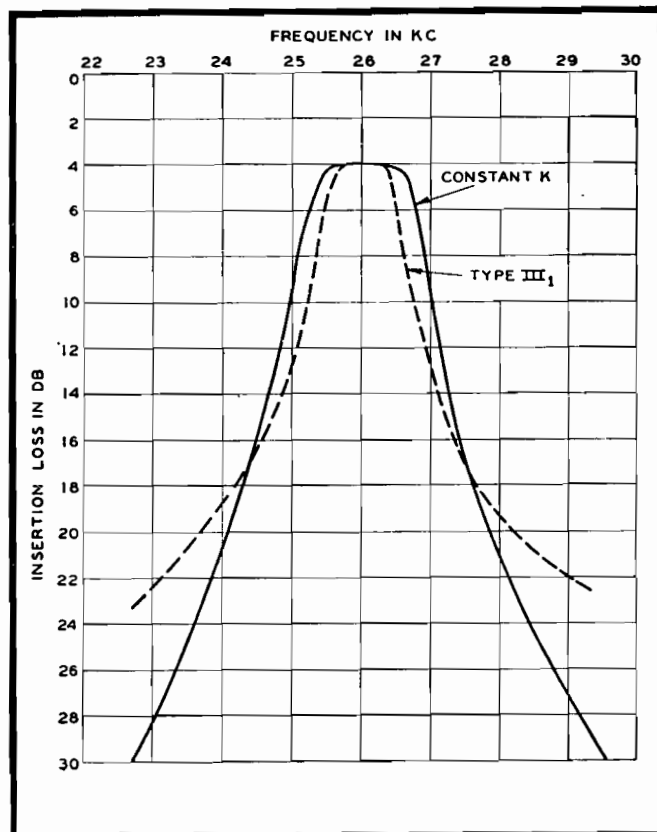


Fig. 8.—Calculated performance of constant- $k$  versus type III<sub>1</sub> filters when coil  $Q$  is assumed equal to 50.

the values obtained by means of these nomograms.

To compare the performance of the two types of filters, calculated performances of type III<sub>1</sub> and of the constant- $k$  type are shown in Fig. 8.

The  $Q$  of the coils were assumed to be 50, and the ratio  $F_2/F_1$  for the two types was selected so as to give the same mid-band insertion loss. The ratios are 1.09 for the constant- $k$  type and 1.04 for the unsymmetrical type. From the curve we can see that if the performance in the vicinity of the mid-band is more important the unsymmetrical filter may be used. The saving in space, weight, and cost will be approximately 20 per cent.

## Attenuation Charts for Band-pass and Band-rejection Filters

By H. HOLUBOW

THE following discussion represents simplifications in methods of calculating the performance of band-pass and band-elimination filters, especially when it is necessary to allow for the dissipation in

the coils. The usual notation holds, *i.e.*,  $F_1$  and  $F_2$  are the critical frequencies (cutoff),  $F_m$  is the median frequency in the critical band, and  $R$  is the terminating resistance.

#### Band-pass Filters

Although there are a number of networks that may be used as band-pass filters, the constant- $k$  type, shown in

Fig. 1, is most commonly employed. In this structure, the product of the series and shunt element impedances  $Z_1$  and  $Z_2$ , respectively, is a constant equal to  $K^2$ . The expected performance of the band-pass filter is usually obtained graphically from the values of  $Z_1/4Z_2$ . These values are usually given in texts and handbooks in terms of the cutoff frequencies. The calculation of  $Z_1/4Z_2$  becomes quite cumbersome when dissipation must be taken into account, but the simplifications that follow are useful in that they do not entail much sacrifice in accuracy.

The impedance of the series arm  $Z_1$  at any frequency  $F_{11}$  may be expressed as follows by substituting for  $L_1$  and  $C_1$  the values given in Fig. 1:

$$Z_1 = j2\pi F_{11}L_1 - j \frac{1}{2\pi F_{11}C_1} = j \left[ \frac{2\pi R F_{11}}{\pi(F_2 - F_1)} - \frac{4\pi F_2 F_1 R}{2\pi F_{11}(F_2 - F_1)} \right]$$

Simplifying,

$$Z_1 = j2R \frac{(F_{11}^2 - F_2 F_1)}{F_{11}(F_2 - F_1)}$$

The impedance of the shunt arm

$$Z_2 = \frac{1}{\frac{1}{j2\pi F_{11}L_2} + j2\pi F_{11}C_2} = j \frac{2\pi F_{11}L_2}{1 - 4\pi^2 F_{11}^2 L_2 C_2}$$

Substituting for  $L_2$  and  $C_2$  their values from Fig. 1,

$$Z_2 = j \frac{R F_{11}(F_2 - F_1)}{2(F_2 F_1 - F_{11}^2)}$$

whence

$$\frac{Z_1}{2Z_2} = \frac{2(F_{11}^2 - F_2 F_1)(F_2 F_1 - F_{11}^2)}{F_{11}^2(F_2 - F_1)^2} \quad (1)$$

The attenuation of the band-pass filter at any point may now be calculated from the relation

$$\cosh \alpha = 1 + \frac{Z_1}{2Z_2}$$

or graphically from

$$\frac{Z_1}{4Z_2}$$

This equation, however, is cumbersome to use, but the following simplification can be made:

For any point on the filter curve corresponding to  $F_{11}$  there is another point  $F_{22}$  such that  $F_{11}F_{22} = F_1F_2 = F_m^2$ . Substituting  $F_{11}F_{22}$  for  $F_1F_2$  in Eq. (1), the following is obtained:

$$\frac{Z_1}{2Z_2} = \frac{2(F_{11}^2 - F_{11}F_{22})(F_{22}F_{11} - F_{11}^2)}{F_{11}^2(F_2 - F_1)^2} = \frac{2(F_{11} - F_{22})(F_{22} - F_{11})}{(F_2 - F_1)^2} = -2 \frac{(F_2 - F_{11})^2}{(F_2 - F_1)^2} \quad (2)$$

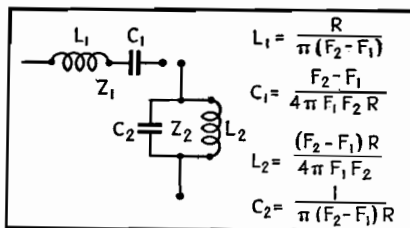


Fig. 1.—Constant- $k$  band-pass filter circuit.

This may now be written as

$$\frac{Z_1}{2Z_2} = -2 \left( \frac{F_{\Delta 1}}{F_{\Delta}} \right)^2 \quad (3)$$

where  $F_{\Delta 1}$  is the band spread at the points of determination ( $F_{22}, F_{11}$ ), while  $F_{\Delta}$  is the band spread of the filter between points  $F_2 - F_1$ . A curve (Fig. 2) may now be made that will give the theoretical determination of the attenuation at any point of any constant- $k$  band-pass filter.

#### Attenuation in Filters with Dissipation

The attenuation of a band-pass filter obtained by means of the curve in Fig. 2 assumes no dissipation either in the reactors or capacitors. The dissipation in capacitors is usually small and can be neglected; the dissipation present in the coils, however, is considerable, especially at the audio frequencies. In the ideal filter there is no attenuation within the pass band, while in an actual filter the attenuation within the pass band may be considerable, especially in the narrow band-pass filters. However, if the attenuations at the mid-frequency  $F_m = F_1F_2$ , and at  $F_1$  and  $F_2$  are known, the response of the filter may easily be determined.

In the constant- $k$  band-pass filter at the frequency  $F_m$ ,  $X_{L1} = X_{C1}$ , and  $Z_1 = 2\pi F_m L_1 d$ , or  $Z_1 = (2\pi F_m L_1)/Q$ , where  $d$  is  $r/(2\pi FL)$  or  $Q = (2\pi FL)/r$  ( $r$  is the equivalent series resistance of the reactor and  $L_1$  is the series arm inductance). In terms of the cutoff frequencies (Fig. 1),

$$Z_1 = \frac{2\pi F_m R}{Q\pi(F_2 - F_1)} = \frac{2F_m R}{Q(F_2 - F_1)}$$

In the shunt arm,  $X_{L2} = X_{C2}$ , and assuming dissipation present in the inductances only,

$$Z_2 = \frac{X_{L2}X_{C2} - jrX_{C2}}{r + j(X_{L2} - X_{C2})} = \frac{X_{L2}X_{C2}}{r} - jX_{C2} \quad \text{or} \quad Z_2 = QX_{L2} - jX_{L2}$$

Inasmuch as the  $Q$  of a filter choke is seldom smaller than 20, the reactive component  $jX_2$  may be neglected and, from Fig. 1,

$$Z_2 = QX_{L2} = 2\pi Q \frac{F_m(F_2 - F_1)R}{4\pi F_1 F_2} = \frac{Q(F_2 - F_1)R}{2F_m}$$

and  
and  
at

$$\frac{Z_1}{Z_2} = \frac{4F_m^2}{Q^2(F_2 - F_1)^2}$$

$$\frac{Z_1}{2Z_2} = \frac{2}{Q^2} \left( \frac{F_m}{F_2 - F_1} \right)^2$$

$$F_{11} = F_m$$

#### Attenuation at $f_m$

The attenuation at the mid-band frequency may be found from tables of hyperbolic functions where

$$\cosh \alpha = 1 + \frac{Z_1}{2Z_2}$$

when  $\alpha$  is the attenuation in nepers. However, inasmuch as  $\alpha$  at the mid-band frequency is less than 1 neper, the following approximation may be used:

$$\cosh \alpha = 1 + \frac{\alpha^2}{2!} + \frac{\alpha^4}{4!}$$

Using the first two terms

$$1 + \frac{\alpha^2}{2!} = 1 + \frac{Z_1}{2Z_2}$$

or

$$\alpha = \sqrt{\frac{Z_1}{2Z_2}} = \frac{2}{Q} \times \frac{F_m}{F_2 - F_1} \text{ nepers} \quad (4)$$

$$\alpha = \frac{17.3}{Q} \times \frac{F_m}{F_2 - F_1} \text{ db} \quad (5)$$

The error from using this expression is less than 4 per cent for  $\alpha$  less than 8 db.

#### Attenuation of a Cutoff Frequency $F_1$

In the same manner it may be shown that at  $F_1$

$$\frac{Z_1}{2Z_2} = 2 \frac{\left( d \frac{F_1}{F_m} + j \frac{F_2 - F_1}{F_m} \right)^2}{(1 - jd) \left( \frac{F_2 - F_1}{F_m} \right)^2}$$

where  $d$  is the dissipation factor of the filter components. Performing the indicated operations

$$\frac{Z_1}{2Z_2} = 2 \times \frac{d^2 \left( \frac{F_1}{F_m} \right)^2 + j2d \frac{F_1}{F_m} \left( \frac{F_2 - F_1}{F_m} \right) - \left( \frac{F_2 - F_1}{F_m} \right)^2}{\left( \frac{F_2 - F_1}{F_m} \right)^2 - jd \left( \frac{F_2 - F_1}{F_m} \right)^2}$$

Inasmuch as  $d$  is usually small, all terms containing  $d^2$  or  $d^3$  can be neglected.

$$\frac{Z_1}{2Z_2} = 2 \left( -1 + j2d \frac{F_1}{F_2 - F_1} + jd \right)$$

$$= -2 + j2d \left( \frac{F_2 + F_1}{F_2 - F_1} \right)$$

$$= -2 + j \frac{2}{Q} \left( \frac{F_2 + F_1}{F_2 - F_1} \right)$$

The attenuation at  $F_1$  or  $F_2$  may be obtained from the curve in Fig. 3 where the abscissas are in terms of

$$\frac{F_2 + F_1}{Q(F_2 - F_1)} \quad \text{or} \quad d \frac{F_2 + F_1}{F_2 - F_1}$$

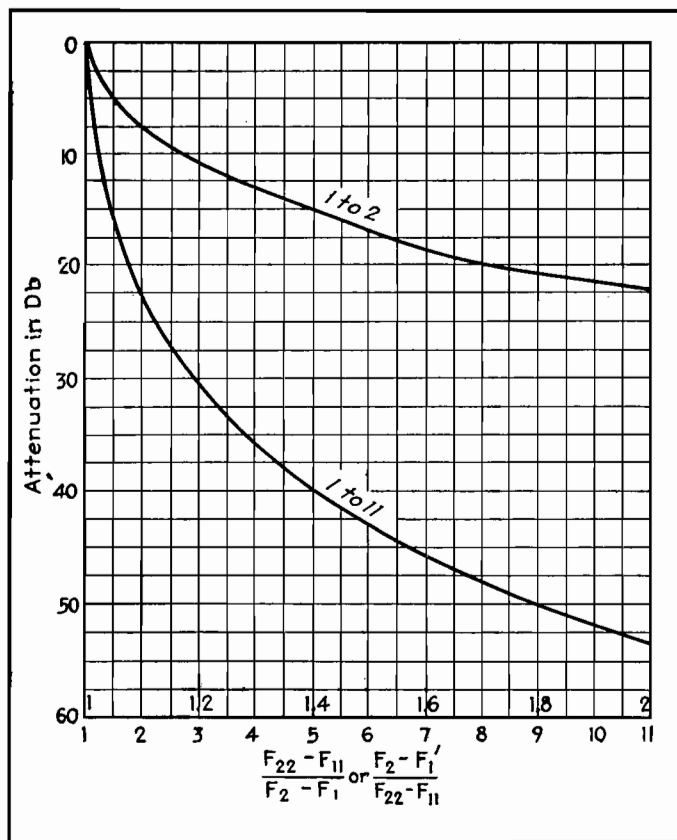


Fig. 2.—Curve showing attenuation of band-pass filter without taking into account resistance in coils or capacitors.

To illustrate the procedure in the design, let us assume that it is required to obtain the expected performance curve for a band-pass filter when  $F_1 = 3,000$  cycles,  $F_2 = 4,000$  cycles, and the dissipation factor of the coils is  $0.04 (Q = 25)$ , and in which  $F_m = \sqrt{4,000 \times 3,000} = 3,450$ . The theoretical performance of the filter may be calculated as shown.

$F_{11}$	$F_{22}$	$\frac{F_{\Delta 1}}{F_{\Delta}}$	Attenuation, db
2,800	4,300	1.5	17
2,600	4,620	2.02	22.5
2,400	5,000	2.6	28.0
2,000	6,000	4.0	36.0
1,500	8,000	6.5	44.5
1,200	10,000	8.8	50

In this table either  $F_{11}$  or  $F_{22}$  is assumed and the other frequency is calculated from

$$\frac{F_1 F_2}{F_{11}} \quad \text{or from} \quad \frac{F_1 F_2}{F_{22}}$$

and

$$\frac{F_{\Delta 1}}{F_{\Delta}} = \frac{F_{22} - F_{11}}{F_2 - F_1}$$

The attenuation in decibels is obtained from Fig. 2. The insertion loss at  $F_m$  is obtained from Eq. (5) and is

$$\frac{17.3}{25} \times \frac{3,450}{1,000} = 2.4 \text{ db}$$

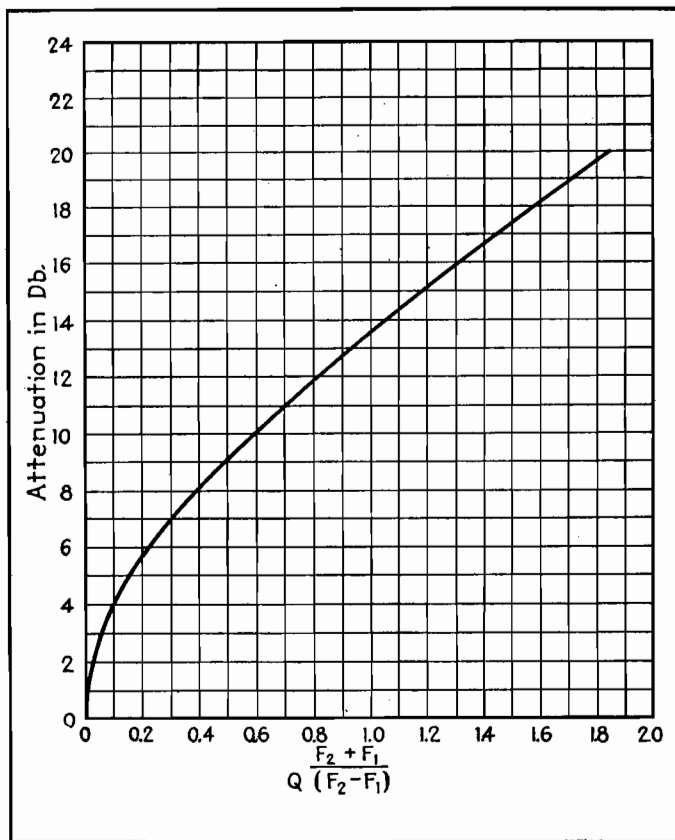


Fig. 3.—Attenuation of band-pass filter at the critical frequencies  $F_1$  and  $F_2$  when the coils have dissipation.

The insertion loss at  $F_2$  and  $F_1$  is 7.6 db (obtained from Fig. 3). The expected performance curve of the filter is as shown in the heavy line on Fig. 4.

#### Band-rejection Filters

The band-rejection filter does not find as wide an application as the band-pass filter. Nevertheless, it is desirable to be

able to predetermine the performance of this type of filter. There is only one type constant- $k$  structure that is commonly used, as shown in Fig. 5.

Using the same method of analysis as in the case of the band-pass filter, it is found that

$$\frac{Z_1}{2Z_2} = -2 \frac{F_2 - F_1}{F_{22} - F_{11}} = -2 \frac{F_{\Delta}}{F_{\Delta 1}}$$

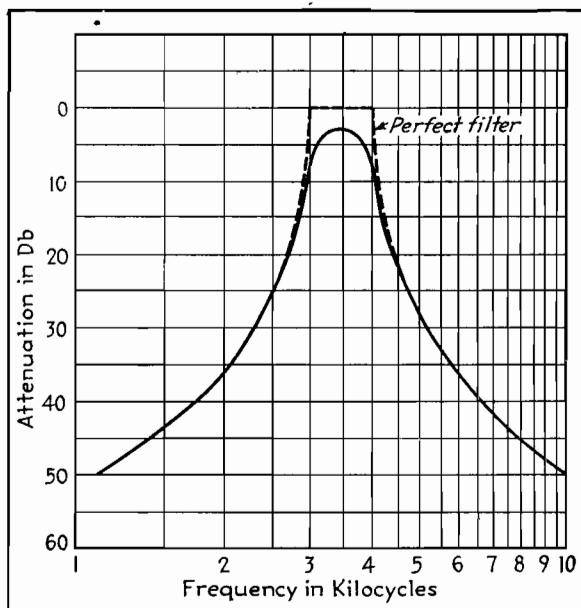


Fig. 4.—Performance curve of band-pass filter as calculated by the methods outlined in this article.

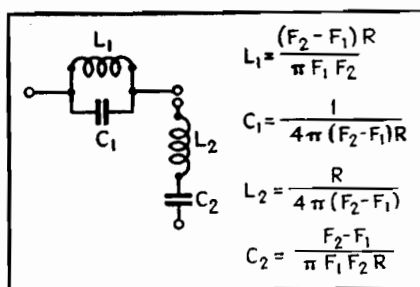


Fig. 5.—Band-elimination filter of the constant K type in which the series and shunt reactances are as shown in terms of the terminal resistance R.

This relation is similar to that obtained for the band-pass filter except that  $F_2 - F_1$  and  $F_{22} - F_{11}$  are interchanged. The theoretical performance of a band-rejection filter may be then obtained from the curve in Fig. 2, using  $F_{\Delta}/F_{\Delta 1}$  for the abscissas.

At mid-band frequency  $2\pi FL = 1/(2\pi FC)$  for both the series and the

shunt arm. At  $F_m$ ,

$$Z_1 = 2\pi F_m L_1 Q = \frac{2F_m(F_2 - F_1)RQ}{F_1 F_2}$$

$$Z_2 = \frac{2\pi F_m L_2}{Q} = \frac{F_m R}{2(F_2 - F_1)Q}$$

$$\frac{Z_1}{2Z_2} = 2 \frac{(F_2 - F_1)^2 Q^2}{F_1 F_2} = 2 \left( \frac{F_2 - F_1}{F_m} \right)^2 Q^2$$

Attenuation  $\alpha$  at mid band may be obtained from the relationship

$$\cosh \alpha = 1 + \frac{Z_1}{2Z_2}$$

where  $\cosh \alpha = \frac{e^\alpha}{2} + \frac{e^{-\alpha}}{2}$

Inasmuch as the attenuation is usually large,

$$\frac{e^\alpha}{2} = \frac{Z_1}{2Z_2} = 2 \frac{(F_2 - F_1)^2 Q^2}{F_m^2}$$

or  $e^\alpha = \left[ 2 \frac{F_2 - F_1}{F_m} Q \right]^2$

The attenuation

$$\alpha = 2 \log_e 2 \frac{F_2 - F_1}{F_m} Q \text{ nepers}$$

or  $\alpha = 40 \log_{10} 2 \frac{F_2 - F_1}{F_m} Q \text{ db}$

At the cutoff frequencies  $F_2$  and  $F_1$

$$\frac{Z_1}{2Z_2} = -2 \frac{\frac{F_2 - F_1}{F_m} - jd \left( \frac{F_2 - F_1}{F_m} \right)^2}{\left( \frac{F_2 - F_1}{F_m} \right)^2 - j2d \frac{F_1}{F_m} \left( \frac{F_2 - F_1}{F_m} \right)}$$

Simplifying and discarding terms containing  $d^2$  and  $d^3$ , we obtain

$$\frac{Z_1}{2Z_2} = -2 - j2d \frac{F_2 + F_1}{F_2 - F_1}$$

$$= -2 - j2 \frac{F_2 + F_1}{Q(F_2 - F_1)}$$

The attenuation at points  $F_2$  and  $F_1$  for a band-rejection filter is obtained in the same manner as for a band-pass filter, from Fig. 3.

## Band-pass Characteristics

By HENRY W. JADERHOLM

Charts relating the coefficient of coupling between two coils to the bandwidth passed, in terms of the reactance-to-resistance ratio ( $Q$  values) of the coils, useful in the measurement of coupling coefficients

THE chart shows the relation of coupling and circuit constants to the bandwidth passed by two coupled tuned circuits. Values of  $Q$  are given for the abscissas; this quantity is defined as

$$Q = \frac{2\pi fL}{R} \quad (1)$$

where  $f$  is the frequency of operation (assumed to be 2,000 kc for this chart),  $L$  is the inductance of the coil, and  $R$  is the resistance of the coil and tuned circuit. If both circuits have the same value of  $Q$ , that value is used. If the two circuits have different  $Q$  values, the geometric mean may be used

$$Q = \sqrt{Q_1 Q_2} \quad (2)$$

where  $Q_1$  and  $Q_2$  are the values for the two circuits, respectively.

### Coupling-bandwidth Relations

The ordinates of Fig. 3 are values of  $k$ , the total coefficient of coupling between

the coils, which is a combination of electromagnetic and electrostatic linkage between the coils and attached circuit elements. The coefficient  $k$  thus repre-

sents the total linkage of the two circuits. The figures on each curve refer to the width in kilocycles of the band passed by the circuits. This bandwidth has been

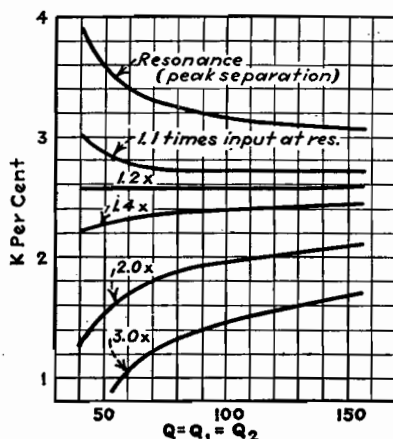


Fig. 1.—Coefficient of coupling  $k$  against circuit  $Q$  for a constant band width of 60 kc and various voltage ratios. Note that the line for 1.2 times input is nearly horizontal.

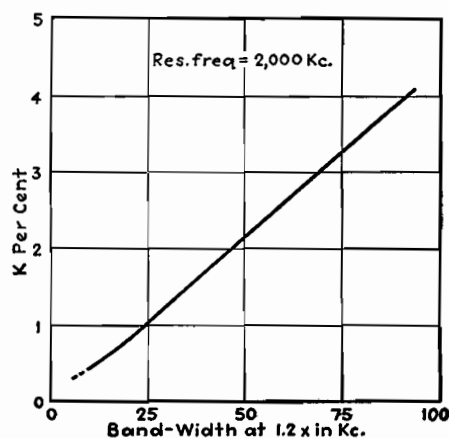


Fig. 2.—Relation between band width (at 1.2 times) and the coefficient of coupling, taken at a resonant frequency of 2,000 kc.

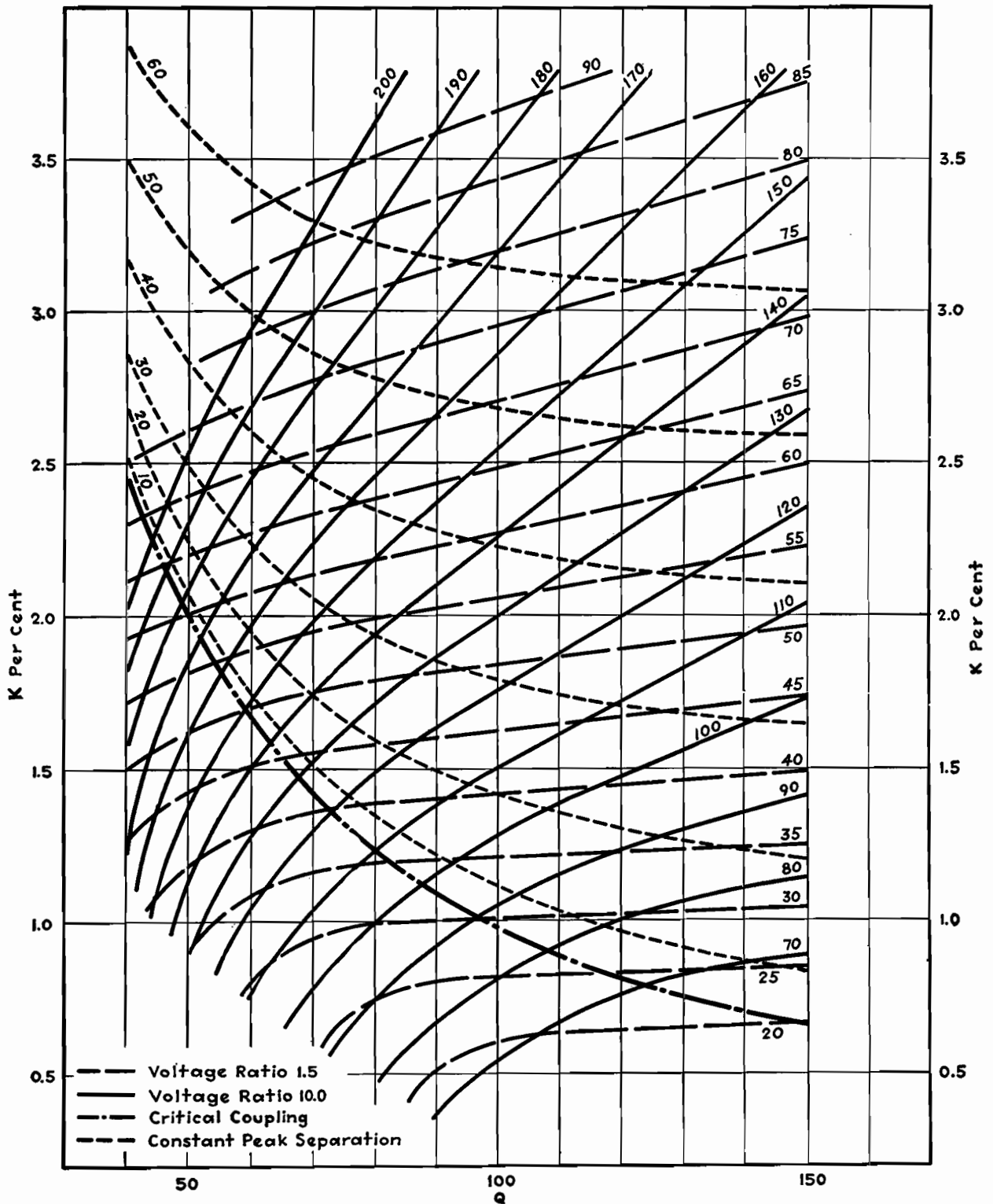


Fig. 3.—Chart giving band-pass filter characteristics.

taken for two values as shown in the legend, one family of curves for a voltage ratio of 1.5 and another for a voltage ratio of 10, where the voltage ratio is the input off resonance for constant output, input at resonance according to the definition of selectivity for receiving apparatus, which is commonly used to define properties of a

single stage as well. A curve for critical coupling is also given, as are lines of constant peak separation for the case of "sufficient" coupling.

If any two of the three quantities represented ( $Q$ ,  $k$ , and bandwidth) are known or can be measured, the third may be found from the chart.

Figure 1 has been calculated for a

constant bandwidth of 60 kc, and shows the relation between  $Q$  and  $k$  for various voltage ratios from 1.1 to 3.0. It will be noticed that the lines for ratios between 1.1 and 1.4 are approximately straight and horizontal. Thus at a voltage ratio of 1.2, the bandwidth can be used for direct measurement of coefficient of coupling. This relation has been shown

in Fig. 2, which gives the total coefficient of coupling directly in terms of bandwidth measured at a voltage ratio of 1.2 times (resonant frequency 2,000 kc).

#### Determining Coupling and Q Values

The total coefficient of coupling and Q value may also be found from two band-

width measurements, in conjunction with the chart (Fig. 3). These bandwidth measurements should be made at voltage ratios of 1.5 and 10 times, to agree with the chart. Where these bandwidth lines intersect, a point is obtained which gives the coefficient of coupling and the value of Q. Should the value of Q in the two

coils be different, the value indicated is the mean value of the two.

Although the chart has been prepared principally to aid in testing and to aid in determining values of Q and k, it may be useful in design, provided that the filter is to operate at 2,000 kc, since this frequency is assumed as a basis for the chart.

## Superheterodyne Oscillator Tracking Chart

By P. C. GARDINER

IN superheterodyne receiver engineering, the oscillator-capacitor tracking design is now considered as one of the more or less cut-and-dried problems. However, the calculations usually involved have been a nuisance to the engineer inasmuch as one value of capacitance per band or less is all he needs to know, and to get this he must wade through one or more rather long formulas.

The results presented here are an effort to simplify the general solution of the problem, together with a chart laid out for rapid design.

In Fig. 1 we have r-f and oscillator circuits whose frequencies are separated by the intermediate frequency. With  $C_v$  the same value of tracked variable capacitance in both circuits, we desire to choose  $C_2$  and  $C_1$  to be such values as to cause the oscillator frequency to track more nearly the r-f circuit than if  $C_2$  were shorted out and  $C_1$  were given the entire tracking responsibility.

The value of inductance of the oscillator circuit must be adjusted to place the circuit in the correct frequency region (e.g., 1 to 1.5 Mc or 10 to 15 Mc, etc.),

but this value can easily be found after the capacitances are known.

The inductance need not clutter up our straightforward reasoning. The capacitances and frequencies are all we need to obtain an equation containing  $C_1$ ,  $C_2$ ,  $C_v$ ,  $F_1$ , and  $F_2$ , where  $F_1$  and  $F_2$  are, respectively, the low and h-f limits of the r-f band. Furthermore, a direct solution for any one of these five quantities need not be made, since for normal given conditions enough values are usually known to produce a quick solution from the following equations, or from the chart.

No attempt has been made to cover the case where  $C_2$  lies between  $C_1$  and  $C_v$ . However, even where  $C_2$  is in the same order of magnitude as  $C_v$ , the solutions given are sufficiently accurate for use with this circuit position of  $C_2$ .

Other special cases, such as that of a coil of high distributed capacitance, are not covered for the simple reason that in practically all cases the results fall very close to those given.

In the r-f circuit

let  $F_1$  = lowest r-f frequency

$F_2$  = highest r-f frequency

$C_v$  =  $\Delta C$  of variable capacitor

$C_t$  = r-f parallel capacitance

$X$  = multiplier of  $C_v$  necessary to give mid-track point

Then

$$\frac{F_2^2}{F_1^2} = \frac{C_t + C_v}{C_t} \text{ or } \frac{C_t}{C_v} = \frac{F_1^2}{F_2^2 - F_1^2} \quad (1)$$

Now assume r-f mid-track frequency  $F_m$  to be the geometric mean of the extreme frequencies. (Calculations show that the arithmetic mean or other approximate center frequencies give practically no error from the following.) Thus,

$$F_m = \sqrt{F_1 F_2} = F_2 \sqrt{\frac{C_t}{C_t + X C_v}}$$

$$\text{or } \frac{C_t}{C_v} = X \frac{F_1}{F_2 - F_1} \quad (2)$$

$$\text{Combining Eqs. (1) and (2) } X = \frac{F_1}{F_1 + F_2}$$

In the oscillator circuit

let  $f_1$  = lowest oscillator frequency

$$= F_1 + I F$$

$f_m$  = oscillator mid-track frequency

$$= F_m + I F$$

$f_2$  = highest oscillator frequency

$$= F_2 + I F$$

$C_1$  = fixed capacitance including trimmer and all minimum capacitance in parallel with  $C_v$

$C_2$  = series capacitance

$$\text{Then } \frac{f_2^2}{f_1^2} = \frac{C_2(C_1 + C_v)}{C_1 + C_2 + C_v} \cdot \frac{C_1 C_2}{C_1 + C_2}$$

$$\text{or } \left( \frac{f_2^2}{f_1^2} - 1 \right) = A = \frac{C_2 C_v}{C_1} \left( \frac{1}{C_1 + C_2 + C_v} \right) \quad (3)$$

$$\frac{f_1^2}{f_m^2} = \frac{C_2(C_1 + X C_v)}{C_1 + C_2 + X C_v} \cdot \frac{C_1 C_2}{C_1 + C_2}$$

$$\text{or } \left( \frac{f_2^2}{f_m^2} - 1 \right) \frac{1}{X} = B = \frac{C_2 C_v}{C_1} \left( \frac{1}{C_1 + C_2 + X C_v} \right) \quad (4)$$

From Eqs. (3) and (4)

$$\frac{A}{B} = \frac{C_1 + C_2 + X C_v}{C_1 + C_2 + C_v} \quad (5)$$

$$C_1 = C_v \left( \frac{A - X B}{B - A} \right) - C_2 \quad (6)$$

Putting this into Eq. (3)

$$\frac{C_2}{C_v} = \frac{(A - X B)}{(1 - X) A B - (A - B)} \quad (7)$$

From Eq. (6) we have

$$\frac{C_1}{C_v} = \frac{A - X B}{B - A} - \frac{C_2}{C_v} \quad (8)$$

Equation (7) is plotted on the chart as a family of straight lines, and  $C_2$  is called

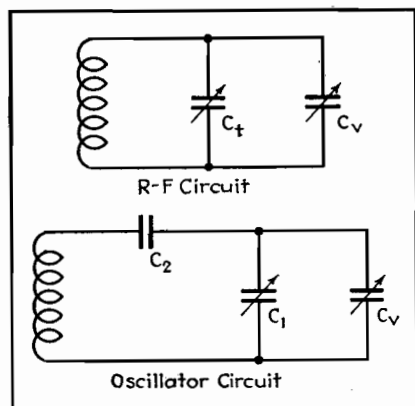


Fig. 1.—Radio-frequency amplifier and oscillator circuits in which are the trimmer and padder capacitors whose relations are outlined in this short cut to the tracking problem.



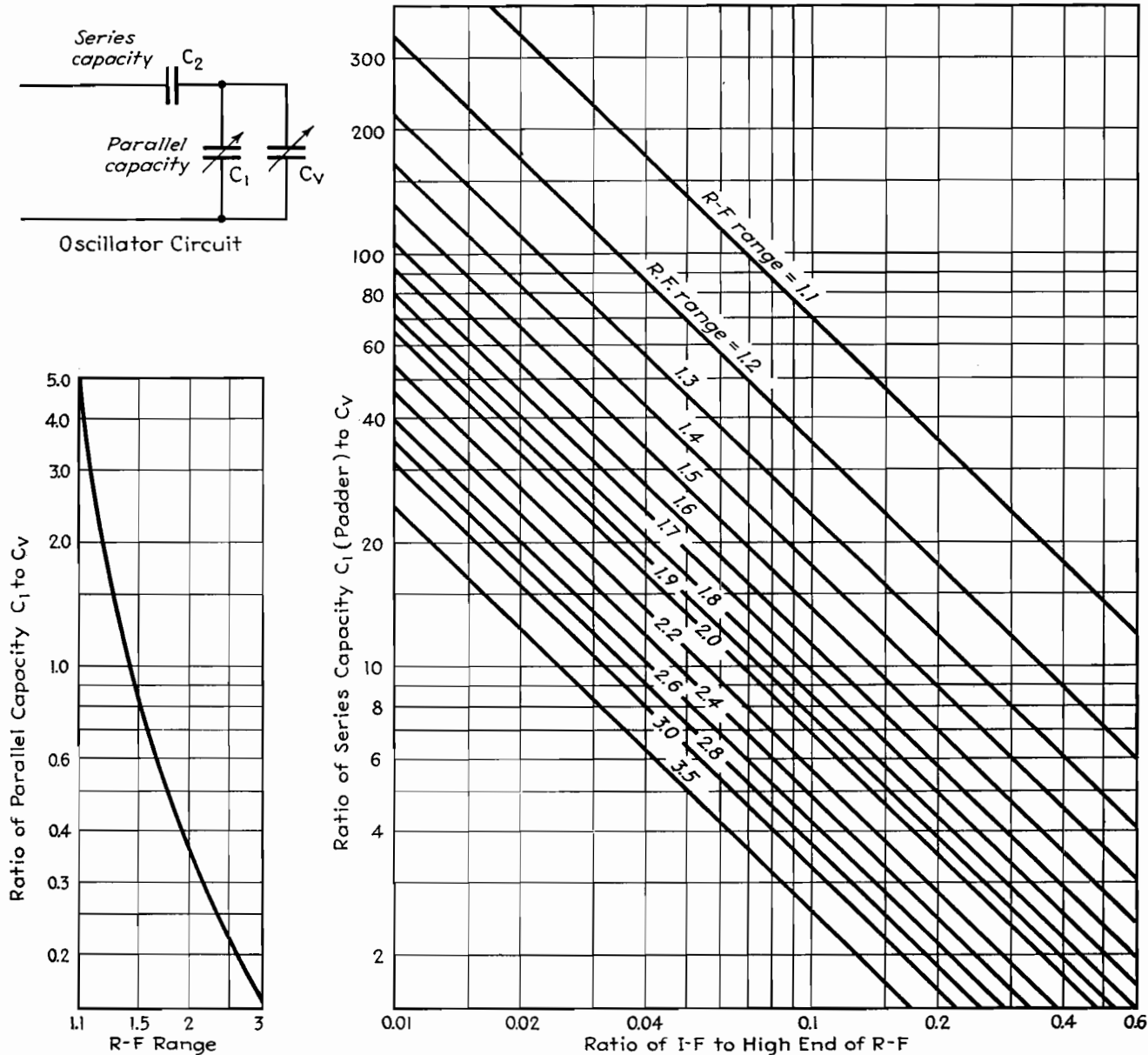


Fig. 2.—Design chart for determining series and shunt capacities for tuned circuits in single-control superheterodyne receivers.

series capacitance or padder. Equation (8) is plotted on the chart as a single curve, and  $C_1$  is called parallel capacitance.

#### Example of Design from Chart

The use of the superheterodyne tracking chart may be made more clear by means of an example involving a numerical result.

Let the upper and lower carrier frequencies be 15 and 10 Mc, respectively, and let the intermediate frequency be 3.0 Mc. Let the tuning capacitor  $C_v$  have a capacitance of 50  $\mu\text{f}$  at 10 Mc.

The problem is to determine  $C_1$  and  $C_2$ , the shunt and series capacitance respectively, and the tuning inductance  $L$ .

The tuning ratio is the ratio of the limits of the r-f spectrum, or  $15/10 = 1.5$ . The ratio of the intermediate frequency to the higher carrier frequency is  $3/15 = 0.20$ . Using the first of these values, we determine for an r-f tuning range of 1.5 that the value of  $(C_1/C_v) = 0.85$ , from the smaller graph. At 10 Mc,  $C_v = 50 \mu\text{f}$  and therefore  $C_1 = 42\frac{1}{2} \mu\text{f}$ .

Using the larger graph, we enter the

chart at the bottom corresponding to a value of 0.2 and follow vertically until we reach the 45-deg line representing an r-f tuning range of 1.5. Then, projecting to the left, we find  $(C_2/C_v) = 0.7$  and hence  $C_2 = 35 \mu\text{f}$  at 10 Mc. The three capacitances are thus determined.

The capacitors  $C_1$  and  $C_v$  in parallel are equivalent to a single capacitor  $C$  of  $92\frac{1}{2} \mu\text{f}$ . The series capacitance,  $C_2$  in series with  $C$ , gives a resultant capacitance of  $26.8 \mu\text{f}$ , so that the required inductance is  $10.7 \mu\text{h}$ .

## SECTION XXVII

# WIDE-BAND AMPLIFIERS

Compensated Amplifier Chart.....	Page
Distortion in Compensated Amplifiers.....	379
D-c Amplifier Design Techniques .....	381
Thermal Noise in a Parallel RC Circuit.....	384
	389

## Compensated Amplifier Chart

By Y. J. LIU and J. D. TRIMMER

THE accompanying chart is designed to give relative values of the gain and phase shift of one stage of a resistance-capacitance coupled amplifier which is compensated by the addition of certain elements to its load impedance. The actual and equivalent circuits of such an amplifier stage are shown in Fig. 1. The chart is based on the equivalent circuit, which includes in the shunt capacitance  $C_s$ , the interelectrode capacitances of the tube, and stray wiring capacitance of the coupling circuit.

The gain of the amplifier stage and also the phase shift between  $E_o$  and  $E_i$  can be determined so that  $(A_f/A_r = 1/\sqrt{X^2 + Y^2})$  and  $\theta_f = \tan^{-1} (Y/X)$ , where  $A_f$  is the gain at any frequency  $f$  and  $A_r$  is some particular value of gain used for reference;  $\theta_f$  is the angle of phase shift between  $E_o$  and  $E_i$ , positive when  $E_o$  lags behind  $E_i$ ; and  $X$  and  $Y$  are quantities depending on frequency and on the various circuit elements.

The expressions for  $X$  and  $Y$  can be simplified, for very high frequencies and for very low frequencies, to the same form, with parameters  $q$ ,  $A$ , and  $B$  to be defined later,

$$X = 1 - A \frac{(q/B)^2}{1 + (q/B)^2} \quad (1)$$

$$Y = q - A \frac{q/B}{1 + (q/B)^2} \quad (2)$$

The chart is simply a graphical method of finding  $X$  and  $Y$  for any given values of  $q$ ,  $A$ , and  $B$  and also of finding  $A_f/A_r$  for any values of  $X$  and  $Y$ .

The simplified forms of Eqs. (1) and (2) are obtained only by making certain assumptions. (1) The ratio  $C_s/C_o$  is considered so small compared with one

that it may be neglected. (2)  $L/C_d R_d R_c$  is much smaller than one. (3)  $R_c$  and  $R_d$  are of the same order of magnitude. (4) The time constants  $C_d R_d$  and  $C_c R_g$  are of the same order of magnitude. These four conditions are easily met in design practice and do not restrict the usefulness of the method.

The values of  $q$ ,  $A$ , and  $B$  for use in Eqs. (1) and (2) and in the chart may be defined more conveniently by first defining the resistances

$$R_H = \frac{1}{\frac{1}{R_g} + \frac{1}{R_p} + \frac{1}{R_c}}$$

$$R_L = R_g + \frac{1}{\frac{1}{R_p} + \frac{1}{R_c}}$$

$$R_{Ld} = R_L \left[ 1 + \frac{R_p R_d}{R_c (R_c + R_p + R_d)} \right]$$

where the subscripts  $H$ ,  $L$ , and  $Ld$  refer, respectively, to high frequencies, low

frequencies, and low frequencies with decoupling.

Then for high frequencies,

$$q_H = 2\pi f C_s R_H$$

$$A_H = \frac{R_H}{R_c}$$

$$B_H = \frac{C_s R_H R_c}{L}$$

and for low frequencies,

$$q_{Ld} = -\frac{1}{2\pi f C_c R_{Ld}}$$

$$A_{Ld} = \frac{R_d R_p R_g}{R_{Ld} R_c (R_c + R_p + R_d)} \left[ 1 - \frac{C_d R_d R_c}{C_c R_g (R_c + R_d)} \right]$$

$$B_{Ld} = \frac{C_d R_d R_c}{C_c R_{Ld} (R_c + R_d)}$$

As previously stated, the value of  $A_f/A_r$  is given on the chart. The reference value is  $A_r = R_H/R_p$ . This, multiplied by the tube's amplification factor, is the gain of the uncompensated amplifier in its medium-frequency range, and, if compensating elements are chosen in accord with the conditions listed above, it is also very closely the gain of the compensated amplifier in its medium-frequency range.

The dotted lines on Fig. 2 serve to illustrate the use of the chart. Suppose the h-f parameters are  $A_H = 0.96$  and  $B_H = 2.0$ . The dotted lines show how values of gain and phase angle are found for two different values of  $q_H$ , i.e., for two different frequencies.

The first step is to locate the value of  $q_H$  on the horizontal scale at the top center of the chart. Starting with  $q_H = 0.8$  and projecting down to the inclined line

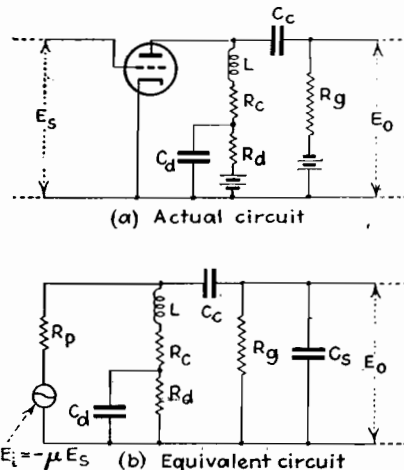


Fig. 1.—Actual and equivalent amplifier circuits.

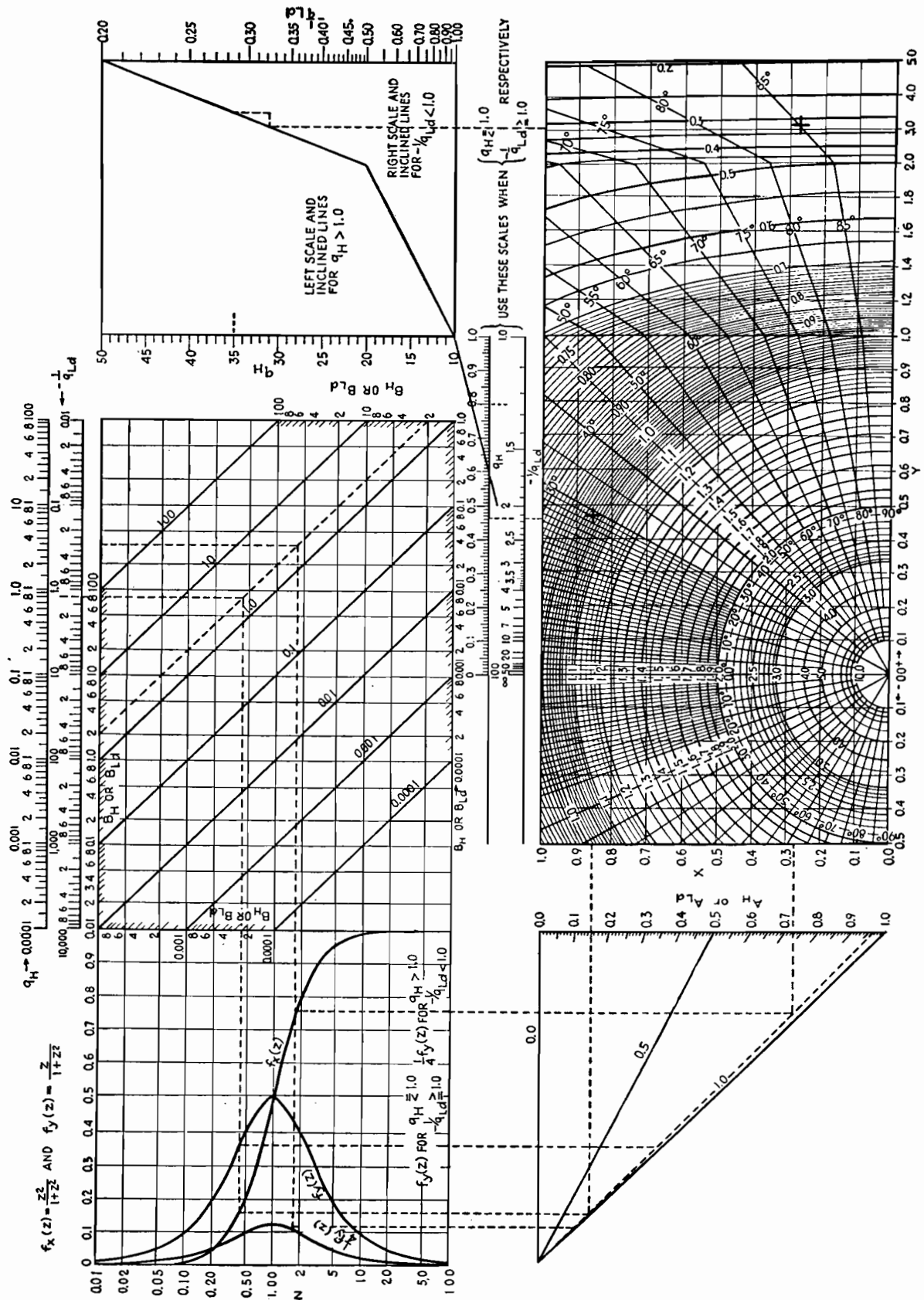


Fig. 2.—Compensated amplifier chart.

drawn for  $B_H = 2.0$ , the projection is then to the left and on to the two curves  $f_x(z)$  and  $f_y(z)$ , thence downward to the inclined line drawn for  $A_H = 0.96$ . Of the two projections, the one from  $f_x(z)$  is carried to the right; the other is used to establish the distance below the line  $A_H = 0$ . This distance is picked up and laid off, on the  $q_H$  scale in the center of the chart, to the left of the point  $q_H = 0.8$ . Projection downward then gives an intersection establishing values of  $X$

and  $Y$ , and also of gain and phase shift. Here  $X = 0.855$ ,  $Y = 0.465$ , relative gain is 1.027, and phase shift is 28.9 deg.

The procedure for  $q_H = 3.5$  ( $q_H$  greater than one) differs in two respects from the above ( $q_H$  less than one). In the upper left of the chart, the  $\frac{1}{4}f_y(z)$  curve is used instead of  $f_y(z)$ , and the length picked up from the projection from this curve to the  $A_H$ -line is laid off along the vertical  $q_H$ -scale. Thus the relative gain

is found to be 0.322 and the phase shift 85 deg.

For high frequencies, positive phase angles read from the chart mean lagging of the output relative to the input voltage. For low frequencies, positive angles on the chart mean leading of the output voltage.

For convenience in using the low-frequency parameters, the frequency scales are plotted in terms of  $-1/q_{Ld}$ , which is directly proportional to frequency; i.e.,  $-1/q_{Ld} = 2\pi f C_c R_{Ld}$ .

## Distortion in Compensated Amplifiers

By J. D. TRIMMER and Y. J. LIU

An approach to the frequency and time-delay discrimination problem in wide-band amplifiers which not only gives a general solution of a given circuit but permits amplifiers to be designed to perform within given tolerances of phase and gain distortion

IN order to provide convenient generalized expressions for the gain and phase characteristics of various combinations of circuit elements and obtain convenient methods of designing resistance-capacitance coupled amplifiers to meet specified distortion tolerances, a quantitative terminology relating to distortion must first be stated.

It is understood here that distortion is a measure of the difference in wave form (i.e., time dependence) between the output voltage  $E_o$  and some standard of comparison  $E_r$ . In many instances,  $E_r$  is the input voltage  $E_i$ . A quantitative definition of distortion would have to be based on a mathematical or physical way of evaluating the quantity  $(E_o - E_r)$ , averaged in some manner over a chosen period of time. In preference to this, it has become customary to measure distortion in terms of its causes, the properties of the network.

In nonlinear networks, the ratio between input and output voltages varies with the amplitude of the input voltage. The resultant change of wave form (due to the presence in the output of frequency components not in the input) represents nonlinear distortion. In linear networks, the ratio of output to input voltage, though independent of the amplitude, still varies with the frequency of the input voltage. The effects of this variation may be called linear distortion.

Of these effects, those due to frequency dependence of relative phase may be called phase distortion; and those due to frequency dependence of relative amplitude may be called gain distortion. (The more directly suggested term amplitude distortion is not suitable because it has, unfortunately, become associated with nonlinear distortion.)

Here we are confined to linear distortion, though many of the statements to be made would apply directly or analogously to

nonlinear distortion as well. In the actual circuit of the compensated amplifier (Fig. 1A), it is the vacuum tube that is the only seat of appreciable nonlinear distortion. Hence, considering only linear distortion, it is possible to use as a basis for discussion the equivalent circuit of Fig. 1B, in which the vacuum tube is replaced by a linear source of voltage  $-\mu E_i$  and internal resistance  $R_p$ . The internal capacitances of the tube are included with wiring capacitances in  $C_c$ .

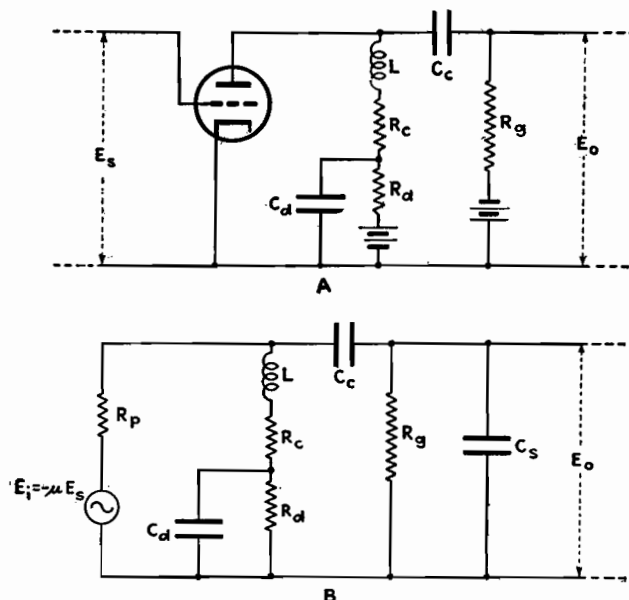


Fig. 1.—Actual (A) and equivalent (B) circuits of the shunt-peaked compensated amplifier on which this analysis is based.

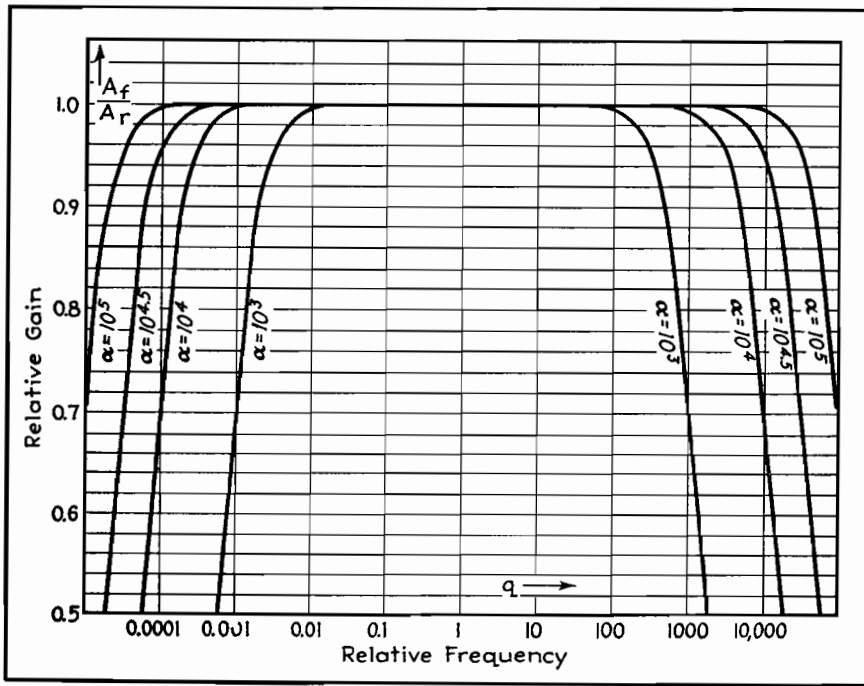


Fig. 2.—Gain-vs.-frequency response characteristic of an uncompensated amplifier plotted in terms of quantities defined in the text.

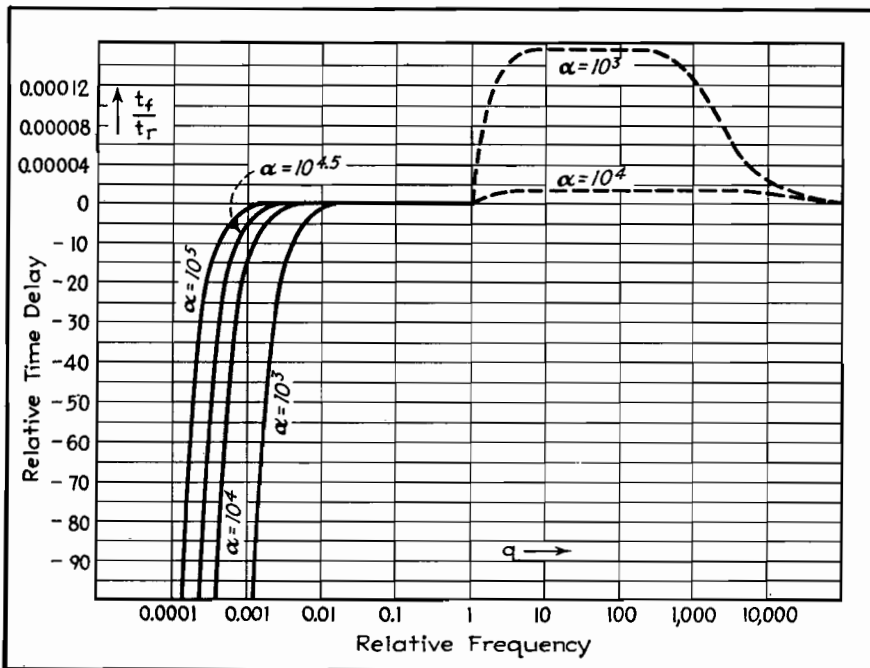


Fig. 3.—Phase shift characteristic of the uncompensated amplifier plotted in terms of relative time delay.

The properties of a network which cause linear distortion may be referred to as variations, with gain variation as a measure of the departure of the gain from a specified frequency dependence and phase variation as a measure of the departure of the phase shift from a specified frequency dependence.

The problem of compensating the resistance-coupled amplifier may be for-

mulated and discussed in terms of these definitions.

#### Compensation of Resistance-coupled Amplifiers

The equivalent circuit diagram for one stage of the uncompensated amplifier would be Fig. 1B, with  $C_d$ ,  $R_d$ , and  $L$  deleted. The gain and time-delay characteristics are plotted, respectively, in Figs. 2 and 3. For computation of these

characteristics, the complex ratio of output to input voltage is reduced to the form<sup>2</sup>

$$\frac{E_o}{E_i} = \left( \frac{A_f}{A_r} \right) e^{-j\theta_f} = \frac{1}{1 + jQ} \quad (1)$$

where  $Q$  is a function of the frequency ratio  $q = f/f_r$  and the nondimensional flatness parameter  $\alpha$ . The quantities are defined as follows:

$$\theta_f = \tan^{-1} Q$$

$$A_r = \frac{R_H}{R_p}$$

$$Q = \frac{q - (1/q)}{\alpha}$$

$$\text{where } q = \frac{f}{f_r} = 2\pi f \sqrt{C_s C_c R_H R_L}$$

$$\alpha = \sqrt{\frac{C_c R_L}{C_s R_H}}$$

$$R_H = \frac{R_o R_p R_c}{R_o + R_p + R_c}$$

$$R_L = R_o + \frac{R_p R_c}{R_p + R_c}$$

Since  $Q = 0$  when  $q = 1$ , the ordinate of Fig. 2 is the gain at any frequency  $f$  divided by the gain at the reference frequency  $f_r$ . In Fig. 3, the ordinate is the phase shift (time delay) at any frequency  $f$  (given as the time  $t_f = \theta_f/2\pi f$ ) divided by a reference time  $t_r = 1/f_r$ . In this figure, the negative ordinate scale applies to values of  $q$  less than one, the magnified positive scale to values of  $q$  greater than one.

It is seen that the time-delay curve (Fig. 3) passes through a maximum positive value at some value of  $q$  greater than one. At this same value of  $q$  (call it  $q_m$ ), the graph of the phase angle  $\theta_f$  has its tangent pass directly through the origin. For the large values of  $\alpha$  occurring in practice,  $q_m$  is given very closely by  $q_m = 1.315 \sqrt{\alpha}$ . So in contrast to the gain characteristics of Fig. 2, which are flat over a frequency range centering about  $q = 1$ , the phase characteristics of Fig. 3 are flat over a range centering about  $q = q_m$ , with  $q_m$  generally much larger than one.

Turning now to the more complicated case of the amplifier with compensating elements added as in Fig. 1, the ratio of output to input voltage can be written in the form:

$$\frac{E_o}{E_i} = \left( \frac{A_f}{A_r} \right) e^{-j\theta_f} = \frac{1}{X + jY} \quad (2)$$

But the quantities  $X$  and  $Y$  are such involved functions of frequency and the circuit elements that it seems feasible to study them only in the simplified forms they assume for the extreme ranges of high and low frequencies.

A suggestion for dealing with the problem of designing compensation to keep the variations within specified limits is embodied in Figs. 4 and 5. These graphs represent a useful and convenient way of summarizing the results of a survey of a large number of gain and phase characteristic curves, drawn for various combinations of parameter values.

In Fig. 4, one ordinate is the compensating advantage  $\eta_c$  which is defined as the ratio of the frequency at which the gain characteristic of the compensated amplifier shows a specified variation ( $\frac{1}{2}$  per cent for Fig. 4) to the frequency at which the uncompensated amplifier shows the same variation. The plotted values of  $\eta_c$  are maximum values, which can be realized only by using optimum amounts of inductance to affect h-f performance. This optimum relation is given by the  $\zeta_H$  curve, where  $\zeta_H$  is inversely proportional to the inductance  $L$ . The parameter  $A_H$  is independent of the compensating elements.

Similarly, in Fig. 5, the ordinate  $\eta_d$  is the low-frequency compensating, or decoupling, advantage, defined as the ratio of the frequency at which the uncompensated amplifier's time-delay characteristic shows a specified variation ( $\frac{1}{2}$  per cent for Fig. 5) to the frequency at which the compensated amplifier shows the same variation. Of the two parameters  $\gamma$  and  $k$ ,  $\gamma$  involves  $R_d$  while  $k$  involves both  $R_d$  and  $C_d$ . The ratio  $R_g/R_L$  does not involve the compensating elements. The optimum relations between  $k$  and  $\gamma$  are given by the  $k$  curves, and the corresponding maximum values of  $\eta_d$  are plotted for the  $\eta_d$  curves.

In Fig. 5, the 0.5 per cent tolerance of phase-time variation is based on the

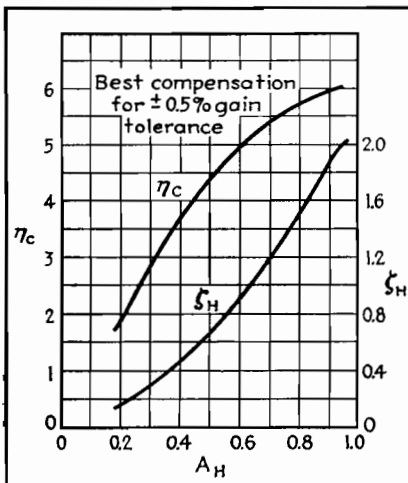


Fig. 4.—Curves for obtaining the best compensation possible in the high-frequency range.

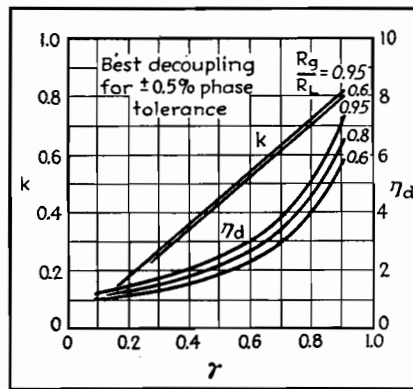


Fig. 5.—Curves for obtaining the best compensation possible in the low-frequency range.

ordinate  $t/t_L$ , where

$$t_L = C_d R_L$$

The parameters  $\zeta_H$ ,  $\gamma$ , and  $k$  of Figs. 4 and 5 are defined

$$\zeta_H = \frac{C_d R_H^2}{L}$$

$$\gamma = \frac{R_p R_d}{(R_c + R_p)(R_c + R_d)}$$

$$k = \frac{C_d}{C_d R_g} \frac{R_c R_d}{(R_c + R_d)}$$

There remains the second problem, which may now be described as relating

the variations of the network to the distortions of the wave forms the network is supposed to handle.

Attention is to be given here primarily to phase distortion. The suggestions proposed concern themselves principally with two questions. First, there is the question of the best way of presenting the phase characteristic so that its variations are obvious and so that it is conveniently useful in predicting phase distortion. The second question is the finding of a method for estimating, from known variations of a given network, the distortion of particular wave forms.

An example that answers both questions to some extent is given in Fig. 6. It is assumed that a perfect saw-tooth input voltage  $E_i$  is applied to one stage of an uncompensated resistance-coupled amplifier. If the fundamental frequency of the input is low enough compared with the middle reference frequency  $f_r$  of the amplifier, the output voltage  $E_o$  will show decided phase distortion. Figures 6A and 6B are drawn, respectively, for fundamental frequencies  $f_r/2,000$  and  $f_r/1,000$ . The amplifier is assumed to have a flatness parameter  $\alpha = 10^4$ .

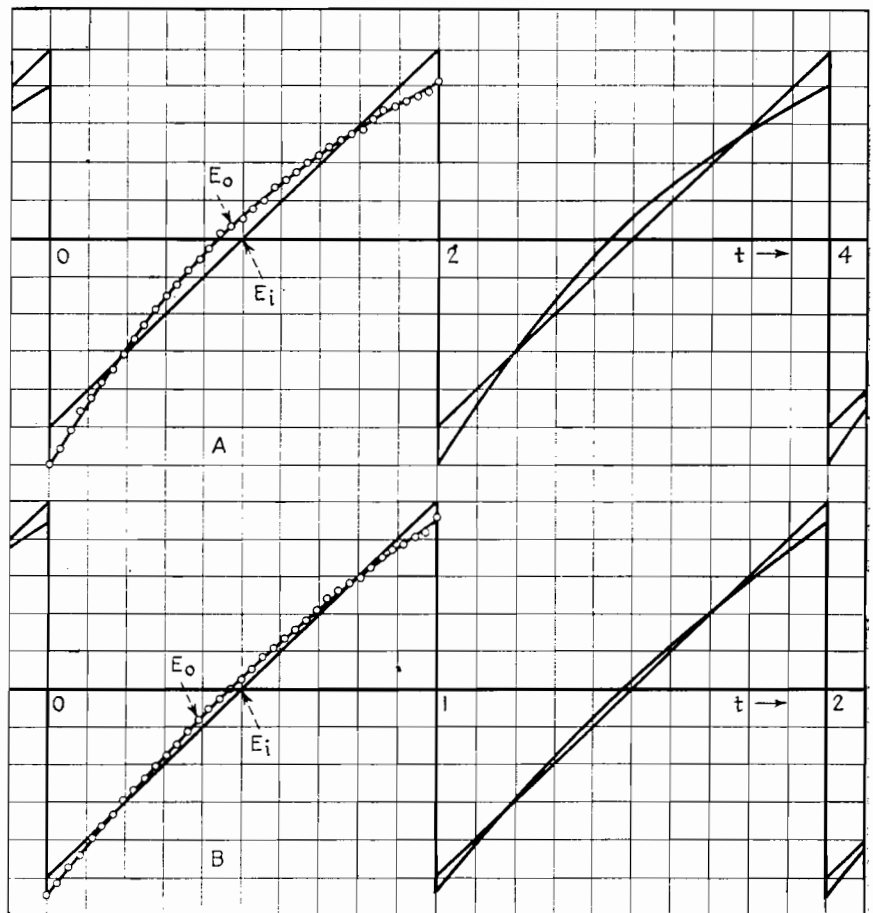


Fig. 6.—Phase distortion of a saw-tooth wave computed by Fourier analysis.

The work summarized in Fig. 6 and in Figs. 2 and 3 may be regarded as a complete solution to the problem of specifying phase distortion tolerances for the uncompensated amplifier. For one has only to look at Fig. 6 and decide whether the amount of distortion shown in  $A$  or in  $B$  (or in another similar graph) is the most that can be tolerated, and the numerical factors of the design are at once determined.

The  $E_o$  curves of Fig. 6 were obtained by replotting the first six harmonic components of  $E_i$ , shifted along the time scale according to the phase characteristic given in Fig. 3, and plotting the higher frequency components as though they had no phase shift at all. The error involved in this approximation is indicated by the slight "ripple" which can be detected in the strings of points. Reference to the appropriate low-frequency points of the gain characteristic for  $\alpha = 10^4$  in Fig. 2 shows that gain variation is quite negligible (less than 2 per cent). One might expect that the gain variation at high frequencies would cause a rounding of the corners as indicated in Fig. 6. How small this effect actually is can be inferred from the fact that for the

same tolerance of 2 per cent,  $q = 2,000$ , and the amplitude of the component at this frequency is one four-millionths of the fundamental amplitude.

This example, therefore, suggests the following general procedure for estimating distortion of periodic waves. The input wave is analyzed into its Fourier components; each component is changed in amplitude according to the relative gain at its frequency, and shifted along the time axis an amount equal to the phase shift at that frequency; the changed components are then added to make up the output wave; and finally, the output wave is compared with the input wave for changes in shape. In general, this would appear to be a very tedious effort. But the above example suggests that, as far as the wave is concerned, usually only a limited number of components are of important amplitude; and, as far as the network is concerned, usually the variations are appreciable only in a limited range of frequency.

#### The Phase Tangent

In conclusion, it may be well to refer to the statement, widely disseminated in the literature, that the phase time shift

(usually called time delay) at a given frequency is equal to the slope of the phase-angle characteristic at that frequency. This is an approximate truth that may be quite useful in many cases, but that may cause serious errors if used injudiciously. The criterion is simple to appreciate and is as follows. The phase time shift is exactly equal to the slope of the phase angle characteristic for a characteristic that consists solely of lines drawn from zero or multiples of  $2\pi$  on the ordinate axis. Hence if a phase characteristic can be closely approximated by tangents drawn from these points, the actual phase distortion will be closely approximated by taking phase time shift equal to the slope of the phase-angle curve. But for cases in which the tangents give a poor approximation (*e.g.*, one stage of a resistance-coupled amplifier), phase time shift at a given frequency may be far from equal to the slope at that frequency.

#### References

- (1) LIU, Y. J., and TRIMMER, J. D., *Electronics*, September, 1939.
- (2) LUCK, D. G. C., A Simplified Method for Resistance-capacity Coupled Amplifier Design, *Proc. IRE*, **20**, 1401, 1932.
- (3) DRAPER, C. S., *Jour. Aeronaut. Sci.*, **5**, 219, 1938.

## D-c Amplifier Design Techniques

By EDWARD L. GINZTON

Design equations with practical examples, stabilization of negative feed-back amplifiers, cathode-follower and phase-inverter considerations, tube-drift problems in high-gain d-c amplifiers, and operation of multistage amplifiers from common power supplies

A METHOD of directly coupling successive stages of a vacuum-tube amplifier without using a common B supply has been described by W. M. Brubaker.<sup>1</sup> In the simplified version of this circuit given in Fig. 1a, a battery is shown tapped near the middle, with a resistor connected across the entire battery. Regardless of the position of the tap on the battery, there is always a point on the resistance that is exactly at the same potential as the tap on the battery. Thus, it is possible to tap a source of voltage  $(E_1 + E_2)$  and, regardless of the load placed on the source of voltage, find a point on the load that will be at the same potential as the tap.

In Fig. 1b, this tap has been applied to the amplifier coupling. A source of voltage  $(E_1 + E_2)$  is tapped, and this point is connected to the cathodes of the two tubes. Then resistances  $R_1$ ,  $R_2$ ,  $R_3$ , and the (d-c) plate resistance  $R_p$  of the tube are so chosen that the junction between resistors  $R_2$  and  $R_3$  is at the same potential as the tap on the source of voltage  $(E_1 + E_2)$ . Any number of tubes may be cascaded in this manner, all using the same power supply.

This method makes it possible to eliminate the zero-signal d-c component from any similar circuit. Several other modifications are illustrated later, with circuit data.

#### Design Equations

The equivalent diagram of Fig. 1b, together with the symbols that are used below, are shown in Fig. 2. It should be noted that  $R_p$  is the d-c plate resistance of the tube, equal to the d-c voltage  $E_o$  at the plate of tube divided by d-c plate current  $I_p$ . The analysis of this circuit should show how the voltage  $E_3$  depends on the various constants shown in Fig. 2, and how this voltage can be adjusted to any desired value. Applying Kirchhoff's law to Fig. 2, one has

$$\left. \begin{aligned} i_p(R_p + R_1) + i_2(R_1) &= E_1 \\ i_p(R_1) + i_2(R_1 + R_2 + R_3) &= E_1 + E_2 \end{aligned} \right\} (1)$$

But  $i_p = \frac{E_o}{R_p}$  and  $i_2 = \frac{E_2 - E_3}{R_3}$



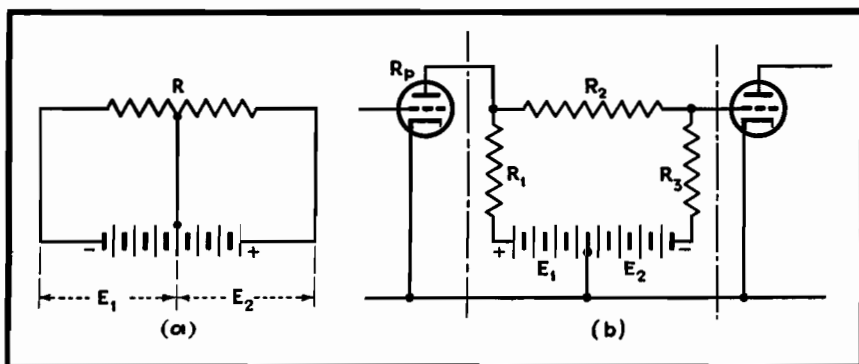


Fig. 1.—Basic bridge circuit and bridge version used for interstage coupling.

By combining these equations and rearranging their terms,

$$R_2 = R_1 \frac{E_0 + E_3}{E_1 - E_0(1 + R_1/R_p)} \quad (2)$$

$$\text{and } R_3 = R_1 \frac{E_2 - E_3}{E_1 - E_0(1 + R_1/R_p)} \quad (3)$$

Equations (2) and (3) are the design equations. If one designs an amplifier for given supply voltages  $E_1$  and  $E_2$ , and a given plate voltage  $E_0$ , and if one knows  $R_1$ , then  $R_2$  and  $R_3$  may be computed to produce the required  $E_3$ . Sometimes, however, one knows all voltages; i.e.,  $E_1$ ,  $E_2$ ,  $E_0$ , and  $E_3$ , but  $R_3$  must not exceed a certain value. Then Eq. (3) can be inverted

$$R_1 = R_3 \frac{E_1 - E_0}{E_2 - E_3 + E_0(R_3/R_p)} \quad (4)$$

Now, from Eqs. (2) and (3),

$$R_2 = R_3 \frac{E_0 + E_3}{E_2 - E_3} \quad (5)$$

forming an alternate set of design equations.

If a resistance-capacitance coupled amplifier is designed to produce a certain amplification  $A_0$ , and is converted into a d-c amplifier by means of the circuit described above, the amplification  $A$  of the d-c amplifier will be less than  $A_0$  owing to the voltage drop across  $R_2$ . Efficiency of amplification may then be defined as  $\eta = A/A_0$ . While an exact expression for the efficiency can be derived, it is more significant to use an

expression based upon a few assumptions. If the resistance-capacitance coupled amplifier is a pentode tube with an infinite dynamic plate resistance, load resistance  $R_1$ , and grid leak resistance  $R_3$ , and a transconductance  $g_m$ , its amplification is

$$A_0 = g_m \frac{R_1 R_3}{R_1 + R_3} \quad (6)$$

If a d-c amplifier is now designed using the same load resistance  $R_1$  and the same grid leak resistance  $R_3$ , then the amplification of the d-c amplifier will be

$$A = g_m \frac{R_1(R_2 + R_3)}{R_1 + R_2 + R_3} \frac{R_3}{R_2 + R_3} = g_m \frac{R_1 R_3}{R_1 + R_2 + R_3} \quad (7)$$

#### Efficiency of Amplification

The efficiency of amplification  $\eta$  can be computed by combining Eqs. (3), (5), (6), and (7), giving

$$\eta = \frac{1}{1 + \frac{E_0 + E_3}{E_2 - E_3 + E_1 - E_0(1 + R_1/R_p)}} \quad (8)$$

The significance of this relation can be seen more clearly when  $E_3 = 0$  and the supply voltage  $E_B = (E_1 + E_2) \gg E_0(1 + R_1/R_p)$ , all of which is accurate enough for qualitative discussion, remembering that  $R_p$  can be considered infinite. Then

$$\eta \approx \frac{1}{1 + E_0/E_B}$$

This means that for best efficiency  $E_0$  should be as small as possible in comparison to the supply voltage. As an example, a 6SJ7 may be operated under the following conditions:

$$\begin{aligned} E_B &= 400 \text{ volts} \\ E_1 &= E_2 = 200 \text{ volts} \\ E_0 &= 100 \text{ volts} \\ E_3 &= 0 \text{ volts} \\ \frac{R_1}{R_p} &= 0.5 \end{aligned}$$

Using Eq. (8), the comparative amplification is found to be 71.4 per cent. By means of more careful design, efficiencies in the neighborhood of 80 per cent can be realized.

#### Example

As an example, Fig. 3 shows a two-stage amplifier using two 6J7 tubes. Suppose a 400-volt power supply is available. From a tube manual, one finds the recommended operating conditions for such a tube. For 6J7:

Plate supply voltage....	180	volts
Screen voltage.....	30	volts
Grid voltage.....	1.55	volts
Plate voltage ( $E_0$ ).....	60	volts
Plate current ( $i_p$ ).....	0.24	ma
Screen current.....	0.08	ma
Plate load ( $R_1$ ).....	0.5	megohm
Grid leak ( $R_3$ ).....	0.5	megohm
Cathode resistor.....	4,850	ohms
Voltage amplification...	93	
Transconductance $g_m$ ....	375	$\mu$ mhos

The d-c amplifier operating under similar conditions will have the following modifications in its design formulas, obtained from the above data and the notation previously given:

$$\begin{aligned} R_p &= \frac{E_0}{i_p} = \frac{60}{0.24 \times 10^{-3}} = 0.25 \text{ megohm} \\ E_0 &= 60 \text{ volts} \\ E_2 &= 150 \text{ volts} \\ E_1 &= 250 \text{ volts} \\ E_3 &= 0 \text{ volt} \\ R_1 &= 0.5 \text{ megohm} \end{aligned}$$

$E_3$  may be any practical value, zero being the most convenient. From Eqs. (2) and (3),  $R_2 = 1.07$  megohms and  $R_3 = 0.428$  megohm. The amplification per stage can be computed from Eq. (7), and is found to be 100. This is higher than the corresponding resistance-capacitance coupled stage because of the higher grid-leak resistance. If the resistance-capacitance coupled amplifier were to use the same grid-leak resistance, its amplification would be about 125 for the same value of plate current.

It should be noticed that in single-ended amplifiers with cathode resistors, there is a loss in amplification due to negative feedback introduced by the cathode resistors, so that the effective amplification per stage is  $A_{eff} = A_0/(1 + R_c g_m)$ , where  $R_c$  is the cathode resistance. In the example shown in Fig. 3, this reduction in amplification is from 100 to 37. If the screen voltage is obtained by means of a series dropping resistor, even a further reduction of gain could be expected.<sup>2</sup>

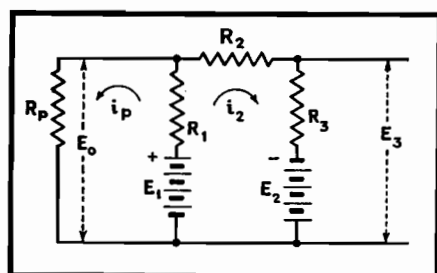


Fig. 2.—Equivalent circuit of the coupling network in Fig. 1b.

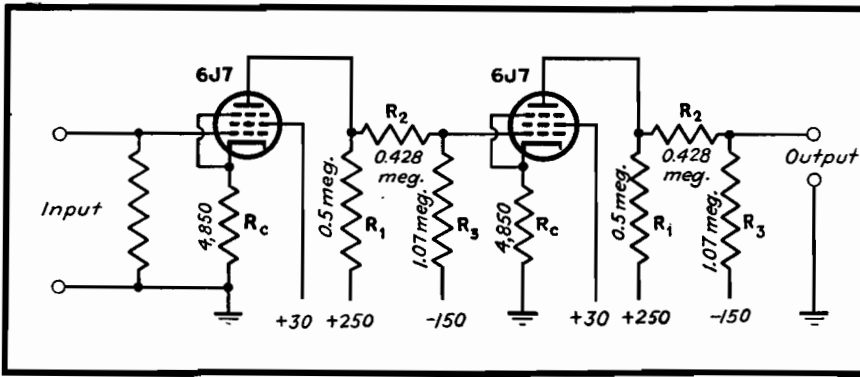


Fig. 3.—A two-stage d-c amplifier using pentode tubes.

The decrease in amplification due to negative feedback introduced by the cathode and screen resistors can be eliminated either by using push-pull amplifiers, in which case there is no degeneration, or by using fixed grid bias and screen supplies.

The amplifier shown in Fig. 3 should have an over-all amplification of about 1,400, a uniform frequency response from zero to 20,000 cycles, and should be able to deliver about 50 volts peak without appreciable distortion.

#### Stabilization of Negative Feed-back Amplifiers

Since the output of the Brubaker amplifier can be adjusted to have a zero d-c component, conventional negative feed-back circuits can be used to stabilize the amplifier. In applying negative feedback, the same oscillation criterion applies as in the case of the ordinary resistance-capacitance coupled amplifiers: unlimited feedback can be applied in one or two stages without any oscillation troubles, and over a larger number of stages if proper care is taken.<sup>3</sup> In general, application of feedback to one stage does not produce great benefits, and more than two stages require a compromise design between frequency response and the degree of stabilization. It is the two-stage amplifier that is easiest to handle if audio frequencies as well as direct current have to be amplified.

If negative feedback is applied to a two-stage amplifier (or any even number of stages), such as shown in Fig. 4, the feedback resistor  $R_4$  has to be connected from the plate circuit of the last stage to the cathode resistor of the first stage. As a result of this, there is an undesirable loss of amplification due to two effects: (1) the un-bypassed cathode resistor  $R_c$  in the first stage, and (2) the loss in gain of the second stage due to the shunting of the plate load by  $(R_4 + R_c)$ .

As was shown in the preceding section,

the first of these could be appreciable, while the effect of the second depends on the magnitude of the feedback desired. These two effects are interrelated in such a way that the greater one attempts to make  $\beta$  (the fraction of output that is introduced into the input), the lower is the amplification of the two stages. This just means that in order to obtain a high degree of the stability, and at the same time the highest possible amplification, these two effects must be minimized.

In practice, this can be done by (1)

designing the output stage to operate with the lowest possible impedance so that the shunting effect of a given  $(R_4 + R_c)$  is as small as possible, (2) designing the input stage with the highest possible impedances so that for a given  $\beta$ ,  $R_4$  becomes as high as possible, (3) adjusting the operation of the first stage so that its gain is obtained for the lowest possible value of  $g_m$ , to reduce the degenerative effects of  $R_c$ , the un-bypassed cathode resistance of the first stage, (4) obtaining the bias for the second stage either with a bias cell, or merely by choosing the proper value of  $E_3$ .

If properly designed, it is possible to obtain both a stabilization factor of 100 and an amplification of approximately 100 with a two-tube pentode amplifier. Figure 4 shows the circuit and frequency response of an amplifier similar to one of Fig. 3, but stabilized by means of negative feedback. It will be observed that in order to connect resistance  $R_4$  without disturbing the potentials of the circuit, a tap on resistance  $R_2$  had to be used which had the same potential with respect to ground as the upper terminal of  $R_c$  of the first stage.

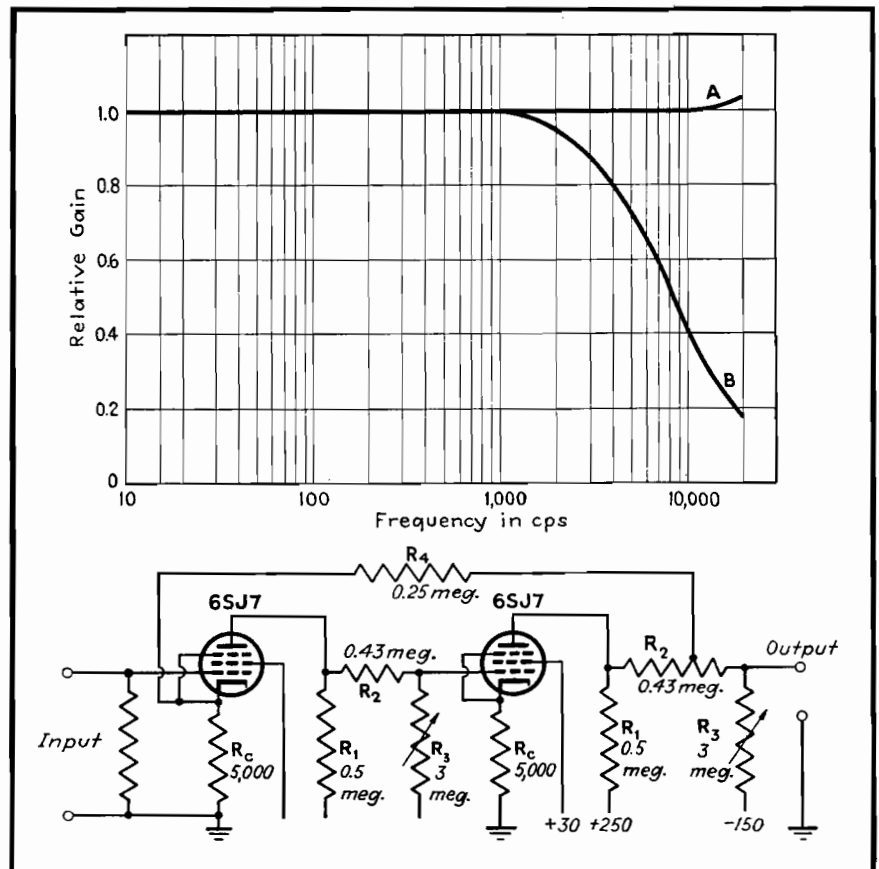


Fig. 4.—A two-stage direct-coupled amplifier employing negative feedback. Curve A shows the frequency response with feedback; B, without feedback.

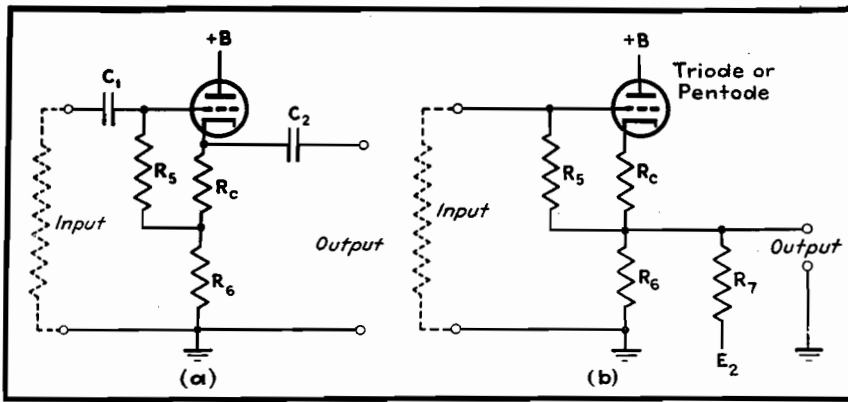


Fig. 5.—The conventional R-C coupled cathode follower (a) and the Brubaker equivalent of the conventional cathode follower (b).

#### Cathode-follower Considerations

Cathode followers of the type shown in Fig. 5a find application in circuits where a high impedance has to be converted into a low one without the use of transformers. In most such cases, in addition to the bias resistor  $R_c$ , a resistance  $R_6$  is added which allows greater output voltages and at the same time develops degenerative feedback which tends to stabilize the action of the tube against voltage and tube characteristic changes.

In conventional cathode followers, the proper bias voltage developed across  $R_c$  is introduced to the grid through the resistance  $R_5$ . The voltage across  $R_6$  is kept from altering the situation by a blocking capacitor  $C_1$  on the input side. Capacitor  $C_2$  prevents the direct voltage across  $(R_c + R_6)$  from appearing at the output terminals.

Figure 5b shows the d-c equivalent of Fig. 5a. Here the capacitors are omitted and the undesired direct voltage across  $R_6$  is eliminated by connecting  $R_7$  to  $E_2$ , which may be the same voltage as is used in the amplifier proper. The proper value of resistance  $R_7$  is chosen so that the current supplied from  $E_2$  through  $R_6$  and  $R_7$  just equals the total cathode current of the tube; i.e.,

$$i_p = \frac{E_2}{R_6 + R_7} \quad \text{or} \quad R_7 = \frac{E_2}{i_p} - R_6 \quad (9)$$

#### Phase-inverter Considerations

Push-pull arrangements have even greater advantages in d-c amplifiers than in resistance-capacitance coupled ones. Single-ended input voltages can be converted to push-pull ones by means of phase inverters, which are shown in Fig. 6. It will be seen that these are again merely modifications of the well-known a-c circuits.

Figure 6a shows a push-pull amplifier in

which one grid is driven by the unbalanced input and the second grid from the output circuit of the first one. The circuit to the left of the line *aa* is designed in the obvious manner using formulas previously given. If this is done, then the d-c potential from point *b* to ground will be zero, and point *c* can be chosen so that the ratio  $(R_{10} + R_{11})/R_{10}$  equals the voltage amplification of the driven stage. If properly designed and adjusted, the input to both tubes will be

balanced, there will be no degeneration due to cathode resistance  $R_c$ , and the gain will be the highest possible with the tubes used.

The phase inverter shown in Fig. 6b is perhaps the more useful of the two. If one were to bisect the circuit by a horizontal line into two symmetrical parts, then each one would again be designed along the general principles outlined before. Each half of the circuit could possess a high degree of stability due to degenerative feedback developed by the resistor  $R_c$ . In the form shown in Fig. 6b the lower tube is driven by the signal voltage developed across  $R_c$  due to the driver tube. If

$$\frac{R_c R_8}{R_c + R_8} q_m > 1$$

then the output of the device will be balanced to the same degree as the above inequality. The balance, of course, can be made perfect by adjusting the tap *b* to the proper point.

It should be pointed out that resistors  $R_{11}$  and  $R_{12}$  provide the proper bias voltages for the two tubes, whereas  $R_c$  and  $R_8$  are so adjusted as to give the highest

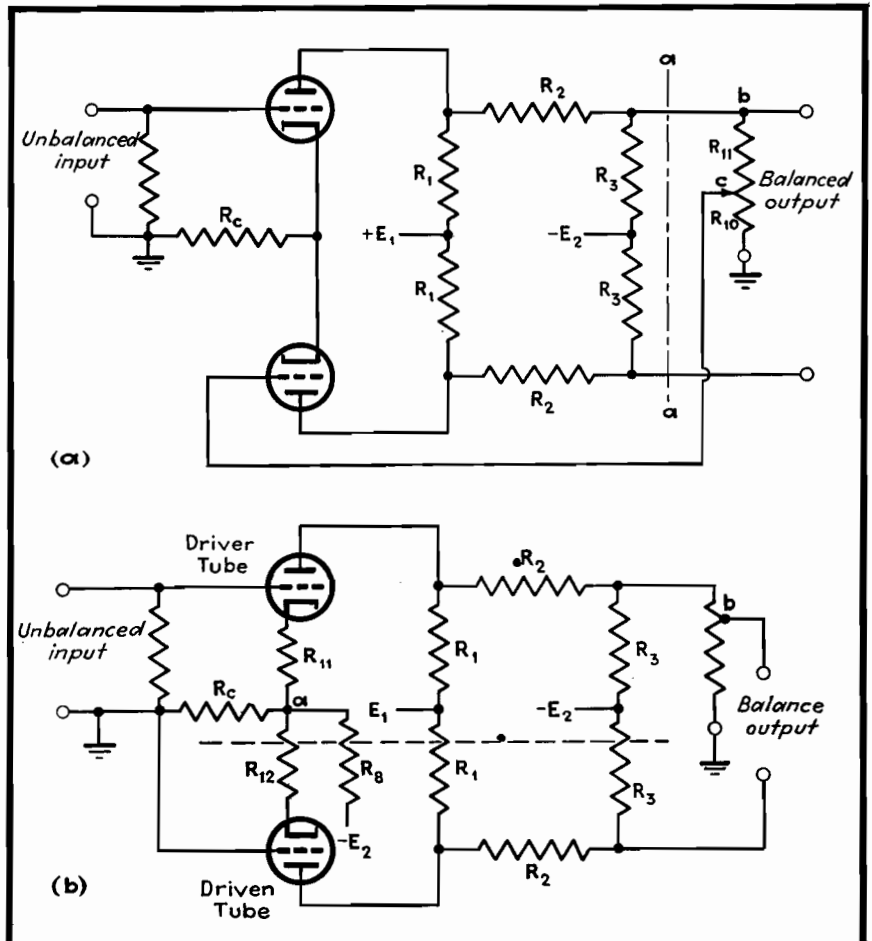


Fig. 6.—Two types of d-c phase inverters. The tubes can be either triodes or pentodes in the circuit at (a).

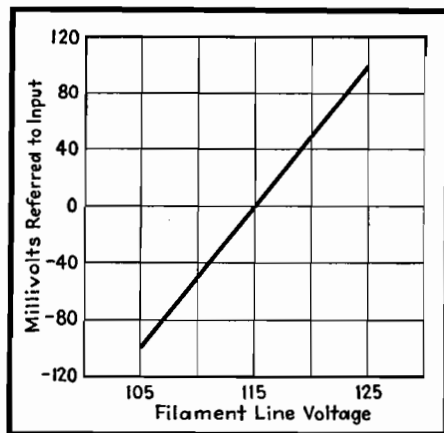


Fig. 7.—Output voltage variation of the amplifier shown in Fig. 4 due to filament voltage changes.

possible value of  $R_c R_8 / (R_c + R_8)$  and still maintain the potential from point  $a$  to ground zero, to provide for the condition that  $R_c R_8 / (R_c + R_8) \gg R_{11}$  or  $R_{12}$ . Other types of phase inverters often used in a-c circuits can be easily converted for d-c applications.

#### Tube Drift Problems in High-gain Amplifiers

The most difficult problem in a high-gain d-c amplifier is the change in the plate current of the first tube due to random changes in the work function of the cathode surface. These current changes are usually small, but are always present. Negative feedback cannot eliminate these changes because they act as if they were input signal variations and as such cannot be distinguished from the signal itself.

The most serious immediate cause of these current changes is the filament voltage; although ambient temperature affects the current also. (In addition, there seem to be other causes that are not yet understood.) To illustrate the magnitude of these changes, Fig. 7 shows the variation of the output voltage due to changes in filament voltage. The ordinate is an equivalent input voltage, i.e., change in output voltage amplification.

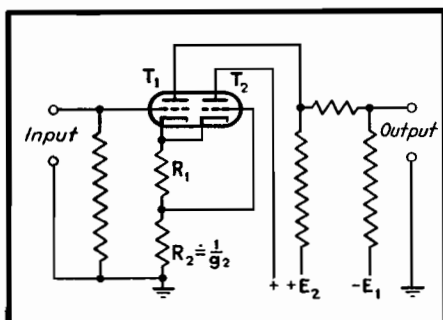


Fig. 8.—The basic Miller circuit which improves the drift problem of the input stage of the d-c amplifier. If  $g_2$  is the transconductance of  $T_2$ , then  $R_2$  is nearly equal to  $1/g_2$ .

A great improvement can be realized by means of a circuit described by Miller.<sup>1</sup> Miller uses a double triode with a common cathode, and the circuit is so arranged that, if one triode behaves in the same manner as the other, cancellation of the variation takes place. The basic circuit is shown in Fig. 8. If  $R_2 = 1/g_2$ , then  $\Delta e = \Delta i_1 R_1 - (g_2 \Delta i_1 R_1) R_2 = 0$ , and changes in emitter characteristics that are common to both sections will produce no net change in the plate current of the active amplifier  $T_1$ . An amplifier built with the first stage modified in this manner is shown in Fig. 9. Figure 10 shows the variation of the output voltage (again referred to input) as a function of the filament voltage of the first tube. It is seen that for a proper value of the resistance  $R_2$ , a marked improvement is produced.

#### Operation of Multistage Amplifiers from Common Power Supplies

If many stages are used in an amplifier, currents flowing through the source of voltage ( $E_2$  and  $E_1$ ) from the last stages can introduce voltages into the earlier stages. This causes regeneration which can express itself either in oscillation or other undesirable effects. There are two ways to avoid the trouble: (1) use of low-impedance power supplies, (2) separately filtered lines to groups of stages. The former can be accomplished by means of either batteries or properly designed electronic voltage regulators, and the second by voltage regulator tubes such as VR-105.

The general method described is useful in extending practically all known techniques now used in a-c amplifiers to zero frequency. These methods are not restricted to amplification alone.

One of the objectionable features of

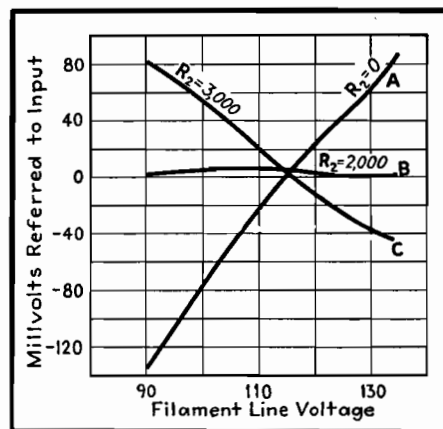


Fig. 10.—The effect of Miller compensation on the stability of the amplifier shown in Fig. 9 in respect to filament voltage changes.

this method is the necessity of two voltages, positive and negative with respect to ground. Miller<sup>4</sup> attempts to get around this difficulty by using cold-cathode regulating tubes as circuit elements. The use of these tubes in this manner brings up other problems, however. The VR tubes need a fairly high voltage to start them and draw heavy currents. This causes troubles in design, adjustment, and operation. The VR tubes also tend to be noisy, so that their use is usually restricted in amplifiers, at least as circuit elements. The two required voltages can be obtained from one power supply and do not require additional parts.

#### References

- (1) BRUBAKER, W. M., D-C Amplifier. *Bull. Amer. Phys. Soc.*, Vol. 14, No. 6, Dec. 7, 1939. (Program for the University of California meeting.)
- (2) THERMAN, F. E., HEWLETT, W. R., PALMER, C. W., and WEN-YUAN PAN, Calculation and Design of Resistance-coupled Amplifiers Using Pentode Tubes, *Trans. AIEE*, Vol. 59, 1940.
- (3) THERMAN, F. E., *Electronics*, January, 1937.
- (4) MILLER, STEWART, E., Sensitive D-C Amplifier with A-C Operation, *Electronics*, November, 1941.

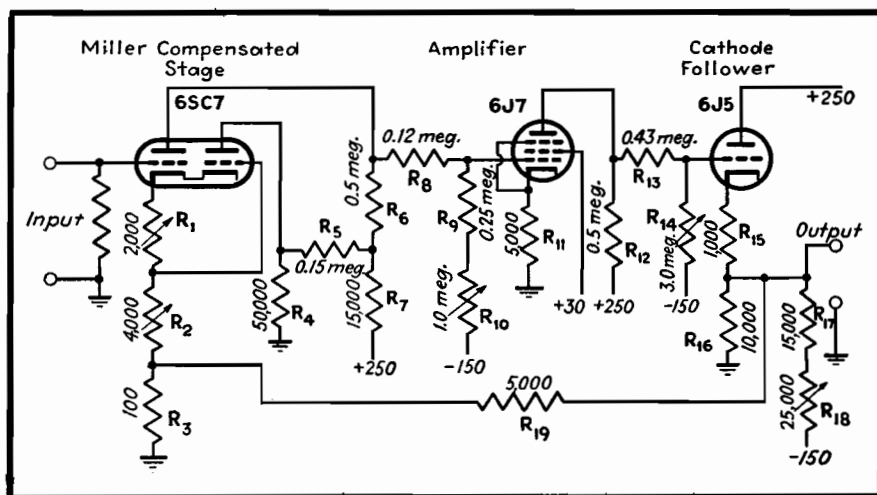


Fig. 9.—A two-stage d-c amplifier using a Miller compensated stage, a cathode follower, and stabilized negative feedback.

# Thermal Noise in a Parallel RC Circuit

By C. J. MERCHANT

Chart giving thermal noise voltage in microvolts produced by random electron movement in a circuit composed of resistance shunted by capacitance, for any desired bandwidth and for the entire frequency spectrum

**T**HE lower limit to the magnitude of voltages that can be measured is set by the so-called thermal-agitation voltages which arise spontaneously in the measuring apparatus itself. When listened to, this noise manifests itself as a rushing, hissing sound, and is familiar to all who have worked with high-gain wide-band audio amplifiers.

## Basic Formula

This voltage is a result of the random movement of electrons in a conductor, and is a function of the temperature of the conductor, its resistance, and the bandwidth over which the voltage is measured. Since components of all frequencies and random phasing are present, one can only specify this voltage in terms of its rms value. The formula relating the above variables is as follows:

$$E = \sqrt{4kTR\Delta f} \quad (1)$$

In this formula,  $E$  is the rms voltage appearing across the terminals of the resistance,  $k$  is Boltzmann's constant, equal to  $1.374 \times 10^{-23}$  joule per °K,  $T$  is the temperature in degrees Kelvin,  $R$  is the resistance in ohms, and  $\Delta f$  is the bandwidth over which the voltage is measured. At room temperature this formula becomes

$$E = 1.28 \times 10^{-10} \sqrt{R\Delta f} \quad (2)$$

This formula holds only for pure wire-wound resistances of zero phase angle. In the case of a general two-terminal impedance containing reactances as well as resistance, F. C. Williams has shown\* that one may compute the thermal noise voltage in either of two ways: (1) one may consider that only the resistances in the impedance give rise to thermal-agitation voltages, and that the reactances serve only as filtering agents by suppressing or reinforcing certain frequency bands; (2) one may reduce the

impedance to the equivalent series circuit, integrate the resistive component of the impedance over the desired frequency band, and substitute the result in place of  $R\Delta f$  in formula (2). This formula then becomes

$$E = 1.28 \times 10^{-10} \sqrt{\int_{f_1} R df} \quad (3)$$

Using either method leads to identical results.

## Noise in Crystal or Condenser Microphone Circuit

A case which arises frequently is that of computing the noise voltage, over a given bandwidth, which arises from a resistor shunted by a capacitor. This is the case of a crystal or condenser microphone which, together with its grid leak, acts as the input circuit of an amplifier. Since such microphones, if their frequency characteristic is flat over a wide range, have relatively low output, the thermal noise output of the microphone and its grid leak often determine the minimum signal that can be measured. The other limiting factors are the ambient noise of the room and the shot noise of the first tube of the following amplifier.

The resistive component of the impedance of a resistor and capacitor in parallel is given by

$$Re(Z) = R \left( \frac{1}{1 + \phi^2} \right) \quad (4)$$

where  $R$  is the value of the resistor in ohms, and  $\phi = f/f_0$ , where  $f_0$  is the frequency at which  $X_C = R$ , and is given by  $f_0 = 1/2\pi RC$ , where  $C$  is in farads. Substituting this expression in Eq. (3) and rewriting  $f_1$ ,  $f_2$ , and  $df$  in terms of  $\phi$  expressed in radians, one has

$$E = 1.28 \times 10^{-10} \sqrt{\int_{\phi_1}^{\phi_2} \left( \frac{R}{1 + \phi^2} \right) \left( \frac{d\phi}{2\pi RC} \right)} \\ = \frac{1.28 \times 10^{-10}}{\sqrt{2\pi C}} \sqrt{\arctan \phi_2 - \arctan \phi_1} \quad (5)$$

Equation (5) shows that the h-f regions contribute very little to the total noise

voltage output. Thus, if one computes the voltage developed across a given resistor in parallel with a given capacitor between  $f_0$  and  $100 f_0$ , it is found to be equal to  $44.7 \times 10^{-12}/\sqrt{C}$ . For the same  $R$  and  $C$ , the total rms voltage developed between  $f_0$  and infinity equals  $45 \times 10^{-12}/\sqrt{C}$ . Thus, the entire region between  $100 f_0$  and infinity contributes less than 1 per cent to the total output. Hence if, as is generally the case, one desires to know the total noise output from a resistor and capacitor in parallel as measured by an amplifier whose lower cutoff frequency is in the vicinity of  $f_0$  and whose upper cutoff frequency is many times  $f_0$ , it will be substantially correct to take this upper cutoff frequency as infinity.

## Basis of Chart

The chart was constructed by taking the lower frequency limit  $f_1$  as some multiple  $N$  of  $f_0$ , and the upper frequency limit as infinity. It gives the value of the rms fluctuation voltage  $E$  between the frequency limits  $\phi_1$  (in radians) =  $N$  and  $\phi_2 = \infty$ , where  $\phi_1 = f/f_0$ ,  $f_0 = 1/2\pi RC$ , and the value of  $E$  is obtained from the following transformation of Eq. (5), in which  $E$  is in microvolts and  $C$  is in micromicrofarads:

$$E = \frac{128}{\sqrt{C}} \sqrt{\frac{\arctan \cot \phi_1}{2\pi}} \quad (6)$$

To accomplish this transformation,  $\phi_2$  is set equal to infinity, so that  $\arctan \phi_2$  equals  $\pi/2$  radians or 90 deg. The resulting expression under the radical is then equal to  $\arctan \cot \phi_1$ . The change in the numerical coefficient is a consequence of expressing  $E$  in microvolts and  $C$  in micromicrofarads in Eq. (6).

Thus, suppose it were desired to find the rms noise-voltage developed across a 20- $\mu\mu\text{f}$  capacitor and a 10-megohm resistor in parallel, between the frequency limits of  $f = 400$  cycles and infinity. Here  $f_0$  is the frequency at which  $X_C = R = 10$  megohms, and from

\* WILLIAMS, F. C., Thermal Fluctuations in Complex Networks, Wireless Section, *Jour. IEE*, 13, 53, March, 1938.

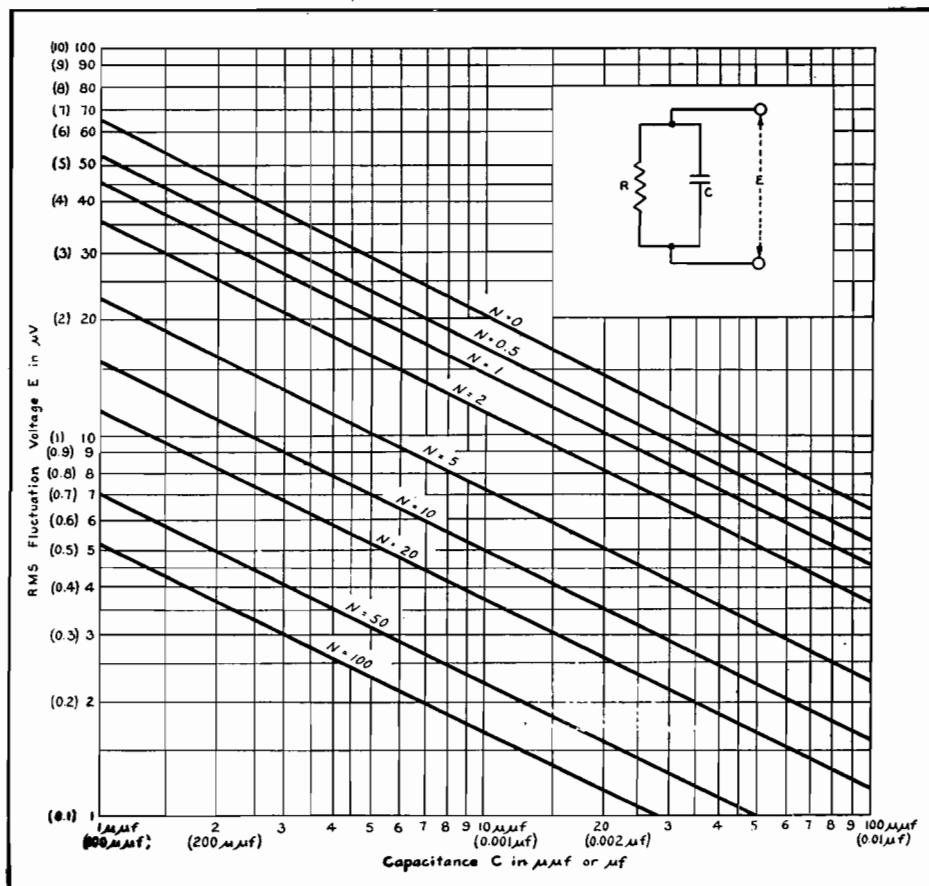


Chart giving rms value of fluctuation voltage across R and C in parallel between a given frequency limit and infinity. The frequency limit is converted into a value N as explained in the accompanying article. When values in parentheses are used on one scale, the parenthesis values on the other scale must be used.

the equation  $f_0 = 1/2\pi RC$  we get 800 cycles as the value of  $f_0$ . Hence  $N = f/f_0 = 400/800 = 0.5$ , and the intersection of the abscissa  $C = 20 \mu\text{f}$  and the contour  $N = 0.5$  is found to occur on the ordinate marked 12  $\mu\text{V}$ .

#### Example of Chart Use

By taking advantage of the fact that noise voltages add as the square root of

the sum of the squares of the component voltages, the chart can be used to find the noise voltage developed when neither of the frequency limits can be considered infinite. Suppose, for example, it were desired to find the voltage developed across the above R and C between the frequency limits of 400 and 800 cycles. From the above, the rms voltage de-

veloped between 400 and 800 cycles equals  $\sqrt{5^2 - 3.5^2}$  or approximately 3.6  $\mu\text{V}$ .

#### Effect of R on Noise Output Voltage

It is worthwhile noting that the total noise voltage output of a given resistor and capacitor in parallel, measured between the frequency limits of zero and infinity, is independent of the value of R, and depends solely on the value of C, as long as R is some finite value different from zero. The value of R serves only to determine the distribution in the spectrum of the total energy, which is determined by C. Stated in a somewhat different fashion, for any given value of C, the voltage output measured between  $f = 0$  and  $f = f_0$  is the same as the output measured between  $f = f_0$  and  $f = \text{infinity}$ . Either of these statements may be verified by reference to Eq. (5).

#### Total Fluctuation Voltage up to Infinite Frequencies

Although no amplifier or meter can be made that will indicate to infinite frequency, the concept of total noise generated over the total spectrum is useful, since it sets an upper limit to the thermal agitation voltage to be expected from an impedance, no matter what the bandwidth over which the actual measurement is made. Thus, by referring to the contour labeled  $N = 0$  on the chart, it is seen that irrespective of either the resistor or the bandwidth, if  $C = 10 \mu\text{f}$ , the total fluctuation voltage will be less than 20  $\mu\text{V}$ . In some cases, this might be all the information needed, as, for example, in the case where the following amplifier itself had a noise or hum level of several times this quantity.